AFRL-ML-WP-TR-2005-4239

(Also Identified As)

AFRL-ML-WP-TP-2005-409



IMPROVING THE D2512 LOX COMPATIBILITY OF COMPOSITES BY USING THERMALLY CONDUCTIVE GRAPHITE FIBERS

Roger Gerzeski
AFRL/MLBC
2941 Hobson Way, Rm 136
Wright-Patterson AFB OH 45433-7750

SEPTEMBER 2005

Approved for public release; distribution is unlimited.

MATERIALS AND MANUFACTURING DIRECTORATE
AIR FORCE RESEARCH LABORATORY
AIR FORCE MATERIEL COMMAND
WRIGHT-PATTERSON AIR FORCE BASE, OH 45433-7750

NOTICE

Using Government drawings, specifications, or other data included in this document for any purpose other than Government procurement does not in any way obligate the U.S. Government. The fact that the Government formulated or supplied the drawings, specifications, or other data does not license the holder or any other person or corporation; or convey any rights or permission to manufacture, use, or sell any patented invention that may relate to them.

This report was cleared for public release by the Air Force Research Laboratory Wright Site Public Affairs Office (AFRL/WS) and is releasable to the National Technical Information Service (NTIS). It will be available to the general public, including foreign nationals.

THIS TECHNICAL REPORT IS APPROVED FOR PUBLICATION.

ROGER GERZESKI, Principal Investigator
Structural Materials Branch
Nonmetallic Materials Division

TIA BENSON TOLLE, Chief
Structural Materials Branch
Nonmetallic Materials Division

PERSIS A. ELWOOD, Deputy Chief
Nonmetallic Materials Division
Materials and Manufacturing Directorate

This report is published in the interest of scientific and technical information exchange and its publication does not constitute approval or disapproval of its ideas or findings.

Table Of Contents

Main Report — Page

Preamble

Part A - Introduction 1-44

Part B - Theory 45-78

Part C - Experimental 79-189

Part D - Results 190-471

Part E - Discussion 472-488

Part F - Conclusion 489

Part G - Bibliography 490-525

Appendix A1-A311

Part H - Residuals A1-A295
- Part I – Disc Residuals
- Part J – Cup Residuals
- Part K – Moat Residuals
- Part L – BagTag Residuals

Part M - Designed Equipment A296-A311

Titles and Signature Page

REPORT DOCUMENTATION PAGE	Form Approved OMB No. 0704-0188

The public reporting burden for this collection of information is estimated to average 1 hour per response, including the time for reviewing instructions, searching existing data sources, gathering and maintaining the data needed, and completing and reviewing the collection of information. Send comments regarding this burden estimate or any other aspect of this collection of information, including suggestions for reducing the burden, to the Department of Defense, Executive Services and Communications Directorate (0704-0188). Respondents should be aware that notwithstanding any other provision of law, no person shall be subject to any penalty for failing to comply with a collection of information if it does not display a currently valid OMB control number.

PLEASE DO NOT RETURN YOUR FORM TO THE ABOVE ORGANIZATION.

1. REPORT DATE *(DD-MM-YYYY)*	2. REPORT TYPE	3. DATES COVERED *(From - To)*
30-09-2005	Tech Report	Jul 01 - Apr 05

4. TITLE AND SUBTITLE
Improving the D2512 LOX Compatibility of Composites by Using Thermally Conductive Graphite Fibers

5a. CONTRACT NUMBER
N/A

5b. GRANT NUMBER

5c. PROGRAM ELEMENT NUMBER
62102F

6. AUTHOR(S)
Roger Gerzeski

5d. PROJECT NUMBER
N/A

5e. TASK NUMBER
N/A

5f. WORK UNIT NUMBER
N/A

7. PERFORMING ORGANIZATION NAME(S) AND ADDRESS(ES)
AFRL/MLBC
2941 Hobson Way, Rm 136
Wright-Patterson AFB OH 45433-7750

8. PERFORMING ORGANIZATION REPORT NUMBER
AFRL-ML-WP-TR-2005-4239
(Also Identified As)
AFRL-ML-WP-TP-2005-409

9. SPONSORING/MONITORING AGENCY NAME(S) AND ADDRESS(ES)
Materials and Manufacturing Directorate
Air Force Research Laboratory
Air Force Materiel Command
Wright-Patterson Air Force Base, Ohio 45433-7750

10. SPONSOR/MONITOR'S ACRONYM(S)
AFRL/MLBC

11. SPONSOR/MONITOR'S REPORT NUMBER(S)
AFRL-ML-WP-TR-2005-4239
(Also Identified As)
AFRL-ML-WP-TP-2005-409

12. DISTRIBUTION/AVAILABILITY STATEMENT
Approved for public release; distribution unlimited.

13. SUPPLEMENTARY NOTES
This report contains color.

14. ABSTRACT
This effort demonstrated that using a thermally conductive fiber substantially enhances a composite's ASTM D2512 mechanical impact liquid oxygen compatibility. It repeatedly achieved 90% of the goal of passing D2512 with a 1700% improvement over baseline. This effort also documented the types of fracture surfaces routinely found in the residuals of the materials investigated. These fracture surfaces indicate that hertzian fracture is the mechanism by which a specimen fractured and failed. The fracture surfaces routinely indicated that kinetic friction associated with signs of intense heating occurred. Kinetic frictiion's mechanical-to-thermal transformation mechanism provided the only phenomenological explanation for the extremely rapid and large temperature rises required for conditions recognizable as ignition to occur in the time frame of a D2512 test. The effort crystallized the sequence from fracture to heating to ignition. First a series of Hertzian fractures develop. These allow kinetic friction of the Hertzian fractured material to occur. Kinetic friction transforms mechanical energy into temperature rising thermal energy. This thermal energy causes the material to degrade by radical chain scission and oxidize by radical addition peroside chemistry to a degree detectable as ignition.

15. SUBJECT TERMS
liquid oxygen, LOX, DE2512, mechanical impact, ignition, launch vehicle, polymer matrix composite, thermal conductivity, thermally conductive fiber, graphite fiber, YSH 50, YSH 60, carbon fiber, T650-35, 5250-4 RTM, Hertzian fracture, conchoidal fracture, kinetic friction, peroxide chemistry, radical chain scission, thermal degradation

16. SECURITY CLASSIFICATION OF:			17. LIMITATION OF ABSTRACT	18. NUMBER OF PAGES	19a. NAME OF RESPONSIBLE PERSON
a. REPORT	b. ABSTRACT	c. THIS PAGE			Roger Gerzeski
UNCLAS	UNCLAS	UNCLAS	SAR	888	19b. TELEPHONE NUMBER *(Include area code)* (937) 255-9068

Standard Form 298 (Rev. 8/98)
Prescribed by ANSI Std. Z39.18

Table Of Contents

Main Report	Page
Abbreviations	iv
List Of Figures	v-xii
List Of Tables	xiii
Executive Summary	xiv-xvii
Introduction ……	1-44
Theory ……	45-78
Ignition Event	45-56
Hertzian Fracture	57-66
Kinetic Friction	67-78
Experimental ……..	79-189
Material Selection	79-87
Lab Room, Equipment And Material Handling Cleaning Procedures	88-89
Prepreging	90-93
Prepreg Cutting And Additional Measurements	94-105
Composite Panel Lay Up Sequence And Sizes	106-107
Bleed Flow Composite Plate Lay Up And Cure Profile Development	108-124
Specimen Composite Plate Lay Up And Cure Profile Development	125-148
5250-4 RTM Neat Resin Specimen Plate Casting	138
D2512 Specimen Fabrication	149-172
Specimen Cleaning And Packaging	173-179
Thermal Conductivity Specimen Fabrication And Testing	180-189
D2512 Laod Versus Time Plots	188-189
Results ……	190-471
D2512 LOX Compatibility Tests	190-191
Contaminated D2512 LOX Compatibility Test Specimen Rejection	190, 192
Thermal Conductivity Tests	193-194
Fractography	194-467
D2512 Load Versus Time Plots	468-471
Discussion ……	472-488
Conclusion	489
Bibliography	490-525
Appendix ……..	A1-A311
Residuals	A1-A295
Designed Equipment	A296-A311

Abbreviations

Prepreg Areal Weight; PAW
Fiber Areal Weight: FAW
Resin Content: RC
Fiber Volume: V_f
Resin Volume: V_r
Void Volume: V_v
Dry Filtered Nitrogen: DFN_2
Liquid Oxygen: LOX
Liquid Nitrogen: LN_2
Expendable Launch Vehicle: ELV
Fresh, Clean and New: FC&N
Polyethylene: PE
Polypropylene: PP
Bismaleimides: BMI
Author and Principal Investigator: A&PI
Bend To Failure: BTF
Safeskin Purple Nitrile: SPN
Triple Distilled Water: TDW
Isopropyl Alcohol: IPA
Methylethylketone: MEK
Thermal Conductivity: K

List Of Figures Page

Introduction
Figure 1, Launch Vehicles Which Use LOX 1
Figure 2, Launch Vehicle LOX Tankage Sizes 2-3
Figure 3, Local Site Temperature Rise And Thermal Transport Mechanisms 5
Figure 4, Thermal Conductivity Of Materials Used In Making Common LOX Components. 5
Figure 5, Ambient Pressure D2512 LOX Impact Sensitivity Tester 8-10
Figure 6, Thermal Conductivity Of Conventional PAN Based Carbon Fiber Composites. 41
Figure 7, Pitch Graphite Fiber Composites Thermal Conductivity 43
Figure 8, Thermal Conductivity Of Granoc XN Graphite Fibers Versus Temperature 44
Figure 9, Room Temp Thermal Conductivity Of Various PAN Carbon And Pitch Graphite Fibers 44
Figure 10, Estimated Thermal conductivity window for making a D2512 LOX compatible composite. 44

Theory: Ignition Event
Figure 11, Initial Ignition Event Step 45
Figure 12, Ignition Event
Figure 13, Temperature Vs Time Rises In NaCl and PTFE Resulting From Mechanical Impacts 47-48, 53-55
Figure 14, Chemical Thermal Degradation Breakdown Products Vs Temperature 51-52

Theory: Hertzian Fracture
Figure 15, Hertzian Loading Indenters 57
Figure 16, Hertzian Stress Field And Stress Trajectories 58
Figure 17, Ring Crack 58-59
Figure 18, Hertzian Cone Crack Development 59
Figure 19, Hertzian Cone Crack Development In Glass 60
Figure 20, Hertzian Cone Crack Parameters 60
Figure 21, Extreme Hertzian Fracture: Conchoidal Fracture 61
Figure 22, Compressive Zone Vent Crack Development 61
Figure 23, Flaw Density 62
Figure 24, Ring Crack Initiation Load Probabilities 62
Figure 25, Effect Of Load Duration And Environment On Hertzian Fracture Initiation Load 63
Figure 26, Impacter Miss Alignment Effects 64
Figure 27, Sharp Pointed Indenter Generated Cracks 64-65
Figure 28, Sliding Impacter Hertzian Stress Fields 66
Figure 29, Stacked Hertzian Crescent Shaped Cone Cracks And Flares 66

Theory: Kinetic Friction
Figure 30, Real Area Of Contact 67
Figure 31, Kinetic Friction's Mechanical Behavior 68
Figure 32, Kinetic Friction Thermal Transport Model 68
Figure 33, Sheared Asperity Temperature Rises "Hot Spot": Magnitude and Duration 69
Figure 34, Hot Spot Temperature Rise Distributions 70
Figure 35, Temperature Rise Versus Sliding Material's Thermal Conductivity 72
Figure 36, WLF Type Correlation 73-74
Figure 37, Initial versus Steady State Coefficients Of Friction 75
Figure 38, Reinforcement Incorporation Effects On Coefficients Of Friction 76

List Of Figures Continued Page

Figure 39, Distinctive Physical Traces Of Kinetic Friction 78

Experimental
Figure 40, Selected Carbon-Graphite Fibers 83
Figure 41, YSH50A and YSH60A Fiber Surface Metal Properties 84
Figure 42, Lab Room 89
Figure 43, 72 inch x 12 Inch Drum Wound Prepreg Tape Cutting 90
Figure 44, Prepreg Individual Ply Cutting Dimensions: 12x9 Specimen Plate 95-98
Figure 45, Prepreg Individual Ply Cutting Dimensions: 6x6 Bleed Flow Plate 99-100
Figure 46, Prepreg Cutting Table and Tools 101
Figure 47, Prepreg Cutting Templates 101
Figure 48, Resin Extraction 102
Figure 49, Proposed Specimen Plate Lay Up Sequence And Dimensions 107
Figure 50, Uncured Composite Bleed Flow Plate Stack Assembly And Initial Vacuum Debulk 111-113
Figure 51, Actual Bleed Flow Plate 3 Cure Profile Used 115
Figure 52, Bleed Flow 3 Composite Plate C Scans 116-118
Figure 53, Cured Bleed Flow 3 Composite Plates 119-121
Figure 54, Microscopy and Digital Picture Capture Equipment 122
Figure 55, Bleed Flow 3 Composite Plate Micrographs 123
Figure 56, Uncured Composite Specimen Plate Stack Assembly And Initial Vacuum Debulk 128-130
Figure 57, Actual D2512 Specimen Composite Panel Cure Profile 132
Figure 58, Cured Specimen Plates In Bagging 133
Figure 59, Perforated Kapton Bagged For Post Cure Specimen Plates 133
Figure 60, Perforated Kapton Bagged Post Cured Specimen Plates 133
Figure 61, Actual Specimen Panel Post Cure Profile Used 133
Figure 62, Specimen Plate C Scans 134-136
Figure 63, Backscatter Unfinished D2512 Specimens C Scans 137
Figure 64, Cured Specimen Plates 139-144
Figure 65, Specimen Plate Micrographs 145-147
Figure 66, Core Drill and Clean Storage Container 150
Figure 67, Coolant Adapter 151
Figure 68, Coolant Pump and Reservoir 152
Figure 69, Cutting Jig, Jig Assembly Tools, Catch Basin and Mill Clamp Plate 153
Figure 70, T650-35 Fiber Composite Specimen Plate Coring 155
Figure 71, Specimen Storage Between Processing Steps From Coring To Final Cleaning 156
Figure 72, Unfinished “Slightly Trapezoidal” Cylinder D2512 Specimens 157-158
Figure 73, Cored Composite Specimen Plate Edges 159-161
Figure 74, Cored Unfinished D2512 Specimen Abrasion: 50X Magnified 163-165
Figure 75, Cored Unfinished D2512 Specimens 166-170
Figure 76, D2512 Specimen Surface Finish 171
Figure 77, Sanded and Beveled D2512 Specimens 172
Figure 78, Clean Glassware Storage 175
Figure 79, Clean Glassware, Specimen Handling Tools, Bagging Tools And Storage 176
Figure 80, Ultrasonic Washing And Rinsing 177
Figure 81, Vacuum Elevated Temperature Drying 178
Figure 82, Aclar Bagged D2512 Specimens 179
Figure 84, X and Y Axis Thermal Conductivity Measurement Specimen Assembly 182
Figure 85, Thermal Conductivity Specimen Vacuum Bag Tear Prevention Damming 183

List Of Figures Continued Page

Figure 86, Thermal Conductivity Measurement Cube Cubes AF191 Bond Line Cure Profile 183
Figure 87, X and Y Axis Cured Thermal Conductivity Measurement Cube Specimens 184
Figure 88, Thermal Conductivity Cube Specimen C Scans 184
Figure 89, Thermal Conductivity Specimen Micrographs: Bond line And Adjacent Composite 185-187
Figure 90, Final Thermal Conductivity Measurement Specimens Orientation 189

Results
Figure 91, Rejected Due To Contamination D2512 Specimen 192
Figure 92, Composite Thermal Conductivity 193
Figure 93, Specimen residual clamping and holding tool dimension 195
Figure 94, External To The Indenting Impacter Fracture Surfaces: Ring Cracks: 5250-4 RTM D2512 Specimen 201-206
Figure 95, External To The Indenting Impacter Fracture Surfaces: Ring Cracks: T650-35 / 5250-4 RTM D2512 Specimen 207-209
Figure 96, External To The Indenting Impacter Fracture Surfaces: Ring Cracks: YSH50 / 5250-4 RTM D2512 Specimen 210-212
Figure 97, External To The Indenting Impacter Fracture Surfaces: Ring Cracks: YSH60 / 5250-4 RTM D2512 Specimen 213-216
Figure 98, External To The Indenting Impacter Fracture Surfaces: Transverse And In Plane Cracks: 5250-4 RTM D2512 Specimen 217-223
Figure 99, External To The Indenting Impacter Fracture Surfaces: Transverse And In Plane Cracks: T650-35 / 5250-4 RTM D2512 Specimen 224-229
Figure 100, External To The Indenting Impacter Fracture Surfaces: Transverse And In Plane Cracks: YSH50 / 5250-4 RTM D2512 Specimen 230-236
Figure 101, External To The Indenting Impacter Fracture Surfaces: Transverse And In Plane Cracks: YSH60 / 5250-4 RTM D2512 Specimen 237-243
Figure 102, External To The Indenting Impacter Fracture Surfaces: Knobs: 5250-4 RTM D2512 Specimen 244-246
Figure 103, External To The Indenting Impacter Fracture Surfaces: Knobs: T650-35 / 5250-4 RTM D2512 Specimen 247-250
Figure 104, External To The Indenting Impacter Fracture Surfaces: Knobs: YSH50 / 5250-4 RTM D2512 Specimen 251-254
Figure 105, External To The Indenting Impacter Fracture Surfaces: Knobs: YSH60 / 5250-4 RTM D2512 Specimen 255-256
Figure 106, External To The Indenting Impacter Fracture Surfaces: Straight Cracks: 5250-4 RTM D2512 Specimen 257-262
Figure 107, External To The Indenting Impacter Fracture Surfaces: Straight Cracks: T650-35 / 5250-4 RTM D2512 Specimen 263-265
Figure 108, External To The Indenting Impacter Fracture Surfaces: Straight Cracks: YSH50 / 5250-4 RTM D2512 Specimen 266-268
Figure 109, External To The Indenting Impacter Fracture Surfaces: Straight Cracks: YSH60 / 5250-4 RTM D2512 Specimen 269-271
Figure 110, External To The Indenting Impacter Fracture Surfaces: Abrasion: 5250-4 RTM D2512 Specimen 272-276
Figure 111, External To The Indenting Impacter Fracture Surfaces: Abrasion: T650-35 / 5250-4 RTM D2512 Specimen 277-279
Figure 112, External To The Indenting Impacter Fracture Surfaces: Abrasion: YSH50 / 5250-4 RTM D2512 Specimen 280-281
Figure 113, External To The Indenting Impacter Fracture Surfaces: Abrasion: YSH60 / 5250-4 RTM D2512 Specimen 282-283

List Of Figures Continued Page

Figure 114, External To The Indenting Impacter Fracture Surfaces: Intense Heat: 5250-4 RTM D2512 Specimen 284-287
Figure 115, External To The Indenting Impacter Fracture Surfaces: Intense Heat: T650 / 5250-4 RTM D2512 Specimen 288-290
Figure 116, External To The Indenting Impacter Fracture Surfaces: Intense Heat: YSH50 / 5250-4 RTM D2512 Specimen 291-293
Figure 117, External To The Indenting Impacter Fracture Surfaces: Intense Heat: YSH60 / 5250-4 RTM D2512 Specimen 294-295
Figure 118, External To The Indenting Impacter Fracture Surfaces: Tensile Hoop Failure: YSH50 / 5250-4 RTM D2512 Specimen 296-298
Figure 119, External To The Indenting Impacter Fracture Surfaces: Tensile Hoop Failure: T650-35 / 5250-4 RTM D2512 Specimen 299-304
Figure 120, External To The Indenting Impacter Fracture Surfaces: Tensile Hoop Failure: YSH50 / 5250-4 RTM D2512 Specimen 305-312
Figure 121, External To The Indenting Impacter Fracture Surfaces: Tensile Hoop Failure: YSH60 / 5250-4 RTM D2512 Specimen 313-317
Figure 122, Internal To The Indenting Impacter Fracture Surfaces: Crescents And Arcs: T650-35 / 5250-4 RTM D2512 Specimen 318-324
Figure 123, Internal To The Indenting Impacter Fracture Surfaces: Crescents And Arcs: YSH50 / 5250-4 RTM D2512 Specimen 325-328
Figure 124, Internal To The Indenting Impacter Fracture Surfaces: Crescents And Arcs: YSH60 / 5250-4 RTM D2512 Specimen 329-333
Figure 125, Internal To The Indenting Impacter Fracture Surfaces: Knobs / Conchoidal Failure: T650-35 / 5250-4 RTM D2512 Specimen 334-339
Figure 126, Internal To The Indenting Impacter Fracture Surfaces: Knobs / Conchoidal Failure: YSH50 / 5250-4 RTM D2512 Specimen 340-343
Figure 127, Internal To The Indenting Impacter Fracture Surfaces: Knobs / Conchoidal Failure: YSH60 / 5250-4 RTM D2512 Specimen 344-347
Figure 128, Internal To The Indenting Impacter Fracture Surfaces: Straight Edged Fragments: T650-35 / 5250-4 RTM D2512 Specimen 348-355
Figure 129, Internal To The Indenting Impacter Fracture Surfaces: Straight Edged Fragments: YSH50 / 5250-4 RTM D2512 Specimen 356-358
Figure 130, Internal To The Indenting Impacter Fracture Surfaces: Straight Edged Fragments: YSH60 / 5250-4 RTM D2512 Specimen 359-363
Figure 131, Internal To The Indenting Impacter Fracture Surfaces: Abrasion: T650-35 / 5250-4 RTM D2512 Specimen 364-369
Figure 132, Internal To The Indenting Impacter Fracture Surfaces: Abrasion: YSH50 / 5250-4 RTM D2512 Specimen 370-372
Figure 133, Internal To The Indenting Impacter Fracture Surfaces: Abrasion: YSH60 / 5250-4 RTM D2512 Specimen 373-376
Figure 134, Internal To The Indenting Impacter Fracture Surfaces: Heat Exposure: T650-35 / 5250-4 RTM D2512 Specimen 377-382
Figure 135, Internal To The Indenting Impacter Fracture Surfaces: Heat Exposure: YSH50 / 5250-4 RTM D2512 Specimen 383-384
Figure 136, Internal To The Indenting Impacter Fracture Surfaces: Heat Exposure: YSH60 / 5250-4 RTM D2512 Specimen 385-390
Figure 137, Internal To The Indenting Impacter Fracture Surfaces: Specimen Original Surface: T650-35 / 5250-4 RTM D2512 Specimen 391-396
Figure 138, Internal To The Indenting Impacter Fracture Surfaces: Specimen Original Surface: YSH50 / 5250-4 RTM D2512 Specimen 397-400
Figure 139, Internal To The Indenting Impacter Fracture Surfaces: Specimen Original Surface: YSH60 / 5250-4 RTM D2512 Specimen 401-404
Figure 140, Internal To The Indenting Impacter: Powder Fracture Surfaces: 5250-4 RTM D2512 Specimen 405-407

List Of Figures Continued Page

Figure 141, Internal To The Indenting Impacter: Powder Fracture Surfaces: T650-35 / 5250-4 RTM D2512 Specimen 408-409
Figure 142, Internal To The Indenting Impacter: Powder Fracture Surfaces: YSH50 / 5250-4 RTM D2512 Specimen 410-411
Figure 143, Internal To The Indenting Impacter: Powder Fracture Surfaces: YSH60 / 5250-4 RTM D2512 Specimen 412-413
Figure 144, Internal To The Indenting Impacter: Powder Fracture Surfaces: Crescents: 5250-4 RTM D2512 Specimen 414-416
Figure 145, Internal To The Indenting Impacter: Powder Fracture Surfaces: Crescents: T650-35 / 5250-4 RTM D2512 Specimen 417-418
Figure 146, Internal To The Indenting Impacter: Powder Fracture Surfaces: Crescents: YSH50 / 5250-4 RTM D2512 Specimen 419-420
Figure 147, Internal To The Indenting Impacter: Powder Fracture Surfaces: Crescents: YSH60 / 5250-4 RTM D2512 Specimen 420-421
Figure 148, Internal To The Indenting Impacter: Powder Fracture Surfaces: Abrasion: 5250-4 RTM D2512 Specimen 422-423
Figure 149, Internal To The Indenting Impacter: Powder Fracture Surfaces: Abrasion: T650-35 / 5250-4 RTM D2512 Specimen 424
Figure 150, Internal To The Indenting Impacter: Powder Fracture Surfaces: Abrasion: YSH50 / 5250-4 RTM D2512 Specimen 425
Figure 151, Internal To The Indenting Impacter: Powder Fracture Surfaces: Abrasion: YSH60 / 5250-4 RTM D2512 Specimen 426-427
Figure 152, Internal To The Indenting Impacter: Powder Fracture Surfaces: Intense Heat: 5250-4 RTM D2512 Specimen 428-431
Figure 153, Internal To The Indenting Impacter: Powder Fracture Surfaces: Intense Heat: T650-35 / 5250-4 RTM D2512 Specimen 432-433
Figure 154, Internal To The Indenting Impacter: Powder Fracture Surfaces: Intense Heat: YSH50 / 5250-4 RTM D2512 Specimen 433-434
Figure 155, Internal To The Indenting Impacter: Powder Fracture Surfaces: Intense Heat: YSH60 / 5250-4 RTM D2512 Specimen 435-436
Figure 156, Internal To The Indenting Impacter: Powder Fracture Surfaces: Specimen Original Surface: 5250-4 RTM D2512 Specimen 437
Figure 157, Internal To The Indenting Impacter: Powder Fracture Surfaces: Specimen Original Surface: T650-35 / 5250-4 RTM D2512 Specimen 438
Figure 158, Internal To The Indenting Impacter: Powder Fracture Surfaces: Specimen Original Surface: YSH50 / 5250-4 RTM D2512 Specimen 439-440
Figure 159, Internal To The Indenting Impacter: Powder Fracture Surfaces: Specimen Original Surface: YSH60 / 5250-4 RTM D2512 Specimen 441-442
Figure 160, Cup Wall And Specimen Interaction: Back Side Impact: 5250-4 RTM D2512 Specimen: In LOX 443-445
Figure 161, Cup Wall And Specimen Interaction: Back Side Impact: T650-35 / 5250-4 RTM D2512 Specimen 446-448
Figure 162, Cup Wall And Specimen Interaction: Back Side Impact: YSH50 / 5250-4 RTM D2512 Specimen 449-452
Figure 163, Cup Wall And Specimen Interaction: Back Side Impact: YSH60 / 5250-4 RTM D2512 Specimen 453-456
Figure 164, Cup Wall And Specimen Interaction: Material Jetting: 5250-4 RTM D2512 Specimen 457-458
Figure 165, Cup Wall And Specimen Interaction: Material Jetting: T650-35 / 5250-4 RTM D2512 Specimen 458

List Of Figures Continued Page

Figure 166, Cup Wall And Specimen Interaction: Material Jetting: YSH50 / 5250-4 RTM D2512 Specimen 459-461
Figure 167, Cup Wall And Specimen Interaction: Material Jetting: YSH60 / 5250-4 RTM D2512 Specimen 462-464
Figure 168, Fiber Resolution Imaging Location 465
Figure 169, Fiber Resolution Fracture Surface Images 465-467
Figure 170, First Bounce Load Versus Time Curves 468-471

Discussion
Figure 171, Conceptual D2512 Striker Specimen Cup Alignment and Its Effects 473
Figure 172, Conceptual SLCLS Derived Stacked Hertzian Cone Crack Development Cycle 474
Figure 173, Conceptual Straight, Knobs And Conchoidal Fractures Residuals 475
Figure 174, Conceptual Crescent Residuals 476
Figure 175, Conceptual Fractured Residuals Force Gradient Driven Movement 477
Figure 176, Conceptual Parabolically Increasing Load And Powder Residuals 478
Figure 177, Notional Kinetic Friction Induced Temperature Rise Distribution Curves 482
Figure 178, Conceptual Low Height Knobed Residual Creation 483
Figure 179, Conceptual Powder Jets Creation 484
Figure 180, Conceptual Severe Fracturing Under The Impacter 485
Figure 181, Conceptual Tensile Hoop Loads 486
Figure 182, Conceptual Tensile Hoop Failure 487
Figure 183, Conceptual Backside Impact Damage 488

Appendix: Residuals
Figure R1, 5250-4 RTM D2512 72 FtLb LOX Tested Specimen Residuals A1-A21
Figure R2, 5250-4 RTM D2512 72 FtLb In LN2 Tested Specimen Residuals A22-A27
Figure R3, T650-35-UC309 / 5250-4 RTM D2512 72 FtLb LOX Tested Specimen Residuals A28-A47
Figure R4, T650-35-UC309 / 5250-4 RTM D2512 72 FtLb In LN2 Tested Specimen Residuals A48-A54
Figure R5, YSH50A / 5250-4 RTM D2512 72 FtLb LOX Tested Specimen Residuals A55-A74
Figure R6, YSH50A / 5250-4 RTM D2512 72 FtLb In LN2 Tested Specimen Residuals A75-A81
Figure R7, YSH60A / 5250-4 RTM D2512 72 FtLb LOX Tested Specimen Residuals A82-A103
Figure R8, YSH60A / 5250-4 RTM D2512 72 FtLb In LN2 Tested Specimen Residuals A104-A108
Figure R9, 5250-4 RTM D2512 72 FtLb LOX Tested Specimen Disc Residuals A109-A128
Figure R10, 5250-4 RTM D2512 72 FtLb In LN2 Tested Specimen Disc Residuals A129-A131
Figure R11, T650-35-UC309 / 5250-4 RTM D2512 72 FtLb LOX Tested Specimen Disc Residuals A132-A151
Figure R12, T650-35-UC309 / 5250-4 RTM D2512 72 FtLb In LN2 Tested Specimen Disc Residuals A152-A154
Figure R13, YSH50A / 5250-4 RTM D2512 72 FtLb LOX Tested Specimen Disc Residuals A155-A174
Figure R14, YSH50A / 5250-4 RTM D2512 72 FtLb In LN2 Tested Specimen Disc Residuals A175-A178
Figure R15, YSH60A / 5250-4 RTM D2512 72 FtLb LOX Tested Specimen Disc Residuals A179-A198

List Of Figures Continued Page

Figure R16, YSH60A / 5250-4 RTM D2512 72 FtLb In LN2 Tested Specimen Disc Residuals A199-A202
Figure R17, 5250-4 RTM D2512 72 FtLb LOX Tested Specimen Cup Residuals A203-A222
Figure R18, 5250-4 RTM D2512 72 FtLb In LN2 Tested Specimen Cup Residuals A223-A225
Figure R19, T650-35-UC309 / 5250-4 RTM D2512 72 FtLb In LN2 Tested Specimen Cup Residuals A226-A228
Figure R20, YSH50A / 5250-4 RTM D2512 72 FtLb LOX Tested Specimen Cup Residuals A229-A248
Figure R21, YSH50A / 5250-4 RTM D2512 72 FtLb In LN2 Tested Specimen Cup Residuals A249-A252
Figure R22, YSH60A / 5250-4 RTM D2512 72 FtLb LOX Tested Specimen Cup Residuals A253-A272
Figure R23, YSH60A / 5250-4 RTM D2512 72 FtLb In LN2 Tested Specimen Cup Residuals A273-A276
Figure R24, T650-35-UC309 / 5250-4 RTM D2512 72 FtLb LOX Tested Specimen From Moat Residuals A277-A280
Figure R25, YSH50A / 5250-4 RTM D2512 72 FtLb LOX Tested Specimen From Moat Residuals A281-A282
Figure R26, YSH60A / 5250-4 RTM D2512 72 FtLb LOX Tested Specimen From Moat Residuals A283-A286
Figure R27, 5250-4 RTM D2512 LOX Tested Specimen Return Bag Tags Residuals A287-A288
Figure R28, T650-35-UC309 / 5250-4 RTM D2512 LOX Tested Specimen Return Bag Tags Residuals A289-A290
Figure R29, YSH50A / 5250-4 RTM D2512 LOX Tested Specimen Return Bag Tags Residuals A291-A293
Figure R30, YSH60A / 5250-4 RTM D2512 LOX Tested Specimen Return Bag Tags Residuals A293-A295

Appendix: Designed Equipment
Figure D1, Designed Specimen Plate Holding Jig A296-A306
Figure D2, Diamond Core Drill A307
Figure D3, Coolant Adapter A308
Figure D4, Core Drill Wash Stand And Storage A309
Figure D5, Resin Extraction Tray A310-A311

Volume I List Of Tables Page

Introduction
Table 1, High Thermal Conductivity Correlates to Greater Ignition in LOX Resistance 6-7
Table 2, LOX Compatibility Of Polymers And Composites Tested Via D2512 Mechanical Impact 11-40

Theory: Ignition Event
Table 3, Localized Energy Injection Mechanisms 45
Table 4, Ignition Starts At A Local Small Site 46
Table 5, Peroxide Oxidation Chemistry 50
Table 6, Impact of Contaminants 51
Table 7, Possible Correlation Of Ignition Event Sequence To D2512 Reaction Indications 56

Theory: Hertzian Fracture
Table 8, Material Toughness Influences On Hertzian Fracture Initiation Loads 63

Theory: Kinetic Friction
Table 9: $T_{Max_{Avg}}$ and $T_{Max_{Max}}$ Hot Spot Temperature Rise Predictive Formulas 71

Experimental
Table 10, Procured 5250-4 RTM Matrix Resin Specifications 79
Table 11, T650-35 Properties 80
Table 12, Procured T650-35-US309 Fiber Lot Properties And Specifications 81
Table 13, YSH50A and YSH60A General Fiber Properties 85
Table 14, YSH50A Procured Fiber Lot Properties 86
Table 15, YSH60A Procured Fiber Lot Properties 87
Table 16, Prepreg Properties: As Delivered (Fabricator Measured): 91-93
Table 17, Prepreg Properties: As (Author / Principal Investigator) Measured: 103-105
Table 18, Bleed Flow Plate 3 Prepreg Lay Up Sequence And Properties: 108-110
Table 19, Bleed Flow Composite Plate 3: Physical Properties 124
Table 20, Prepreg Specimen Plate 1Lay Up Sequence And Subsequent Properties 125-127
Table 21, D2512 Specimen And Specimen Plate Physical Properties 148
Table 22, Thermal Conductivity Specimens Physical Properties 188

Results
Table 23, D2512 LOX Compatibility Test Results: 191
Table 24, Thermal Conductivity At LOX's Boiling Point 194

Executive Summary

The vast majority of all presently used expendable launch vehicles (ELVs) and reusable launch vehicles along with all future planned ELVs designed to use liquid propellants use the oxidizer liquid oxygen (LOX). It is contained in the LV's airframe forming aluminum (Al) tanks. It is also piped to and thru the engines of these LVs via ducts and lines made of Al and nickel (Ni) alloys.

Avoiding an ignition event altogether and / or the deleterious effects of an ignition event is the critical design factor in the selection of a material to fabricate LOX components. Ignition occurs when a sufficient amount of energy is injected at a site on the surface of the component in contact with the LOX. It has been found that the most common energy injection mechanism leading to ignition occurs when an object strikes a LOX tank, duct, or line. That mechanical energy is converted into thermal energy at the site of the strike. This thermal energy raises the temperature of the tank, duct, or line material at the local site and this creates the necessary conditions for ignition to occur as *"all ignitions are thermal in that a local hot spot must be created for ignition to occur*." Hust and Clark 73.

Effectively, all present LV LOX tanks, ducts, and lines are made out of Al or Ni alloys that exhibit significant thermal conductivity (K) at LOX temperatures in spite of the fact that they are designed to hold a cryogenic liquid which will boil off when heated. The K of a LOX tank, duct, or line and various thermal transport mechanisms significantly aid in suppressing these ignitions by transporting the injected energy away. In fact high K in the LOX tank, duct, or line correlates to greater ignition resistance.

ASTM D2512 is the standard test used to determine if a material is compatible with LOX when subjected to a mechanical impact. If twenty 0.689 inch in diameter specimens of a material are capable of having 72 Ft-Lbs (98 joules) of mechanical energy injected by the D2512 apparatus into them without any indication of an ignition event occurring or sixty specimens with only one indication of an ignition event occurring then the test states that it is suitable for use with LOX. Save for heavily halogenated polymers, polyimides, and polypyrlene (better known as graphite) all polymers to date fail these required mechanical impact LOX compatibility test standards. Unfortunately to date all of the PMCs considered for use in making a LOX vehicle component out of have also failed to pass these test standards.

A significant factor explaining why all of the polymer and PMCs failed is their very low in-plane K. None of the PMCs used any reinforcing fibers that exhibit K superior to Ni and all exhibited K inferior to Al. None of the polymeric matrix resins used in these same PMCs exhibit Ks greater than 0.3 W/mK; which is three orders of magnitude less than that of Al. Overall the in-plane K of these PMCs were no greater than 3 to 5 W/mK and the out of plane K was at best 0.5 W/mK due to the matrix resin's very low K. With in-plane and out-of-plane Ks so low the energy injected into these PMCs by the mechanical impacter could not be transported away from the local injection site and instead caused the temperature of the PMC to significantly rise and set up ignition conditions.

Since a high intrinsic K is, with only a few notable exceptions, the hall mark of a LOX compatible material, it stands to reason that it will be necessary to at least increase the in-plane K of a PMC up to that exhibited by Al alloys at LOX's boiling temperature. Fortunately some thermally conductive, highly ordered, and graphitized fibers have been developed over the past decade. Highly ordered graphite, also known as polypyrlene, is the most LOX compatible polymer known. When a PMC is fabricated with one of these high K fibers using one of the more LOX compatible matrix resin systems available, which also exhibits a high Tg, it should exhibit the overall in-plane K of Al alloys. Since the in-plane K of a PMC is a straight rule of mixtures formula and the K of all resin matrixes is roughly the same, it is a very good assumption to expect that any 60+% volume fraction PMC using these high K fibers would also exhibit the Al alloy like in-plane K. To make a D2512 LOX compatible PMC will require that it exhibit a K in the same range as Al and Ni.

The core objective of this research effort is to determine if a PMC, using thermally conductive reinforcement fibers instead of the standard conventional carbon fibers used to date, suitable to the fabrication of axisymmetric tanks, ducts, and lines and exhibiting in-plane Ks comparable to those metals which regularly pass D2512, can be found which either passes or comes close to passing D2512. A secondary objective will then be to deduce and to better understand what happened to the specimens during the D2512 test.

To accomplish the core objective four materials were needed: a matrix resin, a baseline carbon-graphite fiber, and two thermally conductive fibers to provide the experimental variables.

Cytec "Rigidite 5250-4 RTM" was the toughened, easily process able, imide class, matrix resin selected for use in this effort. Toughened imides usually exhibit good D2512 LOX compatibility.

The baseline fiber selected for this effort was the Cytec T650-35. The T650 class of carbon fibers had been used in other published attempts to make D2512 LOX compatible composites. Its selection allowed a connection and comparison of this efforts results to those previous efforts.

Nippon Graphite Fiber Corps' GRANOC graphite YSH50A and YSH60A fibers were selected for use in this effort as the thermally conductive experimental fibers.

Through out the entire experimental portion of this effort numerous situations, circumstances and events presented themselves which might lead to the materials used, their interim fabricated forms, the equipment used to work on or process them and the generated D2512 specimens becoming contaminated by dust, fingerprints, solvents, etc. If not eliminated or stringently mitigated these contaminates would skew the final generated D2512 specimen's LOX compatibility results towards lower compatibility. To eliminate and or mitigate these contaminates and their effects meticulous, exhaustive, thorough, arduous, rigorous, and careful cleaning steps and efforts were always taken at every experimental step to assure that "LOX" clean D2512 specimens were created.

D2512 requires the generation of flat specimens. To assure that the composite panels out of which the D2512 specimens where to be made were flat, the quasi isotropic lay up sequence $(-45.\ 0, +45, 90)_{3S}$ was selected. A common per ply thickness routinely attained by the composites industry is 5 mils. Based upon circa 2002 fabricated LOX LV tank thicknesses in the range of 100 to 250 mils, the final targeted composite thickness was selected to be 120 mils. This set the number of plies in the composite plates to be made for this effort at twenty-four.

All three types of the D2512 specimen generating 12 inch by 9 inch composite plates were laid up and cured simultaneously by a slightly modified Cytec standard 5250-4 RTM cure profile. They were all post cured by the Cytec standard 440°F post cure cycle. A 5250-4 RTM neat resin plate was also cast, cured and post cued by the Cytec standard cure and post cure cycles.

Good quality composite plates were created. The composites were extremely uniform; Fiber Volume was 63.6 to 63.7 for all three composites! Also the composites exhibited excellent Void Volume of less than 1 percent.

Seventy-two D2512 specimens were then clean and contamination free cut from the four specimen plates before the plates were transmission c-scanned or cut up for further property measurements. Coring was used to cut D2512 specimens out of the four specimen plates.

D2512 requires that the tested specimens be free of ragged edges, burrs, fins, or other irregularities. Deburred and beveled specimens were "LOX" quality cleaned, cleanly and uniformly vacuum dried and then placed into prepurchased "LOX" clean Aclar bags while inside a glove box purged with filtered dry nitrogen.

The four particular D2512 specimen type sets generated by this effort were shipped to NASA Johnson Spaceflight Center's White Sands Testing Facilities in these cans for D2512 Mechanical Impact Ignition testing. A sufficient number of D2512 specimens were shipped to accomplish the D2512 LOX compatibility test requirement of 20 impacted in ambient pressure LOX at 72 Ft-Lbs specimens plus an additional 3 to 4 specimens for impact in LN_2 at 72 Ft-Lbs for non-ignition-able comparison and 3 to 4 "just in case" spare specimens.

To obtain an exact measure of the K of the composites created by this effort specimens were sent to Dr. Khairul Alam of Ohio University, Athens Ohio. Dr Alam measured the in and out of plane K of all three types of composites. The x and y axis Ks of the YSH fiber reinforced composites are roughly twenty-three hundred and twenty-six hundred percent greater than the T650-35 fiber reinforced composites. The z axis Ks of the YSH fiber reinforced composites are roughly two hundred percent greater than that of the T650-35 fiber reinforced composites.

The results of the D2512 Mechanical Impact tests conducted by NASA White Sands Test Facility indicated that both of the experimental YSH fibers improved the D2512 LOX compatibility of their respective composites by seventeen hundred percent over the baseline T650-35 fiber reinforced composite's D2512 LOX compatibility. Also the one hundred percent D2512 ignition rate exhibited by the 5250-4 RTM neat resin specimens implies that the seventeen hundred percent improvement in the YSH fiber reinforced 5250-4 RTM matrix composite's D2512 LOX compatibility over that exhibited by the T650-35 fiber reinforced 5250-4 RTM matrix composite specimens is directly attributable to the use of these moderately, thermally conductive, primarily graphite YSH type fibers.

Upon receipt of the residuals of the four D2512 tested types of materials back from White Sands Test Facility the fracture surfaces of these residuals were examined and documented. Any specific residual item could be grouped into four major categories. The residual item originated from either outside of the area of the specimen contacted by the D2512 striker-impacter, under the area contacted by the impacter, a powder of the finely crushed original specimen or the result of an interaction between a specimen residual and the cup.

Additional examination of the specimen residuals originating from outside of the impacter-specimen contacting area found that they could be further grouped into these seven subcategories: ring shaped cracks, transverse and in plane cracks, knob like extreme cone cracks, straight cracks, kinetic friction induced abrasion, intense heat exposure and tensile hoop failure.

Further examination of the larger specimen residuals originating from under the impacter and specimen contacting area found that they could be further assigned to these six subcategories: crescents and arcs, knobs, straight sided, kinetic friction induced abrasion, intense heat exposure, and surface effects. .

All of the returned D2512 tested specimens contained residuals of coarse powder. Examination of these coarse powder residuals found that they could be further grouped into these four subcategories: narrow crescent shapes, abrasion, intense heat exposure, and surface effects.

The final category of residuals consists of the specimen's interaction with the LOX containment cup. The residuals in this category can be broken out into these two subcategories: back edge damage on some of the residuals and particles of the specimens affixed to cup's inner surface.

All of the failure types and phenomenon exhibited by the returned residuals were found in all four types of the D2512 tested specimens. They were also found regardless of the medium, LOX or LN_2, in which the specimen was impacted and regardless of whether or not the material exhibited an ignition reaction. The two exceptions are the prominence of the knobs produced when the D2512 test occurs in LN_2 and the severity of the intense heat or high temperature exposure when a reaction is detected in LOX D2512 tested specimens.

Load versus time plots of the first bounce of a typical D2512 mechanical impact test were collected on samples of the created D2512 specimen with an instrumented UDRI impacter. A series of distinct features repeatedly appear in all of the load versus time plots collected regardless of the material type tested or the number of a specific material's D2512 specimens tested. These distinct features can be grouped into four categories: initial jitter, sharp spike, sloping plateau, and parabolic climb and descent.

This research effort has successfully achieved its two objectives. In achieving these, it has accomplished a series of world firsts.

This effort successfully and repeatedly demonstrated that using a thermally conductive fiber could substantially enhance the mechanical impact LOX compatibility of a composite as measured by ASTM D2512. It repeatedly achieved 90 percent of the goal of passing the ASTM standard D2512 mechanical impact ignition test which is a 1700 percent improvement over the experimental baseline.

This effort also documented and cataloged the types of fracture surfaces which are routinely found in residuals (of the types of materials investigated by this effort) remaining after the impact test fractures and possibly causes the ignition of a specimen. Based upon these fracture surfaces, Hertzian fracture was shown to be mechanism by which a specimen fractured and failed in a D2512 test.

The exhaustive analysis of the residual fracture surfaces also lead to the understanding of the mechanical-to-thermal transformation mechanism. The examined fracture surfaces of the residuals routinely indicated that kinetic friction had occurred during a D2512 test. The examination also indicated that signs of intense heating were associated with the signs of kinetic friction. Kinetic friction's mechanical-to-thermal transformation mechanism provided the only phenomenological explanation for the extremely rapid and large temperature rises required for conditions recognizable as ignition to occur in the time frame of a D2512 mechanical impact test. It also provided the correlation of the various physical parameters varied by this effort to the D2512 testing results obtained.

Overall the effort crystallized the sequence from fracture to heating to possible ignition. It starts first with the development of a series of Hertzian fractures. These allow for heavy kinetic friction of the Hertzian fractured material to occur. This kinetic friction then provides a means for the mechanical energy to become temperature rising thermal energy. This temperature rising thermal energy causes the material to degrade by radical chain scission and then oxidize by radical addition peroxide chemistry to a degree possibly detectable as ignition

Introduction

The vast majority of all presently used expendable launch vehicles (ELVs) and reusable launch vehicles along with all future planned ELVs designed to use liquid propellants use the oxidizer liquid oxygen (LOX).[I1-I29] (The only other oxidizer used is DiNitrogen Tetroxide. It is used by legacy ELVs whose design evolution originates in the 1960's.) As depicted in figure 1, it is contained in Al tanks, which usually forms the LV's airframe. It is also piped to and thru the engines of these LVs via ducts and lines made of Al and Ni alloys.

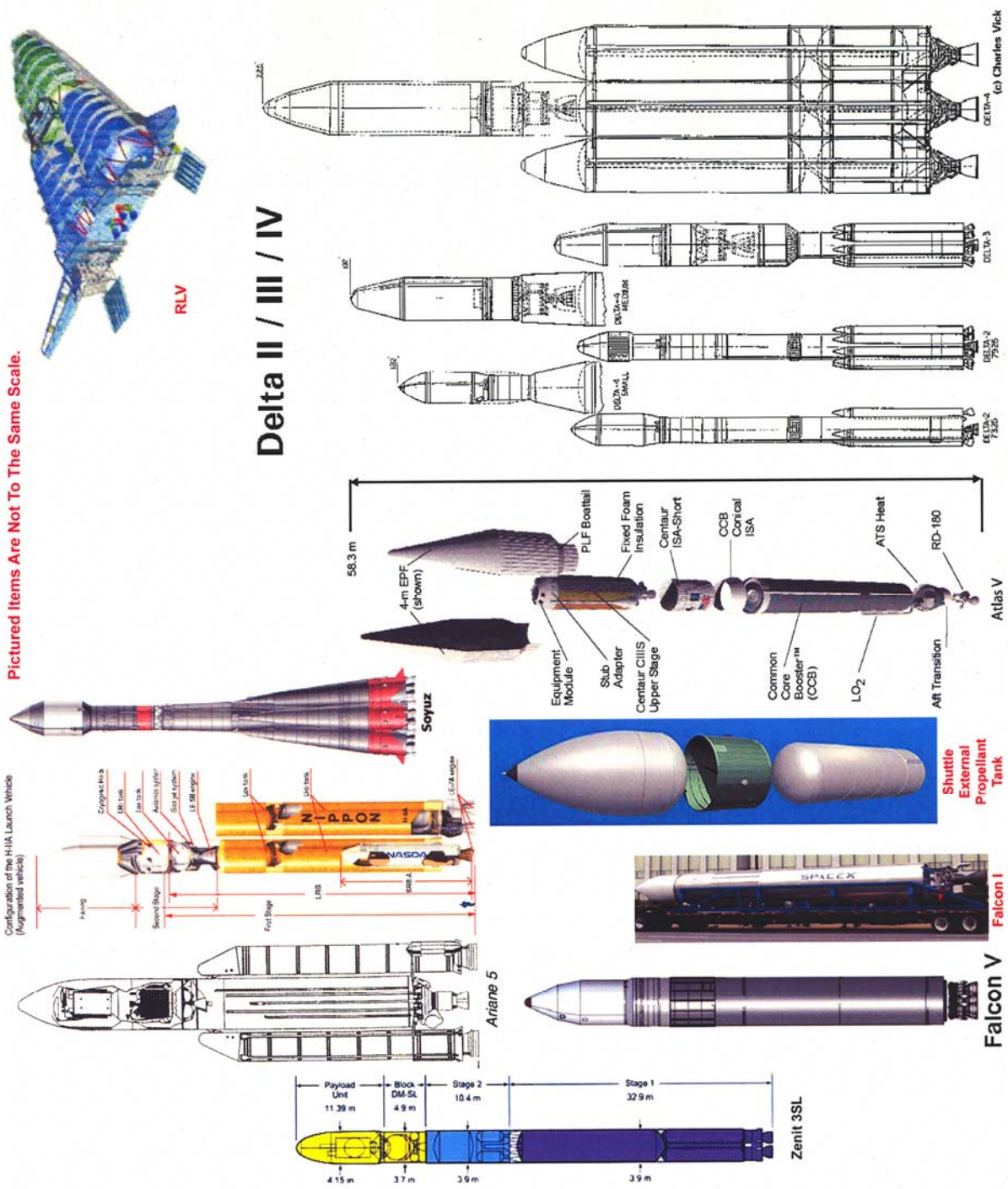


Figure 1, Launch Vehicles Which Use LOX

The LOX tanks on LVs, particularly those on the boost stage, are large. As figure 2 depicts the boost stage tanks on these LVs are comparable or larger in size to railroad tanker cars.[I30-I31] LOX tanks can weight roughly 1000 Lbs when used to make the upper stages of medium and heavy lift LVs or the boost stages of small lift LVs, to thousands of Lbs when used to make the boost stages of medium lift LVs, and as much as ten thousand Lbs when used to make the boost stages of heavy lift LVs.

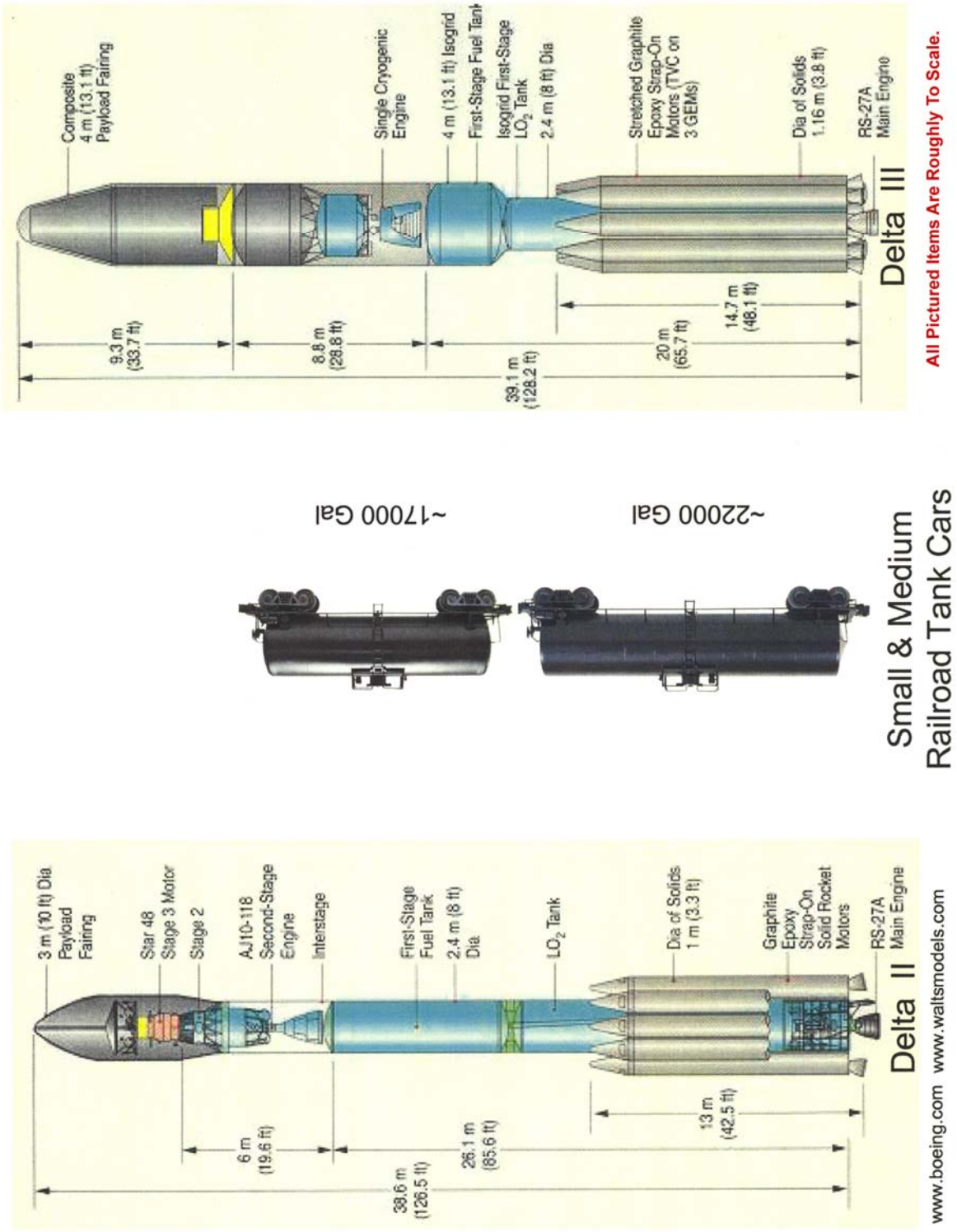
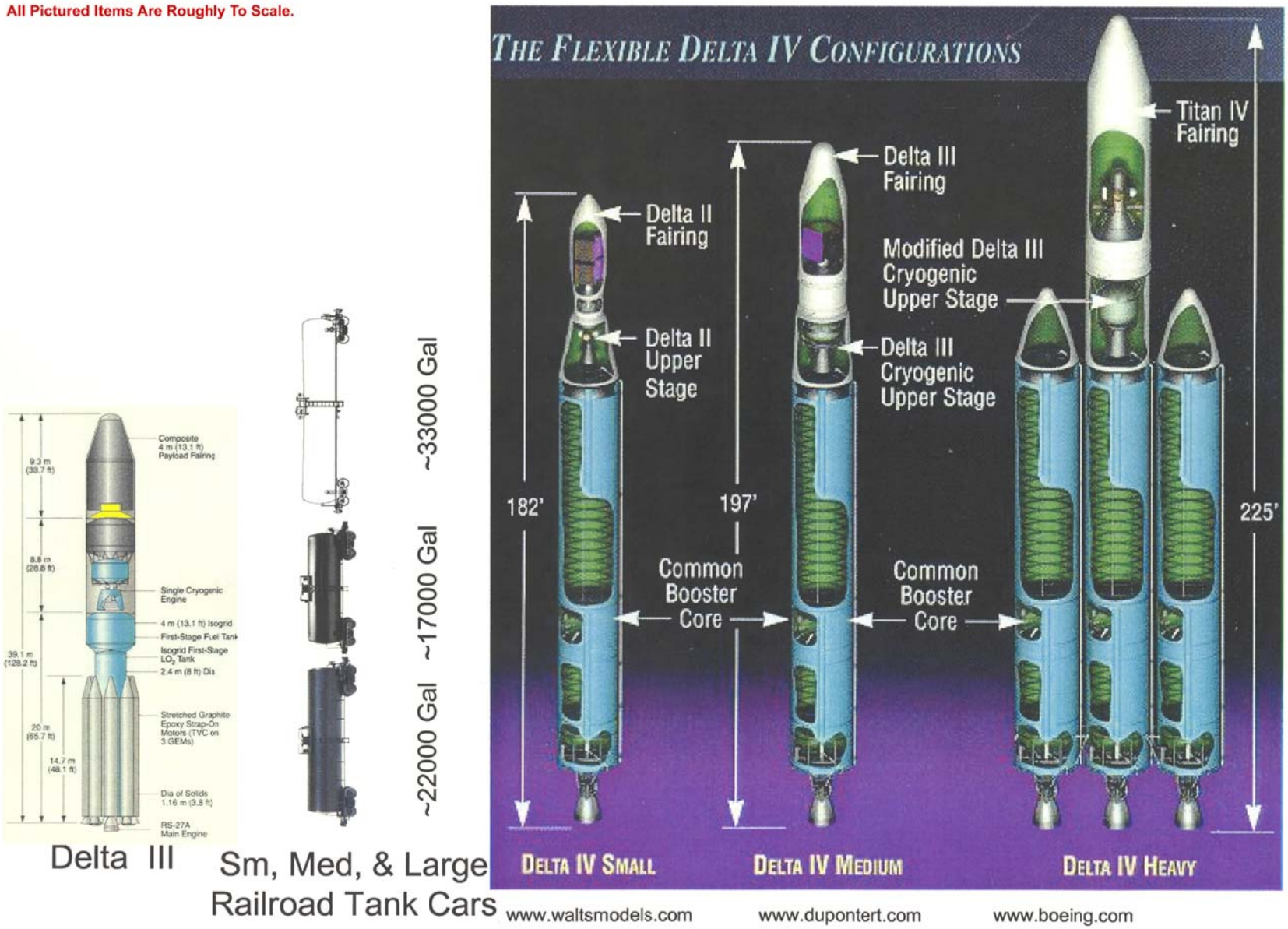


Figure 2a, Launch Vehicle LOX Tankage Sizes

Figure 2b, Launch Vehicle LOX Tankage Sizes



Lifting items into space is very expensive. To lift 1 Lb of material into low earth orbit costs the equivalent of 1 Lb of gold. To put that same Lb into geostationary orbit costs the equivalent of 3 Lbs of gold. To lift that same Lb out of the Earth-Moon gravity well costs the equivalent 10+ lbs of gold. An ELV's mass lifting capacity is routinely increased by 8 additional Lbs for every 100 Lbs of mass removed from the boost stage. Also an 80 additional Lbs of lifted mass is usually gained for every 100 Lbs of mass removed from the second stage and above. Since large fractions of the dry mass of these LVs is in the LOX tanks, ducts, and engine lines it is imperative that the LV building and using community strive to remove as much weight as possible from the weight of these components while maintaining the lightweight, strong, stiff, and LOX compatibility requirements of these components to improve their lifting performance. The only available class of materials which presently meet most of these requirements are polymer matrix composites (PMCs). Within use temperature and other component specific requirements, a twenty five percent reduction in the weight of a component can routinely be had by redesigning it to be built out of PMCs.

Additionally all present ELV Al LOX tanks cost millions of dollars to build and require 3 plus years of scheduling for their fabrication, testing, and delivery. If a LOX compatible PMC can be found the cost and time associated with building and procuring these tanks would drop by an order of magnitude. When Boeing, in the middle 90's, went from fabricating Delta II fairings, and payload support adapters out of Al to fabricating them out of PMCs, the cost to fabricate them dropped from roughly 10 million dollars to roughly 2.5 million dollars and the time to fabricate and qualify them dropped from 3 years to roughly 9 months.[I32] Since these components exhibit many similar aspects, they are both basically axisymmetric components and both require a similar intensity of qualification testing, cost and scheduling, reductions in the fabrication of these low volume production run LOX tanks will be realized. Developing a LOX compatible PMC would directly translate into reducing the cost and scheduling associated with fabricating the LVs.

Avoiding an ignition event altogether and or the deleterious effects of an ignition event is the critical design factor in the selection of a material to fabricate LOX tanks, ducts, and line components.[O1-O214] Ignition occurs when a sufficient amount of energy is injected at a site on the surface of the component in contact with the LOX. It has been found that the most common energy injection mechanism leading to ignition in LOX components is mechanical impact. When an object strikes a LOX tank, duct, or line it injects mechanical energy. That energy is converted into thermal energy at the site of the strike. This usually occurs when a foreign object is inadvertently introduced into the tank, duct, or line or a sub-component breaks off and strikes at some local site. This thermal energy raises the temperature of the tank, duct, or line material at the local site as shown in figure 3 and this creates the necessary conditions for ignition to occur as *"all ignitions are thermal in that a local hot spot must be created for ignition to occur*." Hust and Clark 73.

Effectively, all present vehicle LOX tanks, ducts, and lines are made out of aluminum or nickel alloys that exhibit significant thermal conductivity at cryogenic LOX temperatures. Figure 4 graphs their thermal conductivity over a range of temperatures from LOX's boiling point up. The thermal conductivity of a LOX tank, duct, or line and various thermal transport mechanisms significantly aid in suppressing these ignitions by transporting the injected energy away as shown in figure 3. In fact high thermal conductivity in the LOX tank, duct, or line correlates to greater ignition resistance for the reasons delineated in table 1. This explains why effectively all present vehicle LOX tanks, ducts, and lines have been made out of high thermal conductivity materials, in spite of the fact that they are designed to hold a cryogenic liquid which will boil off when heated. To safely contain the LOX this trade off dictated their use.

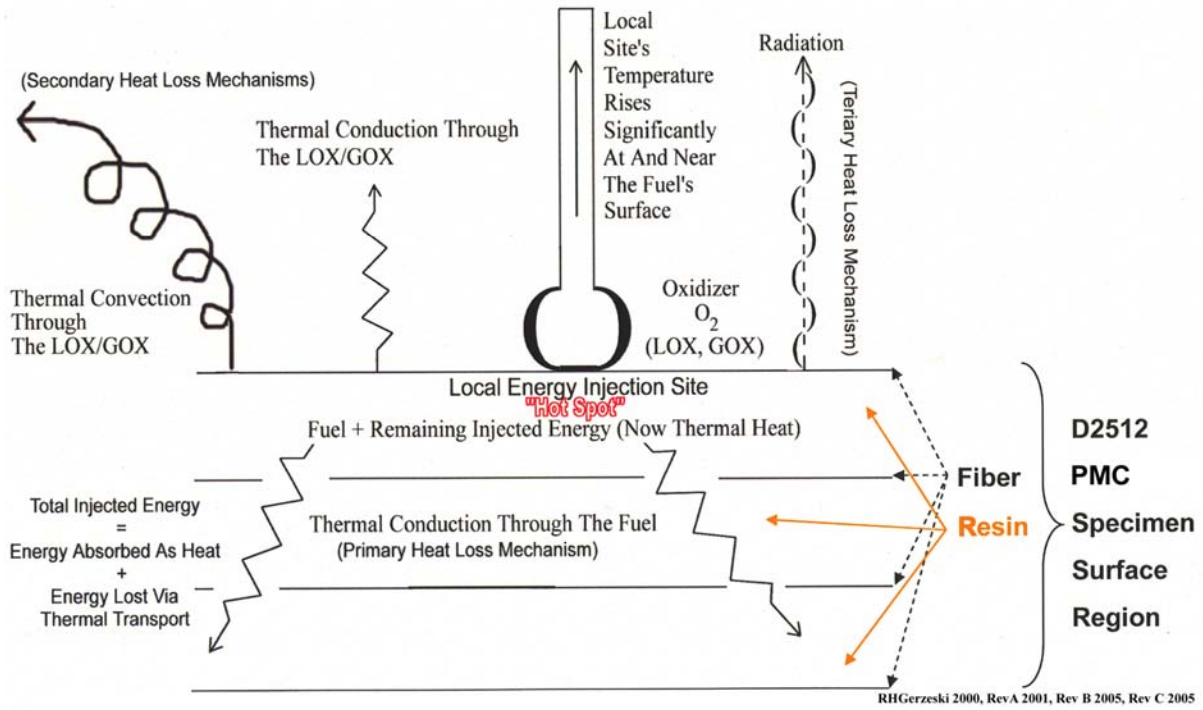


Figure 3, Local Site Temperature Rise And Thermal Transport Mechanisms

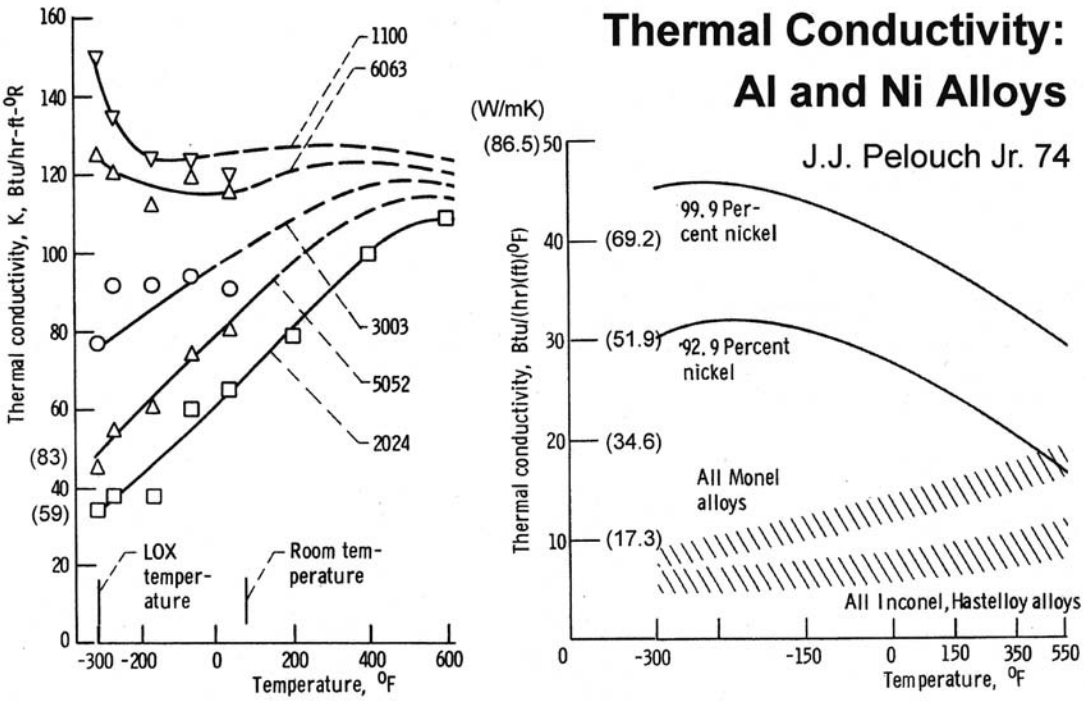


Figure 4, Thermal Conductivity Of Materials Used In Making Common LOX Handling Components.

Table 1, High Thermal Conductivity Correlates to Greater Ignition in LOX Resistance

"Most materials in contact with oxygen will not ignite *without a source of ignition energy.* When an **energy-input rate, as converted to heat, is greater than the rate of heat dissipation, and the temperature increase is continued for sufficient time, ignition and combustion will occur**."
Standard Guide For Evaluating Nonmetallic Materials For Oxygen Service, ASTM G 63 - 1992

"…design for **efficient dissipation of heat**."
Standard Guide For Designing Systems For Oxygen Service, ASTM G 88 – 90, 1990

"…it is also desirable to use materials and design criteria that would provide for **maximum possible heat dissipation by thermal conduction**."
"The apparent **ignition temperature of a given material is affected by its heat capacity, thermal conductivity, heat of reaction and the rate of heat input**, "
"The **thermal diffusivity parameters**, (ie thermal conductivity, density, and specific heat) may be used to calculate energy input rate or power input to reach the ignition temperature of the material. As the **thermal conductivity, density and heat capacity increase, the rate of energy power input to reach an ignition temperature increases**. "
Harold W. Schmidt, and Forney , ASRDI Oxygen Technological Survey. Vol 9: Oxygen Systems Engineering Review, NASA SP-3090, 1-218, 1975

"**Electric arcs and sparks produce temperatures well in excess of all reported autoignition temperatures for aluminum**. They are highly localized and should be effective in delivering energy to the metal. However, despite the high temperature and localization of the heat, the total energy present in sparks from static charge separation or in arcs from low voltage wiring tends to be small, and **aluminum, because of its high thermal conductivity, dissipates heat very effectively**."
Barry L. Werley, Herve' Barthelemy, Robert Gates, Joseph W. Slusser, Keith B. Wilson, and Robert Zawierucha, "A Critical Review Of Flammability Data For Aluminum", Flamibility And Sensitivity Of Materials In Oxygen-Enriched Atmospheres: Sixth Volume, ASTM STP 1197, Pg 300-345, 1993

"…thermal conductivity of metals and alloys is viewed with only casual interest in most structural applications. However**, thermal conductivity in a structure in an oxygen system becomes a direct measure of the resistance of structure to fire**. The structure ignites because sudden energy from some source is momentarily supplied to the surface raising it to the ignition temperature. **High thermal conductivity will** lower the surface temperature and will therefore increase the resistance to ignition."
James J. Pelouch, Jr., ASRDI Oxygen Technological Survey. Vol VII: Characteristics Of Metals That Influence System Safety, NASA SP-3077, Pg 1-68, 1974

"**Metals have high thermal conductivities that help dissipate local heat inputs that might easily ignite nonmetals**"
"Heat is generated from the conversion of mechanical work when a gas is compressed from a low to a high pressure. This can occur when high pressure oxygen is released into a dead-ended tube or pipe, quickly compressing the residual oxygen that was in the tube ahead of it. An effective ignition mechanism with polymers, the much higher heat capacity and thermal conductivity of significantly sized metals greatly attenuates high temperature produced this way."
"**Acoustic oscillations within resonant cavities are associated with rapid gas temperature rise**. This rise is more rapid and achieves higher values where particulates are present or where there are high gas velocities. **Ignition can result if the heat transferred is not rapidly dissipated**,"
Standard Guide For Evaluating Metals For Oxygen Service, ASTM G 94 – 1992

Table 1, High Thermal Conductivity Correlates to Greater Ignition in LOX Resistance cont.

"Other **properties such as specific heat, thermal conductivity, density, and thermal diffusivity influence material compatibility**. For example, nickel-copper alloys are rapidly replacing stainless steels in high pressure (ie 3000 Psi) oxygen systems because of the increased thermal conductivity and diffusivity of nickel-copper alloys. The **higher thermal conductivity results in lower reaction sensitivity**. Also, mechanical properties may be altered in the presence of high pressure oxygen, for example, crack propagation may be enhanced."

"**The use of materials with high thermal diffusivity and high heat capacity are most beneficial since the most rapid rates of heating, from sources such as adiabatic compression, are not appreciably faster than the effective surface cooling rate of good heat conductors**."

"**Material with a high thermal diffusivity are better in dynamic systems since local energy impulses will result in less pronounced hot spots** than materials with low diffusivity. **In a static system high thermal conductivity materials are more desirable for essentially the same reason**. … The presence of sharp edges may result in hot spots for ignition."

"**Whether ignition actually occurs is determined by the temperature of the material … The thermal diffusivity, heat capacity, and other factors such as the existence of sharp edges, determine the peak temperature of the material**."

J.G. Hust, and A.F. Clark, "A Survey Of Compatibility Of Materials With High Pressure Oxygen Service", Cryogenics, Pg 325-336, June 1973

"**Metals with good thermal conductivities, should be more difficult to ignite because local hot spots can be dissipated before ignition occurs**."

"Sharp corners and thin sections promote easier ignition … they heat up more quickly than thicker sections. Metal thickness of less than 0.032 in should be avoided."

"Also**, in design, the nonmetal components are well heat-sunk** in metal and **this impedes their ignition by removing heat** from the area around the nonmetal."

Joseph W. Slusser, and Keith A. Miller, "Selection Of Metals For Gaseous Oxygen Service", Flamibility And Sensitivity Of Materials In Oxygen-Enriched Atmospheres: ASTM STP 812, Pg 167-191, 1983

ASTM D2512 is the standard test used to determine if a material is compatible with LOX and G86 with pressurized LOX when subjected to a mechanical impact. If twenty 0.689 inch in diameter specimens of a material are capable of having 98 joules (72 Ft-Lbs, 10 $kg_f m$, and 43 inch drop height) of mechanical energy injected by the D2512-G86-F371-D2540-NASA STD 6001 Test 13A (Previously NHB 8060.1C Test 13A)-NASA STD 6001 Test 13B (Previously NHB 8060.1C Test 13B)-USAF Spec. Bull. 527 basic apparatus shown in figure 5 into them without any indication of an ignition event occurring or sixty specimens with only one indication of an ignition event occurring then the test states that it is suitable for use with LOX. Table 2 lists the results of numerous polymeric and composite materials published in various open source government documents that have been D2512 and G86 tested. Save for heavily halogenated polymers, polyimides, and polypyrlene (better known as graphite) all polymers to date fail these required mechanical impact LOX compatibility test standards. Unfortunately to date all of the composite materials considered for use in making a LOX vehicle component out of have also failed to pass these test standards.

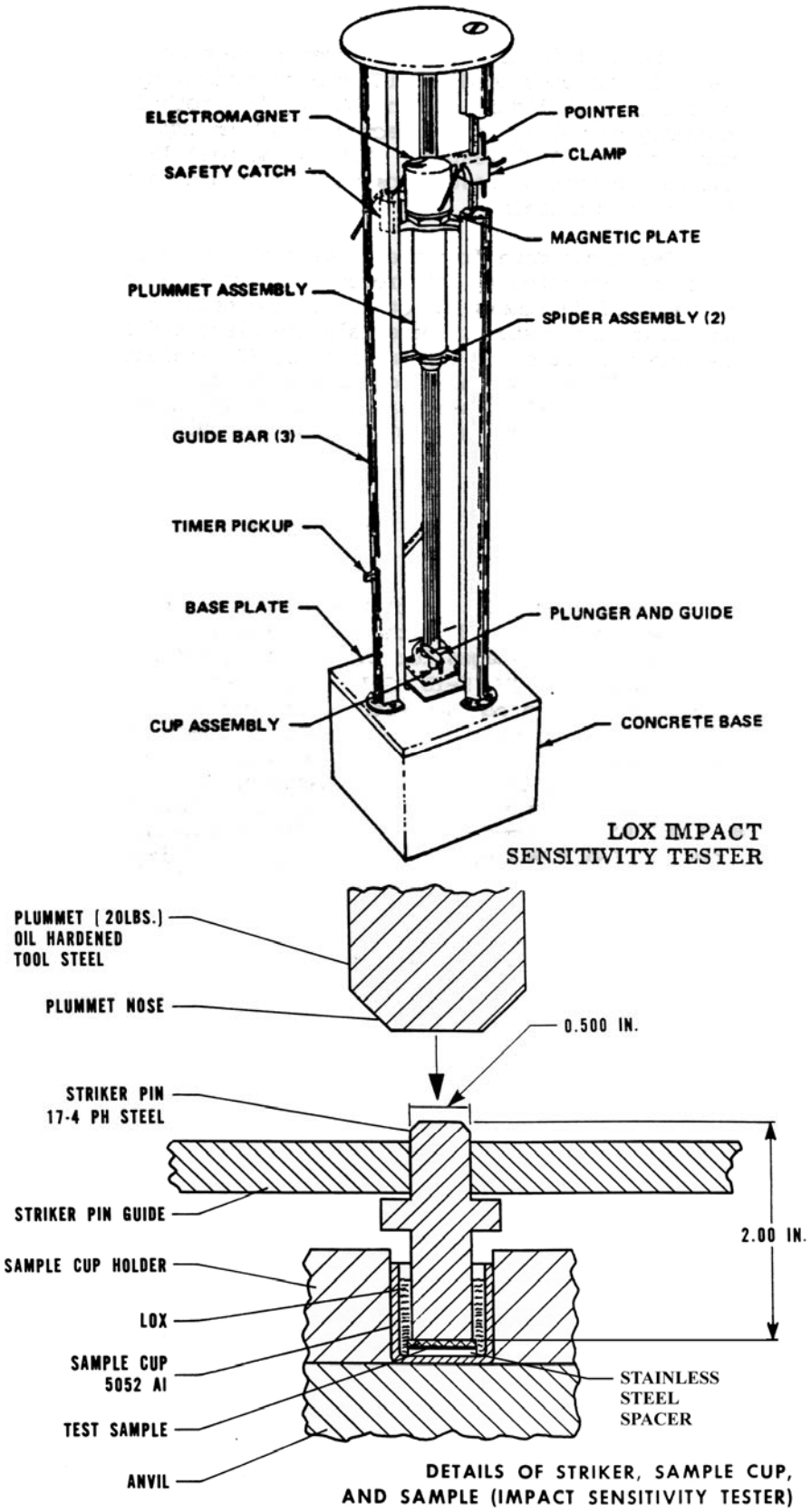


Figure 5a, Ambient Pressure D2512 LOX Impact Sensitivity Tester: Apparatus And Striker Zone

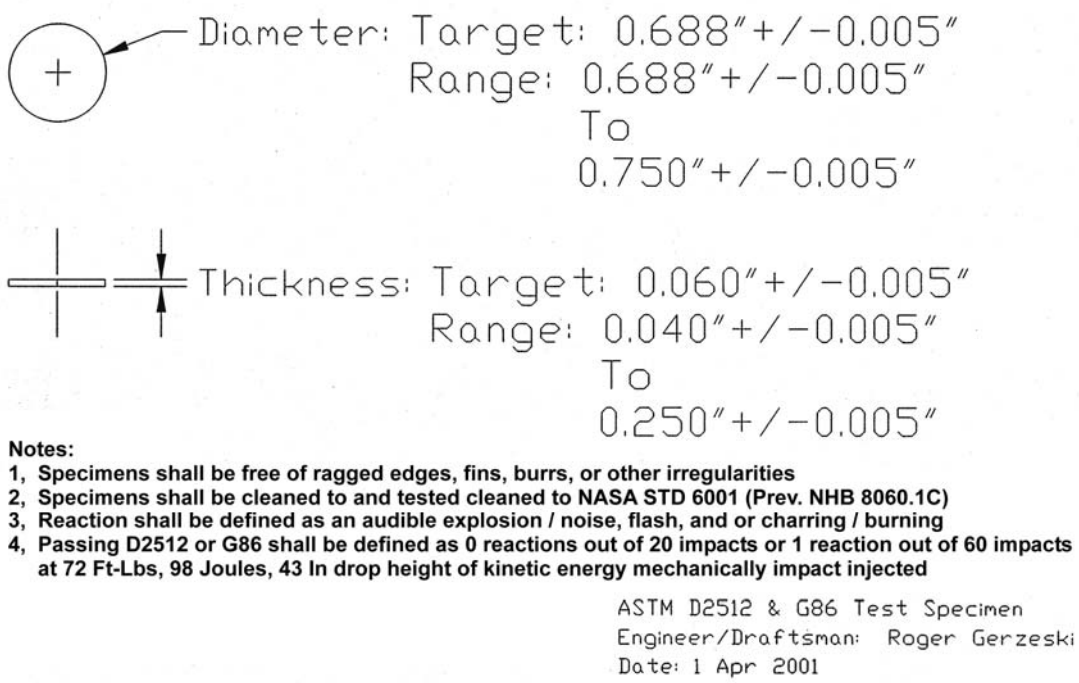


Figure 5b, Ambient Pressure D2512 LOX Impact Sensitivity Tester: Test Specimen



Figure 5c, Ambient Pressure D2512 LOX Impact Sensitivity Tester: Unused Fresh Spacer Disc

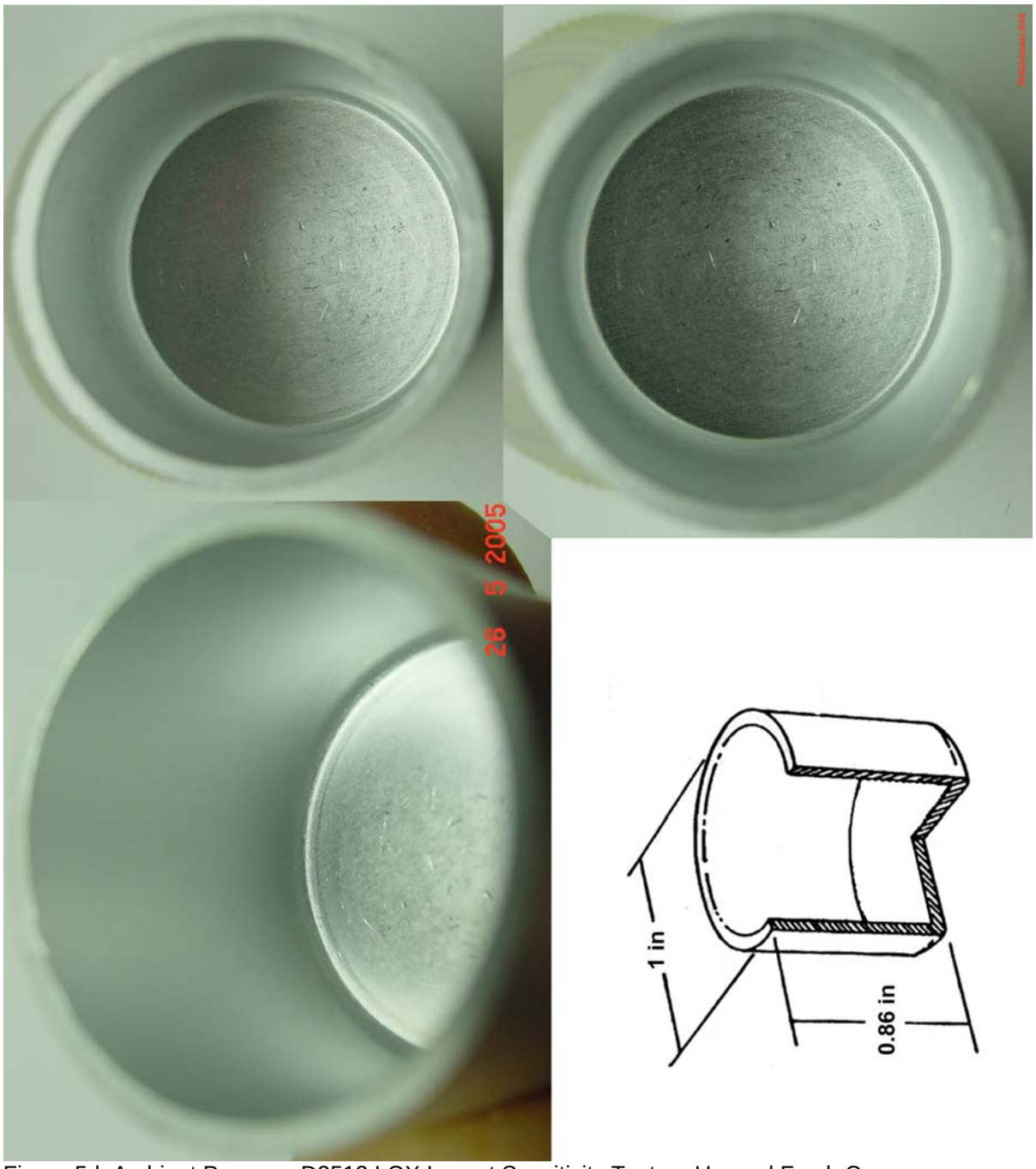


Figure 5d, Ambient Pressure D2512 LOX Impact Sensitivity Tester: Unused Fresh Cup

Table 2, LOX Compatibility Of Polymers And Composites Tested Via D2512 Mechanical Impact (98 Joules=10 Kg_f m=43inchs drop height)

Table 2a, LOX Compatibility Tested Via D2512 Mechanical Impact: NASA TM X-985

Material	Oxygen Phase	Temp	Pressure Psi	Impact Energy	Specimen Thickness	Results Reactions / Impacts
Phenolic resin,	LOX		14.7	10 Kg_f m	0.313 in	2/2
fiberglass honeycomb,	LOX		14.7	5 Kg_f m	0.313 in	11/11
epoxy fiberglass sealer,	LOX		14.7	2 Kg_f m	0.313 in	20/20
epoxy adhesive	LOX		14.7	1 Kg_f m	0.313 in	7/20
	LOX		14.7	1/2 Kg_f m	0.313 in	0/20
Polyurethane	LOX		14.7	10 Kg_f m	0.050 in	6/20
Dyna Therm D-904	LOX		14.7	5 Kg_f m	0.050 in	2/15
	LOX		14.7	4 Kg_f m	0.050 in	0/20
Polyurethane	LOX		14.7	10 Kg_f m	0.063 in	2/20
Dyna Therm D-100	LOX		14.7	2 Kg_f m	0.063 in	1/40
Honey comb phenolic	LOX		14.7	10 Kg_f m	0.063 in	20/20
epoxy (Hexcell 91 LD)	LOX		14.7	5 Kg_f m	0.063 in	20/20
	LOX		14.7	3 Kg_f m	0.063 in	20/20
	LOX		14.7	1 Kg_f m	0.063 in	15/20
Polyurethane	LOX		14.7	10 Kg_f m	0.250 in	20/20
Hexcell Insulation	LOX		14.7	5 Kg_f m	0.250 in	19/20
1414-2	LOX		14.7	3 Kg_f m	0.250 in	8/20
	LOX		14.7	2 Kg_f m	0.250 in	0/20
Quartz spheres and epoxy	LOX		14.7	10 Kg_f m	0.125 in	15/20
(Isowood)	LOX		14.7	7 Kg_f m	0.125 in	7/20
	LOX		14.7	5 Kg_f m	0.125 in	2/20
	LOX		14.7	3 Kg_f m	0.125 in	0/20
Asbestos felt saturated	LOX		14.7	10 Kg_f m	0.063 in	11/20
with phenolic resin and	LOX		14.7	5 Kg_f m	0.063 in	6/20
inorganic filler	LOX		14.7	3 Kg_f m	0.063 in	5/20
	LOX		14.7	2 Kg_f m	0.063 in	3/20
	LOX		14.7	1 Kg_f m	0.063 in	0/20
Phenylated Nylon	LOX		14.7	10 Kg_f m	0.050 in	11/20
	LOX		14.7	5 Kg_f m	0.050 in	8/10
	LOX		14.7	3 Kg_f m	0.050 in	4/10
Polyurethane (Coast Pro Seal 793)	LOX		14.7	10 Kg_f m	0.063 in	2/7
Teflon impregnated silicone rubber (Compound Rubber X-58)	LOX		14.7	10 Kg_f m	0.063 in	2/3
Epoxy and polysulfide	LOX		14.7	10 Kg_f m	0.050 in	10/20
LP/32 activator	LOX		14.7	5 Kg_f m	0.050 in	14/20
(E-Bond Rubber Sealant)	LOX		14.7	1 Kg_f m	0.050 in	10/20
Epibond 123 and Hardner 952A (Furane Plastics Inc)	LOX		14.7	10 Kg_f m	0.050 in	5/20
EPON Glass Terminal	LOX		14.7	10 Kg_f m	0.050 in	2/3
Board	LOX		14.7	5 Kg_f m	0.050 in	1/1
Epoxy Potting Comp	LOX		14.7	10 Kg_f m	0.063 in	1/1
	LOX		14.7	5 Kg_f m	0.063 in	1/1
	LOX		14.7	2 Kg_f m	0.063 in	1/1
Fibrous Glass Tubing	LOX		14.7	10 Kg_f m	0.063 in	4/4
	LOX		14.7	5 Kg_f m	0.063 in	4/4
	LOX		14.7	2 Kg_f m	0.063 in	4/6

Table 2a, LOX Compatibility Tested Via D2512 Mechanical Impact: NASA TM X-985 cont.

Material	Oxygen Phase	Temp	Pressure Psi	Impact Energy	Specimen Thickness	Results Reactions / Impacts
Epoxy Filled Glass Fabric	LOX		14.7	10 Kg_f m	0.063 in	39/40
(Type GEE Grade G-10)	LOX		14.7	5 Kg_f m	0.063 in	4/20
	LOX		14.7	2 Kg_f m	0.063 in	3/20
	LOX		14.7	1 Kg_f m	0.063 in	0/20
Nylon Epoxy	LOX		14.7	10 Kg_f m	0.010 in	17/20
(FM 1000 adhesive)	LOX		14.7	5 Kg_f m	0.010 in	11/20
	LOX		14.7	2 Kg_f m	0.010 in	9/20
Epoxy Phenolic	LOX		14.7	10 Kg_f m	0.013 in	20/20
(HT-424 adhesive)	LOX		14.7	5 Kg_f m	0.013 in	20/20
	LOX		14.7	3 Kg_f m	0.013 in	20/20
	LOX		14.7	1 Kg_f m	0.013 in	6/20
Epoxy Adhesive	LOX		14.7	10 Kg_f m	0.050 in	2/3
(Hysol Cement 6020)	LOX		14.7	5 Kg_f m	0.050 in	2/2
	LOX		14.7	2 Kg_f m	0.050 in	2/4
Kel F Plasticized (PolyTrifluorochloroethylene)	LOX		14.7	10 Kg_f m	0.032 in	0/20
Kel F UnPlasticized (PolyTrifluorochloroethylene)	LOX		14.7	10 Kg_f m	0.032 in	0/20
Kel F L-1380 (PTFCE)	LOX		14.7	10 Kg_f m	0.005 in	0/20
Kel F L-1381 (PTFCE)	LOX		14.7	10 Kg_f m	0.005 in	0/20
Kel F Film Type 8105 (PTFCE)	LOX		14.7	10 Kg_f m	0.005 in	0/20
Kel F Film Type KX202 (PTFCE)	LOX		14.7	10 Kg_f m	0.002 in	0/20
Kel F Film Type KX8110 (PTFCE)	LOX		14.7	10 Kg_f m	0.010in	0/20
Kel F Film Type 8210 (PTFCE)	LOX		14.7	10 Kg_f m	0.010 in	0/20
Kel F Film Type 8205 (PTFCE)	LOX		14.7	10 Kg_f m	0.005 in	0/20
Kel F 81 (PTFCE)	LOX		14.7	10 Kg_f m	0.063 in	0/20
Kel F 800 (PTFCE)	LOX		14.7	10 Kg_f m	0.063 in	0/40
Kel F Film Dispersion 625 (PTFCE)	LOX		14.7	10 Kg_f m	0.005 in	0/20
Kel F Film Dispersion KX 633 (PTFCE)	LOX		14.7	10 Kg_f m	0.002 in	0/20
Kel F Elastomer (PTFCE)	LOX		14.7	10 Kg_f m	0.125 in	0/20
Kel F Elastomer (PTFCE)	LOX		14.7	10 Kg_f m	0.063 in	0/20
Vinyl Rubber (Koroseal) (B.F.Goodrich Co)	LOX		14.7	10 Kg_f m	0.125 in	2/20
Acrylic Resin and	LOX		14.7	10 Kg_f m	0.002 in	2/3
aromatic hydrocarbons	LOX		14.7	5 Kg_f m	0.002 in	2/6
(Krylon Crystal Clear Spray Coating)	LOX		14.7	1 Kg_f m	0.002 in	0/20
Kynar RC2525 (PVF)	LOX		14.7	10 Kg_f m	0.063 in	0/10
Polycarbonate	LOX		14.7	10 Kg_f m	0.063 in	20/20
(GE Lexan)	LOX		14.7	5 Kg_f m	0.063 in	16/20
	LOX		14.7	4 Kg_f m	0.063 in	3/17
	LOX		14.7	2 Kg_f m	0.063 in	0/20
Mylar Insulation Tape	LOX		14.7	10 Kg_f m		2/2
	LOX		14.7	5 Kg_f m		2/13

Table 2a, LOX Compatibility Tested Via D2512 Mechanical Impact: NASA TM X-985 cont.

Material	Oxygen Phase	Temp	Pressure Psi	Impact Energy	Specimen Thickness	Results Reactions / Impacts
Phenolic Laminate	LOX		14.7	10 Kg_f m	0.063 in	16/20
fabric base (Micarta)	LOX		14.7	5 Kg_f m	0.063 in	16/20
(Westinghouse)	LOX		14.7	2 Kg_f m	0.063 in	6/20
	LOX		14.7	1 Kg_f m	0.063 in	0/20
Polyester Mylar Film	LOX		14.7	10 Kg_f m	0.006 in	2/22
(Dupont)	LOX		14.7	5 Kg_f m	0.006 in	2/28
	LOX		14.7	3 Kg_f m	0.006 in	0/20
	LOX		14.7	10 Kg_f m	0.002 in	2/22
	LOX		14.7	5 Kg_f m	0.002 in	2/20
	LOX		14.7	3 Kg_f m	0.002 in	0/20
	LOX		14.7	10 Kg_f m		2/7
	LOX		14.7	5 Kg_f m		0/13
	LOX		14.7	10 Kg_f m		8/10
Mylar 25C Film	LOX		14.7	10 Kg_f m		2/20
Mylar 25UA Film	LOX		14.7	10 Kg_f m		2/11
Mylar 50A Film	LOX		14.7	10 Kg_f m		2/20
	LOX		14.7	5 Kg_f m		0/9
Mylar 50C Film	LOX		14.7	10 Kg_f m		2/20
Mylar 50K Film	LOX		14.7	10 Kg_f m		2/20
Mylar 50T Film	LOX		14.7	10 Kg_f m		2/4
	LOX		14.7	5 Kg_f m		2/3
	LOX		14.7	2 Kg_f m		0/12
Mylar 100T Film	LOX		14.7	10 Kg_f m		3/20
Mylar R22 Film	LOX		14.7	10 Kg_f m		2/20
Mylar Film	LOX		14.7	10 Kg_f m	0.001 in	4/20
Chlorinated Polyester	LOX		14.7	10 Kg_f m	0.050 in	7/10
cured with 2% MEK,	LOX		14.7	5 Kg_f m	0.050 in	4/10
peroxide and cobalt	LOX		14.7	3 Kg_f m	0.050 in	2/20
naphtenate	LOX		14.7	2 Kg_f m	0.050 in	0/20
Chlorinated Polyester	LOX		14.7	10 Kg_f m	0.050 in	9/10
cured with 2% MEK,	LOX		14.7	5 Kg_f m	0.050 in	2/5
peroxide and cobalt	LOX		14.7	3 Kg_f m	0.050 in	1/10
naphtenate filled	LOX		14.7	2 Kg_f m	0.050 in	2/10
with 33.3% antiomony trichloride	LOX		14.7	1 Kg_f m	0.050 in	0/20
ERL 0625 epoxy cured	LOX		14.7	10 Kg_f m	0.050 in	7/10
with 10.6 phr mPDA	LOX		14.7	5 Kg_f m	0.050 in	2/10
	LOX		14.7	3 Kg_f m	0.050 in	0/20
ERL 0625 epoxy cured	LOX		14.7	10 Kg_f m	0.050 in	6/10
with 14.5 phr chlorendic	LOX		14.7	5 Kg_f m	0.050 in	6/20
anhydride and 0.5%	LOX		14.7	3 Kg_f m	0.050 in	2/10
benzyldimethylamine	LOX		14.7	2 Kg_f m	0.050 in	1/10
Narmco Resin 3135	LOX		14.7	10 Kg_f m	0.050 in	3/3
(Adhesive 50% epoxy	LOX		14.7	5 Kg_f m	0.050 in	2/2
50% polyamide)	LOX		14.7	2 Kg_f m	0.050 in	2/7
Narmco Resin 3170	LOX		14.7	10 Kg_f m	0.050 in	16/24
(Adhesive 50% filled	LOX		14.7	5 Kg_f m	0.050 in	2/8
epoxy 50% polyamide)	LOX		14.7	3 Kg_f m	0.050 in	2/14
	LOX		14.7	1 Kg_f m	0.050 in	0/20

Table 2a, LOX Compatibility Tested Via D2512 Mechanical Impact: NASA TM X-985 cont.

Material	Oxygen Phase	Temp	Pressure Psi	Impact Energy	Specimen Thickness	Results Reactions / Impacts
Nylon Basket Weave	LOX		14.7	10 Kg_f m	0.032 in	2/2
No 1803	LOX		14.7	5 Kg_f m	0.032 in	2/2
(Polyamide)	LOX		14.7	2 Kg_f m	0.032 in	2/2
	LOX		14.7	1 Kg_f m	0.032 in	2/12
Nylon Type 127-1	LOX		14.7	10 Kg_f m	0.250 in	8/20
(Polyamide)	LOX		14.7	5 Kg_f m	0.250 in	1/1
	LOX		14.7	3 Kg_f m	0.250 in	1/2
	LOX		14.7	1 Kg_f m	0.250 in	0/20
Nylon "C"	LOX		14.7	10 Kg_f m	0.001 in	13/20
Zytel Nylon	LOX		14.7	10 Kg_f m	0.001 in	10/20
Zytel Nylon	LOX		14.7	10 Kg_f m	0.002 in	3/20
Zytel Nylon	LOX		14.7	10 Kg_f m	0.004 in	8/20
Nylon Extruded Rod	LOX		14.7	10 Kg_f m	0.063 in	2/2
	LOX		14.7	5 Kg_f m	0.063 in	2/2
	LOX		14.7	2 Kg_f m	0.063 in	2/3
Glass and Polyester	LOX		14.7	10 Kg_f m		2/5
Plaskon Alkyd 440	LOX		14.7	5 Kg_f m		2/13
Sheet Plastic	LOX		14.7	1 Kg_f m		0/2
Dyed Polyethylene	LOX		14.7	10 Kg_f m	0.063 in	4/11
	LOX		14.7	5 Kg_f m	0.063 in	2/10
	LOX		14.7	3 Kg_f m	0.063 in	2/14
	LOX		14.7	1 Kg_f m	0.063 in	0/20
Plastic Steel Putty Type A	LOX		14.7	10 Kg_f m	0.050 in	5/5
(80% steel 20% epoxy)	LOX		14.7	5 Kg_f m	0.050 in	5/5
	LOX		14.7	2 Kg_f m	0.050 in	9/12
	LOX		14.7	1 Kg_f m	0.050 in	4/20
Plexiglass (PMMA)	LOX		14.7	10 Kg_f m		2/2
	LOX		14.7	5 Kg_f m		1/3
	LOX		14.7	3 Kg_f m		1/4
Polyethylene	LOX		14.7	10 Kg_f m	0.032 in	4/7
	LOX		14.7	5 Kg_f m	0.032 in	2/19
	LOX		14.7	2 Kg_f m	0.032 in	1/3
	LOX		14.7	1 Kg_f m	0.032 in	0/17
Polyurethane Wiping	LOX		14.7	10 Kg_f m	0.016 in	2/3
Material	LOX		14.7	3 Kg_f m	0.016 in	2/9
	LOX		14.7	1 Kg_f m	0.016 in	0/20
PVC	LOX		14.7	10 Kg_f m	0.125 in	2/2
	LOX		14.7	5 Kg_f m	0.125 in	2/9
	LOX		14.7	2 Kg_f m	0.125 in	2/14
	LOX		14.7	1 Kg_f m	0.125 in	0/20
	LOX		14.7	10 Kg_f m	0.063 in	2/3
	LOX		14.7	5 Kg_f m	0.063 in	2/3
	LOX		14.7	2 Kg_f m	0.063 in	2/11
	LOX		14.7	3 Kg_f m	0.063 in	1/3
Epoxy Potting Compound	LOX		14.7	10 Kg_f m	0.063 in	1/1
	LOX		14.7	5 Kg_f m	0.063 in	1/1
	LOX		14.7	2 Kg_f m	0.063 in	1/1
	LOX		14.7	1 Kg_f m	0.063 in	1/2
Polyurethane PRC 1525	LOX		14.7	10 Kg_f m	0.063 in	3/20
	LOX		14.7	5 Kg_f m	0.063 in	0/20
Polyurethane PRC 1525	LOX		14.7	10 Kg_f m	0.125 in	3/20

Table 2a, LOX Compatibility Tested Via D2512 Mechanical Impact: NASA TM X-985 cont.

Material	Oxygen Phase	Temp	Pressure Psi	Impact Energy	Specimen Thickness	Results Reactions / Impacts
Polyurethane PRC 1527	LOX		14.7	10 Kg_f m	0.125 in	7/20
	LOX		14.7	5 Kg_f m	0.125 in	3/20
Polyurethane PRC 1527	LOX		14.7	10 Kg_f m	0.032 in	11/20
Polyurethane PRC 1538	LOX		14.7	10 Kg_f m	0.063 in	10/20
Polyurethane PRC 1538-T	LOX		14.7	10 Kg_f m	0.063 in	5/20
	LOX		14.7	5 Kg_f m	0.063 in	1/20
Phenolic Epoxy (PT-201	LOX		14.7	10 Kg_f m		1/1
and Solvent PT-1001)	LOX		14.7	5 Kg_f m		1/1
	LOX		14.7	2 Kg_f m		1/2
Fluorosilicone Rubber	LOX		14.7	10 Kg_f m	0.050 in	2/20
Q9-0002A and B adhesive						
Fluorosilicone Rubber	LOX		14.7	10 Kg_f m	0.050 in	1/140
Q9-0046 adhesive	LOX		14.7	10 Kg_f m	0.025 in	38/40
Epoxy (Relco 50%A	LOX		14.7	10 Kg_f m	0.063 in	2/20
and 50%B)						
Epoxy (Relco 50%A	LOX		14.7	10 Kg_f m	0.063 in	3/5
and 50%B and Grit)	LOX		14.7	5 Kg_f m	0.063 in	2/5
	LOX		14.7	3 Kg_f m	0.063 in	2/3
	LOX		14.7	2 Kg_f m	0.063 in	1/8
Scotch Resin No CRP-235	LOX		14.7	10 Kg_f m		3/6
Epoxy 1 part A 2 Part B	LOX		14.7	5 Kg_f m		1/14
cured at 30 C for 1/2 Hr						
Stycast 2651 Epoxy	LOX		14.7	10 Kg_f m	0.063 in	2/2
	LOX		14.7	5 Kg_f m	0.063 in	2/2
	LOX		14.7	3 Kg_f m	0.063 in	2/3
	LOX		14.7	1 Kg_f m	0.063 in	0/20
Teflon PTFE	LOX		14.7	10 Kg_f m	0.002 in	0/20
	LOX		14.7	10 Kg_f m	0.006 in	0/20
Copper Filled Teflon	LOX		14.7	10 Kg_f m	0.028 in	5/40
PTEF adhesive						
PTFE Teflon	LOX		14.7	10 Kg_f m	0.032 in	0/20
PTFE Teflon	LOX		14.7	10 Kg_f m	0.063 in	0/40
Pigmented PTFE Teflon	LOX		14.7	10 Kg_f m		2/20
PTFE Teflon	LOX		14.7	10 Kg_f m	0.016 in	0/20
FEP Teflon Film 0.005 in	LOX		14.7	10 Kg_f m	0.255 in	0/40
between Two Pieces PTFE Teflon felt						
FEP Teflon Type 544	LOX		14.7	10 Kg_f m	0.001 in	0/20
FEP Teflon	LOX		14.7	10 Kg_f m	0.010 in	0/20
	LOX		14.7	10 Kg_f m	0.021 in	0/20
	LOX		14.7	10 Kg_f m	0.005 in	0/20
PTFE Teflon	LOX		14.7	10 Kg_f m	0.001 in	0/20
Enamel 852-202						
Viton A On Glass Fibers	LOX		14.7	10 Kg_f m	0.011 in	2/2
85001	LOX		14.7	5 Kg_f m	0.011 in	2/5
	LOX		14.7	2 Kg_f m	0.011 in	2/3
Viton A On Dacron Fabric	LOX		14.7	10 Kg_f m		2/2
	LOX		14.7	5 Kg_f m		2/4
	LOX		14.7	1 Kg_f m		2/11
Viton A Elastomer	LOX		14.7	10 Kg_f m		0-4/20
(PVdiFandHexaFPP)						

Table 2a, LOX Compatibility Tested Via D2512 Mechanical Impact: NASA TM X-985 cont.

Material	Oxygen Phase	Temp	Pressure Psi	Impact Energy	Specimen Thickness	Results Reactions / Impacts
Epoxy (XR 5038)	LOX		14.7	10 Kg_f m	0.063 in	2/25
	LOX		14.7	5 Kg_f m	0.063 in	0/35
Teflon and Asbestos	LOX		14.7	10 Kg_f m	0.063 in	0/40
Armalon 97-001	LOX		14.7	10 Kg_f m	0.010 in	0/20
0.005 in PTFE Fiber 0.005 in FEP film						
Armalon PDX 7550	LOX		14.7	10 Kg_f m	0.125 in	0/20
PTFE felt and FEP Film						
Armalon No.410-128	LOX		14.7	10 Kg_f m	0.016 in	0/20
Teflon and Glass						
Armalon Teflon	LOX		14.7	10 Kg_f m	0.016 in	2/2
And Glass	LOX		14.7	5 Kg_f m	0.016 in	2/5
	LOX		14.7	3 Kg_f m	0.016 in	1/13
Armalon	LOX		14.7	10 Kg_f m	0.063 in	0/20
Fluorocarbon Felt Bleached Sheet						
Armalon	LOX		14.7	10 Kg_f m	0.063 in	2/4
Fluorocarbon Felt UnBleached Sheet						
Neoprene Latex and	LOX		14.7	10 Kg_f m	0.032 in	2/3
Asbestos Fibers	LOX		14.7	5 Kg_f m	0.032 in	2/2
Duroid Sheet 3102	LOX		14.7	3 Kg_f m	0.032 in	0/14
Neoprene Latex and	LOX		14.7	10 Kg_f m	0.032 in	2/2
Asbestos Fibers	LOX		14.7	5 Kg_f m	0.032 in	2/2
Duroid Sheet 3110	LOX		14.7	3 Kg_f m	0.032 in	1/16
Buna N Latex and	LOX		14.7	10 Kg_f m	0.032 in	2/2
Asbestos Fibers	LOX		14.7	5 Kg_f m	0.032 in	2/2
Duroid 3200	LOX		14.7	3 Kg_f m	0.032 in	2/3
Buna N Latex and	LOX		14.7	10 Kg_f m	0.032 in	2/2
Asbestos Fibers	LOX		14.7	5 Kg_f m	0.032 in	2/2
Duroid 3210	LOX		14.7	3 Kg_f m	0.032 in	2/16
Buna S Latex and	LOX		14.7	10 Kg_f m	0.032 in	2/2
Asbestos Fibers	LOX		14.7	5 Kg_f m	0.032 in	2/2
Duroid 3300	LOX		14.7	3 Kg_f m	0.032 in	2/16
Buna S Latex and	LOX		14.7	10 Kg_f m	0.032 in	2/3
Asbestos Fibers	LOX		14.7	5 Kg_f m	0.032 in	2/3
Duroid 3310	LOX		14.7	3 Kg_f m	0.032 in	0/14
Buna S Latex and	LOX		14.7	10 Kg_f m	0.063 in	2/2
Asbestos Fibers	LOX		14.7	5 Kg_f m	0.063 in	2/6
Duroid 3350	LOX		14.7	3 Kg_f m	0.063 in	0/11
Viton A and Asbestos	LOX		14.7	10 Kg_f m	0.063 in	0/20
Fibers Duroid 3400						
Teflon and Ceramic	LOX		14.7	10 Kg_f m	0.063 in	0/20
Fibers Duroid 5600						
Teflon and Asbestos	LOX		14.7	10 Kg_f m	0.030 in	0/20
Fluorobestos LS-7598						
Teflon and Asbestos	LOX		14.7	10 Kg_f m	0.063 in	0/20
Unsintered						
Fluorogreen E-600	LOX		14.7	10 Kg_f m	0.063 in	0/60
Teflon and Inorganic filler						
Asbestos and Rubber	LOX		14.7	10 Kg_f m	0.063 in	2/2
Composite (Garlock 900)	LOX		14.7	5 Kg_f m	0.063 in	2/3
	LOX		14.7	2 Kg_f m	0.063 in	2/4

Table 2a, LOX Compatibility Tested Via D2512 Mechanical Impact: NASA TM X-985 cont.

Material	Oxygen Phase	Temp	Pressure Psi	Impact Energy	Specimen Thickness	Results Reactions / Impacts
Teflon Reinforced With Glass Fiber (Lo Flo Sheet)	LOX		14.7	10 Kg_f m	0.032 in	0/20
Teflon Reinforced With Ground Glass (Lo Flo Sheet)	LOX		14.7	10 Kg_f m	0.063 in	0/20
Asbestos and Rubber	LOX		14.7	10 Kg_f m	0.063 in	2/2
Composite	LOX		14.7	5 Kg_f m	0.063 in	2/3
(Garlock 7021)	LOX		14.7	2 Kg_f m	0.063 in	2/2
	LOX		14.7	1 Kg_f m	0.063 in	0/2
Asbestos And Neoprene	LOX		14.7	10 Kg_f m	0.063 in	2/2
Rubber (Garlock 7228)	LOX		14.7	5 Kg_f m	0.063 in	0/14
Teflon Impregnated With Asbestos	LOX		14.7	10 Kg_f m	0.063 in	0/20
Asbestos With Sulfur free neoprene binder	LOX		14.7	10 Kg_f m	0.063 in	0/20
Asbestos With Sulfur free neoprene binder	LOX		14.7	10 Kg_f m	0.094 in	4/20
Teflon impregnated with asbestos cloth	LOX		14.7	10 Kg_f m	0.125 in	0/40
Teflon impregnated with asbestos cloth	LOX		14.7	10 Kg_f m	0.063 in	0/40
Polyglycol 15-200	LOX		14.7	10 Kg_f m		2/12
Polyoxyalkylene ethers with methyl side chains and terminal hydroxyl groups						
Polypropylene glycol 174-500	LOX		14.7	10 Kg_f m		1/20
Polypropylene glycol P-400	LOX		14.7	10 Kg_f m		2/20
Polypropylene glycol P-2000	LOX		14.7	10 Kg_f m		2/2
Quartz (Clear Fused)	LOX		14.7	10 Kg_f m		0/20

Table 2b, LOX Compatibility Tested Via D2512 Mechanical Impact: NASA TM X-53533

Material	Oxygen Phase	Temp	Pressure Psi	Impact Energy	Specimen Thickness	Results Reactions / Impacts
DC 33 (Silicone Grease)	LOX		14.7	10 Kg_fm	0.050 in	4/20
	LOX		14.7	7.62 Kg_fm	0.050 in	3/20
	LOX		14.7	5.54 Kg_fm	0.050 in	1/20
	LOX		14.7	4.16 Kg_fm	0.050 in	1/20
	LOX		14.7	3.46 Kg_fm	0.050 in	0/20
	LOX		14.7	10 Kg_fm	0.050 in	6/20
	LOX		14.7	7.62 Kg_fm	0.050 in	5/20
	LOX		14.7	5.54 Kg_fm	0.050 in	2/20
	LOX		14.7	4.16 Kg_fm	0.050 in	1/20
	LOX		14.7	3.46 Kg_fm	0.050 in	0/20
Drilube Type 822 (Fluorinated Silicone)	LOX		14.7	10 Kg_fm	0.050 in	2/20
FS-1280 (Fluorosilcone)	LOX		14.7	10 Kg_fm	0.050 in	0/60
FS-1281	LOX		14.7	10 Kg_fm	0.050 in	33/722
Various batches of (Fluorosilicone)						
Kel F 90 Grease	LOX		14.7	10 Kg_fm	0.050 in	1/120
Anaconda AI-200	LOX		14.7	10 Kg_fm	0.005 in	6/20
Magnet Wire (Amide-Imide copolymer on Copper)						

Table 2b, LOX Compatibility Tested Via D2512 Mechanical Impact: NASA TM X-53533 cont.

Material	Oxygen Phase	Temp	Pressure Psi	Impact Energy		Specimen Thickness	Results Reactions / Impacts
Styrofoam	LOX		14.7	10	Kg_fm	0.401 in	4/20
	LOX		14.7	8	Kg_fm	0.401 in	3/20
	LOX		14.7	6	Kg_fm	0.401 in	4/20
	LOX		14.7	4	Kg_fm	0.401 in	8/20
	LOX		14.7	2	Kg_fm	0.401 in	10/20
	LOX		14.7	1	Kg_fm	0.401 in	7/20
Styrofoam	LOX		14.7	10	Kg_fm	0.401 in	2/20
	LOX		14.7	8	Kg_fm	0.401 in	2/20
	LOX		14.7	6	Kg_fm	0.401 in	5/20
	LOX		14.7	4	Kg_fm	0.401 in	10/20
	LOX		14.7	2	Kg_fm	0.401 in	16/20
	LOX		14.7	1	Kg_fm	0.401 in	7/20
Aclar 22C	LOX		14.7	10	Kg_fm	0.0015 in	0/20
Aclar 33C	LOX		14.7	10	Kg_fm	0.001 in	0/20
(Fluorochloropolymer)	LOX		14.7	10	Kg_fm	0.002 in	0/20
	LOX		14.7	10	Kg_fm	0.005 in	0/20
CS2727 Epoxy 100 gms	LOX		14.7	10	Kg_fm	0.050 in	9/20
and 9817 Accelerator	LOX		14.7	8	Kg_fm	0.050 in	8/20
27 gms 72 hrs air dry	LOX		14.7	6	Kg_fm	0.050 in	6/20
(Chem-seal Corporation)	LOX		14.7	4	Kg_fm	0.050 in	6/20
Eimac 221	LOX		14.7	10	Kg_fm	0.2 in	6/20
(Para polyphenyl)							
Silicone	LOX		14.7	10	Kg_fm	0.050 in	16/20
(Air dried 72 hrs)	LOX		14.7	8	Kg_fm	0.050 in	10/20
	LOX		14.7	6	Kg_fm	0.050 in	9/20
	LOX		14.7	4	Kg_fm	0.050 in	8/20
	LOX		14.7	2	Kg_fm	0.050 in	4/20
Ethyl Cellulose	LOX		14.7	10	Kg_fm	0.005 in	17/20
	LOX		14.7	8	Kg_fm	0.005 in	9/20
	LOX		14.7	6	Kg_fm	0.005 in	8/20
	LOX		14.7	4	Kg_fm	0.005 in	3/20
	LOX		14.7	2	Kg_fm	0.005 in	0/20
Ethyl Cellulose	LOX		14.7	10	Kg_fm	0.010 in	19/20
	LOX		14.7	8	Kg_fm	0.010 in	16/20
	LOX		14.7	6	Kg_fm	0.010 in	10/20
	LOX		14.7	4	Kg_fm	0.010 in	6/20
	LOX		14.7	2	Kg_fm	0.010 in	0/20
Ethyl Cellulose	LOX		14.7	10	Kg_fm	0.020 in	18/20
	LOX		14.7	8	Kg_fm	0.020 in	11/20
	LOX		14.7	6	Kg_fm	0.020 in	12/20
	LOX		14.7	4	Kg_fm	0.020 in	7/20
	LOX		14.7	2	Kg_fm	0.020 in	0/20
Ethyl Cellulose	LOX		14.7	10	Kg_fm	0.030 in	16/20
	LOX		14.7	8	Kg_fm	0.030 in	14/20
	LOX		14.7	6	Kg_fm	0.030 in	11/20
	LOX		14.7	4	Kg_fm	0.030 in	7/20
	LOX		14.7	2	Kg_fm	0.030 in	3/20
	LOX		14.7	2	Kg_fm	0.030 in	1/20

Table 2b, LOX Compatibility Tested Via D2512 Mechanical Impact: NASA TM X-53533 cont.

Material	Oxygen Phase	Temp	Pressure Psi	Impact Energy		Specimen Thickness	Results Reactions / Impacts
Ethyl Cellulose	LOX		14.7	10	$Kg_f m$	0.050 in	16/20
	LOX		14.7	8	$Kg_f m$	0.050 in	12/20
	LOX		14.7	6	$Kg_f m$	0.050 in	7/20
	LOX		14.7	4	$Kg_f m$	0.050 in	4/20
	LOX		14.7	2	$Kg_f m$	0.050 in	2/20
	LOX		14.7	2	$Kg_f m$	0.050 in	0/20
Ethyl Cellulose	LOX		14.7	10	$Kg_f m$	0.060 in	14/20
	LOX		14.7	8	$Kg_f m$	0.060 in	10/20
	LOX		14.7	6	$Kg_f m$	0.060 in	9/20
	LOX		14.7	4	$Kg_f m$	0.060 in	3/20
	LOX		14.7	2	$Kg_f m$	0.060 in	0/20
Ethyl Cellulose	LOX		14.7	10	$Kg_f m$	0.080 in	17/20
	LOX		14.7	8	$Kg_f m$	0.080 in	13/20
	LOX		14.7	6	$Kg_f m$	0.080 in	9/20
	LOX		14.7	4	$Kg_f m$	0.080 in	2/20
	LOX		14.7	2	$Kg_f m$	0.080 in	0/20
Teflon with 0.05% carbon black	LOX		14.7	10	$Kg_f m$	0.050 in	0/20
Teflon	LOX		14.7	10	$Kg_f m$	0.010 in	1/60
Kel F	LOX		14.7	10	$Kg_f m$	0.042 in	0/20
	LOX		14.7	10	$Kg_f m$	0.63 in	0/20
Kel F 800 Spray Coated	LOX		14.7	10	$Kg_f m$		0/20
Kel F Unplasticized	LOX		14.7	10	$Kg_f m$	0.075 in	0/20
Mylar (Polyester)	LOX		14.7	10	$Kg_f m$		17/20
Mylar (Polyester) (Doped with 10%FEP 90% PET)	LOX		14.7	10	$Kg_f m$	0.08 in	7/20
Mylar A (Trike Cleaned)	LOX		14.7	10	$Kg_f m$	0.003 in	4/20
	LOX		14.7	7.62	$Kg_f m$	0.003 in	1/20
	LOX		14.7	6.93	$Kg_f m$	0.003 in	1/40
	LOX		14.7	6.24	$Kg_f m$	0.003 in	1/40
	LOX		14.7	5.54	$Kg_f m$	0.003 in	0/20
Mylar A	LOX		14.7	10	$Kg_f m$	0.005 in	50/100
	LOX		14.7	8	$Kg_f m$	0.005 in	44/100
	LOX		14.7	6	$Kg_f m$	0.005 in	34/100
	LOX		14.7	4	$Kg_f m$	0.005 in	10/100
	LOX		14.7	2	$Kg_f m$	0.005 in	3/100
Mylar A (Trike Cleaned)	LOX		14.7	10	$Kg_f m$	0.005 in	5/20
	LOX		14.7	7.62	$Kg_f m$	0.005 in	5/20
	LOX		14.7	5.54	$Kg_f m$	0.005 in	2/20
	LOX		14.7	4.16	$Kg_f m$	0.005 in	1/20
	LOX		14.7	3.46	$Kg_f m$	0.005 in	2/40
	LOX		14.7	2.08	$Kg_f m$	0.005 in	1/20
Mylar A	LOX		14.7	10	$Kg_f m$	0.005 in	2/120
Mylar A (Trike Cleaned)	LOX		14.7	10	$Kg_f m$	0.0075 in	2/20
	LOX		14.7	7.62	$Kg_f m$	0.0075 in	5/20
	LOX		14.7	6.93	$Kg_f m$	0.0075 in	1/20
	LOX		14.7	6.24	$Kg_f m$	0.0075 in	1/40
	LOX		14.7	5.54	$Kg_f m$	0.0075 in	1/40
	LOX		14.7	3.46	$Kg_f m$	0.0075 in	1/20
	LOX		14.7	2.77	$Kg_f m$	0.0075 in	1/40

Table 2b, LOX Compatibility Tested Via D2512 Mechanical Impact: NASA TM X-53533 cont.

Material	Oxygen Phase	Temp	Pressure Psi	Impact Energy	Specimen Thickness	Results Reactions / Impacts
Mylar A (Trike Cleaned)	LOX		14.7	10 $Kg_f m$	0.010 in	7/20
	LOX		14.7	7.62 $Kg_f m$	0.010 in	7/20
	LOX		14.7	6.93 $Kg_f m$	0.010 in	2/20
	LOX		14.7	6.24 $Kg_f m$	0.010 in	2/20
	LOX		14.7	5.54 $Kg_f m$	0.010 in	2/40
	LOX		14.7	4.85 $Kg_f m$	0.010 in	1/20
	LOX		14.7	4.16 $Kg_f m$	0.010 in	1/60
	LOX		14.7	3.46 $Kg_f m$	0.010 in	0/40
Mylar D	LOX		14.7	10 $Kg_f m$	0.003 in	2/20
	LOX		14.7	8 $Kg_f m$	0.003 in	1/20
Mylar D (Trike Cleaned)	LOX		14.7	10 $Kg_f m$	0.003 in	5/20
	LOX		14.7	7.62 $Kg_f m$	0.003 in	4/20
	LOX		14.7	6.93 $Kg_f m$	0.003 in	1/20
	LOX		14.7	6.24 $Kg_f m$	0.003 in	1/20
	LOX		14.7	5.54 $Kg_f m$	0.003 in	0/60
Mylar D (Trike Cleaned)	LOX		14.7	10 $Kg_f m$	0.005 in	3/20
	LOX		14.7	7.85 $Kg_f m$	0.005 in	2/20
	LOX		14.7	6.93 $Kg_f m$	0.005 in	1/20
	LOX		14.7	6.24 $Kg_f m$	0.005 in	2/20
	LOX		14.7	5.54 $Kg_f m$	0.005 in	2/60
	LOX		14.7	3.46 $Kg_f m$	0.005 in	1/20
	LOX		14.7	2.77 $Kg_f m$	0.005 in	1/60
	LOX		14.7	2.08 $Kg_f m$	0.005 in	0/20
Mylar D (Trike Cleaned)	LOX		14.7	10 $Kg_f m$	0.0075 in	3/20
	LOX		14.7	7.62 $Kg_f m$	0.0075 in	1/20
	LOX		14.7	5.54 $Kg_f m$	0.0075 in	3/40
	LOX		14.7	4.85 $Kg_f m$	0.0075 in	1/20
	LOX		14.7	4.16 $Kg_f m$	0.0075 in	1/20
	LOX		14.7	3.46 $Kg_f m$	0.0075 in	0/60
Mylar D	LOX		14.7	10 $Kg_f m$	0.010 in	14/20
	LOX		14.7	8 $Kg_f m$	0.010 in	11/20
	LOX		14.7	6 $Kg_f m$	0.010 in	11/20
	LOX		14.7	4 $Kg_f m$	0.010 in	9/20
	LOX		14.7	2 $Kg_f m$	0.010 in	2/20
	LOX		14.7	1 $Kg_f m$	0.010 in	0/20
Mylar D (Trike Cleaned)	LOX		14.7	10 $Kg_f m$	0.010 in	10/20
	LOX		14.7	7.62 $Kg_f m$	0.010 in	8/20
	LOX		14.7	5.54 $Kg_f m$	0.010 in	6/20
	LOX		14.7	3.46 $Kg_f m$	0.010 in	1/20
	LOX		14.7	2.08 $Kg_f m$	0.010 in	2/20
	LOX		14.7	1.39 $Kg_f m$	0.010 in	0/20
Neoprene Rubber A-522	LOX		14.7	10 $Kg_f m$	0.065 in	3/20
	LOX		14.7	8 $Kg_f m$	0.065 in	3/20
	LOX		14.7	6 $Kg_f m$	0.065 in	0/20
Nitroso Copolymer	LOX		14.7	10 $Kg_f m$	0.190 in	0/12
Nitroso Vulcanizate	LOX		14.7	10 $Kg_f m$	0.080 in	1/6
Nylon	LOX		14.7	10 $Kg_f m$	0.004 in	2/40
RTV-S-53V-70 Foam	LOX		14.7	10 $Kg_f m$	0.400 in	20/20
	LOX		14.7	8 $Kg_f m$	0.400 in	20/20
	LOX		14.7	6 $Kg_f m$	0.400 in	20/20
	LOX		14.7	4 $Kg_f m$	0.400 in	20/20
	LOX		14.7	2 $Kg_f m$	0.400 in	11/20
	LOX		14.7	1 $Kg_f m$	0.400 in	0/20

Table 2b, LOX Compatibility Tested Via D2512 Mechanical Impact: NASA TM X-53533 cont.

Material	Oxygen Phase	Temp	Pressure Psi	Impact Energy		Specimen Thickness	Results Reactions / Impacts
Rulon A Lot PA-2	LOX		14.7	10	$Kg_f m$	0.050 in	0/20
Fluorosilicone S-2273 (Rubber)	LOX		14.7	10	$Kg_f m$	0.200 in	10/20
Silastic RTV 94-002 (Lot 162116 Cured 30 days at 110 C)	LOX		14.7	10	$Kg_f m$	0.111 in	7/20
SP-1 Unfilled (Polyimide)	LOX		14.7	10	$Kg_f m$	0.050 in	0/20
SP-21 15% Graphite Fill	LOX		14.7	10	$Kg_f m$	0.050 in	0/20
SP-41 40% Bronze Fill	LOX		14.7	10	$Kg_f m$	0.050 in	0/20
Teflon Fiber 400-60-0	LOX		14.7	10	$Kg_f m$		6/40
Teflon Fiber 1350-180-0	LOX		14.7	10	$Kg_f m$		0/20
Teflon Hose #1	LOX		14.7	10	$Kg_f m$	0.070 in	0/20
Teflon Hose #2	LOX		14.7	10	$Kg_f m$	0.070 in	0/20
Teflon Sewing Thread	LOX		14.7	10	$Kg_f m$		14/20
Tenite II	LOX		14.7	10	$Kg_f m$	0.040 in	2/20
(Cellulose Acetate	LOX		14.7	8	$Kg_f m$	0.040 in	5/20
Butyrate)	LOX		14.7	6	$Kg_f m$	0.040 in	4/20
	LOX		14.7	4	$Kg_f m$	0.040 in	3/20
	LOX		14.7	2	$Kg_f m$	0.040 in	0/20
Viton A	LOX		14.7	10	$Kg_f m$	0.125 in	0/20
Viton A, A-34470	LOX		14.7	10	$Kg_f m$	0.065 in	0/20
Viton A Compound V702-0	LOX		14.7	10	$Kg_f m$	0.047 in	2/20
Viton A Compound 17107A	LOX		14.7	10	$Kg_f m$	0.144 in	0/20
Carbon Seal from Bingham LOX Pump Seal	LOX		14.7	10	$Kg_f m$	0.062 in	0/20
Carbon Seal from Bingham LOX Pump Seal Ground To Powder	LOX		14.7	10	$Kg_f m$	0.062 in	5/20
Fluorogreen E-600	LOX		14.7	10	$Kg_f m$	0.062 in	0/20
	LOX		14.7	10	$Kg_f m$	0.065 in	0/20
	LOX		14.7	10	$Kg_f m$	0.066 in	0/20
	LOX		14.7	10	$Kg_f m$	0.072 in	0/20
	LOX		14.7	10	$Kg_f m$	0.080 in	0/20
	LOX		14.7	10	$Kg_f m$	0.120 in	0/20
	LOX		14.7	10	$Kg_f m$	0.125 in	0/20
	LOX		14.7	10	$Kg_f m$	0.130 in	0/20
	LOX		14.7	10	$Kg_f m$	0.132 in	0/20
	LOX		14.7	10	$Kg_f m$	0.135 in	0/20
	LOX		14.7	10	$Kg_f m$	0.150 in	0/20
F-33 Detergent Concentrate	LOX		14.7	10	$Kg_f m$	0.5 ml	2/20

Table 2c, LOX Compatibility Of Composites Tested Via D2512 Mechanical Impact: NASA TM X-53773

Material	Oxygen Phase	Temp	Pressure Psi	Impact Energy		Specimen Thickness	Results Reactions / Impacts
DC 94-018	LOX		14.7	10	$Kg_f m$	0.050 in	2/20
Fluorosilicone	LOX		14.7	10	$Kg_f m$	0.075 in	0/20
	LOX		14.7	10	$Kg_f m$	0.106 in	4/20
DC 94-018	LOX		14.7	10	$Kg_f m$	0.050 in	5/20
Fluorosilicone	LOX		14.7	10	$Kg_f m$	0.084 in	4/20
	LOX		14.7	10	$Kg_f m$	0.100 in	4/20

Table 2c, LOX Compatibility Tested Via D2512 Mechanical Impact: NASA TM X-53773,cont.

Material	Oxygen Phase	Temp	Pressure Psi	Impact Energy	Specimen Thickness	Results Reactions / Impacts
Eimac 221(Polyphenyl)	LOX		14.7	10 Kg_f m	0.280 in	6/20
Epoxy	LOX		14.7	10 Kg_f m	0.35in	11/20
Ethylene Propylene	LOX		14.7	10 Kg_f m	0.078 in	7/20
Polyvinylchloride	LOX		14.7	10 Kg_f m	0.080 in	5/20
	LOX		14.7	7.7 Kg_f m	0.080 in	2/20
	LOX		14.7	7.0 Kg_f m	0.080 in	0/20
	LOX		14.7	5.6 Kg_f m	0.080 in	0/20
	LOX		14.7	10 Kg_f m	0.060 in	6/20
	LOX		14.7	7.7 Kg_f m	0.060 in	5/20
	LOX		14.7	5.6 Kg_f m	0.060 in	4/20
	LOX		14.7	4.9 Kg_f m	0.060 in	1/20
	LOX		14.7	4.2 Kg_f m	0.060 in	0/20
	LOX		14.7	3.5 Kg_f m	0.060 in	0/20
	LOX		14.7	10 Kg_f m	0.050 in	2/20
	LOX		14.7	7.7 Kg_f m	0.050 in	1/20
	LOX		14.7	5.6 Kg_f m	0.050 in	5/20
	LOX		14.7	4.9 Kg_f m	0.050 in	3/20
	LOX		14.7	2.8 Kg_f m	0.050 in	1/20
	LOX		14.7	2.1 Kg_f m	0.050 in	0/20
	LOX		14.7	1.4 Kg_f m	0.050 in	0/20
	LOX		14.7	10 Kg_f m	0.040 in	6/20
	LOX		14.7	7.7 Kg_f m	0.040 in	5/20
	LOX		14.7	5.6 Kg_f m	0.040 in	3/20
	LOX		14.7	2.8 Kg_f m	0.040 in	0/20
	LOX		14.7	2.1 Kg_f m	0.040 in	0/20
	LOX		14.7	1.4 Kg_f m	0.040 in	0/20
	LOX		14.7	10 Kg_f m	0.030 in	9/20
	LOX		14.7	7.7 Kg_f m	0.030 in	5/20
	LOX		14.7	5.6 Kg_f m	0.030 in	6/20
	LOX		14.7	3.5 Kg_f m	0.030 in	2/20
	LOX		14.7	2.8 Kg_f m	0.030 in	0/20
	LOX		14.7	2.1 Kg_f m	0.030 in	0/20
	LOX		14.7	10 Kg_f m	0.020 in	10/20
	LOX		14.7	7.7 Kg_f m	0.020 in	10/20
	LOX		14.7	5.6 Kg_f m	0.020 in	7/20
	LOX		14.7	3.5 Kg_f m	0.020 in	3/20
	LOX		14.7	2.8 Kg_f m	0.020 in	1/20
	LOX		14.7	2.1 Kg_f m	0.020 in	0/20
	LOX		14.7	10 Kg_f m	0.010 in	11/20
	LOX		14.7	7.7 Kg_f m	0.010 in	8/20
	LOX		14.7	5.6 Kg_f m	0.010 in	8/20
	LOX		14.7	3.5 Kg_f m	0.010 in	3/20
	LOX		14.7	1.4 Kg_f m	0.010 in	2/20
	LOX		14.7	0.7 Kg_f m	0.010 in	1/20
Fiberglass Epoxy Pipe	LOX		14.7	10 Kg_f m	0.22 in	20/20
Polyethylene	LOX		14.7	10 Kg_f m	0.006 in	88/100
	LOX		14.7	8 Kg_f m	0.006 in	50/100
	LOX		14.7	6 Kg_f m	0.006 in	42/100
	LOX		14.7	4 Kg_f m	0.006 in	30/100
	LOX		14.7	2 Kg_f m	0.006 in	9/100
	LOX		14.7	1 Kg_f m	0.006 in	0/100

Table 2c, LOX Compatibility Tested Via D2512 Mechanical Impact: NASA TM X-53773,cont.

Material	Oxygen Phase	Temp	Pressure Psi	Impact Energy	Specimen Thickness	Results Reactions / Impacts
Ceramic Filled PTFE	LOX		14.7	10 Kg_f m	0.025 in	4/20
Neoprene Rubber	LOX		14.7	10 Kg_f m	0.040 in	16/20
	LOX		14.7	7.7 Kg_f m	0.040 in	10/20
	LOX		14.7	5.6 Kg_f m	0.040 in	8/20
	LOX		14.7	4.9 Kg_f m	0.040 in	2/20
	LOX		14.7	4.2 Kg_f m	0.040 in	2/20
	LOX		14.7	3.5 Kg_f m	0.040 in	0/20
	LOX		14.7	2.8 Kg_f m	0.040 in	0/20
Polypropylene	LOX		14.7	10 Kg_f m	0.080 in	15/20
	LOX		14.7	7.7 Kg_f m	0.080 in	12/20
	LOX		14.7	5.6 Kg_f m	0.080 in	4/20
	LOX		14.7	4.9 Kg_f m	0.080 in	2/20
	LOX		14.7	4.2 Kg_f m	0.080 in	0/20
	LOX		14.7	3.5 Kg_f m	0.080 in	0/20
	LOX		14.7	10 Kg_f m	0.060 in	17/20
	LOX		14.7	7.7 Kg_f m	0.060 in	12/20
	LOX		14.7	5.6 Kg_f m	0.060 in	6/20
	LOX		14.7	3.5 Kg_f m	0.060 in	3/20
	LOX		14.7	2.8 Kg_f m	0.060 in	1/20
	LOX		14.7	1.4 Kg_f m	0.060 in	0/20
	LOX		14.7	10 Kg_f m	0.050 in	17/20
	LOX		14.7	7.7 Kg_f m	0.050 in	12/20
	LOX		14.7	5.6 Kg_f m	0.050 in	8/20
	LOX		14.7	3.5 Kg_f m	0.050 in	7/20
	LOX		14.7	1.4 Kg_f m	0.050 in	2/20
	LOX		14.7	10 Kg_f m	0.040 in	18/20
	LOX		14.7	7.7 Kg_f m	0.040 in	15/20
	LOX		14.7	5.6 Kg_f m	0.040 in	9/20
	LOX		14.7	3.5 Kg_f m	0.040 in	7/20
	LOX		14.7	1.4 Kg_f m	0.040 in	3/20
	LOX		14.7	10 Kg_f m	0.030 in	18/20
	LOX		14.7	7.7 Kg_f m	0.030 in	17/20
	LOX		14.7	5.6 Kg_f m	0.030 in	14/20
	LOX		14.7	3.5 Kg_f m	0.030 in	14/20
	LOX		14.7	1.4 Kg_f m	0.030 in	8/20
	LOX		14.7	10 Kg_f m	0.020 in	19/20
	LOX		14.7	7.7 Kg_f m	0.020 in	18/20
	LOX		14.7	5.6 Kg_f m	0.020 in	15/20
	LOX		14.7	3.5 Kg_f m	0.020 in	14/20
	LOX		14.7	1.4 Kg_f m	0.020 in	8/20
	LOX		14.7	10 Kg_f m	0.010 in	18/20
	LOX		14.7	7.7 Kg_f m	0.010 in	18/20
	LOX		14.7	5.6 Kg_f m	0.010 in	16/20
	LOX		14.7	3.5 Kg_f m	0.010 in	12/20
	LOX		14.7	1.4 Kg_f m	0.010 in	8/20
	LOX		14.7	0.7 Kg_f m	0.010 in	3/20
Polysulfide	LOX		14.7	10 Kg_f m	0.017 in	20/20
Plaskon (PTFCE)	LOX		14.7	10 Kg_f m	0.080 in	2/20
Polypropylene	LOX		14.7	10 Kg_f m	0.063 in	20/20
Polyphenylene Oxide	LOX		14.7	10 Kg_f m	0.065 in	20/20
Polyimide	LOX		14.7	10 Kg_f m	0.005 in	0/40
Rulon (Filled PTFE)	LOX		14.7	10 Kg_f m	0.063 in	0/20

Table 2c, LOX Compatibility Tested Via D2512 Mechanical Impact: NASA TM X-53773,cont.

Material	Oxygen Phase	Temp	Pressure Psi	Impact Energy	Specimen Thickness	Results Reactions / Impacts
Scotch Ply Tape 1002	LOX		14.7	10 Kg_f m	0.113 in	20/20
(Epoxy Resin w/non woven glass filament)	LOX		14.7	4 Kg_f m	0.113 in	20/20
Vespel SP-1 (Polyimide)	LOX		14.7	10 Kg_f m	0.050 in	6/20
	LOX		14.7	10 Kg_f m	0.050 in	1/60
	LOX		14.7	10 Kg_f m	0.050 in	4/20
	LOX		14.7	10 Kg_f m	0.050 in	0/20
	LOX		14.7	10 Kg_f m	0.050 in	3/20
Vespel SP-3 (Polyimide)	LOX		14.7	10 Kg_f m	0.050 in	0/20
Vespel SP21 (Polyimide	LOX		14.7	10 Kg_f m	0.050 in	0/20
W/15% graphite)	LOX		14.7	10 Kg_f m	0.050 in	0/20
	LOX		14.7	10 Kg_f m	0.050 in	0/20
	LOX		14.7	10 Kg_f m	0.050 in	0/20
Vespel SP-21 (Polyimide w/10% graphite)	LOX		14.7	10 Kg_f m	0.050 in	0/20
Vespel SP-21 (Polyimide w/5% graphite)	LOX		14.7	10 Kg_f m	0.050 in	0/20
Viton Molded Dics	LOX		14.7	10 Kg_f m	0.070 in	0/20
	LOX		14.7	10 Kg_f m	0.070 in	2/20
Viton Strips	LOX		14.7	10 Kg_f m	0.070 in	0/20
Viton Discs	LOX		14.7	10 Kg_f m	0.070 in	0/20
	LOX		14.7	10 Kg_f m	0.070 in	0/20
	LOX		14.7	10 Kg_f m	0.070 in	0/20
Viton A New	LOX		14.7	10 Kg_f m	0.070 in	2/20
Viton A Old	LOX		14.7	10 Kg_f m	0.070 in	5/20
Viton A	LOX		14.7	10 Kg_f m	0.070 in	5/20
Ceramic Filled Teflon	LOX		14.7	10 Kg_f m	0.025 in	4/20
PTFE-FEP Composite	LOX		14.7	10 Kg_f m	0.125 in	0/20
Rulon A	LOX		14.7	10 Kg_f m	0.063 in	0/20
Activated Charcoal	LOX		14.7	10 Kg_f m	0.050 in	30/40
	LOX		14.7	5.6 Kg_f m	0.050 in	11/20
	LOX		14.7	3.5 Kg_f m	0.050 in	2/20
	LOX		14.7	1.4 Kg_f m	0.050 in	4/20
	LOX		14.7	0.7 Kg_f m	0.050 in	1/20
	LOX		14.7	10 Kg_f m	0.050 in	12/20
	LOX		14.7	10 Kg_f m	0.050 in	12/20
	LOX		14.7	7.7 Kg_f m	0.050 in	10/20
	LOX		14.7	5.6 Kg_f m	0.050 in	10/20
	LOX		14.7	3.5 Kg_f m	0.050 in	13/20
	LOX		14.7	1.4 Kg_f m	0.050 in	9/20
	LOX		14.7	0.7 Kg_f m	0.050 in	3/20
	LOX		14.7	10 Kg_f m	0.050 in	4/20
	LOX		14.7	7.7 Kg_f m	0.050 in	2/20
	LOX		14.7	6.7 Kg_f m	0.050 in	1/20
	LOX		14.7	5.6 Kg_f m	0.050 in	0/20
Paper	LOX		14.7	10 Kg_f m	0.009 in	7/20

Table 2d, LOX Compatibility Tested Via D2512 Mechanical Impact: NASA TM X-64711

Material	Oxygen Phase	Temp	Pressure Psi	Impact Energy	Specimen Thickness	Results Reactions / Impacts
Teflon	LOX		14.7	10 Kg_f m	0.0035	0/40
Sintered Teflon	LOX		14.7	10 Kg_f m	0.004	0/20
“	LOX		14.7	10 Kg_f m	0.003	0/340

Table 2d, LOX Compatibility Tested Via D2512 Mechanical Impact: NASA TM X-64711,cont.

Material	Oxygen Phase	Temp	Pressure Psi	Impact Energy	Specimen Thickness	Results Reactions / Impacts
Teflon	LOX		14.7	10 Kg_f m	0.010	0/20
TFE Teflon	LOX		14.7	10 Kg_f m	0.003	0/20
Amide-imide copolymer on 0.008in Aluminum	LOX		14.7	10 Kg_f m	0.001	8/20
Amide-imide coploymer On 0.02 in Aluminum	LOX		14.7	10 Kg_f m	0.007	6/20
Amide–imide copolymer On Copper	LOX		14.7	10 Kg_f m	0.005	6/20
Phenolic resin, fiberglass	LOX		14.7	10 Kg_f m	0.313	2/2
honeycomb, epoxy	LOX		14.7	5 Kg_f m	0.313	11/11
fiberglass sealer, epoxy	LOX		14.7	2 Kg_f m	0.313	20/20
adhesive	LOX		14.7	1 Kg_f m	0.313	7/20
	LOX		14.7	½ Kg_f m	0.313	0/20
Isocyanate Foam	LOX		14.7	10 Kg_f m	0.100	3/20
	LOX		14.7	10 Kg_f m	0.500	10/20
	LOX		14.7	10 Kg_f m	0.250	4/20
	LOX		14.7	10 Kg_f m	0.250	2/20
	LOX		14.7	10 Kg_f m	0.500	7/20
Polyurethane	LOX		14.7	10 Kg_f m	0.250	3/40
	LOX		14.7	9 Kg_f m	0.250	2/40
	LOX		14.7	8 Kg_f m	0.250	2/20
	LOX		14.7	7 Kg_f m	0.250	0/20
	LOX		14.7	5 Kg_f m	0.250	0/20
Filled Polyurethane Fiberglass Braid	LOX		14.7	10 Kg_f m	0.075	0/20
EPI Resin 560 Applied to 0.012 in copper (Epoxy)	LOX		14.7	10 Kg_f m	0.005	9/20
EPI Resin 560 Applied to 0.008 in Al (Epoxy)	LOX		14.7	10 Kg_f m	0.001	9/20
Hexcell 91LD	LOX		14.7	10 Kg_f m	0.063	20/20
Honeycomb phenolic	LOX		14.7	5 Kg_f m	0.063	20/20
Epoxy	LOX		14.7	3 Kg_f m	0.063	20/20
	LOX		14.7	1 Kg_f m	0.063	15/20
Polyurethane	LOX		14.7	10 Kg_f m	0.250	20/20
	LOX		14.7	5 Kg_f m	0.250	19/20
	LOX		14.7	3 Kg_f m	0.250	8/20
	LOX		14.7	2 Kg_f m	0.250	0/20
Polyurethane foam	LOX		14.7	10 Kg_f m	0.050	34/40
Quartz spheres and	LOX		14.7	10 Kg_f m	0.125	15/20
Epoxy	LOX		14.7	7 Kg_f m	0.125	7/20
	LOX		14.7	5 Kg_f m	0.125	2/20
	LOX		14.7	3 Kg_f m	0.125	0/20
Silicone	LOX		14.7	10 Kg_f m	0.250	4/20
	LOX		14.7	5 Kg_f m	0.250	3/20
	LOX		14.7	3 Kg_f m	0.250	0/20
Phenylated Nylon	LOX		14.7	10 Kg_f m		11/20
	LOX		14.7	5 Kg_f m		8/10
	LOX		14.7	3 Kg_f m		4/10
Araldrite 6010	LOX		14.7	10 Kg_f m	0.050	3/3
And catalyst 125	LOX		14.7	5 Kg_f m	0.050	2/4
	LOX		14.7	2 Kg_f m	0.050	2/2
Armalon PDX 7700B (PTFE Bleached Felt)	LOX		14.7	10 Kg_f m	0.063	0/20

Table 2d, LOX Compatibility Tested Via D2512 Mechanical Impact: NASA TM X-64711,cont.

Material	Oxygen Phase	Temp	Pressure Psi	Impact Energy	Specimen Thickness	Results Reactions / Impacts
Fabric impregnated	LOX		14.7	10 Kg_f m		4/6
With butyl rubber	LOX		14.7	5 Kg_f m		2/20
100 gms CS 2727 Epoxy	LOX		14.7	10 Kg_f m	0.050	9/20
and 21 grms	LOX		14.7	8 Kg_f m	0.050	8/20
accelerated 9817	LOX		14.7	6 Kg_f m	0.050	6/20
	LOX		14.7	4 Kg_f m	0.050	6/20
Polyurethane	LOX		14.7	10 Kg_f m	0.063	2/7
Teflon Impreganted	LOX		14.7	10 Kg_f m		2/3
With silicone rubber						
Fluorinated Silicone	LOX		14.7	10 Kg_f m	0.100	15/20
	LOX		14.7	8 Kg_f m	0.100	10/20
	LOX		14.7	6 Kg_f m	0.100	11/20
	LOX		14.7	4 Kg_f m	0.100	3/20
	LOX		14.7	2 Kg_f m	0.100	0/20
Polyvinyl fluoride	LOX		14.7	10 Kg_f m	0.005	9/20
On steel discs						
Silicone	LOX		14.7	10 Kg_f m	0.050	3/3
	LOX		14.7	5 Kg_f m	0.050	2/11
	LOX		14.7	4 Kg_f m	0.050	1/13
	LOX		14.7	3 Kg_f m	0.050	1/2
	LOX		14.7	2 Kg_f m	0.050	0/21
DC 94-017	LOX		14.7	10 Kg_f m	0.050	2/20
(Fluorosilicone)	LOX		14.7	10 Kg_f m	0.075	0/20
	LOX		14.7	10 Kg_f m	0.106	4/20
DC 94-018	LOX		14.7	10 Kg_f m	0.050	5/20
(Fluorosilicone)	LOX		14.7	10 Kg_f m	0.084	4/20
	LOX		14.7	10 Kg_f m	0.100	4/20
DC 94-019	LOX		14.7	10 Kg_f m	0.060	3/20
(Fluorosilicone)	LOX		14.7	10 Kg_f m	0.090	0/20
	LOX		14.7	10 Kg_f m	0.224	1/60
Silicone	LOX		14.7	10 Kg_f m	0.050	16/20
Air dried 72 hrs	LOX		14.7	8 Kg_f m	0.050	10/20
	LOX		14.7	6 Kg_f m	0.050	9/20
	LOX		14.7	4 Kg_f m	0.050	8/20
	LOX		14.7	2 Kg_f m	0.050	4./20
Epoxy and Polysulfide	LOX		14.7	10 Kg_f m	0.050	10/20
LP/32 activator	LOX		14.7	5 Kg_f m	0.050	14/20
	LOX		14.7	1 Kg_f m	0.050	10/20
Ecco Bond No. 45 and	LOX		14.7	10 Kg_f m	0.050	2/2
Cat. No. 15	LOX		14.7	5 Kg_f m	0.050	2/2
(Epoxy Cement)	LOX		14.7	2 Kg_f m	0.050	2/2
Polyphenyl	LOX		14.7	10 Kg_f m	0.280	6/20
Epibond 123 and	LOX		14.7	10 Kg_f m	0.050	5/20
Hardener 952A (Epoxy)						
Epoxy Glass	LOX		14.7	10 Kg_f m		2/3
Terminal Board	LOX		14.7	5 Kg_f m		1/1
Epoxy potting Compound	LOX		14.7	10 Kg_f m	0.063	1/1
	LOX		14.7	5 Kg_f m	0.063	1/1
	LOX		14.7	2 Kg_f m	0.063	1/1
Parapolyphenyl	LOX		14.7	10 Kg_f m	0.2	6/20
Fiberglass Epoxy Pipe	LOX		14.7	10 Kg_f m	0.22	20/20
Fiberglass with A	LOX		14.7	10 Kg_f m	0.012	20/20
Fluorosilicone coating						

Table 2d, LOX Compatibility Tested Via D2512 Mechanical Impact: NASA TM X-64711,cont.

Material	Oxygen Phase	Temp	Pressure Psi	Impact Energy	Specimen Thickness	Results Reactions / Impacts
EPON 901 and 11parts	LOX		14.7	10 Kg_f m	0.050	27/40
B-3 ½ hr 240 F 1.5 hr	LOX		14.7	8 Kg_f m	0.050	10/40
350 F	LOX		14.7	6 Kg_f m	0.050	4/20
	LOX		14.7	4 Kg_f m	0.050	5/20
	LOX		14.7	2 Kg_f m	0.050	2/20
	LOX		14.7	1 Kg_f m	0.050	0/20
Teflon with 0.05%	LOX		14.7	10 Kg_f m	0.050	0/20
Carbon black						
Teflon and ground glass	LOX		14.7	10 Kg_f m		0/20
Fluorosilicone	LOX		14.7	10 Kg_f m	0.070	7/20
FM 1000 adhesive	LOX		14.7	10 Kg_f m	0.010	17/20
(Nylon Epoxy)	LOX		14.7	5 Kg_f m	0.010	11/20
	LOX		14.7	2 Kg_f m	0.010	9/20
Teflon	LOX		14.7	10 Kg_f m	0.010	1/60
HT-424	LOX		14.7	10 Kg_f m	0.013	20/20
(Epoxy Phenolic)	LOX		14.7	5 Kg_f m	0.013	20/20
	LOX		14.7	3 Kg_f m	0.013	20/20
	LOX		14.7	1 Kg_f m	0.013	6/20
Hysol Cement 6020	LOX		14.7	10 Kg_f m	0.050	2/3
(Epoxy)	LOX		14.7	5 Kg_f m	0.050	2/2
	LOX		14.7	2 Kg_f m	0.050	2/4
Kel –F Plasticized	LOX		14.7	10 Kg_f m	0.032	0/20
(PtFClethylene)						
Kel –F Unplasticized	LOX		14.7	10 Kg_f m	0.032	0/20
(PtFClethylene)						
Kel –F Unplasticized	LOX		14.7	10 Kg_f m	0.075	0/20
(PtFClethylene)						
Kel-F (Sheet)	LOX		14.7	10 Kg_f m	0.63	0/20
Kel-F L-1380	LOX		14.7	10 Kg_f m	0.005	0/20
Kel-F L-1381	LOX		14.7	10 Kg_f m	0.005	0/20
Kel-F Film type 8105	LOX		14.7	10 Kg_f m	0.005	0/20
Kel-F Film type KX202	LOX		14.7	10 Kg_f m	0.002	0/20
Kel-F Film type KX8110	LOX		14.7	10 Kg_f m	0.010	0/20
Kel-F Film type 8210	LOX		14.7	10 Kg_f m	0.010	0/20
Kel-F Film type 8205	LOX		14.7	10 Kg_f m	0.005	0/20
Kel-F81Plastic	LOX		14.7	10 Kg_f m	0.063	0/20
Kel-F800 Plastic	LOX		14.7	10 Kg_f m	0.063	0/20
Kel-F800 Plastic	LOX		14.7	10 Kg_f m	0.063	0/20
Kel-F Dispersion 625	LOX		14.7	10 Kg_f m	0.005	0/20
Kel-F Dispersion KX633	LOX		14.7	10 Kg_f m	0.003	0/20
Kel-F Elastomer	LOX		14.7	10 Kg_f m	0.125	0/20
Kel-F Elastomer	LOX		14.7	10 Kg_f m	0.063	0/20
Vinyl Rubber	LOX		14.7	10 Kg_f m	0.125	2/20
Kynar	LOX		14.7	10 Kg_f m	0.063	0/10
(PolyVinylidene Fluoride)						
Kynar	LOX		14.7	10 Kg_f m	0.016	5/20
Kynar	LOX		14.7	8 Kg_f m	0.016	2/20
Kynar	LOX		14.7	10 Kg_f m	0.016	5/20
Kynar	LOX		14.7	8 Kg_f m	0.016	2/20
Kynar	LOX		14.7	6 Kg_f m	0.016	2/20
Kynar	LOX		14.7	11.3 Kg_f m	0.032	4/20
Kynar	LOX		14.7	10 Kg_f m	0.032	11/40
Kynar	LOX		14.7	10 Kg_f m	0.063	2/20

Table 2d, LOX Compatibility Tested Via D2512 Mechanical Impact: NASA TM X-64711,cont.

Material	Oxygen Phase	Temp	Pressure Psi	Impact Energy		Specimen Thickness	Results Reactions / Impacts
Kynar	LOX		14.7	10	Kg_f m	0.025	2/20
Kynar	LOX		14.7	8	Kg_f m	0.025	1/20
Kynar	LOX		14.7	6	Kg_f m	0.025	1/20
Kynar	LOX		14.7	10	Kg_f m	0.063	1/60
Kynar	LOX		14.7	10	Kg_f m	0.025	21/40
Kynar	LOX		14.7	10	Kg_f m	0.025	18/20
Kynar	LOX		14.7	10	Kg_f m	0.002	20/20
Kynar	LOX		14.7	10	Kg_f m	0.002	20/20
PTFE fabric impregnated	LOX		14.7	10	Kg_f m	0.015	4/20
With Kynar	LOX		14.7	8	Kg_f m	0.015	3/20
	LOX		14.7	6	Kg_f m	0.015	3/20
	LOX		14.7	4	Kg_f m	0.015	3/20
	LOX		14.7	2	Kg_f m	0.015	0/20
PTFE fabric impregnated With Kynar	LOX		14.7	10	Kg_f m	0.015	0/20
PTFE fabric impregnated With Kynar	LOX		14.7	10	Kg_f m	0.015	1/20
PTFE fabric impregnated With Kynar	LOX		14.7	10	Kg_f m	0.015	0/20
LS-53	LOX		14.7	10	Kg_f m	0.070	4/20
(Fluorosilicone	LOX		14.7	8	Kg_f m	0.070	6/20
Elastomer)	LOX		14.7	6	Kg_f m	0.070	3/20
	LOX		14.7	4	Kg_f m	0.070	8/20
LS-53	LOX		14.7	10	Kg_f m	0.035	11/20
(Fluorosilicone	LOX		14.7	8	Kg_f m	0.035	10/20
Elastomer)	LOX		14.7	6	Kg_f m	0.035	6/20
	LOX		14.7	4	Kg_f m	0.035	4/20
	LOX		14.7	2	Kg_f m	0.035	5/20
	LOX		14.7	1	Kg_f m	0.035	0/20
LS-53	LOX		14.7	10	Kg_f m	0.016	16/20
(Fluorosilicone	LOX		14.7	8	Kg_f m	0.016	13/20
Elastomer)	LOX		14.7	6	Kg_f m	0.016	9/20
	LOX		14.7	4	Kg_f m	0.016	10/20
	LOX		14.7	2	Kg_f m	0.016	6/20
	LOX		14.7	1	Kg_f m	0.016	2/20
LS-70	LOX		14.7	10	Kg_f m	0.070	2/20
(Fluorosilicone	LOX		14.7	8	Kg_f m	0.070	8/20
Elastomer)	LOX		14.7	6	Kg_f m	0.070	4/20
	LOX		14.7	4	Kg_f m	0.070	0/20
LS-53	LOX		14.7	10	Kg_f m	0.035	4/20
(Fluorosilicone	LOX		14.7	8	Kg_f m	0.035	6/20
Elastomer)	LOX		14.7	6	Kg_f m	0.035	3/20
	LOX		14.7	4	Kg_f m	0.035	8/20
	LOX		14.7	2	Kg_f m	0.035	7/20
	LOX		14.7	1	Kg_f m	0.035	7/20
LS-53	LOX		14.7	10	Kg_f m	0.016	16/20
(Fluorosilicone	LOX		14.7	8	Kg_f m	0.016	15/20
Elastomer)	LOX		14.7	6	Kg_f m	0.016	8/20
	LOX		14.7	4	Kg_f m	0.016	11/20
	LOX		14.7	2	Kg_f m	0.016	4/20
Polycarbonate	LOX		14.7	10	Kg_f m	0.063	20/20
	LOX		14.7	5	Kg_f m	0.063	16/20

Table 2d, LOX Compatibility Tested Via D2512 Mechanical Impact: NASA TM X-64711,cont.

Material	Oxygen Phase	Temp	Pressure Psi	Impact Energy		Specimen Thickness	Results Reactions / Impacts
Polyimide from pyrolytic anhydride	LOX		14.7	10	Kg_f m	0.005	3/20
Phenolic Laminate,	LOX		14.7	10	Kg_f m	0.063	31/40
Fabric base	LOX		14.7	8	Kg_f m	0.063	16/20
	LOX		14.7	6	Kg_f m	0.063	7/20
	LOX		14.7	5	Kg_f m	0.063	16/20
	LOX		14.7	4	Kg_f m	0.063	4/20
	LOX		14.7	2	Kg_f m	0.063	6/20
	LOX		14.7	1	Kg_f m	0.063	0/20
Polyester	LOX		14.7	10	Kg_f m		17/20
Mylar A (Polyester)	LOX		14.7	10	Kg_f m	0.005	2/120
Mylar D (Polyester)	LOX		14.7	10	Kg_f m	0.003	2/20
	LOX		14.7	8	Kg_f m	0.003	1/20
Mylar Film	LOX		14.7	10	Kg_f m	0.001	4/20
Chlorinated Polyester	LOX		14.7	10	Kg_f m	0.050	7/10
Cured with 2% MEK	LOX		14.7	5	Kg_f m	0.050	4/10
Peroxide and cobalt	LOX		14.7	3	Kg_f m	0.050	2/20
Naphtenate	LOX		14.7	2	Kg_f m	0.050	0/20
Chlorinated Polyester	LOX		14.7	10	Kg_f m	0.050	9/10
Cured with 2% MEK	LOX		14.7	5	Kg_f m	0.050	2/5
Peroxide and cobalt	LOX		14.7	3	Kg_f m	0.050	1/10
Naphtenate and with	LOX		14.7	2	Kg_f m	0.050	2/10
33.3% Antimony Trichloride	LOX		14.7	1	Kg_f m	0.050	0/20
ERL 0625 epoxy cured	LOX		14.7	10	Kg_f m	0.050	7/10
With 10.6 Phr mPDA	LOX		14.7	5	Kg_f m	0.050	2/10
	LOX		14.7	3	Kg_f m	0.050	0/20
ERL 0625 epoxy cured	LOX		14.7	10	Kg_f m	0.050	6/10
With 14.5 Phr chlorendic	LOX		14.7	5	Kg_f m	0.050	6/20
Anhydride and 0.5%	LOX		14.7	3	Kg_f m	0.050	2/10
Benzyldimethylamine	LOX		14.7	2	Kg_f m	0.050	1/10
	LOX		14.7	1	Kg_f m	0.050	0/20
Adhesive 50% Epoxy	LOX		14.7	10	Kg_f m	0.050	3/3
And 50% polyamide	LOX		14.7	5	Kg_f m	0.050	2/2
	LOX		14.7	2	Kg_f m	0.050	2/7
	LOX		14.7	1	Kg_f m	0.050	0/12
Adhesive 50% Epoxy	LOX		14.7	10	Kg_f m	0.050	16/24
And 50% polyamide	LOX		14.7	5	Kg_f m	0.050	2/8
	LOX		14.7	3	Kg_f m	0.050	2/14
	LOX		14.7	1	Kg_f m	0.050	0/20
Nylon (Polyamide)	LOX		14.7	10	Kg_f m	0.032	2/2
	LOX		14.7	5	Kg_f m	0.032	2/2
	LOX		14.7	2	Kg_f m	0.032	2/2
	LOX		14.7	1	Kg_f m	0.032	2/12
Nylon (Polyamide)	LOX		14.7	10	Kg_f m	0.250	8/20
	LOX		14.7	5	Kg_f m	0.250	1/1
	LOX		14.7	3	Kg_f m	0.250	1/2
	LOX		14.7	1	Kg_f m	0.250	0/20
Nylon (Polyamide)	LOX		14.7	10	Kg_f m	0.001	13/20
Nylon (Polyamide)	LOX		14.7	10	Kg_f m	0.001	10/20
Nylon (Polyamide)	LOX		14.7	10	Kg_f m	0.002	3/20
Nylon (Polyamide)	LOX		14.7	10	Kg_f m	0.004	8/20
Viton A	LOX		14.7	10	Kg_f m	0.063	0/20

Table 2d, LOX Compatibility Tested Via D2512 Mechanical Impact: NASA TM X-64711,cont.

Material	Oxygen Phase	Temp	Pressure Psi	Impact Energy	Specimen Thickness	Results Reactions / Impacts
Plaskon 2200 CTFE Caps	LOX		14.7	10 Kg_f m	0.080	2/20
Polyphenylene Oxide	LOX		14.7	10 Kg_f m	0.065	20/20
Polysulfide	LOX		14.7	10 Kg_f m	0.017	20/20
Epoxy Potting Compound	LOX		14.7	10 Kg_f m	0.063	1/1
	LOX		14.7	5 Kg_f m	0.063	1/1
	LOX		14.7	2 Kg_f m	0.063	1/1
	LOX		14.7	1 Kg_f m	0.063	1/2
Polyethylene	LOX		14.7	10 Kg_f m	0.032	4/7
	LOX		14.7	5 Kg_f m	0.032	2/19
	LOX		14.7	2 Kg_f m	0.032	1/3
	LOX		14.7	1 Kg_f m	0.032	0/17
Polyethylene Tubing	LOX		14.7	10 Kg_f m		2/11
	LOX		14.7	5 Kg_f m		2/10
	LOX		14.7	2 Kg_f m		2/20
Polyethylene	LOX		14.7	11.3 Kg_f m	0.137	3/20
	LOX		14.7	10 Kg_f m	0.137	1/20
	LOX		14.7	8 Kg_f m	0.137	1/20
	LOX		14.7	6 Kg_f m	0.137	0/20
	LOX		14.7	10 Kg_f m	0.020	15/20
	LOX		14.7	8 Kg_f m	0.020	16/20
	LOX		14.7	6 Kg_f m	0.020	13/20
	LOX		14.7	4 Kg_f m	0.020	11/20
	LOX		14.7	2 Kg_f m	0.020	7/20
	LOX		14.7	1 Kg_f m	0.020	3/20
	LOX		14.7	11.3 Kg_f m	0.075	4/20
	LOX		14.7	10 Kg_f m	0.075	7/20
	LOX		14.7	8 Kg_f m	0.075	3/20
	LOX		14.7	6 Kg_f m	0.075	6/20
	LOX		14.7	4 Kg_f m	0.075	0/20
High Density PE	LOX		14.7	10 Kg_f m	0.063-0.075	7/20
	LOX		14.7	8 Kg_f m	0.063-0.075	2/20
	LOX		14.7	6 Kg_f m	0.063-0.075	1/20
	LOX		14.7	4 Kg_f m	0.063-0.075	2/20
	LOX		14.7	2 Kg_f m	0.063-0.075	1/20
	LOX		14.7	1 Kg_f m	0.063-0.075	0/20
Polyethylene Film	LOX		14.7	10 Kg_f m	0.006	88/100
	LOX		14.7	8 Kg_f m	0.006	50/100
	LOX		14.7	6 Kg_f m	0.006	42/100
	LOX		14.7	4 Kg_f m	0.006	30/100
	LOX		14.7	2 Kg_f m	0.006	9/100
	LOX		14.7	1 Kg_f m	0.006	0/100
Polyvinylchloride	LOX		14.7	10 Kg_f m	0.125	2/2
	LOX		14.7	5 Kg_f m	0.125	2/9
	LOX		14.7	2 Kg_f m	0.125	2/14
	LOX		14.7	1 Kg_f m	0.125	0/20
	LOX		14.7	10 Kg_f m	0.063	2/3
	LOX		14.7	5 Kg_f m	0.063	2/3
	LOX		14.7	2 Kg_f m	0.063	2/11
	LOX		14.7	3 Kg_f m	0.063	1/3

Table 2d, LOX Compatibility Tested Via D2512 Mechanical Impact: NASA TM X-64711,cont.

Material	Oxygen Phase	Temp	Pressure Psi	Impact Energy	Specimen Thickness	Results Reactions / Impacts
Polypropylene	LOX		14.7	10 Kg_f m	0.080	15/20
	LOX		14.7	7.7 Kg_f m	0.080	12/20
	LOX		14.7	5.6 Kg_f m	0.080	4/20
	LOX		14.7	4.9 Kg_f m	0.080	2/20
	LOX		14.7	4.2 Kg_f m	0.080	0/20
	LOX		14.7	3.5 Kg_f m	0.080	0/20
	LOX		14.7	10 Kg_f m	0.060	17/20
	LOX		14.7	7.7 Kg_f m	0.060	12/20
	LOX		14.7	5.6 Kg_f m	0.060	6/20
	LOX		14.7	3.5 Kg_f m	0.060	3/20
	LOX		14.7	2.8 Kg_f m	0.060	1/20
	LOX		14.7	1.4 Kg_f m	0.060	0/20
	LOX		14.7	10 Kg_f m	0.050	17/20
	LOX		14.7	7.7 Kg_f m	0.050	12/20
	LOX		14.7	5.6 Kg_f m	0.050	8/20
	LOX		14.7	3.5 Kg_f m	0.050	7/20
	LOX		14.7	1.4 Kg_f m	0.050	2/20
	LOX		14.7	10 Kg_f m	0.040	18/20
	LOX		14.7	7.7 Kg_f m	0.040	15/20
	LOX		14.7	5.6 Kg_f m	0.040	9/20
	LOX		14.7	3.5 Kg_f m	0.040	7/20
	LOX		14.7	1.4 Kg_f m	0.040	3/20
	LOX		14.7	10 Kg_f m	0.030	18/20
	LOX		14.7	7.7 Kg_f m	0.030	17/20
	LOX		14.7	5.6 Kg_f m	0.030	14/20
	LOX		14.7	3.5 Kg_f m	0.030	14/20
	LOX		14.7	1.4 Kg_f m	0.030	8/20
	LOX		14.7	10 Kg_f m	0.020	19/20
	LOX		14.7	7.7 Kg_f m	0.020	18/20
	LOX		14.7	5.6 Kg_f m	0.020	15/20
	LOX		14.7	3.5 Kg_f m	0.020	14/20
	LOX		14.7	1.4 Kg_f m	0.020	8/20
	LOX		14.7	10 Kg_f m	0.010	18/20
	LOX		14.7	7.7 Kg_f m	0.010	18/20
	LOX		14.7	5.6 Kg_f m	0.010	16/20
	LOX		14.7	3.5 Kg_f m	0.010	12/20
	LOX		14.7	1.4 Kg_f m	0.010	8/20
	LOX		14.7	0.7 Kg_f m	0.010	3/20
PROSEAL 994	LOX		14.7	10 Kg_f m	0.050	8/20
(Polyurethane)	LOX		14.7	10 Kg_f m	0.063	7/20
	LOX		14.7	5 Kg_f m	0.063	6/20
	LOX		14.7	2 Kg_f m	0.063	2/20
	LOX		14.7	1 Kg_f m	0.063	0/20
PR-1525	LOX		14.7	10 Kg_f m	0.063	3/20
(Polyurethane)	LOX		14.7	5 Kg_f m	0.063	0/20
	LOX		14.7	10 Kg_f m	0.125	2/20
PR-1527	LOX		14.7	10 Kg_f m	0.063	7/20
(Polyurethane)	LOX		14.7	5 Kg_f m	0.063	3/20
	LOX		14.7	10 Kg_f m	0.032	11/20
PR-1538 (Polyurethane)	LOX		14.7	10 Kg_f m	0.063	10/20
PR-1910	LOX		14.7	10 Kg_f m	0.050	2/2
(Silicone)	LOX		14.7	5 Kg_f m	0.050	2/2
	LOX		14.7	2 Kg_f m	0.050	0/16

Table 2d, LOX Compatibility Tested Via D2512 Mechanical Impact: NASA TM X-64711,cont.

Material	Oxygen Phase	Temp	Pressure Psi	Impact Energy		Specimen Thickness	Results Reactions / Impacts
Phenolic Impregnated	LOX		14.7	10	Kg_f m	0.060	2/2
Fiberglass	LOX		14.7	5	Kg_f m	0.060	2/2
	LOX		14.7	3	Kg_f m	0.060	2/3
Polyimide	LOX		14.7	10	Kg_f m	0.005	0/40
Q90-002A/B	LOX		14.7	10	Kg_f m	0.050	2/7
(Fluorosilicone)	LOX		14.7	5	Kg_f m	0.050	2/20
	LOX		14.7	4	Kg_f m	0.050	0/20
Q90-031	LOX		14.7	10	Kg_f m	0.050	2/5
(Fluorosilicone)	LOX		14.7	5	Kg_f m	0.050	2/6
	LOX		14.7	4	Kg_f m	0.050	0/18
	LOX		14.7	3	Kg_f m	0.050	0/20
Q94-002	LOX		14.7	10	Kg_f m	0.050	2/20
(Fluorosilicone)	LOX		14.7	11.3	Kg_f m	0.013	1/20
	LOX		14.7	10	Kg_f m	0.013	0/20
	LOX		14.7	10	Kg_f m	0.058	3/20
	LOX		14.7	8	Kg_f m	0.058	3/20
	LOX		14.7	10	Kg_f m	0.032	12/20
	LOX		14.7	8	Kg_f m	0.032	12/20
	LOX		14.7	10	Kg_f m	0.020	13/20
	LOX		14.7	8	Kg_f m	0.020	15/20
	LOX		14.7	10	Kg_f m	0.050	3/20
	LOX		14.7	10	Kg_f m	0.050	2/20
	LOX		14.7	10	Kg_f m	0.050	4/20
	LOX		14.7	10	Kg_f m	0.050	11/20
	LOX		14.7	10	Kg_f m	0.085	10/20
	LOX		14.7	10	Kg_f m	0.105	5/20
Relco A50% + B 50% (Epoxy)	LOX		14.7	10	Kg_f m	0.063	2/20
(Epoxy and Grit)	LOX		14.7	10	Kg_f m	0.063	3/5
	LOX		14.7	5	Kg_f m	0.063	2/5
	LOX		14.7	3	Kg_f m	0.063	2/3
	LOX		14.7	2	Kg_f m	0.063	1/8
Scotch Ply Type 1002	LOX		14.7	10	Kg_f m	0.113	20/20
(Epoxy with non woven glass filament)	LOX		14.7	10	Kg_f m	0.113	20/20
Scotch Resin	LOX		14.7	10	Kg_f m		3/6
No CRP-235 (Epoxy 30C ½ hr)	LOX		14.7	5	Kg_f m		1/14
Silastic No. 50 Rubber	LOX		14.7	10	Kg_f m		2/2
(Silicone Rubber)	LOX		14.7	5	Kg_f m		2/6
	LOX		14.7	2	Kg_f m		2/4
Silastic No. 675	LOX		14.7	10	Kg_f m		2/3
(Silicone Rubber)	LOX		14.7	5	Kg_f m		2/2
	LOX		14.7	2	Kg_f m		1/1
Silastic No50-24-480 (Silicone Rubber)	LOX		14.7	10	Kg_f m		8/10
Silastic No 80-24-480 (Silicone Rubber)	LOX		14.7	10	Kg_f m		7/10
Silastic No 290-24-480	LOX		14.7	10	Kg_f m		2/10
(Silicone Rubber)	LOX		14.7	5	Kg_f m		1/10
Silastic No 916-4-480	LOX		14.7	10	Kg_f m		2/2
(Silicone Rubber)	LOX		14.7	5	Kg_f m		3/15

Table 2d, LOX Compatibility Tested Via D2512 Mechanical Impact: NASA TM X-64711,cont.

Material	Oxygen Phase	Temp	Pressure Psi	Impact Energy		Specimen Thickness	Results Reactions / Impacts
Silastic LS-53	LOX		14.7	10	Kg_f m		2/7
(Silicone Rubber)	LOX		14.7	5	Kg_f m		2/8
	LOX		14.7	2	Kg_f m		0/5
Silastic LS-53-24-300	LOX		14.7	10	Kg_f m		2/3
(Silicone Rubber)	LOX		14.7	5	Kg_f m		2/5
Silastic LS-13-8-400	LOX		14.7	10	Kg_f m		2/8
(Silicone Rubber)	LOX		14.7	5	Kg_f m		3/10
	LOX		14.7	2	Kg_f m		0/2
Stycast 2651	LOX		14.7	10	Kg_f m	0.063	2/2
(Epoxy)	LOX		14.7	5	Kg_f m	0.063	2/2
	LOX		14.7	3	Kg_f m	0.063	2/3
	LOX		14.7	1	Kg_f m	0.063	0/20
PTFE	LOX		14.7	10	Kg_f m	0.002	0/20
	LOX		14.7	10	Kg_f m	0.006	0/20
Tedlar 200 AM 30 WH	LOX		14.7	10	Kg_f m	0.002	4/29
(Polyvinylfluoride)	LOX		14.7	9	Kg_f m	0.002	1/20
	LOX		14.7	8	Kg_f m	0.002	0/20
	LOX		14.7	5	Kg_f m	0.002	0/13
Tedlar 200BG 30 WH	LOX		14.7	10	Kg_f m	0.002	4/25
(Polyvinylfluoride)	LOX		14.7	8	Kg_f m	0.002	1/20
	LOX		14.7	7	Kg_f m	0.002	0/20
	LOX		14.7	5	Kg_f m	0.002	1/35
Tedlar 200BP	LOX		14.7	10	Kg_f m	0.002	3/60
(Polyvinylfluoride)							
Tedlar 2005 50 WH	LOX		14.7	10	Kg_f m	0.002	3/20
(Polyvinylfluoride)							
Tedlar 2005 40	LOX		14.7	10	Kg_f m	0.002	5/20
(Polyvinylfluoride)							
Teflon Sheet	LOX		14.7	10	Kg_f m	0.002	0/20
Teflon Sleeve Adel Clamp	LOX		14.7	10	Kg_f m	0.032	0/20
Fluorinated ethylene	LOX		14.7	10	Kg_f m	0.015	0/20
Propylene polymer (Teflon FEP)							
Teflon TFE	LOX		14.7	10	Kg_f m	0.032	0/20
Teflon White Sheet Stock	LOX		14.7	10	Kg_f m	0.063	0/40
Teflon tube	LOX		14.7	10	Kg_f m	0.016	0/20
Teflon FEP Type 544	LOX		14.7	10	Kg_f m	0.001	0/20
Teflon FEP	LOX		14.7	10	Kg_f m	0.010	0/20
“	LOX		14.7	10	Kg_f m	0.021	0/20
“	LOX		14.7	10	Kg_f m	0.005	0/20
Teflon 856-200 (PTFE)	LOX		14.7	10	Kg_f m	0.006	0/20
Teflon DuPont Enamel	LOX		14.7	10	Kg_f m	0.001	0/20
852-202 (PTFE)							
Teflon Covering	LOX		14.7	10	Kg_f m	0.020	0/20
from cable (PTFE)							
Teflon O-Ring (PTFE)	LOX		14.7	10	Kg_f m		0/20
Vespel SP-1	LOX		14.7	10	Kg_f m	0.050	6/20
(Polyimide)	LOX		14.7	10	Kg_f m	0.050	1/60
	LOX		14.7	10	Kg_f m	0.050	4/20
	LOX		14.7	10	Kg_f m	0.050	0/20
	LOX		14.7	10	Kg_f m	0.050	3/20
Vespel SP-3 (Polyimide)	LOX		14.7	10	Kg_f m	0.050	0/20

Table 2d, LOX Compatibility Tested Via D2512 Mechanical Impact: NASA TM X-64711,cont.

Material	Oxygen Phase	Temp	Pressure Psi	Impact Energy	Specimen Thickness	Results Reactions / Impacts
Vespel SP-21(Polyimide	LOX		14.7	10 Kg_f m	0.050	0/20
And 15% graphite)	LOX		14.7	10 Kg_f m	0.050	0/20
	LOX		14.7	10 Kg_f m	0.050	0/20
	LOX		14.7	10 Kg_f m	0.050	0/20
	LOX		14.7	10 Kg_f m	0.050	0/20
Epoxy	LOX		14.7	10 Kg_f m	0.063	2/25
	LOX		14.7	5 Kg_f m	0.063	0/35
Viton A Hose	LOX		14.7	10 Kg_f m	0.063	3/20
Viton Sponge	LOX		14.7	10 Kg_f m	0.250	9/20
Viton A	LOX		14.7	10 Kg_f m	0.125	0/20
	LOX		14.7	10 Kg_f m	0.065	0/20
Viton	LOX		14.7	10 Kg_f m	0.047	2/20
Viton A	LOX		14.7	10 Kg_f m	0.144	0/20
Viton Strips	LOX		14.7	10 Kg_f m	0.070	0/20
Viton Discs	LOX		14.7	10 Kg_f m	0.070	0/20
Viton Sheet Mat Discs	LOX		14.7	10 Kg_f m	0.070	0/20
Viton Sheet Mat Strip	LOX		14.7	10 Kg_f m	0.070	0/20
Viton A Discs	LOX		14.7	10 Kg_f m	0.070	2/20
Viton A Discs	LOX		14.7	10 Kg_f m	0.070	5/20
Viton A Discs	LOX		14.7	10 Kg_f m	0.070	5/20
Viton A Elastomer	LOX		14.7	10 Kg_f m		4/20
(Copolymer vinylidene fluoride and hexafluoropropylene)						
Fluorosilicone Rubber	LOX		14.7	10 Kg_f m	0.125	2/20
	LOX		14.7	10 Kg_f m	0.100	0/20
	LOX		14.7	10 Kg_f m	0.033	19/20
	LOX		14.7	10 Kg_f m	0.035	19/20
	LOX		14.7	10 Kg_f m	0.070	2/20
	LOX		14.7	8 Kg_f m	0.070	2/20
	LOX		14.7	10 Kg_f m	0.125	2/40
	LOX		14.7	10 Kg_f m	0.064	1/20
	LOX		14.7	8 Kg_f m	0.064	1/20
	LOX		14.7	10 Kg_f m	0.030	20/20
	LOX		14.7	10 Kg_f m	0.125-0.130	2/20
XR5038 (Epoxy)	LOX		14.7	10 Kg_f m	0.003	2/25

Table 2e, LOX Compatibility Tested Via D2512 Mechanical Impact: NASA, MSC-02681 (1972) In (NASA CR 120221 1974)

Material	Oxygen Phase	Temp	Pressure Psi	Impact Energy	Specimen Thickness	Results Reactions / Impacts
Krytox 280-AB	LOX		100	10 Kg_f m	0.030 in	0/20
	LOX		500	10 Kg_f m	0.030 in	0/20
	LOX		1000	10 Kg_f m	0.030 in	0/20
Austin 1972	LOX		1500	10 Kg_f m	0.030 in	0/20
E-617-9	LOX		14.7	50 Ft-Lb/sqin	0.075in	0/4
(PolyEthylenePropylene)	LOX		14.7	200 Ft-Lb/sqin	0.075in	0/4
EpiBond 123/ Hardner 931	LOX		14.7	50 Ft-Lb/sqin	0.005 in	0/8
Kynar	LOX		14.7	50 Ft-Lb/sqin		0/4
(PolyvinylideneFluoride)	LOX		14.7	200 Ft-Lb/sqin		0/4
LS-53	LOX		14.7	50 Ft-Lb/sqin		0/4
(Fluorosilicone Rubber	LOX		14.7	200 Ft-Lb/sqin		0/4
TFE and PTFE Filled)						

Table 2e, LOX Compatibility Tested Via D2512 Mechanical Impact: NASA, MSC-02681 (1972) In (NASA CR 120221 1974), cont.

Material	Oxygen Phase	Temp	Pressure Psi	Impact Energy	Specimen Thickness	Results Reactions / Impacts
Polyisoprene	LOX		14.7	50 Ft-Lb/sqin		0/4
Silastic 601 RTV	LOX		14.7	200 Ft-Lb/sqin		0/4
(2 Part Silicone Rubber)	LOX		14.7	50 Ft-Lb/sqin		0/4
Silicone S-355-7	LOX		14.7	50 Ft-Lb/sqin		0/4
(1 Part Silicone Rubber)	LOX		14.7	200 Ft-Lb/sqin		0/4
Teflon Glass Filled	LOX		14.7	50 Ft-Lb/sqin		0/4
(PTFE)	LOX		14.7	200 Ft-Lb/sqin		0/4
Epoxy	LOX		15	1.1 Kg_f m	0.050 in	20/20
Epoxy Fiberglass	LOX		15	1.1 Kg_f m	0.050 in	20/20
	LOX		15	0.76 Kg_f m	0.050 in	20/20
	LOX		15	0.48 Kg_f m	0.050 in	20/20
	LOX		15	0.19 Kg_f m	0.050 in	4/20
	LOX		15	0.094 Kg_f m	0.050 in	2/20
	LOX		15	10 Kg_f m	0.050 in	20/20
	LOX		15	7.62 Kg_f m	0.050 in	20/20
	LOX		15	5.54 Kg_f m	0.050 in	20/20
	LOX		15	3.46 Kg_f m	0.050 in	20/20
	LOX		15	1.38 Kg_f m	0.050 in	4/20
	LOX		15	0.68 Kg_f m	0.050 in	2/20

Table 2f, LOX Compatibility Tested Via D2512 Mechanical Impact: MSFC HDBK 527 Rev F JSC 09604 Rev F, Sep 1988

Material	Oxygen Phase	Temp	Pressure Psi	Impact Energy	Specimen Thickness	Results Reactions / Impacts
Adhesive EPON 828/	LOX	-297 F	14.7	10 Ft-Lb	0.010 in	0/20
EPOCAST HN951	LOX	-297 F	14.7	10 Ft-Lb	0.020 in	1/9
(Epoxy)	LOX	-297 F	50	10 Ft-Lb	0.020 in	1/13
Adhesive Loctite LO555	LOX	-297 F	1500	72 Ft-Lb	0.007 in	0/20
Clamp Sleeve Teflon TFE	LOX	-297 F	14.7	72 Ft-Lb	0.031 in	0/20
	LOX	-297 F	14.7	72 Ft-Lb	0.046 in	0/20
Coating 850-204 TFE	LOX	-297 F	600	72 Ft-Lb	0.064 in	0/20
Green						
Coating 850-204 /	LOX	-297 F	1000	72 Ft-Lb	0.003 in	0/20
851-225 / 856 - 204	LOX	-297 F	15	72 Ft-Lb	0.003 in	0/20
Coating 851-204 /	LOX	-297 F	14.7	72 Ft-Lb	0.003 in	0/20
851-224 TFE						
Coating 851-224 Green	LOX	-297 F	400	72 Ft-Lb	0.065 in	0/20
850-204 Green (PTFE)						
Coating 851-225	LOX	-297 F	1050	72 Ft-Lb	0.002 in	0/20
850-201 (PTFE)						
Coating 851-245	LOX	-297 F	1000	72 Ft-Lb	0.065 in	0/20
850-204 (PTFE)						
Coating DAPCO 2031	LOX	-297 F	14.7	15 Ft-Lb	0.071 in	0/20
(Fluoroelastomer)						
Coating TRV DC Q36077	LOX	-297 F	14.7	10 Ft-Lb	0.045 in	1/6
Ablative / EPON 828 /	LOX	-297 F	14.7	10 Ft-Lb	0.095 in	1/1
EPOCAST 951	LOX	-297 F	14.7	10 Ft-Lb	0.145 in	1/1
(Silicone And Epoxy)						
Coating Silicone	LOX	-297 F	14.7	10 Ft-Lb	0.132 in	1/1
SEA200G	LOX	-314 F	14.7	35 Ft-Lb	0.131 in	0/20

Table 2f, LOX Compatibility Tested Via D2512 Mechanical Impact: MSFC HDBK 527 Rev F JSC 09604 Rev F, Sep 1988, cont.

Material	Oxygen Phase	Temp	Pressure Psi	Impact Energy	Specimen Thickness	Results Reactions / Impacts
Coating TFE 1 Coat Gray	LOX	-297 F	275	72 Ft-Lb	0.003 in	0/20
Fabric TFE Glass TG 4060	LOX	-297 F	14.7	10 Ft-Lb	0.006 in	0/20
Film Aclar 933A	LOX	-297 F	14.7	72 Ft-Lb	0.002 in	0/20
	LOX	-297 F	14.7	72 Ft-Lb	0.005 in	0/20
Polyimide/Aramid	LOX	-297 F	14.7	15 Ft-Lb	0.007 in	1/13
FEP/Polyimide	LOX	-297 F	14.7	10 Ft-Lb	0.006 in	1/2
Polyimide/Glass	LOX	-297 F	14.7	20 Ft-Lb	0.006 in	0/20
Mylar "S"	LOX	-297 F	14.7	10 Ft-Lb	0.010 in	0/20
Mylar Type A	LOX	-297 F	14.7	10 Ft-Lb	0.009 in	1/20
Teflon FEP	LOX	-297 F	14.7	72 Ft-Lb	0.003 in	0/20
Teflon FEP T160	LOX	-297 F	14.7	72 Ft-Lb	0.010 in	0/20
Fluorogold (75% PTFE/25% Glass)	LOX	-297 F	14.7	72 Ft-Lb	0.016 in	0/20
	LOX	-297 F	14.7	72 Ft-Lb	0.047 in	0/40
	LOX	-297 F	14.7	72 Ft-Lb	0.060 in	0/40
	LOX	-297 F	14.7	72 Ft-Lb	0.063 in	0/60
	LOX	-297 F	14.7	72 Ft-Lb	0.065 in	0/40
	LOX	-297 F	14.7	72 Ft-Lb	0.090 in	0/20
	LOX	-297 F	50	72 Ft-Lb	0.090 in	0/20
Fluoroloy SL (PTFE/Graphite)	LOX	-297 F	14.7	72 Ft-Lb	0.175 in	0/20
Graphite	LOX	-297 F	12.4	72 Ft-Lb	0.060 in	0/40
	LOX	-297 F	500	72 Ft-Lb	0.060 in	0/40
	LOX	-297 F	14.7	72 Ft-Lb	0.160 in	0/20
	LOX	-297 F	300	72 Ft-Lb	0.160 in	0/20
PDL4034 FR Foam (Polyurethane)	LOX	-297 F	14.7	72 Ft-Lb	0.250 in	2/5
Solimide TA301 Foam (Polyimide)	LOX	-297 F	14.7	72 Ft-Lb	0.250 in	2/20
Kel F 81	LOX	-297 F	14.7	72 Ft-Lb	0.060 in	0/60
	LOX	-297 F	14.7	72 Ft-Lb	0.125 in	0/20
	LOX	-297 F	1500	10 Ft-Lb	0.060 in	1/17
Kel F 81/6061 Resin	LOX	-297 F	14.7	72 Ft-Lb	0.010 in	0/20
Kel F 81/AR-7	LOX	-297 F	14.7	30 Ft-Lb	0.070 in	0/20
Kel F Unplasticized (Poly Trifluoro ChloroEthylene)	LOX	-297 F	14.7	35 Ft-Lb	0.006 in	0/20
	LOX	-297 F	14.7	65 Ft-Lb	0.010 in	0/20
	LOX	-297 F	14.7	72 Ft-Lb	0.060 in	0/20
	LOX	-297 F	200	72 Ft-Lb	0.050 in	0/20
	LOX	-297 F	400	72 Ft-Lb	0.040 in	0/60
	LOX	-297 F	400	72 Ft-Lb	0.088 in	0/60
	LOX	-297 F	50	72 Ft-Lb	0.051 in	0/20
Laminated Epoxy/Glass (NEMA G11)	LOX	-297 F	14.7	10 Ft-Lb	0.250 in	1/1
Kritox 240AC Grease	LOX	-297 F	1000	72 Ft-Lb	0.050 in	0/160
Rulon A (TFE/Glass)	LOX	-297 F	600	72 Ft-Lb	0.031 in	0/80
Potting Compound Polyurethane PRP1538	LOX	-297 F	14.7	72 Ft-Lb	0.047 in	2/2
Potting Compound Stycast 1095/17 (Epoxy)	LOX	-297 F	15	72 Ft-Lb	0.062 in	2/3

Table 2f, LOX Compatibility Tested Via D2512 Mechanical Impact: MSFC HDBK 527 Rev F JSC 09604 Rev F, Sep 1988, cont.

Material	Oxygen Phase	Temp	Pressure Psi	Impact Energy	Specimen Thickness	Results Reactions / Impacts
60% Bronze Filled TFE	LOX	-297 F	14.7	72 Ft-Lb	0.060 in	0/20
Teflon / 25% Glass	LOX	-297 F	1000	72 Ft-Lb	0.060 in	0/20
	LOX	-297 F	1500	72 Ft-Lb	0.610 in	0/40
EPR Rubber E688-70	LOX	-297 F	14.7	72 Ft-Lb	0.045 in	2/6
	LOX	-297 F	147	72 Ft-Lb	0.045 in	2/6
EPR Rubber E692-75	LOX	-297 F	14.7	72 Ft-Lb	0.087 in	1/20
Fluorosilicone Rubber L677-70	LOX	-297 F	14.7	72 Ft-Lb	0.066 in	0/22
Kalrez 1050	LOX	-290 F	414.7	72 Ft-Lb	0.187 in	0/20
Neoprene BC CWB10	LOX	-297 F	14.7	72 Ft-Lb	0.090 in	8/25
Silicone RTV 577	LOX	-314 F	14.7	65 Ft-Lb	0.118 in	0/20
Silicone 577/9811	GOX	70 F	1500	72 Ft-Lb	0.060 in	2/27
Silicone RTV 651	LOX	-297 F	14.7	72 Ft-Lb	0.065 in	1/20
Silicone RTV DC3-6077	LOX	-297 F	14.7	10 Ft-Lb	0.025 in	1/1
	LOX	-314 F	14.7	30 Ft-Lb	0.075 in	0/20
	LOX	-314 F	14.7	35 Ft-Lb	0.125 in	0/20
Viton 2702-75	LOX	-297 F	400	10 Ft-Lb	0.5 in	1/20
Viton 3-912V	LOX	-297 F	400	10 Ft-Lb	0.115 in	0/20
Viton 3-916V	LOX	-297 F	400	10 Ft-Lb	0.113 in	1/20
Viton 75	LOX	-297 F	400	10 Ft-Lb	0.050 in	1/1
Viton 9009-90	LOX	-297 F	14.7	72 Ft-Lb	0.072 in	5/20
	LOX	-297 F	1500	72 Ft-Lb	0.072 in	0/20
Viton A	LOX	-297 F	14.7	72 Ft-Lb	0.031 in	4/30
	LOX	-297 F	14.7	72 Ft-Lb	0.062 in	22/220
Viton Fluid Resistant	LOX	-297 F	14.7	72 Ft-Lb	0.070 in	59/100
Viton O-Ring	LOX	-297 F	14.7	10 Ft-Lb	0.086 in	2/2
	LOX	-297 F	14.7	72 Ft-Lb	0.135 in	0/20
Viton O-Ring 19357	LOX	-297 F	400	10 Ft-Lb	0.012 in	1/1
Viton O-Ring CPD 19447	LOX	-297 F	14.7	10 Ft-Lb	0.070 in	1/1
Viton O-Ring S/A 2-012	LOX	-297 F	14.7	10 Ft-Lb	0.070 in	1/6
Viton O-Ring S/A 2-014	LOX	-297 F	14.7	10 Ft-Lb	0.070 in	1/4
Viton O-Ring S/A 2-016	LOX	-297 F	14.7	10 Ft-Lb	0.070 in	1/1
Viton O-Ring S/A 2-020	LOX	-297 F	14.7	10 Ft-Lb	0.070 in	1/7
Viton O-Ring S/A 2-024	LOX	-297 F	14.7	10 Ft-Lb	0.070 in	1/1
Viton O-Ring S/A 2-035	LOX	-297 F	14.7	15 Ft-Lb	0.070 in	1/4
	LOX	-297 F	230	10 Ft-Lb	0.070 in	0/20
Viton O-Ring S/A 343	LOX	-297 F	14.7	10 Ft-Lb	0.210 in	1/6
Viton O-Ring S/A2-214	LOX	-297 F	400	10 Ft-Lb	0.140 in	1/1
Viton V709-90	LOX	-297 F	1000	72 Ft-Lb	0.117 in	1/60
	LOX	-297 F	14.7	72 Ft-Lb	0.117 in	1/20
	LOX	-297 F	1500	72 Ft-Lb	0.117 in	1/60
	LOX	-297 F	500	72 Ft-Lb	0.117 in	0/20
Viton V747-75	LOX	-297 F	14.7	72 Ft-Lb	0.070 in	8/20
PTFE 15% Glass Fill	LOX	-297 F	14.7	72 Ft-Lb	0.060 in	0/20
PTFE 25% Glass Fill	LOX	-297 F	14.7	72 Ft-Lb	0.060 in	0/20
Graphitar 114 Carbon	LOX	-297 F	14.7	72 Ft-Lb	0.250 in	0/20
	LOX	-297 F	14.7	72 Ft-Lb	0.578 in	0/20
	LOX	-297 F	300	72 Ft-Lb	0.250 in	0/20
	LOX	-297 F	300	72 Ft-Lb	0.578 in	0/20

Table 2f, LOX Compatibility Tested Via D2512 Mechanical Impact: MSFC HDBK 527 Rev F JSC 09604 Rev F, Sep 1988, cont.

Material	Oxygen Phase	Temp	Pressure Psi	Impact Energy	Specimen Thickness	Results Reactions / Impacts
Neoprene DAPCO 2030	LOX	-297 F	14.7	15 Ft-Lb	0.005 in	1/12
	LOX	-314 F	45	15 Ft-Lb	0.005 in	0/20
Tape FEP/ARIMID	LOX	-297 F	14.7	10 Ft-Lb	0.010 in	1/2
Tape FEP/Polyimide/ ARAMID	LOX	-297 F	14.7	10 Ft-Lb	0.011 in	2/5
Tape Teflon Antiseize	LOX	-297 F	14.7	72 Ft-Lb	0.003 in	0/60
TPE 11% Metal Ox Fill	LOX	-297 F	275	72 Ft-Lb	0.025 in	0/40
Teflon FEP	LOX	-297 F	1000	72 Ft-Lb	0.062 in	0/6
	LOX	-297 F	1050	72 Ft-Lb	0.010 in	0/40
	LOX	-297 F	275	72 Ft-Lb	0.018 in	0/20
Teflon G-83 PTFE	LOX	-297 F	14.7	72 Ft-Lb	0.018 in	0/20
Teflon PTFE Discs	LOX	-297 F	14.7	10 Ft-Lb	0.016 in	1/1
Powdered PTFE	LOX	-297 F	14.7	72 Ft-Lb	0.050 in	0/20
Teflon TFE 3602	LOX	-297 F	14.7	72 Ft-Lb	0.060 in	0/20
Virgin PTFE Teflon	LOX	-297 F	1050	72 Ft-Lb	0.010 in	0/60
	LOX	-297 F	14.7	72 Ft-Lb	0.250 in	0/60
	LOX	-297 F	200	50 Ft-Lb	0.018 in	0/20
	LOX	-297 F	200	72 Ft-Lb	0.018 in	0/20
	LOX	-297 F	275	72 Ft-Lb	0.020 in	0/20
Teflon 25% Glass Fill	LOX	-297 F	1050	72 Ft-Lb	0.128 in	0/20
Aramid Thread	LOX	-297 F	14.7	10 Ft-Lb	0.020 in	1/1
FEP 100 HST Tubing	LOX	-297 F	14.7	72 Ft-Lb	0.012 in	0/360
Korvex FEP HS Tubing	LOX	-297 F	14.7	72 Ft-Lb	0.055 in	0/20
	LOX	-297 F	45	72 Ft-Lb	0.007 in	0/20
Korvex PTFE HS Tubing	LOX	-297 F	100	72 Ft-Lb	0.095 in	0/20
Tubing Laminated/	LOX	-297 F	600	72 Ft-Lb	0.070 in	0/20
Rolled PTFE/Glass Fabric Base	LOX	-297 F	600	72 Ft-Lb	0.090 in	0/280
PTFE Shrinkable Tubing	LOX	-297 F	14.7	72 Ft-Lb	0.004 in	0/20
PTFE HST Tubing	LOX	-297 F	14.7	72 Ft-Lb	0.095 in	0/20
	LOX	-297 F	100	72 Ft-Lb	0.086 in	0/20
	LOX	-297 F	14.7	72 Ft-Lb	0.080 in	3/99
FEP HST Tubing	LOX	-297 F	14.7	72 Ft-Lb	0.018 in	0/360
Vespel SP-1 Polyimide	LOX	-297 F	300	72 Ft-Lb	0.057 in	0/20
Vespel SP-21	LOX	-297 F	100	72 Ft-Lb	0.053 in	0/20
15% Graphite Fill	LOX	-297 F	1050	55 Ft-Lb	0.060 in	0/20
	LOX	-297 F	14.7	72 Ft-Lb	0.060 in	0/20
	LOX	-297 F	275	55 Ft-Lb	0.040 in	2/33
Vespel SP-211 Polyimide /Graphite/PTFE	LOX	-297 F	14.7	72 Ft-Lb	0.060 in	0/40

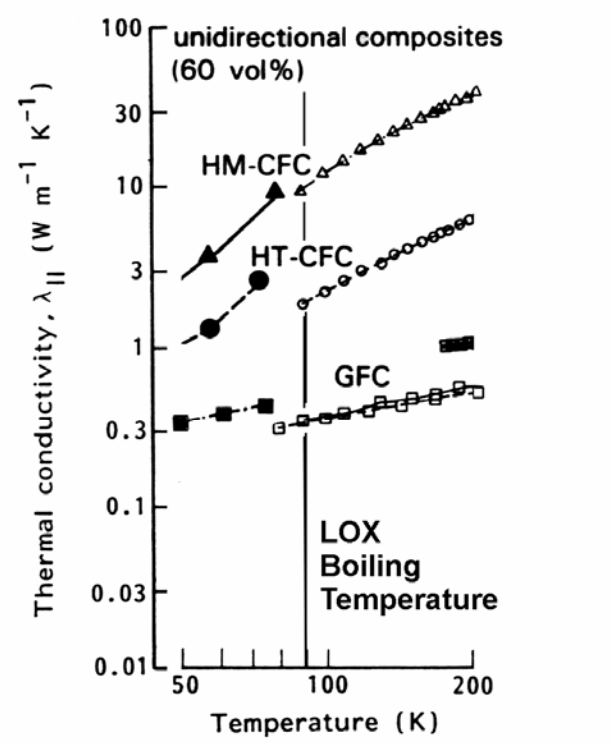
Table 2g, LOX Compatibility Tested Via D2512 Mechanical Impact: NASA, JSC, WSTF-IR-93-0024

Material	Oxygen Phase	Temp	Pressure Psi	Impact Energy	Specimen Thickness	Results Reactions / Impacts
Gr/F655	LOX	-183 C	12.4	72 Ft-Lbf	0.768 cm	6/16 Flash and
(Toughened	"	(-297 F)	(85.5 kPa)	62.7 Ft-Lbf	(0.302 in)	0/7 Charring
Bismaleimide),						RXNs
Woven Fabric						
Gr/F650	LOX	-183 C	12.4	72 Ft-Lbf	0.564 cm	7/10 Flash,
(Bismaleimide),	"	(-297 F)	(85.5 kPa)	62.7 Ft-Lbf	(0.222 in)	2/8 Audible, and
Laminate	"	"	"	54.4 Ft-Lbf	"	0/2 Charring
	"	"	"	47.4 Ft-Lbf	"	0/1 RXNs
	"	"	"	31.1 Ft-Lbf	"	0/1
Gr/BtCy-3	LOX	-183 C	12.4	72 Ft-Lbf	0.746 cm	1/1 Flash,
(Cyanate Ester),	"	(-297 F)	(85.5 kPa)	54.4 Ft-Lbf	(0.294 in)	1/1 Audible, and
Woven Fabric	"	"	"	40.7 Ft-Lbf	"	1/1 Charring
	"	"	"	35.7 Ft-Lbf	"	1/2 RXNs
	"	"	"	23.4 Ft-Lbf	"	1/1
	"	"	"	20.4 Ft-Lbf	"	2/3
	"	"	"	17.7 Ft-Lbf	"	5/8
	"	"	"	15.4 Ft-Lbf	"	2/7
	"	"	"	13.4 Ft-Lbf	"	0/2
	"	"	"	11.6 Ft-Lbf	"	0/1
	"	"	"	8.7 Ft-Lbf	"	0/1
Gr/F3900	LOX	-183 C	12.4	72 Ft-Lbf	0.636 cm	3/6 Flash
(Toughened Epoxy),	"	(-297 F)	(85.5 kPa)	62.7 Ft-Lbf	(0.250 in)	1/4 and
Woven Fabric	"	"	"	54.4 Ft-Lbf	"	5/6 Charring
	"	"	"	47.4 Ft-Lbf	"	0/5 RXNs
	"	"	"	40.7 Ft-Lbf	"	1/2
	"	"	"	35.7 Ft-Lbf	"	0/1
	"	"	"	31.1 Ft-Lbf	"	0/1
	"	"	"	27.1 Ft-Lbf	"	0/1
IM7 / 8551-7A	LOX	-183 C	12.4	72 Ft-Lbf	0.549 cm	3/6 Flash
(Toughened Epoxy),	"	(-297 F)	(85.5 kPa)	62.7 Ft-Lbf	(0.216 in)	2/3 and
Laminate	"	"	"	54.4 Ft-Lbf	"	4/6 Charring
	"	"	"	47.4 Ft-Lbf	"	3/6 RXNs
	"	"	"	40.7 Ft-Lbf	"	0/3
	"	"	"	35.7 Ft-Lbf	"	0/2
AS4/3501-6	LOX	-183 C	12.4	72 Ft-Lbf	0.654 cm	1/1 Flash,
(Epoxy), Woven Fabric	"	(-297 F)	(85.5 kPa)	54.4 Ft-Lbf	(0.258 in)	1/1 Audible
	"	"	"	47.4 Ft-Lbf	"	1/1 and
	"	"	"	35.7 Ft-Lbf	"	3/4 Charring
	"	"	"	31.1 Ft-Lbf	"	8/10 RXNs
	"	"	"	27.1 Ft-Lbf	"	2/10
	"	"	"	23.4 Ft-Lbf	"	3/5
	"	"	"	20.4 Ft-Lbf	"	4/5
	"	"	"	17.7 Ft-Lbf	"	1/6
	"	"	"	15.4 Ft-Lbf	"	0/1
	"	"	"	11.6 Ft-Lbf	"	0/1
AS4/LRF387,	LOX	-183 C	12.4	72 Ft-Lbf	0.301 cm	1/1 Flash,
(Epoxy), Teflon Coated,	"	(-297 F)	(85.5 kPa)	35.7 Ft-Lbf	(0.119 in)	2/2 Audible,
Laminate	"	"	"	23.4 Ft-Lbf	"	6/6 and Charring
	"	"	"	20.4 Ft-Lbf	"	5/11 RXNs
	"	"	"	17.7 Ft-Lbf	"	2/8
	"	"	"	15.4 Ft-Lbf	"	0/2

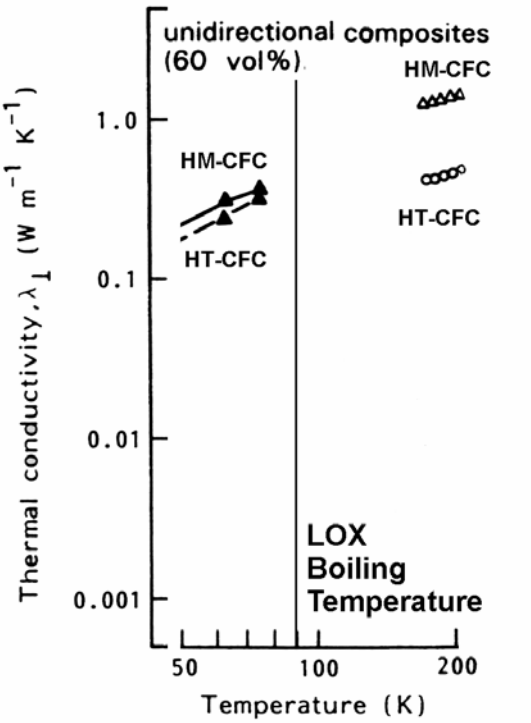
Table 2g, LOX Compatibility Tested Via D2512 Mechanical Impact: NASA, JSC, WSTF-IR-93-0024, cont.

Material	Oxygen Phase	Temp	Pressure Psi	Impact Energy	Specimen Thickness	Results Reactions / Impacts
Glass/Phenolic, Woven Fabric	LOX	-183 C	12.4	72 Ft-Lbf	0.788 cm	1/1 Flash,
	"	(-297 F)	(85.5 kPa)	40.7 Ft-Lbf	(0.310 in)	1/1 Audible,
	"	"	"	35.7 Ft-Lbf	"	5/6 and Charring;
	"	"	"	31.1 Ft-Lbf	"	5/8 Chunks Blown
	"	"	"	27.1 Ft-Lbf	"	1/6 Out Of Cups
	"	"	"	23.4 Ft-Lbf	"	0/3 due to RXNs
	"	"	"	17.7 Ft-Lbf	"	0/1
Glass/NRL-1 (Fluorinated Epoxy), Woven Fabric	LOX	-183 C	12.4	72 Ft-Lbf	0.562 cm	1/1 Flash,
	"	(-297 F)	(85.5 kPa)	35.7 Ft-Lbf	(0.221 in)	2/2 Audible, and
	"	"	"	31.1 Ft-Lbf	"	2/2 Charring;
	"	"	"	27.1 Ft-Lbf	"	7/9 Chunks
	"	"	"	23.4 Ft-Lbf	"	1/8 Blown
	"	"	"	20.4 Ft-Lbf	"	2/4 Out Of
	"	"	"	17.7 Ft-Lbf	"	1/5 Cups due
	"	"	"	8.7 Ft-Lbf	"	0/1 to RXNs
IM7/PEEK, Laminate	LOX	-183 C	12.4	72 Ft-Lbf	0.154 cm	1/1 Flash,
	"	(-297 F)	(85.5 kPa)	35.7 Ft-Lbf	(0.061 in)	1/1 Audible,
	"	"	"	17.7 Ft-Lbf	"	3/3 and Charring
	"	"	"	15.4 Ft-Lbf	"	3/4 RXNs
	"	"	"	13.4 Ft-Lbf	"	3/6
	"	"	"	11.6 Ft-Lbf	"	3/6
	"	"	"	10.1 Ft-Lbf	"	1/6
	"	"	"	8.7 Ft-Lbf	"	0/3
T650-42 / V-25 (Epoxy), Laminate	LOX	-183 C	12.4	72 Ft-Lbf	0.180 cm	7/16 Flash and
	"	(-297 F)	(85.5 kPa)	62.7 Ft-Lbf	(0.071 in)	3/9 Charring
	"	"	"	54.4 Ft-Lbf	"	0/4 RXNs
	"	"	"	35.7 Ft-Lbf	"	0/1
Gr/Avimid N (Polyimide), Woven Fabric	LOX	-183 C	12.4	72 Ft-Lbf	0.084 cm	1/1 Flash and
	"	(-297 F)	(85.5 kPa)	47.4 Ft-Lbf	(0.033 in)	4/4 Charring
	"	"	"	40.7 Ft-Lbf	"	6/13 RXNs
	"	"	"	35.7 Ft-Lbf	"	4/6
	"	"	"	31.1 Ft-Lbf	"	4/7
	"	"	"	27.1 Ft-Lbf	"	1/6
	"	"	"	23.4 Ft-Lbf	"	0/2
	"	"	"	20.4 Ft-Lbf	"	0/1
	"	"	"	17.7 Ft-Lbf	"	0/2

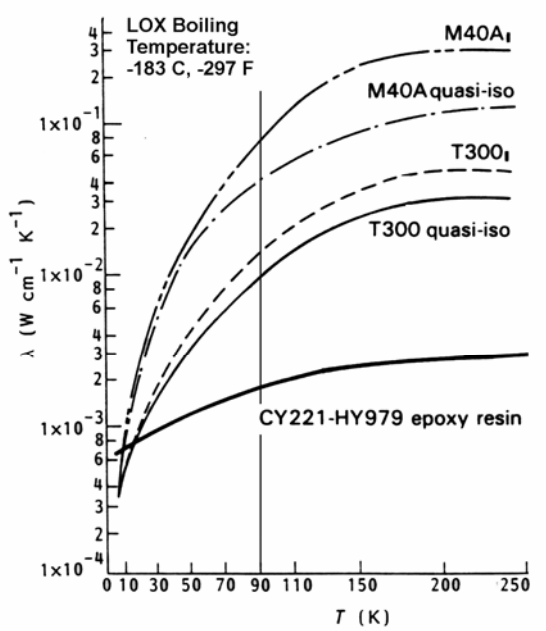
A significant factor explaining why all of the polymer and composite materials in table 2 failed is their very low in-plane thermal conductivity. None of the composite materials used any reinforcing fibers that exhibit thermal conductivity superior to nickel and all exhibited thermal conductivity inferior to aluminum. In fact none of the fibers making up the composites listed on table 2 exhibit axial thermal conductivities greater than 15 W/mK; which is 1/20th that of aluminum.[FP1-FP40, C1-C45] Figure 6 depicts the in and out-of-plane thermoconductivity of various similar low thermoconductivity PAN carbon fiber uni and quasi-isotropic composites. None of the polymeric matrix resins used in these same composite materials exhibit thermal conductivities greater than 0.3 W/mK; which is three orders of magnitude less than that of aluminum. Overall the in-plane thermal conductivity of these composites were no greater than 3 to 5 W/mK and the out-of-plane thermal conductivity of these composites was at best 0.5 W/mK due to the matrix resin's very low thermal conductivity. With in and out-of-plane thermal conductivities so low the energy injected into these composites by the mechanical impacter could not be transported away from the local injection site and instead, as shown in figure 3, caused the temperature of the composite fuel at the energy injection site to significantly rise and set up ignition conditions.



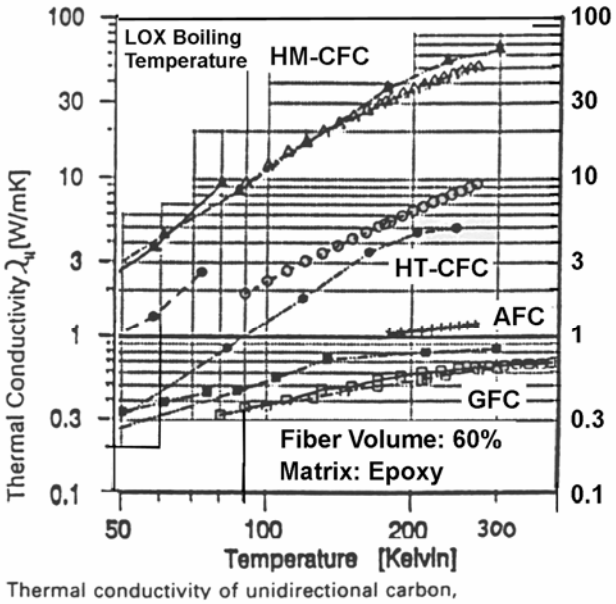
Thermal conductivity in fibre direction
H.Bansemir and O.Haider 1991



Thermal conductivity in fibres of carbon
H.Bansemir and O.Haider 1991



Thermal conductivity of M40A-T300 epoxy and CY221-HY979 epoxy resin (60 vol%).
H.Bansemir and O.Haider 1991



Thermal conductivity of unidirectional carbon, glass and aramid laminates in fibre direction
H.Bansemir and O.Haider 1998

Figure 6, Thermal Conductivity Of Conventional PAN Based Carbon Fiber Composites.

Since a high intrinsic thermal conductivity is, with only a few notable exceptions, the hall mark of a LOX compatible material, it stands to reason that it will be necessary to at least increase the in-plane thermal conductivity of a composite material up to that which is exhibited by Aluminum alloys at LOX's boiling temperature. Fortunately some thermally conductive, highly ordered, and graphitized fibers have been developed over the past decade. Highly ordered graphite, also known as polypyrlene, is the most LOX compatible polymer known. When a composite is fabricated with one of these high thermal conductivity fibers using one of the more LOX compatible matrix resin systems available, which also exhibits a high Tg, it should exhibit the overall in-plane thermal conductivity of Aluminum alloys. While little data is available on the thermal conductivity of such composites at LOX's boiling temperature, figure 7 provides a good indication of the in-plane thermal conductivity over a range of temperatures of various lay up schemes of composites using K13D and K13C and YS95 and YS90 fiber composites also implies roughly the same measure of in-plane thermal conductivity. Figures 8 depicts the thermoconductivity of Granoc graphite XN fibers over a span of temperatures and figure 9 depicts the room temperature conductivity of various other Granoc graphite XN fibers and various Toray Pan fibers. Since the in-plane thermoconductivity of a composite is a straight rule of mixtures formula and the thermal conductivity of all resin matrixes is roughly the same, it is a very good assumption to expect that any 60+% volume fraction composite using these high thermal conductivity fibers would also exhibit aluminum alloy like in-plane thermal conductivity. Comparing the results listed in table 2 and numerous other published composite material's mechanical impact LOX compatibility to the thermal conductivities depicted in figures 4 and 6 and published in numerous other efforts which measured the thermal conductivity of composite materials, the window of thermal conductivity needed in order to make a D2512 LOX compatible composite is shown in figure 10.

The core objective of this research effort is to determine if a composite, using thermally conductive reinforcement fibers instead of the standard conventional carbon fibers used to date, suitable to the fabrication of axisymmetric tanks, ducts, and lines and exhibiting in-plane thermal conductivities comparable to those metals which regularly pass D2512, can be found which either passes or comes close to passing D2512. A secondary objective will then be to deduce and to better understand what happened to the specimens during the D2512 test.

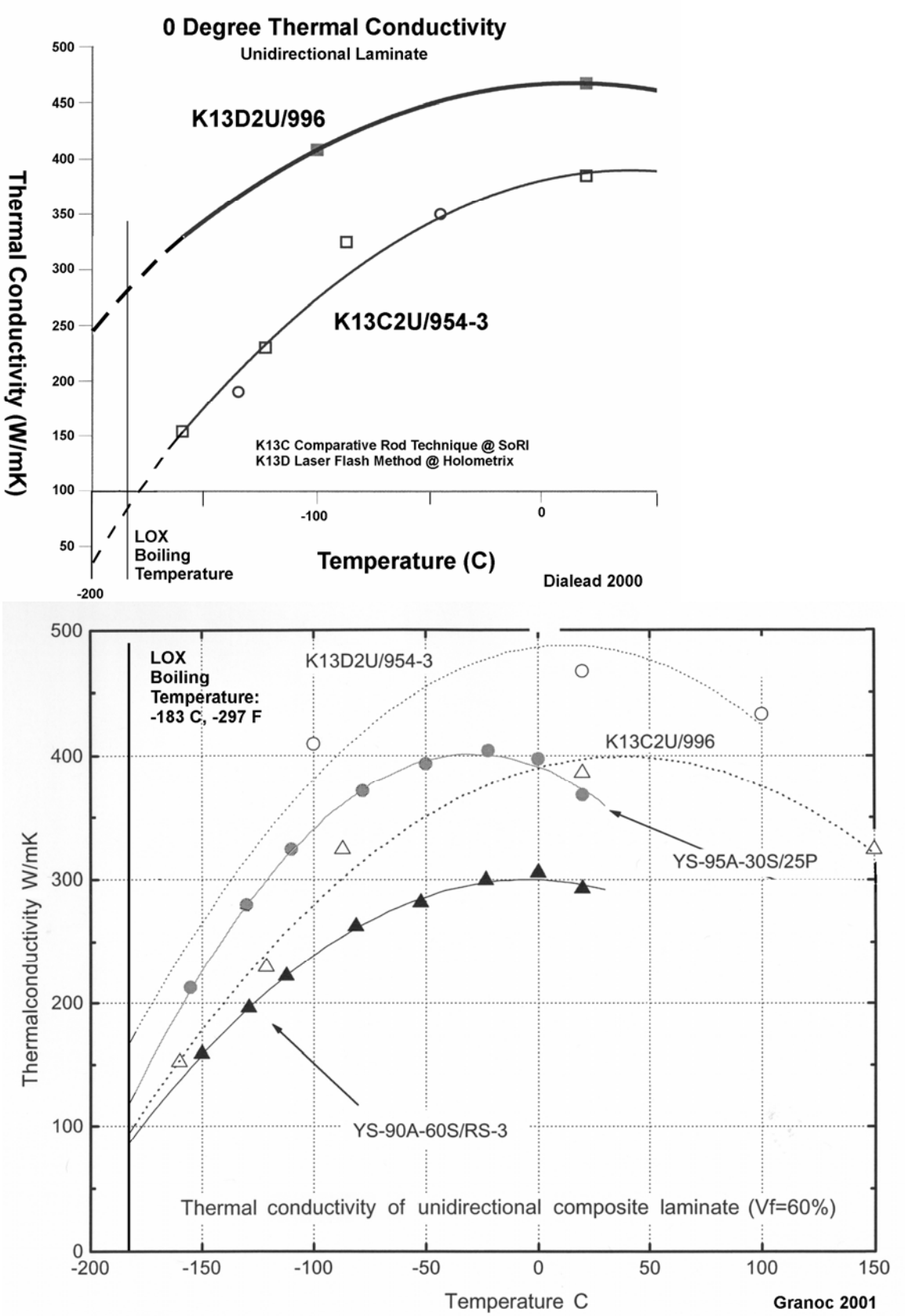
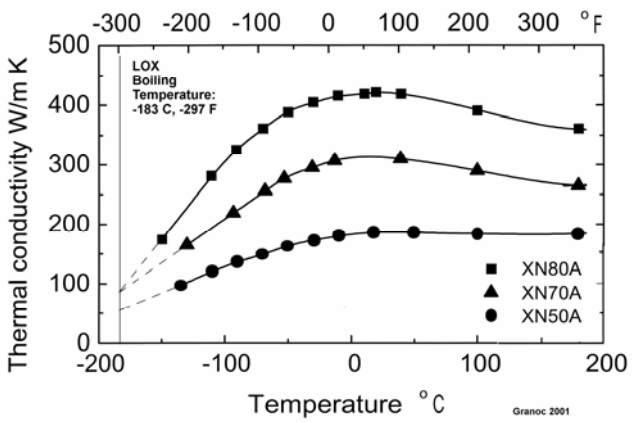


Figure 7, Pitch Graphite Fiber Composites Thermal Conductivity



Thermal conductivity as a function of temperature.

Figure 8, Thermal Conductivity Of Granoc XN Graphite Fibers Versus Temperature

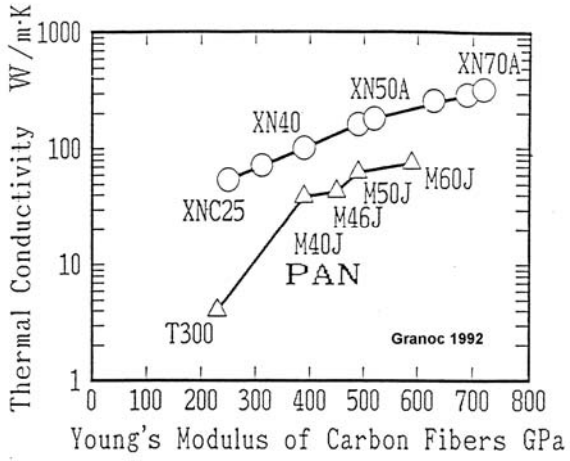


Figure 9, Room Temperature Thermal Conductivity Of Various PAN Carbon And Pitch Graphite Fibers

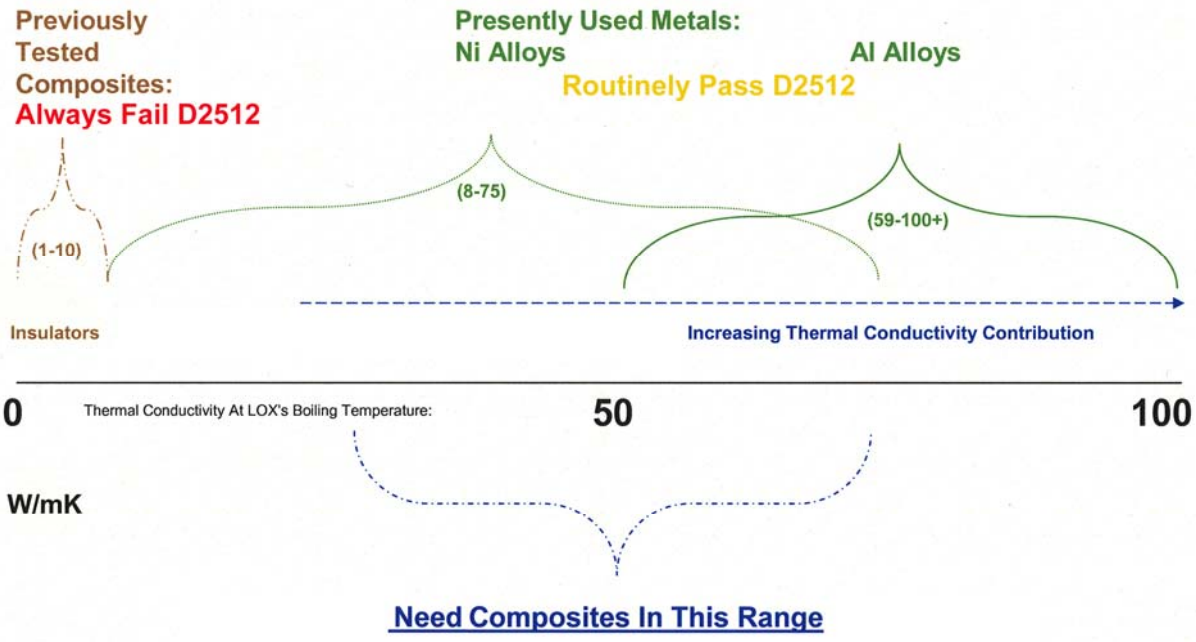


Figure 10, Estimated Thermal conductivity window for making a D2512 LOX compatible composite.

Theory Section: Ignition Event

An ignition event always begins when energy is delivered as shown in Figure 11 by one of the mechanisms listed in Table 3 to a small local site as indicated from Table 4's quotes on a fuel source's surface which is in intimate contact with oxygen or any other oxidizer.[O1-O214] (Without the input of energy as described, oxygen in intimate contact with a fuel source is chemically inert.) The magnitude of the energy required to kick off the ignition event is dependent upon the delivery mechanism's ability to concentrate that energy at the local energy injection site.

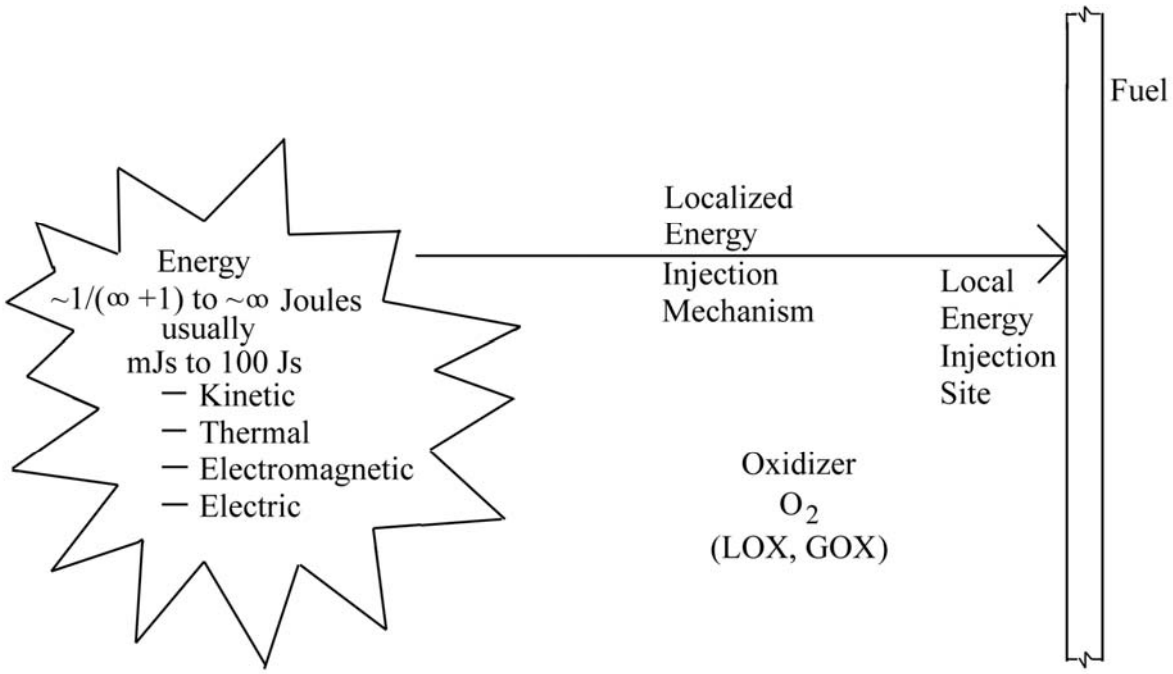


Figure 11, Initial Ignition Event Step

Table 3, Localized Energy Injection Mechanisms

External Continuum Energy Flux:

Bulk Heating
FRICTION: ROTATIONAL RUBBING
GALLING
Acoustic Vibration
Abrasion
Electromagnetic Outside Source Radiation

One Time Energy Packets:
ADIABATIC COMPRESSION "TRAPPED VOLUME PRESSURIZATION"
MECHANICAL IMPACT: BLUNT IMPACT "HAMMER BLOW"
POINT IMPACT "CONTAMINANT PARTICLE IMPACT"
Electric Discharge: Arcing: Failing Electronic Equipment
Static Discharge: Flowing LOX/GOX Across Containment Vessel's Surface
High Shear Rates: Mechanical Rupture / Fracture
Shock Waves

MOST COMMON LOCALIZED ENERGY INJECTION MECHANISMS LEADING TO AN IGNITION EVENT

Table 4, Ignition Starts At A Local Small Site

"Mechanical Impact: **Generates local "Hot Spot" regions via energy localization processes like shear bands ie high rate shear regions**. These regions are between 1/150TH and 1/1000TH of the total of the impacted material." P.J. Miller, C.S. Coffey, and V.F. DeVost, Heating In Crystalline Solids Due To Rapid Deformation, J.Appl.Phys. 59(3),Pg 913-916, Feb 1986

"When the surface of a specimen is exposed to heat sources such as thermal radiation or hot air, the temperature in the solid increases gradually… . As a result, **the hot part in the polymer is decomposed thermally with a rate depending upon the local temperature at each point, and gaseous products are released into the atmosphere through the polymer surface**. Sometimes this pyrolysis process is accompanied by small heat generation. … **Next, a combustible gas - air mixture is formed at the adjacent solid surface**, and flaming combustion occurs spontaneously in the gas phase, ..." K. Akita, Ignition Of Polymers And Flame Propagation On Polymer Surfaces, Chapter 10, Aspects Of Degradation And Stabilization Of Polymers, Edited By H.H.G. Jellinek, Elsevier Scientific Publishing Co., Amsterdam Oxford NY 1978, Pg 501-525, 1978

"Adiabatic compression of gaseous phase oxygen from pressure spikes due to water hammer, fast operation of valves in high pressure systems, oscillatory flow, or other **sudden pressurization can cause localized temperature increases sufficient to ignite many materials**, especially organic contaminants or fire particles. "

"**Water hammer forces in turn can cause adiabatic compression of gaseous pockets which can produce localized high temperatures**." Harold W. Schmidt, and Forney , ASRDI Oxygen Technological Survey. Vol 9: Oxygen Systems Engineering Review, NASA SP-3090, 1-218, 1975

"**Electric arcs and sparks produce temperatures well in excess of all reported autoignition temperatures for aluminum. They are highly localized** and should be effective in delivering energy to the metal. However, despite the high temperature and localization of the heat, the total energy present in sparks from static charge separation or in arcs from low voltage wiring tends to be small, and aluminum, because of its high thermal conductivity, dissipates heat very effectively." Barry L. Werley, Herve' Barthelemy, Robert Gates, Joseph W. Slusser, Keith B. Wilson, and Robert Zawierucha, A Critical Review Of Flammability Data For Aluminum, Flamibility And Sensitivity Of Materials In Oxygen-Enriched Atmospheres: Sixth Volume, ASTM STP 1197, Pg 300-345, 1993

"**Ignition usually begins as a small event** and grows into a fire through the kindling chain sequence. **A small amount of energy ignites a material with a low ignition temperature** … Once ignited, the material gives off enough heat to ignite bulk materials with higher ignition temperatures - which generate more heat - until the process is self-sustaining. " Standard Guide For Control Of Hazards And Risks In Oxygen Enriched Systems, ASTM G 128 - 95, 1995

"Material with **a high thermal diffusivity are better in dynamic systems since local energy impulses will result in less pronounced hot spots** than materials with low diffusivity. In a static system high thermal conductivity materials are more desirable for essentially the same reason. … The presence of sharp edges may result in hot spots for ignition." J.G. Hust, and A.F. Clark, A Survey Of Compatibility Of Materials With High Pressure Oxygen Service, Cryogenics, Pg 325-336, June 1973

"Metals have **high thermal conductivities that help dissipate local heat inputs** that might easily ignite nonmetals" Standard Guide For Evaluating Metals For Oxygen Service, ASTM G 94 – 92, 1992

"Metals with **good thermal conductivities, should be more difficult to ignite because local hot spots can be dissipated before ignition occurs**." Joseph W. Slusser, and Keith A. Miller, Selection Of Metals For Gaseous Oxygen Service, Flamibility And Sensitivity Of Materials In Oxygen-Enriched Atmospheres: ASTM STP 812, Pg 167-191, 1983

Thermal chemical equilibrium between oxygen and a polymer based fuel source such as a PMC causes the oxygen to first adsorb onto the surface of the PMC fuel at the nominal surface and then to diffuse into the PMC and form a gradient through the fuel's thickness. This gradient's highest concentration is at the nominal surface, where liquid/gaseous oxygen predominates to one side and the PMC to the other, and lowest at the other side where atmospheric conditions usually exist. This concentration usually exhibits an exponential decay thru the thickness of a polymer because the oxygen molecules interact with the various groups on the polymers and fall into energy minimization wells where they get "stuck" until energy becomes available to bump them out and move them further through the material. This condition constitutes intimate contact between the oxygen and the PMC fuel. The contacting immediate surface is schematically depicted in figure 12a.

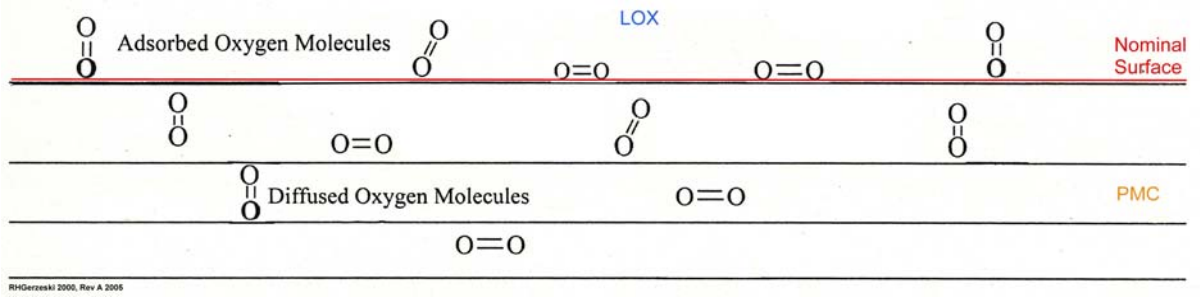


Figure 12a, Ignition Event: Intimate Contact Of PMC Fuel and Oxygen Preliminary Condition

The beginning step in the ignition event, as previously mentioned, is the injection of some type of energy at a local site. For this effort the injection mechanism is mechanically injected kinetic energy. The means of injecting this energy is the D2512 ambient tester apparatus shown in figure 5 and the magnitude of the injected energy is 98 joules. This energy is mostly transformed into thermal energy forming a local hot spot via a mechanism which will be elaborated on in the discussion section. As shown in figure 3 some of this energy is removed via various thermal transport mechanisms. The more removed the better because the remaining energy causes the PMC fuel's temperature to drastically and rapidly rise. As indicated in figure 13, this local hot spot temperature rise can be in the hundreds of ^{o}C and occur in time spans of one thousandth of a second or less.

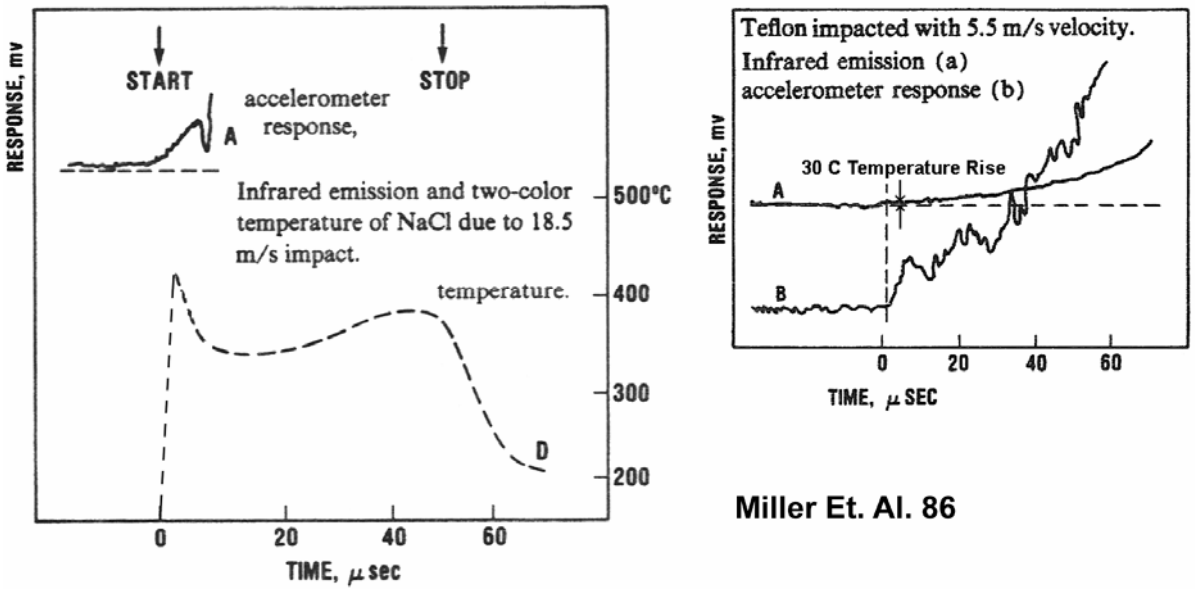


Figure 13, Temperature Vs Time Rises In NaCl and PTFE Resulting From Mechanical Impacts

When the PMC fuel's temperature at the local hot spot has climbed sufficiently the next step in the ignition event occurs: the fuel begins to break down (degrade) into small segments via radical chain scission as depicted in figure 12b. The onset of this degradation is solely dependent upon the thermal stability (ie the temperature at which decomposition begins) of the matrix used in the composition of the PMC fuel. Matrixes made from more aliphatic constituents break down at lower temperatures. Matrixes made from more aromatic constituents break down at somewhat higher temperatures. Matrixes made of various heterocyclic groups such as imides break down at significantly higher temperatures. And matrixes made with halogens amongst their constituents break down at even higher temperatures. Many of the oxygen molecules adsorbed onto and diffused into the PMC are now excited into Triplet, Singlet, etc states and into the diradical state.

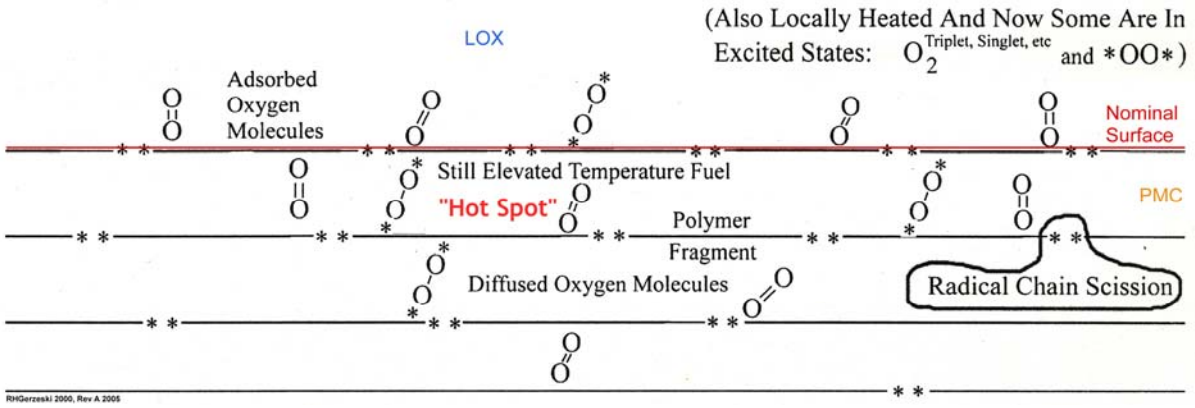


Figure 12b, Ignition Event: Radical Chain Scission Breakdown Of PMC Fuel

Almost instantaneously with the radical chain scission breakdown of the PMC fuel the chemistry of the ignition event depicted in figure 12c begins. This chemistry is that of peroxides and the diverse chemical reaction paths and end products that this chemistry takes and generates is described in table 5.

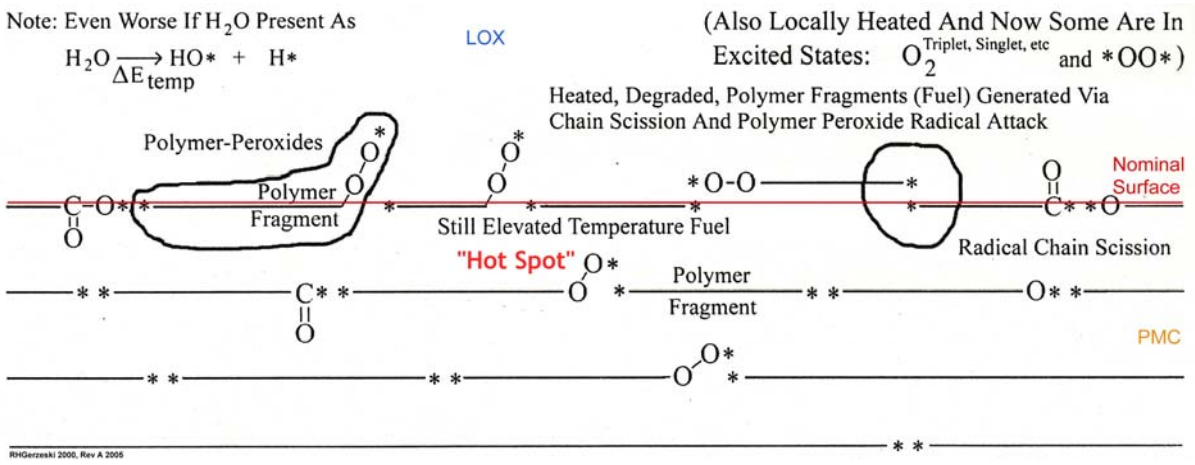


Figure 12c, Ignition Event: Peroxide Oxidation Radical Addition Chemistry

Radical addition is the mechanism of reaction for the oxidation of an organic material such as the PMC's matrix. For all effects and purposes this chemistry is only possible after radicals have been generated in the fuel as direct initiation is highly endothermic. This accounts for oxygen's chemical inertness when in contact with a fuel without an ignition event initiating energy injection. The addition reaction mechanism which generates primarily peroxide chemicals out of the PMC fuel is extremely fast: almost one million times faster than other addition chemical reactions. It also generates a significant amount of heat: the heat of formation of carbon oxygen bonds is between 75 and 100 kcals per mole. This heat gets dumped into the small local site where the original ignition event kick off energy was injected and makes the local hot spot's temperature rapidly rise (due to the peroxide chemistries' rapid reaction rate) to become a really hot spot. This temperature rise induces even more thermal degradation of the PMC fuel and more peroxide oxidation occurs. In addition to the heat, the peroxide radicals formed attack the PMC fuel and causes even more of it to be broken down into a reactable chemical state.

Metal complexes catalyze the breakdown of peroxide chemicals into peroxide radical chemicals. These in turn attack and further degrade the PMC fuel into even more peroxide chemicals, and peroxide radical chemicals generating and dumping even more heat into the PMC fuel which further degrades the fuel. Trace quantities of metals amounting to no more then 100 parts per million (PPM) can significantly accelerate the peroxide oxidation chemistry and the breakdown of the PMC fuel.

The impact of contaminants and poor cleaning on the safe use of a LOX components first manifest themselves at the radical chain scission thermal breakdown and peroxide radical addition oxidation stages of the ignition event. After human error, the most common contributing factor to catastrophic ignition events in LOX components is a failure to properly clean and maintain them contaminant free. The presence of contaminants usually takes the chemical form of lower molecular weight aliphatics in the physical form of cutting oils, lubricant greases, the oils from fingerprints etc. As shown in Table 6 and Figure 14 aliphatics begin thermally breaking down and producing the chemical byproducts of peroxide oxidation chemistry at temperatures 100°Cs lower than materials making up LOX components made from aromatics, heterocyclics and halogens. When these contaminants get to the thermal breakdown and peroxide oxidation stages of the ignition event they generate heat even faster than said same stages for the main LOX component constituting material, which raises the local hot spot's temperature rapidly up to those material's breakdown and oxidation stages. This is known as the kindling chain effect and is the reason for the imperative need for meticulous cleaning and contamination elimination.

The combination of metal complexes and contaminants can, at these two stages of an ignition event, cause very extreme increases in the rate of thermal fuel breakdown and peroxide oxidation. These increases can be so severe that the ignition event takes on the characteristics of an explosion with all of an explosion's deleterious results.

Overall for the reasons and causes elaborated above it is imperative that any material intended for use in a LOX handling component absolutely must be meticulously cleaned and maintained clean. It also must exhibit a metal content below 100 PPM. Failure to achieve these will skew the material towards a tendency to progress farther down the ignition event sequence towards lesser desirable end results and falsely imply a greater tendency for the uncontaminated material to react.

Table 5, Peroxide Oxidation Chemistry

Peroxide Chemistry:

Primary:

$$RH \xrightarrow[\text{Weak Links / Bonds}]{h\nu,\Delta} R\cdot$$

$$R\cdot + \cdot O{-}O\cdot \rightarrow RO_2\cdot$$

$$RO_2\cdot + RH \xrightarrow{k_p} ROOH + R\cdot$$

Secondary:

Thermal Decomposition Of Hydroperoxide

$$ROOH \xrightarrow{\Delta} RO\cdot + \cdot OH$$

Yields

Aldehydes, Carboxyls, Carbenes, Alcohols, Oxygenated Compounds:

$$RO\cdot + RH \xrightarrow{k_a} ROH + R\cdot$$

$$RO_2\cdot + RH \xrightarrow{k_p'} ROO\dot{R}H \xrightarrow{k_p''} R(R{=}O)R + :C{=}O$$

Interesting Notes:

Its Fast:

$$\sim\!\!\underset{\underset{Ph}{|}}{CH}\cdot + CH_2{=}\underset{\underset{Ph}{|}}{CH} \xrightarrow{k_p} \sim\!\!\underset{\underset{Ph}{|}}{CH}CH_2\underset{\underset{Ph}{|}}{CH}\cdot$$

$$\sim\!\!\underset{\underset{Ph}{|}}{CH}\cdot + O_2 \xrightarrow{k_0} \sim\!\!\underset{\underset{Ph}{|}}{CH}OO\cdot \qquad \frac{k_0}{k_p} \approx 1 \times 10^6$$

Metal Salts Catalyze It:

$$M + O_2 \rightarrow M^{\delta+}O_2{}^{\delta-} \qquad (M = \text{metal complex})$$

$$MO_2 + RH \rightarrow M + R\cdot + HO_2\cdot$$

$$RH + O_2 \underset{k_{-a}}{\overset{k_a}{\rightleftharpoons}} \underset{\text{substrate and oxygen complex}}{[RH \ldots O_2]} + RH \xrightarrow{k_b} 2\,R\cdot + H_2O_2$$

$$ROOH + [M]_n \xrightarrow{k_1} \text{radical}$$

$$ROOH + M(II) \xrightarrow{k_{1a}} RO\cdot + M(III) + HO^-$$

$$ROOH + M(III) \xrightarrow{k_{1b}} RO_2\cdot + M(II) + H^+$$

Noteworthy Exception:

Initiation by direct reaction of the organic substrate and molecular oxygen,

$$RH + O_2 \rightarrow R\cdot + HO_2\cdot \qquad \text{(D.I.)}$$

is, for most hydrocarbons, thermodynamically and kinetically, unfavorable. Reaction (D.I.) is highly endothermic and must be a very slow reaction at low temperatures, because the bond dissociation energy of the C—H bond (>75 kcal mole^{-1}) is much higher than that of the H—O_2 bond (45 kcal mole^{-1}).

Kamiya and Niki 78

Table 6, Impact of Contaminants

PTFE tape contaminated with Mobil DTE 25 oil tested with FTIR spectrometer.

Temperature, °C	Gaseous products
<175	Nothing Detectable
175	Hydrocarbons
260	Hydrocarbons, CO_2, $C_xH_yO_z$
280	Hydrocarbons, CO_2, $C_xH_yO_z$, CO, H_2O
285	Ignition
>285	Hydrocarbons, CO_2, $C_xH_yO_z$, CO, HF, COF_2, CF_4, SiF_4

Clean PTFE tested with FTIR spectrometer.

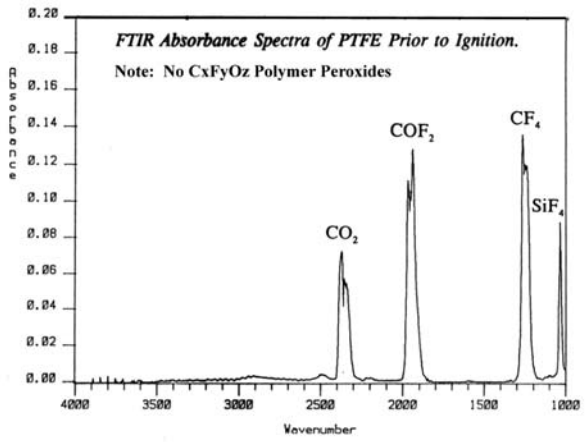
Temperature, °C	Gaseous products
327	Nothing Detectable
<390	Nothing Detectable
450	CO_2, COF_2
520	CO_2, COF_2, CF_4, SiF_4
525	Ignition
610	CO_2, CO, COF_2, CF_4, SiF_4
660	SiF_4

Shelly Et Al 93

PTFE tested with FTIR spectrometer.[a]

Temperature K	Temperature (°C)	Gaseous Products	DSC Features
600	(327)	Nothing Detectable	Melting point
<663	(<390)	Nothing Detectable	Not tested
723	(450)	CO_2, COF_2	"
793	(520)	CO_2, COF_2, CF_4, SiF_4[b]	"
798	(525)	Ignition	"
883	(610)	CO_2, CO, COF_2, CF_4, SiF_4	"
933	(660)	SiF_4	"

[a]PTFE (Teflon grade 8A), 250-mg samples, 10 K/minute, 150-SCCM oxygen.
[b]SiF_4 is an artifact of quartz tube reaction with fluorine.



HDPE tested with FTIR spectrometer.[a]

Temperature K	Temperature (°C)	Gaseous Products[b]	DSC Features
408	(135)	Nothing Detectable	Melting point
473	(200)	Nothing Detectable	Pre-exotherm
523	(250)	$C_xH_yO_z$, CO_2, CO	Beginning of exotherm
548	(275)	$C_xH_yO_z$↑, CO_2↑, CO↑, H_2O	Plateau of exotherm
568	(295)	Ignition	"
573	(300)	$C_xH_yO_z$↑, CO_2↑, CO↑, H_2O	"
758	(485)	$C_xH_yO_z$↓, CO_2↑, CO↑, H_2O	"

[a]HDPE (Quantum, LR 720), 250-mg samples, 10 K/minute, 150-SCCM oxygen
[b]↑: Quantity increasing at that temperature; ↓: Quantity decreasing at that temperature

Tapphorn Et Al 91

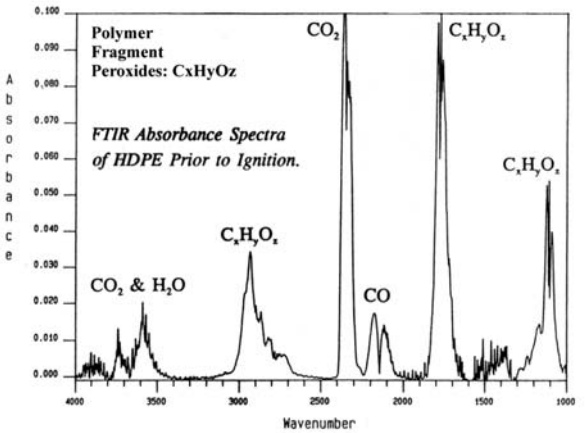


Figure 14a, Chemical Thermal Degradation Breakdown Products Vs Temperature: PTFE and HDPE

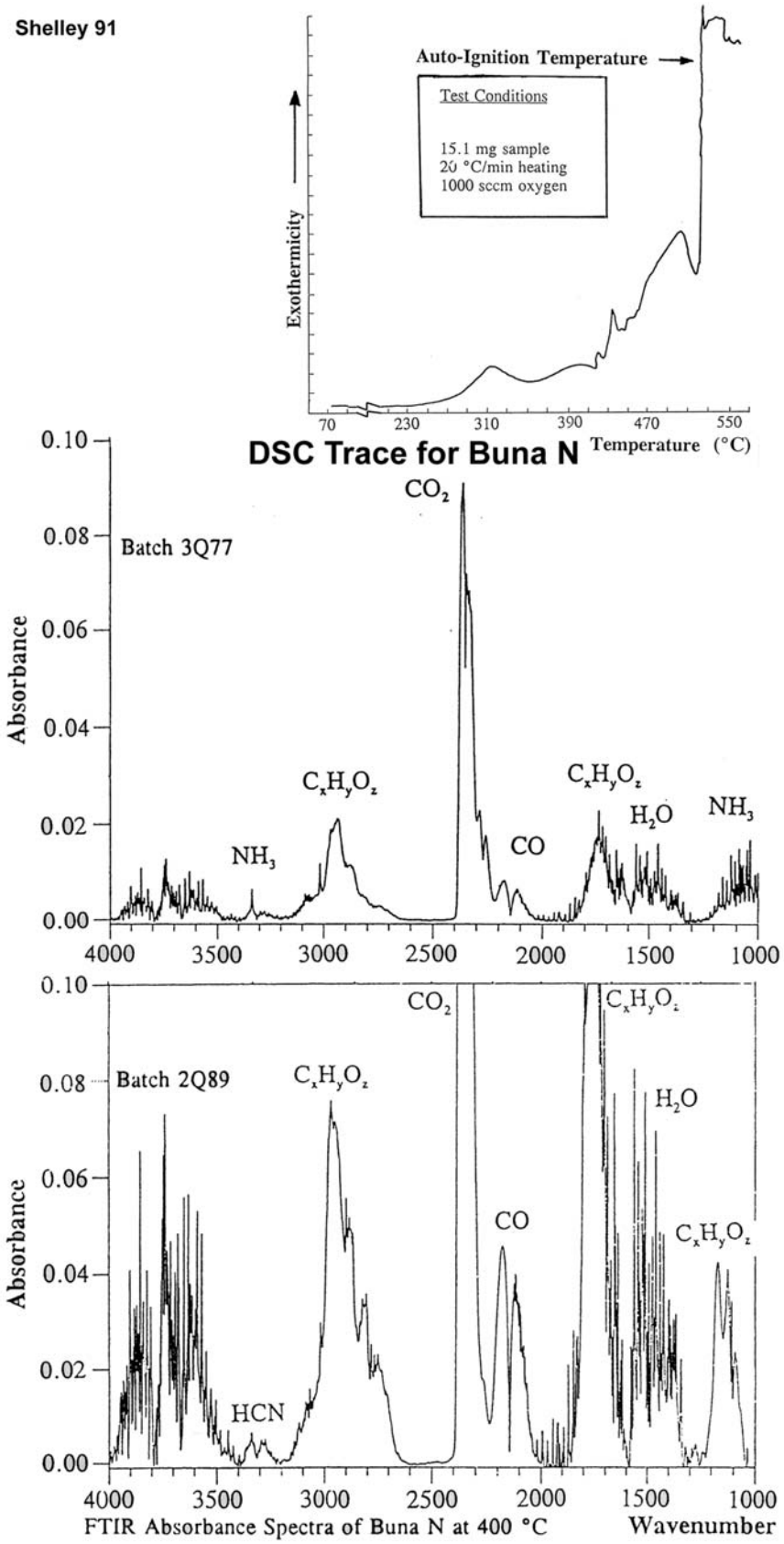


Figure 14b, Chemical Thermal Degradation Breakdown Products Vs Temperature: BUNA N

The chemical by products of the fuel breakdown and peroxide oxidation chemistry are now very hot, small molecular weight chemicals in a gaseous physical state. These gaseous state compounds then evolve their way to the fuel's nominal surface and then into the LOX as shown in figure 12d. The rate at which this emanation of the oxidized volatile fuel into the adjoining LOX as a gas progresses is governed by the material and circumstance specific gasification rate. This next step in the ignition event of a PMC fuel is known as gasification.

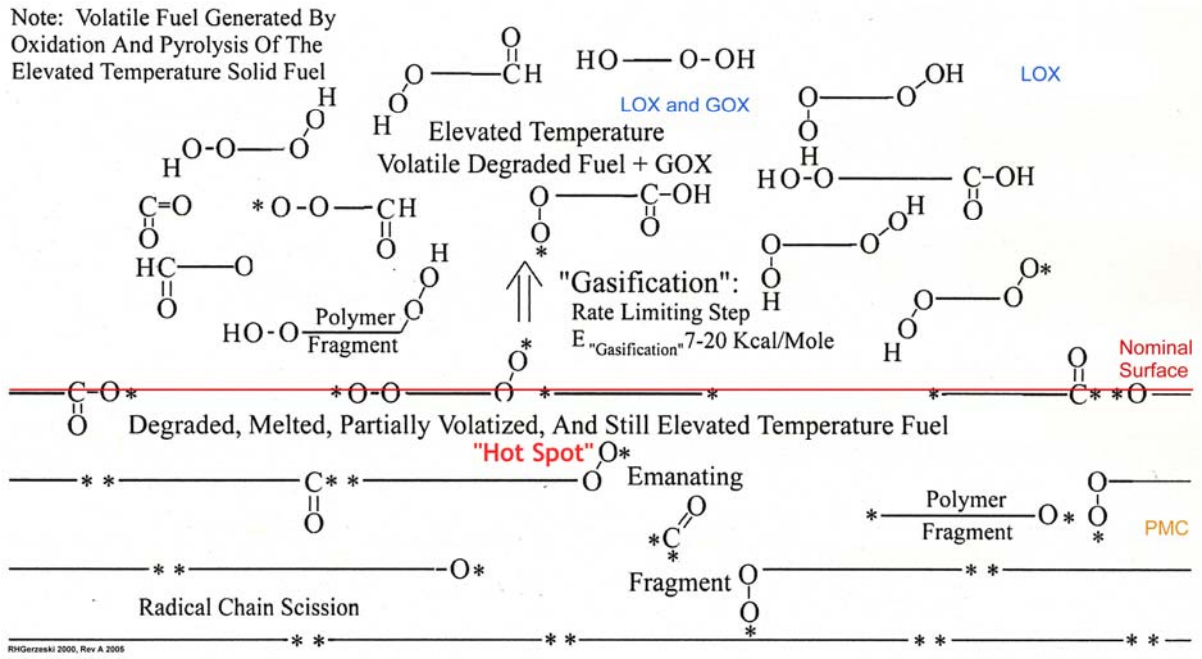


Figure 12d, Ignition Event: Gasification

When a solid material is transformed directly into a gaseous material, as is happening to the PMC fuel during the chain scission and oxidation steps of the ignition event, the resultant gas is formed directly into an above atmospheric pressure physical state. This pressure pulse is such in metals, that have progressed to this point in the ignition event, that the evolving gas creates microscopic blow-holes through to the surface of metals. These have been reported as evidence of LOX micro reactions, and are not considered to be counted as reactions in various LOX compatibility tests such as D2512-G86. These pressure pulses of emanating gas (ie the gasification ignition event step) occurring in PMC fuels would act on the composites' laminate plys like a wedge being driven into them from the edge. This would be like a double cantilever beam loading on the composite. The resultant would be ply delamination in the PMC starting at the edge of the hot spot and progressing away from there into that part of the PMC fuel which did not experience the ignition event.

The emanation of the degraded and peroxide chemistry oxidized PMC fuel out of the PMC via the mechanism of gasification continues building up a gaseous bubble. The bubble forms just above the local energy injection site above the hot spot in the PMC as shown in figure 12e. This is the next step in the ignition event called fuel bubble formation. The fuel bubble consists of the degraded and peroxide oxidized PMC fuel and a mix of LOX and now GOX (as the emanating fuel is hot and it heats the LOX into GOX).

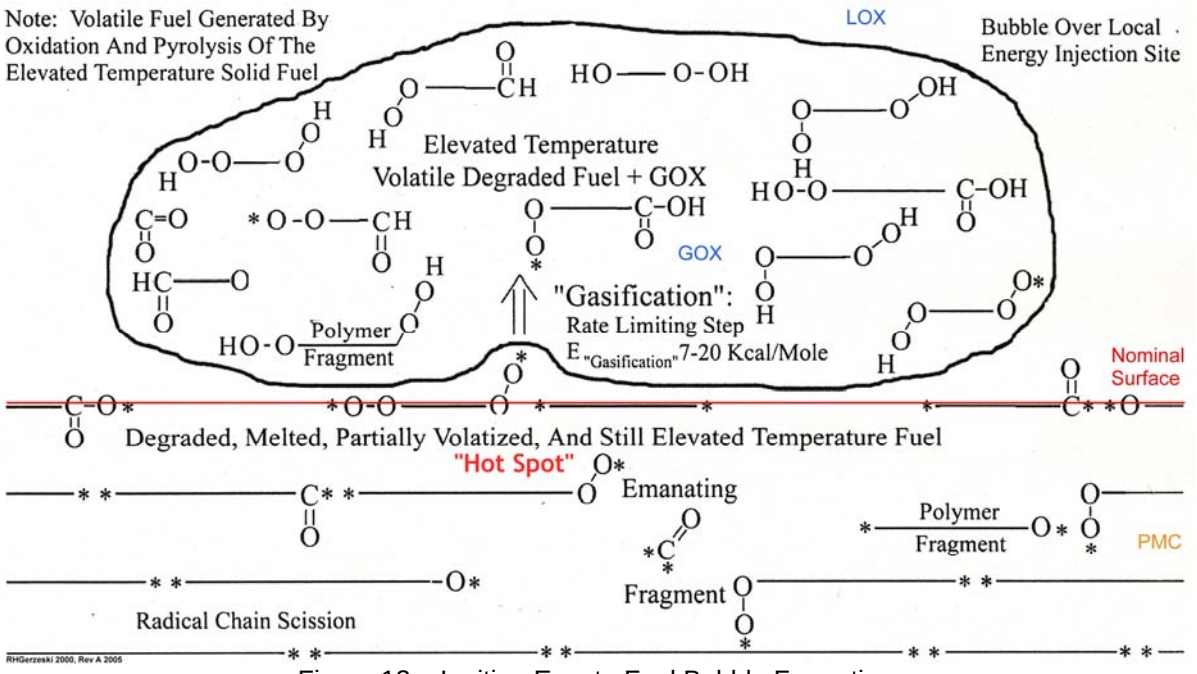


Figure 12e, Ignition Event: Fuel Bubble Formation

If the temperature in the PMC fuel's hot spot is sustained long enough, the concentration of the degraded and peroxide chemistry oxidized PMC fuel in the fuel bubble will continue to increase as shown in figure 12f until it reaches its lean burn flammability limit. Also all of the oxygen in the fuel bubble will have been heated into gaseous oxygen. When this minimum fuel / GOX mix condition is met combustion begins. This combustion completes the oxidation of the degraded and peroxide chemistry oxidized PMC fuel in the bubble into the final combustion products of CO_2 and H_2O. This marks the next step in the ignition event: lean burn combustion. When it happens it usually generates extremely rapid spike like rises in the temperature of the fuel bubble and the remaining PMC in the original local hot spot and a rise in the pressure of the fuel bubble.

If the combustion of the degraded and peroxide chemistry oxidized PMC fuel in the fuel bubble generates a sufficient amount of heat, radiated back onto the PMC, then the formation and gasification of degraded and peroxide chemistry oxidized PMC fuel will continue and expedite. This fuel will then be combusted in the fuel bubble and raise the bubble's and the PMC's temperature. If this cycle sustains itself until the temperature of the fuel bubble and the PMC rises up to the matrixes' adiabatic flame temperature then the final step in the ignition event depicted in figure 12g occurs: sustained combustion. If this final step in an ignition event occurs then the PMC is on fire as all organic materials (such as PMCs) burn in the vapor phase above the fuel.

Table 7 attempts to correlate the physical chemical processes occurring at various ignition event sequence steps to D2512's indication of reactions types. The table implies that flash reaction indications should be more frequent than char or explosion/noise type reaction indications. It also implies that when explosion/noise type reactions are detected, flash type reaction indications should also be simultaneously detected.

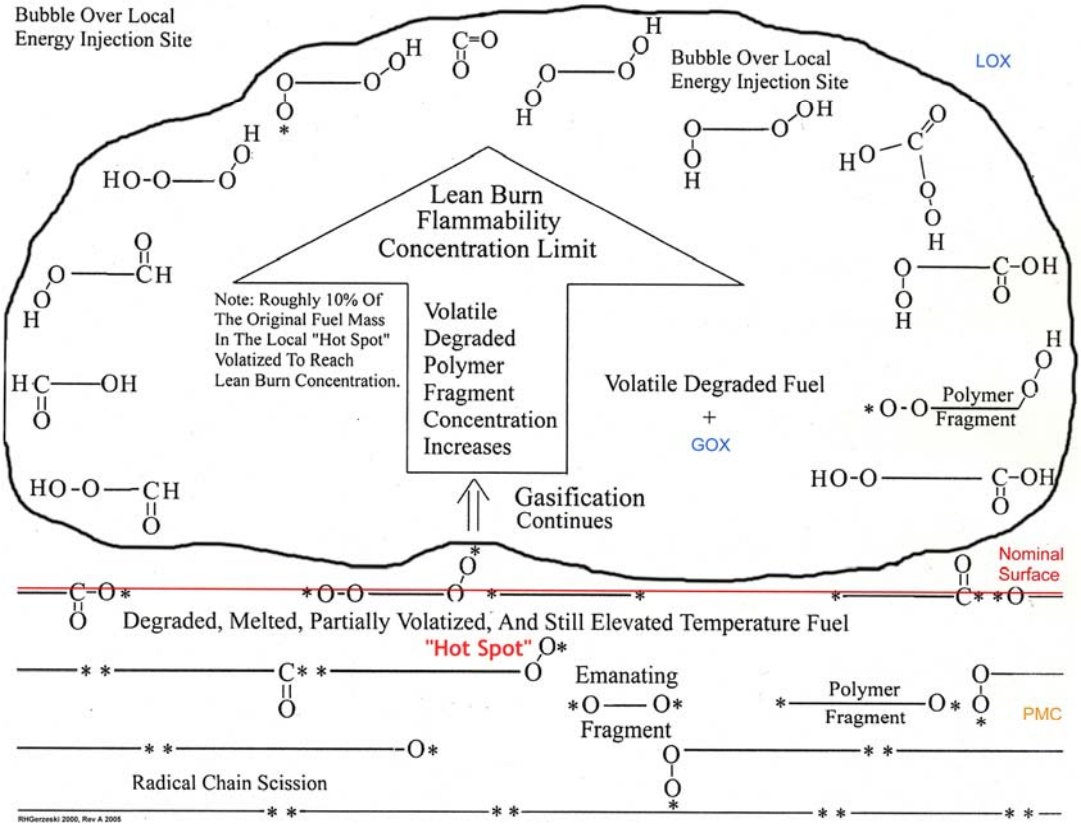


Figure 12f, Ignition Event: Lean Burn Combustion

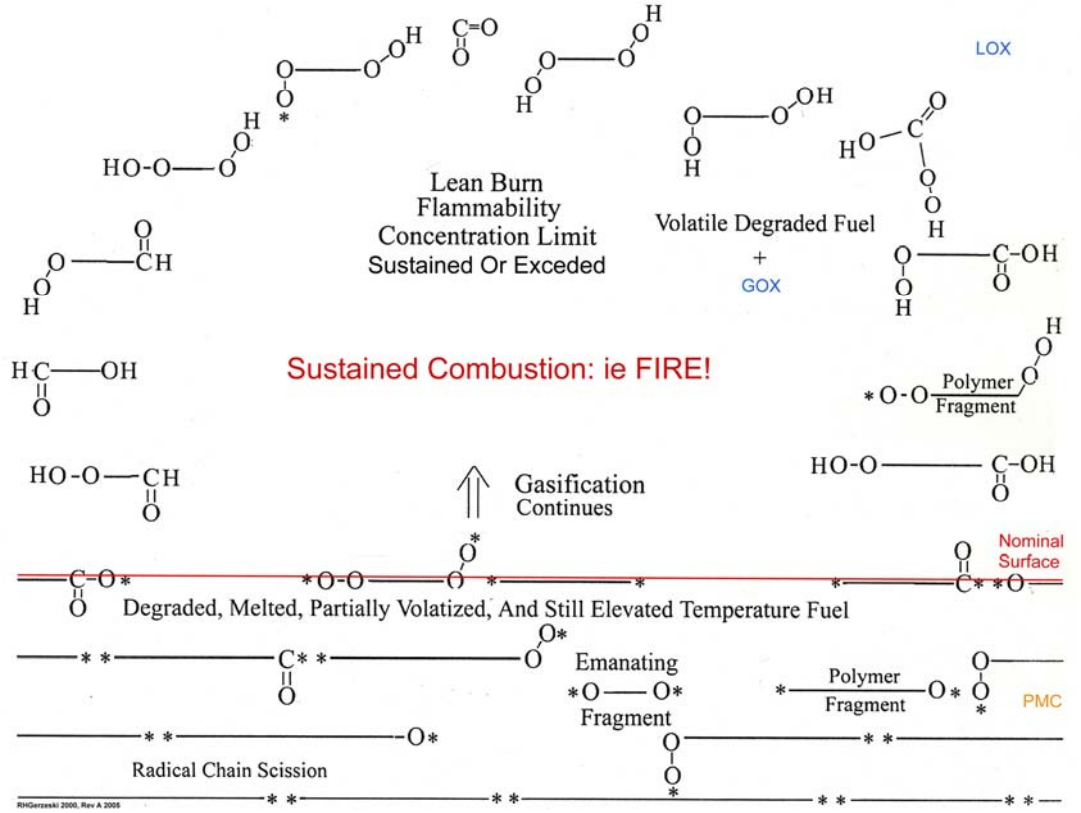


Figure 12g, Ignition Event: Sustained Combustion: Fire

Table 7, Possible Correlation Of Ignition Event Sequence To D2512 Reaction Indications

Ignition Event Sequence	**Mechanism**	**D2512 Reaction Indication**
Possible Source: Radical Chain Scission Peroxide Oxidation Chemistry <u>Probable Source:</u> Gasification Fuel Bubble Formation Lean Burn Combustion Sustained Combustion	Changes In The Electron's (ie The Radical's) Wave Function Between Various Excited and Excited And Ground States Caused By The High Temperature Of Their Environment	Flash
Possible Source: Radical Chain Scission Peroxide Oxidation Chemistry <u>Probable Source:</u> Gasification Fuel Bubble Formation Lean Burn Combustion Sustained Combustion	Freezing Out Of The Radical Chain Scissioned And Peroxide Chemistry Oxidized PMC Fuel, When Either It Diffuses Out Of The Fuel Bubble Into The LOX and Cools Down Or When Insufficient Heat Is Generated At The Local Energy Injection Site's Hot Spot And The Degraded Oxidized Fuel Subsequently Cools	Char
Possible Source: Gasification Fuel Bubble Formation <u>Probable Source:</u> Lean Burn Combustion Sustained Combustion	Generation Of Hot Gas Phase Scissioned And Peroxide Chemistry Oxidized PMC Fuel Generation Of Very Hot High Pressure CO_2 and H_2O Gas Resulting From The Combustion Of The Scissioned And Peroxide Chemistry Oxidized PMC Fuel	Noise / Explosion

Theory Section: Hertzian Fracture

When an object makes forceful contact with the surface of a brittle material it sets up a unique stress field in the brittle material under and around the contacting location. [H1-H18] The object causing the contact is generically known as an indenter. Its shape can be best approximated, relative to the D2512 impact test, by a sphere or a cylinder as shown in figure 15. Also relative to this effort's interest it can also be called an "impacting indenter", "impacter", or "indenter".

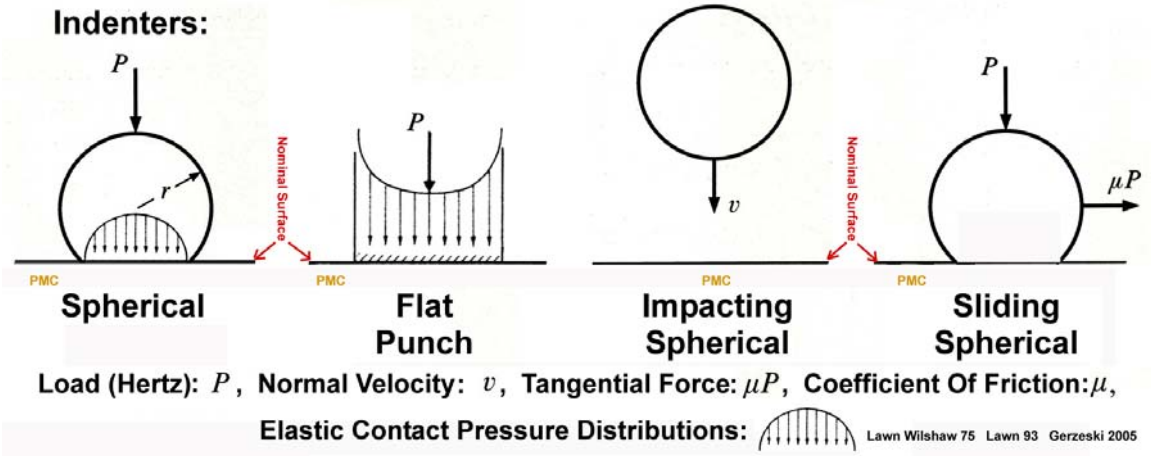


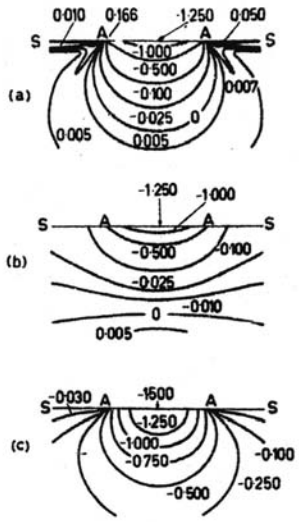
Figure 15, Hertzian Loading Indenters

The nature of the force can be static, constantly building dynamic, or impact. Figure 16 schematically depicts the unique stress field that the indenter sets up in the linear elastic up to fracture brittle material. This stress field is known as a Hertzian stress field and the mechanics that define it have been known since the late 19TH century.

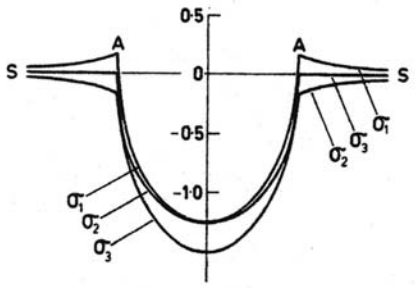
Some interesting aspects of a Hertzian stress field are the location, intensity and type of stresses developed. The zone immediately under the indenter is in compression and shear to a depth into the brittle material roughly equal to the diameter of the indenter. But of significant interest to this effort are the stresses outside of the indenter's contact zone. Forming rings of constant stress immediately outside of the indenter's contact zone, the dominate stresses are primarily a radial tension stress and secondarily a hoop tension stress.

If the load applied by the indenter is increased, then a crack develops in the surface of the brittle material in the region of high tensile stress immediately outside of the indenter's contacting zone. This crack follows a trajectory defined by the surface hoop stress and forms a ring around the indenter as shown in figure 17a. If the material exhibits anisotropy, such as crystal planes, then the ring crack can take on a noncircular with linear runs shape as shown in figure 17b as these anisotropies distort the Hertzian stress field. As the load is further increased, the crack first opens up in the downward direction and then moves outward following a trajectory defined by the hoop and compressive stresses. Figure 18 schematically depicts the development of these Hertzian fractures. This trajectory causes the resulting Hertzian crack to take the shape of a cone as depicted in figure 19 and schematically defined in figure 20. The speed at which this cone portion of the Hertzian fracture develops is extremely fast, calculations by Lawn et al 74 indicate that its duration is between 20 and 70 millionths of a second The angle which the cone portion of the crack makes to the free nominal surface is dependent on the isotropic material's poissons ratio: the higher the poissons ratio, the shallower the cone.

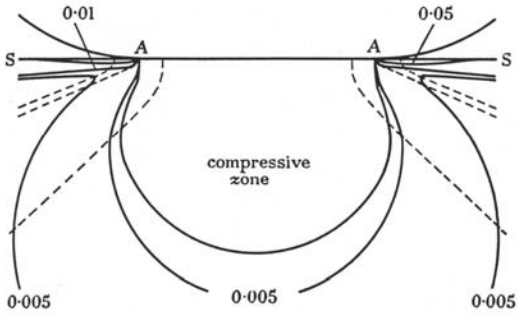
In cases of extreme load or indenter misalignment from normal to the brittle material's nominal surface, this cone crack turns again, first running parallel to, then sloping towards and eventually intersecting the closest free nominal surface as seen in figure 21. These extreme case Hertzian fractures tend to produce flakes that are dislodged from the brittle material's surface and exhibit very sharp edges. Extreme case Hertzian fracture is known as Conchoidal fracture.



Contours of principal normal stresses, (a) σ_{11}, (b) σ_{22}, (c) σ_{33}, in Hertzian field, shown in plane containing contact axis. Plotted for $\nu = 0.33$. Unit of stress is p_0, contact diameter AA is $2a$. Lawn 68 Lawn, Wilshaw 75

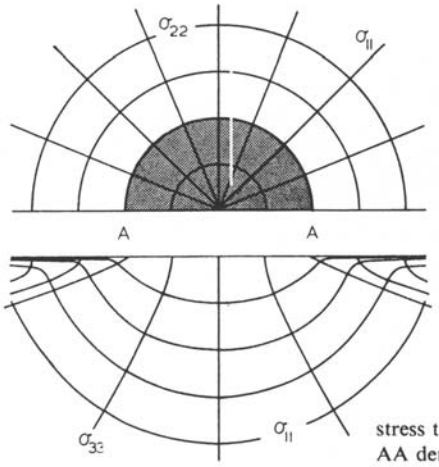


Variation of principal stresses in the surface of a semi-infinite elastic medium (SS) in contact with a spherical indenter. The stresses are measured along a line coincident with a diameter (AA) of the contact circle. p_0 is the unit of stress. **Lawn 68**



Contours of greatest principal stress, σ_1, in semi-infinite elastic medium (surface SS) in contact (diameter of contact AA) with spherical indenter. p_0 is taken as the unit of stress. Broken lines are σ_3 stress trajectories drawn from surface at distances $0{\cdot}8a$, a, $1{\cdot}2a$ from centre of circle of contact.

Frank Lawn 67



Half-surface view (top) and side view (bottom) of stress trajectories in Hertzian field. Plotted for $\nu = 0.33$. AA denotes diameter of contact. Lawn, Wilshaw 75 Lawn 68

RHGerzeski 2005

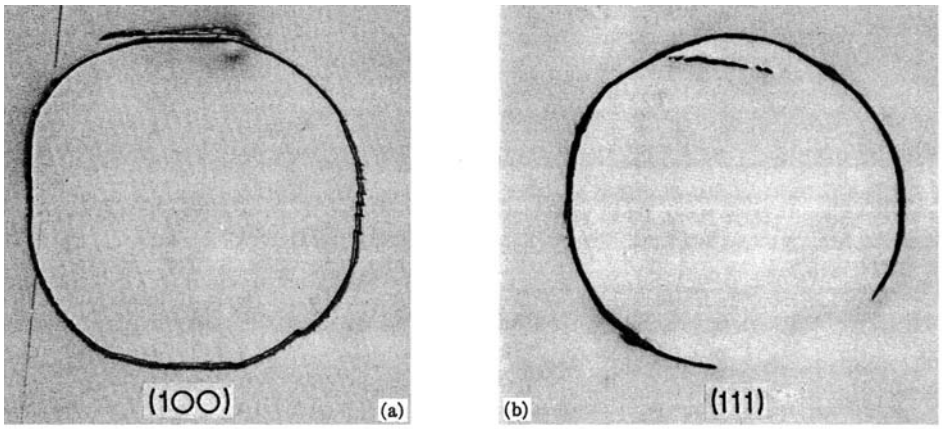
Figure 16, Hertzian Stress Field And Stress Trajectories



Surface view (reflected light) of a ring crack formed by dropping a steel ball, radius $r = 0{\cdot}875$ cm, onto a glass plate. The grease patch, radius $a = 0{\cdot}061$ cm, reveals area of contact.

Frank Lawn 67

Figure 17a, Ring Crack: Impact Generated



Diameter surface cracks 1.0 mm

Traces of Hertzian cracks on (a) (100), (b) (111), (c) (110) surfaces of silicon. Specimens lightly abraded, indented, etched, and viewed in normally reflected light. $r=0.64$ cm, $a=0.05$ cm.

Straighter Segments of surface cracks lie along traces of {111} planes.
Width of field 1500 μm.
Gaps In b and c due to impacter misalignment.

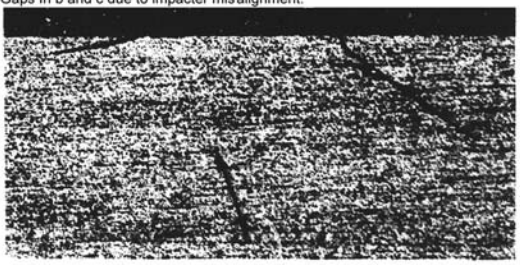
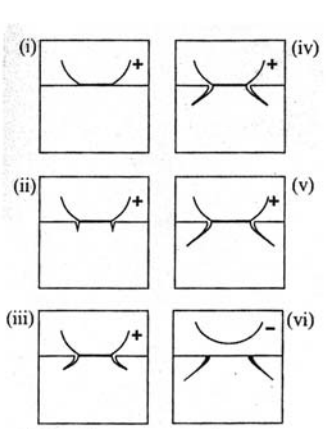


FIG. 5. Cross-sectional profile of Hertzian crack made on the (111) surface in b. Plane of diagram is (01$\bar{1}$). Double arrow indicates trace of {111} easy-cleavage plane. Specimen sawn through crack, ground, lightly etched, and viewed in obliquely reflected light.

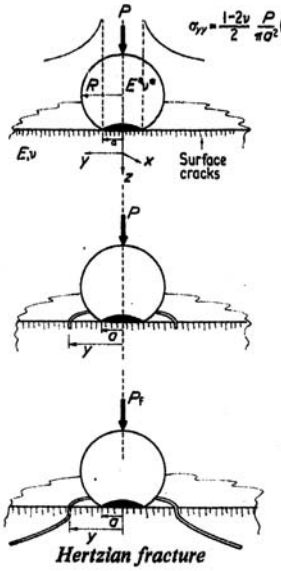
Lawn 93 Lawn 68 Lawn Wilshaw 75

Figure 17b, Ring Crack: Material Anisotropy Effects



Hertzian cone crack system. complete loading (+) and unloading parameters. Evolution of cone during (−) cycle.

Lawn 93

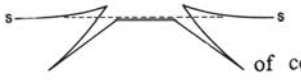


Hertzian loading arrangement showing a schematic array of surface cracks.

Hertzian ring crack development around the σ_{yy} principal stress trajectories, from one of the surface cracks.

Hertzian cone crack fully developed along a schematic representation of a principal stress trajectory from a surface crack at a position y/a in the field.

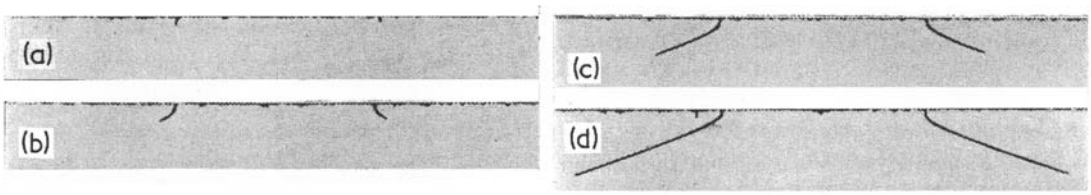
Wilshaw 71



Schematic showing displacement configuration of cone crack walls at incompletely closed interface. Lawn Et Al 84

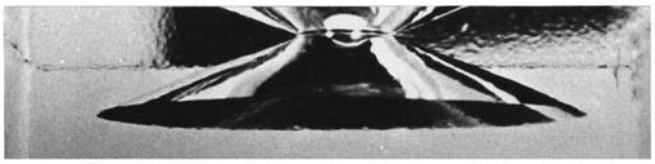
RHGerzeski 2005

Figure 18, Hertzian Cone Crack Development



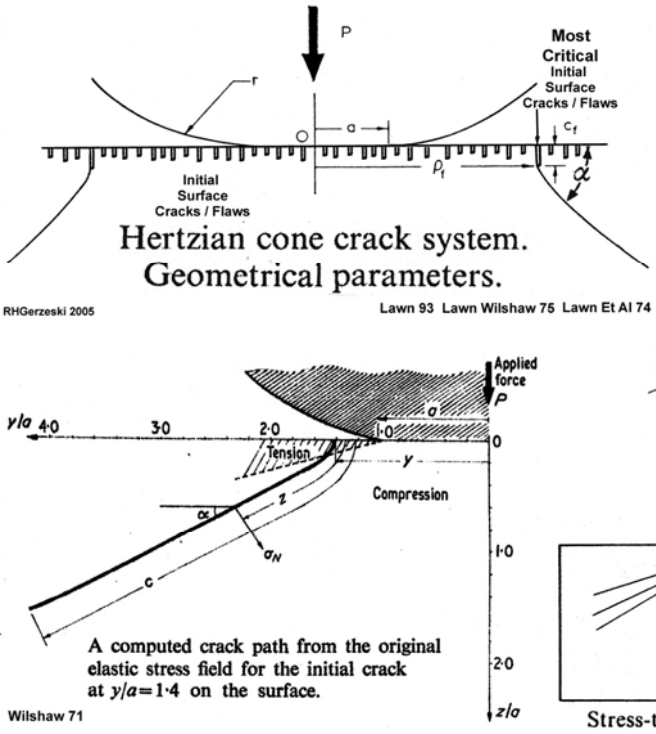
Section-and-etch sequence of Hertzian cone- crack growth in soda-lime glass in air. Load durations, (a) 0.5 sec, (b) 1.4 sec, (c) 1.7 sec, and (d) 100 sec. Note growth of "embryo" crack in (a) and (b) prior to sudden full development in (c) and (d). Width of surface ring crack 0.86 mm. Lawn, Wilshaw 75

Figure 19a, Hertzian Cone Crack Development In Glass: Section And Etch View



Cone crack in soda-lime glass. Photographed under load ($P = 40$ kN) from cylindrical punch, optical micrograph (block edge length 50 mm). Crack makes angle $\simeq 22°$ to free surface. (After Roesler, F. C. (1956) *Proc. Phys. Soc. Lond.* **B69** 981.) **Lawn 93**

Figure 19b, Hertzian Cone Crack Development In Glass: Edge View

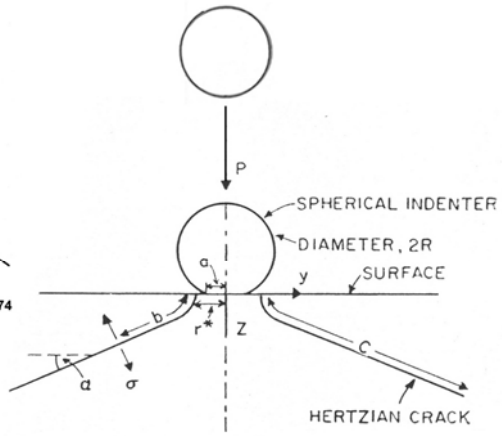


Hertzian cone crack system. Geometrical parameters.

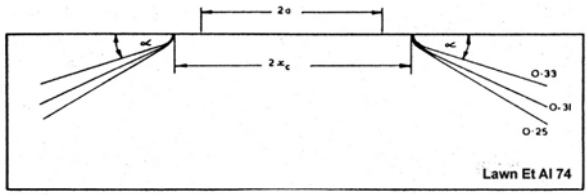
RHGerzeski 2005 Lawn 93 Lawn Wilshaw 75 Lawn Et Al 74

A computed crack path from the original elastic stress field for the initial crack at $y/a = 1{\cdot}4$ on the surface.

Wilshaw 71



Hertzian crack formed by spherical impacted indenter; σ is maximum principal tensile stress Evans 73



Stress-trajectory pattern, for three values of ν (labelled).

The Hertzian stress field has the property of geometrical similarity if all spatial coordinates are normalised to the contact radius a, and all stresses are normalised to the mean contact pressure $p_0 = P/\pi a^2$. The stresses in the OXZ plane are given by Huber as follows:

$$\frac{\sigma_{xx}}{p_0} = \left(\frac{1-2\nu}{2}\right)\frac{a^2}{r^2}\left[1-\left(\frac{z}{\sqrt{u}}\right)^3\right]+1.5\left(\frac{z}{\sqrt{u}}\right)^3\left(\frac{a^2u}{u^2+a^2z^2}\right)$$

$$+1.5\,\frac{z}{\sqrt{u}}\left[(1-\nu)\frac{u}{a^2+u}+(1+\nu)\frac{\sqrt{u}}{a}\arctan\left(\frac{a}{\sqrt{u}}\right)-2\right]$$

$$\frac{\sigma_{zz}}{p_0} = -1.5\left(\frac{z}{\sqrt{u}}\right)^3\left(\frac{a^2u}{u^2+a^2z^2}\right)$$

$$\frac{\sigma_{xz}}{p_0} = -1.5\left(\frac{xz^2}{u^2+a^2z^2}\right)\left(\frac{a^2\sqrt{u}}{a^2+u}\right)$$

where

$$u = \tfrac{1}{2}\{(x^2+z^2-a^2)+[(x^2+z^2-a^2)^2+4a^2z^2]^{\frac{1}{2}}\}.$$

The principal stresses across the crack path are $\sigma_N(x,z) = \sigma_{xx}\sin^2\alpha+\sigma_{zz}\cos^2\alpha-2\sigma_{xz}\sin\alpha\cos\alpha$ where the angle α between the crack path and specimen surface is found from $\tan 2\alpha = -2\sigma_{xz}/(\sigma_{xx}-\sigma_{zz})$. Lawn Et Al 74 RHGerzeski 2005

Figure 20, Hertzian Cone Crack Parameters

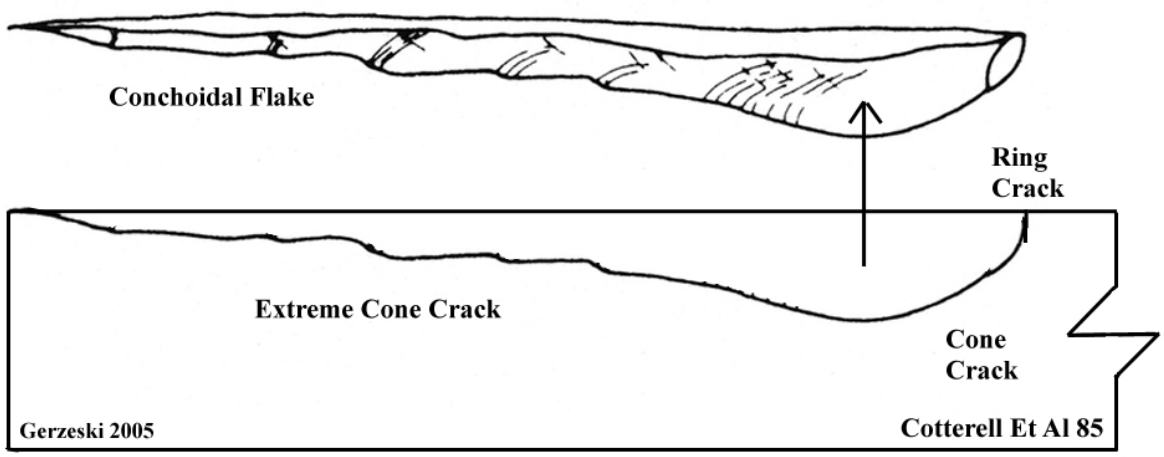


Figure 21, Extreme Hertzian Fracture: Conchoidal Fracture

If the load applied by the indenter is increased beyond the point of full Hertzian cone crack development, then compressive and shear stresses develop in the brittle material under the indenter. As depicted in figure 22 these stresses fracture the brittle material into a course powder which subsequently behaves like a "pressurized" fluid. In essence this fracturing now creates a "new" nominal bulk brittle surface from which additional cone cracks can develop. If the course powder creating fracturing in the compressive zone under the indenter continues long enough, then the stresses in the remaining bulk original material become tensile stresses. At this point the entire remaining original bulk material is in essence functioning as a miniature pressure vessel containing the fractured "pressurized" course powder. The remaining original bulk material then fails in tension at its weakest or most stressed points. These points are located directly below the center of the indenter and directly below the edge of the indenter forming what are know as "vent" cracks. These tension cracks plunge straight down relative to the original bulk material's nominal surface.

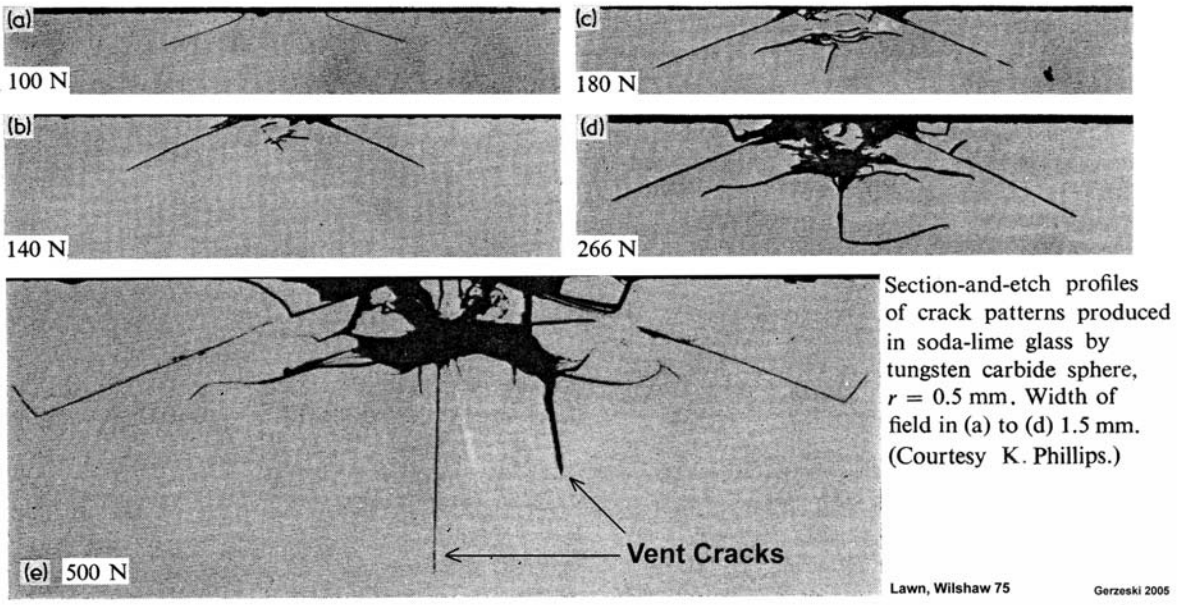
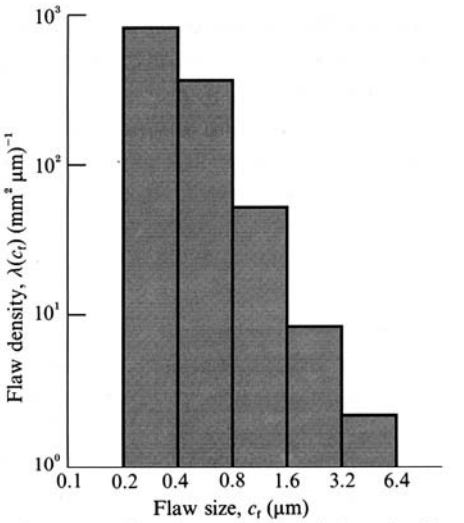


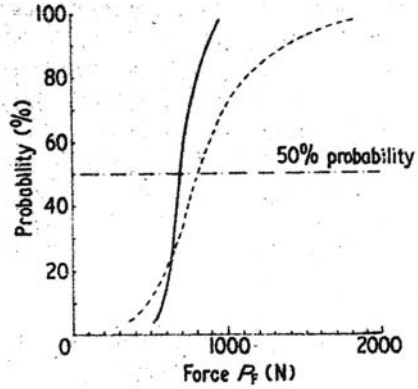
Figure 22, Compressive Zone Vent Crack Development

Initiation of the development of the Hertzian cone crack is dependent upon the size and distribution of initial inherent flaws in the surface of the brittle material. All Hertzian cone cracks initiate at the site of a preexisting flaw in the surface of the original bulk material. When a critical load is imparted to the brittle material by the indenter, the most critical of the surface cracks originally in the surface of the material near the indenter as seen in figure 20 begins to open up from the resulting surface Hertzian tensile stress and forms the ring crack. The sizes of these original surface cracks come in a gaussian distribution as shown in figure 23 over the nominal surface of the material. The existence of any particular size of flaw found at any particular point on the surface of a brittle material in the high Hertzian surface tensile stress zone resulting form an indenter's loading of the material depicted in figure 16 is probabilistic. This causes the magnitude of the necessary indenter load to initiate the development of the Hertzian ring crack and subsequent cone crack to have a distribution as shown in figure 24. This distribution can cause the ring crack initiation load to vary as much as the magnitude of the 50 percent mean probability load. This distribution can be minimized by flaw size normalizing techniques like grinding, polishing etc but the probabilistic nature of this load will always remain.

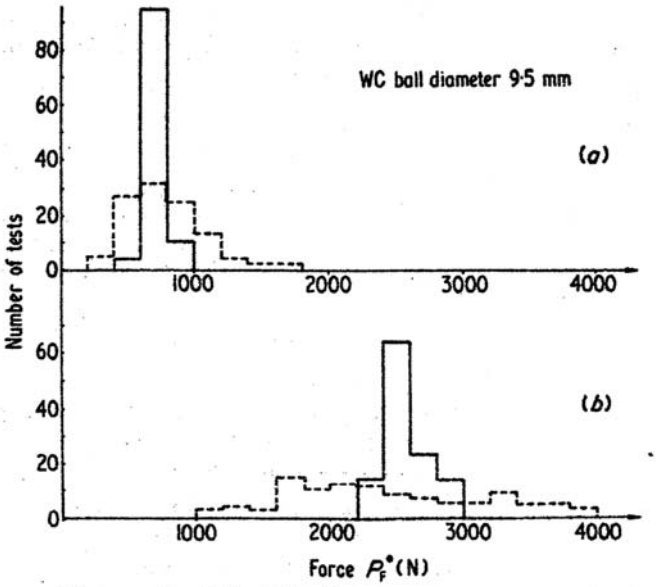


Histogram showing variation of flaw density with flaw size for 'as-received' plate glass. Results from Hertzian tests, tungsten carbide ball $r = 0.35$ mm, $N = 99$, $N' = 97$. (After Poloniecki, Wilshaw, (1971) *Nature* **229** 226.) **Wilshaw 71 Lawn 93**

Figure 23, Flaw Density



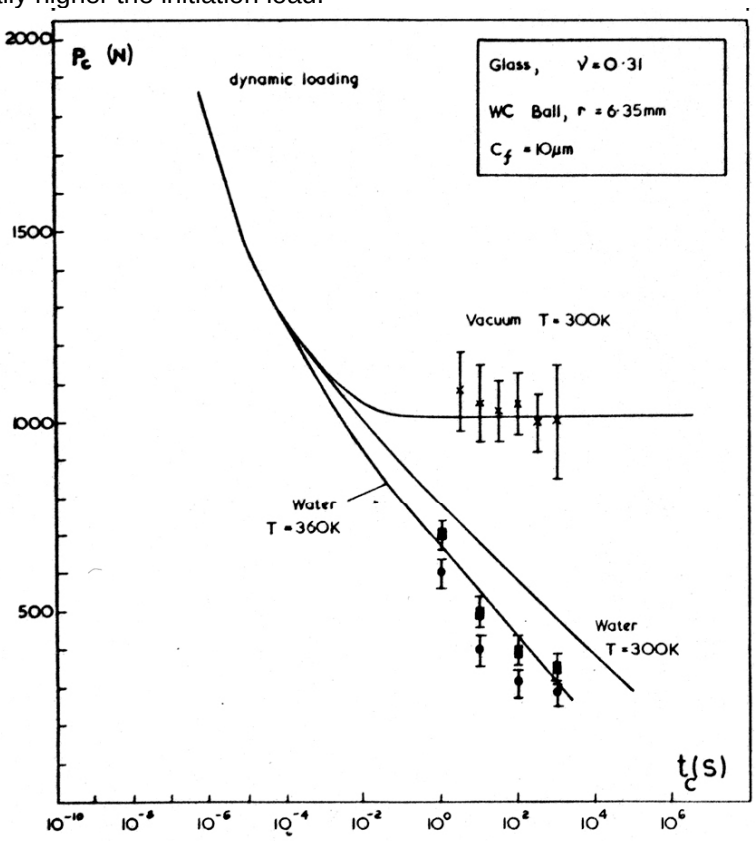
Hertzian fracture forces of as received and abraded untoughened glass. — abraded, - - as-received cumulative distributions.



The results of Hertzian fracture tests on as-received and thermally toughened, abraded and unabraded glass specimens. — abraded, – – as-received. (*a*) toughened, (*b*) thermally toughened.

Figure 24, Ring Crack Initiation Load Probabilities

In addition to the dependence of the Hertzian cone crack fracture initiating load being dependent upon the availability and size of initial surface cracks in the original brittle material, the rate of loading, the environment in which the loading occurs, and the innate toughness of the material also shift the magnitude of this load. Figure 25 depicts the effect which the rate of loading and the environment of the loading has upon the magnitude of the load necessary to initiate the development of the Hertzian cone crack fracture. The magnitude of the fracture initiation load increases with faster loading rates such as impact indention and can be substantially changed by the presence of a fluid like water. The toughness of the original brittle material can also significantly impact the magnitude of the fracture initiation load. As implied by the results in figure 24 and table 8 the tougher the material the substantially higher the initiation load.



Lawn Et Al 74

Variation of fracture load with load duration and environment. Smooth curves indicate computer predictions, data points indicate test results in water $T = 300$ K (squares), $T = 360$ K (circles) and vacuum (data courtesy J. J. H. Beek and M. V. Swain).

Figure 25, Effect Of Load Duration And Environment On Hertzian Fracture Initiation Load

Table 8, Material Toughness Influences On Hertzian Fracture Initiation Loads

Critical Loads for Hertzian Crack Formation

Material	Surface finish	Sphere diameter (mm)	Critical load (N)
SiC	Ground	5	$4.8 \pm 0.6 \times 10^2$
”	”	10	$1.0 \pm 0.1 \times 10^3$
”	”	20	$2.1 \pm 0.2 \times 10^3$
Al_2O_3	Ground	5	$9.0 \pm 0.8 \times 10^3$
”	”	10	$1.8 \pm 0.1 \times 10^4$
”	”	20	$4.0 \pm 0.3 \times 10^4$
Soda-lime glass	Abraded	5	$3.0 \pm 0.4 \times 10^2$
”	”	10	$5.9 \pm 0.8 \times 10^2$
”	”	20	$1.4 \pm 0.1 \times 10^3$
”	As-received	10	$7.2 \pm 1.0 \times 10^3$

Evans 73

Throughout this discussion the orientation of the main concentric axis of the indenter has been implicitly parallel to the normal of the original brittle material's nominal surface plane. But if the indenter's axis is even marginally misaligned, the shape of the resulting Hertzian fracture is changed. The gaps in the Hertzian ring cracks depicted in figure 17b are the result of a very slight (roughly one degree of angle) misalignment of the central axis of the punch (cylindrical) indenter used to initiate them. As depicted in figure 26 this would generate Hertzian ring and cone cracks with the appearance of crescents or half moons. The misalignment of a circular cylindrical indenter, such as the striker of the D2512 testing apparatus, would also cause the indenter contact area to become a truncated circle with sharp stress concentrating points like those found on Vickers and Knoop hardness indenters. Since they generate straight "flare" cracks as seen in figure 27 from these sharp points it can be expected that misaligned cylindrical indenters would also create straight "flare" cracks attached to the Hertzian cone crack.

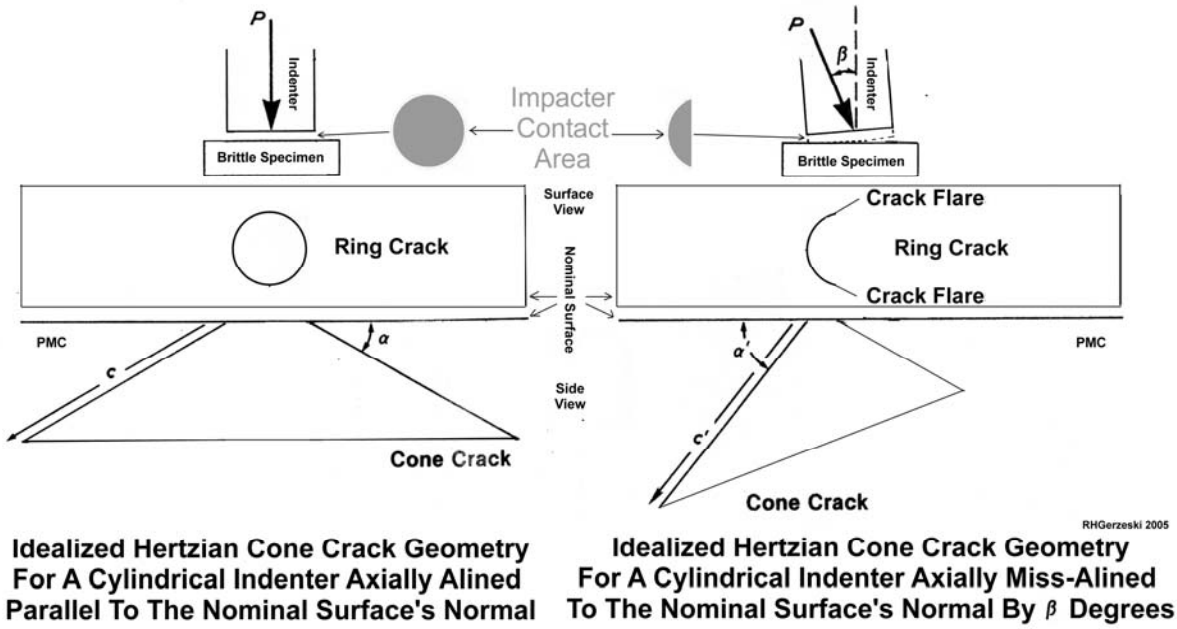
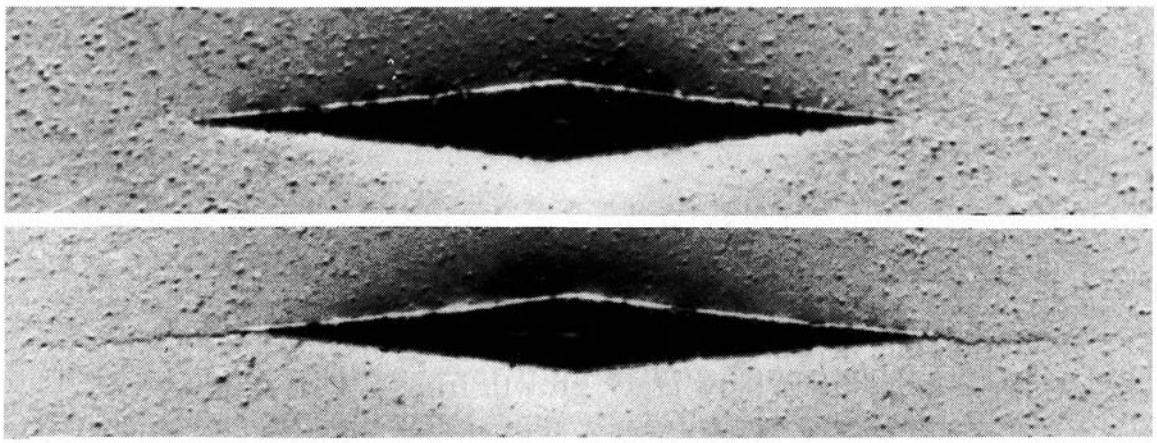


Figure 26, Impacter Miss Alignment Effects



Micrographs showing Knoop indentation in hot-pressed silicon nitride before (above) and after (below) application of stress. Width of field 400 μm. (Courtesy D. B. Marshall.) **Lawn 93**

Figure 27a, Sharp Pointed Indenter Generated Cracks: Knoop Hardness Indenter Developed

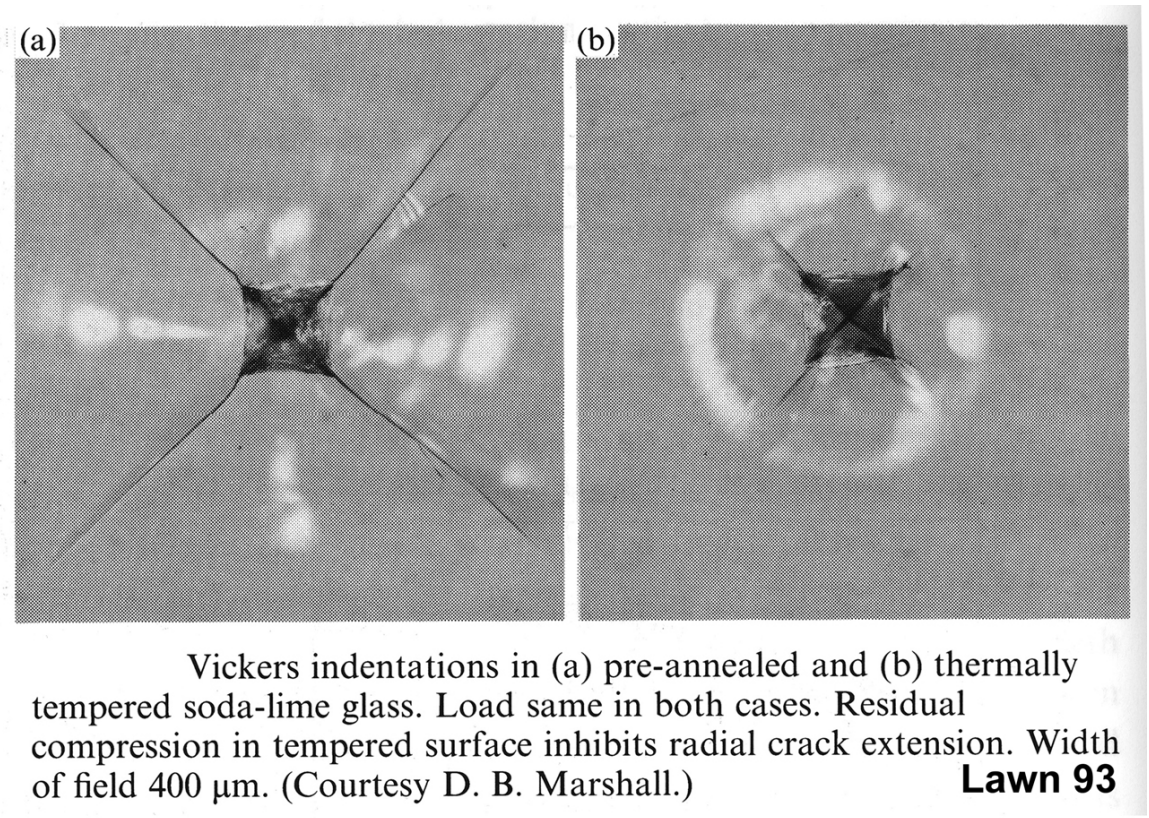


Figure 27b, Sharp Pointed Indenter Generated Cracks: Vickers Hardness Indenter Developed

If either the indenter or the brittle material it is loading or both should slide tangentially to one another during the loading then the sliding will substantially change the shape and magnitudes of Hertzian stress field. Figure 28 depicts these changes. The sliding, depending upon the coefficient of friction between the indenter and the brittle material, causes a significant reduction in the magnitude of the radial tension stress in the brittle material ahead of the direction of sliding and a dramatic increase in the radial tension stresses in the brittle material behind the indenter's travel direction. The increases in these rear tension stresses can be as much as 400+ percent at coefficients of friction of as little as 0.4. Due to these substantial increases in the radial tension stresses, any normal load which would ordinarily not initiate the development of a Hertzian ring crack now does. Also because the gradient of the stress fields are significantly compressed to the rear of the indenter and relieved to the front of the indenter the ring cracks formed take the shape of crescents or half moons. Additionally the sliding changes the shape and distribution of the Hertzian hoop and compressive stress fields such that if and when a Hertzian cone crack develops it will follow the trajectories of the lesser stress at a significantly steeper angle on its downward plunge into the brittle material forming steep sided crescent shaped cone cracks. These fully developed Hertzian ring and cone cracks do not form complete circular structures around the original indenter site. When the coefficient of friction climbs above 0.1 the Hertzian stress fields become so distorted that they cause the ring and cone cracks to flare off to the sides and forward of the direction of sliding and form straight ring and cone cracks to these flanks. Additionally, because of the relative movement of the indenter brittle material pair, fresh material is constantly moving into the Hertzian stress field developed by the indenter. This causes new crescents of Hertzian ring and cone cracks to develop and leaves a series of these cracks stacked adjacent to and on top of one another in the direction of sliding as seen in figure 29. The higher the coefficient of friction the more and closer packed and the steeper the cone angle are the resulting Hertzian ring and cone cracks, causing the residual Hertzian fractured brittle material left in the wake of the indenter's passing to take the form of steep sided, crescent, partial cone shaped sleeves with flares of brittle material on their flanks.

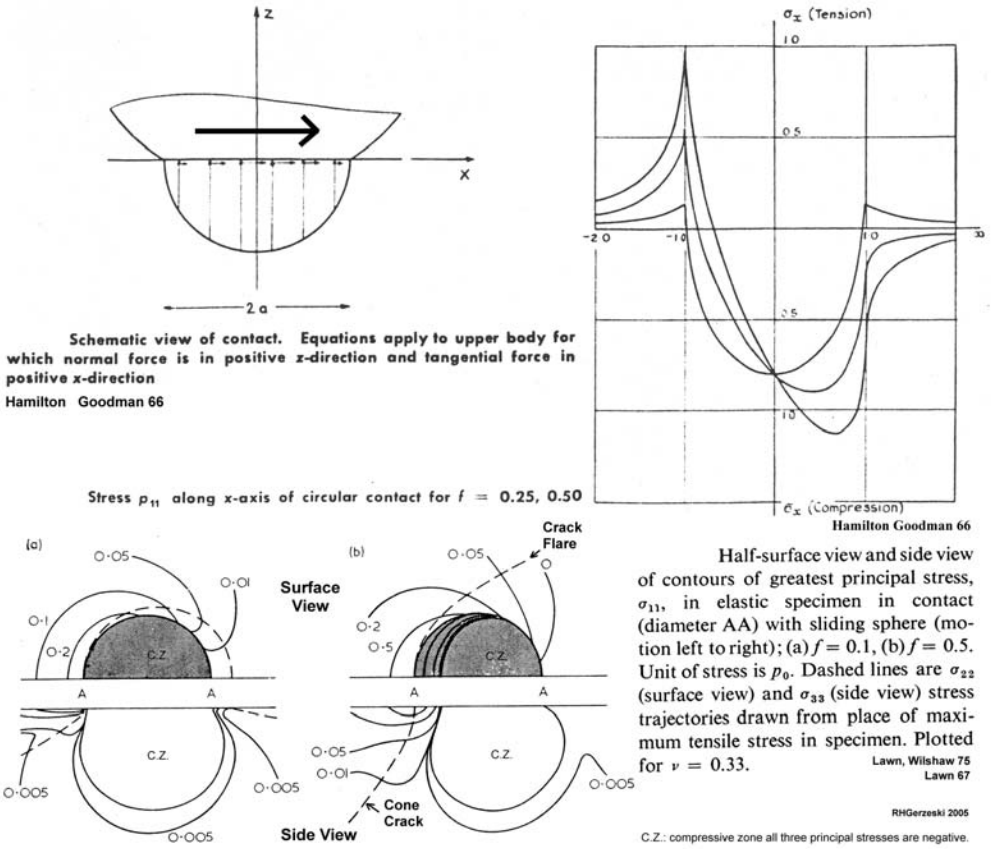
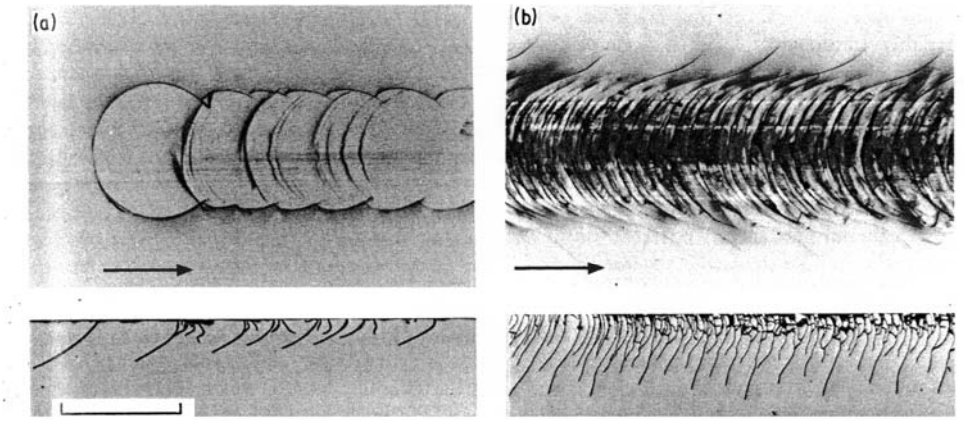


Figure 28, Sliding Impacter Hertzian Stress Fields



Micrographs showing surface (top) and side (bottom) views of sliding damage on soda-lime glass caused by steel sphere of radius 3.17 mm under normal load $P = 20$ N, for (a) $f = 0.1$, (b) $f = 0.5$. Cf. traces of deep cracks in side views. Index marker 0.5 mm. Width of field 2000 μm.

Lawn 93 Lawn Et Al 84



Crack patterns on soda-lime glass produced by sliding tungsten carbide sphere, $r = 1.5$ mm, $P = 10$ N, across surface, in n-decanol, $f \approx 0.12$. Etched surfaces, viewed in transmitted light. Width of field 1.25 mm. (Courtesy of G. M. Crimes.) Lawn, Wilshaw 75

Wear track on quartz made by a tungsten-carbide rider. (Courtesy W. F. Brace.) McClintock Argon 66

Direction of sliding shown by the arrow.

RHGerzeski 2005

Figure 29, Stacked Hertzian Crescent Shaped Cone Cracks And Flares

Theory Section: Kinetic Friction

When two physical items are pressed or loaded against each other they make real physical contact at junctions depicted in figure 30, called asperities, at only a fraction of their apparent measurable surface.[F1-F131] This real contact area is usually no more than one hundredth at extreme loads and can be as small as one millionth at light loads of the apparent measurable surface. These asperities are usually measured by secondary inference techniques to be lengths of 100 to 1000 10^{-6} m. Due to the nature of surfaces, increasing the load marginally increases the size of these asperities but normally increases their number.

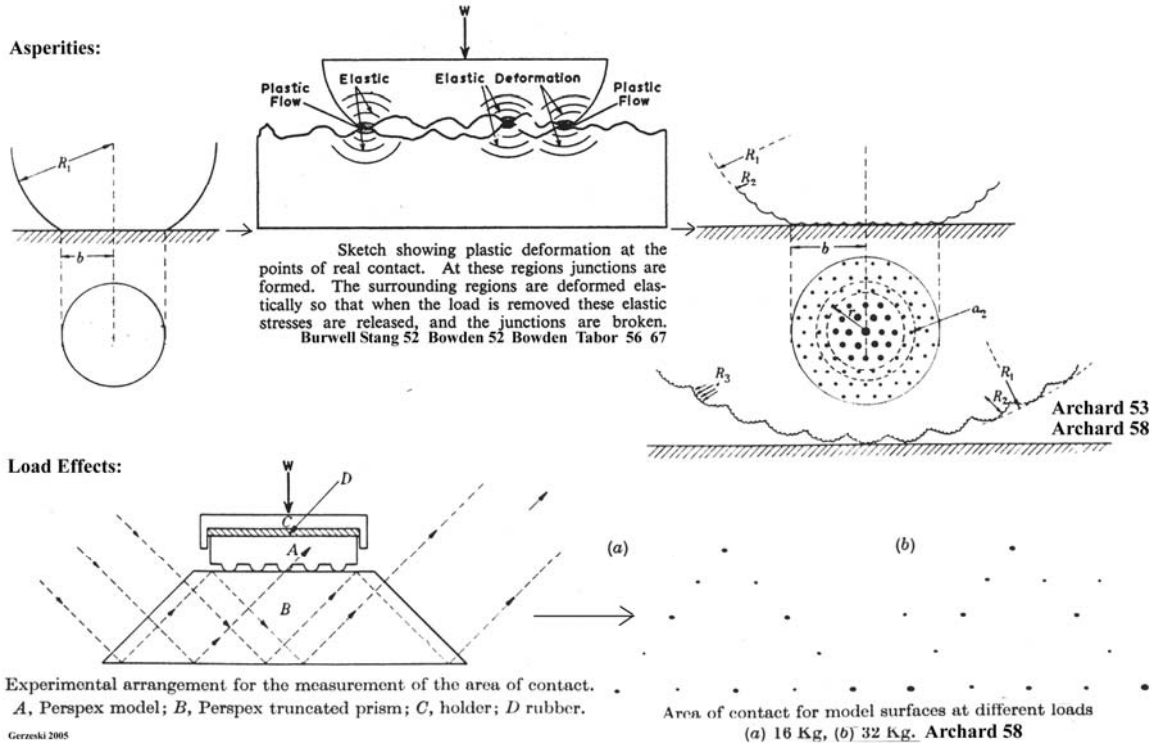


Figure 30, Real Area Of Contact

To move the two items tangentially relative to each other at a constant rate requires a tangential load be applied. The correlation between these two loads is $W = \mu F$. This resistive load is independent of the apparent area of contact and directly proportional to the pressing or normal load. This physical behavior is known as kinetic friction. The resistive load is known as the friction force and it is the only mechanical property exhibited by materials that is completely area independent.

A force versus time plotting of this friction force reveals that two types of kinetic friction motion occur: smooth slip and stick slip. Figure 31 depicts these two behaviors. For all real world normal loads and relative movement rates (sliding speeds), the stick slip behavior is most commonly displayed. This stick slip behavior arises from the constant shearing and reforming of the asperities. This behavior requires the input of energy and reveals itself as shown in figure 32 as if it were a sheet heat energy source appearing at the contacting asperities' surfaces.

This heat causes the temperatures of the immediate surfaces of the now sheared asperities to climb. The magnitude and the time for these temperature rises are astonishingly large and brief.
Figure 33 depicts examples of the magnitudes and times of the temperature rises at the sheared asperities known as "hot spots". It is very typical to measure hot spot temperature rises on the order of 100s to sometimes 1000+ degrees C under even low normal loads of a few Kgs or less and sliding speeds measured in the single digits m/sec or less. Also these temperature rises occur in millionths of a second with an average time of ~30 millionths of a second and a range of as little as 1 and as large as 50 millionths of a second. While the magnitude of these temperature rises is significantly

influenced by numerous physical properties of the sliding materials the duration of the rises is not. For all materials the typical rise time is usually roughly 30 millionths of a second and the literature does not indicate that any material physical property modifies or influences this significantly.

These temperature rises are completely localized at the sheared asperities surfaces. Work by Jaeger 42 and Bowden Et AL has shown that the temperature rise drops rapidly down to the bulk background material's temperature at no more than four to five asperity sliding lengths depth into the material. Because of this the heating and temperature rises associated with kinetic friction, or shearing of the asperities, are exclusively surface effects.

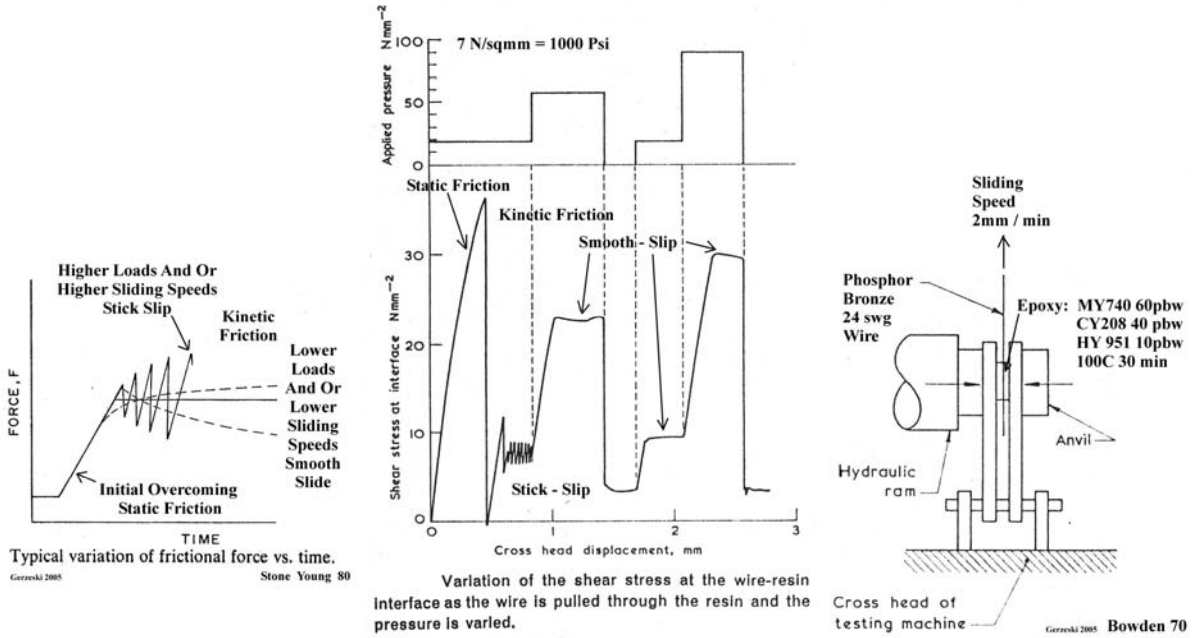


Figure 31, Kinetic Friction's Mechanical Behavior

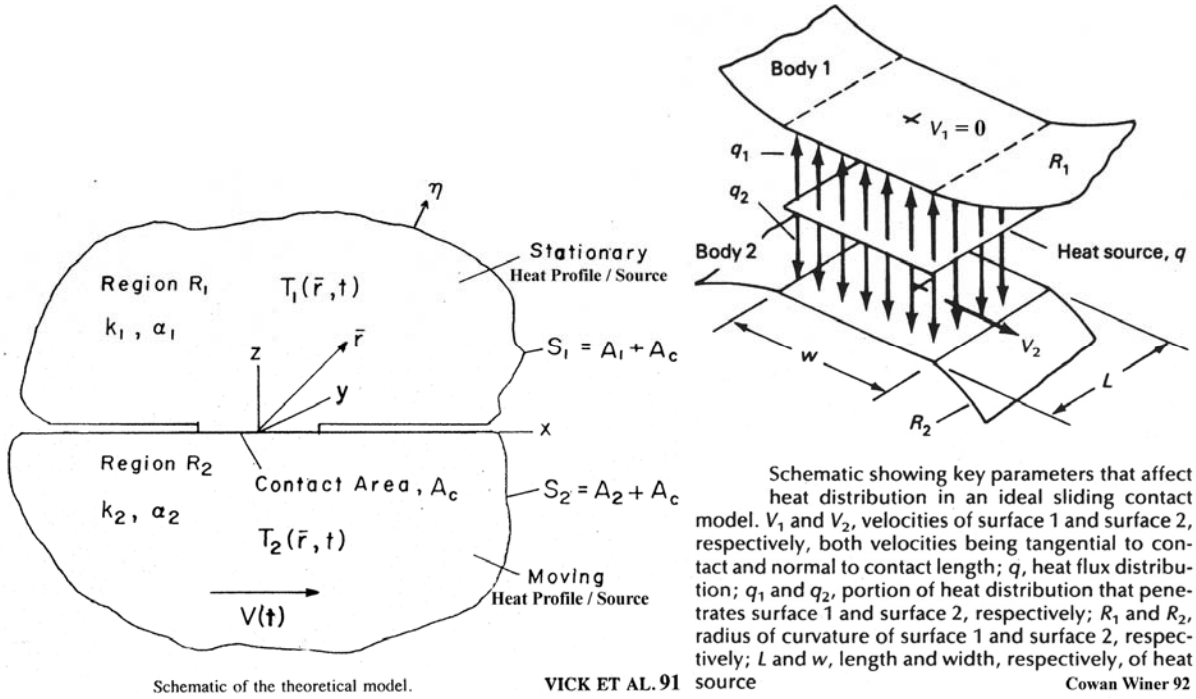


Figure 32, Kinetic Friction Thermal Transport Model

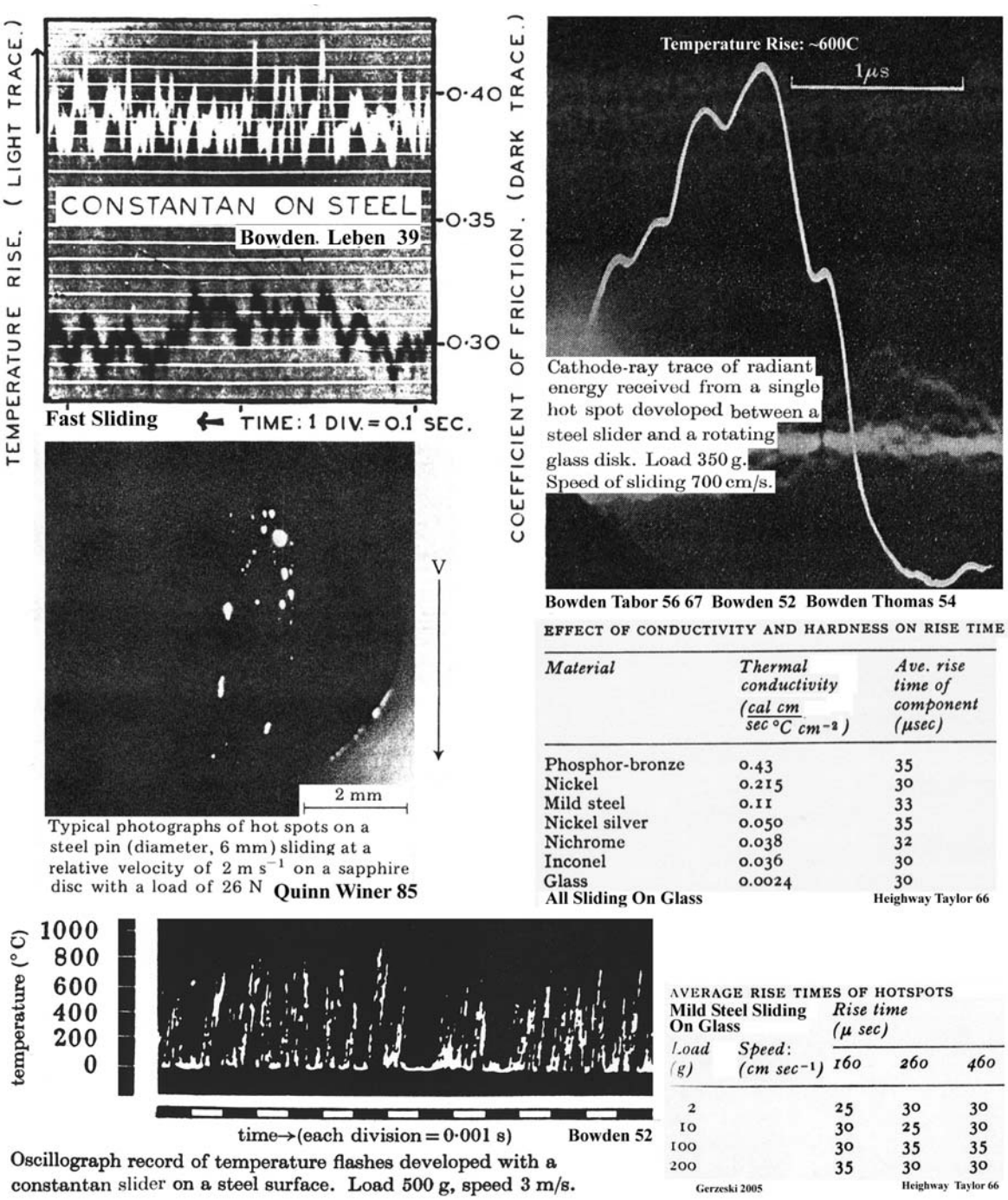
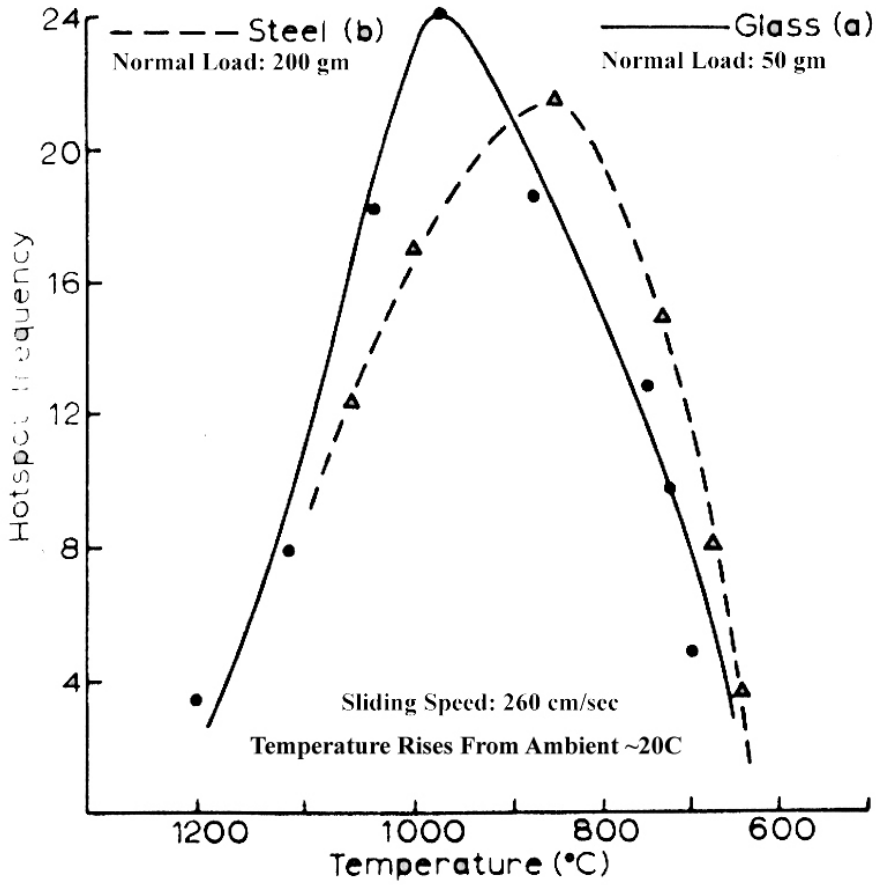


Figure 33, Sheared Asperity Temperature Rises “Hot Spot”: Magnitude and Duration

As implied by the series of hot spot temperature rises shown in figure 33, the magnitude of these rises for all of the asperities formed and sheared during the kinetic friction sliding takes on the form of a distribution function. While actually measuring the individual temperature rises at each formed and sheared asperity is in practicality extremely difficult, one effort was reported. By carefully selecting materials and detection/measurement techniques, Heighway and Taylor 66 collected and plotted the general distribution of these rises as shown in figure 34. The distribution takes on the form of a parabola bounded by the average temperature rise ($\triangle T_{Max_{Avg}}$) at its apex and the maximum ($\triangle T_{Max_{Max}}$) and minimum temperature rises defining its feet.



Temperature distributions for
(a) glass rubbing on glass and
(b) steel rubbing on glass. Heighway Taylor 66

Figure 34, Hot Spot Temperature Rise Distributions

Analytical models have been developed by Bowden, Thomas, Ridler, Archard, Blok and most importantly Jaeger over the past 75 years to predict the apex and feet conditions of the parabolic distribution of probabilistic temperatures depicted in figure 34. All of these models begin with a round, square, blade or rectangle asperity shape model and energy balance depicted in figure 32 assuming that the entire normal load is supported by one sliding asperity. While the real world probability of any real surface kinetically sliding on one asperity is very small, the developed models have provided an insight into the critical variables associated with the hot spot temperature rises. These models have been perfected by Cowan, Winer, Quinn, Tian, Kennedy, Vick, Furey, and Foo to take into account different asperity shapes, such as additionally parabola, the impact of different sliding speed regimes, and the effect of multiple sliding asperity contacts.

Basically the hot spot $\triangle T_{Max_{Avg}}$ temperature rise equations developed by Bowden and Jaeger in the late 1930s and early 1940s still apply. They predict the formulas shown in table 9 for circular and square like asperities for the same material sliding on itself.

Predicting $\triangle T_{Max_{Max}}$ is a far more difficult and imprecise thing. Effectively the works of the latter above group and Jaeger have shown it to have the values indicated in table 9 relative to the associated $\triangle T_{Max_{Avg}}$ values.

Table 9, $\triangle T_{Max_{Avg}}$ and $\triangle T_{Max_{Max}}$ Hot Spot Temperature Rise Predictive Formulas

$\triangle T_{Max_{Avg}}$ Formula:

For Slow Sliding Speed: μ: coefficient of sliding friction: P: normal load
$\triangle T_{Max_{Avg}} = 0.236\ \mu\ P\ v / l\ 2\ K$ v: sliding speed; l: ½ asperity sliding direction length
For Fast Sliding Speed: D: density; S: specific heat
$\triangle T_{Max_{Avg}} = 0.236\ \mu\ P\ v / l(K+0.88K(sqrt(vlDs/K)))$. K: thermal conductivity
(Circular or Square Asperities) Bowden, Ridler, And Jaeger

$\triangle T_{Max_{Max}}$ Formula:

For Slow Sliding Speed: $\triangle T_{Max_{Max}}$ ~= 1.1 to 3.0 times $\triangle T_{Max_{Avg}}$ Jaeger
(Square and Blade Shaped Asperities)
$\triangle T_{Max_{Max}}$ ~= 2.1 to 2.5 times $\triangle T_{Max_{Avg}}$ Tian, Kennedy
(Circular and Parabola Shaped Asperities)
$\triangle T_{Max_{Max}}$ ~= 1.5 to 1.7 times $\triangle T_{Max_{Avg}}$ Vick, Furey, and Foo
(Square Shaped Asperities)

For Fast Sliding Speed: $\triangle T_{Max_{Max}}$ ~= 1.3 to 1.5 times $\triangle T_{Max_{Avg}}$ Jaeger
(Square and Blade Shaped Asperities)
$\triangle T_{Max_{Max}}$ ~= 3.0 to 3.3 times $\triangle T_{Max_{Avg}}$ Tian, Kennedy
(Circular and Parabola Shaped Asperities)

These early analytical models confirm and explain some key observations reported by the early researchers in kinetic friction. These researchers noted that while kinetic friction obviously caused dramatic hot spot temperature rises at the surface of the sliding materials, those same material's bulk temperatures barely rose above their starting ambient original temperatures. The models also confirmed the impressions of the early researchers that the greatest hot spot temperature rise from kinetic friction occurred at the back edge of the sliding asperity and that small changes in the sliding direction length of the asperity caused significant increases in the hot spot temperature rises. Jaeger's models detailed that a one order of magnitude reduction in the sliding direction length of the asperity caused a two order of magnitude rise in the hot spot temperature rise due to kinetic friction. Also the models confirmed the linear correlation in the hot spot temperature rises due to kinetic friction with linear changes in the normal load. They also confirmed the low power (almost linear in some conditions) correlation in the hot spot temperature rises due to kinetic friction with linear changes in the sliding speed. And most importantly they also confirmed the inverse low power (almost linear in some conditions) correlation in the hot spot temperature rises due to kinetic friction with changes in the sliding material's thermal conductivity as shown in figure 35: ie the more thermally conductive the materials sliding the significantly lower the hot spot temperature rise.

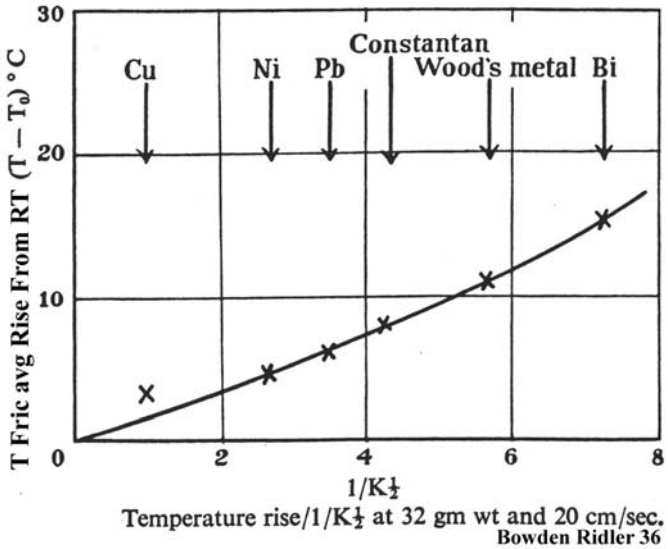


Figure 35, Temperature Rise Versus Sliding Material's Thermal Conductivity

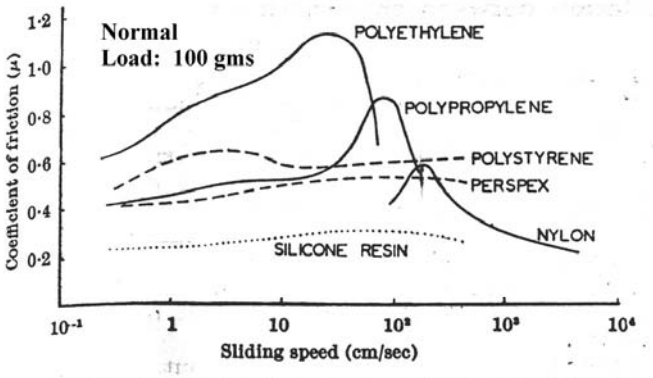
The later models confirmed the hot spot temperature rise suppressing effects which having the same load supported by numerous asperities having the same area has. The enhanced models developed by Vick, Furey and Foo, Tian and Kennedy, and Quinn, Cowan and Winer detailed that the original models predicted significantly higher hot spot temperature rises than observations indicated. In fact the enhanced models indicated that with multiple asperities the temperature rises were suppressed by a factor of N^{-1} for slow speed sliding and as much as $N^{-0.25}$ for fast speed sliding. N being the number of asperities. These suppressions were also shown to be relevant so long as the broken up multiple asperities were spaced at least five (predicted by Vick et al) and as much as fifty sliding length diameters apart from each other.

All of the analytical models also imply a linear correlation between the bulk coefficient of kinetic friction (μ) for the sliding materials and the hot spot temperature rise. What the models did not predict and which the bulk of past kinetic friction studies have worked on is determining the variation in the μ of materials with seemingly every possible imaginable variable.

The coefficient of friction has a distinct correlation to the kinetic friction sliding speed and the bulk material's temperature. The correlation, as shown in figure 36, is identical to the second order Williams Landel Ferry (WLF) time temperature superposition transition with the transition temperature being defined as $T_s=T_g + 50^oC$. The μ of a material tends to be at a stable and lowest value at low bulk temperatures and low sliding speeds and after the transition returns to this low. But when the asperities' sliding surface temperature rises to the transition temperature the μ can for some materials spike as much as 400 percent. The implication of this is that the hot spot temperature rise will also spike by the same percent when the right combination of sliding surface material temperature and sliding speed are met. While little work has been reported on it seems that increased normal load also can have this effect.

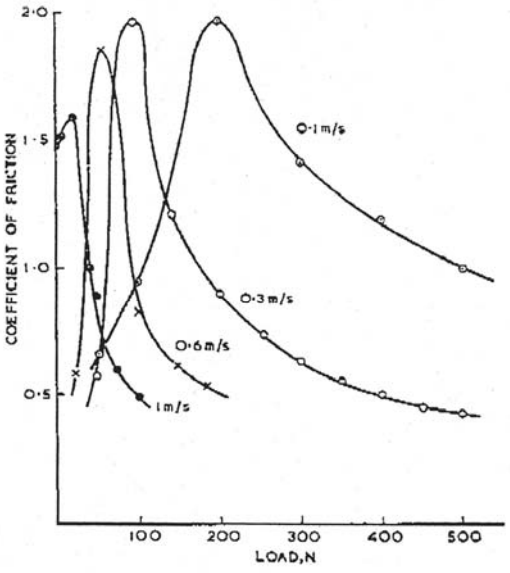
An interesting side correlation of note is the realization that the only two general types of polymeric materials, not already heavily oxidized by the incorporation of halogens, which pass the D2512 G86 mechanical impact ignition test do not exhibit a classic Tg. The polypyromellitimide known as Vespel and the polypyrlene known as graphite do not exhibit a Tg with increasing temperature. Instead when their temperatures are steadily ramped up they reach a point at which they simply begin degrading.

Overall significant increases in the normal load usually cause the μ of a material to drop by percentage points. But this correlation is very material specific and some efforts have reported the opposite. The reduced μ would cause the magnitude of the hot spot temperature rises to drop, but the large, usually order of magnitude, increases in the normal load associated with this reduced μ cause substantial increases in the resulting hot spot temperature rises.



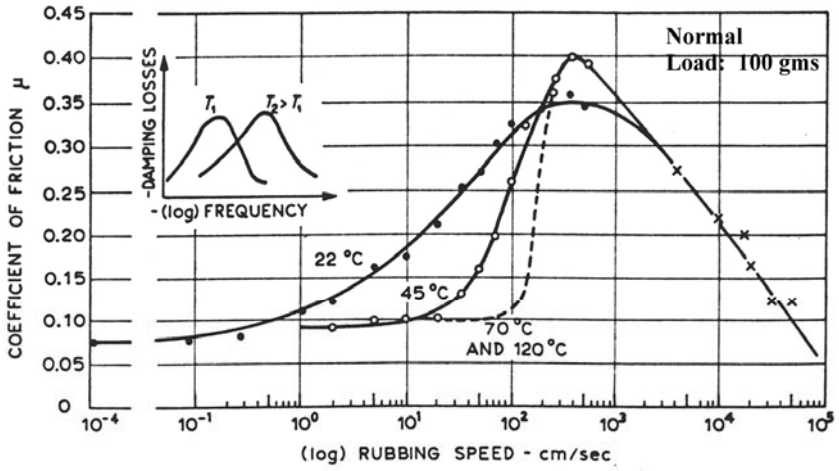
Variation of friction with speed at room temperature for thermoplastic crystalline polymers (polyethylene, polypropylene, 6,6-nylon), for thermoplastic amorphous polymers (polystyrene, 'Perspex') and for a typical thermo-setting polymer (silicone-resin). With the first group there is a marked rise in friction and a drop when the speed exceeds about 100 cm/sec. The resin shows the least effect of speed on friction

McLaren Tabor 63



Variation of friction with load for nylon 6 sliding on steel at various speeds (from Wanatabe *et al.*)

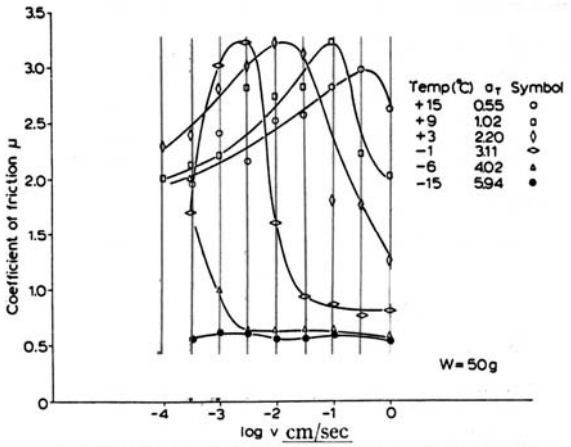
Lancaster 73



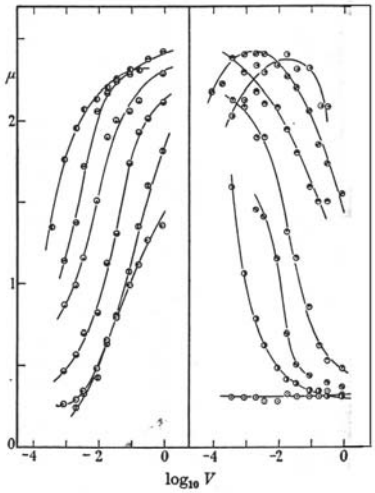
Friction of p.t.f.e. on p.t.f.e. (49% crystalline) as a function of speed. Speeds above 1000 cm/sec are from BOWDEN AND PERSSON[2]. The insert shows damping losses for a viscoelastic material as a function of frequency. If the temperature is raised the peak is shifted to a higher frequency.

McLaren Tabor 65

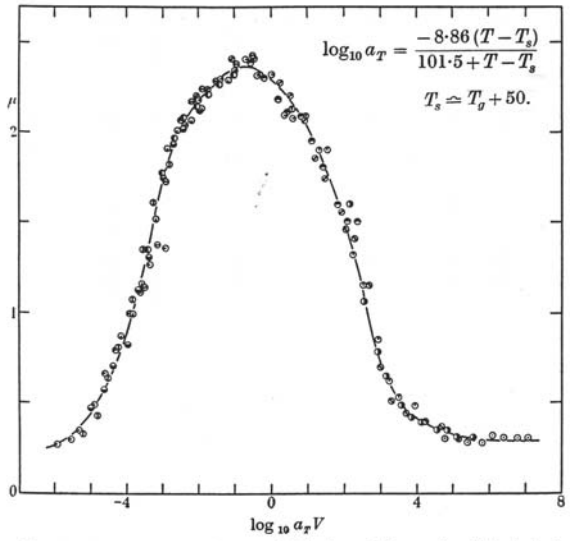
Figure 36a, WLF Type Correlation: Indications



Friction of a glass hemisphere sliding over a clean surface of acrylonitrile butadiene rubber **Ludema Tabor 66**



Coefficient of friction as function of the sliding velocity at various temperatures of the acrylonitrile-butadiene rubber *C*, on wavy glass. Curves are shown in two groups for clarity. ⊖, 85 °C; ⊕, 70 °C; ◒, 55 °C; ⊙, 40 °C; ⊖, 30 °C; ◐, 20 °C; ⊖, 10 °C; ⊘, 5 °C; ◓, 0 °C; ⊙, −5 °C; ⊘, −10 °C; ◑, −12·5 °C; ⊙, −15 °C.



Master curve of the coefficient of friction of the acrylonitrile-butadiene rubber compound *C* on wavy glass, reference temperature $T_0 = 20$ °C. **Grosch 63**

Figure 36b, WLF Type Correlation: Actuality

The values of μ during the initial kinetic friction sliding differ from those when said sliding has achieved a steady state. Figure 37 depicts these differences. The differences in these values can vary by as much as one hundred to two hundred percent. These differences would directly translate into said same changes in the hot spot temperature rises.

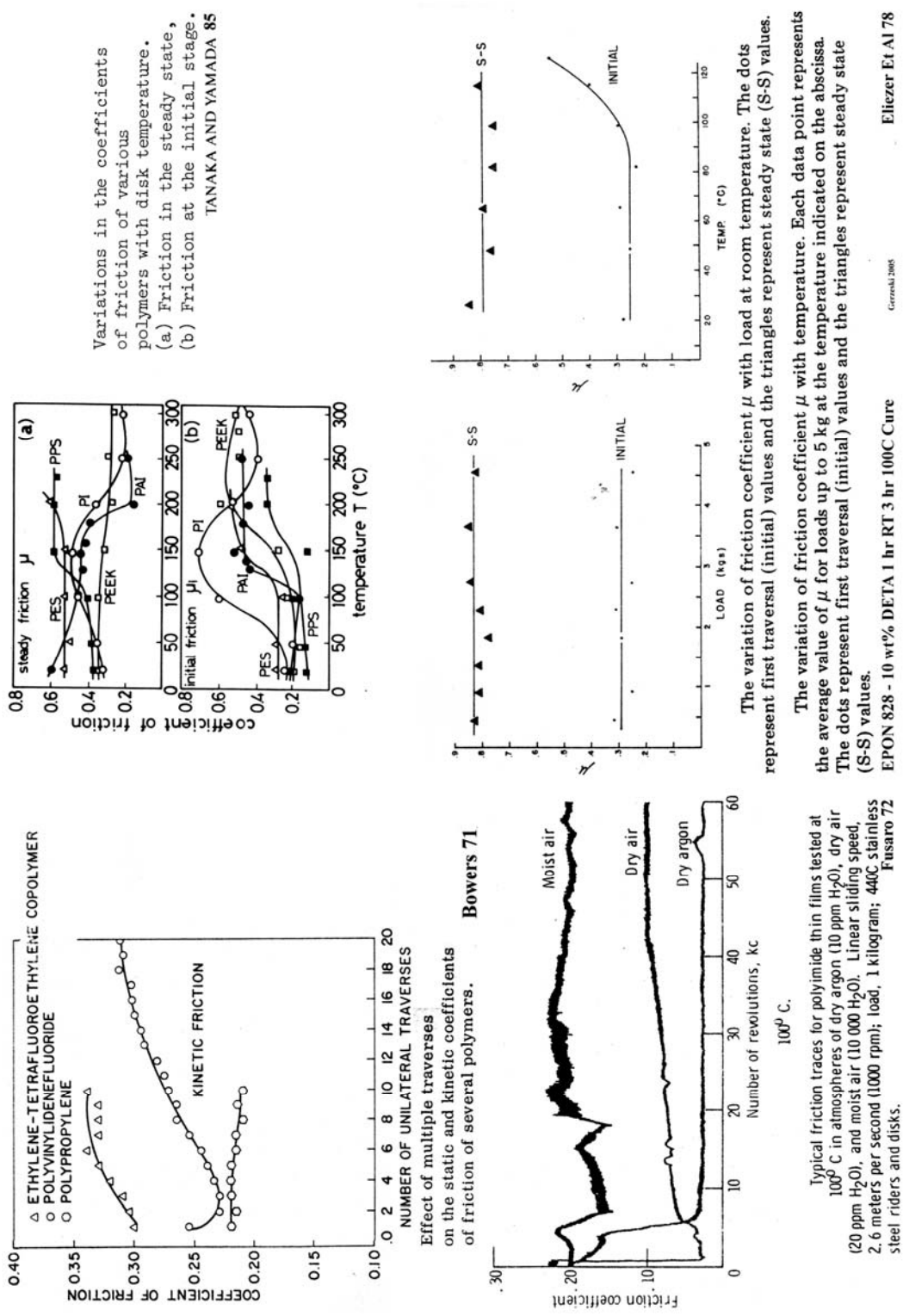


Figure 37, Initial versus Steady State Coefficients Of Friction

Work conducted by Fusaro, Bowden Et Al, Savage and Lancaster have decisively shown that trace quantities of low molecular weight gases and chemicals can have a significant impact on the value of μ. Gases and chemicals like oxygen, hydrogen, and water can suppress the μ exhibited by the sliding sheared asperities by almost 80 to 90 percent. These reduced μ would translate into lower hot spot temperature rises.

The addition of fillers or reinforcing fibers also changes the μ exhibited by the matrix material in a PMC in that the overall material rapidly takes on the μ of the reinforcement. As shown in figure 38 the reinforcement of a matrix material by a carbon-graphite pan fiber can suppress the resulting material's μ by upwards of eighty percent. This is due to the presence of very low μ graphite in the reinforcement. Other works have indicated that for other types of reinforcements or fillers the exact opposite can occur. When the percentage of the reinforcement or filler becomes the majority of the PMC composition, works by Tripathy and Furey, Shim Et Al, and Jianjun Et Al have indicated that the sliding asperities consist of the reinforcement or filler sliding on itself. The matrix, because it is almost always softer than the reinforcement, gets either pressed out of the contacting reinforcement or filler sliding surface contacting asperities or acts as a very poor boundary lubricant. Overall these changes in the PMC's μ would cause a corresponding linear change in the hot spot temperature rises.

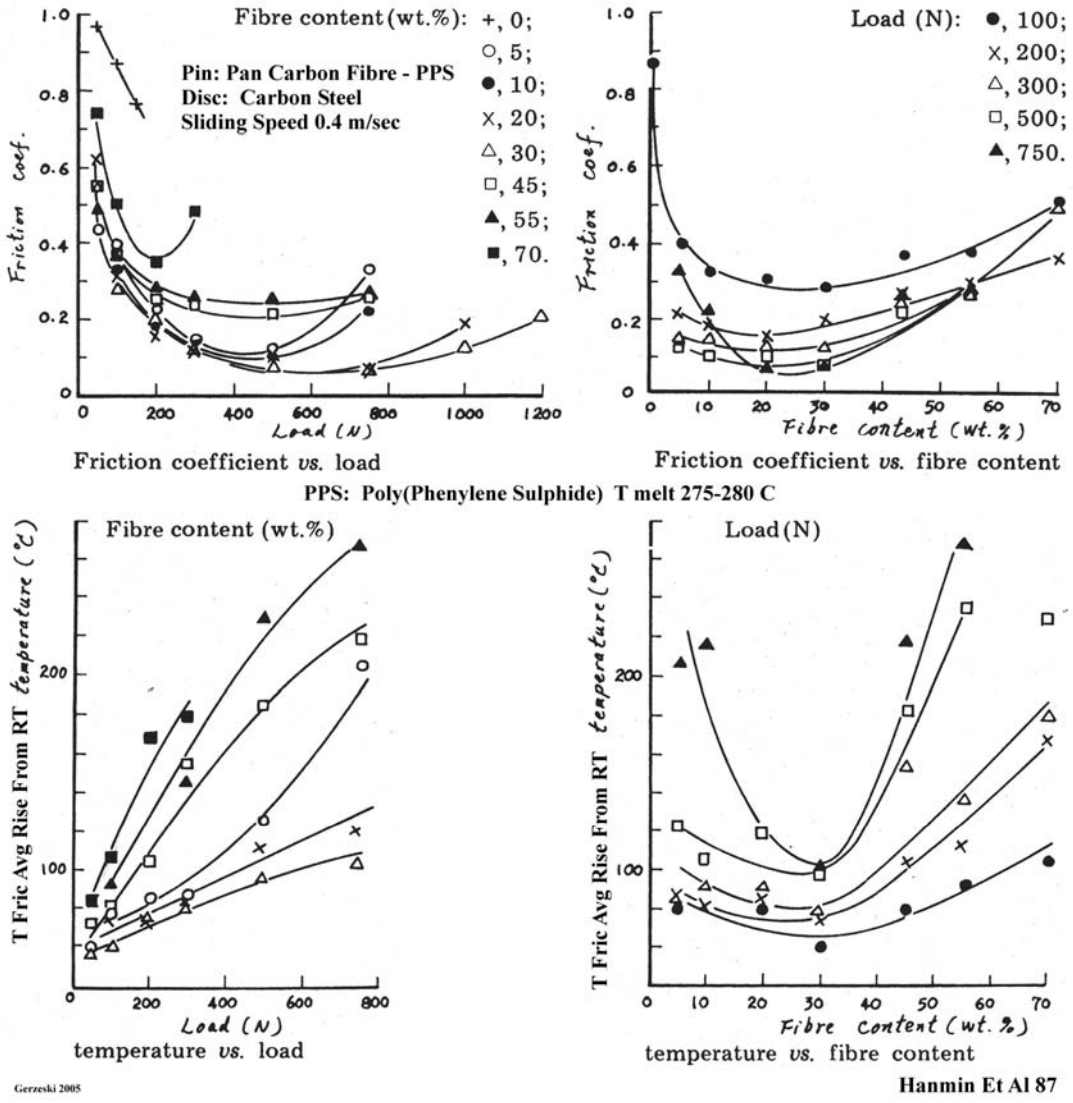


Figure 38, Reinforcement Incorporation Effects On Coefficients Of Friction

Along with the second order WLF associated changes in μ some materials also exhibit peculiar third order transition changes in μ with temperature, sliding speed, etc. The polypyromellitimide Vespel and carbon exhibit odd third order changes in μ with changes in temperature and asperity sliding speed. Vespel goes through a third order transition at around 60°C that causes its μ to increase by almost 2500 percent and then return to its common μ of roughly 0.05 at higher bulk material temperatures. Materials consisting of carbon-graphite go through a similar third order transition at 175 to 185°C. Their exhibited μ can climb by as much as 500 percent and the increase is correlative to the amount of carbon in the carbon-graphite: the more carbon the higher the μ climb; all graphite no increase in μ. Unlike Vespel, the μ exhibited by carbon–graphite materials does not return to its pre 175-185°C value at higher material temperatures but remains high. Because of the extremely rapid nature of the hot spot temperature rise induced by sliding asperities, the temperature of sliding Vespel asperities would rapidly transition this third order transition and the final apparent hot spot temperature rises would be representative of its intrinsic common low μ. For materials with carbon in their composition, if the asperities' sliding surface temperature meets or exceeds 175 to 185°C, their final exhibited hot spot temperature rises would dramatically increase as per the implied linear correlations listed in table 9: the more carbon in their composition the dramatically higher the hot spot temperature rise.

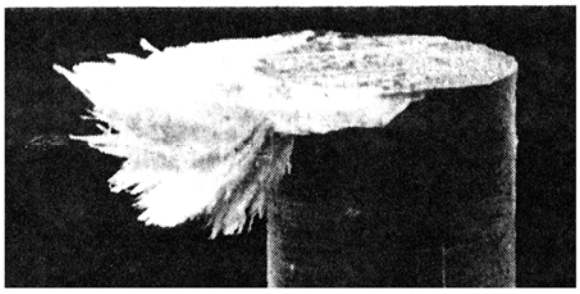
Materials exhibiting crystalline anisotropy, also exhibit widely varying μ's depending upon the orientation of the sliding asperities' surface to the crystalline axis. Both diamond and graphite exhibit one to three order of magnitude changes in their μ depending upon these relative orientations. (For diamond these μ changes go from 0.05 to 0.25; for graphite these changes go from 0.005 to 0.02 for sliding with/along the basal plane to 0.3 for sliding perpendicular to the basal plane.) Such μ differences would, as per table 9, translate into significantly large differences in the hot spot temperature rises exhibited by the same material, being solely dependent upon the orientation the sliding asperity surface had relative to a crystalline axis.

Different types and classes of polymeric materials exhibit different μ. A brief comparison and relative ranking of various polymers' μs indicates that those with amide groups and or large bulky side groups exhibit the highest, epoxies exhibit μs that are roughly equivalent, BMIs, carbon and phenolics exhibit μ's lower then the previous groups, and graphite, Vespel like polyimides, highly linear "smooth molecular shaped" and halogenated polymers exhibit the lowest μ. As these different μs range from lows of 0.005 to highs of 1.2, the hot spot temperature rises that different polymers would exhibit experiencing the same kinetic friction sliding conditions would vary by the same linear ratios. This can and does mean hot spot temperature rise differences of 100s and occasionally as much as 1000°C occur just with the selection of a different polymer.

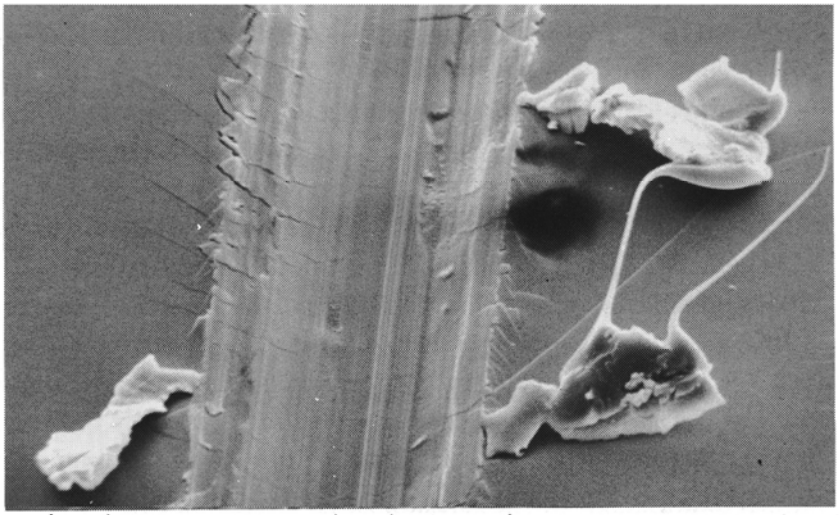
The kinetic friction sliding of polymeric materials, at real world sliding speeds and normal loads, leaves distinctive physical traces of its having occurred. Figure 39 depicts three of the most common of these traces. The single pass sliding of a material leaves a trail of melted and refrozen "puddles" of material in its wake. The long duration, one direction, sliding of a material produces a tail of "feathered" material extruded from the rear of the sliding surface. All leave a sporadic trail of tendril like, melted and drawn out, filaments thrown out and along side the sliding track. The appearance of these physical traces is proof that the hot spot temperature rises occurring at the sliding asperities' surfaces exceeded the melting point of one or both of the materials involved in the kinetic friction.



Optical micrograph of a flat surface of polyvinylchloride after a hemispherical slider of the same material has slid over it once at a very slow sliding speed and under a load of a few kg. The strongly attached fragments of slider material are clearly revealed. (Magnification × 13.) **Pascoe Tabor 56 Hearle Tabor 59**



Appearance of a worn sample of pmma where appreciable surface melting has occurred. The pin is about 10mm in diameter and has been sliding at high speeds on 'smooth' steel from left to right. The characteristic tail of extruded material is evident at the rear of the contact **Briscoe 81**



Polishing groove on glass produced by translating diamond tool at 10 m s^{-1}. Direction of sliding from bottom to top. Note extrusion layer inside groove and molten 'stringers' outside. Width of field 75 μm. (After Schinker, M. G. & Doll, W. (1985), in *Strength of Glass*, ed. C. R. Kurkjian, Plenum, New York, p. 67.) **Lawn 93**

Figure 39, Distinctive Physical Traces Of Kinetic Friction

Experimental: Material Selection

The core objective of this effort was to determine if the D2512 LOX compatibility of composites could be improved by using thermally conductive reinforcement fibers instead of the standard conventional carbon fibers used to date. To accomplish this four materials were needed to be acquired: a matrix resin, a baseline carbon-graphite fiber, and two thermally conductive fibers to provide the experimental variables.

This effort's matrix resin needed to come from a general class which usually exhibit good D2512 LOX compatibility. A through reading of the LOX literature by the author and Principal Investigator (A&PI) narrowed the selection of the matrix resin class to imides. Since ability by the LOX using industry to fabricate the resulting composite via conventional techniques like filament winding needed to be considered, the selected resin also needed to exhibit processing characteristics which lended themselves to easy incorporation into existing fabrication facilities and processes. This qualification further narrowed the class of resins down from imides to bismaleimides (BMIs), which are routinely used by industry to fabricate composites. Also as indicated in table 2g and numerous other published efforts to find a D2512 LOX compatible composite, resin systems that exhibited greater toughness tended to come closer to passing D2512 then those that didn't. This finding further narrowed the class of resins from BMI's to toughened BMIs. Circa 2001-2, the starting time frame for this effort, the number of commercially available toughened BMIs was limited, but one made by Cytec "Rigidite 5250-4 RTM" was available in neat resin form.[B1-B17] This was the resin system selected for use as the matrix in this effort. Table 10 delineates the specifics of the actual lot of resin procured from Cytec and used in this effort.

Table 10, Procured 5250-4 RTM Matrix Resin Specifications

Cytec ENGINEERED MATERIALS

Cytec Engineered Materials Inc.
1440 N. Kraemer Blvd.
Anaheim, CA 92806
Telephone (714)630-9400
FAX (714)666-4345

Date: September 25, 2002

CERTIFICATION

We certify that this Cytec Engineered Materials product ordered on the indicated purchase order has been tested in accordance with the applicable specification procedures and found to possess the following properties, therefore meeting the requirements of your requested specification.

Cytec Eng Matl Part No.:	407816
Product Name:	RIGIDITE 5250-4-RTM RESIN, AGGREGATE (1G)
Lot Name:	7688300
Specification:	CSP (407816)
Date Shipped:	9/25/2002
QTY Shipped:	20 LB
Customer PO:	R0201971
Sales Order No.:	0010272-001
Packing Slip No.:	0010272-001
Date of Manufacture:	9/19/2002
Shelf Life:	6 MONTHS FROM DATE OF SHIPMENT WHEN STORED AT 10°F OR BELOW.

Notes:	**Result**	**Units**	**Minimum**	**Maximum**	**Result Type**
Sublot: 1 ST DRAW OFF					
Segment: BUCKET					
VOLATILES / 1 350°F Test Temperature					
VOL-AVG / 1	0.1	%	0.0	1.0	
Sublot: LAST DRAW OFF					
Segment: BUCKET					
VOLATILES / 1 350°F Test Temperature					
VOL-AVG / 1	0.1	%	0.0	1.0	
Sublot: 014					
Segment: BUCKET					
VISCOSITY / 1 50°C TEST TEMP.					
Min Viscosity / 1	25	cP	0	300	
Gel Time / 1	72	min	55	95	

J Blackford 9/30/02
Quality Representative

Report Number: ORDER-000036883

RHGerzeski 07/05

All fibers procured for this effort were procured in the 6K tow quantity, as this is the lower boundary for the commercially economical fabrication of composites.

A baseline reinforcement fiber needed to be selected and used to make a baseline composite so that a possible connection to previous composite LOX compatibility efforts could be established. As indicated in table 2g and numerous other published efforts to find a D2512 LOX compatible composite, the reporting of the exact type of fiber used was almost always missing. But a rare few of the published efforts did report using the T650-42 class of carbon graphite fiber and indicated that it did impart some degree of D2512 LOX compatibility to a composite. Unfortunately by the time this effort got underway the T650-42 fiber made by Amoco (and subsequently Cytec) was no longer in production but a sister fiber T650-35 was available. This fiber was only available with the UC309 epoxy-urethane finish on it. Epoxies and most particularly urethanes exhibit poor D2512 LOX compatibility and would certainly via the kindling chain effect skew the D2512 compatibility of any composite made with it as a finish. All attempts by the author to procure the T650-35 fiber from Cytec without the UC309 finish were ignored. Also due to the small (roughly $85K) budget and limited time available to the A&PI to complete this effort it was impossible to strip the finish off in house. So the baseline fiber selected for this effort was the Cytec T650-35 with the UC309 finish. Table 11 delineates some of T650-35's properties of relevance to this effort and Table 12 delineates the specifics of the T650-35-UC309 lot procured from Cytec for this effort.

Table 11, T650-35 Properties

THORNEL® Pan Based

Fiber Charactersitcs, Units	**Fiber Type**	
	T-650/35	**T-650/42**
Tensile Strength[2], ksi (GPa)	660 (4.55)	730 (5.03)
Tensile Modulus, Msi (Gpa)	35 (241)	42 (290)
Density, lbs/in³ (g/cc)	0.064 (1.77)	0.064 (1.78)
Elongation at Break[3] %	1.75	1.7
Filament Diameter, μ	6.8	5.1
Carbon Assay, %	94	94
Surface Area, m²/g	0.5	0.5
Electrical Resistivity[4], μ ohm-m	14.9	14.2
Thermal Conductivity[4], BTU/hr ft °F (W/m K)	8 (14)	9 (15)
CTE at 70 °F (21 °C)[4] (ppm/°F) (ppm/°C)	−0.3 (−0.5)	−0.3 (−0.5)
Strand Construction and Properties		
Available Forms[5]	3k, 6k, 12k	6k, 12k
Yield, yd/lb	2534, 1271, 650	2219, 1127
Linear Density, g/m	0.196, 0.391, 0.763	0.224, 0.440
Twist, tpi	0[6], 0[6], 0	0[6], 0[6]
Fiber Area in Yarn Cross Section, in² × 10^{-5}	17.2, 34.1, 66.9	19.5, 38.2

Table 12, Procured T650-35-US309 Fiber Lot Properties And Specifications

05/14/02

Thornel® Carbon Fiber Certification

CYTEC Carbon Fibers,
Post Office Box 849
Greenville, SC
29602-0849

CYTEC Ref. Number: 603000863

Customer Order No.:R0201037

Product: T-650/35 6K 309 NT

Based on random lot samplings, listed are the average physical properties of the lots included in this shipment.

Trace Number B6Y0411	Yield	Fiber Density	Tensile Strength	Sacma | Young's Modulus		Elong**	Sizing
	G/M	G/CC	(psi x 10^3)	(psi x 10^6)		%	WT. %
AVG	.3944	1.773	623	34.5	37.1	1.7	1.02
SD	0.0046	0.0055	30.84	0.3197	0.3465	0.0795	0.2130
CV%	1.17	0.31	4.95	0.93	0.93	4.74	20.79
N=	65	65	65	65	65	65	65
MIN	0.3817	1.760	553	33.6	36.2	1.5	0.75
MAX	0.4019	1.789	668	35.3	38.2	1.8	1.74

[Mfg on GP2 Production Line] [Lbs Shipped =8.44]
[Mfg, Date APR 2002] [Release Date 20020423]

The material shipped on this order is in compliance with Cytec Carbon Fibers' PAN product specification requirements.

** Elongation is a calculated value based on T. S./Young's Mod. x 100.

This certification has been reviewed and approved by Linda Fuller in the Quality Assurance Department. For questions or assistance, please call (864) 299-9363.

Item: 60658479

Description: T650/35 6K 309 NT P2

Specifications:

Cytec Carbon Fibers' Pan product specification requirements

	Lot/Sublot No		Delivery Qty UOM
1	B6Y0411-0139		8.4400 lb
Lot:	B6Y0411	**Total:**	8.4400 lb
Sublot Count:	1		
Total (Lots):	1		8.4400 lb

A reasonably through reading of the literature on fiber properties and the interface indicated that almost all of the commercially available fibers used by the composites industry have substantial quantities, routinely measurable in the 100s to 1000s PPM, of metal oxides and salts on their surfaces as a residual of their fabrication.[FP1-FP40 and FI1-FI 50] As was discussed in the Ignition section of the Theory Section, metal salts and oxides act as oxidation catalysts and so any fiber selected as an experimental variable for this effort needed to be very clean: exhibit a very low concentration of metals on its surface. Also, so as not to have the finish skew the resulting D2512 LOX compatibility of the resulting composites made from these experimental variable fibers, they need to be acquirable without finishes. Unfortunately almost all fibers that exhibit thermal conductivity are highly graphitic and graphitic fibers usually exhibit very poor interface and transverse mechanical properties when made into composites. Finsihes usually overcome this deficit in graphite fiber reinforced composites but they and the associated additional variable effects they would have on the D2512 LOX compatibility of any composite made with them needed to be eliminated from this effort. To assure that the composites made from these experimental variable fibers exhibited reasonable to at least minimally acceptable interface and transverse properties a surface treatment of the thermally conductive experimental fibers would have to suffice. Based upon the knowledge that highly preoxidized (i.e. preburned) organic materials exhibit good D2512 LOX compatibility and that small durations of oxygen plasma exposure to the surface of a freshly fabricated fiber significantly improved its interfacial and transverse composite properties, all of the experimental fibers were purchased after having a five minute oxygen plasma treatment by the fabricator.

Almost all highly graphitic thermally conductive fibers are very inflexible. Most have bend to failure (BTF) radii measured in inches. They can usually be barely wrapped around a soda can without breaking. In order for the acquired thermally conductive experimental fibers to be of future practical commercial fabrication use, and since all of the fibers would need to be sent off for prepregging which would entail extensive bending (all would also need to survive extensive handling through out their conversion from prepreg to finished D2512 composite) experimental fibers that were pliable exhibiting tight BTF radii of less than one inch needed to be acquired.

A through reading of the available commercial fiber literature and extensive discussions during 2001 with various fiber manufacturing representatives narrowed the possible experimental fiber providers down to Nippon Graphite Fiber Corps' Granoc fibers. Of the GRANOC fibers available two were selected for use in this effort as the experimental fibers. Those two were YSH50A and YSH60A. As can be seen in figure 40 they both exhibit BTF radii that are tight enough to meet the requirements listed in the previous paragraph E mail correspondence with GRANOC personal during 2001 and a review of the GRANOC fiber literature indicated that the YSH fibers had the necessary low amounts of metals on their surfaces (as detailed in the e mail reproduced in figure 41) and exhibited low but sufficient interface and transverse properties when incorporated into a composite. Also as seen in table 13 the two selected experimental fibers also exhibited thermal conductivities which when made into 60 plus percent fiber volume (V_f) composites would exhibit the figure 10 targeted axial thermal conductivities suspected to be needed in order to improve a composite's D2512 LOX compatibility. Nippon Graphite Fiber Corps was also cooperative in that they were willing to provide the fibers without any surface finish and also treat their surfaces with a five minute oxygen plasma exposure before shipping them. The actual properties of the lots of the 6K tow YSH50 and YSH60 experimental fibers delivered by Nippon Graphite Fiber Corps and used in this effort are detailed in tables 14 and 15.



Figure 40, Selected Carbon-Graphite Fibers

Gerzeski Roger H Civ AFRL/MLBCO

From: Takayuki Matsumoto
Sent: Tuesday, May 15, 2001 9:24 PM
To: roger.gerzeski
Cc: Gen Ishikawa (E-mail); TGWongConsulting (E-mail); Tetsuji Watanabe (E-mail); NGF????? (E-mail)
Subject: Metal content of GRANOC carbon fiber

Dear Mr. Gerzeski,

Thank you for visiting our booth at the SAMPE show last week.
We are back in Japan and ready to answer your questions.

1. Metal content
According to the EDX test results, GRANOC fiber is considered to have the following amount of metal (not ion form but mainly oxide form).

Mg 0.5 ppm
Al 2.8 ppm
K 0.2 ppm
Ca 0.6 ppm
Na 0 ppm

Please note that the above values are approximate ones.

2. Compatibility with imides
Unfortunately we have no actual data of bonding strength between our fiber and polyimides or bismaleimides. But according to our laboratory people, it would be just a little lower than that with epoxy resin. What is more important would be the thermal stress after curing since the process temperature is way higher than epoxy system.

I hope the above information is of some help to you.
We are happy to provide some free sample if you want.

Your comments or further questions would be very much appreciated. Thank you again.

Best regards,

Takayuki Matsumoto
****
Takayuki Matsumoto
Manager, Sales Division
Nippon Graphite Fiber Corp.
Nisseki Mitsubishi Building
1-3-12, Nishi-shimbashi, Minato-ku,
Tokyo, 105-8412, Japan
Tel:03-3502-9251 Fax:03-3502-9253
****

Figure 41, YSH50A and YSH60A Fiber Surface Metal Properties

Table 13, YSH50A and YSH60A General Fiber Properties

Granoc YSH-ASeries PITCHBASEDCARBONFIBER

		YSH-50A	YSH-60A
TensileStrength	ksi	560	560
	kgf/mm^2	390	390
	MPa	3830	3830
TensileModulus	msi	75	92
	$10^3 kgf/mm^2$	53	64.5
	GPa	520	630
UltimateElongation	%	0.7	0.6
Density	g/cm^3	2.10	2.12
FilamentDiameter	μm	7	7
FilamentsperYarn		1000/3000/6000	1000/3000/6000
Yield	g/km	75/250/520	75/250/520
CTE	$10^{-6}/K$	-1.4	-1.4
ThermalConductivity	W/m·K	140	200
Electrical Resistivity	10^{-4} Ω·cm	7	6

Table 14, YSH50A Procured Fiber Lot Properties

Nippon Graphite Fiber

Nippon Graphite Fiber Corporation

3-12, NISHI-SHINBASHI 1-CHOME, MINATO-KU, TOKYO 105-8412, JAPAN
PHONE : 81-3-3502-9251
FAX : 81-3-3502-9253

No. S140083-001
March 08 , 2002

GRANOC YARN CERTIFICATION

<LOT AVERAGE TEST DATA>

Fiber Type	YSH-50A-60Z
Lot No.	130901382302
Tensile Strength	562 ksi 3870 MPa 395 kgf/mm^2
Tensile Modulus	74.5 msi 514 GPa 52.4 tf/mm^2
Density	2.10 g/cm^3
Mass Per Unit Length	521 g/km
Size Content	0.0 mass %
Surface Treatment	Yes

Yutaka Arai

GENERAL MANAGER
QUALITY ASSURANCE DIV.

Table 15, YSH60A Procured Fiber Lot Properties

Nippon Graphite Fiber

Nippon Graphite Fiber Corporation

3-12, NISHI-SHINBASHI 1-CHOME, MINATO-KU, TOKYO 105-8412, JAPAN
PHONE : 81-3-3502-9251
FAX : 81-3-3502-9253

No. S140228-001
July 05 , 2002

GRANOC YARN CERTIFICATION

<LOT AVERAGE TEST DATA>

Fiber Type	YSH-60A-60Z
Lot No.	1317B1470102
Tensile Strength	528 ksi 3640 MPa 371 kgf/mm^2
Tensile Modulus	90.6 msi 625 GPa 63.7 tf/mm^2
Density	2.12 g/cm^3
Mass Per Unit Length	509 g/km
Size Content	0.0 mass %
Surface Treatment	Yes

PO No. R0201402

Yutaka Arai

Yutaka Arai
GENERAL MANAGER
QUALITY ASSURANCE DIV.

Experimental: Lab Room, Equipment And Material Handling Cleaning Procedures

Through out the entire experimental portion of this effort numerous situations, circumstances and events presented themselves which might lead to the materials used, their interim fabricated forms, the equipment used to work on or process them and the generated D2512 specimens becoming contaminated by dust, fingerprints, solvents, etc. If not eliminated or stringently mitigated these contaminates would as described in the Theory Section: Ignition Event skew the final generated D2512 specimen's LOX compatibility results towards lower compatibility. To eliminate and or mitigate these contaminates certain steps and efforts were always taken. Fresh, clean and new (FC&N) Safeskin Purple Nitrile (SPN) gloves were always worn during any step in this research effort. Thousands of pairs of FC&N SPN gloves were used by the author throughout this entire effort to prevent contamination. Also whenever possible, any step in the this effort was done in the lab room shown in figure 42 which was cleaned again before that step was to be accomplished by being wiped down with FC&N cheese cloth wipes soaked in isopropyl alcohol (IPA) and mopped. And finally any piece of equipment or tool that came into contact with the materials used, their interim forms or the generated D2512 specimens was wiped down with FC&N cheese cloth wipes soaked in IPA, triple distilled water (TDW) or whatever was a relevant or only available means of cleaning it. Other cleaning techniques were used throughout this effort and they will be discussed when they were used. These contamination control efforts will be indicated to have been taken throughout the remainder of this report by the moniker: Meticulous Cleaning Procedures

Prior to the build up of the lab room shown in figure 42 the entire room, from ceiling to floor, was blown down with high pressure dry filtered nitrogen (DFN_2) gas. This blew away years of accumulated dust which might have migrated into the D2512 specimens via the tools, general contact, or retaking to the air and skew the specimen's D2512 LOX compatibility results erroneously lower. Abrasives skew the D2512 LOX compatibility of any material that they are in contact with towards more reactions: ie lower D2512 LOX compatibility. Dust is an abrasive and would skew the D2512 LOX compatibility results of any of the D2512 specimens generated in this effort towards more reactions if it was not kept off of them. The lab room was also washed and scrubbed twice with soap and water and numerous water rinses before the build up. Also throughout the entire experimental effort, dust traps consisting of open trays of soapy water as shown in figure 42 were put out throughout the lab to humidify the air and catch dust from the air. These needed to be cleaned once every month and put roughly one to two gallons of TDW into the lab room's air every day. This caused the lab room's relative humidity to be somewhat uniform throughout the entire effort.

SPN gloves were selected as the barrier glove material of choice to prevent or minimize the contamination of the materials used, their interim fabricated forms, the equipment used to work on or process them and the generated D2512 specimens by the oils and metal salts left behind by fingerprints. They are made out of nitrile rubber which exhibits modestly good D2512 LOX compatibility as seen in table 2. SAFESKIN Corporation's literature indicates that they are both "LATEX FREE" and clean enough to be used as medical examination gloves, implying that they contain minute quantities of low molecular weight organics. These organics, if accreted onto a D21512 specimen, would as described in the Theory Section: Ignition Event skew any subsequent D2512 test results towards more reactions. They are also powder free. Powder being an abrasive, this indicates that they are free of a key class of contaminating material (Abrasives) which as stated previously skew the D5212 LOX compatibility results of any material towards more reactions. Also, while being moderately expensive, they were affordable in the thousands of pairs quantities that the A&PI realized would be needed to accomplish this effort.



Legend:

a, Triple Distilled Water Generation And Storage
b, Vacuum Oven
c, Ultrasonic Cleaners
d, Nitrogen Purged Glove Box
e, 40 Micron Nitrogen Gas Filters
f, Open Ivory Soap And Water Humidifiers And Dust Catchers
g, Clean Prepreg Cutting Table
h, Room Cleaning Equipment
i, Prepreg Storage Deep Freeze

Figure 42, Lab Room

Experimental: Prepregging

As composites using the selected fibers (baseline and most particularly experimental) and 5250-4 RTM matrix had never been made before or even attempted to be prepregged before, all needed to be prepregged for the first time. The selected matrix resin and all three fibers were sent to Michigan State Universities' Advanced Materials Engineering Experiment Station during the summer and fall of 2002 to be prepregged by Mr. Bob Jurek senior technician. The desired prepreg specifications sought were prepreg areal weight (PAW) of 145 +/- 5 gms/cm^2, resin content (RC) of 35 weight percent, and 5 mil thickness. To avoid the potential of contaminating the prepregs with metal salts from finger prints or low molecular weight organics, which as described in the Theory Section: Ignition Event would skew any subsequent D2512 test results, Mr. Jurek was instructed to take meticulous care to clean and keep clean the prepregging area during prepregging with cheesecloth wipes and ACS grade clean acetone and always wear clean SPN gloves during all handling of the resin, fiber and prepreg. The wipes and gloves were provided by the A&PI. Prepregging was done by drum winding and kinetic friction was used to impregnate the resin into the fiber. Figure 43 delineates the size of the drum wound tapes generated. These tapes were further cut up into smaller strips/sheets also detailed in figure 43 for flat storage and shipment in dry nitrogen purged FC&N polyethylene (PE) bags. The fabricator also made one data point measurement of the prepreg's properties from the surplus. Table 16 details these fabricator measurements, the prepregging temperature of the resin and the date of the prepregging of the three fibers.

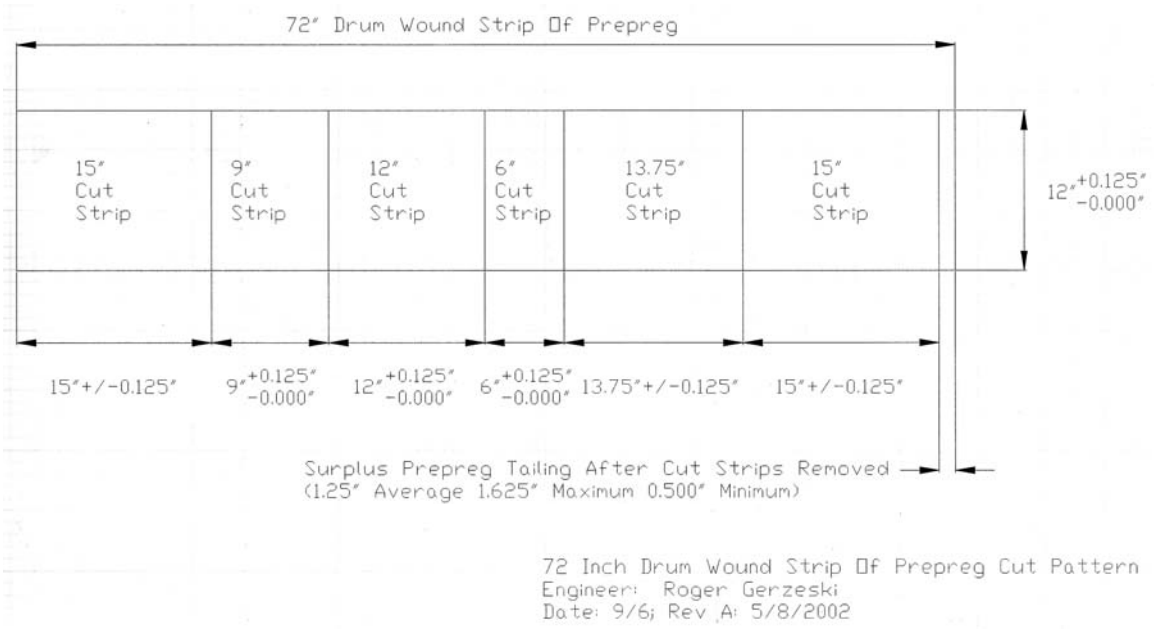


Figure 43, 72 inch x 12 Inch Drum Wound Prepreg Tape Cutting

As table 16 details, the resulting prepregs made exhibited significantly varying PAW and for the experimental fibers were very resin rich. Also subsequent attempts to further handle many of the generated tapes showed that they sometimes broke up when handled.

Table 16-a, T650-35 Prepreg Properties: As Delivered (Fabricator Measured):

Tape (Number)	Fiber Areal Weight (gms/sqm)	Resin Content ($\%_{Weight}$)	V_f (%)	Impregnation Temperature ($^{\circ}F$)	Fabrication Date
1	NA	43	NA	194	07/02
2	NA	43	NA	194	07/02
3	146.4	41.4	49.9	194	07/02
4	144.9	37.8	53.7	190	07/02
5	144.9	35.9	55.7	190	07/02
6	144.6	37.8	53.7	190	07/02
7	144.6	36.2	55.4	190	07/02
8	137.1	31.6	60.4	194	07/02
9	137.1	31.9	60.1	194	07/02
10	137.1	32.2	59.8	194	07/02
11	152.1	32.8	59.1	194	07/02
12	152.1	32.5	59.4	194	07/02
13	152.1	33.0	58.9	194	07/02
14	152.1	33.6	58.2	194	07/02
15	130.0	32.4	59.5	194	07/02
16	130.0	31.6	60.4	194	07/02
17	130.0	30.9	61.2	194	07/02
18	158.1	34.3	57.5	194	07/02
19	158.1	34.2	57.6	194	07/02
20	158.1	37.5	54.0	194	07/02
21	140.2	33.8	58.0	194	07/02
22	140.2	34.3	57.5	194	07/02
23	140.2	35.2	56.5	194	07/02
24	144.6	33.9	57.9	194	07/02
25	144.6	34.9	56.8	194	07/02
26	144.6	35.0	56.7	194	07/02
27	145.8	32.6	59.3	194	07/02
28	145.8	30.5	61.6	194	07/02
29	153.0	36.7	54.9	194	07/02
30	153.0	36.7	54.9	194	07/02
31	153.0	36.7	54.9	194	07/02

Notes: 1 Unusable: Lost
2 Unusable: Jigsawed* When Removed From Shipping Bag.
15 Unusable. Too Low A FAW
16 Unusable. Too Low A FAW
17 Unusable. Too Low A FAW. Jigsawed* When Removed From Shipping Bag.
18 Unusable. Too High A FAW
19 Unusable. Too High A FAW
20 Unusable. Too High A FAW
28 Unusable. Too Resin Thin
* Jigsawed meaning the prepreg broke up into numerous small strips of prepreg tape.

Table 16-b, YSH50 Prepreg Properties: As Delivered (Fabricator Measured):

Tape (Number)	Fiber Areal Weight (gms/sqm)	Resin Content ($\%_{Weight}$)	V_f (%)	Impregnation Temperature (^{o}F)	Fabrication Date
1	181.9	35.0	52.5	194	21/10/02
2	154.1	42.3	44.8	190	12/11/02
3	148.3	42.4	44.7	191	12/11/02
4	147.9	42.8	44.3	192	12/11/02
5	142.3	45.0	42.1	187	20/11/02
6	142.3	45.0	42.1	188	20/11/02
7	142.3	43.8	43.3	189	20/11/02
8	146.0	39.1	48.1	190	25/11/02
9	144.9	41.2	45.9	192	25/11/02
10	144.2	41.1	46.0	188	26/11/02
11	147.2	40.4	46.8	190	26/11/02
12	148.0	40.4	46.8	190	26/11/02
13	151.2	45.4	41.7	190	26/11/02
14	135.6	45.5	41.6	190	26/11/02
15	150.2	45.6	41.5	187	10/12/02
16	147.1	44.9	42.2	189	10/12/02
17	140.1	44.2	42.9	190	10/12/02
18	147.0	41.7	45.4	187	12/12/02
19	140.1	45.4	41.7	189	12/12/02
20	147.1	42.7	44.4	190	12/12/02
21	150.9	41.0	46.1	187	13/12/02
22	161.5	44.3	42.8	189	13/12/02
23	153.9	44.3	42.8	188	13/12/02
24	150.0	43.0	44.1	187	16/12/02
25	143.5	41.9	45.2	189	16/12/02
26	145.8	42.9	44.2	188	16/12/02
27	144.1	41.6	45.5	187	17/12/02
28	139.8	44.4	42.7	189	17/12/02
29	147.7	44.4	42.7	188	17/12/02
30	147.5	42.4	44.7	187	18/12/02
31	148.4	46.1	41.0	187	18/12/02
32	139.0	46.4	40.7	187	18/12/02
33	149.0	41.7	45.4	187	19/12/02

Notes:
- 1 Unusable: FAW Too High
- 2 Unusable: FAW Too High
- 7 Unusable: Tape Jigsawed* Into 30~40 Separate Pieces When Removed From The Shipping Bag
- 10 Unusable: Tape Jigsawed* Into ~10 Separate Pieces When Removed From The Shipping Bag
- 12 Unusable: Tape Jigsawed* Into ~10 Separate Pieces When Removed From The Shipping Bag
- 14 Unusable: FAW Too Low
- 22 Unusable: FAW Too High
- 23 Unusable: FAW Too High
- 31 Unusable: Resin Too High
- 32 Unusable: Resin Too High

* Jigsawed meaning the prepreg broke up into numerous small strips of prepreg tape.

Table 16-c, YSH60 Prepreg Properties: As Delivered (Fabricator Measured):

Tape (Number)	Fiber Areal Weight (gms/sqm)	Resin Content ($\%_{Weight}$)	V_f (%)	Impregnation Temperature (^{o}F)	Fabrication Date
1	131.0	55.0	32.5	200	30/10/02
2	167.2	38.0	49.0	192	08/11/02
3	163.9	44.9	42.0	194	11/11/02
4	144.0	37.9	49.1	191	11/11/02
5	146.3	44.5	42.4	188	13/11/02
6	142.9	44.1	42.8	189	13/11/02
7	143.5	44.1	42.8	190	13/11/02
8	147.2	39.2	47.8	188	19/11/02
9	147.2	41.0	45.9	189	19/11/02
10	140.3	44.9	42.0	190	19/11/02
11	140.3	43.9	43.0	191	19/11/02
12	138.4	39.6	47.3	188	27/11/02
13	139.0	37.4	49.7	189	27/11/02
14	140.9	43.9	43.0	189	27/11/02
15	140.0	43.1	43.8	188	27/11/02
16	140.5	40.1	46.8	188	02/12/02
17	155.2	45.1	41.8	189	02/12/02
18	146.6	41.5	45.4	190	02/12/02
19	152.0	45.7	41.2	188	03/12/02
20	145.4	42.9	44.0	189	03/12/02
21	146.7	41.8	45.1	190	03/12/02
22	157.4	42.2	44.7	188	04/12/02
23	172.3	41.2	45.7	189	04/12/02
24	169.4	39.9	47.0	190	04/12/02
25	160.9	44.7	42.2	188	05/12/02
26	150.5	42.2	44.7	189	05/12/02
27	148.7	43.5	43.4	190	05/12/02
28	147.4	45.4	41.5	188	06/12/02
29	149.3	43.3	43.6	189	06/12/02
30	137.0	44.1	42.8	190	06/12/02
31	137.3	49.0	38.0	188	09/12/02
32	142.9	47.3	39.6	189	09/12/02

Notes:
- 1 Unusable: Jigsawed* On Removal From The Shipping Bag.
- 2 Unusable: FAW Too High
- 3 Unusable: FAW Too High
- 12 Unusable: Jigsawed* Into Strips ~ 1 Inch Wide When Removed From The Shipping Bag
- 16 Unusable: Severe Gapping Between Tows And Jigsawed On Removal From The Shipping Bag
- 18 Unusable: Jigsawed* Into Strips ~ 1Inch Wide When Removed From The Shipping Bag
- 21 Unusable: Jigsawed* Into Strips ~1Inch Wide When Removed From The Shipping Bag
- 23 Unusable: FAW Too High
- 24 Unusable: FAW Too High
- 25 Unusable: FAW Too High

* Jigsawed meaning the prepreg broke up into numerous small strips of prepreg tape.

Experimental: Prepreg Cutting And Additional Measurements

Plus 45°, minus 45°, 0°, and 90°, 12 inch by 9 inch and 6 inch by 6 inch plies of the prepregs were subsequently cut by the A&PI from the locations shown in figures 44 and 45 from a series of the strips from various prepreg tapes during the winter of 2003. Meticulous Cleaning Procedures were taken by the A&PI to avoid contaminating the cut prepreg plies during the cutting. The surface upon which cutting occurred was wiped down with FC&N cheese cloth wipes soaked in IPA before each days cutting and kept free of potential dust contamination by being covered as shown in figure 46 with opened up FC&N CLEANLINER PE bags made by CLEAN FILM conforming to NASA JPG 5322.1 Level 100. All of the cutting tools shown in figure 46 and cutting templates shown in figure 47 used were cleaned by the same technique used to clean D2512 specimens, which will be described later in this report. The cutting tools were stored when not in use under ACS grade FC&N acetone in jars cleaned by the same technique (the cutting tools). Meticulous Cleaning Procedures were used on the templates and they were stored in FC&N PE Zip lock bags when not being used. Meticulous Cleaning Procedures were used on the cutting board and it was stored under a FC&N CLEANLINER PE bag when not being used.

The various prepreg tapes' thickness, fiber areal weight (FAW), PAW, and RC were measured by cutting three to six roughly 10 square inch pieces from the areas in figures 44 and 45 labeled "Eliminate Prepreg". The thickness was measured with a micrometer accurate to 0.0001 inch. The remaining properties were measured using the resin extraction technique depicted in figure 48 developed by the A&PI. Detailed drawings of the sub components shown in figure 48 are given in the Designed Equipment appendix. The area of the sampled prepreg was first measured with a caliper accurate to 0.001 inch and then weighted to 0.0001 gm accuracy. The resin extraction tray was also weighed to the same accuracy. The prepreg was placed into the tray and the tray with prepreg in it was placed into the Qorpac quart jar. The jar was then filled with ACS grade acetone and left in a hood. The resin was both dissolved and displaced from the surface of the fibers and settled to the bottom of jar. After roughly 12 hours the tray was removed from the jar and allowed to sit until the acetone had evaporated. The tray was then weighted to the same accuracy as above described.

Table 17 lists the measured prepreg properties for the cut tapes from each particular fiber's prepreg. All of the prepregs were very thick, ranging from 6.6 to 16.2 mils thick with a typical thickness of 11 mils. The FAWs of all of the prepregs ranged widely between the 125s and 155s gms/sqm, also usually exhibiting substantial standards of deviation within tapes. The RCs of the prepreg tapes measured showed that, particularly for the YSH fiber containing prepregs, all of the prepregs were extremely resin rich with some tapes having RCs well into the 50 plus percent range. This resin rich aspect implied that a substantial amount of resin would need to be bled off of any composite laid up using these prepregs. To obtain the targeted fiber volume (V_f) for this effort of between 60 and 65 percent, the amount of resin needing to be removed from these prepregs was as high as 120 plus gms/sqm and routinely between 60 and 80. This high RC and the large thickness of the tapes meant that a significant amount of trial and error modifications to the standard Cytec 5250-4 RTM cure cycle would need to be done in order to make good cured composites from these prepregs.

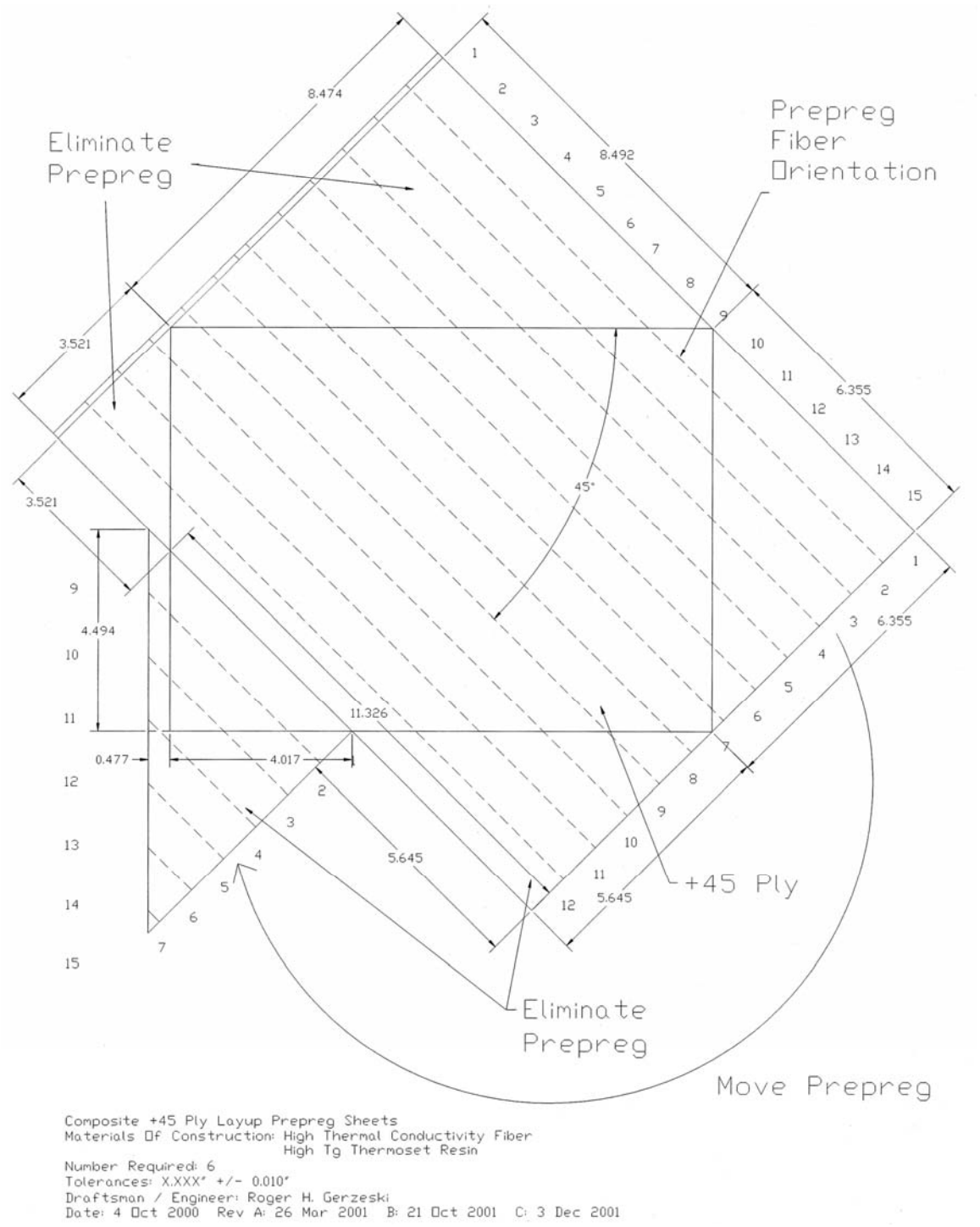


Figure 44-a, Prepreg Individual Ply Cutting Dimensions: 12x9 Specimen Plate

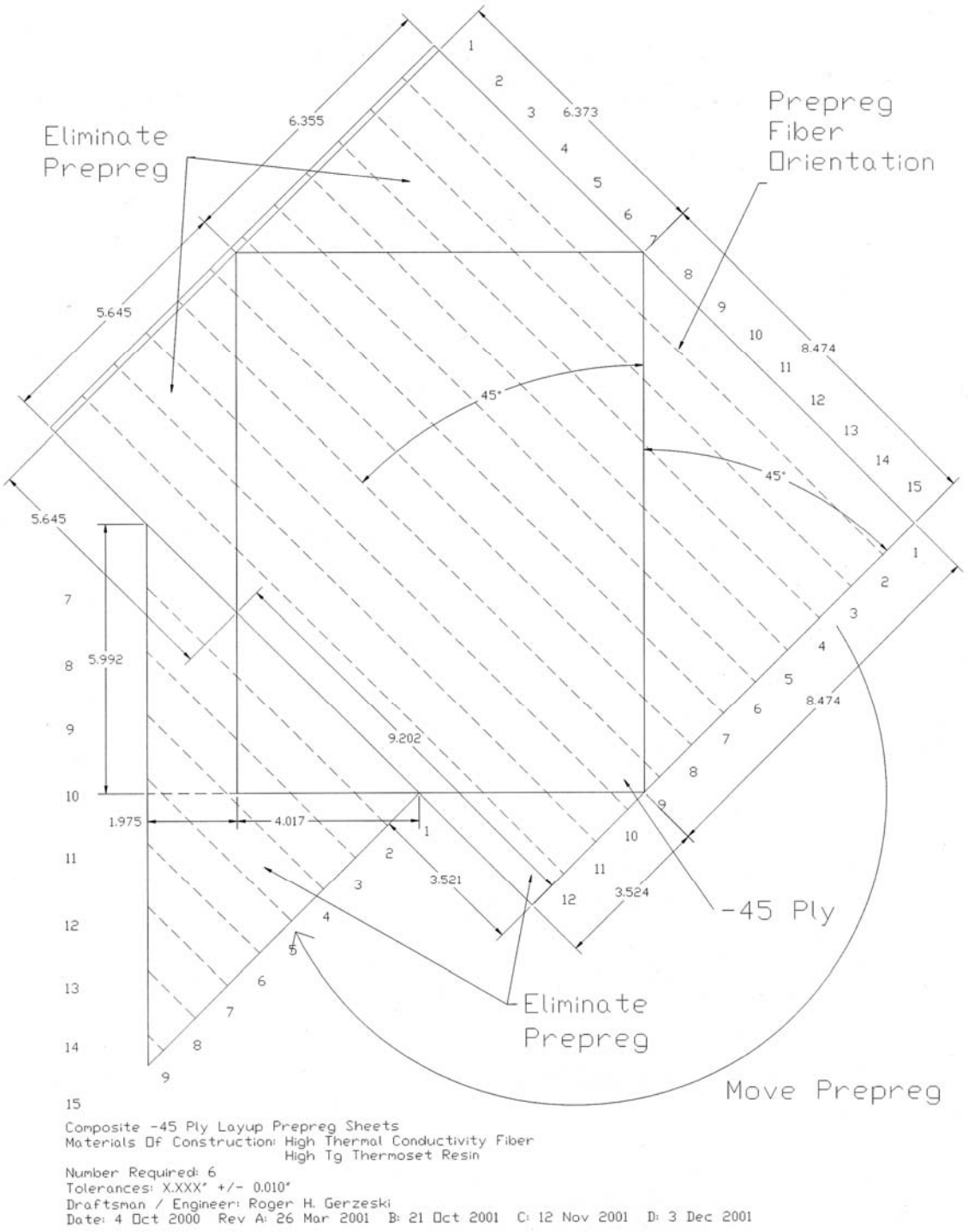


Figure 44-b, Prepreg Individual Ply Cutting Dimensions: 12x9 Specimen Plate

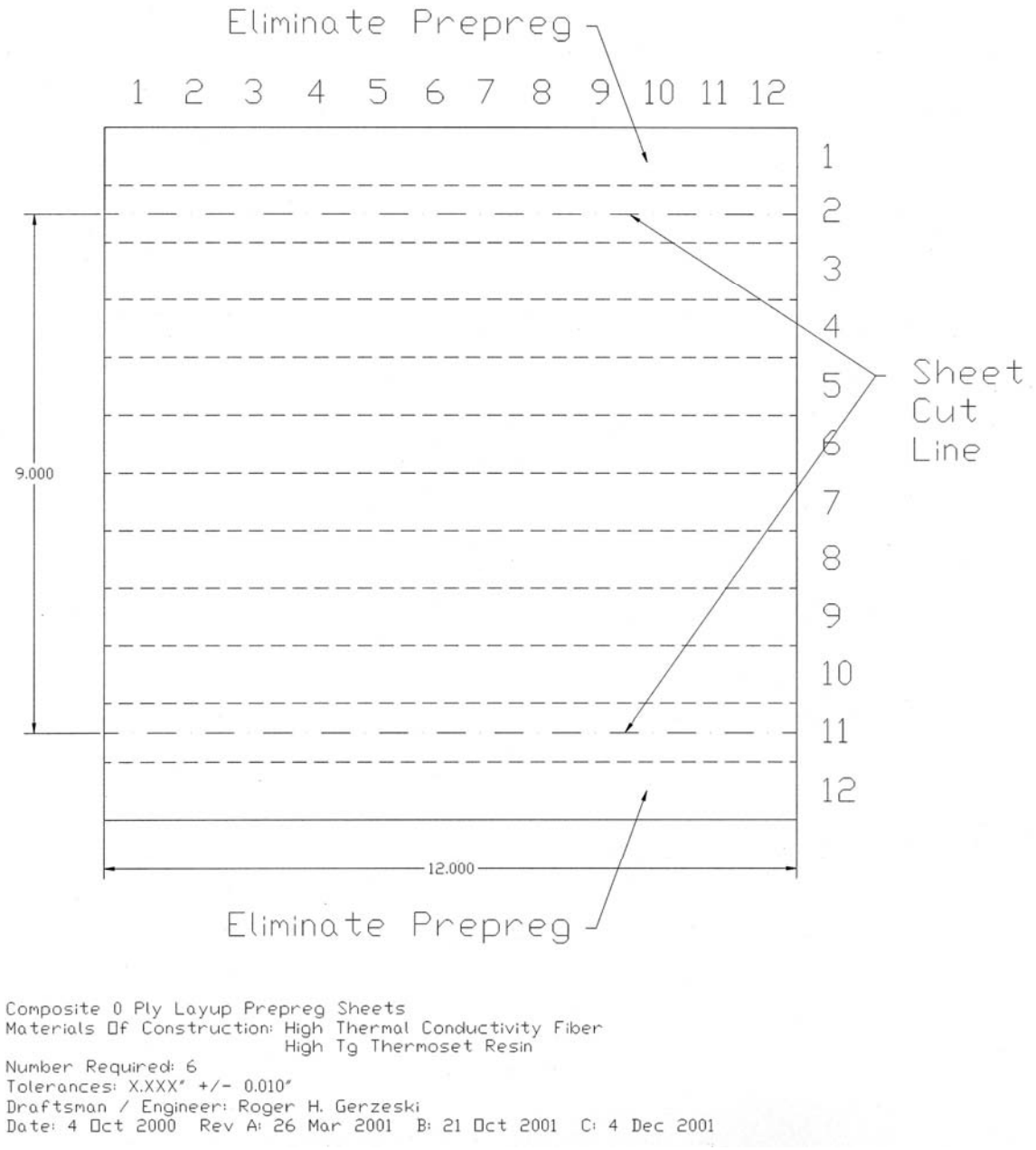


Figure 44-c, Prepreg Individual Ply Cutting Dimensions: 12x9 Specimen Plate

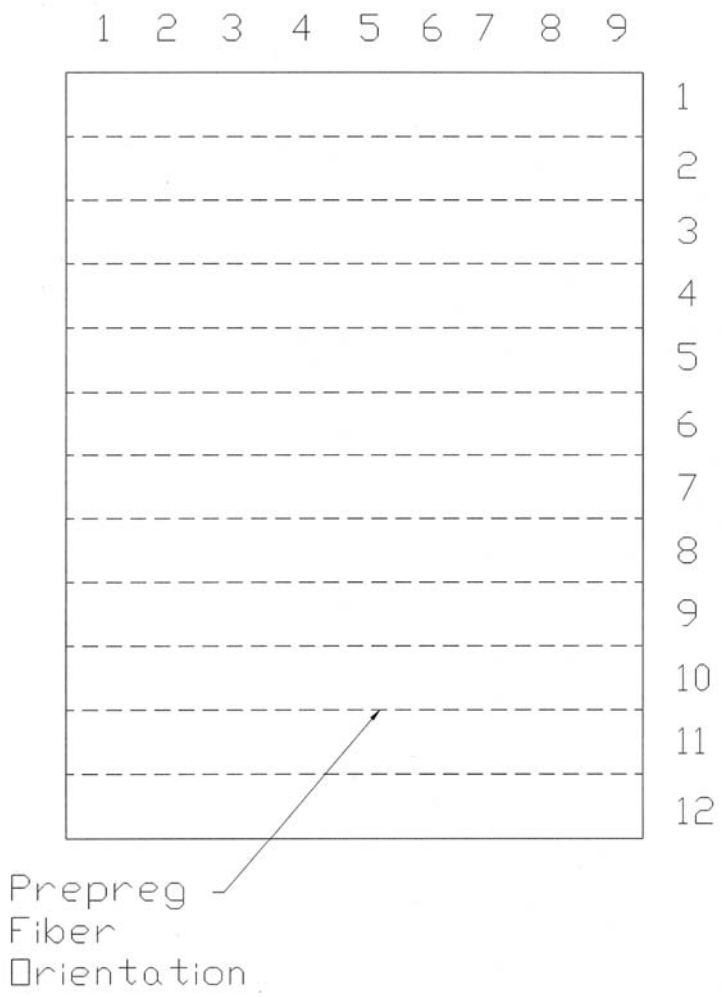


Figure 44-d, Prepreg Individual Ply Cutting Dimensions: 12x9 Specimen Plate

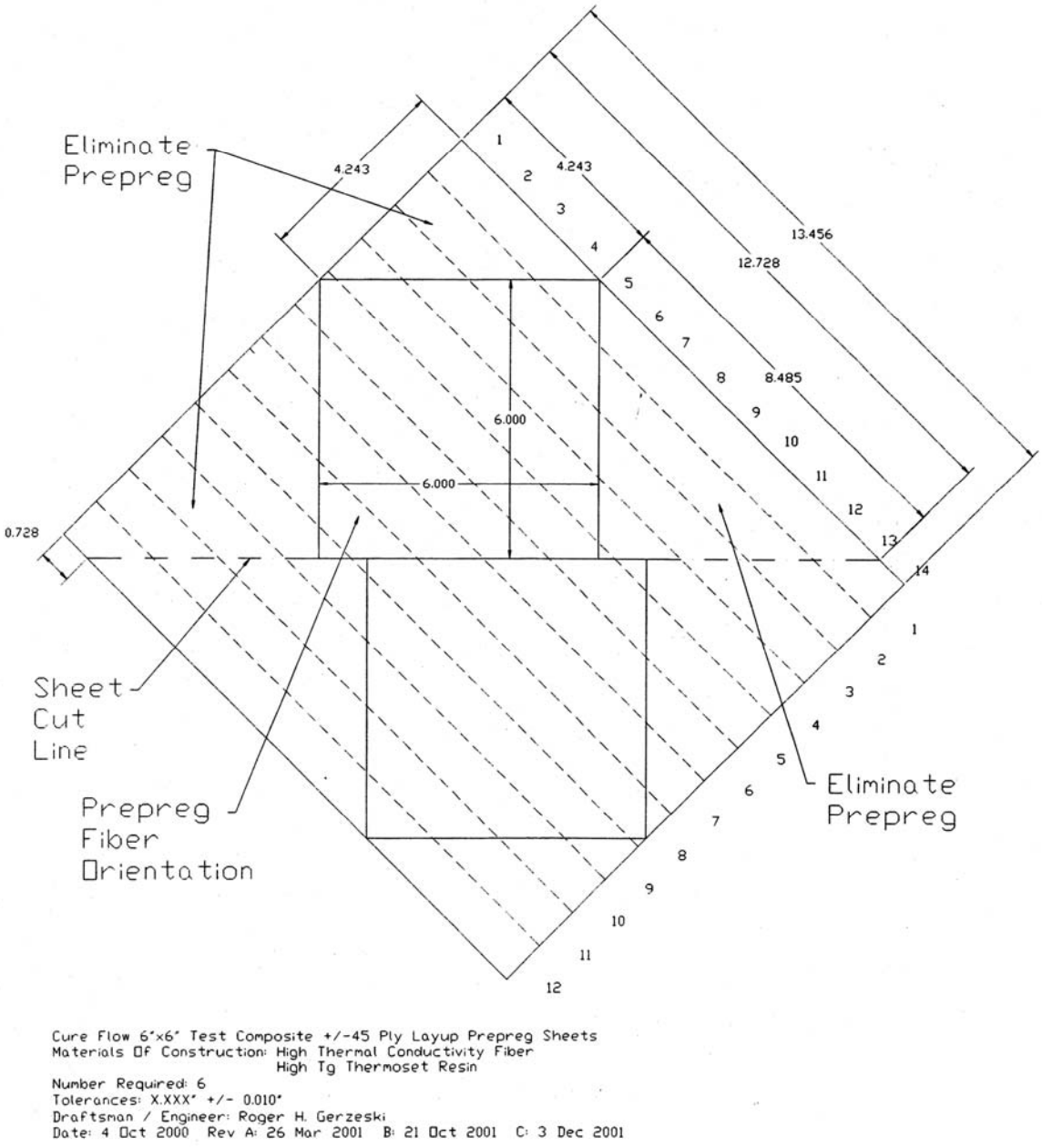
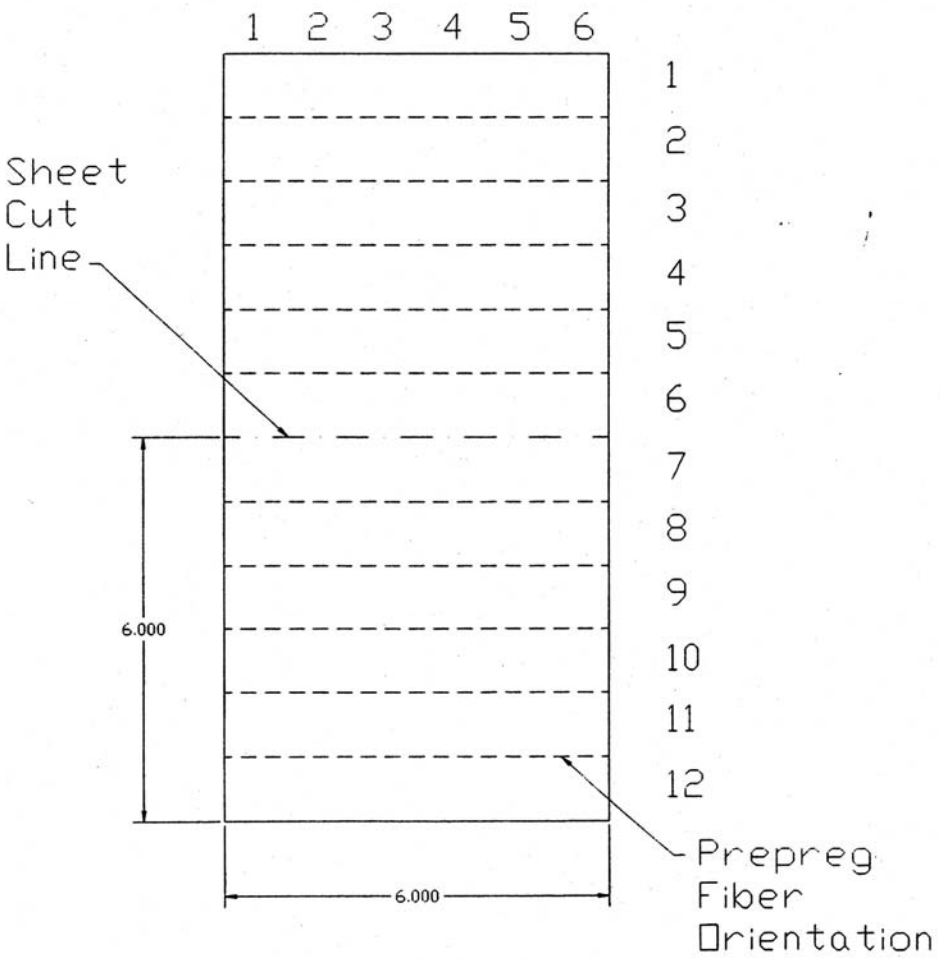


Figure 45-a, Prepreg Individual Ply Cutting Dimensions: 6x6 Bleed Flow Plate



Cure Flow 6"x6" Test Composite 0 and 90 Ply Layup Prepreg Sheets
Materials Of Construction: High Thermal Conductivity Fiber
High Tg Thermoset Resin
Number Required: 6
Tolerances: X.XXX" +/- 0.010"
Draftsman / Engineer: Roger H. Gerzeski
Date: 4 Oct 2000 Rev A: 26 Mar 2001 B: 21 Oct 2001 C: 4 Dec 2001

Figure 45-b, Prepreg Individual Ply Cutting Dimensions: 6x6 Bleed Flow Plate



Figure 46, Prepreg Cutting Table and Tools

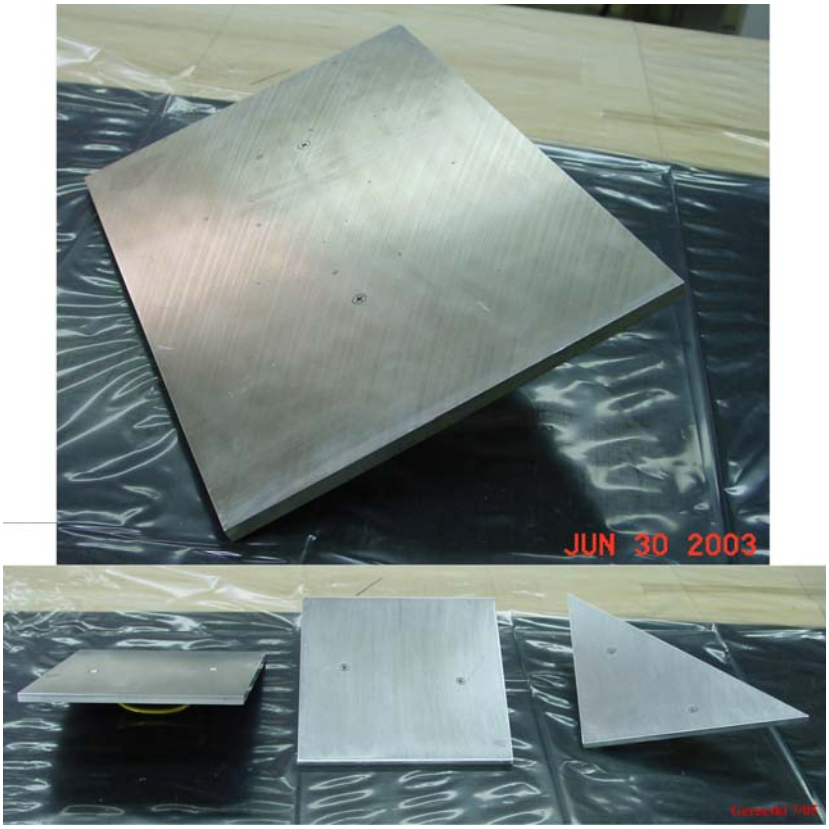
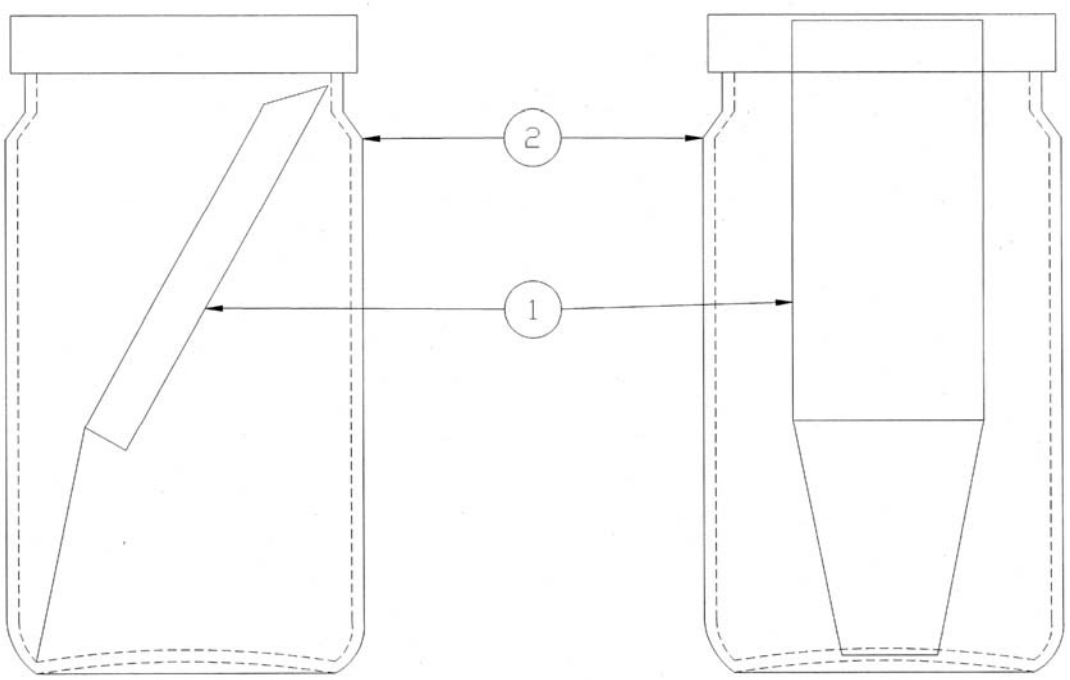


Figure 47, Prepreg Cutting Templates



Parts List:
1. Prepreg Extraction Tray
2. QorPac 1 Quart Jar With Teflon Lined Lid

Prepreg Resin Extraction Assemnly
Engineer: Roger Gerzeski
Date: 22 Dec 2002 Rev A: 2 Feb 2003

Figure 48, Resin Extraction

Table 17-a, T650-35 Prepreg Properties: As (Author / Principal Investigator) Measured:

Tape	Fiber Areal Weight (gms/sqm)			Resin Content ($\%_{Weight}$)	V_f (%)
Number	Avg +/- Std	Data Points	Max – Min	Max – Min	Max – Min
3	131.9 +/- 11.8	3	145.6 – 125.0	38.9 – 35.4	56.4 – 52.5
4	149.5 +/- 3.3	3	152.5 – 146.0	36.6 – 35.9	55.6 – 54.9
5	139.0 +/- 6.5	4	145.9 – 132.9	38.7 – 37.9	49.2 – 48.8
6	151.3 +/- 0.4	3	151.6 – 150.8	38.1 – 37.7	49.7 – 49.0
7	134.3 +/- 3.6	3	138.4 – 131.9	38.5 – 37.7	49.4 – 48.8
8	130.4 +/- 0.5	3	131.0 – 130.1	31.9 – 31.7	56.2 – 56.0
10	133.1 +/- 0.5	3	133.6 – 132.7	32.2 – 31.6	60.2 – 59.7
11	156.2 +/- 1.8	3	158.3 – 155.1	32.4 – 31.9	56.0 – 55.4
12	162.3 +/- 0.5	3	162.8 – 161.8	33.0 – 32.7	59.1 – 58.8
13	151.3 +/- 1.5	3	152.9 – 150.0	33.4 – 32.4	59.4 – 58.5
14	153.9 +/- 1.0	3	155.0 – 153.0	34.3 – 33.7	57.8 – 57.3
18	156.2 +/- 2.2	3	157.8 – 153.7	34.8 – 33.8	57.8 – 56.7
19	158.5 +/- 7.0	3	166.6 – 154.0	36.4 – 33.8	57.7 – 55.5
20	165.6 +/- 2.7	3	168.7 – 164.0	38.6 – 37.1	54.6 – 53.1
21	129.0 +/- 2.4	3	131.5 – 126.7	35.1 – 34.2	53.2 – 52.2
22	137.0 +/- 1.3	4	138.3 – 135.3	35.9 – 34.3	53.3 – 51.5
23	140.9 +/- 0.3	3	141.1 – 140.6	35.8 – 35.5	52.0 – 51.5
24	140.7 +/- 1.5	3	142.2 – 139.2	34.0 – 33.8	53.8 – 53.7
25	138.5 +/- 0.5	3	139.0 – 138.0	35.9 – 34.6	52.8 – 51.3
26	146.0 +/- 9.4	3	156.8 – 140.5	36.1 – 35.2	56.6 – 55.7
27	144.3 +/- 1.1	3	145.1 – 143.1	33.6 – 32.7	55.0 – 53.9
28	147.3 +/- 0.9	4	148.3 – 146.2	31.3 – 29.5	62.8 – 60.7
29	150.9 +/- 2.4	3	153.6 – 149.2	37.4 – 36.2	55.4 – 54.3
30	156.6 +/- 2.7	3	159.4 – 154.0	38.4 – 37.1	54.7 – 53.0
31	165.0 +/- 6.4	3	172.4 – 160.6	37.9 – 37.1	54.8 – 53.5

Tape Number	Resin Removal (gms/sqm) To Achieve V_f Of		Thickness (mils)	
	65% Max – Min	60% Max – Min	Max – Min	Data Points
3	37.5 – 20.6	24.4 – 9.3	9.7 – 7.3	12
4	30.3 – 27.6	16.5 – 14.0	10.6 – 9.0	10
5	43.5 – 39.2	32.6 – 29.1	10.3 – 7.8	19
6	45.3 – 42.7	33.7 – 31.2	10.0 – 8.6	22
7	40.0 – 40.0	30.0 – 29.5	9.6 – 8.2	22
8	19.3 – 18.6	9.3 – 8.6	9.1 – 7.4	23
10	12.8 – 11.6	0.8 – -0.5	9.2 – 7.9	12
11	24.7 – 23.2	12.9 – 11.1	9.6 – 8.1	21
12	18.5 – 17.6	3.9 – 2.9	9.3 – 7.9	12
13	18.6 – 15.5	4.7 – 1.9	10.4 – 8.5	12
14	22.3 – 20.7	8.5 – 6.8	10.3 – 8.5	12
18	25.0 – 21.3	10.7 – 7.1	10.8 – 8.9	12
19	30.7 – 21.0	15.7 – 7.1	10.8 – 9.1	12
20	39.7 – 34.8	24.9 – 19.5	10.6 – 9.1	12
21	29.5 – 25.7	19.5 – 16.0	9.5 – 6.6	18
22	32.4 – 27.5	22.1 – 17.0	11.6 – 8.4	16
23	33.7 – 32.2	23.0 – 21.5	10.5 – 8.1	19
24	27.1 – 26.9	16.3 – 16.1	10.2 – 8.0	15
25	33.7 – 29.2	23.1 – 18.7	11.6 – 8.6	19
26	25.5 – 22.8	12.8 – 10.1	12.7 – 9.7	12
27	27.0 – 24.1	16.1 – 13.0	10.1 – 8.5	17
28	11.1 – 5.7	NA	10.0 – 8.5	17
29	32.0 – 28.0	18.4 – 14.5	10.8 – 9.6	12
30	37.7 – 32.6	23.8 – 18.2	11.6 – 9.5	12
31	40.3 – 32.3	24.8 – 17.8	16.2 – 9.0	12

Table 17-b, YSH50 Prepreg Properties: As (Author / Principal Investigator) Measured:

Tape	Fiber Areal Weight (gms/sqm)			Resin Content ($\%_{Weight}$)	V_f (%)
Number	Avg +/- Std	Data Points	Max – Min	Max – Min	Max – Min
3	146.9 +/- 1.8	3	148.8 – 145.2	45.9 – 45.3	41.7 – 41.5
4	145.5 +/- 2.4	3	147.9 – 143.2	45.7 – 45.0	42.4 – 41.5
5	137.1 +/- 10.0	3	148.6 – 130.5	47.1 – 46.3	40.9 – 39.8
6	133.5 +/- 2.8	3	135.3 – 130.3	46.6 – 46.2	40.9 – 40.7
7	142.7 +/- 3.9	3	146.9 – 139.2	45.6 – 38.9	48.4 – 41.4
8	141.5 +/- 3.0	3	144.2 – 138.3	49.9 – 48.8	38.1 – 37.2
10	144.9 +/- 2.6	3	147.7 – 142.7	42.7 – 41.2	45.8 – 44.3
11	147.5 +/- 1.3	3	148.9 – 146.3	42.4 – 41.8	45.2 – 45.0
12	146.8 +/- 0.8	3	147.6 – 146.0	42.5 – 41.5	45.3 – 44.8
14	136.7 +/- 2.1	5	139.0 – 134.2	51.0 – 41.1	46.1 – 36.3
15	136.9 +/- 1.7	3	138.8 – 135.6	49.3 – 46.9	40.0 – 38.2
16	144.0 +/- 7.0	3	152.0 – 139.3	47.4 – 46.5	40.5 – 40.0
17	144.9 +/- 0.1	3	145.0 – 144.8	45.1 – 44.2	43.0 – 42.4
19	140.6 +/- 3.4	3	143.6 – 136.9	47.2 – 45.1	42.0 – 39.9
20	139.9 +/- 1.6	3	141.4 – 138.3	44.7 – 44.5	42.7 – 42.4
21	149.4 +/- 3.8	3	153.5 – 146.1	45.3 – 41.5	45.6 – 41.8
22	159.5 +/- 4.6	4	162.9 – 152.8	45.9 – 44.6	42.5 – 41.1
24	148.0 +/- 2.5	3	150.7 – 145.8	51.9 – 51.6	35.8 – 35.5
25	142.0 +/- 2.4	3	144.8 – 140.4	52.3 – 49.8	37.5 – 35.3
27	140.9 +/- 3.6	3	143.9 – 136.9	45.6 – 42.3	45.0 – 41.7
28	128.3 +/- 1.4	3	129.2 – 126.6	50.5 – 50.1	37.4 – 36.9
29	146.3 +/- 2.0	3	147.8 – 144.1	47.5 – 45.4	41.7 – 39.6
30	145.3 +/- 1.6	3	146.5 – 143.5	44.1 – 43.5	43.8 – 43.0
31	149.8 +/- 4.0	4	154.1 – 144.4	52.1 – 49.1	38.1 – 35.5
32	144.4 +/- 3.3	3	147.4 – 140.8	49.9 – 44.4	42.7 – 37.4
33	146.5 +/- 3.8	3	150.9 – 143.9	43.3 – 42.4	44.5 – 43.8

Tape Number	Resin Removal (gms/sqm) To Achieve V_f Of		Thickness (mils)	
	65% Max – Min	60% Max – Min	Max – Min	Data Points
3	77.2 – 74.3	65.8 – 63.2	12.3 – 8.1	12
4	75.1 – 72.0	64.0 – 60.7	12.6 – 8.9	12
5	86.4 – 71.4	75.0 – 61.3	12.3 – 8.1	12
6	73.5 – 71.4	63.2 – 61.5	12.2 – 7.7	12
7	72.5 – 46.1	61.9 – 34.9	12.5 – 9.0	12
8	98.4 – 89.2	87.4 – 78.6	14.5 – 8.5	12
10	63.1 – 55.0	51.8 – 44.1	11.2 – 8.2	12
11	60.6 – 58.9	49.2 – 47.6	11.0 – 8.7	12
12	61.1 – 58.1	49.8 – 47.0	11.5 – 7.4	12
14	100.3 – 50.9	89.7 – 40.6	11.7 – 8.7	12
15	87.4 – 79.3	77.0 – 68.7	11.6 – 8.8	12
16	87.1 – 77.0	75.5 – 66.4	13.2 – 9.6	12
17	70.9 – 67.7	59.8 – 56.6	11.4 – 7.5	12
19	78.7 – 72.1	68.3 – 61.1	12.1 – 9.5	12
20	67.7 – 67.2	56.9 – 56.5	12.8 – 9.5	12
21	74.1 – 57.8	62.9 – 46.5	10.9 – 7.7	12
22	86.5 – 73.9	74.1 – 62.3	11.9 – 9.2	10
24	112.7 – 111.3	101.2 – 100.1	12.8 – 9.3	12
25	111.6 – 94.7	100.5 – 83.9	12.3 – 9.1	12
27	73.5 – 55.6	62.5 – 45.2	10.6 – 8.0	12
28	90.0 – 85.6	80.1 – 76.0	10.3 – 8.5	12
29	84.7 – 75.2	73.7 – 64.0	11.6 – 10.3	12
30	68.5 – 63.7	57.4 – 52.8	13.1 – 8.1	12
31	114.4 – 93.5	102.9 – 82.5	14.9 – 10.5	9
32	99.7 – 69.1	88.4 – 58.1	12.8 – 9.4	9
33	64.2 – 62.2	53.2 – 51.2	9.3 – 7.5	12

Table 17-c, YSH60 Prepreg Properties: As (Author / Principal Investigator) Measured:

Tape	Fiber Areal Weight (gms/sqm)			Resin Content ($\%_{Weight}$)	V_f (%)
Number	Avg +/- Std	Data Points	Max – Min	Max – Min	Max – Min
4	136.4 +/- 0.7	3	137.1 – 135.8	50.0 – 48.9	38.1 – 37.6
5	144.1 +/- 6.7	3	151.6 – 138.7	47.5 – 46.0	41.3 – 39.4
6	138.4 +/- 5.1	3	144.3 – 135.4	45.6 – 45.3	41.9 – 41.3
7	136.5 +/- 1.0	3	137.6 – 135.9	45.8 – 45.2	41.6 – 41.3
8	138.1 +/- 2.3	3	139.7 – 135.5	43.4 – 43.3	43.9 – 43.6
9	137.6 +/- 0.9	3	138.6 – 136.8	42.6 – 41.4	45.2 – 44.8
10	133.1 +/- 2.0	3	134.7 – 130.9	48.0 – 44.3	42.9 – 39.3
11	131.3 +/- 1.8	3	133.3 – 129.8	48.5 – 48.2	39.2 – 38.4
12	133.2 +/- 0.5	3	133.7 – 132.7	40.8 – 40.1	47.1 – 46.3
14	137.1 +/- 3.7	3	140.7 – 133.4	54.9 – 52.7	34.6 – 33.2
15	141.3 +/- 1.4	3	142.1 – 139.7	44.3 – 41.5	45.2 – 42.6
16	142.4 +/- 3.5	3	145.8 – 138.8	40.3 – 39.7	47.5 – 46.9
17	153.3 +/- 3.4	5	157.2 – 148.8	46.5 – 38.7	48.3 – 40.5
18	145.0 +/- 4.9	3	150.6 – 142.0	41.3 – 40.3	47.1 – 45.8
19	145.8 +/- 3.6	3	149.9 – 143.2	49.0 – 48.1	38.9 – 38.6
20	141.7 +/- 1.8	3	143.7 – 140.6	44.4 – 43.3	43.7 – 43.1
21	143.1 +/- 1.4	3	144.7 – 142.1	44.8 – 39.2	47.6 – 42.6
22	150.5 +/- 3.0	3	153.8 – 147.8	43.6 – 43.2	43.8 – 43.6
26	150.1 +/- 1.8	3	152.0 – 148.5	44.8 – 43.5	43.5 – 42.5
27	150.0 +/- 4.5	3	155.2 – 147.0	45.0 – 40.6	46.8 – 41.9
28	145.5 +/- 1.7	3	147.4 – 144.1	47.3 – 46.7	40.4 – 39.4
29	146.5 +/- 2.9	3	148.9 – 143.3	48.2 – 43.6	43.3 – 39.3
30	139.5 +/- 5.1	3	143.2 – 133.6	44.7 – 44.4	42.9 – 42.2
31	130.9 +/- 2.3	6	134.1 – 128.7	55.8 – 50.4	37.0 – 32.3
32	139.3 +/- 1.5	5	141.1 – 137.5	49.5 – 48.1	39.1 – 37.6

Tape Number	Resin Removal (gms/sqm) To Achieve V_f Of		Thickness (mils)	
	65% Max – Min	60% Max – Min	Max – Min	Data Points
4	90.9 – 88.9	80.5 – 78.4	12.4 – 8.9	12
5	82.7 – 79.4	72.2 – 67.8	12.1 – 9.2	12
6	75.6 – 68.6	64.6 – 58.3	11.7 – 9.8	12
7	71.6 – 70.7	61.2 – 60.2	11.2 – 8.8	12
8	62.5 – 61.1	51.9 – 50.6	11.4 – 7.4	12
9	57.3 – 55.0	46.7 – 44.5	11.2 – 8.6	12
10	80.3 – 61.9	70.1 – 52.0	10.7 – 8.1	12
11	82.2 – 80.2	72.3 – 70.0	10.5 – 8.2	12
12	49.2 – 46.4	39.0 – 36.2	16.7 – 7.3	12
14	123.6 – 110.3	112.9 – 99.8	12.2 – 6.4	12
15	67.3 – 56.9	56.7 – 46.0	11.6 – 8.6	12
16	51.7 – 48.0	40.5 – 37.1	11.2 – 5.9	12
17	85.9 – 48.8	74.0 – 37.0	12.9 – 9.3	12
18	54.7 – 52.4	43.8 – 40.9	12.2 – 7.7	12
19	93.8 – 88.5	82.3 – 77.6	12.4 – 9.4	12
20	66.9 – 62.8	56.0 – 52.1	12.2 – 7.7	12
21	68.4 – 47.5	57.5 – 36.6	12.5 – 8.3	12
22	69.0 – 65.3	57.3 – 54.0	11.3 – 9.0	12
26	72.6 – 67.2	61.1 – 55.9	12.1 – 8.7	12
27	74.5 – 55.4	63.2 – 43.5	11.0 – 7.8	12
28	85.7 – 82.0	74.7 – 70.8	13.2 – 8.4	12
29	88.4 – 68.4	77.1 – 57.0	11.9 – 8.2	12
30	70.8 – 63.2	59.9 – 53.0	10.8 – 7.2	12
31	121.2 – 92.6	111.2 – 82.5	12.9 – 10.4	16
32	93.3 – 84.2	82.5 – 73.7	12.8 – 9.2	22

Experimental: Composite Panel Lay Up Sequence and Sizes

D2512 requires the generation of flat specimens. To assure that the composite panels out of which the D2512 specimens where to be made were flat, a quasi isotropic lay up sequence of the prepreg plies was selected. A reasonably through reading by the A&PI of the literature concerning cryogenic temperature exposure and cryogenic cycling of composites indicated that an optimal fiber orientation difference between adjacent plies to minimize cracking and delamination was roughly 35°.[C1-C45] This orientation minimizes the stresses in the matrix resulting from the temperature excursions experienced by the composite during cure, post cure and cryogenic LOX D2512 testing. If these residual and temperature induced stresses exceed the matrixes' tensile strength and or the composite's interfacial strength, then cracks and delaminations would occur in the composite. What effect they have on the D2512 LOX compatibility of a composite is unknown, and not a variable desired to be experimentally investigated by this effort. Unfortunately a quasi isotropic lay up sequence with the fiber orientations of the adjacent ply orientated no more than 35° apart is not possible. The closest that is possible, for the least number of plies to be used, is 45°. This fiber orientation difference was settled upon by the A&PI.

A common per ply thickness routinely attained by the composites industry is 5 mils. Based upon circa 2002 fabricated LOX LV tank thicknesses in the range of 100 to 250 mils thickness, the final thickness of the composite plates made to generate the D2512 specimens needed to fall in this range. Due to the limited quantity of prepreg available to this effort, the targeted composite thickness was selected by the A&PI to be 120 mils. This set the number of plies in the composite plates to be made for this effort at twenty-four.

Based upon the above restrictions the final lay up sequence settled on by the A&PI was the twelve ply symmetric spiral lay up detailed in figure 49. This lay up sequence would generate the desired quasi isotropic flat composite plates. This sequence would also assure that the fiber orientations between individual adjacent plies would be no more than 45° and so reduce the possibility of microcracking the matrix and delaminating the composite with cryogenic LOX exposure.

For reasons associated with the cutting of D2512 specimens out of the composite plates that will be discussed later in the report, an additional eight ply symmetric spiral lay up identical to that in figure 49 minus the outer four plies was also settled upon. This lay up was used to make backing composite plates for use during the cutting of burr free D2512 specimens from the twenty-four ply specimen generating composite plates.

Two different sizes of composite plates were laid up. Initially 6 inch by 6 inch bleed flow plates were laid up and cured out by various permutations on the standard Cytec 5250-4 RTM cure cycle. When an acceptable cure cycle was developed with these bleed flow plates, then the 12 inch by 9 inch specimen composite plates were laid up and cured out. As depicted in figure 49, seventy-two D2512 specimens could be cut out of these specimen composite plates for subsequent examination and mechanical impact LOX compatibility testing.

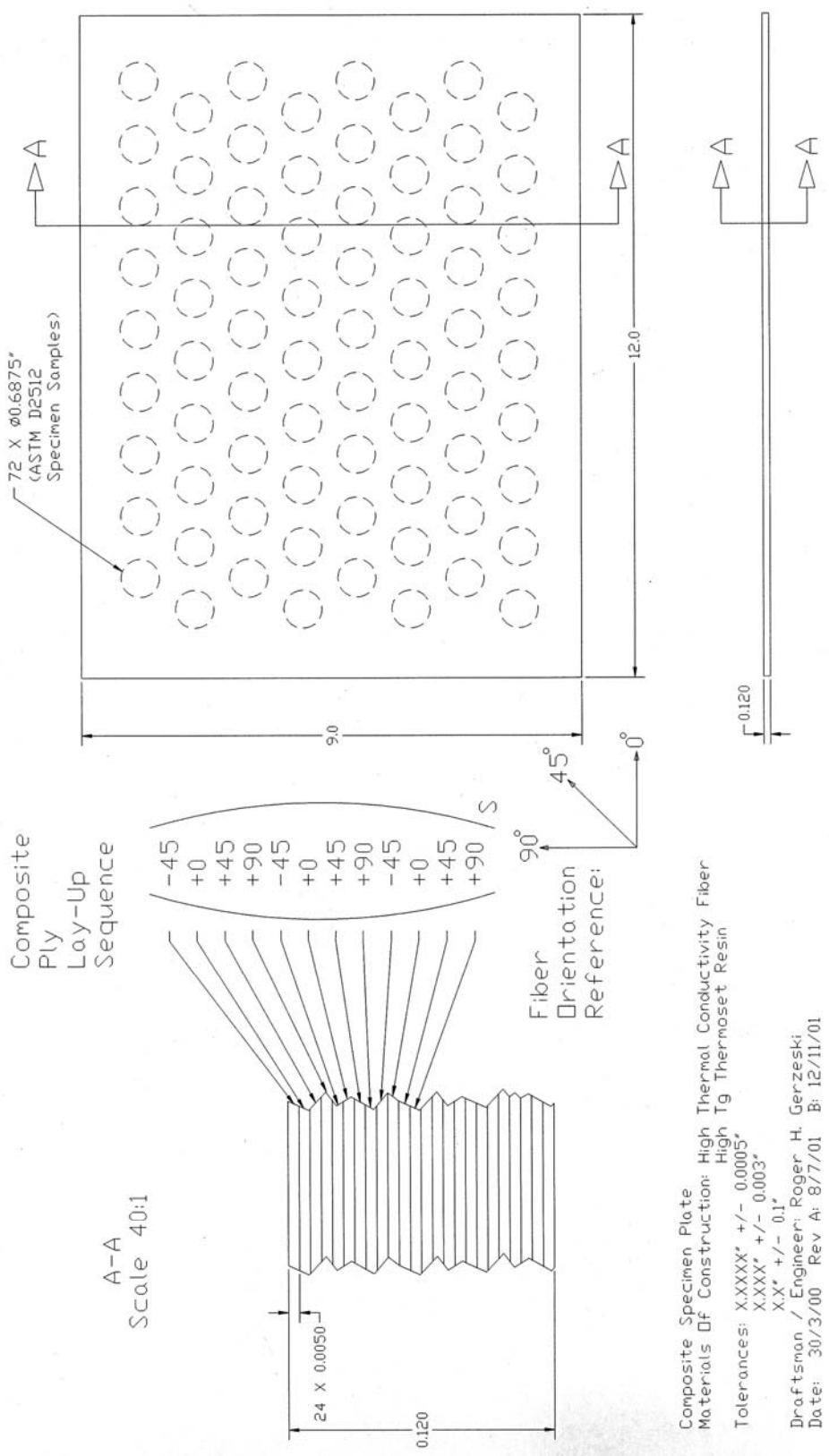


Figure 49, Proposed Specimen Plate Lay Up Sequence And Dimensions

Experimental: Bleed Flow Composite Plate Lay Up and Cure Profile Development

Four sets of bleed flow plates were laid up and cured out under various permutations of the Cytec standard 5250-4 RTM cure profile with various numbers of bleeder plies to extract the high excess resin content of the very resin rich prepregs. Vacuum was lost in the vacuum bag on one plate set and so only three successful bleed flow plate set runs were made.

Due to the extreme variance of the FAW and RC of the cut and measured prepregs listed in table 17 the A&PI was forced to devise a scheme for interleaving the various prepregs from the various cut tapes to attempt to get a uniform consistency, wrinkle free, well bled final composite exhibiting the targeted V_f. The objective of the interleaving scheme was to place high RC prepregs next to low RC prepregs and high FAW prepregs next to low FAW prepregs to attempt to create a balanced lay up while making sure that an equal number of prepregs originating from the same tape were on both symmetric sides of the final lay up. Stacks of the prepregs were planned which generated a targeted average FAW of roughly 145 gms/sqm. Table 18 lists the prepreg stacking scheme and the final uncured laid up bleed flow plate 3's prepreg properties.

Table 18, Bleed Flow Plate 3 Prepreg Lay Up Sequence And Properties:

Table 18-a-i, T650 Uncured Composite Bleed Flow Plate 3 Prepreg Lay Up Sequence:

Stacking Sequence: Top (24) to Bottom (1)	Ply Orientation	Measured Prepreg Tape Used	Reason Prepreg Tape Was Selected	
24	-45	26	Average FAW;	Average Resin Content
23	0	26	Average FAW;	Average Resin Content
22	45	13	Average FAW;	Low Resin Content
21	90	18	High FAW;	Average Resin Content
20	-45	22	Low FAW;	Average Resin Content
19	0	25	Low FAW;	Average Resin Content
18	45	18	High FAW;	Average Resin Content
17	90	25	Low FAW;	Average Resin Content
16	-45	14	High FAW;	Average Resin Content
15	0	26	Average FAW;	Average Resin Content
14	45	25	Low FAW;	Average Resin Content
13	90	26	Average FAW;	Average Resin Content
12	90	25	Low FAW;	Average Resin Content
11	45	26	Average FAW;	Average Resin Content
10	0	25	Low FAW;	Average Resin Content
9	-45	13	Average FAW;	Low Resin Content
8	90	14	High FAW;	Average Resin Content
7	45	22	Low FAW;	Average Resin Content
6	0	13	Average FAW;	Low Resin Content
5	-45	25	Low FAW;	Average Resin Content
4	90	26	Average FAW;	Average Resin Content
3	45	14	High FAW;	Average Resin Content
2	0	22	Low FAW;	Average Resin Content
1	-45	18	High FAW;	Average Resin Content

Table 18-a-ii, T650 Uncured Composite Bleed Flow Plate 3 Laid Up Prepreg Properties:

Fiber Areal Weight (gms/sqm)		Resin Content (%Weight)		V_f (%)		Thickness (mils)
Avg +/- Std	Max – Min	Avg +/- Std	Max – Min	Avg +/- Std	Max – Min	~Avg
145.6 +/- 8.1	157.8 – 135.3	34.8 +/- 1.0	36.1 – 32.4	55.3 +/- 2.6	59.4 – 51.3	0.2346

Resin Removal To Achieve V_f Of:	65% (gms)	60% (gms)
	Max – Min	Max – Min
	47.9 – 34.7	59.3 – 43.0

Bleeders Used To Achieve Resin Removal: 2

Table 18-b-i, YSH50 Uncured Composite Bleed Flow Plate 3 Prepreg Lay Up Sequence:

Stacking Sequence: Top (24) to Bottom (1)	Ply Orientation	Measured Prepreg Tape Used	Reason Prepreg Tape Was Selected	
24	-45	22	Very High FAW	High Resin Content
23	0	28	Very Low FAW	Very High Resin Content
22	45	31	Average FAW	Very High Resin Content
21	90	15	Low FAW	High Resin Content
20	-45	5	Low FAW	High Resin Content
19	0	6	Low FAW	High Resin Content
18	45	28	Very Low FAW	Very High Resin Content
17	90	31	Average FAW	Very High Resin Content
16	-45	6	Low FAW	High Resin Content
15	0	22	Very High FAW	High Resin Content
14	45	15	Low FAW	High Resin Content
13	90	5	Low FAW	High Resin Content
12	90	6	Low FAW	High Resin Content
11	45	5	Low FAW	Average Resin Content
10	0	15	Low FAW	High Resin Content
9	-45	31	Average FAW	Very High Resin Content
8	90	28	Very Low FAW	Very High Resin Content
7	45	22	Very High FAW	High Resin Content
6	0	5	Low FAW	High Resin Content
5	-45	28	Very Low FAW	Very High Resin Content
4	90	22	Very High FAW	High Resin Content
3	45	6	Low FAW	High Resin Content
2	0	31	Average FAW	Very High Resin Content
1	-45	15	Low FAW	High Resin Content

Table 18-b-ii, YSH50 Uncured Composite Bleed Flow Plate 3 Laid Up Prepreg Properties:

Fiber Areal Weight (gms/sqm)		Resin Content ($\%_{Weight}$)		V_f (%)		Thickness (mils)
Avg +/- Std	Max – Min	Avg +/- Std	Max – Min	Avg +/- Std	Max – Min	~Avg
142.2 +/- 11.8	162.9 – 126.6	47.9 +/- 2.1	52.1 – 44.6	39.4 +/- 2.0	42.5 –35.5	0.2496

Resin Removal To Achieve V_f Of:	65% (gms)	60% (gms)
	Max – Min	Max – Min
	114.4 – 71.4	102.9 – 61.3

Bleeders Used To Achieve Resin Removal: 17

Table 18-c-i, YSH60 Uncured Composite Bleed Flow Plate 3 Prepreg Lay Up Sequence:

Stacking Sequence: Top (24) to Bottom (1)	Ply Orientation	Measured Prepreg Tape Used	Reason Prepreg Tape Was Selected	
24	-45	31	Very Low FAW	Very High Resin Content
23	0	4	Low FAW	High Resin Content
22	45	10	Low FAW	High Resin Content
21	90	7	Low FAW	High Resin Content
20	-45	11	Very Low FAW	High Resin Content
19	0	31	Very Low FAW	Very High Resin Content
18	45	7	Low FAW	High Resin Content
17	90	31	Very Low FAW	Very High Resin Content
16	-45	4	Low FAW	High Resin Content
15	0	11	Very Low FAW	High Resin Content
14	45	31	Very Low FAW	Very High Resin Content
13	90	10	Low FAW	High Resin Content
12	90	4	Low FAW	High Resin Content
11	45	11	Very Low FAW	High Resin Content
10	0	31	Very Low FAW	Very High Resin Content
9	-45	10	Low FAW	High Resin Content
8	90	11	Very Low FAW	High Resin Content
7	45	31	Very Low FAW	Very High Resin Content
6	0	7	Low FAW	High Resin Content
5	-45	31	Very Low FAW	Very High Resin Content
4	90	31	Very Low FAW	Very High Resin Content
3	45	4	Low FAW	High Resin Content
2	0	10	Low FAW	High Resin Content
1	-45	7	Low FAW	High Resin Content

Table 18-c-ii, YSH60 Uncured Composite Bleed Flow Plate 3 Laid Up Prepreg Properties:

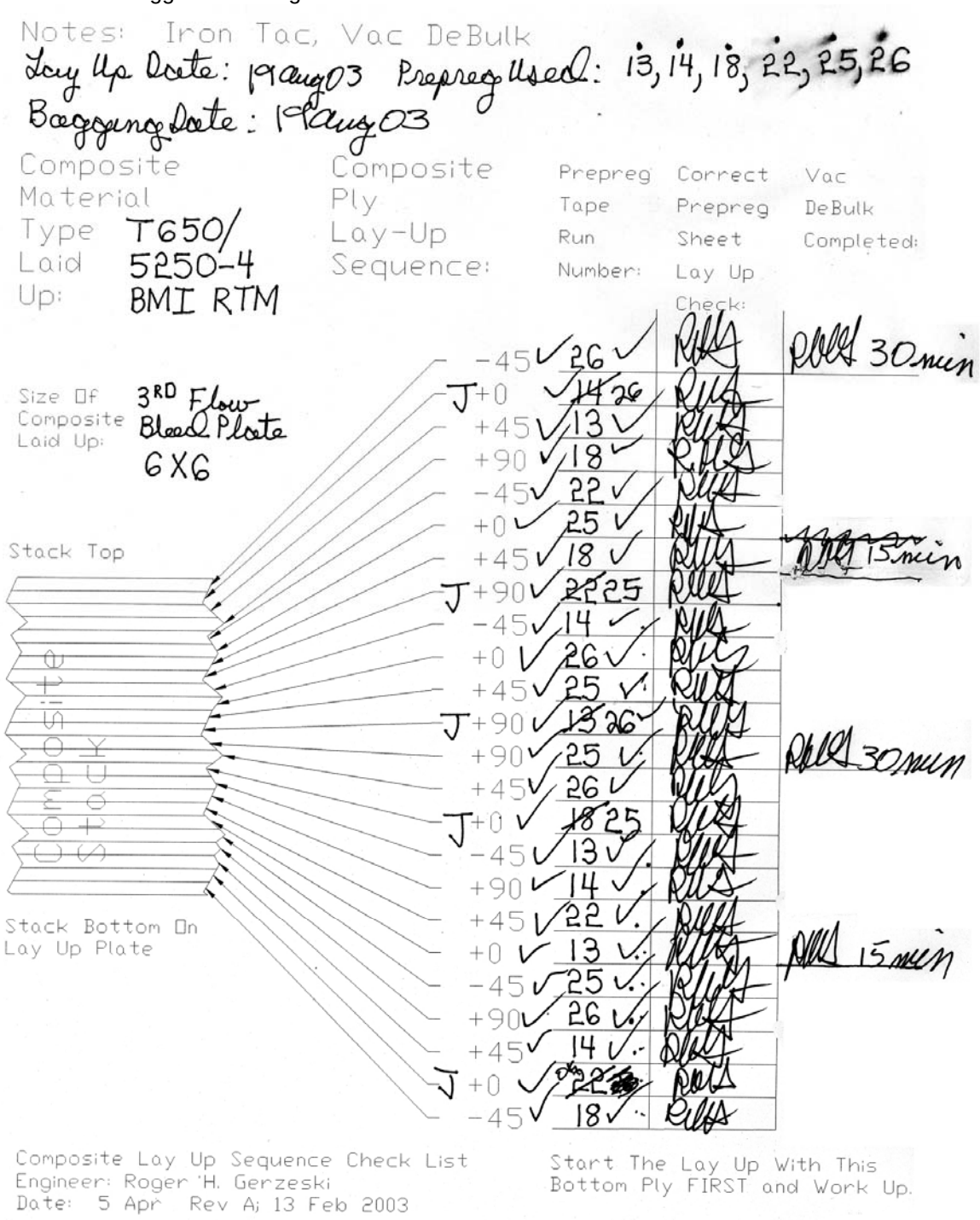
Fiber Areal Weight (gms/sqm)			Resin Content ($\%_{Weight}$)			V_f (%)		Thickness (mils)
Avg	+/- Std	Max – Min	Avg	+/- Std	Max – Min	Avg +/- Std	Max – Min	~Avg
132.6	+/- 2.9	137.6 – 128.7	50.2	+/- 3.2	55.8 – 44.3	37.2 +/- 3.0	42.9 – 32.3	0.2484

Resin Removal To Achieve V_f Of:	65% (gms)	60% (gms)
	Max – Min	Max – Min
	121.2 – 61.9	111.2 – 52.0

Bleeders Used To Achieve Resin Removal: 16

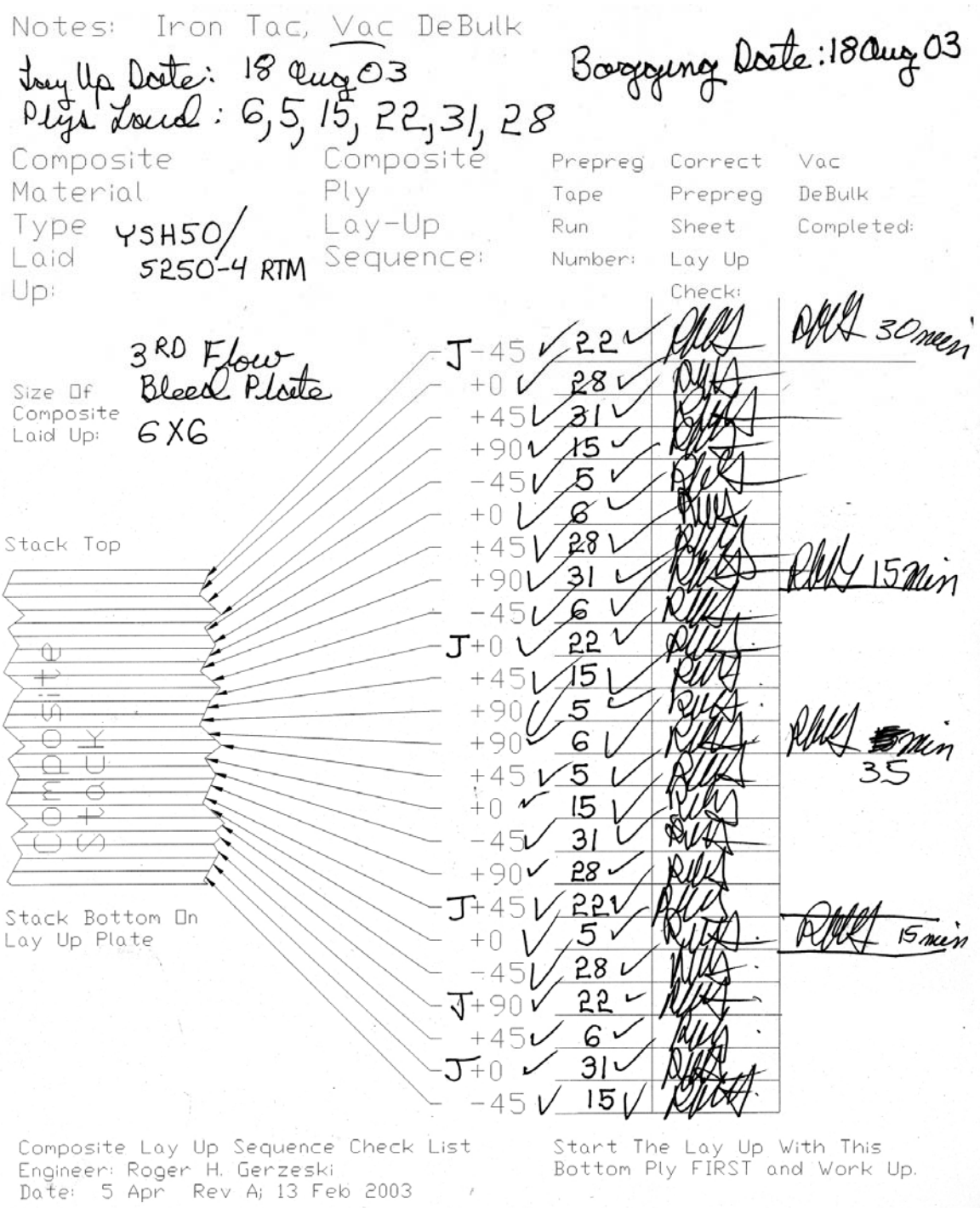
To assure that the correct cut prepregs were laid up in the correct orientation during the lay up assembly of the bleed flow composite plates and to assure that vacuum debulking was done in a systematic manner the A&PI used templates and check lists. Figure 50 depicts the checklists generated during the lay up of the bleed flow 3 composite plates. As seen in figure 50 many more of the prepregs broke up during lay up. Also four vacuum debulks were done during each composite lay up with durations of 15 to 60 minutes. Each ply was tacked down by first putting a clean sheet of Teflon peal ply on the already laid up stack and then lightly running a previously cleaned with cheese cloth wipes soaked in IPA heated clothing iron over the just laid down prepreg. The entire lay up was done using the Meticulous Cleaning Procedures. These cleaning and handling procedures were done on the bleed flow composite plates to keep the 12 inch by 9 inch prepregs, stored in the same freezer bag with these 6 inch by 6 inch prepregs per prepregged tape number, uncontaminated for future use in making the specimen composite plates.

The laid up bleed flow 3 composite plates then had the number of bleeder sheets indicated in table 18 spaced as equally as possible on each side of the laid up composite. The composite plate with bleeders were then placed on a Teflon coated stainless steel caul plate and wrapped in bagging. The wrapped specimen composite plates were then transferred to an on site autoclave and vacuum bagged for curing.



Note: J designates the Jigsaw breakup of the ply when removed from the storage bag for lay up.

Figure 50-a, Uncured Composite Bleed Flow Plate Stack Assembly And Initial Vacuum Debulk



Note: J designates the Jigsaw breakup of the ply when removed from the storage bag for lay up.

Figure 50-b, Uncured Composite Bleed Flow Plate Stack Assembly And Initial Vacuum Debulk

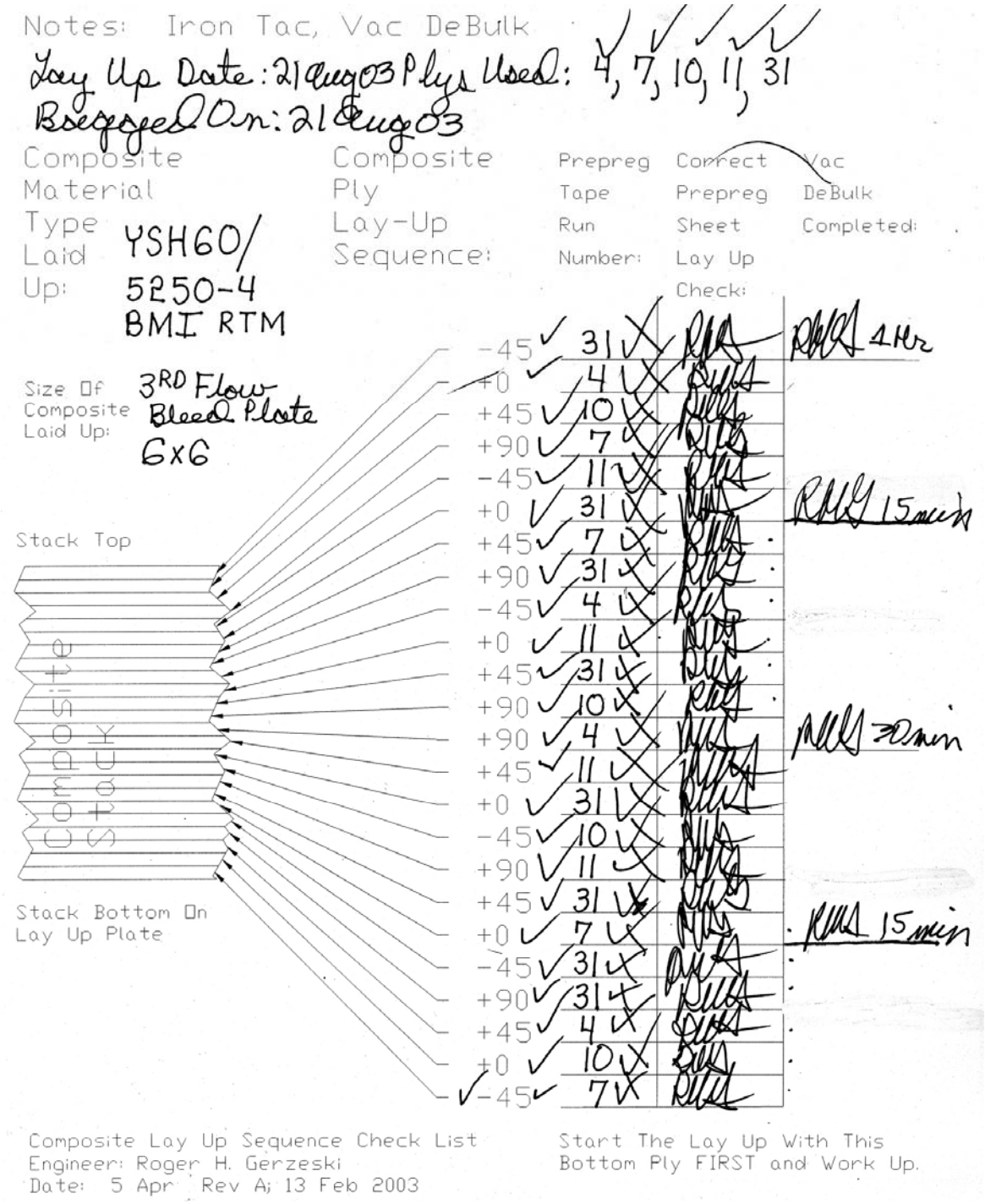


Figure 50-c, Uncured Composite Bleed Flow Plate Stack Assembly And Initial Vacuum Debulk

All three types of bleed flow 3 composites were cured simultaneously by the A&PI modified 5250-4 RTM cure profile depicted in figure 51. The key changed features of this cure profile was the 15 hour vacuum debulk and the fast ramp up to roughly 200°F followed by a slower ramp up to the first 1 hour bleed hold. The 200°F rate change point was selected because that was always above the resin impregnation temperature as listed in table 16. This assured that the composite's through the thickness temperature was reasonably uniform and the resin's temperature was not excessively high when the cure's scheduled timing arrived at the bleed hold. It also assured that the resin was at as low a viscosity as it could get and would have a good chance of bleeding / flowing out of the curing composite.

The cured bleed flow 3 composite plates were then removed from their wrapping and vacuum bagging material. The plates were then post cured in an air convection oven by a 6 hour 440°F post cure with a 2°F per minute ramp up to the post curing temperature and a 15 hour natural cool down.

The three bleed flow 3 composite plates were c-scanned to determine the uniformity of the composite cure and determine how effective the combination of figure 51's cure profile and table 18's bleeder sheets used was at uniformly removing the excess resin. Figure 52 shows the results of the c-scans. They indicate that the profile and bleeders used generated good uniform composite plates.

The bleed flow 3 composite plates were then cut along the lines shown in figure 52 to generate pieces for subsequent different types of testing and examination. Examination of the cut surfaces and overall composite plates shown in figure 53 indicated that the cure profile and bleeders used generated low waviness, wrinkle free, flat composite plates. Some of the cut surfaces, indicated by an arrow in figure 52, were polished. Micrographs, taken at 200X with the microscope indicated in figure 54, were made of them. Figure 55 shows a micrograph of one each of these examined surfaces for the bleed flow 3 composite plates. These micrographs indicated that there was no resin wash of the fibers, that there were no large pockets of resin, no large void pockets, good and uniform bleed flow of the resin, good and uniform consolidation of the prepreg plies and that the prepreg interleaving scheme generated roughly uniform thickness plies.

Three of the cut pieces were sampled to determine the density, V_f, resin volume (V_r) and void volume (V_v) for each of the bleed flow 3 composite plates. An acid digestion technique was used to measure these values. The results are listed in table 19. The developed figure 51 cure profile and indicated in table 18 bleeder sheets used generated composites with V_fs in or slightly greater than the targeted objective. Also the composites exhibited acceptable V_vs of around 1 percent.

Thicknesses were measured at numerous points on the cut pieces of the three bleed flow 3 composite plates with a micrometer accurate to 0.0001 inch. Table 19 lists the overall measured and per ply calculated thicknesses. All of the plates met or exceeded, by being thinner, the targeted overall composite thickness. Additionally the calculated individual ply thicknesses were commensurate with composites industry standards of 5 mils, with the bleed flow 3 composite plates made from the experimental fibers having thickness of slightly more than 4 mils.

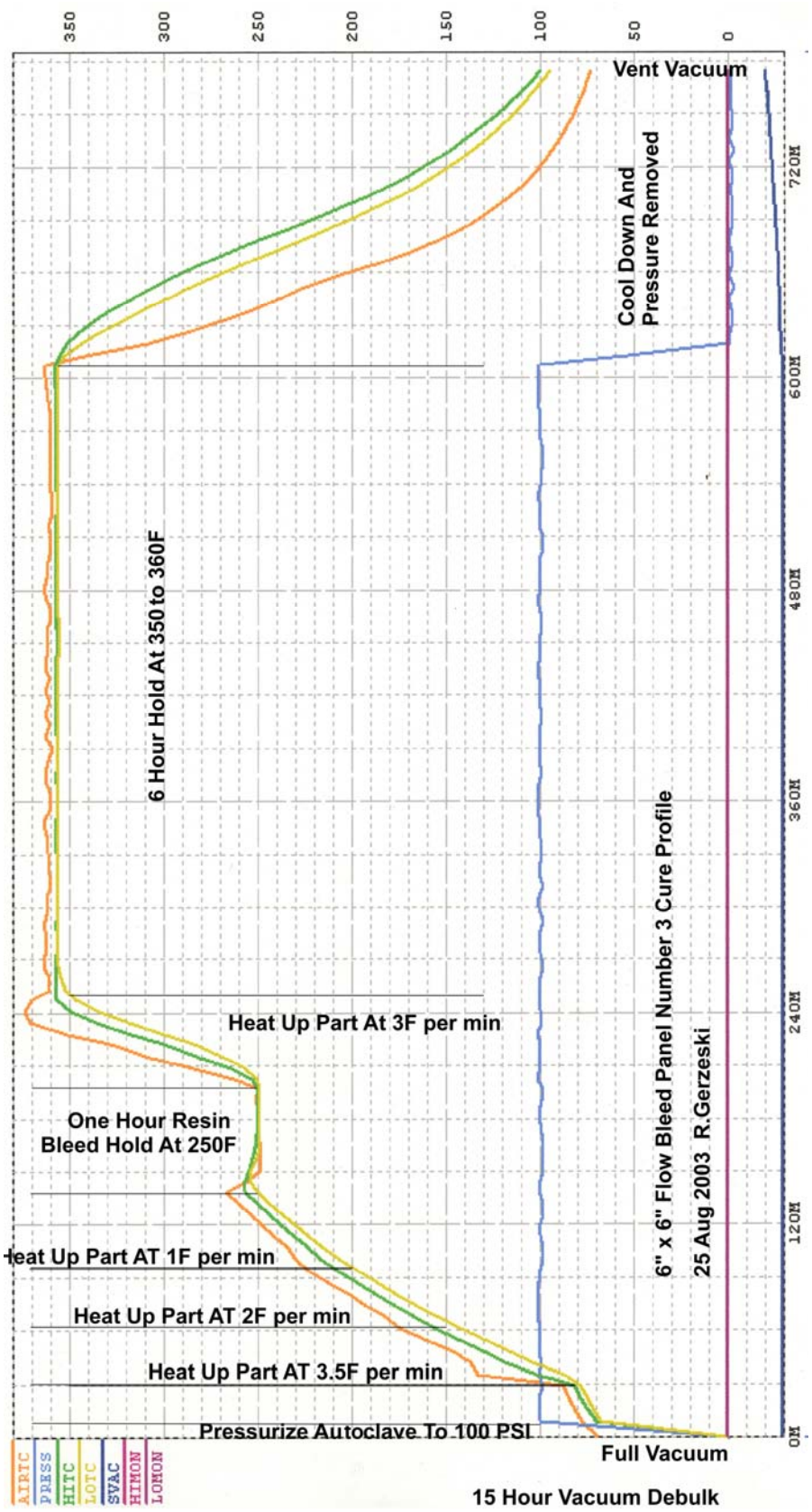


Figure 51, Actual Bleed Flow Plate 3 Cure Profile Used

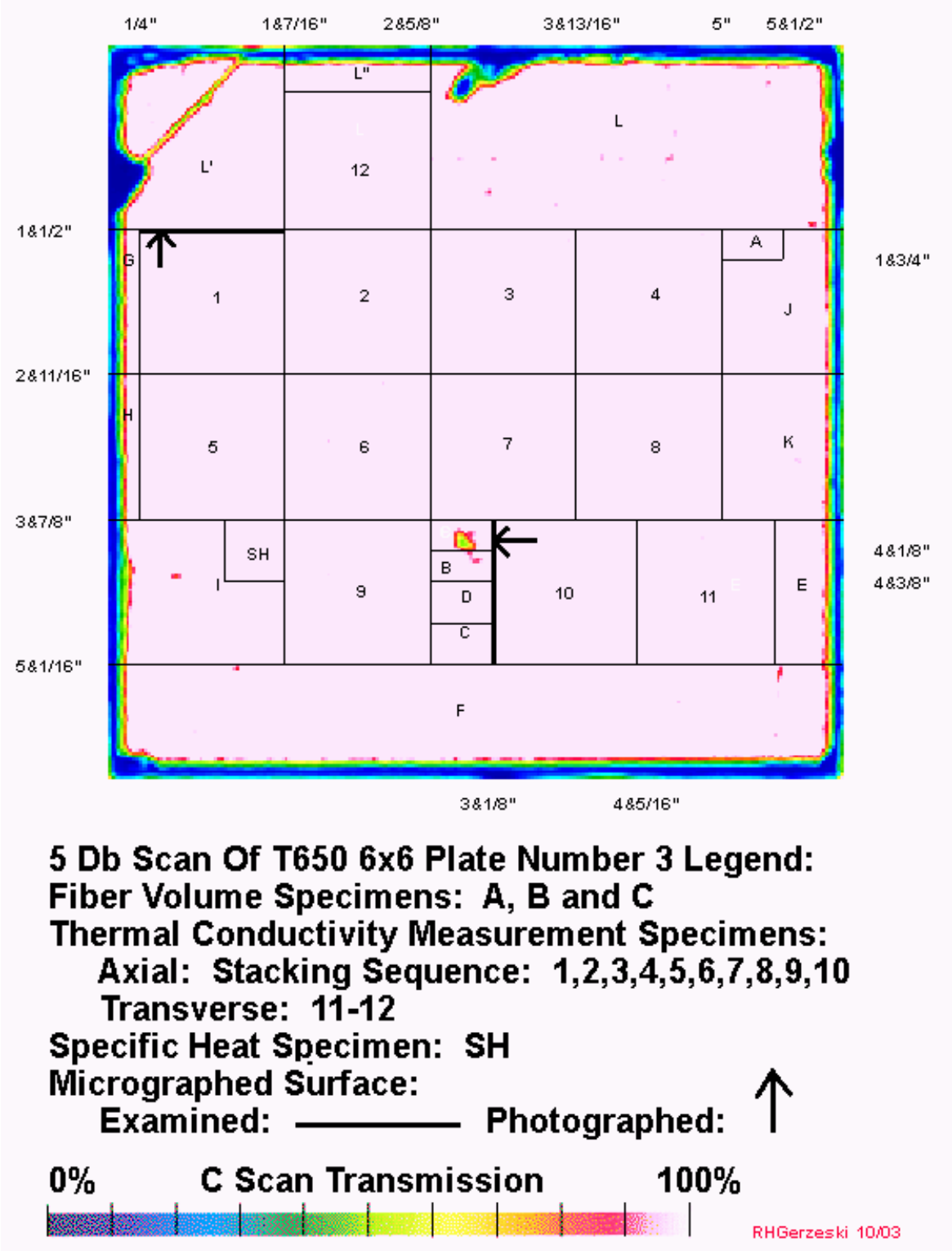


Figure 52-a, Bleed Flow 3 Composite Plate C Scans

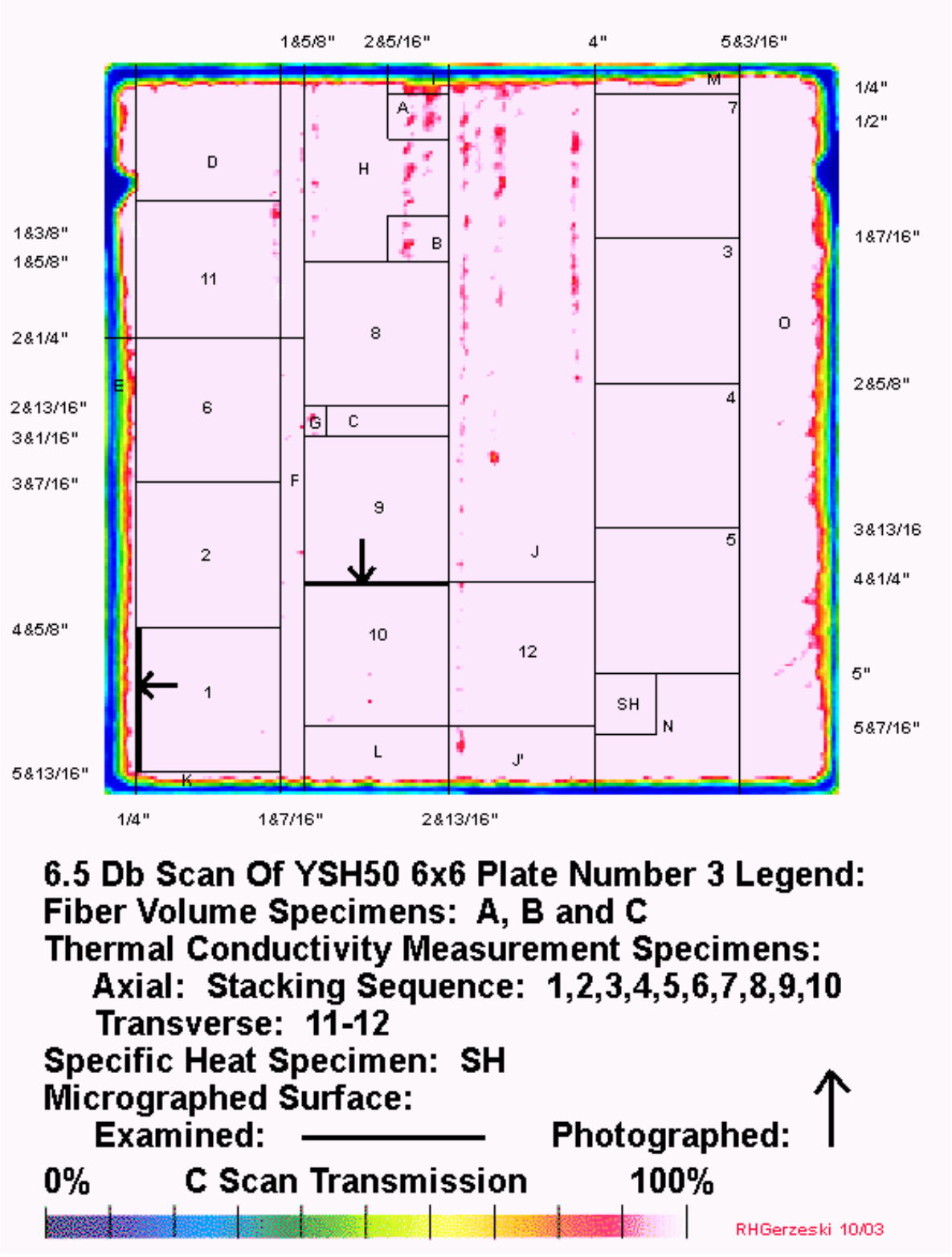


Figure 52-b, Bleed Flow 3 Composite Plate C Scans

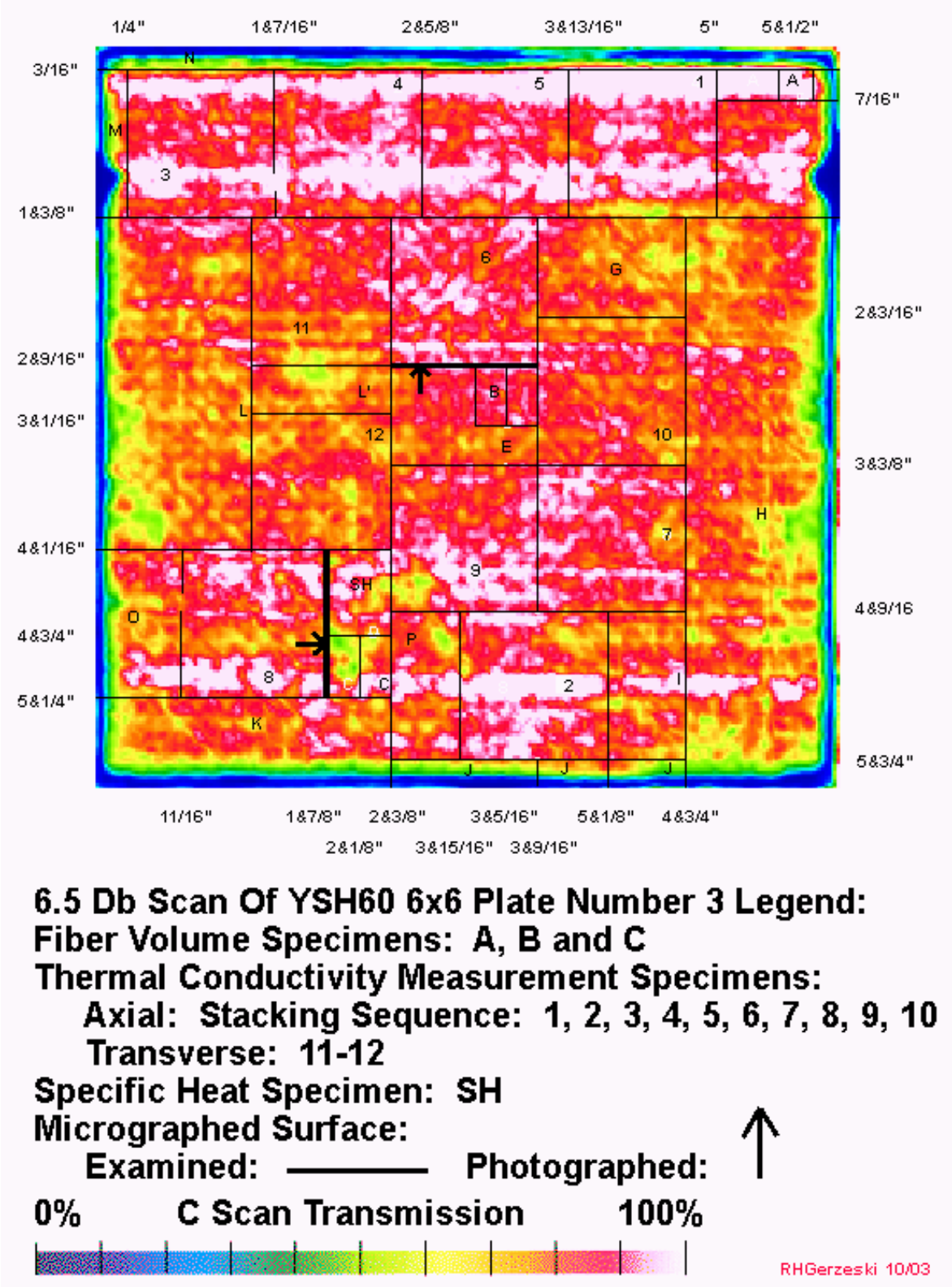


Figure 52-c, Bleed Flow 3 Composite Plate C Scans

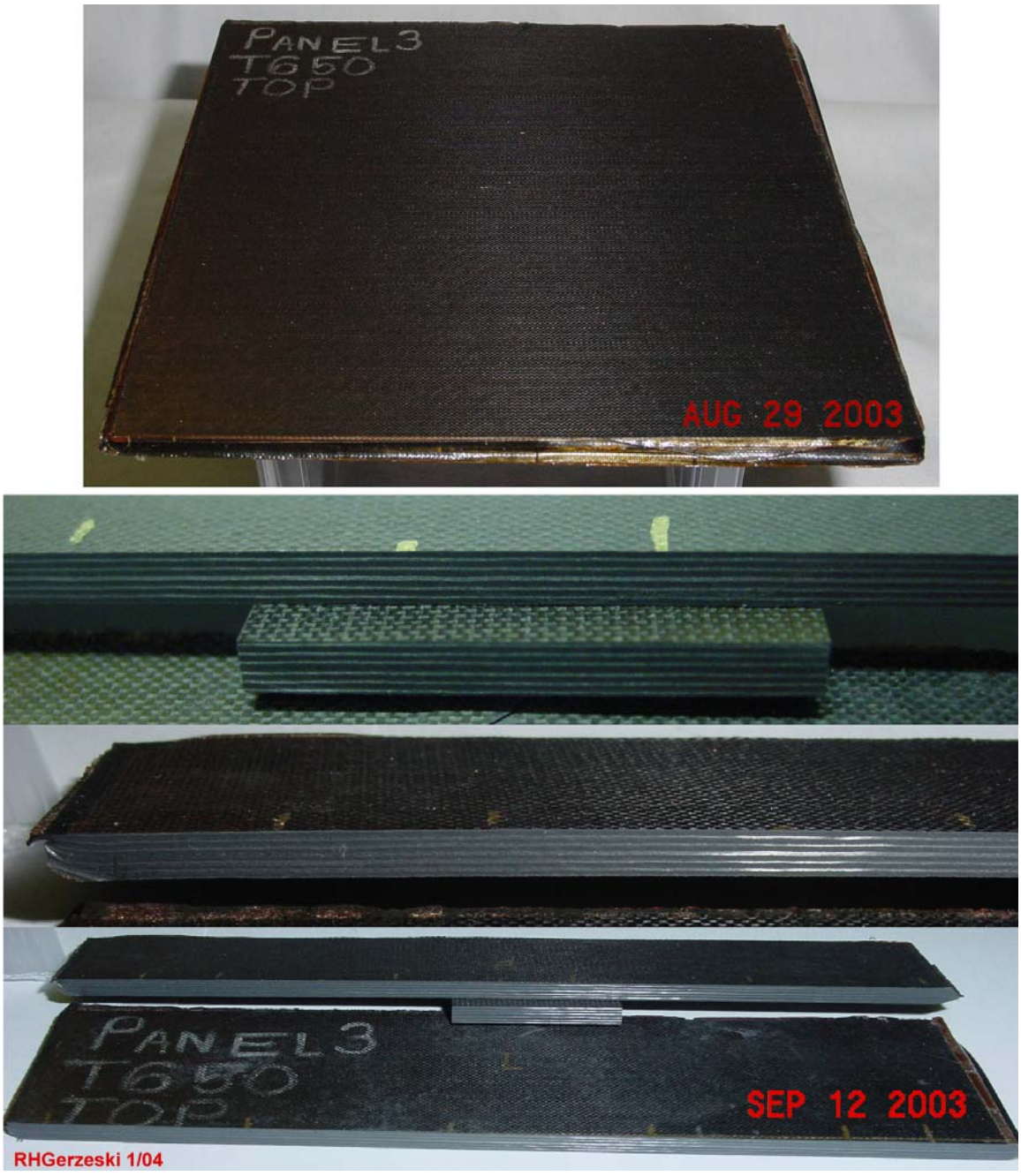


Figure 53-a, Cured Bleed Flow 3 Composite Plates

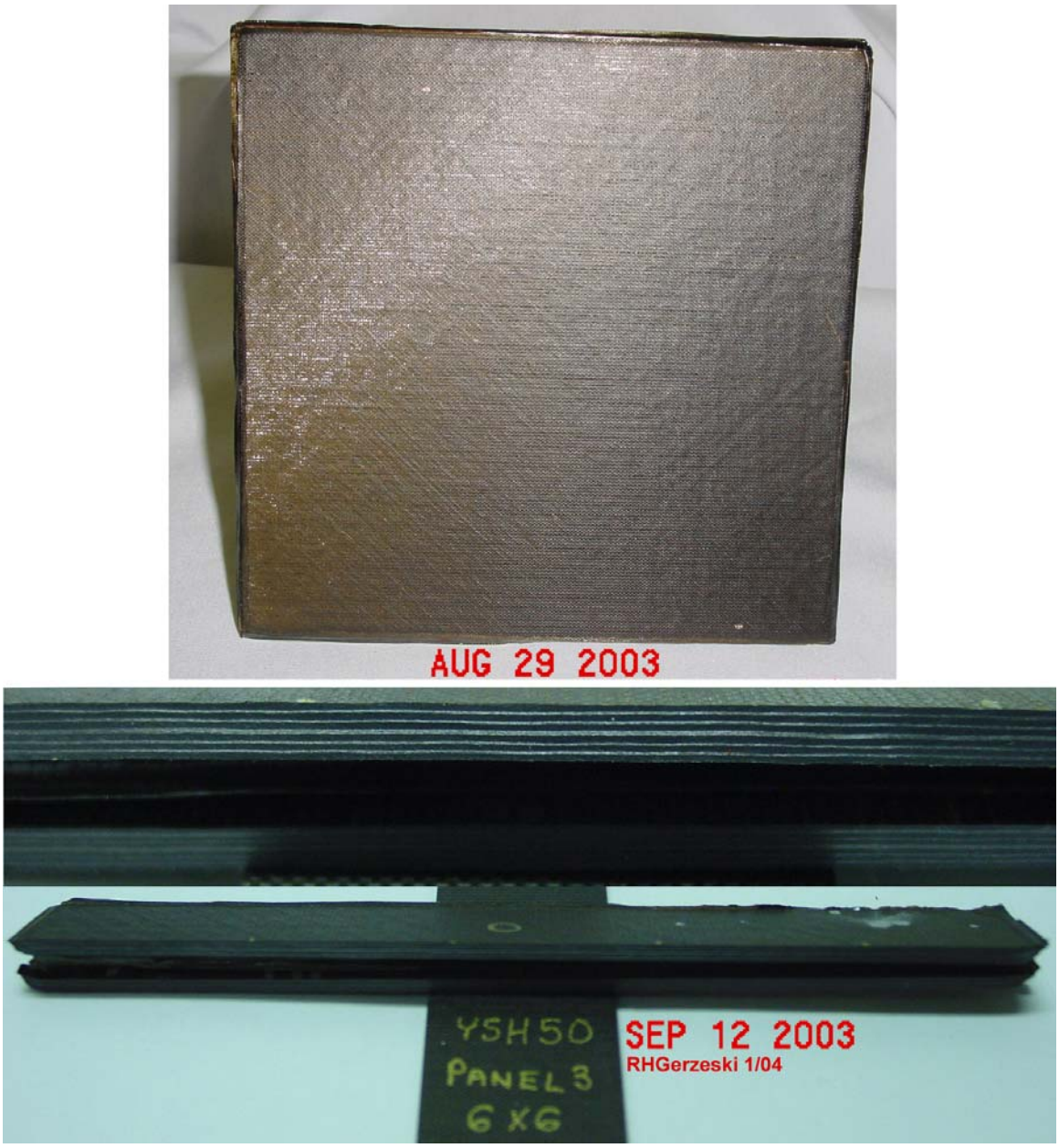


Figure 53-b, Cured Bleed Flow 3 Composite Plates

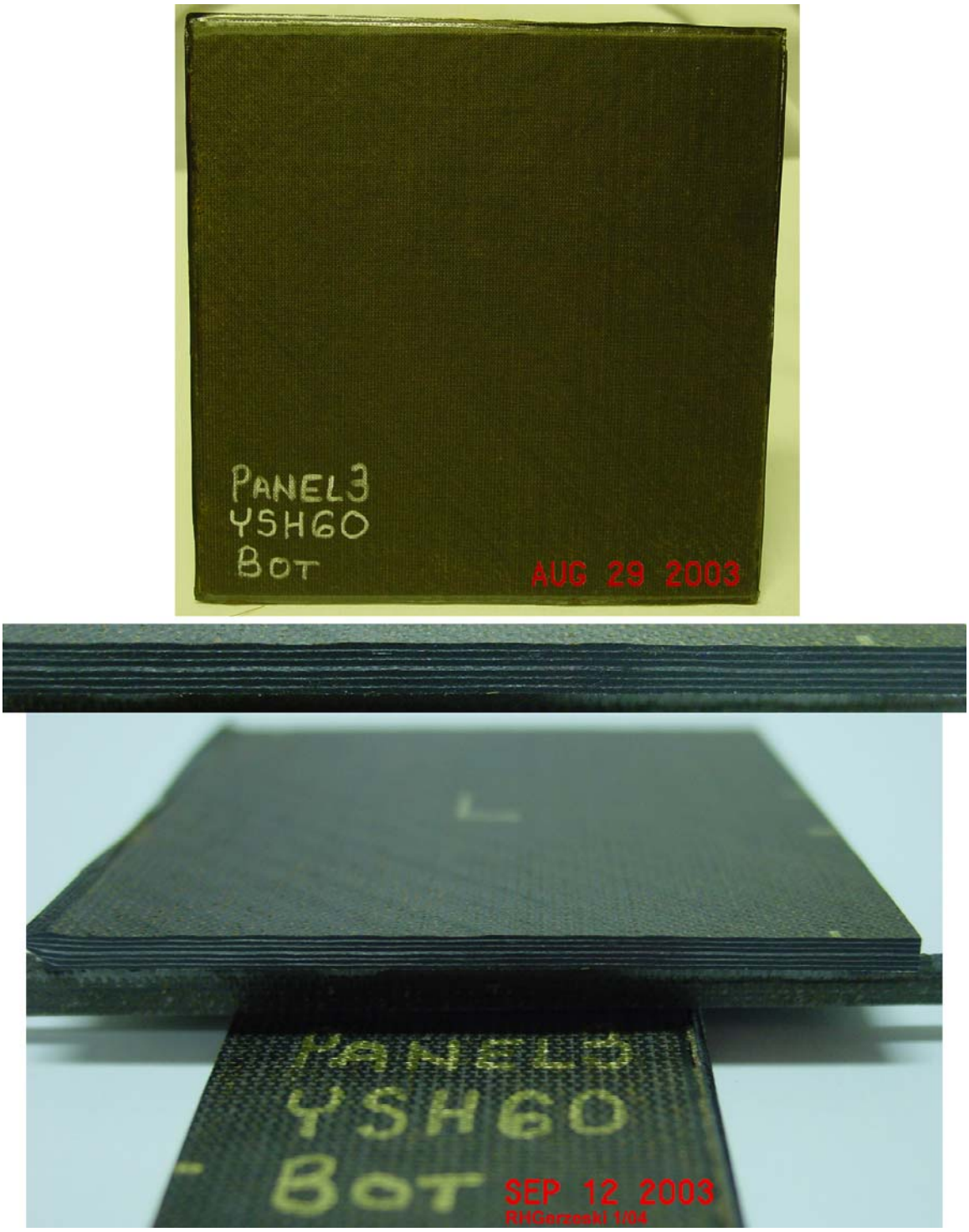


Figure 53-c, Cured Bleed Flow 3 Composite Plates

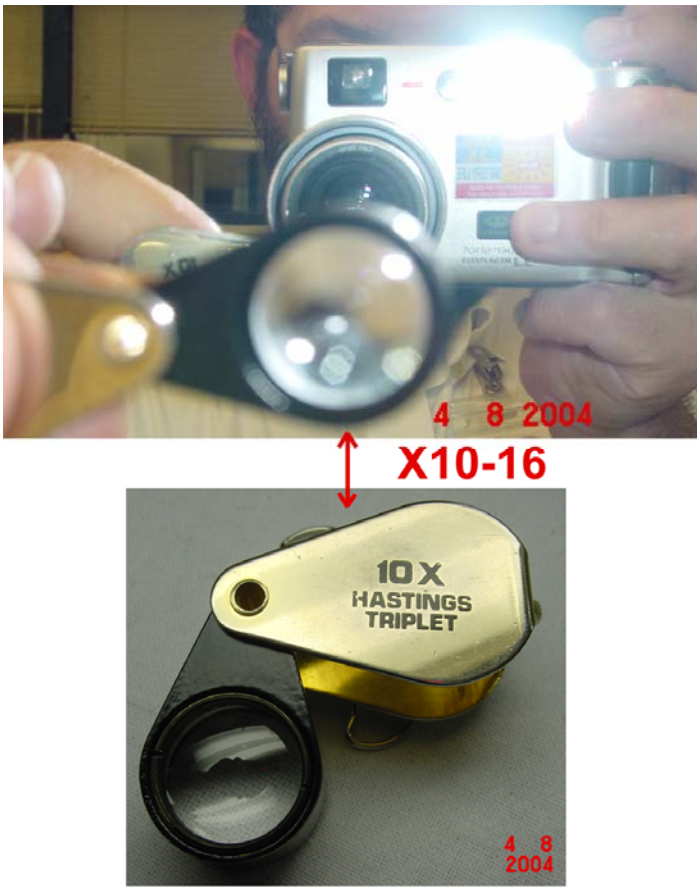


Figure 54, Microscopy and Digital Picture Capture Equipment

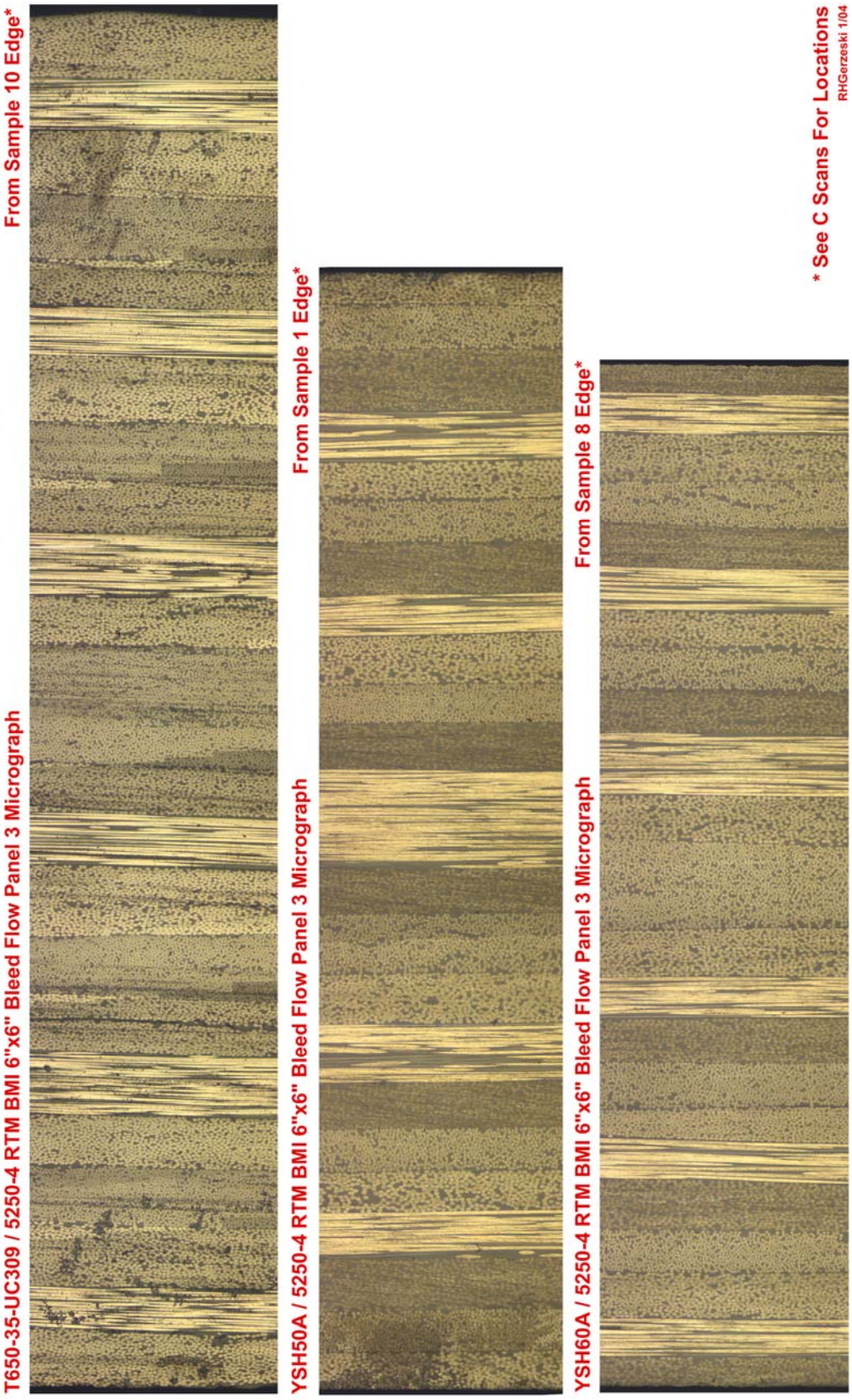


Figure 55, Bleed Flow 3 Composite Plate Micrographs

Table 19, Bleed Flow Composite Plate 3: Physical Properties:

Material:		T650-35 / 5250-4 RTM	YSH50A / 5250-4 RTM	YSH60A / 5250-4 RTM
Property: Density:	Avg:	1.5844	1.7738	1.7904
(gms/cc)	Max:	1.5990	1.7808	1.7966
	Min:	1.5706	1.7654	1.7852
	Std:	0.0142	0.0078	0.0058
Data Points:		3	3	3
Property: Fiber Volume:	Avg:	65.9963	63.2238	63.1442
(%)	Max:	66.5681	63.3994	63.4561
	Min:	65.1784	62.8714	62.7809
	Std:	0.6238	0.2425	0.2853
Data Points:		3	3	3
Property: Resin Volume:	Avg:	32.9507	35.5241	35.9478
(%)	Max:	33.4734	35.9217	36.3114
	Min:	32.2635	35.1827	35.6554
	Std:	0.3919	0.2276	0.2017
Data Points:		3	3	3
Property: Void Volume:	Avg:	1.0530	1.2521	0.9080
(%)	Max:	2.0161	1.9459	1.3067
	Min:	0.0000	0.6789	0.4680
	Std:	0.7414	0.4033	0.2556
Data Points:		3	3	3
Property: Thickness:	Avg:	0.1225	0.1038	0.0969
Overall:	Max:	0.1245	0.1064	0.1000
(inches)	Min:	0.1200	0.1019	0.0941
Data Points:		22	22	22
Property: Thickness:	Avg:	0.0051	0.0043	0.0040
Per Ply:	Max:	0.0052	0.0044	0.0042
(inches)	Min:	0.0050	0.0042	0.0039
Data Points:		22	22	22

Experimental: Specimen Composite Plate Lay Up and Cure Profile Development

One set of D2512 specimen generating composite plates were laid up and cured out under one final permutation to the cure profile developed for the bleed flow plates with a larger number of bleeder plies versus the amount of excess resin needed to be removed than that used during bleed flow 3 plate's cure.

The same scheme for interleaving the various prepregs used to make the bled flow plates was used again to overcome the extreme variance of the FAW and RC of the cut and measured prepregs. With it a prepreg stacking sequence for the specimen composite plates was developed. As with the bleed flow plates, stacks of the prepregs were planned which generated a targeted average FAW of roughly 145 gms/sqm. Table 20 lists the prepreg stacking scheme and the final laid up uncured composite specimen plate's prepreg stack properties.

Table 20, Prepreg Specimen Plate 1Lay Up Sequence And Subsequent Properties

Table 20-a-i, T650 Uncured Composite Specimen Plate 1 Prepreg Lay Up Sequence:

Stacking Sequence: Top (24) to Bottom (1)	Ply Orientation	Measured Prepreg Tape Used	Reason Prepreg Tape Was Selected	
24	-45	6	High FAW;	Low Resin Content
23	0	4	High FAW;	High Resin Content
22	45	27	High FAW;	High Resin Content
21	90	28	Average FAW;	High Resin Content
20	-45	24	Low FAW;	Average Resin Content
19	0	6	High FAW;	Low Resin Content
18	45	28	Average FAW;	High Resin Content
17	90	23	Average FAW;	Average Resin Content
16	-45	4	High FAW;	High Resin Content
15	0	24	Low FAW;	Average Resin Content
14	45	23	Average FAW;	Average Resin Content
13	90	27	High FAW;	High Resin Content
12	90	4	High FAW;	High Resin Content
11	45	24	Low FAW;	Average Resin Content
10	0	23	Average FAW;	Average Resin Content
9	-45	27	High FAW;	High Resin Content
8	90	24	Low FAW;	Average Resin Content
7	45	6	High FAW;	Low Resin Content
6	0	28	Average FAW;	High Resin Content
5	-45	23	Average FAW;	Average Resin Content
4	90	6	High FAW;	Low Resin Content
3	45	4	High FAW;	High Resin Content
2	0	27	High FAW;	High Resin Content
1	-45	28	Average FAW;	High Resin Content

Table 20-a-ii, T650 Uncured Composite Specimen Plate 1 Laid Up Prepreg Properties:

Fiber Areal Weight (gms/sqm)		Resin Content ($\%_{Weight}$)		V_f (%)		Thickness (mils)
Avg +/- Std	Max – Min	Avg +/- Std	Max – Min	Avg +/- Std	Max – Min	~Avg
145.7 +/- 4.2	152.5 – 139.2	34.4 +/- 2.5	38.1 – 29.5	54.7 +/- 4.1	62.8 –49.0	0.2248

Resin Removal To Achieve V_f Of:	65% (gms)	60% (gms)
	Max – Min	Max – Min
	75.8 – 9.5	56.4 – 0

Bleeders Used To Achieve Resin Removal: 2

Table 20-b-i, YSH50 Uncured Composite Specimen Plate 1 Prepreg Lay Up Sequence:

Stacking Sequence: Top (24) to Bottom (1)	Ply Orientation	Measured Prepreg Tape Used	Reason Prepreg Tape Was Selected	
24	-45	16	High FAW	Low Resin Content
23	0	3	High FAW	High Resin Content
22	45	29	High FAW	High Resin Content
21	90	11	Average FAW	High Resin Content
20	-45	17	Low FAW	Average Resin Content
19	0	16	High FAW	Low Resin Content
18	45	11	Average FAW	High Resin Content
17	90	20	Average FAW	Average Resin Content
16	-45	3	High FAW	High Resin Content
15	0	17	Low FAW	Average Resin Content
14	45	20	Average FAW	Average Resin Content
13	90	29	High FAW	High Resin Content
12	90	3	High FAW	High Resin Content
11	45	17	Low FAW	Average Resin Content
10	0	20	Average FAW	Average Resin Content
9	-45	29	High FAW	High Resin Content
8	90	17	Low FAW	Average Resin Content
7	45	16	High FAW	Low Resin Content
6	0	11	Average FAW	High Resin Content
5	-45	20	Average FAW	Average Resin Content
4	90	16	High FAW	Low Resin Content
3	45	3	High FAW	High Resin Content
2	0	29	High FAW	High Resin Content
1	-45	11	Average FAW	High Resin Content

Table 20-b-ii, YSH50 Uncured Composite Specimen Plate 1Laid Up Prepreg Properties:

Fiber Areal Weight (gms/sqm)		Resin Content ($\%_{Weight}$)		V_f (%)		Thickness (mils)
Avg +/- Std	Max – Min	Avg +/- Std	Max – Min	Avg +/- Std	Max – Min	~Avg
144.9 +/- 3.6	152.0 – 138.3	45.0 +/- 1.6	47.5 – 41.8	42.1 +/- 1.7	45.2 –39.6	0.2512

Resin Removal To Achieve V_f Of:	65% (gms)	60% (gms)
	Max – Min	Max – Min
	145.7 – 98.5	126.3 – 79.6

Bleeders Used To Achieve Resin Removal: 16

Table 20-c-i, YSH60 Uncured Composite Specimen Plate 1 Prepreg Lay Up Sequence:

Stacking Sequence: Top (24) to Bottom (1)	Ply Orientation	Measured Prepreg Tape Used	Reason Prepreg Tape Was Selected	
24	-45	27	High FAW	Low Resin Content
23	0	28	Average FAW	High Resin Content
22	45	26	High FAW	High Resin Content
21	90	29	Average FAW	Average Resin Content
20	-45	5	Low FAW	Average Resin Content
19	0	9	High FAW	High Resin Content
18	45	28	Average FAW	High Resin Content
17	90	26	High FAW	High Resin Content
16	-45	9	High FAW	High Resin Content
15	0	27	High FAW	Low Resin Content
14	45	29	Average FAW	Average Resin Content
13	90	5	Low FAW	Average Resin Content
12	90	9	High FAW	High Resin Content
11	45	5	Low FAW	Average Resin Content
10	0	29	Average FAW	Average Resin Content
9	-45	26	High FAW	High Resin Content
8	90	28	Average FAW	High Resin Content
7	45	27	High FAW	Low Resin Content
6	0	5	Low FAW	Average Resin Content
5	-45	29	Average FAW	Average Resin Content
4	90	27	High FAW	Low Resin Content
3	45	9	High FAW	High Resin Content
2	0	26	High FAW	High Resin Content
1	-45	28	Average FAW	High Resin Content

Table 20-c-ii, YSH60 Uncured Composite Specimen Plate 1Laid Up Prepreg Properties:

Fiber Areal Weight (gms/sqm)		Resin Content ($\%_{Weight}$)		V_f (%)		Thickness (mils)
Avg +/- Std	Max – Min	Avg +/- Std	Max – Min	Avg +/- Std	Max – Min	~Avg
144.5 +/- 5.8	155.2 – 133.6	44.6 +/- 2.1	47.5 – 40.6	42.5 +/- 2.1	46.8 –39.4	0.2436

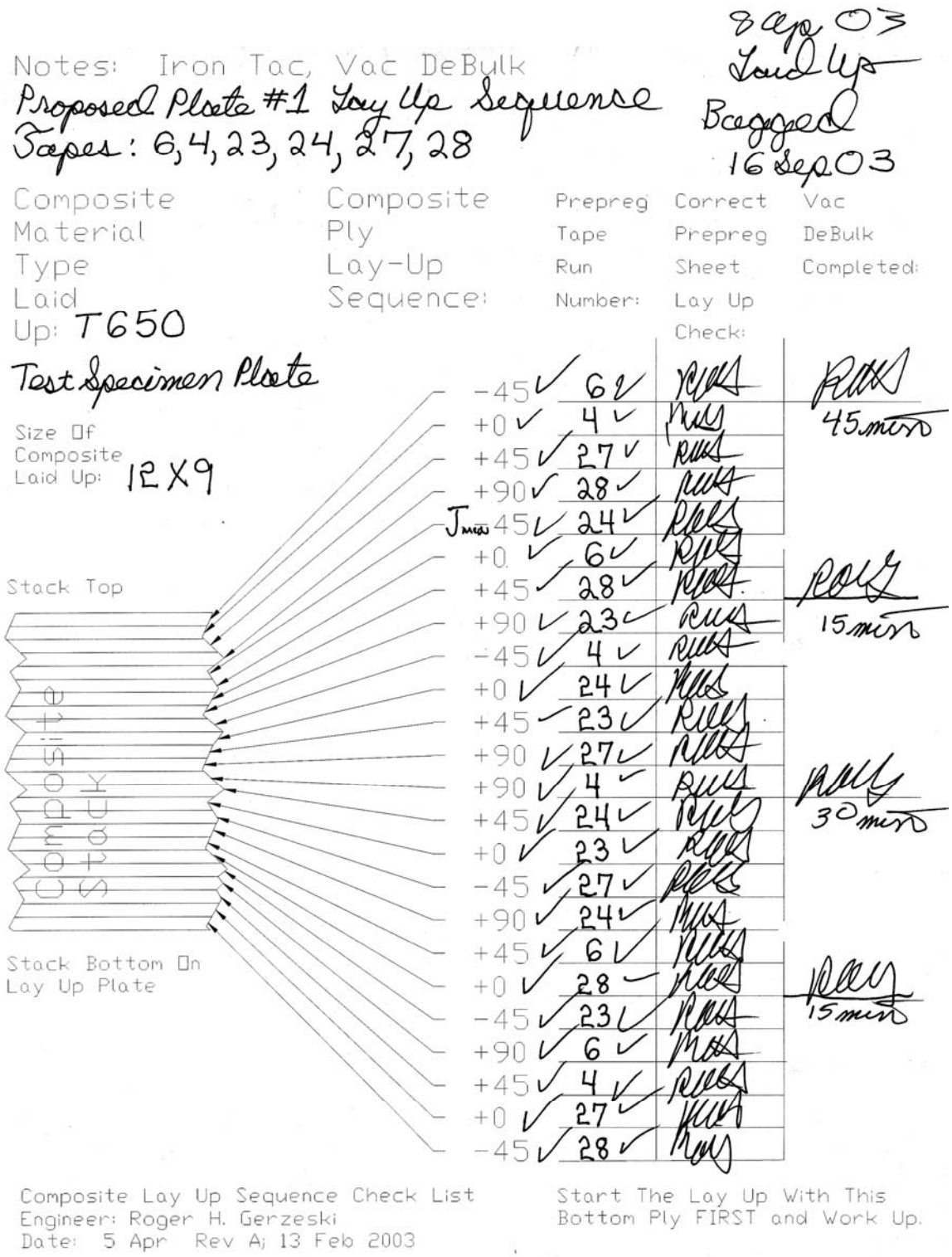
Resin Removal To Achieve V_f Of:	65% (gms)	60% (gms)
	Max – Min	Max – Min
	143.3 – 92.0	124.9 – 72.7

Bleeders Used To Achieve Resin Removal: 14

To assure that the correct cut prepregs were laid up in the correct orientation during the lay up assembly of the specimen composite plates and to assure that vacuum debulking was done in a systematic manner the A&PI once again used templates and check lists. Figure 56 depicts the checklists generated during the lay up of the specimen composite plates. As seen in figure 56 even more of the prepregs broke up during lay up. Also four vacuum debulks were done during each composite lay up with durations of 15 to 45 minutes. Each ply was tacked down by first putting a clean sheet of Teflon peal ply on the already laid up stack and then lightly running a heated clothing iron over the just laid down prepreg. Meticulous Cleaning Procedures were used during the entire lay up.

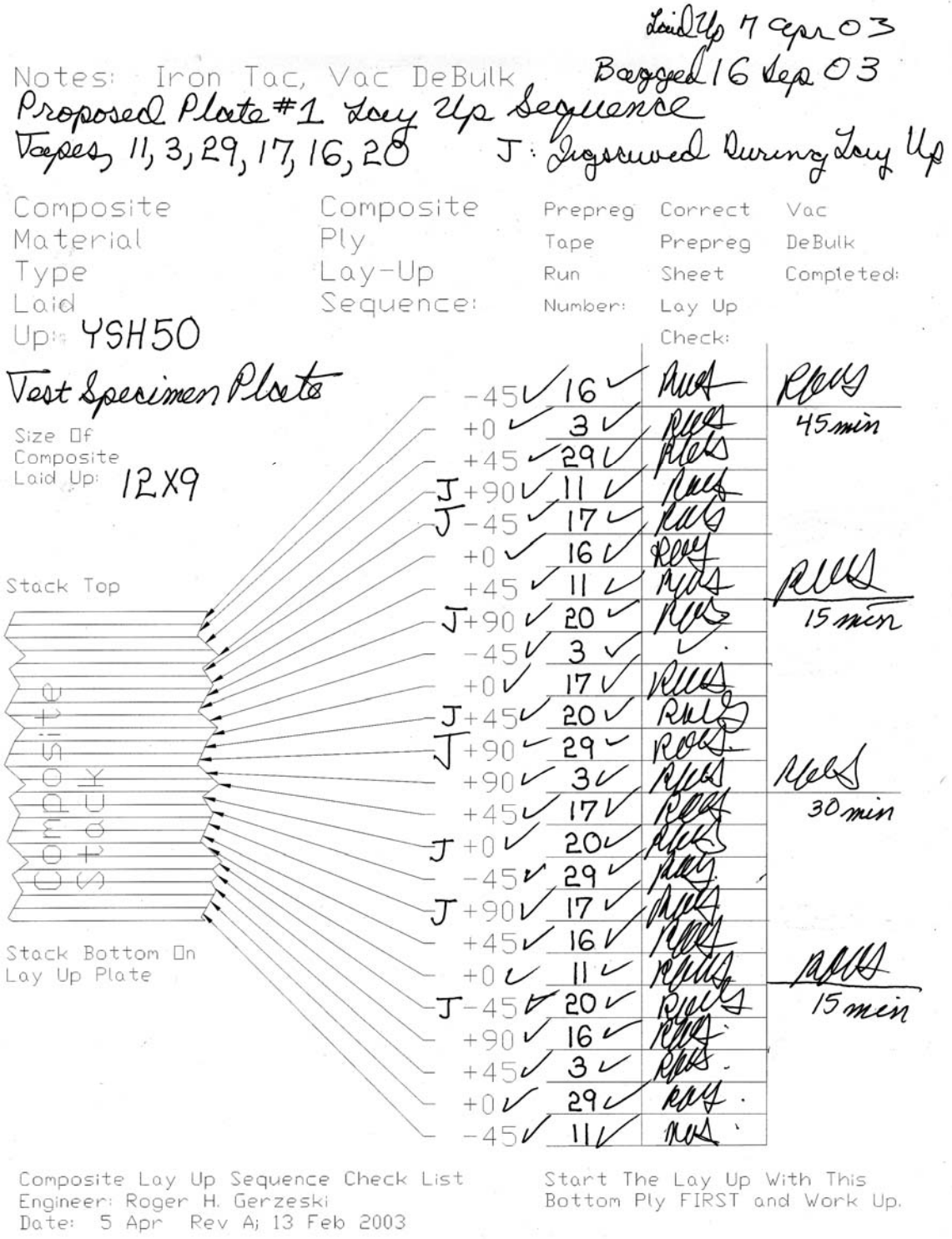
The laid up specimen composite plates then had the number of bleeder sheets indicated in table 20 spaced as equally as possible on each side of the laid up composite. The composite plate with bleeders was then placed on a Teflon coated stainless steel caul plate. The caul plate had been previously cleaned by the same procedure used to clean the D2512 LOX compatibility specimens. This cleaning procedure will be described in a later subsection. This assemblage

was then wrapped with FC&N conventional bagging materials. Meticulous Cleaning Procedures were used during the entire wrapping.



Note: J designates the Jigsaw breakup of the ply when removed from the storage bag for lay up.

Figure 56-a, Uncured Composite Specimen Plate Stack Assembly And Initial Vacuum Debulk



Note: J designates the Jigsaw breakup of the ply when removed from the storage bag for lay up.

Figure 56-b, Uncured Composite Specimen Plate Stack Assembly And Initial Vacuum Debulk

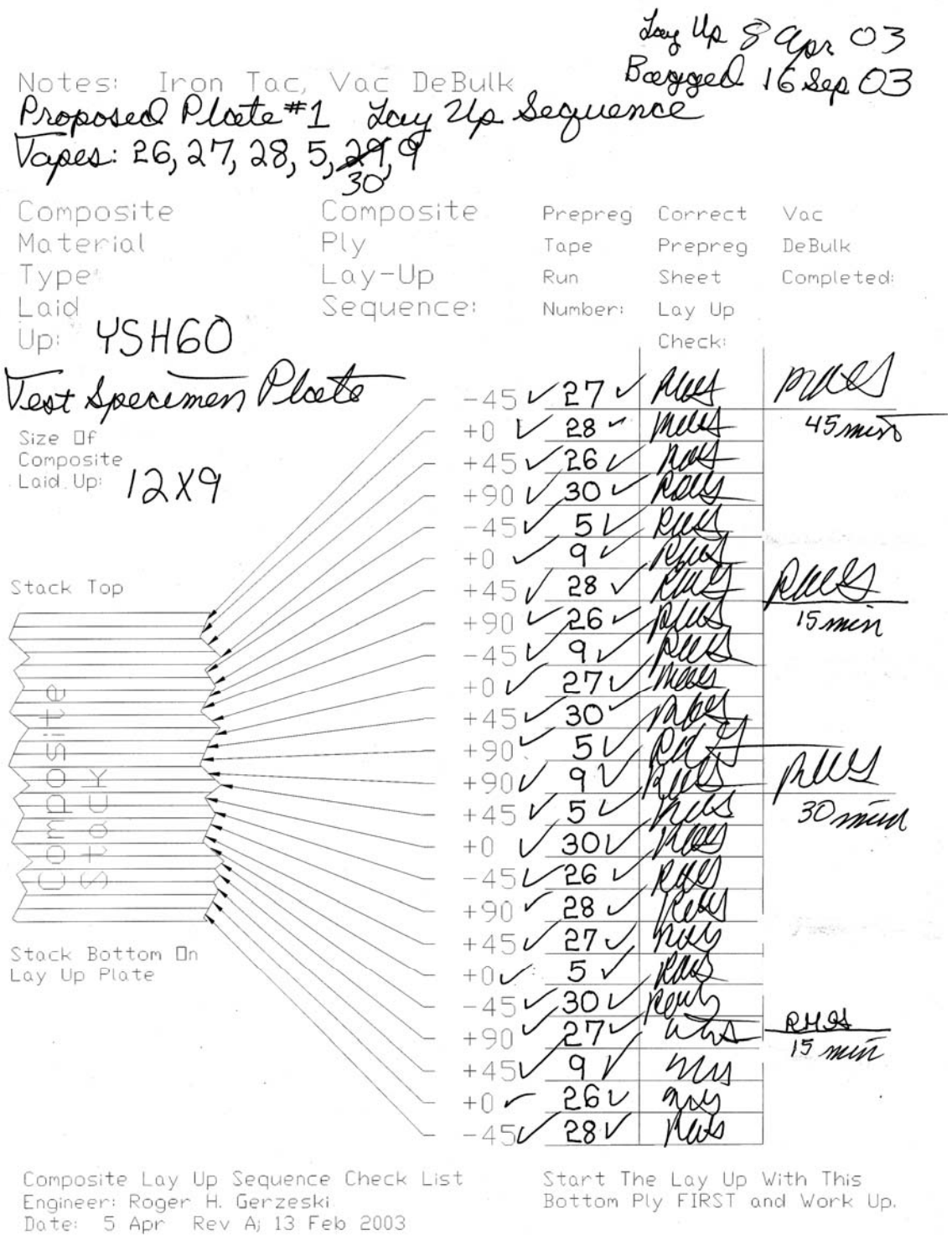


Figure 56-c, Uncured Composite Specimen Plate Stack Assembly And Initial Vacuum Debulk

The wrapped specimen composite plates were then transferred to an on site autoclave and vacuum bagged for curing.

All three types of the D2512 specimen generating composites were cured simultaneously by the final modification to the 5250-4 RTM cure profile depicted in figure 57. This was essentially the

same cure profile used to cure the bleed flow 3 composite plates with a few key changes. The autoclave temperature ramp rates between 150 to 200°F and 200 to 250°F were reduced from 2 and 1°F per minute to 1.25 and 0.75°F. This assured that the composite's through the thickness temperature was reasonably uniform and the resin's temperature was not excessively high when the cure's scheduled timing arrived at the bleed hold. It also assured that the resin was at as low a viscosity as it could get and would have a good chance of bleeding/flowing out of the curing composite.

The cured specimen composite plates were kept in their vacuum bagging as seen in figure 58 and moved into the lab room depicted in figure 42. Once in the lab room Meticulous Cleaning Procedures were followed and the wrapping and vacuum bagging material was then removed with tools which were previously cleaned by the same technique used to clean the D2512 LOX compatibility specimens. The resulting specimen composite plates were then rebagged in FC&N perforated Kapton as shown in figure 59. The perforated Katon bagging was done to minimize the potential for contamination during the post curing of the specimen composite plates in the air convection heated post curing oven. The Kapton bagged plates were then placed on top of FC&N glass fabric as shown in figure 60 so as to avoid contaminating contact with the oven's dirty surfaces and post cured in an air convection oven by the post cure profile shown in figure 61. This profile was in essence a 6 hour 440°F post cure with a 2°F per minute ramp up to the post curing temperature and a 15 hour natural cool down. The plates were actually removed from the oven when their temperature had dropped to 193°F and placed into FC&N CLEANLINER PE bags for both the remainder of their cool down and until D2512 specimens could be clean and contamination free cut from them.

Seventy-two D2512 specimens were then clean and contamination free cut from the composite specimen plates before the plates were transmission c-scanned or cut up for further property measurements. A detailed description of this cutting will be given in a later subsection of this report. Some of the cut, unfinished D2512 specimens, designated as "Friction Specimens", were retained for backscatter c-scanning and microscopy. The D2512 specimens were cut first from the composite plates since all of the subsequent testing needed to be done on the composite plates to determine their relevant physical properties and quality involve dirty processes which would contaminate the plates and subsequently the generated D2512 specimens. The c-scanning process uses tap water which would leave unacceptable quantities of contaminating metal containing chemicals and organic compounds on the plates. The diamond saw cutting of the plates would cause cross contamination of the plate's surfaces with the residue of other items previously cut by the saw. These contaminates would skew the D2512 specimen's D2512 LOX compatibility testing results towards more reactions.

The three specimen composite plates were, after they had had the D2512 specimens cut from them, transmission c-scanned to determine the uniformity of the composite cure and determine how effective the combination of figure 57's cure profile and table 20's number of bleeder sheets used was at uniformly removing the excess resin. Figure 62 depicts the results of the c-scans. They indicate that the profile and bleeders used generated good uniform composite plates.

Five to ten selected samples of the cut D2512 specimens were also backscatter c-scanned. The exact location in the specimen composite plates where they came from is designated by "FS#" (Friction Specimen #). Figure 63 depicts the results of these c-scans. They too indicated that the profile and bleeders used generated good uniform composite plates and D2512 specimens.

Both types of c-scans indicated that cutting the D2512 specimens out of the composite specimen plates caused some damage to the composites. The c-scans indicate that this damage was localized to a narrow zone near the edges cut to generate of the D2512 composite specimens.

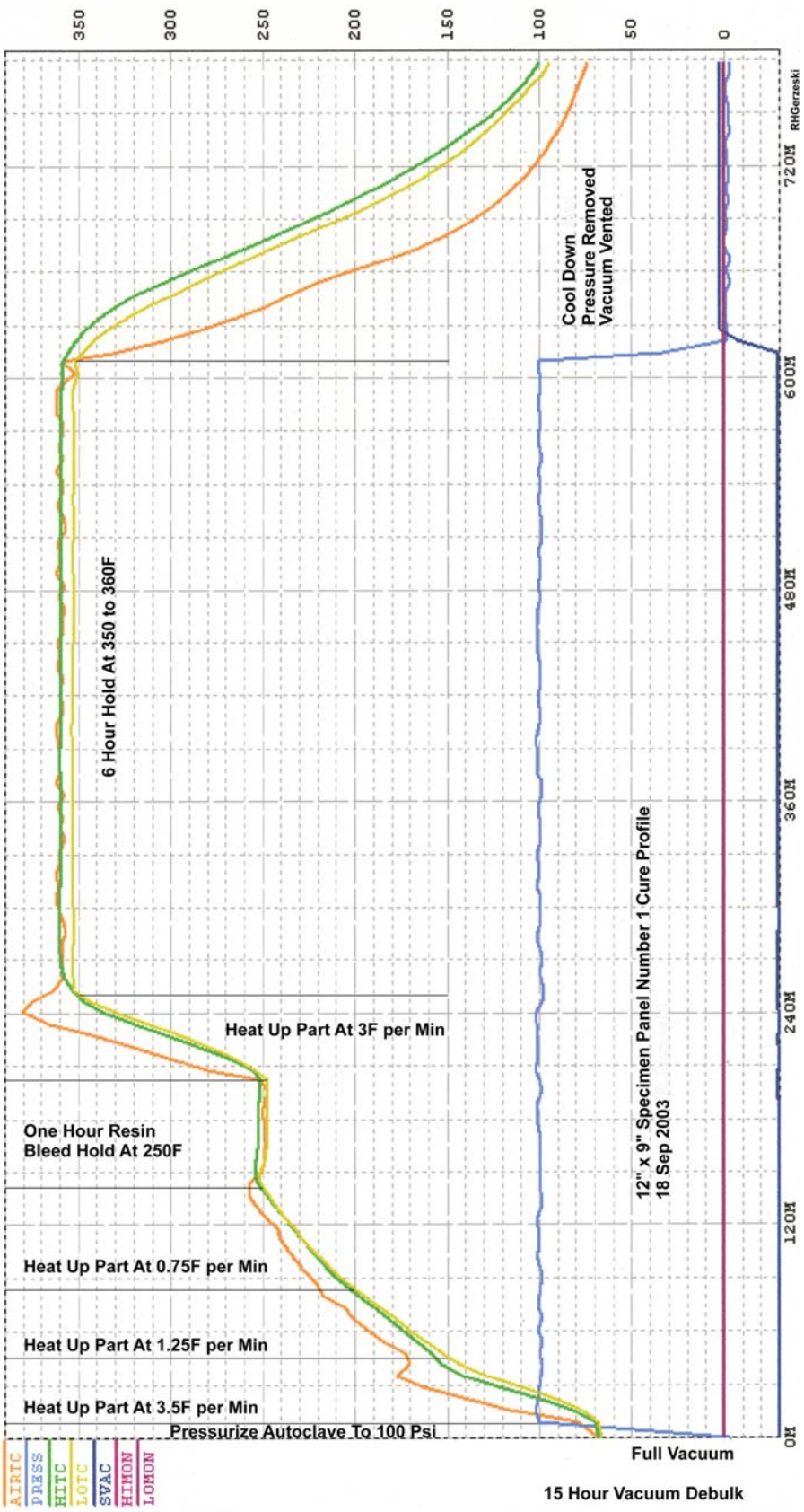


Figure 57, Actual D2512 Specimen Composite Panel Cure Profile



Figure 58, Cured Specimen Plates In Bagging

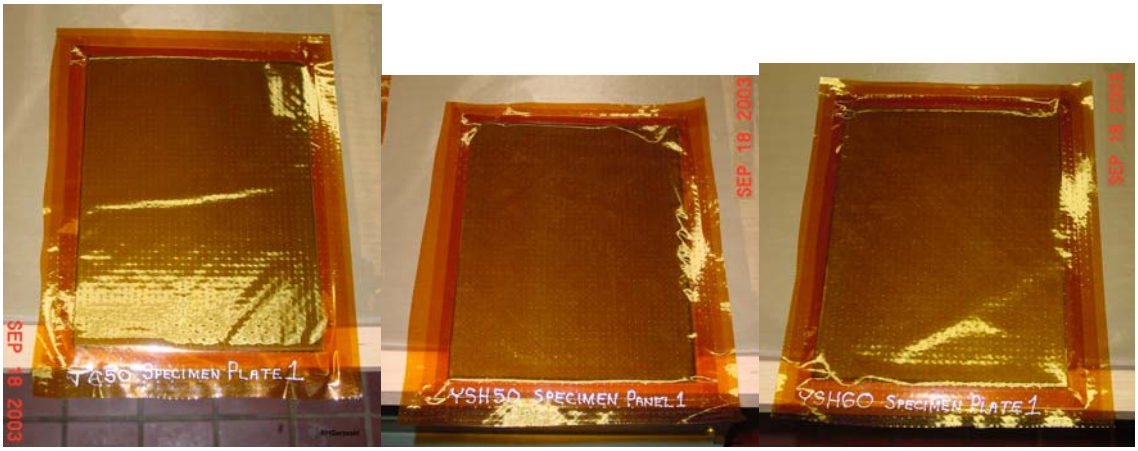


Figure 59, Perforated Kapton Bagged For Post Cure Specimen Plates



Figure 60, Perforated Kapton Bagged Post Cured Specimen Plates

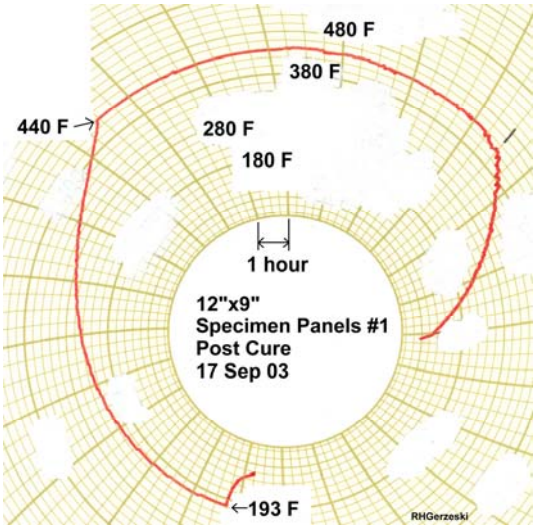


Figure 61, Actual Specimen Panel Post Cure Profile Used

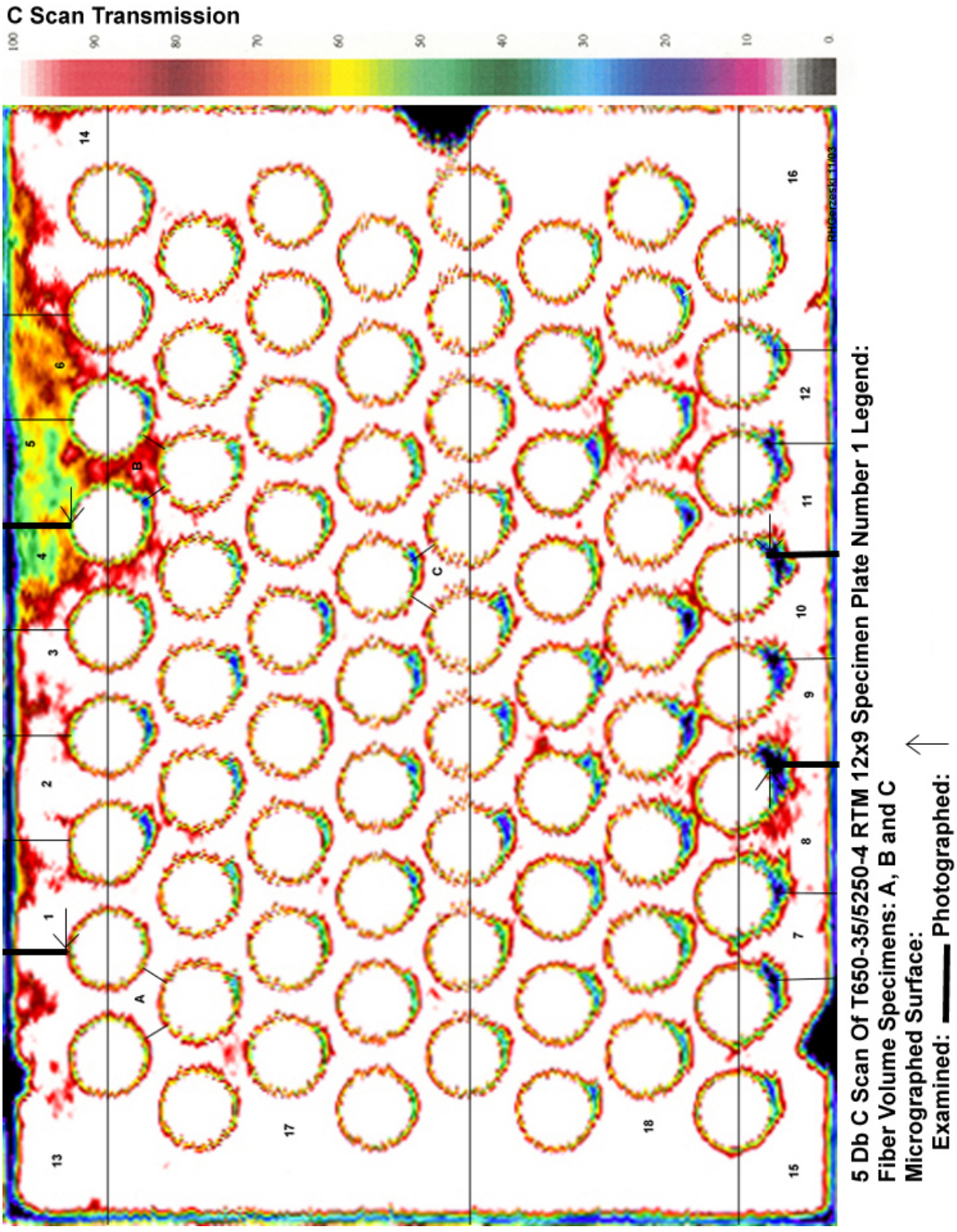


Figure 62-a, Specimen Plate C Scans

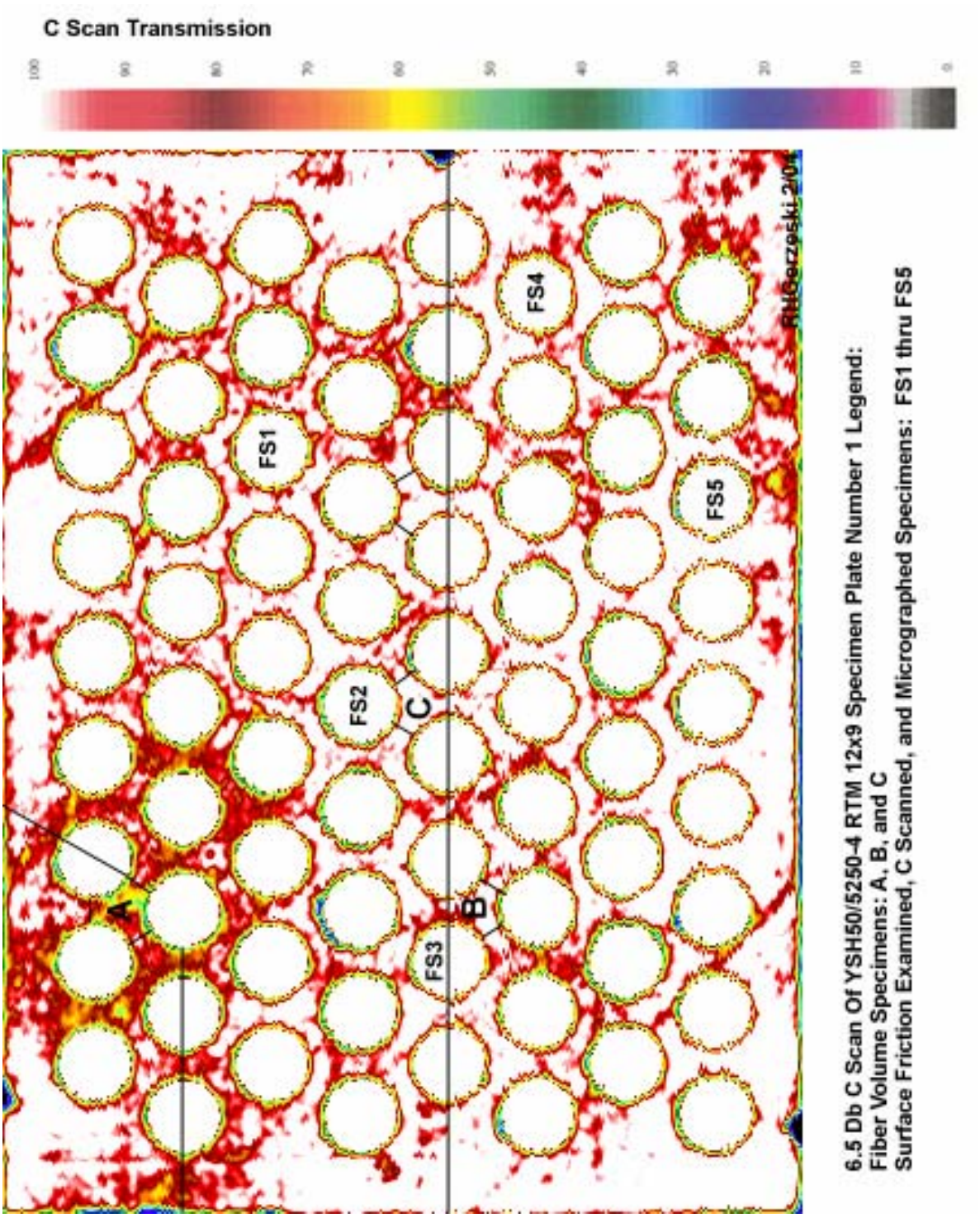


Figure 62-b, Specimen Plate C Scans

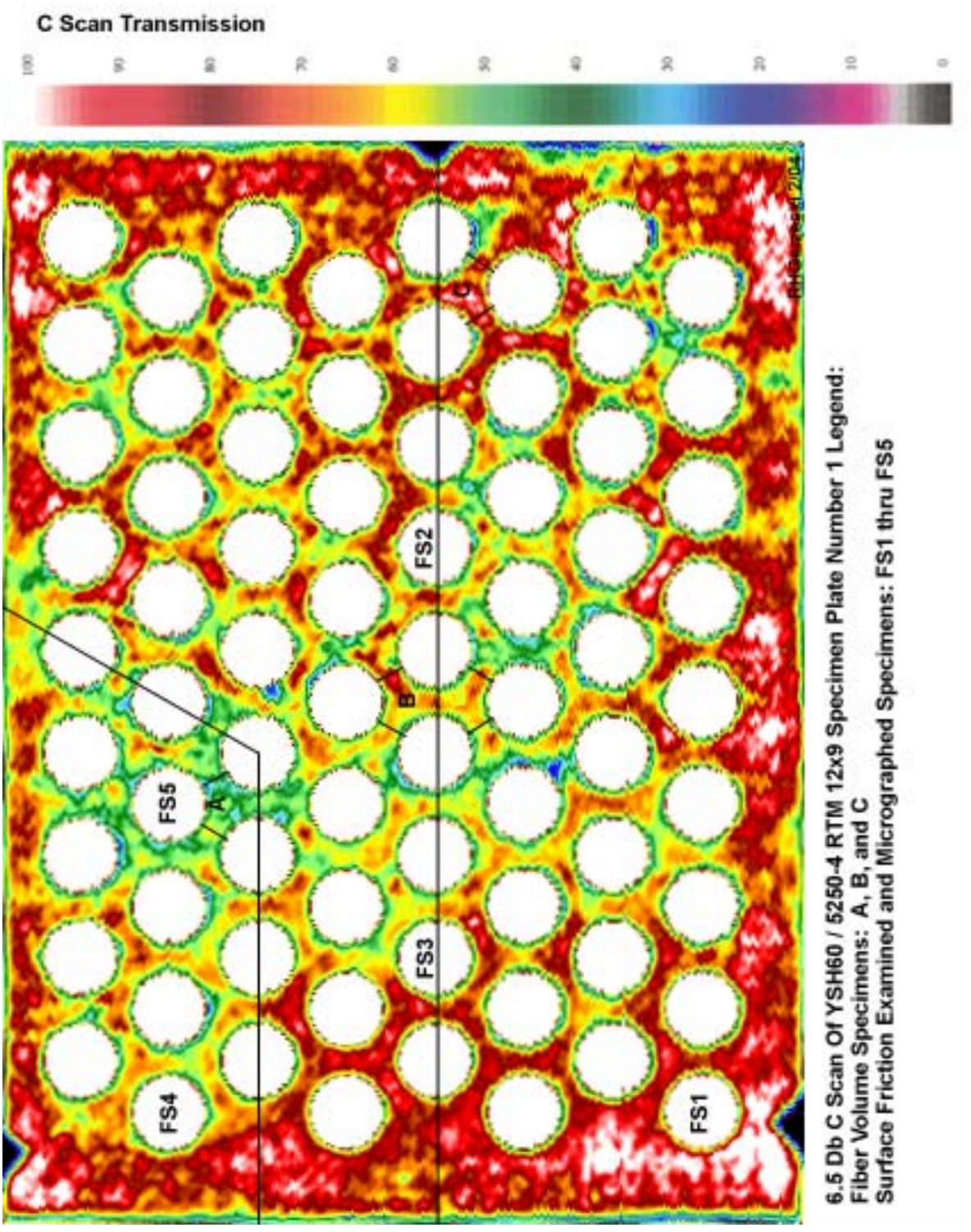


Figure 62-c, Specimen Plate 1 C Scans

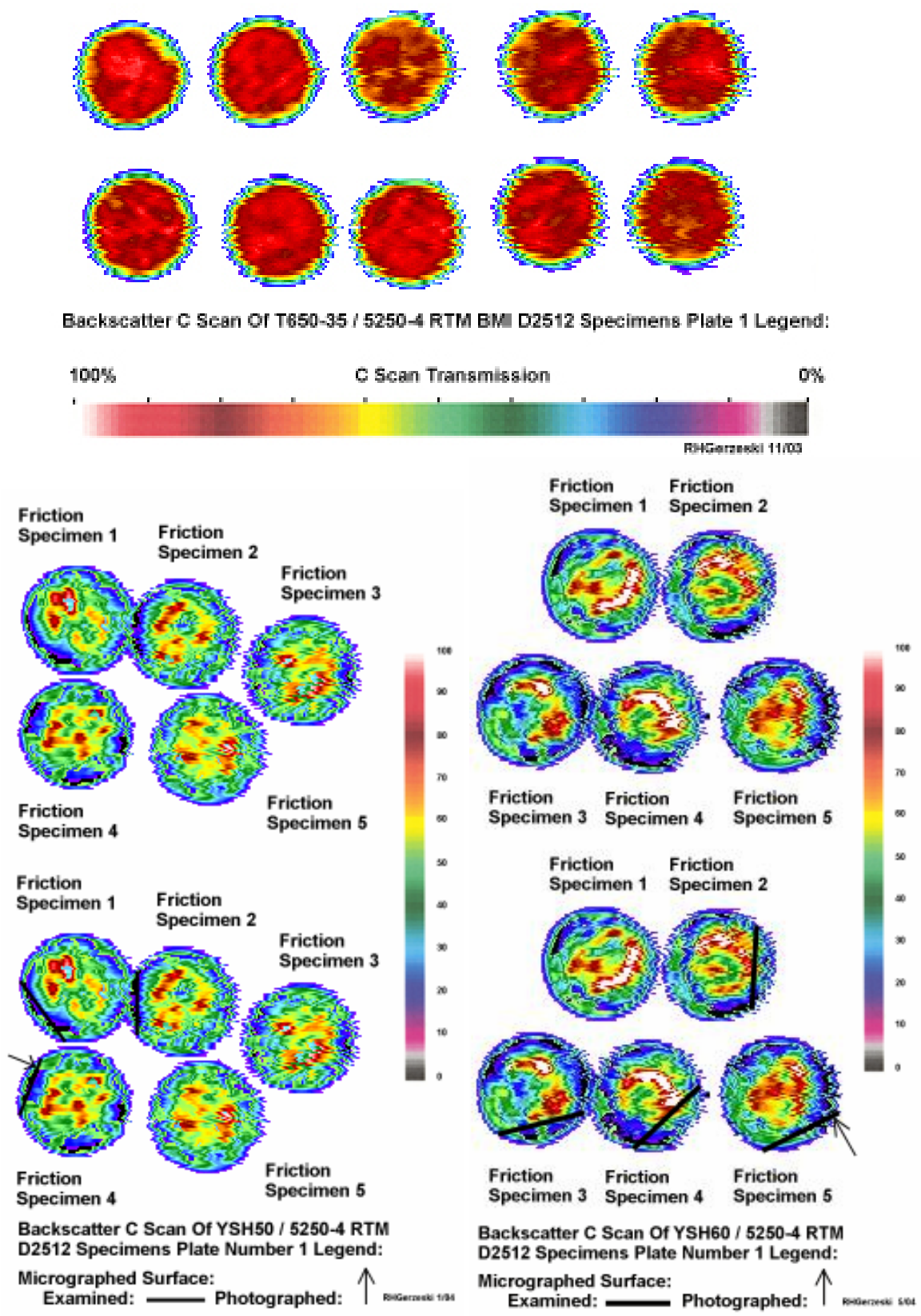


Figure 63, Backscatter Unfinished D2512 Specimens C Scans

The specimen composite plates and the friction specimens were then cut along the lines shown in figures 62 and 63 to generate pieces for subsequent different types of testing and examination. Examination of the cut surfaces and overall composite plates shown in figure 64 indicated that the cure profile and bleeders used generated moderate to low waviness, wrinkle free, flat composite plates. While the waviness was worse than that exhibited by the bleed flow 3 plates it was no worse than that which is found in most composites made by filament winding. Some of the cut surfaces, indicated by an arrow in figures 62 and 63, were polished. Micrographs, taken at 200X with the microscope indicated in figure 54, were made of them. Figure 65 shows a micrograph of one each of these examined surfaces. These micrographs indicated that there was no resin wash of the fibers, that there were no large pockets of resin, no large void pockets, good and uniform bleed flow of the resin, good and uniform consolidation of the prepreg plies and that the prepreg interleaving scheme generated roughly uniform thickness plies. They also show that the cutting of the D2512 specimens caused substantial in ply cracks to develop in the specimens and the composite plates at the third ply up from the bottom. These in ply cracks penetrated into the composite plates and specimens to a length roughly equal to the thickness of the composite.

Three of the cut pieces were sampled to determine the density, V_f, V_r and V_v for each of the specimen composite plates. An acid digestion technique was used to measure these physical values. The results are listed in table 21. The developed figure 57 cure profile and indicated in table 20 bleeder sheets used generated composites with extremely uniform V_f (differing between the composites by less a tenth of a percent!). These V_f were almost precisely in the middle of the targeted objective. Also the composites exhibited excellent V_v of less than 1 percent.

Meticulous Cleaning Procedures were used to measure the thicknesses and diameters of numerous D2512 specimens cut from each of the three types of specimen composite plates with a micrometer accurate to 0.0001 inch. Table 21 lists the overall measured and per ply calculated thicknesses and diameters. All of the plates met or exceeded, by being thinner, the targeted overall composite thickness. Additionally the calculated individual ply thicknesses were again commensurate with composite industry standards of 5 mils with the specimen composite plates made from the experimental fibers having thickness marginally greater than 4 mils.

Experimental: 5250-4 RTM Neat Resin Specimen Plate Casting

A 12 inch by 9 inch plate of 5250-4 RTM neat resin was made by casting. The resin was first heated to 130°C and degassed for 30 minutes in a container which was previously cleaned by the same technique used to clean the specimens for D2512 LOX testing. This cleaning technique will be discussed in a later subsection. The resin was then cast between two Teflon lined borosilicate glass sheets spaced apart by silicone rubber strips. The two sheets and the rubber were cleaned prior to the casting by the same technique used to clean the specimens for D2512 LOX testing. The resin was then cured in an air convection oven by a 2°F temperature ramp up to 350°F followed by a 6 hour hold at 350°F followed by a 2°F temperature ramp up to 440°F followed by a 6 hour hold at 440°F and then cooled by a 20 hour natural cool down in the then turned off oven.

The resin plate was then moved into the Lab room shown in figure 42. The cured neat resin plate was cleanly removed with tools, which were previously cleaned by the same technique used to clean the D2512 LOX compatibility specimens, from between the glass sheets. Meticulous Cleaning Procedures were used during the entire removal. The plate was then put into a FC&N CLEANLINER PE bag until D2512 specimens could be clean and contamination free cut out.

Seventy-two D2512 specimens were then clean and contamination free cut from the neat resin plate. Meticulous Cleaning Procedures were used to measure the thicknesses and diameters of numerous D2512 specimens cut from the neat resin plate with a micrometer accurate to 0.0001 inch. Table 21 lists the overall measured thickness and diameters. The plate and the specimens met the targeted overall thickness. Additionally the density of five cut out D2512 specimens of the neat resin were also measured by the Archimedes principle. Table 21 lists the measured density results.

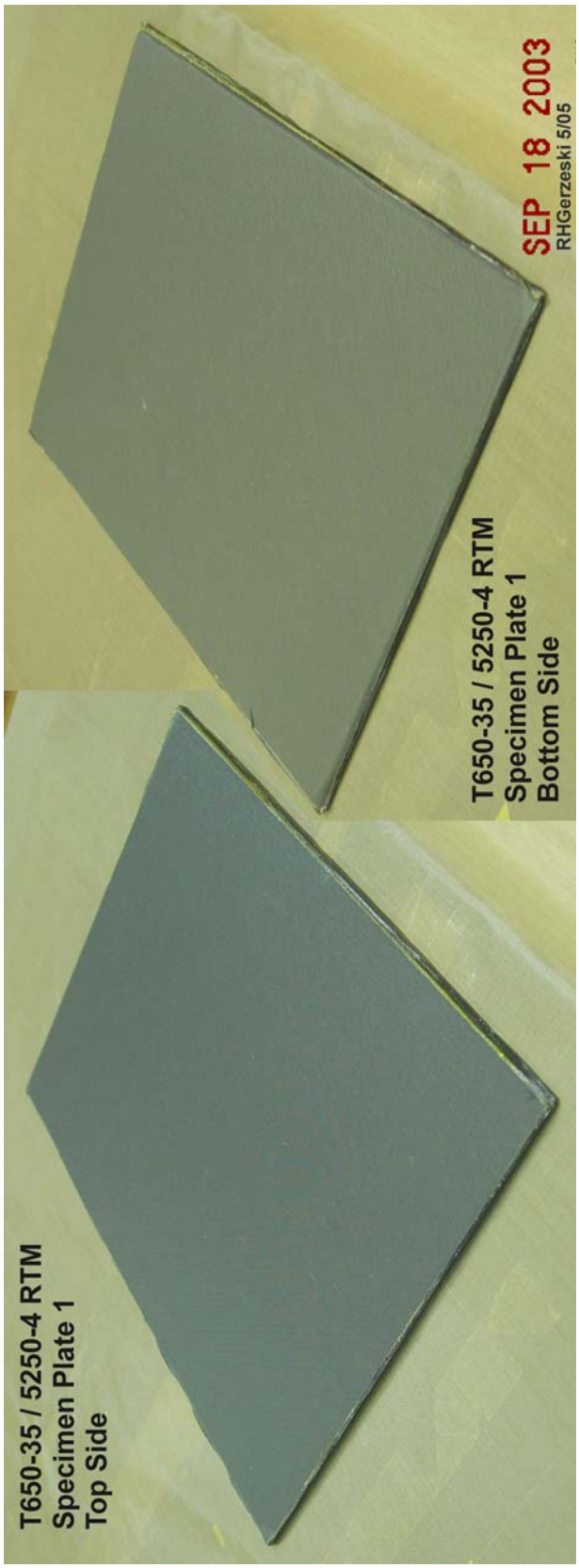


Figure 64-a-i, Cured Specimen Plates

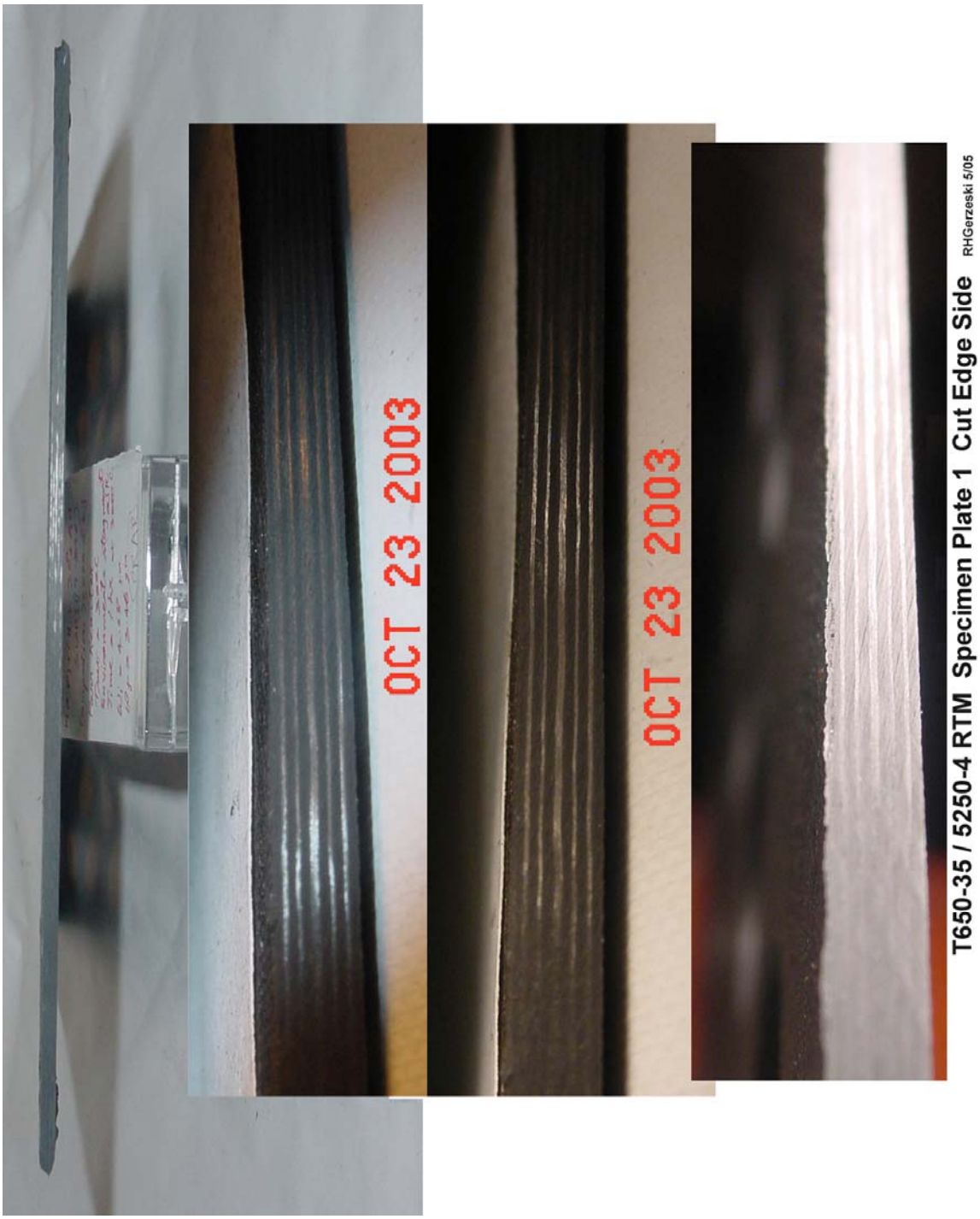


Figure 64-a-ii, Cured Specimen Plates

Figure 64-b-i, Cured Specimen Plates



Figure 64-b-ii, Cured Specimen Plates

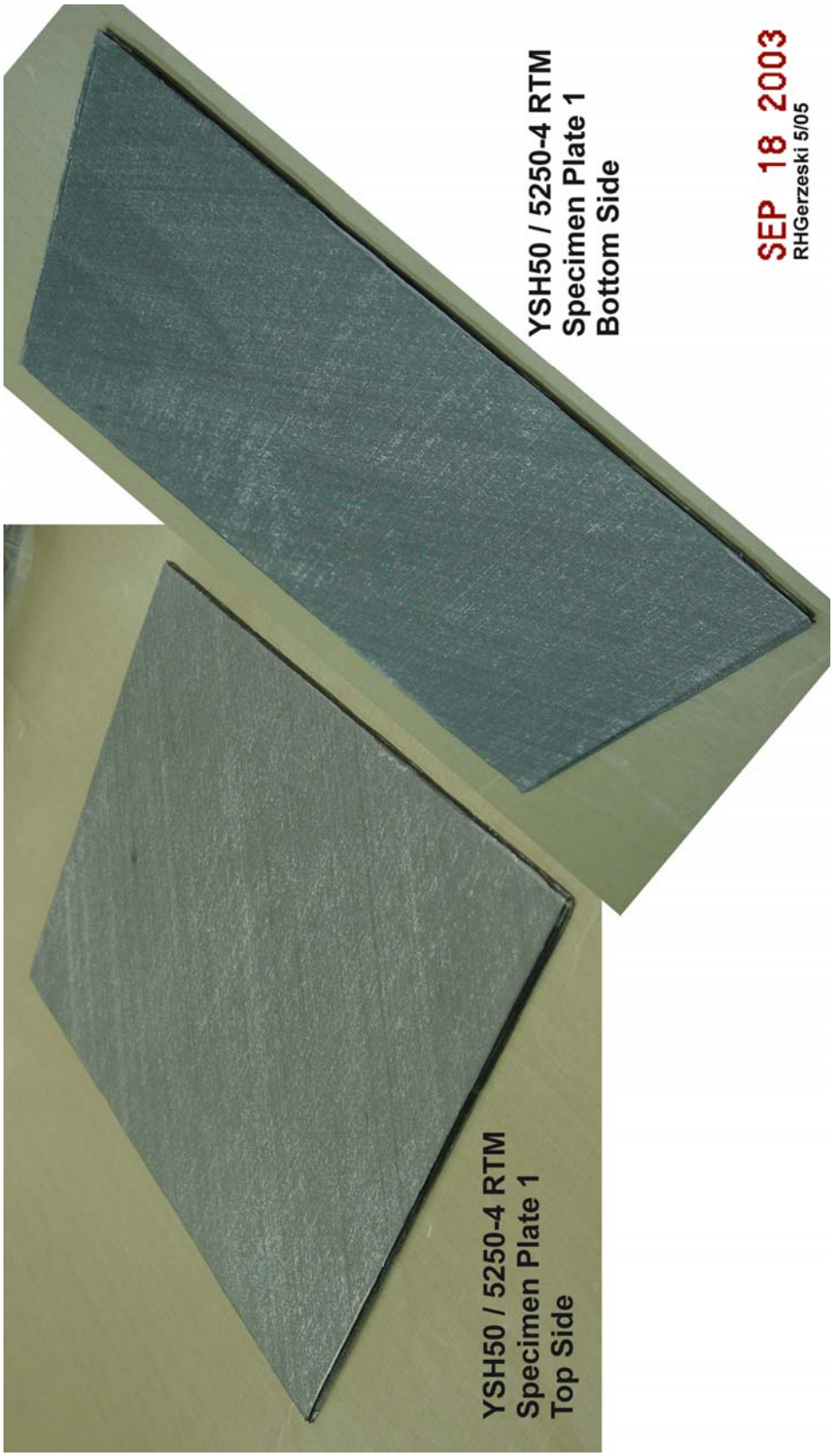


Figure 64-c-i, Cured Specimen Plates



Figure 64-c-ii, Cured Specimen Plates

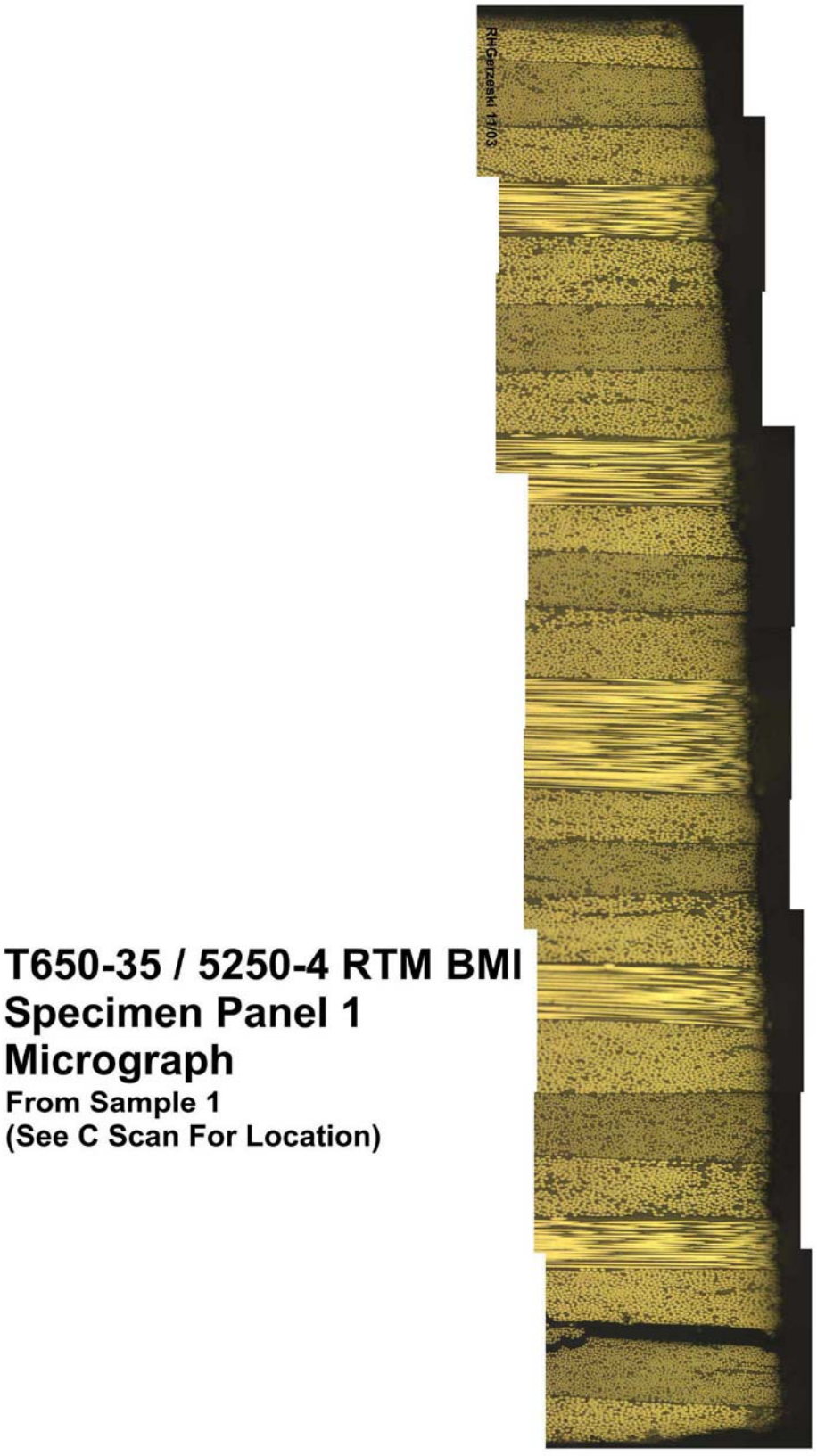


Figure 65-a, Specimen Plate Micrographs



Figure 65-b, Specimen Plate Micrographs

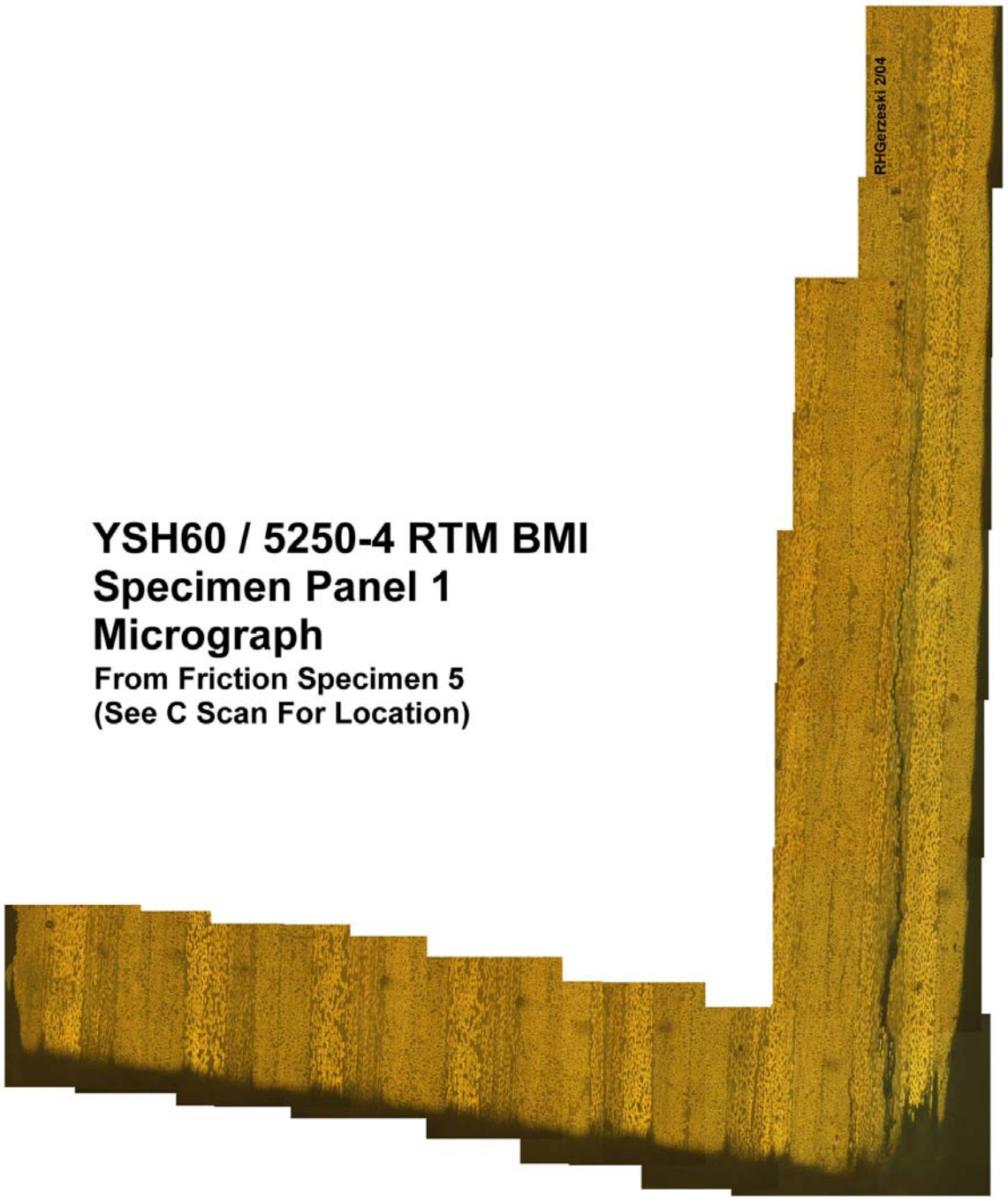


Figure 65-c, Specimen Plate Micrographs

Table 21, D2512 Specimen And Specimen Plate Physical Properties

Physical Properties			5250-4 RTM	T650-35 / 5250-4 RTM	YSH50A / 5250-4 RTM	YSH60A / 5250-4 RTM
Density: (gms/cc)	Specimen*	A:	Five Data	1.5846	1.7807	1.7977
		B:	Points	1.5747	1.7867	1.7945
		C:	Collected	1.5694	1.7886	1.7917
	Avg:		1.2573	1.5763	1.7853	1.7946
	Std:		0.0051	0.0077	0.0041	0.0030
	Max:		1.2650	1.5846	1.7886	1.7977
	Min:		1.2511	1.5694	1.7807	1.7917
Fiber Volume: (%)	Specimen*	A		64.4745	63.3973	63.7189
		B		63.3962	63.7146	63.6820
		C		63.1818	63.8335	63.5218
	Avg:			63.6842	63.6485	63.6409
	Std:			0.6928	0.2255	0.1048
	Max:			64.4745	63.8335	63.7189
	Min:			63.1818	63.3973	63.5218
Resin Volume: (%)	Specimen*	A:		35.1101	35.7409	35.5441
		B:		35.8494	35.6877	35.3479
		C:		35.7287	35.6415	35.3951
	Avg:			35.5627	35.6900	35.4290
	Std:			0.3966	0.0498	0.1024
	Max:			35.8494	35.7409	35.5441
	Min:			35.1101	35.6415	35.3479
Void Volume: (%)	Specimen*	A:		0.4154	0.8617	0.7370
		B:		0.7544	0.5977	0.9701
		C:		1.0896	0.5250	1.0831
	Avg:			0.7531	0.6615	0.9301
	Std:			0.3371	0.1772	0.1765
	Max:			1.0896	0.8617	1.0831
	Min:			0.4154	0.5250	0.7370
Cut D2512 Specimen Thickness: (inches) Overall:						
	Avg:		0.117	0.1240	0.1047	0.1004
	Std:		0.002	0.0011	0.0009	0.0015
	Max:		0.121	0.1263	0.1062	0.1037
	Min:		0.114	0.1223	0.1024	0.0971
	Data Points:		28	32	22	30
	Per Ply:					
	Avg:			0.0052	0.0044	0.0042
	Std:			0.00005	0.00004	0.00006
	Max:			0.0053	0.0044	0.0043
	Min:			0.0051	0.0043	0.0040
Cut D2512 Specimen Diameter: (inches) Overall:						
	Avg:		0.684	0.6763	0.6882	0.6846
	Std:		0.002	0.0029	0.0030	0.0022
	Max:		0.688	0.6852	0.6965	0.6920
	Min:		0.680	0.6709	0.6852	0.6818
	Data Points:		28	32	22	30

* See Specimen Plate C Scan Figures for exact location of these samples.

Experimental: D2512 Specimen Fabrication

The machining technique of coring was used to cut D2512 specimens out of the four specimen plates. Coring was settled upon because it presented the least prospects for specimen contamination and damage resulting from fabrication. Other possible techniques like water jet, end mill and continuous blade thru cutting were rejected. Water jet cutting would contaminate the surface of the D2512 specimens with tap water residue and impaled cutting abrasives; both of which are known to skew the results of D2512 testing towards lower compatibility. End milling and continuous blade thru cutting would both contaminate the surface of the D2512 specimens with cutting fluid residue and cause substantial cracking and delamination damage to the composites. The cutting fluid residue contamination would skew the D2512 LOX compatibility testing results towards more ignitions. The substantial cracking and delamination damage would be a completely unknown added variable not desired to be investigated by this effort.

D2512, as described in figure 5-b, requires that the tested specimens be free of ragged edges, burrs, fins, or other irregularities. Coring can cause the creation of substantial burrs on the bottom edges of a composite specimen if the core drill's axis is normal to the composites' surface. This is called a blow out and is the result of a delaminating bending fracture of the last few plies in a composite. To overcome this and to reduce the magnitude of the size of the residual burrs on the cored specimens, some trial and error coring was done on scrap composite plates by the A&PI and Mr. John Camping of University Of Dayton Research Institute in 2000. The results of these trails and errors was that burring could be almost completely eliminated by implementing two procedures during the coring of circular samples like the D2512 specimens out of a composite plate. First the composite plate to be cored would need to be placed on a backing or supporting plate during the coring. Second the core drill would need to intersect the plate during the coring at an angle of 4° off of normal to the plate's surface.

D2512 also requires that the tested specimens have a diameter of 0.688 inchs; though this can range up to 0.750 inches. To eliminate the possibility that varying a specimen's diameter might change the D2512 LOX compatibility results and to assure that the D2512 compatibility results generated by this effort would be relatable to previously reported results which used 0.688 inch diameter specimens, the A&PI settled upon making 0.688 inch diameter specimens. Unfortunately circa late 2001 no maker of core drills routinely provided them with internal diameters of 0.688 inch. This forced the A&PI to design and have tailor built core drills with this diameter. The detail drawing of this core drill design titled "Diamond Core Drill" is in the Designed Equipment appendix. Three core drills meeting the design were procured from Continental Diamond Tool Corp. Continental assigned them stock part number 232002A. One of these core drills is depicted in its clean storage container in figure 66.

To initially clean and cleanly store the core drills, so as to not damage their diamond abrasive cutting surfaces, a storage container was devised and assembled. The container was also needed to prevent the core drills from striking the walls of their container during storage, which would cause the diamond abrasive to pick up parts of that container and transfer it to the D2512 specimens during coring. The design and use of this storage container eliminated this D2512 LOX compatibility reducing cross contamination potential. A detail drawing of it titled "Core Drill Wash Stand Assembly" is provided in the Designed Equipment appendix. It is also depicted in figure 66; it is the container and suspending subcomponents that the core drill is shown within. When the core drill was not in use it was stored in the storage container, immersed under FC&N ACS grade methylethylketone (MEK) or Acetone to keep it clean and uncontaminated. The storage container with the core drill inside of it was placed into the sealed paint bucket for safe storage. The glass Qorpac quart jar part of the storage container was caustic etched and all of the components were subsequently cleaned by the same technique used to clean the D2512 specimens before they were used to store core drills.

A core drill cuts by kineticly running an abrasive (diamond for this effort) across the cutting surface. This generates heat at the cutting surface interface and a continuous stream of coolant is needed to carry the heat away. TDW was used as the coolant during the coring of D2512 specimens from all four plates. To get the TDW coolant into the core drill required that a coolant injection collar, which could be cleaned, used clean and kept clean, need to also be designed. The detail drawing of this coolant injection collar titled “Coolant Adapter” is also in the Designed Equipment appendix. It is depicted disassembled in figure 67-a and assembled and mounted onto the core drill in figure 67-b. When it was not in use it and its’ subcomponents were stored in caustic etched and subsequently cleaned by the same technique used to clean the D2512 specimens Qorpac pint jars to keep it clean and uncontaminated.

The TDW coolant flow was maintained from the injection port on the collar (the barbed brass hose couple shown in figure 67-b) into the core drill intake port (the hole in the upper core drill shaft also shown in figure 67-b) by using grease smeared o-rings as seals. This was necessary as spraying TDW onto the mill would damage it. As the collar remained stationary and the core drill spun at roughly 3000 rpms these o-rings degraded from frictional abrasion and had to be changed out after all of each composite specimen plate’s D2512 specimens had been cut. The o-ring abrasion products and worn off grease had but one direction to go: onto the top surface of the cored D2512 specimens. If these o-rings and grease where made of low LOX compatibility materials then they would potentially contaminate the D2512 specimens and skew the specimen’s D2512 LOX compatibility towards more reactions. To avoid that, the o-rings were made out of Viton and the grease was 240AB Krytox. Both routinely pass D2512. Their presence on the D2512 specimens, if the best efforts to clean them off of the specimens failed, would not result in any skewing of the specimen’s intrinsic D2512 LOX compatibility.

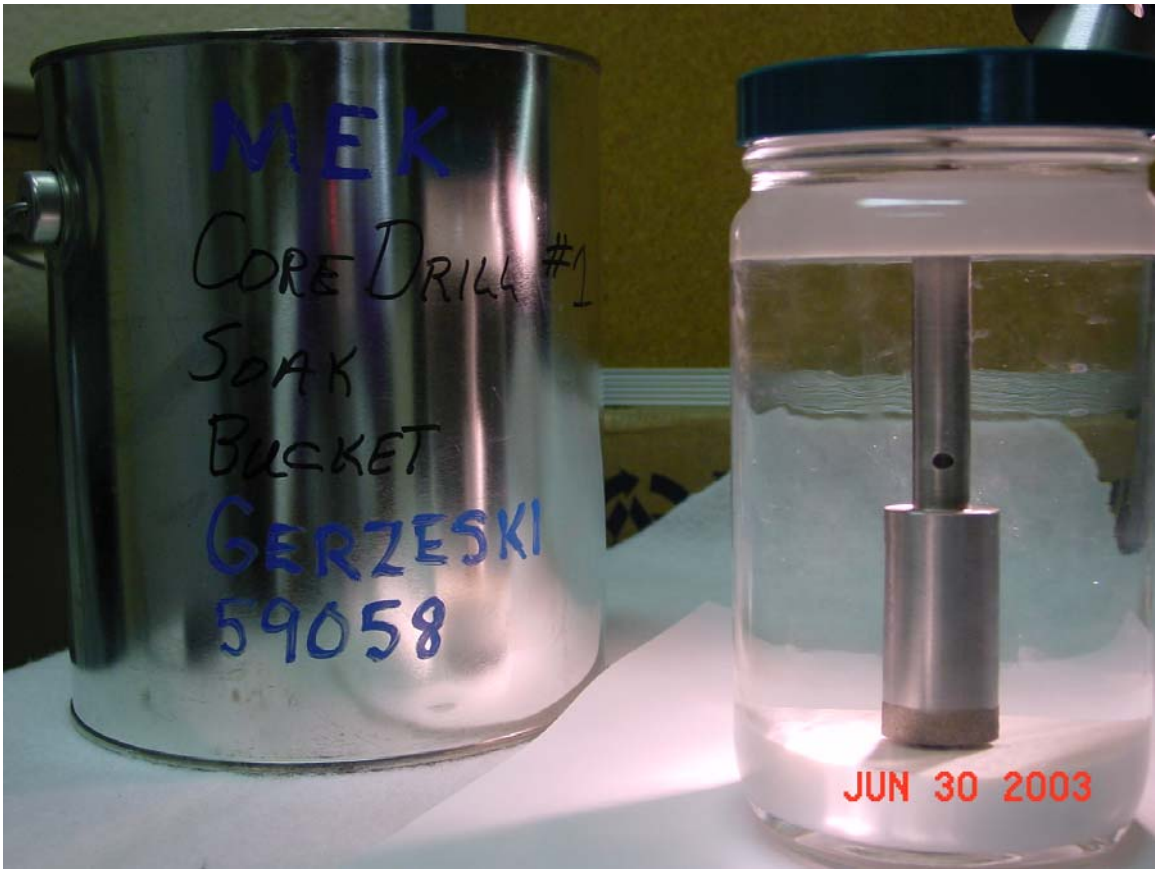


Figure 66, Core Drill and Clean Storage Container



Figure 67-a, Coolant Adapter: Disassembled



Figure 67-b, Coolant Adapter: Assembled And Core Drill Mounted



Figure 68, Coolant Pump and Reservoir

To get the TDW coolant into the coolant injection collar, thru the core drill and across the cutting surface interface required a pump and a TDW coolant supply reservoir. A submersible pump and a PE tank were procured to accomplish this. They are depicted in figure 68. When not in use they were stored in FC&N PE Ziplock bags (the pumps) or filled with TDW and enclosed in a sealed FC&N CLEANLINER PE bag (the tank) to kept them clean and uncontaminated.



Figure 69, Cutting Jig, Jig Assembly Tools, Catch Basin and Mill Clamp Plate

To burr free core the D2512 specimens out of the specimen plates required that a jig be designed and tailor built to hold them during the machining at the 4° angle. The detail drawings of this jig and its' related subcomponents are in the Designed Equipment appendix. It is depicted in figure 69 along with the cleanly stored tools required to assemble it. When not in use it was stored after being cleaned in a DFN_2 purged thermal impulse sealed FC&N CLEANLINER PE bag to keep it clean and uncontaminated. The tools were stored when not in use in caustic etched and subsequently cleaned by the same technique used to clean the D2512 specimens Qorpac quart jars to keep them clean and uncontaminated.

To seal the CLEANLINER PE bags and other specimen and prepreg related PE bag containers, a 12 inch Thermo Impulse sealer was acquired. When it arrived from the vendor it was initially scrubbed with IPA saturated FC&N cheese cloths, scrubbed again with TDW saturated FC&N

cheese cloths, dried with FC&N cheese cloths and then stored in a DFN_2 purged CLEANLINER PE bags. Whenever it was to be used, the first three cleaning steps were repeated. When not in use it was stored in a FC&N DFN_2 purged CLEANLINER PE bag.

The TDW coolant, once it had passed by the cutting surface interface, needed to be caught and returned to the TDW coolant supply reservoir. This was accomplished by anchoring the jig to the bottom of a catch basin (also depicted in figure 69) and another submersible pump drew the TDW coolant out of the basin back into the reservoir.

Tygon High Purity Tubing shown in figure 68 was used to transport the TDW coolant from the reservoir to the coring site and from the catch basin back into the reservoir. For the coring of D2512 specimens from each specimen plate, FC&N out of the box Tygon High Purity Tubing was used. It was discarded after the coring was completed so as to not cross contaminate the D2512 specimens cored from a particular specimen plate with abrasion particles from a previous plates's coring. All barbed brass hose couples used during the coring of D2512 specimens from any particular specimen plate were also discarded after that plate's coring for the same reasons.

To drive the core drill and to precisely locate it over the specimen plates during the coring of the D2512 specimens required a mill. The catch basin and jig were themselves mounted to together onto a mill clamp plate as shown in figure 69. They were then precisely mounted onto the bed of the mill. The core drill with the assembled coolant adapter mounted on it would then be inserted and clamped into the mill's chuck.

All most all of the designed equipment components and their subcomponents were made out of aluminum and stainless steel. As all of the components were in contact with TDW, this was done to reduce the potential of forming metal ion corrosion products. These metal ion corrosion products could potentially contaminate the surfaces of the cored D2512 specimens and, as detailed in the Theory Section: Ignition Event, skew the specimen's LOX compatibility towards more reactions.

The jig and collar subcomponents and the tools used to assemble them were cleaned by the same procedure used to clean the D2512 specimens. This procedure will be described in a later subsection of this report. They were first cleaned when they were initially received from their fabricators and after they were used to core D2512 specimens out of a specimen plate. After being used to core a specimen plate the jig and collar were allowed to soak in a solution of Ivory soap and TDW until a day later when they were cleaned.

Due to the way in which the diamond abrasive was attached to the core drills shank it needed to be cleaned in a different way. They were cleaned by being placed in the already cleaned storage containers described above filled with FC&N ACS grade MEK. Then the container with the core drill in it was gently agitated for 5 hours. The MEK was drained from the storage container and replaced with FC&N MEK. This entire process was repeated four times for each of the three core drills before they were used.

The TDW reservoir tank and the submersible pumps were cleaned when they were first received by first scrubbing them out with TDW saturated cheese cloths and then using the pumps to vigorously circulate for ½ to 1 hour 3 gallons of a cleaner solution and then rinse them five times. This cleaned the pumps and the tank simultaneously. The cleaner solution consisted of ½ ounce of Ivory dish soap to 1 gallon of TDW. The rinse consisted of 3 gallons of TDW. Within one day after being used as the coolant reservoir for the coring of D2512 specimen from a specimen plate, the tank was drained and the same cleaning procedure was done again.

These cleaning procedures for the jig, collar, tools, pumps and tank were done so as to not allow the abrasion products from the previous days coring to cake up on them. This caking would have made the cleaning even more difficult. It would also have potentially resulted in the cross contamination of the D2512 specimens cored from the next specimen plate or plates to be cored

with the abrasion products from previously cored plates. This cross contamination needed to be avoided as it might possibly skew later cored D2512 specimen's LOX compatibility towards more reactions.

Prior to the setting up of the jig, collar, core drill, pumps, tubing and tank on and around the mill in preparation for coring D2512 specimens from a specimen plate, a slight modification to the Meticulous Cleaning Procedures was implemented. The mill was not located in the lab room described in the Meticulous Cleaning Procedures section, it was located in another general specimen prep lab room. The Meticulous Clearing Procedures were done on the mill and that quarter of the specimen prep lab room in which it sat. Then the coring equipment was set up.

After the coring equipment was set up and made ready, a specimen plate and a backing plate made from the same material was removed from their storage bags and clamped into the jig. The backing plates, when used, were placed under the specimen plates.

The D2512 specimens were cored out of the four specimen plates in the following sequence: First the neat resin plate, then the T650 plate, then the YSH50 plate and finally the YSH60 plate. Figure 70 depicts the coring of the T650 specimens. Using one core drill to core out the D2512 specimens from more than one of the composite specimen plates would result in the cross contamination of the D2512 specimens cored out of the subsequent composite specimen plates. This would skew the D2512 LOX compatibility testing results of those subsequently cored D2512 specimens towards more reactions. To eliminate this, three separate core drills were used. Each composite specimen plate's D2512 specimens were cored out with a different FC&N core drill. The same core drill used to core the D2512 specimens out of the 5250-4 RTM neat resin specimen plate was also used to core the specimens out of the T650-35 composite specimen plate. Since the T650-35 composite specimen plate's matrix was 5250-4 RTM the A&PI decided that this would result in no D2512 LOX compatibility results skewing cross contamination.

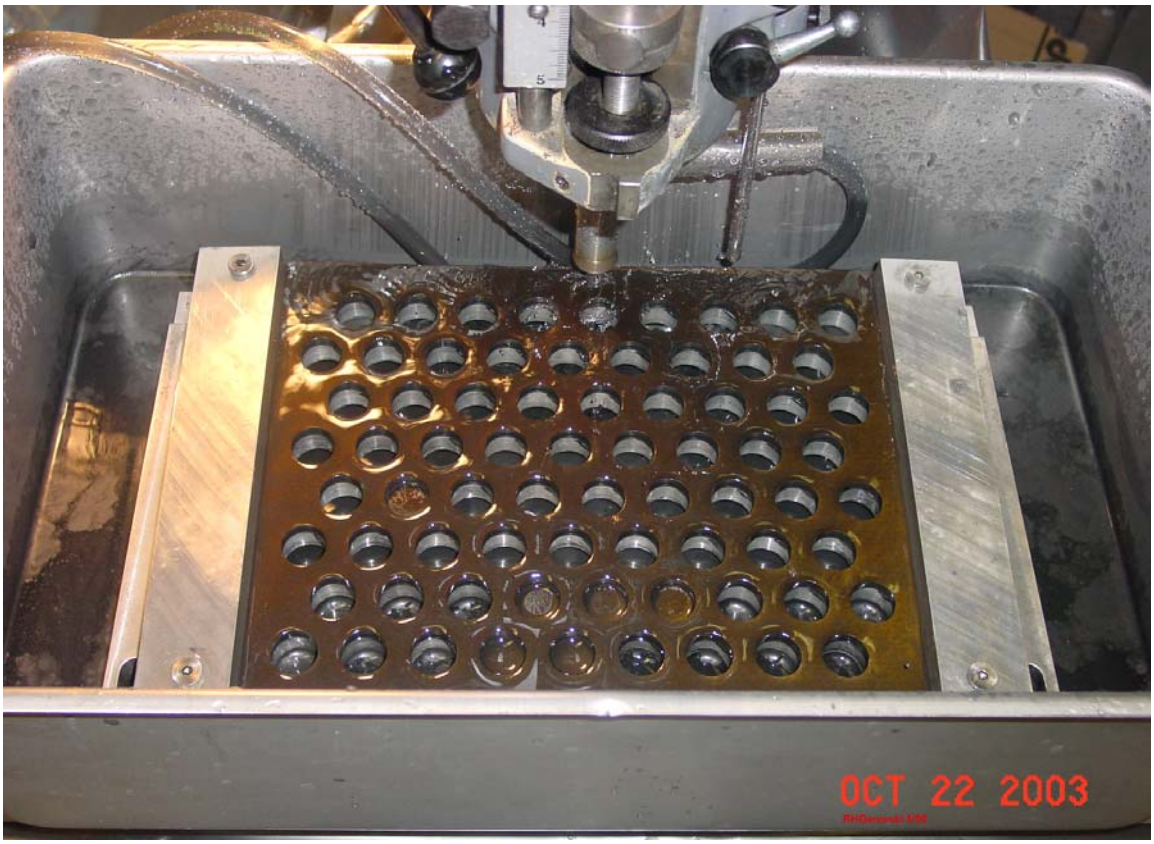


Figure 70, T650-35 Fiber Composite Specimen Plate Coring

Seventy-two D2512 specimens were each cored out of the four specimen plates. Except for the five to ten previously mentioned “Friction Specimens” retained for additional examination, the specimens were collected out of the catch basin with clean forceps, rinsed with TDW, placed into Qorpac pint jars and stored under TDW as depicted in figure 71. These jars had been previously cleaned by first caustic etch and then the same procedure used to clean the D2512 specimens. This D2512 specimen cleaning procedure will be detailed in a later subsection of this report. Storage under TDW was done so as to not allow the abrasion products to cake up on the D2512 specimens. This caking would have made the cleaning even more difficult. The abrasion products might also skew the resulting D2512 LOX compatibility results and this was another variable that this effort did not intend to measure.



Figure 71, Specimen Storage Between Processing Steps From Coring To Final Cleaning

As depicted in figure 72 the unfinished freshly cored D2512 specimens had a “slightly trapezoidal” cylindrical shape. D2512 specimens created from the 5250-4 RTM neat resin plates were cored without the use of a backing plate. This generated substantial burrs on the bottoms of the resulting neat resin specimens. The composite specimen plates were cored with backing plates made from the same composite material. Using the backing plates substantially reduced the degree of burring on the D2512 specimens cored from the composite specimen plates.

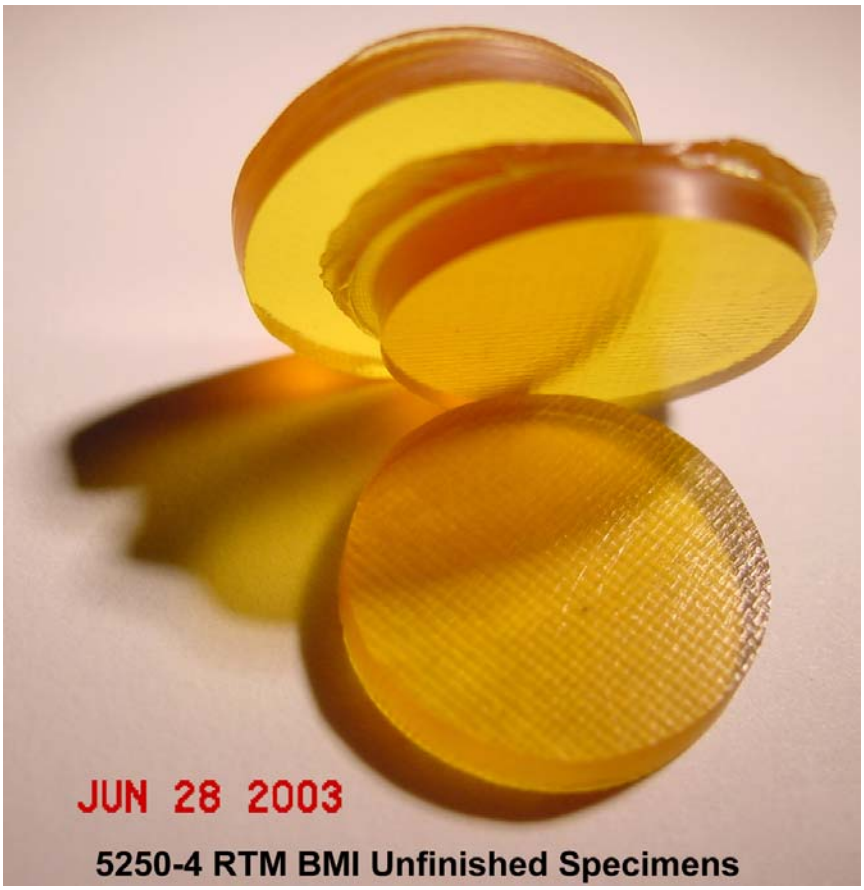


Figure 72-a, Unfinished “Slightly Trapezoidal” Cylinder D2512 Specimens



Figure 72-b, Unfinished “Slightly Trapezoidal” Cylinder D2512 Specimens



Figure 72-c, Unfinished “Slightly Trapezoidal” Cylinder D2512 Specimens



Figure 72-d, Unfinished “Slightly Trapezoidal” Cylinder D2512 Specimens

Some random and sporadic delamination and removal of the outer most plies on the outer bottom edges of the D2512 specimens cored from the composite specimen plates can be inferred from figure 73. This occurred in spite of the use of the backing plates. It indicates that the interface between the 5250-4 RTM matrix and the all of the fibers used was at best marginal.



Figure 73-a, Cored Composite Specimen Plate Edges

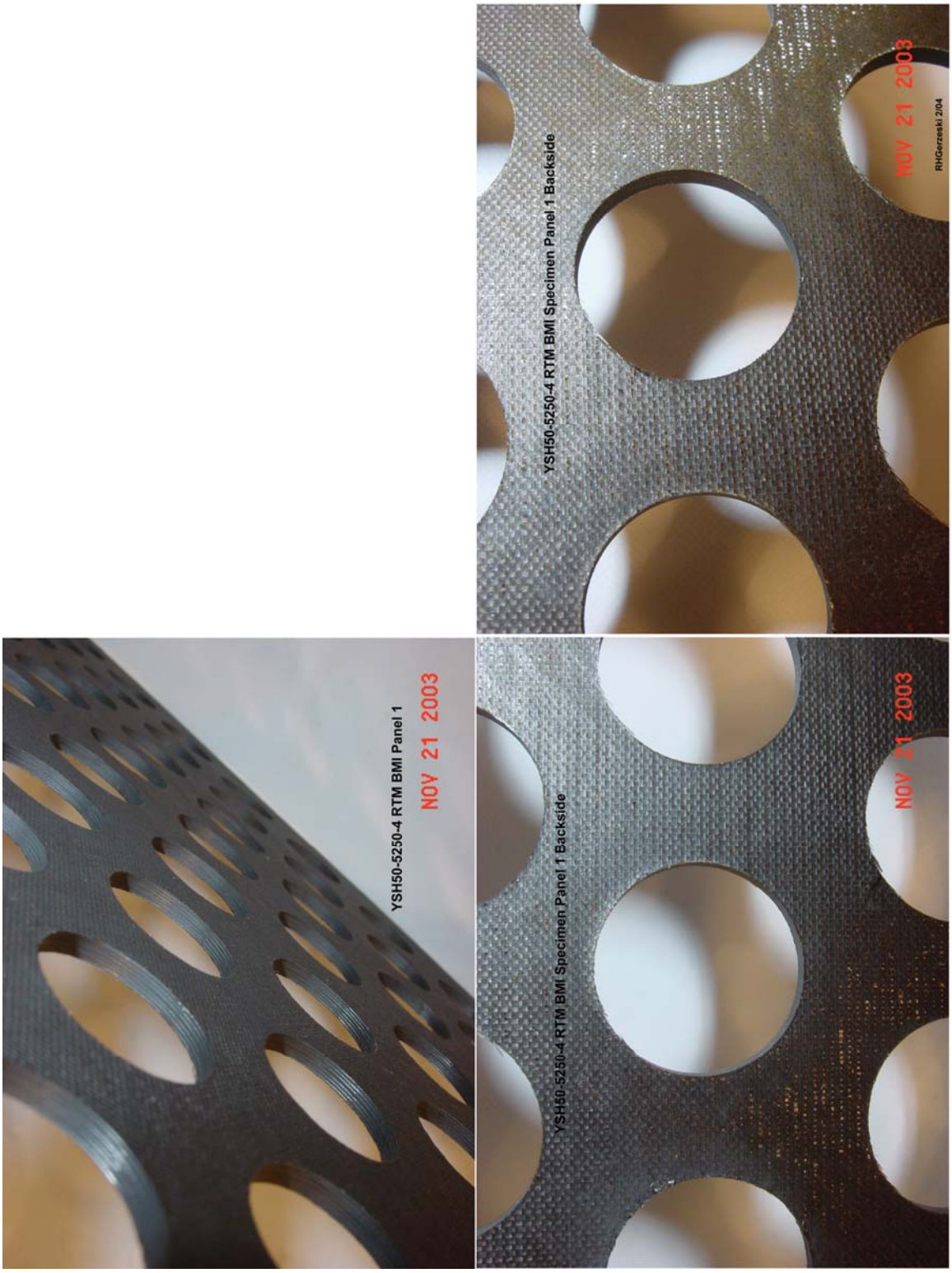


Figure 73-b, Cored Composite Specimen Plate Edges

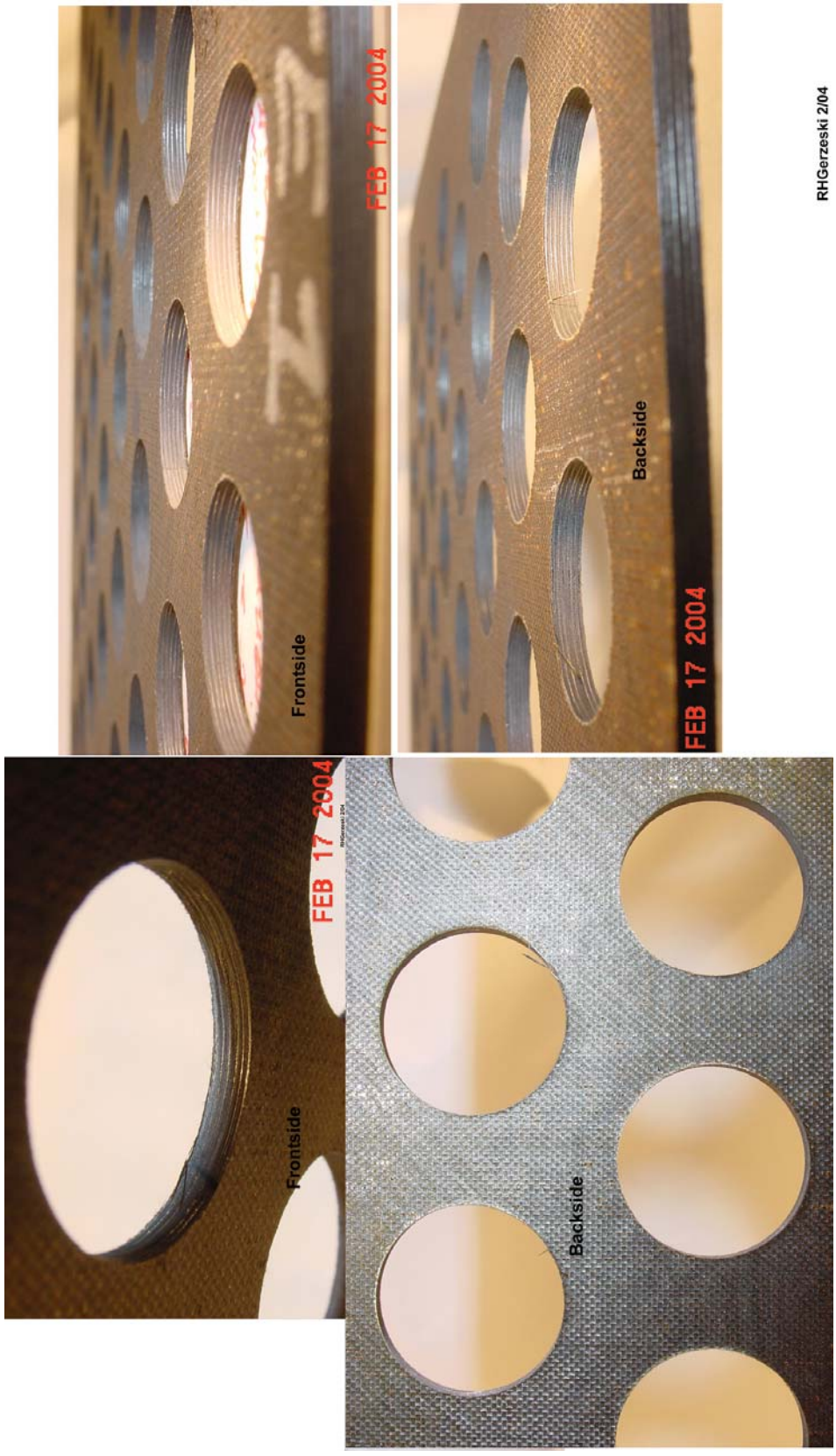


Figure 73-c, Cored Composite Specimen Plate Edges

50X micrographs of the outer bottom surfaces of the D2512 specimens cored from the three composite specimen plates were taken using the microscope shown in figure 54. They are depicted in figure 74. These micrographs indicate the following. The coring of the composites made with the YSH fibers caused a feathering extraction or lifting of the fibers away from the outer edge of the main body of the specimen. The YSH fiber containing composites also have a loosely adhered resin rich coating on them which is easily removed. All of the D2512 composite specimens exhibit indications of frictional abrasion on their bottom surfaces.

Figure 75 depicts the tops and bottoms of the "Friction Specimens" taken from the composite specimen plates without magnification. The ease of removing the resin coating on the D2512 specimens made from the YSH fiber composites is confirmed by figure 75. Figure 75 shows that the resin rich coating was even removed to a minor degree from the tops of the YSH50 fiber composites and significantly more so from the top of the YSH60 fiber composites. The indication of frictional abrasion is also seen without magnification in figure 75 at the outer edges of the bottom of all of the D2512 composite specimens.

The resin removal from the tops of the YSH fiber containing D2512 specimens could only have come about as a result of the flowing coolant. Other then being handled by SPN gloved hands and being placed into PE bags until they could be examined, nothing else came into contact with them. This is an indication of the quality of the interface between the matrix and the fibers. It was marginal for the YSH50 fiber composite specimens and poor for the YSH60 fiber composite specimens.

The feathering extraction or lifting of the fibers away from the outer edge of the main body of the sides of the YSH fiber D2512 specimens is due to the frictional abrasion cutting of the diamond powder on the core drill. The degree of extraction is an indication of the YSH fibers to matrix interfacial strength. This also supports the conclusion reached in the previous paragraph: marginal interface strength for the YSH 50 fiber composites and poor for the YSH60.

The indication of frictional abrasion on the bottoms of the YSH fiber D2512 specimens is the result of their "slightly trapezoidal" shape and coolant flow through the core drill. The combination, caused the cored D2512 specimens to both be pressed against the backing plate, wedged against the inner walls of the core drill and then dragged downward as the core drill continued coring into the backing plate. The author/PI anticipated that this friction and its' resulting abrasion between the composite specimen plate and the backing plate might occur. This frictional abrasion will cause the transfer of material from the backing plate's top surface onto the D2512 specimen's bottom surface. Since the backing plates were fabricated out of the same composite material as the specimen composite plates this transfer consisted of the same to the same. Had the backing plates been made of a different material, it would have been the different material of the backing plate being transferred into the surface of the specimen plates. This would have been a possible cause of cross contamination. If not eliminated by making both the specimen composite plates and the backing composite plates out of the same material, it would have possibly skewed the final D2512 LOX compatibility results of the cored specimens.

The deep gouge in Friction Specimen 4 of figure 75-c-ii was the result of the A&PIs effort to extract it from the core drill. Frictional heat generated by the diamond abrasives coring of the specimens was carried into the D2512 specimens during their coring. This heat and how effectively it was carried into the D2512 specimens caused them to expand. With the increased thermal conductivity of the YSH fibers their main specimen bodies would heat up enough during the coring to expand and "wedge" themselves into the sides of the core drill. This was primarily overcome by bringing the TDW coolant's temperature down to that of ice water by adding TDW ice to the reservoir. But occasionally a specimen would still get wedged and needed to be knocked out with a stainless steel rod. As the striking of the specimen would cause mechanically degrading damage and possible contamination, both of which might skew the D2512 LOX compatibility of that specimen, these wedged specimens were usually relegated to display and presentation use. They were not processed on for D2512 LOX compatibility testing.

The TDW ice was made by filling FC&N Ziplock PE bags with TDW and freezing them. Roughly 10 pounds of TDW ice was used to during the coring of the YSH fiber containing composite specimen plates.

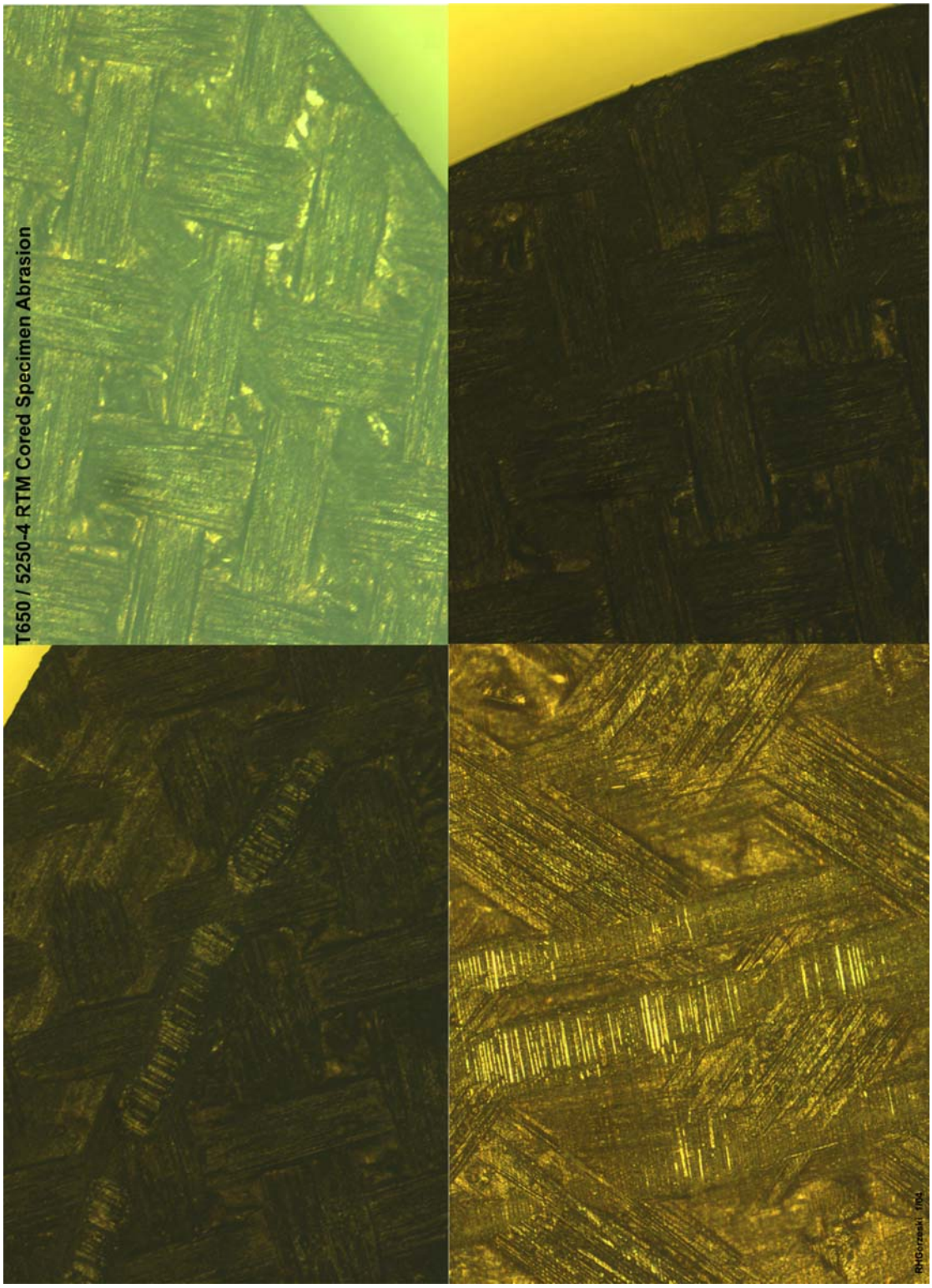


Figure 74-a, Cored Unfinished D2512 Specimen Abrasion: 50X Magnified

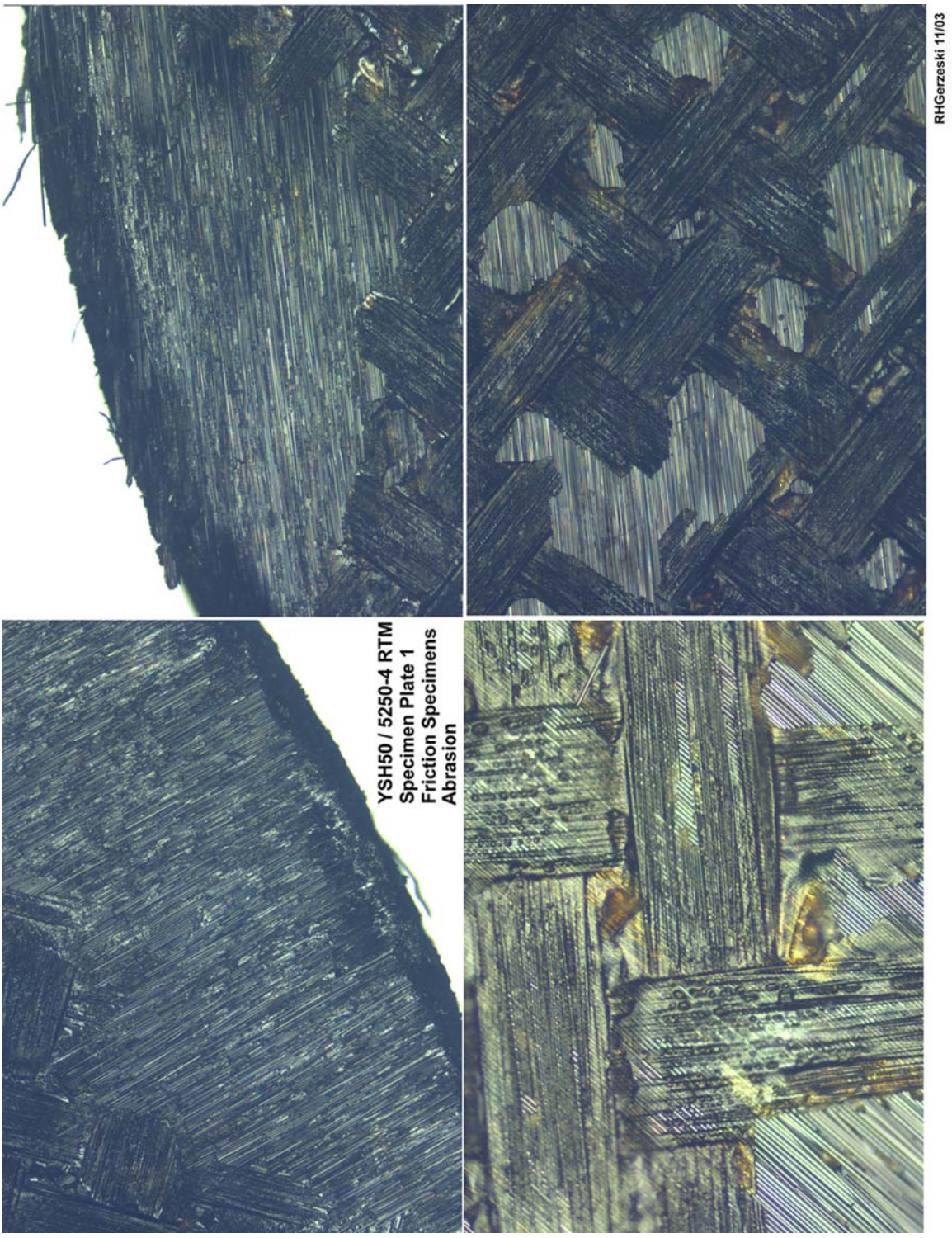


Figure 74-b, Cored Unfinished D2512 Specimen Abrasion: 50X Magnified

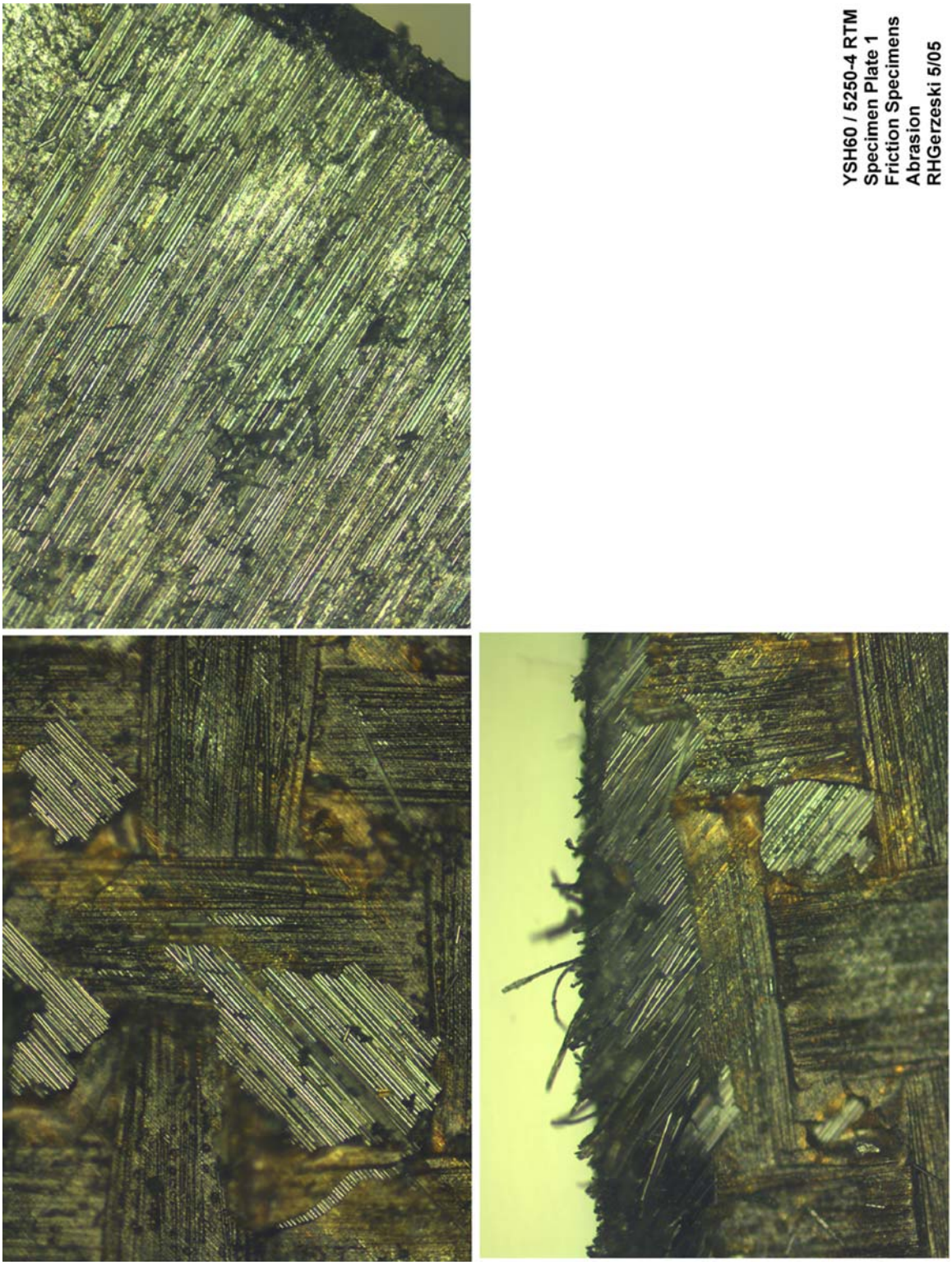


Figure 74-c, Cored Unfinished D2512 Specimen Abrasion: 50X Magnified



Figure 75-a-I, Cored Unfinished D2512 Specimens



Figure 75-a-ii, Cored Unfinished D2512 Specimens

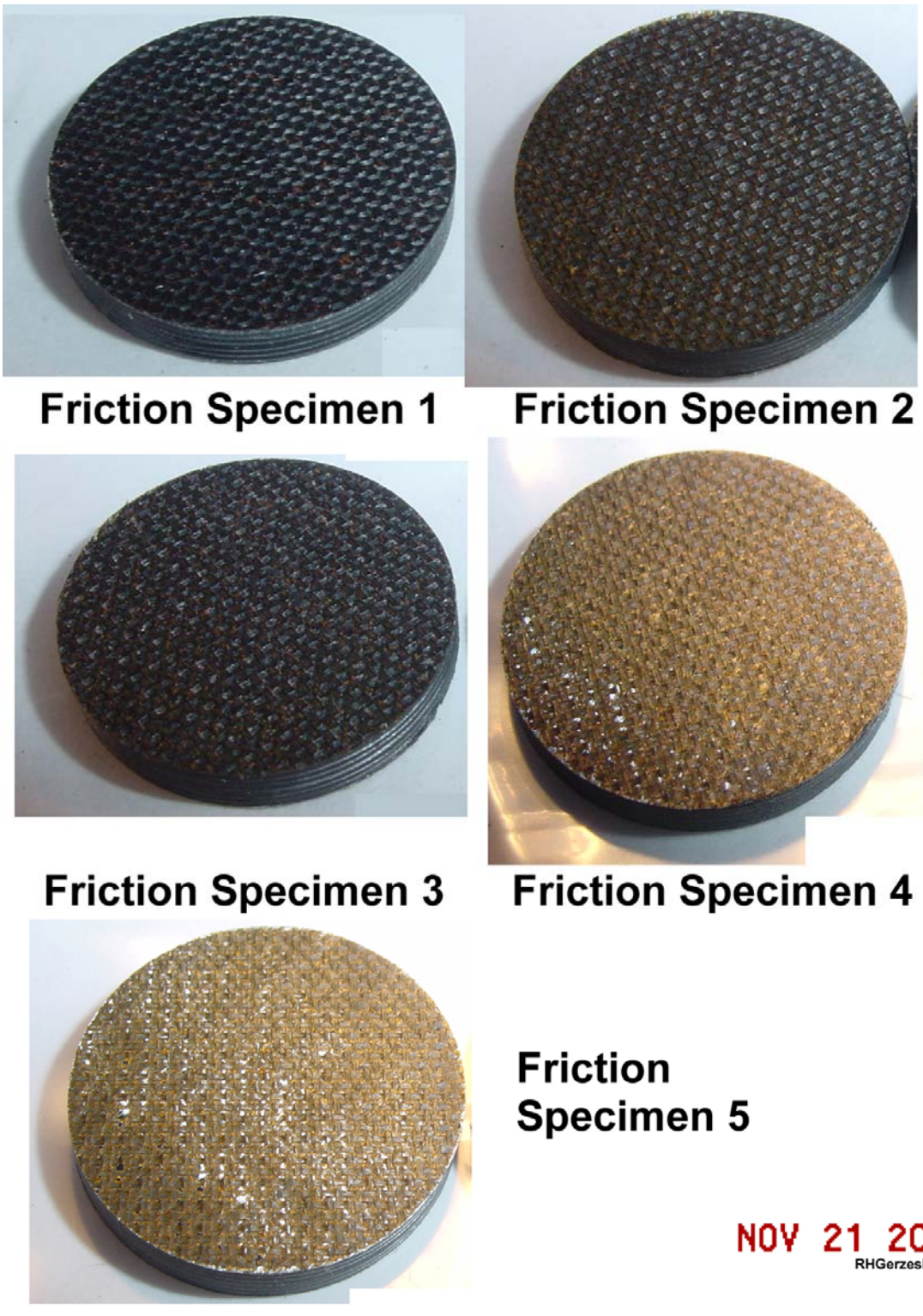


Figure 75-b-i, Cored Unfinished D2512 Specimens

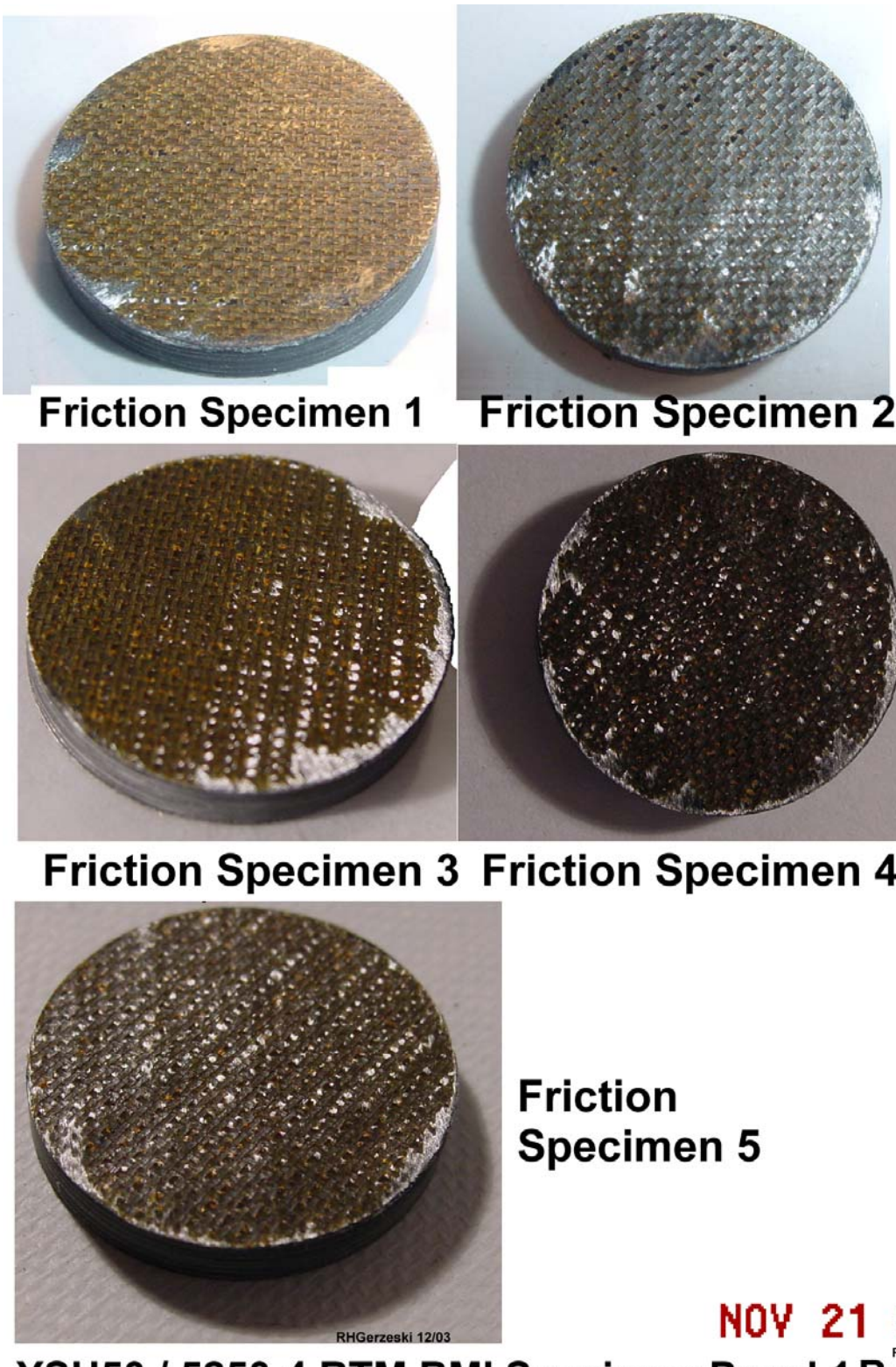


Figure 75-b-ii, Cored Unfinished D2512 Specimens

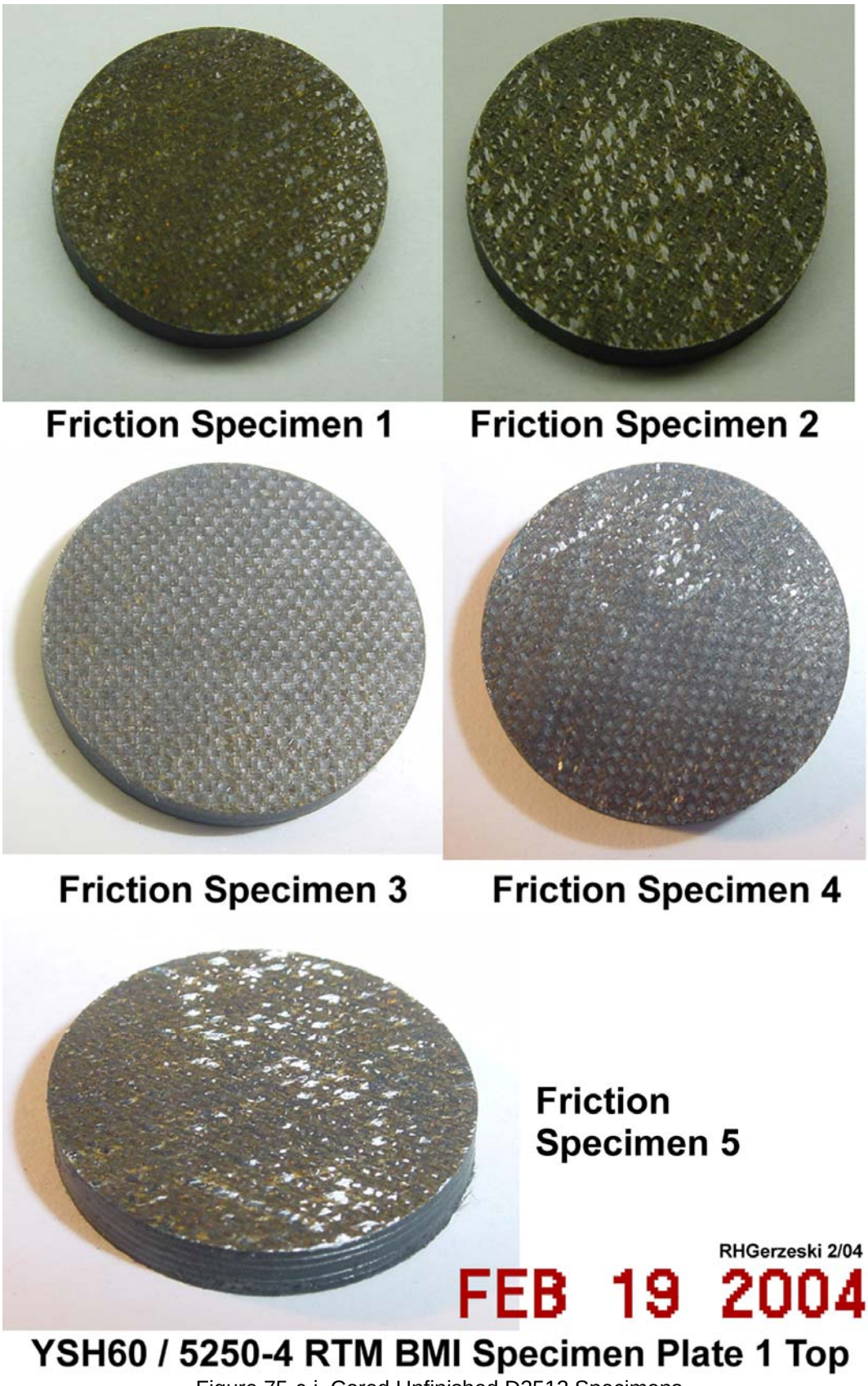


Figure 75-c-i, Cored Unfinished D2512 Specimens

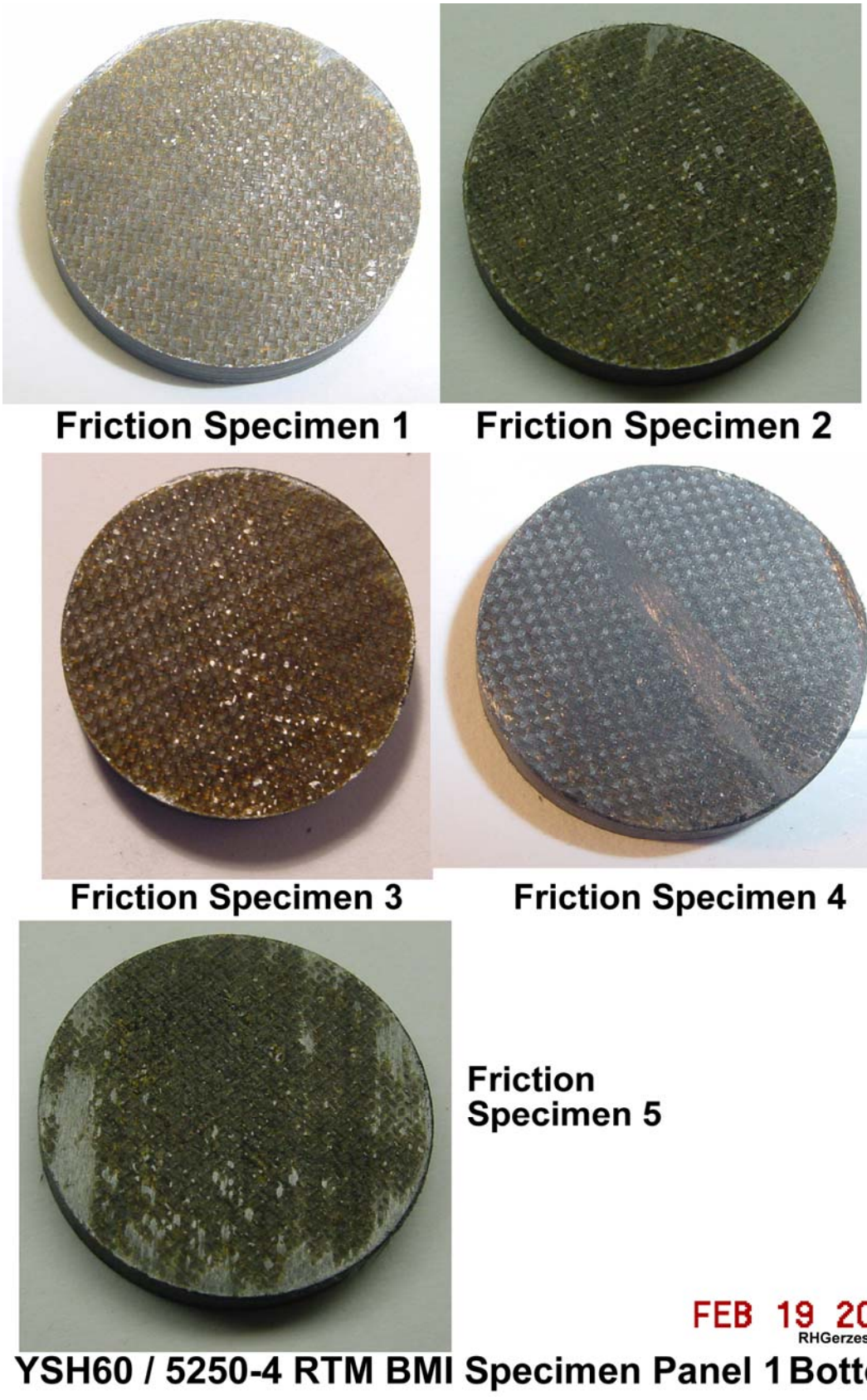


Figure 75-c-ii, Cored Unfinished D2512 Specimens

A comparator roughness gage was used to determine the top and bottom surface roughness of the various D2512 specimens. Figure 76 depicts the best fit between the surface roughness of one of the 5250-4 RTM D2512 specimens and the various roughnesses on the gage. All D2512 specimens and the plates that they were fabricated out of exhibited similar surface roughnesses of approximately 63. This roughness was a residual of the peal plies used during the specimen plates curing.

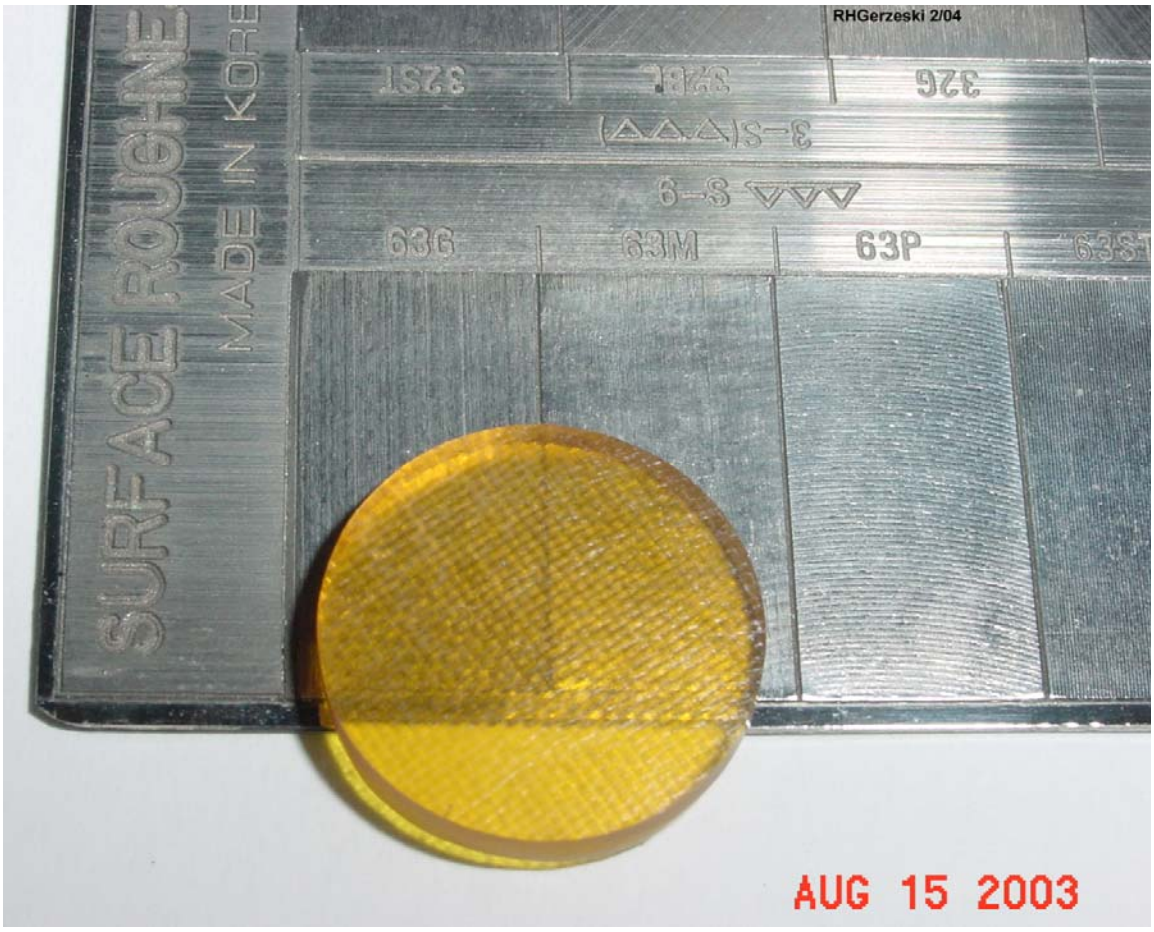


Figure 76, D2512 Specimen Surface Finish

The burrs and feathering on the D2512 specimens were removed by wet sanding. Also during this sanding, a light (barely perceivable) to mild (just perceivable) beveled edge on the top and bottom of all specimens was ground into them. Figure 77 depicts one example of each type of these sanded and beveled specimens. TDW was used as the wetting coolant for the sanding wheel. 600 grit abrasive sand paper was used as the abrasive. SPN gloves were worn through out the sanding of all of the D2512 specimens. No attempt was made to remove the loosely attached resin coating on the top and bottom surfaces of either of the experimental fibers D2512 specimens. To minimize the frictional transfer of abrasive into the surface of the D2512 specimens, the contact force was light and accompanied by a constant rolling of the specimen in the direction of the rotating sanding wheel. This was done to suppress the skewing, by increasing the reported number of ignitions, effects which abrasives are known to have on D2512 LOX compatibility test results. The specimens were rinsed by numerous squirts of TDW. They were then stored under TDW in FC&N Qorpac pint jars which had been previously caustic etched and cleaned by the same technique used to clean D2512 specimens for D2512 LOX compatibility testing.



Figure 77, Sanded and Beveled D2512 Specimens

Experimental: Specimen Cleaning and Packaging

As was alluded to in the Introduction and the Theory Section, contaminating materials like oils, abrasives, and or other inadvertently picked up materials skew a specific material's D2512 LOX compatibility testing results. These contaminating materials almost always cause more ignition results in D2512 testing. To assure that the D2512 specimens generated by this effort were at the necessary uniform state of high cleanliness needed for D2512 LOX compatibility testing, all of them and any and all tools and equipment used to fabricate, handle, and store them were cleaned by the meticulous procedure detailed in this section.

Prior to setting up the D2512 specimen cleaning equipment, Meticulous Cleaning Procedures were used on the lab room shown in figure 42 were the cleaning was done. Applicable Meticulous Cleaning Procedures were used in each of the following steps described below.

Each time components or D2512 specimens needed to be cleaned roughly 40 gallons of TDW was required to be generated by the distillers depicted in figure 42. Twenty gallons of TDW was initially generated by each paired single-to-double and double-to-triple distillers depicted in figure 42 after they were first acquired to clean them. The single to double stage distillers usually had a slight oil residue left in them after 1 gallon had been processed. This was wiped out of them with a FC&N cheese cloth before the next gallon was processed. After this initial cleaning was done, the TDW generated by the distillers was stored in 5 and 8 gallon PE jugs equipped with spigots. After the jugs were acquired they were initially cleaned by being agitation washed after being filled with 2 gallons of the previously described room temperature TDW and Ivory dish soap solution. The solution was then drained through the spigot. They were then filled with TDW and allowed to stand for three days. This rinse was also drained through the spigot. This standing rinse was repeated five times. Externally accreted dust and other organic contamination of the spigots through out the effort was prevented by enclosing them in FC&N PE bags.

Two large capacity Ultrasonic cleaners were used in the cleaning procedure. After receipt from the vendor and before being used to clean other items the tanks were initially cleaned by the following procedure. Each tank was washed by ultrasonicating a full tank of TDW and Ivory dish soap solution previously described at 150°F for 5 minutes. This was repeated once again. Each tank was then rinsed by filling the tank with TDW at 150°F and ultrsonicating for 5 minutes. This was repeated five more times. At the end of each cleaning activity in this effort, the ultrasonicater tanks were drained, blown down with DFN_2, wiped dry with FC&N cheesecloth wipes and placed inside of FC&N CLEANLINER (see figure 78 and 42) PE bags for clean, no corrosion, contamination free storage.

All glassware used in this effort was, when it was received from the vendor, first cleaned by the following procedure before being used to clean or contain other items. Every glassware item was first caustic etched. Each glassware item was then ultrasonication washed by filling or immersing it with or in the previously described TDW and Ivory dish soap solution at 150°Ffor 5 minutes. This was repeated once again. Each glassware item was then rinsed by filling or immersing it with or in TDW at 150°F and ultrsonicating for 5 minutes. This was repeated nine additional times. The large 4 liter Pyrex beakers and the 15 inch and 9 inch Pyrex casserole dishes shown in figure 78 were filled to accomplish the above steps. They were primarily used to clean other items or to heat TDW for other cleaning activities. When not in use they were stored immersed under TDW in the 5 gallon polypropylene (PP) tanks shown in figure 78 and 42 which were placed inside of CLEANLINER PE bags for clean, contamination free storage. The large casserole dishes were stored in FC&N CLEANLINER PE bags as also shown in figure 78. These large casserole dishes were used for cleaning the D2512 specimen coring related equipment, prepreg cutting related tools, caul plates, autoclave cure related wrapping and bagging removal tools, and neat resin casting equipment. The 1 liter Pyrex beakers, Qorpac jars and the 6 inch and 3 inch diameter Petri dishes were immersed in the 4 liter beakers to accomplish the above cleaning steps. Since they were used in direct contact with the D2512 specimen's surface during those specimens cleaning they needed to be stored in the clean DFN_2 purged glove box shown in

figure 78, as their entire surface needed to be clean. The 1 liter beakers and the 6 inch Petri dishes used during the wash steps of the D2512 specimen cleaning were stored immersed under TDW in the 5 gallon PP tanks shown in figure 78 and 42 which were then placed inside of CLEANLINER PE bags.

The 5 gallon PP tanks, when they were first acquired, were scrubbed and washed with FC&N cheese cloths soaked in the room temperature TDW and Ivory dish soap solution described above. They were then filled with TDW and allowed to stand for three days. This standing rinse was repeated four times. The TDW in these tanks, when they were being used, was drained and replaced every third month.

During D2512 specimen cleaning the specimens themselves were only actively manipulated by contact with the clean 9 inch long stainless steel tweezers depicted in figure 79. During the packaging of the specimens for clean and contamination free storage and shipping they were manipulated by contact with the clean 6 inch long stainless steel tweezers depicted in figure 79-b. Both of these along with the scissors depicted in figure 79 needed to be cleaned before they could be used. They were cleaned by the same procedures described for glassware cleaning except for the caustic etch step. Since they were used in direct contact with the D2512 specimen's surface during those specimen's cleaning and packaging they needed to be stored in the clean DFN_2 purged glove box.

To prevent recontamination of D2512 specimens with dust and other organics after they have been cleaned they need to be handled and packaged in a controlled clean environment. To provide this environment a glove box was purchased. The glove box was cleaned when it arrived from the vendor by being hand scrubbed and washed with FC&N cheese cloths soaked in the room temperature TDW and Ivory dish soap solution described above. The glove box was then rinsed out by scrubbing it again with FC&N cheese cloths soaked in the room temperature TDW. It was then hooked up to a DFN_2 line as shown in figure 42. As the glove box was made of polymethylmethacrylate, a high rate of DFN_2 flow purge was flushed through it for three months prior to its first use. This was done to assure that any low molecular weight residual solvents in or on the polymethylmethacrylate had time to diffuse out and be blown out of the glove box by the DFN_2 purge. The high DFN_2 flow was continuously maintained throughout the entire effort to assure that the clean environment inside of the glove box was maintained.

Long term clean storage, packaging and shipping of clean D2512 specimens requires that they be placed and sealed in Aclar bags meeting NASA JPG 5322.1 Level 100 cleanliness. To seal the Aclar bags a 4 inch Thermo Impulse sealer was acquired. It is the blue piece of equipment shown in figure 79-b. When it arrived from the vendor it was initially scrubbed with IPA saturated FC&N cheese cloths, scrubbed again with TDW saturated FC&N cheese cloths, dried with FC&N cheese cloths and then placed, used and stored for the duration of this effort in the DFN_2 glove box. It was placed near and used near a purge port. To attempt to allow any organic residual contaminates to evolve off of it before its first use, it sat unused for an additional 3 months in the glove box after this initial cleaning in the high flow DFN_2 purge stream.

3 inch by 2 inch Aclar bags were purchased from CLEAN FILM. They also make the previously mentioned CLEAN LINERS. They were fabricated clean to the appropriate NASA standard and shipped in outer wrapping similar to the CLEANLINER packaging shown in figure 78. This wrapping was removed in the glove boxes' airlock using applicable Meticulous Cleaning Procedures. The Aclar bags were then immediately placed into a Qorpac pint jar, previously cleaned by caustic etch and the D2512 specimen cleaning technique, inside the glove box for clean and contamination free storage until needed.



Figure 78, Clean Glassware Storage



Figure 79-a, Clean Glassware, Specimen Handling Tools, And Storage



Figure 79-b Clean Bagging Tools And Storage

After having generated the necessary 40 gallons of TDW and set up all of the equipment needed to clean D2512 specimens, the specimens were removed from their Qorpac jars and placed into clean 1 liter Pyrex beakers. Applicable Meticulous Cleaning Procedures were used during their cleaning. No more than fifteen D2512 specimens were put into any one beaker. As shown in figure 80 up to four beakers with specimens could be simultaneous run through an ultrasonic cleaning step. Each beaker's D2512 specimens was then washed after filling the beaker with ½ liter of the previously described solution of TDW and Ivory dish soap by ultrasonicating at 150°F for 5 minutes. This step was repeated once again. Each beaker's D2512 specimens was then rinsed by filling the beaker with ½ liter of TDW at 150°F and ultrsonicating for 5 minutes. This step was repeated nine additional times. During these cleaning steps a clean 6 inch Petri dish was placed on top of each beaker. This was done to reduce the possibility of contaminating dust falling into the beakers. It also aided in stopping any D2512 specimens from being entrained out of the beaker when the hot cleaning fluid was poured out.



Figure 80, Ultrasonic Washing And Rinsing

When the twelve ultrasonic cleaning steps were done, the Petri dish capped beakers with D2512 specimens in them were placed in the glove box. Once in the glove box, the D2512 specimens were transferred into clean 3 inch Petri dishes. They were arrayed in the bottom half of the Petri dishes in a single layer. The Petri dish tops were then placed on the dish bottoms.

To uniformly and cleanly dry the cleaned D2512 specimens, the Vacuum oven shown in figure 42 and 81 was purchased. When it arrived from the vendor it was scrubbed out with IPA saturated FC&N cheese cloths and baked out under vacuum at 300°F for 72 hours. Applicable Meticulous Cleaning Procedures were used during its initial cleaning. When not being used, it was continuously flushed with DFN_2. This flushing prevented dust and contaminating oils from getting into the oven. A plastic cover was also placed on it when it was not in use to channel the nitrogen flow and reduce contaminate ingress possibilities. Prior to drying any set of D2512 specimens, it was scrubbed out with IPA saturated FC&N cheese cloths and wiped dry with FC&N cloths.

The Petri dishes containing the D2512 specimens were next transferred from the glove box directly into the Vacuum oven depicted in figure 81. Once in the vacuum oven, the D2512 specimens were baked at 125°C under a low grade vacuum for 36 hours. When this drying step was completed the Petri dishes containing the D2512 specimens were next transferred directly back into the glove box were they were allowed to cool to room temperature.



Figure 81, Vacuum Elevated Temperature Drying

Once the cleaned and dried D2512 specimens cooled to room temperature in the glove box they were then placed and sealed into the 3 inch by 2 inch precleaned Aclar bags. Due to the high cost of each Aclar bag (roughly 2 dollars apiece) two to four specimens were sealed in individual subsections of each Aclar bag as shown in figure 82. These Aclar bagged specimens were then transfered from the main glove box into a FC&N Zip lock PE bag which was in the glove boxes' airlock. The Zip lock bag was then purged with DFN_2 and thermo impulse sealed.

The Zip lock bag containing the D2512 specimens was wrapped in FC&N bubble pack and then placed into a FC&N 1 gallon paint can. The 1 gallon paint cans had been cleaned before this by being scrubbed with IPA soaked FC&N cheese cloths, then TDA soaked FC&N cheese cloths and then finally dried with FC&N cheese cloths. The can was purged with DFN_2 and sealed.

The four particular D2512 specimen type sets generated by this effort were shipped to NASA Johnson Spaceflight Center's White Sands Testing Facilities in these cans for D2512 Mechanical Impact Ignition testing. A sufficient number of D2512 specimens were shipped to accomplish the D2512 LOX compatibility test requirement of 20 impacted in LOX at 72 Ft-Lbs specimens plus an additional 3 to 4 specimens for impact in LN_2 at 72 Ft-Lbs for non-ignition-able comparison and 3 to 4 "just in case" spare specimens.



Figure 82-a, Aclar Bagged D2512 Specimens: 5250-4 RTM Neat Resin



Figure 82-b, Aclar Bagged D2512 Specimens: T650-35 Specimens

Experimental: Thermal Conductivity Specimen Fabrication And Testing

To obtain an exact measure of the thermal conductivity of the composites created by this effort required the fabrication of specimens tailored for that measurement. This measurement was needed to determine whether or not the estimated range of thermal conductivity depicted in figure 10, which a composite needed to exhibit in order to pass D2512, had in fact been achieved using the YSH experimental fibers.

Measuring the thermal conductivity of anything at or near the cryogenic temperatures of LOX is very difficult. As the thermal conductivity of a material is derived from,

Thermal Conductivity (W/mK) = Thermal Diffusivity(m^2/sec)*Specific Heat(J/kgK)*Density(Kg/m^3).

It requires that the material's density, specific heat and thermal diffusivity be measurable over the desired temperature range. Specific heats of materials are routinely measured by DSC down to these and lower temperatures. As the density of a material changes very little over a wide range of temperatures, the density at room temperature can be used for all calculations of a material's thermal conductivity. Measuring thermal diffusivity at or as close as possible to the boiling point of LOX requires the use of tailor built thermal flash diffusivity equipment. Fortunately Dr. Khairul Alam of Ohio University, Athens Ohio has tailor built high speed Xenon flash thermal diffusivity measurement equipment capable of measurements down to -164°C. Dr Alam's device requires, as a starting point, composite specimens which are slightly larger than 1 inch on a side cubes for the in-plane x and y axis and slightly larger than 1 inch on a square plates for the z axis thermal diffusivity measurement.

Dr Alam's flash thermal diffusivity measurement equipment has a measurement accuracy of plus or minus 3 percent. The accuracy of his DSC measurements of the specific heat are plus or minus 6 percent.

From discussions with Dr Alam during mid 2003 the A&PI learned the following concerning the prediction and measurement of a composite's thermal conductivity. According to Dr Alam predicting the in-plane thermal conductivity of a composite is simply a rule of mixtures of the fiber and the matrix by their V_f and V_r with the added variable of the fiber's orientation. This orientation variance of the fiber's thermal conductivity contribution is simply the sine function of the fiber's orientation with the maximum fiber thermal conductivity contribution at 0° (axial thermal conductivity) and minimum contribution at 90° (transverse thermal conductivity). According to Dr Alam predicting the transverse or out-of-plane thermal conductivity of a composite is simply a rule of mixtures of the fiber's transverse thermal conductivity and the matrix by their V_f and V_r. This rule of thumb rule of mixtures way of predicting a composite's thermal conductivity is according to Dr Alam accurate to within single percentage points of the true measured value.

Fabricating the 1 inch specimen composite cubes out of prepreg was ruled out by the A&PI as being probably not doable. After discussions with Dr Alam it was determined that simply bonding a stack of the already available bleed flow composite plates would suffice. The V_f and V_r results would be within roughly 10 percent of a full up 1 inch cube lay up composite stack if the nine bond lines between the plates could be kept to standard bond line thicknesses. These are routinely around 5 mils; roughly equivalent to the thickness of a ply. The measured in-plane thermal conductivity could then simply be scaled up to the V_f and V_r of the D2512 LOX compatibility specimens already fabricated with almost no effective deviation from their actual values.

Discussions with Dr Greg Schoeppner during the same time period determined that the best material to bond the composite plates together would be 3M's AF191 with a 0.085 psf knit carrier.

As the bleed flow 3 composite plates shown in figure 53 were made from the same composite prepreg material as the specimen composite plates out of which the D2512 specimens had been cored, the A&PI cut twelve roughly 1 plus inch squares out of their remains to make the 1 inch

thermal conductivity measurement specimen cubes and plates. Figure 52 shows the locations on these plates from whence the 1 plus inch plates were taken. These cut out 1 plus inch square plates were then sanded. The sanding removed the loosely attached resin coating which all of the composite plates made by this effort had on them. The sanding also made the surfaces more uniformly flat so as to allow the bond line material the best chance to flow and achieve the 5 mil or less desired bond line thickness. The plates were then cleaned of sanding residue by an ultrasonic wash with the Ivory soap and room temperature TDW solution previously described followed by an ultrasonic rinse in room temperature TDW. For each of the three types of composites the 1 plus inch square composite plates numbered one through ten in figure 52 were then stacked up with sheets of the AF191 between them. Figure 84 depicts the locations on the YSH50 bleed flow 3 composite plate from where the ten 1 plus inch plates came from and the uncured stack of these sanded and cleaned plates with the AF191 bond line material between them.

The three cubes were then wrapped in bagging material using one bleeder ply wrapped around the four edges revealing the AF191 bond line material. As the cubes were now over 1 inch tall and had relatively sharp edges on them that combination might tear the vacuum bag. To over come this possibility the cubes were situated inside the pockets of the dam structure depicted in figure 85 and vacuum bagging was completed. The AF191 bond line material in all three types of composite thermal conductivity cube specimens was simultaneously cured using an onsite autoclave by the cure profile depicted in figure 86. After being cured the three cubes were removed from their wrapping and vacuum bagging material. As can be seen in figure 87 the AF191bond line material did flow.

The three composite thermal conductivity cube specimens were c-scanned to determine the uniformity of the overall bonded material and determine if large voids in the bond lines or large delaminations in the constituent composite plates had occurred. Figure 88 shows the results of the c-scans. They indicate that good uniform bonded composite cube specimens with no voids or delaminations had been made.

One of the four edges revealing the AF191 bond line material of each of the three composite thermal conductivity cube specimens was polished. Micrographs, taken at 200X with the microscope indicated in figure 54, were made of them. Figure 89 shows micrographs of each of these polished and examined surfaces. These micrographs indicated that there were no large void pockets in the bond line AF191 material, that the bond line material did form a good bond to the composite plates and that the bond line material did flow to some degree forming the desired fillets representative of a good bond at the edges of the cubes. Unfortunately they also indicate that the bond line AF191 material did not flow to a sufficient degree to make the desired thin bond lines. Comparing the thickness of the bond lines to the thickness of the plies in the adjacent composite plates the bond lines were at least 11 and possibly as much as 14 mils thick. This was probably the result of the damming material shown in figure 85 being pushed up against the cubes during their cure and preventing the squeezing out of the bond line material during the cure. The micrographs also revealed that this one thermal cycling caused in-plane in ply cracks in the two composite cubes made from the YSH experimental fibers. This substantiates the observation from the fabrication section that the interface between the YSH fibers and the 5250-4 RTM was minimal at best.

Unfortunately this set of cubes was the A&PI's second attempt to generate the thermal conductivity cube specimens having used up the available material from bleed flow 1 plate in an initial failed attempt. Discussions with Dr Alam indicated that these specimens would probably suffice and so a third attempt with the last remaining bleed flow 2 composite plates was held off and reserved for a last ditch effort if the cubes failed during thermal diffusivity measurement at the desired cryogenic temperatures.

The three composite thermal conductivity cube specimens, along with two 1 plus inch square composite plates numbered 11 and 12 (See figure 52) from the three types of bleed flow 3 composite plates and one smaller specimen from each of the three plates labeled “SH” for specific heat (See figure 52 again) were shipped to Dr Alam for thermal conductivity measurement. The cubes would be used to measure the in-plane x and y axis thermal diffusivity of the three types composites. The square plates would be used to measure the transverse z axis thermal diffusivity of the three types composites. The smaller SH specimens would be used to measure the specific heats of the three types of composites. The specific heats and the x axis thermal diffusivity were to be measured at -164, -162, -157, -151, -146, -136, -126, -100, -50, 1, 25, 50, 101, 150, and 204°C. The y axis thermal diffusivities were to be measured at 25, 50, 101, 150, and 204°C. The z axis thermal diffusivities were to be measured at -162, -157, -151, -146, -136, -126, -100, -50, 1, 25, 50, 101, 150, and 204°C. If the x and the y axis thermal diffusivities differed on average by more than 5 percent at the same measured temperature then the y axis thermal diffusivity would be measured and reported at all of the remaining x axis temperatures.

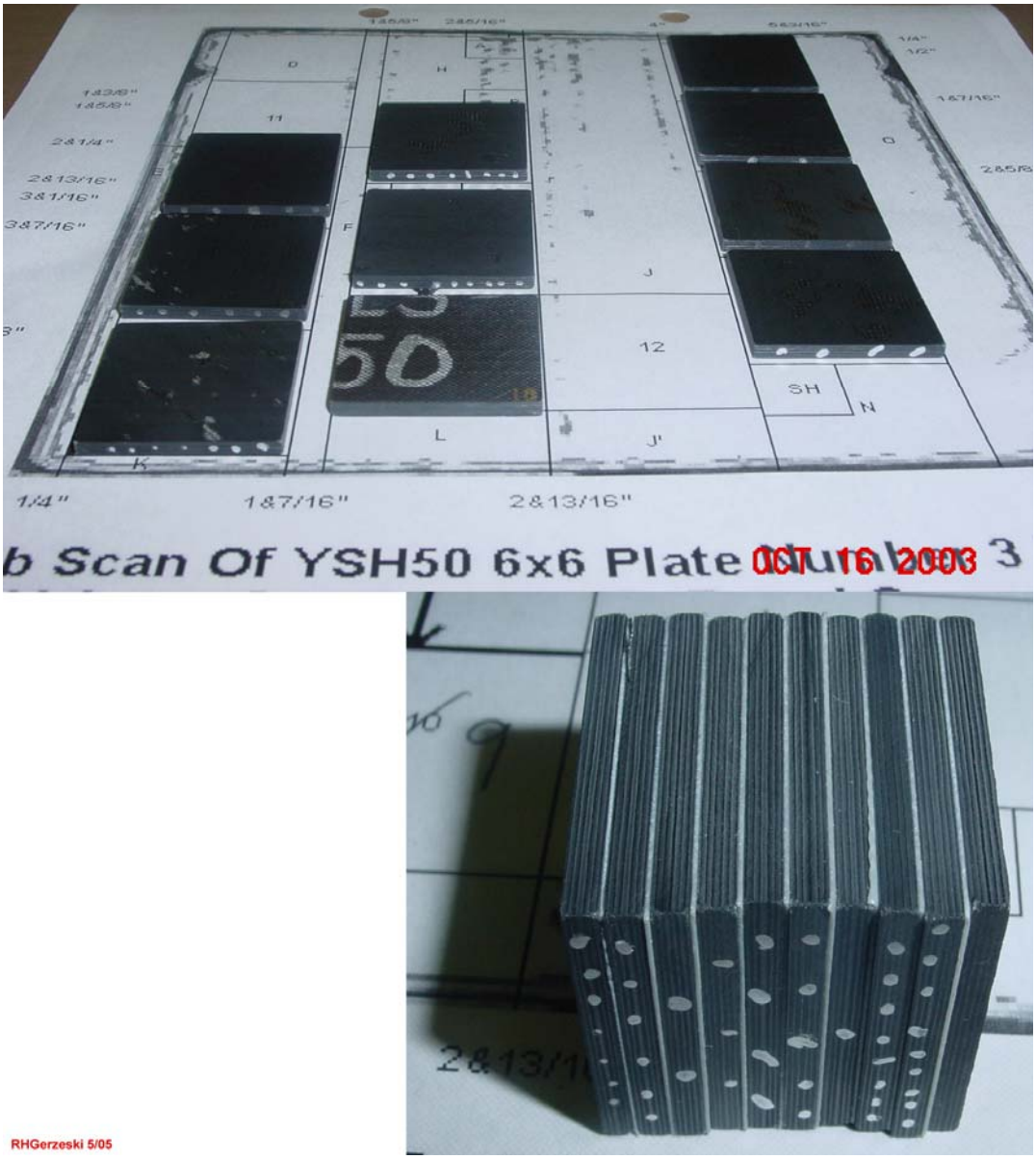


Figure 84, X and Y Axis Thermal Conductivity Measurement Specimen Assembly



Figure 85, Thermal Conductivity Specimen Vacuum Bag Tear Prevention Damming

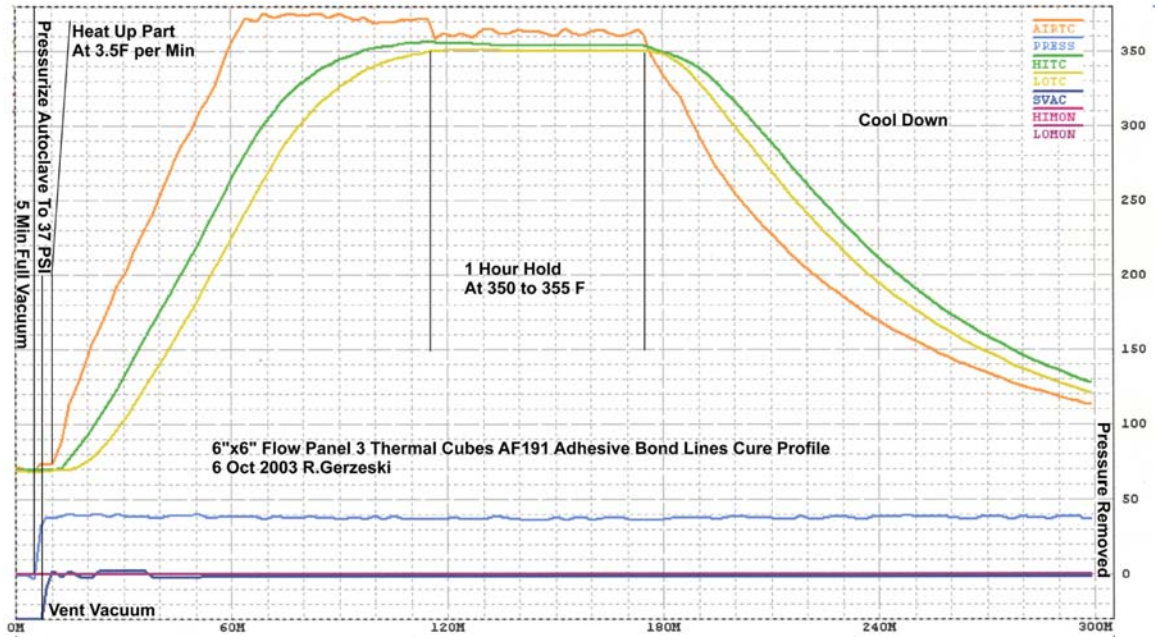


Figure 86, Thermal Conductivity Measurement Cube Cubes AF191 Bond Line Cure Profile

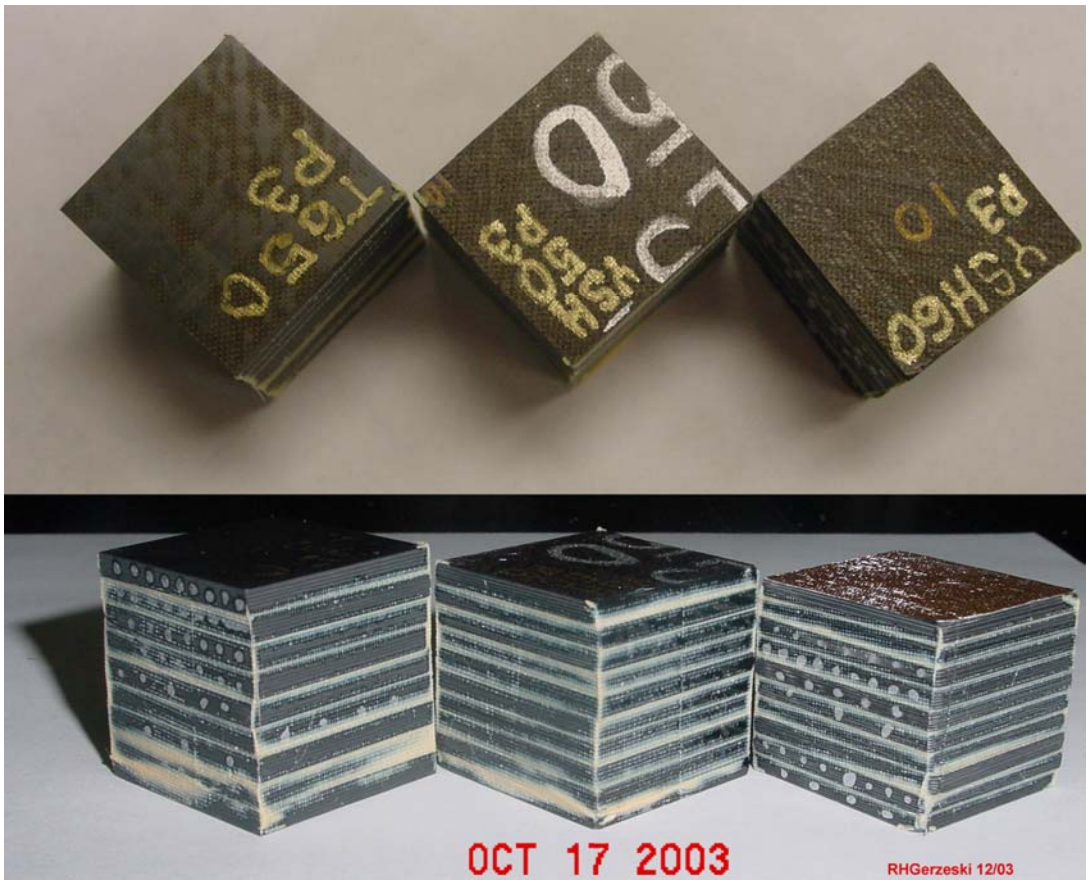


Figure 87, X and Y Axis Cured Thermal Conductivity Measurement Cube Specimens

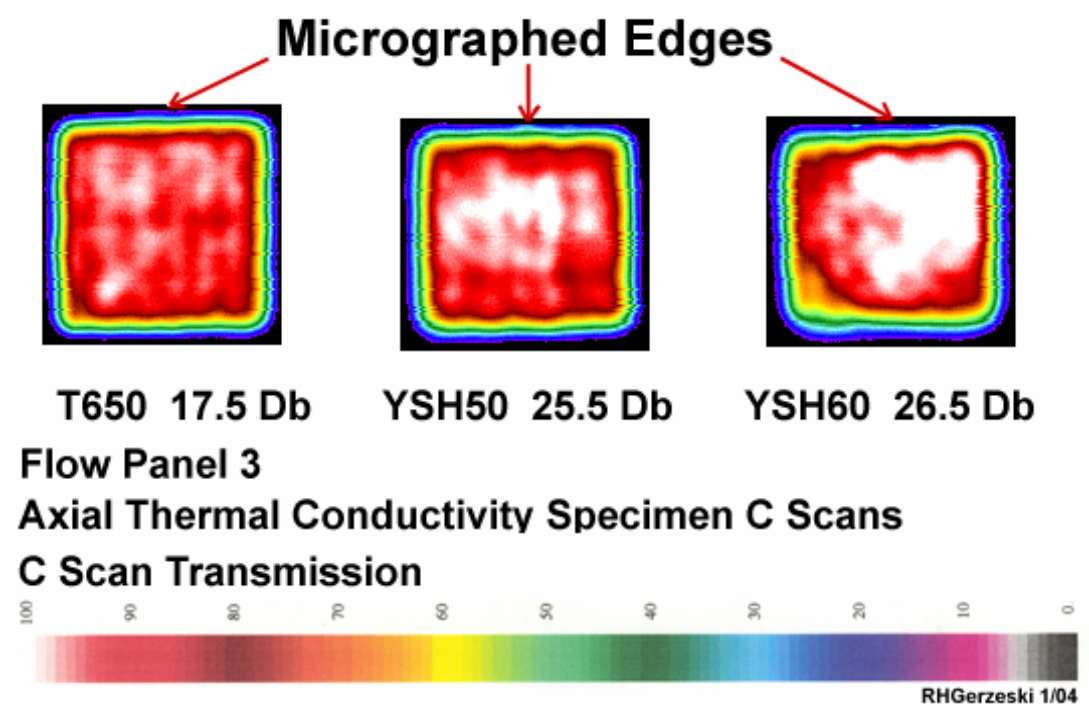


Figure 88, Thermal Conductivity Cube Specimen C Scans

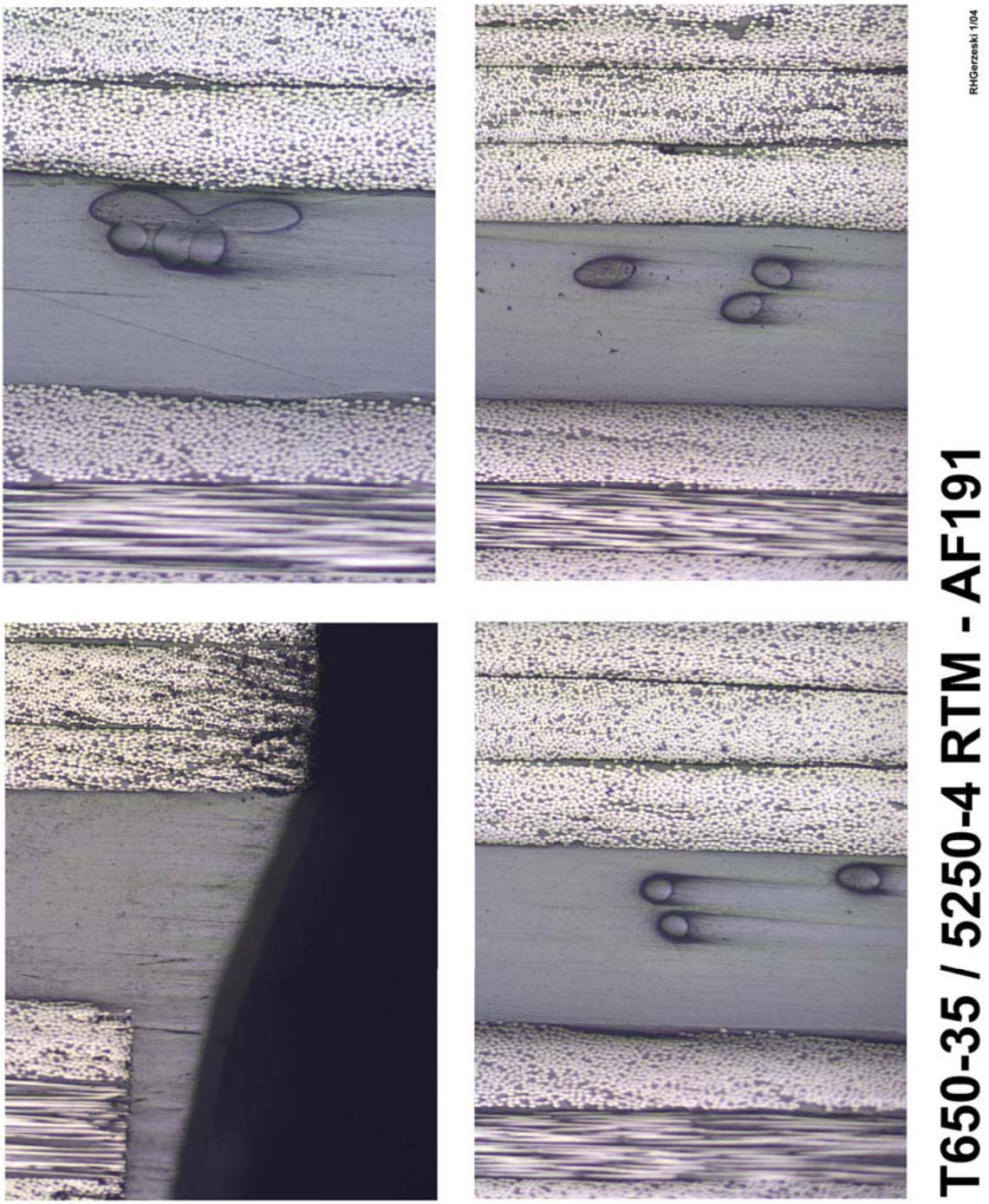


Figure 89-a, Thermal Conductivity Specimen Micrographs: Bond line And Adjacent Composite

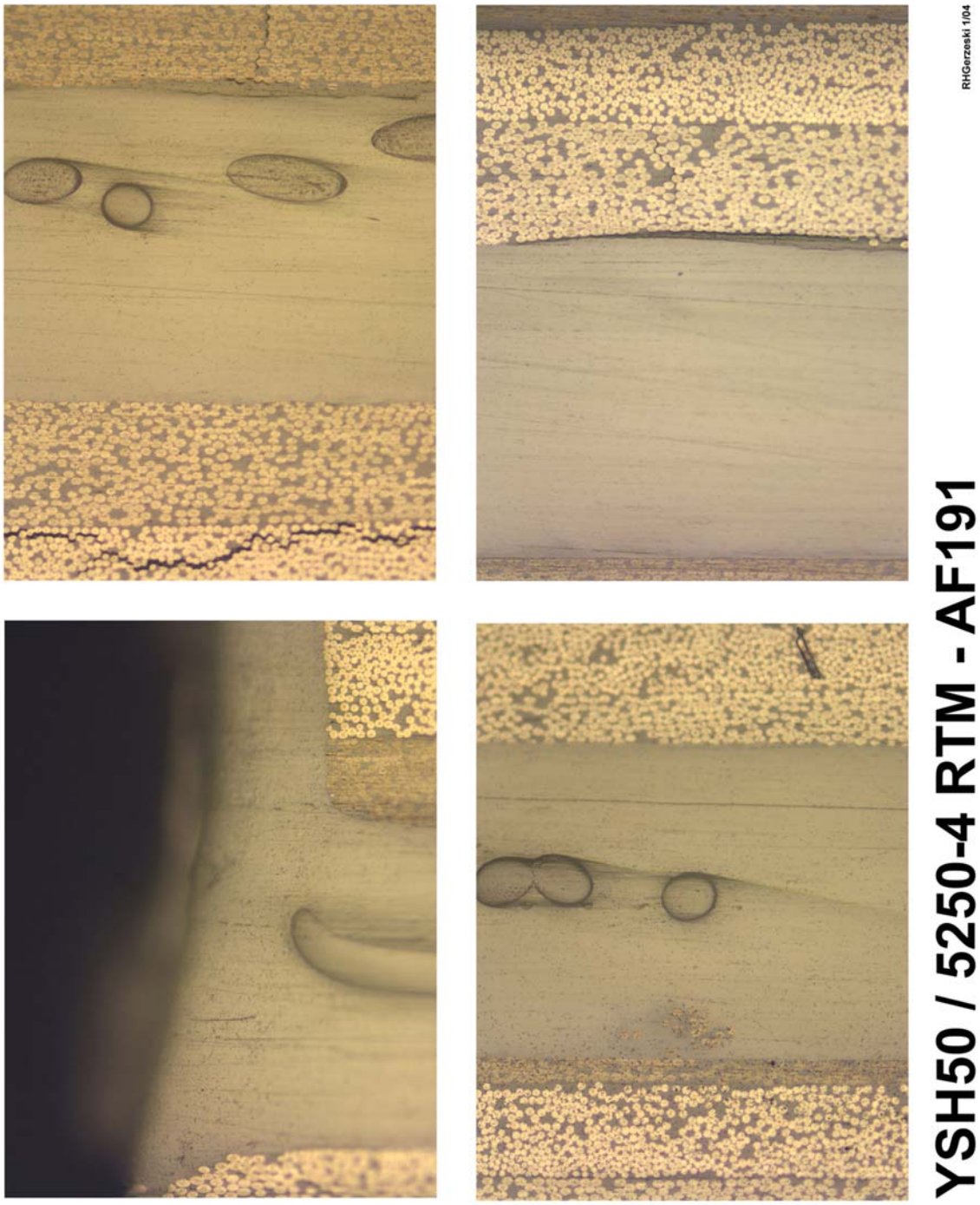


Figure 89-b, Thermal Conductivity Specimen Micrographs: Bond line And Adjacent Composite

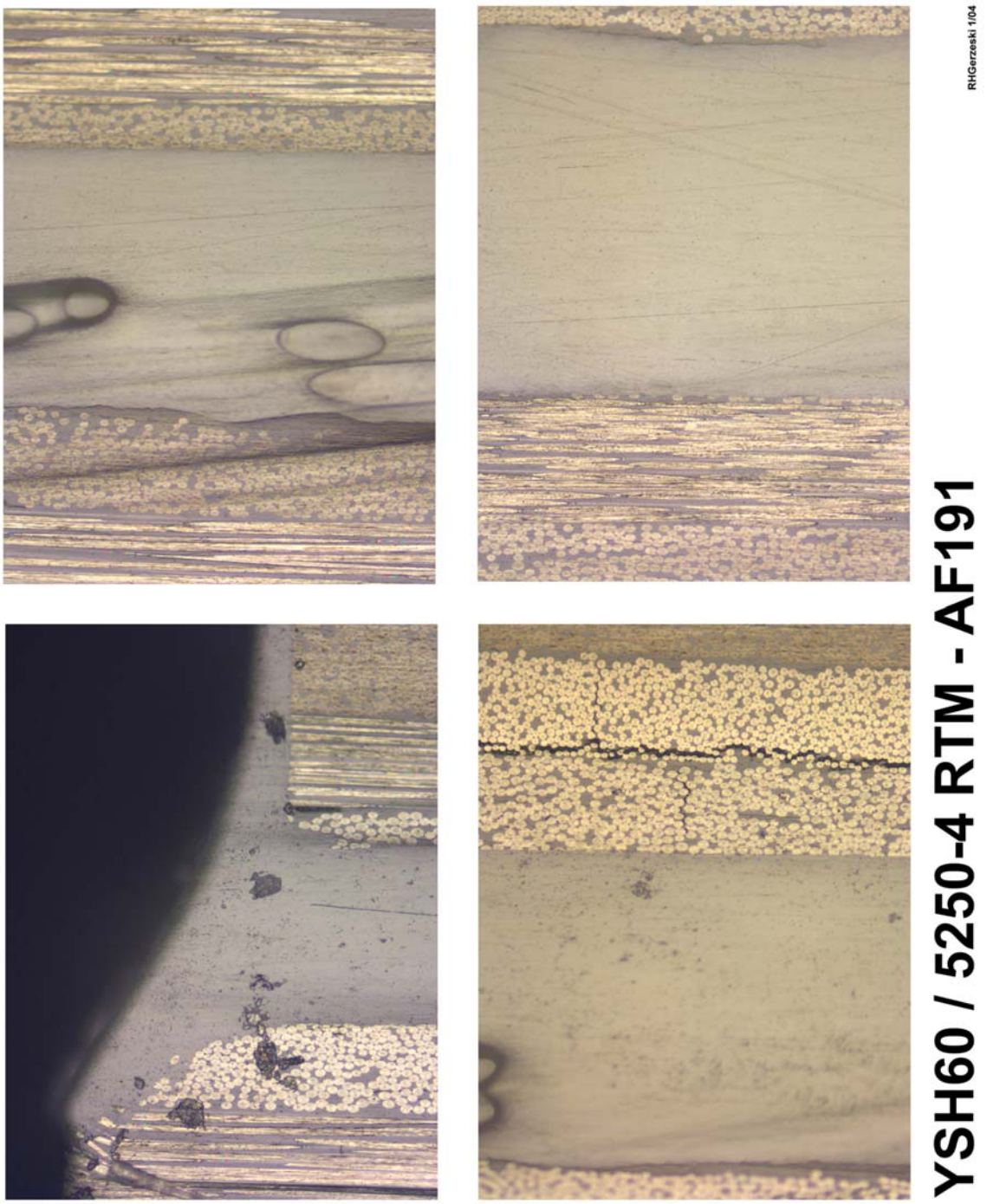


Figure 89-c, Thermal Conductivity Specimen Micrographs: Bond line And Adjacent Composite

Dr Alam's initial efforts to measure the x and y axis thermal diffusivities of the three composite cube specimens sent to him were unsuccessful. The thermal diffusivity of all of the specimens was too low for a sufficiently strong temperature rise signal to get through the 1 inch cube specimens and be accurately detected by his flash diffusivity equipment. To overcome this Dr Alam cut the cubes into the smaller thickness specimens shown in figure 90.

The small roughly ¾ inch by ¾ inch by 1 inch tall residual cube shown in figure 90 remaining after Dr Alam's fabricated usable thermal diffusivity specimens from the three original 1 inch cubes

were sent back to the A&PI for density, V_f, V_r and V_v measurements. These smaller cubes were further cut by the A&PI into three additional pieces. The density, V_f, V_r and V_v of these three pieces for each of the three types of bleed flow 3 x and y axis thermal conductivity specimen composite cubes was measured. The Archimedes principle was used to measure the density and an acid digestion technique was used to measure the volume values. The results are listed in table 22. The density, V_f, V_r and V_v of the three types of bleed flow 3 z axis thermal conductivity specimen composite square plates are the same as those reported in table 19. These values were reported back to Dr Alam so that he could complete his calculations of the three types of composite specimen's three different axial thermal conductivities.

Table 22, Thermal Conductivity Specimens Physical Properties:

X and Y Axis:	Material:	T650-35 / 5250-4 RTM	YSH50A / 5250-4 RTM	YSH60A / 5250-4 RTM
Property: Density: (gms/cc)	Avg:	1.5571	1.7257	1.7346
	Max:	1.5579	1.7279	1.7351
	Min:	1.5566	1.7230	1.7343
	Std:	0.0007	0.0025	0.0005
Property: Fiber Volume: (%)	Avg:	60.5294	57.0439	56.6460
	Max:	60.5865	57.2405	56.8022
	Min:	60.4136	56.8210	56.4922
	Std:	0.0796	0.1814	0.1310
Property: Resin Content: (%)	Avg:	38.4783	41.9564	42.4362
	Max:	38.8066	42.3421	42.9577
	Min:	38.1681	41.5708	41.9051
	Std:	0.1960	0.2314	0.3122
Property: Void Volume: (%)	Avg:	0.9923	0.9996	0.9177
	Max:	1.2669	1.3022	1.2927
	Min:	0.7523	0.7268	0.5501
	Std:	0.1774	0.1945	0.2237

Z Axis Physical Properties Are Those of Bleed Flow Plate 3:

Experimental: D2512 Load Versus Time Plots

Circa the early 2000s no effort had been reported which measured the actual load versus time curves exhibited by D2512 specimens as they were being impacted in the standard D2512 apparatus depicted in figure 5. To remedy this, the Air Force funded an effort by the University of Dayton Research Institute to develop an instrumented D2512 impacter. The core goal of this effort was to take D2512 type Load versus time impact data on various types of materials at initially LN_2 and ambient temperatures and eventually LOX. The contract PI for this effort was Dr William Lee and the chief technician was Mr John Camping. By late 2003 they had successfully designed, built, instrumented, and set up the impacter equipment and were collecting data. In April 2004 the A&PI was invited to collect load versus time plots on the D2512 specimens generated by this report's efforts.

Fifteen specimens in all were provided by the A&PI. They were impacted at various conditions and the instrumented load versus time data for the first impact bounce were collected. Any single specimen's impacted test in the D2512 apparatus almost always involves numerous bounces of the plummet and subsequently numerous impact loads by the indenting D2512 striker pin shown in figure 5. The instrumented equipment developed could only collect data on the first of these impacting bounces. Of the tested specimens, eight were impacted at conditions directly relevant to this reported effort's interests and the D2512 testing conditions. These specimens were not

progressed past the sanding and beveling point on towards fully cleaned and packaged D2512 specimens. Two of each type of D2512 specimen cored from the four types of specimen plates generated for this effort were tested at 72 Ft-Lb impact in LN_2 and the load versus time plots were collected.

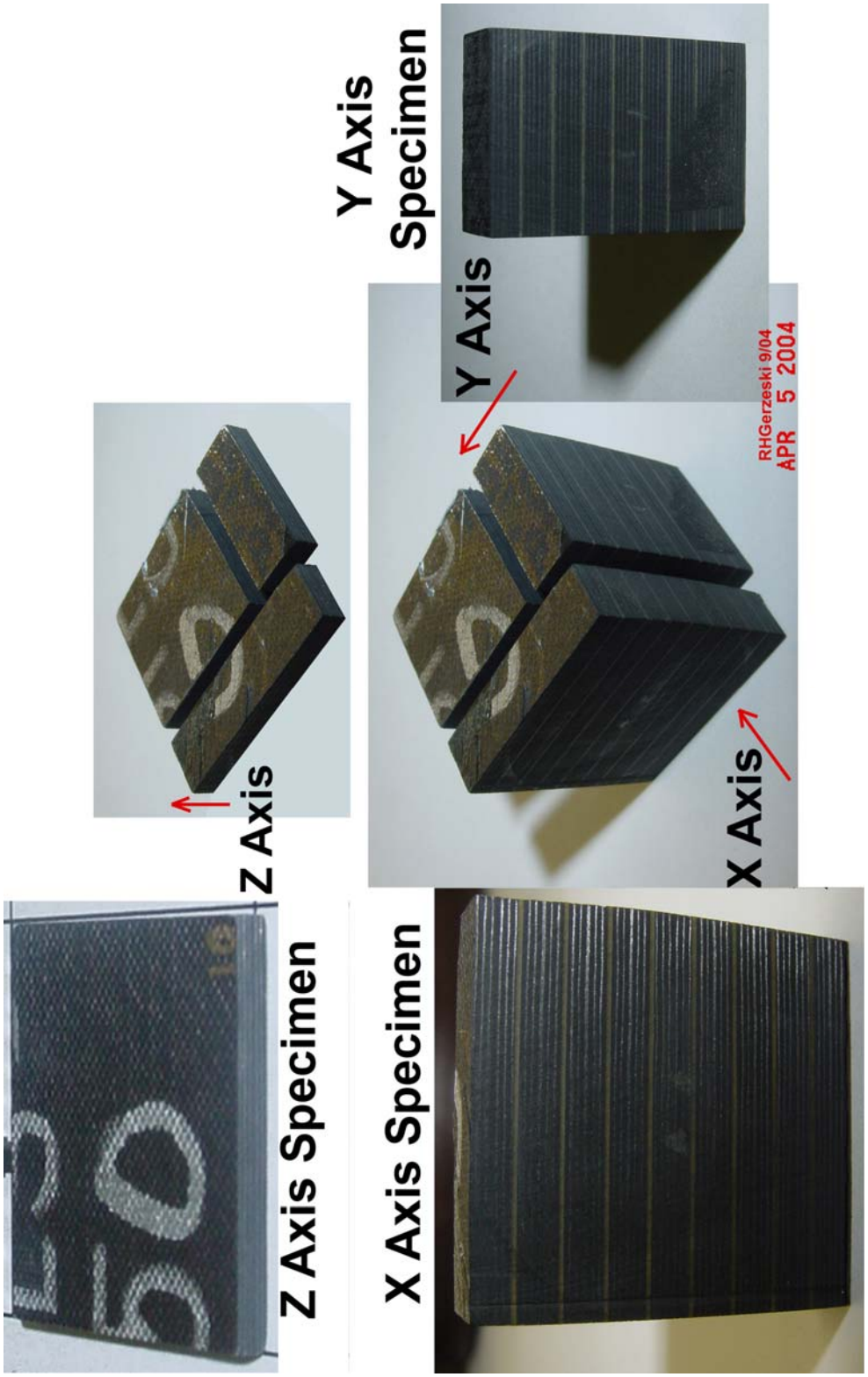


Figure 90, Final Thermal Conductivity Measurement Specimens Orientation

Results Section: D2512 LOX Compatibility Tests

Table 23 lists the results of the D2512 Mechanical Impact tests conducted by NASA White Sands Test Facility at 72 Ft-Lbs in ambient pressure LOX on the four sets of prepared specimens. The results indicated that both of the experimental YSH fibers improved the D2512 LOX compatibility of their respective composites by seventeen hundred percent over the baseline T650-35 fiber reinforced composite's D2512 LOX compatibility. Also only the flash type of reaction was detected for the YSH fibered specimens, where as, flash, char and noise types of reactions where detected for the T650-35 fibered specimens. This implies that the ignition events (See Table 7) of reaction indicating YSH fibered composites did not progress as far as those in T650-35 fibered specimens. Also the one hundred percent D2512 ignition rate exhibited by the 5250-4 RTM neat resin specimens implies that the seventeen hundred percent improvement in the YSH fiber reinforced 5250-4 RTM matrix composite's D2512 LOX compatibility over that exhibited by the T650-35 fiber reinforced 5250-4 RTM matrix composite specimens is directly attributable to the use of these moderately, thermally conductive, primarily graphite YSH type fibers.

Results Section: Contaminated D2512 LOX Compatibility Test Specimen Rejection

In spite of the extreme use of meticulous cleaning procedures and clean specimen preparation and handling techniques one of the eighty tested in LOX specimens was inadvertently tested in a contaminated condition. Sample 12 of the prepared 5250-4 RTM neat resin specimen was determined to have been D2512 tested in a contaminated condition. Since contaminates severely skew LOX compatibility test results it was rejected and its' results were also removed from the final tabulations, examinations, depictions and basis of interpretation. This determination was based on the very harsh and extreme magnitude of the mechanical impact initiated ignition reaction results exhibited by Sample 12's residuals as compared to the residuals of all other reaction indicating tested specimens.

Figure 91 and figures R1l, R9l, and R17l in the residuals appendix depict sample 12's returned residuals. The images in figures 91, R9l and R17l were taken at a magnification of somewhere between X10 and X16 using the X10-16 technique depicted in figure 54. Many final results, only seen in this sample's residuals, are depicted in these figures. Sample 12's returned residual 304 stainless steel support disc was the only returned disc exhibiting a melted and gouged out flow streak in its surface. Sample 12's returned residual 5052 aluminum cup was the only returned cup exhibiting either impaled or melted and refrozen metal particles adhering to its inner walls and bottom surface. Sample 12's returned 5250-4 RTM residual specimen pieces were the only containing scalloped out and melted and refrozen metal flakes.

The types of residuals resulting from Sample 12's testing indicate that a very high temperature and high pressure pulse generating ignition reaction had occurred near the disc's surface. This pulse melted out or scalloped out a jet or flow of metal from the disc's surface. This jet of scalloped out, melted metal flakes were thrust into the wall of the LOX containing cup where some of them remained. Those metal flakes that were not impaled into the cup's wall or blown out of the D2512 testing apparatus, cooled and formed obviously refrozen flakes admixed in with the shattered remains of the 5250-4 RTM specimen. This high temperature and pressure pulse could only have been generated by some type of contaminating material which exhibited a very low radical chain scission degradation temperature, a very low ignition temperature, a metal catalyzed peroxide oxidation of the degraded material and achieved a full sustained combustion ignition. Since none of the other 19 D2512 tested neat resin specimens generated residuals even remotely looking like this, residuals like sample 12's could only have been generated by the ignition of some extraneous contaminating material like fingerprint oil or a hair follicle or some flammable solvent.

Table 23, D2512 LOX Compatibility Test Results:

Material:	5250-4 RTM Neat Resin		T650-35 / 5250-4 RTM	
Sample	Result:	Reaction Type:	Result:	Reaction Type:
1	Reaction	FCN	Reaction	FCN
2	Reaction	FCN	Reaction	FCN
3	Reaction	FCN	Reaction	FCN
4	Reaction	FCN	Reaction	FCN
5	Reaction	FCN	Reaction	FCN
6	Reaction	FCN	Reaction	FCN
7	Reaction	FCN	Reaction	FCN
8	Reaction	FCN	Reaction	FCN
9	Reaction	FCN	Reaction	FCN
10	Reaction	FCN	No Reaction	
11	Reaction	FCN	Reaction	FCN
12	Rejected Due To Contamination		Reaction	FCN
13	Reaction	FCN	Reaction	FCN
14	Reaction	FCN	Reaction	FCN
15	Reaction	FCN	Reaction	FCN
16	Reaction	FCN	Reaction	FCN
17	Reaction	FCN	Reaction	FCN
18	Reaction	FCN	Reaction	FCN
19	Reaction	FCN	Reaction	FCN
20	Reaction	FCN	Reaction	FCN
	Reactions/Impacts		Reactions/Impacts	
Overall:	19/19	FCN	19/20	FCN

Material:	YSH50A / 5250-4 RTM		YSH60A / 5250-4 RTM	
Sample	Result:	Reaction Type:	Result:	Reaction Type:
1	No Reaction		No Reaction	
2	No Reaction		No Reaction	
3	No Reaction		No Reaction	
4	No Reaction		Reaction	F
5	No Reaction		No Reaction	
6	Reaction	F	No Reaction	
7	No Reaction		No Reaction	
8	No Reaction		No Reaction	
9	No Reaction		No Reaction	
10	No Reaction		No Reaction	
11	No Reaction		No Reaction	
12	No Reaction		No Reaction	
13	No Reaction		Reaction	F
14	Reaction	F	No Reaction	
15	No Reaction		No Reaction	
16	No Reaction		No Reaction	
17	No Reaction		No Reaction	
18	No Reaction		No Reaction	
19	No Reaction		No Reaction	
20	No Reaction		No Reaction	
	Reactions/Impacts		Reactions/Impacts	
Overall:	2/20	F	2/20	F

Reaction Type: F: Flash C: Char N: Noise



Figure 91-a, Rejected Due To Contamination D2512 Specimen: Cup and Disc Residuals

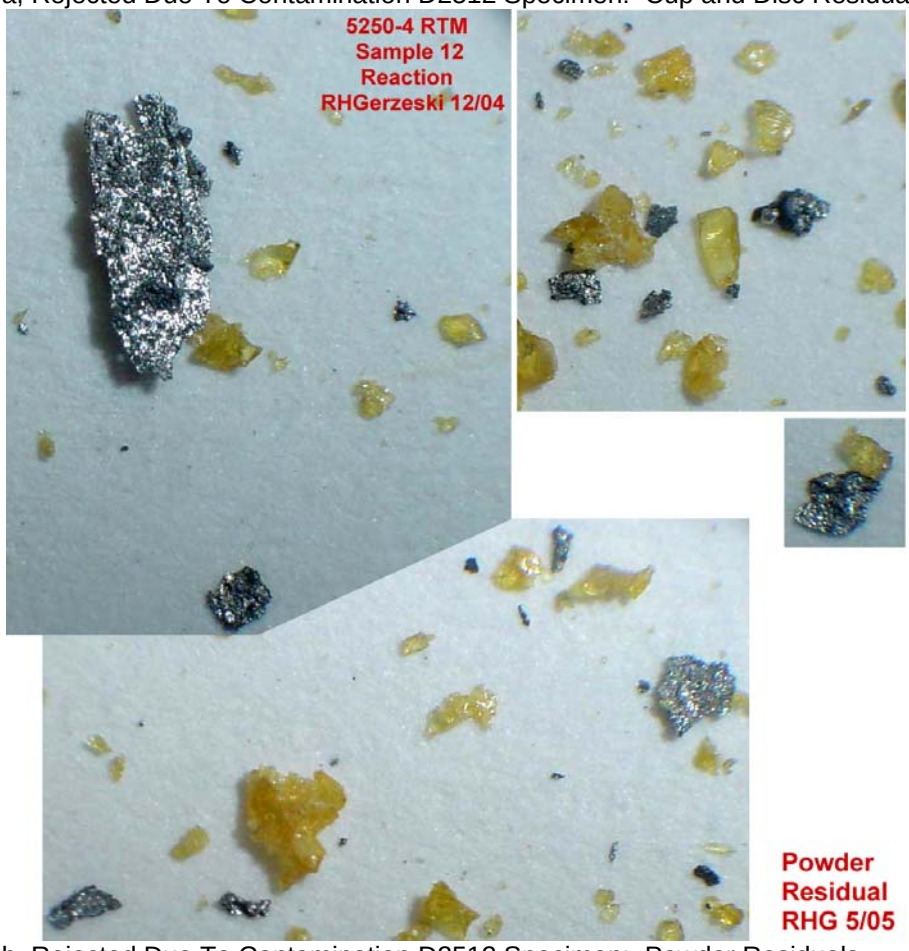


Figure 91-b, Rejected Due To Contamination D2512 Specimen: Powder Residuals

Results Section: Thermal Conductivity Tests

Figure 92 graphically depicts the various axial thermal conductivities as measured by Dr Alam of the three types of composites listed in table 22.

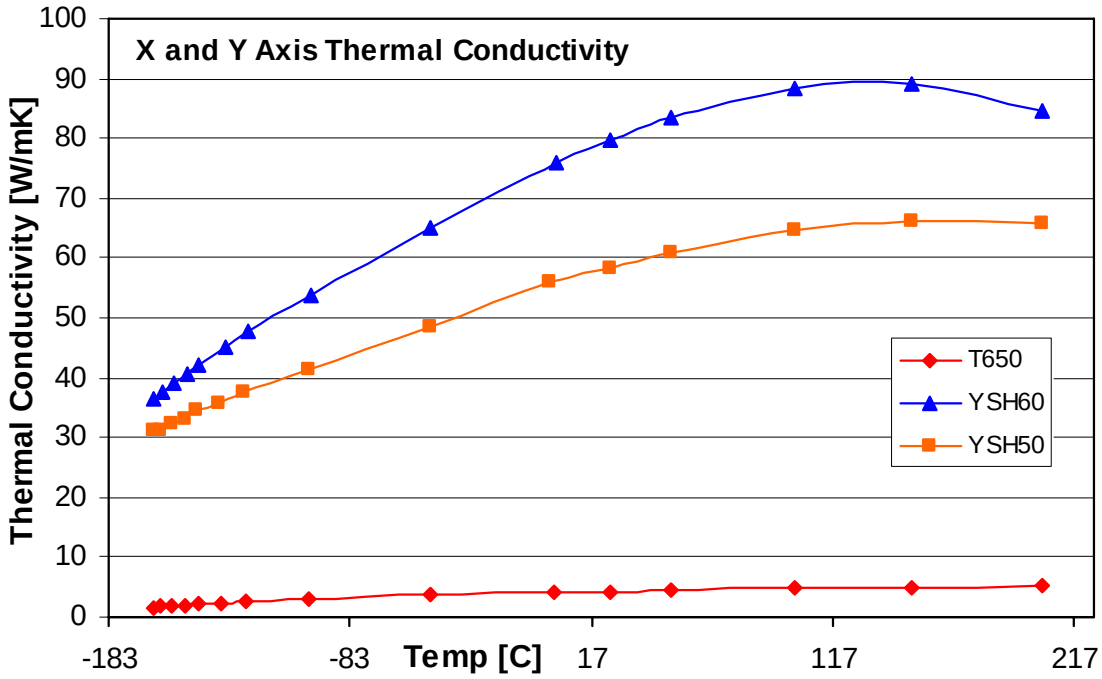


Figure 92-a, Composite Thermal Conductivity: X and Y Axis

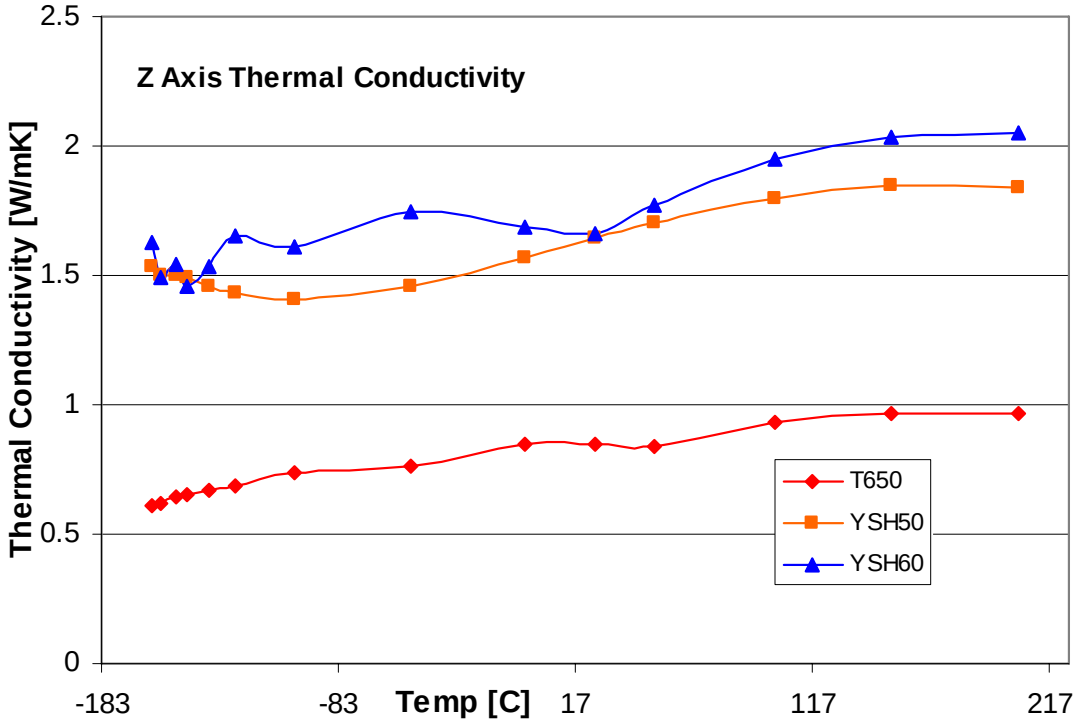


Figure 92-b, Composite Thermal Conductivity: Z Axis

To determine the thermal conductivities at LOX's boiling point and the V_f listed in table 21 of the three types of D2512 tested composite specimens, Dr Alam's rule of thumbs mixture approach and a linear regression extrapolation for the x and y axis measured thermal conductivity to LOX's boiling point was used. The linear regression extrapolation was based on the last seven, lowest temperature data points in figure 92-A for each of the three separate composite types. Table 24 lists these extrapolated and scaled thermal conductivities. The x and y axis extrapolated and scaled thermal conductivities of the YSH fiber reinforced composites are roughly twenty-three hundred and twenty-six hundred percent greater than the T650-35 fiber reinforced composites. An examination of figure 92-B indicates that the z axis thermal conductivity for the three composites are as listed in Table 24. The z axis thermal conductivities of the YSH fiber reinforced composites are roughly two hundred percent greater than that of the T650-35 fiber reinforced composites.

Table 24, Thermal Conductivity At LOX's Boiling Point

X and Y Axis:			
	Material:	T650-35 / 5250-4 RTM	YSH50A / 5250-4 RTM	YSH60A / 5250-4 RTM
K At LOX's BP: (W/mK) (Measured And Scaled To 63.7% FV)		1.34	31.22	35.24
Z Axis:				
	Material:	T650-35 / 5250-4 RTM	YSH50A / 5250-4 RTM	YSH60A / 5250-4 RTM
K At LOX's BP: (W/mK) (Rough Estimate From Figure 92-B)		~0.55	~1.60	~1.60

Results Section: Fractography

Upon receipt of the residuals of the four D2512 tested types of materials back from White Sands Test Facility in early 2004 the A&PI began an exhaustive fifteen month effort to examine and document the fracture surfaces of these residuals. This fractography effort was essential to finally acquiring images of the fracture surfaces of D2512 tested specimens since like images had never before been published.

All of the images reported in this Fractography subsection and also most of those depicted in the Residuals Appendix were taken with the X10-16 image magnification and digital picture capture technique shown in figure 54. As figure 54's X10-16 system was incapable of incorporating a length scale into the magnified images the same specimen residual clamping and holding technique tool used through out the fractography sub effort was dimensioned. The dimensions of this tool are shown in figure 93. As this tool appears in many of the residual specimen images it can give the reader a rough estimate of feature lengths.

A thorough examination of the returned specimen residuals found that any specific residual item could be grouped into four major categories. The residual item originated from either outside of the area of the specimen contacted by the D2512 striker-impacter, under the area contacted by the impacter, a powder of the finely crushed original specimen or the result of an interaction between a specimen residual and the cup.

Results Section: Fractography: Impacter External

Additional examination of the specimen residuals originating from outside of the impacter-specimen contacting area found that they could be further grouped into these seven subcategories: ring shaped cracks, transverse and in plane cracks, knob like extreme cone cracks, straight cracks, kinetic friction induced abrasion, intense heat exposure and tensile hoop failure. The determination that these residuals originated from outside of the impacter was based upon their possessing a portion of the original specimen's cylindrical edge.

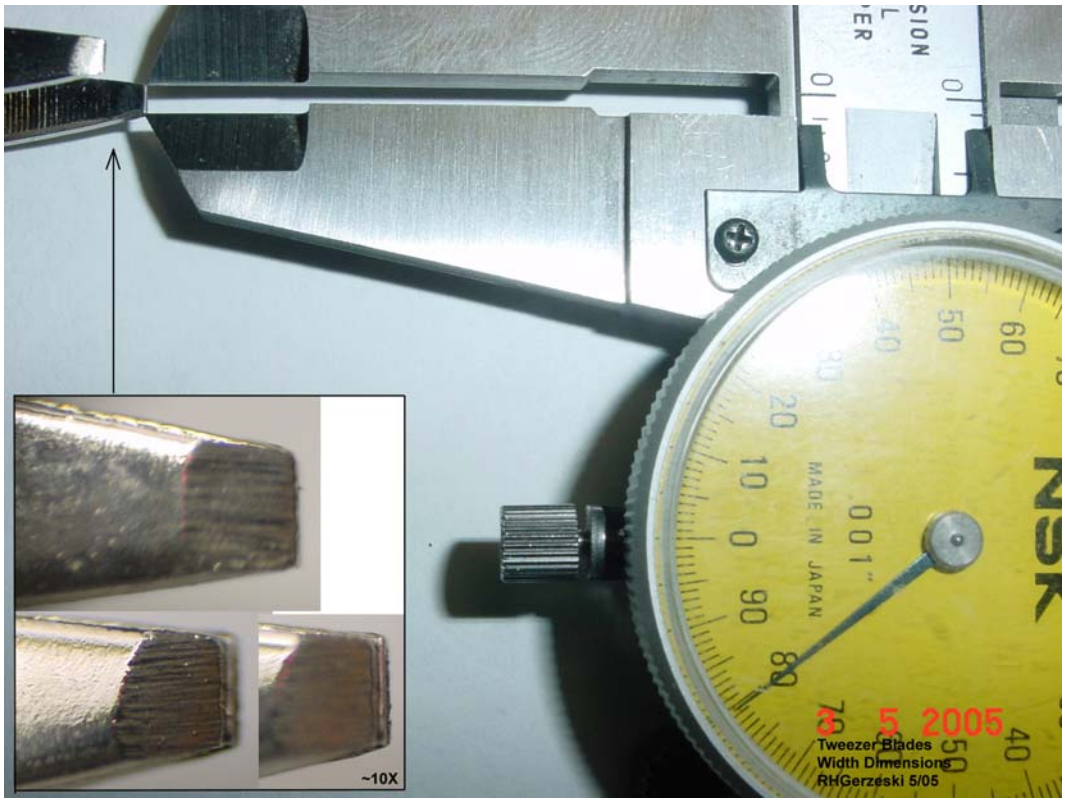


Figure 93-a, Specimen residual clamping and holding tool dimension: Width



Figure 93-b, Specimen residual clamping and holding tool dimension: Thickness

Figures 94 thru 97 show examples of the ring shaped cracks found in many of the returned residuals. In many residuals a series of ring shaped cracks are seen stacked across what was the original specimen's surface or stacked downwards at various plies thru the original specimen's surface. These ring cracks routinely plunge straight downward normal to the original specimen's surface or to a ply. In the composite specimens these ring shaped cracks had sub segments which were "straighter" giving the crack a slightly octagonal shape. Overall these ring shape cracks and their location on the original specimens is analogous to the Hertzian ring cracks described in the Theory Section: Hertzian Fracture.

Figures 98 thru 101 show examples of transverse and in plane cracks found in many of the returned residuals. In many residuals a series of these transverse and in plane cracks are seen stacked on top of each other progressing downwards thru the original specimen's thickness. These transverse and in plane cracks always start at the bottom edge of the previously described ring cracks and then follow one of three distinct paths. Almost all of the transverse and in plane cracks found in the neat resins initially progress at an angle in a direction straight downwards through the thickness of the specimen. Some continue along this path until they terminate. Others deviate from this and curl in an arc back in a direction which would cause them to terminate in a region of the original specimen that would have been under the impacter. For the residuals which came from the composite specimens the transverse and in plane cracks initially progress at an angle in a direction straight downwards thru the thickness of the specimen. They progress on this downward path for the thickness of only a very few plys. They then and progress parallel to the fiber reinforcement outwards towards the original specimen's edge. These outward ranging transverse cracks occur both along a ply to ply interface and through the interior thickness of an individual ply. Overall these transverse and in plane cracks and their location on the original specimens is analogous to the Hertzian cone cracks described in the Theory Section: Hertzian Fracture. The transverse ranging along the reinforcements of these cracks are the result of the Hertzian cone crack's propagation direction being normal to the material's weakest tensile vector. For composites the weakest tensile properties are transverse to the reinforcements.

Figures 102 thru 105 show examples of the knob shapes found on many of the returned residuals. These knobs look to be a series stacked combination of an extreme version of the above Hertzian cone crack followed by a typical cone crack stacked closer to the original specimen's center. The knobs found on the specimens impacted in LN2 were usually larger and more prominent than those found on specimens impacted in LOX. Overall the outer extreme cone crack's shape and their location on the original specimens is analogous to the negative surface which Conchoidal flakes leave behind in an impacted or indented material as described in the Theory Section: Hertzian Fracture. In essence the outer fracture crack surface is an extreme Hertzian cone crack and a negative resulting from the evolution of a conchoidal flake from the specimen and the stacking of it with another typical Hertzian cone crack creates the knob structures.

Figures 106 thru 109 show examples of the straight shaped cracks found in many of the returned residuals. These straight cracks exhibit a combination of the simpler features of the Hertzian ring and cone cracks: they plunge straight downward normal to the original specimen's surface and then progress at an angle in a straight direction downwards thru the thickness of the specimen until they terminate. They also stack up one on another with the first starting at the original specimen's surface and then a series of new straight cracks develop through the thickness. For the composite residuals exhibiting these straight cracks they always occur at the outer edges of the residuals and flow out from the more centrally occurring Hertzian ring and cone cracks. Overall these straight shape cracks and their location on the original specimens is analogous to the flare cracks coming off of Hertzian cone cracks developed in a specimen which slid relative to the impacter as described in the Theory Section: Hertzian Fracture.

Figures 110 thru 113 show examples of the signs of abrasion found on many of the returned residuals. The presence of oriented flakes consisting of the neat resin on the neat resin residual

samples are classic indicator products of past light to moderate kinetic friction abrasion. The appearance of smooth gentle contour changing surfaces on the various composite's residuals where their should be jagged fracture surfaces, with or without light or heavy traces of particulate residue, are another classic indicator that light to moderate kinetic friction had abrasion normalized the surface profile. These smooth gentle contour changing surfaces give the same appearance under X10-16 magnification as the beveled edges that the A&PI put onto the specimens for burr removal. Overall these traces of abrasion indicate that kinetic friction movement occurred between some of the residuals and some other portion or residual of the original specimen.

Figures 114 thru 117 show examples of the signs of intense heat or high temperature exposure found on many of the returned residuals. A pebbled and pock marked surface of spherical nodules with spherical craters and or a refrozen smear, sometimes in the shape of a feathered extrusion, are the classic signs of a polymeric material that has been exposed to intense heat or high temperature. These signs were always located adjacent to signs of abrasion on the residuals exhibiting them. As described in the Theory Section: Kinetic Friction heavy kinetic friction abrasion can produce the intense heat and correspondingly high temperatures which create many of these features. This caused portions of the residuals to become a degraded "melt" which was then either smeared and rapidly "refrozen or resolidified" or was not smeared and had time to form partial spheres and spherical craters.

Figures 118 thru 121 show examples of tensile hoop failure in the returned residuals. All of the composite residuals exhibit a combination of a tensile failure and an in towards the center of the original specimen bending of the fibers. These tensile hoop failures always occur at the outer wing edge of the residual. The neat resin residuals all exhibit the classic flat and usually clean tensile fractures characteristics of a brittle material failing in tension. They too always occur at the outer edges of the residual. This type of failure would occur if the original specimen was being compression loaded in the general location of its center causing was left of, or remaining in, the center region under the impacter to press outward. Essentially this tensile hoop failure is basically identical to the rupture failure of an over pressurized vessel.

Figure 118-a-iv provides an important clue as to the relative timing of all of the above described failure types and phenomenon. It depicts stacked Hertzian ring and cone cracks with an incomplete tensile failure progressing through them. This indicates that the tensile hoop failure occurs last in the previously listed sequence of failure types and phenomenon. .

Many of the neat resin residuals in figures 94, 98, 102, 106, 110 and 114 exhibit an arc or arc-like tensile failures on the side of the residual which would have been closest to the center of the original specimen. The Hertzian fracture mechanism described in the Theory Section: Hertzian Fracture, indicates that these arc-like tensile failures are vent cracks. They locate the side of the residual opposite to the impacter's point of contact on the original specimen.

Results Section: Fractography: Under The Impacter

Further examination of the larger specimen residuals originating from under the impacter and specimen contacting area found that they could be further assigned to these six subcategories: crescents and arcs, knobs, straight sided, kinetic friction induced abrasion, intense heat exposure, and surface effects. These residuals were determined to have originated from under the impacter by the lack of the existence of a portion of the original specimen's cylindrical edge or, in the case of the straight sided residuals, by the length of the residual relative to the remaining original specimen's edge.

As no large neat resin residuals were returned which exhibited the characteristics of having come from some location on the original specimen located under the impacter, no figures of the fracture effects and phenomenon can be provided in this sub section.

Figures 122 thru 124 show examples of crescent and arc shaped returned residuals. The crescent shaped residuals are found in a multitude of thicknesses and widths but all have the appearance of being made by a series of Hertzian cone cracks. As previously described in the Theory Section Hertzian Fracture, they are the crescent shapes produced in the area of a material under an indenter which has been slid over it. The arc shaped residuals represent the last of the Hertzian cone cracks generated when the specimen stopped sliding due the restricted room available in the cup (see figure 5) for the original specimen to move through. Their existence indicates that kinetic friction sliding occurred between the impacter and the specimen during the D5212 testing.

Figures 125 thru 127 show examples of Knobs on the returned residuals. These residuals usually exhibit a long sloping fracture surface which moves towards the original specimen's surface. These sloping cracks are the extreme cone or conchoidal cracks described in the Theory Section Hertzian Fracture. These knobbed residuals are a stacked in series combination of a standard Hertzian cone crack and an extreme Hertzian cone crack. Both being created as the original specimen slid under the impacter during the D2512 test. The knobs formed on the residuals impacted in LN2 were usually larger and more prominent than those found on residuals impacted in LOX.

Figures 128 thru 130 show examples of straight sided returned residuals. Most of these straight sided residuals exhibit a portion of the outer edge of the original specimen and they are also usually of a length that is a substantial portion of the original specimen's diameter. They are created by a stacked series of the straight flare cracks, described in the Theory Section: Hertzian Fracture, originating in the original specimen under the impacter and progressing outwards towards the specimen's edge as it slid during the D2512 testing.

Figures 131 thru 133 show examples of the signs of abrasion found on many of the returned residuals. The appearance of smooth gentle contour changing surfaces on the various residuals where their should be jagged fracture surfaces, without traces of particulate residue, are an indicator that light to moderate kinetic friction had abrasion normalized the surface profile. Overall these traces indicate that kinetic friction abrasion inducing movement occurred between some of these residuals and some other portion of the original specimen under the impacter during D2512 testing.

Figures 134 thru 136 show examples of the signs of intense heat or high temperature exposure found on many of the returned residuals. A pebbled and pock marked surface of spherical nodules combined with spherical craters or a "refrozen or resolidified" smear are the signs of a polymer containing material that has been exposed to intense heat or high temperature. A majority of these signs were found on the surfaces of residuals which were parallel to the original specimen's impacted surface. The remainder were always located adjacent to signs of abrasion. No residuals presented both. As described in the Theory Section: Kinetic Friction heavy kinetic friction abrasion can produce intense heat and or high temperatures creating these features. This caused portions of the residuals to become a melt which was then either smeared and rapidly "refrozen or resolidified" or was not smeared and had time to form partial spheres and spherical craters.

Figures 137 thru 139 show examples of the surface of the returned residuals. Determining whether or not these surfaces were in direct contact with the impacter is impossible due to the way in which they were fabricated and the way in which D2512 testing is conducted. But based upon the previously noted failure types and phenomenon mechanisms, the specimens slid during the D2512 impact loading. As both sides of the specimen are in contact with steel during D2512 testing (see figure 5) a similar degree of kinetic friction occurred on both sides of the specimen. This steel on specimen sliding caused remarkably little damage to the resin rich and in the case of the YSH composites poorly adhering surfaces. The only traces of interaction consist of a light abrasion which ground the high points down into flattened plateaus .

Results Section: Fractography: Powder

All of the returned D2512 tested specimens contained residuals of course powder. Figures 140 through 143 depict these course powders. Additional examination of these course powder residuals found that they could be further grouped into these four subcategories: narrow crescent shapes, abrasion, intense heat exposure, and surface effects.

Figures 144 through 147 show examples of narrow crescent shaped powder residuals. These appear to have two sides shaped like the Hertzian ring or cone cracks described in the Theory Section: Hertzian Fracture. The sliding of the specimen under impacter during a D2512 test would create a series of stacked Hertzian ring and cone cracks in the specimen. Some would be narrowly spaced together and create crescent shaped narrow sleeves of the material between the Hertzian cracks.

Figures 148 thru 151 show examples of the signs of abrasion found on many of the returned powder residuals. The appearance of smooth gentle contour changing surfaces on the various residuals where the typical powder residuals presented jagged fracture surfaces, with or without traces of light particulate residue, are an indicator that light to moderate kinetic friction had abrasion normalized the surface profile. Overall these traces of abrasion indicate that kinetic friction movement occurred between some of the powder residuals and some other portion of the original specimen.

Figures 152 thru 155 show examples of signs of intense heat or high temperature exposure found on many of the returned powder residuals. The pebbled and pock marked surface of spherical nodules and spherical craters and or the refrozen smear, as previously described, are signs that these residuals experienced intense heat or high temperature exposure. Many of the neat resin powder residuals as shown in figure 152 also exhibited drawn out tendrils. These neat resin residuals appear to have been heated up to a state were they became a viscose fluid, were drawn out and then “refrozen or resolidified” into the tendril shapes on many of the powder residuals. Also cakes of neat resin powder residuals as seen in figures 152-a-i, 152-a-ii, and 152-c-I were common. They appear to be an agglomeration of individual powder residuals who’s edges had been rendered a viscose fluid, pressed into one another and then “refrozen or resolidified”. Many of the composite powder residuals also exhibit the appearance of char on their surfaces. As described in the Theory Section: Kinetic Friction heavy kinetic friction abrasion can produce the high temperatures which would create these features.

Figures 156 thru 159 show examples of the original specimen’s surface in the returned powder residuals. For the same reasons detailed to describe the surfaces shown in figures 137 through 139, these powder residuals exhibit remarkably little damage from the D2512 testing besides the high point flattening kinetic friction abrasion between the sliding specimen’s surface and the steel impacter and disc of the testing apparatus.

Results Section: Fractography: Specimen Cup Interactions

The final category of residuals consists of the specimen’s interaction with the LOX containment cup depicted in figure 5. The residuals in this category can be broken out into these two subcategories: back edge damage on some of the residuals and particles of the specimens affixed to cup’s inner surface.

Figures 160 thru 163 show examples of returned residuals which exhibited compressive crushing done to the original specimen’s cylindrical edge. All of the residuals exhibiting these signs of back edge crushing originate from areas on the original specimen originally outside of the impacter’s contact. Usually the crushes are located directly behind the residual’s Hertzian cone cracked inner edge typically along the middle of the remaining original specimen’s cylindrical edge. The actual crushed areas present the same features which appear on the edge of a brittle isotropic material or the edge of a composite laminate which has been impacted by a blow

aligned normal to that edge. For the brittle material these features generate conchoidal flakes and the extreme Hertzian cone crack negatives described in the Theory Section: Hertzian Fracture. For the composite these features are bent backwards and or snapped over reinforcement fibers. As the only surface available for these edges to contact during a D2512 test are the cup's inner walls, these crushing impacts must have occurred when the residual forcefully contacted the cup.

Figures 164 thru 167show examples of returned residual cups which have bands of impaled powder residuals or scorch marks on their inner walls. The bands are usually narrow and located on the lower third of the cup's walls. They seldom range for more than one quarter of the cup's inner circumference. The scorch marks routinely take a more circular shape whose size ranges between a pinprick and a blotch occupying between five and fifteen degrees of the cup's inner circumference.

Results Section: Fractography: Global Observations

For all of the failure types and phenomenon previously exhibited by the returned residuals, with a rare few exceptions, all were found in all four types of the D2512 tested specimens. They were also found regardless of the medium, LOX or LN_2, in which the specimen was impacted and regardless of whether or not the material exhibited an ignition reaction. The only exceptions to these observations occurred when the paucity of returned relevant residuals (no returned no reaction detected 5250-4 RTM specimens, only one returned no reaction detected T650-35 specimen and two returned reaction detected YSH50 and YSH60 specimens each were available for examination) precluded finding examples of these failure types and phenomenon at a specific overall D2512 testing condition. Based upon these observations the failure types and phenomenon described in the Impacter External, Under The Impacter, Powder and Specimen Cup Interactions Fractography subsections, with only two notable exceptions, occur independent of the testing conditions and whether or not a reaction occurs. The two exceptions are the prominence of the knobs produced when the D2512 test occurs in LN_2 and the severity of the intense heat or high temperature exposure when a reaction is detected in LOX D2512 tested specimens.

Results Section: Fractography: Fiber Resolution Fracture Surface Imaging

Numerous attempts were made to acquire fiber resolution images using the X25-200 system depicted in figure 54 of the various fracture surfaces described in the previous fractography subsections. Due to the X25-200 system's extremely limited field of depth almost all created nothing more than blotchy black, grey and white images which were indecipherable. One exception was a series of images taken at X200 of the fracture surface depicted in figure 168. These images were taken from the only sample made of the T650-35 / 5250-4 RTM composite which did not react when D2512 tested. Figure 169 depicts this fracture surface. This fracture surface is also shown in figure 115-b. Based on the fracture mechanism detailed in the Theory Section; Hertzian Fracture, it is a straight flare off of a hertzian cone crack. Based on the smeared instead of jagged surface it has been intensely heated to a high temperature probably by the kinetic friction mechanism detailed in the Theory Section: Kinetic Friction. The images in figure 169 show no fiber pull out and clean transversely fractured fibers. The images also show that the crack's propagation is anisotropically influenced by the orientation of the fibers. It forms parallel to the fibers when extending laterally along a fiber bed. It extends transversely thru the fiber beds by fracturing segments of the composite as small as ten fiber diameters in length at orientations parallel or perpendicular to the fibers.

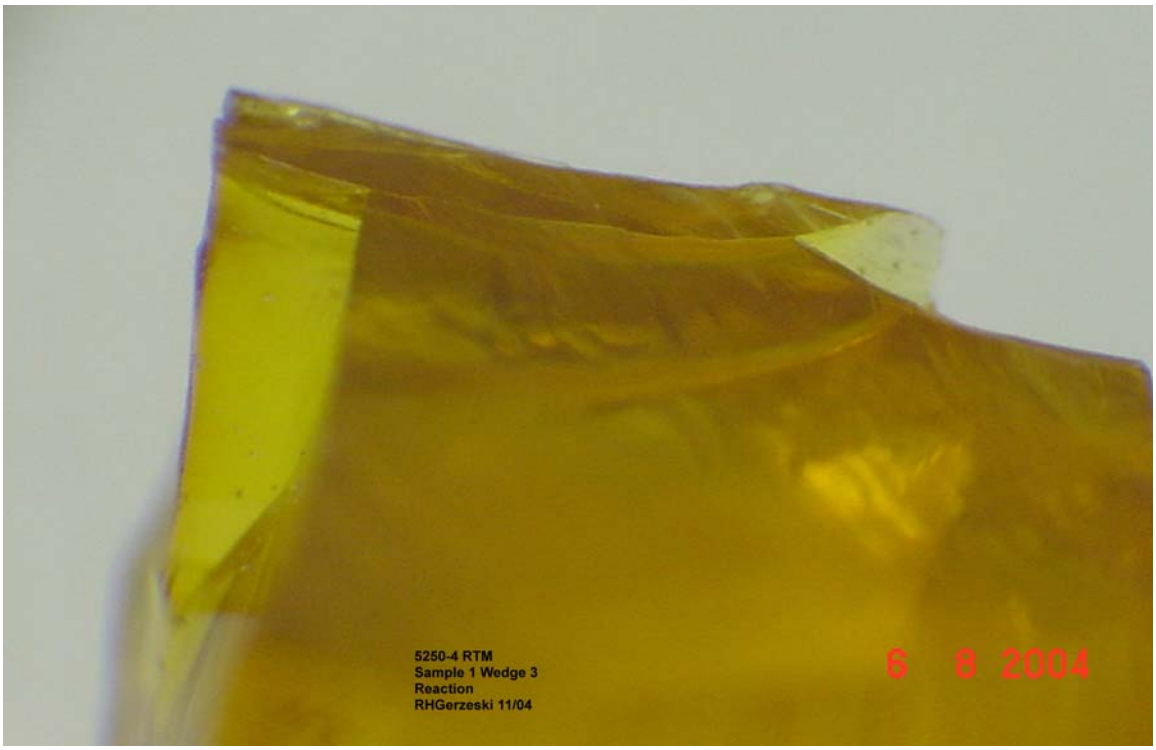


Figure 94-a-i, External To The Indenting Impacter Fracture Surfaces: Ring Cracks: 5250-4 RTM D2512 Specimen: In LOX: Reaction Detected

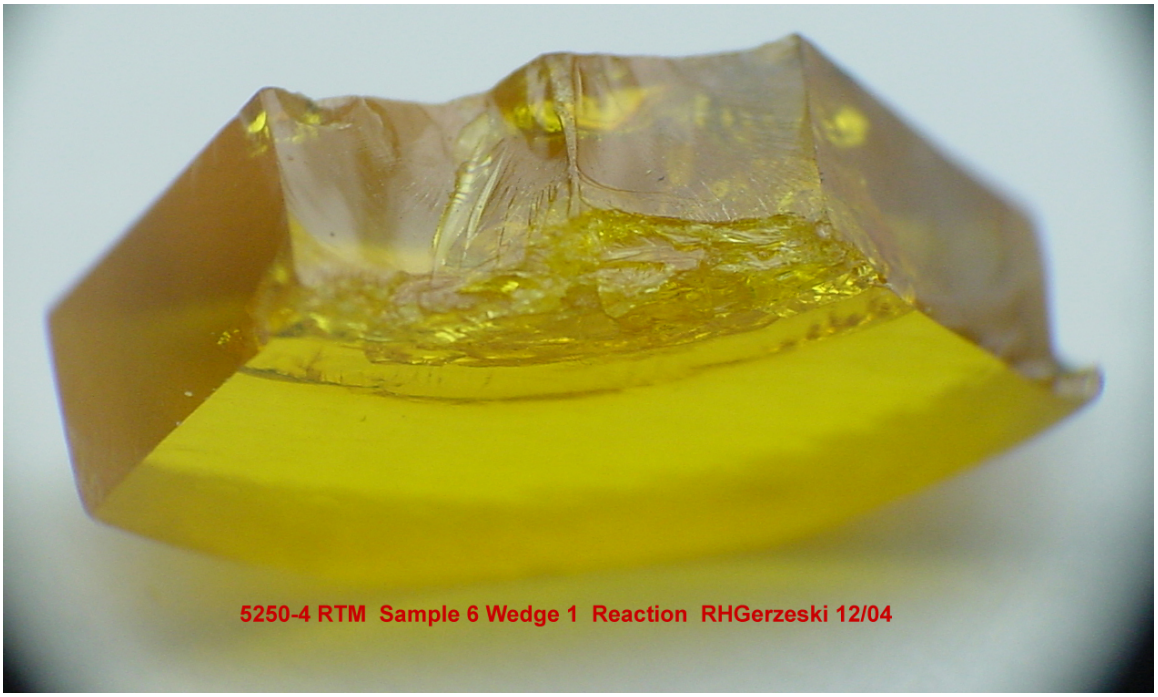


Figure 94-a-ii, External To The Indenting Impacter Fracture Surfaces: Ring Cracks: 5250-4 RTM D2512 Specimen: In LOX: Reaction Detected



Figure 94-a-iii, External To The Indenting Impacter Fracture Surfaces: Ring Cracks: 5250-4 RTM D2512 Specimen: In LOX: Reaction Detected

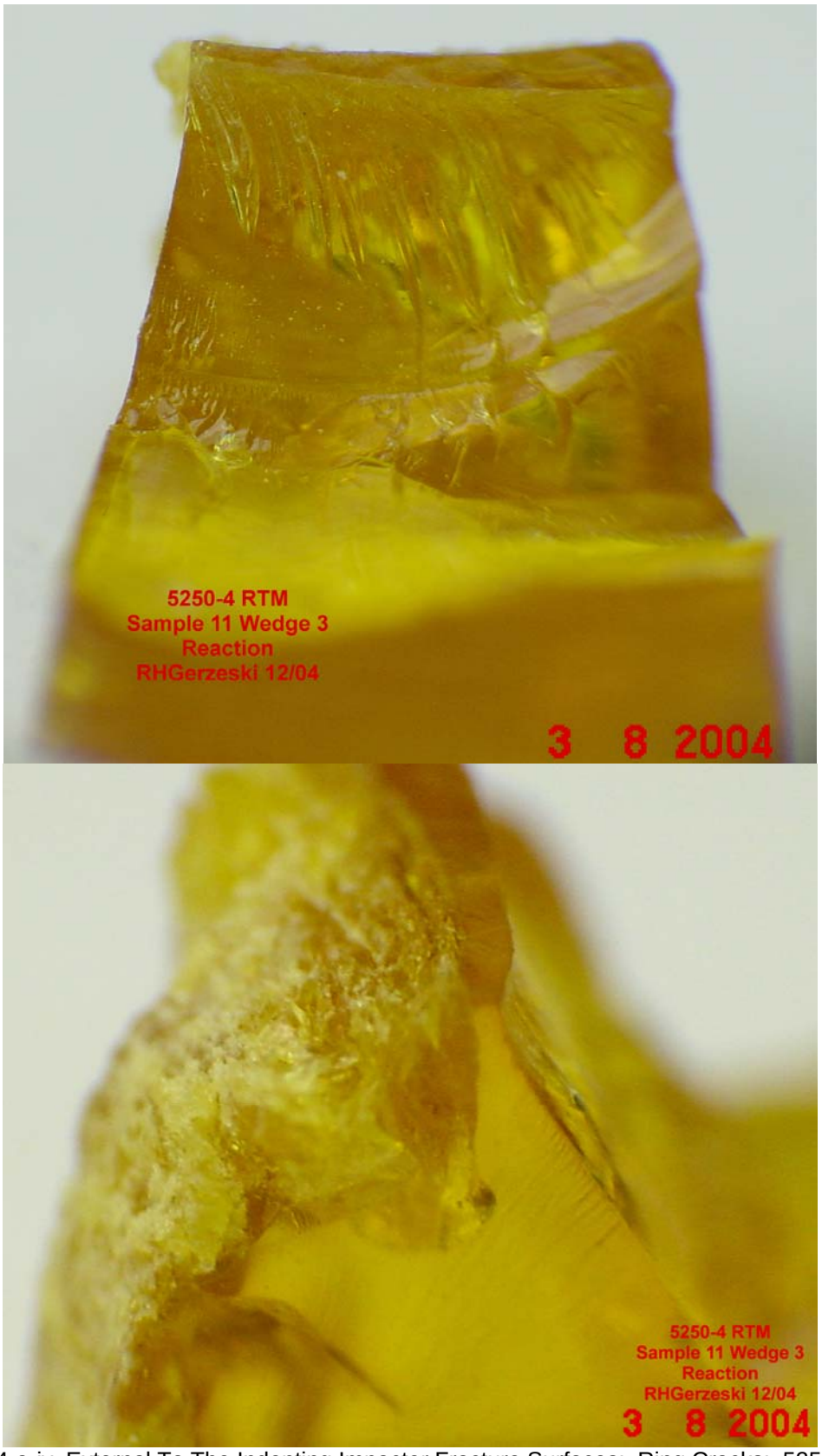


Figure 94-a-iv, External To The Indenting Impacter Fracture Surfaces: Ring Cracks: 5250-4 RTM D2512 Specimen: In LOX: Reaction Detected



Figure 94-a-v, External To The Indenting Impacter Fracture Surfaces: Ring Cracks: 5250-4 RTM D2512 Specimen: In LOX: Reaction Detected

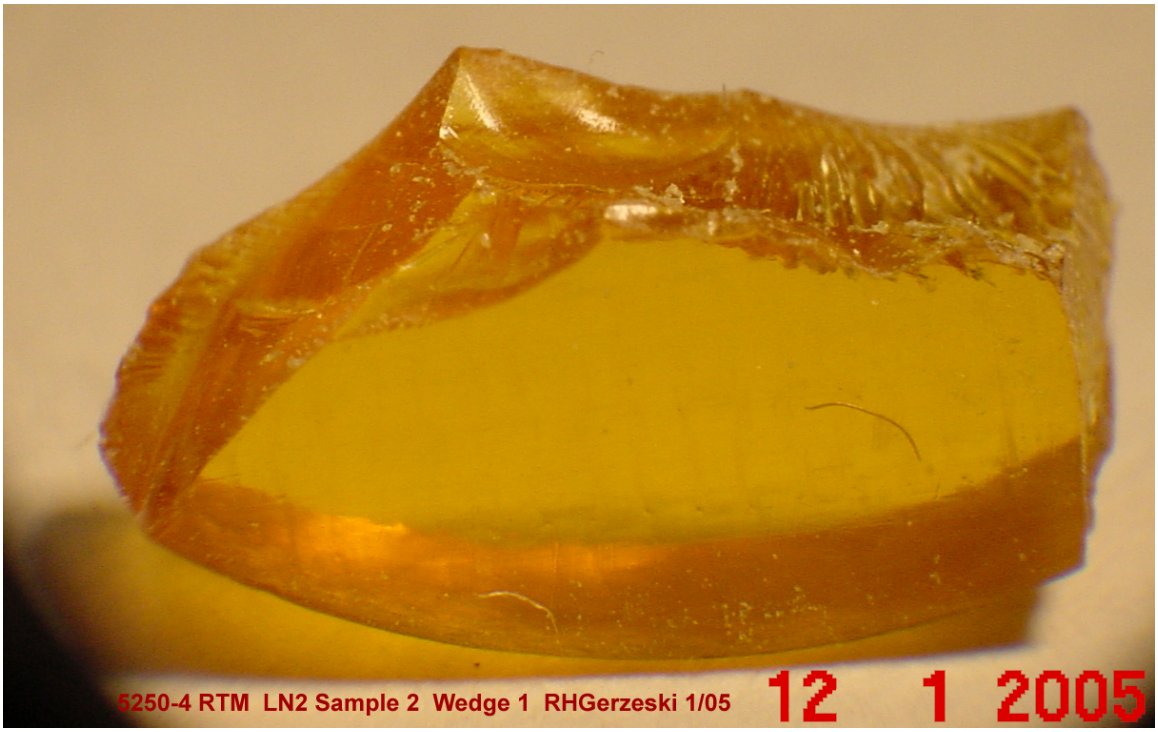


Figure 94-b-i, External To The Indenting Impacter Fracture Surfaces: Ring Cracks: 5250-4 RTM D2512 Specimen: In LN2

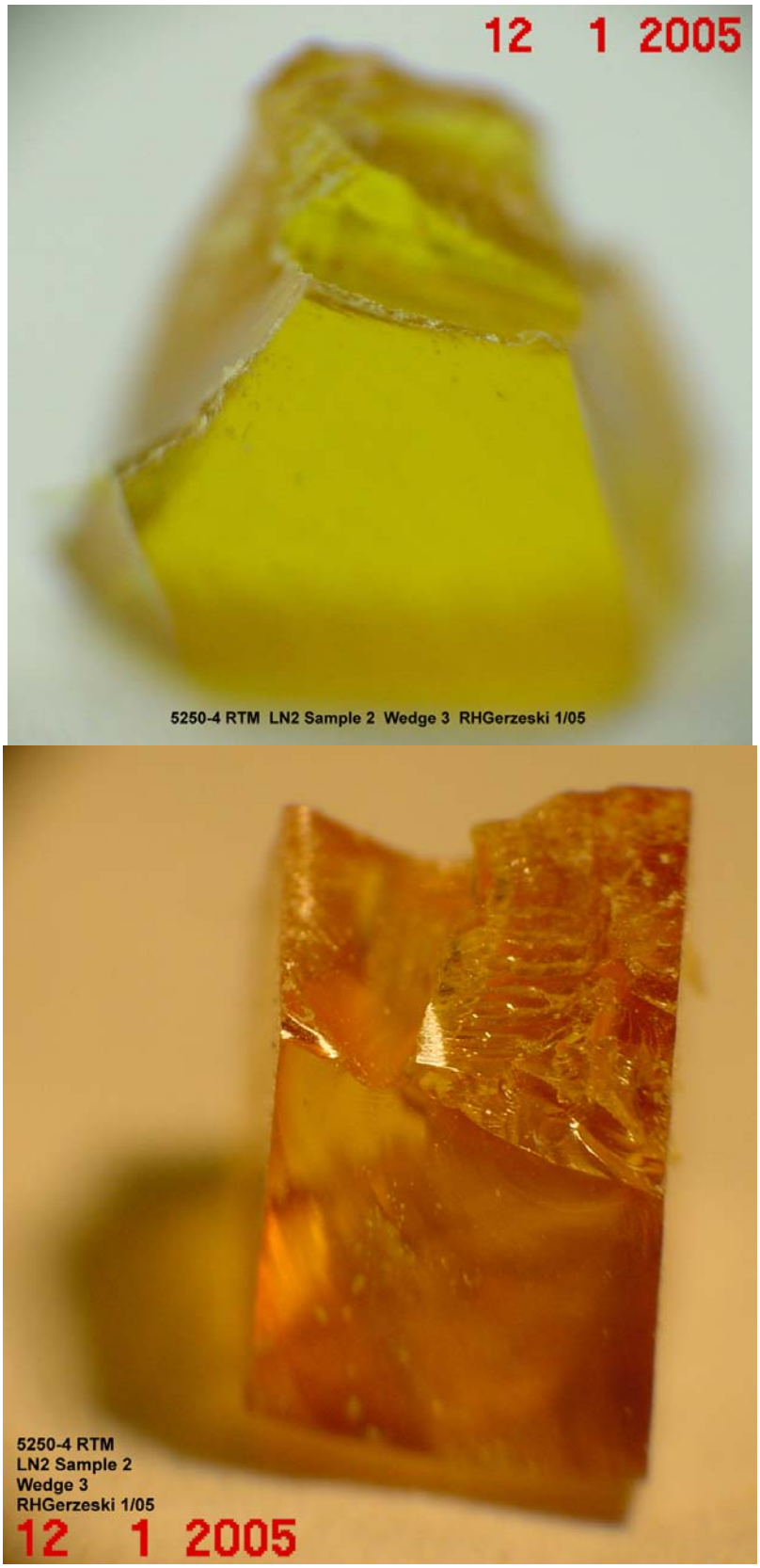
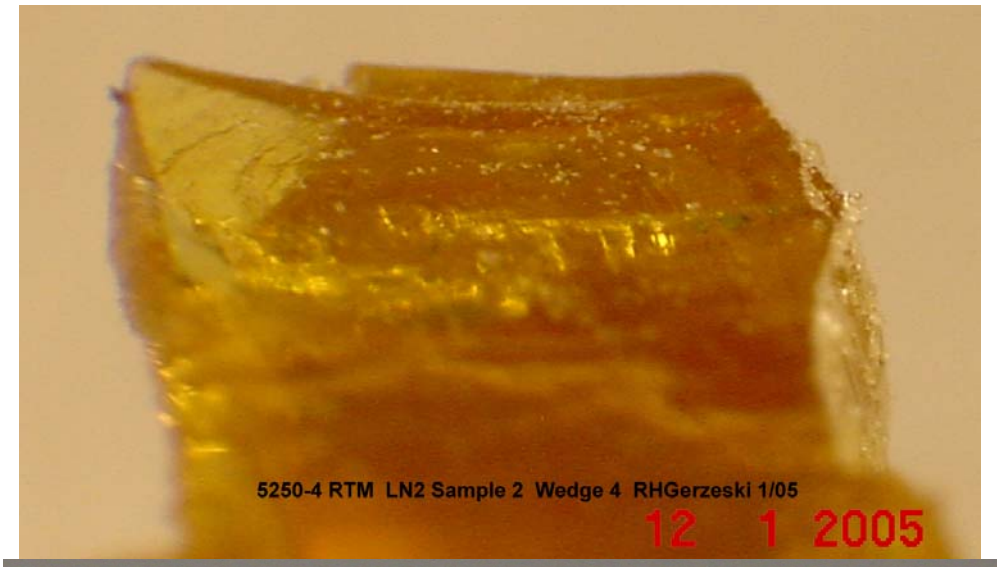


Figure 94-b-ii, External To The Indenting Impacter Fracture Surfaces: Ring Cracks: 5250-4 RTM D2512 Specimen: In LN2



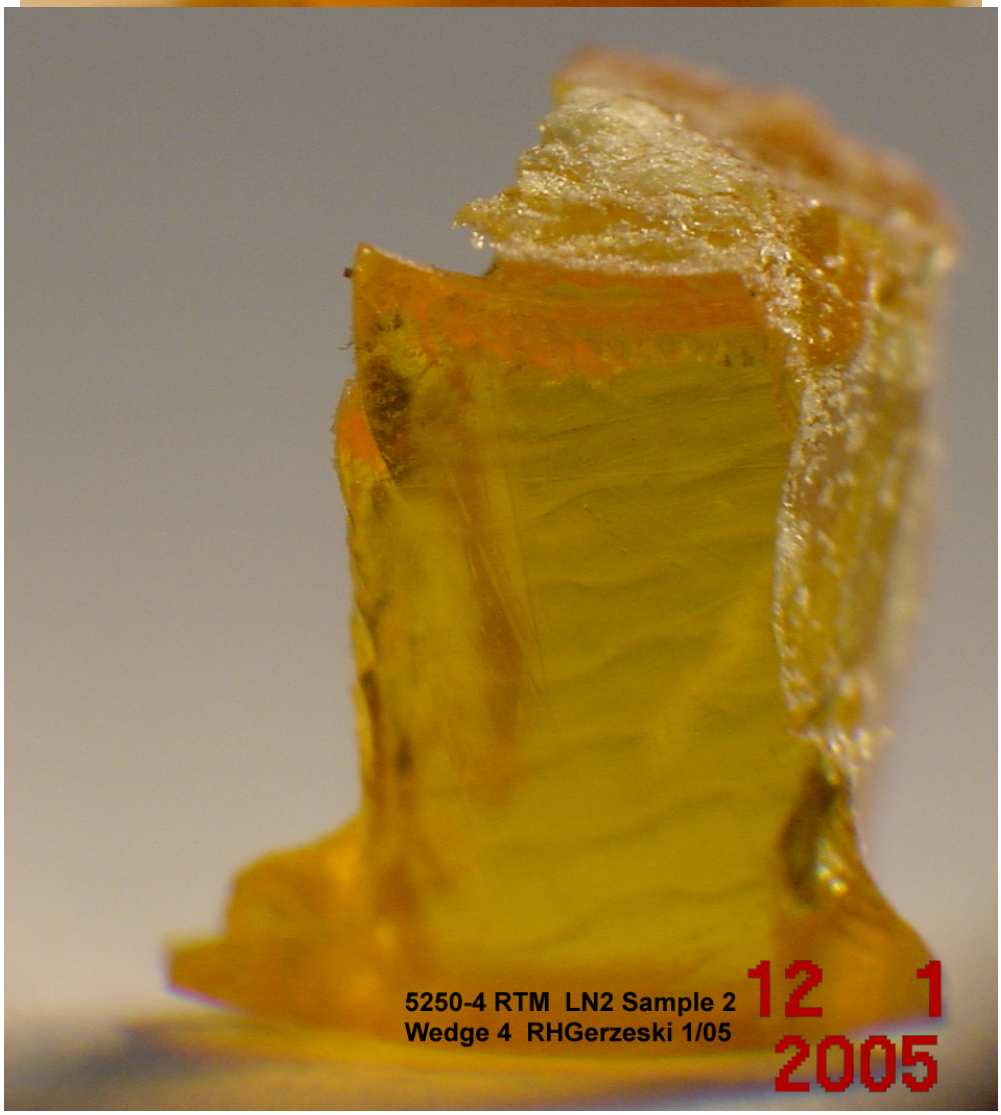


Figure 94-b-iii, External To The Indenting Impacter Fracture Surfaces: Ring Cracks: 5250-4 RTM D2512 Specimen: In LN2



Figure 95-a-i, External To The Indenting Impacter Fracture Surfaces: Ring Cracks: T650-35 / 5250-4 RTM D2512 Specimen: In LOX: Reaction Detected



Figure 95-a-ii, External To The Indenting Impacter Fracture Surfaces: Ring Cracks: T650-35 / 5250-4 RTM D2512 Specimen: In LOX: Reaction Detected



Figure 95-a-iii, External To The Indenting Impacter Fracture Surfaces: Ring Cracks: T650-35 / 5250-4 RTM D2512 Specimen: In LOX: Reaction Detected



Figure 95-b-i, External To The Indenting Impacter Fracture Surfaces: Ring Cracks: T650-35 / 5250-4 RTM D2512 Specimen: In LOX: No Reaction Detected



Figure 95-c-i, External To The Indenting Impacter Fracture Surfaces: Ring Cracks: T650-35 / 5250-4 RTM D2512 Specimen: In LN2



Figure 95-c-ii, External To The Indenting Impacter Fracture Surfaces: Ring Cracks: T650-35 / 5250-4 RTM D2512 Specimen: In LN2

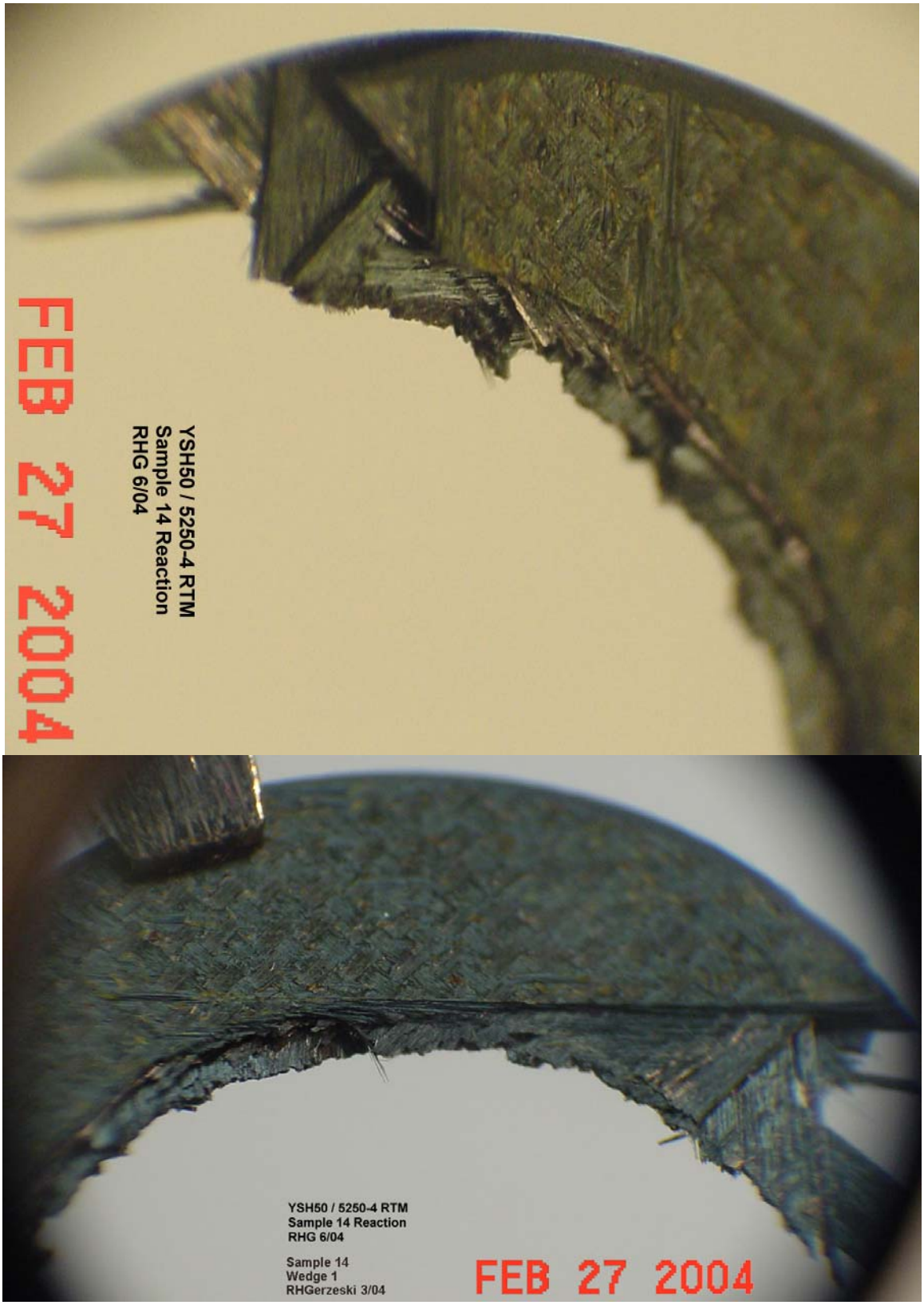


Figure 96-a, External To The Indenting Impacter Fracture Surfaces: Ring Cracks: YSH50 / 5250-4 RTM D2512 Specimen: In LOX: Reaction Detected



Figure 96-b-i, External To The Indenting Impacter Fracture Surfaces: Ring Cracks: YSH50 / 5250-4 RTM D2512 Specimen: In LOX: No Reaction Detected

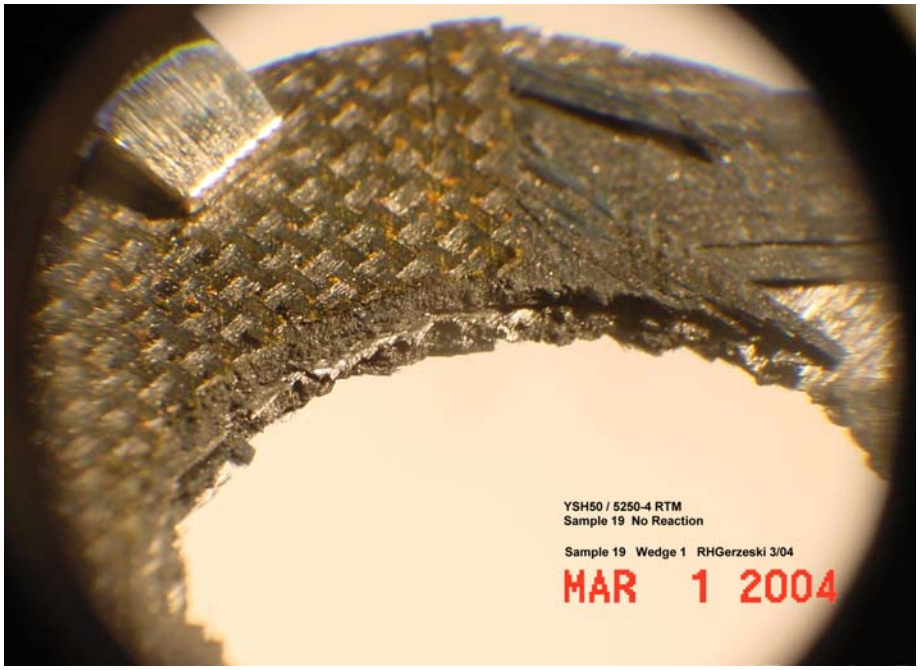


Figure 96-b-ii, External To The Indenting Impacter Fracture Surfaces: Ring Cracks: YSH50 / 5250-4 RTM D2512 Specimen: In LOX: No Reaction Detected



Figure 96-c-i, External To The Indenting Impacter Fracture Surfaces: Ring Cracks: YSH50 / 5250-4 RTM D2512 Specimen: In LN2



Figure 96-c-ii, External To The Indenting Impacter Fracture Surfaces: Ring Cracks: YSH50 / 5250-4 RTM D2512 Specimen: In LN2

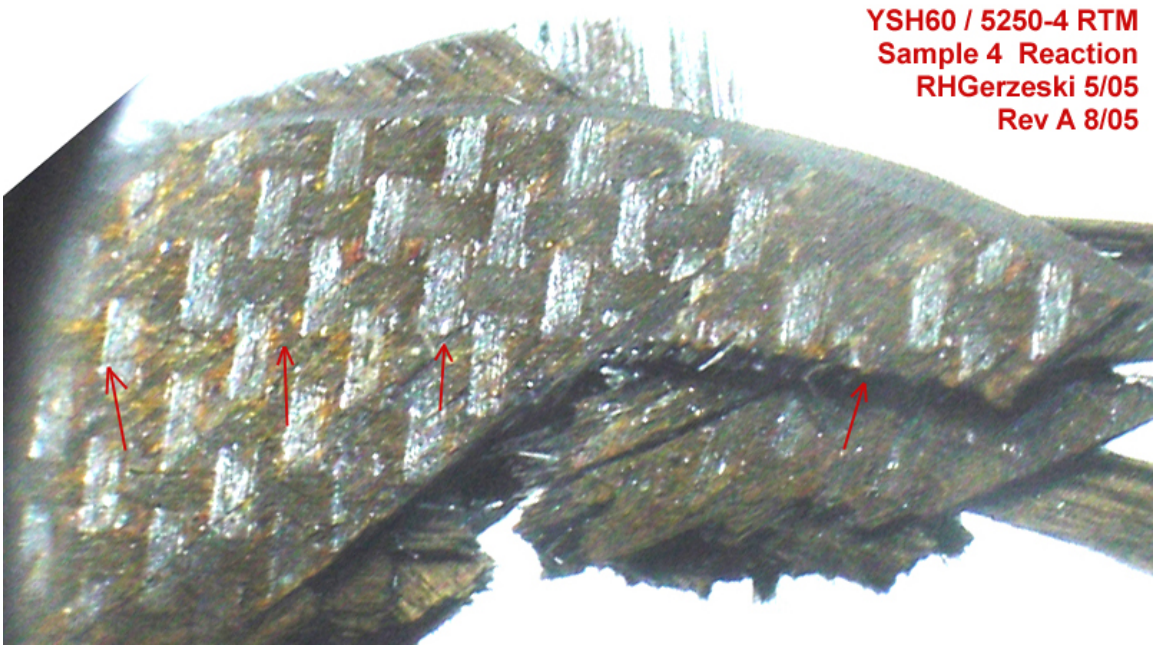


Figure 97-a-i, External To The Indenting Impacter Fracture Surfaces: Ring Cracks: YSH60 / 5250-4 RTM D2512 Specimen: In LOX: Reaction Detected

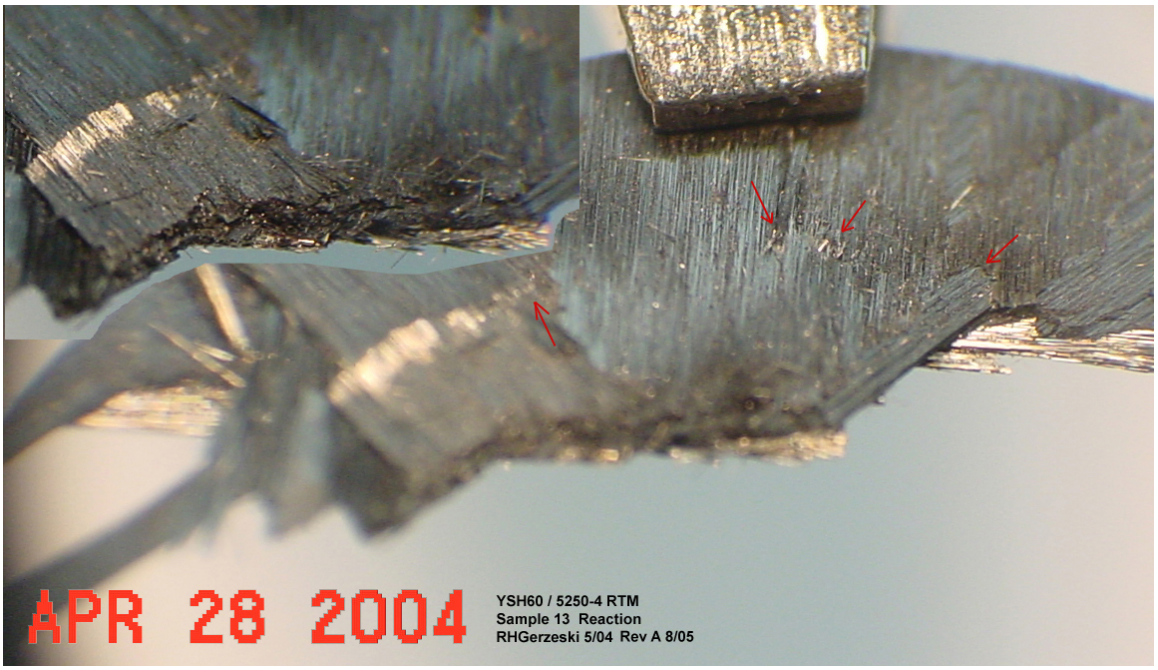


Figure 97-a-ii, External To The Indenting Impacter Fracture Surfaces: Ring Cracks: YSH60 / 5250-4 RTM D2512 Specimen: In LOX: Reaction Detected

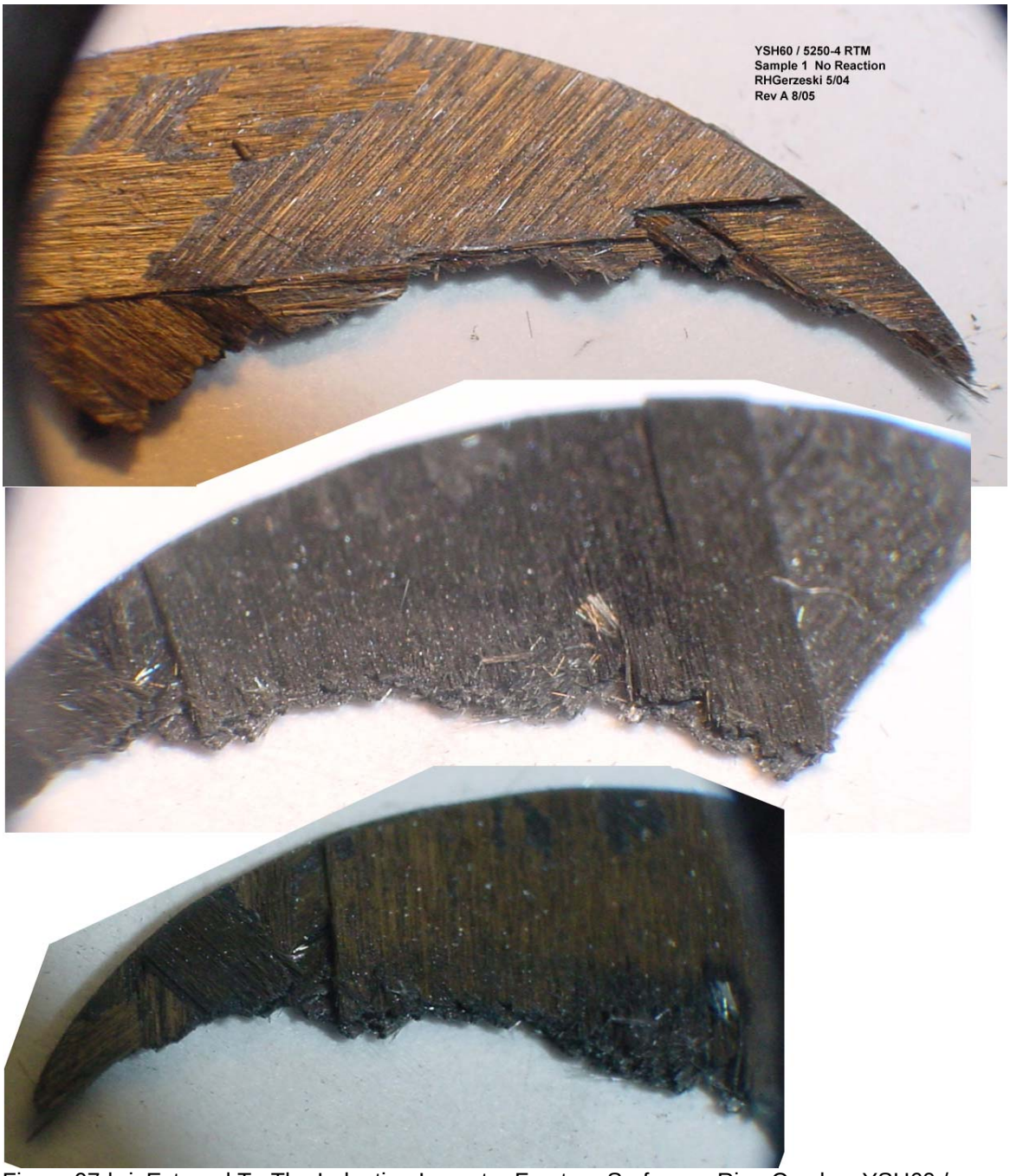


Figure 97-b-i, External To The Indenting Impacter Fracture Surfaces: Ring Cracks: YSH60 / 5250-4 RTM D2512 Specimen: In LOX: No Reaction Detected



Figure 97-b-ii, External To The Indenting Impacter Fracture Surfaces: Ring Cracks: YSH60 / 5250-4 RTM D2512 Specimen: In LOX: No Reaction Detected



Figure 97-c-i, External To The Indenting Impacter Fracture Surfaces: Ring Cracks: YSH60 / 5250-4 RTM D2512 Specimen: In LN2

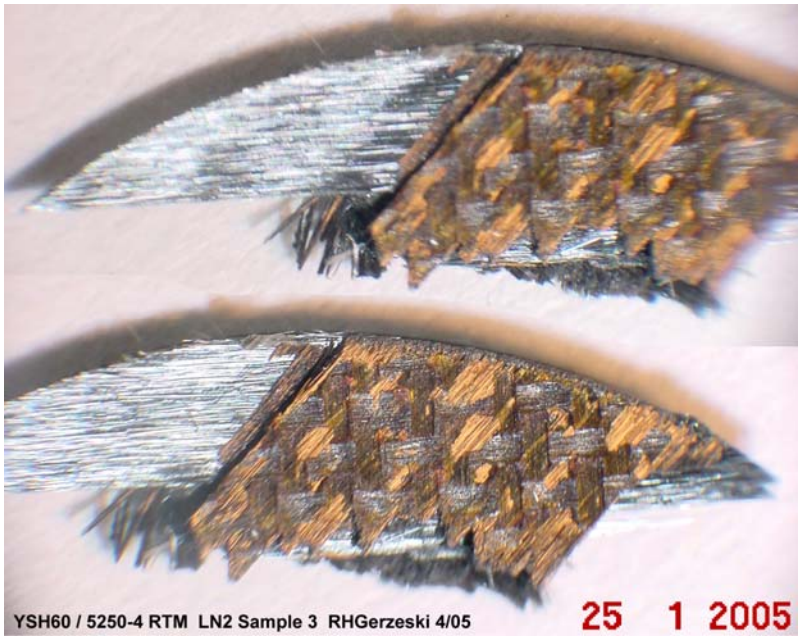


Figure 97-c-ii, External To The Indenting Impacter Fracture Surfaces: Ring Cracks: YSH60 / 5250-4 RTM D2512 Specimen: In LN2



Figure 98-a-i, External To The Indenting Impacter Fracture Surfaces: Transverse And In Plane Cracks: 5250-4 RTM D2512 Specimen: In LOX: Reaction Detected



Figure 98-a-ii, External To The Indenting Impacter Fracture Surfaces: Transverse And In Plane Cracks: 5250-4 RTM D2512 Specimen: In LOX: Reaction Detected



Figure 98-a-iii, External To The Indenting Impacter Fracture Surfaces: Transverse And In Plane Cracks: 5250-4 RTM D2512 Specimen: In LOX: Reaction Detected



Figure 98-a-iv, External To The Indenting Impacter Fracture Surfaces: Transverse And In Plane Cracks: 5250-4 RTM D2512 Specimen: In LOX: Reaction Detected

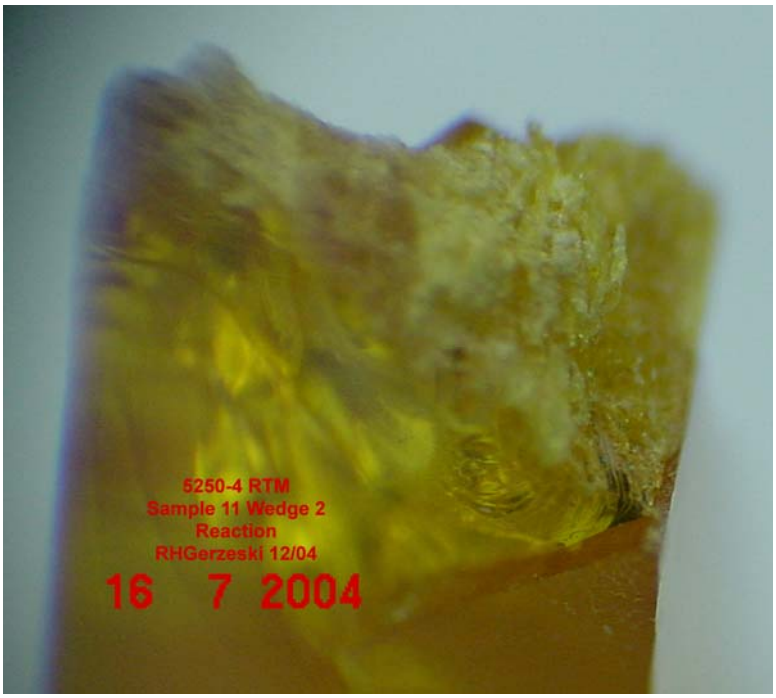


Figure 98-a-v, External To The Indenting Impacter Fracture Surfaces: Transverse And In Plane Cracks: 5250-4 RTM D2512 Specimen: In LOX: Reaction Detected

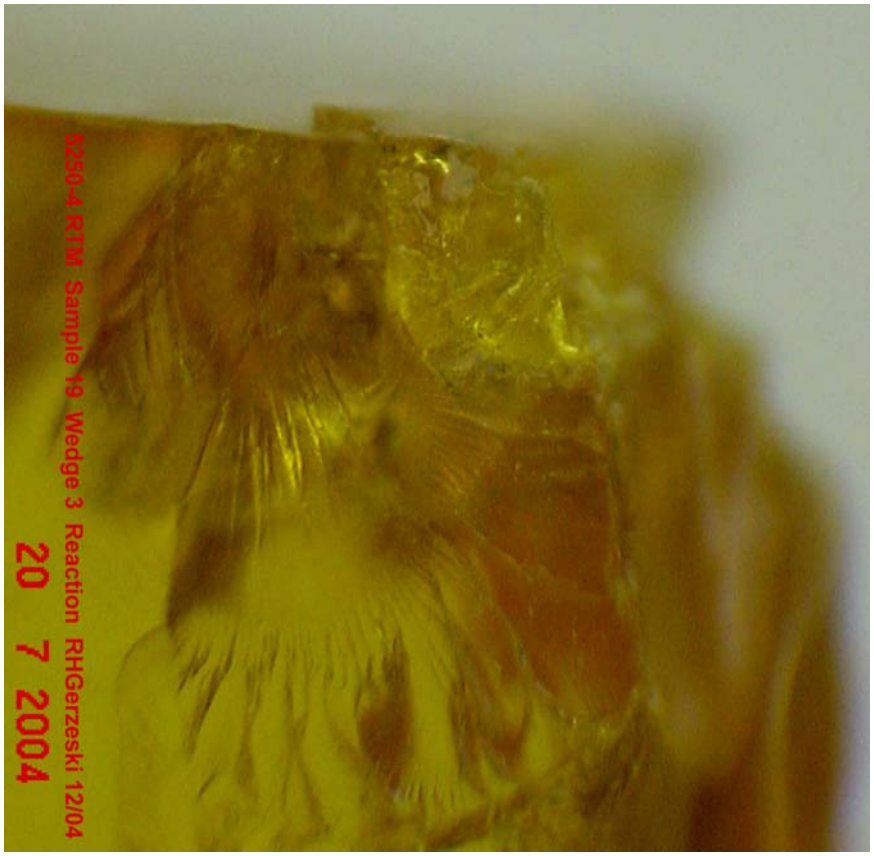


Figure 98-a-vi, External To The Indenting Impacter Fracture Surfaces: Transverse And In Plane Cracks: 5250-4 RTM D2512 Specimen: In LOX: Reaction Detected

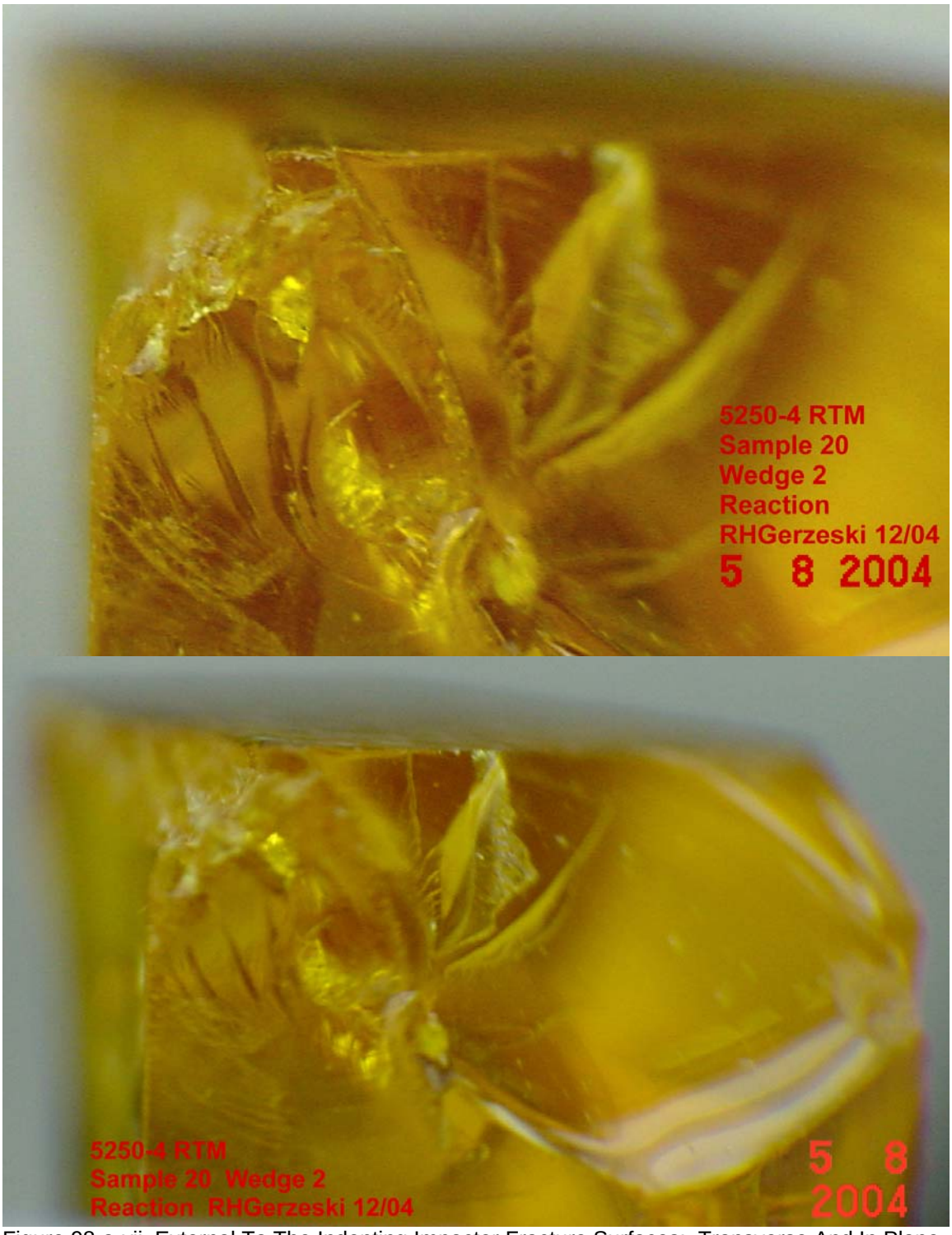


Figure 98-a-vii, External To The Indenting Impacter Fracture Surfaces: Transverse And In Plane Cracks: 5250-4 RTM D2512 Specimen: In LOX: Reaction Detected



Figure 98-b-i, External To The Indenting Impacter Fracture Surfaces: Transverse And In Plane Cracks: 5250-4 RTM D2512 Specimen: In LN2



Figure 98-b-ii, External To The Indenting Impacter Fracture Surfaces: Transverse And In Plane Cracks: 5250-4 RTM D2512 Specimen: In LN2

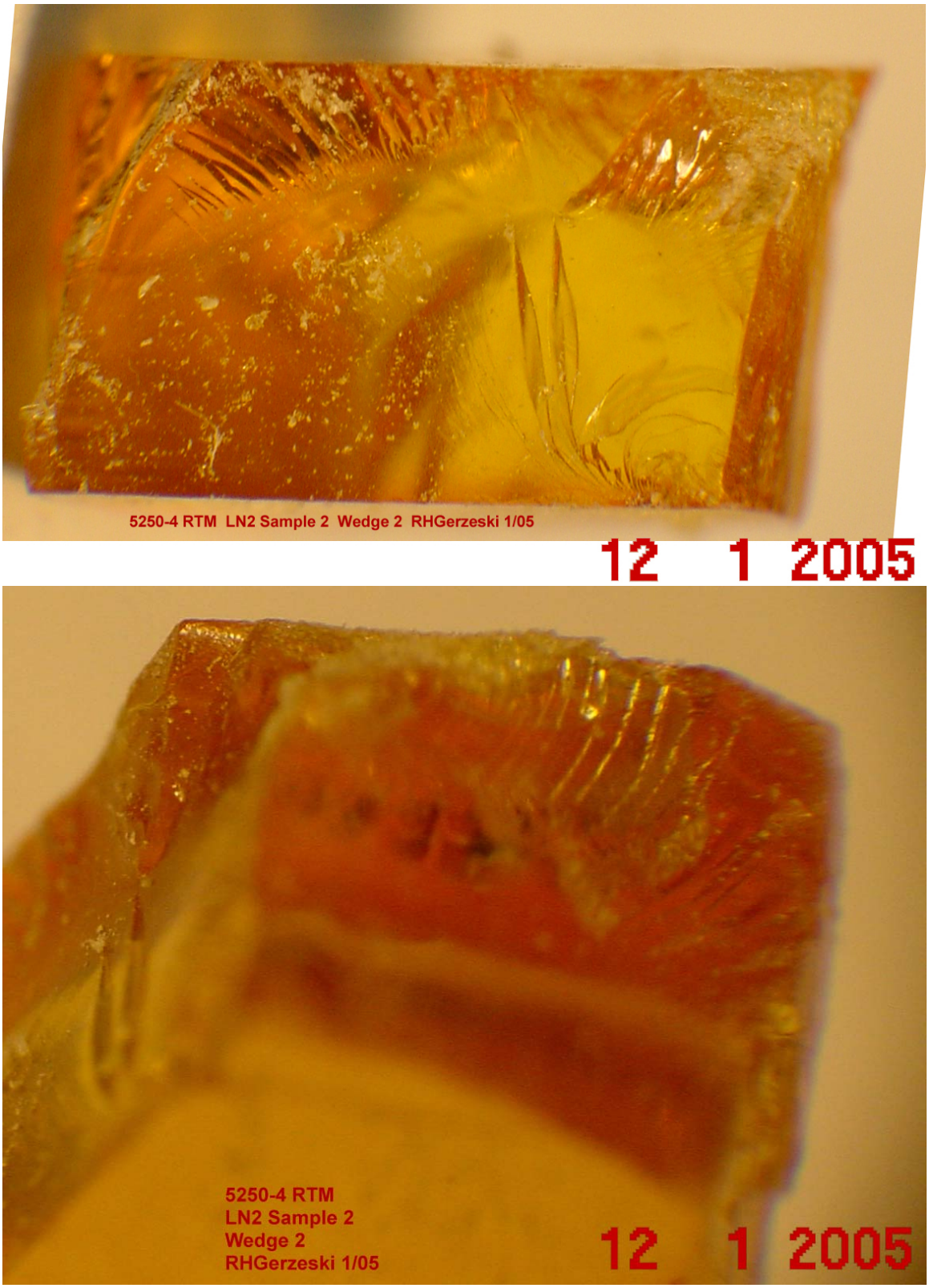
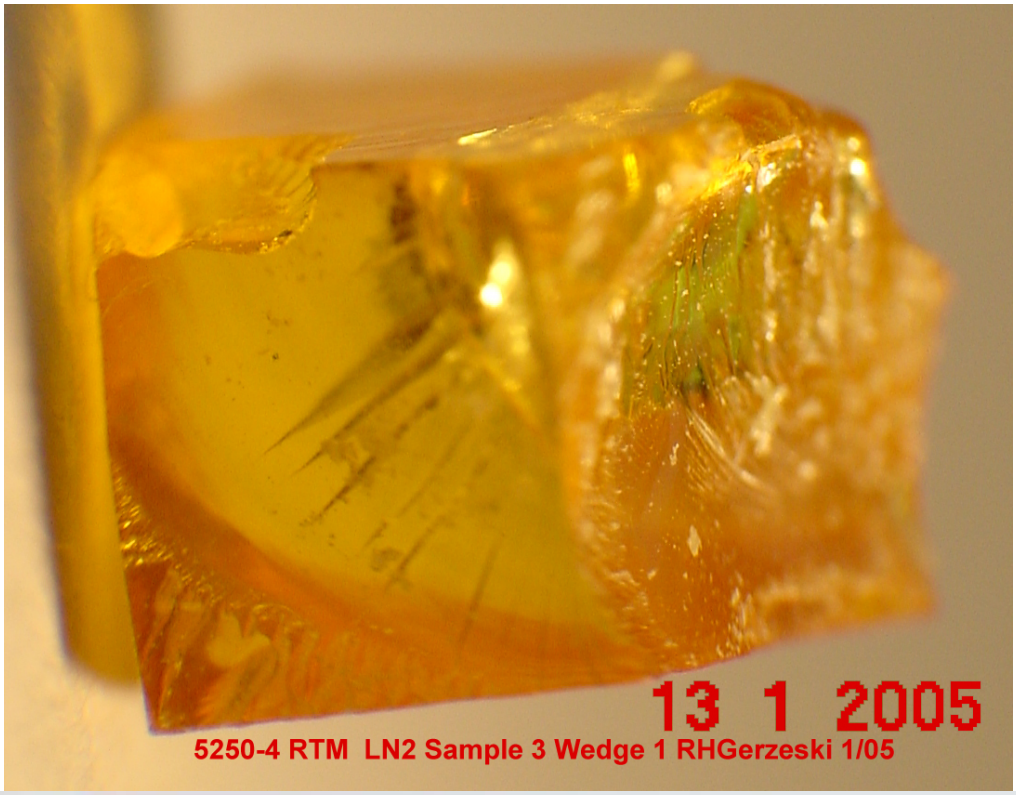


Figure 98-b-iii, External To The Indenting Impacter Fracture Surfaces: Transverse And In Plane Cracks: 5250-4 RTM D2512 Specimen: In LN2



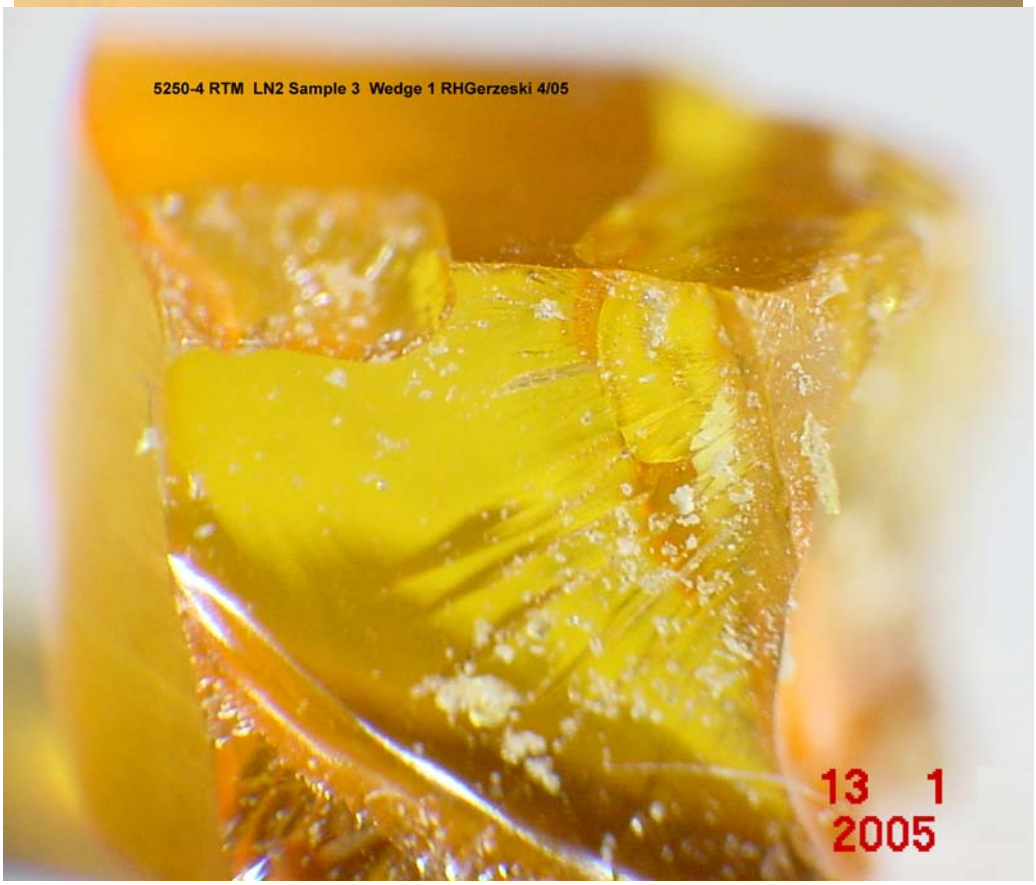


Figure 98-b-iv, External To The Indenting Impacter Fracture Surfaces: Transverse And In Plane Cracks: 5250-4 RTM D2512 Specimen: In LN2



Figure 99-a-i, External To The Indenting Impacter Fracture Surfaces: Transverse And In Plane Cracks: T650-35 / 5250-4 RTM D2512 Specimen: In LOX: Reaction Detected



Figure 99-a-ii, External To The Indenting Impacter Fracture Surfaces: Transverse And In Plane Cracks: T650-35 / 5250-4 RTM D2512 Specimen: In LOX: Reaction Detected



Figure 99-a-iii, External To The Indenting Impacter Fracture Surfaces: Transverse And In Plane Cracks: T650-35 / 5250-4 RTM D2512 Specimen: In LOX: Reaction Detected



Figure 99-a-iv, External To The Indenting Impacter Fracture Surfaces: Transverse And In Plane Cracks: T650-35 / 5250-4 RTM D2512 Specimen: In LOX: Reaction Detected



Figure 99-a-v, External To The Indenting Impacter Fracture Surfaces: Transverse And In Plane Cracks: T650-35 / 5250-4 RTM D2512 Specimen: In LOX: Reaction Detected



Figure 99-a-vi, External To The Indenting Impacter Fracture Surfaces: Transverse And In Plane Cracks: T650-35 / 5250-4 RTM D2512 Specimen: In LOX: Reaction Detected



Figure 99-b-i, External To The Indenting Impacter Fracture Surfaces: Transverse And In Plane Cracks: T650-35 / 5250-4 RTM D2512 Specimen: In LOX: No Reaction Detected



Figure 99-b-ii, External To The Indenting Impacter Fracture Surfaces: Transverse And In Plane Cracks: T650-35 / 5250-4 RTM D2512 Specimen: In LOX: No Reaction Detected



Figure 99-c-i, External To The Indenting Impacter Fracture Surfaces: Transverse And In Plane Cracks: T650-35 / 5250-4 RTM D2512 Specimen: In LN2



Figure 99-c-ii, External To The Indenting Impacter Fracture Surfaces: Transverse And In Plane Cracks: T650-35 / 5250-4 RTM D2512 Specimen: In LN2

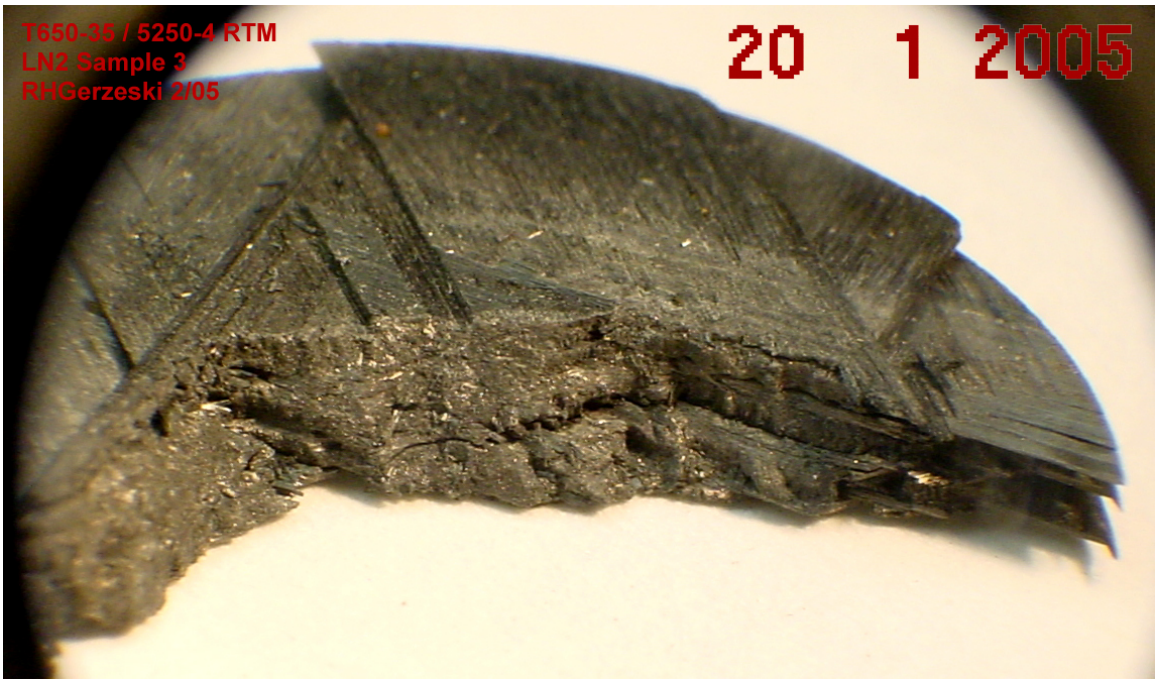


Figure 99-c-iii, External To The Indenting Impacter Fracture Surfaces: Transverse And In Plane Cracks: T650-35 / 5250-4 RTM D2512 Specimen: In LN2

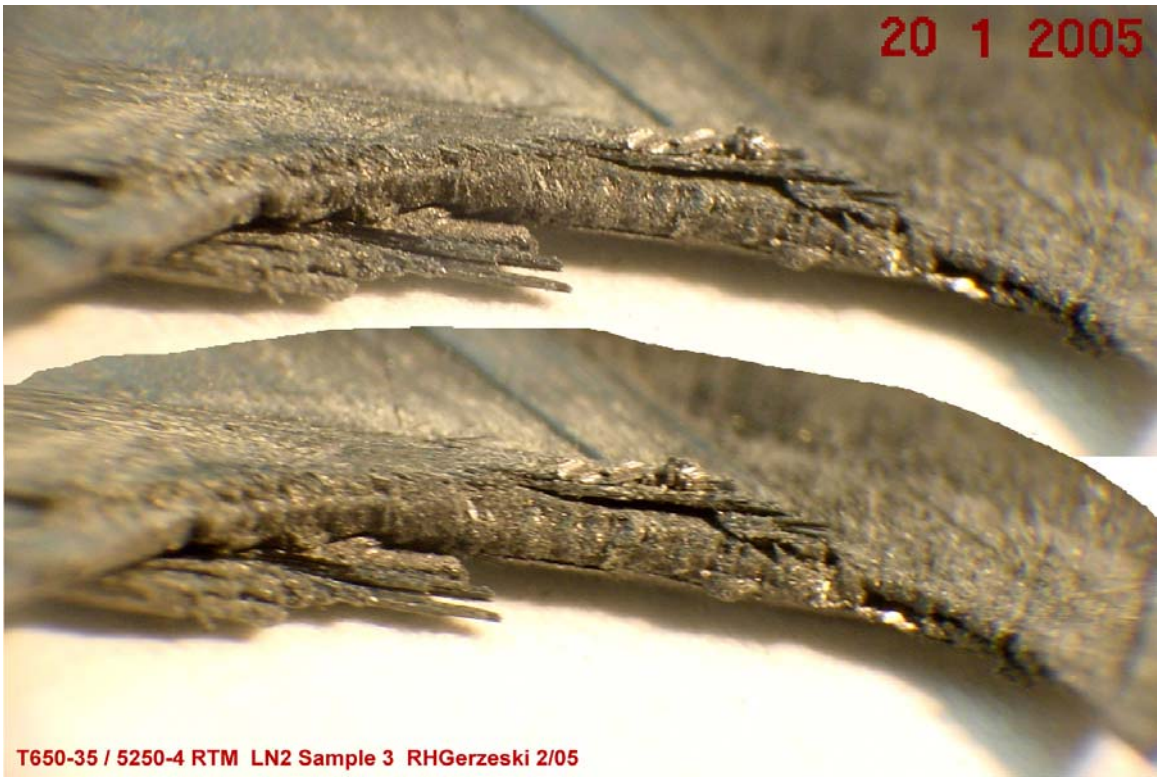


Figure 99-c-iv, External To The Indenting Impacter Fracture Surfaces: Transverse And In Plane Cracks: T650-35 / 5250-4 RTM D2512 Specimen: In LN2

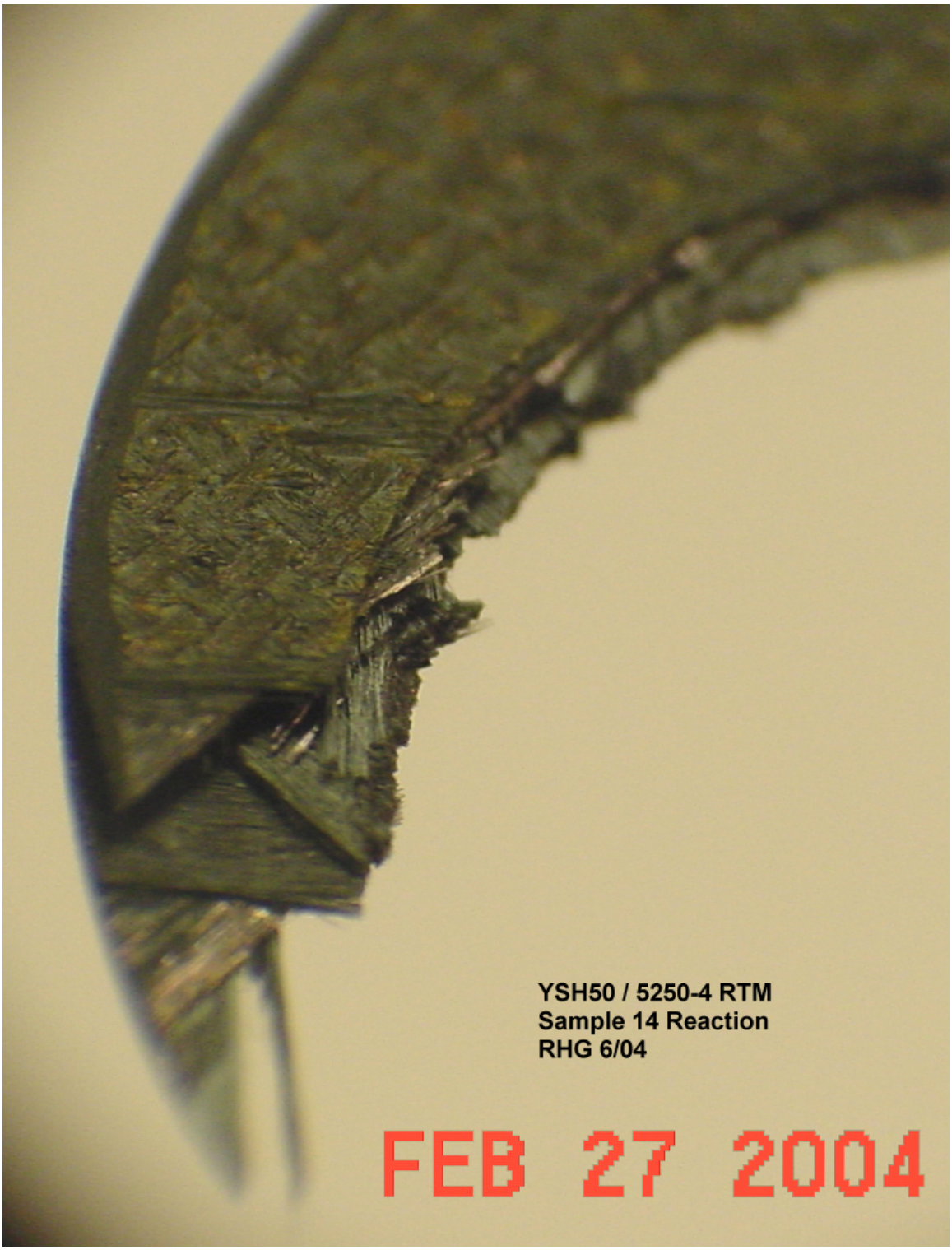


Figure 100-a-i, External To The Indenting Impacter Fracture Surfaces: Transverse And In Plane Cracks: YSH50 / 5250-4 RTM D2512 Specimen: In LOX: Reaction Detected

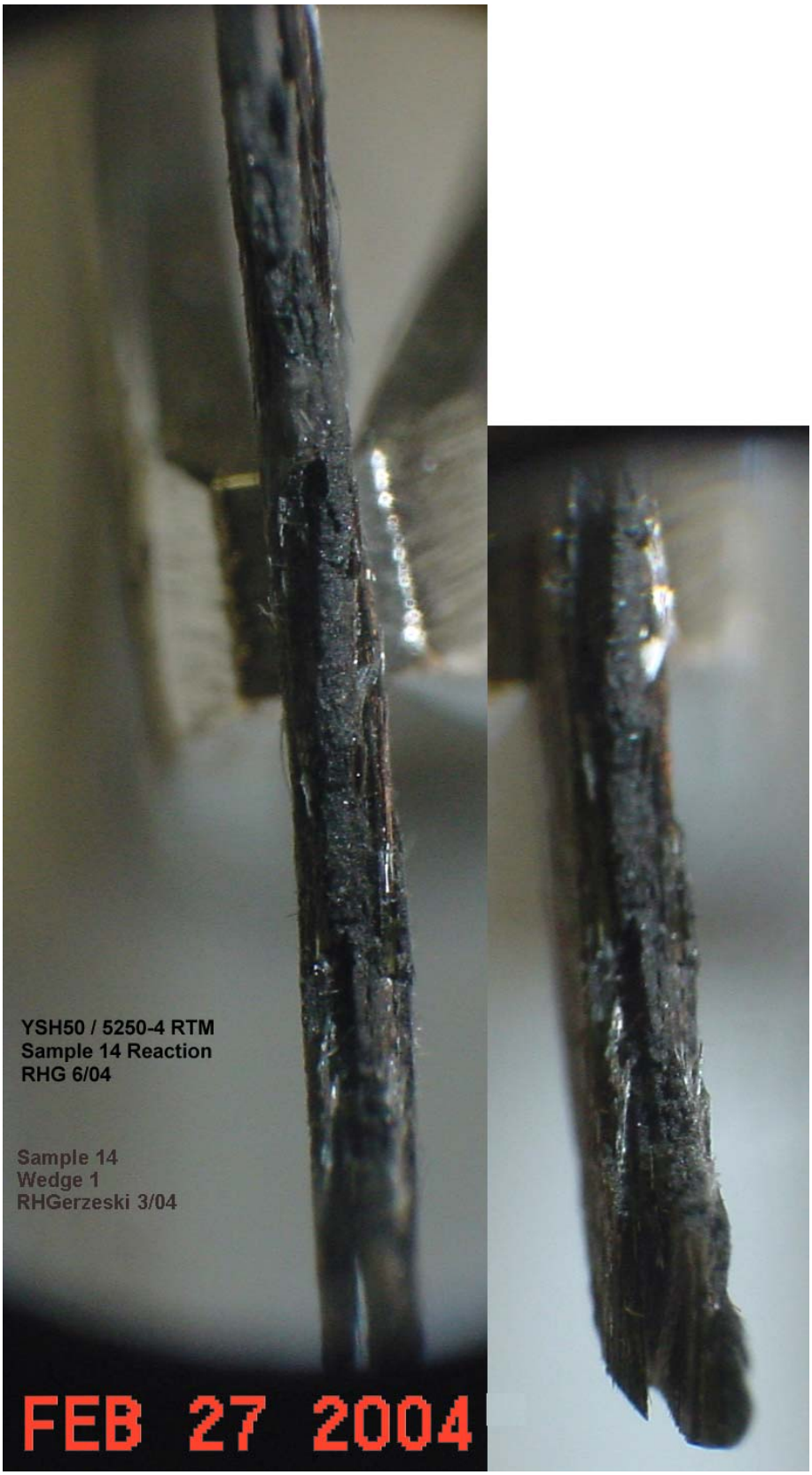


Figure 100-a-ii, External To The Indenting Impacter Fracture Surfaces: Transverse And In Plane Cracks: YSH50 / 5250-4 RTM D2512 Specimen: In LOX: Reaction Detected



Figure 100-b-i, External To The Indenting Impacter Fracture Surfaces: Transverse And In Plane Cracks: YSH50 / 5250-4 RTM D2512 Specimen: In LOX: No Reaction Detected



Figure 100-b-ii, External To The Indenting Impacter Fracture Surfaces: Transverse And In Plane Cracks: YSH50 / 5250-4 RTM D2512 Specimen: In LOX: No Reaction Detected



Figure 100-b-iii, External To The Indenting Impacter Fracture Surfaces: Transverse And In Plane Cracks: YSH50 / 5250-4 RTM D2512 Specimen: In LOX: No Reaction Detected

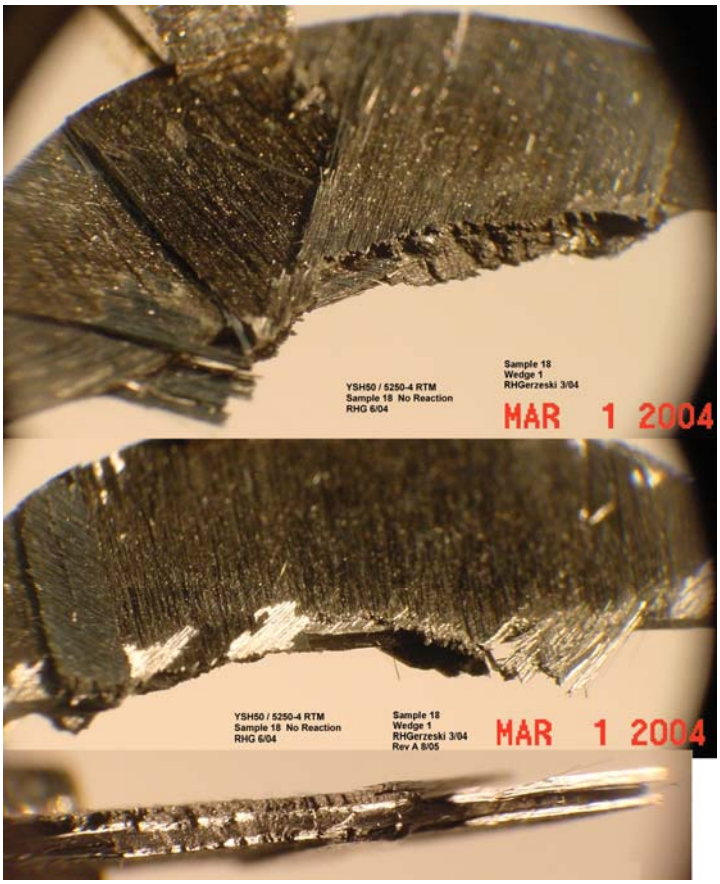


Figure 100-b-iv, External To The Indenting Impacter Fracture Surfaces: Transverse And In Plane Cracks: YSH50 / 5250-4 RTM D2512 Specimen: In LOX: No Reaction Detected

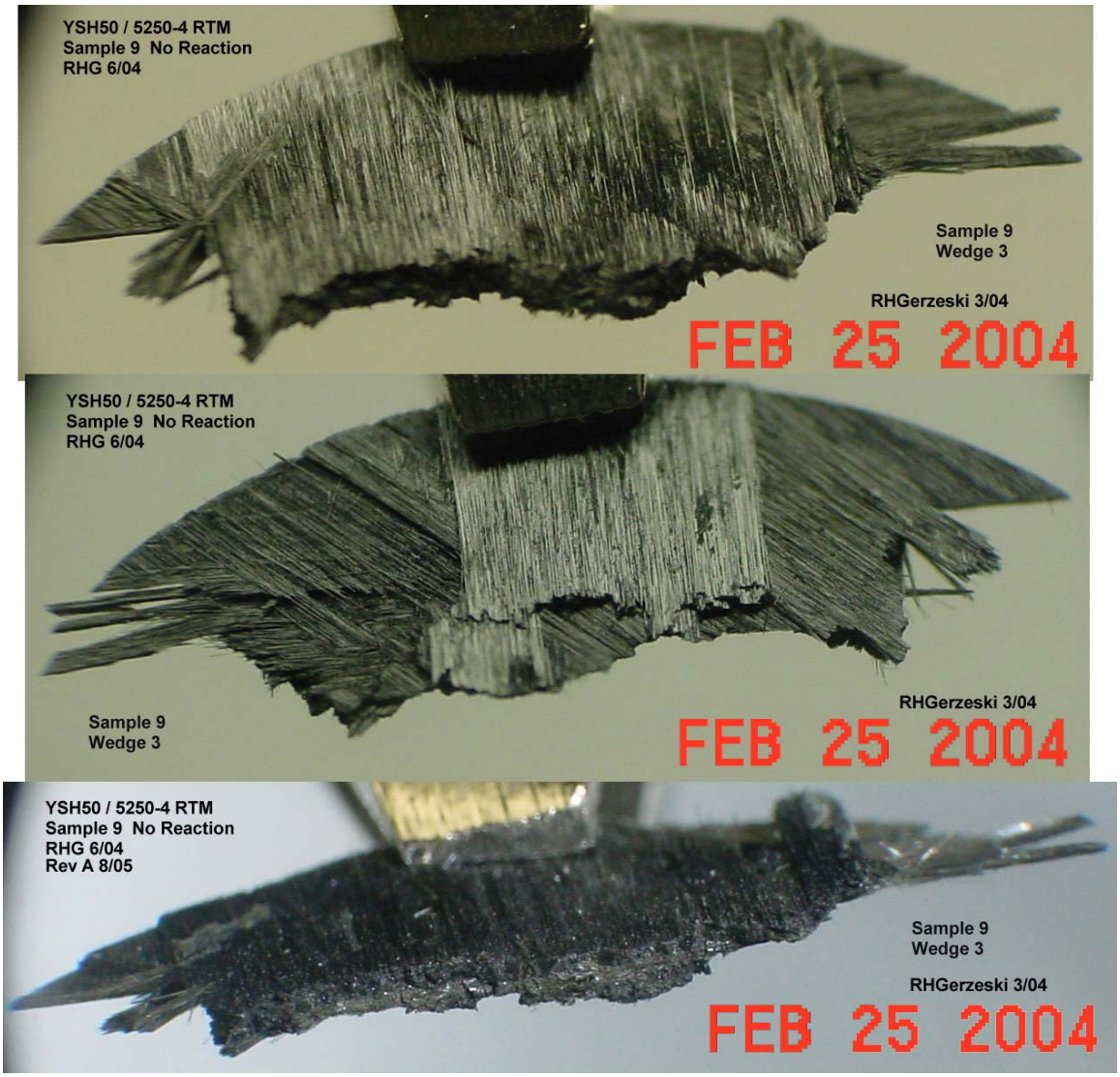


Figure 100-b-v, External To The Indenting Impacter Fracture Surfaces: Transverse And In Plane Cracks: YSH50 / 5250-4 RTM D2512 Specimen: In LOX: No Reaction Detected

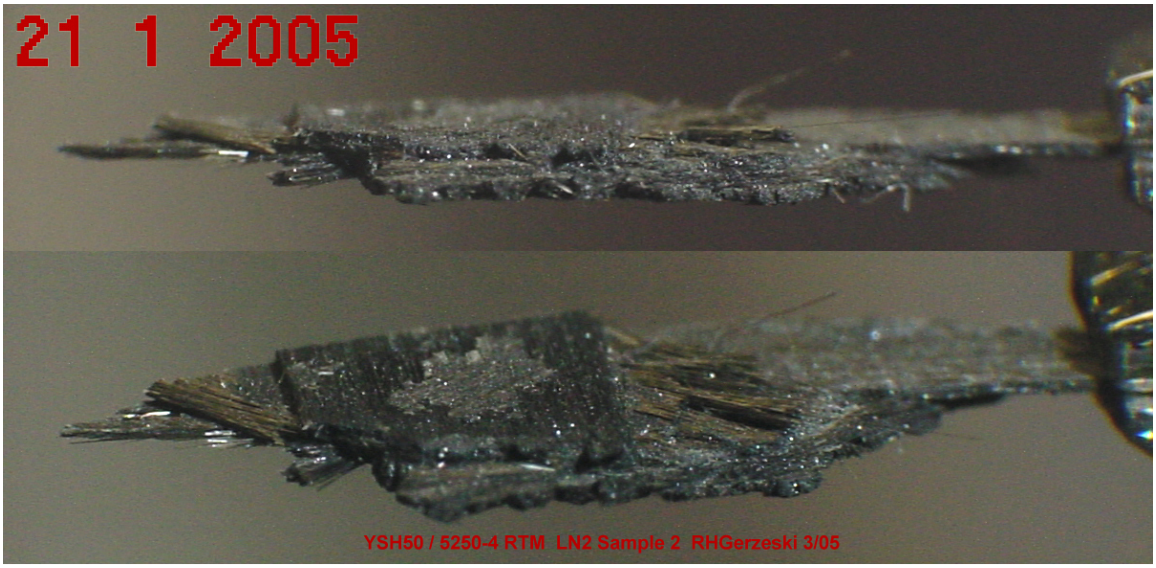


Figure 100-c-i, External To The Indenting Impacter Fracture Surfaces: Transverse And In Plane Cracks: YSH50 / 5250-4 RTM D2512 Specimen: In LN2

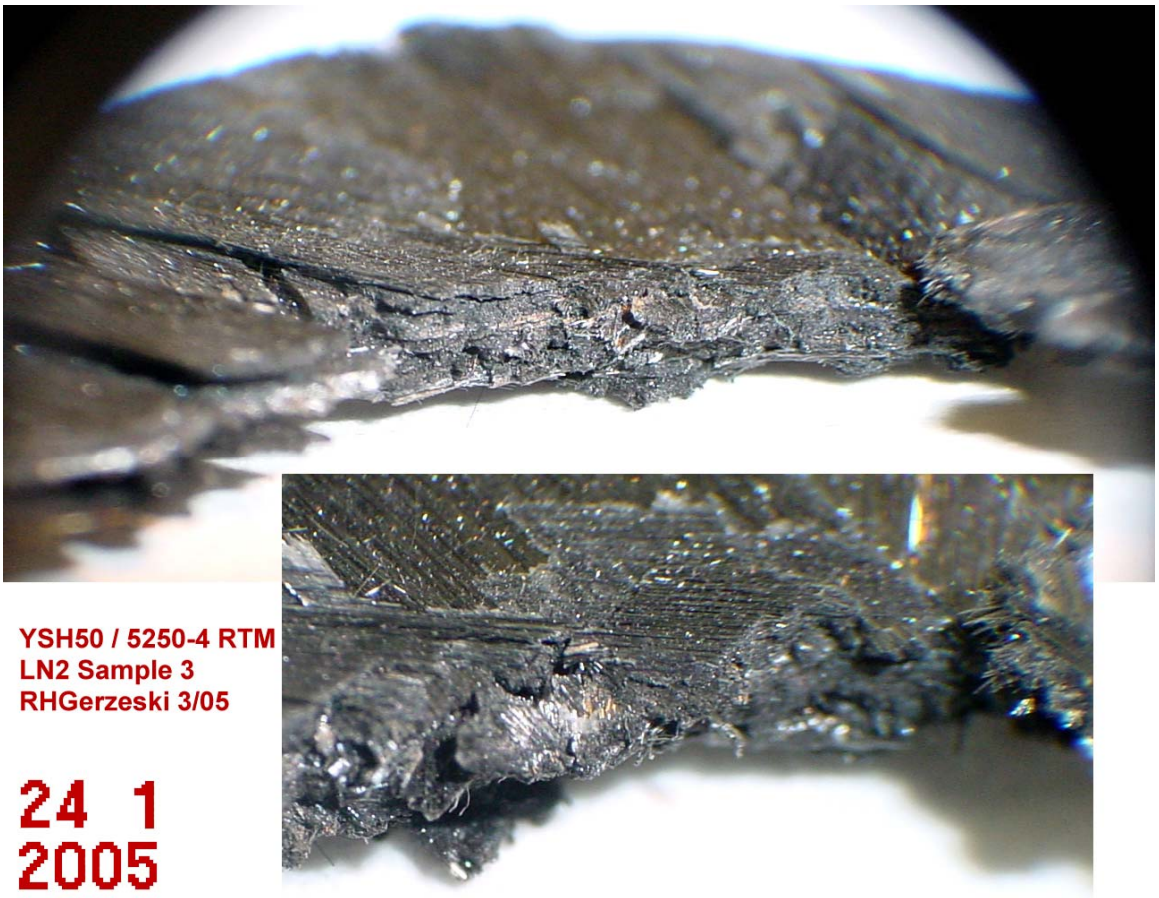


Figure 100-c-ii, External To The Indenting Impacter Fracture Surfaces: Transverse And In Plane Cracks: YSH50 / 5250-4 RTM D2512 Specimen: In LN2



Figure 100-c-iii, External To The Indenting Impacter Fracture Surfaces: Transverse And In Plane Cracks: YSH50 / 5250-4 RTM D2512 Specimen: In LN2

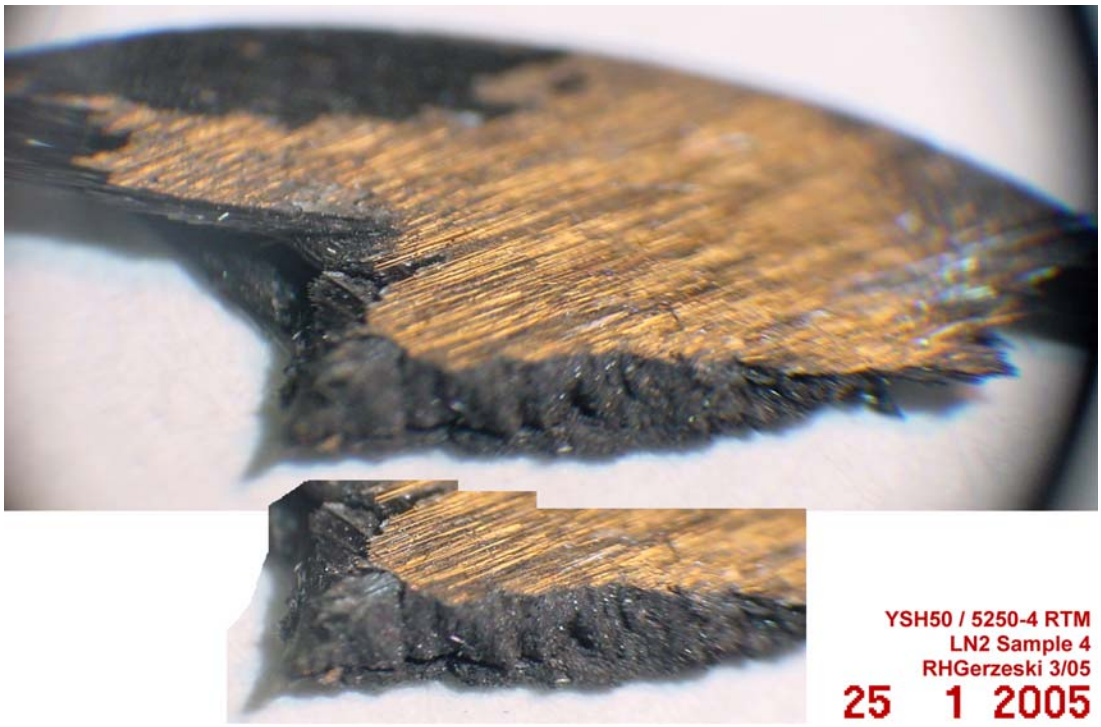


Figure 100-c-iv, External To The Indenting Impacter Fracture Surfaces: Transverse And In Plane Cracks: YSH50 / 5250-4 RTM D2512 Specimen: In LN2



Figure 101-a-i, External To The Indenting Impacter Fracture Surfaces: Transverse And In Plane Cracks: YSH60 / 5250-4 RTM D2512 Specimen: In LOX: Reaction Detected

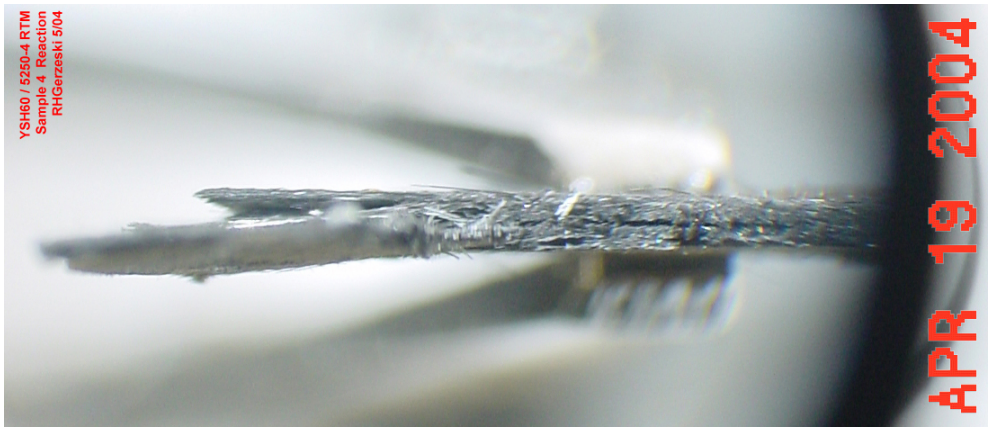


Figure 101-a-ii, External To The Indenting Impacter Fracture Surfaces: Transverse And In Plane Cracks: YSH60 / 5250-4 RTM D2512 Specimen: In LOX: Reaction Detected

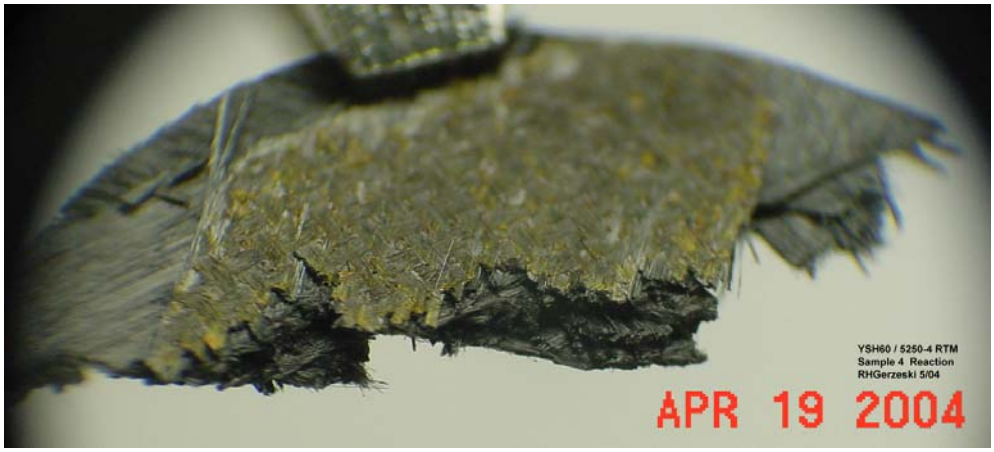


Figure 101-a-iii, External To The Indenting Impacter Fracture Surfaces: Transverse And In Plane Cracks: YSH60 / 5250-4 RTM D2512 Specimen: In LOX: Reaction Detected



Figure 101-a-iv, External To The Indenting Impacter Fracture Surfaces: Transverse And In Plane Cracks: YSH60 / 5250-4 RTM D2512 Specimen: In LOX: Reaction Detected

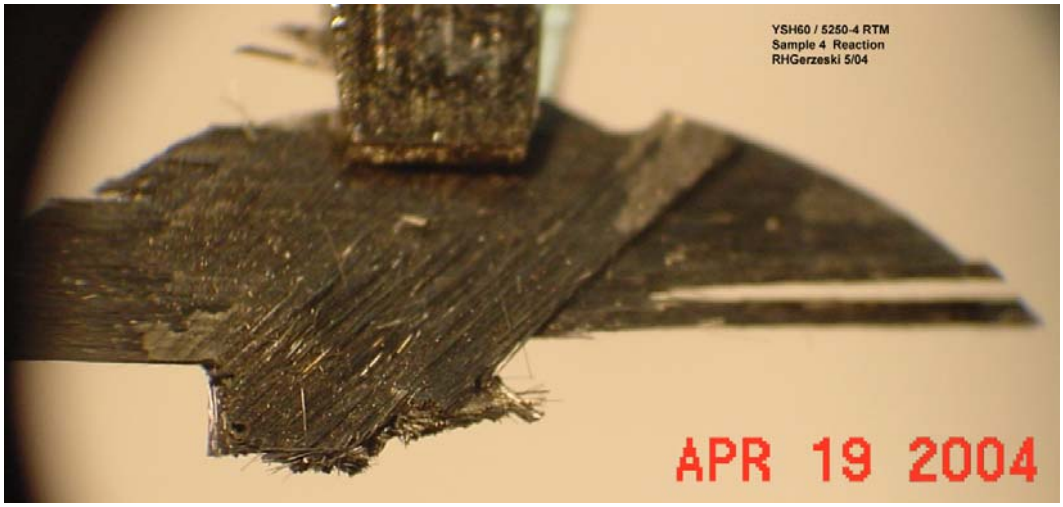


Figure 101-a-v, External To The Indenting Impacter Fracture Surfaces: Transverse And In Plane Cracks: YSH60 / 5250-4 RTM D2512 Specimen: In LOX: Reaction Detected

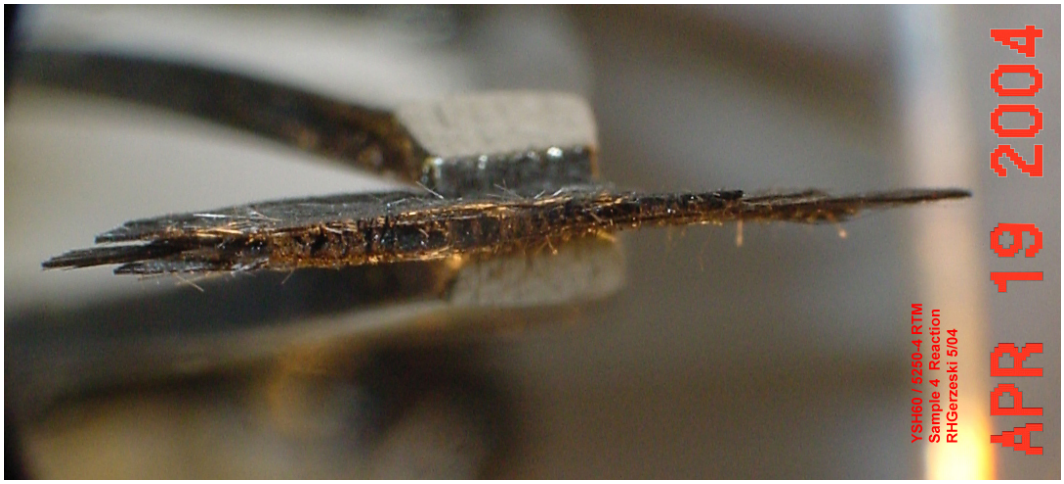


Figure 101-a-vi, External To The Indenting Impacter Fracture Surfaces: Transverse And In Plane Cracks: YSH60 / 5250-4 RTM D2512 Specimen: In LOX: Reaction Detected

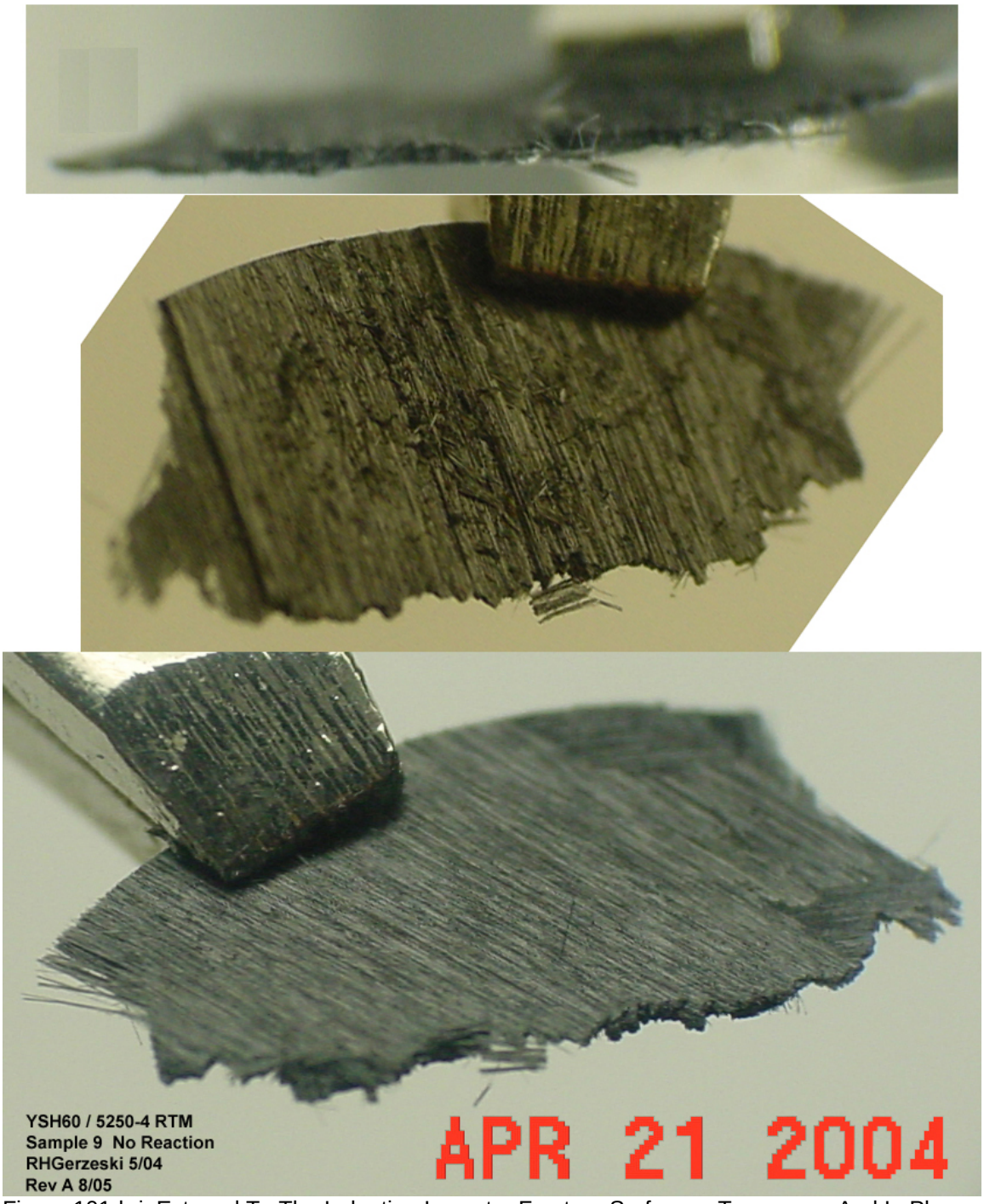


Figure 101-b-i, External To The Indenting Impacter Fracture Surfaces: Transverse And In Plane Cracks: YSH60 / 5250-4 RTM D2512 Specimen: In LOX: No Reaction Detected



Figure 101-b-ii, External To The Indenting Impacter Fracture Surfaces: Transverse And In Plane Cracks: YSH60 / 5250-4 RTM D2512 Specimen: In LOX: No Reaction Detected

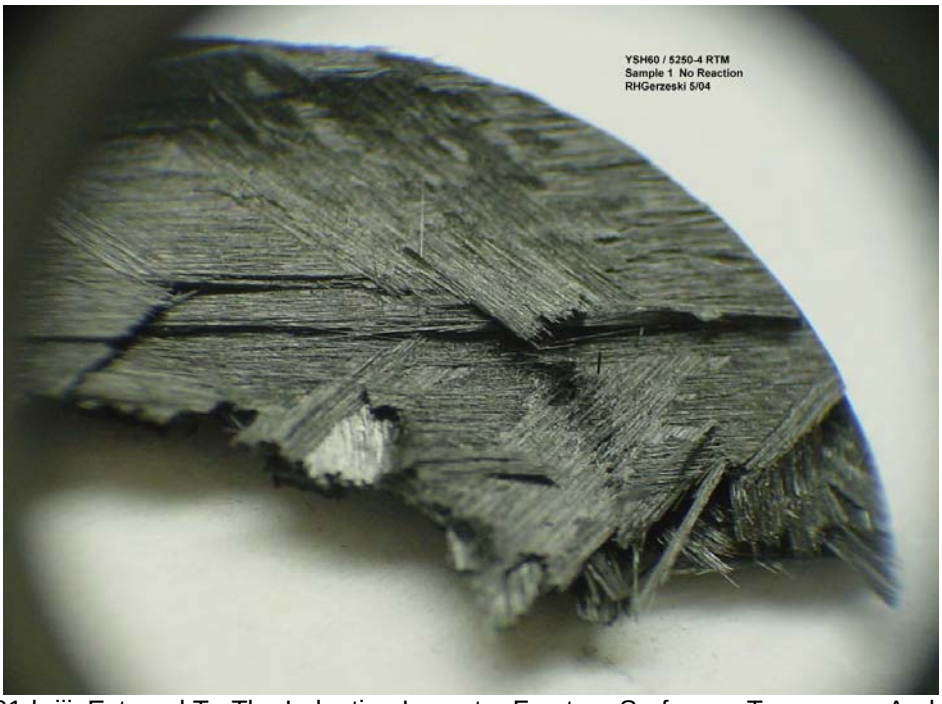


Figure 101-b-iii, External To The Indenting Impacter Fracture Surfaces: Transverse And In Plane Cracks: YSH60 / 5250-4 RTM D2512 Specimen: In LOX: No Reaction Detected



Figure 101-b-iv, External To The Indenting Impacter Fracture Surfaces: Transverse And In Plane Cracks: YSH60 / 5250-4 RTM D2512 Specimen: In LOX: No Reaction Detected



Figure 101-c-i, External To The Indenting Impacter Fracture Surfaces: Transverse And In Plane Cracks: YSH60 / 5250-4 RTM D2512 Specimen: In LN2

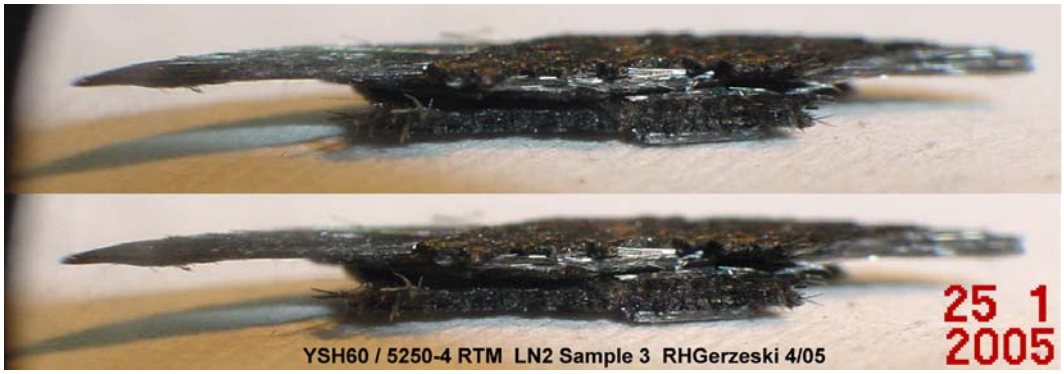


Figure 101-c-ii, External To The Indenting Impacter Fracture Surfaces: Transverse And In Plane Cracks: YSH60 / 5250-4 RTM D2512 Specimen: In LN2



Figure 101-c-iii, External To The Indenting Impacter Fracture Surfaces: Transverse And In Plane Cracks: YSH60 / 5250-4 RTM D2512 Specimen: In LN2

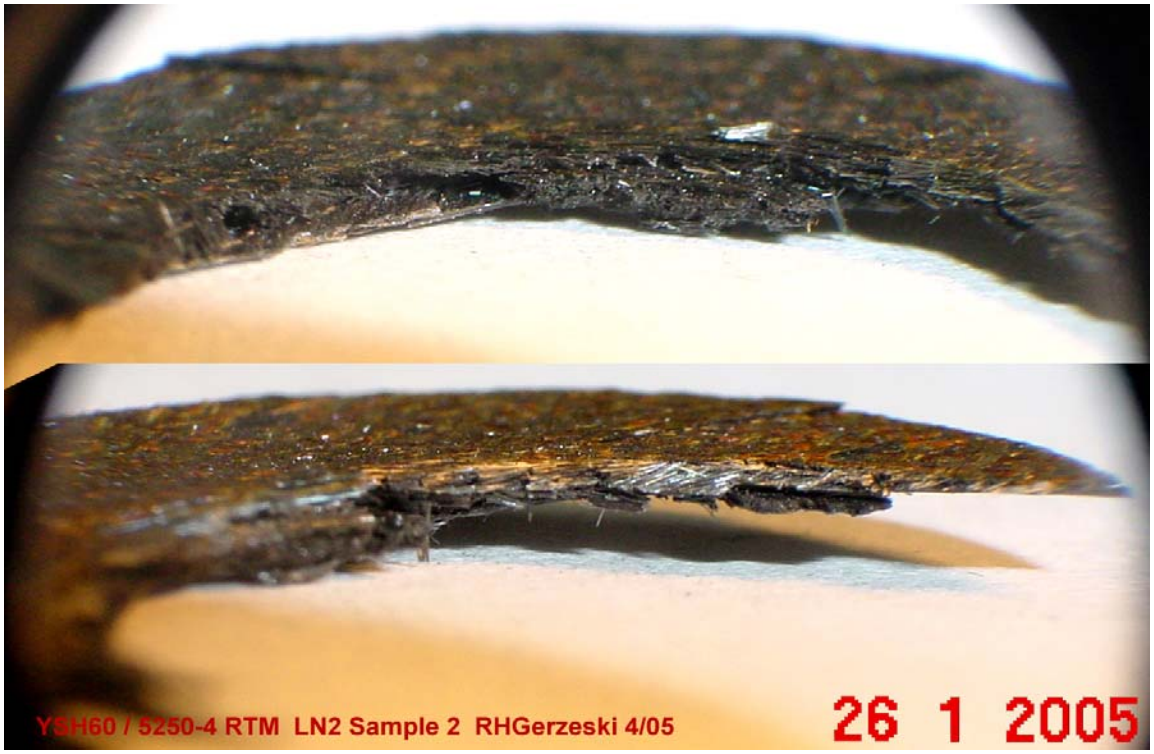


Figure 101-c-iv, External To The Indenting Impacter Fracture Surfaces: Transverse And In Plane Cracks: YSH60 / 5250-4 RTM D2512 Specimen: In LN2



Figure 102-a-i, External To The Indenting Impacter Fracture Surfaces: Knobs: 5250-4 RTM D2512 Specimen: In LOX: Reaction Detected



Figure 102-a-ii, External To The Indenting Impacter Fracture Surfaces: Knobs: 5250-4 RTM D2512 Specimen: In LOX: Reaction Detected



Figure 102-a-iii, External To The Indenting Impacter Fracture Surfaces: Knobs: 5250-4 RTM D2512 Specimen: In LOX: Reaction Detected

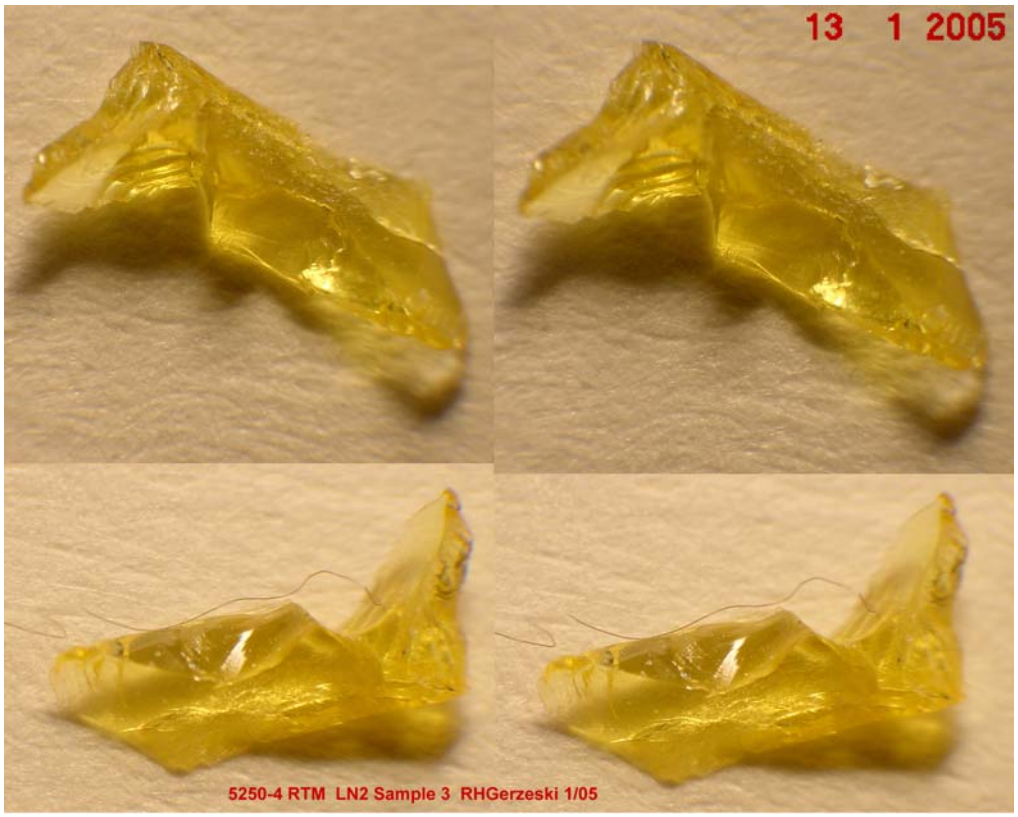


Figure 102-b-i, External To The Indenting Impacter Fracture Surfaces: Knobs: 5250-4 RTM D2512 Specimen: In LN2





Figure 102-b-ii, External To The Indenting Impacter Fracture Surfaces: Knobs: 5250-4 RTM D2512 Specimen: In LN2



Figure 103-a-i, External To The Indenting Impacter Fracture Surfaces: Knobs: T650-35 / 5250-4 RTM D2512 Specimen: In LOX: Reaction Detected



Figure 103-a-ii, External To The Indenting Impacter Fracture Surfaces: Knobs: T650-35 / 5250-4 RTM D2512 Specimen: In LOX: Reaction Detected



Figure 103-a-iii, External To The Indenting Impacter Fracture Surfaces: Knobs: T650-35 / 5250-4 RTM D2512 Specimen: In LOX: Reaction Detected



Figure 103-b-i, External To The Indenting Impacter Fracture Surfaces: Knobs: T650-35 / 5250-4 RTM D2512 Specimen: In LOX: No Reaction Detected



Figure 103-c-i, External To The Indenting Impacter Fracture Surfaces: Knobs: T650-35 / 5250-4 RTM D2512 Specimen: In LN2

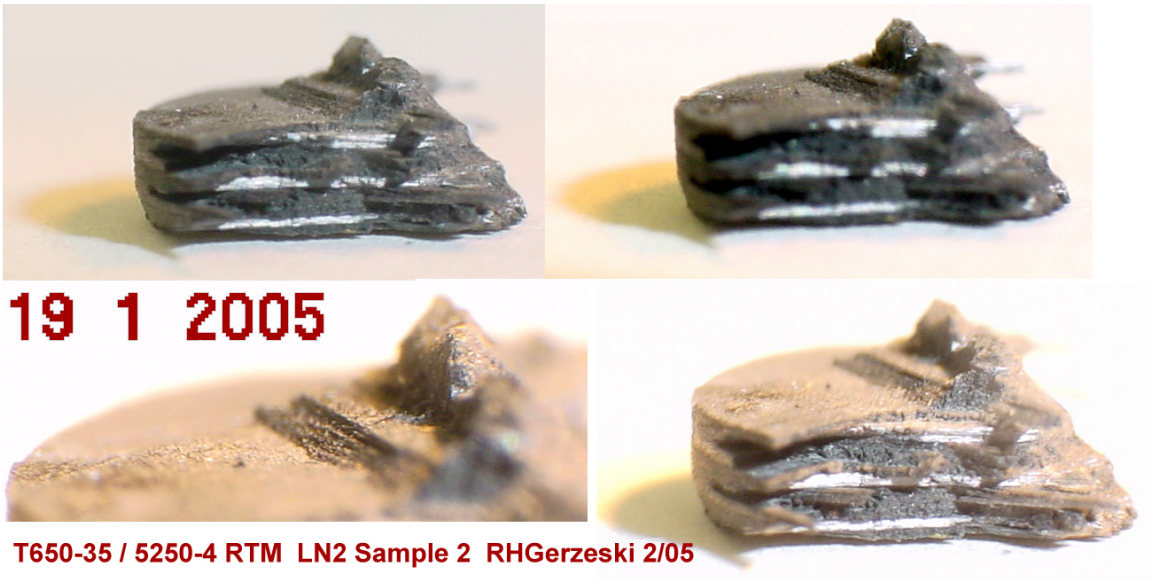


Figure 103-c-ii, External To The Indenting Impacter Fracture Surfaces: Knobs: T650-35 / 5250-4 RTM D2512 Specimen: In LN2



Figure 103-c-iii, External To The Indenting Impacter Fracture Surfaces: Knobs: T650-35 / 5250-4 RTM D2512 Specimen: In LN2

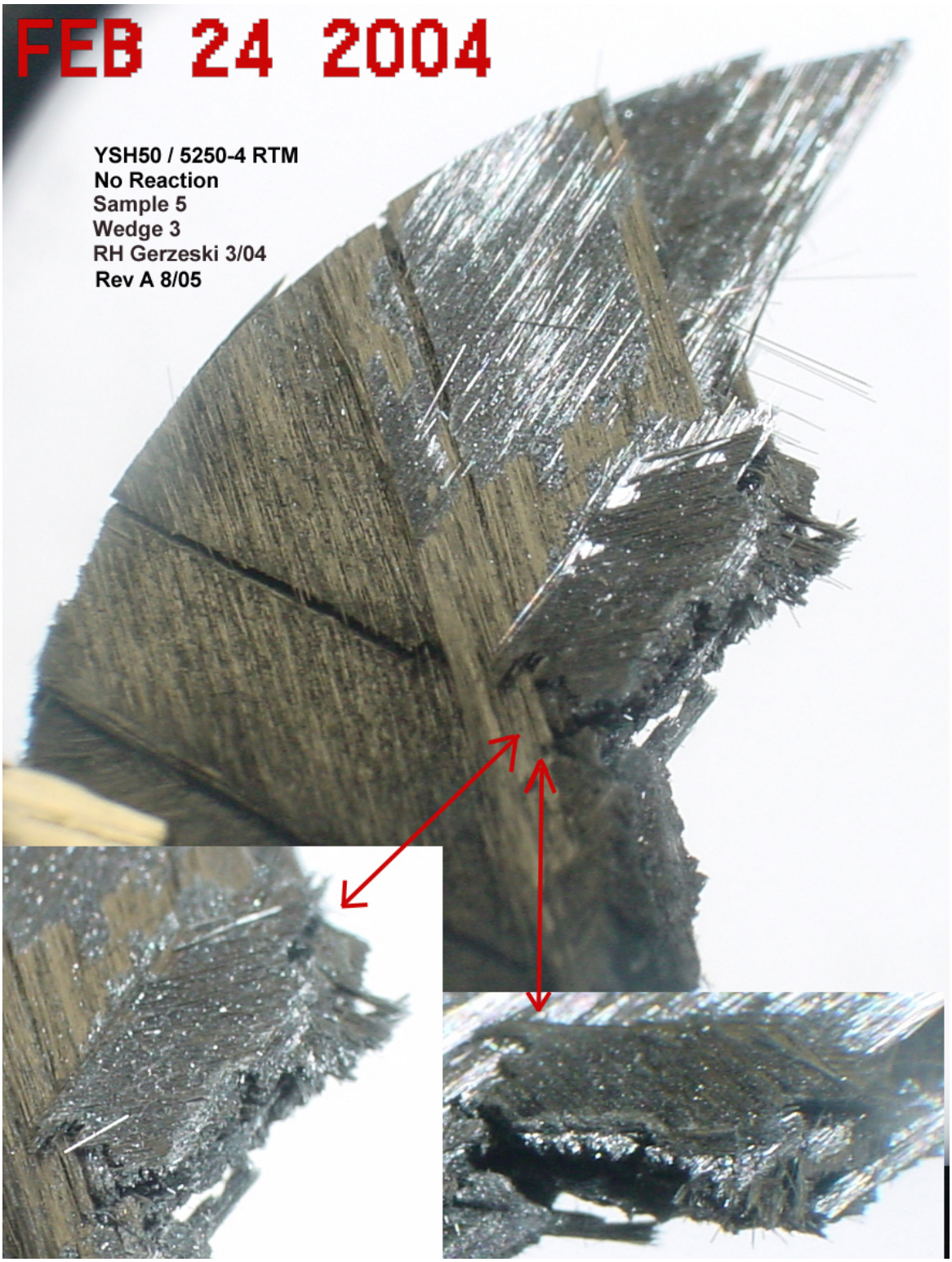


Figure 104-a-i, External To The Indenting Impacter Fracture Surfaces: Knobs: YSH50 / 5250-4 RTM D2512 Specimen: In LOX: No Reaction Detected



Figure 104-a-ii, External To The Indenting Impacter Fracture Surfaces: Knobs: YSH50 / 5250-4 RTM D2512 Specimen: In LOX: No Reaction Detected

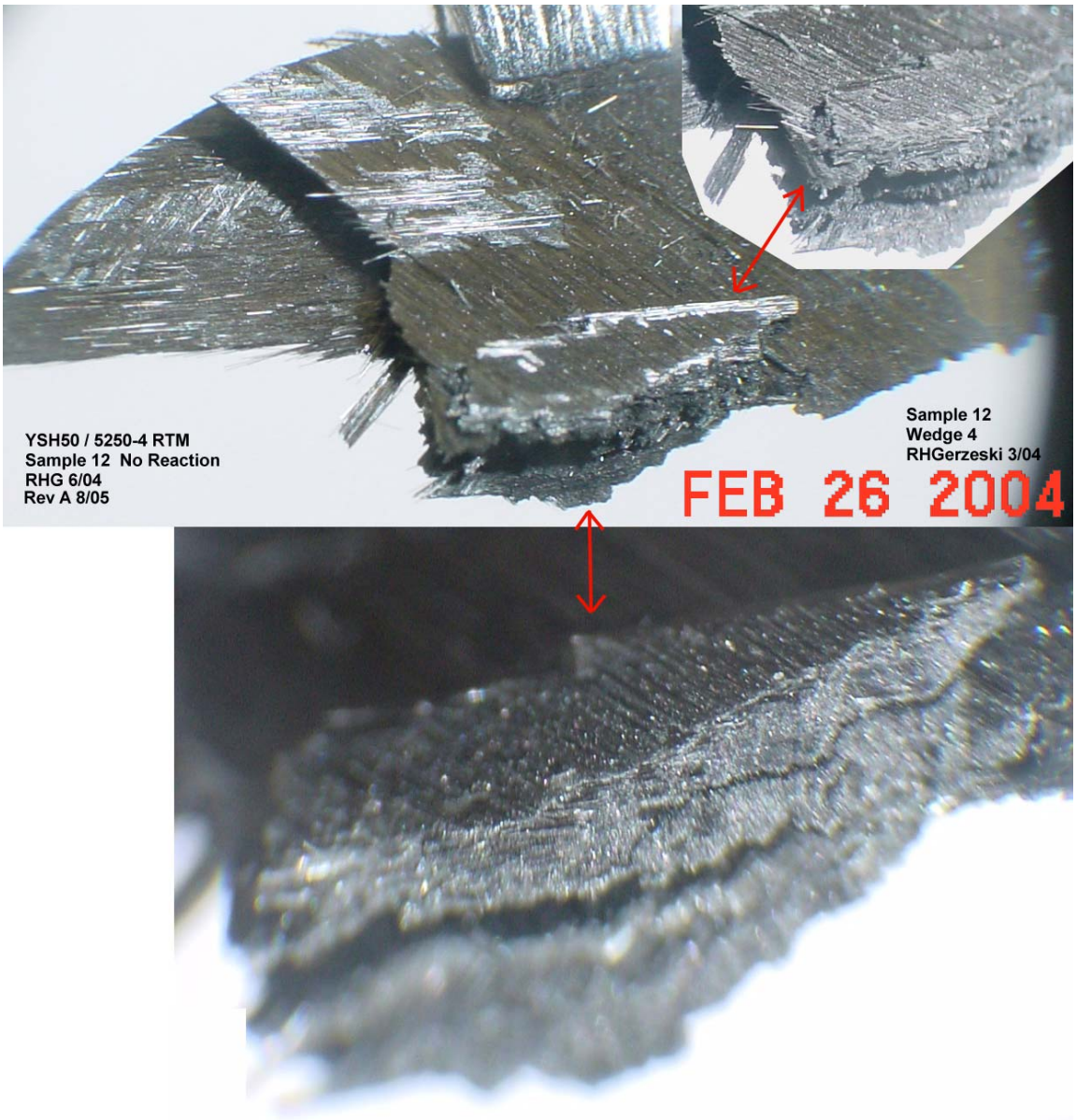


Figure 104-a-iii, External To The Indenting Impacter Fracture Surfaces: Knobs: YSH50 / 5250-4 RTM D2512 Specimen: In LOX: No Reaction Detected



Figure 104-b-i, External To The Indenting Impacter Fracture Surfaces: Knobs: YSH50 / 5250-4 RTM D2512 Specimen: In LN2



Figure 104-b-ii, External To The Indenting Impacter Fracture Surfaces: Knobs: YSH50 / 5250-4 RTM D2512 Specimen: In LN2

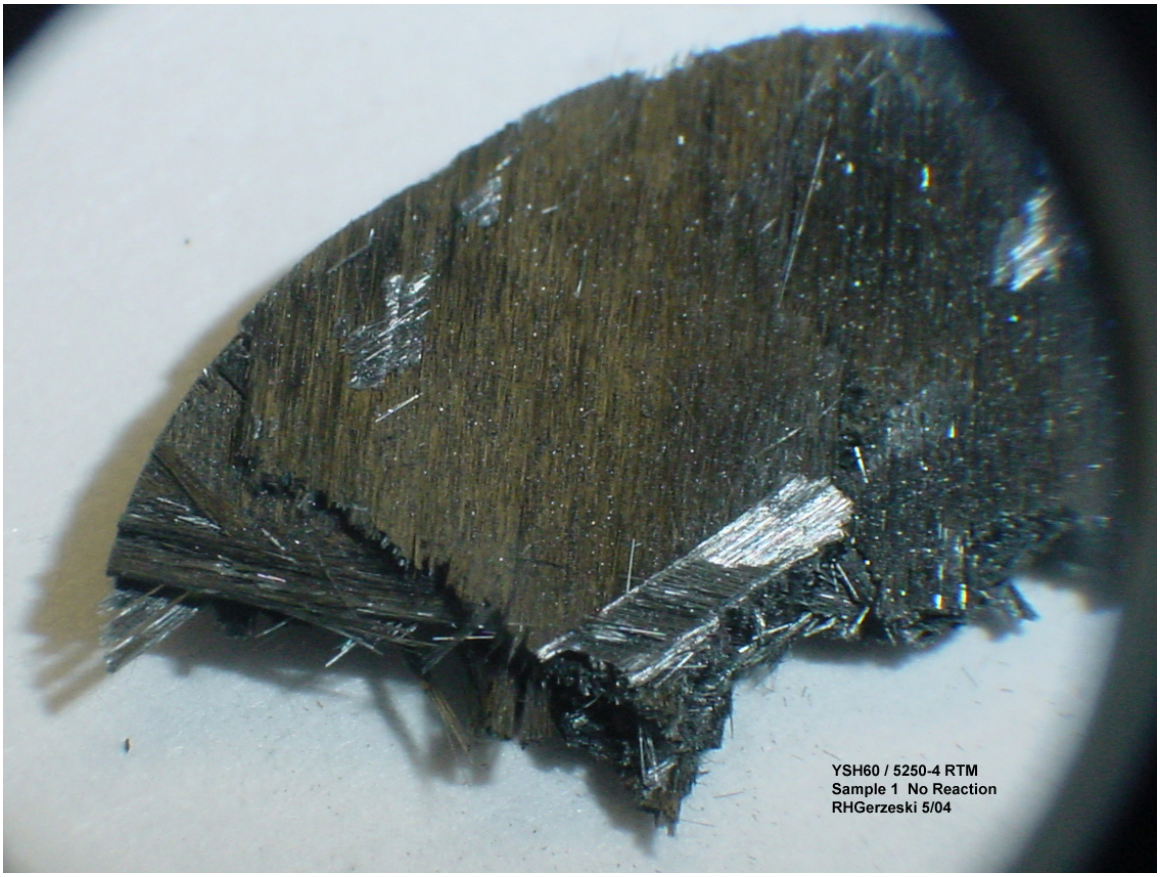


Figure 105-a-i, External To The Indenting Impacter Fracture Surfaces: Knobs: YSH60 / 5250-4 RTM D2512 Specimen: In LOX: No Reaction Detected



Figure 105-a-ii, External To The Indenting Impacter Fracture Surfaces: Knobs: YSH60 / 5250-4 RTM D2512 Specimen: In LOX: No Reaction Detected



Figure 105-a-iii, External To The Indenting Impacter Fracture Surfaces: Knobs: YSH60 / 5250-4 RTM D2512 Specimen: In LOX: No Reaction Detected



Figure 105-b, External To The Indenting Impacter Fracture Surfaces: Knobs: YSH60 / 5250-4 RTM D2512 Specimen: In LN2

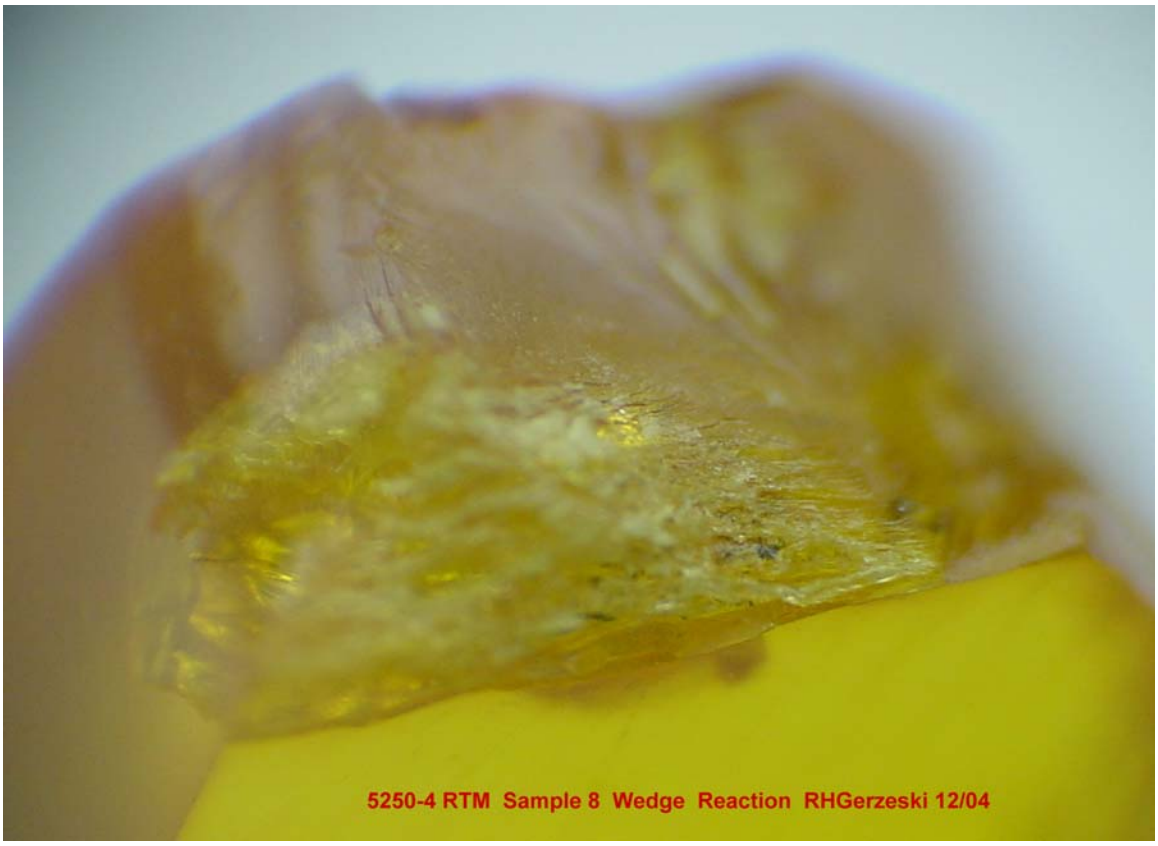
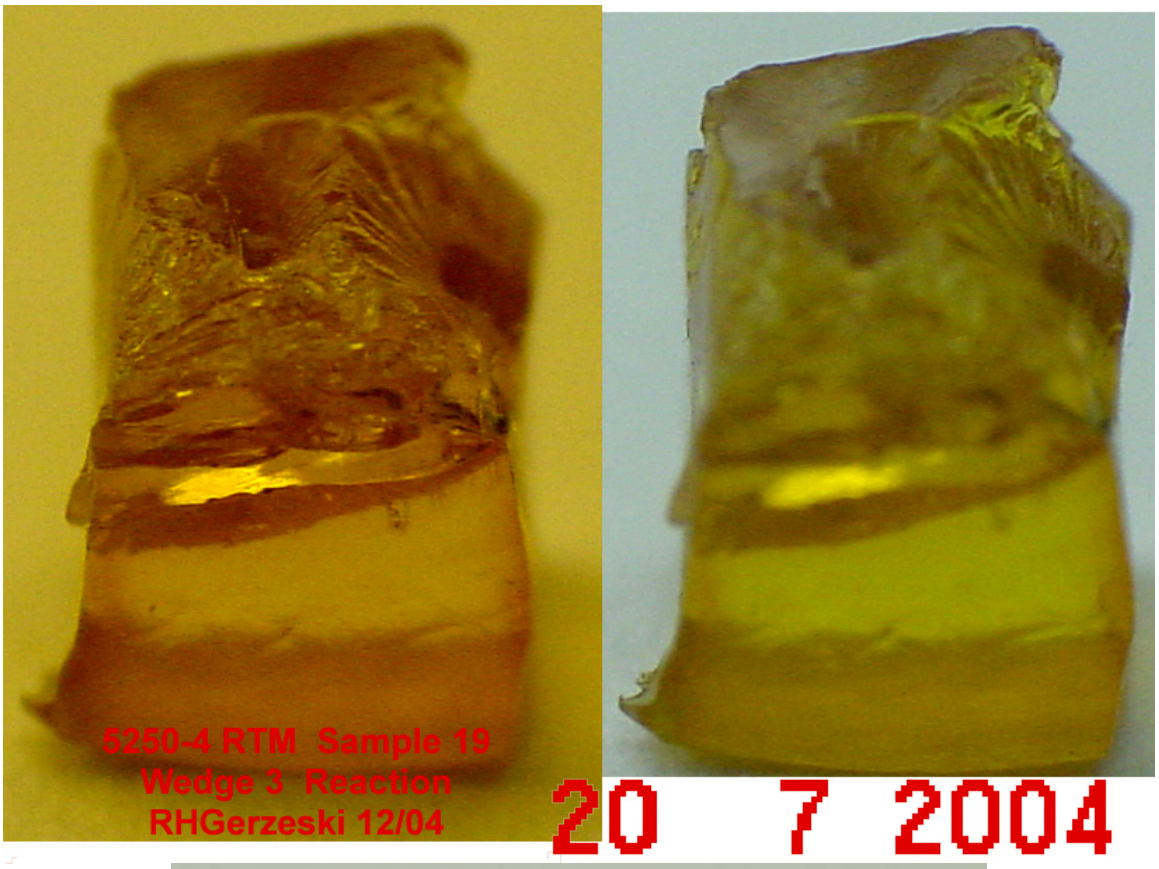


Figure 106-a-i, External To The Indenting Impacter Fracture Surfaces: Straight Cracks: 5250-4 RTM D2512 Specimen: In LOX: Reaction Detected



Figure 106-a-ii, External To The Indenting Impacter Fracture Surfaces: Straight Cracks: 5250-4 RTM D2512 Specimen: In LOX: Reaction Detected



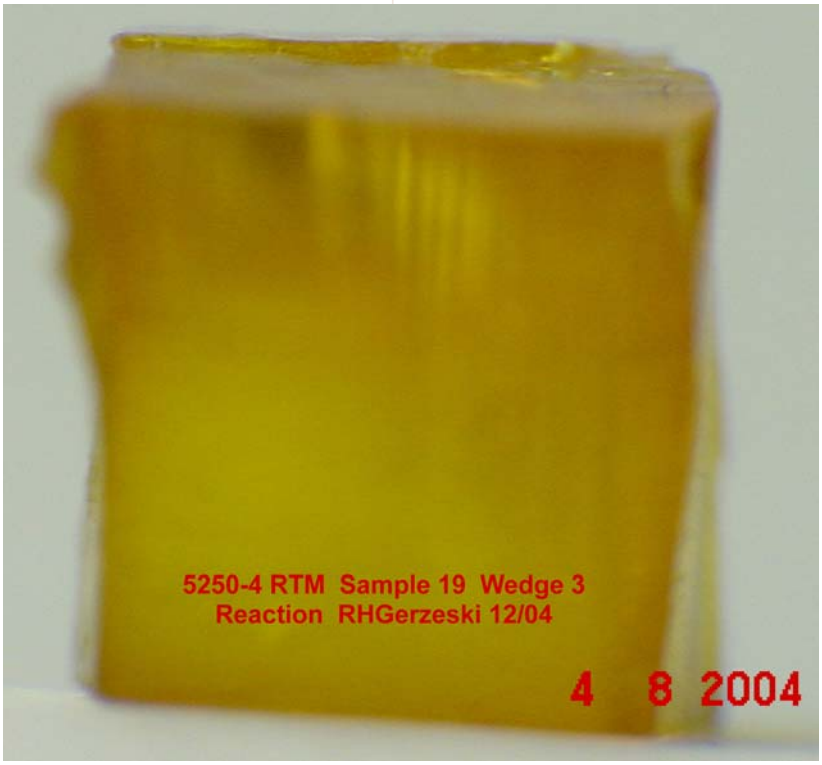


Figure 106-a-iii, External To The Indenting Impacter Fracture Surfaces: Straight Cracks: 5250-4 RTM D2512 Specimen: In LOX: Reaction Detected

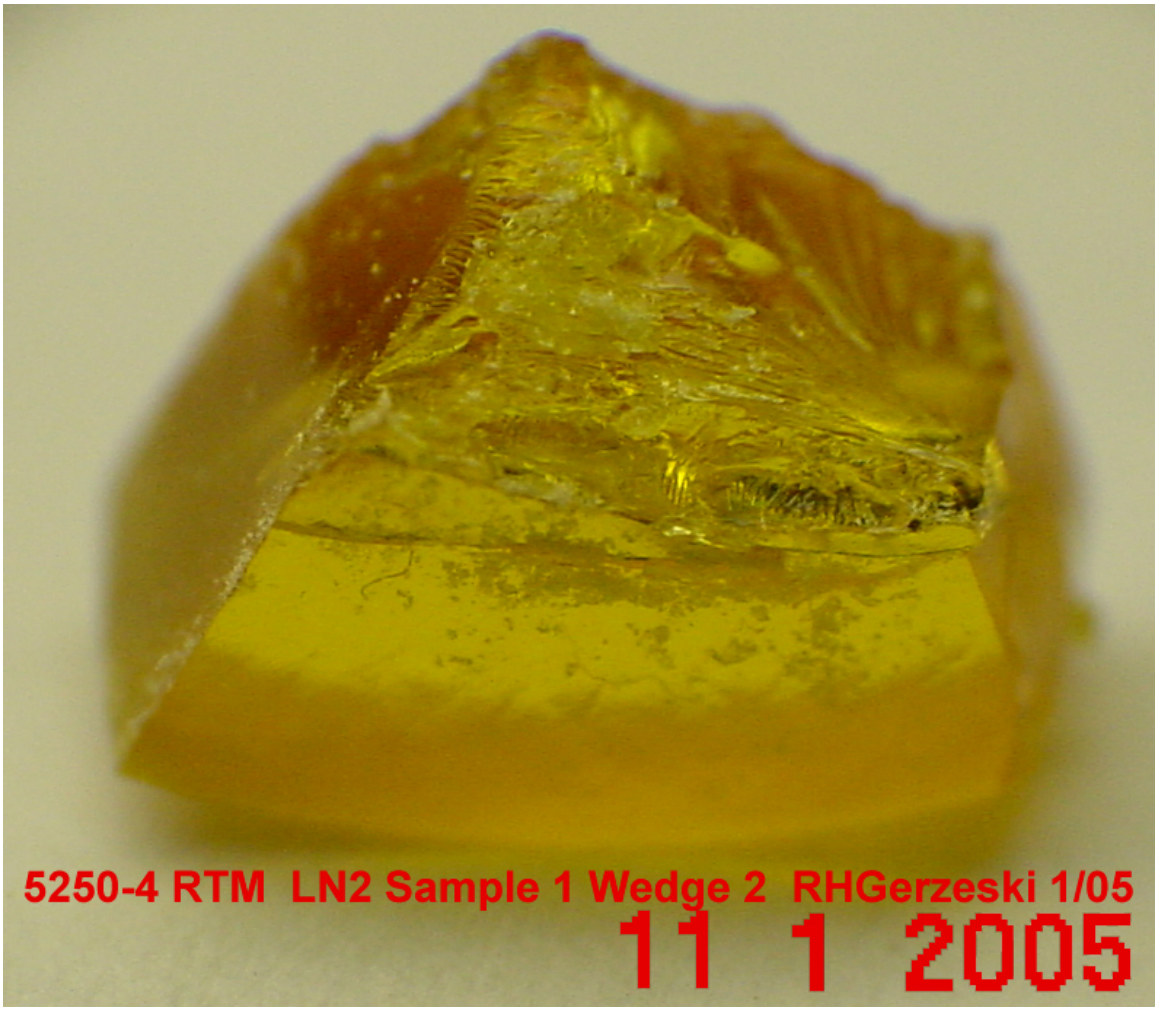


Figure 106-b-i, External To The Indenting Impacter Fracture Surfaces: Straight Cracks: 5250-4 RTM D2512 Specimen: In LN2

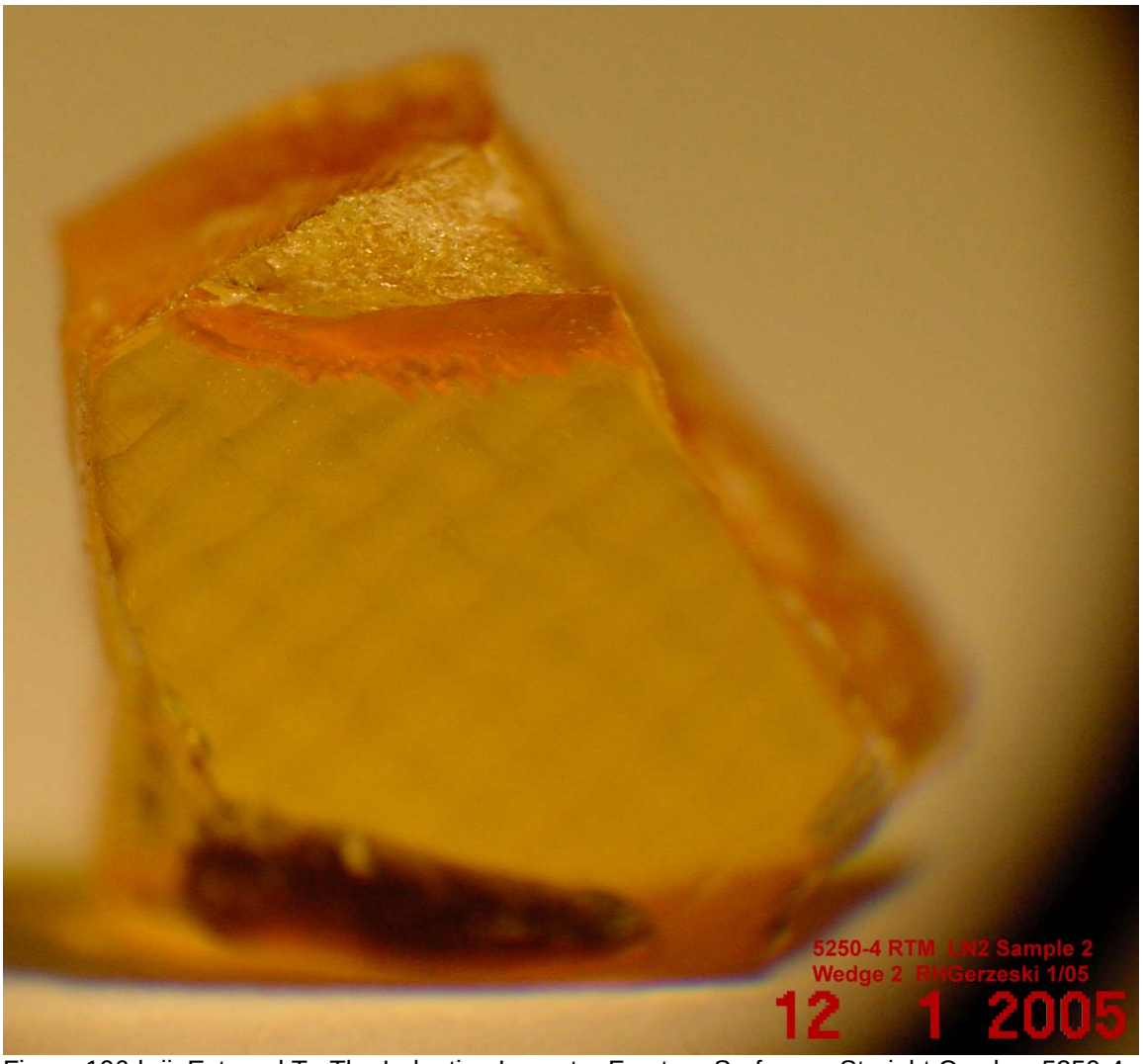


Figure 106-b-ii, External To The Indenting Impacter Fracture Surfaces: Straight Cracks: 5250-4 RTM D2512 Specimen: In LN2



Figure 106-b-iii, External To The Indenting Impacter Fracture Surfaces: Straight Cracks: 5250-4 RTM D2512 Specimen: In LN2



Figure 107-a-i, External To The Indenting Impacter Fracture Surfaces: Straight Cracks: T650-35 / 5250-4 RTM D2512 Specimen: In LOX: Reaction Detected



Figure 107-a-ii, External To The Indenting Impacter Fracture Surfaces: Straight Cracks: T650-35 / 5250-4 RTM D2512 Specimen: In LOX: Reaction Detected



Figure 107-a-iii, External To The Indenting Impacter Fracture Surfaces: Straight Cracks: T650-35 / 5250-4 RTM D2512 Specimen: In LOX: Reaction Detected



Figure 107-b, External To The Indenting Impacter Fracture Surfaces: Straight Cracks: T650-35 / 5250-4 RTM D2512 Specimen: In LOX: No Reaction Detected



Figure 107-c-i, External To The Indenting Impacter Fracture Surfaces: Straight Cracks: T650-35 / 5250-4 RTM D2512 Specimen: In LN2



Figure 107-c-ii, External To The Indenting Impacter Fracture Surfaces: Straight Cracks: T650-35 / 5250-4 RTM D2512 Specimen: In LN2

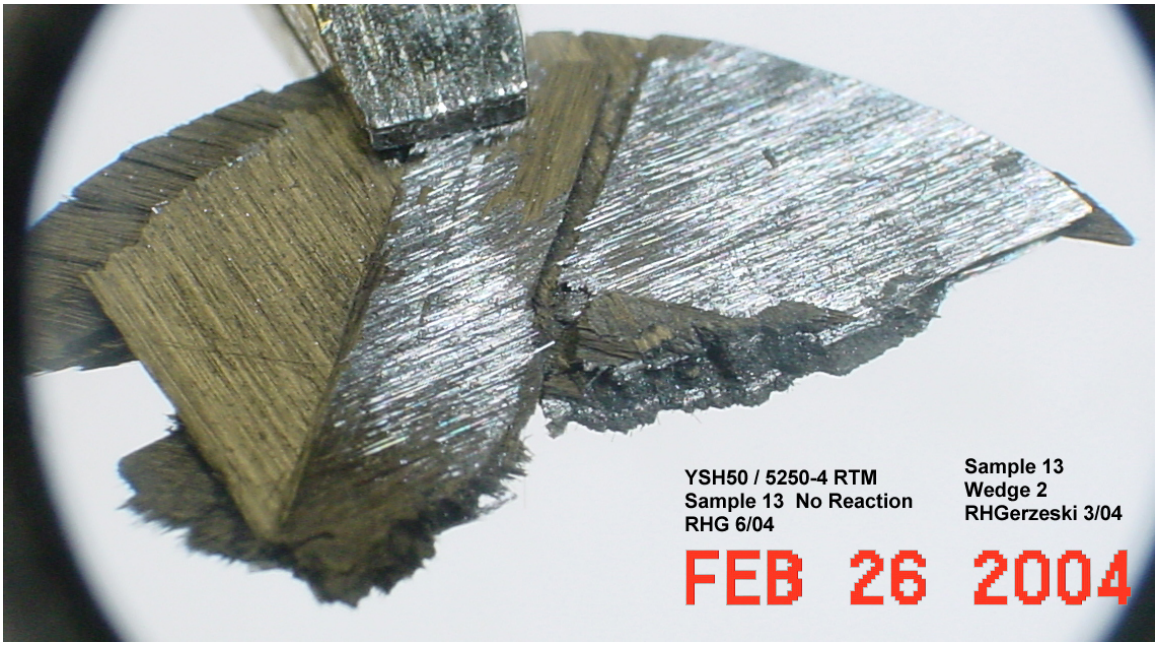


Figure 108-a-i, External To The Indenting Impacter Fracture Surfaces: Straight Cracks: YSH50 / 5250-4 RTM D2512 Specimen: In LOX: No Reaction Detected

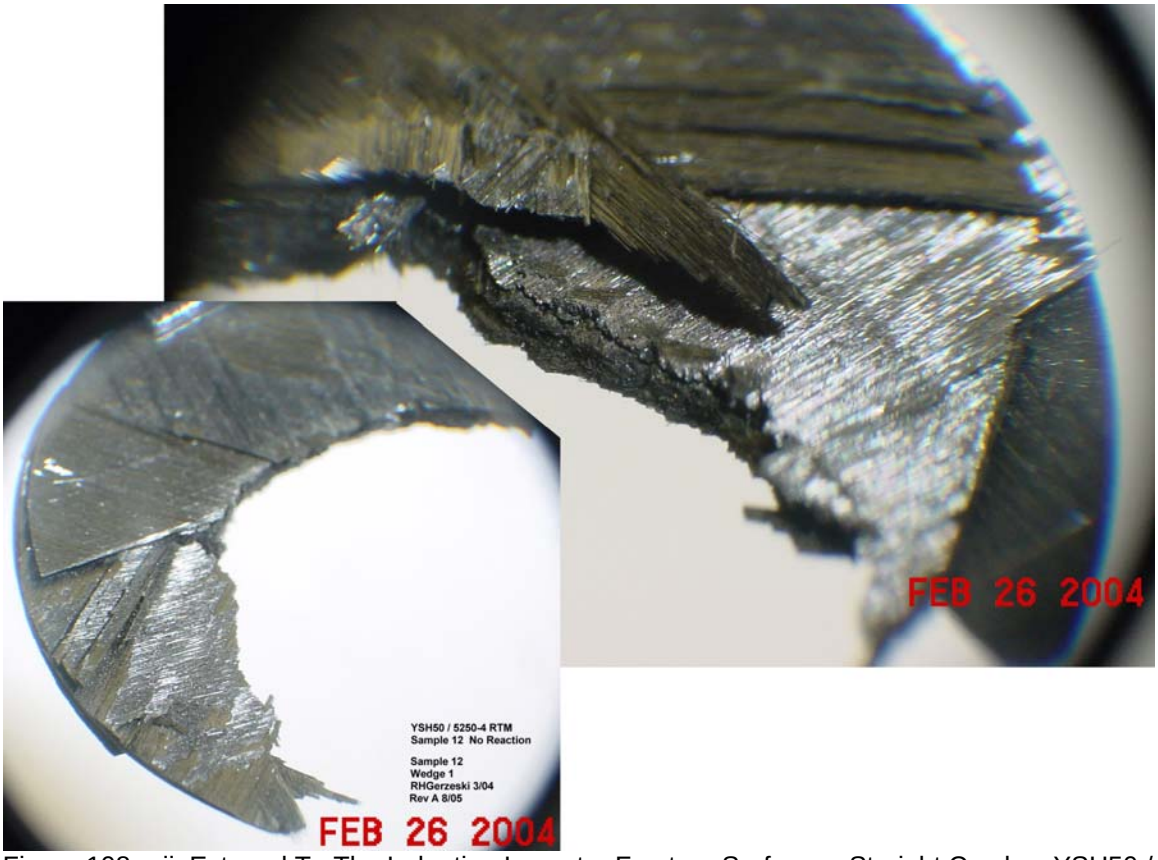


Figure 108-a-ii, External To The Indenting Impacter Fracture Surfaces: Straight Cracks: YSH50 / 5250-4 RTM D2512 Specimen: In LOX: No Reaction Detected

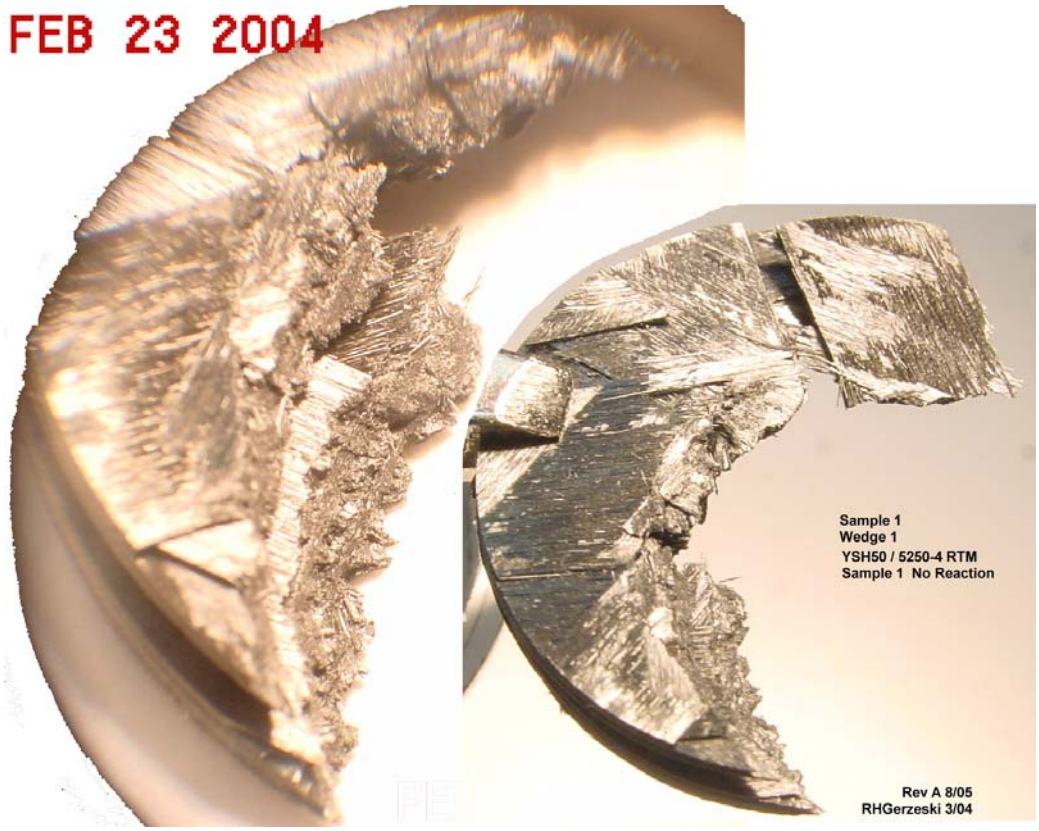


Figure 108-a-iii, External To The Indenting Impacter Fracture Surfaces: Straight Cracks: YSH50 / 5250-4 RTM D2512 Specimen: In LOX: No Reaction Detected



Figure 108-b-i, External To The Indenting Impacter Fracture Surfaces: Straight Cracks: YSH50 / 5250-4 RTM D2512 Specimen: In LN2

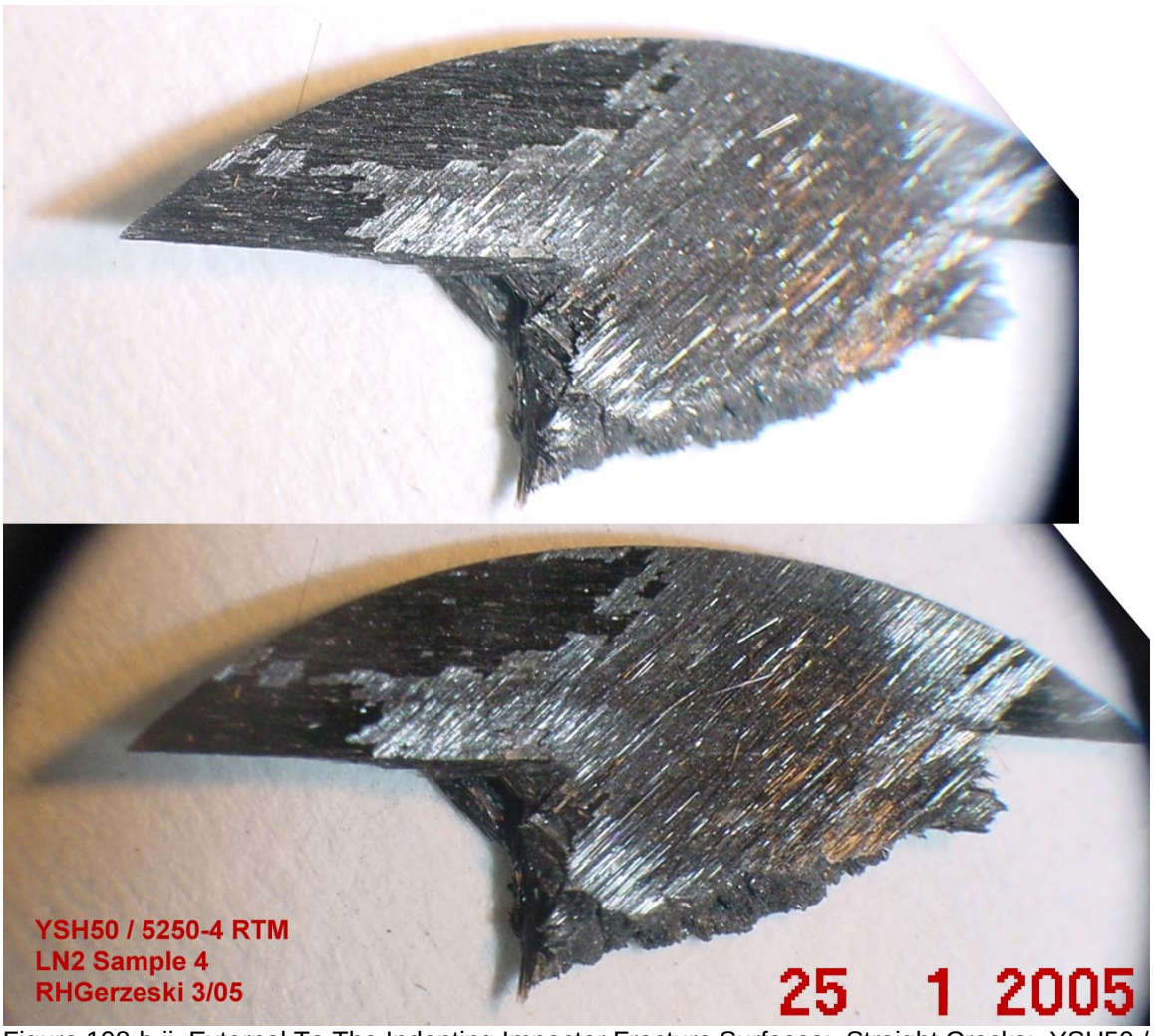


Figure 108-b-ii, External To The Indenting Impacter Fracture Surfaces: Straight Cracks: YSH50 / 5250-4 RTM D2512 Specimen: In LN2



Figure 109-a-i, External To The Indenting Impacter Fracture Surfaces: Straight Cracks: YSH60 / 5250-4 RTM D2512 Specimen: In LOX: Reaction Detected



Figure 109-a-ii, External To The Indenting Impacter Fracture Surfaces: Straight Cracks: YSH60 / 5250-4 RTM D2512 Specimen: In LOX: Reaction Detected

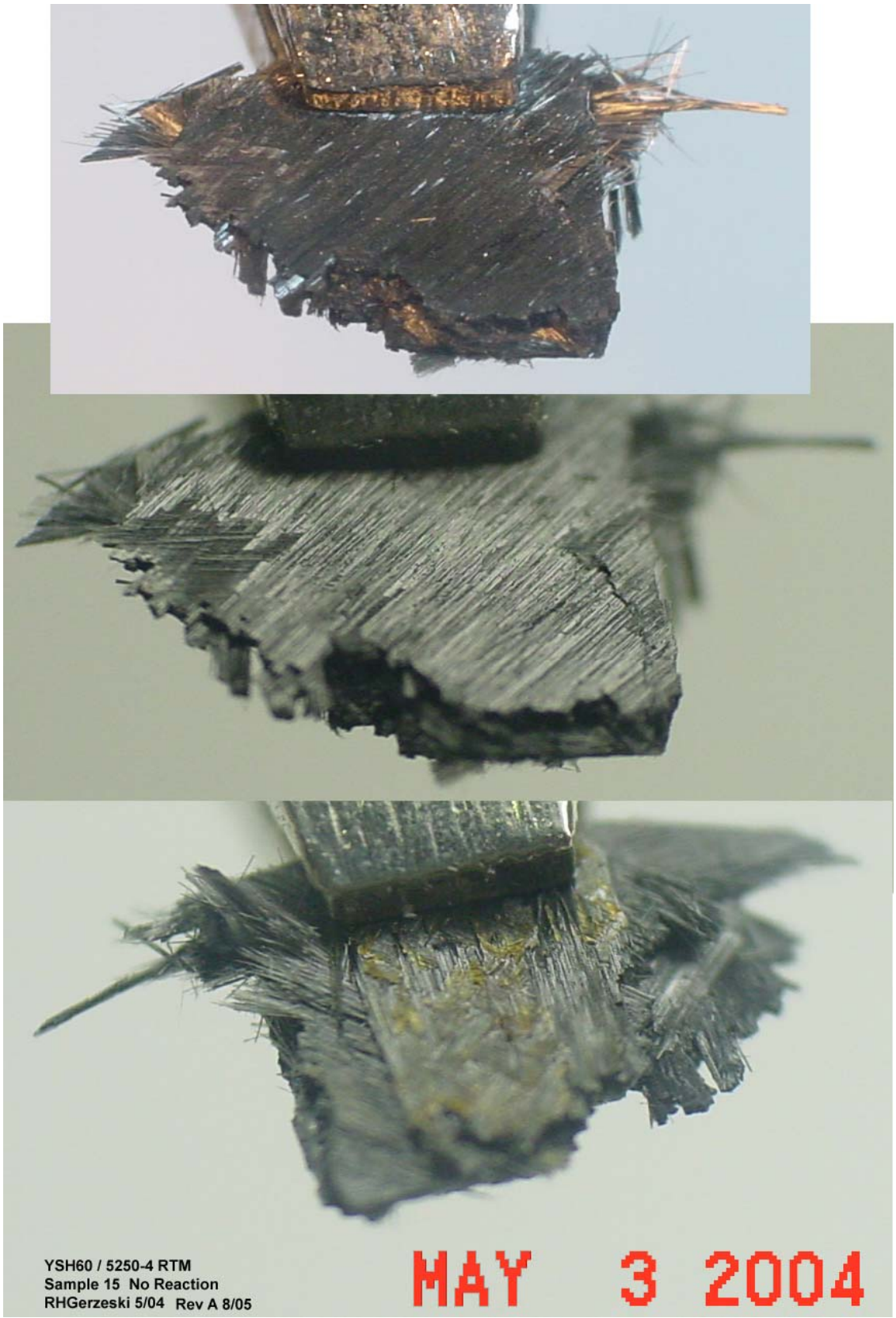


Figure 109-b-i, External To The Indenting Impacter Fracture Surfaces: Straight Cracks: YSH60 / 5250-4 RTM D2512 Specimen: In LOX: No Reaction Detected



Figure 109-b-ii, External To The Indenting Impacter Fracture Surfaces: Straight Cracks: YSH60 / 5250-4 RTM D2512 Specimen: In LOX: No Reaction Detected



Figure 109-b-iii, External To The Indenting Impacter Fracture Surfaces: Straight Cracks: YSH60 / 5250-4 RTM D2512 Specimen: In LOX: No Reaction Detected



Figure 109-c, External To The Indenting Impacter Fracture Surfaces: Straight Cracks: YSH60 / 5250-4 RTM D2512 Specimen: In LN2



Figure 110-a-i, External To The Indenting Impacter Fracture Surfaces: Abrasion: 5250-4 RTM D2512 Specimen: In LOX: No Reaction Detected

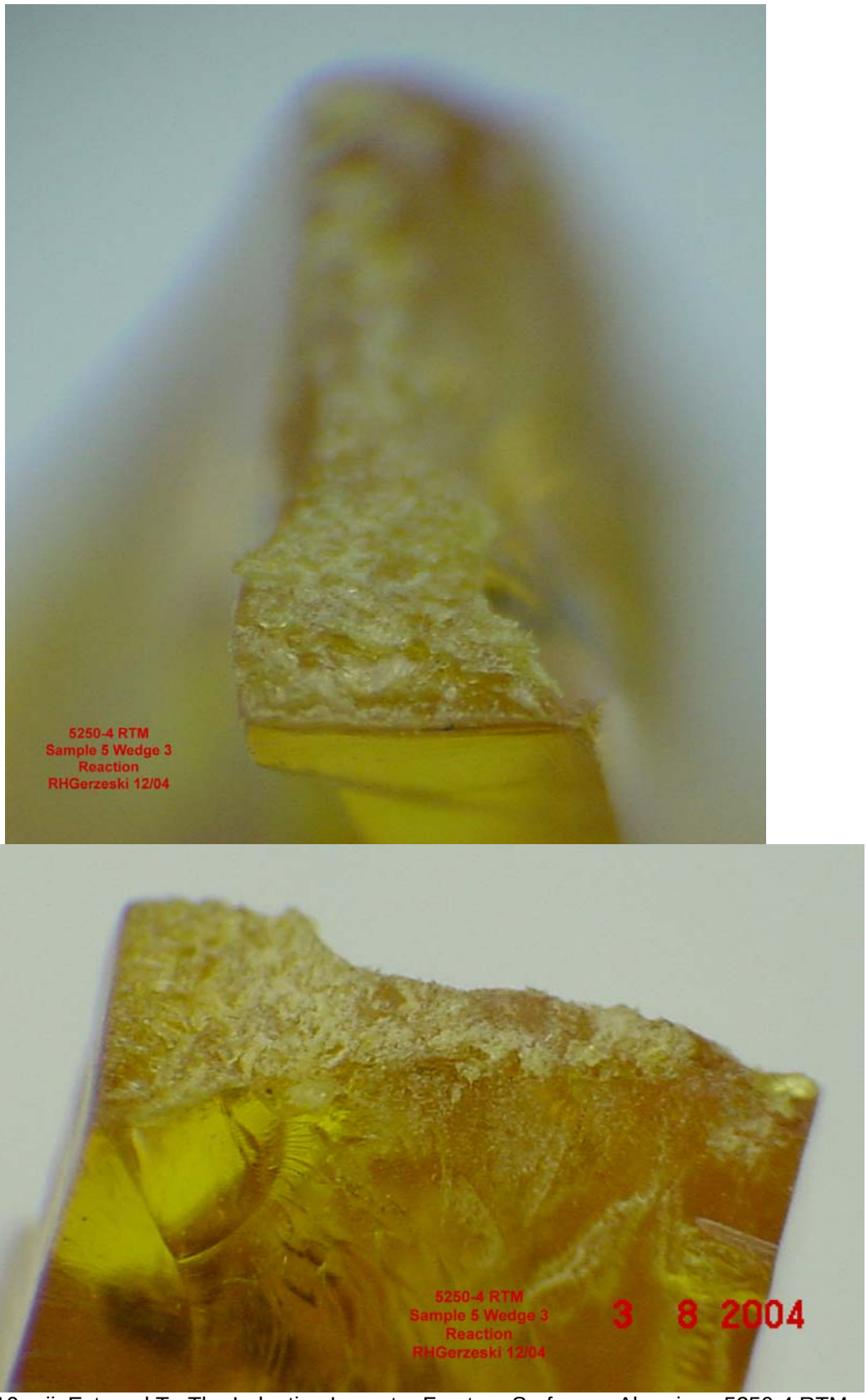


Figure 110-a-ii, External To The Indenting Impacter Fracture Surfaces: Abrasion: 5250-4 RTM D2512 Specimen: In LOX: Reaction Detected

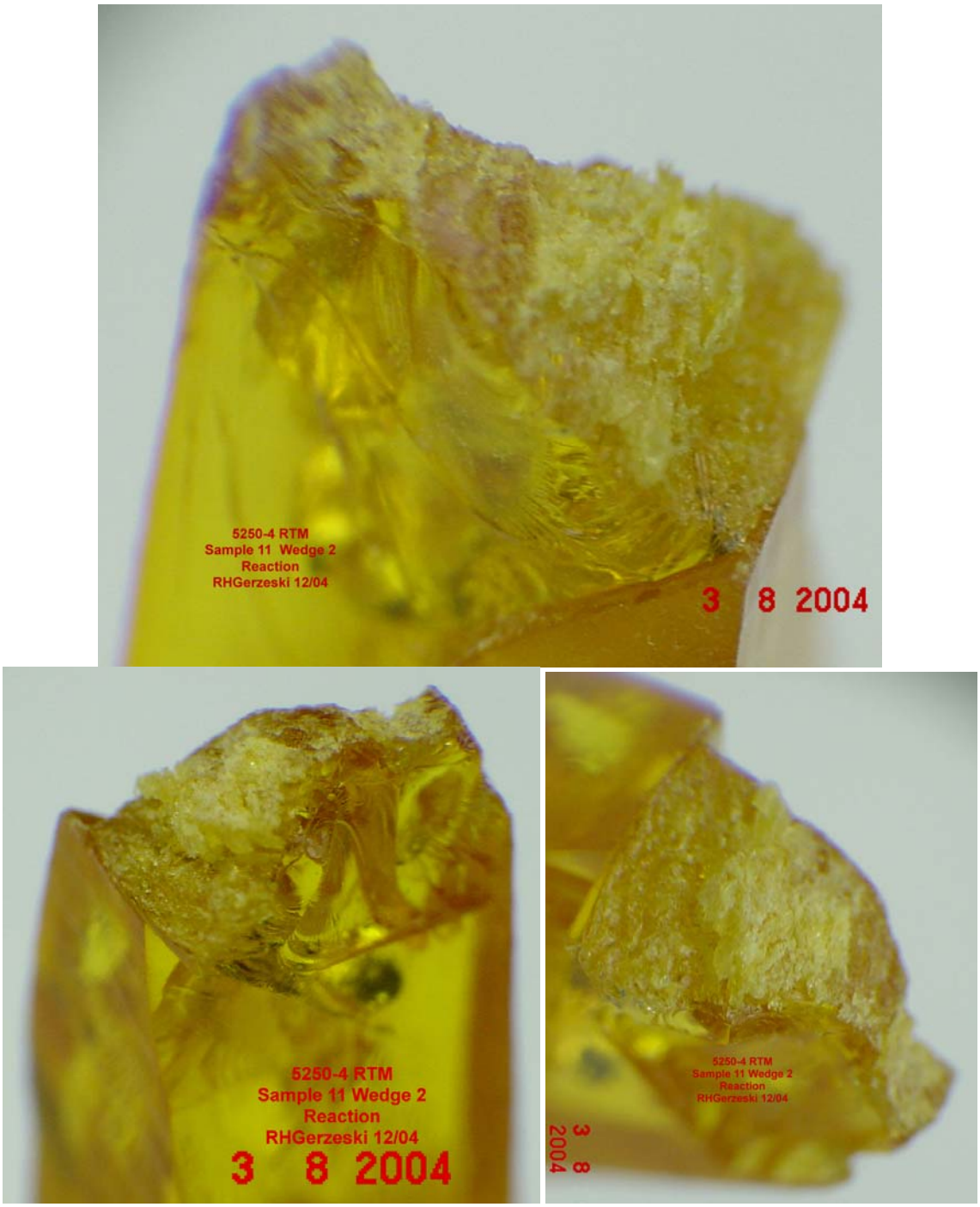


Figure 110-a-iii, External To The Indenting Impacter Fracture Surfaces: Abrasion: 5250-4 RTM D2512 Specimen: In LOX: Reaction Detected



Figure 110-b-i, External To The Indenting Impacter Fracture Surfaces: Abrasion: 5250-4 RTM D2512 Specimen: In LN2

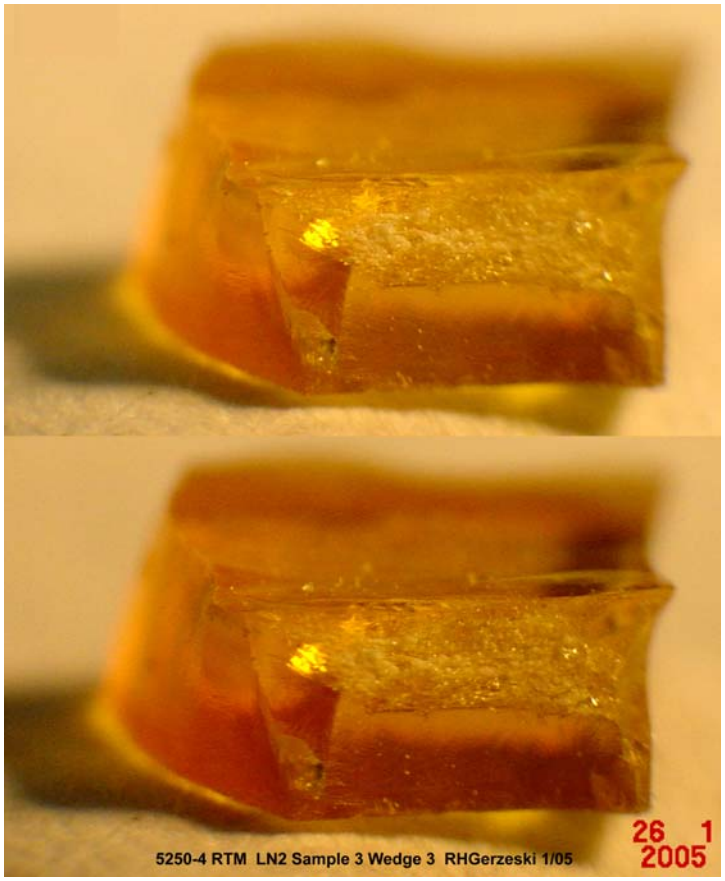


Figure 110-b-ii, External To The Indenting Impacter Fracture Surfaces: Abrasion: 5250-4 RTM D2512 Specimen: In LN2

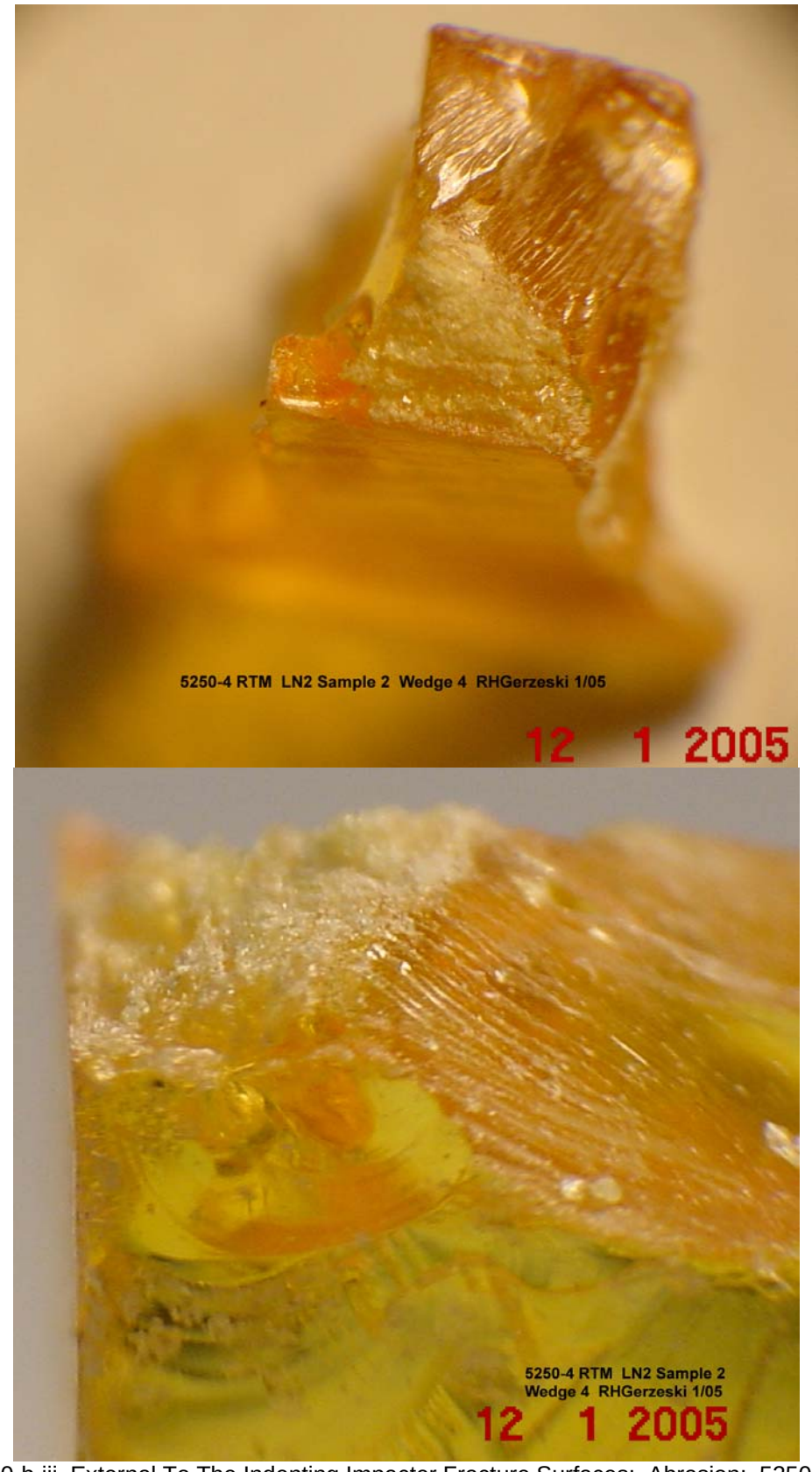


Figure 110-b-iii, External To The Indenting Impacter Fracture Surfaces: Abrasion: 5250-4 RTM D2512 Specimen: In LN2



Figure 111-a-i, External To The Indenting Impacter Fracture Surfaces: Abrasion: T650-35 / 5250-4 RTM D2512 Specimen: In LOX: Reaction Detected



Figure 111-a-ii, External To The Indenting Impacter Fracture Surfaces: Abrasion: T650-35 / 5250-4 RTM D2512 Specimen: In LOX: Reaction Detected



Figure 111-a-iii, External To The Indenting Impacter Fracture Surfaces: Abrasion: T650-35 / 5250-4 RTM D2512 Specimen: In LOX: Reaction Detected

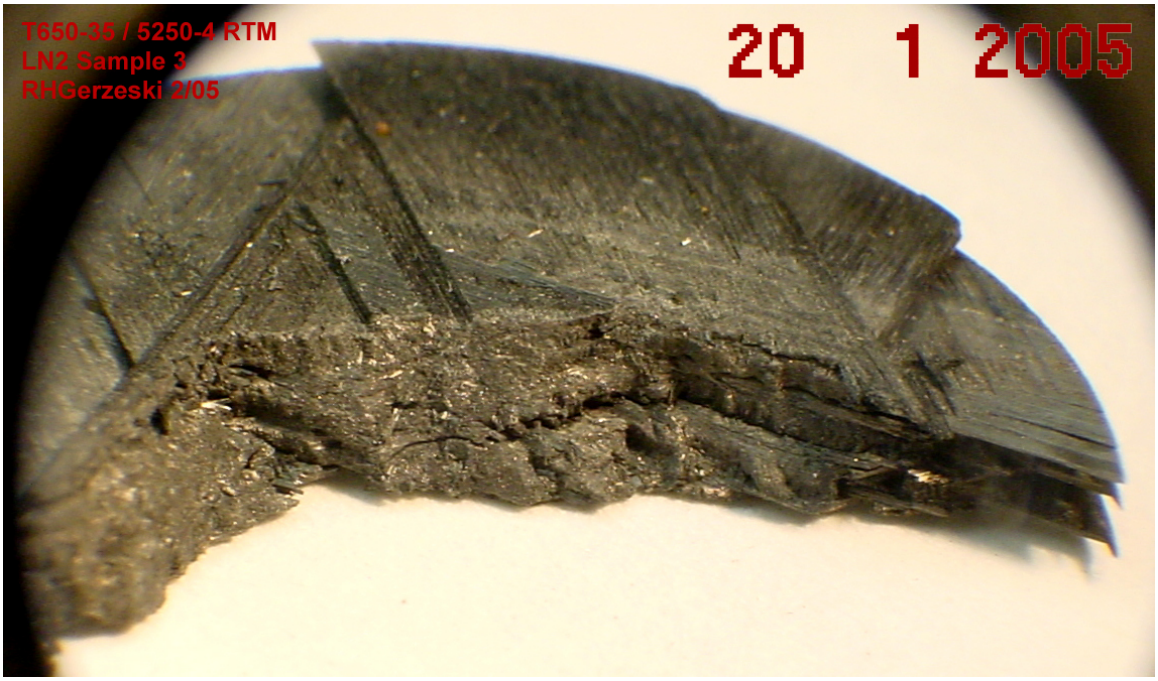


Figure 111-b-i, External To The Indenting Impacter Fracture Surfaces: Abrasion: T650-35 / 5250-4 RTM D2512 Specimen: In LN2



Figure 111-b-ii, External To The Indenting Impacter Fracture Surfaces: Abrasion: T650-35 / 5250-4 RTM D2512 Specimen: In LN2



Figure 111-b-iii, External To The Indenting Impacter Fracture Surfaces: Abrasion: T650-35 / 5250-4 RTM D2512 Specimen: In LN2



Figure 112-a, External To The Indenting Impacter Fracture Surfaces: Abrasion: YSH50 / 5250-4 RTM D2512 Specimen: In LOX: Reaction Detected

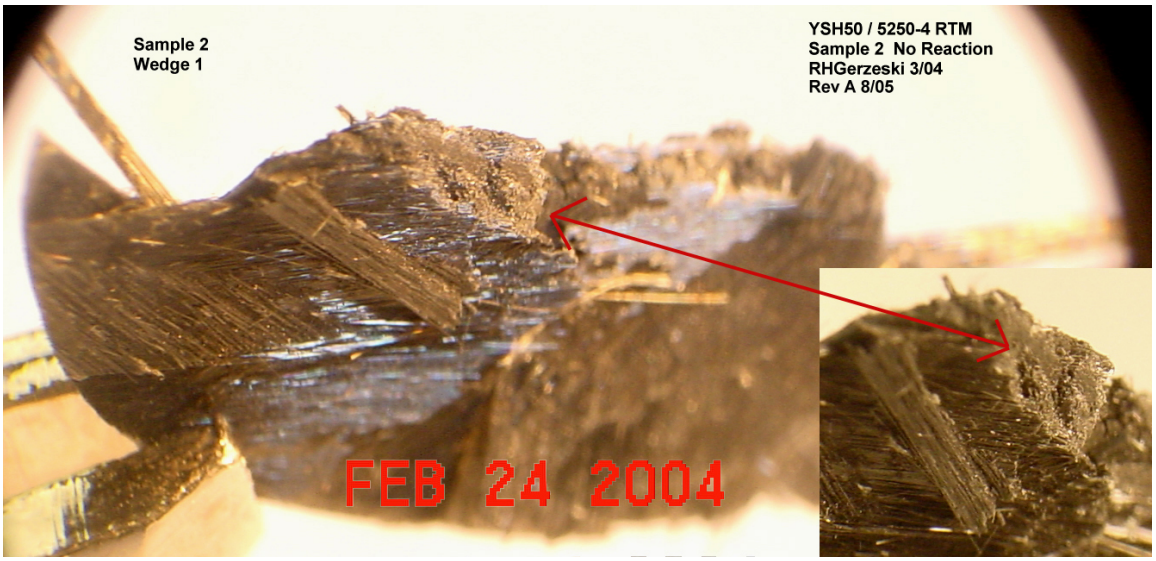


Figure 112-b-i, External To The Indenting Impacter Fracture Surfaces: Abrasion: YSH50 / 5250-4 RTM D2512 Specimen: In LOX: No Reaction Detected

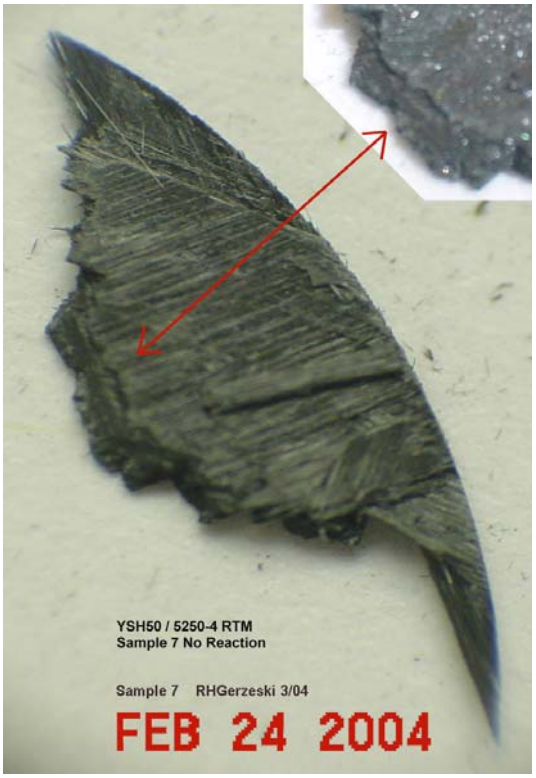


Figure 112-b-ii, External To The Indenting Impacter Fracture Surfaces: Abrasion: YSH50 / 5250-4 RTM D2512 Specimen: In LOX: No Reaction Detected

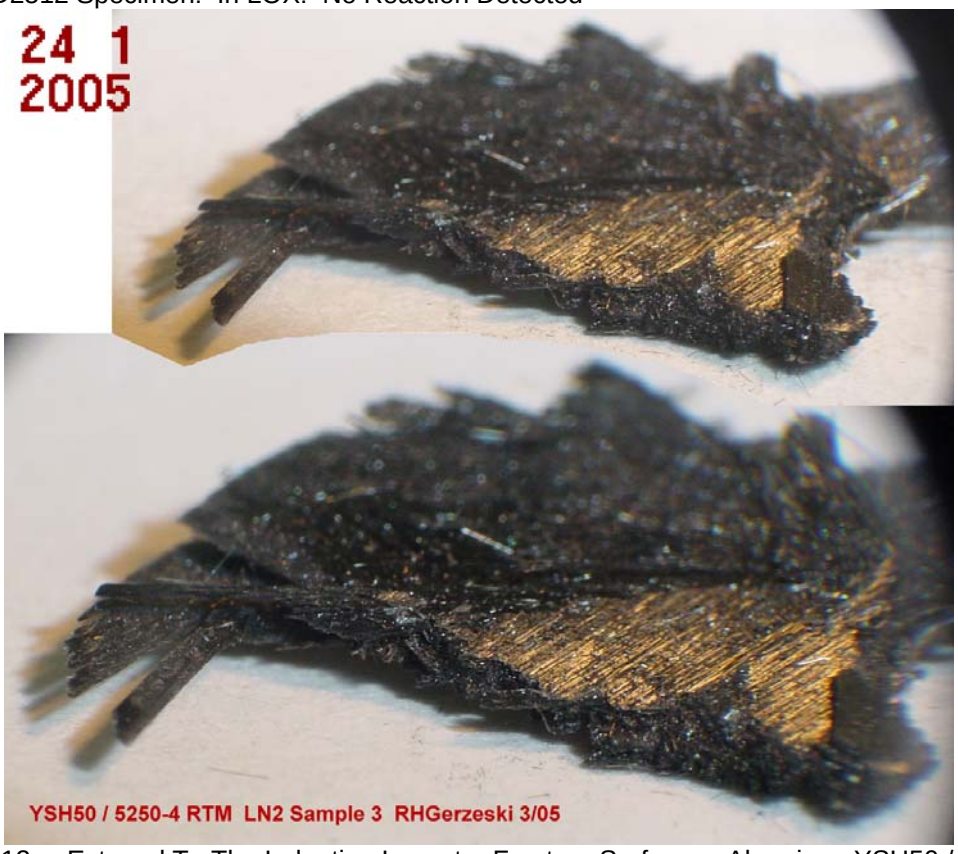


Figure 112-c, External To The Indenting Impacter Fracture Surfaces: Abrasion: YSH50 / 5250-4 RTM D2512 Specimen: In LN2



Figure 113-a-i, External To The Indenting Impacter Fracture Surfaces: Abrasion: YSH60 / 5250-4 RTM D2512 Specimen: In LOX: Reaction Detected



Figure 113-a-ii, External To The Indenting Impacter Fracture Surfaces: Abrasion: YSH60 / 5250-4 RTM D2512 Specimen: In LOX: Reaction Detected



Figure 113-b-i, External To The Indenting Impacter Fracture Surfaces: Abrasion: YSH60 / 5250-4 RTM D2512 Specimen: In LOX: No Reaction Detected



Figure 113-b-ii, External To The Indenting Impacter Fracture Surfaces: Abrasion: YSH60 / 5250-4 RTM D2512 Specimen: In LOX: No Reaction Detected



Figure 113-b-iii, External To The Indenting Impacter Fracture Surfaces: Abrasion: YSH60 / 5250-4 RTM D2512 Specimen: In LOX: No Reaction Detected

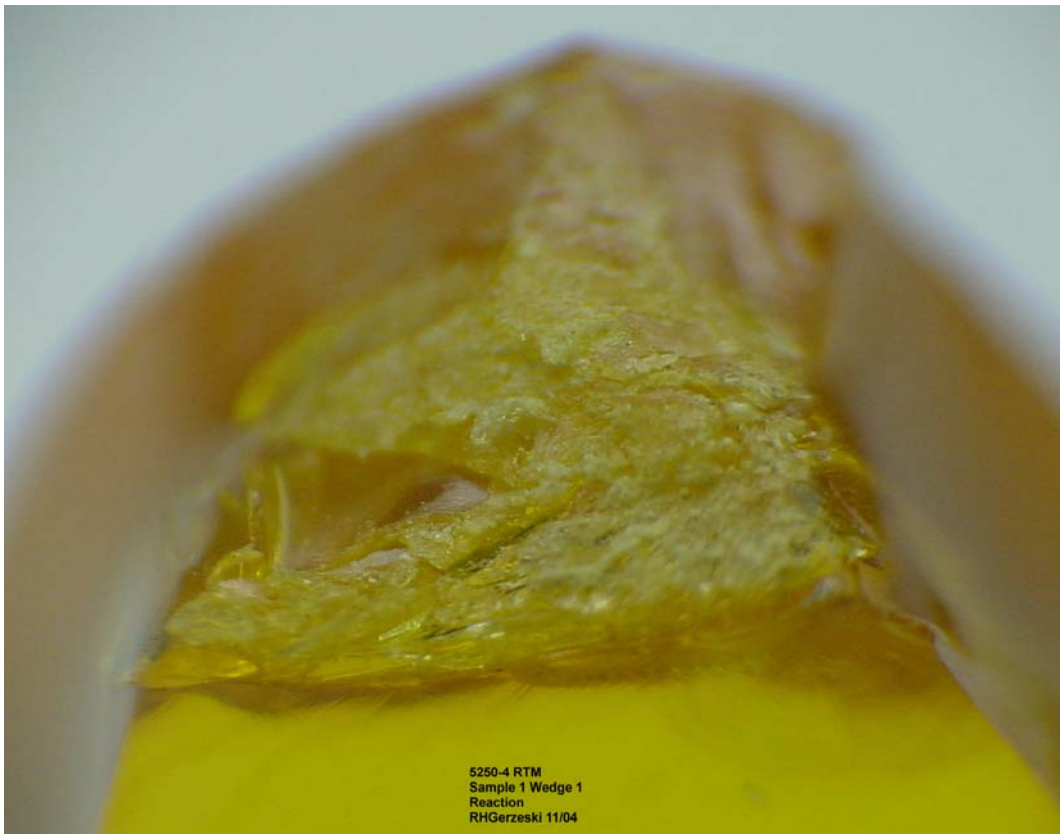


Figure 114-a-i, External To The Indenting Impacter Fracture Surfaces: Intense Heat: 5250-4 RTM D2512 Specimen: In LOX: Reaction Detected



Figure 114-a-ii, External To The Indenting Impacter Fracture Surfaces: Intense Heat: 5250-4 RTM D2512 Specimen: In LOX: Reaction Detected

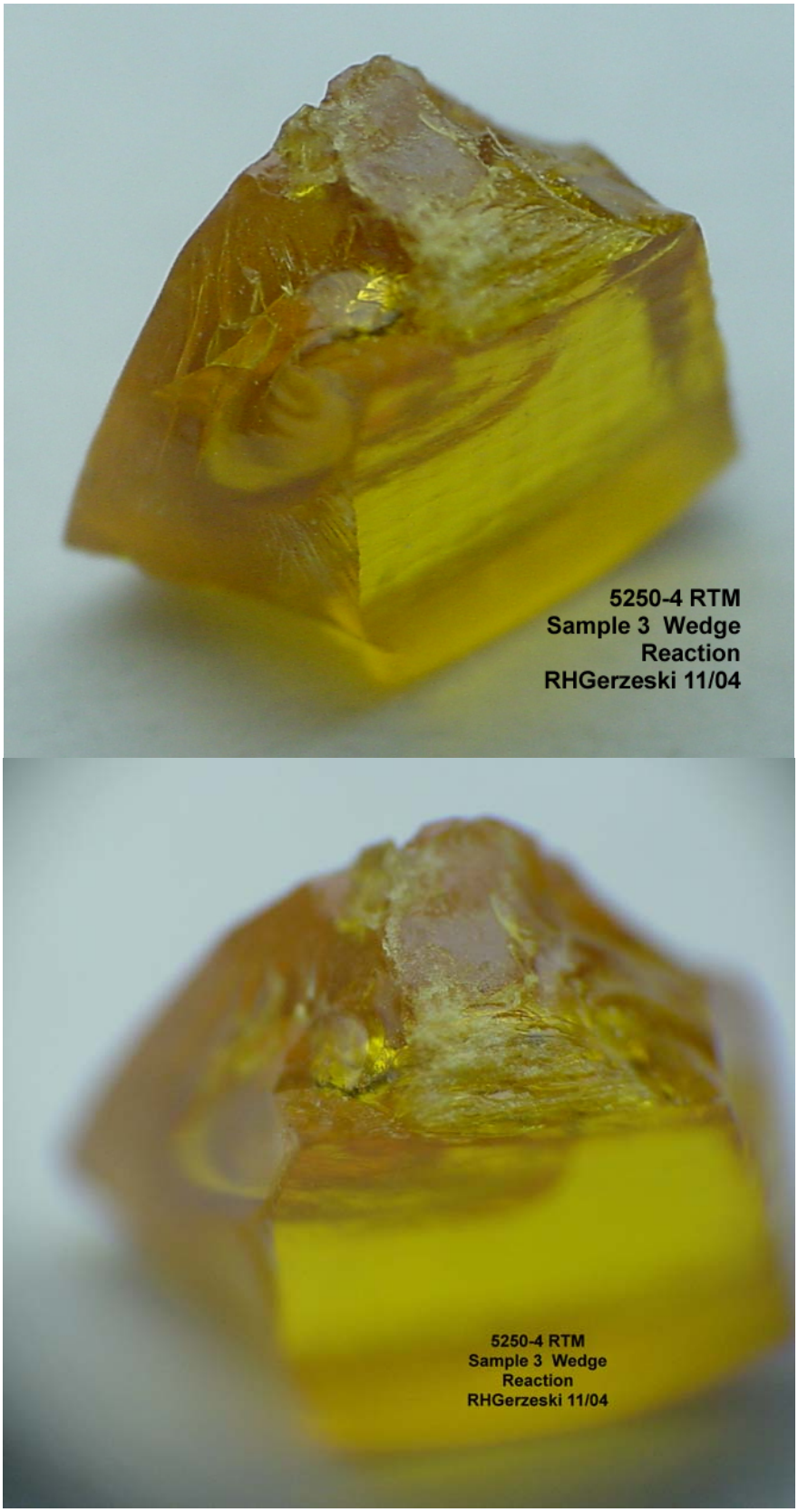


Figure 114-a-iii, External To The Indenting Impacter Fracture Surfaces: Intense Heat: 5250-4 RTM D2512 Specimen: In LOX: Reaction Detected

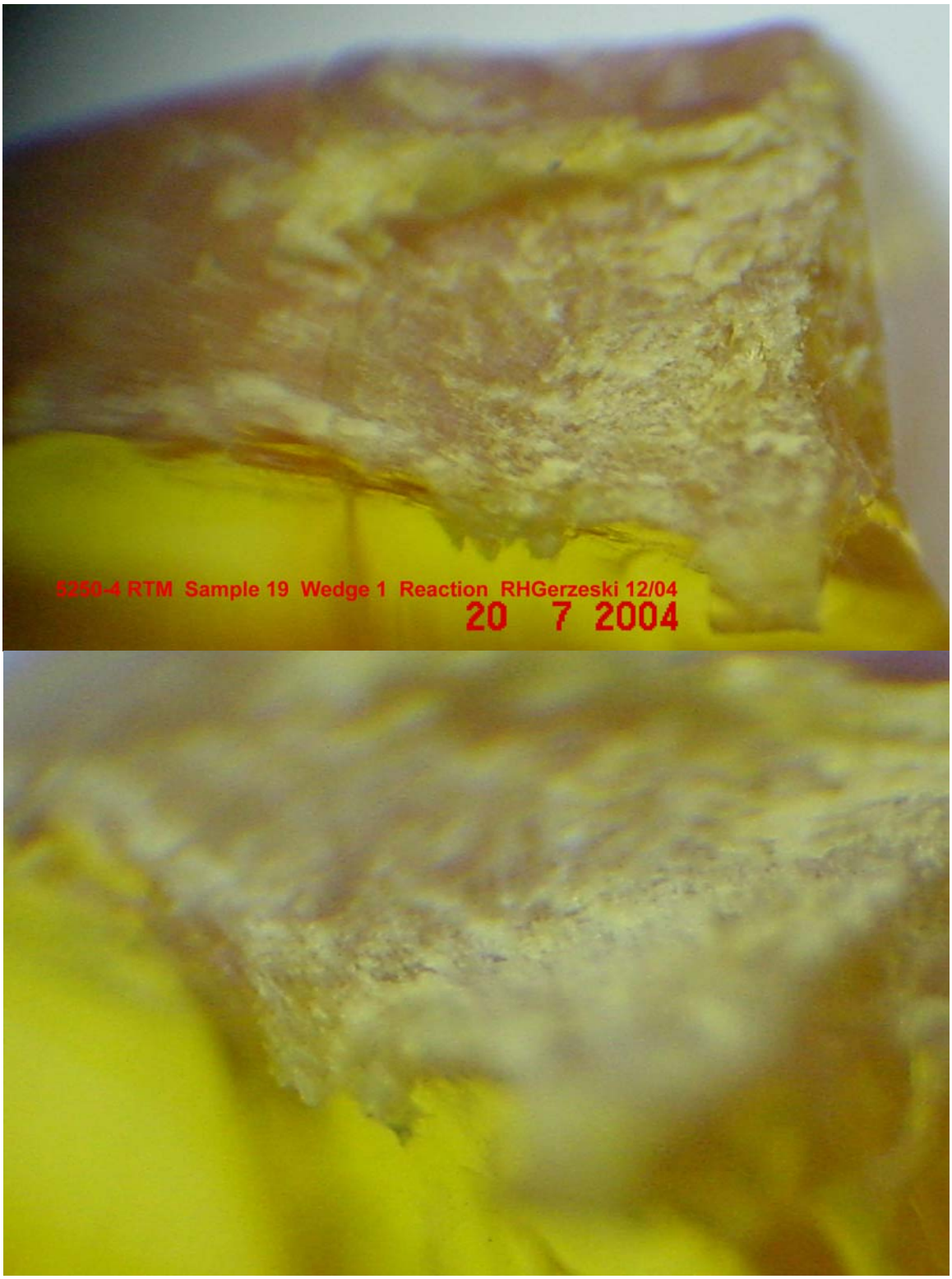


Figure 114-a-iv, External To The Indenting Impacter Fracture Surfaces: Intense Heat: 5250-4 RTM D2512 Specimen: In LOX: Reaction Detected



Figure 114-b-i, External To The Indenting Impacter Fracture Surfaces: Intense Heat: 5250-4 RTM D2512 Specimen: In LN2



Figure 114-b-ii, External To The Indenting Impacter Fracture Surfaces: Intense Heat: 5250-4 RTM D2512 Specimen: In LN2



Figure 115-a-i, External To The Indenting Impacter Fracture Surfaces: Intense Heat: T650 / 5250-4 RTM D2512 Specimen: In LOX: Reaction Detected



Figure 115-a-ii, External To The Indenting Impacter Fracture Surfaces: Intense Heat: T650 / 5250-4 RTM D2512 Specimen: In LOX: Reaction Detected



Figure 115-a-iii, External To The Indenting Impacter Fracture Surfaces: Intense Heat: T650 / 5250-4 RTM D2512 Specimen: In LOX: Reaction Detected



Figure 115-b, External To The Indenting Impacter Fracture Surfaces: Intense Heat: T650 / 5250-4 RTM D2512 Specimen: In LOX: No Reaction Detected



Figure 115-c-i, External To The Indenting Impacter Fracture Surfaces: Intense Heat: T650 / 5250-4 RTM D2512 Specimen: In LN2



Figure 115-c-ii, External To The Indenting Impacter Fracture Surfaces: Intense Heat: T650 / 5250-4 RTM D2512 Specimen: In LN2

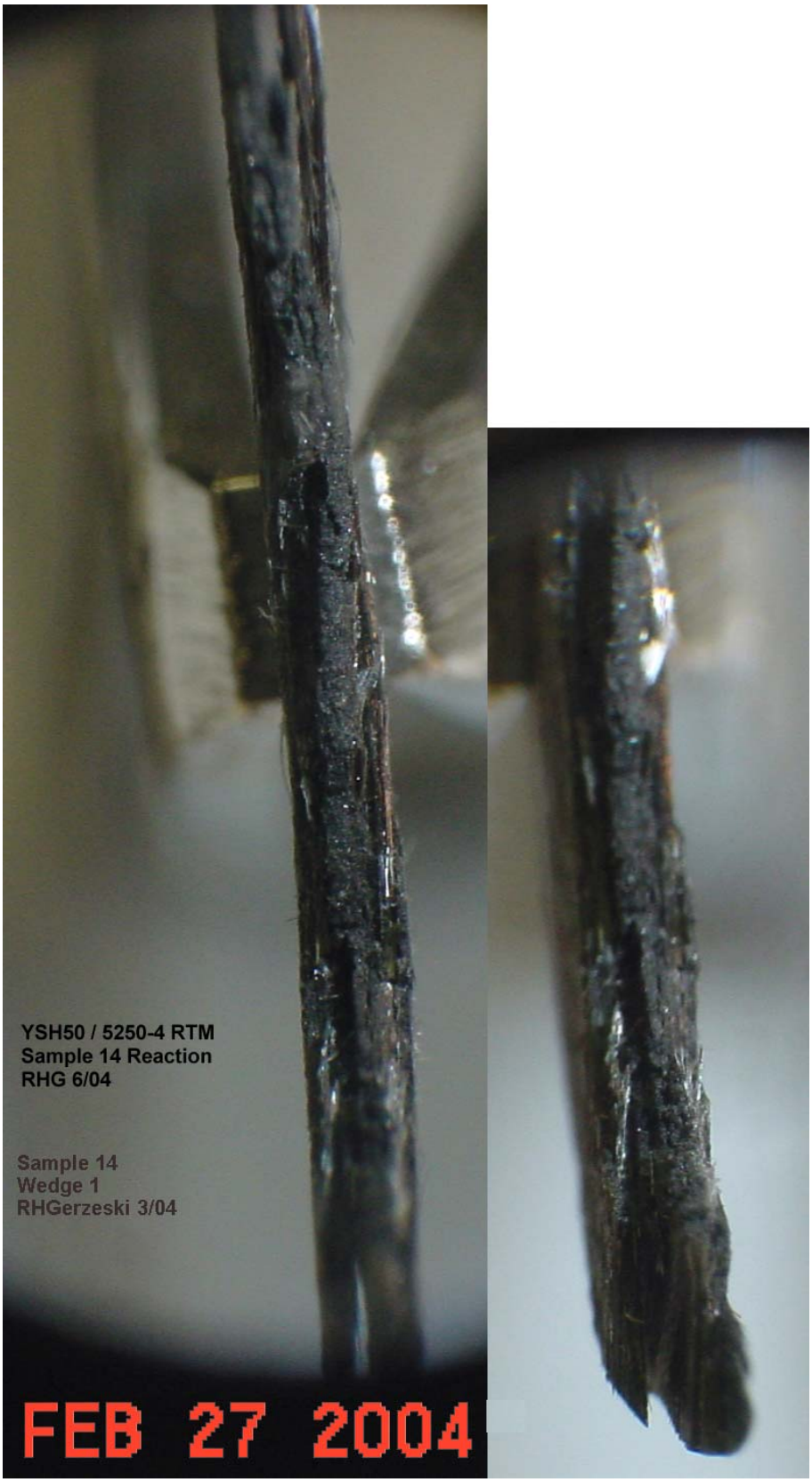


Figure 116-a, External To The Indenting Impacter Fracture Surfaces: Intense Heat: YSH50 / 5250-4 RTM D2512 Specimen: In LOX: Reaction Detected



Figure 116-b-i, External To The Indenting Impacter Fracture Surfaces: Intense Heat: YSH50 / 5250-4 RTM D2512 Specimen: In LOX: No Reaction Detected

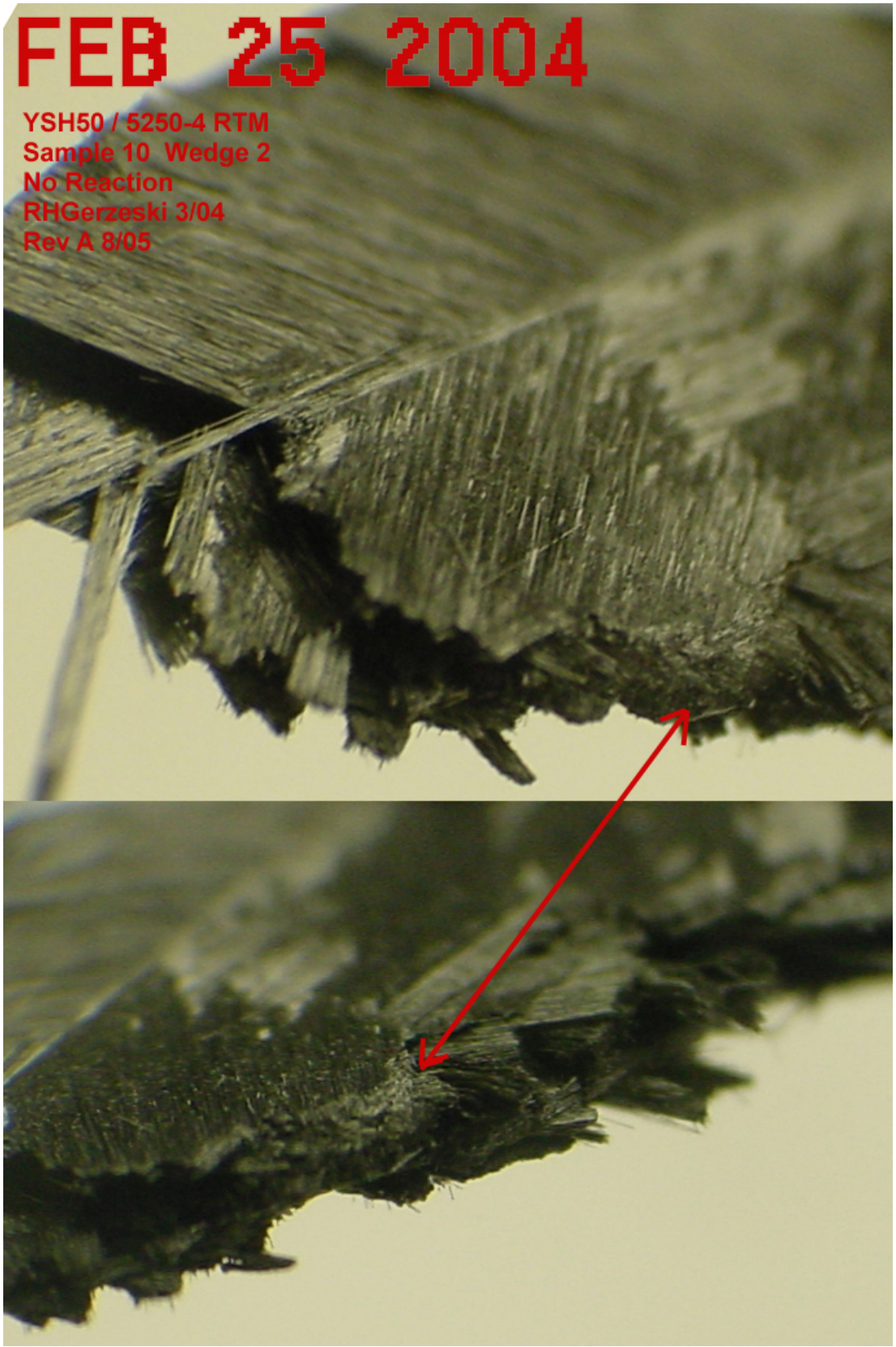


Figure 116-b-ii, External To The Indenting Impacter Fracture Surfaces: Intense Heat: YSH50 / 5250-4 RTM D2512 Specimen: In LOX: No Reaction Detected



Figure 117-a, External To The Indenting Impacter Fracture Surfaces: Intense Heat: YSH60 / 5250-4 RTM D2512 Specimen: In LOX: Reaction Detected

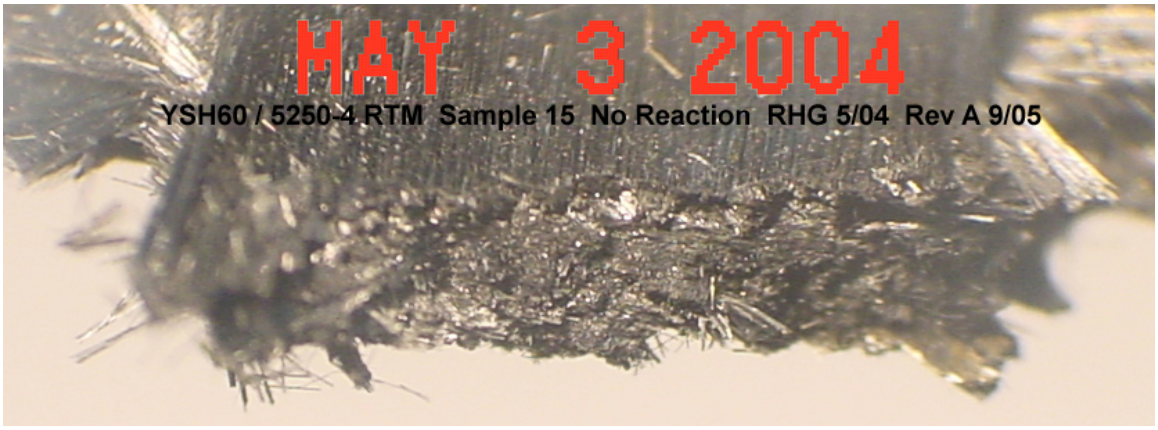


Figure 117-b, External To The Indenting Impacter Fracture Surfaces: Intense Heat: YSH60 / 5250-4 RTM D2512 Specimen: In LOX: No Reaction Detected



Figure 117-c, External To The Indenting Impacter Fracture Surfaces: Intense Heat: YSH60 / 5250-4 RTM D2512 Specimen: In LN2

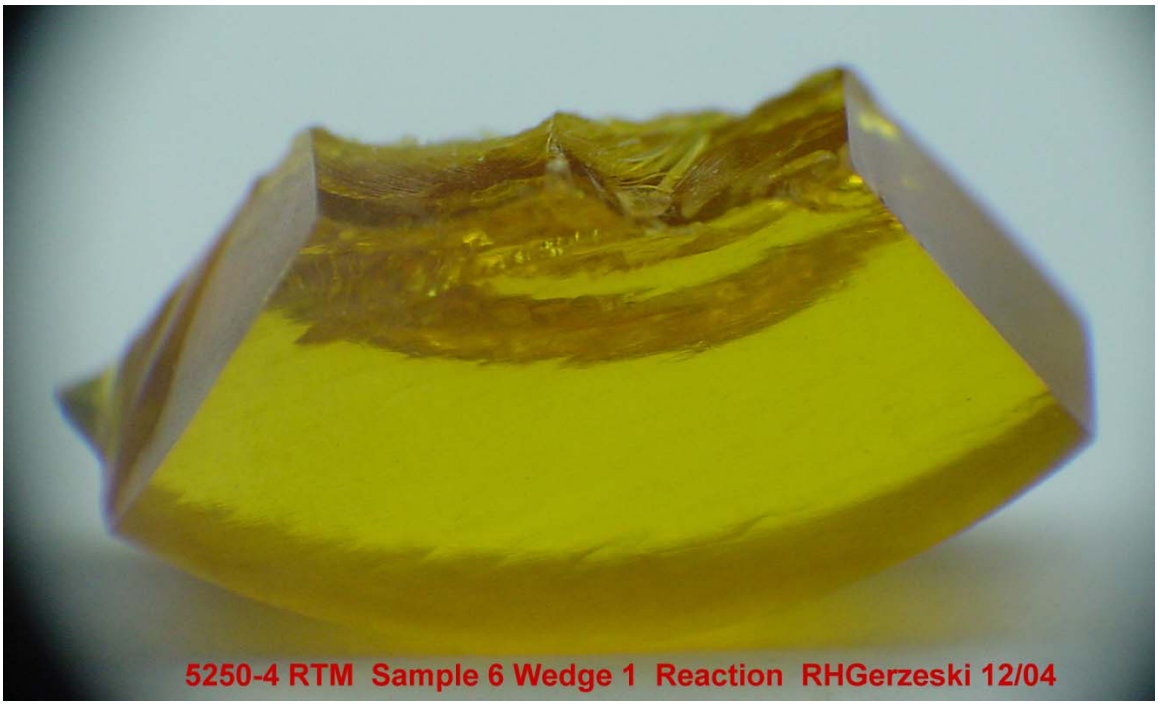


Figure 118-a-i, External To The Indenting Impacter Fracture Surfaces: Tensile Hoop Failure: 5250-4 RTM D2512 Specimen: In LOX: Reaction Detected



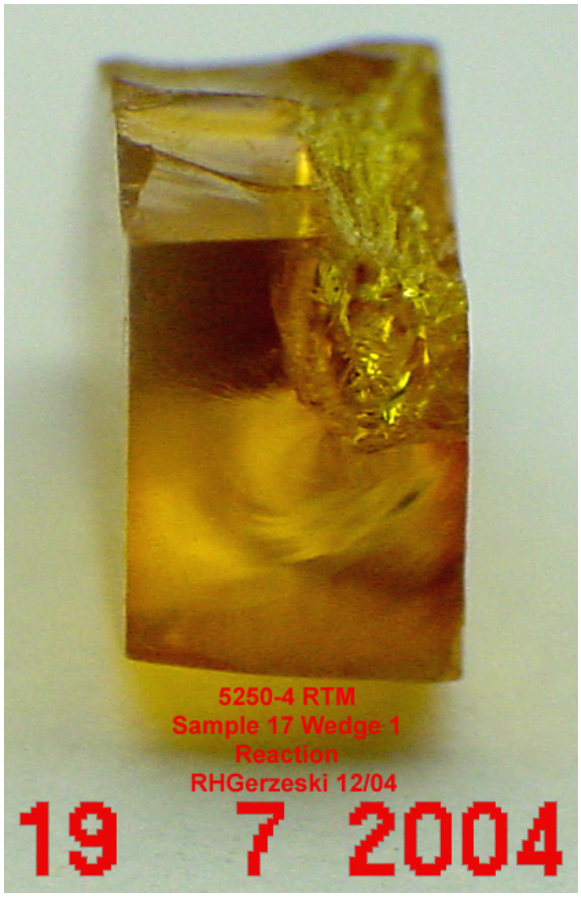


Figure 118-a-ii and iii, External To The Indenting Impacter Fracture Surfaces: Tensile Hoop Failure: 5250-4 RTM D2512 Specimen: In LOX: Reaction Detected

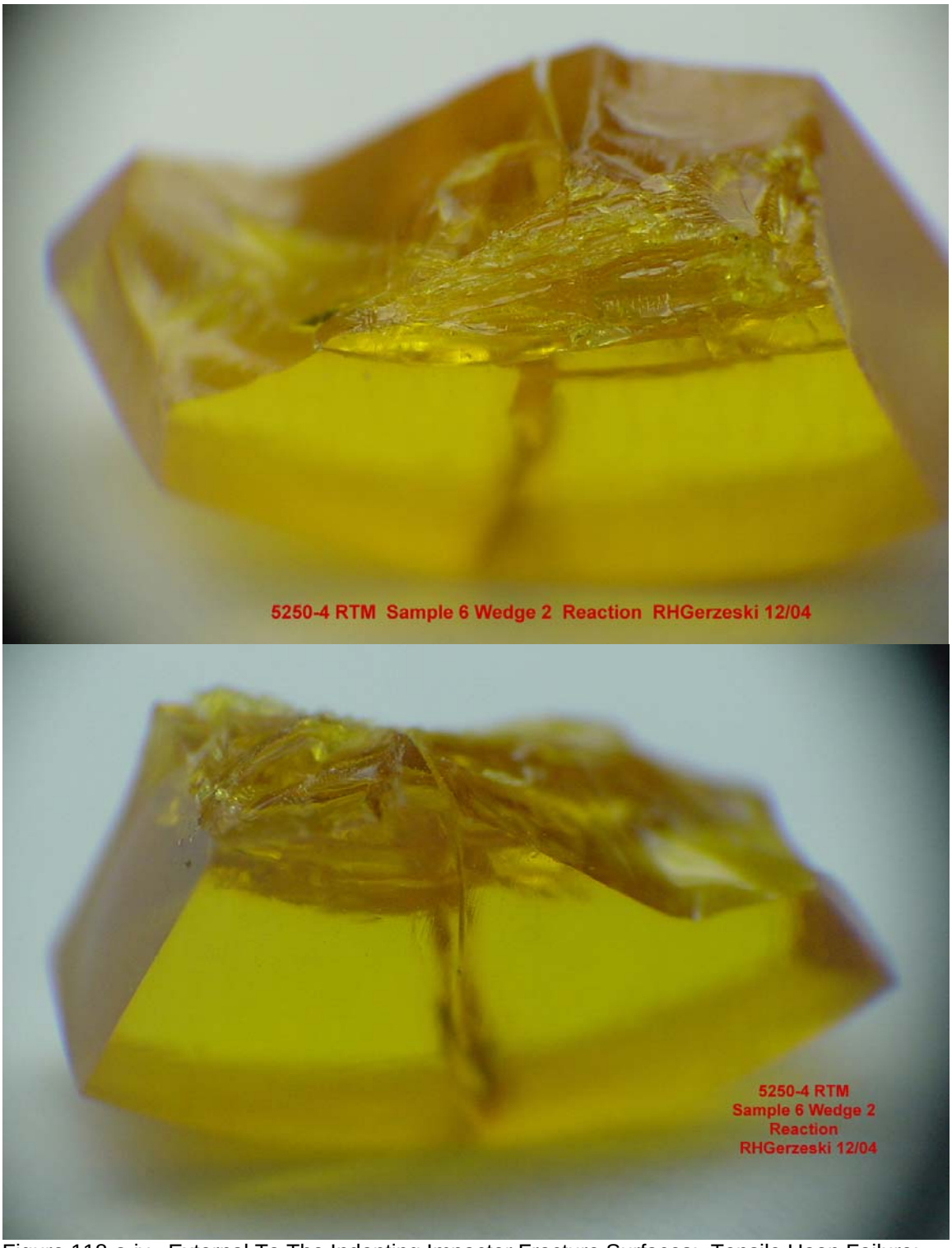


Figure 118-a-iv, External To The Indenting Impacter Fracture Surfaces: Tensile Hoop Failure: 5250-4 RTM D2512 Specimen: In LOX: Reaction Detected

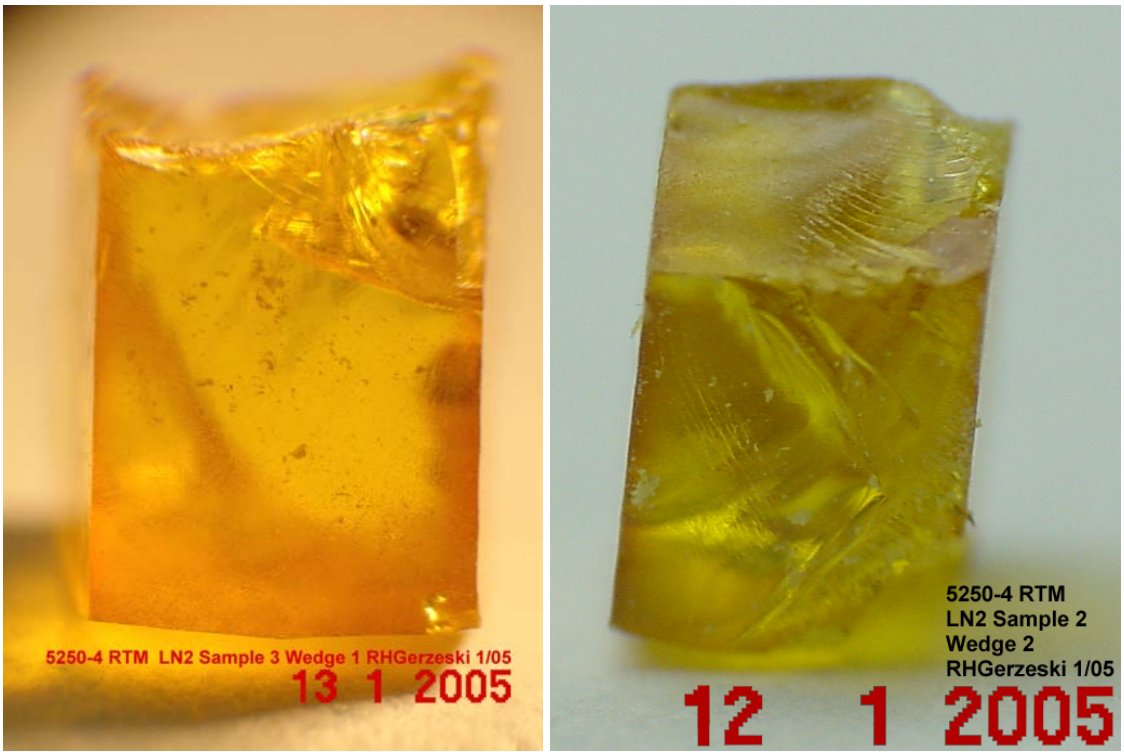


Figure 118-c-i and ii External To The Indenting Impacter Fracture Surfaces: Tensile Hoop Failure: 5250-4 RTM D2512 Specimen: In LN2



Figure 118-c-iii, External To The Indenting Impacter Fracture Surfaces: Tensile Hoop Failure: 5250-4 RTM D2512 Specimen: In LN2



Figure 119-a-i, External To The Indenting Impacter Fracture Surfaces: Tensile Hoop Failure: T650-35 / 5250-4 RTM D2512 Specimen: In LOX: Reaction Detected



Figure 119-a-ii, External To The Indenting Impacter Fracture Surfaces: Tensile Hoop Failure: T650-35 / 5250-4 RTM D2512 Specimen: In LOX: Reaction Detected



Figure 119-a-iii, External To The Indenting Impacter Fracture Surfaces: Tensile Hoop Failure: T650-35 / 5250-4 RTM D2512 Specimen: In LOX: Reaction Detected



Figure 119-a-iv, External To The Indenting Impacter Fracture Surfaces: Tensile Hoop Failure: T650-35 / 5250-4 RTM D2512 Specimen: In LOX: Reaction Detected



Figure 119-b-i, External To The Indenting Impacter Fracture Surfaces: Tensile Hoop Failure: T650-35 / 5250-4 RTM D2512 Specimen: In LOX: No Reaction Detected



Figure 119-b-ii, External To The Indenting Impacter Fracture Surfaces: Tensile Hoop Failure: T650-35 / 5250-4 RTM D2512 Specimen: In LOX: No Reaction Detected



Figure 119-b-iii, External To The Indenting Impacter Fracture Surfaces: Tensile Hoop Failure: T650-35 / 5250-4 RTM D2512 Specimen: In LOX: No Reaction Detected



Figure 119-c-i, External To The Indenting Impacter Fracture Surfaces: Tensile Hoop Failure: T650-35 / 5250-4 RTM D2512 Specimen: In LN2



Figure 119-c-ii, External To The Indenting Impacter Fracture Surfaces: Tensile Hoop Failure: T650-35 / 5250-4 RTM D2512 Specimen: In LN2



Figure 119-c-iii, External To The Indenting Impacter Fracture Surfaces: Tensile Hoop Failure: T650-35 / 5250-4 RTM D2512 Specimen: In LN2



Figure 120-a, External To The Indenting Impacter Fracture Surfaces: Tensile Hoop Failure: YSH50 / 5250-4 RTM D2512 Specimen: In LOX: Reaction Detected

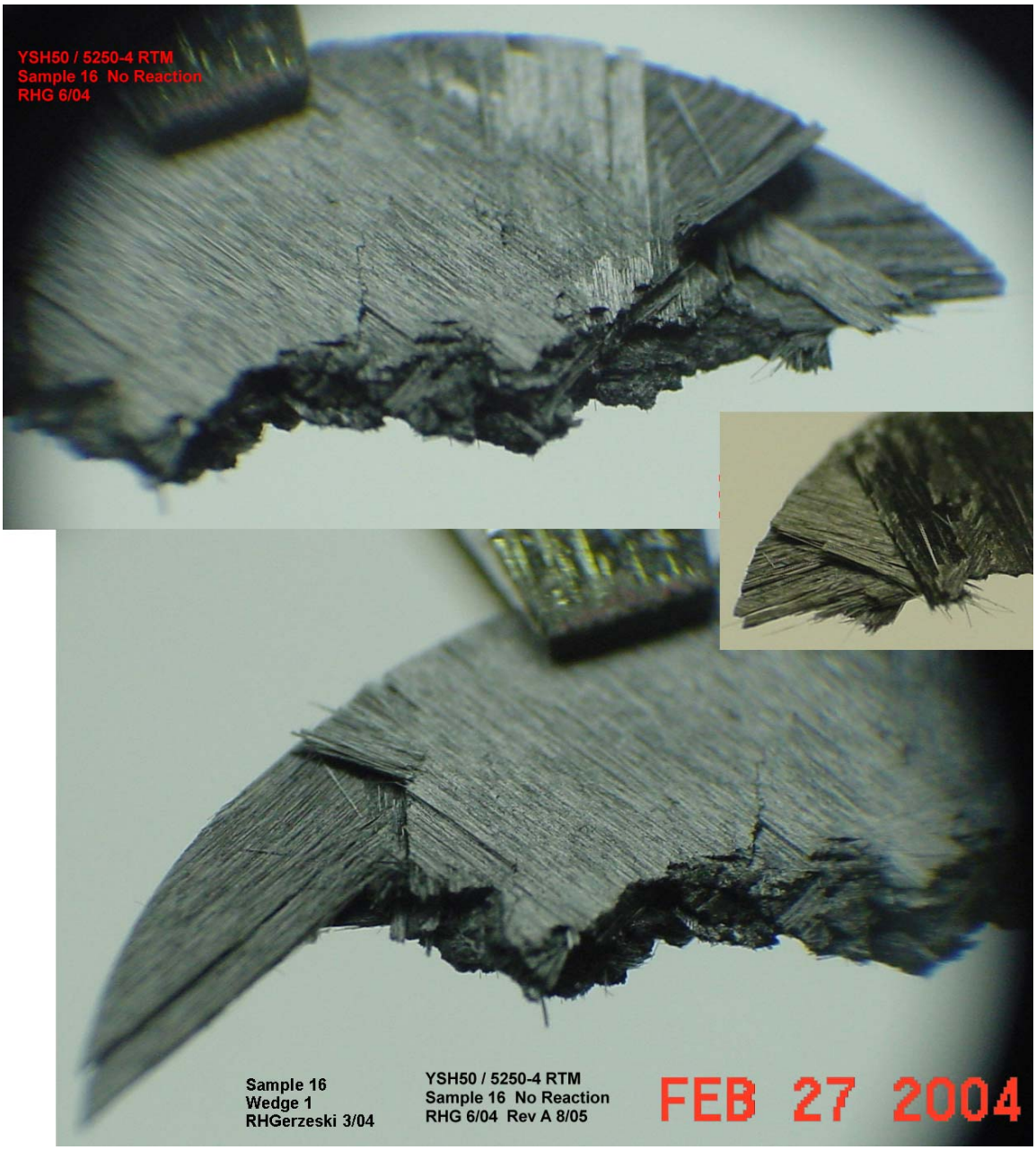


Figure 120-b-i, External To The Indenting Impacter Fracture Surfaces: Tensile Hoop Failure: YSH50 / 5250-4 RTM D2512 Specimen: In LOX: No Reaction Detected

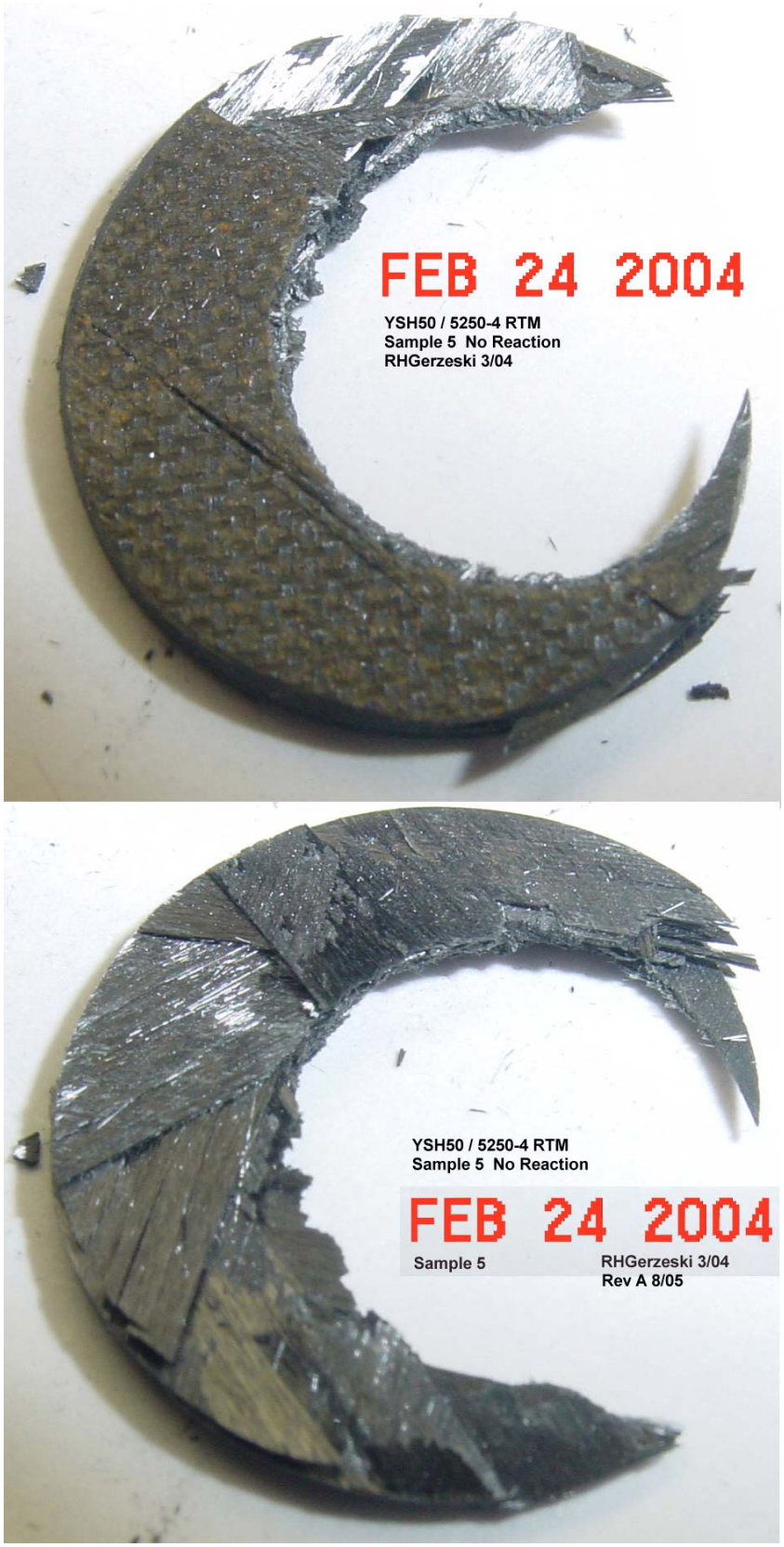


Figure 120-b-ii, External To The Indenting Impacter Fracture Surfaces: Tensile Hoop Failure: YSH50 / 5250-4 RTM D2512 Specimen: In LOX: No Reaction Detected

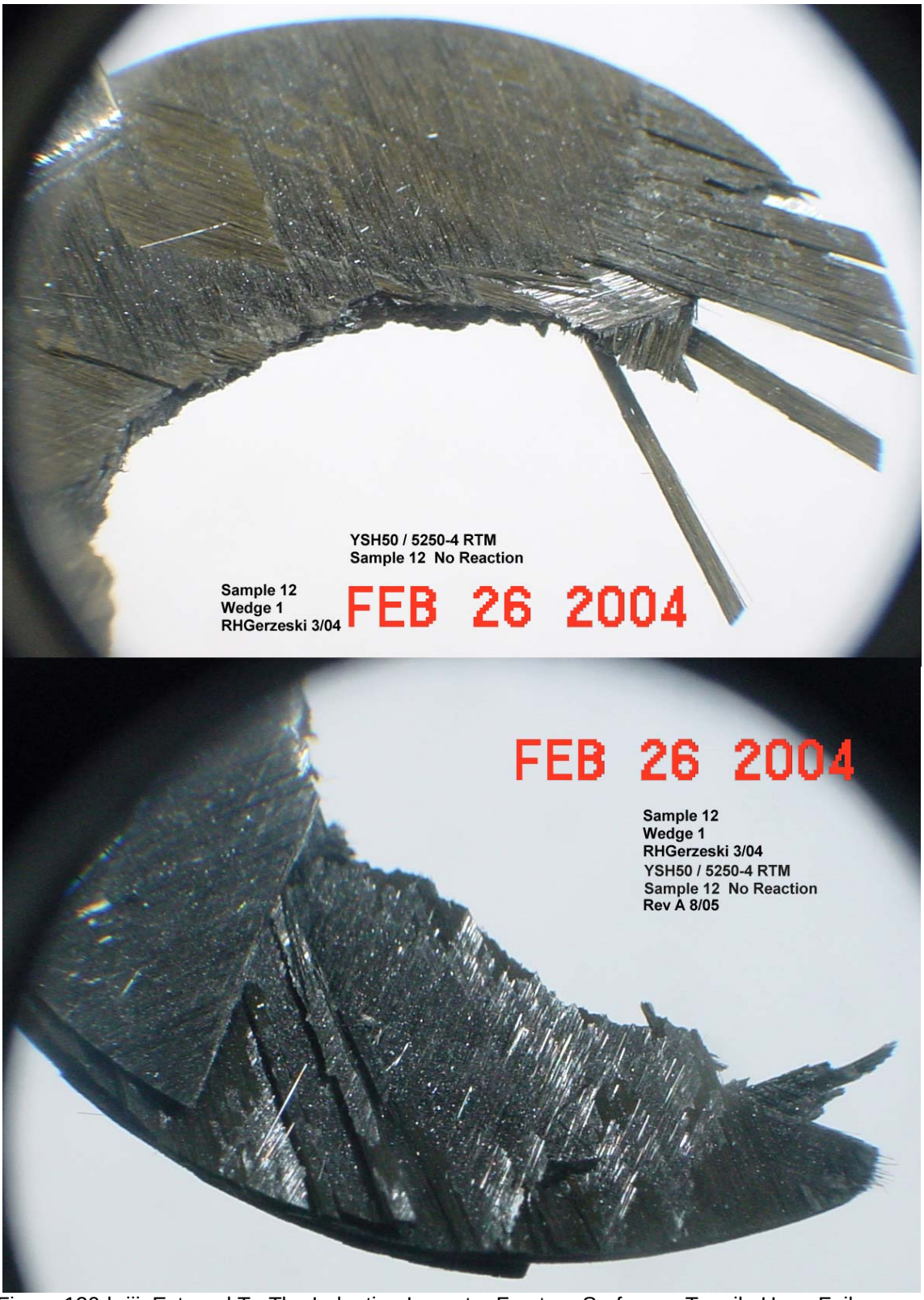


Figure 120-b-iii, External To The Indenting Impacter Fracture Surfaces: Tensile Hoop Failure: YSH50 / 5250-4 RTM D2512 Specimen: In LOX: No Reaction Detected

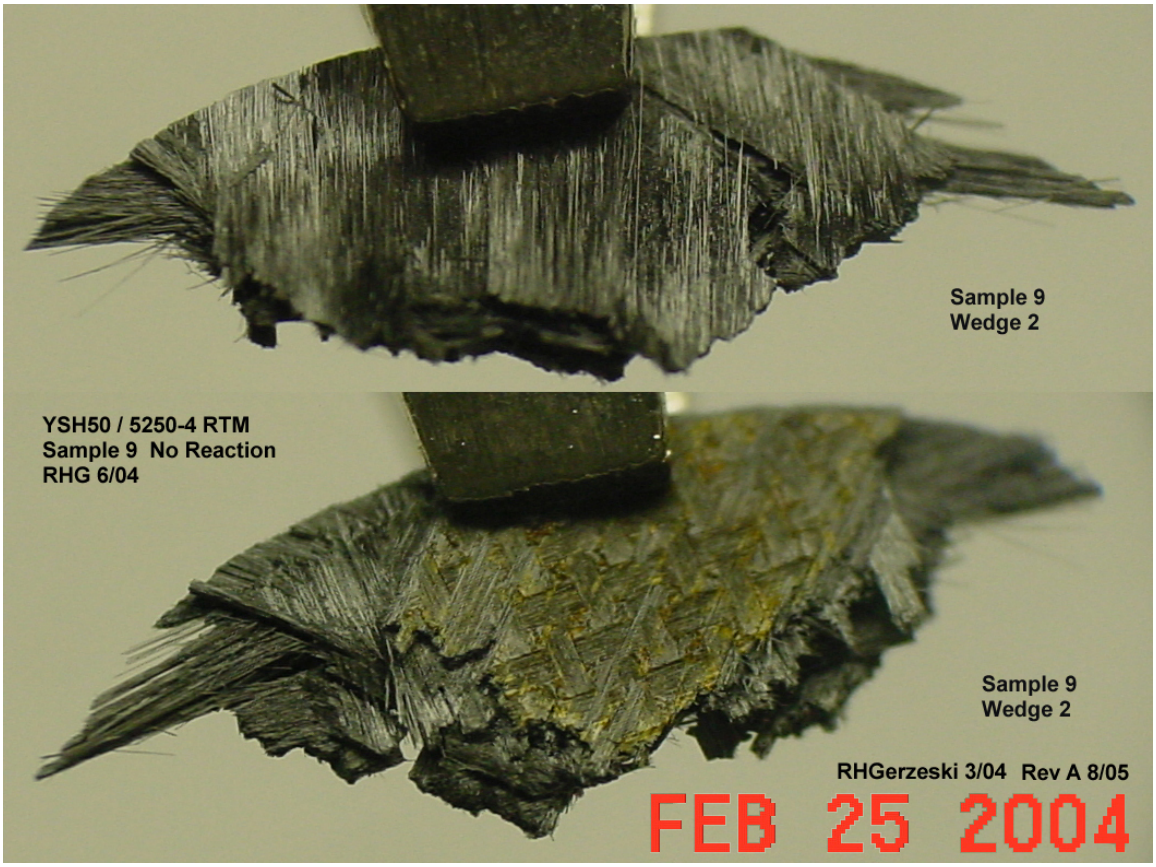


Figure 120-b-iv, External To The Indenting Impacter Fracture Surfaces: Tensile Hoop Failure: YSH50 / 5250-4 RTM D2512 Specimen: In LOX: No Reaction Detected

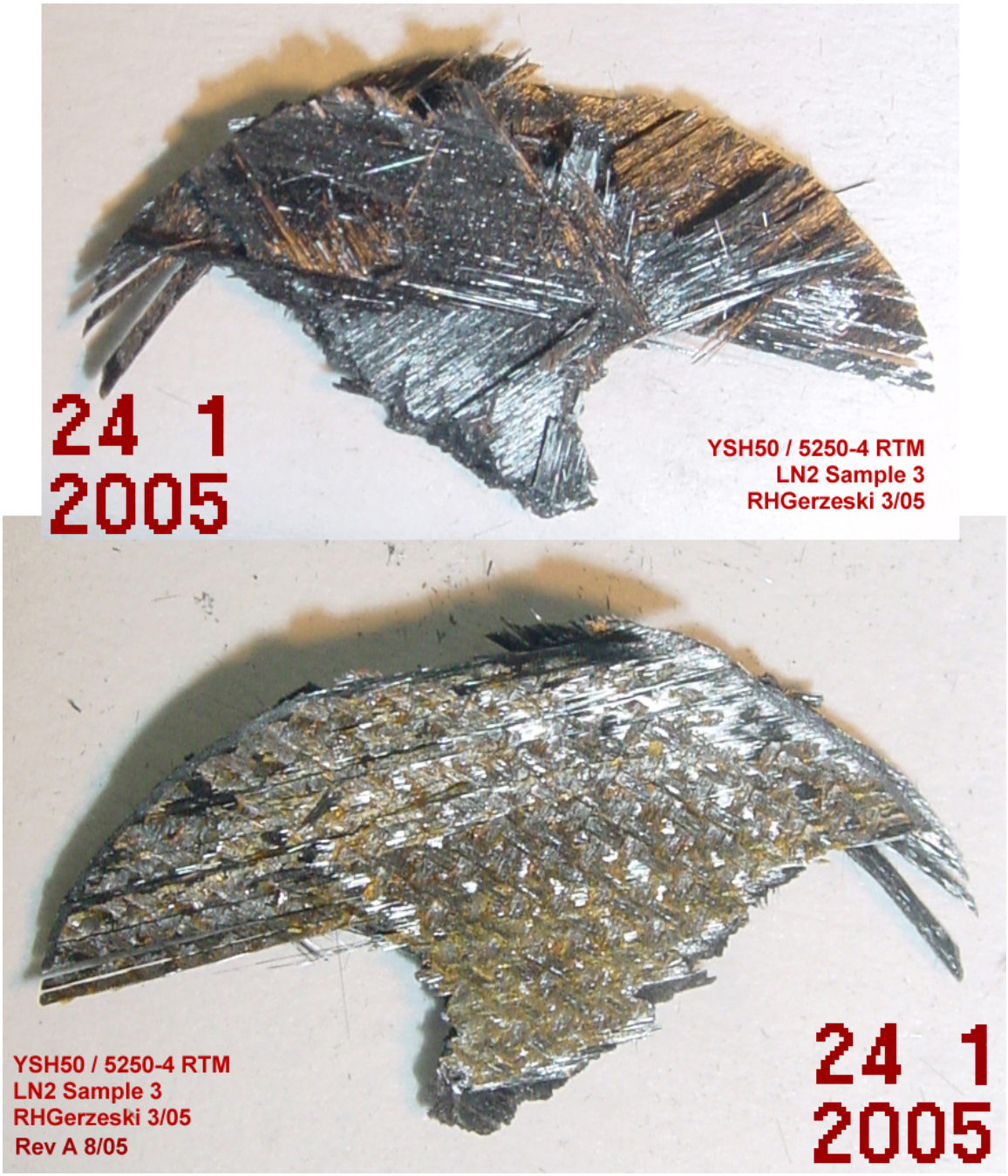


Figure 120-c-i, External To The Indenting Impacter Fracture Surfaces: Tensile Hoop Failure: YSH50 / 5250-4 RTM D2512 Specimen: In LN2

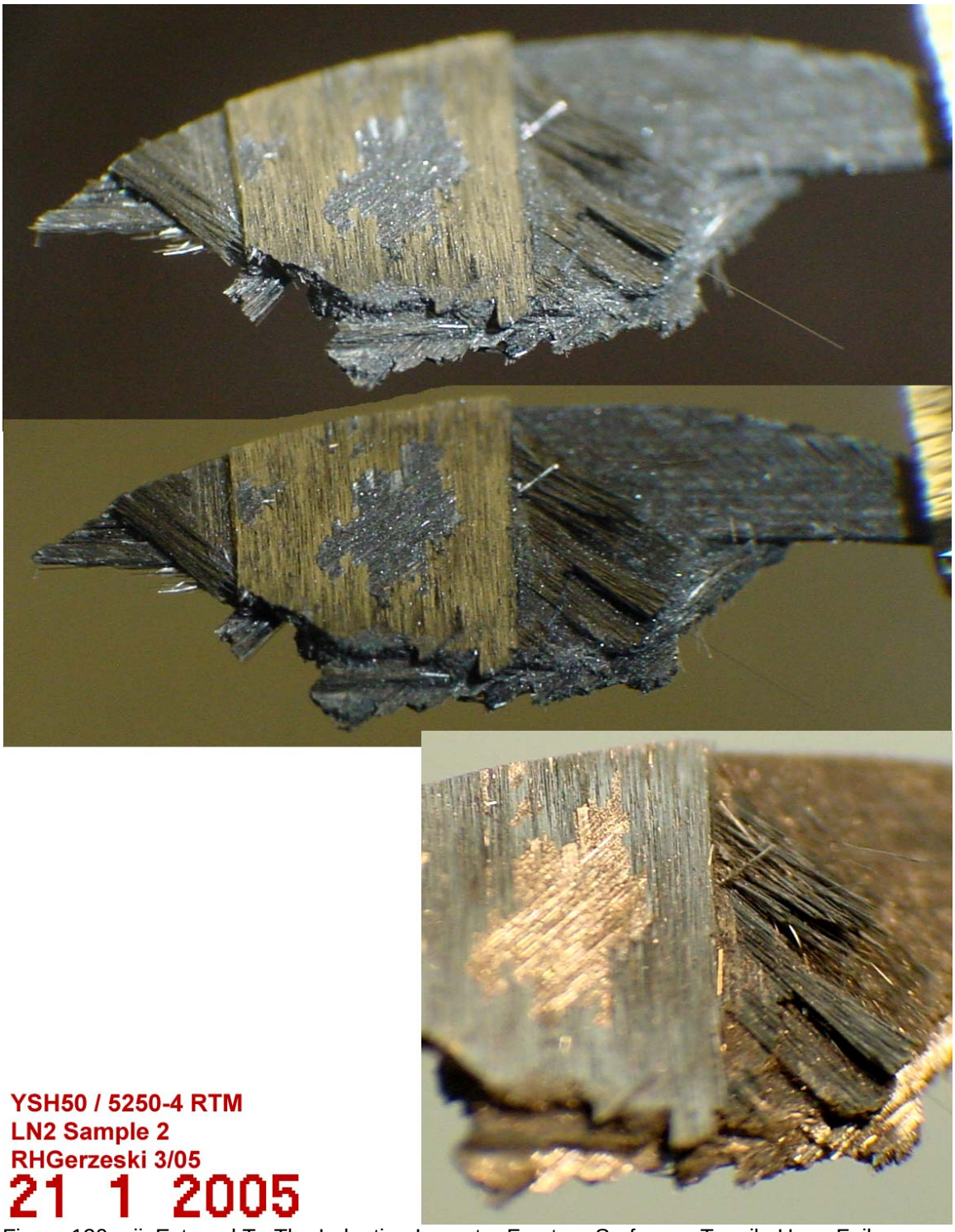


Figure 120-c-ii, External To The Indenting Impacter Fracture Surfaces: Tensile Hoop Failure: YSH50 / 5250-4 RTM D2512 Specimen: In LN2

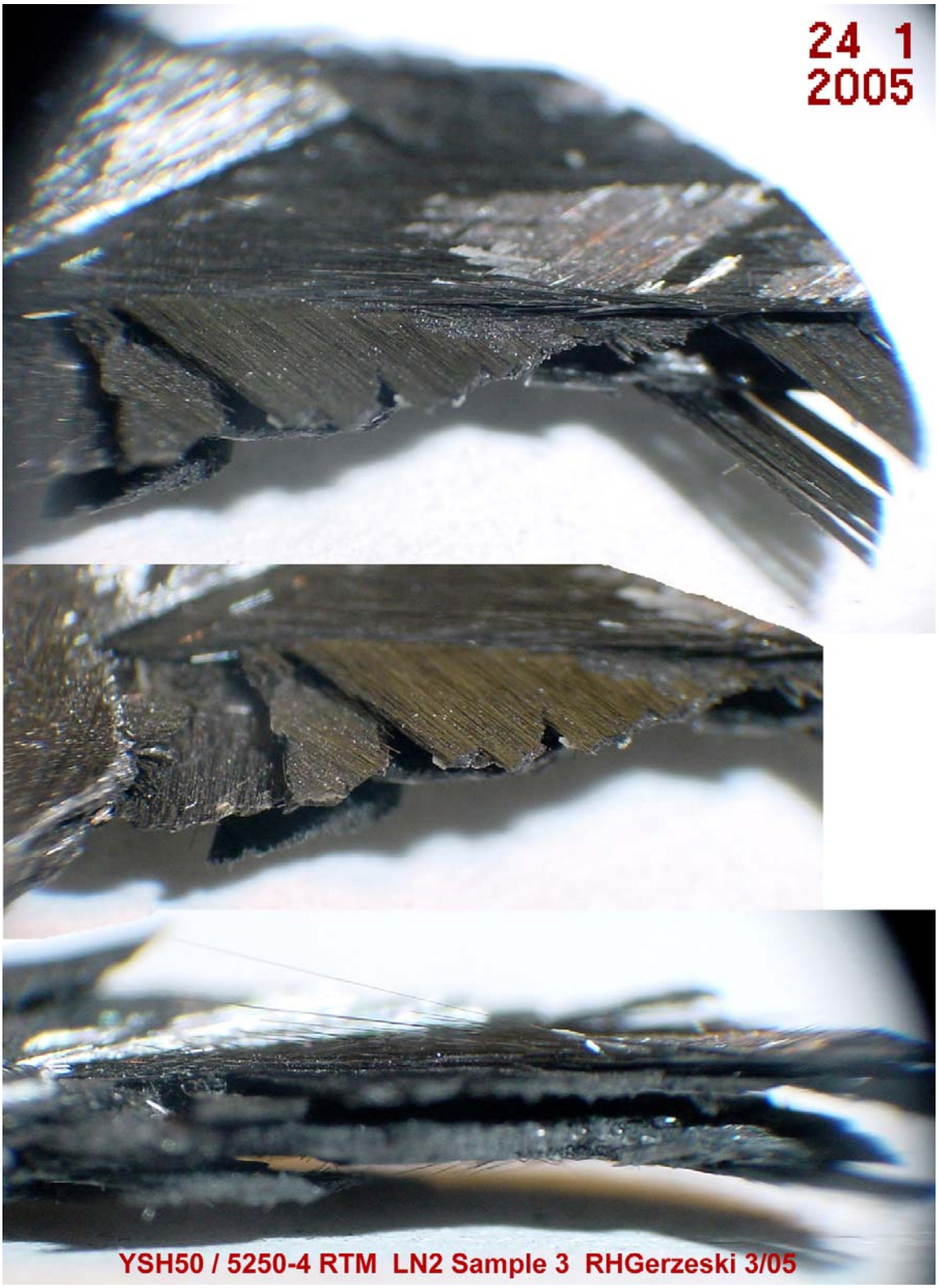


Figure 120-c-iii, External To The Indenting Impacter Fracture Surfaces: Tensile Hoop Failure: YSH50 / 5250-4 RTM D2512 Specimen: In LN2



Figure 121-a-i, External To The Indenting Impacter Fracture Surfaces: Tensile Hoop Failure: YSH60 / 5250-4 RTM D2512 Specimen: In LOX: Reaction Detected



Figure 121-a-ii, External To The Indenting Impacter Fracture Surfaces: Tensile Hoop Failure: YSH60 / 5250-4 RTM D2512 Specimen: In LOX: Reaction Detected



Figure 121-a-iii, External To The Indenting Impacter Fracture Surfaces: Tensile Hoop Failure: YSH60 / 5250-4 RTM D2512 Specimen: In LOX: Reaction Detected



Figure 121-b-i, External To The Indenting Impacter Fracture Surfaces: Tensile Hoop Failure: YSH60 / 5250-4 RTM D2512 Specimen: In LOX: No Reaction Detected



Figure 121-b-ii, External To The Indenting Impacter Fracture Surfaces: Tensile Hoop Failure: YSH60 / 5250-4 RTM D2512 Specimen: In LOX: No Reaction Detected

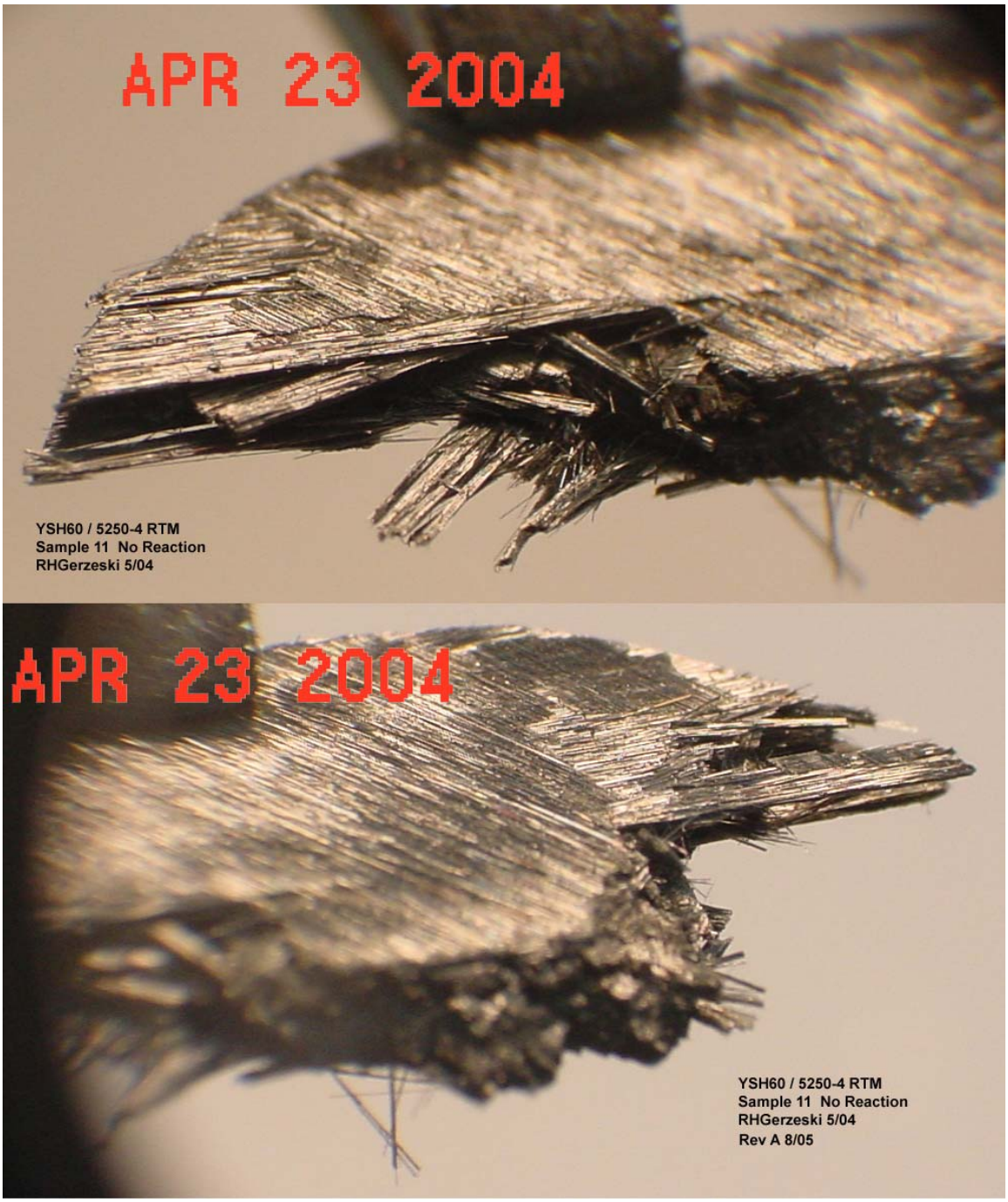


Figure 121-b-iii, External To The Indenting Impacter Fracture Surfaces: Tensile Hoop Failure: YSH60 / 5250-4 RTM D2512 Specimen: In LOX: No Reaction Detected

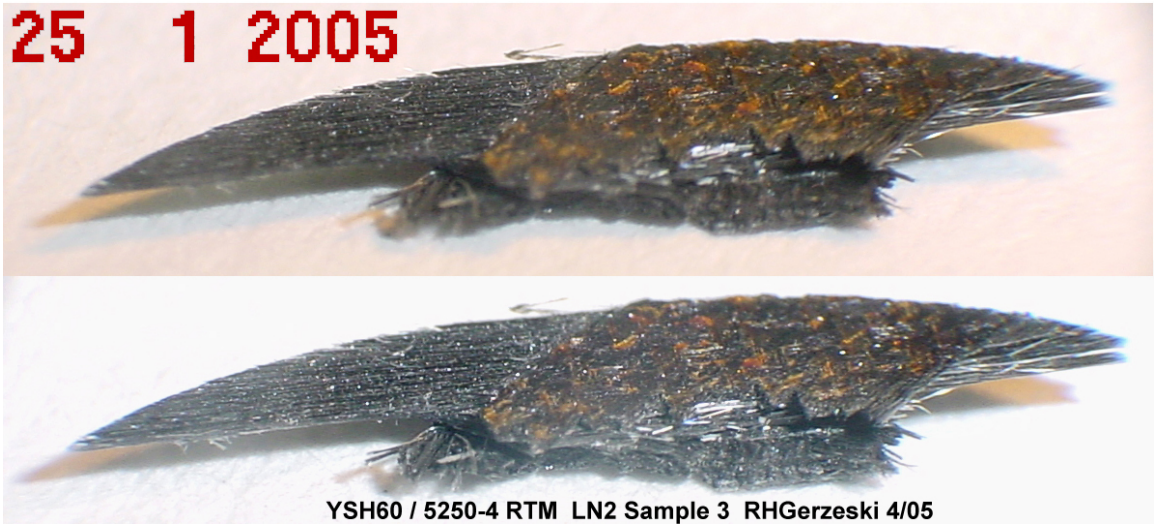


Figure 121-c-i, External To The Indenting Impacter Fracture Surfaces: Tensile Hoop Failure: YSH60 / 5250-4 RTM D2512 Specimen: In LN2

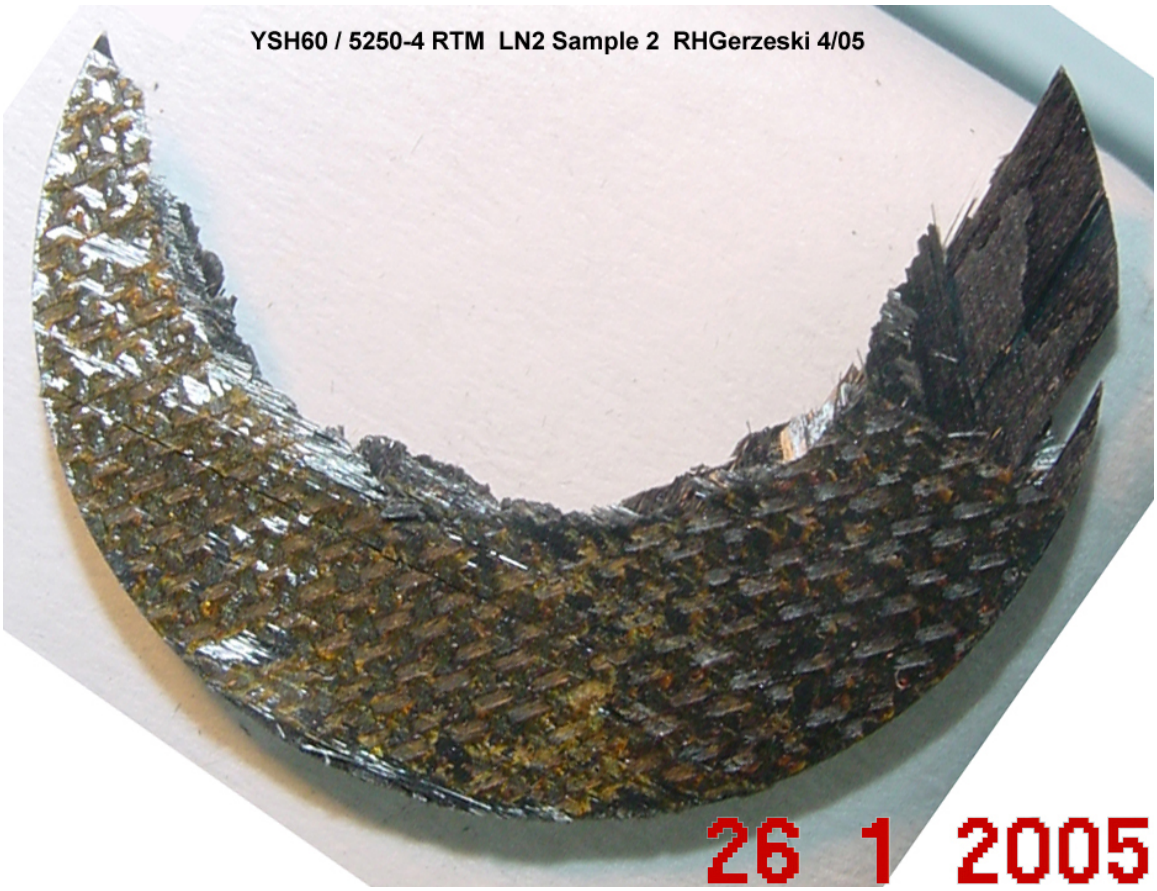


Figure 121-c-ii, External To The Indenting Impacter Fracture Surfaces: Tensile Hoop Failure: YSH60 / 5250-4 RTM D2512 Specimen: In LN2



Figure 121-c-iii, External To The Indenting Impacter Fracture Surfaces: Tensile Hoop Failure: YSH60 / 5250-4 RTM D2512 Specimen: In LN2

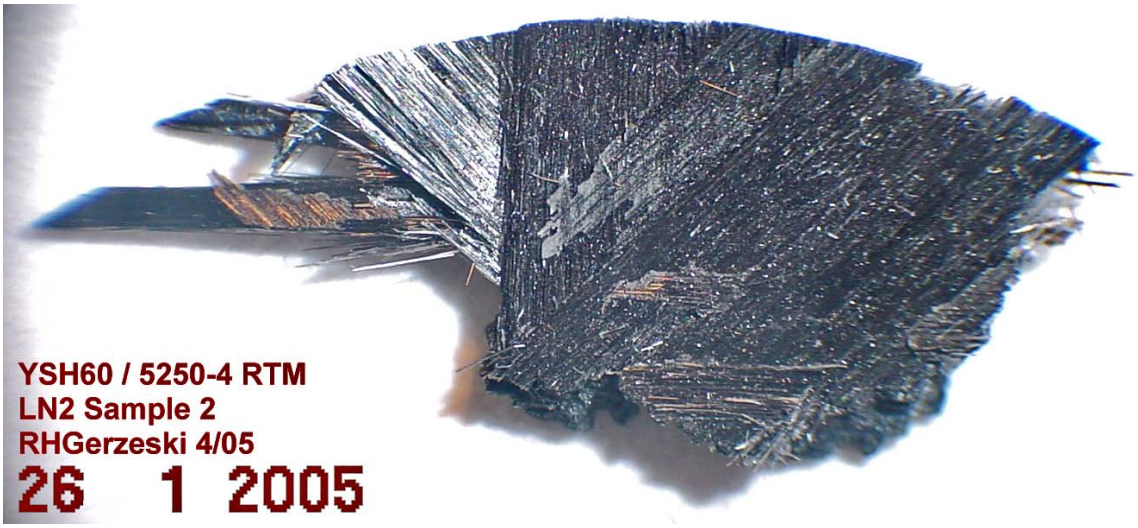


Figure 121-c-iv, External To The Indenting Impacter Fracture Surfaces: Tensile Hoop Failure: YSH60 / 5250-4 RTM D2512 Specimen: In LN2

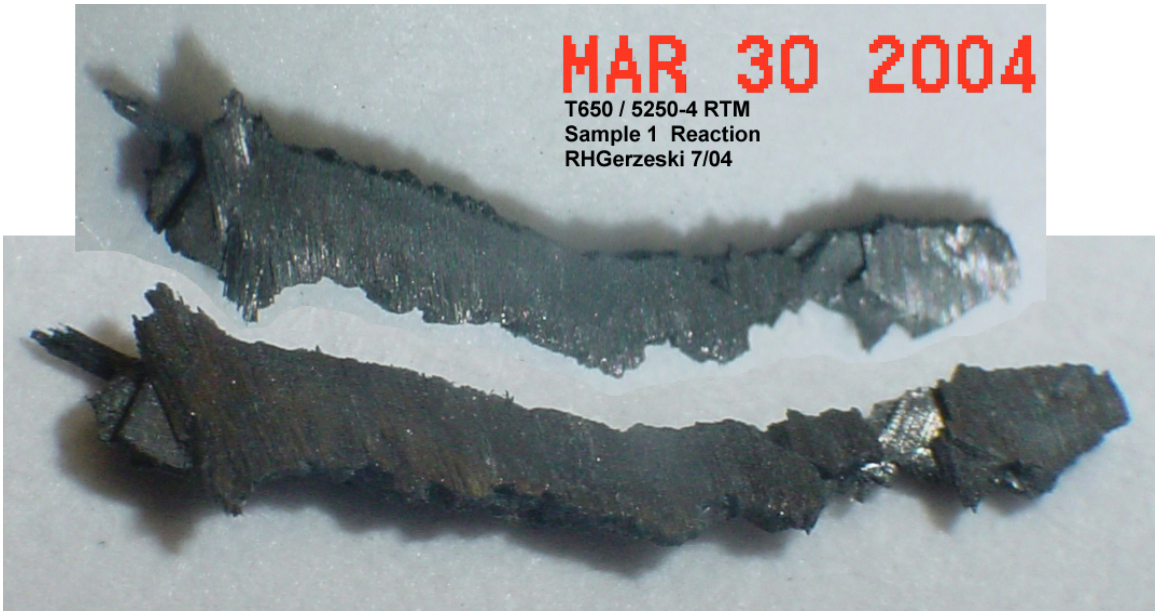


Figure 122-a-i, Internal To The Indenting Impacter Fracture Surfaces: Crescents And Arcs: T650-35 / 5250-4 RTM D2512 Specimen: In LOX: Reaction Detected



Figure 122-a-ii, Internal To The Indenting Impacter Fracture Surfaces: Crescents And Arcs: T650-35 / 5250-4 RTM D2512 Specimen: In LOX: Reaction Detected



Figure 122-a-iii, Internal To The Indenting Impacter Fracture Surfaces: Crescents And Arcs: T650-35 / 5250-4 RTM D2512 Specimen: In LOX: Reaction Detected

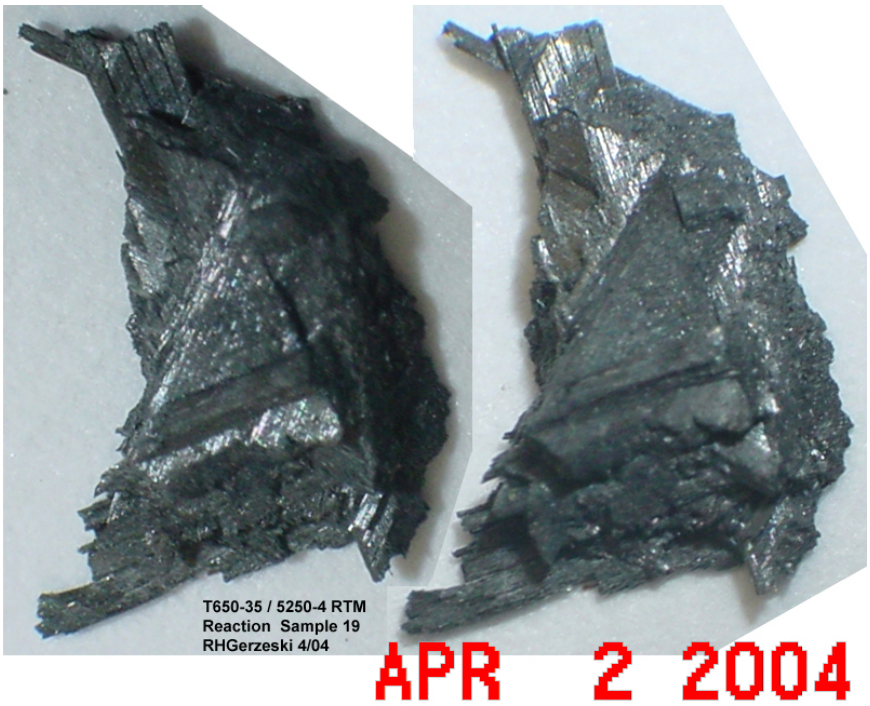


Figure 122-a-iv, Internal To The Indenting Impacter Fracture Surfaces: Crescents And Arcs: T650-35 / 5250-4 RTM D2512 Specimen: In LOX: Reaction Detected

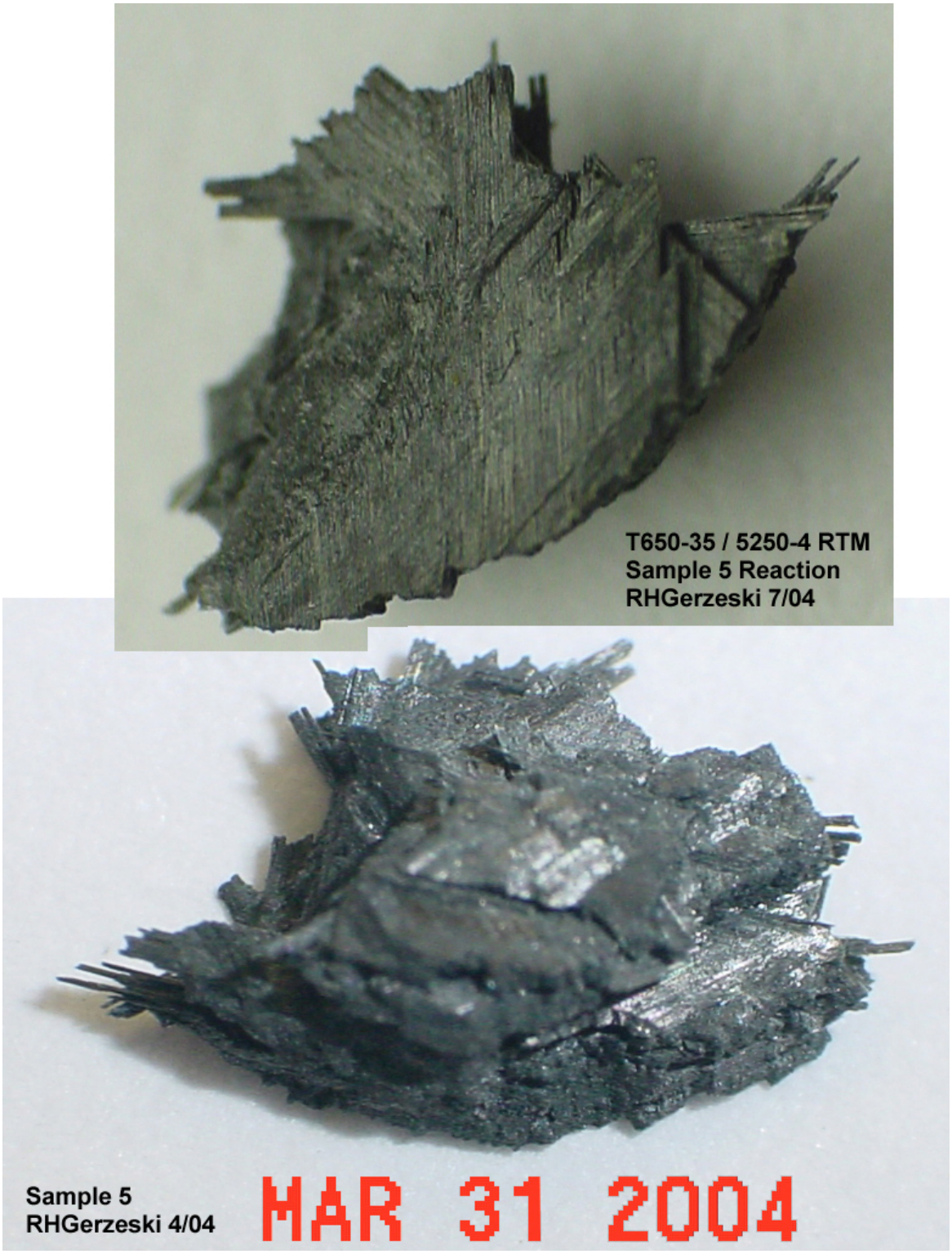


Figure 122-a-v, Internal To The Indenting Impacter Fracture Surfaces: Crescents And Arcs: T650-35 / 5250-4 RTM D2512 Specimen: In LOX: Reaction Detected



Figure 122-b-i, Internal To The Indenting Impacter Fracture Surfaces: Crescents And Arcs: T650-35 / 5250-4 RTM D2512 Specimen: In LOX: No Reaction Detected



Figure 122-b-ii, Internal To The Indenting Impacter Fracture Surfaces: Crescents And Arcs: T650-35 / 5250-4 RTM D2512 Specimen: In LOX: No Reaction Detected



Figure 122-b-iii, Internal To The Indenting Impacter Fracture Surfaces: Crescents And Arcs: T650-35 / 5250-4 RTM D2512 Specimen: In LOX: No Reaction Detected



Figure 122-c-i, Internal To The Indenting Impacter Fracture Surfaces: Crescents And Arcs: T650-35 / 5250-4 RTM D2512 Specimen: In LN2



Figure 122-c-ii, Internal To The Indenting Impacter Fracture Surfaces: Crescents And Arcs: T650-35 / 5250-4 RTM D2512 Specimen: In LN2



Figure 122-c-iii, Internal To The Indenting Impacter Fracture Surfaces: Crescents And Arcs: T650-35 / 5250-4 RTM D2512 Specimen: In LN2

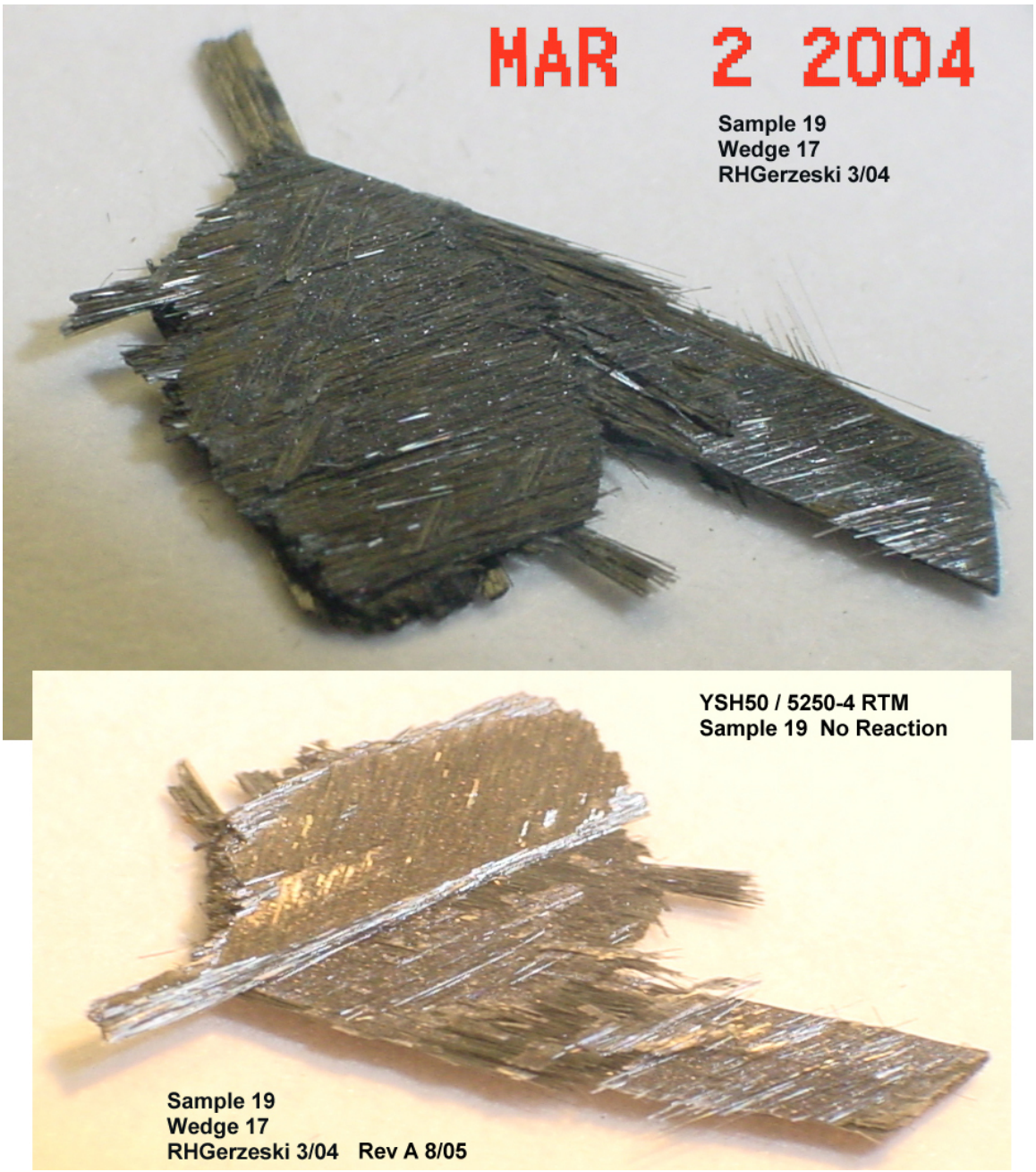


Figure 123-a-i, Internal To The Indenting Impacter Fracture Surfaces: Crescents And Arcs: YSH50 / 5250-4 RTM D2512 Specimen: In LOX: No Reaction Detected



Figure 123-a-ii, Internal To The Indenting Impacter Fracture Surfaces: Crescents And Arcs: YSH50 / 5250-4 RTM D2512 Specimen: In LOX: No Reaction Detected



Figure 123-a-iii, Internal To The Indenting Impacter Fracture Surfaces: Crescents And Arcs: YSH50 / 5250-4 RTM D2512 Specimen: In LOX: No Reaction Detected



Figure 123-a-iv, Internal To The Indenting Impacter Fracture Surfaces: Crescents And Arcs: YSH50 / 5250-4 RTM D2512 Specimen: In LOX: No Reaction Detected



Figure 123-b-i, Internal To The Indenting Impacter Fracture Surfaces: Crescents And Arcs: YSH50 / 5250-4 RTM D2512 Specimen: In LN2



Figure 123-b-ii, Internal To The Indenting Impacter Fracture Surfaces: Crescents And Arcs: YSH50 / 5250-4 RTM D2512 Specimen: In LN2

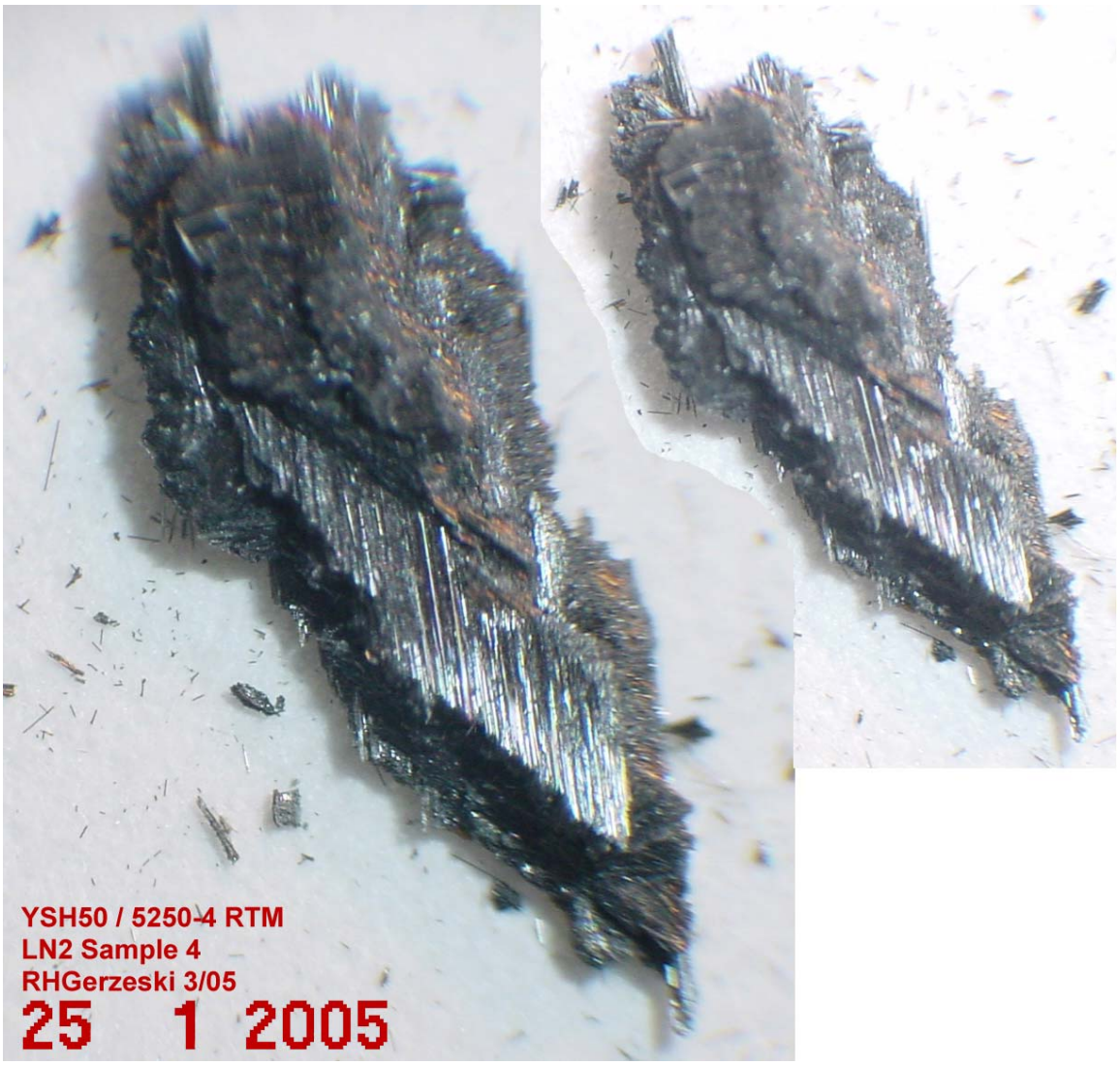


Figure 123-b-iii, Internal To The Indenting Impacter Fracture Surfaces: Crescents And Arcs: YSH50 / 5250-4 RTM D2512 Specimen: In LN2



Figure 124-a-i, Internal To The Indenting Impacter Fracture Surfaces: Crescents And Arcs: YSH60 / 5250-4 RTM D2512 Specimen: In LOX: Reaction Detected

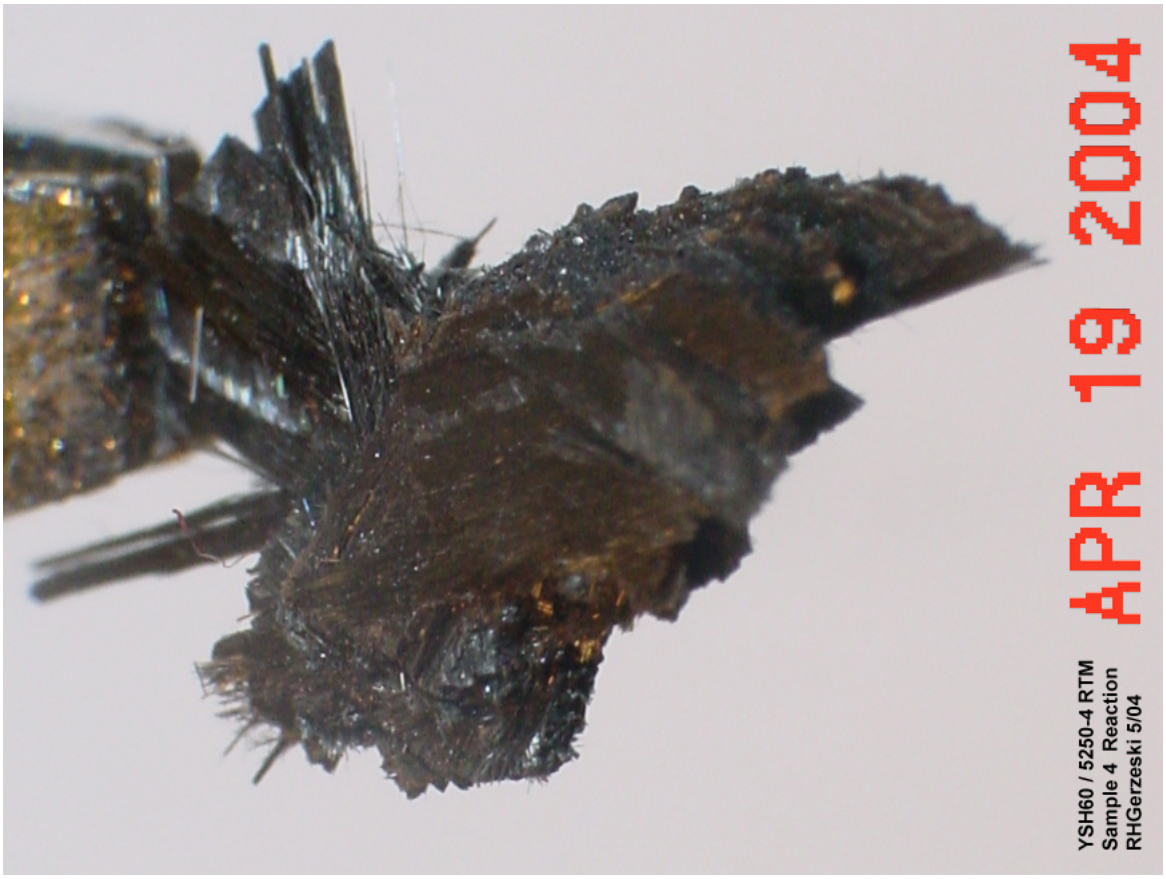


Figure 124-a-ii, Internal To The Indenting Impacter Fracture Surfaces: Crescents And Arcs: YSH60 / 5250-4 RTM D2512 Specimen: In LOX: Reaction Detected



Figure 124-a-iii, Internal To The Indenting Impacter Fracture Surfaces: Crescents And Arcs: YSH60 / 5250-4 RTM D2512 Specimen: In LOX: Reaction Detected

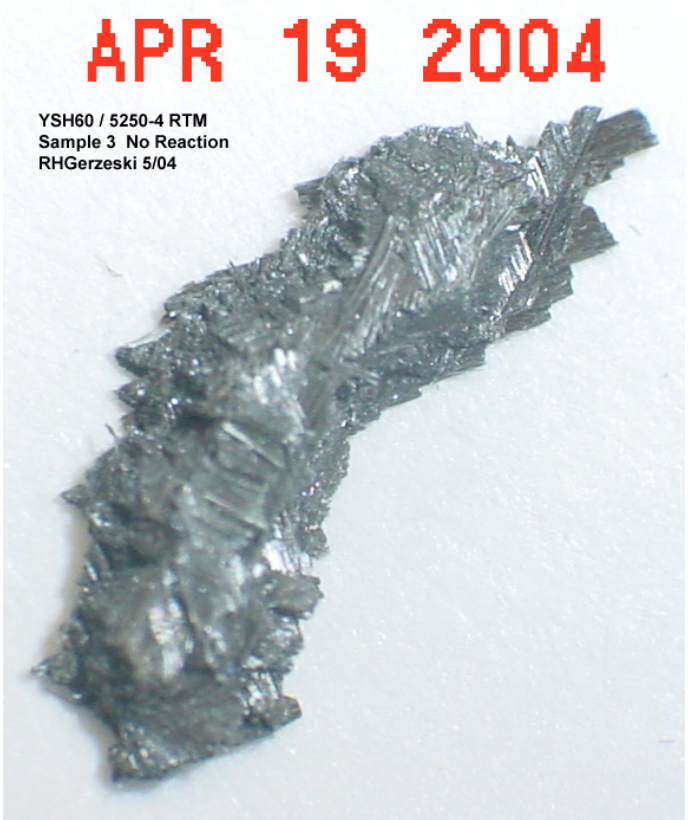


Figure 124-b-i, Internal To The Indenting Impacter Fracture Surfaces: Crescents And Arcs: YSH60 / 5250-4 RTM D2512 Specimen: In LOX: No Reaction Detected



Figure 124-b-ii, Internal To The Indenting Impacter Fracture Surfaces: Crescents And Arcs: YSH60 / 5250-4 RTM D2512 Specimen: In LOX: No Reaction Detected



Figure 124-b-iii, Internal To The Indenting Impacter Fracture Surfaces: Crescents And Arcs: YSH60 / 5250-4 RTM D2512 Specimen: In LOX: No Reaction Detected



Figure 124-b-iv, Internal To The Indenting Impacter Fracture Surfaces: Crescents And Arcs: YSH60 / 5250-4 RTM D2512 Specimen: In LOX: No Reaction Detected



Figure 124-c-i, Internal To The Indenting Impacter Fracture Surfaces: Crescents And Arcs: YSH60 / 5250-4 RTM D2512 Specimen: In LN2



Figure 124-c-ii, Internal To The Indenting Impacter Fracture Surfaces: Crescents And Arcs: YSH60 / 5250-4 RTM D2512 Specimen: In LN2



Figure 124-c-iii, Internal To The Indenting Impacter Fracture Surfaces: Crescents And Arcs: YSH60 / 5250-4 RTM D2512 Specimen: In LN2



Figure 125-a-i, Internal To The Indenting Impacter Fracture Surfaces: Knobs / Conchoidal Failure: T650-35 / 5250-4 RTM D2512 Specimen: In LOX: Reaction Detected

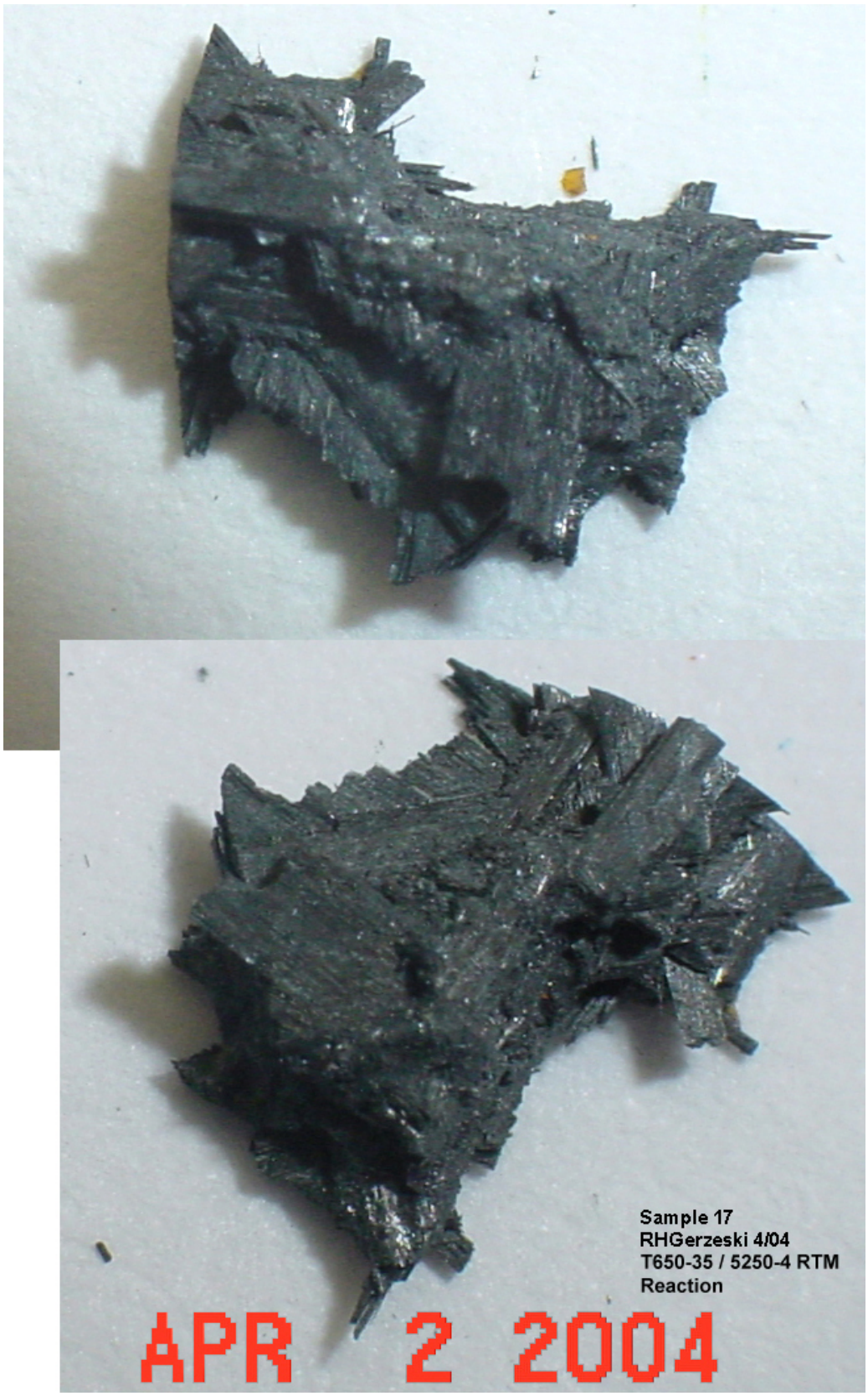


Figure 125-a-ii, Internal To The Indenting Impacter Fracture Surfaces: Knobs / Conchoidal Failure: T650-35 / 5250-4 RTM D2512 Specimen: In LOX: Reaction Detected



Figure 125-a-iii, Internal To The Indenting Impacter Fracture Surfaces: Knobs / Conchoidal Failure: T650-35 / 5250-4 RTM D2512 Specimen: In LOX: Reaction Detected



Figure 125-b-i, Internal To The Indenting Impacter Fracture Surfaces: Knobs / Conchoidal Failure: T650-35 / 5250-4 RTM D2512 Specimen: In LOX: No Reaction Detected



Figure 125-b-ii, Internal To The Indenting Impacter Fracture Surfaces: Knobs / Conchoidal Failure: T650-35 / 5250-4 RTM D2512 Specimen: In LOX: No Reaction Detected



Figure 125-c-i, Internal To The Indenting Impacter Fracture Surfaces: Knobs / Conchoidal Failure: T650-35 / 5250-4 RTM D2512 Specimen: In LN2



Figure 125-c-ii, Internal To The Indenting Impacter Fracture Surfaces: Knobs / Conchoidal Failure: T650-35 / 5250-4 RTM D2512 Specimen: In LN2



Figure 125-c-iii, Internal To The Indenting Impacter Fracture Surfaces: Knobs / Conchoidal Failure: T650-35 / 5250-4 RTM D2512 Specimen: In LN2



Figure 126-a-i, Internal To The Indenting Impacter Fracture Surfaces: Knobs / Conchoidal Failure: YSH50 / 5250-4 RTM D2512 Specimen: In LOX: No Reaction Detected



Figure 126-a-ii, Internal To The Indenting Impacter Fracture Surfaces: Knobs / Conchoidal Failure: YSH50 / 5250-4 RTM D2512 Specimen: In LOX: No Reaction Detected



Figure 126-a-iii, Internal To The Indenting Impacter Fracture Surfaces: Knobs / Conchoidal Failure: YSH50 / 5250-4 RTM D2512 Specimen: In LOX: No Reaction Detected



Figure 126-b-i, Internal To The Indenting Impacter Fracture Surfaces: Knobs / Conchoidal Failure: YSH50 / 5250-4 RTM D2512 Specimen: In LN2

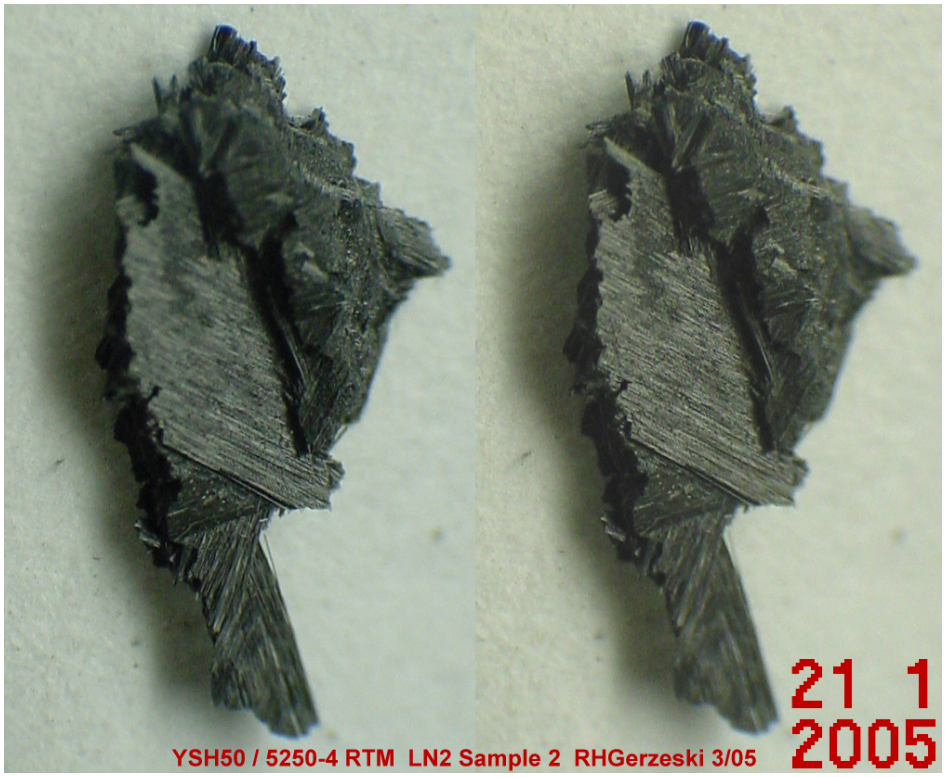


Figure 126-b-ii, Internal To The Indenting Impacter Fracture Surfaces: Knobs / Conchoidal Failure: YSH50 / 5250-4 RTM D2512 Specimen: In LN2

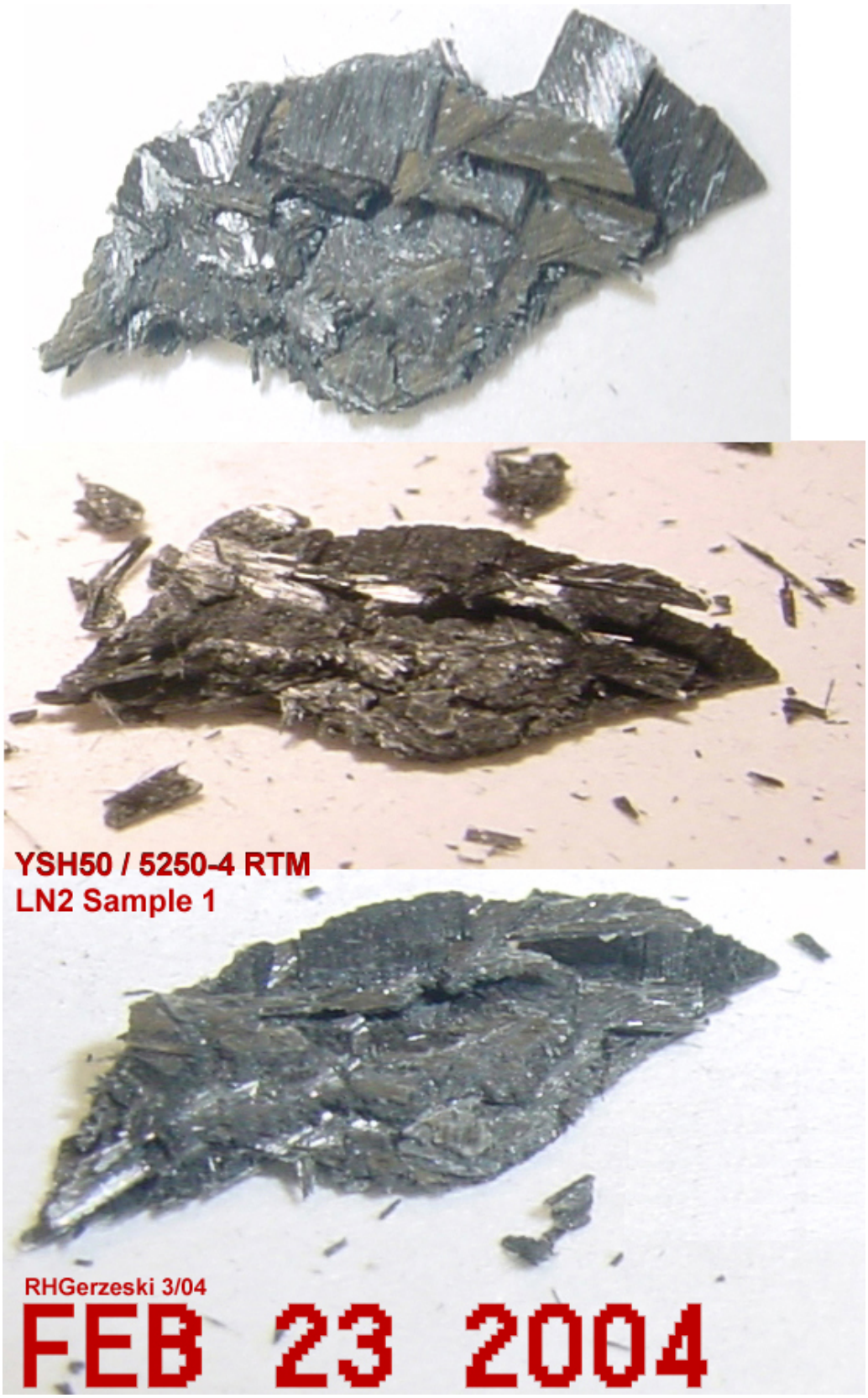


Figure 126-b-iii, Internal To The Indenting Impacter Fracture Surfaces: Knobs / Conchoidal Failure: YSH50 / 5250-4 RTM D2512 Specimen: In LN2



Figure 127-a, Internal To The Indenting Impacter Fracture Surfaces: Knobs / Conchoidal Failure: YSH60 / 5250-4 RTM D2512 Specimen: In LOX: Reaction Detected



Figure 127-b-i, Internal To The Indenting Impacter Fracture Surfaces: Knobs / Conchoidal Failure: YSH60 / 5250-4 RTM D2512 Specimen: In LOX: No Reaction Detected

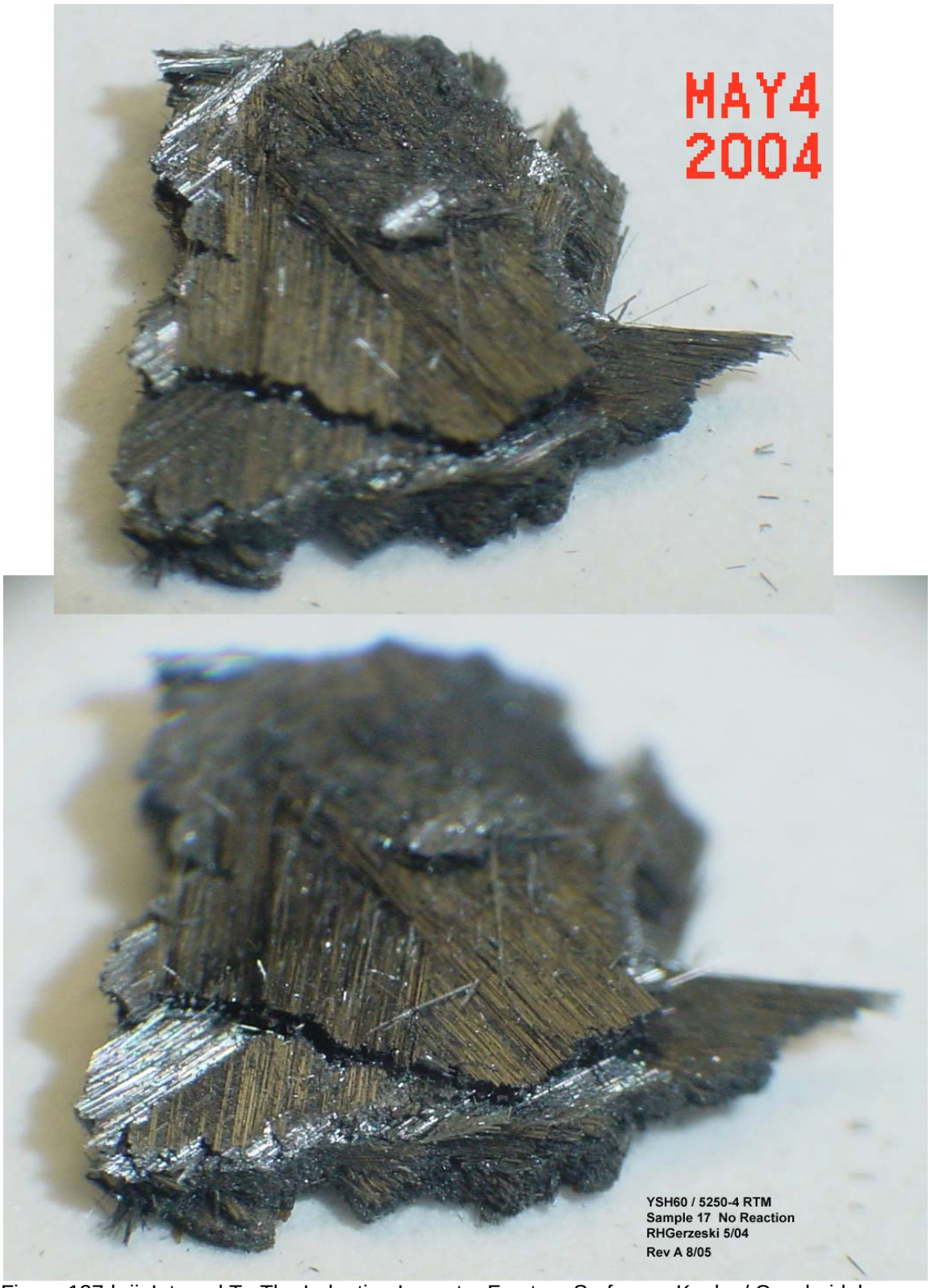


Figure 127-b-ii, Internal To The Indenting Impacter Fracture Surfaces: Knobs / Conchoidal Failure: YSH60 / 5250-4 RTM D2512 Specimen: In LOX: No Reaction Detected



Figure 127-b-iii, Internal To The Indenting Impacter Fracture Surfaces: Knobs / Conchoidal Failure: YSH60 / 5250-4 RTM D2512 Specimen: In LOX: No Reaction Detected



Figure 127-c-i, Internal To The Indenting Impacter Fracture Surfaces: Knobs / Conchoidal Failure: YSH60 / 5250-4 RTM D2512 Specimen: In LN2

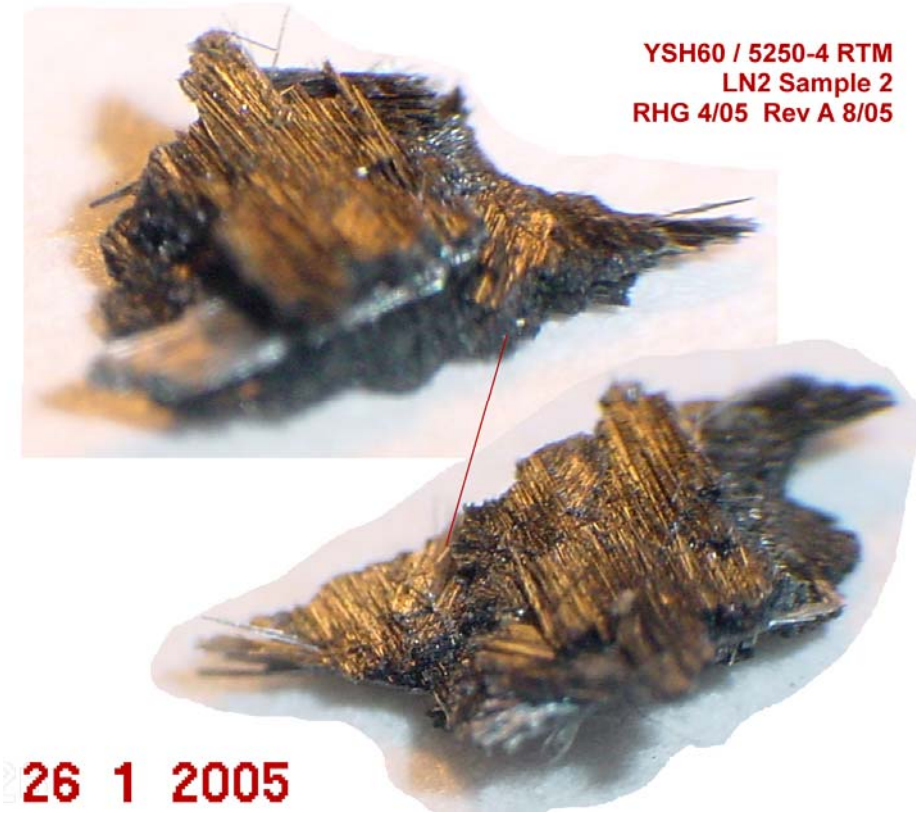


Figure 127-c-ii, Internal To The Indenting Impacter Fracture Surfaces: Knobs / Conchoidal Failure: YSH60 / 5250-4 RTM D2512 Specimen: In LN2



Figure 128-a-i, Internal To The Indenting Impacter Fracture Surfaces: Straight Edged Fragments: T650-35 / 5250-4 RTM D2512 Specimen: In LOX: Reaction Detected



Figure 128-a-ii, Internal To The Indenting Impacter Fracture Surfaces: Straight Edged Fragments: T650-35 / 5250-4 RTM D2512 Specimen: In LOX: Reaction Detected

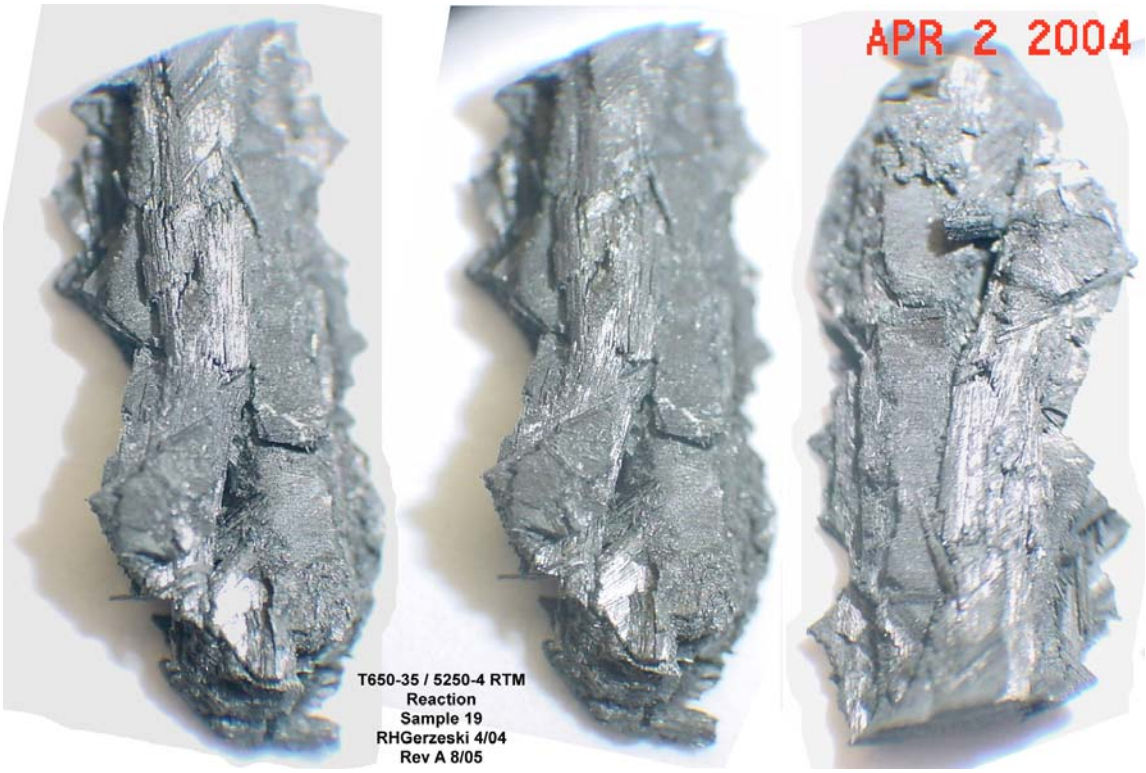


Figure 128-a-iii, Internal To The Indenting Impacter Fracture Surfaces: Straight Edged Fragments: T650-35 / 5250-4 RTM D2512 Specimen: In LOX: Reaction Detected

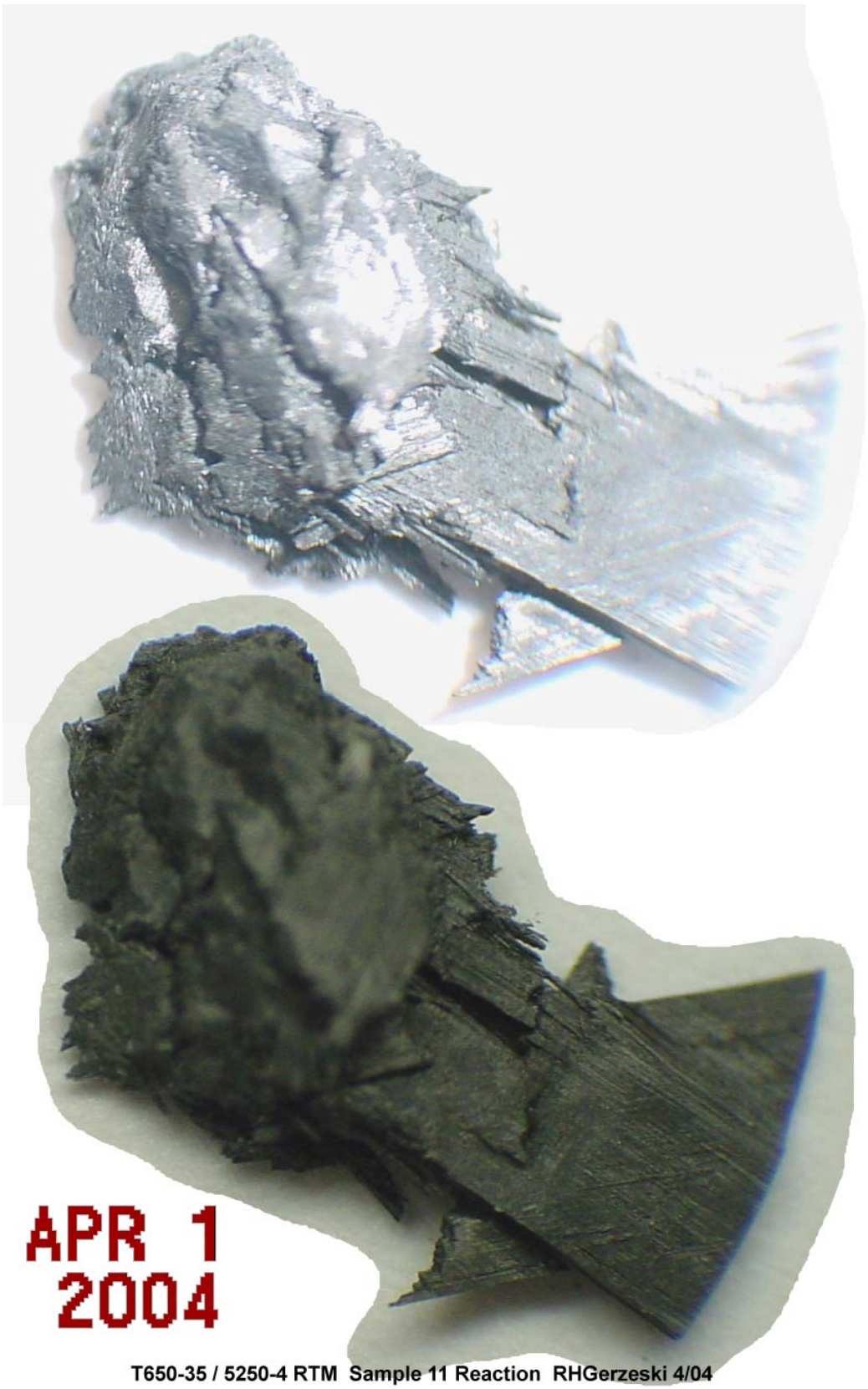


Figure 128-a-iv, Internal To The Indenting Impacter Fracture Surfaces: Straight Edged Fragments: T650-35 / 5250-4 RTM D2512 Specimen: In LOX: Reaction Detected



Figure 128-b-i, Internal To The Indenting Impacter Fracture Surfaces: Straight Edged Fragments: T650-35 / 5250-4 RTM D2512 Specimen: In LOX: No Reaction Detected

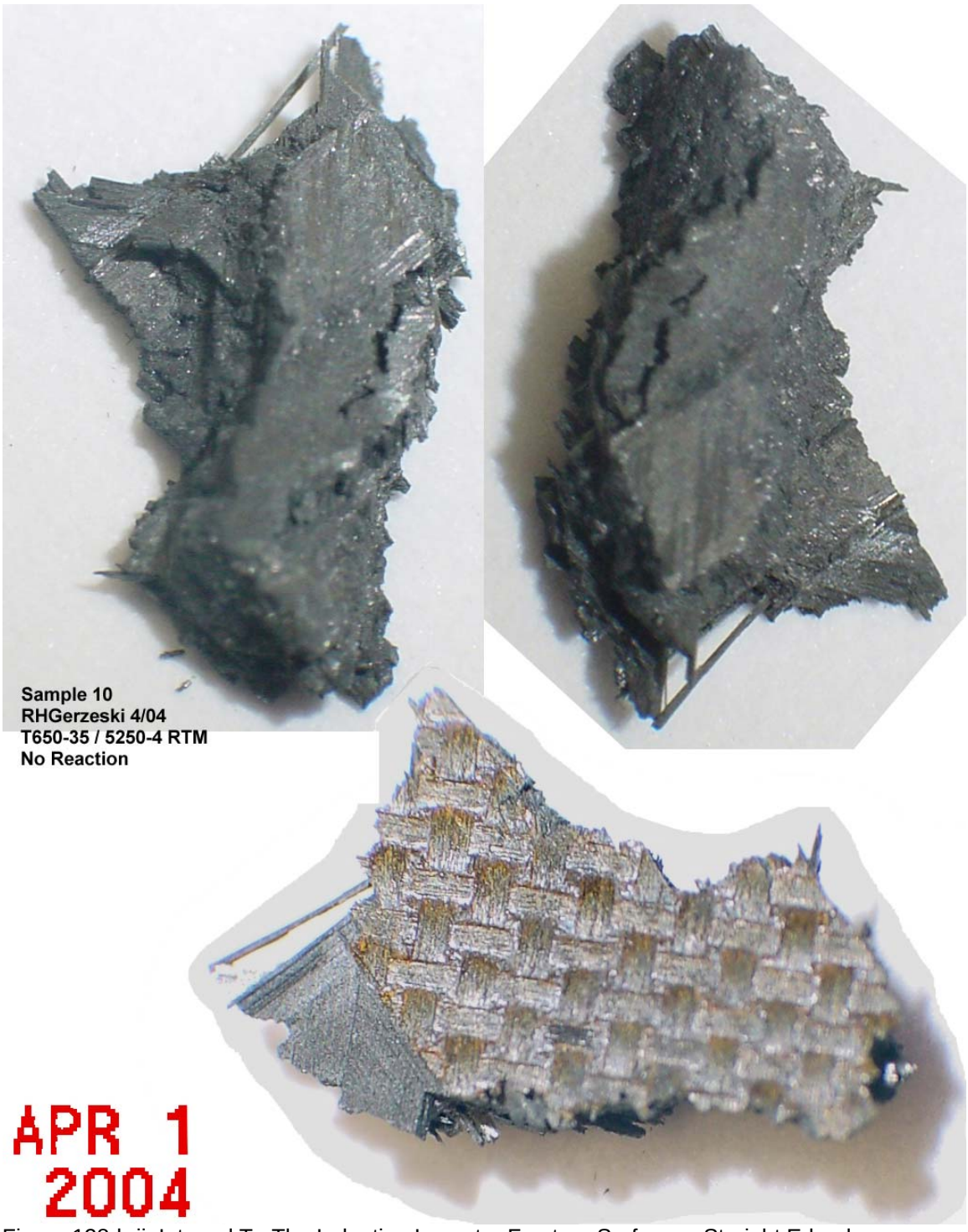


Figure 128-b-ii, Internal To The Indenting Impacter Fracture Surfaces: Straight Edged Fragments: T650-35 / 5250-4 RTM D2512 Specimen: In LOX: No Reaction Detected





Figure 128-c-i, Internal To The Indenting Impacter Fracture Surfaces: Straight Edged Fragments: T650-35 / 5250-4 RTM D2512 Specimen: In LN2

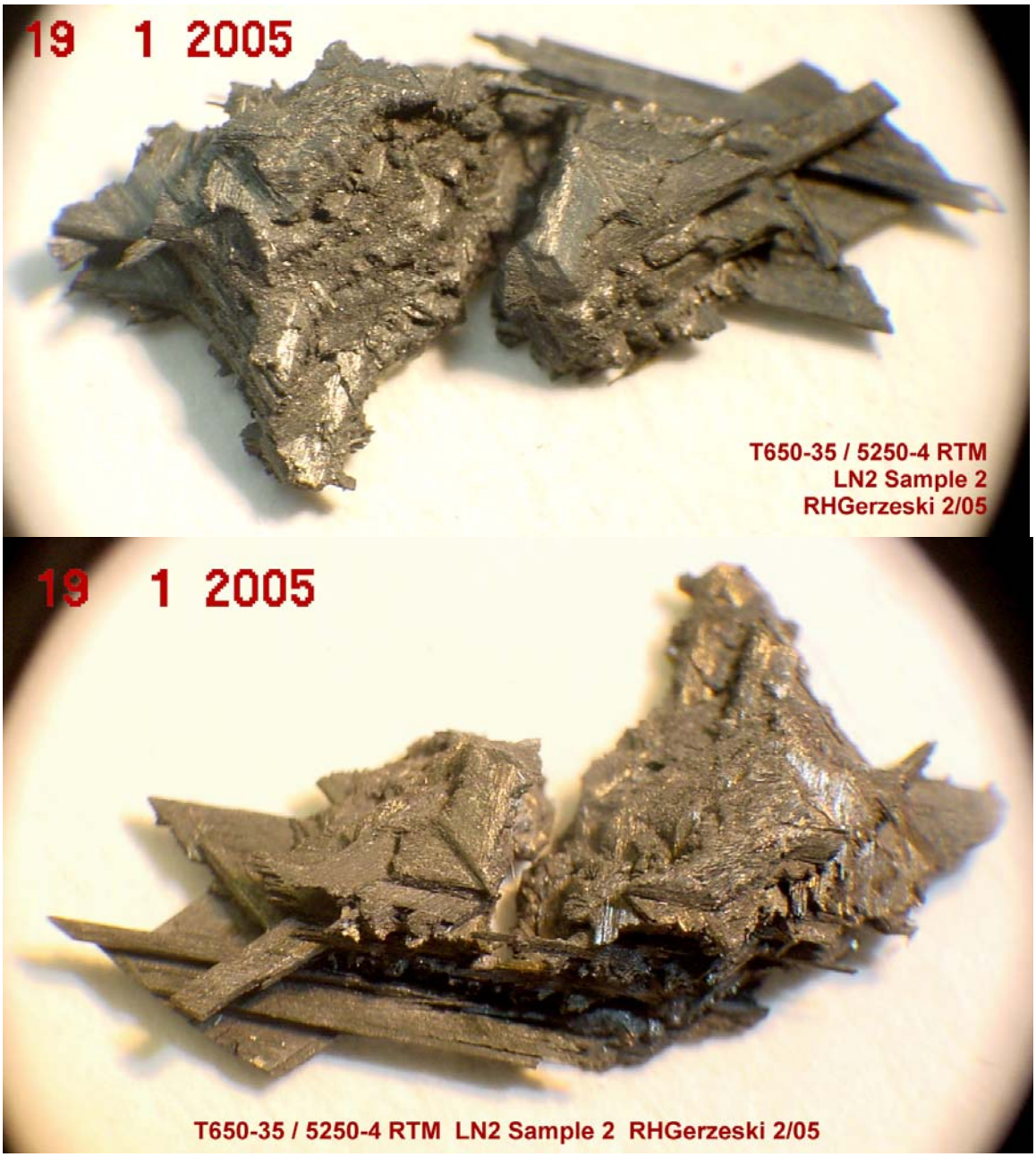


Figure 128-c-ii, Internal To The Indenting Impacter Fracture Surfaces: Straight Edged Fragments: T650-35 / 5250-4 RTM D2512 Specimen: In LN2



Figure 128-c-iii, Internal To The Indenting Impacter Fracture Surfaces: Straight Edged Fragments: T650-35 / 5250-4 RTM D2512 Specimen: In LN2

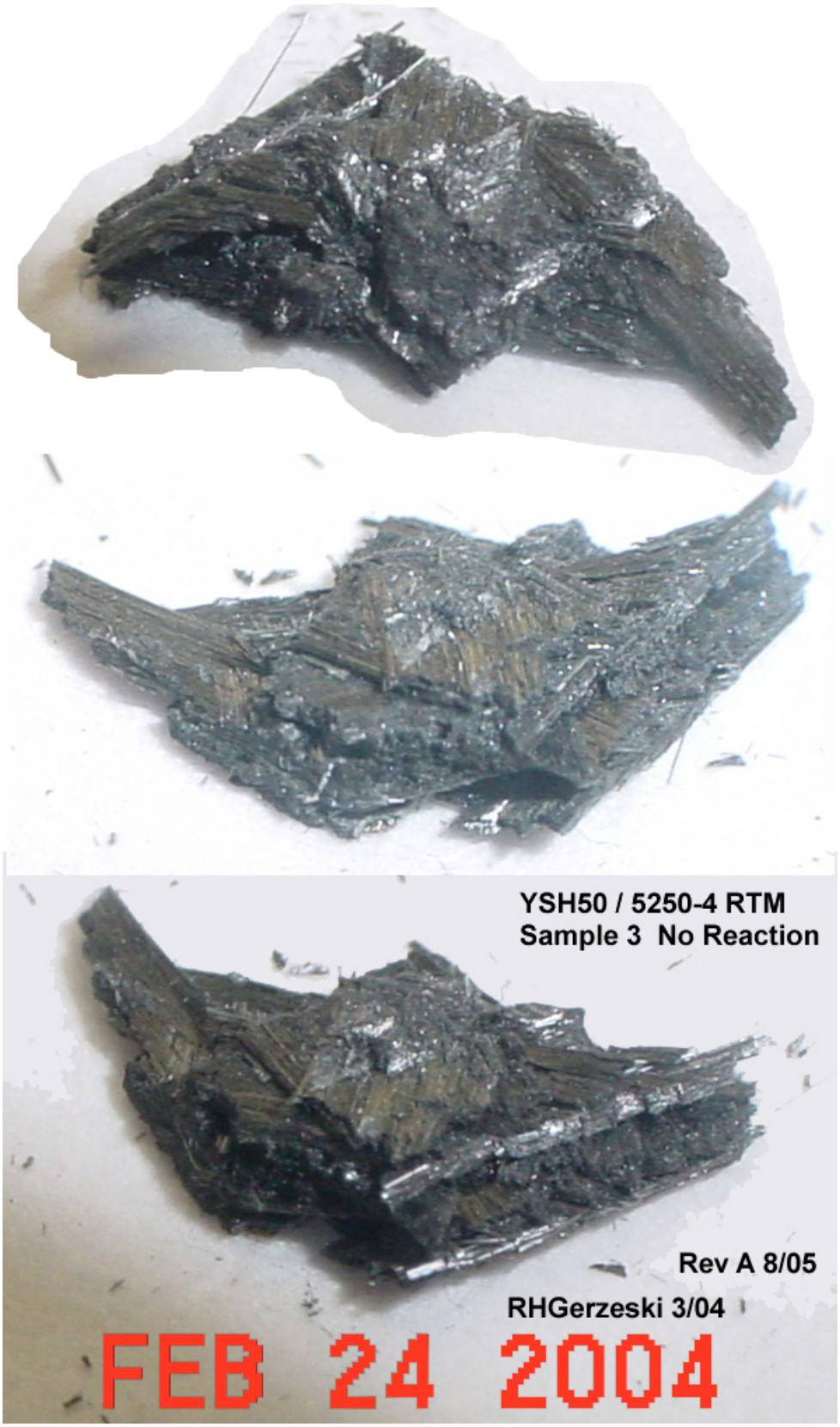


Figure 129-b-i, Internal To The Indenting Impacter Fracture Surfaces: Straight Edged Fragments: YSH50 / 5250-4 RTM D2512 Specimen: In LOX: No Reaction Detected



Figure 129-b-ii, Internal To The Indenting Impacter Fracture Surfaces: Straight Edged Fragments: YSH50 / 5250-4 RTM D2512 Specimen: In LOX: No Reaction Detected

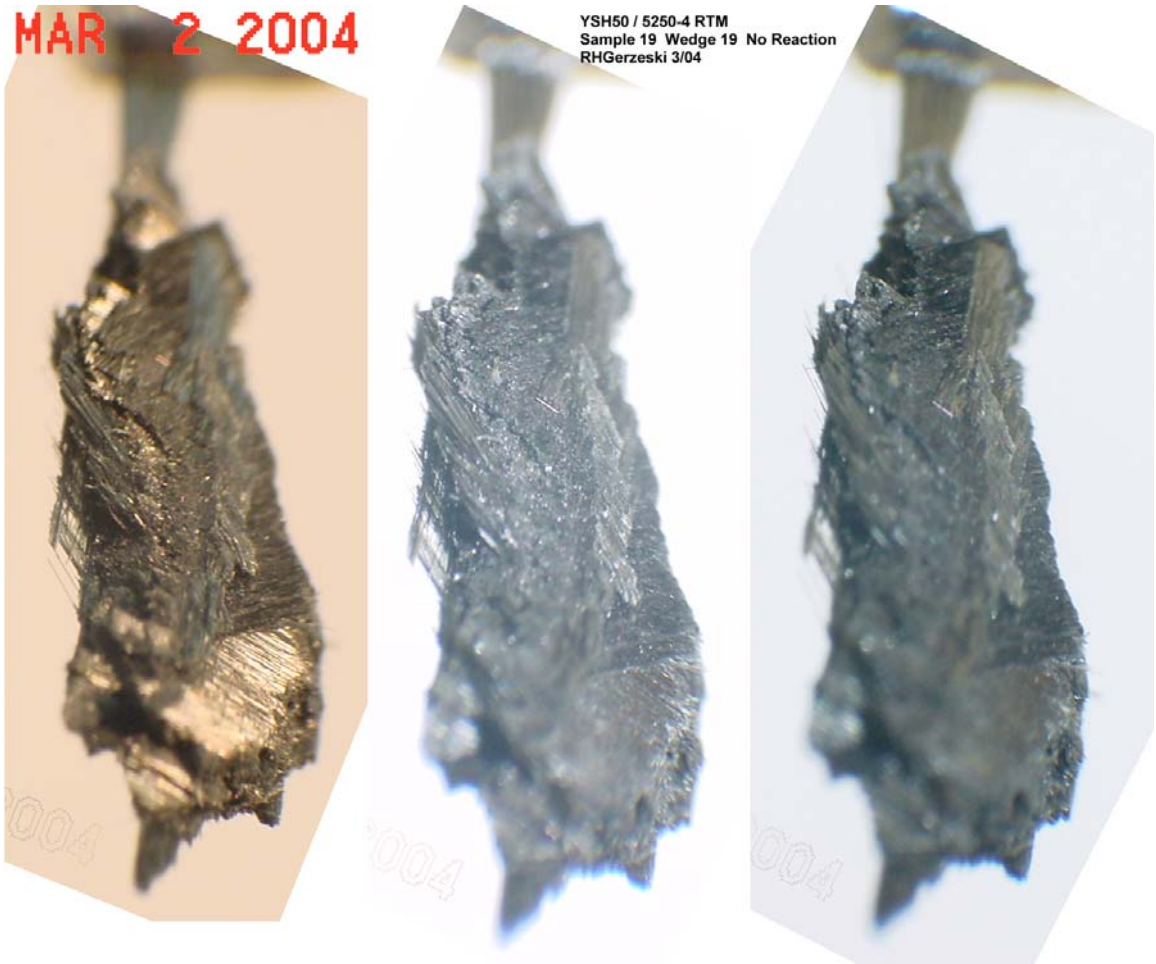


Figure 129-b-iii, Internal To The Indenting Impacter Fracture Surfaces: Straight Edged Fragments: YSH50 / 5250-4 RTM D2512 Specimen: In LOX: No Reaction Detected



Figure 129-c-i, Internal To The Indenting Impacter Fracture Surfaces: Straight Edged Fragments: YSH50 / 5250-4 RTM D2512 Specimen: In LN2

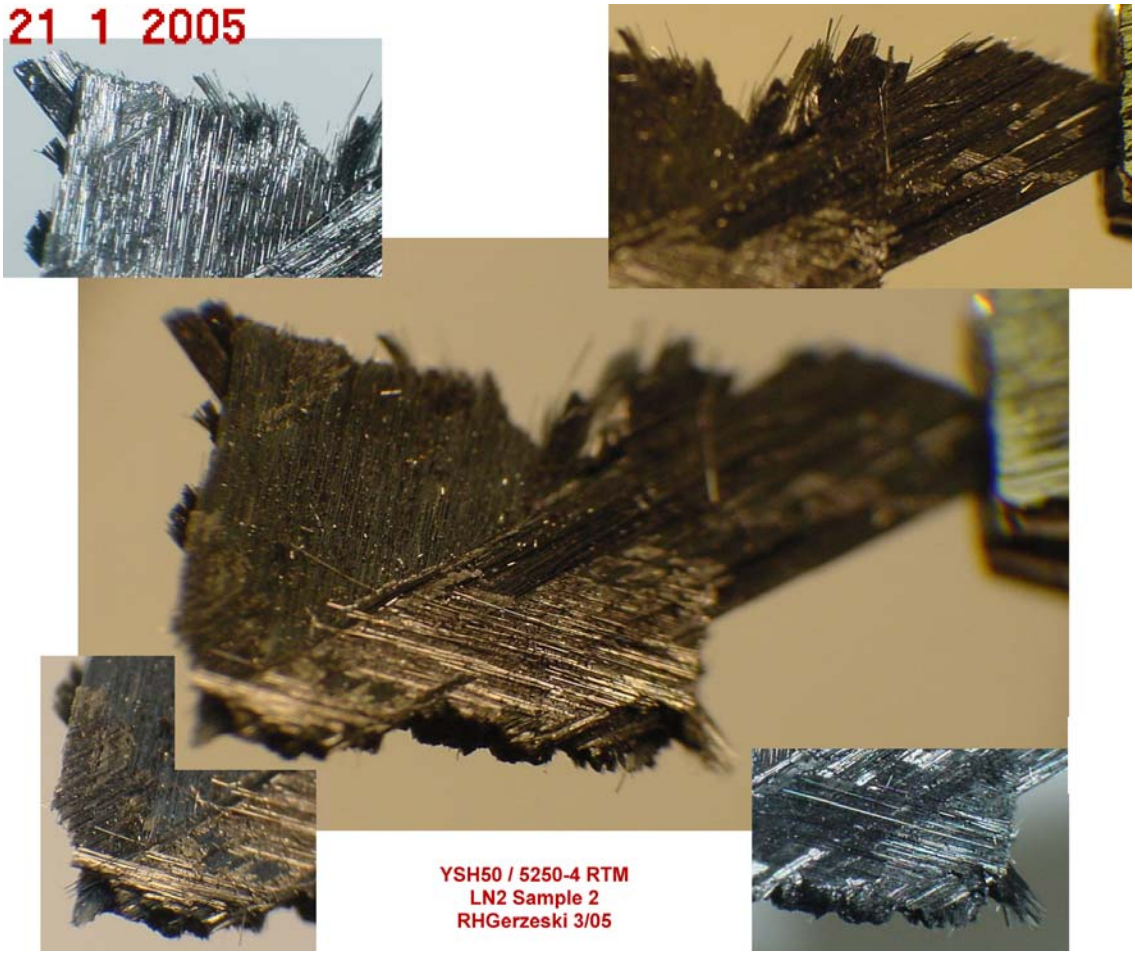


Figure 129-c-ii, Internal To The Indenting Impacter Fracture Surfaces: Straight Edged Fragments: YSH50 / 5250-4 RTM D2512 Specimen: In LN2



Figure 130-a-i, Internal To The Indenting Impacter Fracture Surfaces: Straight Edged Fragments: YSH60 / 5250-4 RTM D2512 Specimen: In LOX: Reaction Detected



Figure 130-a-ii, Internal To The Indenting Impacter Fracture Surfaces: Straight Edged Fragments: YSH60 / 5250-4 RTM D2512 Specimen: In LOX: Reaction Detected



Figure 130-a-iii, Internal To The Indenting Impacter Fracture Surfaces: Straight Edged Fragments: YSH60 / 5250-4 RTM D2512 Specimen: In LOX: Reaction Detected

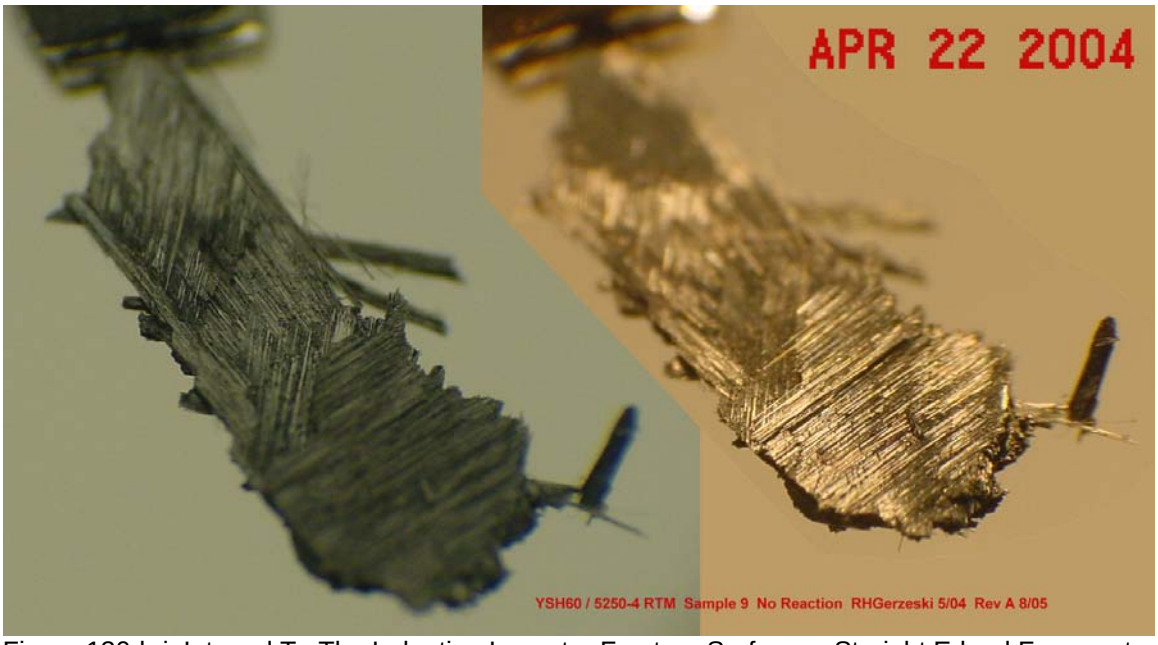


Figure 130-b-i, Internal To The Indenting Impacter Fracture Surfaces: Straight Edged Fragments: YSH60 / 5250-4 RTM D2512 Specimen: In LOX: No Reaction Detected



Figure 130-b-ii, Internal To The Indenting Impacter Fracture Surfaces: Straight Edged Fragments: YSH60 / 5250-4 RTM D2512 Specimen: In LOX: No Reaction Detected

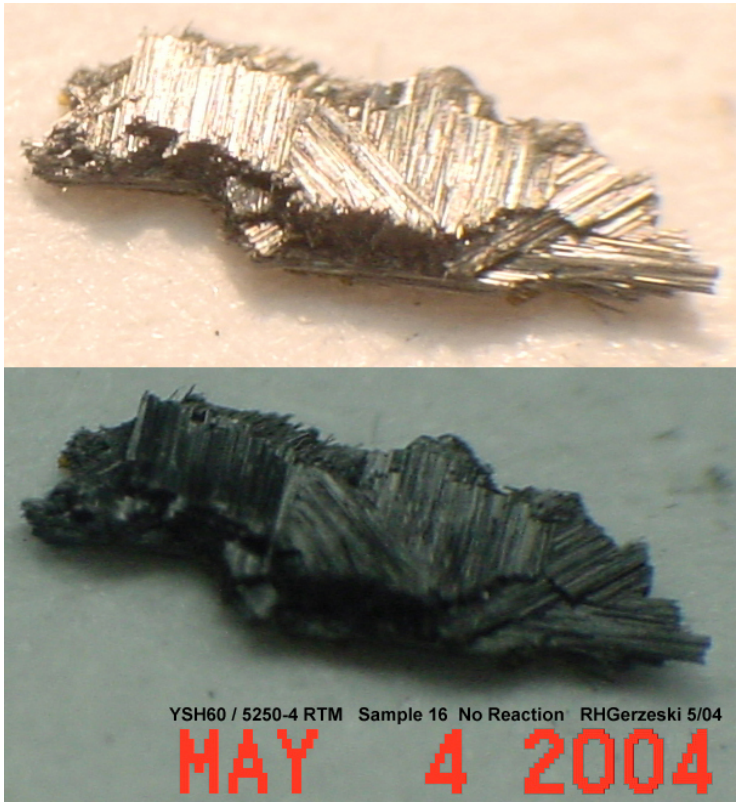


Figure 130-b-iii, Internal To The Indenting Impacter Fracture Surfaces: Straight Edged Fragments: YSH60 / 5250-4 RTM D2512 Specimen: In LOX: No Reaction Detected

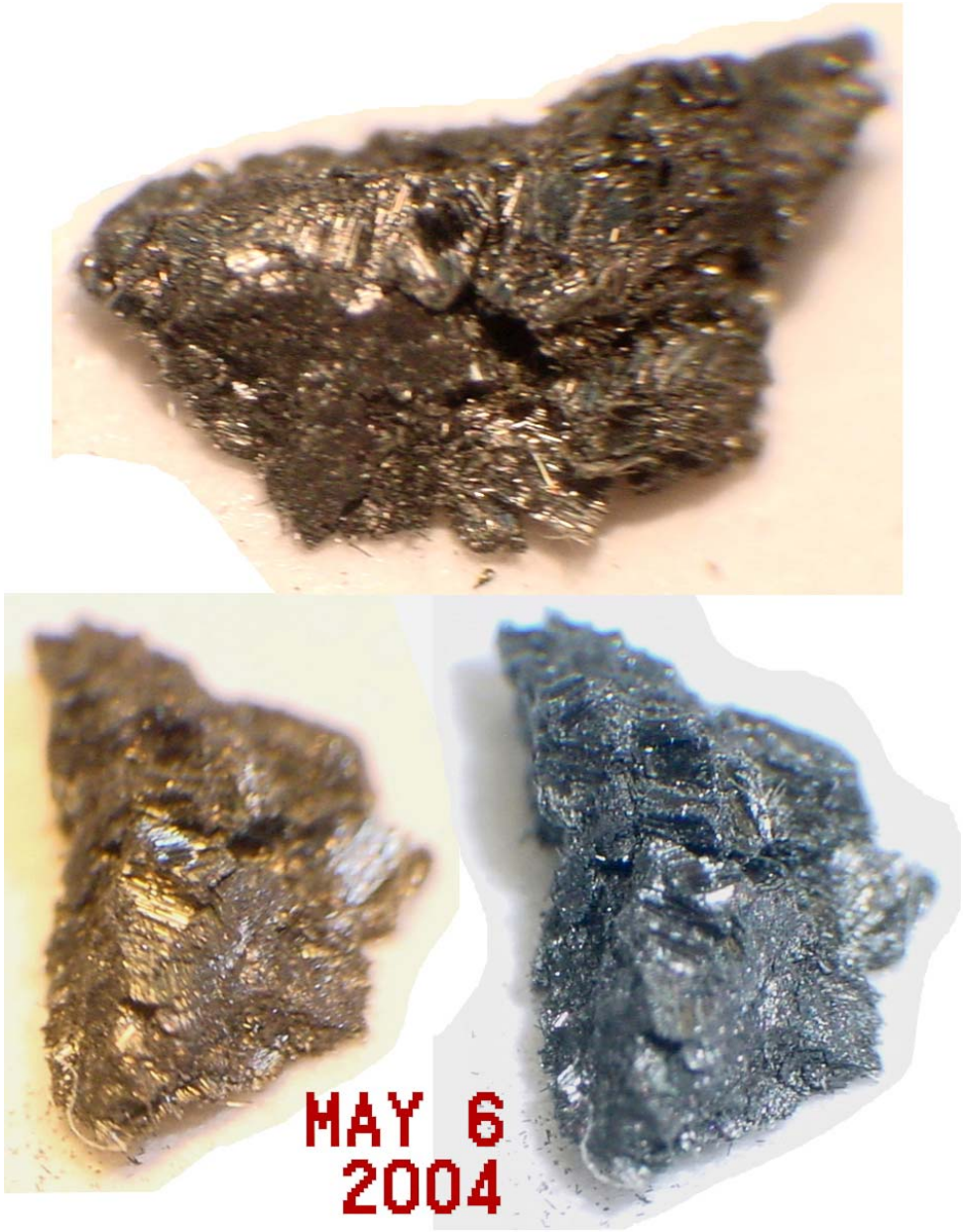


Figure 130-c-i, Internal To The Indenting Impacter Fracture Surfaces: Straight Edged Fragments: YSH60 / 5250-4 RTM D2512 Specimen: In LN2



Figure 130-c-ii, Internal To The Indenting Impacter Fracture Surfaces: Straight Edged Fragments: YSH60 / 5250-4 RTM D2512 Specimen: In LN2



Figure 130-c-iii, Internal To The Indenting Impacter Fracture Surfaces: Straight Edged Fragments: YSH60 / 5250-4 RTM D2512 Specimen: In LN2

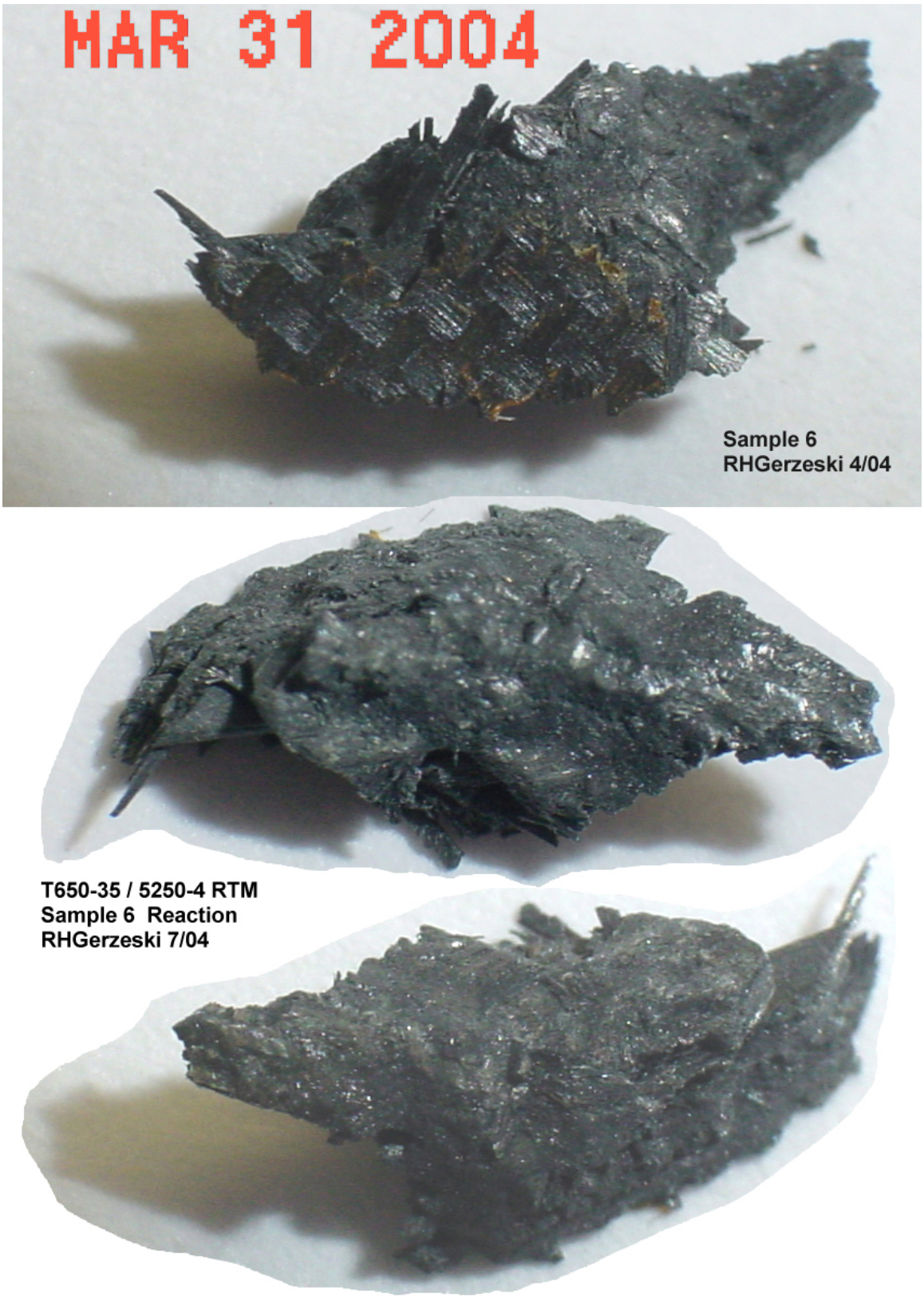


Figure 131-a-i, Internal To The Indenting Impacter Fracture Surfaces: Abrasion: T650-35 / 5250-4 RTM D2512 Specimen: In LOX: Reaction Detected



Figure 131-a-ii, Internal To The Indenting Impacter Fracture Surfaces: Abrasion: T650-35 / 5250-4 RTM D2512 Specimen: In LOX: Reaction Detected



Figure 131-a-iii, Internal To The Indenting Impacter Fracture Surfaces: Abrasion: T650-35 / 5250-4 RTM D2512 Specimen: In LOX: Reaction Detected



Figure 131-a-iv, Internal To The Indenting Impacter Fracture Surfaces: Abrasion: T650-35 / 5250-4 RTM D2512 Specimen: In LOX: Reaction Detected



Figure 131-b-i, Internal To The Indenting Impacter Fracture Surfaces: Abrasion: T650-35 / 5250-4 RTM D2512 Specimen: In LOX: No Reaction Detected

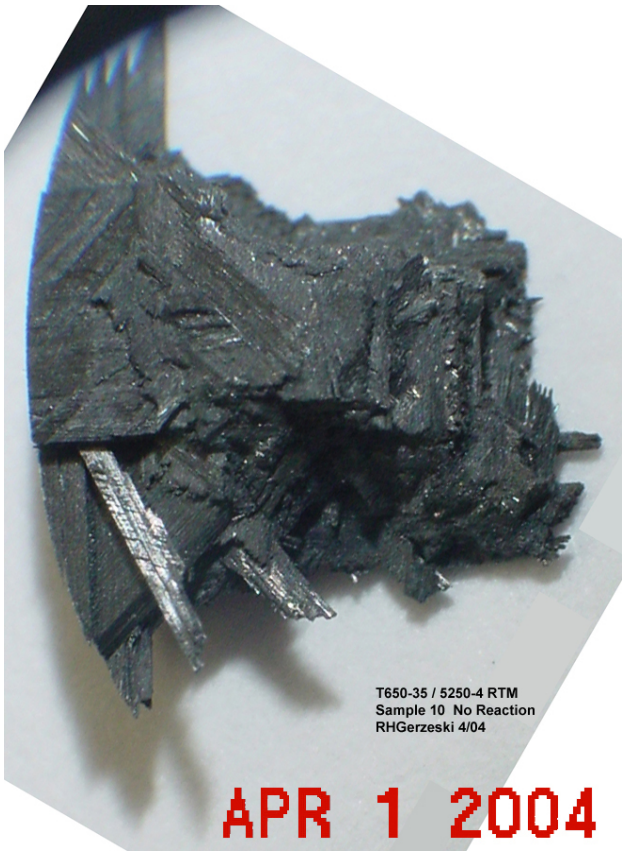


Figure 131-b-ii, Internal To The Indenting Impacter Fracture Surfaces: Abrasion: T650-35 / 5250-4 RTM D2512 Specimen: In LOX: No Reaction Detected



Figure 131-c-i, Internal To The Indenting Impacter Fracture Surfaces: Abrasion: T650-35 / 5250-4 RTM D2512 Specimen: In LN2



Figure 131-c-ii, Internal To The Indenting Impacter Fracture Surfaces: Abrasion: T650-35 / 5250-4 RTM D2512 Specimen: In LN2

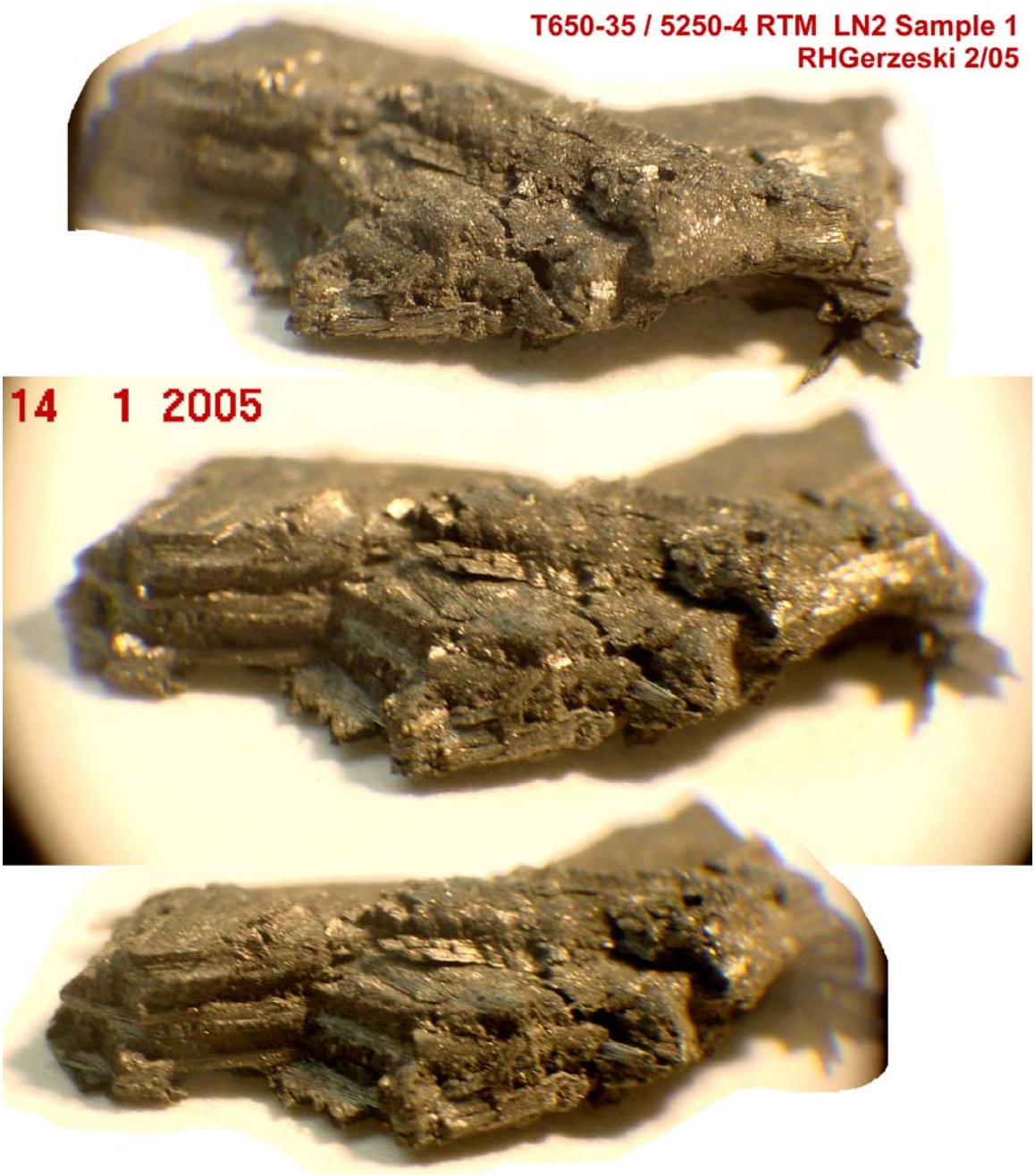


Figure 131-c-iii, Internal To The Indenting Impacter Fracture Surfaces: Abrasion: T650-35 / 5250-4 RTM D2512 Specimen: In LN2



Figure 132-a-i, Internal To The Indenting Impacter Fracture Surfaces: Abrasion: YSH50 / 5250-4 RTM D2512 Specimen: In LOX: No Reaction Detected



Figure 132-a-ii, Internal To The Indenting Impacter Fracture Surfaces: Abrasion: YSH50 / 5250-4 RTM D2512 Specimen: In LOX: No Reaction Detected



Figure 132-a-iii, Internal To The Indenting Impacter Fracture Surfaces: Abrasion: YSH50 / 5250-4 RTM D2512 Specimen: In LOX: No Reaction Detected



Figure 132-b-i, Internal To The Indenting Impacter Fracture Surfaces: Abrasion: YSH50 / 5250-4 RTM D2512 Specimen: In LN2



Figure 132-b-ii, Internal To The Indenting Impacter Fracture Surfaces: Abrasion: YSH50 / 5250-4 RTM D2512 Specimen: In LN2

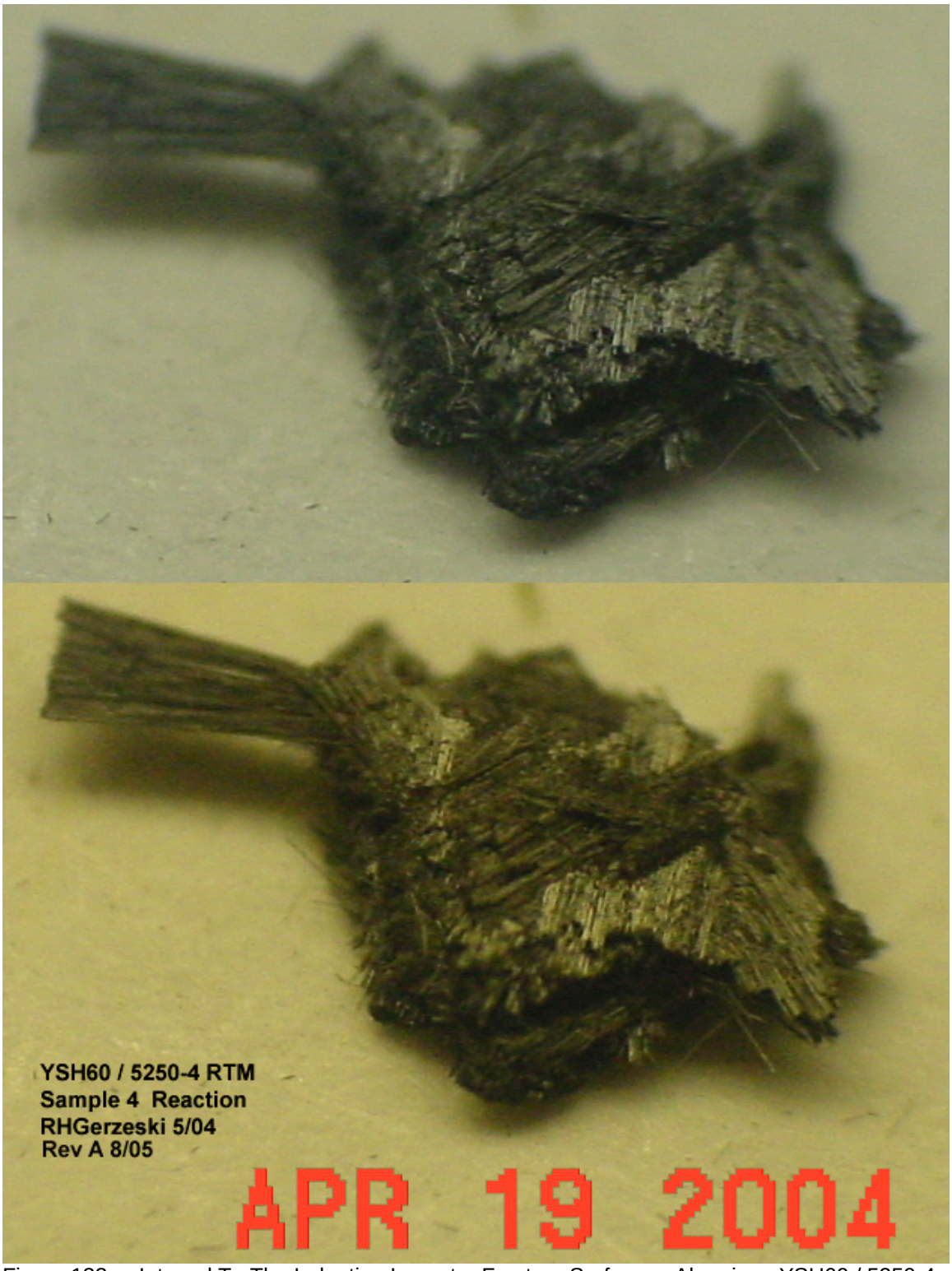


Figure 133-a, Internal To The Indenting Impacter Fracture Surfaces: Abrasion: YSH60 / 5250-4 RTM D2512 Specimen: In LOX: Reaction Detected

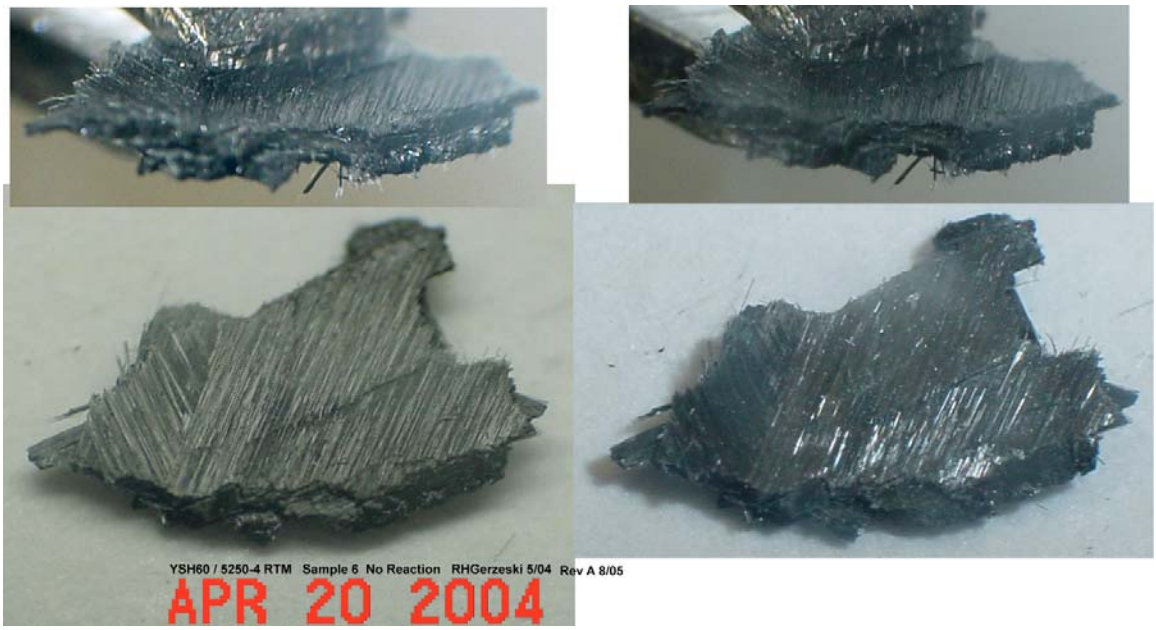


Figure 133-b-i, Internal To The Indenting Impacter Fracture Surfaces: Abrasion: YSH60 / 5250-4 RTM D2512 Specimen: In LOX: No Reaction Detected



Figure 133-b-ii, Internal To The Indenting Impacter Fracture Surfaces: Abrasion: YSH60 / 5250-4 RTM D2512 Specimen: In LOX: No Reaction Detected



Figure 133-b-iii, Internal To The Indenting Impacter Fracture Surfaces: Abrasion: YSH60 / 5250-4 RTM D2512 Specimen: In LOX: No Reaction Detected



Figure 133-c-i, Internal To The Indenting Impacter Fracture Surfaces: Abrasion: YSH60 / 5250-4 RTM D2512 Specimen: In LN2

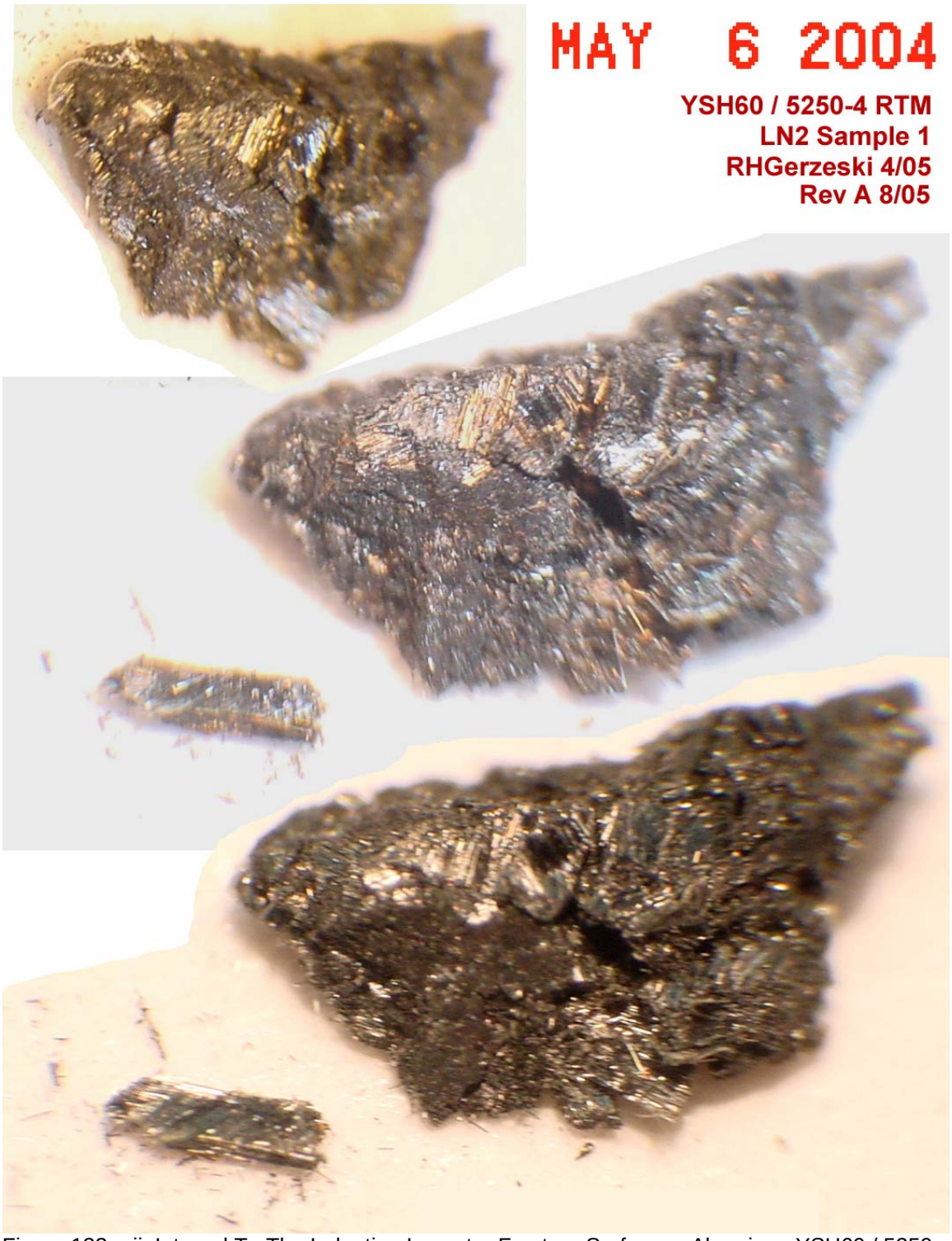


Figure 133-c-ii, Internal To The Indenting Impacter Fracture Surfaces: Abrasion: YSH60 / 5250-4 RTM D2512 Specimen: In LN2

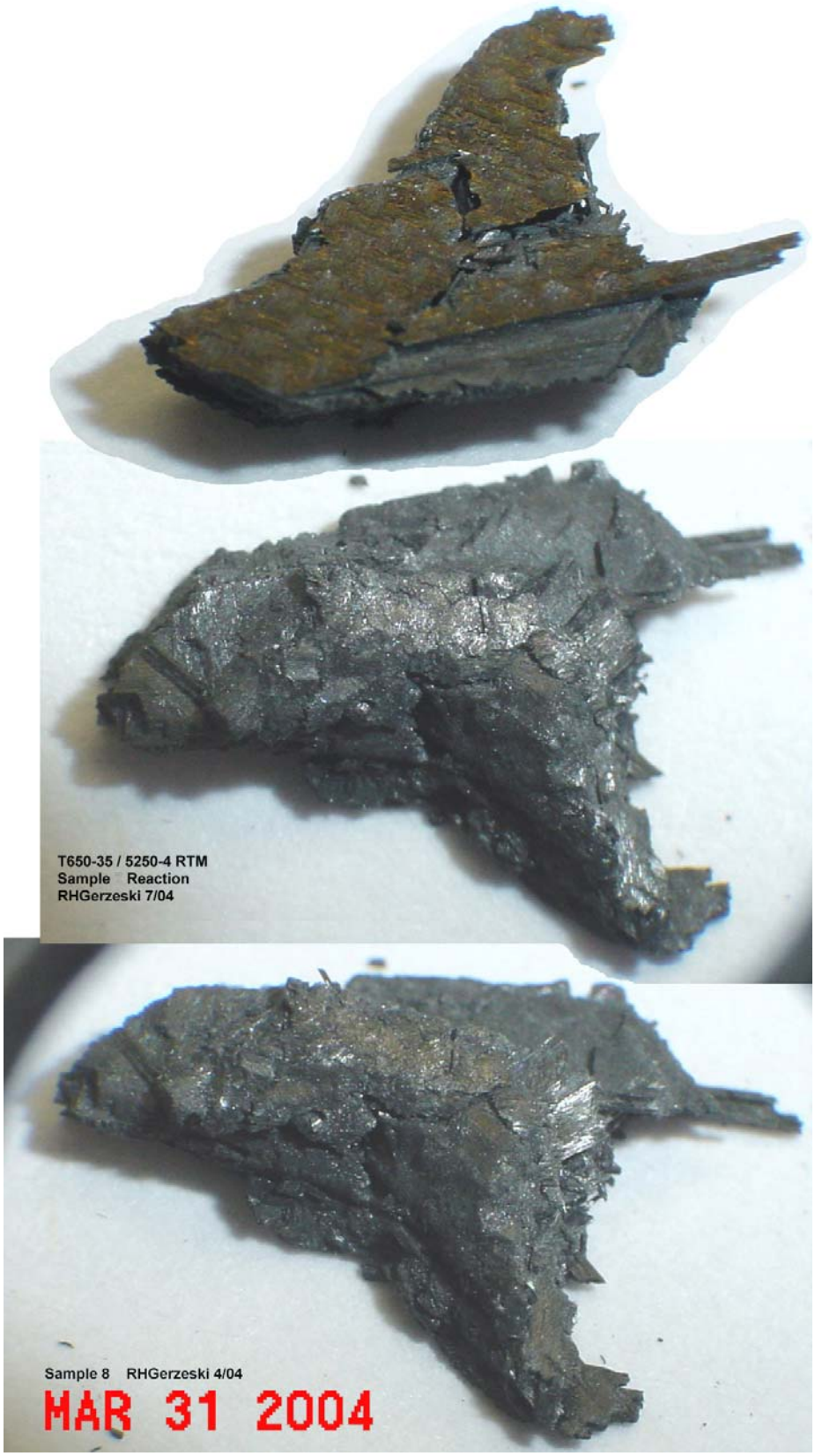


Figure 134-a-i, Internal To The Indenting Impacter Fracture Surfaces: Heat Exposure: T650-35 / 5250-4 RTM D2512 Specimen: In LOX: Reaction Detected



Figure 134-a-ii, Internal To The Indenting Impacter Fracture Surfaces: Heat Exposure: T650-35 / 5250-4 RTM D2512 Specimen: In LOX: Reaction Detected



Figure 134-a-iii, Internal To The Indenting Impacter Fracture Surfaces: Heat Exposure: T650-35 / 5250-4 RTM D2512 Specimen: In LOX: Reaction Detected

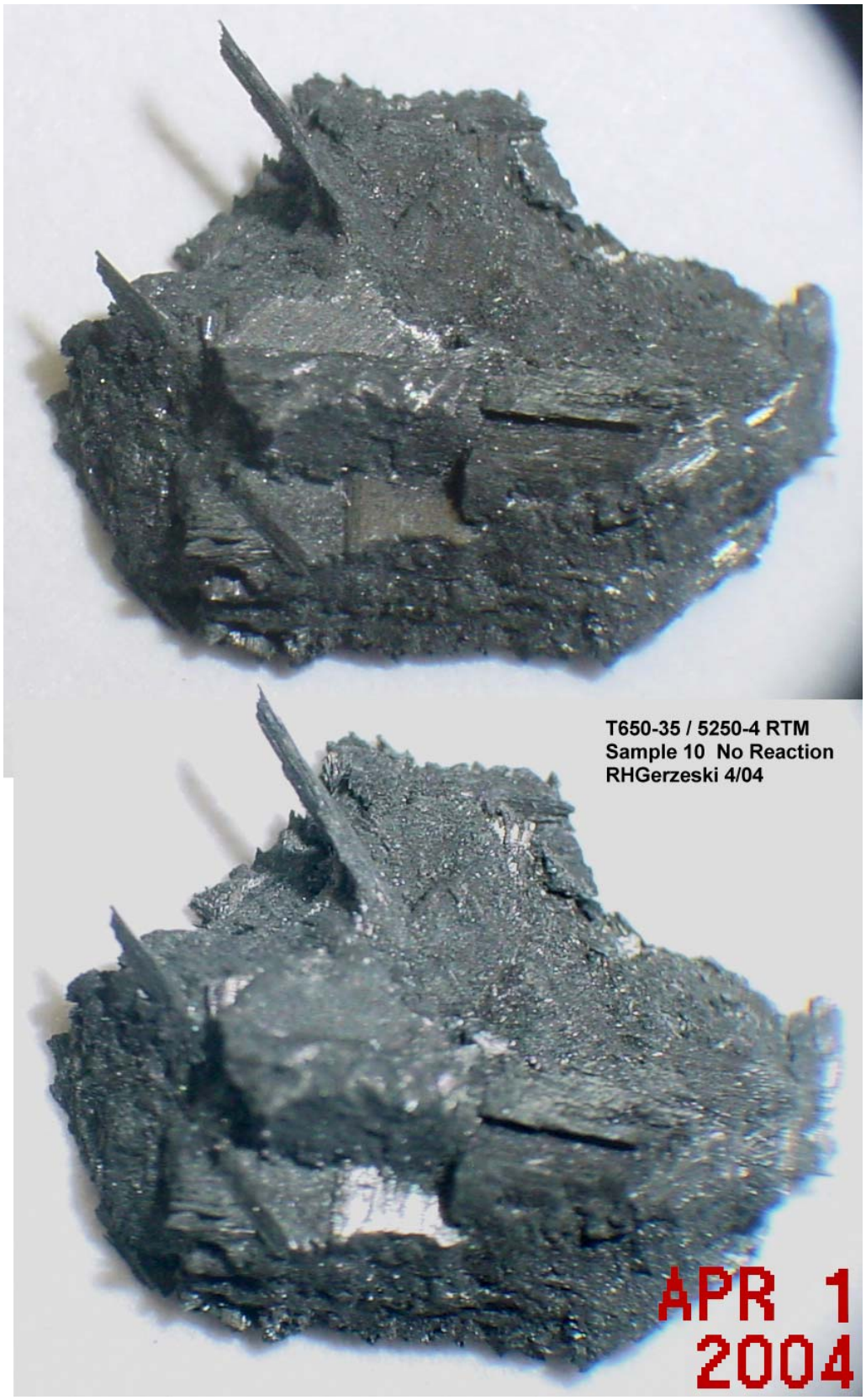


Figure 134-b-i, Internal To The Indenting Impacter Fracture Surfaces: Heat Exposure: T650-35 / 5250-4 RTM D2512 Specimen: In LOX: No Reaction Detected



Figure 134-b-ii, Internal To The Indenting Impacter Fracture Surfaces: Heat Exposure: T650-35 / 5250-4 RTM D2512 Specimen: In LOX: No Reaction Detected



Figure 134-c-i, Internal To The Indenting Impacter Fracture Surfaces: Heat Exposure: T650-35 / 5250-4 RTM D2512 Specimen: In LN2

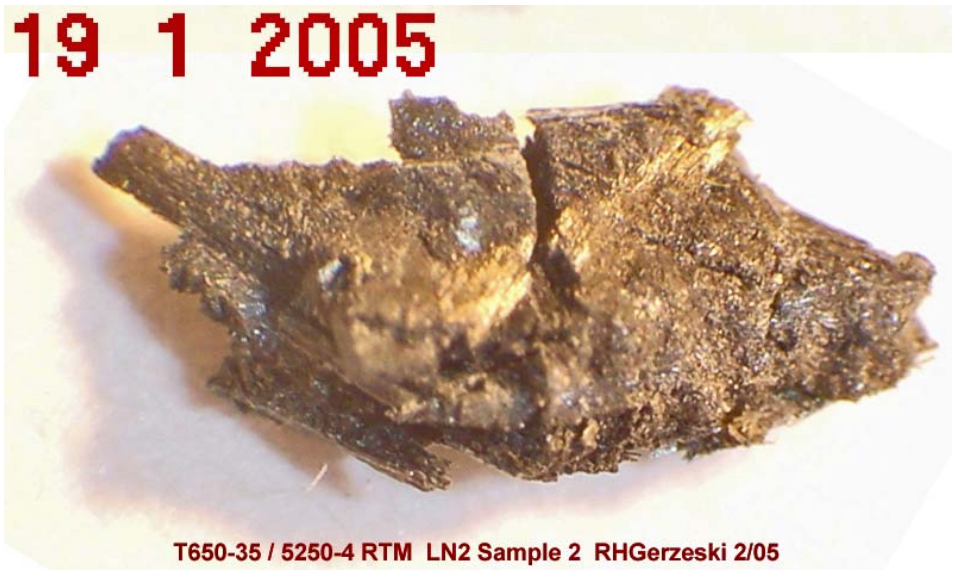


Figure 134-c-ii, Internal To The Indenting Impacter Fracture Surfaces: Heat Exposure: T650-35 / 5250-4 RTM D2512 Specimen: In LN2

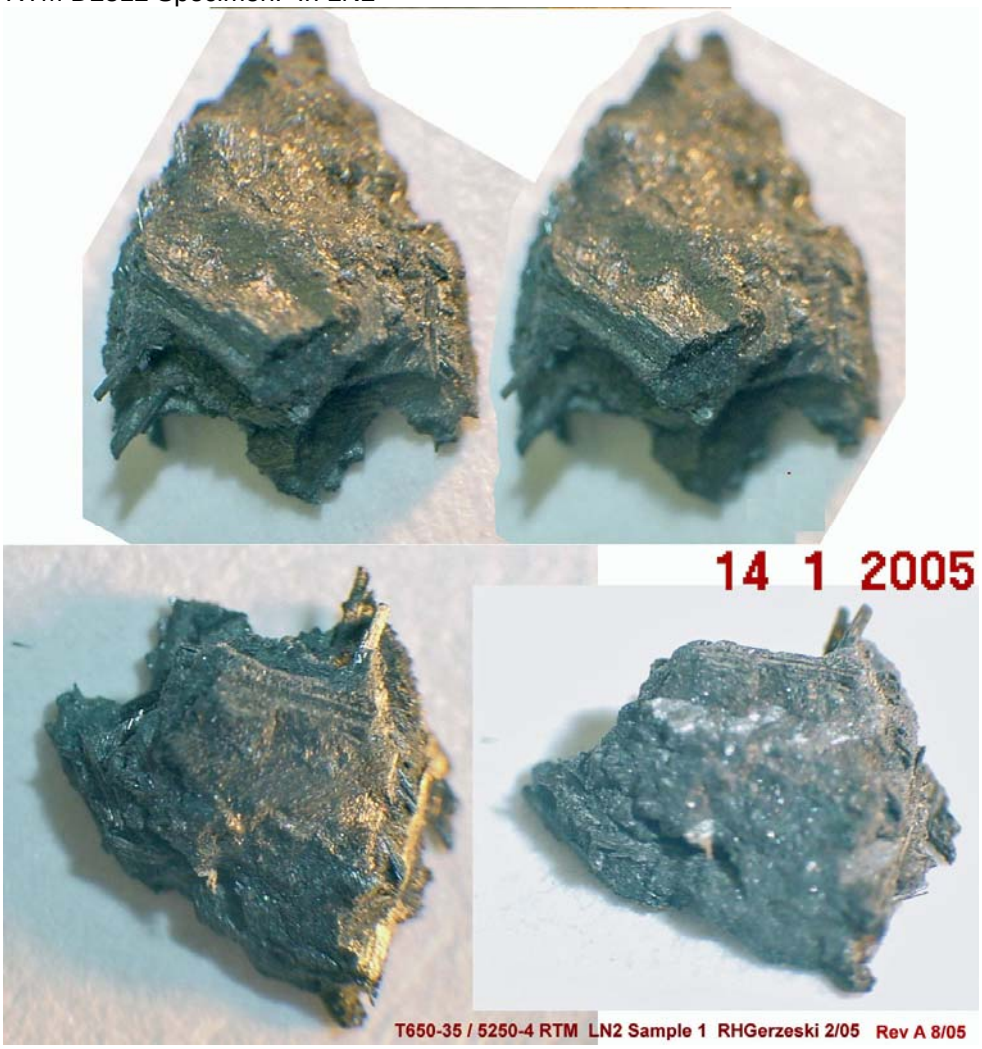


Figure 134-c-iii, Internal To The Indenting Impacter Fracture Surfaces: Heat Exposure: T650-35 / 5250-4 RTM D2512 Specimen: In LN2

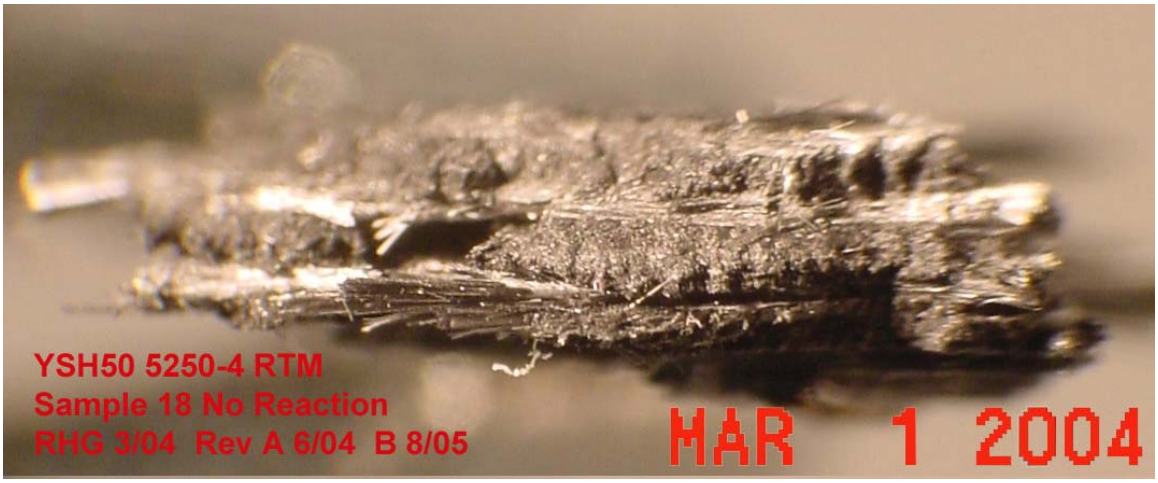


Figure 135-a-i, Internal To The Indenting Impacter Fracture Surfaces: Heat Exposure: YSH50 / 5250-4 RTM D2512 Specimen: In LOX: No Reaction Detected



Figure 135-a-ii, Internal To The Indenting Impacter Fracture Surfaces: Heat Exposure: YSH50 / 5250-4 RTM D2512 Specimen: In LOX: No Reaction Detected



Figure 135-b-i, Internal To The Indenting Impacter Fracture Surfaces: Heat Exposure: YSH50 / 5250-4 RTM D2512 Specimen: In LN2

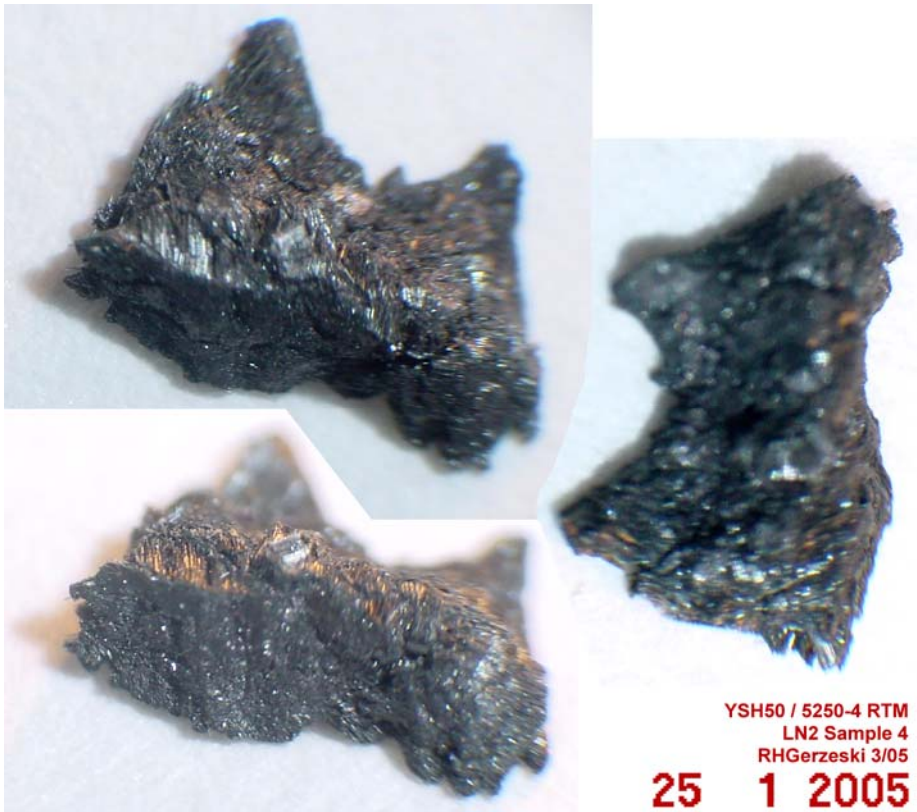


Figure 135-b-ii, Internal To The Indenting Impacter Fracture Surfaces: Heat Exposure: YSH50 / 5250-4 RTM D2512 Specimen: In LN2



Figure 136-a-i, Internal To The Indenting Impacter Fracture Surfaces: Heat Exposure: YSH60 / 5250-4 RTM D2512 Specimen: In LOX: Reaction Detected



Figure 136-a-ii, Internal To The Indenting Impacter Fracture Surfaces: Heat Exposure: YSH60 / 5250-4 RTM D2512 Specimen: In LOX: Reaction Detected



Figure 136-b-i, Internal To The Indenting Impacter Fracture Surfaces: Heat Exposure: YSH60 / 5250-4 RTM D2512 Specimen: In LOX: No Reaction Detected



Figure 136-b-ii, Internal To The Indenting Impacter Fracture Surfaces: Heat Exposure: YSH60 / 5250-4 RTM D2512 Specimen: In LOX: No Reaction Detected



Figure 136-b-iii, Internal To The Indenting Impacter Fracture Surfaces: Heat Exposure: YSH60 / 5250-4 RTM D2512 Specimen: In LOX: No Reaction Detected



Figure 136-b-iv, Internal To The Indenting Impacter Fracture Surfaces: Heat Exposure: YSH60 / 5250-4 RTM D2512 Specimen: In LOX: No Reaction Detected

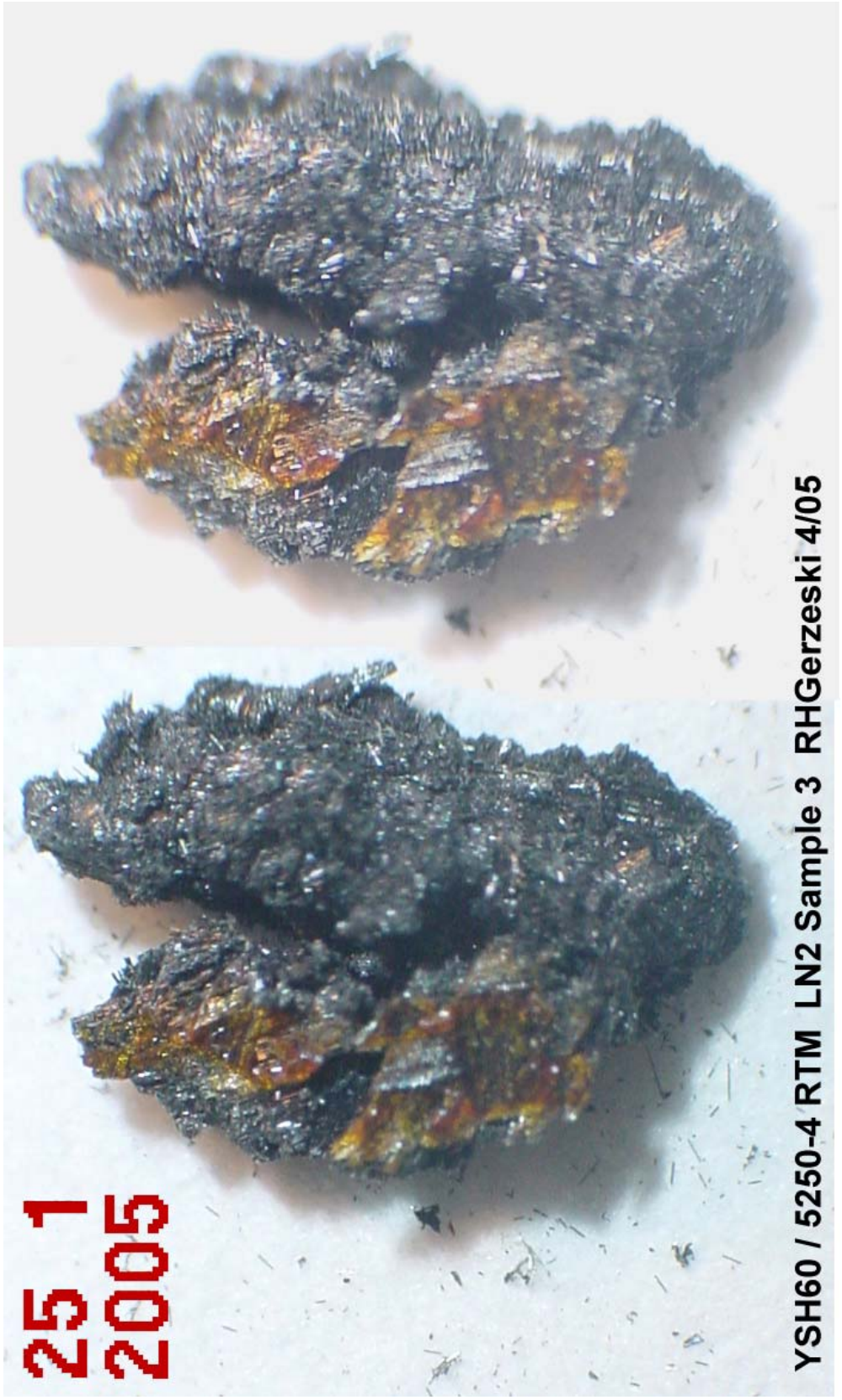


Figure 136-c-i, Internal To The Indenting Impacter Fracture Surfaces: Heat Exposure: YSH60 / 5250-4 RTM D2512 Specimen: In LN2

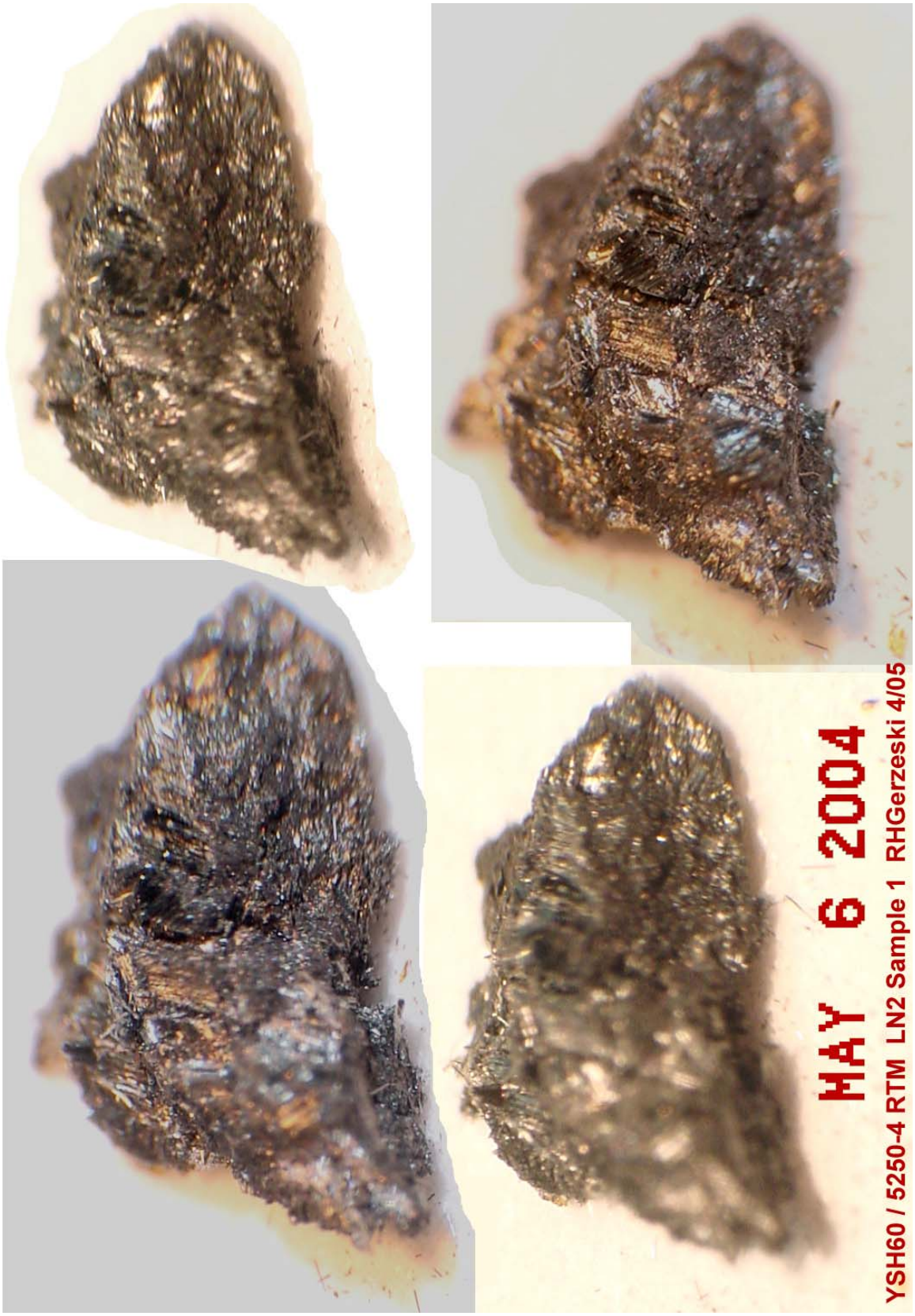


Figure 136-c-ii, Internal To The Indenting Impacter Fracture Surfaces: Heat Exposure: YSH60 / 5250-4 RTM D2512 Specimen: In LN2

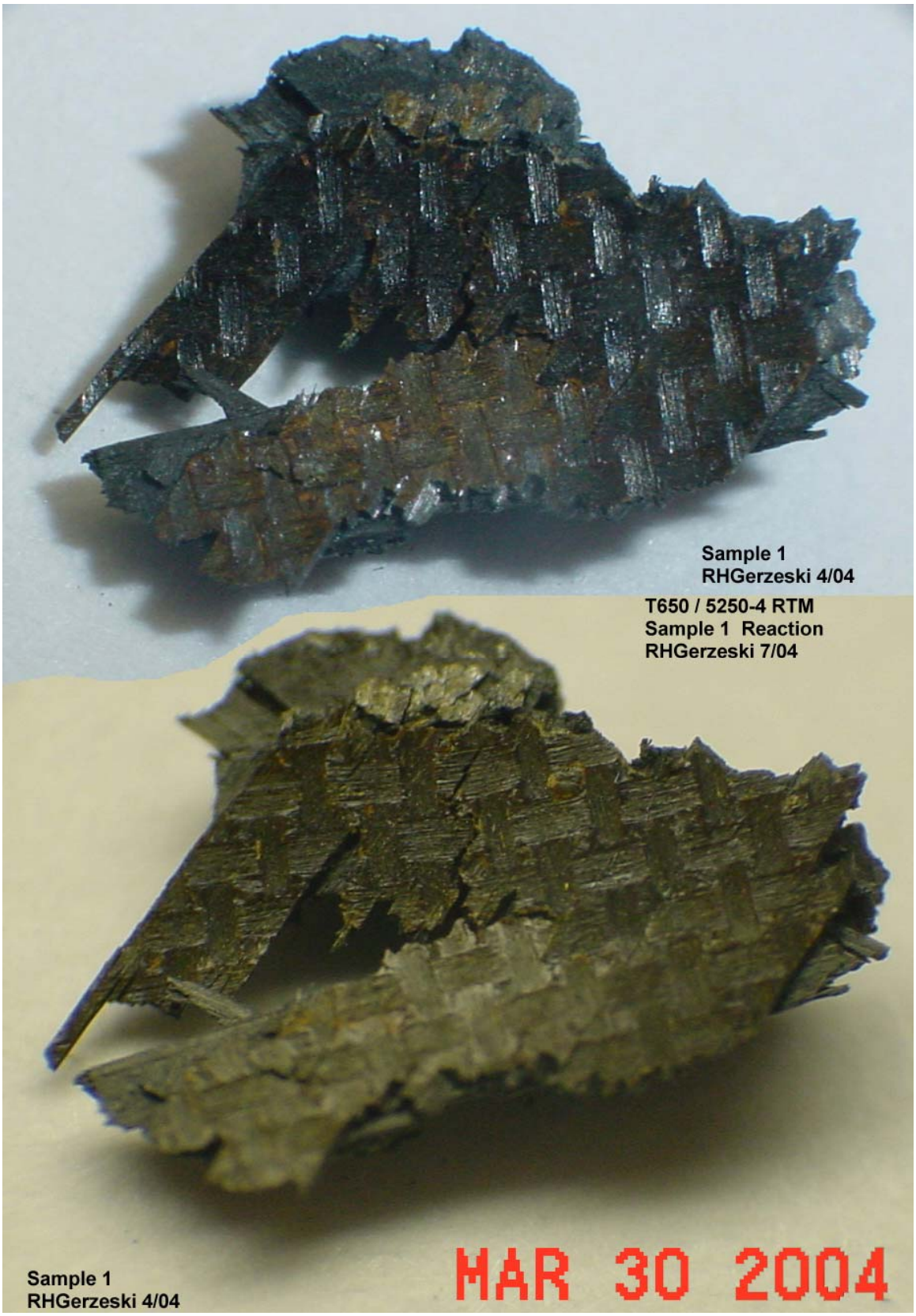


Figure 137-a-i, Internal To The Indenting Impacter Fracture Surfaces: Specimen Original Surface: T650-35 / 5250-4 RTM D2512 Specimen: In LOX: Reaction Detected

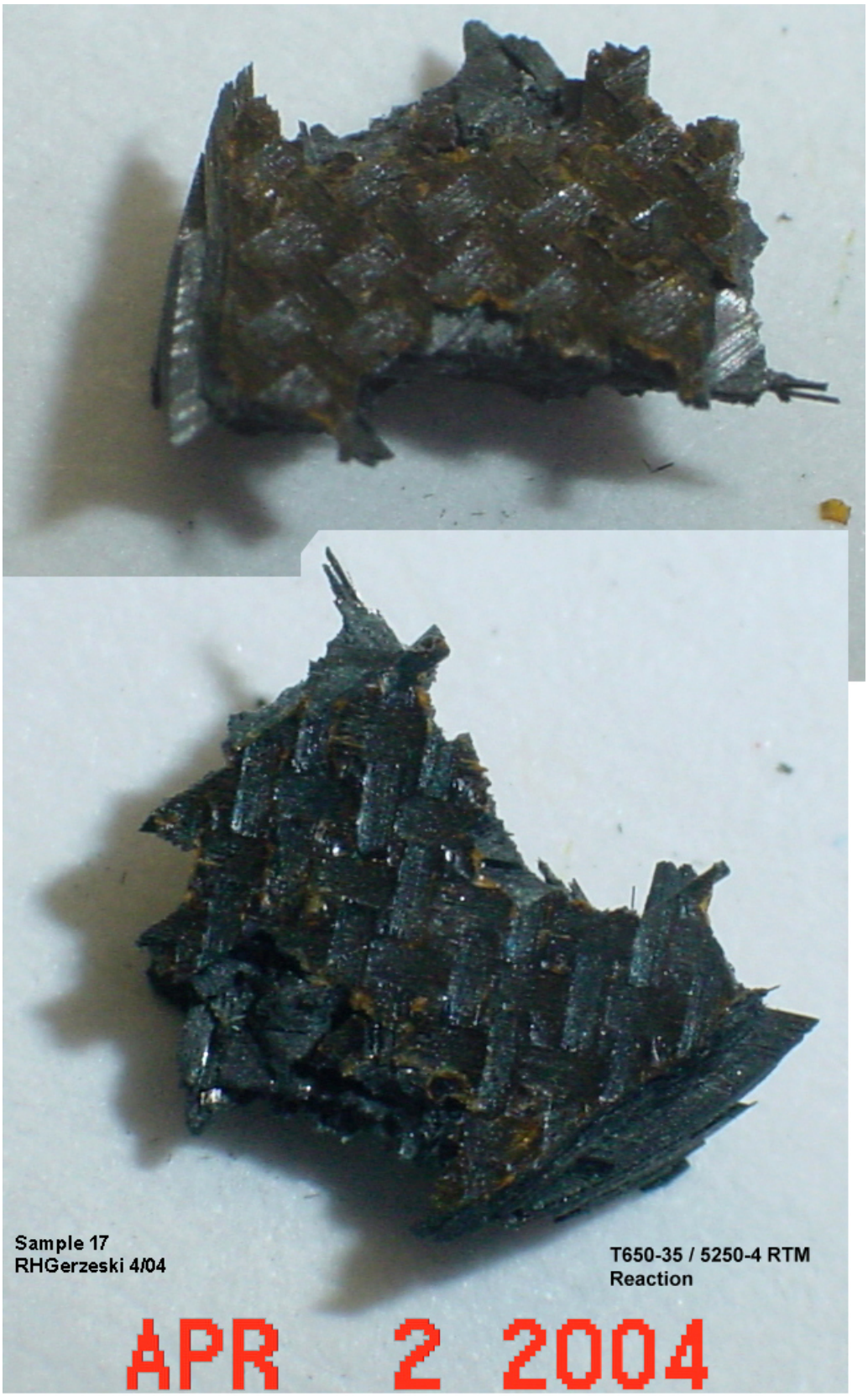


Figure 137-a-ii, Internal To The Indenting Impacter Fracture Surfaces: Specimen Original Surface: T650-35 / 5250-4 RTM D2512 Specimen: In LOX: Reaction Detected

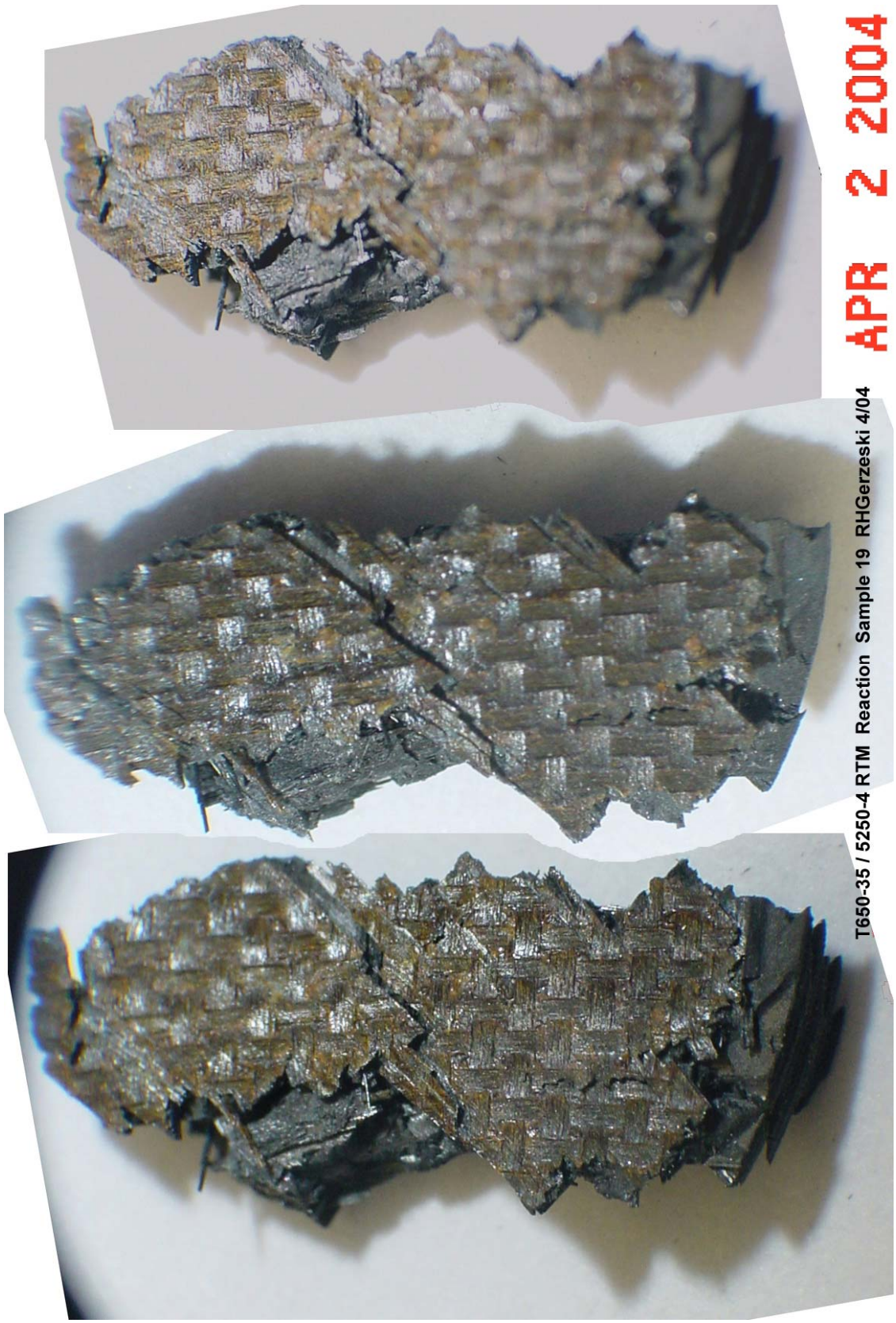


Figure 137-a-iii, Internal To The Indenting Impacter Fracture Surfaces: Specimen Original Surface: T650-35 / 5250-4 RTM D2512 Specimen: In LOX: Reaction Detected

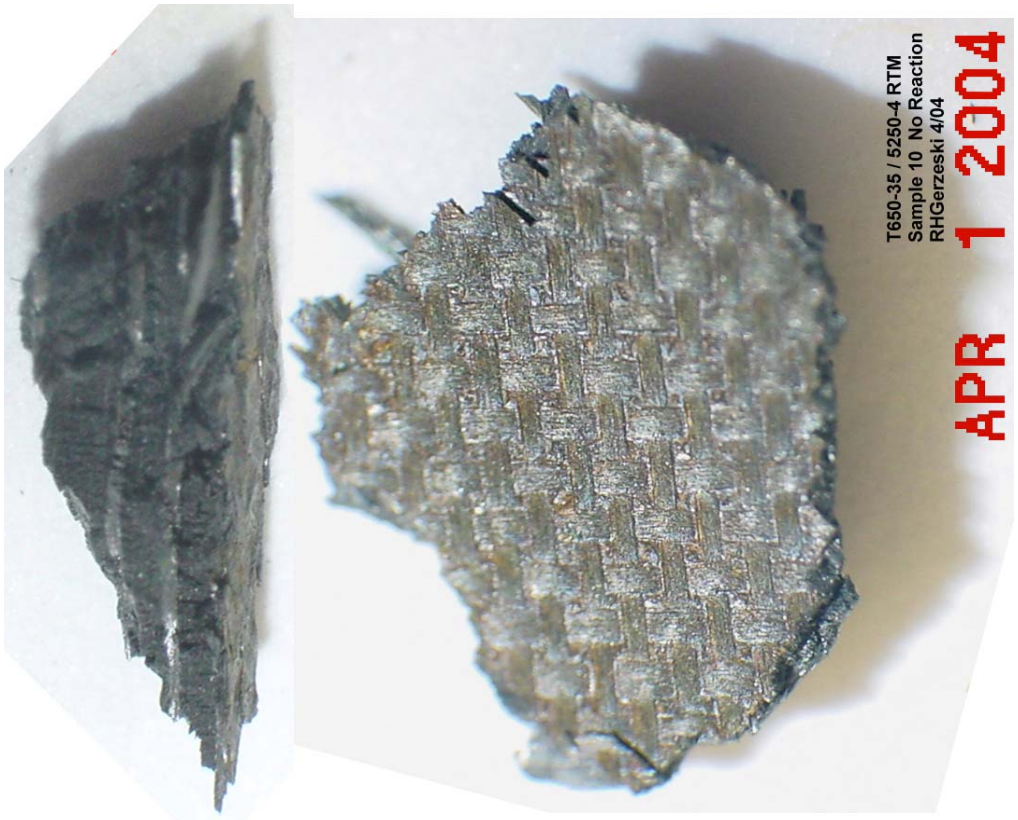


Figure 137-b-i, Internal To The Indenting Impacter Fracture Surfaces: Specimen Original Surface: T650-35 / 5250-4 RTM D2512 Specimen: In LOX: No Reaction Detected

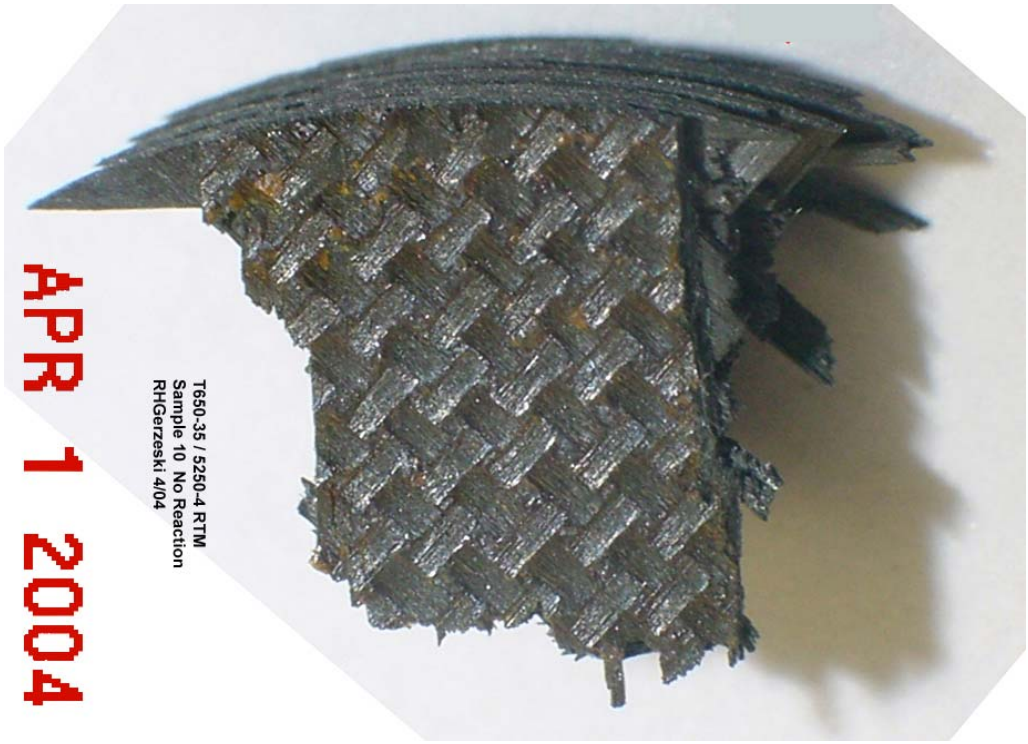


Figure 137-b-ii, Internal To The Indenting Impacter Fracture Surfaces: Specimen Original Surface: T650-35 / 5250-4 RTM D2512 Specimen: In LOX: No Reaction Detected



Figure 137-c-i, Internal To The Indenting Impacter Fracture Surfaces: Specimen Original Surface: T650-35 / 5250-4 RTM D2512 Specimen: In LN2



Figure 137-c-ii, Internal To The Indenting Impacter Fracture Surfaces: Specimen Original Surface: T650-35 / 5250-4 RTM D2512 Specimen: In LN2

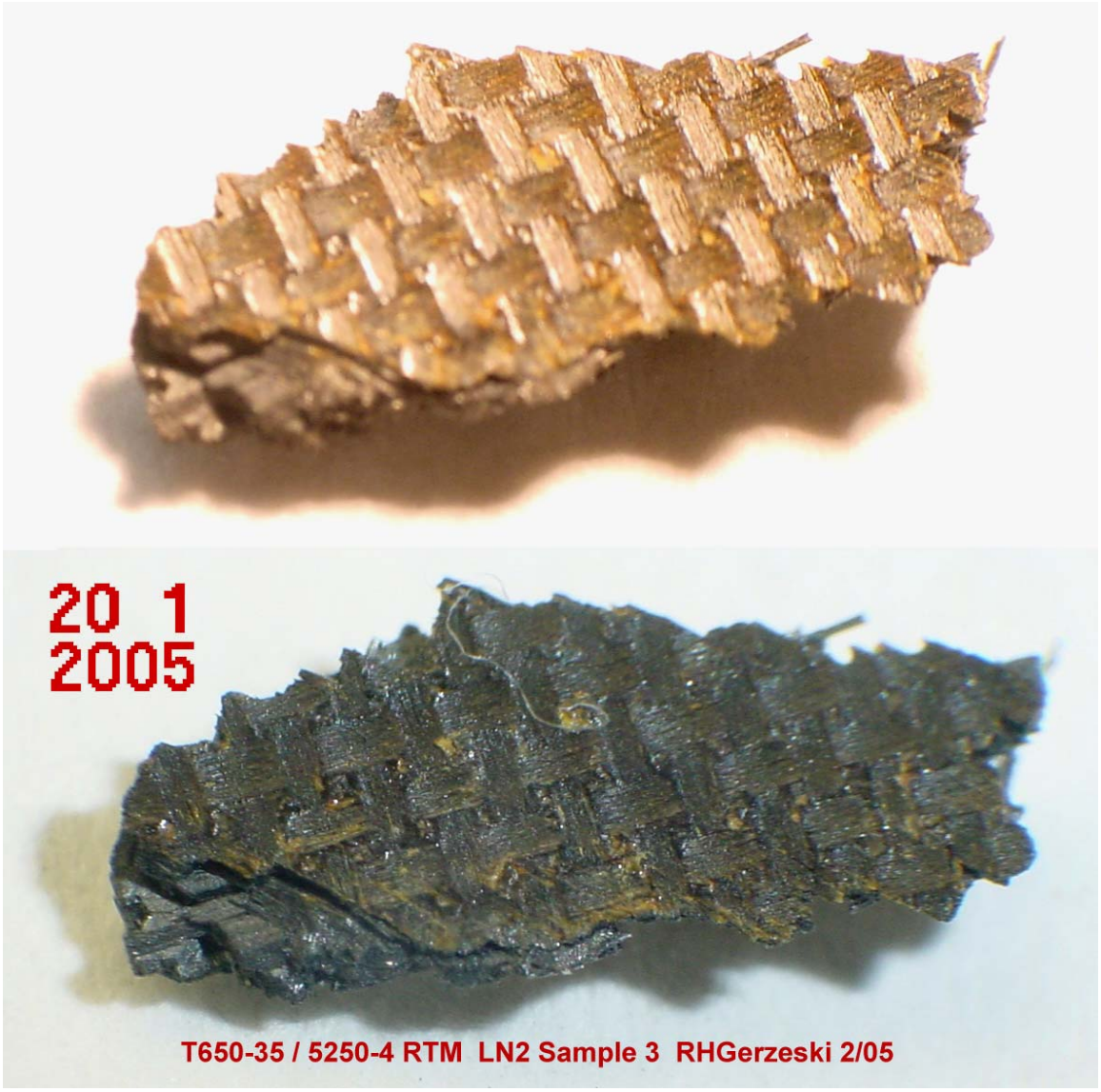


Figure 137-c-iii, Internal To The Indenting Impacter Fracture Surfaces: Specimen Original Surface: T650-35 / 5250-4 RTM D2512 Specimen: In LN2



Figure 138-a, Internal To The Indenting Impacter Fracture Surfaces: Specimen Original Surface: YSH50 / 5250-4 RTM D2512 Specimen: In LOX: Reaction Detected



Figure 138-b-i, Internal To The Indenting Impacter Fracture Surfaces: Specimen Original Surface: YSH50 / 5250-4 RTM D2512 Specimen: In LOX: No Reaction Detected

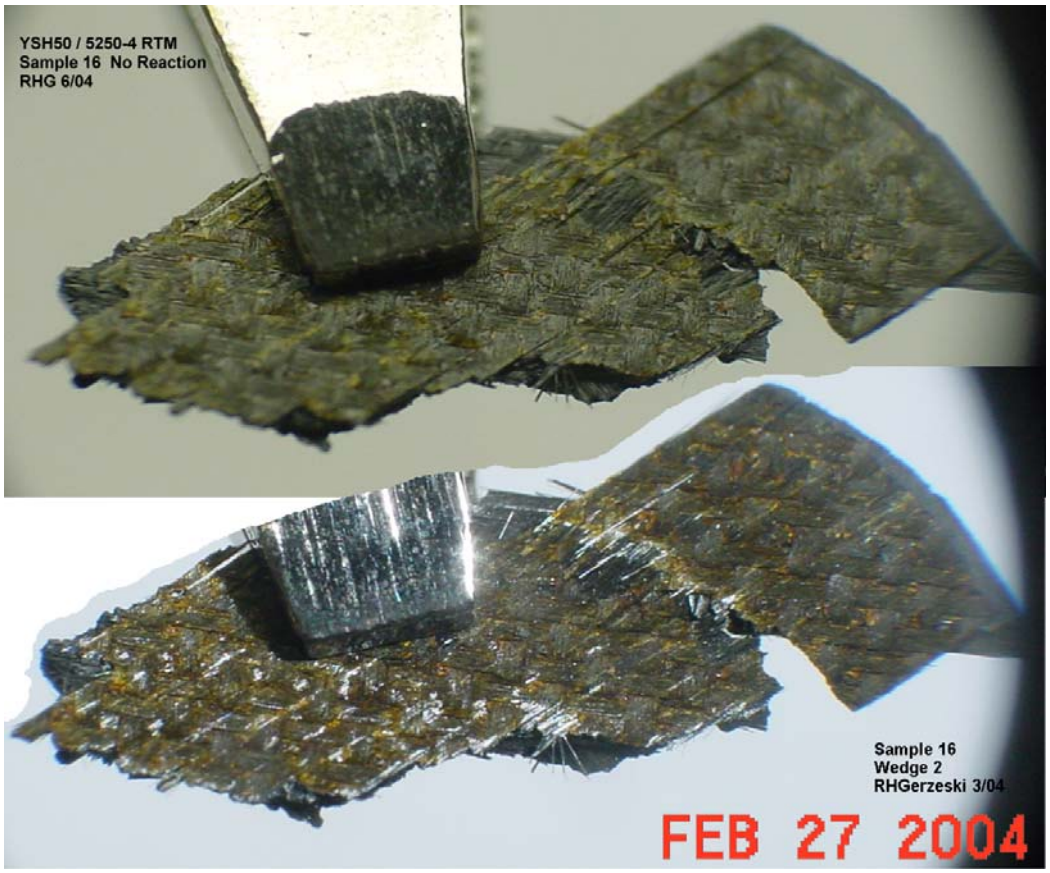


Figure 138-b-ii, Internal To The Indenting Impacter Fracture Surfaces: Specimen Original Surface: YSH50 / 5250-4 RTM D2512 Specimen: In LOX: No Reaction Detected



Figure 138-b-iii, Internal To The Indenting Impacter Fracture Surfaces: Specimen Original Surface: YSH50 / 5250-4 RTM D2512 Specimen: In LOX: No Reaction Detected



Figure 138-c-i, Internal To The Indenting Impacter Fracture Surfaces: Specimen Original Surface: YSH50 / 5250-4 RTM D2512 Specimen: In LN2



Figure 138-c-ii, Internal To The Indenting Impacter Fracture Surfaces: Specimen Original Surface: YSH50 / 5250-4 RTM D2512 Specimen: In LN2

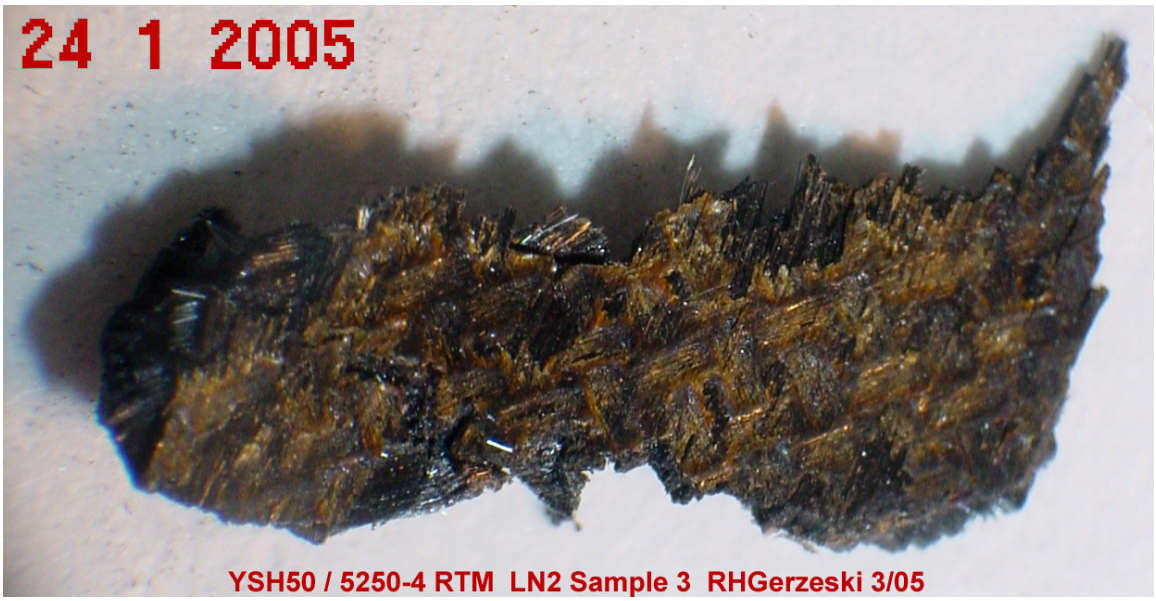


Figure 138-c-iii, Internal To The Indenting Impacter Fracture Surfaces: Specimen Original Surface: YSH50 / 5250-4 RTM D2512 Specimen: In LN2



Figure 139-a-i, Internal To The Indenting Impacter Fracture Surfaces: Specimen Original Surface: YSH60 / 5250-4 RTM D2512 Specimen: In LOX: Reaction Detected

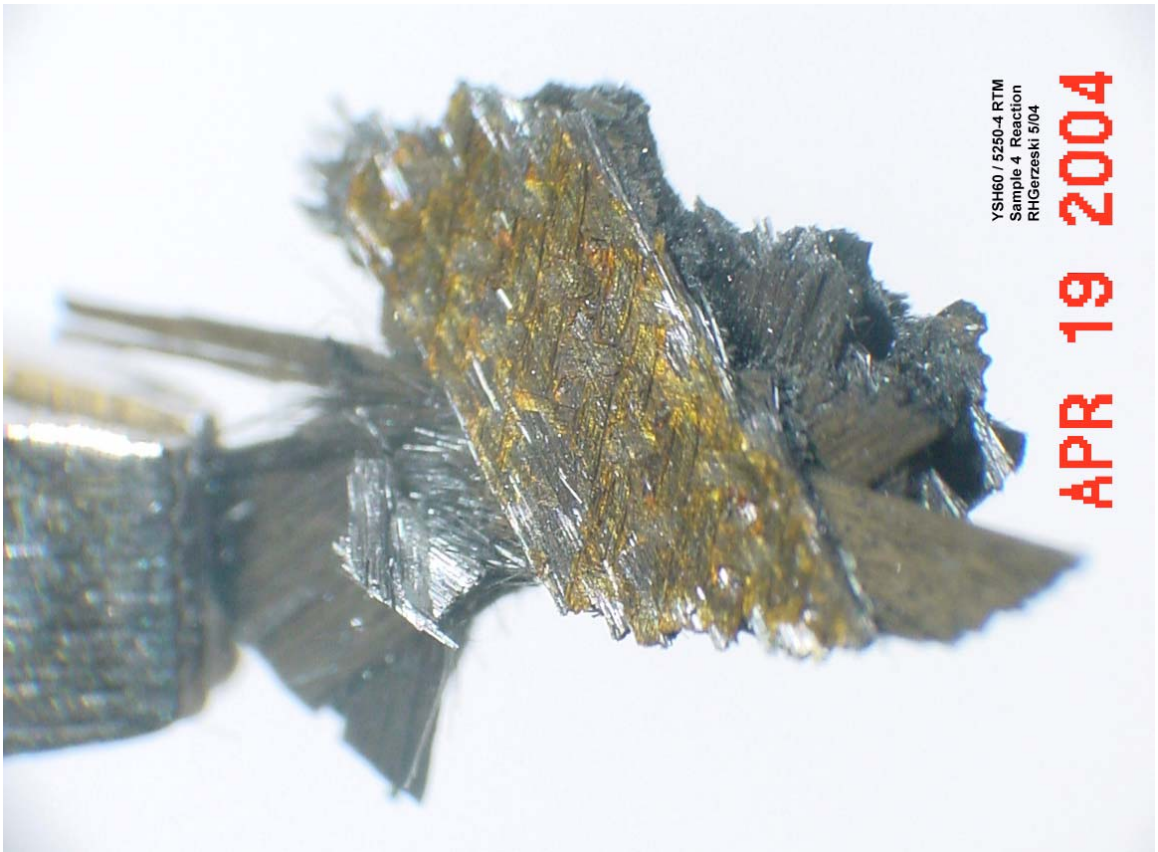


Figure 139-a-ii, Internal To The Indenting Impacter Fracture Surfaces: Specimen Original Surface: YSH60 / 5250-4 RTM D2512 Specimen: In LOX: Reaction Detected

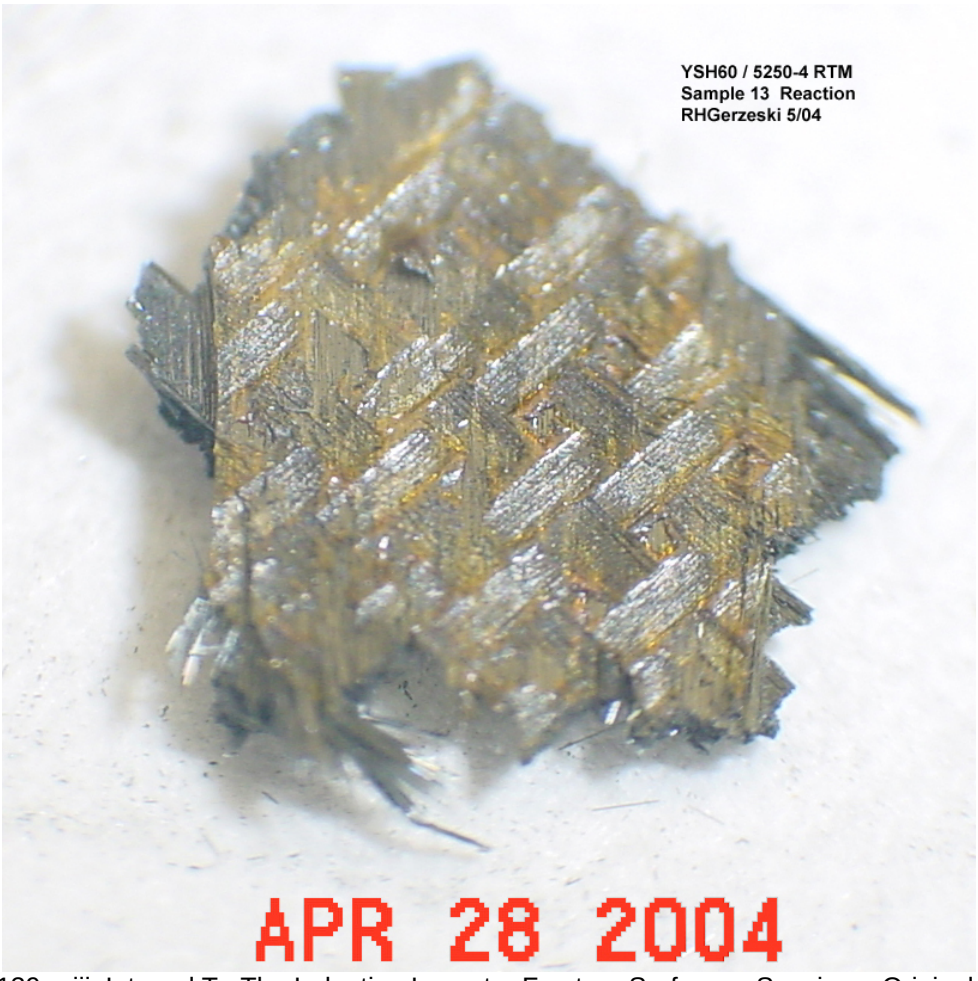


Figure 139-a-iii, Internal To The Indenting Impacter Fracture Surfaces: Specimen Original Surface: YSH60 / 5250-4 RTM D2512 Specimen: In LOX: Reaction Detected



Figure 139-b-i, Internal To The Indenting Impacter Fracture Surfaces: Specimen Original Surface: YSH60 / 5250-4 RTM D2512 Specimen: In LOX: No Reaction Detected



Figure 139-b-ii, Internal To The Indenting Impacter Fracture Surfaces: Specimen Original Surface: YSH60 / 5250-4 RTM D2512 Specimen: In LOX: No Reaction Detected



Figure 139-b-iii, Internal To The Indenting Impacter Fracture Surfaces: Specimen Original Surface: YSH60 / 5250-4 RTM D2512 Specimen: In LOX: No Reaction Detected

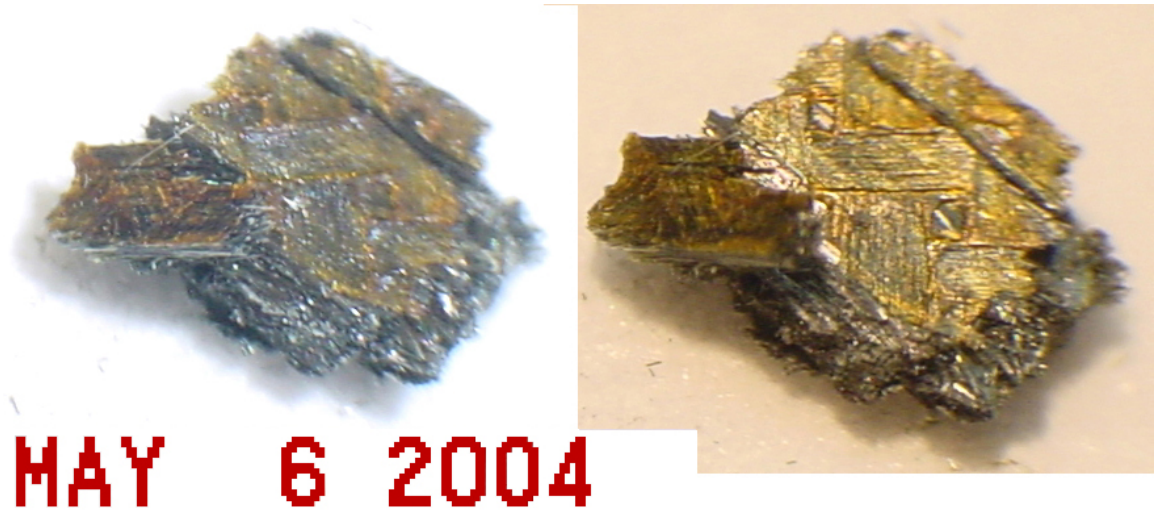


Figure 139-c-i, Internal To The Indenting Impacter Fracture Surfaces: Specimen Original Surface: YSH60 / 5250-4 RTM D2512 Specimen: In LN2



Figure 139-c-ii, Internal To The Indenting Impacter Fracture Surfaces: Specimen Original Surface: YSH60 / 5250-4 RTM D2512 Specimen: In LN2



Figure 140-a-i, Internal To The Indenting Impacter: Powder Fracture Surfaces: 5250-4 RTM D2512 Specimen: In LOX: Reaction Detected

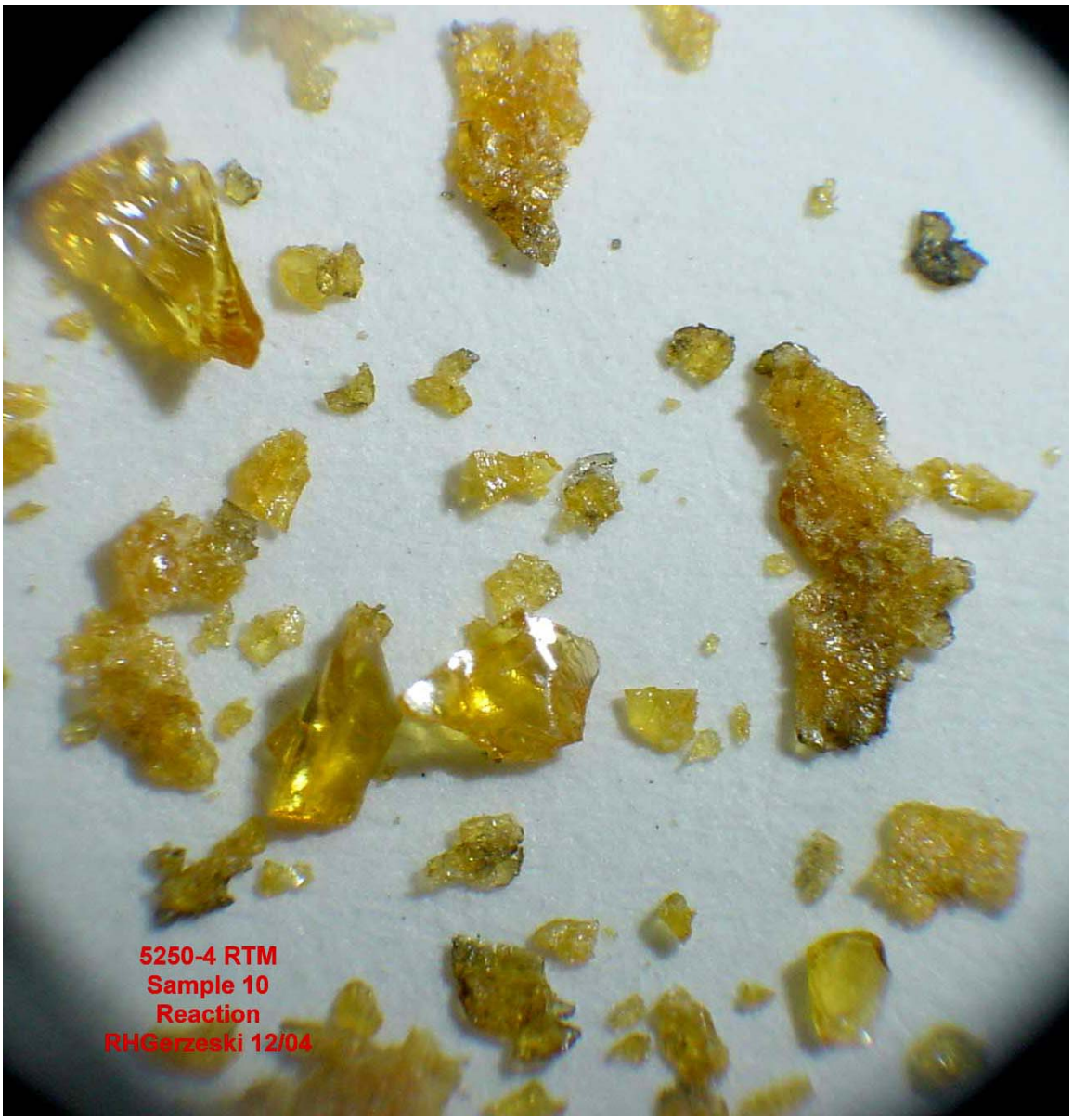


Figure 140-a-ii, Internal To The Indenting Impacter: Powder Fracture Surfaces: 5250-4 RTM D2512 Specimen: In LOX: Reaction Detected



Figure 140-c-i, Internal To The Indenting Impacter: Powder Fracture Surfaces: 5250-4 RTM D2512 Specimen: In LN2



Figure 140-c-ii, Internal To The Indenting Impacter: Powder Fracture Surfaces: 5250-4 RTM D2512 Specimen: In LN2



Figure 141-a, Internal To The Indenting Impacter: Powder Fracture Surfaces: T650-35 / 5250-4 RTM D2512 Specimen: In LOX: Reaction Detected



Figure 141-b, Internal To The Indenting Impacter: Powder Fracture Surfaces: T650-35 / 5250-4 RTM D2512 Specimen: In LOX: No Reaction Detected



Figure 141-c, Internal To The Indenting Impacter: Powder Fracture Surfaces: T650-35 / 5250-4 RTM D2512 Specimen: In LN2



Figure 142-a, Internal To The Indenting Impacter: Powder Fracture Surfaces: YSH50 / 5250-4 RTM D2512 Specimen: In LOX: Reaction Detected



Figure 142-b-i, Internal To The Indenting Impacter: Powder Fracture Surfaces: YSH50 / 5250-4 RTM D2512 Specimen: In LOX: No Reaction Detected



Figure 142-b-ii, Internal To The Indenting Impacter: Powder Fracture Surfaces: YSH50 / 5250-4 RTM D2512 Specimen: In LOX: No Reaction Detected

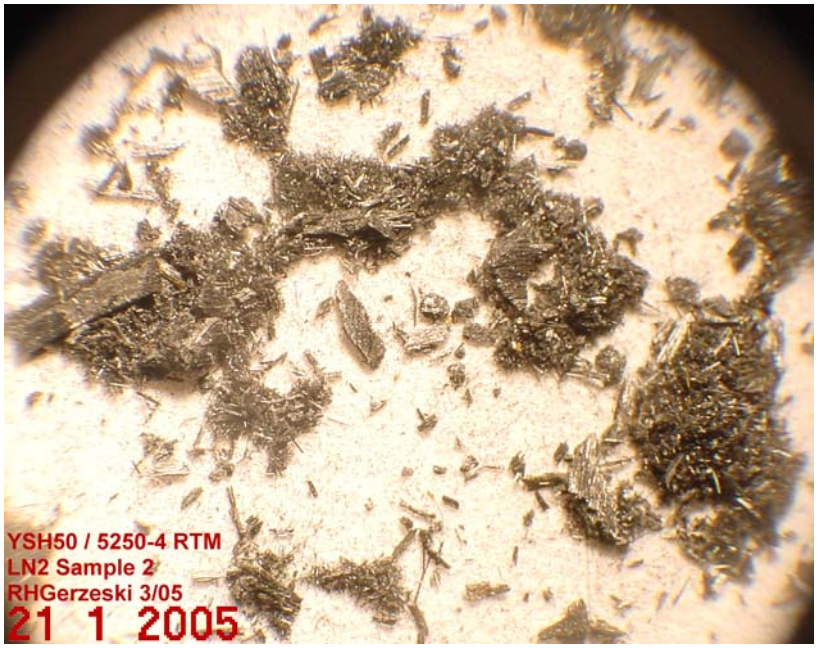


Figure 142-c, Internal To The Indenting Impacter: Powder Fracture Surfaces: YSH50 / 5250-4 RTM D2512 Specimen: In LN2



Figure 143-a-i, Internal To The Indenting Impacter: Powder Fracture Surfaces: YSH60 / 5250-4 RTM D2512 Specimen: In LOX: Reaction Detected



Figure 143-b-i, Internal To The Indenting Impacter: Powder Fracture Surfaces: YSH60 / 5250-4 RTM D2512 Specimen: In LOX: No Reaction Detected

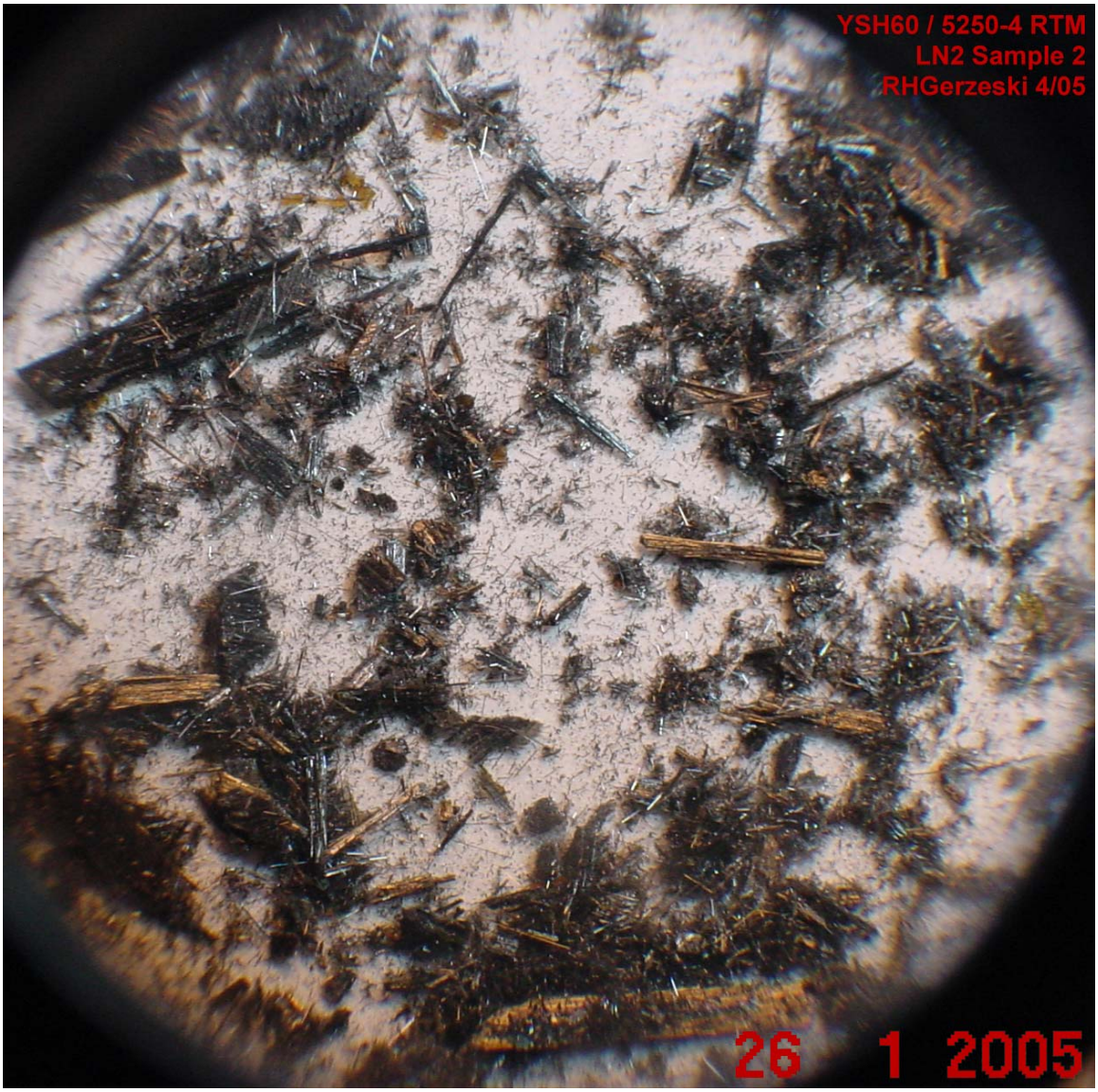


Figure 143-c, Internal To The Indenting Impacter: Powder Fracture Surfaces: YSH60 / 5250-4 RTM D2512 Specimen: In LN2



Figure 144-a-i, Internal To The Indenting Impacter: Powder Fracture Surfaces: Crescents: 5250-4 RTM D2512 Specimen: In LOX: Reaction Detected



Figure 144-a-ii, Internal To The Indenting Impacter: Powder Fracture Surfaces: Crescents: 5250-4 RTM D2512 Specimen: In LOX: Reaction Detected



Figure 144-a-iii, Internal To The Indenting Impacter: Powder Fracture Surfaces: Crescents: 5250-4 RTM D2512 Specimen: In LOX: Reaction Detected



Figure 144-c-i, Internal To The Indenting Impacter: Powder Fracture Surfaces: Crescents: 5250-4 RTM D2512 Specimen: In LN2



Figure 144-c-ii, Internal To The Indenting Impacter: Powder Fracture Surfaces: Crescents: 5250-4 RTM D2512 Specimen: In LN2



Figure 144-c-iii, Internal To The Indenting Impacter: Powder Fracture Surfaces: Crescents: 5250-4 RTM D2512 Specimen: In LN2



Figure 145-a, Internal To The Indenting Impacter: Powder Fracture Surfaces: Crescents: T650-35 / 5250-4 RTM D2512 Specimen: In LOX: Reaction Detected



Figure 145-b, Internal To The Indenting Impacter: Powder Fracture Surfaces: Crescents: T650-35 / 5250-4 RTM D2512 Specimen: In LOX: No Reaction Detected



Figure 145-c, Internal To The Indenting Impacter: Powder Fracture Surfaces: Crescents: T650-35 / 5250-4 RTM D2512 Specimen: In LN2

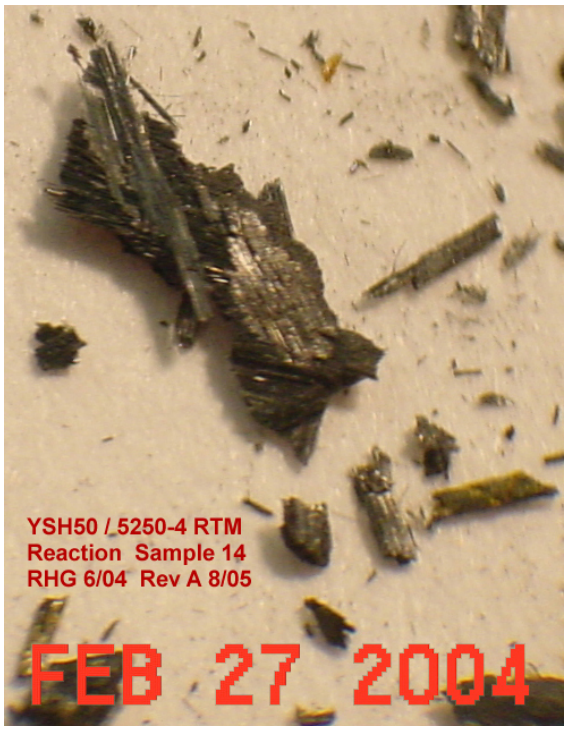


Figure 146-a, Internal To The Indenting Impacter: Powder Fracture Surfaces: Crescents: YSH50 / 5250-4 RTM D2512 Specimen: In LOX: Reaction Detected

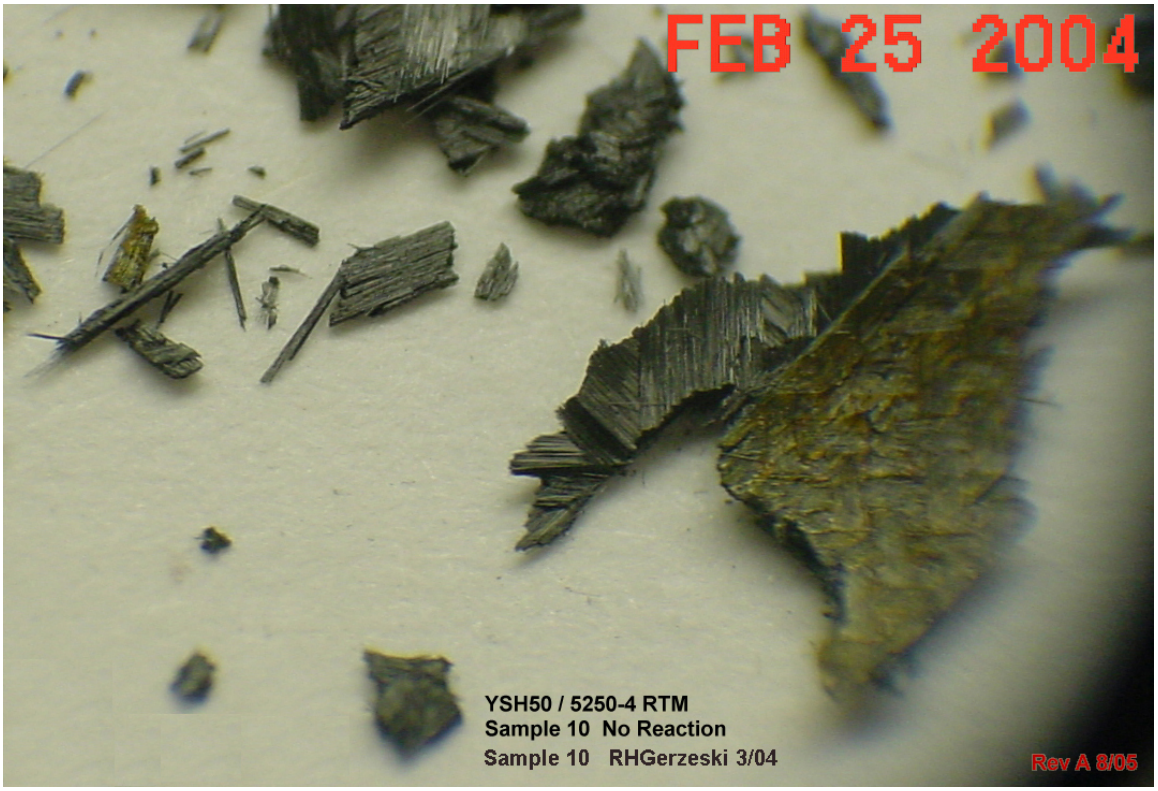


Figure 146-b, Internal To The Indenting Impacter: Powder Fracture Surfaces: Crescents: YSH50 / 5250-4 RTM D2512 Specimen: In LOX: No Reaction Detected

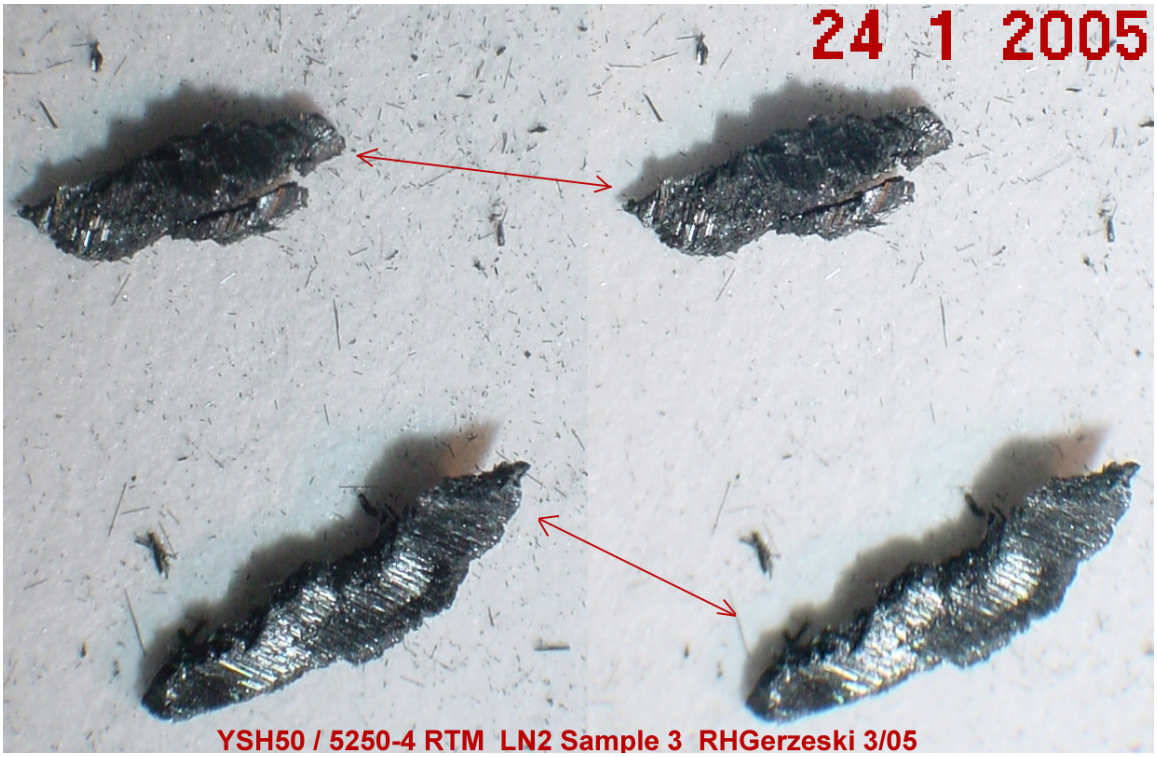


Figure 146-c, Internal To The Indenting Impacter: Powder Fracture Surfaces: Crescents: YSH50 / 5250-4 RTM D2512 Specimen: In LN2



Figure 147-a, Internal To The Indenting Impacter: Powder Fracture Surfaces: Crescents: YSH60 / 5250-4 RTM D2512 Specimen: In LOX: Reaction Detected



Figure 147-b, Internal To The Indenting Impacter: Powder Fracture Surfaces: Crescents: YSH60 / 5250-4 RTM D2512 Specimen: In LOX: No Reaction Detected



Figure 147-c, Internal To The Indenting Impacter: Powder Fracture Surfaces: Crescents: YSH60 / 5250-4 RTM D2512 Specimen: In LN2



Figure 148-a-i, Internal To The Indenting Impacter: Powder Fracture Surfaces: Abrasion: 5250-4 RTM D2512 Specimen: In LOX: Reaction Detected



Figure 148-a-ii, Internal To The Indenting Impacter: Powder Fracture Surfaces: Abrasion: 5250-4 RTM D2512 Specimen: In LOX: Reaction Detected



Figure 148-a-iii, Internal To The Indenting Impacter: Powder Fracture Surfaces: Abrasion: 5250-4 RTM D2512 Specimen: In LOX: Reaction Detected



Figure 148-b-i, Internal To The Indenting Impacter: Powder Fracture Surfaces: Abrasion: 5250-4 RTM D2512 Specimen: In LN2



Figure 148-b-ii, Internal To The Indenting Impacter: Powder Fracture Surfaces: Abrasion: 5250-4 RTM D2512 Specimen: In LN2



Figure 149-a, Internal To The Indenting Impacter: Powder Fracture Surfaces: Abrasion: T650-35 / 5250-4 RTM D2512 Specimen: In LOX: Reaction Detected



Figure 149-b, Internal To The Indenting Impacter: Powder Fracture Surfaces: Abrasion: T650-35 / 5250-4 RTM D2512 Specimen: In LOX: No Reaction Detected



Figure 149-c, Internal To The Indenting Impacter: Powder Fracture Surfaces: Abrasion: T650-35 / 5250-4 RTM D2512 Specimen: In LN2



Figure 150-a, Internal To The Indenting Impacter: Powder Fracture Surfaces: Abrasion: YSH50 / 5250-4 RTM D2512 Specimen: In LOX: Reaction Detected

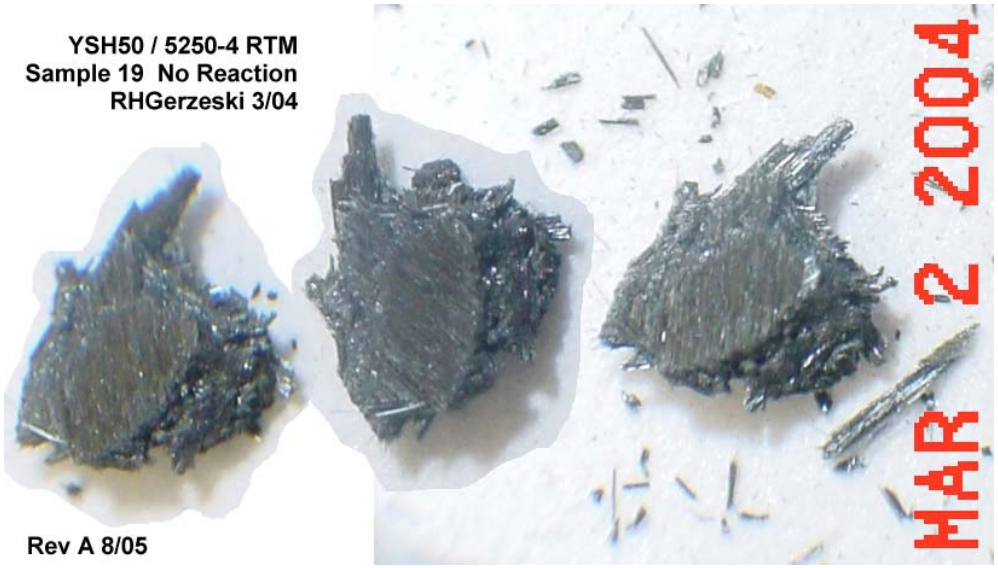


Figure 150-b, Internal To The Indenting Impacter: Powder Fracture Surfaces: Abrasion: YSH50 / 5250-4 RTM D2512 Specimen: In LOX: No Reaction Detected



Figure 150-c, Internal To The Indenting Impacter: Powder Fracture Surfaces: Abrasion: YSH50 / 5250-4 RTM D2512 Specimen: In LN2



Figure 151-a, Internal To The Indenting Impacter: Powder Fracture Surfaces: Abrasion: YSH60 / 5250-4 RTM D2512 Specimen: In LOX: Reaction Detected



Figure 151-b, Internal To The Indenting Impacter: Powder Fracture Surfaces: Abrasion: YSH60 / 5250-4 RTM D2512 Specimen: In LOX: No Reaction Detected



Figure 151-c-i, Internal To The Indenting Impacter: Powder Fracture Surfaces: Abrasion: YSH60 / 5250-4 RTM D2512 Specimen: In LN2



Figure 151-c-ii, Internal To The Indenting Impacter: Powder Fracture Surfaces: Abrasion: YSH60 / 5250-4 RTM D2512 Specimen: In LN2



Figure 152-a-i, Internal To The Indenting Impacter: Powder Fracture Surfaces: Intense Heat: 5250-4 RTM D2512 Specimen: In LOX: Reaction Detected



Figure 152-a-ii, Internal To The Indenting Impacter: Powder Fracture Surfaces: Intense Heat: 5250-4 RTM D2512 Specimen: In LOX: Reaction Detected



Figure 152-a-iii, Internal To The Indenting Impacter: Powder Fracture Surfaces: Intense Heat: 5250-4 RTM D2512 Specimen: In LOX: Reaction Detected



Figure 152-a-iv, Internal To The Indenting Impacter: Powder Fracture Surfaces: Intense Heat: 5250-4 RTM D2512 Specimen: In LOX: Reaction Detected



Figure 152-c-i, Internal To The Indenting Impacter: Powder Fracture Surfaces: Intense Heat: 5250-4 RTM D2512 Specimen: In LN2



Figure 152-c-ii, Internal To The Indenting Impacter: Powder Fracture Surfaces: Intense Heat: 5250-4 RTM D2512 Specimen: In LN2



Figure 152-c-iii, Internal To The Indenting Impacter: Powder Fracture Surfaces: Intense Heat: 5250-4 RTM D2512 Specimen: In LN2



Figure 153-a-i, Internal To The Indenting Impacter: Powder Fracture Surfaces: Intense Heat: T650-35 / 5250-4 RTM D2512 Specimen: In LOX: Reaction Detected

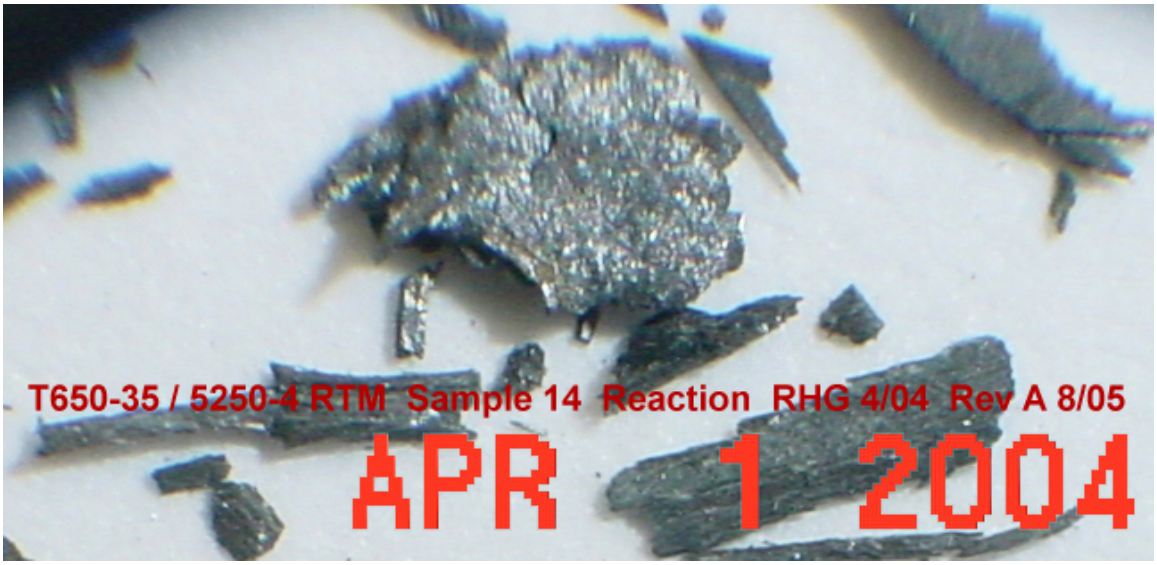


Figure 153-a-ii, Internal To The Indenting Impacter: Powder Fracture Surfaces: Intense Heat: T650-35 / 5250-4 RTM D2512 Specimen: In LOX: Reaction Detected



Figure 153-c, Internal To The Indenting Impacter: Powder Fracture Surfaces: Intense Heat: T650-35 / 5250-4 RTM D2512 Specimen: In LN2



Figure 154-a, Internal To The Indenting Impacter: Powder Fracture Surfaces: Intense Heat: YSH50 / 5250-4 RTM D2512 Specimen: In LOX: Reaction Detected



Figure 154-b, Internal To The Indenting Impacter: Powder Fracture Surfaces: Intense Heat: YSH50 / 5250-4 RTM D2512 Specimen: In LOX: No Reaction Detected

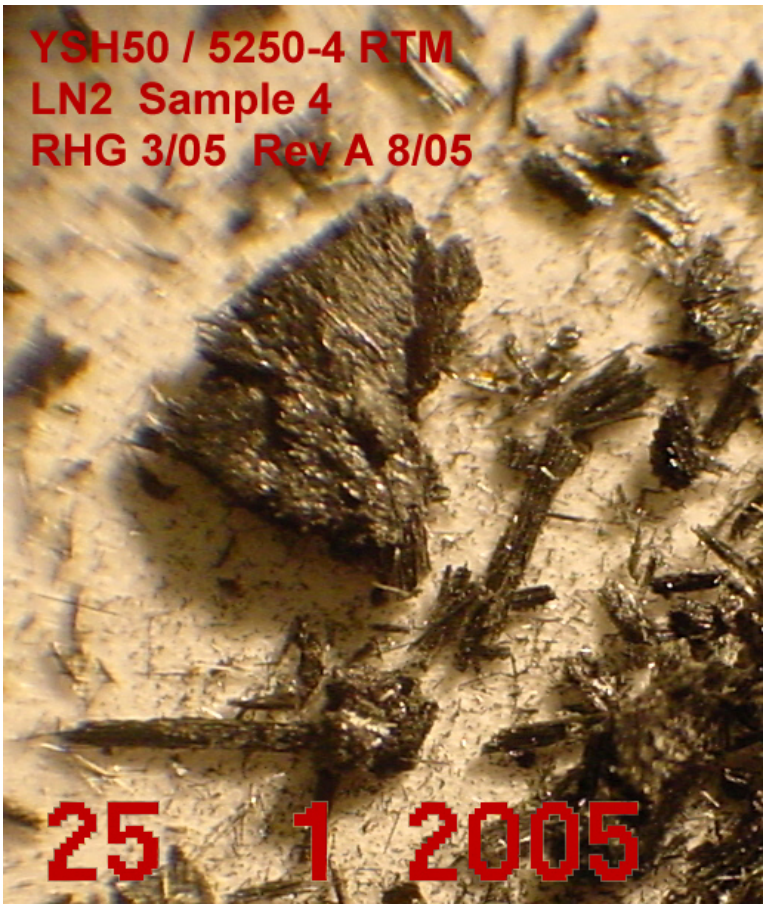


Figure 154-c, Internal To The Indenting Impacter: Powder Fracture Surfaces: Intense Heat: YSH50 / 5250-4 RTM D2512 Specimen: In LN2

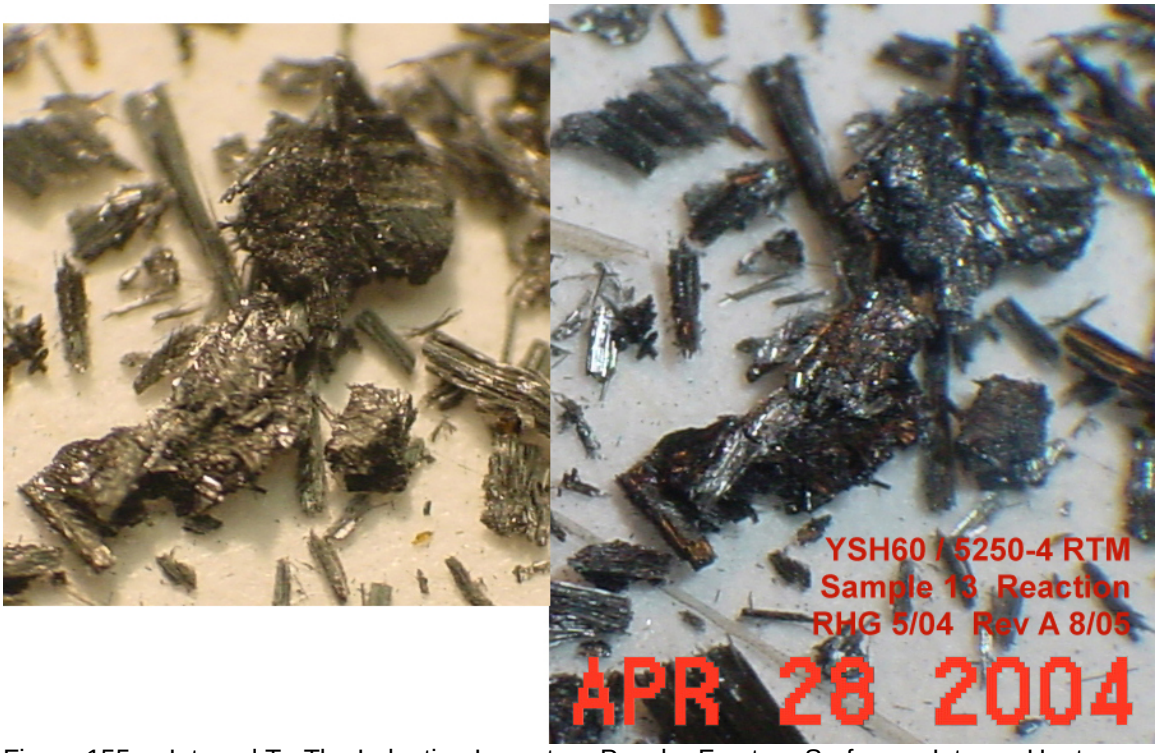


Figure 155-a, Internal To The Indenting Impacter: Powder Fracture Surfaces: Intense Heat: YSH60 / 5250-4 RTM D2512 Specimen: In LOX: Reaction Detected



Figure 155-b, Internal To The Indenting Impacter: Powder Fracture Surfaces: Intense Heat: YSH60 / 5250-4 RTM D2512 Specimen: In LOX: No Reaction Detected



Figure 155-c, Internal To The Indenting Impacter: Powder Fracture Surfaces: Intense Heat: YSH60 / 5250-4 RTM D2512 Specimen: In LN2



Figure 156-a, Internal To The Indenting Impacter: Powder Fracture Surfaces: Specimen Original Surface: 5250-4 RTM D2512 Specimen: In LOX: Reaction Detected



Figure 156-b, Internal To The Indenting Impacter: Powder Fracture Surfaces: Specimen Original Surface: 5250-4 RTM D2512 Specimen: In LN2

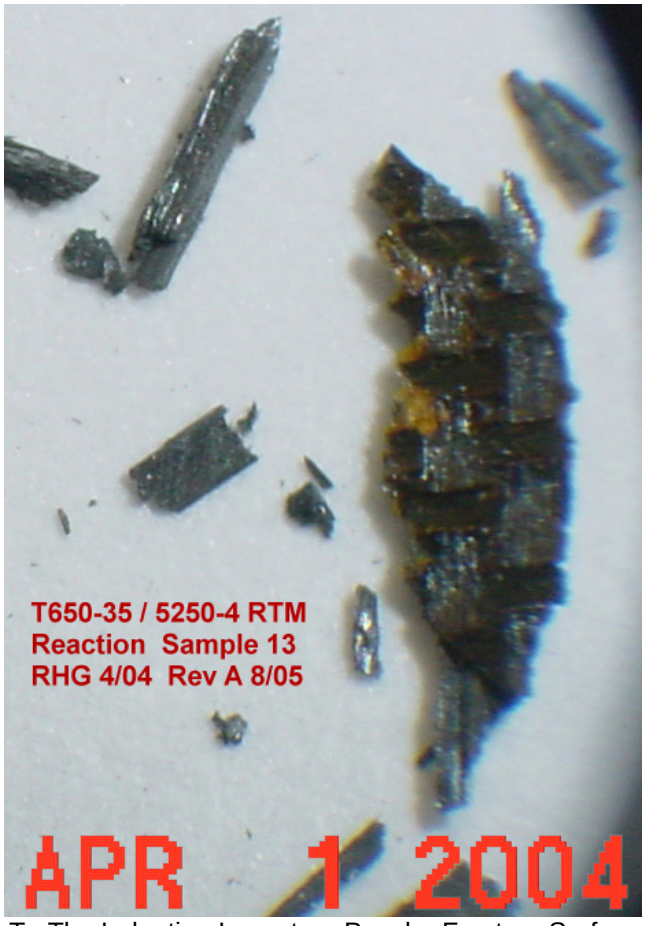


Figure 157-a, Internal To The Indenting Impacter: Powder Fracture Surfaces: Specimen Original Surface: T650-35 / 5250-4 RTM D2512 Specimen: In LOX: Reaction Detected



Figure 157-b, Internal To The Indenting Impacter: Powder Fracture Surfaces: Specimen Original Surface: T650-35 / 5250-4 RTM D2512 Specimen: In LN2



Figure 158-a, Internal To The Indenting Impacter: Powder Fracture Surfaces: Specimen Original Surface: YSH50 / 5250-4 RTM D2512 Specimen: In LOX: Reaction Detected



Figure 158-b, Internal To The Indenting Impacter: Powder Fracture Surfaces: Specimen Original Surface: YSH50 / 5250-4 RTM D2512 Specimen: In LOX: No Reaction Detected

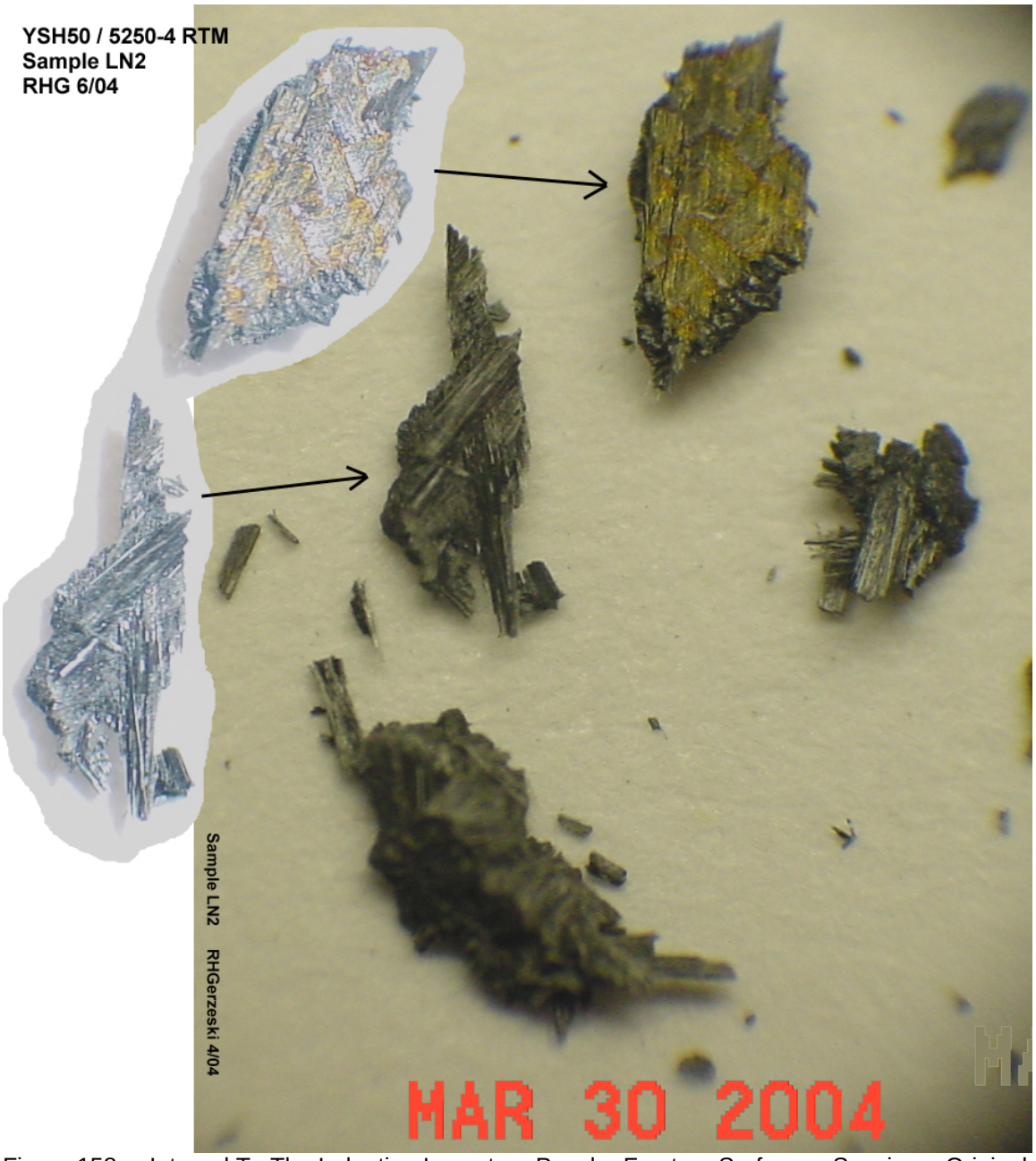


Figure 158-c, Internal To The Indenting Impacter: Powder Fracture Surfaces: Specimen Original Surface: YSH50 / 5250-4 RTM D2512 Specimen: In LN2



Figure 159-a, Internal To The Indenting Impacter: Powder Fracture Surfaces: Specimen Original Surface: YSH60 / 5250-4 RTM D2512 Specimen: In LOX: Reaction Detected

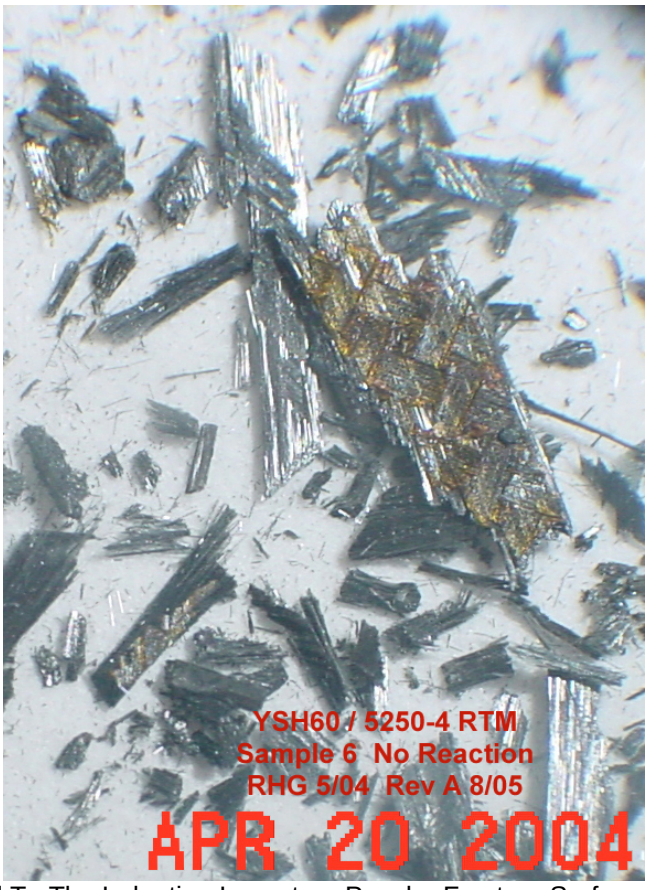


Figure 159-b, Internal To The Indenting Impacter: Powder Fracture Surfaces: Specimen Original Surface: YSH60 / 5250-4 RTM D2512 Specimen: In LOX: No Reaction Detected



Figure 159-c, Internal To The Indenting Impacter: Powder Fracture Surfaces: Specimen Original Surface: YSH60 / 5250-4 RTM D2512 Specimen: In LN2

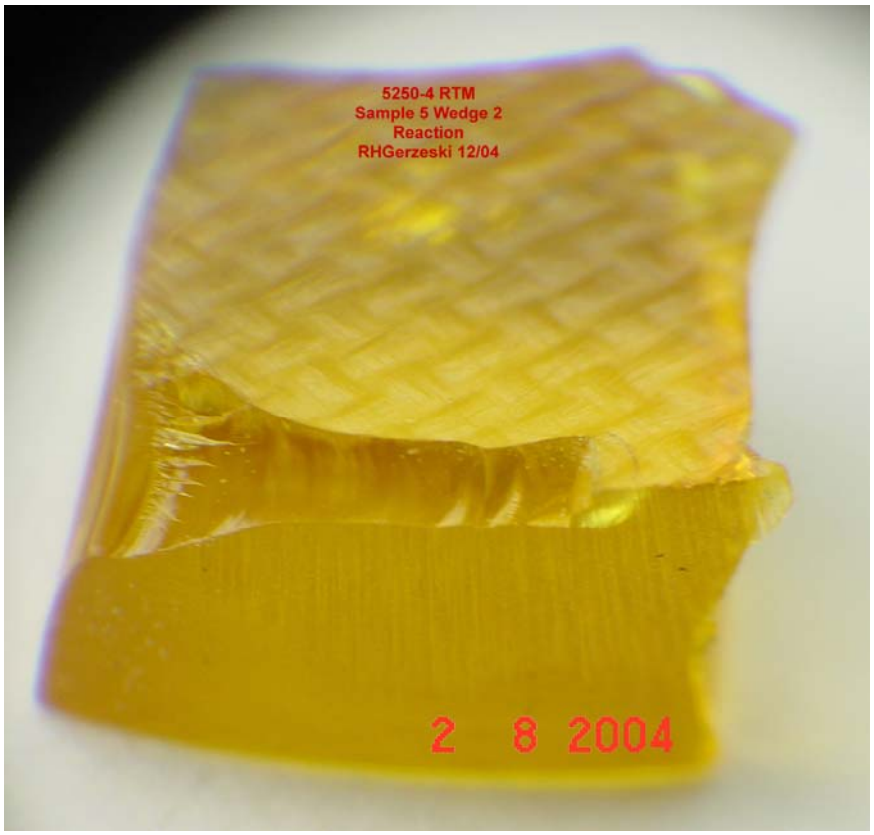


Figure 160-a-i, Cup Wall And Specimen Interaction: Back Side Impact: 5250-4 RTM D2512 Specimen: In LOX: Reaction Detected



Figure 160-a-ii, Cup Wall And Specimen Interaction: Back Side Impact: 5250-4 RTM D2512 Specimen: In LOX: Reaction Detected



Figure 160-a-iii, Cup Wall And Specimen Interaction: Back Side Impact: 5250-4 RTM D2512 Specimen: In LOX: Reaction Detected

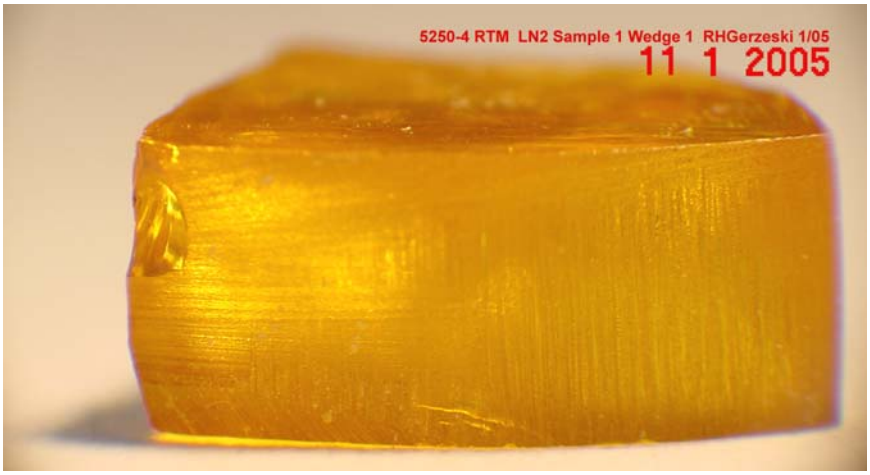


Figure 160-b-i, Cup Wall And Specimen Interaction: Back Side Impact: 5250-4 RTM D2512 Specimen: In LN2



Figure 160-b-ii, Cup Wall And Specimen Interaction: Back Side Impact: 5250-4 RTM D2512 Specimen: In LN2

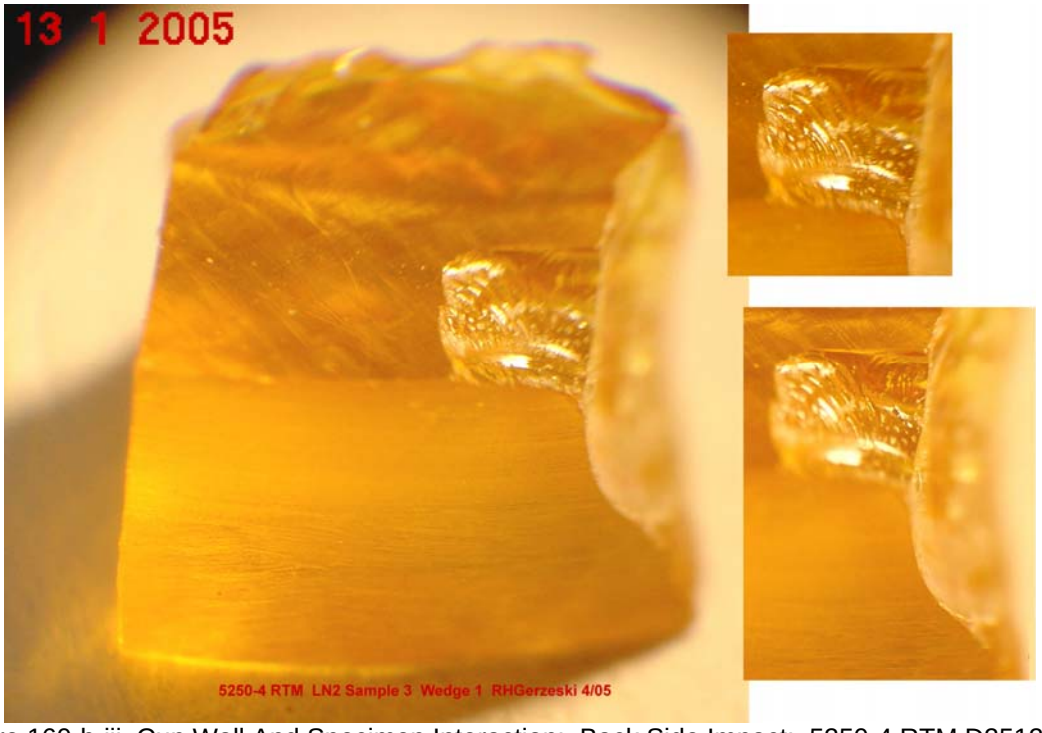


Figure 160-b-iii, Cup Wall And Specimen Interaction: Back Side Impact: 5250-4 RTM D2512 Specimen: In LN2

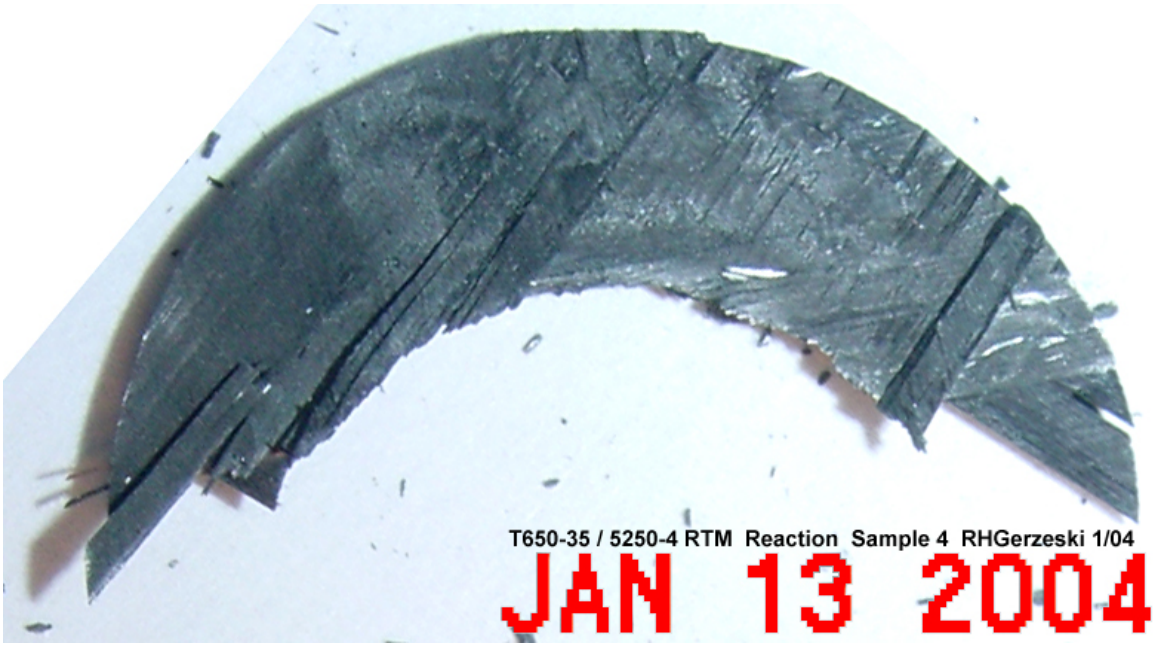


Figure 161-a-i, Cup Wall And Specimen Interaction: Back Side Impact: T650-35 / 5250-4 RTM D2512 Specimen: In LOX: Reaction Detected



Figure 161-a-ii, Cup Wall And Specimen Interaction: Back Side Impact: T650-35 / 5250-4 RTM D2512 Specimen: In LOX: Reaction Detected



Figure 161-b, Cup Wall And Specimen Interaction: Back Side Impact: T650-35 / 5250-4 RTM D2512 Specimen: In LOX: No Reaction Detected



Figure 161-c-i, Cup Wall And Specimen Interaction: Back Side Impact: T650-35 / 5250-4 RTM D2512 Specimen: In LN2

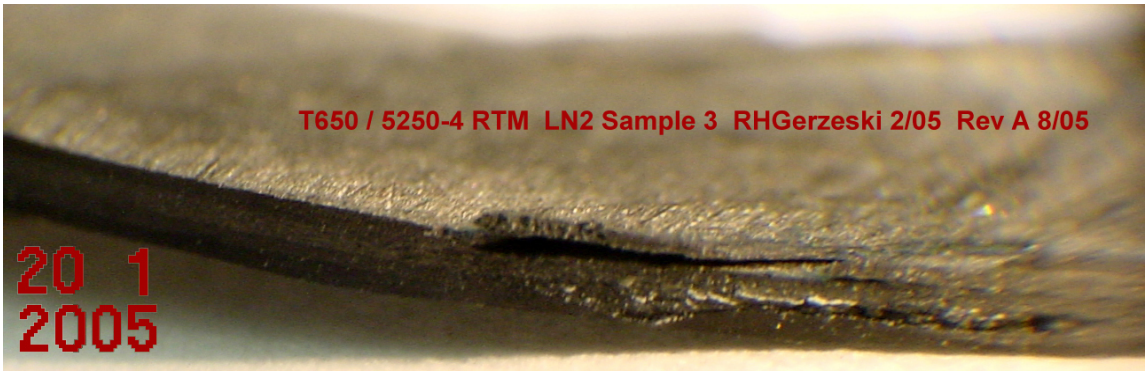


Figure 161-c-ii, Cup Wall And Specimen Interaction: Back Side Impact: T650-35 / 5250-4 RTM D2512 Specimen: In LN2

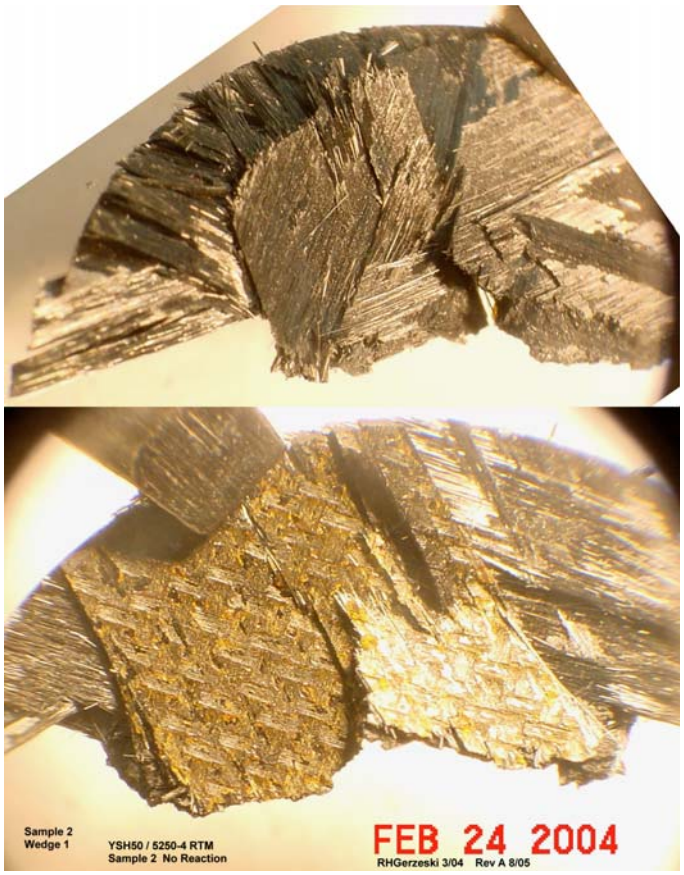


Figure 162-a-i, Cup Wall And Specimen Interaction: Back Side Impact: YSH50 / 5250-4 RTM D2512 Specimen: In LOX: No Reaction Detected

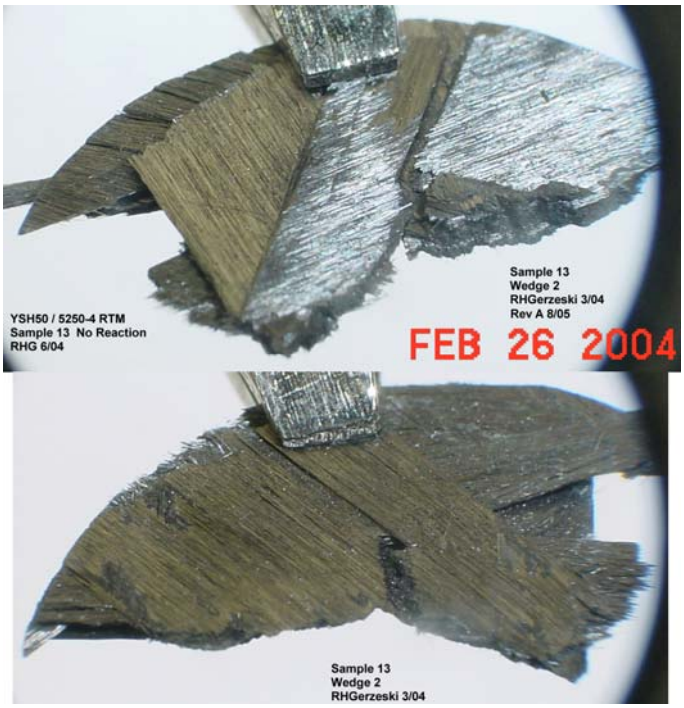


Figure 162-a-ii, Cup Wall And Specimen Interaction: Back Side Impact: YSH50 / 5250-4 RTM D2512 Specimen: In LOX: No Reaction Detected



Figure 162-a-iii, Cup Wall And Specimen Interaction: Back Side Impact: YSH50 / 5250-4 RTM D2512 Specimen: In LOX: No Reaction Detected

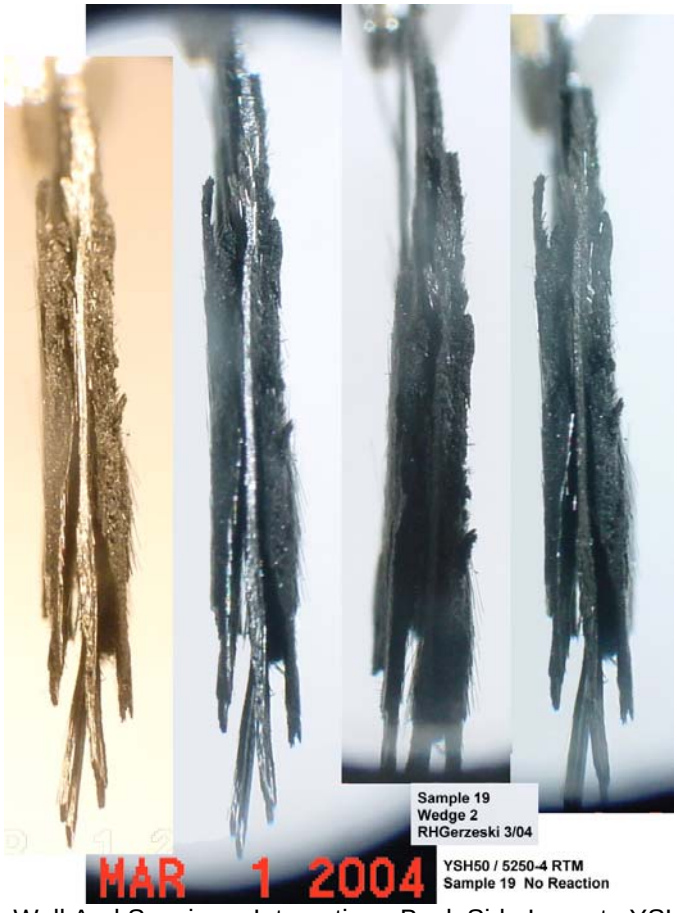


Figure 162-a-iv, Cup Wall And Specimen Interaction: Back Side Impact: YSH50 / 5250-4 RTM D2512 Specimen: In LOX: No Reaction Detected

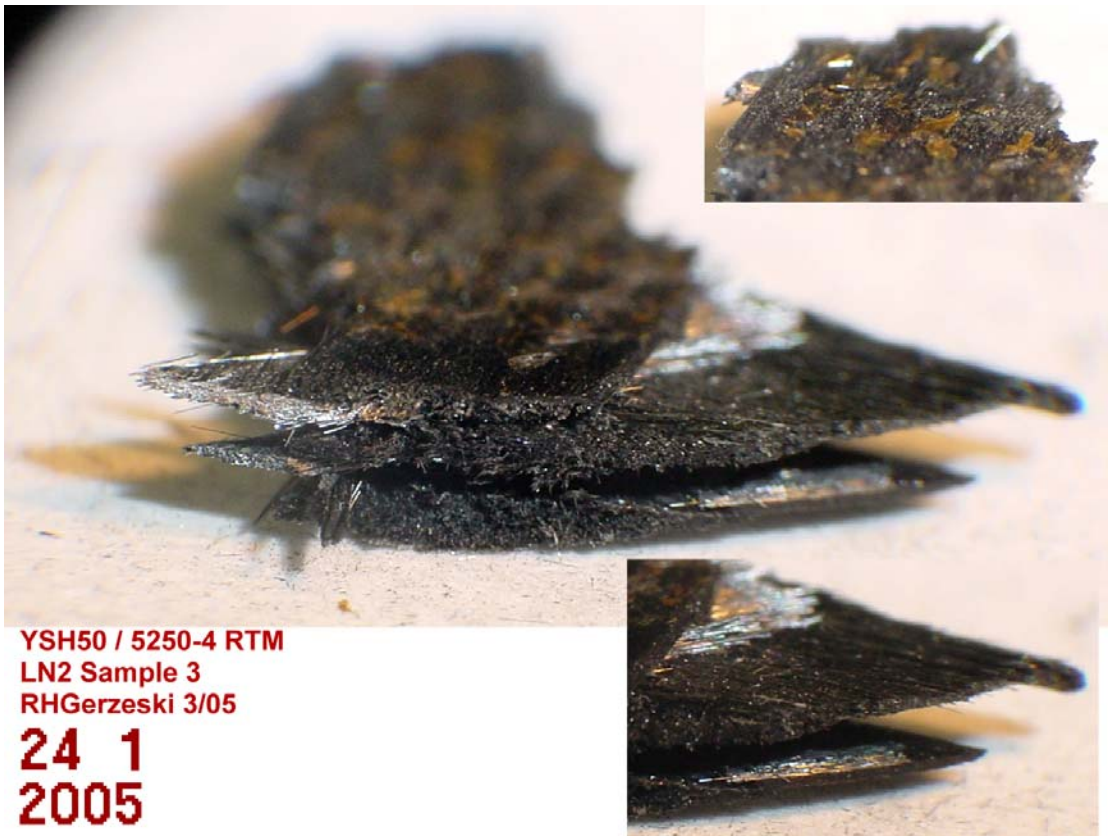


Figure 162-b-i, Cup Wall And Specimen Interaction: Back Side Impact: YSH50 / 5250-4 RTM D2512 Specimen: In LN2



Figure 162-b-ii, Cup Wall And Specimen Interaction: Back Side Impact: YSH50 / 5250-4 RTM D2512 Specimen: In LN2

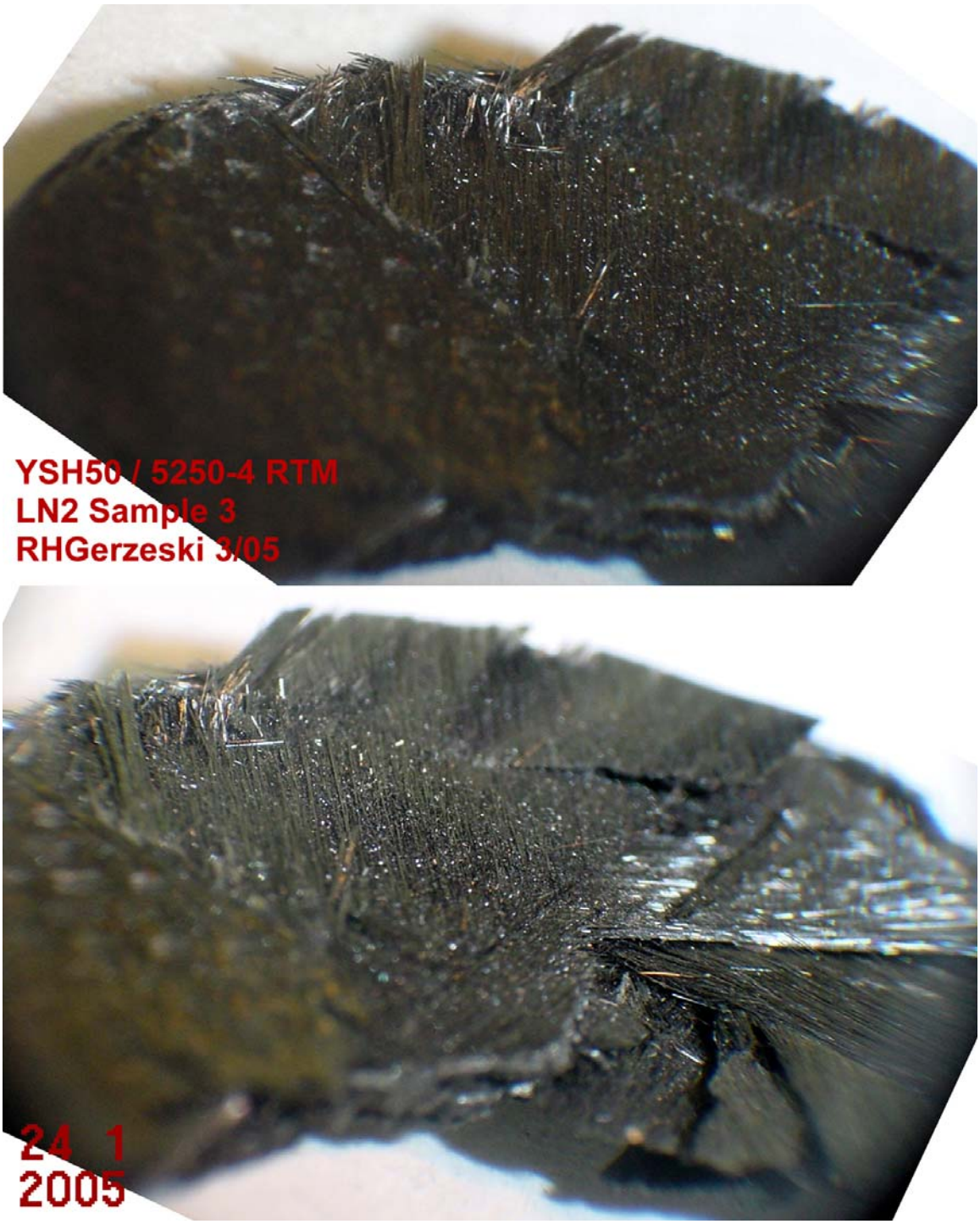


Figure 162-b-iii, Cup Wall And Specimen Interaction: Back Side Impact: YSH50 / 5250-4 RTM D2512 Specimen: In LN2



Figure 163-a-i, Cup Wall And Specimen Interaction: Back Side Impact: YSH60 / 5250-4 RTM D2512 Specimen: In LOX: Reaction Detected



Figure 163-a-ii, Cup Wall And Specimen Interaction: Back Side Impact: YSH60 / 5250-4 RTM D2512 Specimen: In LOX: Reaction Detected



Figure 163-b-i, Cup Wall And Specimen Interaction: Back Side Impact: YSH60 / 5250-4 RTM D2512 Specimen: In LOX: No Reaction Detected



Figure 163-b-ii, Cup Wall And Specimen Interaction: Back Side Impact: YSH60 / 5250-4 RTM D2512 Specimen: In LOX: No Reaction Detected

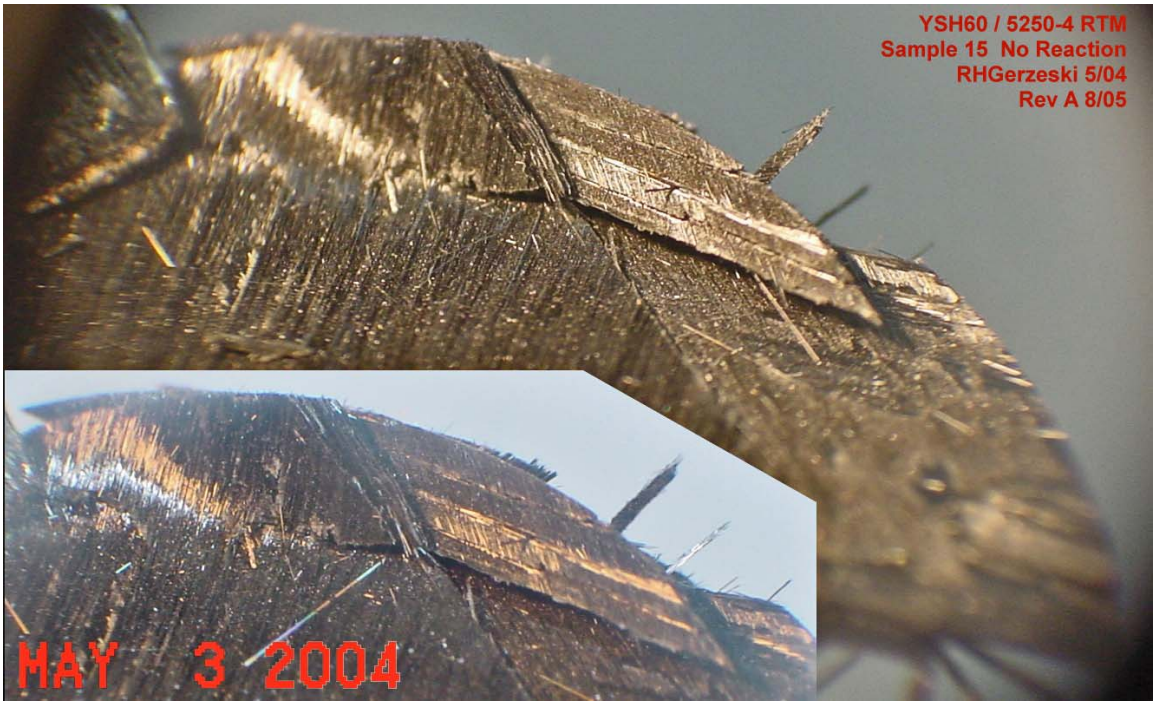


Figure 163-b-iii, Cup Wall And Specimen Interaction: Back Side Impact: YSH60 / 5250-4 RTM D2512 Specimen: In LOX: No Reaction Detected

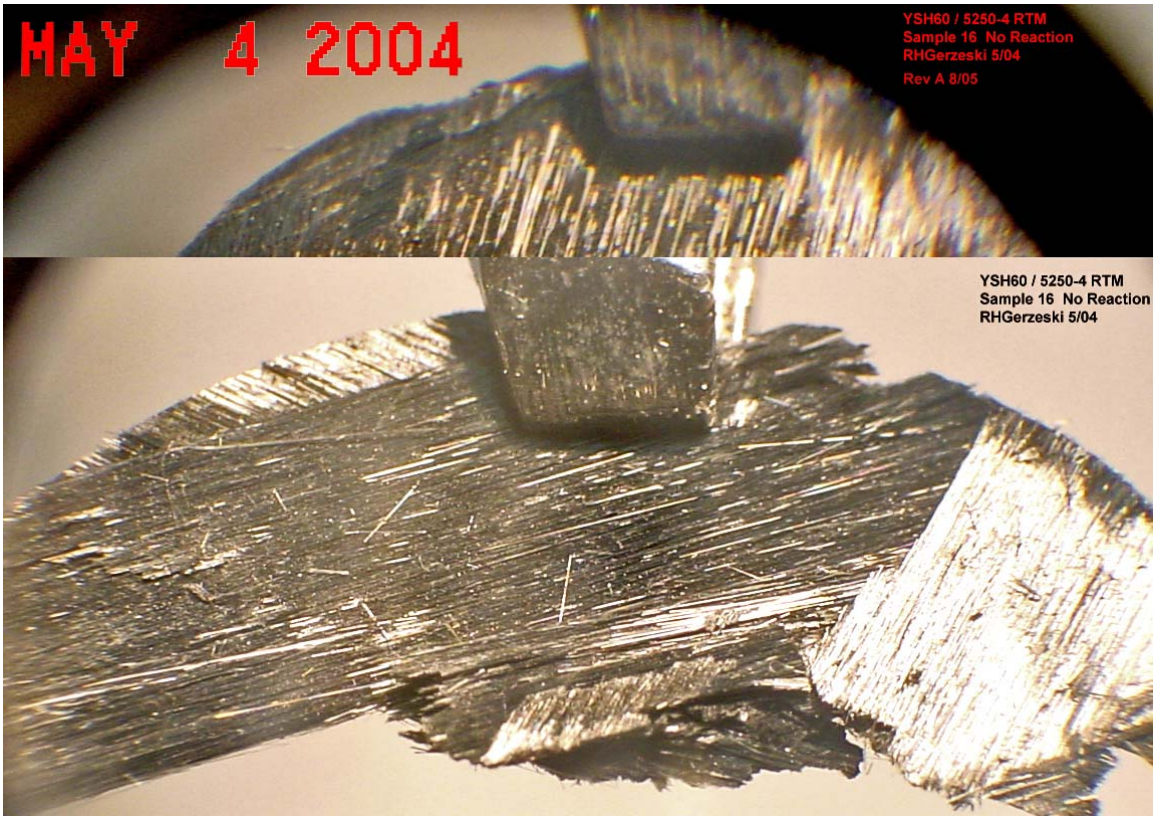


Figure 163-b-iv, Cup Wall And Specimen Interaction: Back Side Impact: YSH60 / 5250-4 RTM D2512 Specimen: In LOX: No Reaction Detected

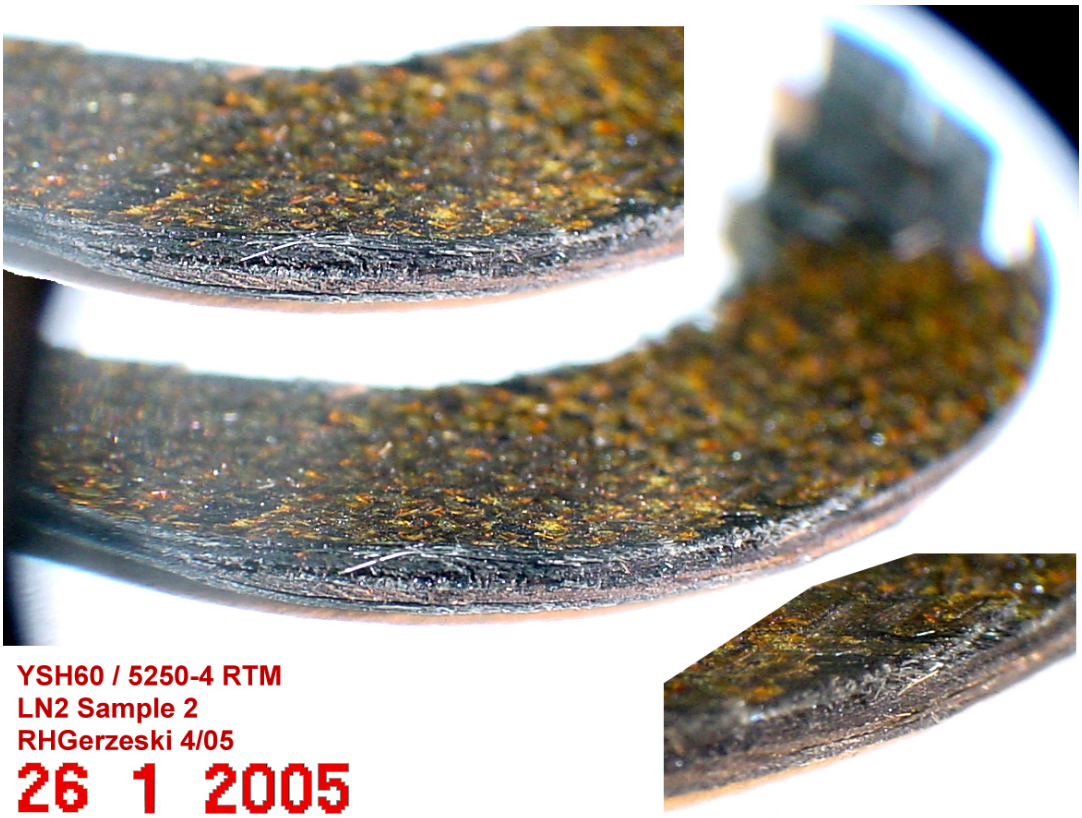


Figure 163-c-i, Cup Wall And Specimen Interaction: Back Side Impact: YSH60 / 5250-4 RTM D2512 Specimen: In LN2



Figure 163-c-ii, Cup Wall And Specimen Interaction: Back Side Impact: YSH60 / 5250-4 RTM D2512 Specimen: In LN2



Figure 164-a-i, Cup Wall And Specimen Interaction: Material Jetting: 5250-4 RTM D2512 Specimen: In LOX: Reaction Detected



Figure 164-a-ii, Cup Wall And Specimen Interaction: Material Jetting: 5250-4 RTM D2512 Specimen: In LOX: Reaction Detected



Figure 164-a-iii, Cup Wall And Specimen Interaction: Material Jetting: 5250-4 RTM D2512 Specimen: In LOX: Reaction Detected



Figure 164-b, Cup Wall And Specimen Interaction: Material Jetting: 5250-4 RTM D2512 Specimen: In LN2



Figure 165-a, Cup Wall And Specimen Interaction: Material Jetting: T650-35 / 5250-4 RTM D2512 Specimen: In LN2



Figure 166-a, Cup Wall And Specimen Interaction: Material Jetting: YSH50 / 5250-4 RTM D2512 Specimen: In LOX: Reaction Detected



Figure 166-b-i, Cup Wall And Specimen Interaction: Material Jetting: YSH50 / 5250-4 RTM D2512 Specimen: In LOX: No Reaction Detected

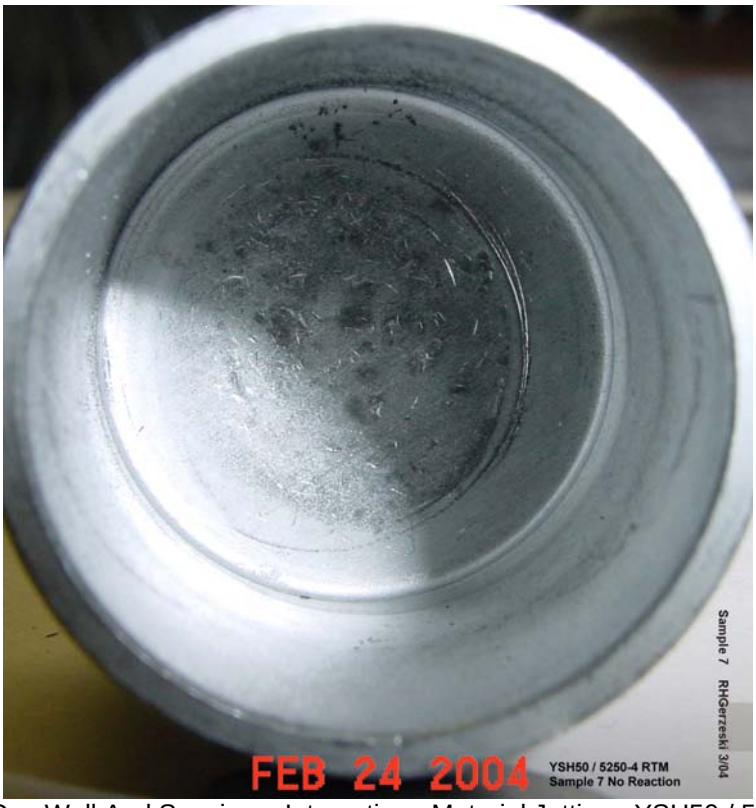


Figure 166-b-ii, Cup Wall And Specimen Interaction: Material Jetting: YSH50 / 5250-4 RTM D2512 Specimen: In LOX: No Reaction Detected



Figure 166-b-iii, Cup Wall And Specimen Interaction: Material Jetting: YSH50 / 5250-4 RTM D2512 Specimen: In LOX: No Reaction Detected



Figure 166-c-i, Cup Wall And Specimen Interaction: Material Jetting: YSH50 / 5250-4 RTM D2512 Specimen: In LN2



Figure 166-c-ii, Cup Wall And Specimen Interaction: Material Jetting: YSH50 / 5250-4 RTM D2512 Specimen: In LN2



Figure 167-a-i, Cup Wall And Specimen Interaction: Material Jetting: YSH60 / 5250-4 RTM D2512 Specimen: In LOX: Reaction Detected



Figure 167-a-ii, Cup Wall And Specimen Interaction: Material Jetting: YSH60 / 5250-4 RTM D2512 Specimen: In LOX: Reaction Detected



Figure 167-b-i, Cup Wall And Specimen Interaction: Material Jetting: YSH60 / 5250-4 RTM D2512 Specimen: In LOX: No Reaction Detected



Figure 167-b-ii, Cup Wall And Specimen Interaction: Material Jetting: YSH60 / 5250-4 RTM D2512 Specimen: In LOX: No Reaction Detected



Figure 167-c-i, Cup Wall And Specimen Interaction: Material Jetting: YSH60 / 5250-4 RTM D2512 Specimen: In LN2



Figure 167-c-ii, Cup Wall And Specimen Interaction: Material Jetting: YSH60 / 5250-4 RTM D2512 Specimen: In LN2



Figure 167-c-iii, Cup Wall And Specimen Interaction: Material Jetting: YSH60 / 5250-4 RTM D2512 Specimen: In LN2

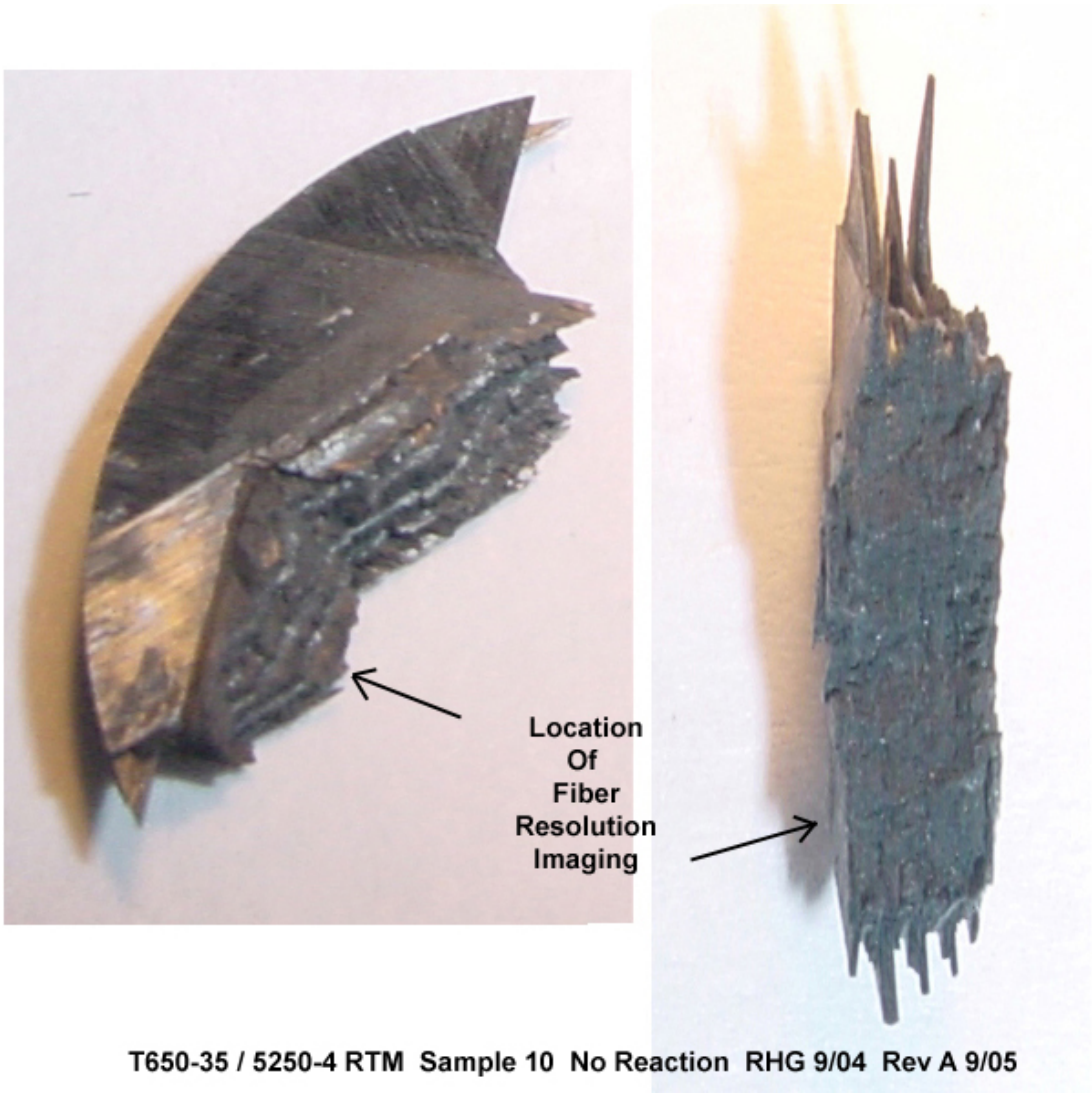


Figure 168, Fiber Resolution Imaging Location

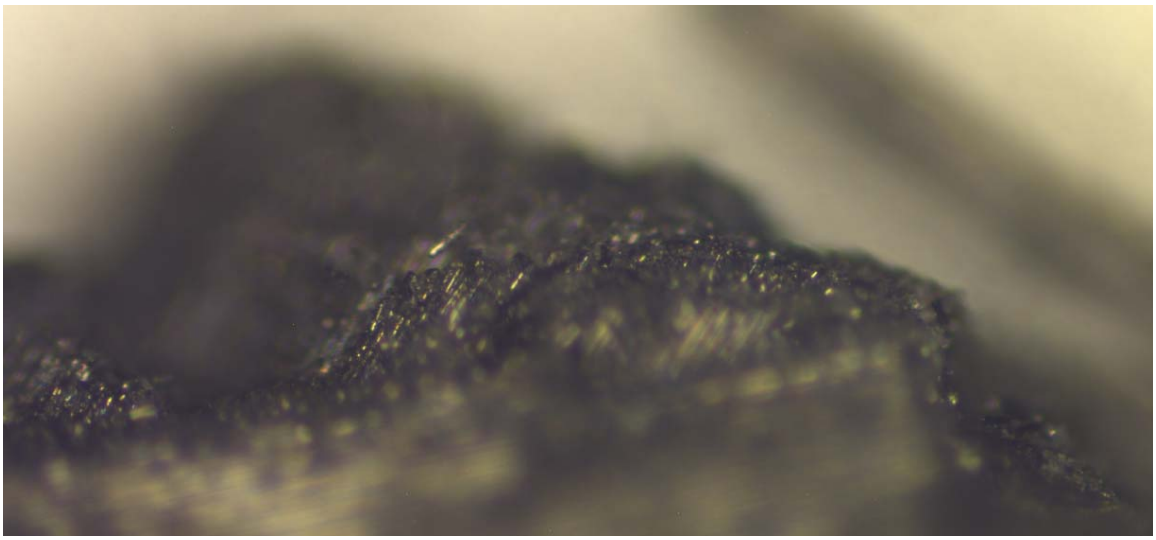


Figure 169, Fiber Resolution Fracture Surface Images

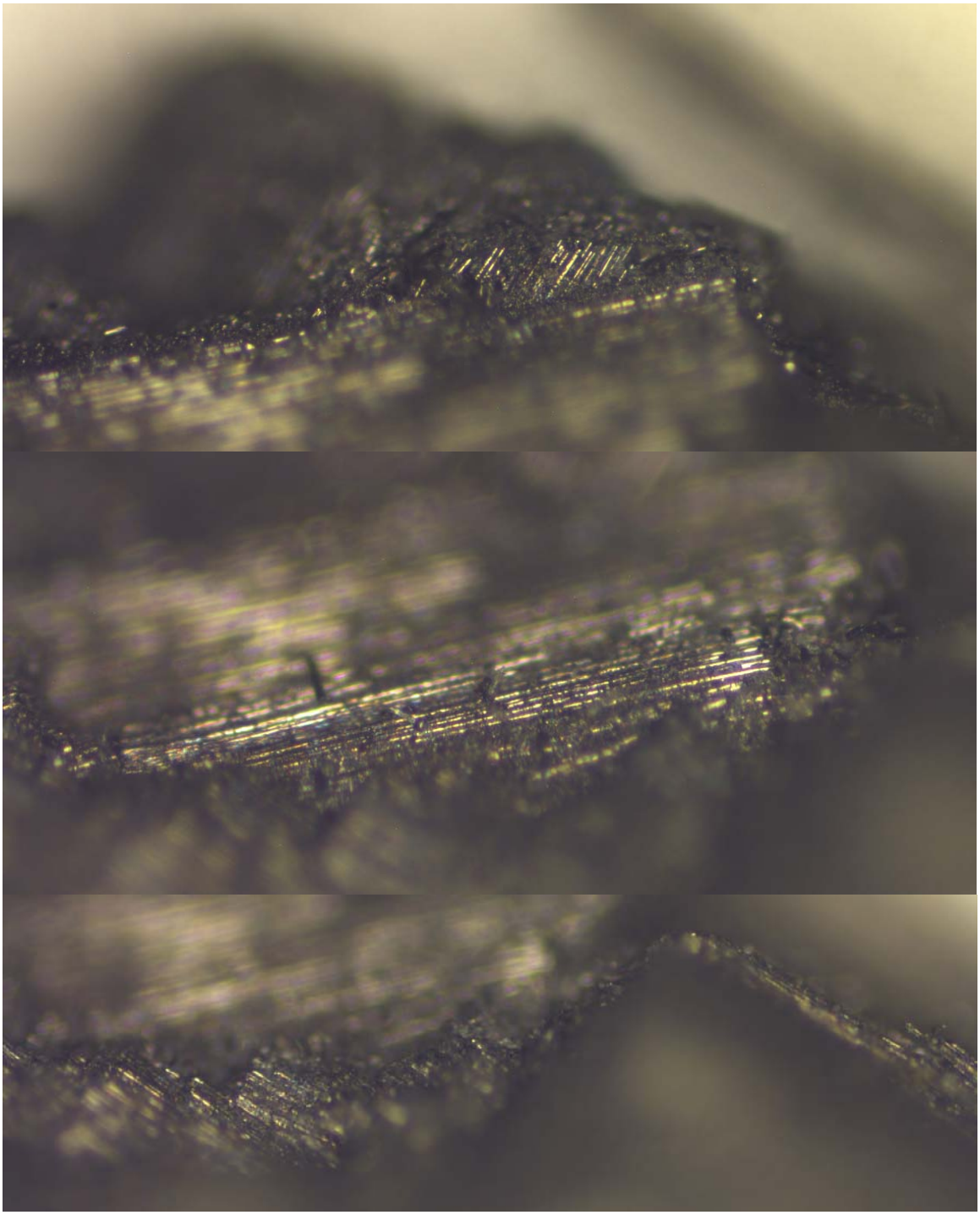


Figure 169, Fiber Resolution Fracture Surface Images Continued

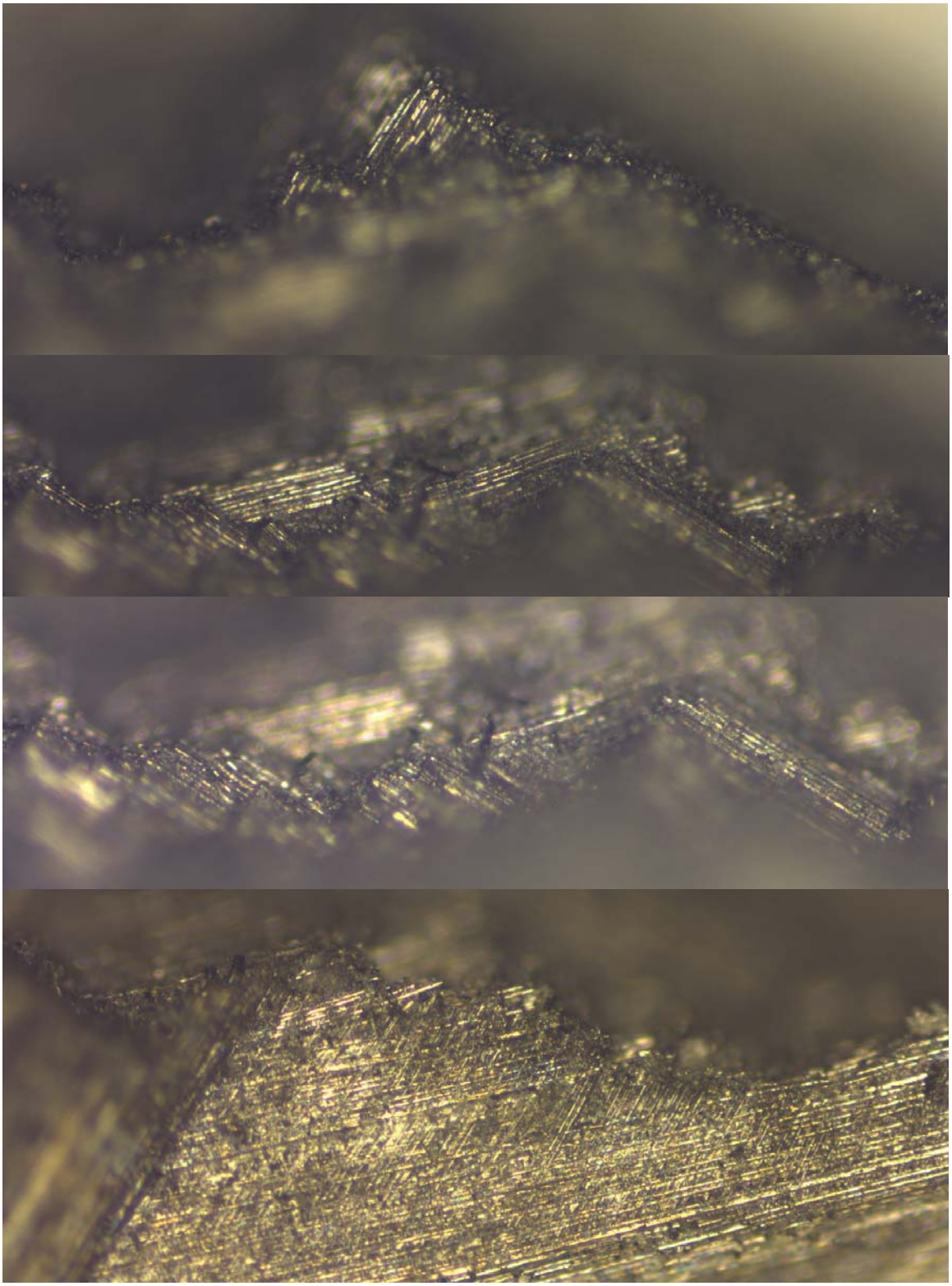


Figure 169, Fiber Resolution Fracture Surface Images Continued

Results Section: D2512 Load Versus Time Plots

Figure 170 presents the load versus time plots of the first bounce of D2512 type mechanical impact tests. Each graphs an individual D2512 specimen's impact test. Two specimens of each of the four types of materials investigated by this effort were tested.

A series of distinct features repeatedly appear in all of the load versus time plots regardless of the material type tested or the number of a specific material's D2512 specimens tested. All plots have an initial small load, short duration jitter. This is followed by a steep linear increase of the load to a sharp inflection point. At the inflection point the load rapidly drops off; usually to zero. The load then increases and cyclically oscillates erratically and non repeatedly, both in period and amplitude, forming a slightly rising ragged plateau. This plateau occupies the largest majority of the plotted impact bounce's duration. The load then commences a parabolic climb to another inflection point after which it descends back down this parabola to a load of zero. These distinct features can be grouped into four categories: initial jitter, sharp spike, sloping plateau, and parabolic climb and descent.

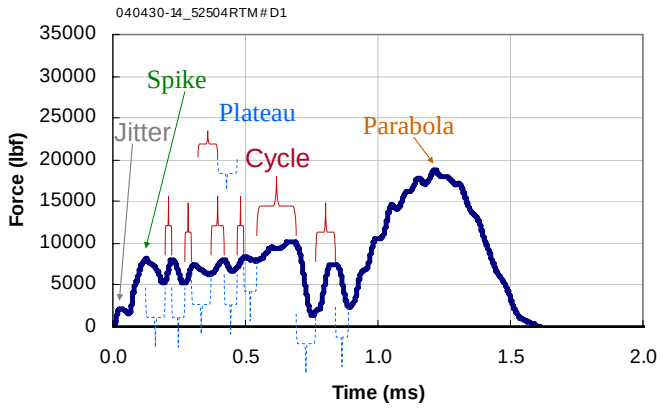


Figure 170-a-i, First Bounce Load Versus Time Curves: 5250-4 RTM

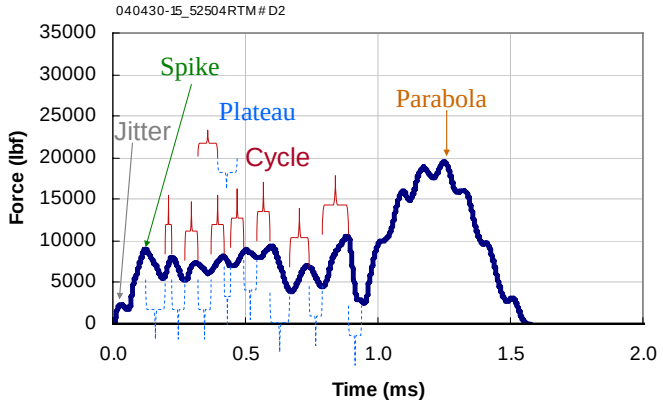


Figure 170-a-ii, First Bounce Load Versus Time Curves: 5250-4 RTM

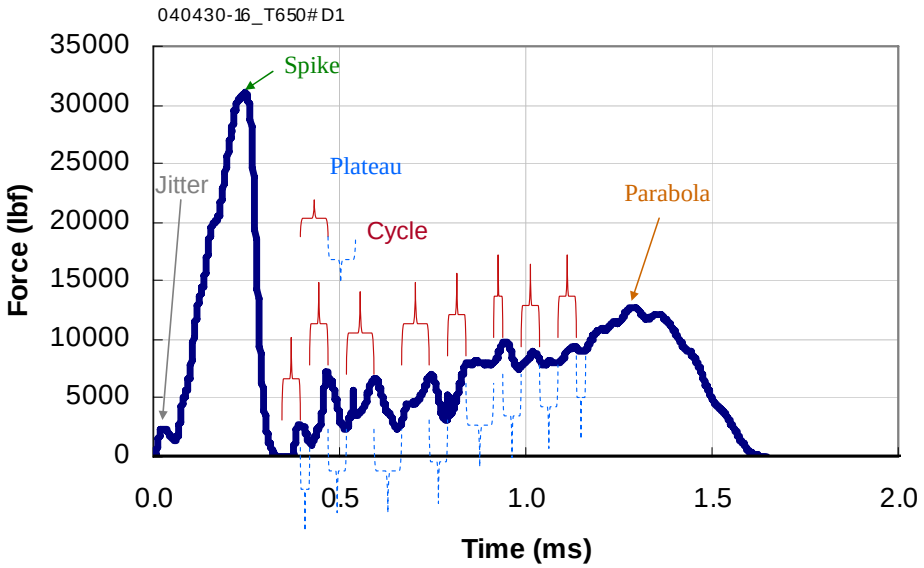


Figure 170-b-i, First Bounce Load Versus Time Curves: T650-35 / 5250-4 RTM

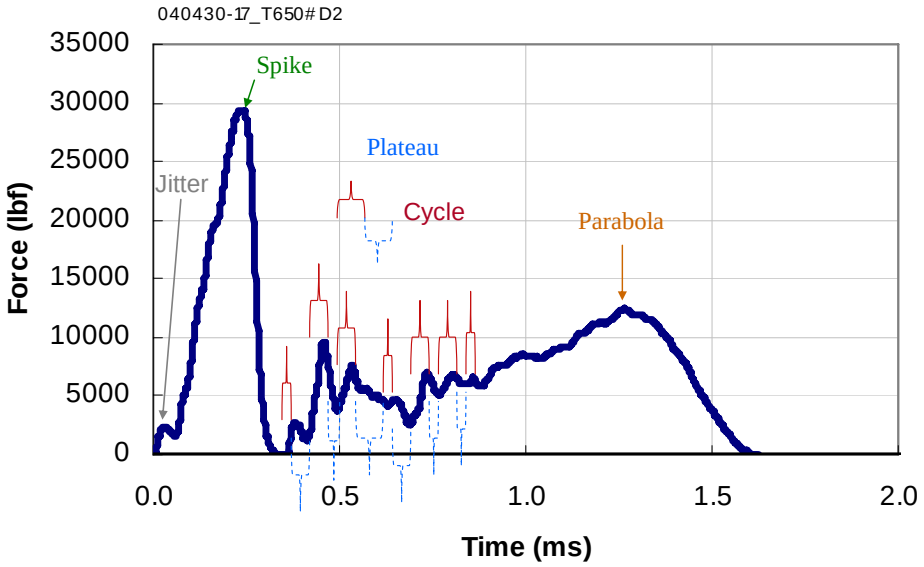


Figure 170-b-ii, First Bounce Load Versus Time Curves: T650-35 / 5250-4 RTM

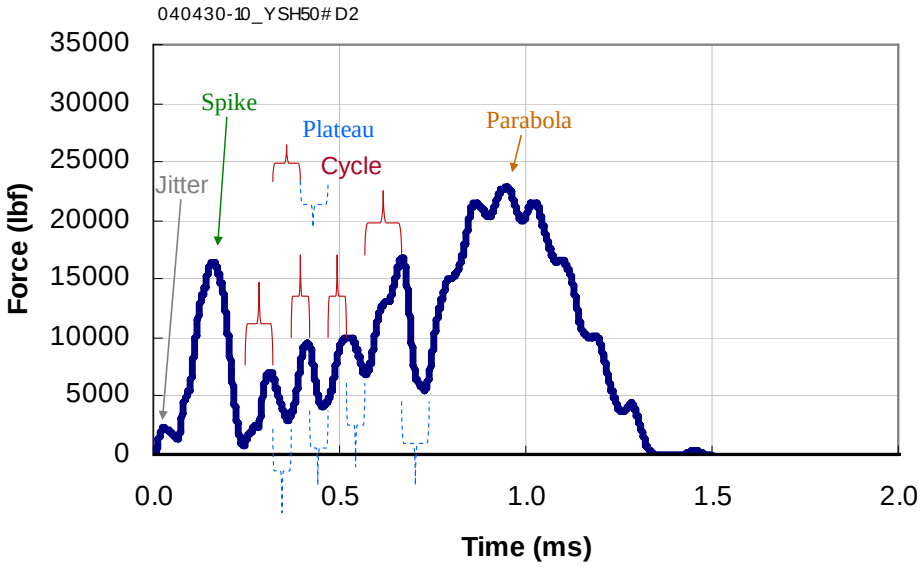


Figure 170-c-i, First Bounce Load Versus Time Curves: YSH50 / 5250-4 RTM

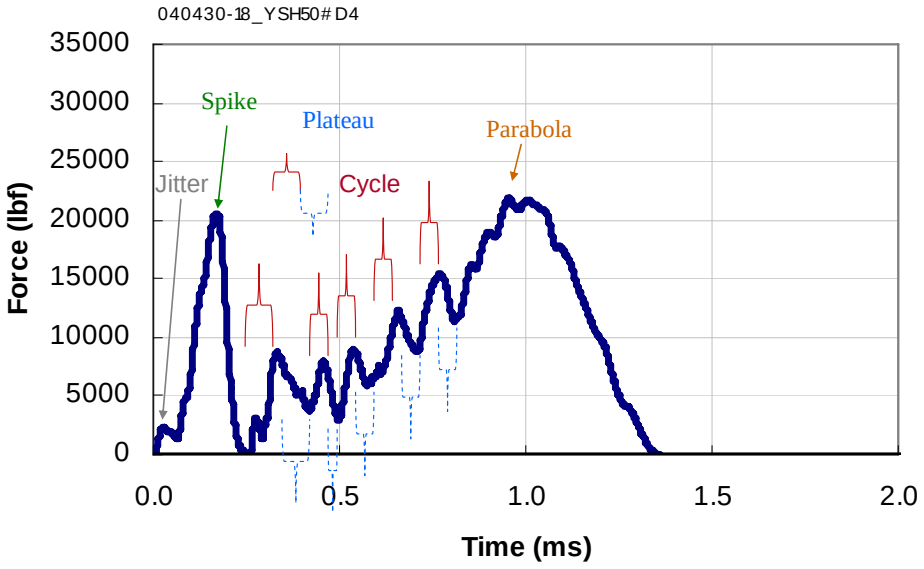


Figure 170-c-ii, First Bounce Load Versus Time Curves: YSH50 / 5250-4 RTM

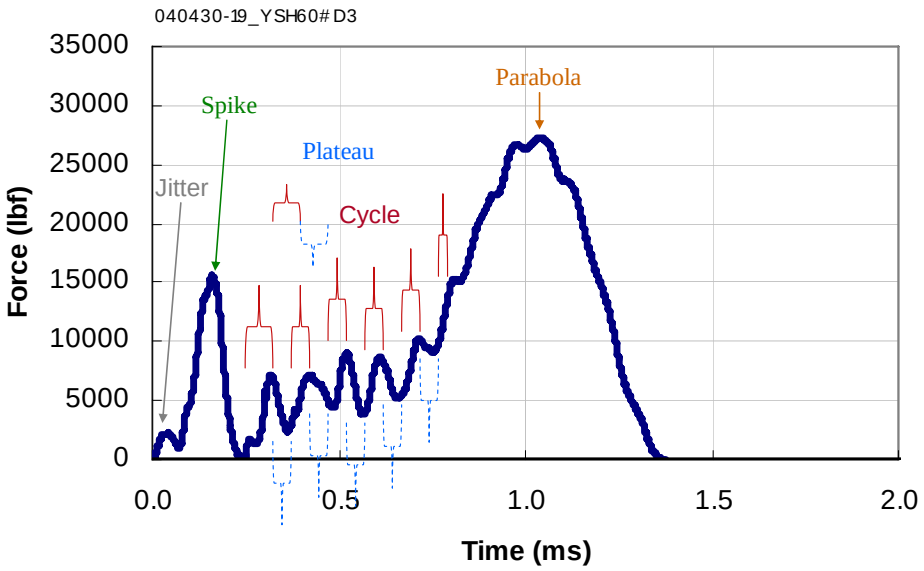


Figure 170-d-i, First Bounce Load Versus Time Curves: YSH60 / 5250-4 RTM

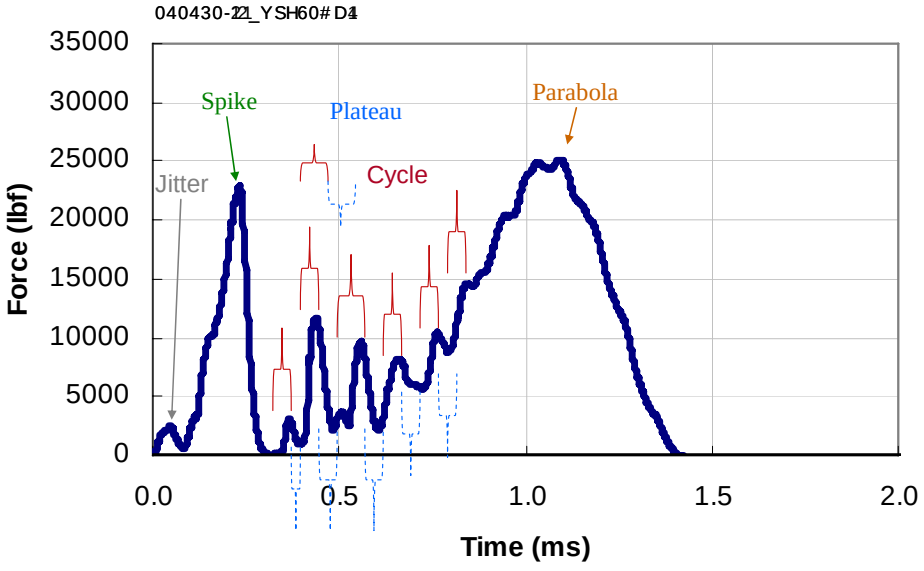


Figure 170-d-ii, First Bounce Load Versus Time Curves: YSH60 / 5250-4 RTM

Discussion

An ignition event initiated by a mechanical impact, such as that which the D2512 and G86 tests attempt to induce, is one final possible result of a cascade of probabilistic mechanisms. These mechanisms usually occur in series with occasional minor overlapping additive effects.

A mechanical impact ignition event begins when an indenting impacter, such as the striker in the D2512 test, starts putting a load onto the surface of the specimen. If the specimen's surface isn't oriented almost exactly normal to the loading angle of the indenter and if the specimen isn't restrained from off load-axis movement but the indenter is, then the specimen will attempt to reorient its' surface to be normal to the indenter's loading axis. In a load versus time plot of a D2512 test this appears as a brief load and unload jitter. It occurs in the D2512 test because extrusion drawn cups and stamped specimen support discs (See figure 5) are used. Their surfaces are not flat nor are they parallel. This would cause the surface of a D2512 specimen to not be aligned parallel as depicted in figure 171 to the flat loading face of a punch like D2512 striker-indenter. Under loading, the specimen and disc would jitter until a sufficiently parallel alignment of the specimen's face to the striker's punch face allowed a sufficient number of the contacting asperity points described in the Theory Section: Kinetic Friction to physically attach or "stick" the specimen to the striker. The jitter would then stop and the impacter or striker contact area would be circular as depicted in figure 171.

The striker would then proceed to load the specimen developing a "Hertzian like" stress field described in figure 16 of the Theory Section: Hertzian Fracture. This stress field development would then proceed until a Hertzian ring crack followed immediately by a cone crack was formed in an area of the specimen external to the striker as conceptionally depicted in figure 172 a. Examples of these in the returned residuals are depicted in figures 94-97. At the inflection point of the sharp spikes in figure 170's Load Versus Time Plots, the most fully developed, and complete Hertzian ring and cone crack appears in the specimen.

The load at which the Hertzian ring and cone crack forms is probabilistic. The load is determined by the size of the most critical surface flaw/crack originally in the specimen's surface. An example of what the original surface flaw/cracks size distribution might look like is shown in figure 23. This size distribution translates into a probabilistic distribution of loads, as implied by figure 24, needed to form the ring and cone cracks. This crack formation absorbs some of the striker's original 72 Ft Lbs of energy. The higher the load, the more energy absorbed and the less energy available to cause future failure types and phenomena. After the crack is formed, the indenting impact load imparted to the specimen drops; usually to zero.

Due to the nature of the D2512 test, the specimen's alignment with the punch-like indenting striker will never be perfectly concentric. As seen in figure 171 the actual concentricity can deviate substantially. With this non-concentricity, the Hertzian stress field developed in the specimen vectorially sums to the net tensile transverse load depicted in figure 171. When the Hertzian crack forms this transverse load causes a spring back movement of the specimen which shears the contacting asperities physically attaching or "sticking" the specimen to the striker. Figures 137-139 provide examples of the real area of these contacting asperities. The flattened plateaus are the small actual physical contact areas between the specimen and the striker. The specimen then moves or "slips" under the still descending striker as conceptionally depicted in the change from figure 172 b to 172 c. The specimen's movement shifts portions of the original surface from under the indenting striker to outside of it. This slippage continues until new contacting asperities physically reattach or "stick" the specimen to the striker. As a result of having experienced the spike compressive and tensile transverse loadings, the original surface cracks in the specimen become larger.

The striker again begins to put load onto the surface of the specimen. The load redevelops an approximation of the Hertzian stress field in the damaged specimen. The specimen now has a previously developed Hertzian ring and cone crack in it and a more diverse set of larger, most

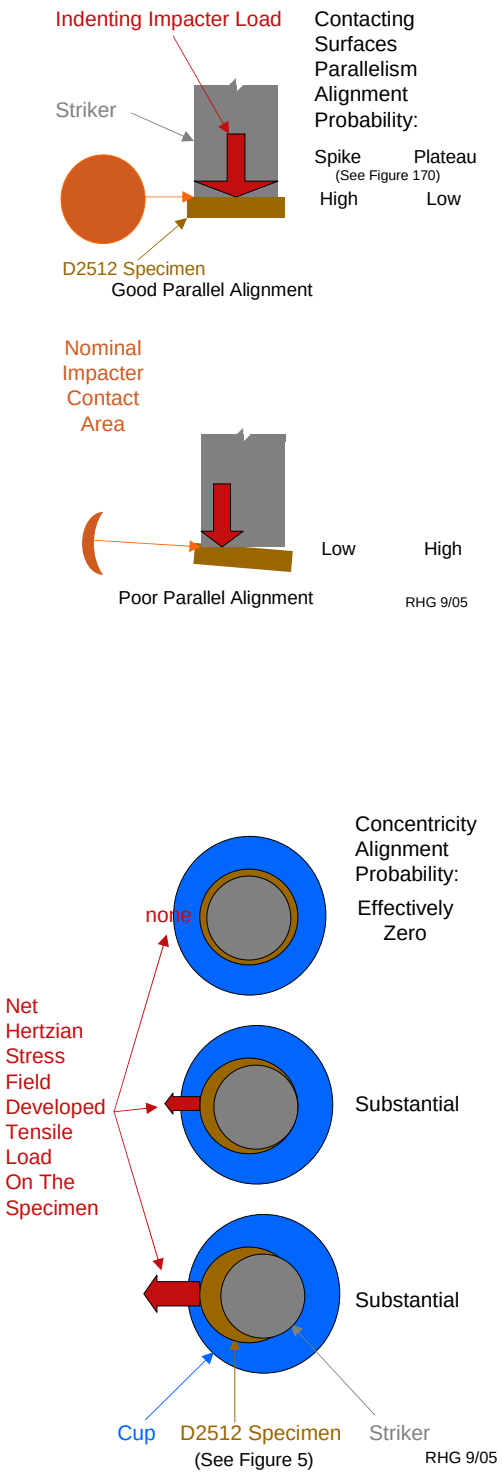
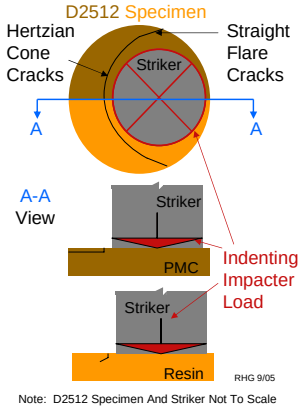
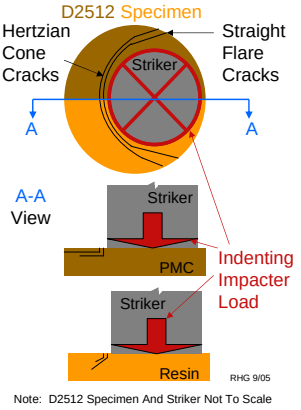


Figure 171, Conceptual D2512 Striker Specimen Cup Alignment and Its Effects

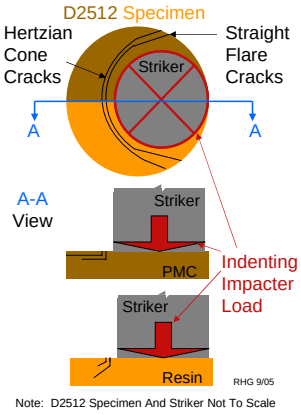
critical surface cracks. The indenting load rises until another Hertzian ring and cone crack develops. The indention load again drops. The specimen slips again. More new surface is exposed. New contacting asperities are created and the load climbs again. This erratic cycle of "sticking, increasing load, Hertzian cracking, falling load with slipping" (SLCLS), conceptionally depicted in figures 172 a thru h, repeats itself many times.



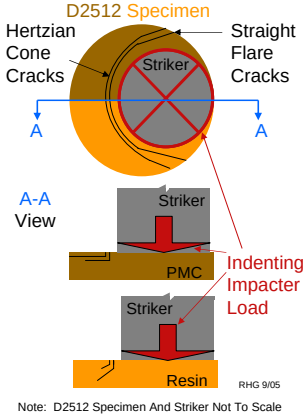
a 1st Plateau SLCLS: Stick And Begin Loading



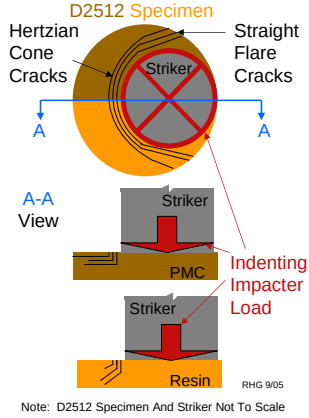
b 1st Plateau SLCLS: Load To Fracture And Asperity Shear



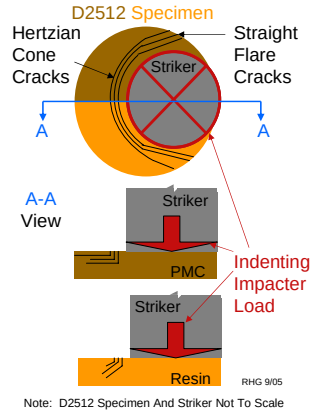
c 1st Plateau SLCLS: Unload And Slip



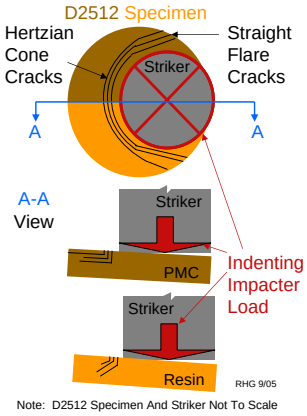
c 2nd Plateau SLCLS: Stick And Begin Loading



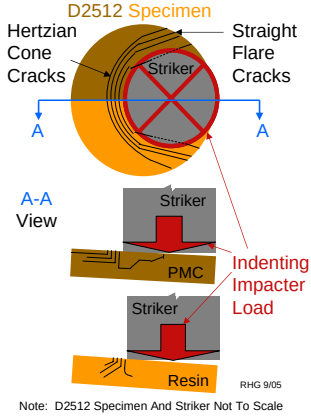
d 2nd Plateau SLCLS: Load To Fracture And Asperity Shear



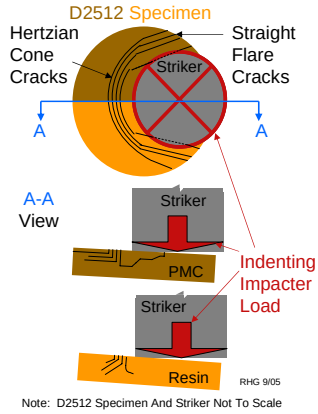
e 2nd Plateau SLCLS: Unload And Slip



f 3rd Plateau SLCLS: Stick And Begin Loading



g 3rd Plateau SLCLS: Load To Fracture And Asperity Shear



h 3rd Plateau SLCLS: Unload And Slip

i etc j etc k etc …

Figure 172, Conceptual SLCLS Derived Stacked Hertzian Cone Crack Development Cycle

Due to the increasing damage and shrinking potential nominal specimen surface contact area of these subsequent SLCLS's the probability of good parallel alignment of the specimen's surface to the striker's flat punch face becomes lower. The resultant nominal impacter contact area during the sticking, loading and cracking portions of these subsequent SLCLSs would look more like the crescent shape depicted in figure 171. (The first and most completely circular shaped Hertzian crack, created during the spike portion of the load versus time portions of figure 170's curves, would be generated by an almost or completely circular shape contact.) This actual loading nominal contact area looks more like that of the Vickers or Knopp indenter depicted in figure 27. It would generate the partially circular Hertzian ring and cone cracks depicted in figure 26 and conceptionally depicted in figure 173. Due to the sharp points on the crescent shaped nominal contact area, these SLCLS's would also generate straight flaring cracks (See figure 26), like those shown in figures 106-109, coming off of these stress concentration points. These straight flaring cracks would produce the straight sided residuals shown in figures 128-130. They, in the initial specimen, span from under to outside of the impacter.

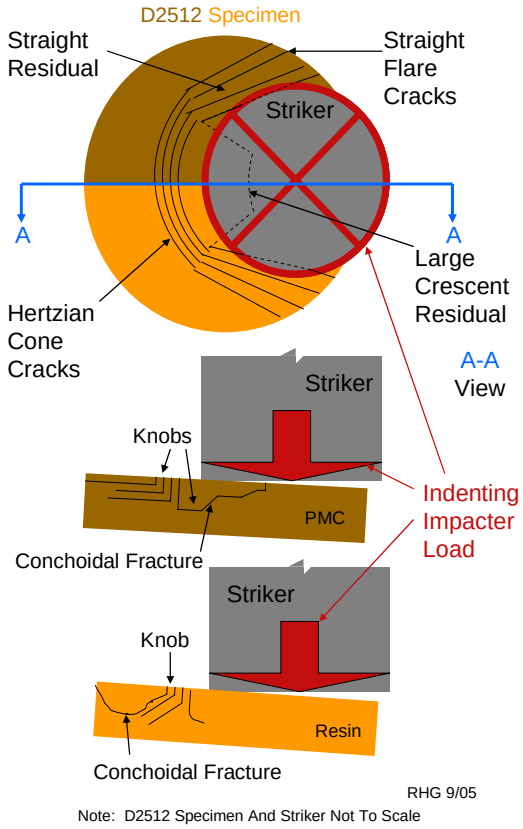
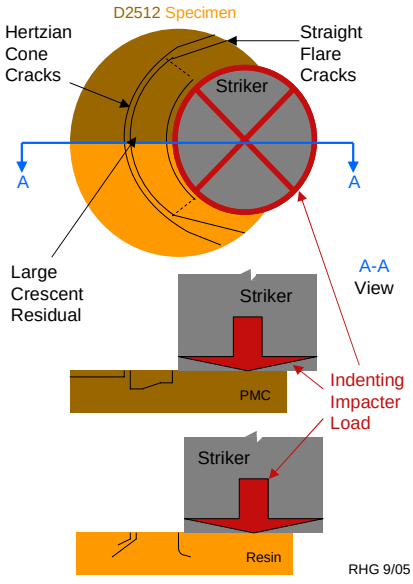


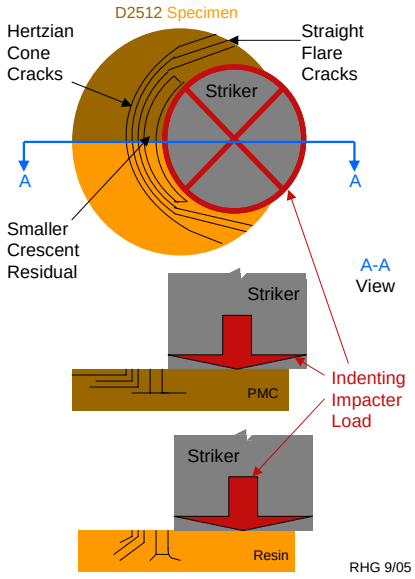
Figure 173, Conceptual Straight, Knobs And Conchoidal Fractures Residuals

The repeated manifestation of the SLCLS cycle phenomena is known as stick slip kinetic friction. Its manifestation indicates that the specimen slides under the striker during a D2512 impact drop test. This kinetic friction sliding happens during the slightly rising plateau region of the load versus time plots described in "Results Section: D2512 Load Versus Time Plots". The sliding of the specimen distorts the Hertzian stress field developed into the shape and distribution described in figure 28. The combination of the stick slip kinetic friction and the resultant distorted hertzian stress field generate a series of stacked partial crescent shaped hertzian ring and cone cracks with straight flare cracks coming off of their extreme edges as depicted in figure 29 and conceptionally depicted in figure 172 h.

Crescent shape residuals of D2512 specimens that had experienced stick slip kinetic friction during the impact test were originally located on the specimen both outside of and under the indenting striker. The differences in their widths is an indication of the distance the specimen slid during a SLCLS cycle. The initial degree of specimen to striker non-concentricity alignment (See figure 171) for a set SLCLS cycle results in a set magnitude of the transverse tensile load on the specimen. When a hertzian crack forms, that transverse load determines the distance of the specimen's movement before the creation of movement restraining contact aspirates. A small transverse load would result in the close stacking of hertzian cracks seen in the residuals originally from outside of the strikers nominal contact area. Figures 98-101 provide examples of these closely stacked Hertzian cracks. If some of the specimen material between those cracks were later broken off that would generate the thin width crescents found in the powder residuals. Figures 144-147 depict examples of these thin crescents. A large transverse load resulting from a substantial initial non-concentricity would result in a large distance between hertzian cracks. It would produce the large width crescent examples shown in Figures 122-124. These crescents are conceptionally depicted in figure 174.



Note: D2512 Specimen And Striker Not To Scale



Note: D2512 Specimen And Striker Not To Scale

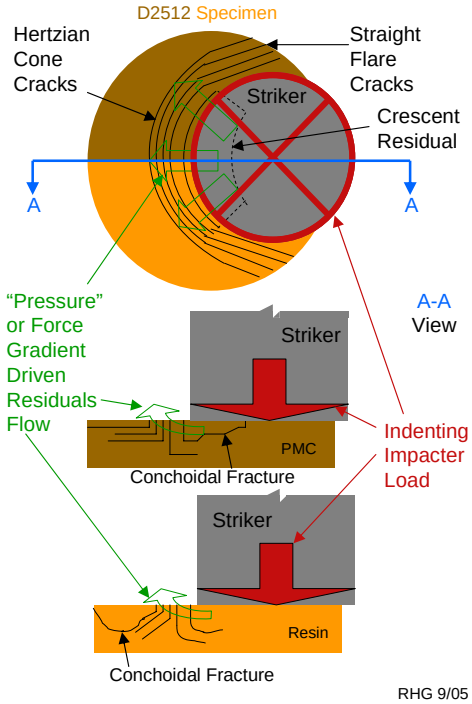
a b

Figure 174, Conceptual Crescent Residuals

An additional consequence of poor parallel alignment of the specimen's surface to the striker's flat punch face is, according to Cotterell et al, an increased tendency of the indenter to generate extreme hertzian cone cracks or conchoidal fractures. The sequential generation of an extreme, followed by a typical, hertzian cone crack from two back-to-back SLCLS cycles would also generate residuals with knob-like structures along one edge. Figures 102-105 and 125-127 depict the knob and conchoidal fractures which this type of sequence would generate. These conchoidal fractures and knobs are conceptionally depicted in figure 173. While these figures only provide examples of the phenomena, the number of composite residuals exhibiting these features which originated from under the impacter and had experienced some SLCLS cycles were roughly equal to the number which originated from outside the impacter and had experienced the first two SLCLS cycles. For the neat resin all of the residuals exhibiting these features originated from outside the impacter and had experienced the first two SLCLS cycles.

Overall the sliding of the specimen during the impact test allows for a more accurate simulation of a real impact event in a LOX component such as a tank etc. In a real impact the impacted item's movement (simulated by the D2512 specimen) will be substantially restrained and the impacter's movement (simulated by the striker) will be completely unrestrained. This is essentially the exact opposite of the specimen and striker's mobility in a D2512 impact test. Also the probability that the impacter will strike the real component at a perfect normal orientation to its' surface is essentially zero. According to the works of Lawn, all impacting indenters will slide to some extent during the indenting impact. The extent of sliding is a function of the deviation from normal of the initial contact (i.e. poor parallel contacting surface alignment) and the speed of the impacter. The D2512 impact test simulates both the sliding and the poor parallel alignment of a real impact event by allowing the specimen to move unrestrained. The final fracture results indicate that the same path in-specific end fractures and sliding occur.

The combination of a specimen exhibiting a series of structurally weakening stacked Hertzian cracks outside of, and not directly loaded by, the impacter with fractured residuals under, and being loaded by, the impacter sets up what in effect amounts to a "pressure" or force gradient as conceptionally depicted in figure 175. The gradient goes from the highly compressively loaded region of the specimen under the indenter to the zero compressively loaded region of the stacked Hertzian cracks outside. This gradient causes the under the impacter residuals to move towards the "vent" presented by the structurally weakened stacked Hertzian cracks area. As they move they slide and rub against one another and the structural remains of the original specimen. This rubbing is a manifestation of kinetic friction known as third body abrasion.



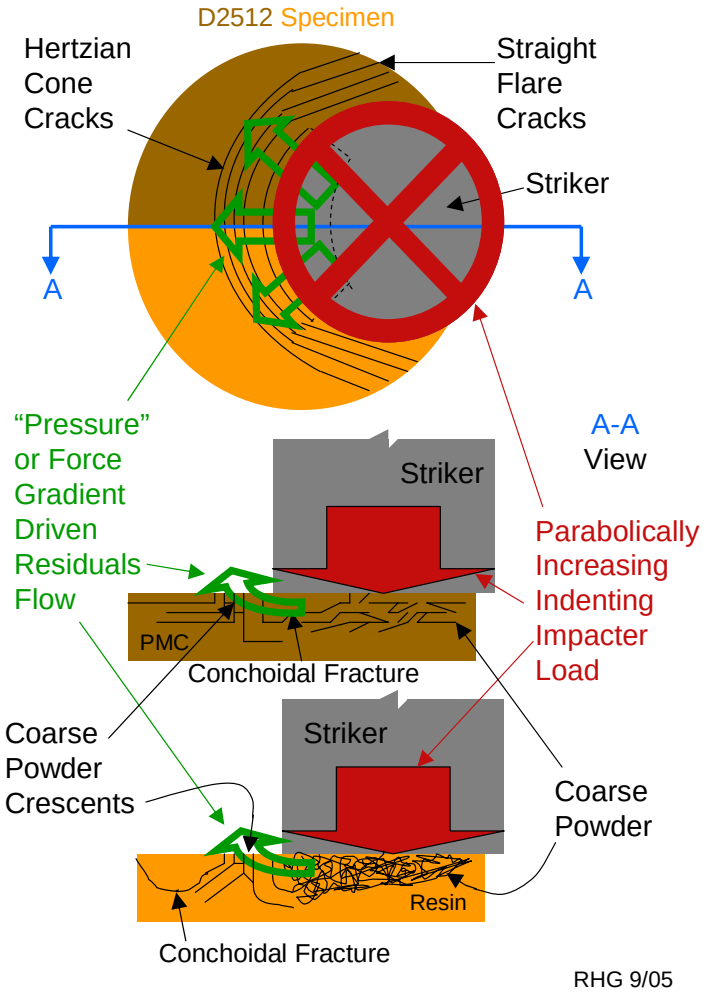
Note: D2512 Specimen And Striker Not To Scale

Figure 175, Conceptual Fractured Residuals Force Gradient Driven Movement

Simultaneous with the flow of residuals from under the indenting impacter the overall SLCLS cycling stops. The overall original specimen stops slipping out from under the impacting striker and a steady parabolic build up or climb of the load on what remains of the specimen begins. This climbing parabolic load build up generates intense compressive and shear loads in the residuals and the remains of the original specimen under the impacting striker. These

compressive and shear loads severely fracture the original specimen under the indenter as depicted in figure 22 c, d and e and conceptionally depicted in figure 176. According to Lawn this fracturing can even progress to comminution in which the individual fractured residuals inflict further fractures on each other. Comminution is common in the particulate size reduction crushing of isotropic materials such as rock. This fracturing generates a substantial portion of the coarse powder residuals depicted in figures 140-143.

The crescent powder residuals occur when the residuals under the parabolically climbing load of the striker are forced by the “pressure” or force gradient depicted in figure 176 to be driven through the sleeves of the original material created by the close stacking of Hertzian cone cracks depicted in figure 172. Some portions of the sleeves are broken off from their tenuous connection with the original specimen by this on rushing flow of other residuals towards the “vent” presented by the structurally weakened stacked Hertzian cracks area. This generates some of the small crescents seen in the powder residuals depicted in figures 144-147. They too slide and rub against one another, the other types of residuals and the remains of the original specimen. This rubbing is once again more third body abrasion kinetic friction.



Note: D2512 Specimen And Striker Not To Scale

Figure 176, Conceptual Parabolically Increasing Load And Powder Residuals

The force gradient induced flow of residuals, from the size of large crescents down to crushed powder, causes them to slide over and against each other and against the “walls” formed by the stacked Hertzian cracks of the original remaining outside of the indenter specimen. This sliding kinetic friction causes their contacting surfaces to abrade, transforming originally jagged fractured surfaces into smooth curves occasionally covered with abrasion residue. Figures 110-113, 131-133, and 148-151 exhibit the signs of this kinetic friction abrasion in residuals originating from outside of and under the impacter and in the powder. For the composite residuals the abrasion occurs at surfaces that are typically oriented roughly perpendicular to the plies or flat along one ply. For the neat resin these abrasion surfaces are oriented roughly in line with the surfaces formed by the stacked Hertzian cracks.

For the transient and brief D2512 mechanical impact event, this kinetic friction abrasion is one pass initial friction as opposed to multiple passes steady state friction. Also the magnitude of the normal loads required to achieve the material removal depicted in figures 110-113, 131-133, and 148-151 in one pass would need to be very large; possibly as large as the loads measured in the increasing portion of the parabolic range of figure 170’s load versus time plots. But the exact measurement of these loads is impossible and they could range from small up to the load depicted in figure 170 at a particular time point on the increasing parabolic portion of the curve. While it is also impossible to directly measure the kinetic friction sliding speeds at which these residuals are sliding on one another, an approximation would be that they are experiencing sliding speeds roughly equivalent to the indenting striker’s descent speed of roughly 3.5 to 1.0 meters per sec. These loads and striker speeds exhibit an inverse correlation at any particular time on the front side of the parabolic portion of the load versus time curves.

At this point in the mechanical impact the kinetic mechanical energy of the impacting striker proceeds to be converted into thermal temperature rising energy by the phenomena of kinetic friction. During the force gradient induced flow of the residuals the temperature of each sliding contacting surface would dramatically rise to a random temperature within a range as a result of the intense local heating generated by kinetic friction. Figures 114-117, 134-136 and 152-155 depict examples of all types of the residuals which exhibit indications of having been intensely heated. In many cases they exhibit the traces of frictional heating depicted in figure 39. As detailed in the Theory Section: Kinetic Friction section this range is defined by a parabolic probabilistic curve. If all relevant kinetic friction parameters can be measured its apex, feet and general shape can be detailed using the equations, some of which are listed, in table 9. Unfortunately, for this effort and for most examples of kinetic friction temperature rises, almost all of these parameters can not be directly measured. Fortunately a notion of their magnitudes and an implication of how they would shape and distort these curves can be inferred.

All possible temperature rises and the relative number of those rises resulting from kinetic friction are described by a parabolic temperature distribution curve of which examples are depicted in figure 34. The area under one of these parabolic temperature distribution curves represents one hundred percent of all of the possible temperature rises. If some key physical transformation, like ignition, occurred at a set temperature that was encompassed by the kinetic friction parabolic temperature rises distribution curve, then the probability of a material’s temperature being risen to or above that temperature by the kinetic friction sliding of any one contacting set of asperities would be the ratio of the area under the parabolic curve above that temperature to the area under the total curve.

The temperature span of the kinetic friction parabolic temperature distribution curve can be determined by first defining its’ apex known as $\triangle T_{Max_{Avg}}$. For the fast kinetic friction sliding which is most likely occurring at this point in a D2512 test and the assumption that the sliding contacting asperities are circular or square in shape this is determined by the following equation from table 9: $\triangle T_{Max_{Avg}} = 0.236\ \mu\ P\ v\ /\ l(K+0.88K(\mathrm{sqrt}(vlDs/K)))$.

where μ: coefficient of sliding friction, P: normal load, v: sliding speed, D: density
l: ½ asperity sliding direction length, s: specific heat, K: thermal conductivity

Once the apex is defined then for any specific set of the above parameters the feet of the parabola can be defined. The highest temperature foot is known as $\triangle T_{Max_{Max}}$ and for the same specific set of parameters it can also be determined. Assuming that the parabolic distribution curve is symmetric, the other foot $\triangle T_{Max_{Min}}$ can also be determined from $\triangle T_{Max_{Avg}}$ and $\triangle T_{Max_{Max}}$. As the time associated with the temperature rises resulting from the sliding of contacting asperities is as per the Theory Section: Kinetic Friction roughly 0.00003 sec and the average time span of the parabolic load rises in the load versus time plots of figure 170 is 0.0003 sec all of the variables needed to calculate $\triangle T_{Max_{Avg}}$ and $\triangle T_{Max_{Max}}$ and define the parabolic temperature distribution curve can be considered constants at an arbitrary "instant". But in any one arbitrary 0.00003 sec "instant" some of these variables will change depending on the type of material making up the sliding contacting asperities and the orientation of any reinforcing fibers to the sliding surface.

The size of the sliding asperities of the composite residuals will differ significantly depending on the orientation of the fibers to the sliding surface. A close study of the residuals depicted in figures 110-113, 131-133, 148-151 and 169 implies that these asperities come in two distinct size classes. For contacting asperities sliding perpendicular to the plies these asperities appear to be of the size of small rounder bundles of fibers. This would imply that these asperities have sliding lengths on the order of 0.0001s meters. For contacting asperities sliding along a ply these asperities appear to be scrapes along the axis of sheets of fibers. This would imply that these asperities have sliding lengths on the order of 0.001s meters.

The thermal conductivity of the sliding asperities of the composite residuals will differ significantly depending on the orientation of the fibers to the sliding surface. The plots of the various composite's in plane and transverse thermal conductivity depicted in figure 92 and tabulated in table 24 indicates substantial differences between the two orientations. The differences between the in plane and transverse bulk thermal conductivities of the YSH 50 and YSH 60 composites are 1850 and 2100 percent, for the T650-35 composite it is 140 percent. For contacting asperities sliding perpendicular to the plies the conductivity would be the highest. For contacting asperities sliding along a ply the conductivity would be the lowest.

For any particular contacting asperity the correlation between the length and the thermal conductivity is inverse. For the contacting asperities sliding perpendicular to the plies they exhibit the largest thermal conductivities associated with the smallest lengths. For contacting asperities sliding along a ply they exhibit the smallest thermal conductivities associated with the largest lengths. The overall implication of this correlation, all other parameters defining $\triangle T_{Max_{Avg}}$ and $\triangle T_{Max_{Max}}$ held constant, would be a flattening and broadening of the parabolic temperature distribution curve and a shifting down towards lower temperatures. Based upon the 1000's of percents increase in the in plane thermal conductivity of the YSH fibered composites over the T650-35 fibered composites detailed in table 24 the width of the YSH fibered composites parabolic temperature rise distribution curve would be substantially broader than that of the T650-35 fibered. But since there is only a roughly 200 percent difference between their very low transverse thermal conductivities both would exhibit high and similar $\triangle T_{Max_{Max}}$ high temperature foots.

The coefficient of friction of the sliding contacting asperities of the composite residuals will differ significantly depending on the type of the fibers used to make the D2512 specimens. Examination of the residuals in figures 114-117, 134-136 and 152-155 implies that many of them experienced temperature rises far in excess of their Tg's. 5250-4 RTM, the matrix material used in all of the D2512 specimens, has a Tg greater than 200°C. As per the Theory Section: Kinetic Friction when the sliding contacting asperities of a carbon containing material causes a temperature rise above 185 ^{o}C the coefficient of friction will experience a substantial step function jump of up to 400 percent. Also as per the same theory section when a filler becomes the major constituent in an end material its' coefficient of friction becomes that of the major constituent. All

of the composite D2512 specimens had Fv's of 63.6 percent, therefore the coefficient of frictions exhibited by their respective sliding contacting asperities was that of the fibers. The T650-35 fiber is predominately carbon, where as, the YSH fiber is predominately graphite. Therefore the temperature rises which the sliding contacting T650-35 fibered composite asperities experienced would dramatically jump when those temperatures exceeded 185°C. The temperature rises which the sliding contacting YSH fibered composite asperities experienced would show no noticeable change when those temperatures exceeded 185°C. This would change the shape of the T650-35 fiber containing sliding asperities' parabolic temperature rise distribution curve by incorporating a canyon-like gap followed by a sharp subsequent spike.

A notional approximation of the relative parabolic kinetic friction temperature rise distribution curves for each of the four materials investigated by this effort and the kinetic friction interaction between the striker and the specimen is presented in figure 177. These curves were created by alloying all of the previous observations concerning the various parameters defining $\triangle T_{Max_{Avg,}}$ $\triangle T_{Max_{Max}}$and curve shape, compounding them with the knowledge that all of the observations of abrasion and intense heating were the result of kinetic friction temperature rises and taking into account the actual D2512 testing results listed in table 23. The area encompassed under each of these curves has been normalized to represent 100 percent of all kinetic friction temperature rise events for that material or component interaction. The curves also incorporate the A&PI's observation that multiple examples of both abrasion and intense heating resulting from kinetic friction were found on the residuals associated with each individual D2512 specimen sample tested. (Due to report page count considerations, which would require hundreds and maybe over a thousand additional pages of substantiating figures to support this observation, these "data point pictures" will not be provided.)

The relative parabolic kinetic friction temperature rise distribution curves in figure 177 provide the clues for why the mildly thermally conductive YSH fibers improve a composite's D2512 LOX compatibility and the carbon T650-35 fibered composites routinely fail the D2512 LOX compatibility test. The 2300 to 2600 percent increase in the in plane thermal conductivity of YSH fibered composites over T650-35 fibered composite's dramatically shifts the $\triangle T_{Max_{Avg}}$ apex and the $\triangle T_{Max_{Min}}$ foot of the temperature rise curves which kinetic friction directed across the plies can generate to significantly lower temperatures. The number and distribution of these types of kinetic friction temperature rises in YSH fibered composites is routinely below the matrix's Radical Chain Scission Degradation and ignition temperature. Unfortunately the 200 percent increase in the transverse thermal conductivity of YSH fibered composites over T650-35 fibered composite's shifts the $\triangle T_{Max_{Max}}$ foot of the temperature rises which kinetic friction along the plies can generate to only marginally lower temperatures. Also for the YSH fibered composites a small but real portion of the kinetic friction temperature rises described by these curves is above the Radical Chain Scission Degradation and Ignition temperatures of the matrix and will leave a rare occasional indication of ignition as described in table 7 of the Theory Section: Ignition Event. The fact that the T650-35 fiber is primarily carbon causes its composite's distribution curve to exhibit a strong bimodal shape split by a canyon like gap. One small mode being below carbon's dramatic coefficient of friction rise at 185+^{o}C and the other larger mode being well above the Radical Chain Scission Degradation and Ignition temperatures of the matrix. With multiple evidences of kinetic friction occurring in any one T650-35 fibered specimen's D2512 test, to find only one out of twenty of those tested specimens with out any indication of ignition as described in table 7 of the Theory Section: Ignition Event is astonishing.

Due to its very poor isotropic thermal conductivity and moderately high coefficient of friction the kinetic friction temperature rise distribution curve of the 5250-4 RTM specimens would be a sharp narrow peaked parabola. All of its kinetic friction induced temperature rises would be definitively detected as ignitions.

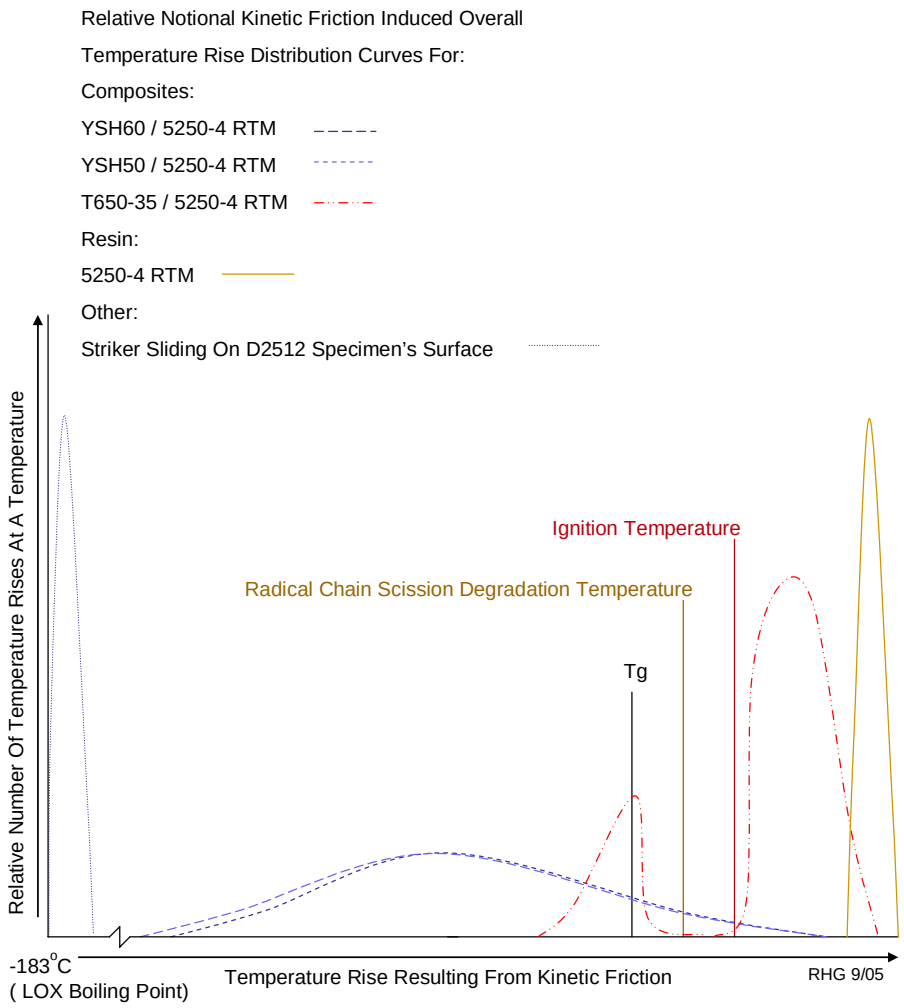
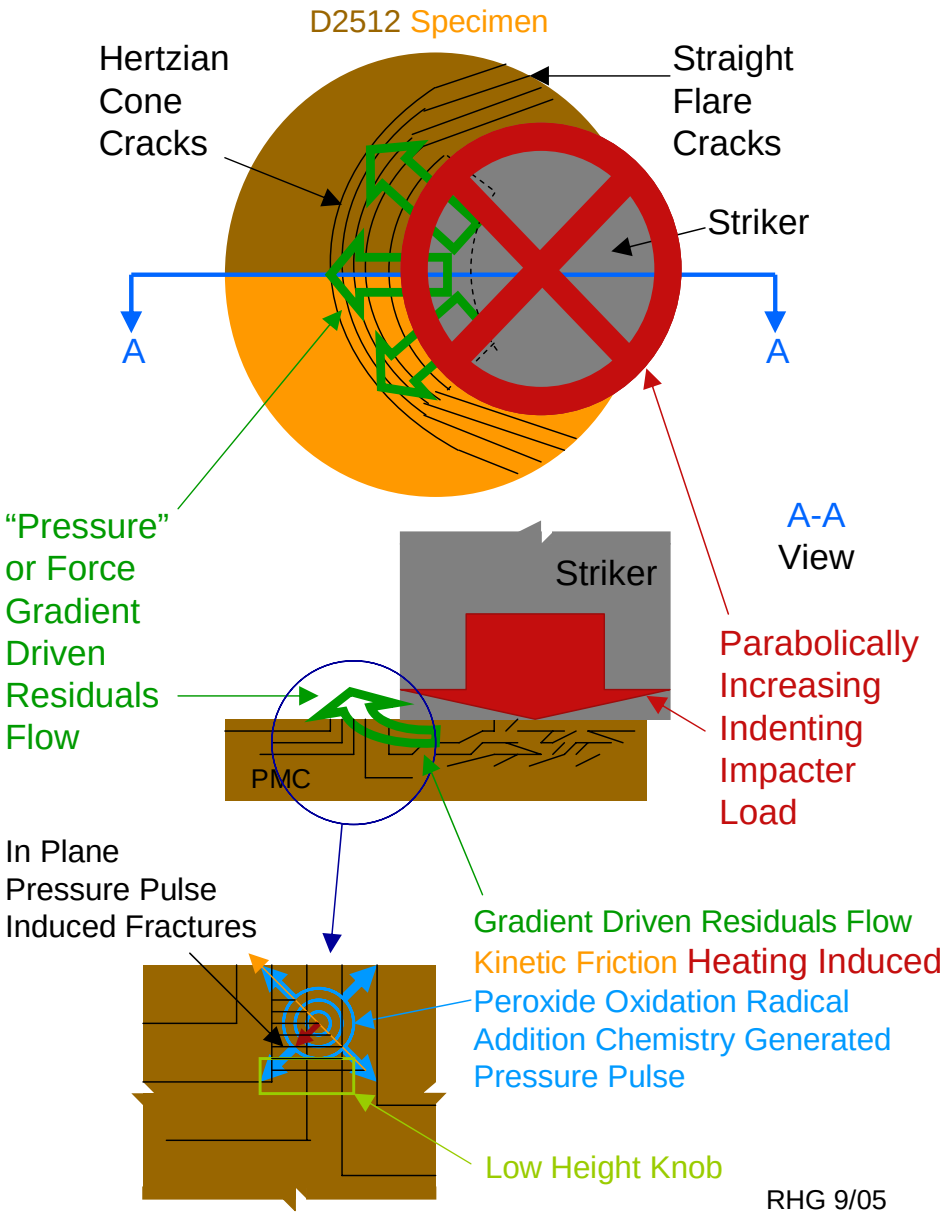


Figure 177, Notional Kinetic Friction Induced Temperature Rise Distribution Curves

The fiber matrix interfaces of composites are essentially clamped interference friction fits consisting of an enormous array of contacting asperities up and down the fiber's length as generally depicted in figure 30. As all D2512 specimens are soaked for 30 to 60 minutes in LOX before the impact test, the LOX will literally flow in from the cored edges along the length of the fiber, around the asperities saturating the entire composite specimen. During the parabolically increasing load portions of the curves in figure 170, the gradient driven flow of the residuals will cause them to slide against the stacked Hertzian cracks. This sliding will result in kinetic friction heating at various contacting asperities points all along the up slope edge of these stacked cracks. Some of the cracks will be bent and break off. Many of these asperities will induce temperature rises at the immediate Hertzian crack surface of these LOX saturated composites high enough to kick off the peroxide oxidation radical addition chemistry depicted in figure 12c of the Theory Section: Ignition Event. When this occurs the gaseous, volatile, partially oxidized, peroxide chemistry fuel products listed in table 5 will be very rapidly generated. This will generate the substantial pressure pulse depicted in figure 178 at the crack surface. This pressure pulse

will act like a wedge causing a double cantilever beam load perpendicular to the fiber plies which will cause them to spilt or crack along the plies and in some instances through a ply. This would break the remaining closely packed Hertzian cracks all along the length of the Hertzian crack and generate the thin thickness (routinely one to three plies thick), thin width crescents found in the powder residuals of the composite specimens. The combination of the pressure pulses and the gradient force residual flow causes these in ply cracks to propagate to the edge of the original specimen or to another Hertzian crack behind kinetic friction surface plunging deeper into the specimen. The later type of in ply cracks would generate low height knob like structures, such as those seen in figures 103-105, on the residuals.



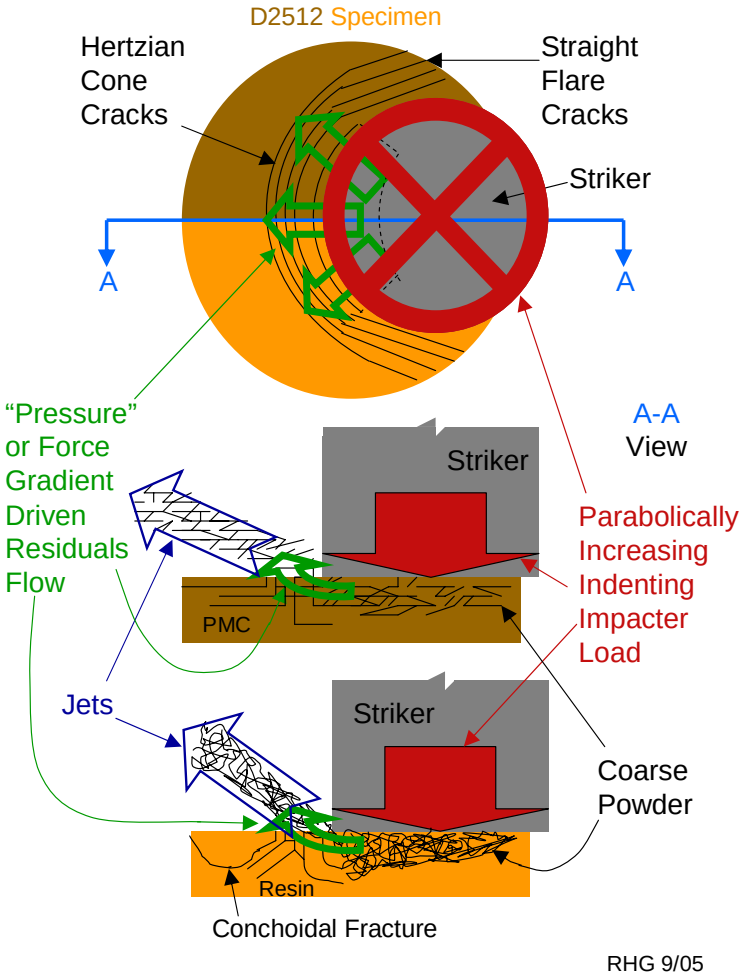
Note: D2512 Specimen And Striker Not To Scale

Figure 178, Conceptual Low Height Knobed Residual Creation

The D2512 specimens impacted in LN_2 did not exhibit these low height knobs. They instead exhibited higher height knobs and many more instances of them. This would indicate that their knobs were created primarily by being broken off by the gradient driven residuals flow as nitrogen does not become reactive until the environment's temperature rises into the low 1000+^{o}C; a temperature only attained by the only sample rejected for being contaminated, 5250-4 RTM neat resin sample 12.

The load imposed on the original specimen continues to climb up the parabolic section of the load versus time curves depicted in figure 170. During this climb the force gradient driven flow of powdered residuals is jetted out the vent formed by the stacked hertzian cracks as depicted in figure 179 and is sprayed onto the inner surface of the LOX containment cups. The form of these sprays can, as depicted in figures 164 through 167, ranges from small spots to diffuse bands.

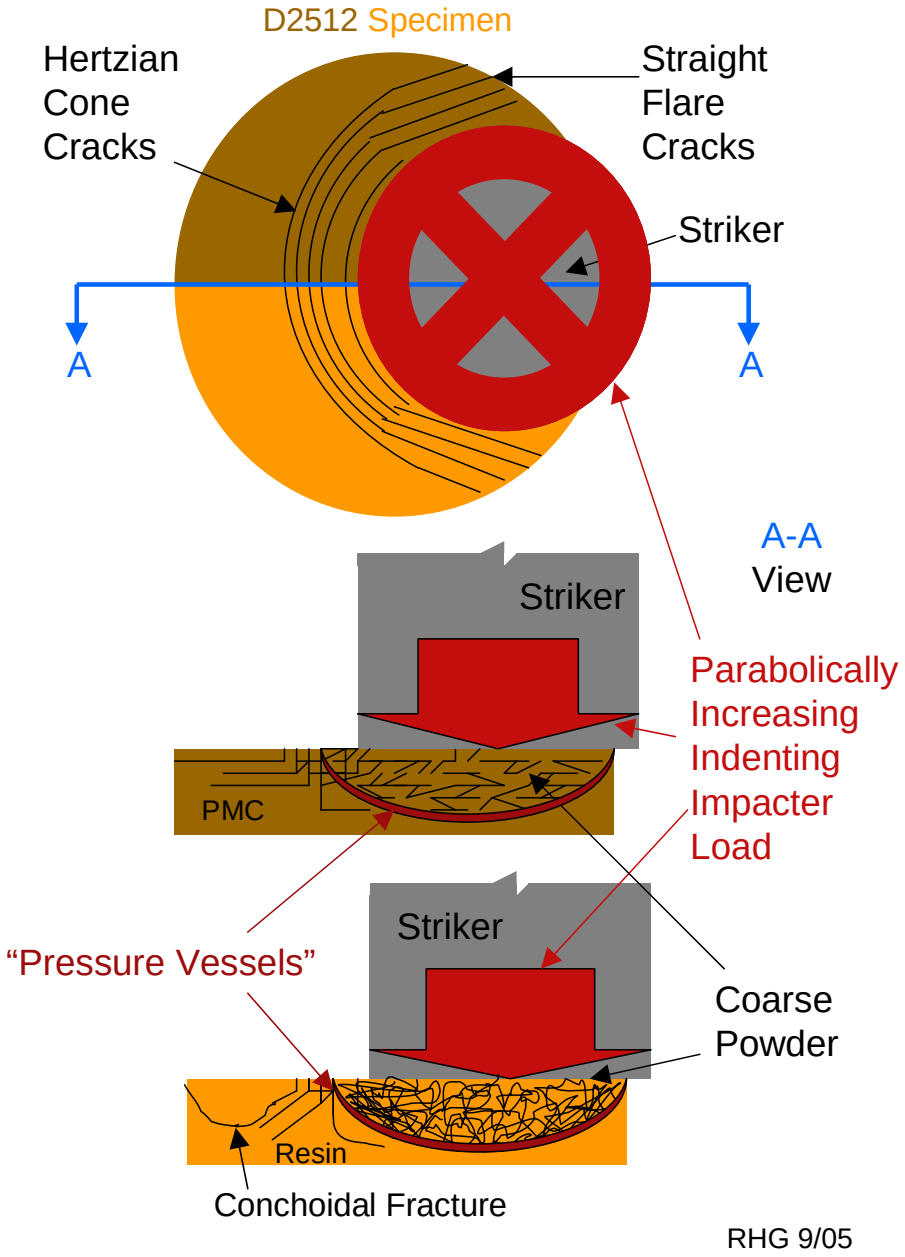
These jets would also leave a smear of particles up the side of the hertzian cracks. They would slide up the side of the hertzian cracks and subsequently heat up from the kinetic friction to temperatures described by the parabolic curves in figure 177. Some of these temperature rises would result in the intense heat exposure exhibited by the powder residuals shown in figures 152-155, some would cause ignitions.



Note: D2512 Specimen And Striker Not To Scale

Figure 179, Conceptual Powder Jets Creation

The climbing parabolic load build up continues. It generates even more intense compressive and shear loads in the residuals and the remains of the original specimen under the impacting striker. These more intense compressive and shear loads severely fracture even more of the original specimen under the indenter as depicted in figure 180. This fracturing erodes away at the original specimen beneath the striker until the loads in it become effectively all tensile. When this occurs, the remains of the original specimen effectively become a miniature “pressure vessel” containing the loaded coarse powder which is now acting like a “pressurized” fluid.



Note: D2512 Specimen And Striker Not To Scale

Figure 180, Conceptual Severe Fracturing Under The Impacter

The climbing parabolic load build up continues, approaching and achieving the apex of the parabolic section of the curves in figure 170. It generates the intense tensile hoop loads depicted in figure 181 in what remains of the original specimen outside of the striker. It also causes vent cracks to form in what remains of the original specimen under the striker. As described in the Theory Section: Hertzian Fracture and depicted in figure 22 these vent cracks are tensile failures occurring in a specimen located below the striker's center and edge. These vent cracks are seen in many of the neat resin residuals but nothing resembling them were detected on any of the composite residual's fracture surfaces.

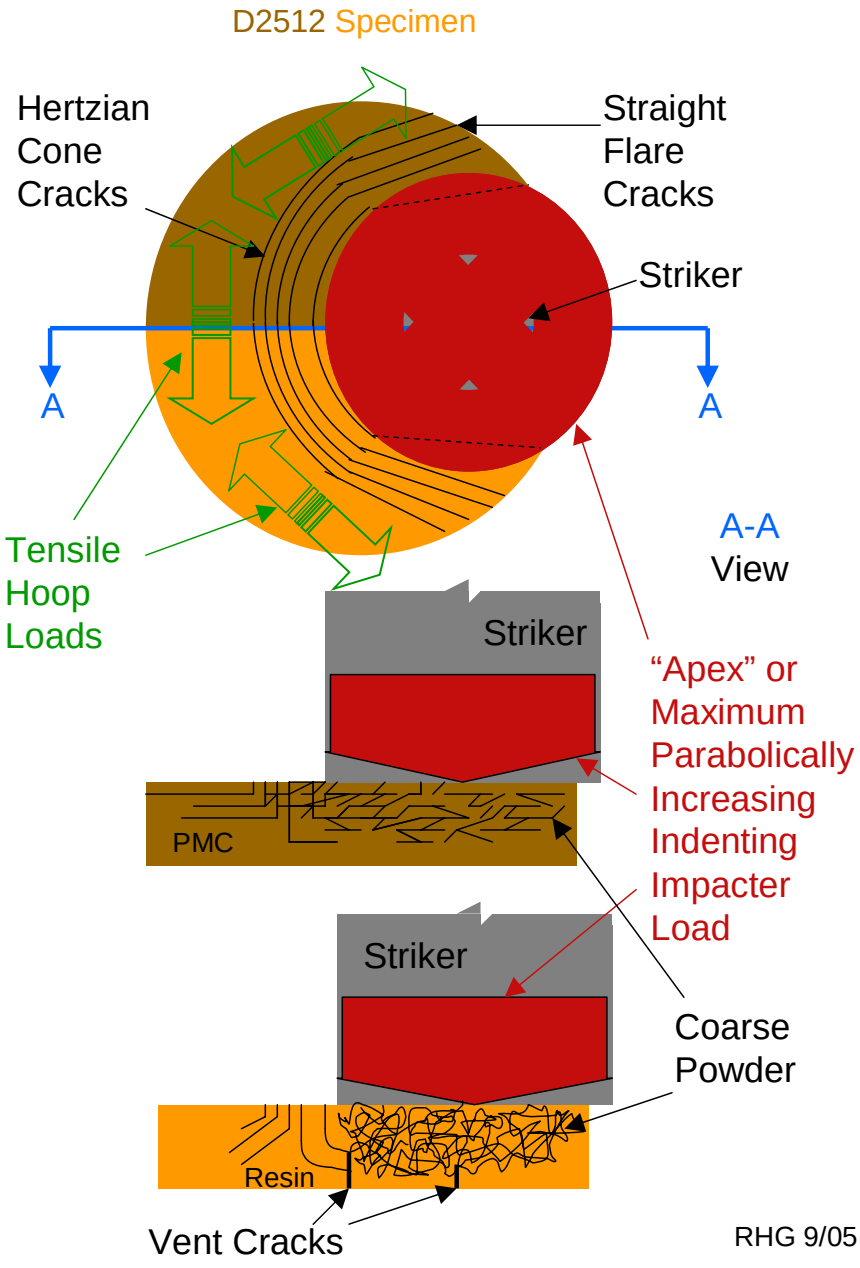
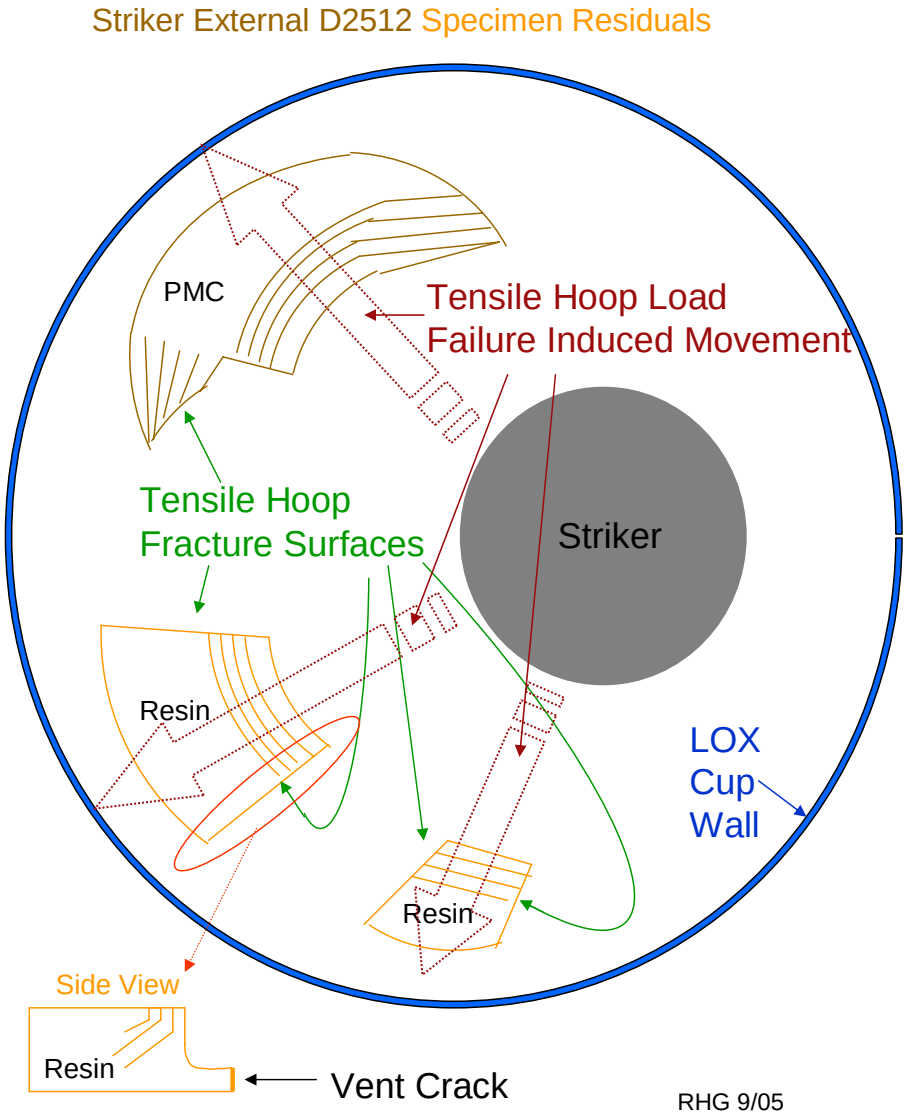


Figure 181, Conceptual Tensile Hoop Loads

When the load increases to the apex of the parabolic section of the load-versus-time curves the remains of the original specimen outside of the striker fail in tension generating the tensile fracture surfaces at the outer “wing” positions of the residuals depicted in figures 118-121. This tensile hoop failure causes the residuals created by it to be thrust out towards the wall of the LOX cup as depicted in figure 182. They then impact the LOX cup’s wall along the original specimen’s cored outer edge. This impact causes the flattening, crushing and chipping damage to the backside cored edges of the residuals depicted in figure 183. Figures 160-163 provide examples of the backside impact damage done to some of the residuals.



Note: D2512 Specimen, Cup And Striker Not To Scale

Figure 182, Conceptual Tensile Hoop Failure

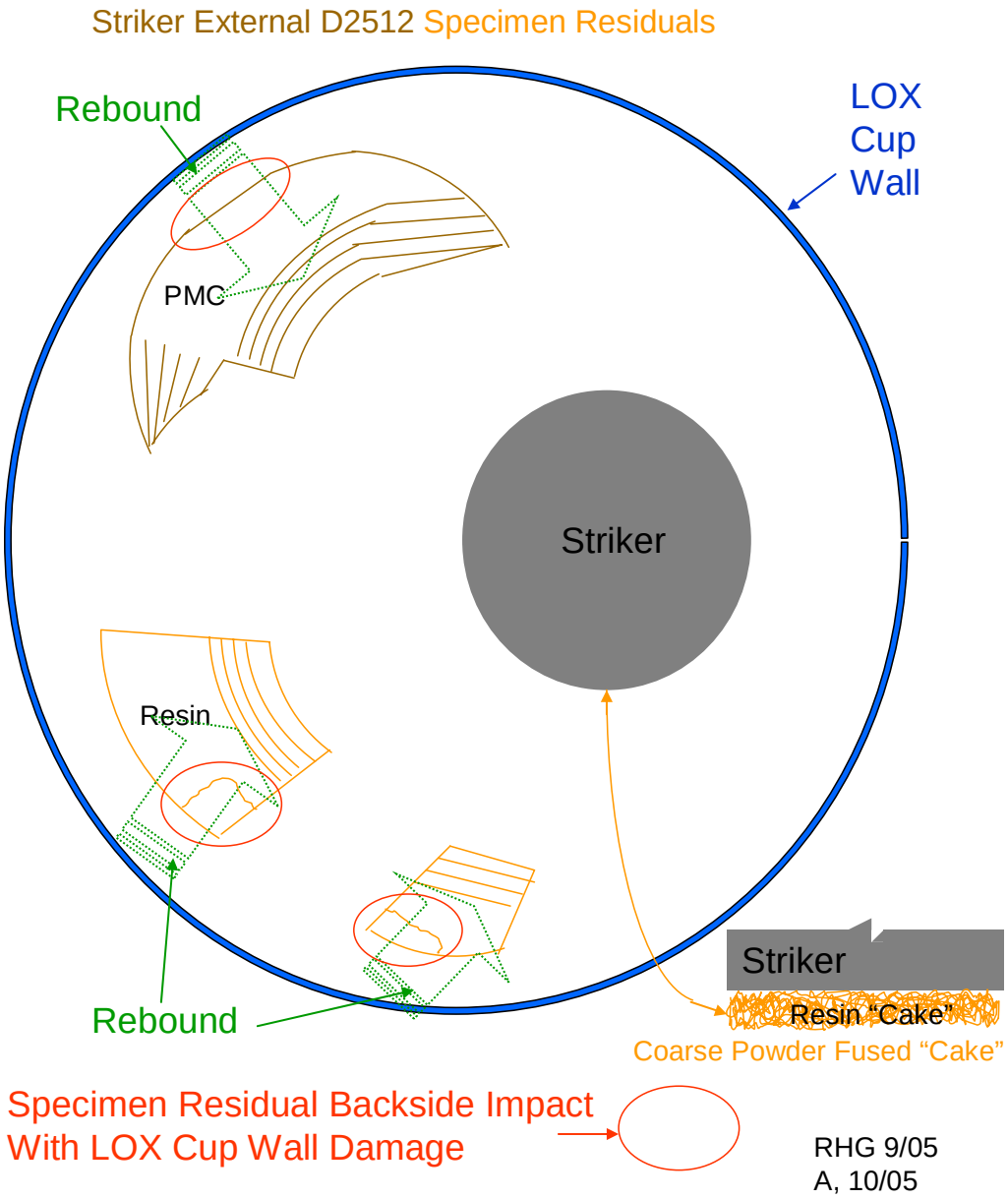


Figure 183, Conceptual Backside Impact Damage

For the neat resin specimens that were D2512 tested, occasionally some of the returned residuals appeared to consist of flat cakes of fused together powder. Some examples of these resin "cakes" are depicted in figure 152. Many also appeared to have had portions that appeared to have melted and flown to form a glossy surface or stringers. These cakes were most likely generated by a mechanism analogous to hot isostatic pressing with the heat being generated by the kinetic friction of the particles sliding over one another.

Conclusion

This research effort has successfully achieved its two objectives. The first was to determine if a composite, using thermally conductive reinforcement fibers instead of the standard conventional carbon fibers used to date, suitable to the fabrication of axisymmetric tanks, ducts, and lines and exhibiting in-plane Ks comparable to metals (which regularly pass D2512), can be found which either passes or comes close to passing D2512. The second objective was deduce and to better understand what happened to the specimens during the D2512 test. In achieving these objectives it has accomplished a series of world firsts.

This effort successfully and repeatedly demonstrated that using a thermally conductive fiber could substantially enhance the mechanical impact LOX compatibility of a composite as measured by ASTM D2512. It repeatedly achieved 90 percent of the goal of passing the ASTM standard D2512 mechanical impact ignition test which is a 1700 percent improvement over the experimental baseline.

This effort also acquired, sorted, documented and cataloged the types of fracture surfaces which are routinely found in residuals (of the types of materials investigated by this effort) remaining after the impact test fractures and possibly causes the ignition of a specimen. Based upon these fracture surfaces, Hertzian fracture was shown to be the mechanism by which a specimen fractured and failed in a D2512 test.

The exhaustive analysis of the residual fracture surfaces also lead to the understanding of the mechanical-to-thermal transformation mechanism. The examined fracture surfaces of the residuals routinely indicated that kinetic friction had occurred during a D2512 test. The examination also indicated that signs of intense heating were associated with the signs of kinetic friction. Kinetic friction's mechanical-to-thermal transformation mechanism provided the only phenomenological explanation for the extremely rapid and large temperature rises required for conditions recognizable as ignition to occur in the time frame of a D2512 mechanical impact test. It also provided the only correlation of the various physical parameters varied by this effort to the D2512 testing results obtained.

Overall the effort crystallized the sequence from fracture to heating to possible ignition. It starts first with the development of a series of Hertzian fractures. These allow for heavy kinetic friction of the Hertzian fractured material to occur. This kinetic friction then provides a means for the mechanical energy to become temperature rising thermal energy. This temperature rising thermal energy causes the material to degrade by radical chain scission and then oxidize by radical addition peroxide chemistry to a degree possibly detectable as ignition.

Introduction Bibliography:

I1, www.fas.org/spp/guide/russia/launch/

I2, www.nkau.gov.ua

I3, www.orbireport.com

I4, www.russianspace.web

I5, www.calt.com.cn/new/english

I6, www.fas.org/spp/guide/china/launch/

I7, www.tbs-satellite.com

I8, www.astronautix.com

I9 www.kevinforsyth.net

I10, www.spaceandtech.com

I11, www.losangeles.af.mil/smc/pa/fact-sheets/eelv.htm

I12, www.geocites.com/capecanaveral/launchpad/1921/launch.com

I13, www.ilslaunch.com

I14, www.daviddarling.info

I15, www.nationmaster.com

I16, www.averillpark.net

I17, www.spacex.com

I18, www.boeing.com

I19, www.nasda.go.jp

I20, Y. Prel, “Composite Materials On Ariane 5 Launcher.”, SAMPE Journal, V35, N5, Pg 13-17, Sep-Oct 99

I21, Michael J. Robinson, Joel M. Stoltzfus, and Thomas N. Owens, “Composite Material Compatibility With Liquid Oxygen”, 38TH AIAA/ASME/ASCE/AHS/ASC Structures, Structural dynamics, and Materials Conference, Kissimmee, Fl., 7-10 April 1997; also, McDonnell Douglas Aerospace, MDC 96H0860, Pg 1-10, 1997

I22, Rollin C. Christianson, “Oxygen Hazards Analysis Of Composite Liquid Oxygen Tanks”, WSTF IR 93 0024, NASA JSC WSTF P.O. Drawer MM, Las Cruces, NM 88004

I23, Mike Shoffstall, Oxygen Hazards Analysis of McDonnell Douglas Composite LOX Tank for the X-33 Vehicle, WSTF-IR-96-0070, Oct 11 1996

I24, Harold W. Schmidt, and Forney, ASRDI Oxygen Technological Survey. Vol 9: Oxygen Systems Engineering Review, NASA SP-3090, Pg 1-218, 1975

I25, R.L.Hauser, G.E.Sykes, and W.F.Rumpel, "Mechanically Initiated Reactions Of Organic Materials In Missile Oxidizers", TR 61-324, Elastomers and Coatings Branch, Nonmetallic Materials Laboratory, Directorate Of Materials And Processes, ASD, AFSC, USAF, WPAFB, Contract # AF 33(616)-7271, The Martin Company, Oct 1961, Pg 1-281

I26, "Liquid Rocket Metal Tanks And Tank Components." NASA Space Vehicle Design Criteria (Chemical Propulsion), NASA SP-8088, Pg 1-156, May 1974

I27, R.P. Reed, N.J. Simon, J.D. McColskey, J.R. Berger, C.N. McCowen, J.W. Bransford, E.S. Drexler, and R.P. Walsh, "Aluminum Alloys For Cryogenic Tanks: Oxygen Compatibility Volume 1.", AL TR 90 063, Pg 1-196, Sep 1990

I28, R.P. Reed, N.J. Simon, J.D. McColskey, C.N.McCowen, and E.S. Drexler, "Aluminum Alloys For ALS Cryogenic Tanks: Oxygen Compatibility Volume 2. Final Report.", AL TR 90 063, Pg 1-118, Sep 1990

I26, James J. Pelouch, Jr., ASRDI Oxygen Technological Survey. Vol VII: Characteristics Of Metals That Influence System Safety, NASA SP-3077, Pg 1-68, 1974

I29, Numerous Meetings and Conversations With LV Community Personnel Mid 1980s thru 2001

I30, www.waltsmodels.com

I31, www.dupontert.com

I32, Conversations With M. Hand Of Boeing 98

Oxygen Compatibility Bibliography:

Theory Related

O1, Standard Guide For Designing Systems For Oxygen Service, ASTM G 88 - 90

O2, Standard Guide For Evaluating Metals For Oxygen Service, ASTM G 94 - 92

O3, Standard Guide For Evaluating Nonmetallic Materials For Oxygen Service, ASTM G 63 - 92

O4, Standard Practice For Aging Oxygen-Service Materials Prior To Flammability Testing, ASTM G 114 - 93

O5, Standard Test Method For Determining Material Ignition And Flame Spread Properties, ASTM E 1321 - 97a

O6, Flammability, Odor, Offgassing, And Compatibility Requirements And Test Procedures For Materials In Environments That Support Combustion., NASA STD 6001 (Previously NHB 8060.1C), Pg 1-62, Feb 1998

O7, Safety Standard For Oxygen And Oxygen Systems: Guidelines for oxygen System Design, Materials Selection, Operations, Storage, and Transportation, NASA NSS 1740.15, Pg 1-220, Jan 1996

O8, Standard General Requirements For Safe Design And Operation Of Pressurized Missile And Space Systems, MIL-STD-1522A (USAF), Pg 1-70, 28 May 1984

O9, NASA JSC Requirements For Flight And Flight Prototype Liquid And High Pressure Oxygen Components And Systems, NASA JSC SE-0-0104, Pg 1-314, 1 May 1983

O10, "Hazards Of Chemical Rockets And Propellants: Oxygen", Chemical Propulsion Information Agency CPIA Pub 394 Volume III, Ch 11, Pg 1-11, Sep 1984

O11, "Liquid Rocket Metal Tanks And Tank Components." NASA Space Vehicle Design Criteria (Chemical Propulsion), NASA SP-8088, Pg 1-156, May 1974

O12, Austin, John G., Hust, J.G., and Clark, A.F., " A Survey Of Compatibility Of Materials With High Pressure Oxygen Service (Final Report).", NASA-CR-120221, Pg 1-178, Oct 1974

O13, J. L. Hopewell, D.J.T. Hill, J.H. O'Donnell, P.J.Pomery, J.E.McGrath, D.B.Priddy Jr, and C.D.Smith, "The radiation chemistry of poly (arylene ether phosphine oxide)s.", Polymer Degradation and Stability, Vol 45 Elsevier Science Limited, Pg 293-299, 1994

O14, Mike Shoffstall, "Oxygen Hazards Analysis Of McDonnell Douglas Composite LOX tank for the X-33 Vehicle.", WSTF IR 96 0070, Pg 1-11, Oct 1996

O15, Barry L. Werley, Herve' Barthelemy, Robert Gates, Joseph W. Slusser, Keith B. Wilson, and Robert Zawierucha, "A Critical Review Of Flammability Data For Aluminum.", Flamibility And Sensitivity Of Materials In Oxygen-Enriched Atmospheres: **Sixth Volume**, ASTM STP 1197, Dwight D. Janoff and Joel M. Stoltzfus, Eds, American Society For Testing and Materials, Philadelphia, Pg 300-345, 1993

O16, Theodore A. Steinberg, D. Bruce Wilson, and Frank J. Benz, "Microgravity And Normal Gravity Combustion Of Metals And Alloys In High Pressure Oxygen.", Flamibility And Sensitivity Of Materials In Oxygen-Enriched Atmospheres: **Sixth Volume**, ASTM STP 1197, Dwight D. Janoff and Joel M. Stoltzfus, Eds, American Society For Testing and Materials, Philadelphia, Pg 133-145, 1993

O17, Frank J. Benz, Ralph E. Williams, and Dan Armstrong, "Ignition Of Metals And Alloys By High-Velocity Particles.", Flamibility And Sensitivity Of Materials In Oxygen-Enriched Atmospheres: **Second Volume**, ASTM STP 910, Michael A. Benning, Eds, American Society For Testing and Materials, Philadelphia, Pg 16-37, 1986

O18, Jess M Waller, Steven D, Hornung, and Harold D. Beeson, "Fuel Cell Elastomertic Materials Oxygen Compatability Testing: Effect Of 450 and 6200 kPA Oxygen.", Flamibility And Sensitivity Of Materials In Oxygen-Enriched Atmospheres: **Eigth Volume**, ASTM STP 1319, W.T. Royals, T.C. Chou, and T.A. Steinberg, Eds, American Society For Testing and Materials, Pg 385-402, 1997

O19, Lawrence H. Haselmaier, and Benjamin A. Powell, "The Seal Configuration Tester, A New Approach To The Evaluation Of Elastomeric Materials For Oxygen Service", Flamibility And Sensitivity Of Materials In Oxygen-Enriched Atmospheres: **Seventh Volume**, ASTM STP 1267, Dwight D. Janoff, William T. Royals, and Mohgan V. Gunaji, Eds, American Society For Testing and Materials, Pg 11-22, 1995

O20, Barry Newton, Wendell C. Hull, and Jack Stradling, "A Database for metallic and nonmetallic matetrials commonly utilized in oxygen service.", Flamibility And Sensitivity Of Materials In Oxygen-Enriched Atmospheres: **Eigth Volume**, ASTM STP 1319, W.T. Royals, T.C. Chou, and T.A. Steinberg, Eds, American Society For Testing and Materials, Pg 458-476, 1997

O21, Theodore A. Steinberg, and Benjamin C. Scown, “New Test Capabilities For The Evaluation Of Material Flammability In Oxygen-Enriched Atmospheres”, Flamibility And Sensitivity Of Materials In Oxygen-Enriched Atmospheres: **Seventh Volume**, ASTM STP 1267, Dwight D. Janoff, William T. Royals, and Mohgan V. Gunaji, Eds, American Society For Testing and Materials, Pg 57-66, 1995

O22, Theodore A. Steinberg, “Combustion Testing Of Non-Metallic Materials In Ambient And Oxygen-Enriched Atmospheres”, Flamibility And Sensitivity Of Materials In Oxygen-Enriched Atmospheres: **Eigth Volume**, ASTM STP 1319, W.T. Royals, T.C. Chou, and T.A. Steinberg, Eds, American Society For Testing and Materials, Pg 370-384, 1997

O23, Jesse Dees, Elliot Forsyth, Mohan V. Gunaji, and Joel M. Stoltzfus, “An Evaluation Of Polymers As Ignition Sources During Particle Impact In Oxygen”, Flamibility And Sensitivity Of Materials In Oxygen-Enriched Atmospheres: **Seventh Volume**, ASTM STP 1267, Dwight D. Janoff, William T. Royals, and Mohgan V. Gunaji, Eds, American Society For Testing and Materials, Pg 143-151, 1995

O24, Wolfgang Wegener, Christain Binder, Peter Hengstenberg, K.-P. Herrmann, and D Weinert, “Tests to evaluate the suitability of materials for Oxygen Service.”, Flamibility And Sensitivity Of Materials In Oxygen-Enriched Atmospheres: **Third Volume**, ASTM STP 986, D.W. Schroll, Eds, American Society For Testing and Materials, Philadelphia, Pg 268-278, 1988

O25, Barry L. Werley, ”An Oxygen Index Update.”, Flamibility And Sensitivity Of Materials In Oxygen-Enriched Atmospheres: **Third Volume**, ASTM STP 986, D.W. Schroll, Eds, American Society For Testing and Materials, Philadelphia, Pg 248-261, 1988

O26, Roland K. Wharton, “An Assessment of the Critical Oxygen Index Test as a Measure of Material Flammability.”, Flamibility And Sensitivity Of Materials In Oxygen-Enriched Atmospheres: **Third Volume**, ASTM STP 986, D.W. Schroll, Eds, American Society For Testing and Materials, Philadelphia, Pg 279-285, 1988

O27, Jose M. Dieguez, Louis Bothorel, Adolfo de Lorenzo, and Albert Faupin, “Ignition Testing of hollow vessels pressurized with gaseous oxygen.”, Flamibility And Sensitivity Of Materials In Oxygen-Enriched Atmospheres: **Third Volume**, ASTM STP 986, D.W. Schroll, Eds, American Society For Testing and Materials, Philadelphia, Pg 368-388, 1988

O28, Rohintan S. Irani, James L. Currie, Neville J. Wilson, and John Sanders, “Dimensional Changes In Elastomers Under High-Pressure Oxygen.”, Flamibility And Sensitivity Of Materials In Oxygen-Enriched Atmospheres: **Third Volume**, ASTM STP 986, D.W. Schroll, Eds, American Society For Testing and Materials, Philadelphia, Pg 346-358, 1988

O29, Walter W. Yuen, Donald Greer, Gary Lin, and Coleman Bryan, “Modeling of the transient ignition of a Nonmetal/oxygen system by heterogeneous reaction: effects of oxygen pressure.”, Flamibility And Sensitivity Of Materials In Oxygen-Enriched Atmospheres: **Third Volume**, ASTM STP 986, D.W. Schroll, Eds, American Society For Testing and Materials, Philadelphia, Pg 191-205, 1988

O30, Leonard Schoenman, Ralph L. Sabiers, and Mel C. McIlwain, “Test Experience with a high-pressure oxygen turbopump and heat exchanger.”, Flamibility And Sensitivity Of Materials In Oxygen-Enriched Atmospheres: **Fifth Volume**, ASTM STP 1111, Joel M. Stoltzfus and Kenneth McIlroy, Eds, American Society For Testing and Materials, Philadelphia, Pg 556-573, 1991

O31, Irvin Glassman, “Combustion Fundamentals Of Low Volatility Materials In Oxygen Enriched Atmospheres.”, Flamibility And Sensitivity Of Materials In Oxygen-Enriched Atmospheres: **Fifth Volume**, ASTM STP 1111, Joel M. Stoltzfus and Kenneth McIlroy, Eds, American Society For Testing and Materials, Philadelphia, Pg 7-25, 1991

O32, David B. Hirsch, Radel L. Bunker, and Dwight Janoff, “Effects of oxygen concentration, diluents and pressure on ignition and flame-spread rates of nonmetals: A Review Paper.”, Flamibility And Sensitivity Of Materials In Oxygen-Enriched Atmospheres: **Fifth Volume**, ASTM STP 1111, Joel M. Stoltzfus and Kenneth McIlroy, Eds, American Society For Testing and Materials, Philadelphia, Pg 179-190, 1991

O33, Ralph M. Tapphorn, Richard Shelley, and Frank Benz, “Test Developments for polymers In Oxygen Enriched Environments.”, Flamibility And Sensitivity Of Materials In Oxygen-Enriched Atmospheres: **Fifth Volume**, ASTM STP 1111, Joel M. Stoltzfus and Kenneth McIlroy, Eds, American Society For Testing and Materials, Philadelphia, Pg 43-59, 1991

O34, Klaus Boddenberg, and Jurgen Waldmann, “Special Construction Features Of Centrifugal Compressors For Oxygen Service.”, Flamibility And Sensitivity Of Materials In Oxygen-Enriched Atmospheres: **Fifth Volume**, ASTM STP 1111, Joel M. Stoltzfus and Kenneth McIlroy, Eds, American Society For Testing and Materials, Philadelphia, Pg 528-545, 1991

O35, John A. Gilbertson, “The Application Of Compatibility Knowledge.”, Flamibility And Sensitivity Of Materials In Oxygen-Enriched Atmospheres: **Second Volume**, ASTM STP 910, Michael A. Benning, Eds, American Society For Testing and Materials, Philadelphia, Pg 7-15, 1986

O36, James W. Bransford, “Ignition And Combustion Temperatures Determined By Laser Heating.”, Flamibility And Sensitivity Of Materials In Oxygen-Enriched Atmospheres: **Second Volume**, ASTM STP 910, Michael A. Benning, Eds, American Society For Testing and Materials, Philadelphia, Pg 78-97, 1986

O37, Walter W. Yuen, “A Model Of Metal Ignition Including The Effect Of Oxide Generation.”, Flamibility And Sensitivity Of Materials In Oxygen-Enriched Atmospheres: **Second Volume**, ASTM STP 910, Michael A. Benning, Eds, American Society For Testing and Materials, Philadelphia, Pg 59-77, 1986

O38, Robert M. Neary, “ASTM G63: A Milestone In A 60 Year Safety Effort.”, Flamibility And Sensitivity Of Materials In Oxygen-Enriched Atmospheres: ASTM STP 812, Berry L. Werley, Eds, American Society For Testing and Materials, Philadelphia PA. Pg 3-8, 1983

O39, Joseph W. Slusser, and Keith A. Miller, “Selection Of Metals For Gaseous Oxygen Service.”, Flamibility And Sensitivity Of Materials In Oxygen-Enriched Atmospheres: ASTM STP 812, Berry L. Werley, Eds, American Society For Testing and Materials, Philadelphia PA. Pg 167-191, 1983

O40, Raymond W. Monroe, Charles E. Bates, and Coultas D. Pears, “Metal Combustion In High-Pressure Flowing Oxygen.”, Flamibility And Sensitivity Of Materials In Oxygen-Enriched Atmospheres: ASTM STP 812, Berry L. Werley, Eds, American Society For Testing and Materials, Philadelphia PA., Pg 126-149, 1983

O41, George K. Ikeda, “Oxygen Index Tests To Evaluate The Suitability Of A Given Material For Oxygen Service.”, Flamibility And Sensitivity Of Materials In Oxygen-Enriched Atmospheres: ASTM STP 812, Berry L. Werley, Eds, American Society For Testing and Materials, Philadelphia PA., Pg 56-67, 1983

O42, Michael A. Benning, “Measurement Of Oxygen Index At Elevated Pressures.”, Flamibility And Sensitivity Of Materials In Oxygen-Enriched Atmospheres: ASTM STP 812, Berry L. Werley, Eds, American Society For Testing and Materials, Philadelphia PA., Pg 68-83, 1983

O43, Billy J. Lockhart, Michael D. Hampton, and Coleman J. Bryan, “The Oxygen Sensitivity / Compatibility Ranking Of Several Materials By Different Test Methods.”, Flamibility And Sensitivity Of Materials In Oxygen-Enriched Atmospheres: **Fourth Volume,** ASTM STP 1040, Joel M. Stoltzfus, Frank J. Benz, and Jack S. Stradling, Eds, American Society For Testing and Materials, Philadelphia PA., Pg 93-105, 1989

O44, Christer V. Hokkanen, “Measurements Of Oxygen Enrichment In Foam Insulation For Liquid Nitrogen Pipelines.”, Flamibility And Sensitivity Of Materials In Oxygen-Enriched Atmospheres: **Fourth Volume,** ASTM STP 1040, Joel M. Stoltzfus, Frank J. Benz, and Jack S. Stradling, Eds, American Society For Testing and Materials, Philadelphia PA., Pg 406-415, 1989

O45, Rohintan S. Irani, Jim L. Currie, and John Sanders, “Evolving Non-swelling Elastomers For High Pressure Oxygen Environments.”, Flamibility And Sensitivity Of Materials In Oxygen-Enriched Atmospheres: **Fourth Volume,** ASTM STP 1040, Joel M. Stoltzfus, Frank J. Benz, and Jack S. Stradling, Eds, American Society For Testing and Materials, Philadelphia PA., Pg 309-331, 1989

O46, Joel Stoltzfus, Jack Stradling, and Frank Benz, “Overview.”, Flamibility And Sensitivity Of Materials In Oxygen-Enriched Atmospheres: **Fourth Volume,** ASTM STP 1040, Joel M. Stoltzfus, Frank J. Benz, and Jack S. Stradling, Eds, American Society For Testing and Materials, Philadelphia PA., Pg 1-8, 1989

O47, Jim L. Currie, Rohintan S. Irani, and John Sanders, “The Ignition Behaviour Of Silicone Greases In Oxygen Atmospheres.”, Flamibility And Sensitivity Of Materials In Oxygen-Enriched Atmospheres: **Fourth Volume,** ASTM STP 1040, Joel M. Stoltzfus, Frank J. Benz, and Jack S. Stradling, Eds, American Society For Testing and Materials, Philadelphia PA., Pg 125-141, 1989

O48, Herve' Barthelemy, Georges Delode, and Gerard Vagnard, “Oxygen Compatibility Of Pressure Regulators For Gas Cylinders.”, Flamibility And Sensitivity Of Materials In Oxygen-Enriched Atmospheres: **Fourth Volume,** ASTM STP 1040, Joel M. Stoltzfus, Frank J. Benz, and Jack S. Stradling, Eds, American Society For Testing and Materials, Philadelphia PA., Pg 267-287, 1989

O49, Angel Abbud-Madrid, Melvyn C. Branch, Thomas J. Feiereisen, and John W. Daily, “Ignition Of Bulk Metals By A Continuous Radiation Source In A Pure Oxygen Atmosphere.”, Flamibility And Sensitivity Of Materials In Oxygen-Enriched Atmospheres: **Sixth Volume**, ASTM STP 1197, Dwight D. Janoff and Joel M. Stoltzfus, Eds, American Society For Testing and Materials, Philadelphia, Pg 211-222, 1993

O50, Aleck C. Bond, Henry O. Pohl, Norman H. Chaffee, Walter W. Guy, Charles S. Allton, and Robert L. Johnston, Design Guide For High Pressure Oxygen Systems, NASA RP 1113, Pg 1-83, 1983

O51, Harold W. Schmidt, and Forney, ASRDI Oxygen Technological Survey. Vol 9: Oxygen Systems Engineering Review, NASA SP-3090, Pg 1-218, 1975

O52, Michael J. Robinson, Joel M. Stoltzfus, and Thomas N. Owens, “Composite Material Compatibility With Liquid Oxygen.”, 38TH AIAA/ASME/ASCE/AHS/ASC Structures, Structural dynamics, and Materials Conference, Kissimmee, Fl., 7-10 April 1997; also, McDonnell Douglas Aerospace, MDC 96H0860, Pg 1-10, 1997

O53, Bert R. Phillips, and Kenneth J. De Witt, “Resonance Tube Ignition Of Aluminum.”, Combustion And Flame, V35, Pg 249-258, 1979

O54, A. G. Merzhanov, Yu. M. Grigorjev, and Yu. A. Gal'chenko, “Aluminum Ignition”, Combustion And Flame, V29, Pg 1-14, 1977

O55, Standard Test Method For Rubber Property - Effect Of Liquids., ASTM D 471 – 98

O56, Standard Test Method For Heat Of Combustion Of Liquid Hydrocarbon Fuels By Bomb Calorimeter, ASTM D 240 - 92 (Reapproved 1997)

O57, Standard Practice For Evaluating The Resistance Of Plastics To Chemical Reagents., ASTM D 543 – 95

O58, Standard Test Method For Rubber Property - Change In Length During Liquid Immersion., ASTM D 1460 - 86

O59, Alan F. Clark, and Jerome G. Hust, “A review Of The Compatibility Of Structural Materials With Oxygen.”, AIAA Journal, V12, N4, Pg 441-454, Apr 1974

O60, K. Kishore, and S. Sankaralingam, “Effect Of Pressure On Polymer Ignition.”, Journal Of Fire Sciences, V4, Pg 94-99, Mar-Apr 1986

O61, D.E. Stuetz, A.H. Diedwardo, F. Zitomer, and B.P. Barnes, “Polymer Combustion.”, Journal Of Polymer Science: Polymer Chemistry Edition, V13, Pg 585-621, 1975

O62, A. L. Breiter, V.M. Mal'tsev, and E.I. Popov, “Models Of Metal Ignition.”, Fizika Goreniya I Vzryva (Combustion, Explosion, And Shock Waves), V13, N4, Pg 558-570, Oct-Dec 1977

O63, Robert Lowrie, “Oxygen Compatibility Of Metals And Alloys.”, Flamibility And Sensitivity Of Materials In Oxygen-Enriched Atmospheres: **Sixth Volume**, ASTM STP 1197, Dwight D. Janoff and Joel M. Stoltzfus, Eds, American Society For Testing and Materials, Philadelphia, Pg 3-23, 1993

O64, James J. Pelouch, Jr., ASRDI Oxygen Technological Survey. Vol VII: Characteristics Of Metals That Influence System Safety, NASA SP-3077, Pg 1-68, 1974

O65, J.G. Hust, and A.F. Clark, “A Survey Of Compatibility Of Materials With High Pressure Oxygen Service.”, Cryogenics, Pg 325-336, June 1973

O66, Fu-Yu Hshieh, Coleman J. Bryan, and Michael D. Pedley,”Communication: Autoignition Temperature Of Carbon filled Fluoroelastomers At Elevated Oxygen Pressure.”, Fire And Materials, V18, Pg 389-39, 1994

O67, Fu-Yu Hshieh, Joel M. Stoltzfus, and Harold D. Beeson, “Note: Autoignition Temperature Of Selected Polymers At Elevated Oxygen Pressure And Their Heat Of Combustion.”, Fire And Materials, V20, Pg 301-303, 1996

O68, I. Glassman, A.M. Mellor, H.F. Sullivan, and N.M. Laurendeau, “A Review Of Metal Ignition And Flame Models.”, Princeton Univ., Princeton USA

O69, K. Akita, ”Ignition Of Polymers And Flame Propagation On Polymer Surfaces.”, Chapter 10, Aspects Of Degradation And Stabilization Of Polymers, Edited By H.H.G. Jellinek, Elsevier Scientific Publishing Co., Amsterdam Oxford NY, Pg 501-525, 1978

O70, K. Kishore, R. Nagarajan, and K. Mohandas, “Polymer Ignition - A Review.”, Polymer Engineering Reviews, V2, N3, Pg 257-293, 1983

O71, K. Kishore, and K. Mohandas, “Polymer Gasification Processes - A Review.”, Polymer Engineering Reviews, V2, N3, Pg 189-210, 1983

O72, K. Kishore, K. Mohandas, and K.S. Annakutty, “Is Gasification Rate Controlling Step In Polymer Ignition?”, Combustion Science And Technology, V31, Pg 183-194, 1983

O73, F.Y. Hshieh, and G.N. Richards, “Factors Influencing Chemisorption And Ignition Of Wood Chars.”, Combustion And Flame, V76, Pg 37-47, 1989

O74, F.Y. Hshieh, and G.N. Richards, ” Factors Influencing Oxygen Chemisorption And Ignition Of Chars From Newsprint.”, Combustion And Flame, V76, Pg 49-56, 1989

O75, Yoshio Kamiya, and Etsuo Niki, “Oxidative Degradation.”, Chapter 3, Aspects Of Degradation And Stabilization Of Polymers, Edited By H.H.G. Jellinek, Elsevier Scientific Publishing Co., Amsterdam Oxford NY, Pg 79-147, 1978 1978

O76, J.H.Kimzey, “Review Of Factors Affecting Ignition Of Metals In High Pressure Oxygen Systems.”, Structures And Mechanics Division Internal Note, NASA Manned Spacecraft Center, Houston, Texas, October 28, 1970

O77, Alan E. Comyns, Jose Sanchez, and Terry N. Myers, “Peroxides and Peroxide Compounds: Inorganic Peroxides; Organic Peroxides.”, Kirk-Othmer Encyclopedia Of Chemical Technology, 4Th Ed, Vol 18, J. I. Kroschwitz, M. Howe-Grant Editors, John Wiley & Sons, Pg 202-310, 1996

O78, Kenneth Kuan-yun Kuo, “Ignition.”, Principles Of Combustion, Ch 10, John Wiley & Sons, Pg 734-790, 1986

O79, Robert A. Frosch, Indra K. Varma, George M. Fohlen, and John A. Parker, “Phosphorus Containing Bisimide Resins.”, US Patent Number: 4,276,344, Pg 1-4, Jun 1981

O80, James E. Mark, Harry R. Allcock, and Robert West, Inorganic Polymers, Prentice Hall, A Division Of Simon & Schuster, Englewood Cliffs, New Jersey 07632, Pg 1-272, 1992

O81, C.Bianca, H.S.Greenberg, and S.E.Johnson, “Reusable LH2 Tank technology demonstration through ground test.”, AIAA Space Programs and Technologies Conference, AIAA 94-4677, Pg 1-12, Sep 1994

O82, Neil A. Graf, Richard J. Hudgins, and Michael McBain, “Oxygen Compatibility Testing Of Composite Materials.”, SAMPE 32ND Internat. Conf. Boston MA, Pg. 1-12, Nov 2000

O83, Neil A. Graf, Richard J. Hudgins, and Michael McBain, “Subscale Composite Liquid Oxygen Tank Testing.”, A NASA Space Transportation Conference, Pg 1-13, 2000

O84, Paul A. Wood, Gregory D. Lyle, Atilla Gungor, Carrington D. Smith, and James E. McGrath, “Synthesis Of New Bismaleimides Derived From Bis(3-Amino Phenoxy) Triphenylphosphine Oxide And Bis (4-Fluoro Benzoyl) Benzene.”, 36Th Internat. SAMPE Symposium, Pg 1355-1367, Apr 1991

O85, Paul A. Wood III, “Synthesis and characterization of novel bismaleimides derived from arylene phosphine oxides and ether-ketones.”, PHD Dissertation Virginia Polytechnic Institute and State University, Pg 1-277, 1991

O86, H.D. Stenzenberger, P. Konig, W. Romer, M. Herzog, and W.V. Breitigam, “BMI / Bis(allylphenoxyphthalimide) - Copolymers: A New Family Of Resins For Advanced Composites With Improvged Thermal Oxidative Stability.”, 36Th Internat. SAMPE Symposium, Pg 1232-1243, Apr 1991

O87, Daniel A. Scola, “Thermo-Oxidative Stability Of Graphite Fiber / PMR - 15 Polyimide Composites At 350 C.”, High Temperature Polymer Matrix Composites, Noyes Data Corp., Pg 214-239, 1987

O88, D. Evans, S.J. Robertson, and J.T. Morgan, ”The Long-Term Effects Of Hydrogen And Oxygen On The Mechanical Properties Of Carbon Fibre Reinforced Composites.”, Advances In Cryogenic Engineering (Materials), Vol. 36, Edited By R.P. Reed and F.R. Fickett, Plenum Press, NY, Pg 937-941, 1990

O89, H.P. Boehm, E.Diehl, and W.Heck, “Identification Of Functional Groups In Surface Oxides Of Carbon.”, Second Conference On Industrial Carbon And Graphite, London, 7-9 Apr 1965, Pg 369-379, 1966

O90, E.I. Courtright, S. Baskaran, D.A. Nelson, and H.C. Reid, “Materials For Advanced Rocket Propulsion - An Assessment Of Materials & Process Development Needs.”, WL-TR-96-4086, Pg. 1-19, 24-67, 141-169, 208-219, Dec 1996

O91, Demetrius A. Kourtides, and John A. Parker, ”Advanced Resin Matrices For Fire resistant Composites.”, Pactec 79, SPE, Pg 51-54, Feb 1979

O92, Demetrius A. Kourtides, and John A. Parker, “Flammability Properties Of Some Thermoplastic And Thermoset Resins.”, 23RD National SAMPE, Pg 36-43, May 1978

O93, John A. Parker, Demitrius A. Kourtides, and George M. Fohlen, “Bismaleimides And Related Maleimido Polymers As Matrix Resins For High Temperature Environments.”, High Temperature Polymer Matrix Composites, Noyes Data Corp., Pg 54-76, 1987

O94, M.E.S. Carvalho, and J.J.C. Cruz-Pinto, “The kinetics of photo-oxidation of low-density polyethylene films.”, Polymer Engineering and Science,, V32, N8, Pg 567-572, Apr. 1992

O95, C.D. Smith, H. Grubbs, H.F. Webster, A. Gungor, J.P. Wightman, and J.E. McGrath, “Unique Characteristics Derived From PolyArylene Ether Phosphine Oxide)s”, High Performance Polymers, V3, N4, Pg 211-229, 1991

O96, Robert Savage, “Graphite Lubrication”, J. Of Applied Physics, V19, N1, Pg 1-10, Jan 1948

O97, R.L.Tobler, “A review of antifriction materials and design for cryogenic environments.”, Advances in Cryogenic Engineering Materials, V26, Editors: A.F. Clark and R.P.Reed, Plenum Press, Pg 66-77, 1980

O98, L.D.Wedeven, and N.C.Miller, “Material and Tribological Considerations for Turbopump Bearings.”, J. of the Society of Tribologists and Lubrication Engineers, V47, N12, Pg 1009-1017, Dec 1991

O99, Roger Gerzeski, “Polymer Ignition In 100% LOX/GOX”, ASC-01-0390, Cleared For Public Release Presentation, 2001

Mechanical Impact Related

O100, Standard Test Method For Compatibility Of Materials With Liquid Oxygen (Impact Sensitivity Threshold And Pass-Fail Techniques), ASTM D 2512 - 95

O101, Standard Test Method For Compatibility Of Materials With Liquid Oxygen (Reaction Intensity Method), ASTM F 371 - 83 (Reapproved 1994)

O102, Standard Test Method For Deteremining Ignition Sensitivity Of Materials To Mechancial Impact In Ambient Liquid Oxygen and Pressurized Liquid And Gaseous Oxygen Environments,ASTM G 86 - 98

O103, Standard Test Method For Drop-Weight Sensitivity Of Liquid Monopropellants. ASTM D 2540 - 93

O104, Ambient LOX Impact Testing NASA-STD-6001: Test 13A, ED36-OWI-032 Rev A, Pg 1-34, Aug 1999

O105, High Pressure Impact Testing NASA-STD-6001: Test 13B, ED36-OWI-033 Rev A, Pg 1-52, Aug 1999

O106, V.V. Bolotin, A.E. Efimov, N.S. Mezentsev, and V.N. Shchugorev, “Experimental Investigation Of The Effect Of Local Impact Loading On The Interlaminar Strength Of Composites.”, Mekhanika Kompozitnykh Materialov, V26, N1, Pg 48-51, Jan-Feb 1990

O107, K. Srimivasan, W.C. Jackson, and J.A. Hinkley, “Response Of Composite Materials To Low Velocity Impact.”, 36Th Internat. SAMPE Symposium, Pg 850-862, Apr 1991

O108, J.W.Bransford, C.J.Bryan, G.W.Frye, and S.L.Stohler, “LOX/GOX Mechanical Impact Tester Assessment.”, NASA TM 74106, JFK Space Center, Feb 1980

O109, William S. Porter, “Test Report metals Ignition Study In Gaseous Oxygen (Particle Impact Technique Relating To The Shuttle Main propulsion System Oxygen Flow Control Valve Tests).”, NASA Document, TR-277-001, WSTF JSC, Oct 1982

O110, Mark Wilenski, “Impact Test Costs At NASA WSTF.”, Conversations As Of 28 June 1999
O111, Key, C.F., and Riehl, W.A., “Compatibility Of Materials With Liquid Oxygen.”, NASA-TM X-985, Pg 1-72, Aug 1964

O112, Key, C.F., “Compatibility Of Materials With Liquid Oxygen I.“, NASA-TM X-64711, Pg 1-221, Oct 1972

O113, Key, C.F., ”Compatibility Of Materials With Liquid Oxygen III.”, NASA-TM X-53533, Pg 1-54, Nov 1966

O114, Key, C.F., “Compatibility Of Materials With Liquid Oxygen IV.”, NASA-TM X-53773, Pg 1-47, Aug 1968

O115, William R. Lucas, and Wilbur A. Riehl, “An Instrument For Determination Of Impact Sensitivity Of Materials In Contact With Liquid Oxygen.”, ASTM Bulletin N244, Pg 29-34, Feb 1960

O116, Riehl, W.A., Key, C.F., and Gayle, J.B, “Reactivity Of Titanium With Oxygen.”, NASA TR R-180, Pg 1-113, Dec 1963

O117, Materials Selection List For Space Hardware Systems, MSFC HDBK 527 Rev F JSC 09604 Rev F, Pg 1-1560, Sep 1988

O118, “Matrix and Coating Polymers for Composite LOX Containers.”, NASA Tech Briefs MFS - 26541, Pg 1-4, Late 1990’s

O119, Wm. Troy Tack, Dave K. McNamara, Joel M. Stoltzfus, and S. Sircar, " Aluminum-Lithium Alloys: Mechanical Property And Composition Effects On Liquid Oxygen Compatibility.", Flamibility And Sensitivity Of Materials In Oxygen-Enriched Atmospheres: **Fifth Volume**, ASTM STP 1111, Joel M. Stoltzfus and Kenneth McIlroy, Eds, American Society For Testing and Materials, Philadelphia, Pg 216-239, 1991

O120, Richard P. Reed, Chris N. McCowan, J. David McColskey, and Nancy J. Simon, "Macro And Microreactions In Mechanical Impact Tests Of Aluminum Alloys.", Flamibility And Sensitivity Of Materials In Oxygen-Enriched Atmospheres: **Fifth Volume**, ASTM STP 1111, Joel M. Stoltzfus and Kenneth McIlroy, Eds, American Society For Testing and Materials, Philadelphia, Pg 240-259, 1991

O121, Rollin C. Christianson, "Oxygen Hazards Analysis Of Composite Liquid Oxygen Tanks.", WSTF-IR-93-0024, NASA,JSC,WSTF, P.O. Drawer MM Las Cruces, NM 88004, Pg 1-117, 1993

O122, W.R.Lucas, and W.A.Riehl, "An Instrument For Determination Of Impact Sensitivity Of Materials In Contact With Liquid Oxygen.", DSN-TR-2-58, Army Ballistic Missile Agency, Redstone Arsenal, Al., Pg 1-20, 15 Oct 1958

O123, R.L.Hauser, G.E.Sykes, and W.F.Rumpel, "Mechanically Initiated Reactions Of Organic Materials In Missile Oxidizers.", TR 61-324, Elastomers and Coatings Branch, Nonmetallic Materials Laboratory, Directorate Of Materials And Processes, ASD, AFSC, USAF, WPAFB, Contract # AF 33(616)-7271, The Martin Company, Pg 1-281, Oct 1961

O124, Harold D. Beeson, and Richard Shelley, "USAF Turbopump Plastics Testing, Oxygen Exposure.", WSTF-91-24845 to 47, NASA,JSC,WSTF, P.O. Drawer MM Las Cruces, NM 88004, Pg 242-267, 10 Oct 1991

O125, R.P. Reed, N.J. Simon, J.D. McColskey, J.R. Berger, C.N. McCowen, J.W. Bransford, E.S. Drexler, and R.P. Walsh, "Aluminum Alloys For Cryogenic Tanks: Oxygen Compatibility Volume 1.", AL TR 90 063, Pg 1-196, Sep 1990

O126, R.P. Reed, N.J. Simon, J.D. McColskey, C.N.McCowen, and E.S. Drexler, "Aluminum Alloys For ALS Cryogenic Tanks: Oxygen Compatibility Volume 2. Final Report.", AL TR 90 063, Pg 1-118, Sep 1990

O127, Gary E. Moffett, Michael D. Pedley, Naomi Schmidt, and Larry J. Linley, "An Evaluation Of The Liquid Oxygen Mechanical Impact Test.", Flamibility And Sensitivity Of Materials In Oxygen-Enriched Atmospheres: **Fourth Volume,** ASTM STP 1040, Joel M. Stoltzfus, Frank J. Benz, and Jack S. Stradling, Eds, American Society For Testing and Materials, Philadelphia PA., Pg 11-22, 1989

O128, Jim L. Currie, Roy S. Irani, and John Sanders, "Factors Affecting The Impact Sensitivity Of Solid Polymer Materials In Contact With Liquid Oxygen.", Flamibility And Sensitivity Of Materials In Oxygen-Enriched Atmospheres: **Third Volume**, ASTM STP 986, D.W. Schroll, Eds, American Society For Testing and Materials, Philadelphia, Pg 233-247, 1988

O129, Coleman J. Bryan, and Melvin G. Olsen, "Procedure for the selection of materials for use in Oxygen systems at the John F. Kennedy Space Center.", Flamibility And Sensitivity Of Materials In Oxygen-Enriched Atmospheres: **Third Volume**, ASTM STP 986, D.W. Schroll, Eds, American Society For Testing and Materials, Philadelphia, Pg 262-267, 1988

O130, J. Chaudhuri, G.H. Choe, and J.R. Vinson, "Impact Characterization of Graphite Fiber Reinforced Thermoplastic Laminates.", Proc. Of The American Society For Composites 6TH Technical Conference Pg 33-42, Oct 1991

O131, Laurence deQuay, and Patrick E. Scheuermann, “Analysis of oxygen mechanical impact test apparatuses and methods.”, Flamibility And Sensitivity Of Materials In Oxygen-Enriched Atmospheres: **Fifth Volume**, ASTM STP 1111, Joel M. Stoltzfus and Kenneth McIlroy, Eds, American Society For Testing and Materials, Philadelphia, Pg 87-125 1991

O132, Richard P. Reed, Nancy J. Simon, John R. Berger, and J. David McColskey, “Influence of specimen absorbed energy in LOX mechanical impact tests.”, Flamibility And Sensitivity Of Materials In Oxygen-Enriched Atmospheres: **Fifth Volume**, ASTM STP 1111, Joel M. Stoltzfus and Kenneth McIlroy, Eds, American Society For Testing and Materials, Philadelphia, Pg 381-398, 1991

O133, Bao K. Nguyen, and Bruce T. Pham, “Assessing LOX Compatibility For Al-Li Alloys.”, Flamibility And Sensitivity Of Materials In Oxygen-Enriched Atmospheres: **Fifth Volume**, ASTM STP 1111, Joel M. Stoltzfus and Kenneth McIlroy, Eds, American Society For Testing and Materials, Philadelphia, Pg 463-474, 1991

O134, J. David McColskey, Richard P. Reed, Nancy J. Simon, and James W. Bransford, “Recommended Changes In ASTM TEST Methods D2512-82 and G86-84 for Oxygen Compatibility Mechanical Impact Tests On Metals.”, Flamibility And Sensitivity Of Materials In Oxygen-Enriched Atmospheres: **Fifth Volume**, ASTM STP 1111, Joel M. Stoltzfus and Kenneth McIlroy, Eds, American Society For Testing and Materials, Philadelphia, Pg 126-153, 1991

O135, Nancy J. Simon, and Richard P. Reed, ” Temperature Increases In Aluminum Alloys Durings Mechanical-Impact Tests For Oxygen Compatibility.”, Flamibility And Sensitivity Of Materials In Oxygen-Enriched Atmospheres: **Fifth Volume**, ASTM STP 1111, Joel M. Stoltzfus and Kenneth McIlroy, Eds, American Society For Testing and Materials, Philadelphia, Pg 367-380, 1991

O136, Frank J. Benz, and Joel M. Stoltzfus, “Ignition Of Metals And Alloys In Gaseous Oxygen By Frictional Heating.”, Flamibility And Sensitivity Of Materials In Oxygen-Enriched Atmospheres: **Second Volume**, ASTM STP 910, Michael A. Benning, Eds, American Society For Testing and Materials, Philadelphia, Pg 38-58, 1986

O137, Coleman J. Bryan, “NASA Mechanical Impact Testing In High-Pressure Oxygen.”, Flamibility And Sensitivity Of Materials In Oxygen-Enriched Atmospheres: ASTM STP 812, Berry L. Werley, Eds, American Society For Testing and Materials, Philadelphia PA. Pg 9-42, 1983

O138, Rudolf Jenny, and Hans R. Wyssmann, “Friction-Induced Ignition In Oxygen.”, Flamibility And Sensitivity Of Materials In Oxygen-Enriched Atmospheres: ASTM STP 812, Berry L. Werley, Eds, American Society For Testing and Materials, Philadelphia PA., Pg 150-166, 1983

O139, Joel M. Stoltzfus, Frank J. Benz, and John Homa, “The Pv Product Required For The Frictional Ignition Of Alloys.”, Flamibility And Sensitivity Of Materials In Oxygen-Enriched Atmospheres: **Fourth Volume,** ASTM STP 1040, Joel M. Stoltzfus, Frank J. Benz, and Jack S. Stradling, Eds, American Society For Testing and Materials, Philadelphia PA., Pg 212-223, 1989

O140, Walter W. Yuen, “Modeling And Data Evaluation Of The WSTF Frictional Heating Test Facility.”, Flamibility And Sensitivity Of Materials In Oxygen-Enriched Atmospheres: **Fourth Volume,** ASTM STP 1040, Joel M. Stoltzfus, Frank J. Benz, and Jack S. Stradling, Eds, American Society For Testing and Materials, Philadelphia PA., Pg 76-90, 1989

O141, Mohan V. Gunaji, and Joel M. Stoltzfus, “Review Of Frictional Heating Test Results In Oxygen-Enriched Environments.”, Flamibility And Sensitivity Of Materials In Oxygen-Enriched Atmospheres: **Sixth Volume**, ASTM STP 1197, Dwight D. Janoff and Joel M. Stoltzfus, Eds, American Society For Testing and Materials, Philadelphia, Pg 146-155, 1993

O142, John M. Homa, and Joel M. Stoltzfus, “The Measurement Of The Friction Coefficient And Wear Of Metals In High Pressure Oxygen.”, Flamibility And Sensitivity Of Materials In Oxygen-Enriched Atmospheres: **Sixth Volume**, ASTM STP 1197, Dwight D. Janoff and Joel M. Stoltzfus, Eds, American Society For Testing and Materials, Philadelphia, Pg 389-402, 1993

O143, P.J. Miller, C.S. Coffey, and V.F. DeVost, “Heating In Crystalline Solids Due To Rapid Deformation.”, J.Appl.Phys. 59(3), Pg 913-916, Feb 1986

O144, H.H. Jamison, “Development Of A Gaseous Oxygen Impact Testing Method.”, Materials Research And Standards, ASTM, V 11, N6, Pg 22-27, Jun 1971

O145, C.F. Key, “An Apparatus For Determination Of Impact Sensitivity Of Materials In Contact With Liquid And Gaseous Oxygen At High Pressures.”, Materials Research And Standards, ASTM, V 11, N6, Pg 28-29 and 51-52, Jun 1971

O146, W.R. Blackstone, and P.M. Ku, “An Assessment Of Impact Test Techniques For Determining The Fire Or Explosion Hazards Of Materials Exposed To Liquid Oxygen.”, Materials Research And Standards, ASTM, V 11, N6, Pg 30-35 and 52, Jun 1971

O147, D.L. Pippen, and J.S. Stradling, “Techniques For Determination Of Flash and Fire Points And Impact Sensitivity Of Materials In A Gaseous Oxygen Environment.”, Materials Research And Standards, ASTM, V 11, N6, Pg 35-43 and 52-53, Jun 1971

O148, H. Bauer, W. Wegener, and K.F. Windgassen, “Fire Tests On Centrifugal Pumps For Liquid Oxygen.”, Cryogenics, V10, N3, Pg 241-248, June 1970

O149, A. Africano, “Maximum Rate Theory Of Impact Sensitivity.”, Advances In Cryogenic Engineering, V5, Plenum Press, NY NY, Pg 533-544, 1960

O150, Marvin A. Guiles, “Liquid Crystal Polymer Cryogenic Storage Tank With Reduced Thermal Loss And Weight.”, AIAA 95-2355, 31ST AIAA / ASME / ASEE Joint Propulsion Conference And Exhibit Jul 10-12 1995, San Diego, Ca, Pg 1-11, 1995

O151, Y.S. Kwon, and B.V. Sankar, “Indentation Damage In Graphite/Epoxy Laminates.”, Proc. Of The American Society For Composites 6TH Technical Conference, Pg 483-492, Oct 1991

Autogenous Ignition Temperature Related

O152, Standard Test For Gross Calorific Value Of Coal And Coke By The Adiabatic Bomb Calorimeter, ASTM D 2015 - 96

O153, Standard Test Method For Heat Of Combustion Of Liquid Hydrocarbon Fuels By Bomb Calorimeter (Precision Method, ASTM D 4809 - 95

O154, Standard Practice For Safe Use Of Oxygen Combustion Bombs, ASTM E 144 - 94 (Reapproved 1995)

O155, Standard Test Method For Autogenous Ignition Temperature Of Liquids And Solids In A High-Pressure Oxygen Enriched Environment, ASTM G 72 - 82 (Reapproved 1996)

O156, Standard Test Method For Determining Ignition Temperature Of Plastics, ASTM D 1929 - 96

O157, Standard Test Method For Flash And fire Points By Cleveland Open Cup, ASTM D 92 - 98a

O158, Beeson, Harold D., Hshieh, Fu-Yu, and Hirsch, David B. “Ignitibility of advanced composites in liquid and gaseous oxygen.”, Flamibility And Sensitivity Of Materials In Oxygen-Enriched Atmospheres: **Eigth Volume**, ASTM STP 1319, W.T. Royals, T.C. Chou, and T.A. Steinberg, Eds, American Society For Testing and Materials, Pg 421-431, 1997

O159, David Hirsch, Fu-Yu Hshieh, Harold Beeson, and Coleman Bryan, “Ignitibility In Air, Gaseous Oxygen, and Oxygen - Enriched Environments Of Polymers Used In Breathing - Air Devices.”, Flamibility And Sensitivity Of Materials In Oxygen-Enriched Atmospheres: **Eigth Volume**, ASTM STP 1319, W.T. Royals, T.C. Chou, and T.A. Steinberg, Eds, American Society For Testing and Materials, Pg 359-369, 1997

O160, Amit Jain, Mohan V. Gunaji, and Coleman J. Bryan, “Evaluation Of The Compatibility Of Materials Used In Breathing Air Devices”, Flamibility And Sensitivity Of Materials In Oxygen-Enriched Atmospheres: **Seventh Volume**, ASTM STP 1267, Dwight D. Janoff, William T. Royals, and Mohgan V. Gunaji, Eds, American Society For Testing and Materials, Pg 184-191, 1995

O161, Ting C. Chou, and Anthony Fiedorowicz, “Oxygen Compatibility of Polymers Including TFE-Teflon, Kel-F 81, Vespel SP-21, Viton A, Viton A-500, Fluorel, Neoprene, EPDM, Buna-N, and Nylon 6,6”, Flamibility And Sensitivity Of Materials In Oxygen-Enriched Atmospheres: **Eigth Volume**, ASTM STP 1319, W.T. Royals, T.C. Chou, and T.A. Steinberg, Eds, American Society For Testing and Materials, Pg 319-349, 1997

O162, Michael J. Yentzen, “Design Of The LOX and GOX Systems For The Stennis Space Center High Heat Flux Facility”, Flamibility And Sensitivity Of Materials In Oxygen-Enriched Atmospheres: **Seventh Volume**, ASTM STP 1267, Dwight D. Janoff, William T. Royals, and Mohgan V. Gunaji, Eds, American Society For Testing and Materials, Pg 36-56, 1995

O163, Vincent J. D'Imperio, and Barry L. Werley, “Oxygen Compatibility of FKM Elastomers”, Flamibility And Sensitivity Of Materials In Oxygen-Enriched Atmospheres: **Eigth Volume**, ASTM STP 1319, W.T. Royals, T.C. Chou, and T.A. Steinberg, Eds, American Society For Testing and Materials, Pg 350-358, 1997

O164, Ian Swindells, Philip F. Nolan, and Roland K. Wharton, “Spontaneous Ignition Temperatures Of Nonmetals In Gaseous Oxygen”, Flamibility And Sensitivity Of Materials In Oxygen-Enriched Atmospheres: **Third Volume**, ASTM STP 986, D.W. Schroll, Eds, American Society For Testing and Materials, Philadelphia, Pg 206-217, 1988

O165, Gerard Vagnard, Georges Delode, and Herve Barthelemy, “Test Methods And Interpretation of results for selecting non-metallic materials for oxygen service.”, Flamibility And Sensitivity Of Materials In Oxygen-Enriched Atmospheres: **Fifth Volume**, ASTM STP 1111, Joel M. Stoltzfus and Kenneth McIlroy, Eds, American Society For Testing and Materials, Philadelphia, Pg 489-505, 1991

O166, Robert Lowrie, Harvy Garcia, and Randall L. Henningson, “Automation Of Autogenous Ignition Equipment.”, Flamibility And Sensitivity Of Materials In Oxygen-Enriched Atmospheres: **Fifth Volume**, ASTM STP 1111, Joel M. Stoltzfus and Kenneth McIlroy, Eds, American Society For Testing and Materials, Philadelphia, Pg 75-85, 1991

O167, Coleman J. Bryan, and Robert Lowrie, “Comparative Results Of Autogenous Ignition Temperature Measurements By ASTM G 72 and Pressurized Scnning Calorimetry In Gaseous Oxygen.”, Flamibility And Sensitivity Of Materials In Oxygen-Enriched Atmospheres: **Second Volume**, ASTM STP 910, Michael A. Benning, Eds, American Society For Testing and Materials, Philadelphia, Pg 108-117, 1986

O168, Kenneth McIlroy, and Robert Zawierucha, “The Use Of The Accelerating Rate Calorimeter In Oxygen Compatibility Testing.”, Flamibility And Sensitivity Of Materials In Oxygen-Enriched Atmospheres: **Second Volume**, ASTM STP 910, Michael A. Benning, Eds, American Society For Testing and Materials, Philadelphia, Pg 98-107, 1986

O169, Richard W. McQuaid, Donald G. Sheets, and Mary J. Bieberich, “Determination Of Autogenous Ignition Temperatures Of A Steam Turbine Lubricating Oil In Nitrogen And Oxygen Mixtures.”, Flamibility And Sensitivity Of Materials In Oxygen-Enriched Atmospheres: ASTM STP 812, Berry L. Werley, Eds, American Society For Testing and Materials, Philadelphia PA., Pg 43-55, 1983

O170, Robert Lowrie, “Heat Of Combustion and Oxygen Compatibility.”, Flamibility And Sensitivity Of Materials In Oxygen-Enriched Atmospheres: ASTM STP 812, Berry L. Werley, Eds, American Society For Testing and Materials, Philadelphia PA., Pg 84-96, 1983

O171, Roland K. Wharton, Philip F. Nolan, and Ian Swindells, “Further Studies Of Factors That Affect The Spontaneous Ignition Temperatures Of Non-Metallic Materials In Gaseous Oxygen.”, Flamibility And Sensitivity Of Materials In Oxygen-Enriched Atmospheres: **Fourth Volume,** ASTM STP 1040, Joel M. Stoltzfus, Frank J. Benz, and Jack S. Stradling, Eds, American Society For Testing and Materials, Philadelphia PA., Pg 106-124, 1989

O172, Richard M. Shelley, Rollin Christianson, and Joel M. Stoltzfus, ” Evaluation Of Buna N Ignition Hazard In Gaseous Oxygen.”, Flamibility And Sensitivity Of Materials In Oxygen-Enriched Atmospheres: **Sixth Volume**, ASTM STP 1197, Dwight D. Janoff and Joel M. Stoltzfus, Eds, American Society For Testing and Materials, Philadelphia, Pg 239-251, 1993

O173, Richard M. Shelley, D. Bruce Wilson, and Harold Beeson, “Combustion Characteristics Of Polymers As Ignition Promoters.”, Flamibility And Sensitivity Of Materials In Oxygen-Enriched Atmospheres: **Sixth Volume**, ASTM STP 1197, Dwight D. Janoff and Joel M. Stoltzfus, Eds, American Society For Testing and Materials, Philadelphia, Pg 223-238, 1993

O174, Richard M. Shelley, “Ignition Of Inconel 718 By Buna N Contamination.”, WSTF-IR-91-0005, NASA, JSC, WSTF, P.O. Drawer MM, Las Cruces, NM 88004, Pg 1-25, 1991

O175, A. Nakagoshi, S. Tomonoh, and Y. Sakamoto, “Mesophase Pitch-Based Carbon Fiber For Improved Inflammability Of CFRP.”, Proceedings Of The International Conference On Composite Materials And Energy (Enercomp 95), Technomic Publishing Co., Lancaster Penn, Pg 260-267, 8-10 May 1995

Pneumatic Impact Related

O176, Standard Test Method For Ignition Sensitivity Of Materials To Gaseous Fluid Impact., ASTM G 74 - 82 (Reapproved 1996)

O177, Gary E. Moffett, Michael D. Pedley, Naomi Schmidt, Ralph E. Williams, David Hirsch, and Frank J. Benz, “Ignition Of Nonmetallic Materials By Impact Of High Pressure Gaseous Oxygen”, Flamibility And Sensitivity Of Materials In Oxygen-Enriched Atmospheres: **Third Volume**, ASTM STP 986, D.W. Schroll, Eds, American Society For Testing and Materials, Philadelphia, Pg 218-232, 1988

O178, Herve Barthelemy, and Gerard Vagnardm “Ignition of PTFE Lined Hoses in High Pressure Oxygen Systems: Test Results and considerations for safe design and use.”, Flamibility And Sensitivity Of Materials In Oxygen-Enriched Atmospheres: **Third Volume**, ASTM STP 986, D.W. Schroll, Eds, American Society For Testing and Materials, Philadelphia, Pg 289-304, 1988

O179, Herve' Barthelemy, Georges Delode, and Gerard Vagnard, “Ignition of materials in oxygen atmospheres: Comparison of different testing methods for ranking materials.”, Flamibility And Sensitivity Of Materials In Oxygen-Enriched Atmospheres: **Fifth Volume**, ASTM STP 1111, Joel M. Stoltzfus and Kenneth McIlroy, Eds, American Society For Testing and Materials, Philadelphia, Pg 506-515, 1991

O180, Ian H. Leslie, “Thermodynamic and fluid mechanic analyses of rapid pressurization in a dead-end tube.”, Flamibility And Sensitivity Of Materials In Oxygen-Enriched Atmospheres: **Fifth Volume**, ASTM STP 1111, Joel M. Stoltzfus and Kenneth McIlroy, Eds, American Society For Testing and Materials, Philadelphia, Pg 399-413, 1991

O181, Dwight Janoff, Michael D. Pedley, and Larry J. Bamford, “Ignition Of Non metallic materials by impact of high pressure oxygen III: New Method Development.”, Flamibility And Sensitivity Of Materials In Oxygen-Enriched Atmospheres: **Fifth Volume**, ASTM STP 1111, Joel M. Stoltzfus and Kenneth McIlroy, Eds, American Society For Testing and Materials, Philadelphia, Pg 60-74, 1991

O182, Laurence deQuay, and Patrick E. Scheuermann, “Use Of Computer Analysis To Predict And Reduce Liquid Hammer Forces In High Pressure, High Flow Liquid Oxygen Systems.”, Flamibility And Sensitivity Of Materials In Oxygen-Enriched Atmospheres: **Fifth Volume**, ASTM STP 1111, Joel M. Stoltzfus and Kenneth McIlroy, Eds, American Society For Testing and Materials, Philadelphia, Pg 414-449, 1991

O183, Barry L. Werley, “A Perspective On Gaseous Impact Tests: Oxygen Compatibility Testing On A Budget.”, Flamibility And Sensitivity Of Materials In Oxygen-Enriched Atmospheres: **Sixth Volume**, ASTM STP 1197, Dwight D. Janoff and Joel M. Stoltzfus, Eds, American Society For Testing and Materials, Philadelphia, Pg 27-42, 1993

O184, Ulrich H. Koch, “Oxygen System Safety.”, Flamibility And Sensitivity Of Materials In Oxygen-Enriched Atmospheres: **Sixth Volume**, ASTM STP 1197, Dwight D. Janoff and Joel M. Stoltzfus, Eds, American Society For Testing and Materials, Philadelphia, Pg 349-359, 1993

O185, Naomi Schmidt, Gary E. Moffett, Michael D. Pedley, and Larry J. Linley, “Ignition Of Nonmetallic Materials By Impact Of High Pressure Oxygen II: Evaluation Of Repeatability Of Pneumatic Impact Test.”, Flamibility And Sensitivity Of Materials In Oxygen-Enriched Atmospheres: **Fourth Volume,** ASTM STP 1040, Joel M. Stoltzfus, Frank J. Benz, and Jack S. Stradling, Eds, American Society For Testing and Materials, Philadelphia PA., Pg 23-37, 1989

O186, Dwight Janoff, Larry J. Bamford, Barry E. Newton, and Coleman J. Bryan, “Ignition Of PTFE-Lined Flexible Hoses By Rapid Pressurization With Oxygen.”, Flamibility And Sensitivity Of Materials In Oxygen-Enriched Atmospheres: **Fourth Volume,** ASTM STP 1040, Joel M. Stoltzfus, Frank J. Benz, and Jack S. Stradling, Eds, American Society For Testing and Materials, Philadelphia PA., Pg 288-308, 1989

O187, J.H. Schafer, and A. Frohn, “Ionization Behind Shock Waves In Nitrogen-Oxygen Mixtures.”, AIAA Journal, V10, N8, Pg 985-987, Aug 1972

O188, Larry J. Bamford, Michelle A. Rucker, and Douglas Dobbin, “Gudie for oxygen component qualification tests.”, NASA Technical Memorandum 104821, Dec 1996

O189, F.P.Bowden, M.Mulcahy, R.Vines, and A.Yoffe, “The detonation of liquid explosives by gentle impact. The effect of minute gas spaces.”, Proc. Royal Soc. London, V.188A, N.1014, London, Pg 291-311, 1947

O190, A.Yoffe, “Influence of entrapped gas on initiation of explosion in liquids and solids.”, Proc. Royal Soc. London, V.198A, N.1054, London, Pg 373-388, 1949

O191, F.P.Bowden, and M.P.McOnie, “Formation Of Cavities and Microjets in Liquids and their role in initiation and growth of explosion.”, Proc. Royal Soc. London, V.298A, London, Pg 38-50, 1967

O192, Coley, G.D., and Field, J.E., “The role of cavities in the initiation and growth of explosion in liquids.”, Proc. Royal Soc. London, V.335A, N.1600, London, Pg 67-86, 1973

O193, Faeth, G.M., “Thermal Environment Of Combustibles During Pneumatic Charging Process.”, Naval Engineers Journal, V77, N2, Pg 299-307, Apr 1965

Contamination Related

O194, Standard Practice For Cleaning Methods And Cleanliness Levels For Material and Equipment Used In Oxygen Enriched Environments, ASTM G 93 - 96

O195, Standard Guide For Control Of Hazzards And Risks In Oxygen Enriched Systems, ASTM G 128 - 95

O196, Standard Guide for the Selection Of Cleaning Agents For Oxygen Systems, ASTM G 127 - 95

O197, Standard Practice For Cleaning Of Materials And Components By Ultrasonic Techniques, ASTM G 131 - 96

O198, Standard Practice For Determination Of Soluble Residual Contamination In Materials And Components By Soxhlet Extraction., ASTM G 120 - 95

O199, Standard Test Method For Evaluating The Effectiveness Of Cleaning Agents., ASTM G 122 - 96

O200, Standard Test Method For Gravimetric Determination Of Nonvolatile Residue (NVR) In Environmentally Controlled Areas For Spacecraft., ASTM E 1235 - 88 (Reapproved 1993

O201, Standard Test Method For Gravimetric Determination Of Nonvolatile Residue (NVR) In Environmentally Controlled Areas For Spacecraft [Metric]., ASTM E 1235M - 95

O202, Test Sample Preparation For Testing In The Materials Combustion research Facility, ED36-OWI-042 Rev A., Pg 1-92, Aug 1999

O203, Receipt, Handling, Prioritization, and Data Requirements for samples submitted for testing in the Materials Combustion Research Facility of the Materials, Processes, and Manufacturing Department, Building 4623. ED36-OWI-051, Pg 1-14, Aug 1999

O204, Ulrich H. Koch, and Christopher J. Kmetko, “Aqueous Cleaning Of Industrial And High-Purity Valves And Fittings: Process Development, Control, And Validation.”, Alternatives To Chlorofluorocarbon Fluids In The Cleaning Of Oxygen And Aerospace Systems And Components, ASTM STP 1181,Coleman J. Bryan and Karen Gebert-Thompson, Eds, American Society For Testing and Materials, Philadelphia,, Pg 49-65, 1993

O205, Dennis E. Griffin, “Cleanliness Of Componrnts For Use In Oxygen, Fuel, And Pneumatic Systems, Specifications For”, MSFC-Spec-164B, Pg 1-16, Nov 1994

O206, R.H. Gompf, “Physical And Chemical Test Results Of Plastic Films.”, NASA TM 103500, Pg 1-71, Sep 1988

O207, Michael S. McIlroy, “An Investigation Of Laboratory Methods For Cleaning Typical Metallic Surfaces Using Aqueous Type Cleaning Agents.”, Flamibility And Sensitivity Of Materials In Oxygen-Enriched Atmospheres: **Sixth Volume**, ASTM STP 1197, Dwight D. Janoff and Joel M. Stoltzfus, Eds, American Society For Testing and Materials, Philadelphia, Pg 373-388, 1993

O208, Ting C. Chou, and Anthony Fiedorowicz, “A protocol for evaluating the cleaning efficiency, corrosion property and oxygen compatibility of non-ozone depleting cleaning agents.”, Flamibility And Sensitivity Of Materials In Oxygen-Enriched Atmospheres: **Seventh Volume**, ASTM STP 1267, Dwight D. Janoff, William T. Royals, and Mohgan V. Gunaji, Eds, American Society For Testing and Materials, Pg 195-221, 1995

O209, Michael D. Pedley, Jenn-Hai Pao, Larry Bamford, Ralph E. Williams, and Barry Plante, “Ignition Of Contaminants By Impact Of High-Pressure Oxygen.”, Flamibility And Sensitivity Of Materials In Oxygen-Enriched Atmospheres: **Third Volume**, ASTM STP 986, D.W. Schroll, Eds, American Society For Testing and Materials, Philadelphia, Pg 305-317, 1988

O210, Coleman J. Bryan, William R. Carman, Thomas A. Schehl, and Lee D. Underhill, “Is "LOX Clean Enough?”, Flamibility And Sensitivity Of Materials In Oxygen-Enriched Atmospheres: **Fifth Volume**, ASTM STP 1111, Joel M. Stoltzfus and Kenneth McIlroy, Eds, American Society For Testing and Materials, Philadelphia, Pg 519-527, 1991

O211, Dennis W. Schroll, “Cleaning Methods And Procedures For Military Oxygen Equipment: Investigation Results.”, Flamibility And Sensitivity Of Materials In Oxygen-Enriched Atmospheres: **Second Volume**, ASTM STP 910, Michael A. Benning, Eds, American Society For Testing and Materials, Philadelphia, Pg 180-203, 1986

O212, John A. Gilbertson, and Robert Lowrie, “Threshold Sensitivities Of Tests To Detect Oil Film Contamination In Oxygen Equipment.”, Flamibility And Sensitivity Of Materials In Oxygen-Enriched Atmospheres: **Second Volume**, ASTM STP 910, Michael A. Benning, Eds, American Society For Testing and Materials, Philadelphia, Pg 204-211, 1986

O213, Barry L. Werley, “Oil Film Hazards In Oxygen Systems.”, Flamibility And Sensitivity Of Materials In Oxygen-Enriched Atmospheres: ASTM STP 812, Berry L. Werley, Eds, American Society For Testing and Materials, Philadelphia PA., Pg 108-125, 1983

O214, Shelley, R.M., Janoff, D.D., and Pedley, M.D., ”Effect Of Hydrocarbon Oil Contamination On The Ignition And Combustion Properties Of PTFE Tape In Oxygen.”, Flamibility And Sensitivity Of Materials In Oxygen-Enriched Atmospheres: **Sixth Volume**, ASTM STP 1197, Dwight D. Janoff and Joel M. Stoltzfus, Eds, American Society For Testing and Materials, Philadelphia, Pg 81-94, 1993

Fiber Property Bibliography:

FP1, YLA K-1100 Prepregs, YLA, INC, 1999

FP2, Dialead Coal Tar Pitch Carbon Fiber, Mitsubishi Chemical, pg 1-26, 2000

FP3, GRANOC Data Package 2001, Ver 1.04, Nippon Graphite Fiber Corp, 2001

FP4, “Granoc Yarn YSH-A Series”, Technical Data 0104YSHA, Nippon Graphite Fiber Corp, 2001

FP5, Noriyuki Kiuchi, Kazuhiro Ozawa, Tatsusaburou Komamiand, Osamu Katch, Yutaka Arai, Tetsuji Watanabe, and Sakuya Iwai, “Pitch Based Carbon Fiber with high thermal conductivity for new advanced thermal design.”, Nippon Graphite Fiber Corp, 2001

FP6, Masatoshi Furuyama,Yutaka Arai, Osamu Katchm, and Michiharu Harakawa, “Pitch based carbon fiber with improved compressive strength.”, Nippon Graphite Fiber Corp, 2001

FP7, “Granoc Prepreg Type: YSH-50A/25P”, Technical Data 9 905, Nippon Graphite Fiber Corp, 2001

FP8, “Mechncical Properties Of Granoc YSH-50A-30S/25P (Modified Epoxy resin) Unidirectional Laminates”, Nippon Graphite Fiber Corp, 1996

FP9, “Mechncical Properties Of Granoc YSH-60A-30S/RS-3 (Polycyanate Resin) Unidirectional Laminates”, Nippon Graphite Fiber Corp, 1996

FP10, “Mechncical Properties Of Granoc YSH-A & YS-A Fibers and Composites”, Nippon Graphite Fiber Corp, 2000

FP11, Tsutomu Kiharam, Noriyuki Kiuchi, Tatsusaburou Komamiand, Osamu Katch, Yutaka Arai, Tsutomu Nakamura, Tetsuji Watanabe, and Gen Ishikawa, “”Mechanical and thermal properties of pitch based carbon fibers with thermal conductivities for space applications.”, Nippon Graphite Fiber Corp, 2001

FP12, “Granoc Prepreg Type: YSH-60A/25P”, Technical Data 9 905, Nippon Graphite Fiber Corp, 2001

FP13, “Mechncical Properties Of Granoc YSH-60A-30S/25P (Modified Epoxy Resin) Unidirectional Laminates”, Nippon Graphite Fiber Corp, 1997

FP14, “Mechncical Properties Of Granoc YSH-60A-30S/EX-1515 (Polycyanate Resin) Unidirectional Laminates”, Nippon Graphite Fiber Corp, 1998

FP15, “Mechncical Properties Of Granoc YSH-60A-30S/RS-3 (Polycyanate Resin) Unidirectional Laminates”, Nippon Graphite Fiber Corp, 1998

FP16, “Granoc Prepreg Type: YSH-70A/25P”, Technical Data 9 905, Nippon Graphite Fiber Corp, 2001

FP17, “Mechncical Properties Of Granoc YSH-70A-30S/25P (Modified Epoxy Resin) Unidirectional Laminates Lot #1”, Nippon Graphite Fiber Corp, 1998

FP18, Takayuki Matsumoto, Metal Content of GRANOC Carbon Fibers, personnel e-mail, May 2001

FP19, GRANOC Data Package 1992, Nippon Graphite Fiber Corp, 1992

FP20, Carbon Fibers For Performance: Product Overview, BP Amoco Polymers, 2000

FP21, “Applications of BP Amoco’s High Thermal Conductivity Graphite Based Materials”, BP Amoco Polymers, INC, 1999

FP22, “Product Information Technical Information THORNEL Carbon Fiber T-300 6K”, F-5409 Rev.3, Union Carbide Corp, 1987

FP23, “Product Information Technical Information THORNEL Carbon Fiber T-300 6K”, F-7013 Rev.9, Union Carbide Corp, 1987

FP24, “Product Information Technical Information THORNEL K-1100X 2K”, F-7298, Amoco Performance Products

FP25, “Product Information Technical Information THORNEL P-100X HTS”, F-7303, Amoco Performance Products

FP26, “THORNEL Product Information”, F-7132, Amoco Performance Products, 1987

FP27, “Product Information Technical Information THORNEL Carbon Fiber T-50 6K”, F-5092 Rev.7, Union Carbide Corp, 1987

FP28, “Product Information Technical Information THORNEL Carbon Fiber T-40 12K”, F-7055 Rev.2, Union Carbide Corp, 1987

FP29, “Product Information Technical Information THORNEL Carbon Fiber P-55S 4K”, F-6374 Rev.3, Union Carbide Corp, 1987

FP30, “Product Information Technical Information THORNEL Carbon Fiber P-75S 2K”, F-5817 Rev.4, Union Carbide Corp, 1987

FP31, “Product Information Technical Information THORNEL Carbon Fiber P-100S 2K”, F-7007 Rev.1, Union Carbide Corp, 1987

FP32, “Product Information Technical Information THORNEL Carbon Fiber P-120S 2K”, F-7010 Rev.2, Union Carbide Corp, 1987

FP33, “THORNEL Carbon Fiber Properties”, Amoco Performance Products, JJB, 1994

FP34, “THORNEL Carbon Fibers”, F-7088, Amoco Performance Products, 1987

FP35, TORAYCA Contact Information and Data Sheets, “TORAY” Carbon Fibers America Inc., Jan 2000

FP36, TORAYCA Quality Carbon Fiber, www.netoray.com/tcf/fiber.htm, 2001

FP37, Scola, Daniel A. “Thermo-Oxidative Stability of Graphite Fiber/PMR-15 Polyimide Composites at 350°C.” High Temperature Polymer Matrix Composites. Noyes Data Corp., 1987, pg 214-239.

FP38, De Pruneda, J.A.H., and R.J. Morgan. “The Effects of Thermal Exposure on the Structural and Mechanical Integrity of Carbon Fibres.” Journal of Materials Science. Vol. 25. 1990, pg 4776-4781.

FP39, A.K.Gupta, D.K.Paliwal and Pushpa Bajaj, Acrylic Precursors for Carbon Fibers, J. Macromolecular Science, Reviews In Macromolecular Chemistry And Physics , C31(1), Marcel Dekker, Inc., 1991, pg 1-89

FP40, “Space Materials Update Seminar: K-1100X Prepregs for Thermal Management and 954-2A and 954-3 Cyanate Ester Prepregs”, ICI Fiberite – Tempe Products, 1994

Cryogenic Exposure Bibliography:

C1. D.J. Radcliffe and H.M. Posenberg, “The Thermal Conductivity Of Glass-fibre and carbon-fibre/epoxy composites from 2 to 80 K.”, Cryogenics, V22 # 5, pg 245-249, May1995

C2. C.I.Nicholis and H.M.Rosenberg, “The Thermal Conductivity Of Carbon-Carbon Fibre Composites Below 80K.”, Cryogenics, V24, #7, pg 355-358, Jul 1984

C3. G.Hartwig and S. Knaak, “Fibre-Epoxy Compsoites At Low Temperatures.”, Cryogenics, V24, #11, pg 639- 647, Nov 1984

C4. G Hartwig, “Overview of advanced fibre composites.”, Cryogenics, V28, #4, pg 216-219, 1988

C5. K. Ahlborn, “Mechanical relaxation of polymers at low temperatures.”, Cryogenics, V28, #4, pg 234-239, 1988

C6. D. Greig, “Low Temperature Thermal Conductivity Of Polymers.”, Cryogenics, V28, #4, pg 243-247, 1988

C7. G. Schwarz, “Thermal expansion of polymers from 4.2 K to room temperature.”, Cryogenics, V28, #4, pg 248-254, 1988

C8. G Hartwig, “Thermal expansion of fibre composites.”, Cryogenics, V28, #4, pg 255-266, 1988

C9. K. Ahlborn, “Fatigue behaviour of carbon fibre reinforced plastic at cryogenic temperatures.”, Cryogenics, V28, #4, pg 267-272, 1988

C10. K. Ahlborn and S. Knaak, “Cryogenic mechanical behavior of a thick-walled carbon fibre reinforced plastic structure.”, Cryogenics, V28, #4, pg 273-277, 1988

C11. D. Evans and J.T. Morgan, “Gas permeability through composite materials.”, Cryogenics, V28, #4, pg 283-284, 1988

C12. S. Nishijima, T.Okada, K. Fujioka and Y. Kuraoka, “Gas Permeation and performance of a fibre reinforced plastic cryostat.”, Cryogenics, V28, #4, pg 285-287, 1988

C13. G. Hartwig and S. Knaak, “Fatigure behaviour of polymers.”, Cryogenics, V31, #4, pg 231-233, 1991

C14. T. Saatkamp and G. Hartwig, “Fracture energy of polymers at low temperatures.”, Cryogenics, V31, #4, pg 234-237, 1991

C15. G. Schwarz, F. Krahn and G. Hartwig, “Thermal expansion of carbon fibre composites with themoplastic matrices.”, Cryogenics, V31, #4, pg 244-247, 1991

C16. K. Pannkoke and H.-J. Wagner, “Fatigue properties of undirectional carbon fibre composites at cryogenic temperatures.”, Cryogenics, V31, #4, pg 248-251, 1991

C17. K. Ahlborn, “Cryogenic mechanical response of carbon fibre reinforced plastics with thermoplastic matrices to quasi-static loads.”, Cryogenics, V31, #4, pg 252-256, 1991

C18. H. Bansemir and O. Haider, “Basic material data and structural analysis of fibre composite components for space application.”, Cryogenics, V31, #4, pg 298-306, 1991

C19. M.T. Callaghan, “Use of resin composites for cryogenic tankage.”, Cryogenics, V31, #4, pg 282-287, 1991

C20. Y. Iwasaki, J.Yasuda, T. Hirokawa, K. Noma, S. Nishijima and T. Okada, “Three dimensional fabric reinforced plastics for cryogenic use.”, Cryogenics, V31, #4, pg 261-264, 1991

C21. E.Tschegg, K.Humer and H.W.Weber, “Influence of test geometry on tensile strength of fibre reinforced plastics at cryogenic temperatures.”, Cryogenics, V31, #4, pg 312-318, 1991

C22. K. Ahlborn, “Durability of carbon fibre reinforced plastics with thermoplastic matrices under cyclic mechanical and cyclic thermal loads at cryogenic temperatures.”, Cryogenics, V31, #4, pg 257-260, 1991

C23. H.Eggers, W.Hartung and S.Knaak, “Damage in carbon fibre reinforced epoxy after thermal cycling and T-fatigue loading.”, Cryogenics, V31, #4, pg 265-268, 1991

C24. T. Hirokawa, J. Yasuda, Y. Iwasaki, K. Noma, S.Nishijima, and T. Okada, “Design Of Support Strap With Advanced Compsoite For Cryogenic Application.”, Cryogenics, V31, #4, pg 288-291, Apr 1991

C25. H. Yamaoka, K. Miyata and O. Yano, “Cryogenic Properties Of Engineering Plastic Films.”, Cryogenics, V35, #11, pg 787-789, NOV 1995

C26. Hirokazu Yokoyama, “Thermal Conductivity of polyimide film at cryogenic temperature.”, Cryogenics, V35, #11, pg 799-800, NOV 1995

C27. Fumio Sawa, Shigehiro Nishijima and Toichi Okada, “Molecular design of an epoxy for cryogenic temperatures.”, Cryogenics, V35, #11, pg 767-769, NOV 1995

C28. U. Escher, “Thermal expansion of epoxy resins with different cross-link densities at low temperatures.”, Cryogenics, V35, #11, pg 775-778, NOV 1995

C29. Takefumi Horiuchi and Tsutomu Ooi, “Cryogenic Properties Of Composite Materials.”, Cryogenics, V35, #11, pg 677-679, NOV 1995

C30. J.B.Schutz, “Properties of composite materials for cryogenic applications.”, Cryogenics, V38, #1, pg 3-12, 1998

C31. R. Heydenreich, “Cryotanks In Future Vehicles.”, Cryogenics, V38, #1, pg 125-130, 1998

C32. S.Disdier, J.M. Rey, P. Pailler and A.R. Bunsell, “Helium Permeation In Composite Materials For Cryogenic Application.”, Cryogenics, V38, #1, pg 135-142, 1998

C33. H.Bansemir and O.Haider, “Fibre composite structures for space applications - recent and future developments.”, Cryogenics, V38, #1, pg 51-59, 1998

C34. G.Hartwig, R.Hubner, S.Knaak and C.Pannkoke, “Fatigue behaviour of composites.”, Cryogenics, V38, #1, pg 75-78, 1998

C35. Toichi Okada, Borauzima Rugaiganisa and Shigehiro Nishijma, “Data Base: Properties Of Organic Compsoite Materials At Low Temperatures.”, Advances In Cryogenic Engineering (Materials), Vol 36 Part B Edited By R.P Reed and F.R. Fickett, pg 1027-1035, 1990

C36. G.Hartwig and K. Pannkoke, “Fatigue Behavior Of UD Carbon Fibre Composites At Cryogenic Temperatures.”, Advances In Cryogenic Engineering (Materials), V38, pg 453-457, 1992

C37. C.Biamca, H.S.Greenberg and S.E.Johnson, “Reusable LH2 Tank Technology Demonstration Through Ground Test.”, AIAA Space Programs And Technologies Conference, AIAA 94-4677, pg 1-12, Sep 27-9 1994

C38. R. Perami, W. Prince and D. Foucher, “Investigation Of Microfracture Process In Composites By Gas Permeability.”, Proceedings Of The International Conference On Composite Materials And Energy (Enercomp 95),Technomic Publishing Co., Lancaster Penn, pg 195-202, 8-10 May 1995

C39. K.Pannkoke, “Experimental Evaluation Of Basic Material Data For Carbon Fibre Reinforced Plastics At 77K.”, Proceedings Of The International Conference On Composite Materials And Energy (Enercomp 95), Technomic Publishing Co., Lancaster Penn, pg 3-10, 8-10 May 1995

C40. Marvin A. Guiles, “Liquid Crystal Polymer Cryogenic Storage Tank With Reduced Thermal Loss And Weight.”, AIAA 95-2355, 31ST AIAA / ASME / ASEE Joint Propulsion Conference And Exhibit Jul 10-12 1995, San Diego, Ca, pg 1-11, 1995

C41. M. Hussain, A. Nakahira, S. Nishijima and K. Niihara, “Evaluation of mechanical behavior of CFRC transverse to the fiber direction at room and cryogenic temperature.”, Composites Part A: Applied Science And Manufacturing, V31, pg 173-179, 2000

C42. S.S.Kessler, T.Matuszeski and H.McManus, “Cryocycling And Mechanical Testing Of CFRP For The X-33 Liquid H2 Fuel Tank Structure.”, ASC 2001 Conference, pg 1-12, 2001

C43. N.J.Pagano, G.A.Schoeppner, R.Kim and F.L.Abrams, “Steady State cracking and edge effects in thermomechanical transverse cracking of cross ply laminates.”, Composites Science and Technology, V58, pg 1811-1825, 1998

C44. C.L.Choy, “Thermal Conductivity of polymers.”, POLYMER, V18, pg 984-1004, Oct 1977

C45. Linda S. Schadler, Juan C. Figueroa and Campbell Laird, “Interphase Behavior In Cyclic Fatigue Of Monofilament Composites.”, Mat. Res. Soc. Symp. Proc. V170, Materials Research Society, pg 345-350, 1990

Hertzian Fracture Bibliography:

H 1, Brian Lawn, “Indentation Fracture”, Fracture of Brittle Solids 2Ed, Ch 8, Cambridge Uni. Press, Pg 249-306, 1993

H 2, B.R. Lawn, and M.V. Swain, “Microfracture beneath point indentations in brittle solids.”, J. of Materials Science, V10, N1, Pg 113-122, Jan 1975

H 3, Brian Lawn, and Rodney Wilshaw, “Review Indentation fracture: principles and applications.”, J. of Materials Science, V10, N6, Pg 1049-1081, Jun 1975

H 4, B.R. Lawn, S.M. Wiederhorn, and D.E. Roberts, “Effect Of Sliding Friction Forces On The Strength Of Brittle Materials. ”, J. of Materials Science, V19, Pg 2561-2569, 1984

H 5, G.M.Hamilton, and L.E.Goodman, “The Stress Field Created By A Circular Sliding Contact.”, J. of Applied Mechanics, V33, Series E, N2, Pg 371-376, Jun 1966

H 6, B.R. Lawn, , “Hertzian Fracture In Single Crystals With The Diamond Structure. ”, J. of Applied Physics, V39, N10, Pg 4828-4836, Sep 1968

H 7, F.B. Langitan, and B.R. Lawn, “Hertzian Fracture Experiments On Abraded Glass Surfaces As Definitive Evidence For An Energy Balance Explanation Of Aurbach's Law. ”, J. of Applied Physics, V40, N10, Pg 4009-4017, Sep 1969

H 8, T.R. Wilshaw, “The Hertzian Fracture Test. ”, J. of Physics D: Applied Physics, V4, Pg 1567-1581, 1971

H 91, F.C.Frank, and B.R. Lawn, “On the theory of Hertzian fracture.”, Proc. Of the Royal Society of London, Series A. Mathematical and Physical Sciences, V299, N1458, Pg 291-306, Jul 1967

H 10, B.R. Lawn, , “Partial Cone Crack Formation In A Brittle Material Loaded With A Sliding Spherical Indenter.”, Proc. Of the Royal Society of London, Series A. Mathematical and Physical Sciences, V299, N1458, Pg 307-316, Jul 1967

H 11, B.R. Lawn, T.R.Wilshaw, and E.W. Hartley, “A computer simulation study of hertzian cone crack growth. ”, Int. J. of Fracture, V10, N1, Pg 1-16, Mar 1974

H 12, F.F.Lange, “Crack extension and arrest in contact stress fields.”, Int. J. of Fracture, V12, N3, Pg 409-417, Jun 1976

H 13, B. Cotterell, J. Kamminga, and F.P. Dickson, “The essential mechanics of conchoidal flaking. ”, Int. J. of Fracture, V29, N4, Pg 205-221, Dec 1985

H 14, A.G. Evans, “Strength Degradation By Projectile Impacts”, J. of the American Ceramic Society, V56, N8, Pg 405-409, Aug 1973

H 15, J.P.A. Tillett, “Fracture Of Glass By Spherical Indenters. ”, Proc Of The Physical Society, Section B, V69, Part 1, N433 B, Pg 47-54, Jan 1956

H 16, F.C.Roesler, “Indentation Hardness Of Glass As An Energy Sealing Law. ”, Proc Of The Physical Society, Section B, V69, Part 1, N433 B, Pg 55-60, Jan 1956

H 17, F.C.Roesler, “Brittle Fractures Near Equilibrium. ”, Proc Of The Physical Society, Section B, V69, Part 1, N433 B, Pg 981-992, Jan 1956

H 18, A.Iwabuchi, T.Honda, and J.Tani, “Tribological properties at temperatures of 293, 77, and 4 K in fretting. ”, Cryogenics, V29, N2, Pg 124-131, Feb 1989

H 19, P.C.Michael, E.Rabinowicz, and Y.Iwasa, “Friction and wear of polymeric materials at 293, 77 and 4.2 K. ”, Cryogenics, V31, N8, Pg 695-704, Aug 1991

H 20, Fumio Sawa, Shigehiro Nishijima, and Toichi Okada, “Molecular design of an epoxy for cryogenic temperatures. ”, Cryogenics, V35, N11, Pg 767-769, Nov 1995

H 21, Kyuichiro Tanaka, and Yoshinori Yamada, “Effect of Tempereature on the Friction and Wear of some Heat - Resistant Polymers. ”, Polymer wear and its control. ACS, Pg 103-128, 1985

H 22, Frank A. McClintock, and Ali S. Argon, “Hardness”, Mechanical Behavior of Materials, Ch 13, Addison-Weslet Publishing Co. Inc., Pg 443 468, 1966

H 23, Frank A. McClintock, and Ali S. Argon, “Friction and Wear”, Mechanical Behavior of Materials, Ch 20, Addison-Weslet Publishing Co. Inc. , Pg 657-673, 1966

Friction Bibliography:

F1, Frank Philip Bowden, and David Tabor, “FRICTION An Introduction to Tribology.”, Robert E. Krieger Publishing Co., Malabar FL, Pg 1-178, 1982

F2, Frank Philip Bowden, and David Tabor, Friction And Lubrication, Methuen & Co. LTD., 11 New Fetter Lane, London EC4, Pg 1-166, 1967

F3, F.P.Bowden, and K.E.W.Ridler, “Physical Properties Of Surfaces III - The Surface Temperature Of Sliding Metals The Temperature Of Lubricated Surfaces.”, Proc Royal Society Of London Series A Mathematical And Physical Sciences, Vol CLIV, Pg 640-656, May 1936

F4, F.P.Bowden, and T.P.Hughes, “Physical Properties Of Surfaces IV - Polishing, Surface Flow and the Formation of the Beilby Layer.”, Proc Royal Society Of London Series A Mathematical And Physical Sciences, V160, Pg 575-587, Jun 1937

F5, F.P.Bowden, and L.Lebin, “The Nature of Sliding and the Analysis of Friction.”, Proc Royal Society Of London Series A Mathematical And Physical Sciences, V167, Pg 371-391, Mar 1939

F6, F.P.Bowden, and D.Tabor, “The area of contact between stationary and between moving surfaces.”, Proc Royal Society Of London Series A Mathematical And Physical Sciences, V167, Pg 391- 413, Mar 1939

F7, F.P.Bowden, M.A.Stone, and G.K.Tudor, “Hot Spots on Rubbing Surfaces and the Detonation of Explosives by Friction.”, Proc Royal Society Of London Series A Mathematical And Physical Sciences, V188, Pg 329-349, Feb 1947

F8, J.S.McFarlane, and D. Tabor, “Relation Between Friction And Adhesion.”, Proc Royal Society Of London Series A Mathematical And Physical Sciences, V202, N A 1069, Pg 244-253, Jul 1950

F9, F.P.Bowden, and J.E.Young, “Friction of diamond, graphite, and carbon and the influence of surface films.”, Proc Royal Society Of London Series A Mathematical And Physical Sciences, V208, Pg 444-455, 1951

F10, F.P.Bowden, J.E.Young, and G.Rowe, “Friction of diamond, graphite, and carbon: the influence of adsorbed films.”, Proc Royal Society Of London Series A Mathematical And Physical Sciences, V212, Pg 485-488, 1952

F11, K.V.Shooter, “Frictional Properties Of Plastics.”, Proc Royal Society Of London Series A Mathematical And Physical Sciences, V212, Pg 488-491, 1952

F12, F.P.Bowden, “The Mechanism Of Friction.”, Proc Royal Society Of London Series A Mathematical And Physical Sciences, V212, Pg 440-449, 1952

F13, A.J.Moore, and W.J.McG.Tegart, “Relation Between Friction And Hardness.”, Proc Royal Society Of London Series A Mathematical And Physical Sciences, V212, Pg 452-458, 1952

F14, J.T.Burwell, and C.D.Strang, “Metallic Wear.”, Proc Royal Society Of London Series A Mathematical And Physical Sciences, V212, Pg 470-477, 1952

F15, D.Tabor, “Note on Professor Blok's Comments.”, Proc Royal Society Of London Series A Mathematical And Physical Sciences, V212, Pg 482, 1952

F16, G.I.Finch, and R.T.Spurr, “Surface Changes Due To Sliding.”, Proc Royal Society Of London Series A Mathematical And Physical Sciences, V212, Pg 462-464, 1952

F17, F.E.Simon, F.P.Bowden, A.J.W.Moore, and D.Tabor, “Comments on the Energetics of the Frictional Process. Reply To Professor Simon's Comments. Comments on the Energy of Deformation During Sliding. Comments On the Work Done in Rolling Friction.”, Proc Royal Society Of London Series A Mathematical And Physical Sciences, V212, Pg 477-479, 1952

F18, Nils Gralen, “Friction Between Single Fibres.”, Proc Royal Society Of London Series A Mathematical And Physical Sciences, V212, Pg 491-495, 1952

F19, K.Rachel Makinson, “Some Comments On The Paper By Dr. N. Gralen.”, Proc Royal Society Of London Series A Mathematical And Physical Sciences, V212, Pg 495-496, 1952

F20, F.P.Bowden, and P.H.Thomas, “The Surface Temperature Of Sliding Solids.”, Proc. Of The Royal Society Of London Series A. Mathematical And Physical Sciences, V223, N1152, Pg 29-40, 1954

F21, R.F. King, and D. Tabor, “The Strength Properties And Frictional Behaviour Of Brittle Solids.”, Proc. Royal Society Of London Series A Mathematical And Physical Sciences, V223, Pg 225-238, 1954

F22, W. Hirst, and J.K. Lancaster, “The influence of oxide and lubricant films on the friction and surface damage of metals.”, Proc Royal Society Of London Series A Mathematical And Physical Sciences, V223, Pg 324-338, 1954

F23, J.A. Chapman, and J.W. Menter, “A Study Of The Shape, Surface Structure And Frictional Wear Of Fibres By Reflexion Electron Microscopy.”, Proc Royal Society Of London Series A Mathematical And Physical Sciences, V226, N1166, Pg 400-407, Nov 1954

F24, M.W.Pascoe, and D.Tabor, “The Friction and Deformation of Polymers.”, Proc Royal Society Of London Series A Mathematical And Physical Sciences, V235, Pg 210-224, Jun 1956

F25, J.F. Archard, “Elastic Deformation and the Laws of Friction.”, Proc Royal Society Of London Series A Mathematical And Physical Sciences, V243, N1233, Pg 190-205 Dec 1957,

F26, F.P.Bowden, and P.A.Persson, “Deformation, heating and melting of solids in high-speed friction.”, Proc Royal Society Of London Series A Mathematical And Physical Sciences, V260, N1303, Pg 433-458, Mar 1961

F27, K.A.Grosch, “The relation between the friction and visco-elastic properties of rubber.”, Proc Royal Society Of London Series A Mathematical And Physical Sciences, V274, N1356, Pg 21-39, Aug 1963

F28, K. Rachel Makinson, and D. Tabor, “The friction and transfer of polytetrafluoroethylene.”, Proc Royal Society Of London Series A Mathematical And Physical Sciences, V281, N1384, Pg 49-61, Aug 1964

F29, J.A.Greenwood, and J.B.P. Williamson, “Contact of Nominally Flat Surfaces.”, Proc Royal Society Of London Series A Mathematical And Physical Sciences, V295, N1442, Pg 300-319, Dec 1966

F30, B.R. Lawn, “Partial Cone Crack Formation In A Brittle Material Loaded With A Sliding Spherical Indenter.”, Proc. Of the Royal Society of London, Series A. Mathematical and Physical Sciences, V299, N1458, Pg 307-316, Jul 1967

F31, Christine M. Pooley, and D. Tabor, “Friction and molecular structure: the behaviour of some thermoplastics.”, Proc Royal Society Of London Series A Mathematical And Physical Sciences, V329, N1578, Pg 251-274, Aug 1972

F32, J.C. Jaeger, “Moving Sources Of Heat And The Temperature At Sliding Contacts.”, Journal and Proceedings Of The Royal Society Of New South Wales, V 76, #28, Pg 203-224, 1942

F33, J.R.Barber, “The conduction of heat from sliding solids.”, Int.J. Heat Mass Transfer, Pergamon Press, V13, Pg 857-868, 1970

F34, M.G.Cooper, B.B.Mikic, and M.M.Yovanovich, “Thermal Contact Conductance.”, Int.J. Heat Mass Transfer, Pergamon Press, V12, Pg 279-300, 1969

F35, Brian Vick, M.J.Furey, and S.J.Foo, “Boundary Element Thermal Analysis Of Sliding Contact.”, Numerical Heat Transfer, Part A, V20, Pg 19-40, 1991

F36, Michael J. Furey, Brian Vick, Ser Jee Foo, and Brian L. Weick, “A Theoretical And Experimental Study Of Surface Temperatures Generated During Fretting.”, Proc of the Japan International Tribology Conference, Nagoya , Vol II, Pg 809-814, Oct-Nov 1990

F37, H. Blok, “Theoretical Study Of Temperature Rise At Surfaces Of Actual Contact Under Oiliness Lubricating Conditions.”, Proc General Discussion On Lubrication And Lubricants, V2, Pg 222-235, Oct 1937

F38, F.P. Bowden, “The Friction Of Sliding Metals.”, Proc General Discussion On Lubrication And Lubricants, V2, Pg 236-240, Oct 1937

F39, H. Blok, “Measurement Of Temperature Flashes On Gear Teeth Under Extreme Pressure Conditions.”, Proc. General Discussion On Lubrication And Lubricants, V2, Pg 14-20, Oct 1937

F40, N.K.Adam, “Molecular Forces In Friction And Boundary Lubrication.”, Proc General Discussion On Lubrication And Lubricants, V2, Pg 197-201, Oct 1937

F41, D. Tabor, “Friction, Lubrication And Wear Of Synthetic Fibres.”, Wear, V1, Pg 5-24, 1957 / 58

F42, Frederick F. Ling, and Edward Saibel, “Thermal Aspects Of Galling Of Dry Metallic Surfaces In Sliding Contact.”, Wear, V1, Pg 80-91, 1957 / 58

F43, F.P.Bowden, “A Review Of The Friction Of Solids.”, Wear, V1, Pg 333-346, 1957 / 58

F44, J.F. Archard, “The Temperature Of Rubbing Surfraces.”, Wear, V2, N6, Pg 438-455, 1958 / 59

F45, H. Blok, “The Flash Temperature Concept.”, Wear, V6, Pg 483-494, 1963

F46, K.G.McLaren, and D.Tabor, “The friction and deformation properties of irradiated polytetrafluoroethylene (PTFE).”, Wear, V8, N1, Pg 3-7, Jan-Feb 1965

F47, K.G.McLaren, and D.Tabor, “Friction of polymers at engineering speeds: Influence of speed, temperature and lubricants.”, Wear, V8, N1, Pg 79-83, Jan-Feb 1965

F48, R.J.Heighway, and D.S.Taylor, “Transient Temperature Rises During The Rubbing Of Metals On Glass.”, Wear, V9, N4, Pg 310-319, 1966

F49, K.C.Ludema, and D.Tabor, “The Friction and Visco-elastic Properties of Polymeric Solids.”, Wear, V9, N5, Pg 329-348, Sep-Oct 1966

F50, D.F.Moore, and W.Geyer, “A Review of Adhesion Theories for Elastomers.” Wear, V22, N2, Pg 113-141, Nov 1972

F51, Z.Eliezer, C.J.Schulz, and J.W.Barlow, “Friction and Wear Properties of An Epoxy-Steel System.”, Wear, V46, N2, Pg 397-403, Feb 1978

F52, T.F Quin, and W.O.Winer, “The Thermal Aspects Of Oxidational Wear.”, Wear, V102, Pg 67-80, 1985

F53, Zeng Hanmin, He Guoren, and Yang Guicheng, “Friction and Wear of Poly(phenylene Sulphide) and Its Carbon Fibre Composites: I Unlubricated.”, Wear, V116, N1, Pg 59-68, Apr 1987

F54, Zeng Hanmin, He Guoren, and Yang Guicheng, “Friction and Wear of Poly(phenylene Sulphide) and Its Carbon Fibre Composites: II Water Lubrication.”, Wear, V116, N1, Pg 69-75, Apr 1987

F55, Bhawani S. Tripathy, and Michael J. Furey, “Tribological behavior of unidirectional graphite-epoxy and carbon-PEEK composites.”, Wear, V162-164, Pg 385-396, Apr 1993

F56, R.Bassani, G.Levita, M.Meozzi, and G.Palla, “Friction and wear of epoxy resin on inox steel: remarks on the influence of velocity, load and induced thermal state.”, Wear, V247, N2, Pg 125-132, Feb 2001

F57, Peter J. Blau, and Rebecca L.Martin, “Friction and wear of carbon-graphite materials against metal and ceramic counterfaces.”, Tribology International, V27, N6, Pg 413-422, Dec 1994

F58, E.Santner, and H.Czichos, “Tribology of polymers.”, Tribology International, V22, N2, Pg 103-109, Apr 1989

F59, K.Friedrich, “Sliding wear performance of different polyimide formulations.”, Tribology International, V22, N1, Pg 25-31, Feb 1989

F60, B.Briscoe, “Wear of polymers: an essay on fundamental aspects.”, Tribology International, Pg 231-243, Aug 1981

F61, U.S.Tewari, S.K.Sharma, and P.Vasudevan, “Friction and wear studies of a bismaleimide.”, Tribology International, V21, N1, Pg 27-30, Feb 1988

F62, B.K.Gupta, J.Janting, and G.Sorensen, “Friction and wear characteristics of ion-beam modified graphite coatings.”, Tribology International, V27, N3, Pg 139-143, Jun 1994

F63, Ragnar Holm, “Calculation of the Temperature Development in a Contact Heated in the Contact Surface, and Application to the Problem of the Temperature Rise In a Sliding Contact.”, J. Of Applied Physics, V19, Pg 361-366, Apr 1948

F64, Ernest F. Fullam, and Robert H. Savage, “Carbon Film Formation And Commutator Brush-Wear As Revealed By The Electron Micxroscope.”, J. Of Applied Physics, V19, Pg 654-661, Jul 1948

F65, Robert Savage, “Graphite Lubrication.”, J. Of Applied Physics, V19, N1, Pg 1-10, Jan 1948

F66, J.F. Archard, “Contact And Rubbing Of Flat Surfaces.”, J.Appl.Phys., V24, Pg 981-988, 1954

F67, A.M. Freudenthal, and J.H. Weinerm, “On The Thermal Aspect Of Fatigue.”, J.Appl.Phys., V27, Pg 44-50, 1956

F68, Robert H. Savage, and D.L.Schaefer, “Vapor Lubrication Of Graphite Sliding Contacts.”, J.Appl.Phys., V27, Pg 136-138, 1956

F69, W.W.Hansen, and D. Tabor, “Role Of Hydrodynamic Lubrication In The Friction Of Fibers And Yarns.”, J.Appl.Phys., V27, Pg 1558-1559, 1956

F70, R.C.Bowers, “Coefficient of friction of high polymers as a friction of pressure.”, J of Applied Physics, V42, N12, Pg 4961-4970, Nov 1971

F71, I.C.Roselman, and D.Tabor, “The friction of carbon fibres.”, J.Phys. D: Appl. Phys., V9, Pg 2517-2532, 1976

F72, J.K.Lancaster, and J.R.Pritchard, “On the "dusting" wear regime of graphite sliding against carbon.”, J.Phys.D: Appl.Phys., V13, Pg 1551-1564, 1980

F73, E.I.Stone, and W.C.Young, “Coefficient of friction measurements of Fiberglass/Epoxy at cryogenic temperatures.”, Advances in Cryogenic Engineering Materials, V26, Editors: A.F. Clark and R.P.Reed, Plenum Press, Pg 315-318, 1980

F74, R.L.Tobler, “A review of antifriction materials and design for cryogenic environments.”, Advances in Cryogenic Engineering Materials, V26, Editors: A.F. Clark and R.P.Reed, Plenum Press, Pg 66-77, 1980

F75, D.W.Wisander, and R.L.Johnson, “Wear and friction of impregnated carbon seal materials in Liquid Nitrogen and Hydrogen.”, Advances in Cryogenic Engineering Materials, V6, Editor: K.D.Timmerhaus, Plenum Press, Pg 210-218, 1961

F76, D.W.Wisander, W.F.Hady, and R.L.Johnson, “Friction studies of various materials in liquid nitrogen.”, Advances in Cryogenic Engineering Materials, V3, Editor: K.D.Timmerhaus, Plenum Press, Pg 390-406, 1960

F77, A.Iwabuchi, T.Honda, and J.Tani, “Tribological properties at temperatures of 293, 77, and 4 K in fretting.”, Cryogenics, V29, N2, Pg 124-131, Feb 1989

F78, P.C.Michael, D.Aized, E.Rabinowicz, and Y.Iwasa, “Mechanical properties and static friction behaviour of epoxy mixes at room temperature and at 77K.”, Cryogenics, V30, Pg 775-786, Sep 1990

F79, P.C.Michael, E.Rabinowicz, and Y.Iwasa, “Friction and wear of polymeric materials at 293, 77 and 4.2 K.”, Cryogenics, V31, N8, Pg 695-704, Aug 1991

F80, Xuefeng Tian, and Francis E. Kennedy, Jr., “Contact Surface Temperature Models For Finite Bodies In Dry And Boundary Lubricated Sliding.”, J. Of Tribology, V115, Pg 411-418, Jul 1993

F81, Xuefeng Tian, and Francis E. Kennedy, Jr., “Maximum and Average Flash Temperatures in Sliding Contacts.”, J. Of Tribology, V116, Pg 167-174, Jan 1994

F82, Qu Jianjun, Luo Yunxia, Zhang Zhiqian, Qi Yulin, and Li Xiaoquang, “Study of sliding friction and wear properties of bismaleimide and its composite against AL.”, Eleventh International Conference on Composite Materials, Vol 4, Composite Processing And Microstructure, Proceedings, Woodhead Pub Limitied, Editor Murray L.Scott, Pg 856-865, 1997

F83, Witold Brostow, Patrick E. Cassidy, Haley E. Hagg, Magdalena Jacklewicz, and Pablo E. Montemartini, “Modification Of Epoxies For Low Friction.”, Annual Tech. Conf. - oc. Plast. Eng., V59, N3, Pg 3214-3218, 2001

F84, Richard S. Cowan, and Ward O. Winer, “Frictional Heating Calculations.”, ASM Handbook, V18, Friction, Lubrication, and Wear Technology. Ch: Soild Friction, Pg 39-44, Oct 1992

F85, William A. Glaeser, “Materials For Tribology”, Tribology Series, 20, Elsevier, Pg 1-7, 114-29, 177-86, 211-45, 1992

F86, D.C. Evans, and J.K. Lancaster, “The Wear Of Polymers.”, Treatise On Materials Science And Technology, V13, Academic Press, Inc., Pg 85-139, 1979

F87, J.K. Lancaster, “Transitions in the Friction and Wear of Carbons and Graphites Sliding Against Themselves.”, ASLE Transactions, Pub Of The American Society Of Lubrication Engineers, V18, N3, Pg 187-200, Jul 1975

F88, Kyuichiro Tanaka, and Yoshinori Yamada, “Effect of Temperature on the Friction and Wear of some Heat - Resistant Polymers.”, Polymer wear and its control. ACS, Pg 103-128, 1985

F89, R.E.Schramm, A.F.Clark, and R.P.Reed, “A Compilation and Evaluation of Mechanical, Thermal, and Electrical Properties of Selected Polymers.”, NBS Monograph 132, Cryogenics Division, Inst. For Basic Standards, NBS, Boulder, Co 80302, Pg 1-848, Sep 1983

F90, D.H.Buckley, and R.L.Johnson, “Degradation of Polymeric Compositions in Vacuum to 10^{-9} mm Hg in Evaporation and Sliding Friction Experiments.”, SPE Transactions, Pg 306-314, Oct 1964

F91, H.H.Shim, O.K.Kwon, and J.R.Youn, “Effects of Structure and Humidiy on Friction and Wear Properties of Carbon Fiber Reinforced Epoxy Composites.”, Conference Proceedings, In Search of Excellence Annual Technical Conference, ANTEC 91, Pg 1997-1999, 1991

F92, K.V.Shooter, and P.H.Thomas, “Frictional Properties Of Some Plastics.”, Research, A Journal of Science and Its Applications., V2, N11, Pg 533-535, Nov 1949

F93, M.J.Devine, and A.E.Kroll, “Aromatic Polyimide Compositions for Solid Lubriction.”, J. Of The American Society of Lubrication Engineers, V20, Pg 225-230, 1964

F94, H.E.Sliney, “High Temperature Solid Lubricants, Part 2: Polymers and Fluoride Coatings And Composites.”, Mechanical Engineering, V96, N3, Pg 34-39, Mar 1974

F95, N.H.Cook, and B.Bhushan, “Sliding Surface Interface Temperatures.”, J. Of Lubrication Technology V95, Series F, N1, Transactions of the ASME, Pg 59-64, Jan 1973

F96, N.H.Cook, and B.Bhushan, “Temperatures In Sliding.”, J. Of Lubrication Technology V95, Series F, N4, Transactions of the ASME, Pg 535-536, Oct 1973

F97, T.A.Dow, and R.A.Burton, ”The Role of Wear in the Initiation of Thermoelastic Instabilities of Rubbing Contact.”, J. Of Lubrication Technology V95, Series F, N1, Transactions of the ASME, Pg 71-75, Jan 1973

F98, Bharat Bushan, Tempperature And Friction Of Sliding Surfaces. Masters Thesis, MIT, Pg 1-116, Aug 1971

F99, J.K.Lancaster, “Basic Mechanisms of Friction and Wear of Polymers.”, Plastics And Polymers, V41, Pg 297-306, Dec 1973

F100, J.W.S. Hearle, and D.Tabor, “Frictional Behaviour Of Textiles.”, Physical Methods Of Investigating Textiles Edited By R. Meredith and J.W.S. Hearle, Interscience Publishers Inc, Ch 11, NY and London, Pg 301-319, 1959

F101, B.Lincoln, “Frictional and elastic properties of high polymeric materials.”, British J. Of Applied Physics, V3, Pg 260-263, Aug 1952

F102, H.G. Howell, and J.Mazur, “Amonton's Law And Fibre Friction.”, J. of the Textile Institute, V44, Pg T59-T69, 1953

F103, R.F. King, and D.Tabor, “The Effect Of Temperature on the Mechanical Properties and the Friction of Plastics.”, Proc. Phys. Soc. London, V B66, Pg 728-736, 1953

F104, K.V.Shooter, and D.Tabor, “The Frictional Properties of Plastics.”, Proc. Phys. Soc. London, V B65, Pg 661-671, 1952

F105, M.W.Pascoe, and D.Tabor, “Friction of Nylon as a Function of Load and Surface Curvature.”, Research Correspondence (A Suppliment issued with "Research: A J. of Sci. And Its Apps."), V8, N4, Pg S15-S17, Apr 1955

F106, Yoshikawa M., Satoh T., Inubushi S., Ikeda T., and Tazuke S., ” Anti-abrasion and Low Friction Properties Of Solid Lubricant- Aminimide Cured Epoxy Resin Composites.”, J. of Materials Science Letters, V5, N5, Pg 1239-1241, Dec 1986

F107, P.B.Bowden, “The effect of hydrostatic pressure on the fibre-matrix bond in a steel-resin model composite.”, J. Of Materials Science, V5, Pg 517-520, 1970

F108, B.Harris, J.Morley, and D.C.Phillips, “Fracture mechanisms in glass-reinforced plastics.”, J. Of Materials Science, V10, Pg 2050-2061, 1975

F109, J.N.Kirk, M.Munro, and P.W.R.Beaumont, “The fracture energy of hybrid carbon and glass fibre composites.” J. Of Materials Science, V13, Pg 2197-2204, 1978

F110, Brian Lawn, and Rodney Wilshaw, “Review Indentation fracture: principles and applications.”, J. of Materials Science, V10, N6, Pg 1049-1081, Jun 1975

F111, B.R. Lawn, S.M. Wiederhorn, and D.E. Roberts, “Effect Of Sliding Friction Forces On The Strength Of Brittle Materials.”, J. of Materials Science, V19, Pg 2561-2569, 1984

F112, Robert, L. Fusaro, “Friction and Wear Life Properties of Polyimide Thin Films.”, NASA TN D-6914, Pg I-14, Aug 1972

F113, Robert L. Fusaro, “Friction Transition in Polyimide Films As Related To Molecular Relaxations And Structure.”, NASA TN D-7954, Pg 1-28, Apr 1975

F114, Robert L. Fusaro, “Tribological Properties At 25 C of Seven Polyimide Films Bonded To 440C High-Temperature Stainless Steel.”, NASA TP-1944, Pg 1-20, Feb 1982

F115, H.G.Howell, “The Laws of Friction.”, Nature, V171, Pg 220, Jan 1953

F116, B.Lincoln, “Elastic Deformation and the Laws Of Friction.”, Nature, V172, Pg 169-170, Jul 1953

F117, K.A.Grosch, “Relation between the friction and visco-elastic properties of rubber.”, Nature, V197, N4870, Pg 858-859, Mar 1963

F118, K.G.McLaren, and D.Tabor, “Friction of polymers: Influence of speed and temperature.”, Nature, V197, N4870, Pg 856-858, Mar 1963

F119, J.Skinner, N.Gane, and D. Tabor, “Micro-friction of Graphite.”, Nature: Physical Science, V232, Pg 195-196, Aug 1971

F120, B.Gecim, and W.O.Winer, “Transient Temperatures In The Vicinity Of An Asperity Contact.”, J. Of Tribology Technology, V107, N3, Pg 333-342, Jul 1985

F121, T.F.J.Quinn, and W.O.Winer, “An Experimental Study of the "Hot Spots" Occurring During The Oxidational Wear of Tool Steel On Sapphire.”, J. Of Tribology Technology, V109, N2, Pg 315- 320, Apr 1987

F122, J.P.Giltrow, “Friction and Wear of some polyimides.”, Tribology, V6, Pg 253-257, Dec 1973

F123, L.D.Wedeven, and N.C.Miller, “Material and Tribological Considerations for Turbopump Bearings.”, J. of the Society of Tribologists and Lubrication Engineers, V47, N12, Pg 1009-1017, Dec 1991

F124, E. Lord, “Frictional Forces Between Fringes Of Fibres.”, Journal Of The Textile Institute, V46, Pg P41-58, 1955

F125, H.L. Roder, “Measurements Of The Influence Of Finishing Agents On The Friction Of Fibers.”, The Journal Of The Textile Institute Transactions, V44, N6, Pg T247-T265, June 1953

F126, Joel Lindberg, and Nils Gralen, “Mesaurement Of Friction Between Single Fibers II. Frictional Properties Of Wool Fibers Measured By The Fiber-Twist Method.”, Textile Research Journal, V18, Pg 287-301, May 1948

F127, D.G. Lyne, “The Dynamic Friction Between Cellulose Acetate Yarn And A Cylindrical Metal Surface.”, The Journal Of The Textile Institute Transactions, V46, Pg P112-P122, 1955

F128, G.M.Hamilton, and L.E.Goodman, “The Stress Field Created By A Circular Sliding Contact.”, J. of Applied Mechanics, V33, Series E, N2, Pg 371-376, Jun 1966

F129, Frank A. McClintock, and Ali S. Argon, “Friction and Wear.”, Ch 20, Mechanical Behavior of Materials, Addison-Weslet Publishing Co. Inc., Pg 657-673, 1966

Bismaleimides Bibliography:

B1, Jason E. Lincoln, Roger J. Morgan, and E. Eugene Shin,”Fundamental Investigation Of Cure-Induced Microcracking In Carbon Fiber/Bismaleimide Cross-Ply Laminates.”, Polymer Composites, V22, N3, Pg 397-419, Jun 2001

B2, C.L. Heisey, P.A. Wood, J.E. McGrath, and J.P. Wightman, “Measurement of adhesion between carbon fibers and Bismaleimide resins”, J Adhesion, V53, Pg 117-147, 1995

B3, C.L. Heisey, P.A. Wood, J.E. McGrath, and J.P. Wightman, “Characterization And Carbon Fiber Adhesion Of A Novel Bismaleimide Containing Phosphine Oxide”, Proceedings Of The ACS Div Of Polymeric Materials-Science and Engineering, V67, Pg 28-29, Fall 1992

B4, Robert A. Frosch, Indra K. Varma, George M. Fohlen, and John A. Parker, “Phosphorus Containing Bisimide Resins”, US Patent Number: 4,276,344, Pg 1-4, Jun 1981

B5, Steven P. Wilkinson, Toughened Bismaleimides, their Carbon Fiber Composites And Interphase Evaluation Studies; Dissertation, Virgina Polytechnic Institute And State Uni., Sep 1991

B6, Paul A. Wood, Gregory D. Lyle, Atilla Gungor, Carrington D. Smith, and James E. McGrath, “Synthesis Of New Bismaleimides Derived From Bis(3-Amino Phenoxy) Triphenylphosphine Oxide And Bis (4-Fluoro Benzoyl) Benzene.”, 36Th Internat. SAMPE Symposium, Pg 1355-1367, Apr 1991

B7, H.D. Stenzenberger, P. Konig, W. Romer, M. Herzog, and W.V. Breitigam, “BMI / Bis(allylphenoxyphthalimide) - Copolymers: A New Family Of Resins For Advanced Composites With Improvged Thermal Oxidative Stability.”, 36Th Internat. SAMPE Symposium, Pg 1232-1243, Apr 1991

B8, R. Jurek, D.E.Larive, M.Wood, R.J.Morgan, C.Tung, and T.Donnellan, ”Processing and toughening of Bismaleimide - Carbon Fiber Composites.”, Proceedins of the American Society for Ccomposites, 5Th Tech Conf., Pg 229-238, Jun 1990

B9, Paul A. Wood III, Synthesis and characterization of novel bismaleimides derived from arylene phosphine oxides and ether-ketones., Dissertation Virginia Polytechnic Institute and State University, 1991

B10, Numerous Meetings and Conversations With Composites Prepreging Community Personnel Mid 1990s thru 2001

B11, Extensive Conversations With AFRL/MLBC government and onsite contract Personnel 2000s thru 2001

B12, 5250-4 Prepreg System Technical Data Product Features, Cytec Engineered Materials Inc, Pg 1-22, Feb 1992

B13, CYCOM 5250-4 RTM Resin System, Cytec Engineered Materials Inc. , Pg 1-9, May 1992

B14, John A. Parker, Demitrius A. Kourtides, and George M. Fohlen, ” Bismaleimides And Related Maleimido Polymers As Matrix Resins For High Temperature Environments.”, High Temperature Polymer Matrix Composites, Noyes Data Corp., Pg 54-76, 1987

B15, Demetrius A. Kourtides, and John A. Parker, “Advanced Resin Matrices For Fire resistant Composites.”, Pactec 79, SPE, Pg 51-4, Feb 1979

B16, Demetrius A. Kourtides, and John A. Parker, “Flammability Properties Of Some Thermoplastic And Thermoset Resins”, 23RD National SAMPE, Pg. 36-43, May 1978

B17, Tao C. Chang, and B.Z. Jang, “The Effects Of Fiber Surface Treatments By A Cold Plasma In Carbon Fiber/BMI Composites”, Mat. Res. Soc. Symp. Proc. Vol. 170, Materials Research Society, Pg 321-326, 1990

Fiber Surface And Interface Bibliography:

FI1, Lawrence T. Drzal, Michale J. Rich and Pamela F. Lloyd, “Adhesion of graphite fibers to epoxy matrices: I. The role of fiber surface treatment.”, J Adhesion, V16, pg 1-30, 1982

FI2, Lawrence T. Drzal, Michale J. Rich and Pamela F. Lloyd, “Adhesion of graphite fibers to epoxy matrices: I. The effect of fiber finish.”, J Adhesion, V16, pg 133-152, 1983

FI3, C.L. Heisey, P.A. Wood, J.E. McGrath and J.P. Wightman, “Measurement of adhesion between carbon fibers and Bismaleimide resins.”, J Adhesion, V53, pg 117-147, 1995

FI4, W. Gutowski, “Thermodynamic Criteria for the Maximum and Minimum Strength of Fibre-Reinforced Composite Materials.”, J Adhesion, V23, pg 187-199, 1987

FI5, J. Schultz, L. Lavielle and C. Martin, “The Role Of The Interface In Carbon Fibre-Epoxy Composites.”, J Adhesion, V23, pg 45-60, 1987

FI6, Nursel Dilsiz and J.P. Wightman, “Effect of acid base properties of unsized and sized carbon fibers on fiber epoxy matrix adhesion.”, Collids and Surfaces A: Physicochemical and Engineering Aspects, V164, pg 325-336, 2000

FI7, E. Mader, K. Grundke, H-J Jacobasch and G. Wachinger, “Surface, interphase and composite property relations in fibre reinforced polymers.”, Composites, V25, #7, pg 739-744, 1994

FI8, G.S. Shul, L.M. Shkirkova, L.A. Shchukina, Yu.A. Gorbatkina, and N.P. Selishcheva,” Effect of modification of the surface of carbon fibers on the reaction with epoxy matrices.”, Mekhanika Kompozitnykh Materialov, #4, pg 600-603, 1987

FI9, Lawrence T. Drzal, M. Madhukar and M.C. Waterbury, “Surface Chemistry And Energetics Of IM6 Carbon Fiber Surfaces And Their Adhesion To Epoxy Matrices.”, Polymer Preprints, V33, #1, pg 453-454, Apr 1992

FI10, C.L. Heisey, P.A. Wood, J.E. McGrath and J.P. Wightman, “Characterization And Carbon Fiber Adhesion Of A Novel Bismaleimide Containing Phosphine Oxide.“, Proceedings Of The ACS Div Of Polymeric Materials-Science and Engineering, V67, pg 28-29, Fall 1992

FI11, Steven P. Wilkinson, Ch 2: Carbon Fiber Characterization, Toughened Bismaleimides, their Carbon Fiber Composites And Interphase Evaluation Studies; Dissertation, Virgina Polytechnic Institute And State Uni., pg 4-48, Sep 1991

FI12, Steven P. Wilkinson, Ch 5: Composite Properties, Toughened Bismaleimides, their Carbon Fiber Composites And Interphase Evaluation Studies; Dissertation, Virgina Polytechnic Institute And State Uni., pg 208-273, Sep 1991

FI13, Steven P. Wilkinson, Ch 6: Interphase Evaluation Studies Using Micro And Meso Indention Techniques, Toughened Bismaleimides, their Carbon Fiber Composites And Interphase Evaluation Studies; Dissertation, Virgina Polytechnic Institute And State Uni., pg 274-337, Sep 1991

FI14, M.R. Piggott, “The Interface - An Overview.”, 36Th Internat. SAMPE Symposium, pg 1773-1786, Apr 1991

FI15, Aharon Moshonov, Hong Li and John D. Muzzy, “Electrochemical Surface treatment Of Carbon Fibers.”, 36Th Internat. SAMPE Symposium, pg.1787-1801, Apr 1991

FI16, M.S. Madhukar and L.T. Drzal, “Effect of fiber matrix adhesion on longitudinal (0 degree) compressive properties of graphite/epoxy composites.”, Proceedins of the American Society For Composites, 5Th Tech Conf., pg 849-858, Jun 1990

FI17, Daniel A. Scola, Bruce L. Laube and John H. Vontell, “Interface Characteristics Of Isothermally Aged High Temperature Graphite Fiber / PMR-15 Composites.”, Controlled Interphases In Composite Materials, Elsevier Science Publishing Co. Inc., pg 17-36, 1990

FI18, E. Fitzer and H.P. Rensch, “Carbon Fibers Surfaces And Their Analysis.”, Controlled Interphases In Composite Materials, Elsevier Science Publishing Co. Inc., pg 241-254, 1990

FI19, W. Gutowski, “Effect Of Fiber-Matrix Adhesion On Mechanical Properties Of Composites.”, Controlled Interphases In Composite Materials, Elsevier Science Publishing Co. Inc., pg 505-520, 1990

FI20, Georg Wachinger, “The Influence Of CFRP-Sizings On Processability And Interphase Properties.”, Controlled Interphases In Composite Materials, Elsevier Science Publishing Co. Inc., pg 457-467, 1990

FI21, I. Verpoest, M. Desaeger and R. Keunings, “Critical Review Od Direct Micromechanical Test Methods For Interfacial Strength Measurements in Composites.”, Controlled Interphases In Composite Materials, Elsevier Science Publishing Co. Inc., pg 653-666, 1990

FI22, Umesh Gaur and Bernard Miller, “Variability Of Fiber/Resin Interfacial Shear Strengths.”, Controlled Interphases In Composite Materials, Elsevier Science Publishing Co. Inc., pg 723-730, 1990

FI23, J.D. DeLong, K.J. Hook, M.J. Rich, J. Kalantar and L.T. Drzal, “Spectroscopic Characterization Of Fiber-Polymer Interphases.”, Controlled Interphases In Composite Materials, Elsevier Science Publishing Co. Inc., pg 87-95, 1990

FI24, L. T. Drzal, “Fiber-Matrix Interphase Structure And Its Effect On Adhesion And Composite Mechanical Properties.”, Controlled Interphases In Composite Materials, Elsevier Science Publishing Co. Inc., pg 309-320, 1990

FI25, M.J. Pitkethly and J.B. Doble, “The effect of surface treatment level on the interfacial properties of carbon fibre reinforced composites.”, Controlled Interphases In Composite Materials, Elsevier Science Publishing Co. Inc., pg 809-818, 1990

FI26, Yue-hen Wei, Zhi-Qian Zhang, Yin Li, Zi-Hai Guo and Bai-Ling Zheng, “A Study Of The Interfacial Bonding Between Carbon Fibre And PMR-15 Resin.”, Controlled Interphases In Composite Materials, Elsevier Science Publishing Co. Inc. pg 167-174, 1990

FI27, H.P. Boehm, E.Diehl and W.Heck, “Identification Of Functional Groups In Surface Oxides Of Carbon.”, Second Conference On Industrial Carbon And Graphite, London, 7-9 Apr 1965, pg 369-379, 1966

FI28, U. Gaur, C.T. Chou and B. Miller, “Interfacial Adhesion In Carbon Reinforced Thermosetting And Thermoplastic Composites.”, Proc. Of The American Society For Composites 6TH Technical Conference, pg 751-758, Oct 1991

FI29, F. Pomies and L.A. Carlsson, “Analysis Of Initiation And Propagation Of A Fiber/Matrix Debond.”, Proc. Of The American Society For Composites 6TH Technical Conference, pg 558-568, Oct 1991

FI30, M.R.Piggott and Z.N. Wang, “Relations Between Polymer And Fibre-Polymer Interface Properties.”, Proc. Of The American Society For Composites 6TH Technical Conference, pg 725-731, Oct 1991

FI31, J. Orso and A.J. Vizzini, “The Effects Of An Expanding Monomer On The Tensile Properties Of Graphite/Epoxy.”, Proc. Of The American Society For Composites 6TH Technical Conference, pg 211-220, Oct 1991

FI32, P.S. Chua and M.R. Piggott, “The Glass Fibre-Polymer Interface: I - Theoretical Consideration For Single Fibre Pull-out Tests.”, Composites Science and Technology, V22 Elsevier Applied Science Publishers Ltd, England, pg 33-42, 1985

FI33, P.S. Chua and M.R. Piggott, “The Glass Fibre-Polymer Interface: II - Work Of Fracture And Shear Stresses.”, Composites Science and Technology, V22 Elsevier Applied Science Publishers Ltd, England, pg 107-119, 1985

FI34, P.S. Chua and M.R. Piggott, “The Glass Fibre-Polymer Interface: III - Pressure And Coefficient Of Fraction.”, Composites Science and Technology, V22 Elsevier Applied Science Publishers Ltd, England, pg 185-196, 1985

FI35, P.S. Chua and M.R. Piggott, “The Glass Fibre-Polymer Interface: IV - Controlled Shrinkage Polymers.”, Composites Science and Technology, V22 Elsevier Applied Science Publishers Ltd, England, pg 245-258, 1985

FI36, Linda S. Schadler, Juan C. Figueroa and Campbell Laird, “Interphase Behavior In Cyclic Fatigue Of Monofilament Composites.”, Mat. Res. Soc. Symp. Proc. V170, Materials Research Society, pg 345-350, 1990

FI37, Tao C. Chang and B.Z. Jang, “The Effects Of Fiber Surface Treatments By A Cold Plasma In Carbon Fiber/BMI Composites.”, Mat. Res. Soc. Symp. Proc. V170, Materials Research Society, pg 321-326, 1990

FI38, P.W. Yip and S.S.Lin, “Effect Of Surface Oxygen On Adhesion Of Carbon Fiber Reinforced Composites.”, Mat. Res. Soc. Symp. Proc. V170, Materials Research Society, pg 339-344, 1990

FI39, Umesh Gaur and Theodore Davidson, “Interfacial Effects Of Plasma Treatment On Fiber Pull-out.”, Mat. Res. Soc. Symp. Proc. V170, Materials Research Society, pg 309-314, 1990

FI40, Lawrence T. Drzal and Madhu S. Madhukar, “Fiber-Matrix adhesion And Its Effect On Composite Mechanical Properties: I. Inplane and Interlaminar Shear Behavior Of Graphite / Epoxy Composites.”, J. Compsoite Materials, V25, pg 932-957, Aug 1991

FI41, Lawrence T. Drzal and Madhu S. Madhukar, “Fiber-Matrix adhesion And Its Effect On Composite Mechanical Properties: II. Longitudinal (0) and Transverse (90) Tensile And Flexure Behavior Of Graphite / Epoxy Composites.”, J. Composite Materials, V25, pg 958-991, Aug 1991

FI42, Bor Z. Jang, “Control Of interfacial adhesion in continuous carbon and kevlar fiber reinforced polymer composites.”, Composites Science And Technology V44, 1992

FI43, K.Pannkoke, ”Experimental Evaluation Of Basic Material Data For Carbon Fibre Reinforced Plastics At 77K.”, Proceedings Of The International Conference On Composite Materials And Energy (Enercomp 95), Technomic Publishing Co., Lancaster Penn, pg 3-10, 8-10 May 1995

FI44, Frank Philip Bowden and David Tabor, FRICTION An Introduction to Tribology, Robert E. Krieger Publishing Co., Malabar FL, pg 1-178, 1982

FI45, Robert Savage, “Graphite Lubrication”, J. Of Applied Physics, V19, #1, pg 1-10, Jan 1948

FI46, A.H.Cottrel, “Strong Solids”, Proceedings Of The Royal Society Of London Series A Mathematical And Physical Sciences, V282, pg 2-9, Dec 1964

FI47, B.Gershon and G.Maron, “Fracture toughness and mechanical properties of glass fibre-epoxy composites.”, J. Materials Science, V10, pg 1549-1556, 1975

FI48, B.Harris, J.Morley and D.C.Phillips, “Fracture mechanisms in glass-reinforced plastics.”, J. Materials Science, V10, pg 2050-2061, 1975

FI49, P.B.Bowden, “The effect of hydrostatic pressure on the fibre-matrix bond in a steel-resin model composite.”, J. Materials Science, V5, pg 517-520, 1970

FI50, J.N.Kirk, M.Munro and P.W.R.Beaumont, “The fracture energy of hybrid carbon and glass fibre composites.”, J. Materials Science, V13, pg 2197-2204, 1978

Appendix: Residuals: Specimens Remaining In The Cup

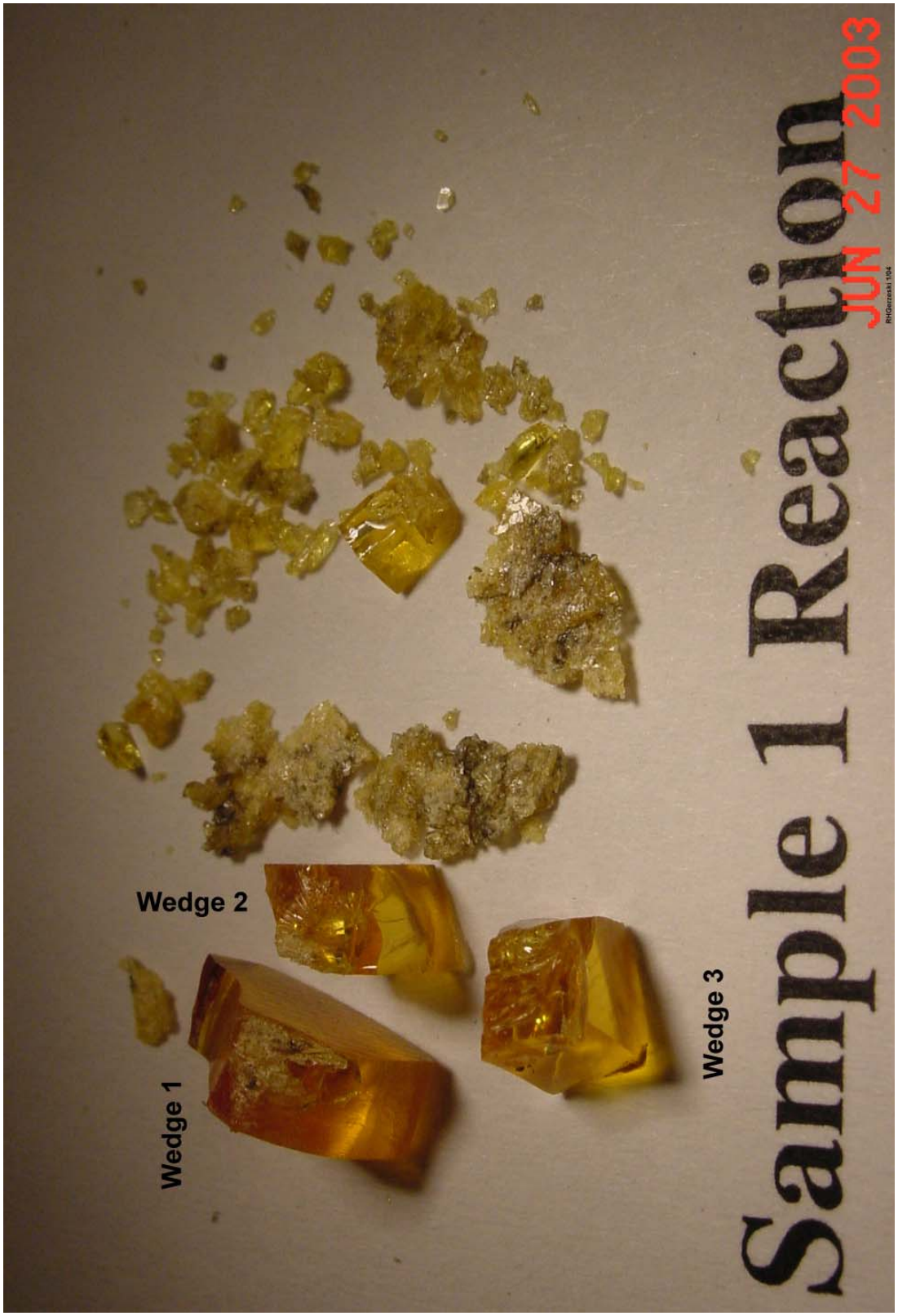


Figure R1a 5250-4 RTM D2512 72 FtLb LOX Tested Specimen Residuals

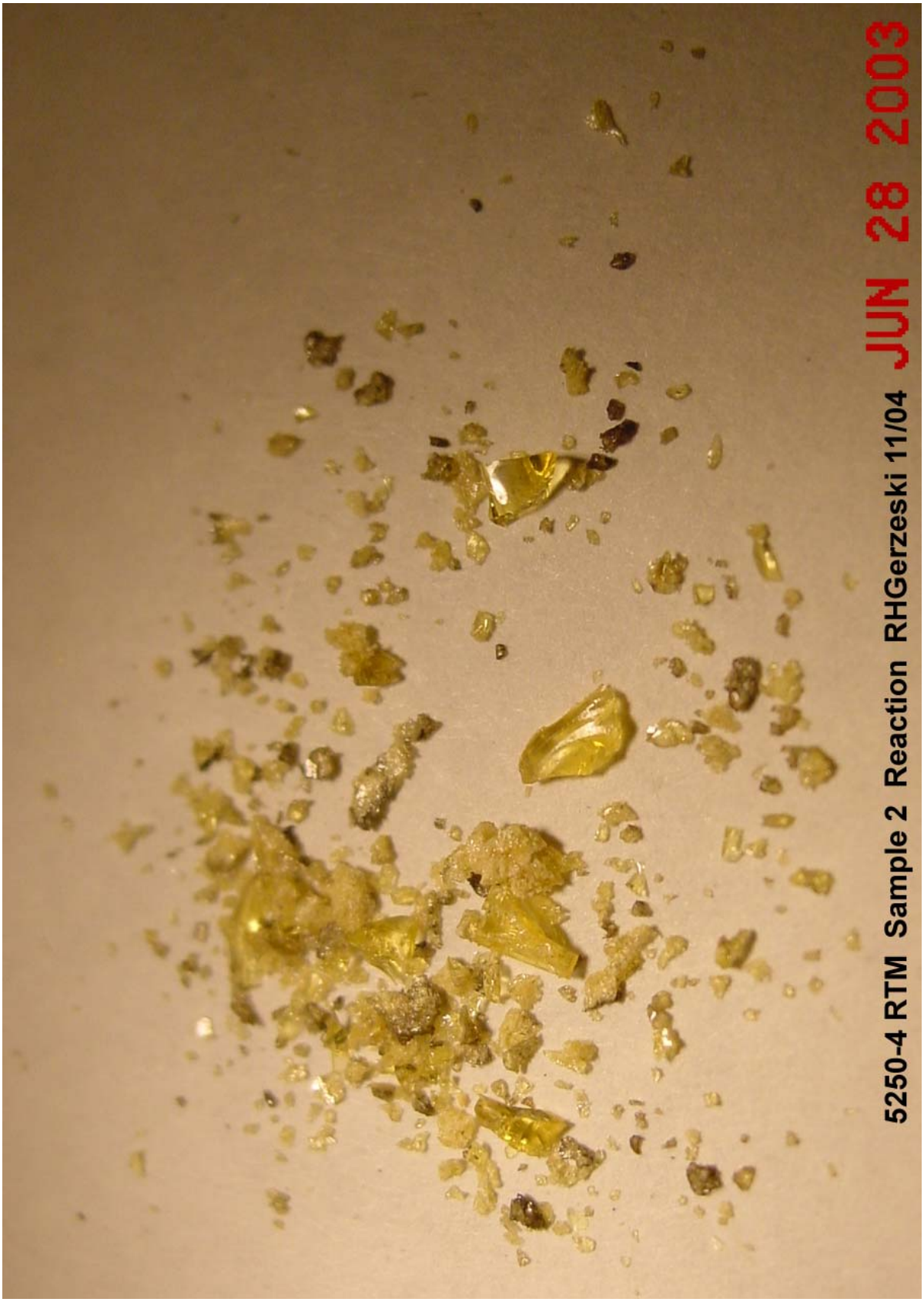


Figure R1b 5250-4 RTM D2512 72 FtLb LOX Tested Specimen Residuals



Figure R1c 5250-4 RTM D2512 72 FtLb LOX Tested Specimen Residuals



Figure R1d 5250-4 RTM D2512 72 FtLb LOX Tested Specimen Residuals



Figure R1e 5250-4 RTM D2512 72 FtLb LOX Tested Specimen Residuals



Figure R1f 5250-4 RTM D2512 72 FtLb LOX Tested Specimen Residuals



Figure R1g 5250-4 RTM D2512 72 FtLb LOX Tested Specimen Residuals



Figure R1h 5250-4 RTM D2512 72 FtLb LOX Tested Specimen Residuals



Figure R1i 5250-4 RTM D2512 72 FtLb LOX Tested Specimen Residuals

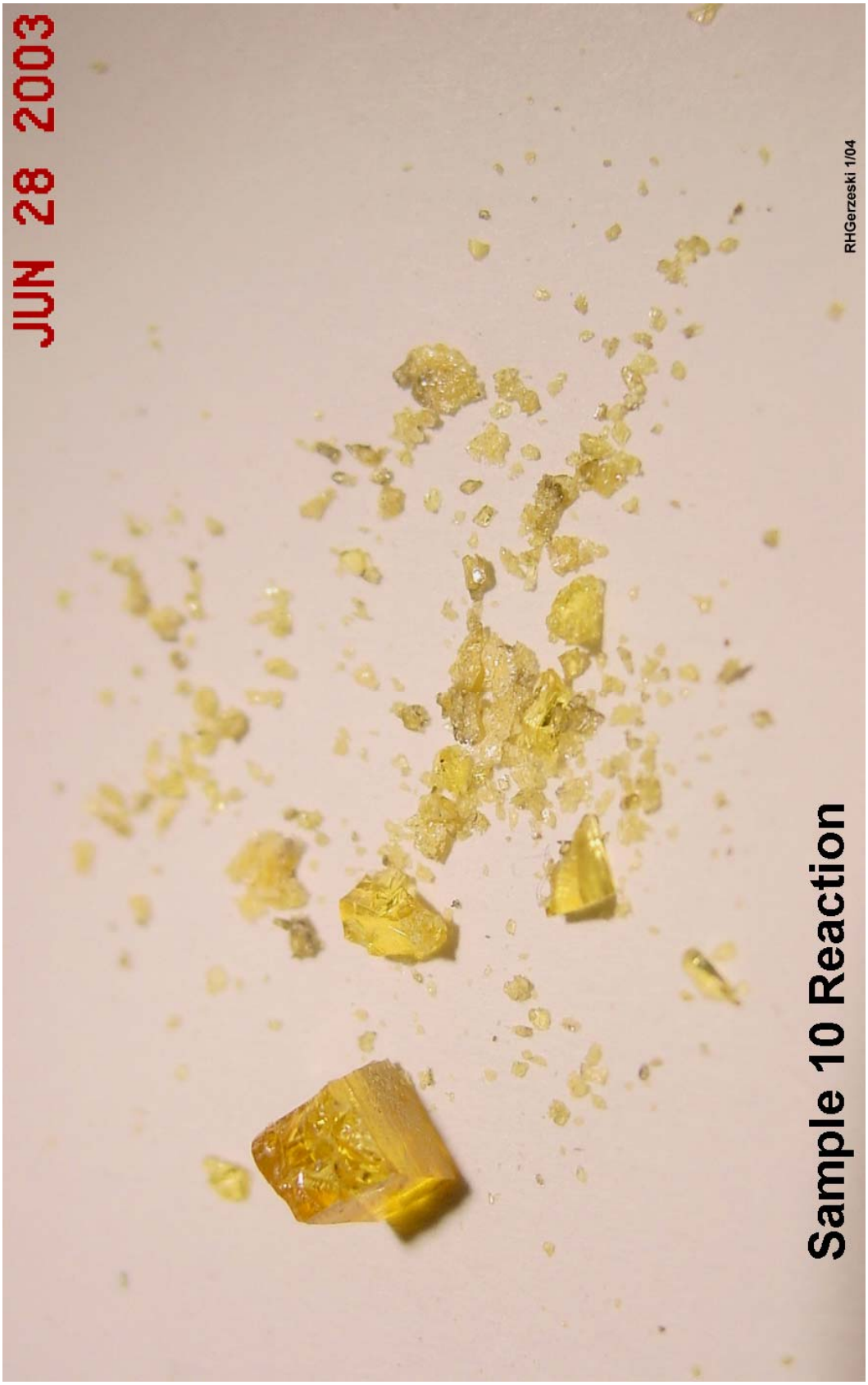


Figure R1j 5250-4 RTM D2512 72 FtLb LOX Tested Specimen Residuals



Figure R1k 5250-4 RTM D2512 72 FtLb LOX Tested Specimen Residuals

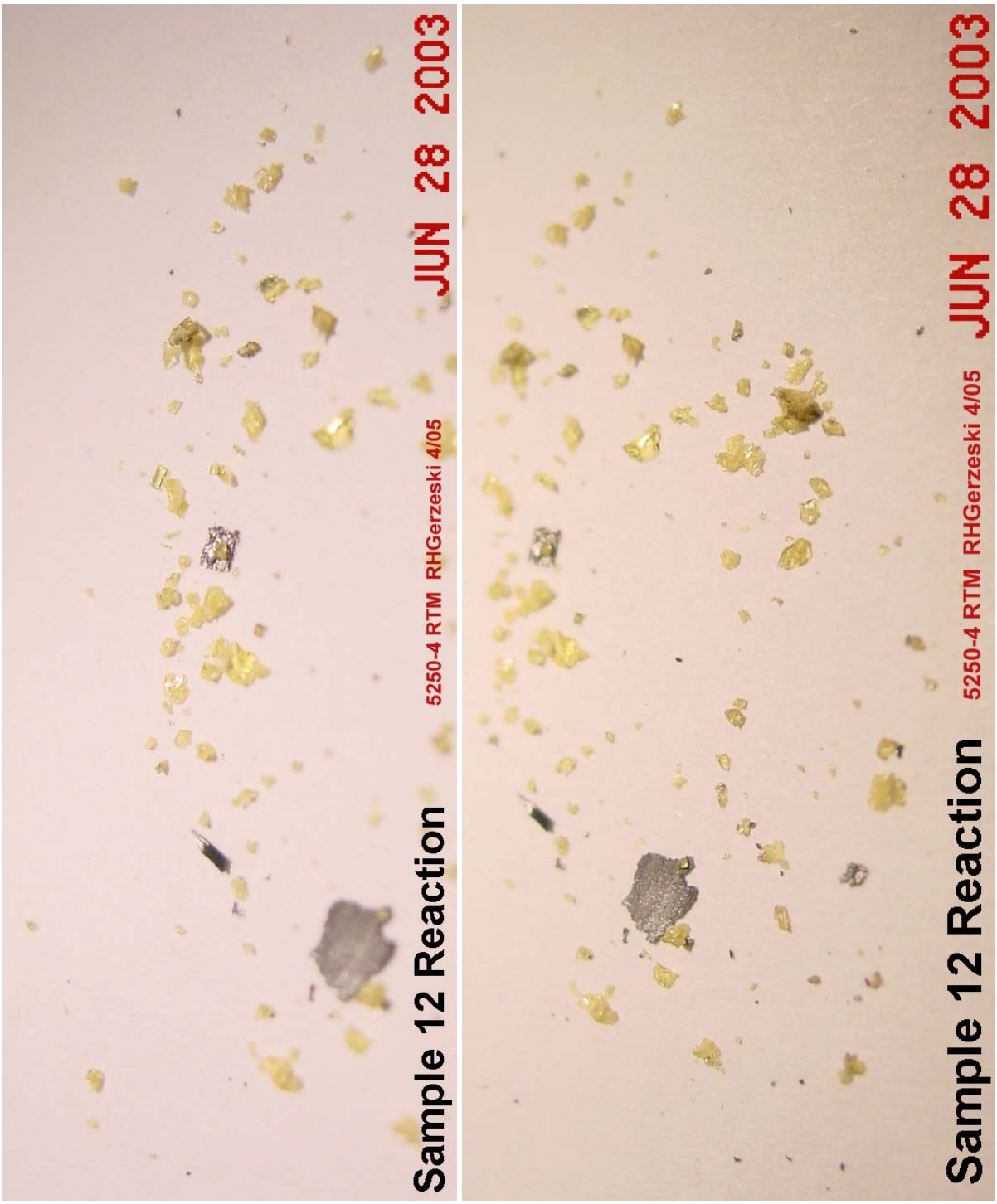


Figure R1l 5250-4 RTM D2512 72 FtLb LOX Tested Specimen Residuals



Figure R1m 5250-4 RTM D2512 72 FtLb LOX Tested Specimen Residuals



Figure R1n 5250-4 RTM D2512 72 FtLb LOX Tested Specimen Residuals



Figure R1o 5250-4 RTM D2512 72 FtLb LOX Tested Specimen Residuals



Figure R1p 5250-4 RTM D2512 72 FtLb LOX Tested Specimen Residuals

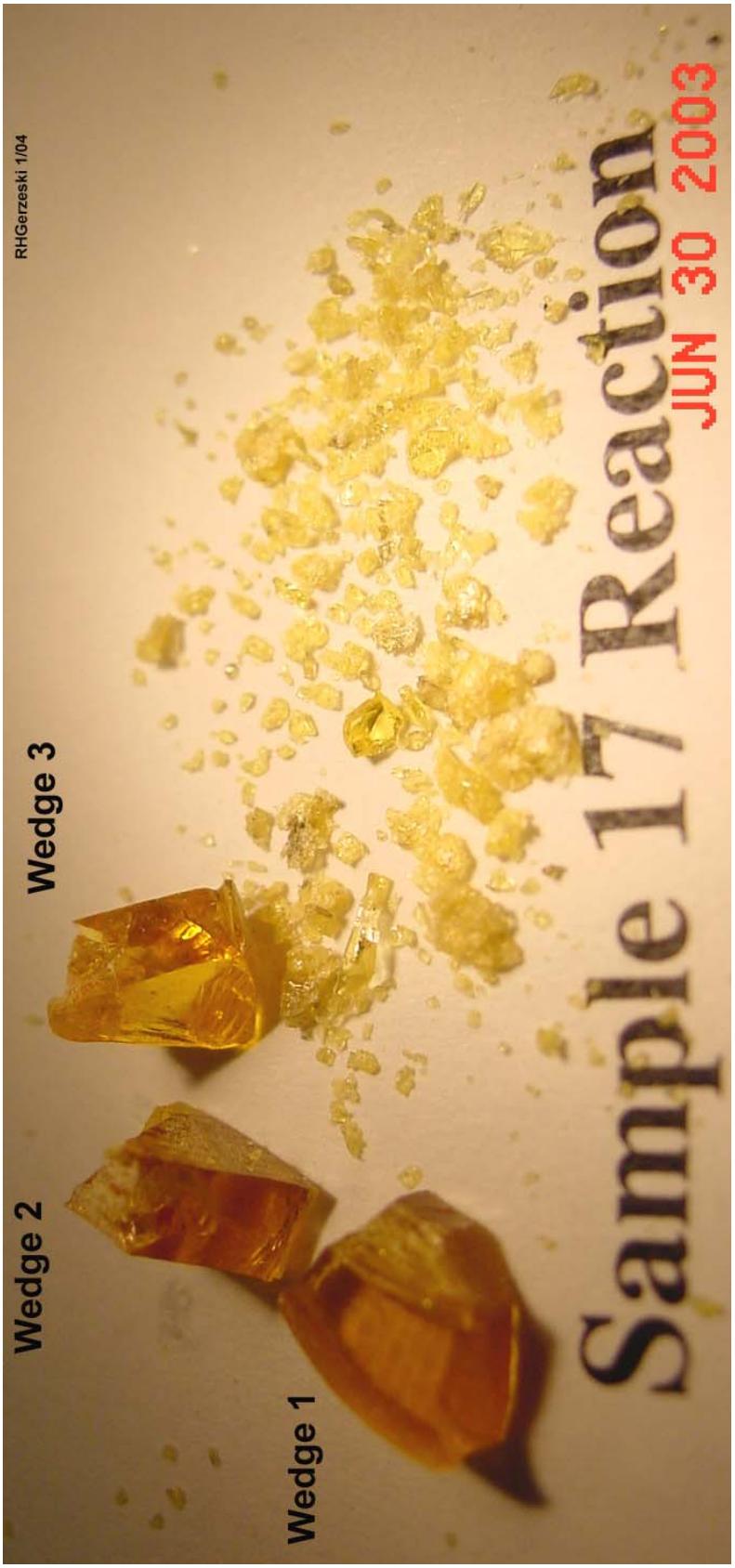


Figure R1q 5250-4 RTM D2512 72 FtLb LOX Tested Specimen Residuals



Figure R1r 5250-4 RTM D2512 72 FtLb LOX Tested Specimen Residuals



Figure R1s 5250-4 RTM D2512 72 FtLb LOX Tested Specimen Residuals



Figure R1t-i 5250-4 RTM D2512 72 FtLb LOX Tested Specimen Residuals



Figure R1t-ii 5250-4 RTM D2512 72 FtLb LOX Tested Specimen Residuals

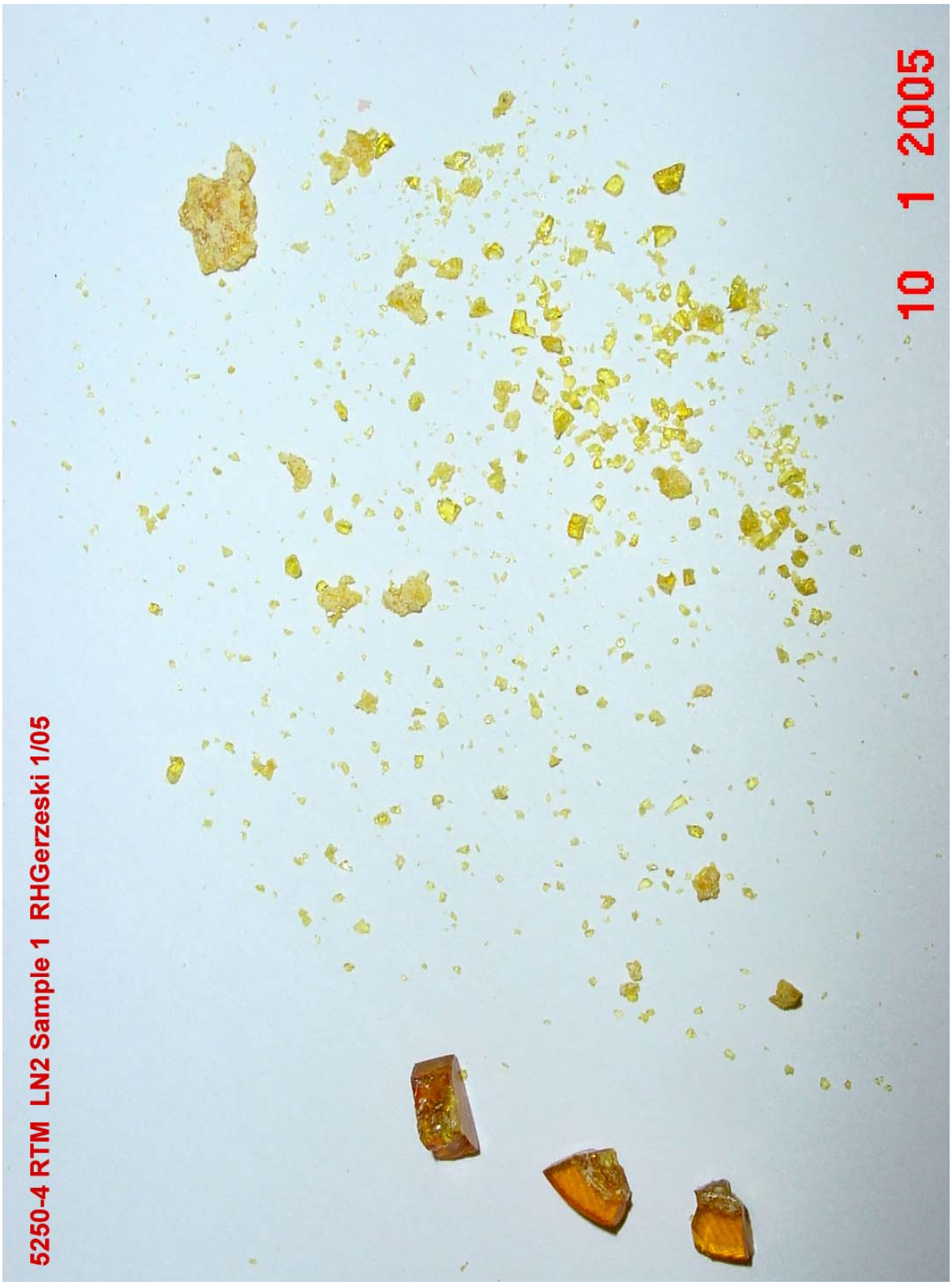


Figure R2a-i 5250-4 RTM D2512 72 FtLb In LN2 Tested Specimen Residuals



Figure R2a-ii 5250-4 RTM D2512 72 FtLb In LN2 Tested Specimen Residuals

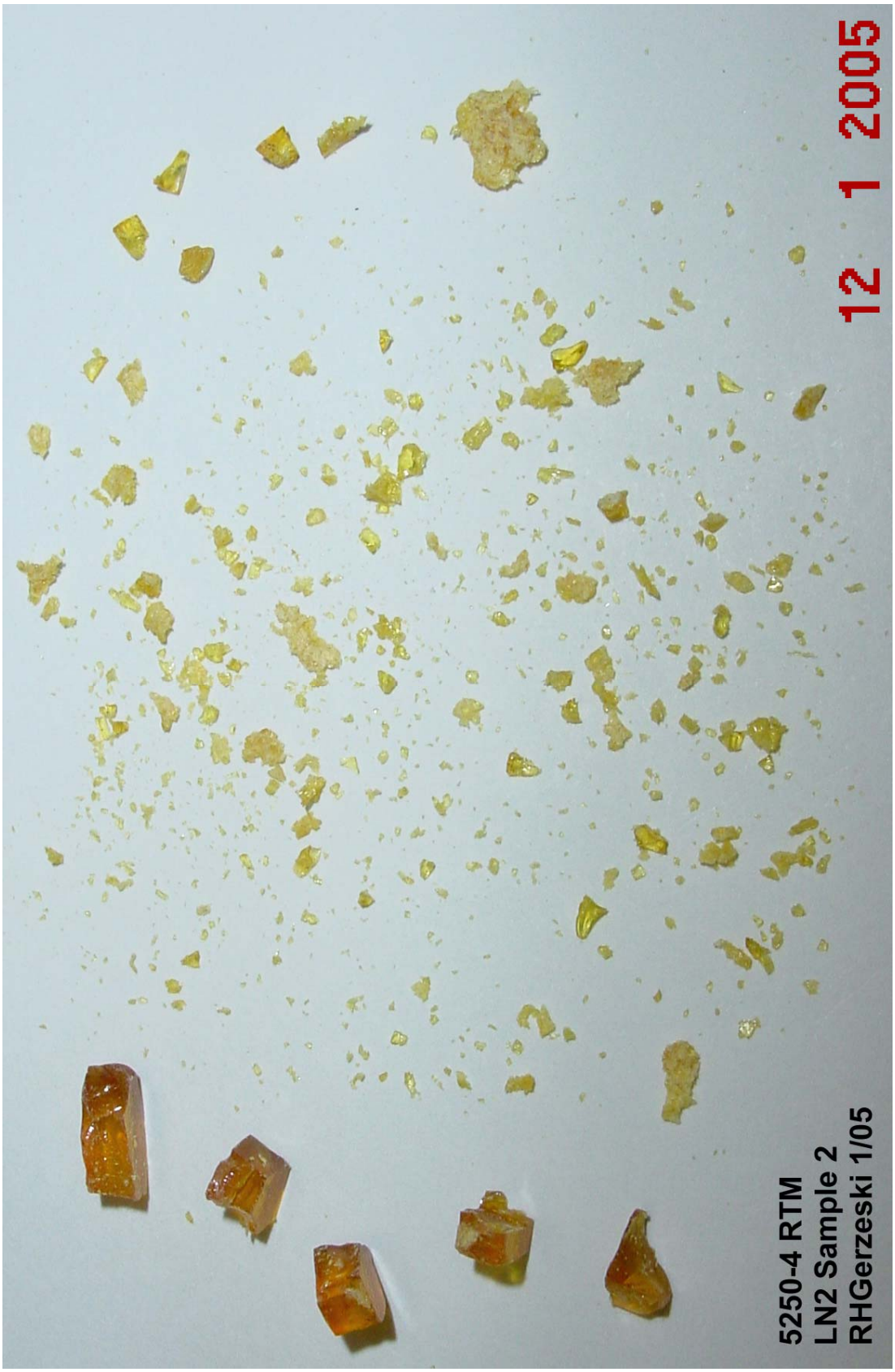


Figure R2b-i 5250-4 RTM D2512 72 FtLb In LN2 Tested Specimen Residuals

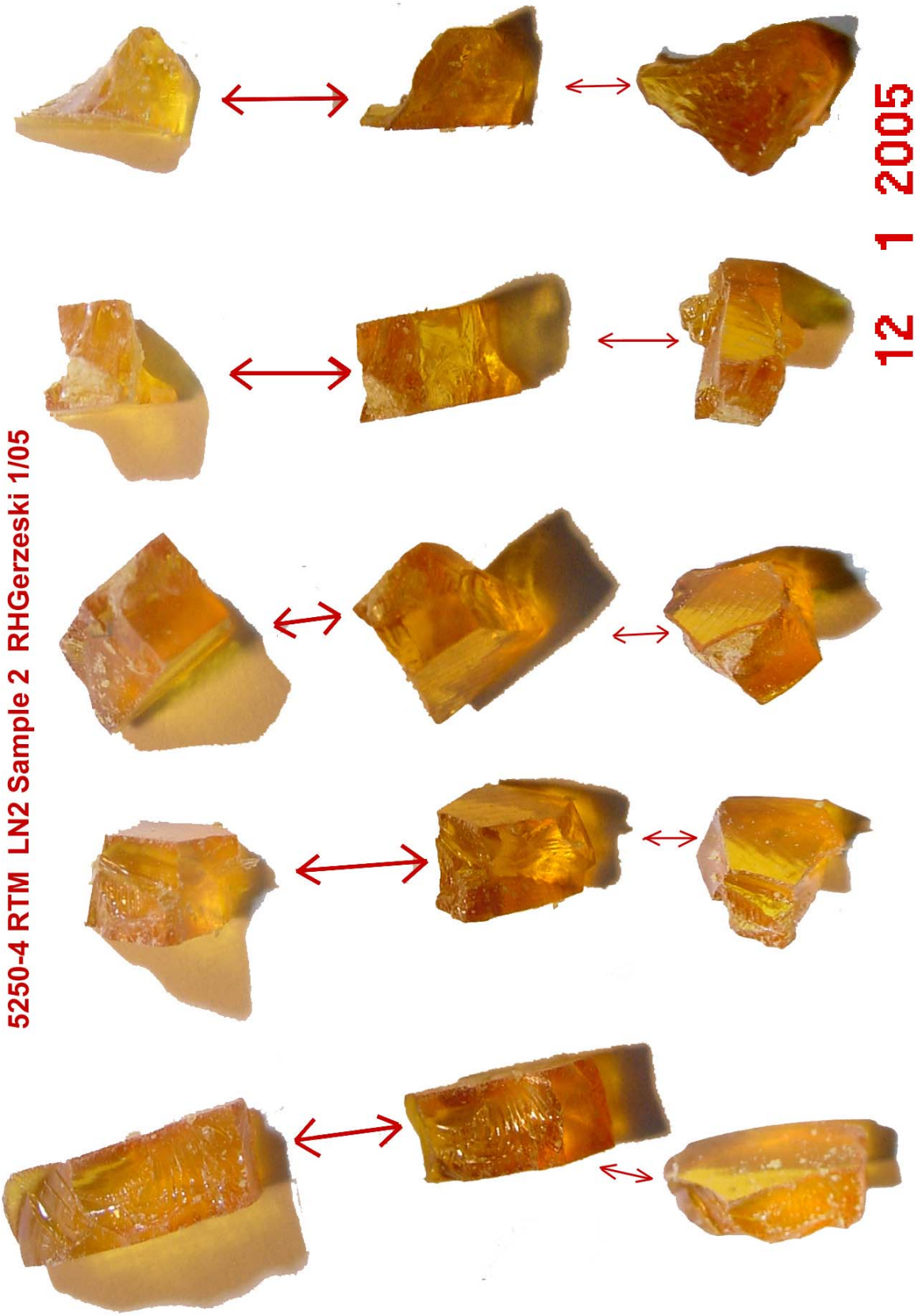


Figure R2b-ii 5250-4 RTM D2512 72 FtLb In LN2 Tested Specimen Residuals

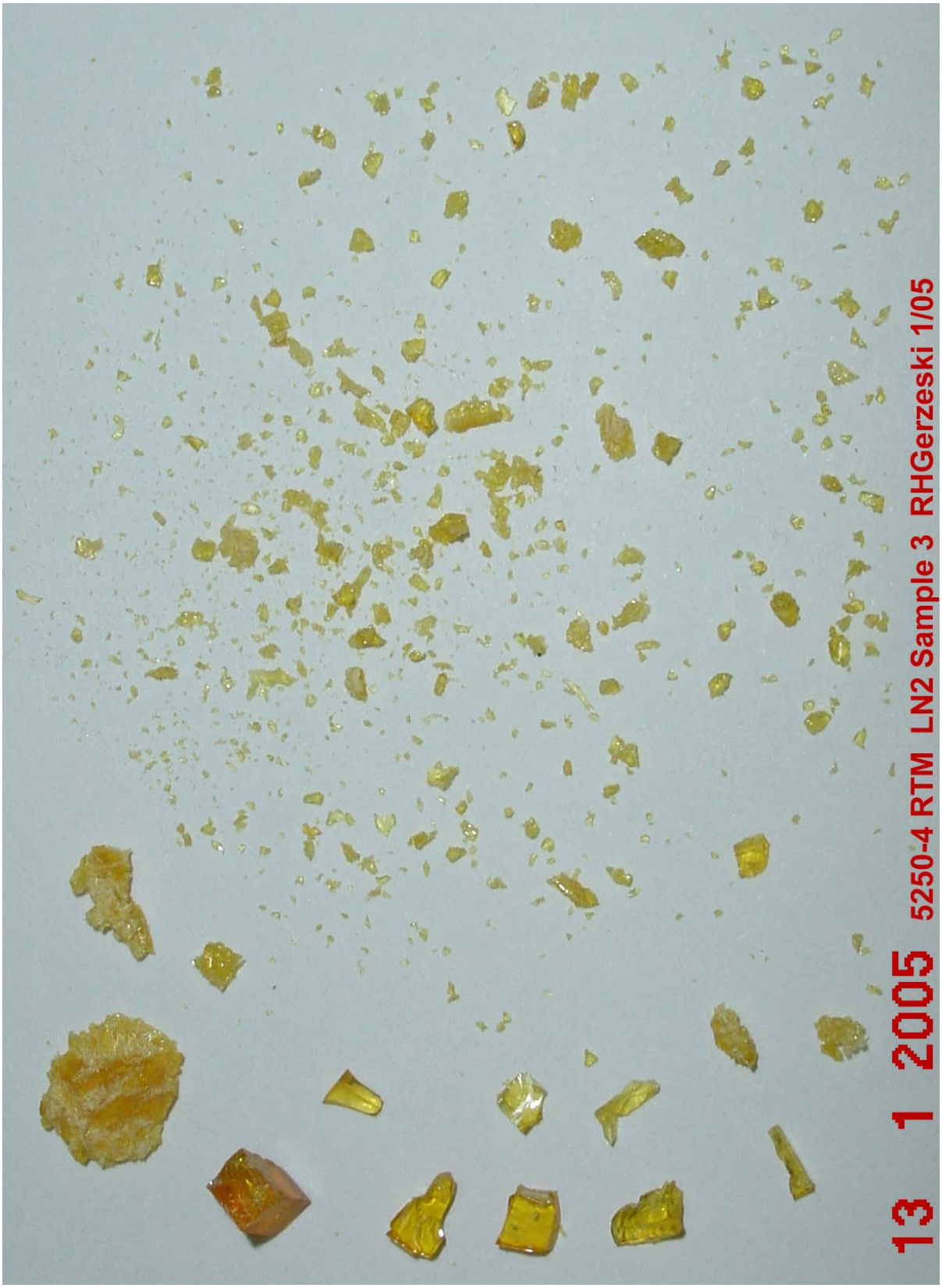


Figure R2c-i 5250-4 RTM D2512 72 FtLb In LN2 Tested Specimen Residuals

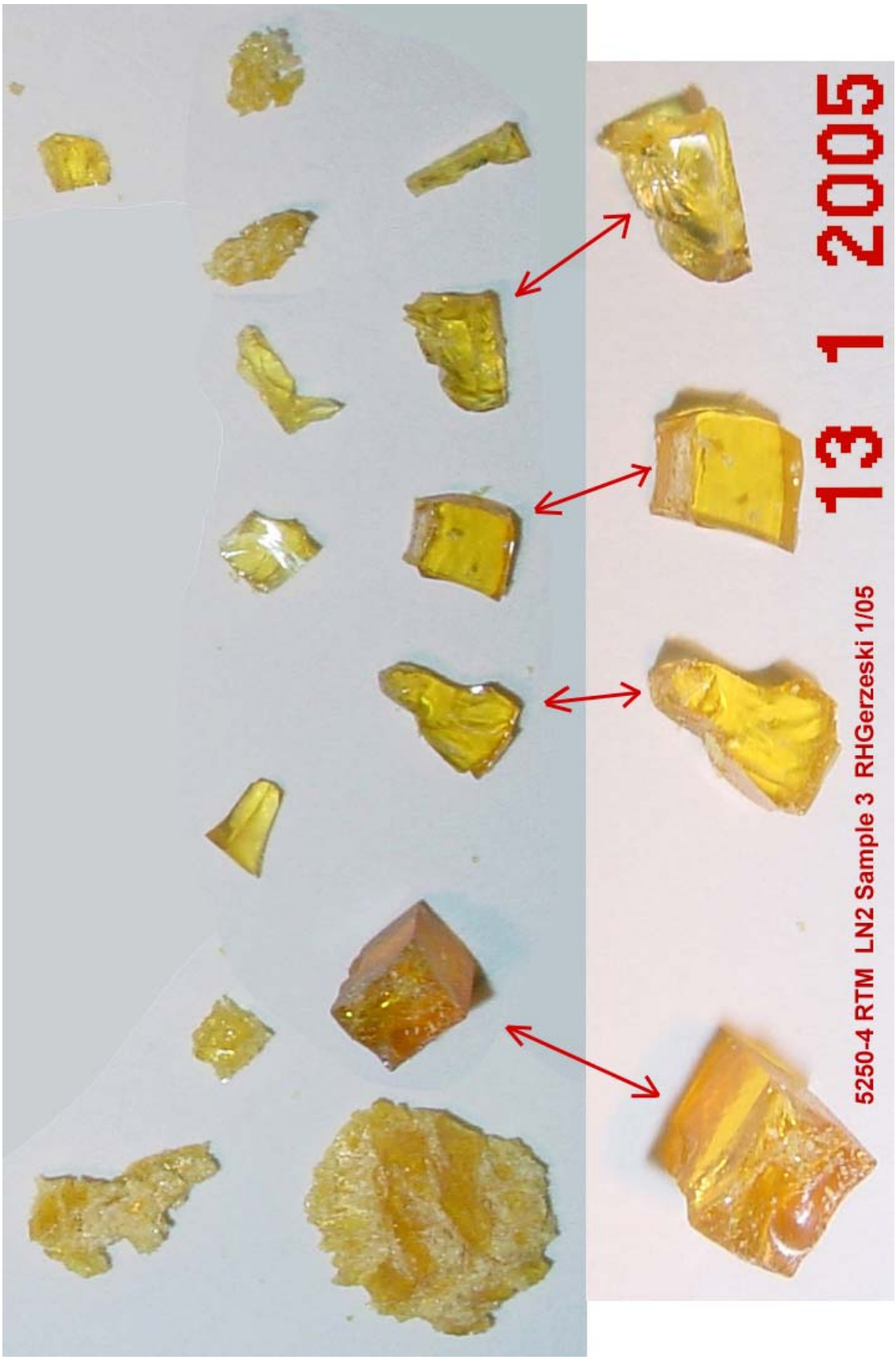


Figure R2c-ii 5250-4 RTM D2512 72 FtLb In LN2 Tested Specimen Residuals



Figure R3a T650-35–UC309 / 5250-4 RTM D2512 72 FtLb LOX Tested Specimen Residuals

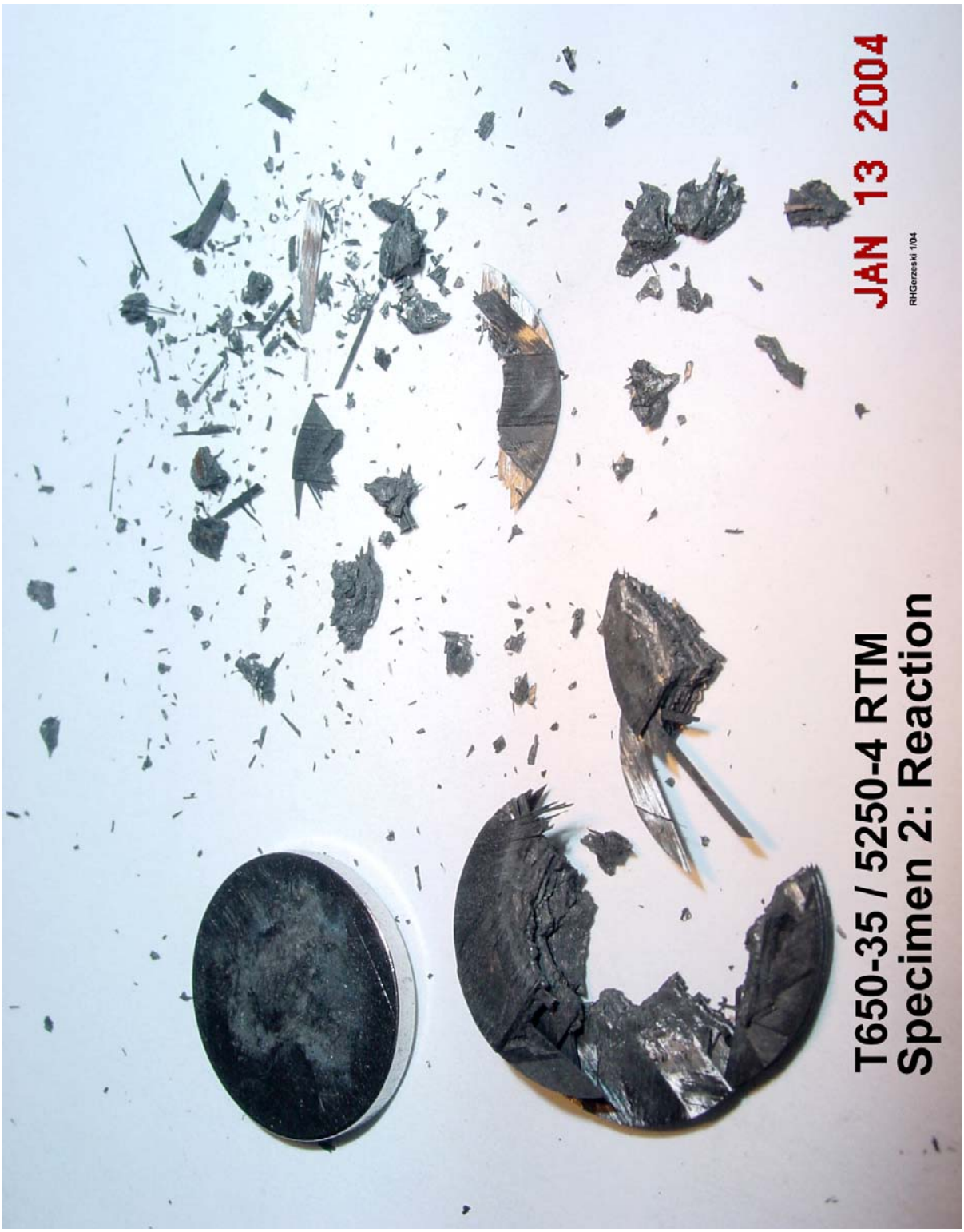


Figure R3b T650-35–UC309 / 5250-4 RTM D2512 72 FtLb LOX Tested Specimen Residuals



Figure R3c T650-35–UC309 / 5250-4 RTM D2512 72 FtLb LOX Tested Specimen Residuals

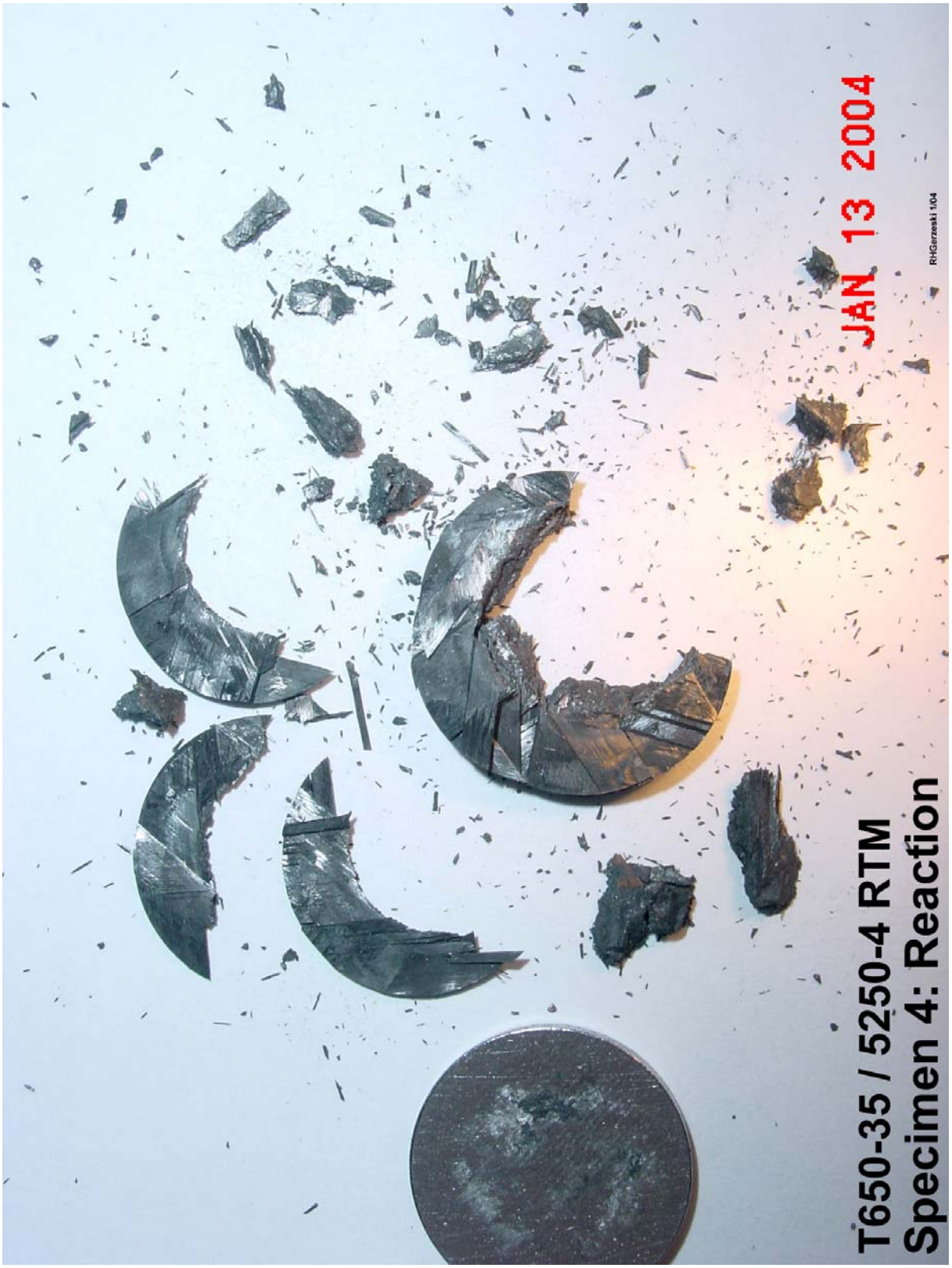


Figure R3d T650-35–UC309 / 5250-4 RTM D2512 72 FtLb LOX Tested Specimen Residuals



Figure R3e T650-35–UC309 / 5250-4 RTM D2512 72 FtLb LOX Tested Specimen Residuals

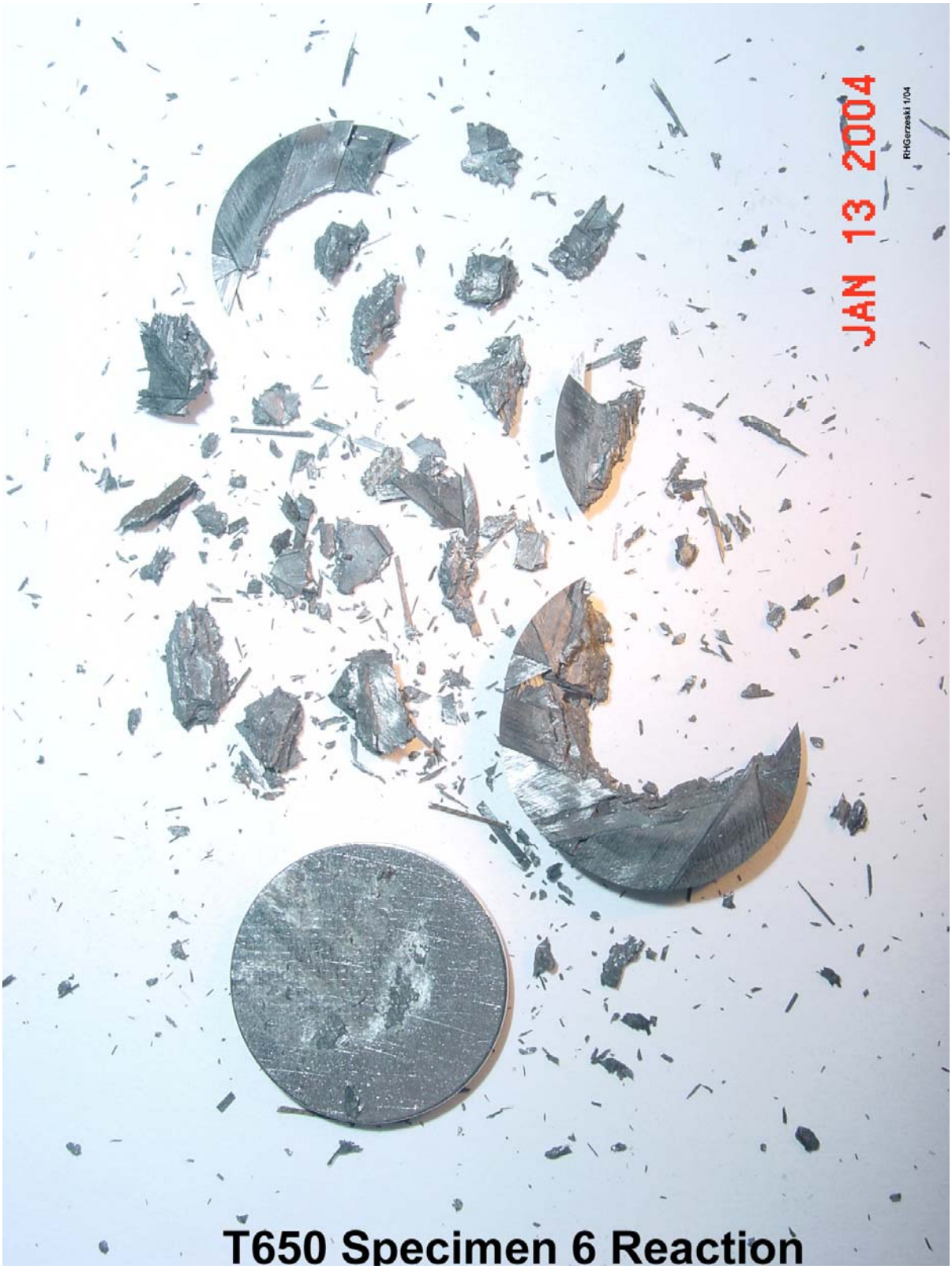


Figure R3f T650-35–UC309 / 5250-4 RTM D2512 72 FtLb LOX Tested Specimen Residuals



Figure R3g T650-35–UC309 / 5250-4 RTM D2512 72 FtLb LOX Tested Specimen Residuals

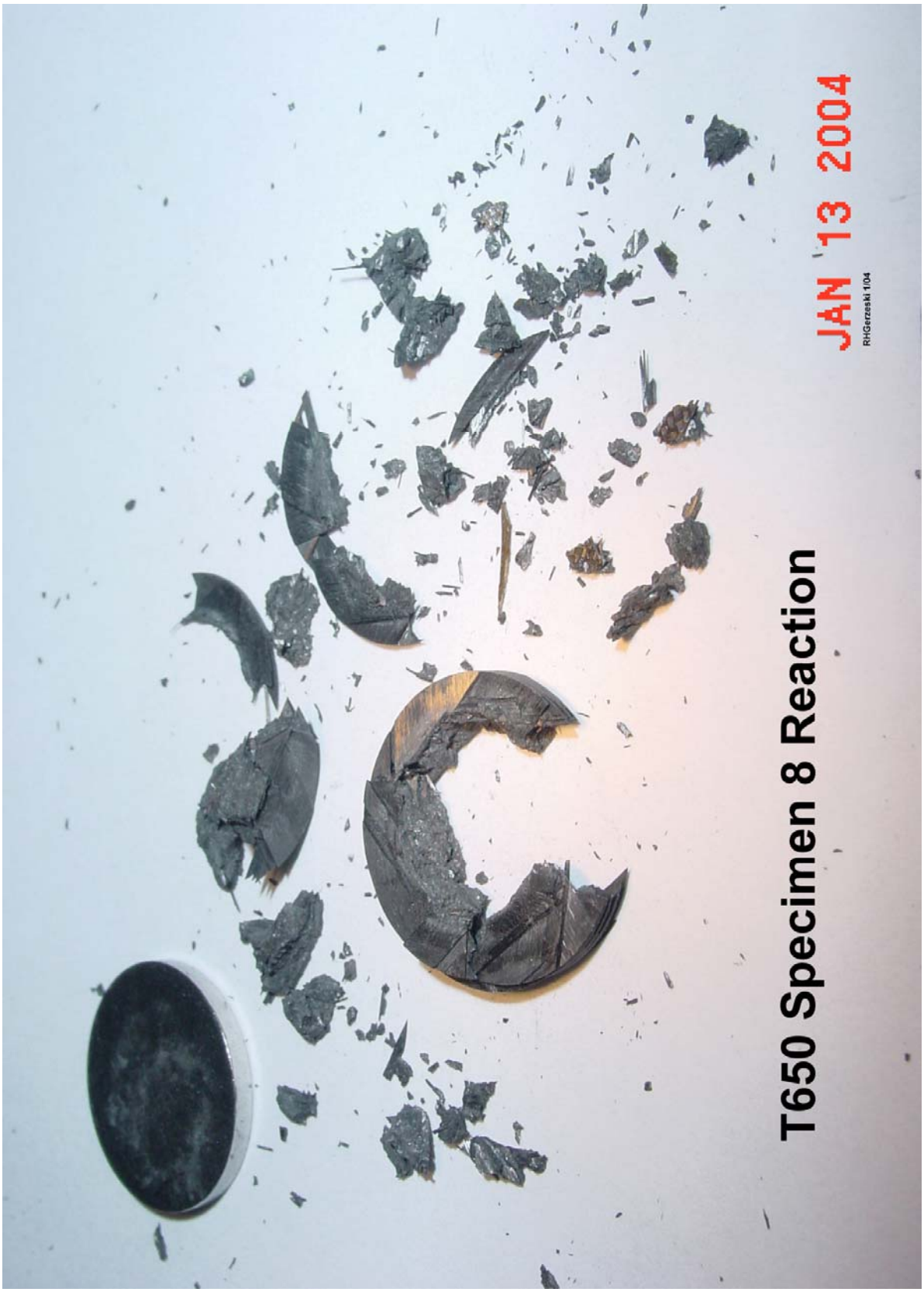


Figure R3h T650-35–UC309 / 5250-4 RTM D2512 72 FtLb LOX Tested Specimen Residuals

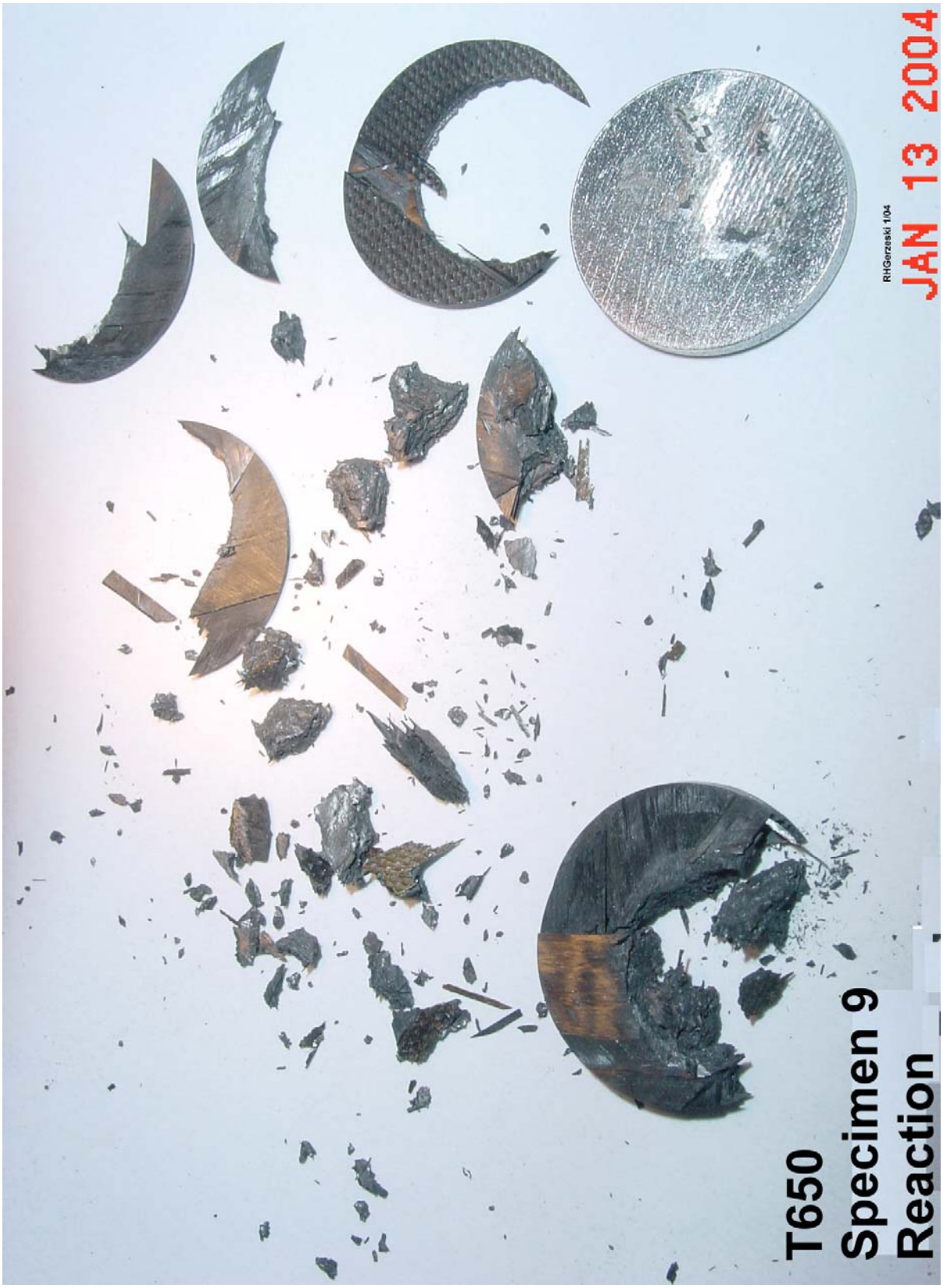


Figure R3i T650-35–UC309 / 5250-4 RTM D2512 72 FtLb LOX Tested Specimen Residuals



Figure R3j T650-35–UC309 / 5250-4 RTM D2512 72 FtLb LOX Tested Specimen Residuals

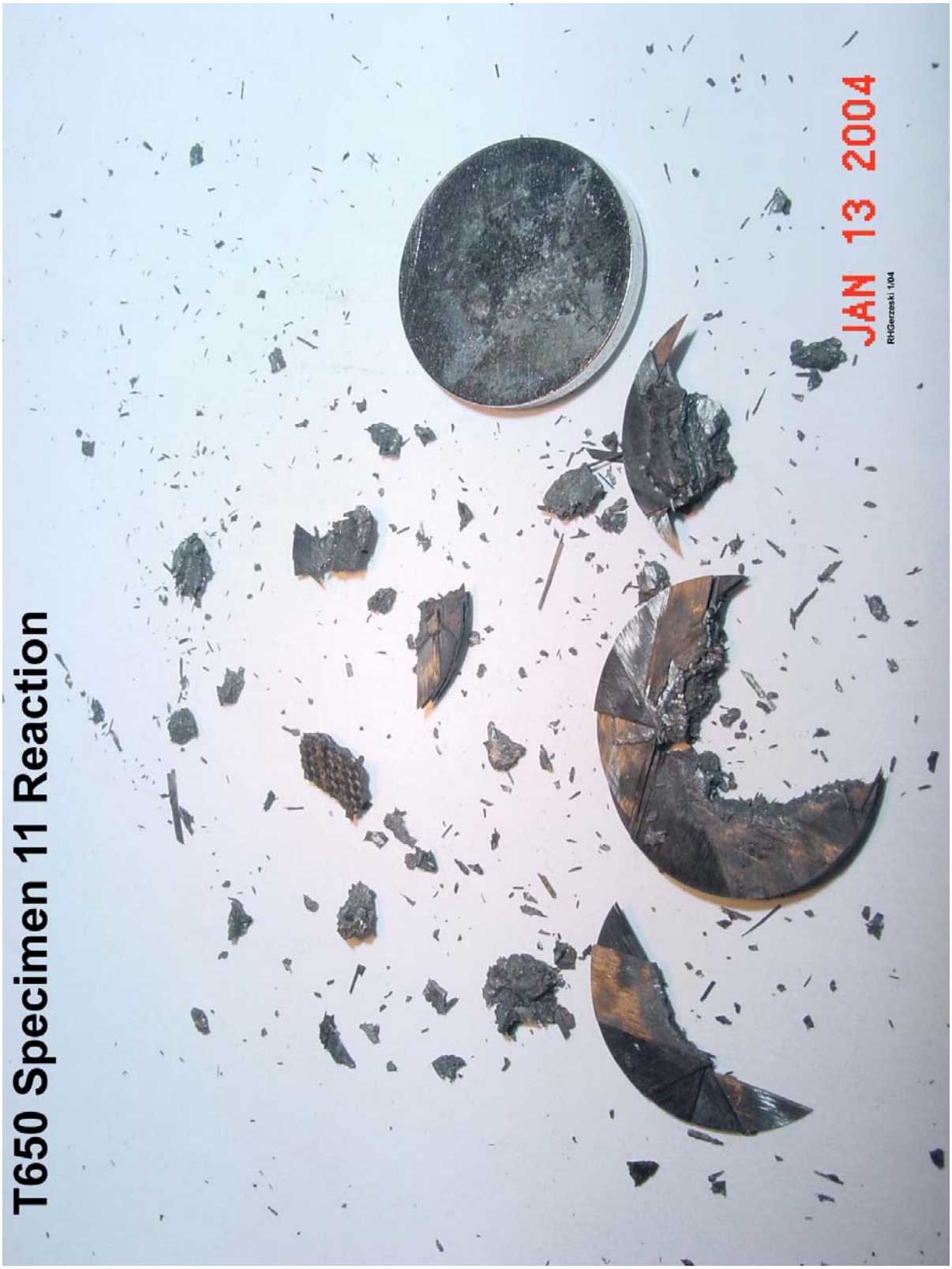


Figure R3k T650-35–UC309 / 5250-4 RTM D2512 72 FtLb LOX Tested Specimen Residuals



Figure R3l T650-35–UC309 / 5250-4 RTM D2512 72 FtLb LOX Tested Specimen Residuals



Figure R3m T650-35–UC309 / 5250-4 RTM D2512 72 FtLb LOX Tested Specimen Residuals



Figure R3n T650-35–UC309 / 5250-4 RTM D2512 72 FtLb LOX Tested Specimen Residuals



Figure R3o T650-35–UC309 / 5250-4 RTM D2512 72 FtLb LOX Tested Specimen Residuals



Figure R3p T650-35–UC309 / 5250-4 RTM D2512 72 FtLb LOX Tested Specimen Residuals

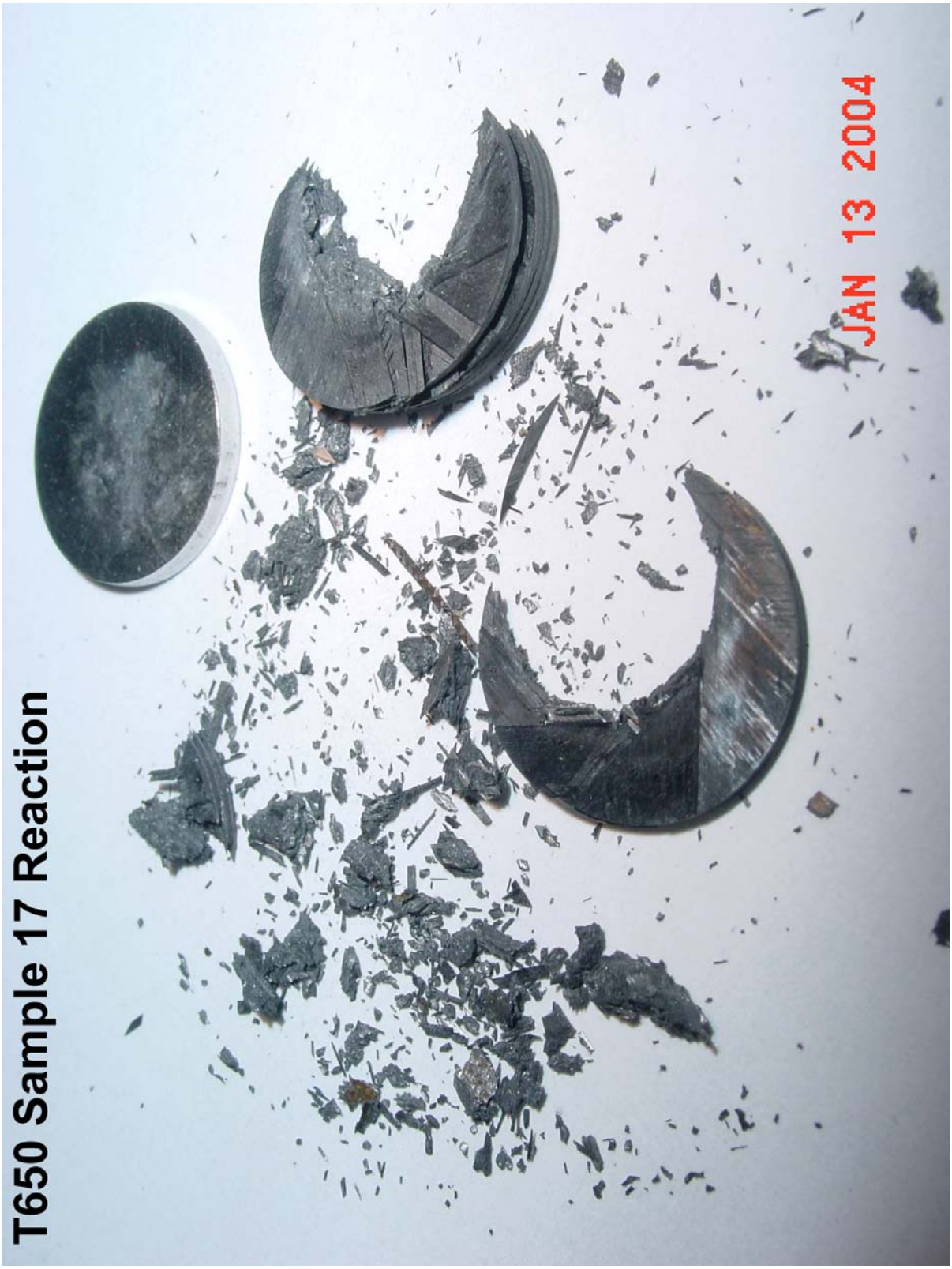


Figure R3q T650-35-UC309 / 5250-4 RTM D2512 72 FtLb LOX Tested Specimen Residuals



Figure R3r T650-35-UC309 / 5250-4 RTM D2512 72 FtLb LOX Tested Specimen Residuals



Figure R3s T650-35-UC309 / 5250-4 RTM D2512 72 FtLb LOX Tested Specimen Residuals



Figure R3t T650-35-UC309 / 5250-4 RTM D2512 72 FtLb LOX Tested Specimen Residuals

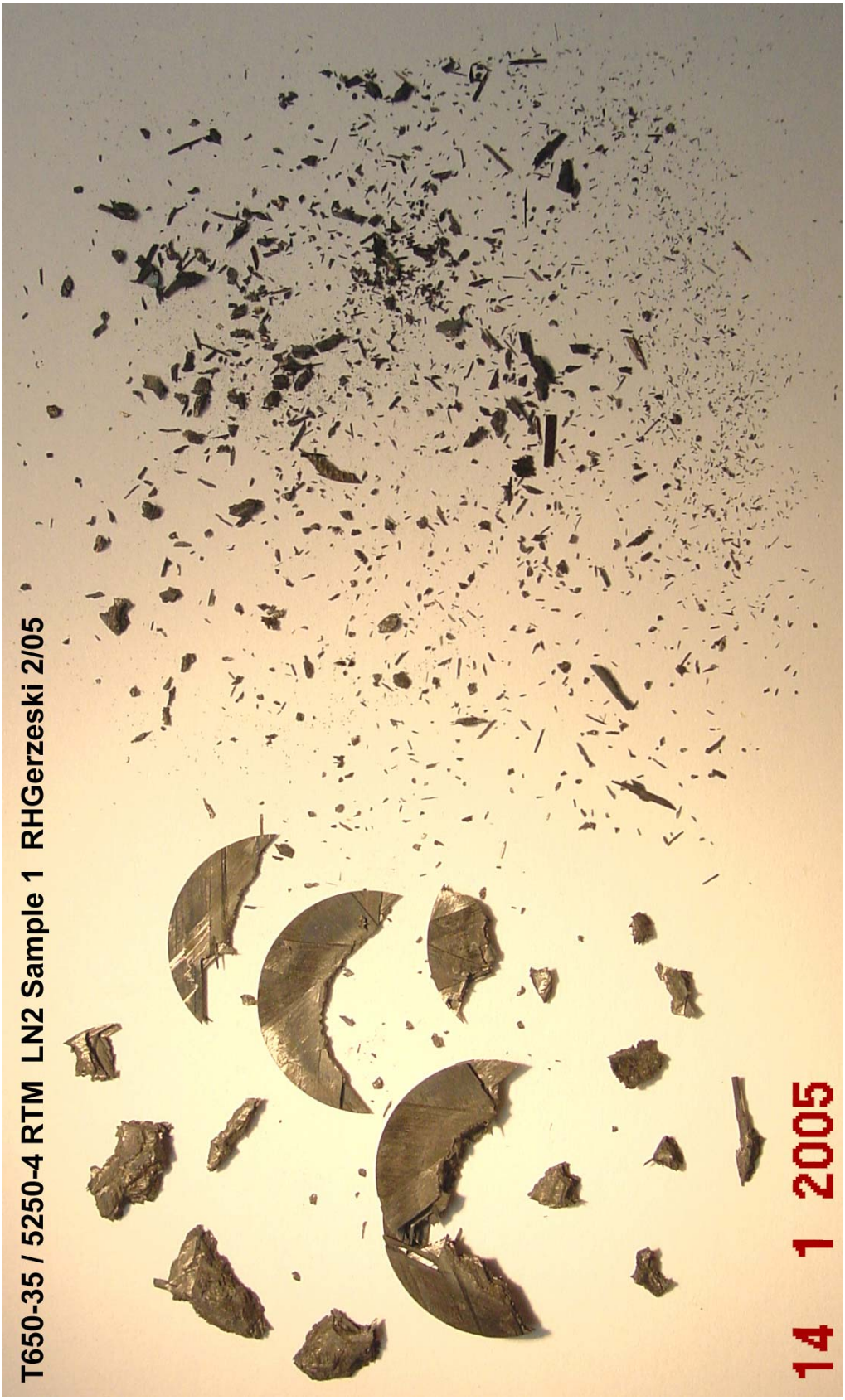


Figure R4a-i T650-35-UC309 / 5250-4 RTM D2512 72 FtLb In LN2 Tested Specimen Residuals

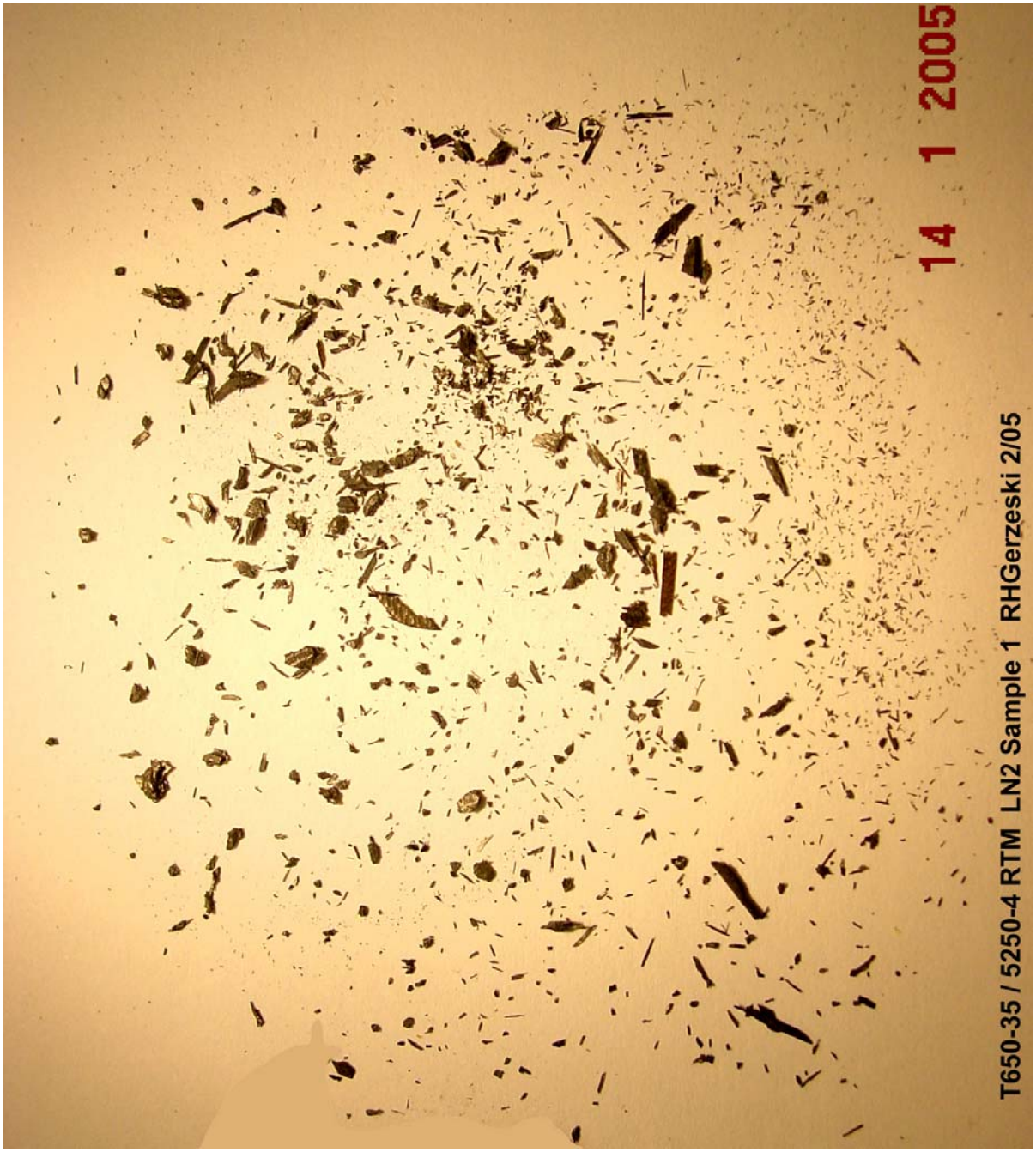


Figure R4a-ii T650-35-UC309 / 5250-4 RTM D2512 72 FtLb In LN2 Tested Specimen Residuals

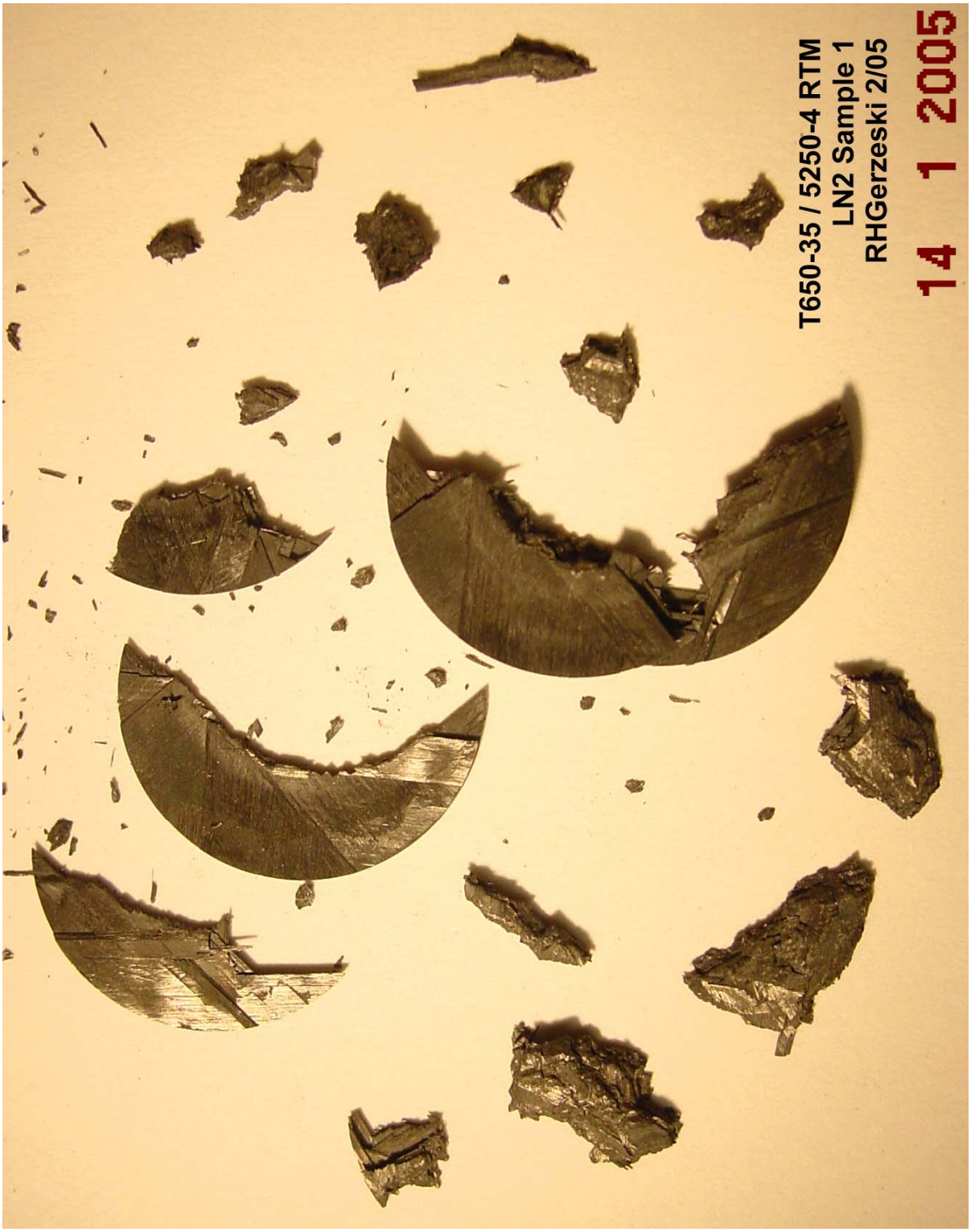


Figure R4a-iii T650-35-UC309 / 5250-4 RTM D2512 72 FtLb In LN2 Tested Specimen Residuals



Figure R4b-i T650-35-UC309 / 5250-4 RTM D2512 72 FtLb In LN2 Tested Specimen Residuals



Figure R4b-ii T650-35-UC309 / 5250-4 RTM D2512 72 FtLb In LN2 Tested Specimen Residuals



Figure R4c-i T650-35-UC309 / 5250-4 RTM D2512 72 FtLb In LN2 Tested Specimen Residuals



Figure R4c-ii T650-35-UC309 / 5250-4 RTM D2512 72 FtLb In LN2 Tested Specimen Residuals



Figure R5a YSH50A / 5250-4 RTM D2512 72 FtLb LOX Tested Specimen Residuals



Figure R5b YSH50A / 5250-4 RTM D2512 72 FtLb LOX Tested Specimen Residuals

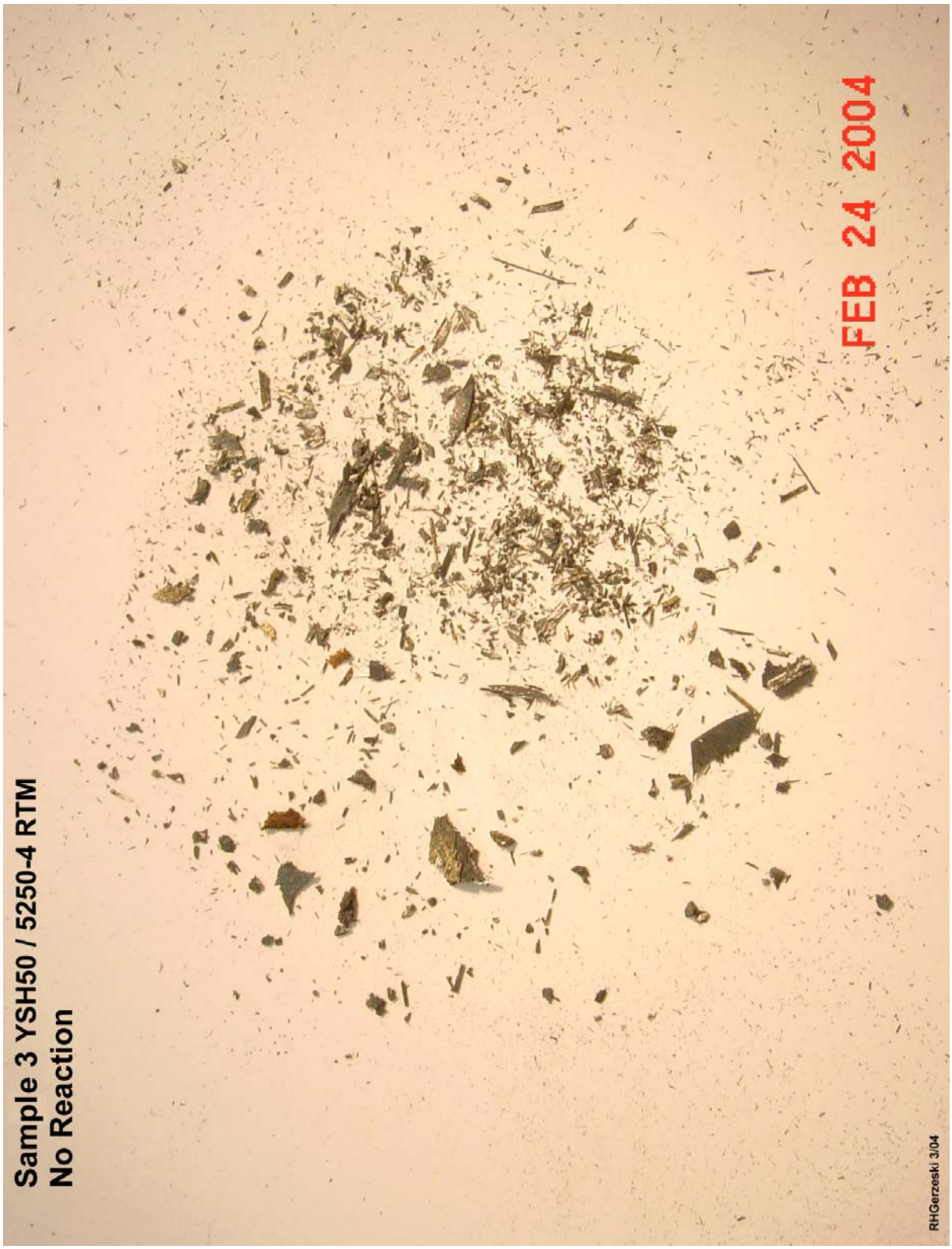


Figure R5c YSH50A / 5250-4 RTM D2512 72 FtLb LOX Tested Specimen Residuals

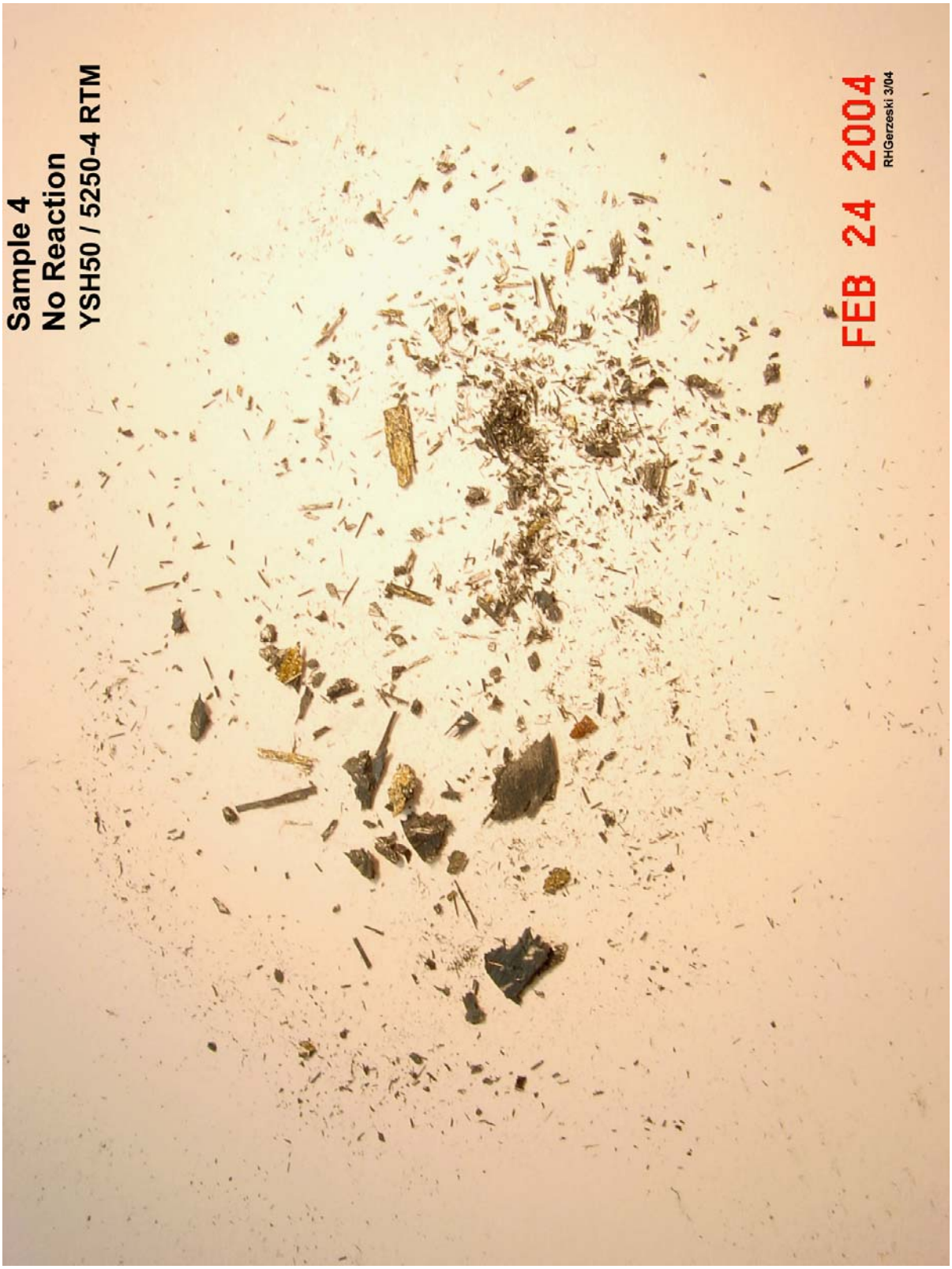


Figure R5d YSH50A / 5250-4 RTM D2512 72 FtLb LOX Tested Specimen Residuals



Figure R5e YSH50A / 5250-4 RTM D2512 72 FtLb LOX Tested Specimen Residuals

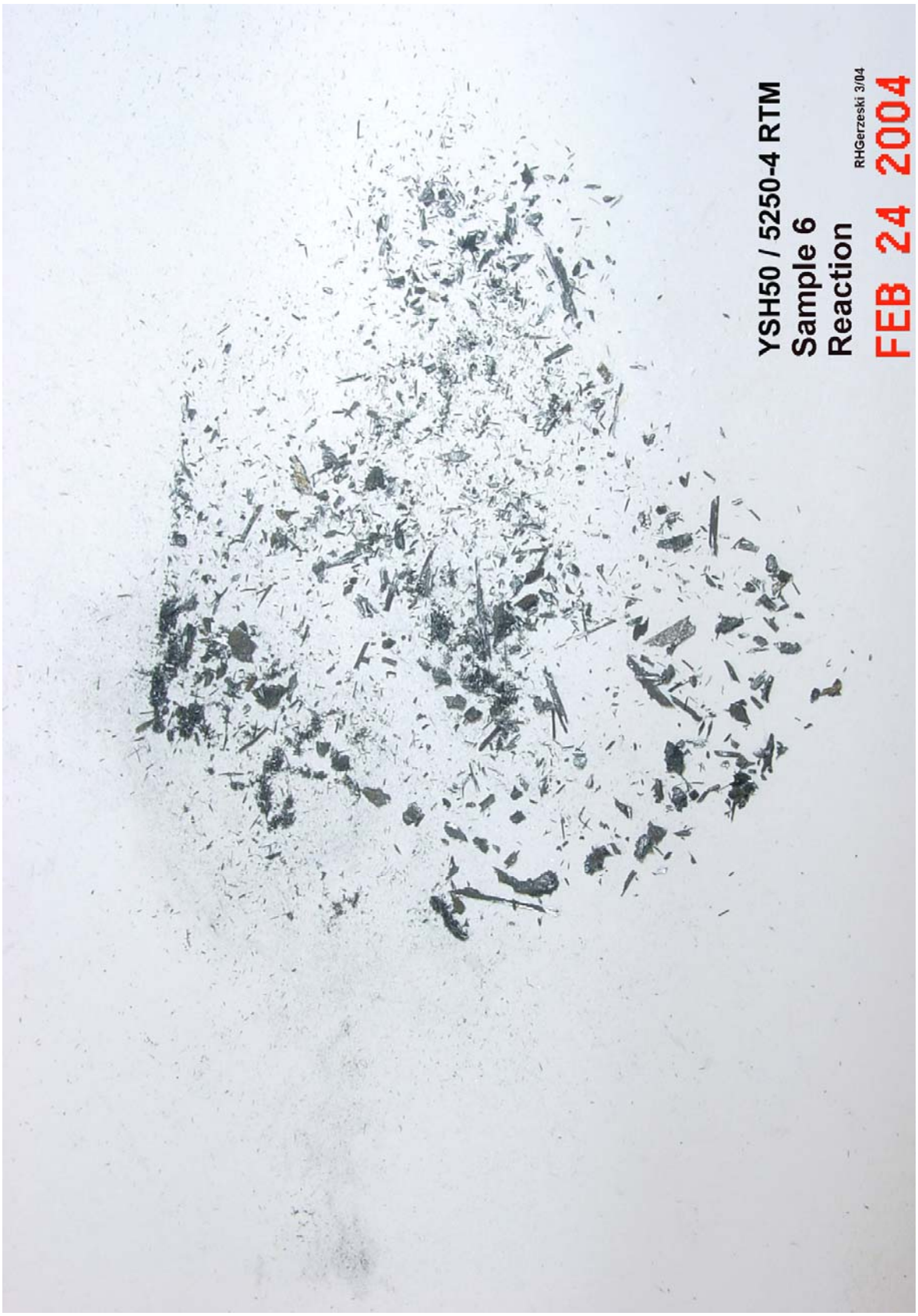


Figure R5f YSH50A / 5250-4 RTM D2512 72 FtLb LOX Tested Specimen Residuals



Figure R5g YSH50A / 5250-4 RTM D2512 72 FtLb LOX Tested Specimen Residuals

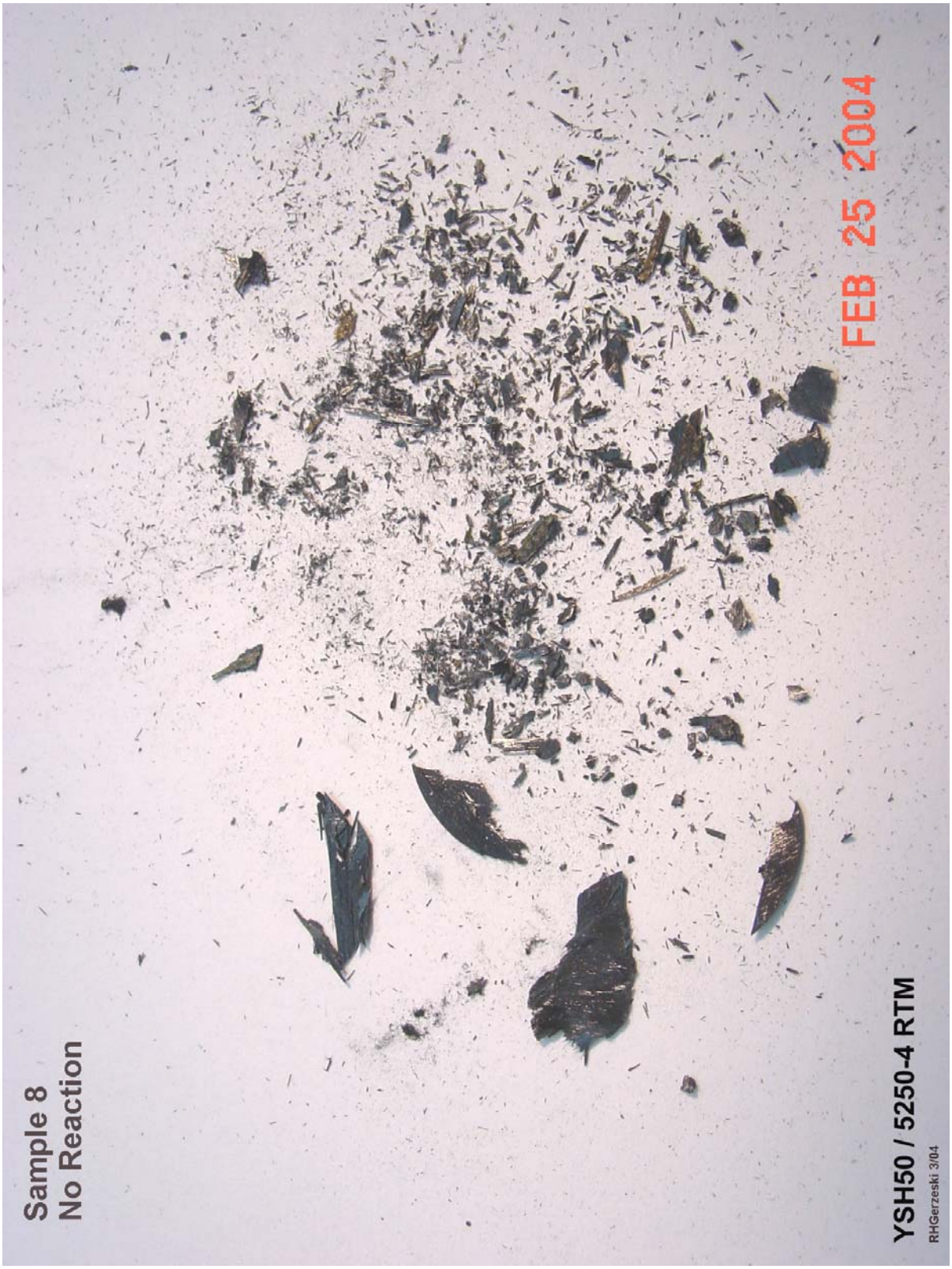


Figure R5h YSH50A / 5250-4 RTM D2512 72 FtLb LOX Tested Specimen Residuals



Figure R5i YSH50A / 5250-4 RTM D2512 72 FtLb LOX Tested Specimen Residuals



Figure R5j YSH50A / 5250-4 RTM D2512 72 FtLb LOX Tested Specimen Residuals

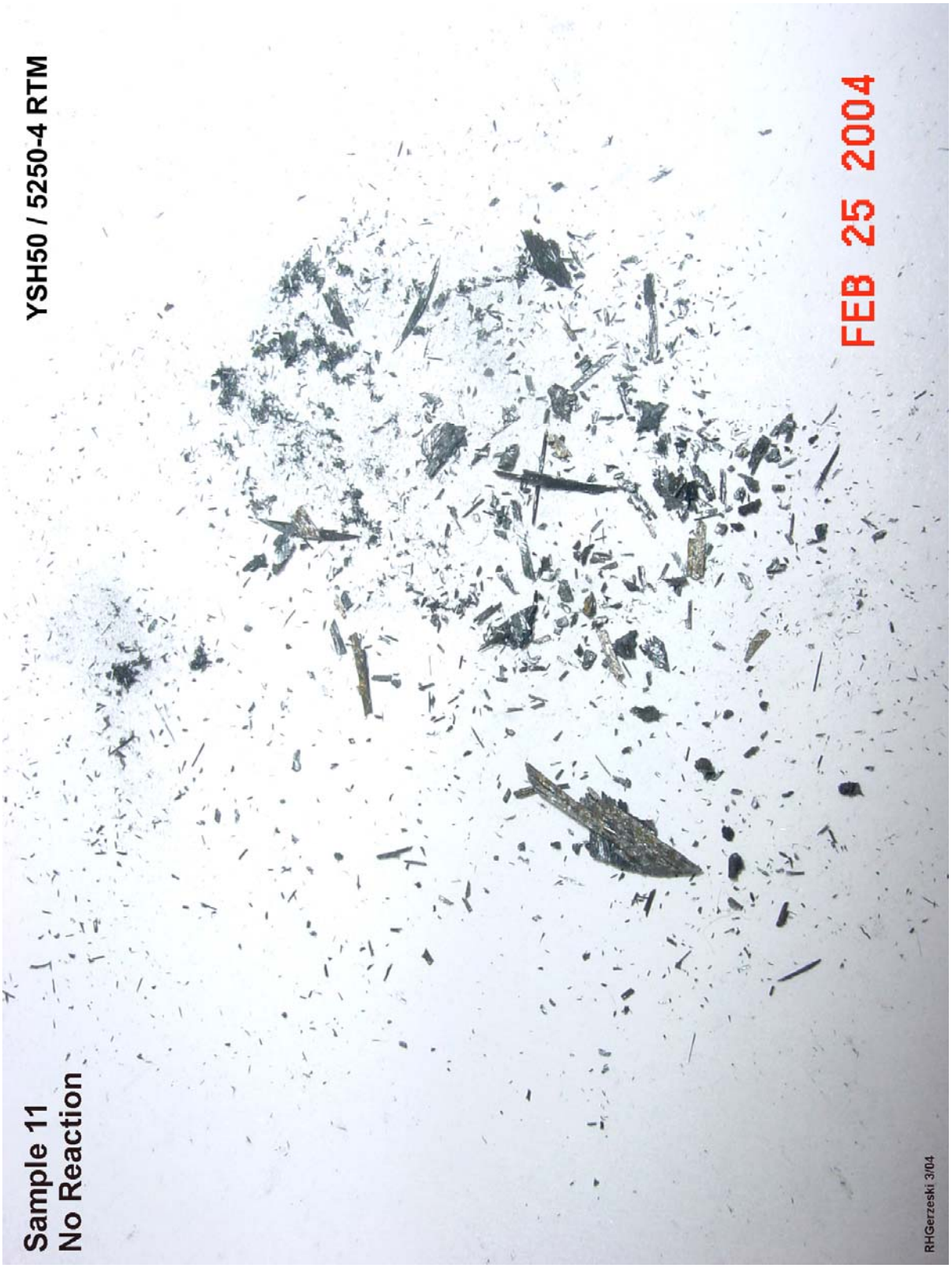


Figure R5k YSH50A / 5250-4 RTM D2512 72 FtLb LOX Tested Specimen Residuals

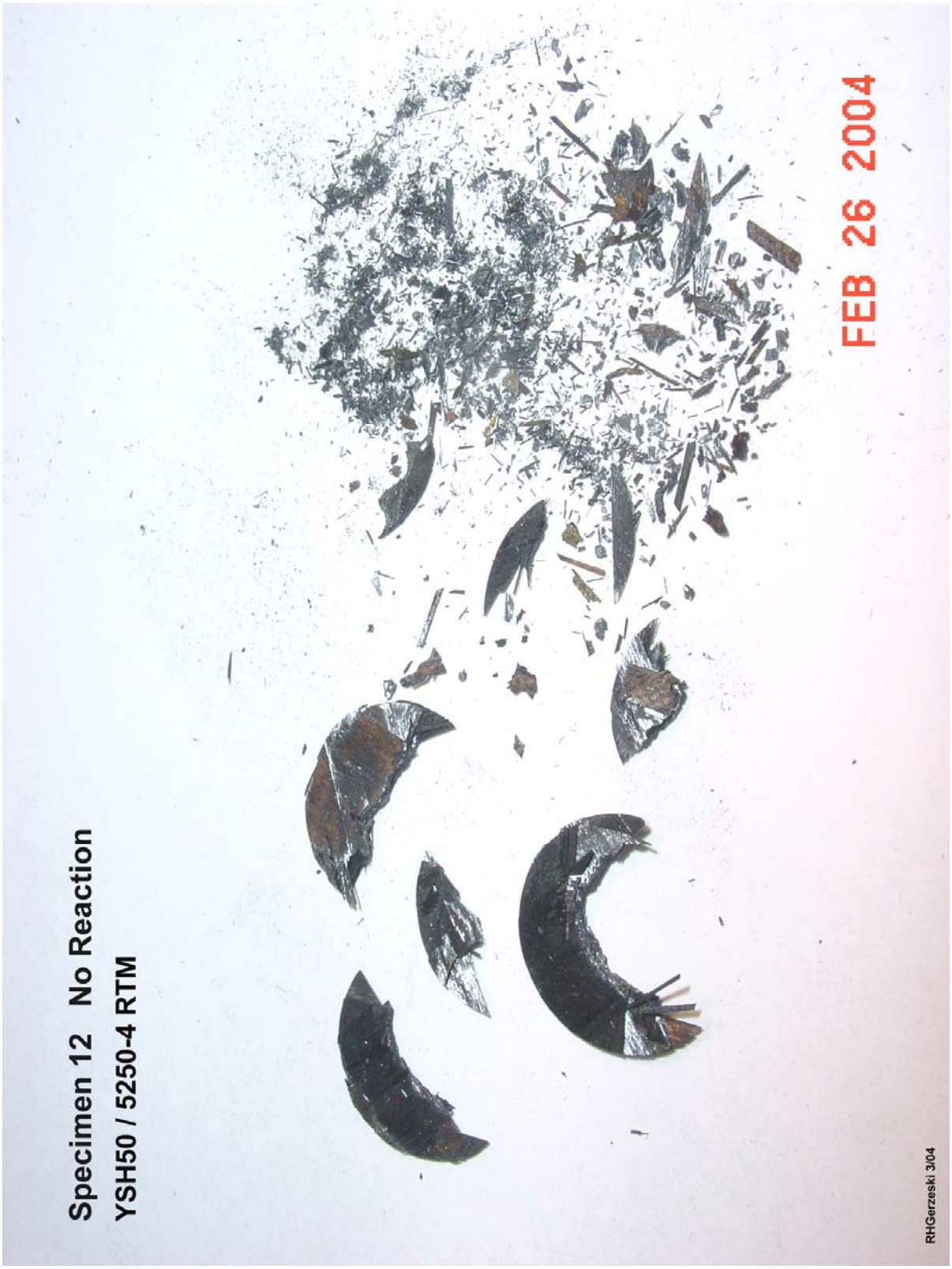


Figure R5l YSH50A / 5250-4 RTM D2512 72 FtLb LOX Tested Specimen Residuals



Figure R5m YSH50A / 5250-4 RTM D2512 72 FtLb LOX Tested Specimen Residuals



Figure R5n YSH50A / 5250-4 RTM D2512 72 FtLb LOX Tested Specimen Residuals

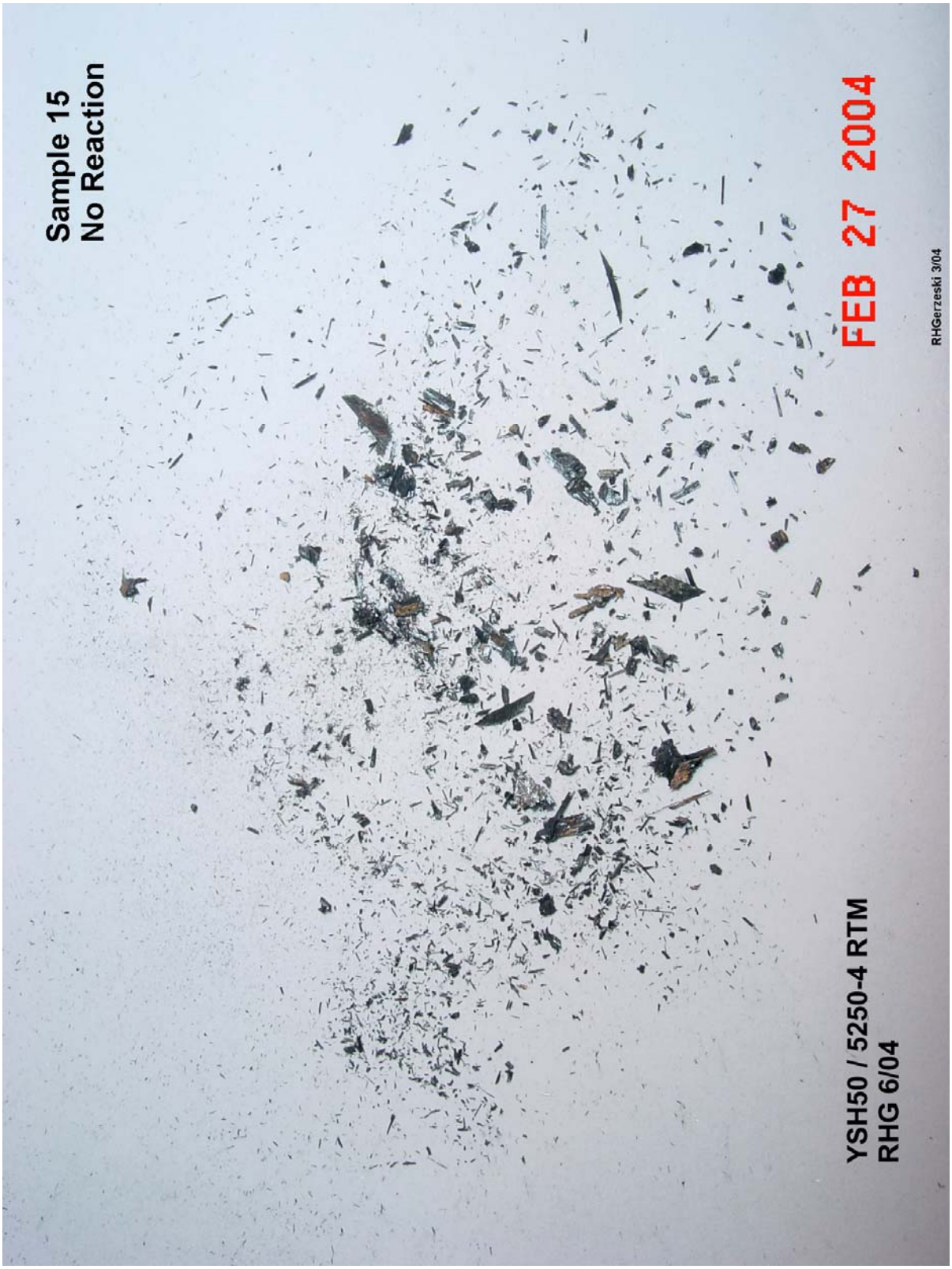


Figure R5o YSH50A / 5250-4 RTM D2512 72 FtLb LOX Tested Specimen Residuals



Figure R5p YSH50A / 5250-4 RTM D2512 72 FtLb LOX Tested Specimen Residuals



Figure R5q YSH50A / 5250-4 RTM D2512 72 FtLb LOX Tested Specimen Residuals



Figure R5r YSH50A / 5250-4 RTM D2512 72 FtLb LOX Tested Specimen Residuals



Figure R5s YSH50A / 5250-4 RTM D2512 72 FtLb LOX Tested Specimen Residuals

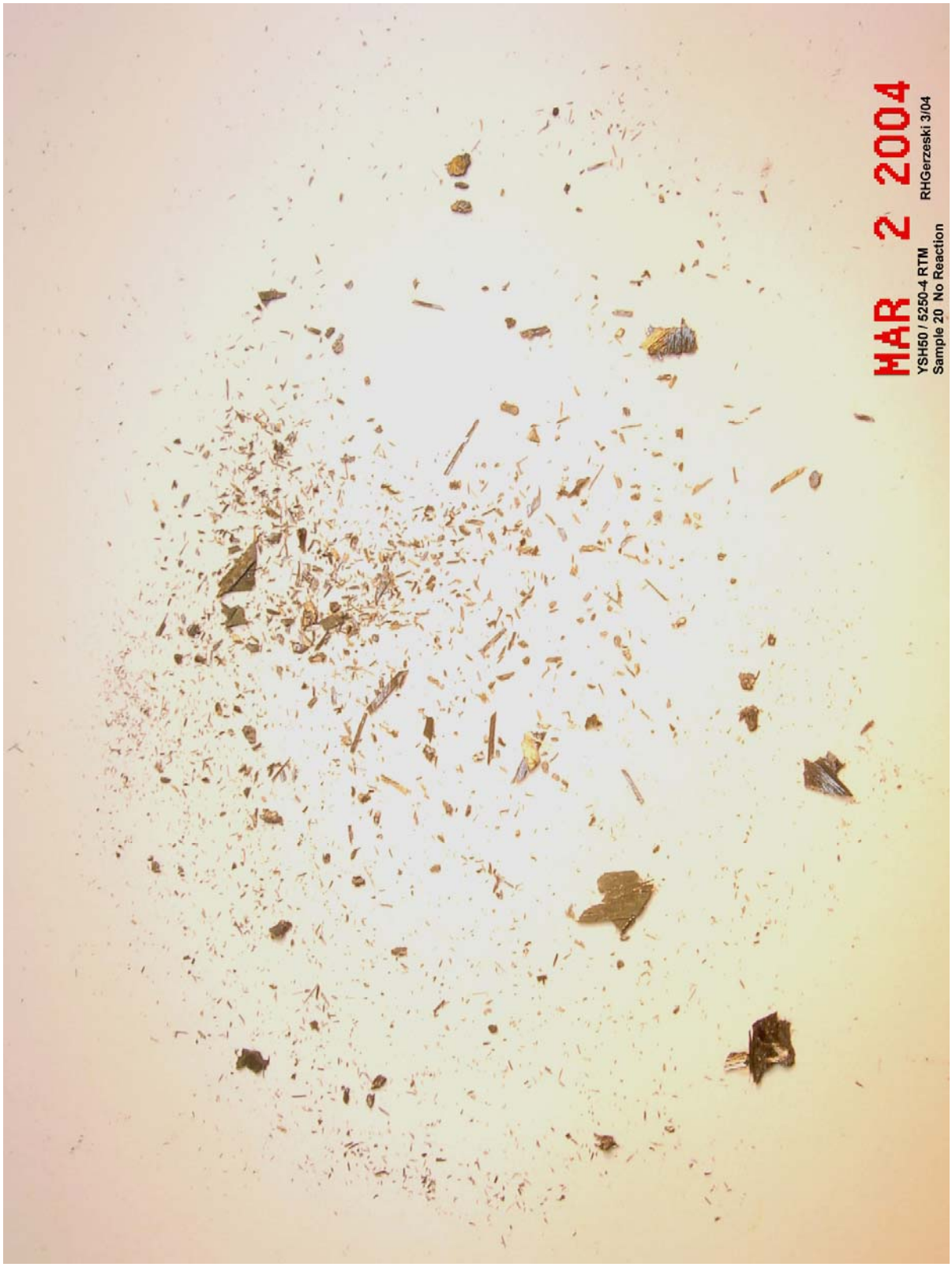


Figure R5t YSH50A / 5250-4 RTM D2512 72 FtLb LOX Tested Specimen Residuals



Figure R6a YSH50A / 5250-4 RTM D2512 72 FtLb In LN2 Tested Specimen Residuals



Figure R6b-i YSH50A / 5250-4 RTM D2512 72 FtLb In LN2 Tested Specimen Residuals



Figure R6b-ii YSH50A / 5250-4 RTM D2512 72 FtLb In LN2 Tested Specimen Residuals



Figure R6c-i YSH50A / 5250-4 RTM D2512 72 FtLb In LN2 Tested Specimen Residuals



Figure R6c-ii YSH50A / 5250-4 RTM D2512 72 FtLb In LN2 Tested Specimen Residuals

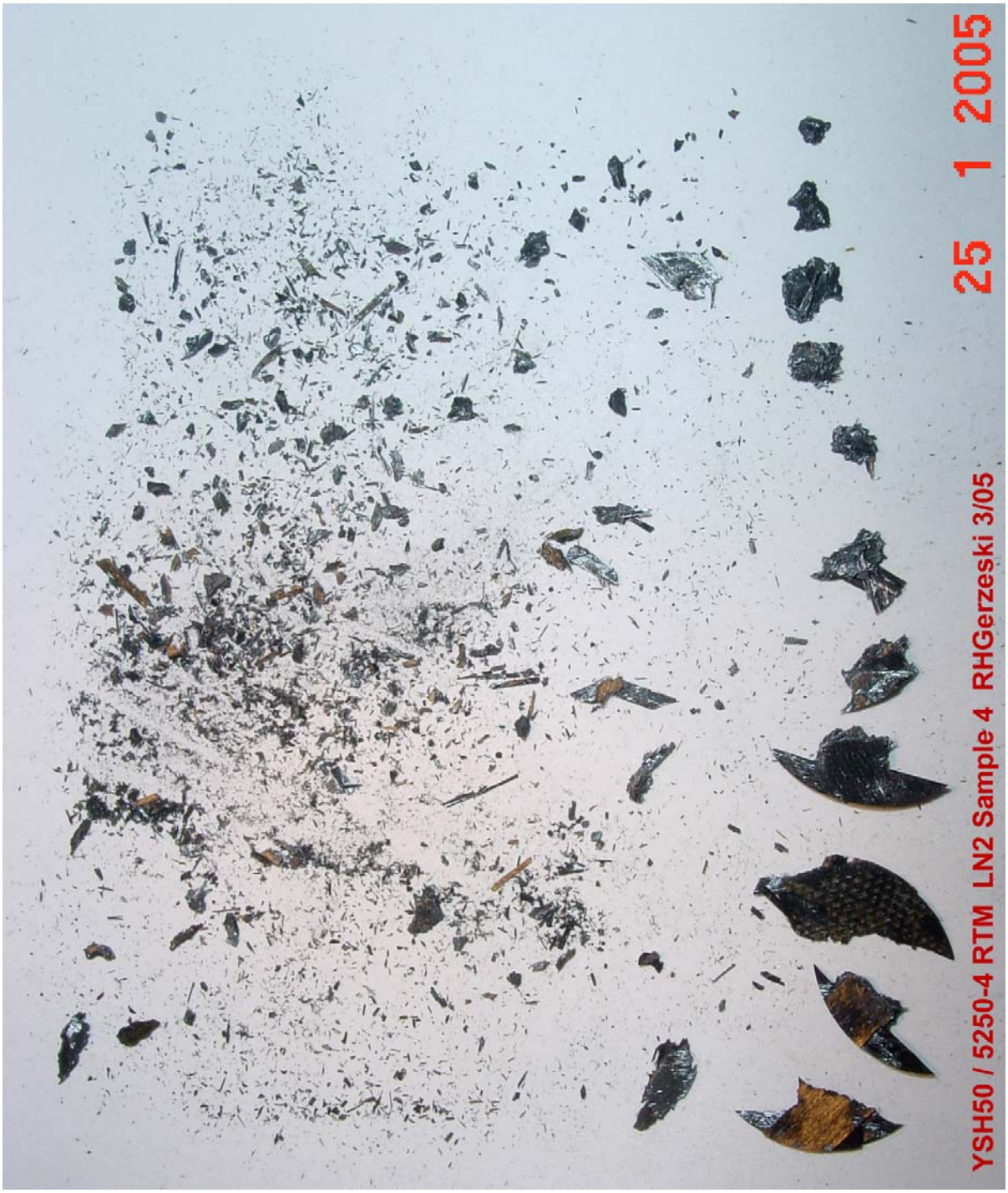


Figure R6d-i YSH50A / 5250-4 RTM D2512 72 FtLb In LN2 Tested Specimen Residuals



Figure R6d-ii YSH50A / 5250-4 RTM D2512 72 FtLb In LN2 Tested Specimen Residuals



Figure R7a YSH60A / 5250-4 RTM D2512 72 FtLb LOX Tested Specimen Residuals

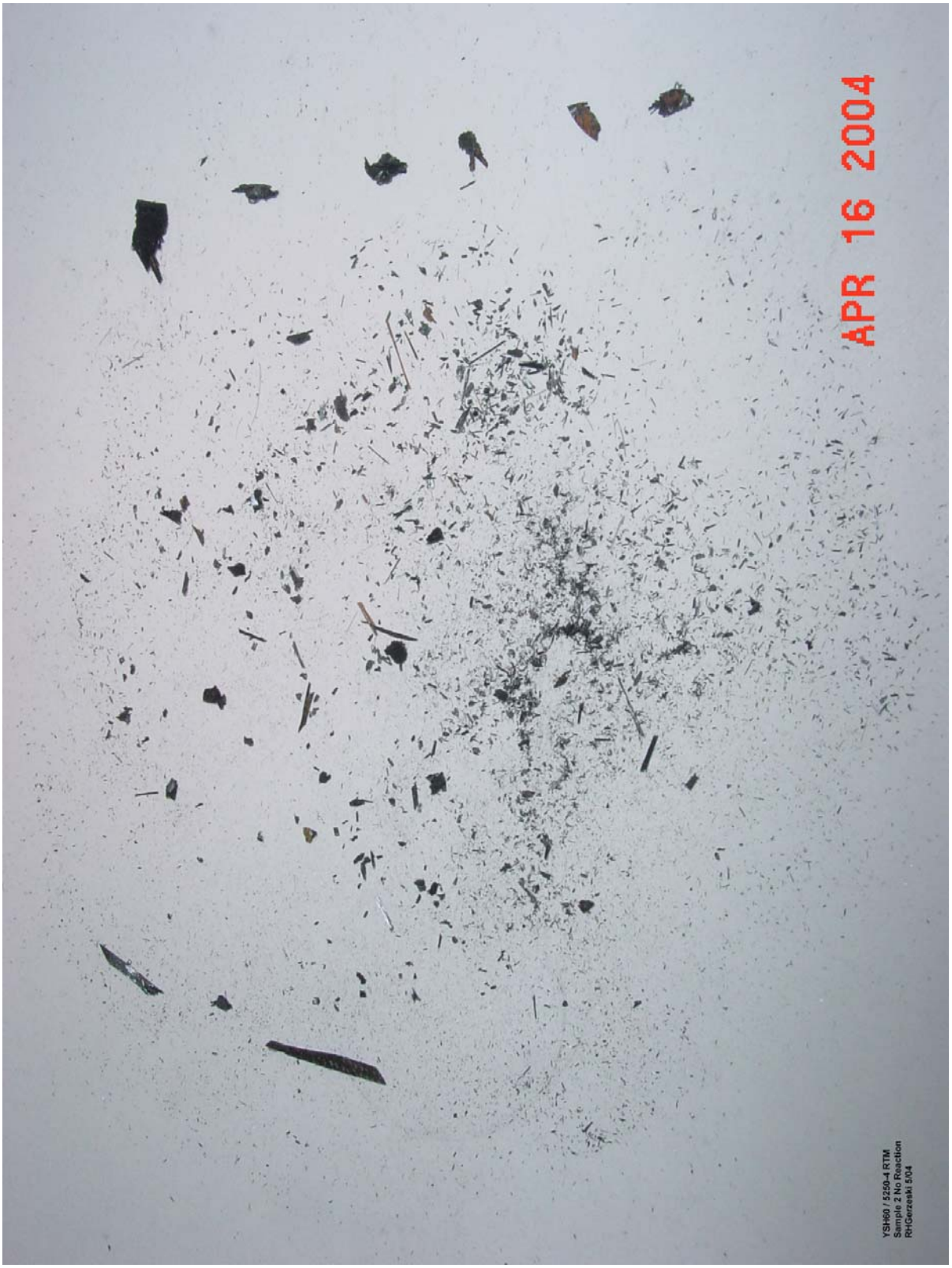


Figure R7b YSH60A / 5250-4 RTM D2512 72 FtLb LOX Tested Specimen Residuals

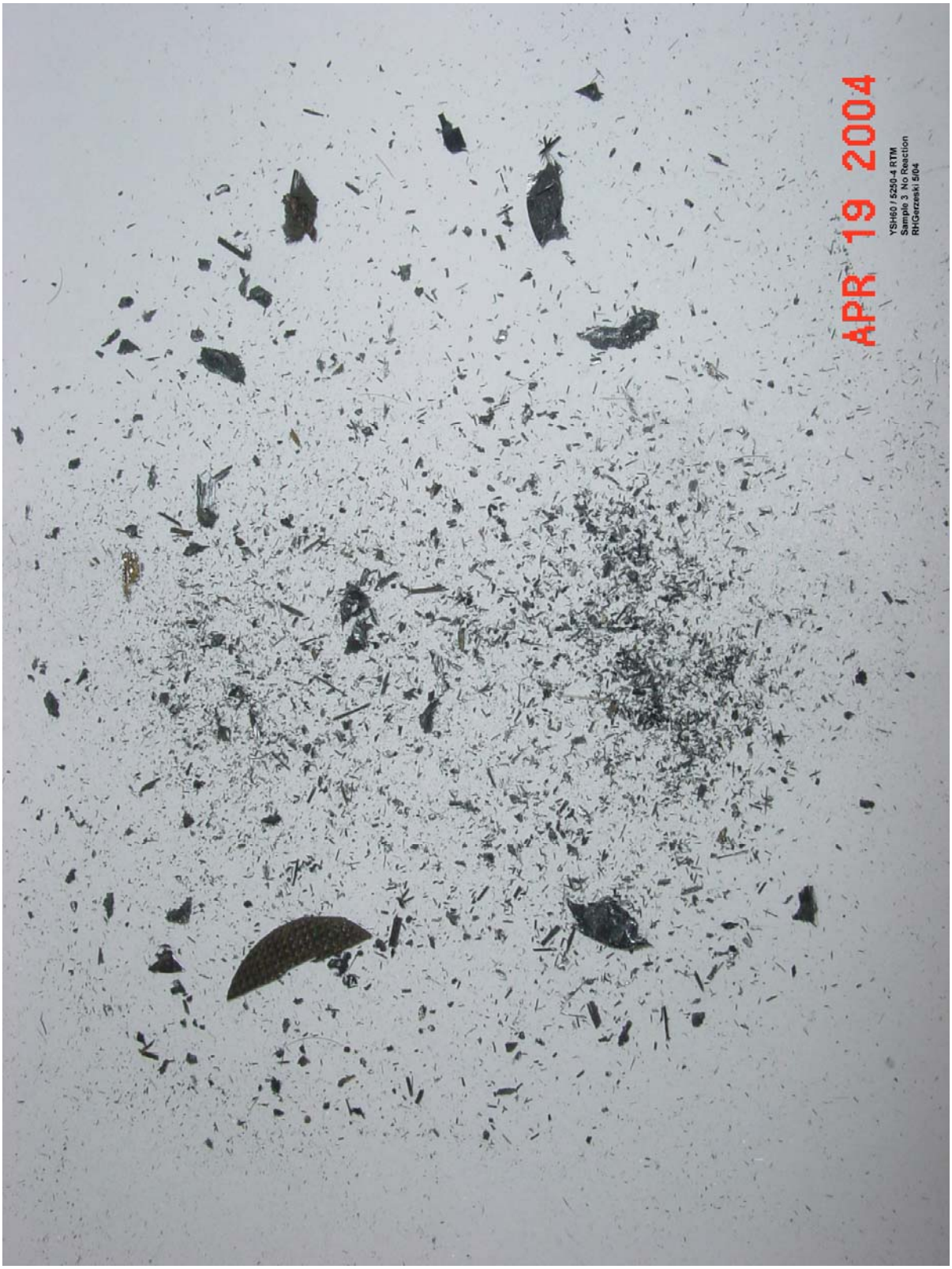


Figure R7c YSH60A / 5250-4 RTM D2512 72 FtLb LOX Tested Specimen Residuals



Figure R7d YSH60A / 5250-4 RTM D2512 72 FtLb LOX Tested Specimen Residuals



Figure R7e YSH60A / 5250-4 RTM D2512 72 FtLb LOX Tested Specimen Residuals



Figure R7f YSH60A / 5250-4 RTM D2512 72 FtLb LOX Tested Specimen Residuals

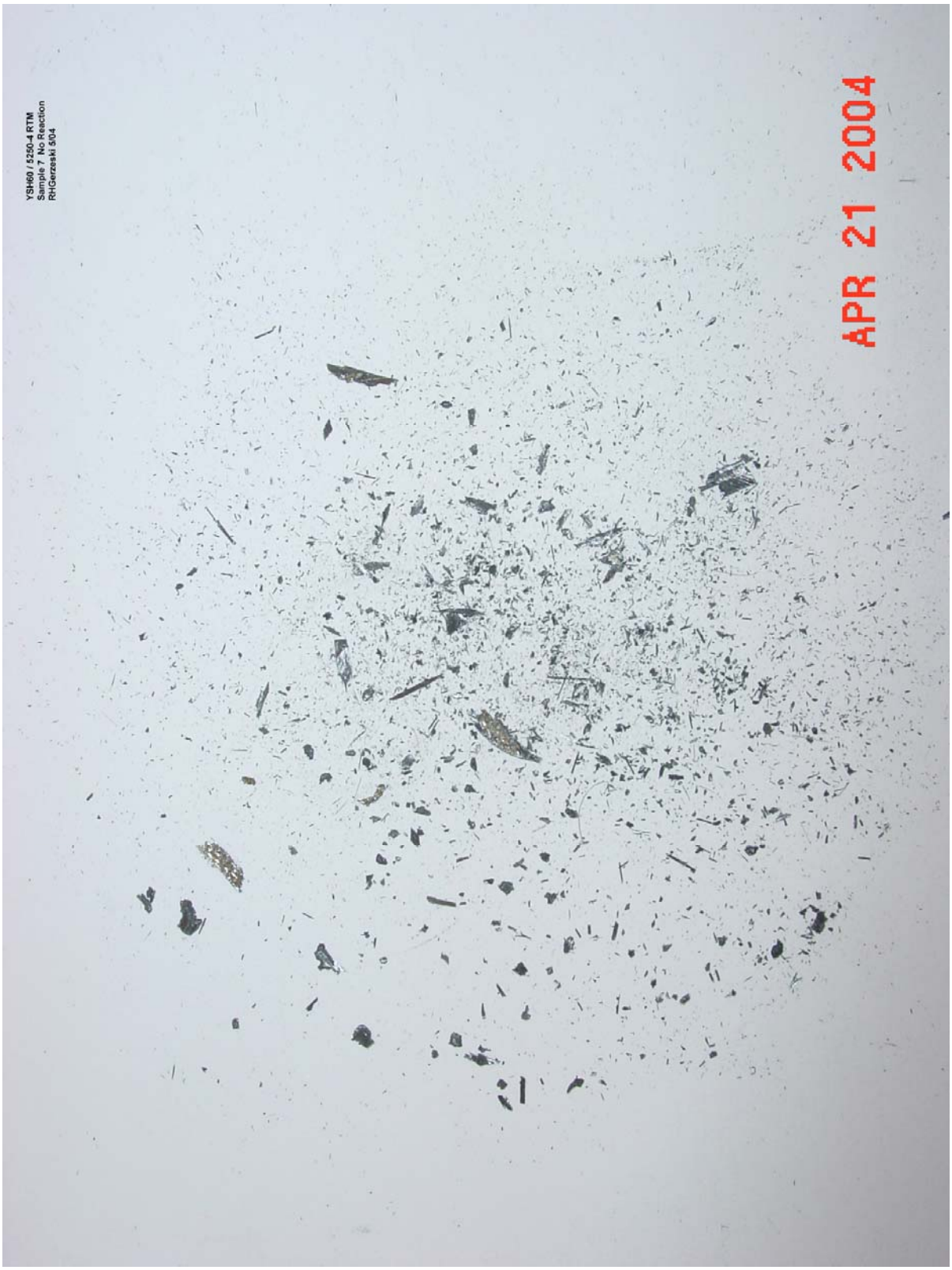


Figure R7g YSH60A / 5250-4 RTM D2512 72 FtLb LOX Tested Specimen Residuals



Figure R7h YSH60A / 5250-4 RTM D2512 72 FtLb LOX Tested Specimen Residuals

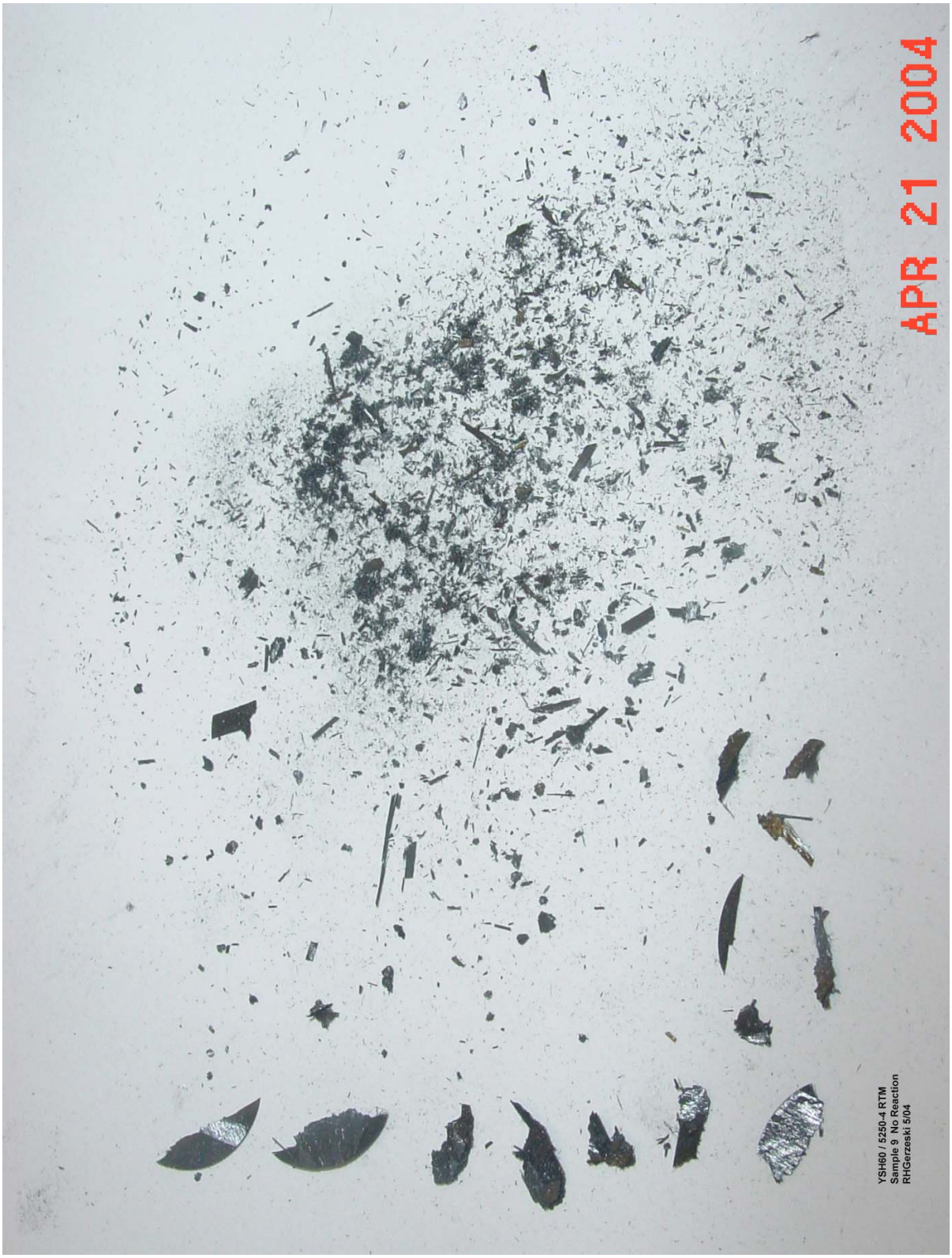


Figure R7i YSH60A / 5250-4 RTM D2512 72 FtLb LOX Tested Specimen Residuals



Figure R7j-i YSH60A / 5250-4 RTM D2512 72 FtLb LOX Tested Specimen Residuals



Figure R7j-ii YSH60A / 5250-4 RTM D2512 72 FtLb LOX Tested Specimen Residuals



Figure R7k YSH60A / 5250-4 RTM D2512 72 FtLb LOX Tested Specimen Residuals



Figure R7l-i YSH60A / 5250-4 RTM D2512 72 FtLb LOX Tested Specimen Residuals



Figure R7I-ii YSH60A / 5250-4 RTM D2512 72 FtLb LOX Tested Specimen Residuals



Figure R7m YSH60A / 5250-4 RTM D2512 72 FtLb LOX Tested Specimen Residuals



Figure R7n YSH60A / 5250-4 RTM D2512 72 FtLb LOX Tested Specimen Residuals

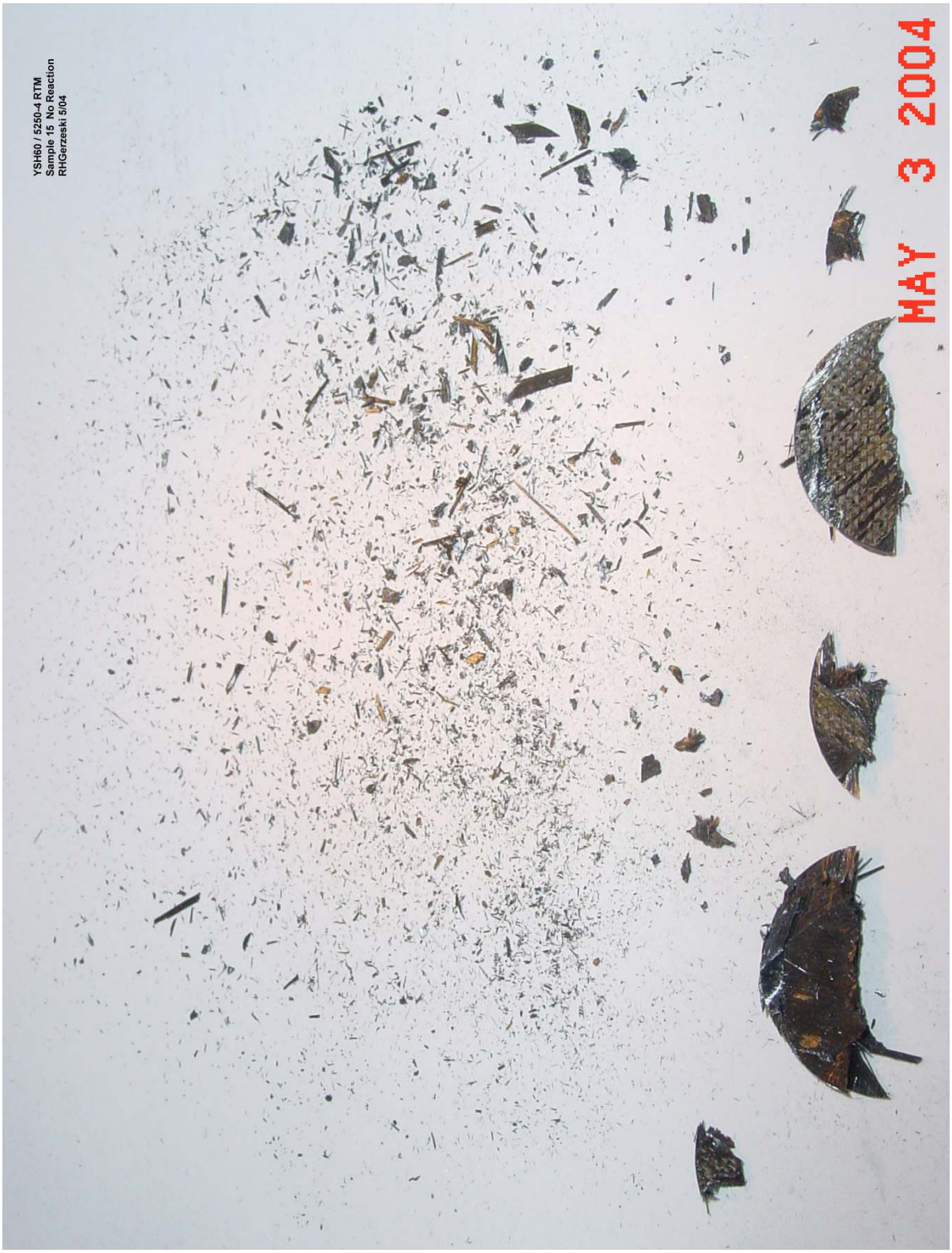


Figure R7o YSH60A / 5250-4 RTM D2512 72 FtLb LOX Tested Specimen Residuals

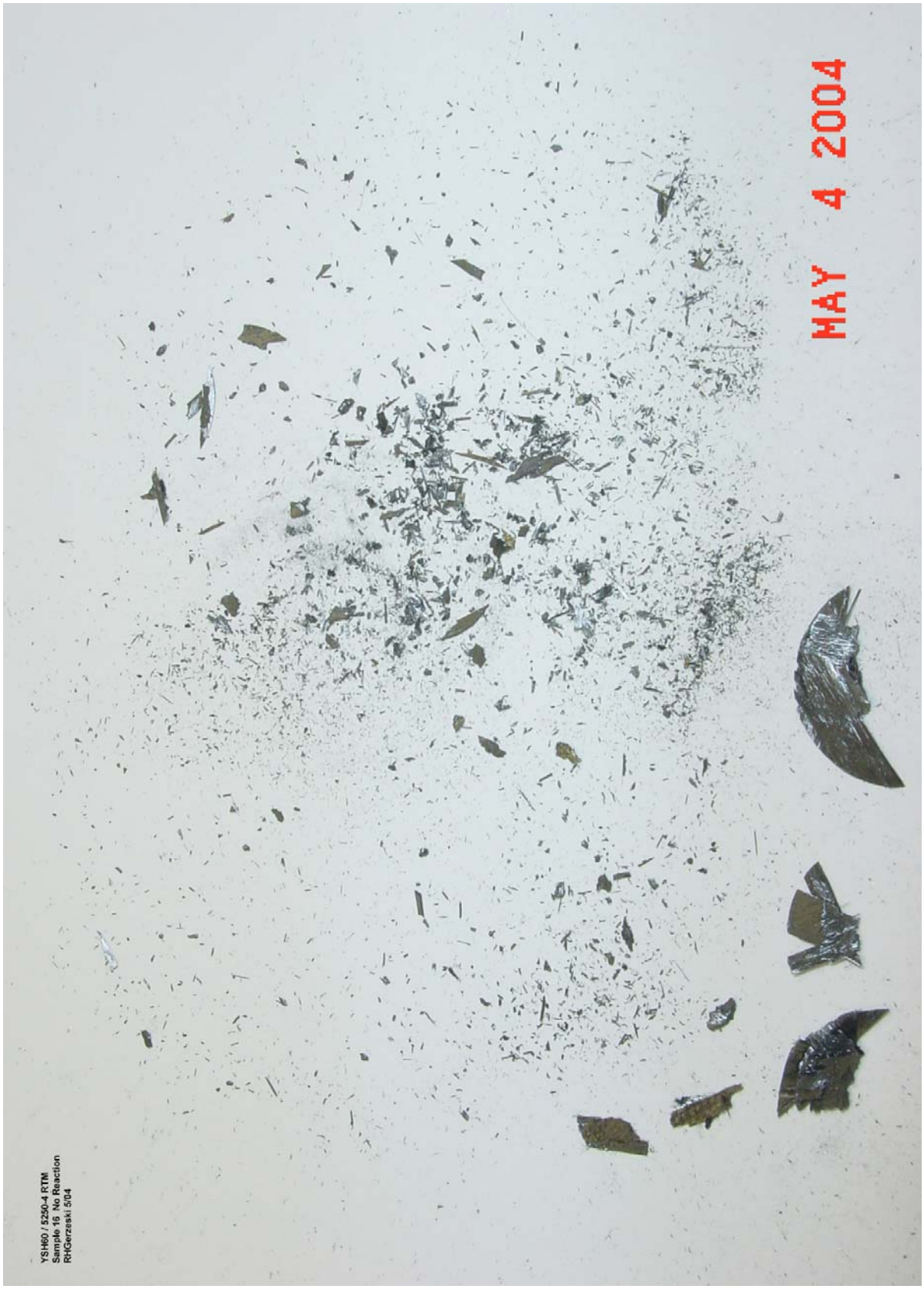


Figure R7p YSH60A / 5250-4 RTM D2512 72 FtLb LOX Tested Specimen Residuals

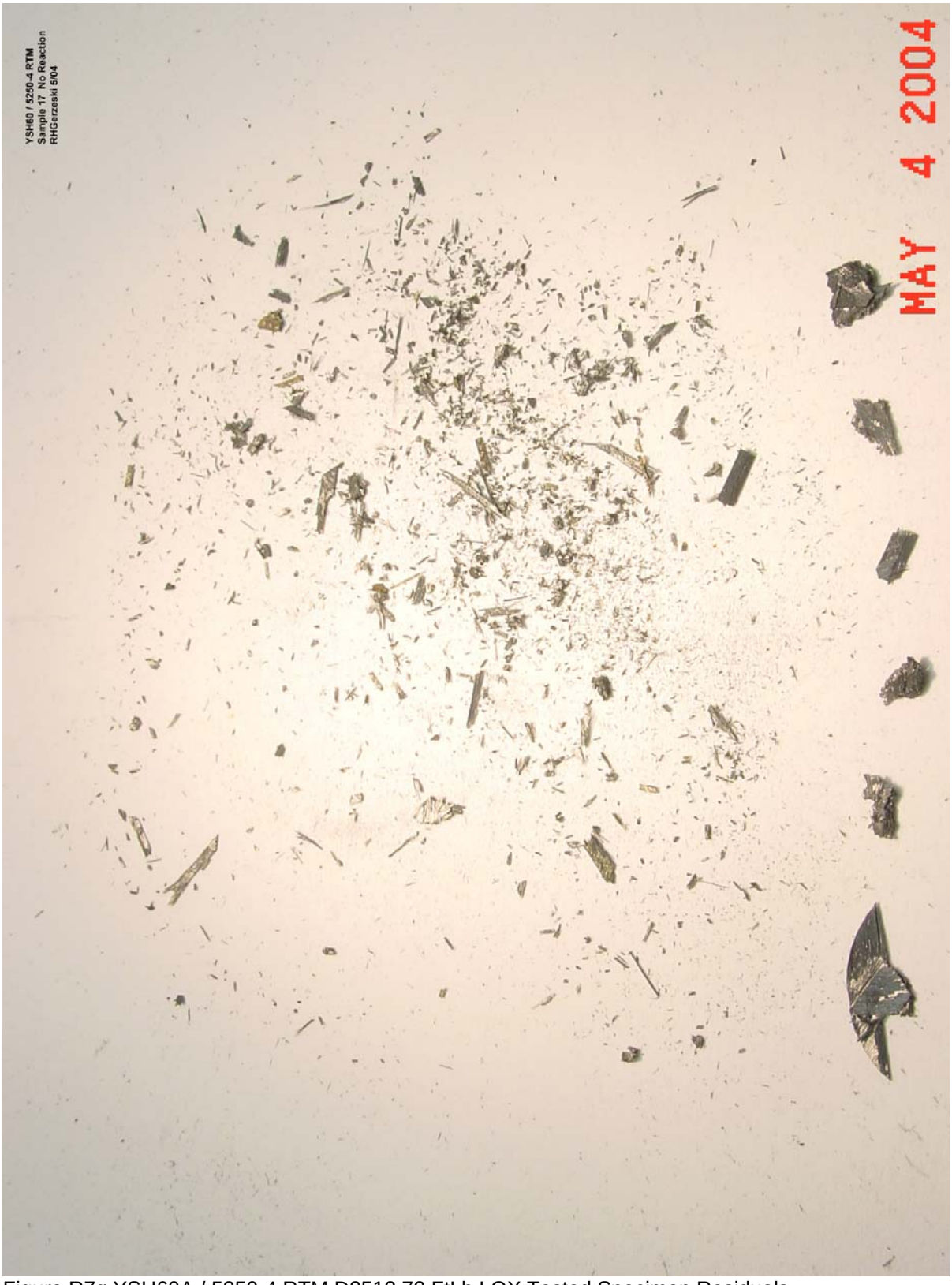


Figure R7q YSH60A / 5250-4 RTM D2512 72 FtLb LOX Tested Specimen Residuals

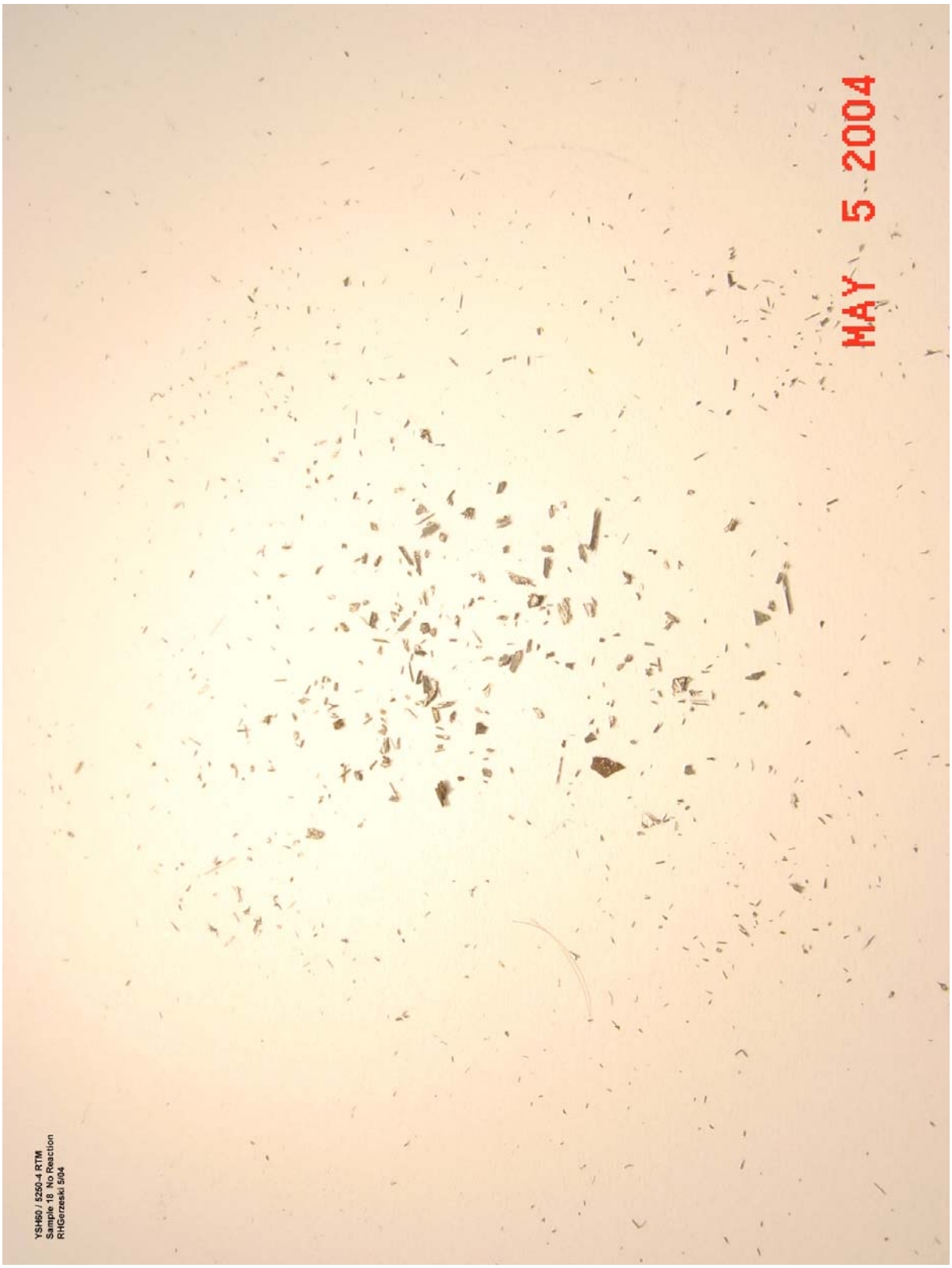


Figure R7r YSH60A / 5250-4 RTM D2512 72 FtLb LOX Tested Specimen Residuals

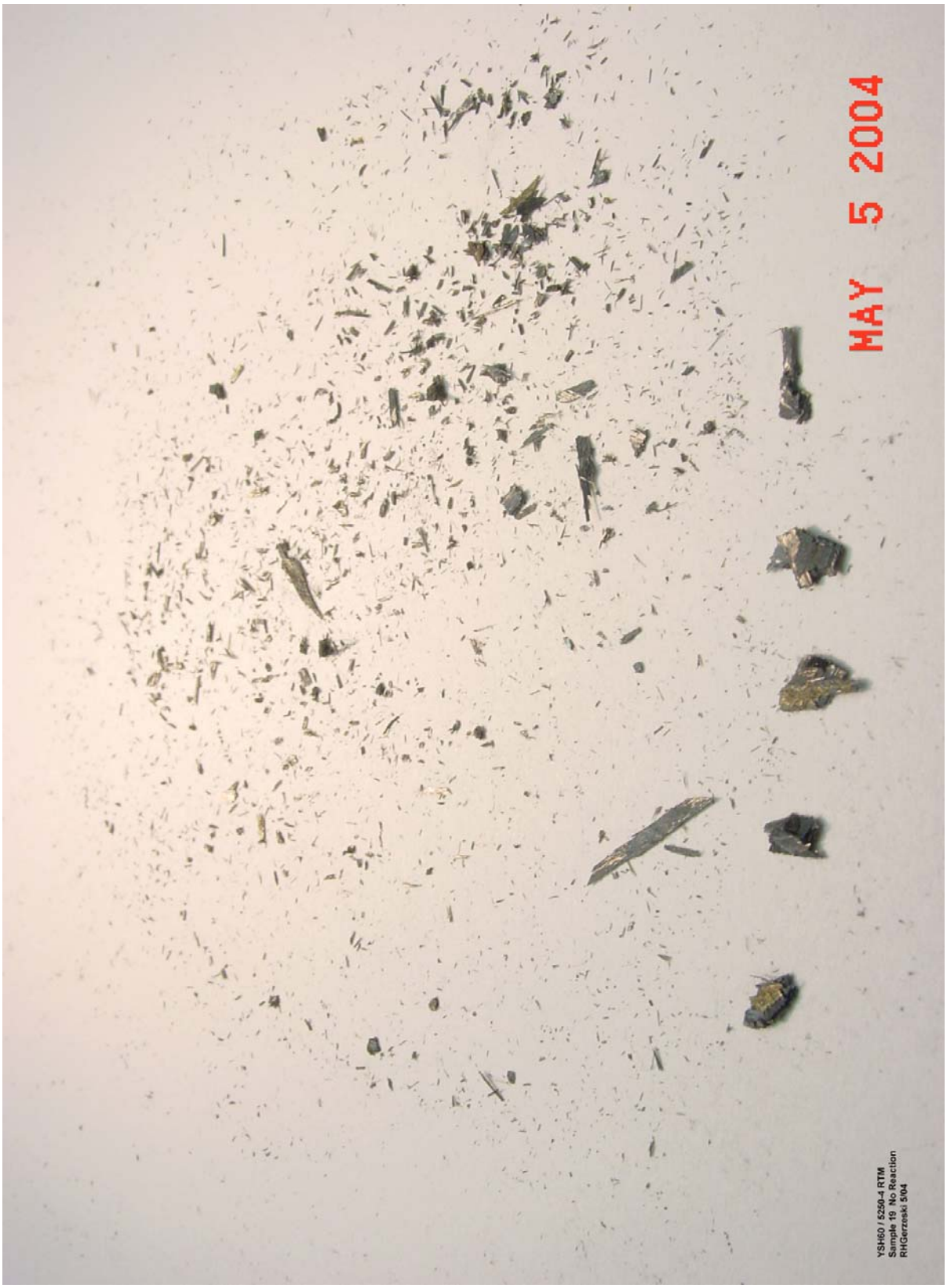


Figure R7s YSH60A / 5250-4 RTM D2512 72 FtLb LOX Tested Specimen Residuals



Figure R7t YSH60A / 5250-4 RTM D2512 72 FtLb LOX Tested Specimen Residuals

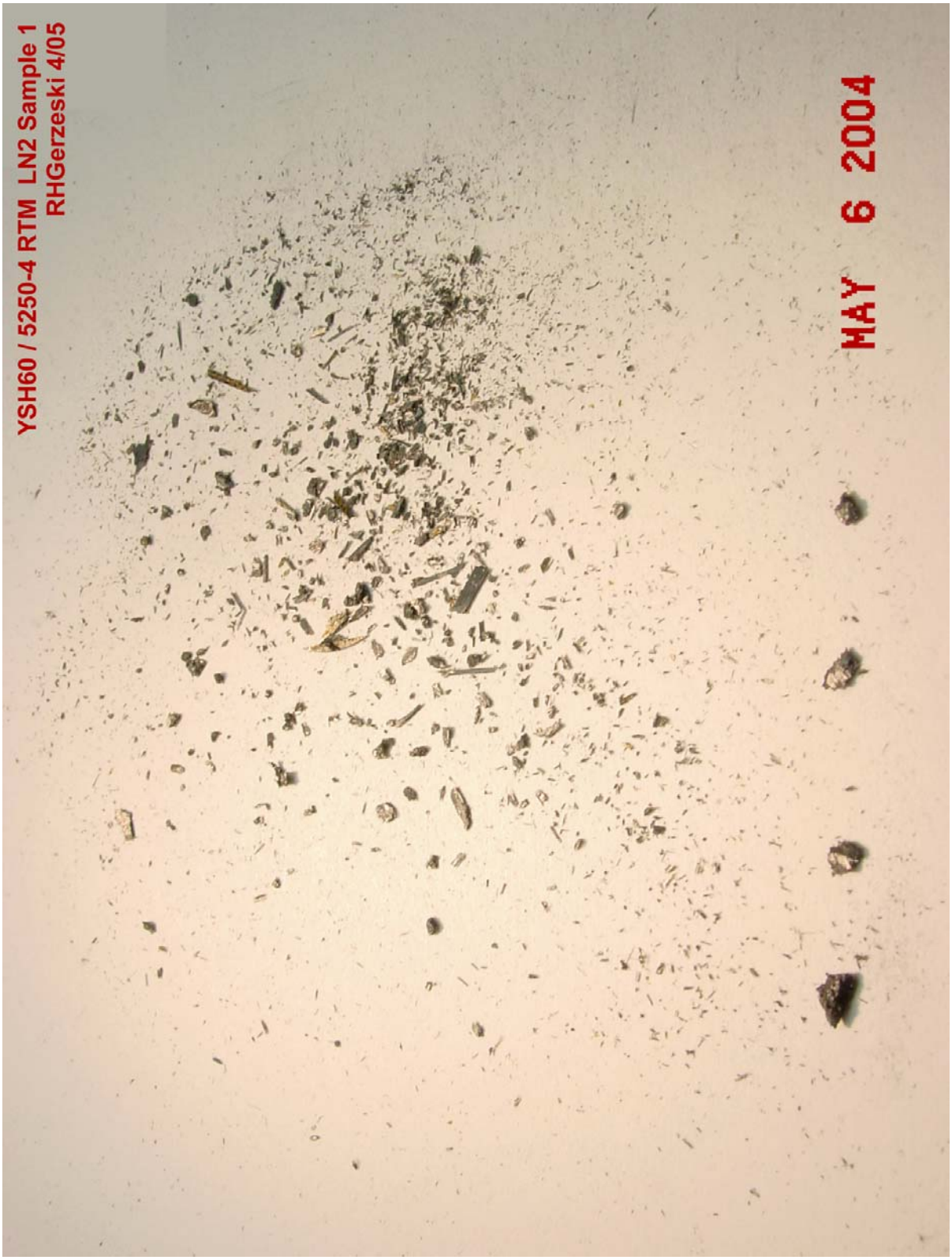


Figure R8a YSH60A / 5250-4 RTM D2512 72 FtLb In LN2 Tested Specimen Residuals



Figure R8b-i YSH60A / 5250-4 RTM D2512 72 FtLb In LN2 Tested Specimen Residuals



Figure R2b-ii YSH60A / 5250-4 RTM D2512 72 FtLb In LN2 Tested Specimen Residuals

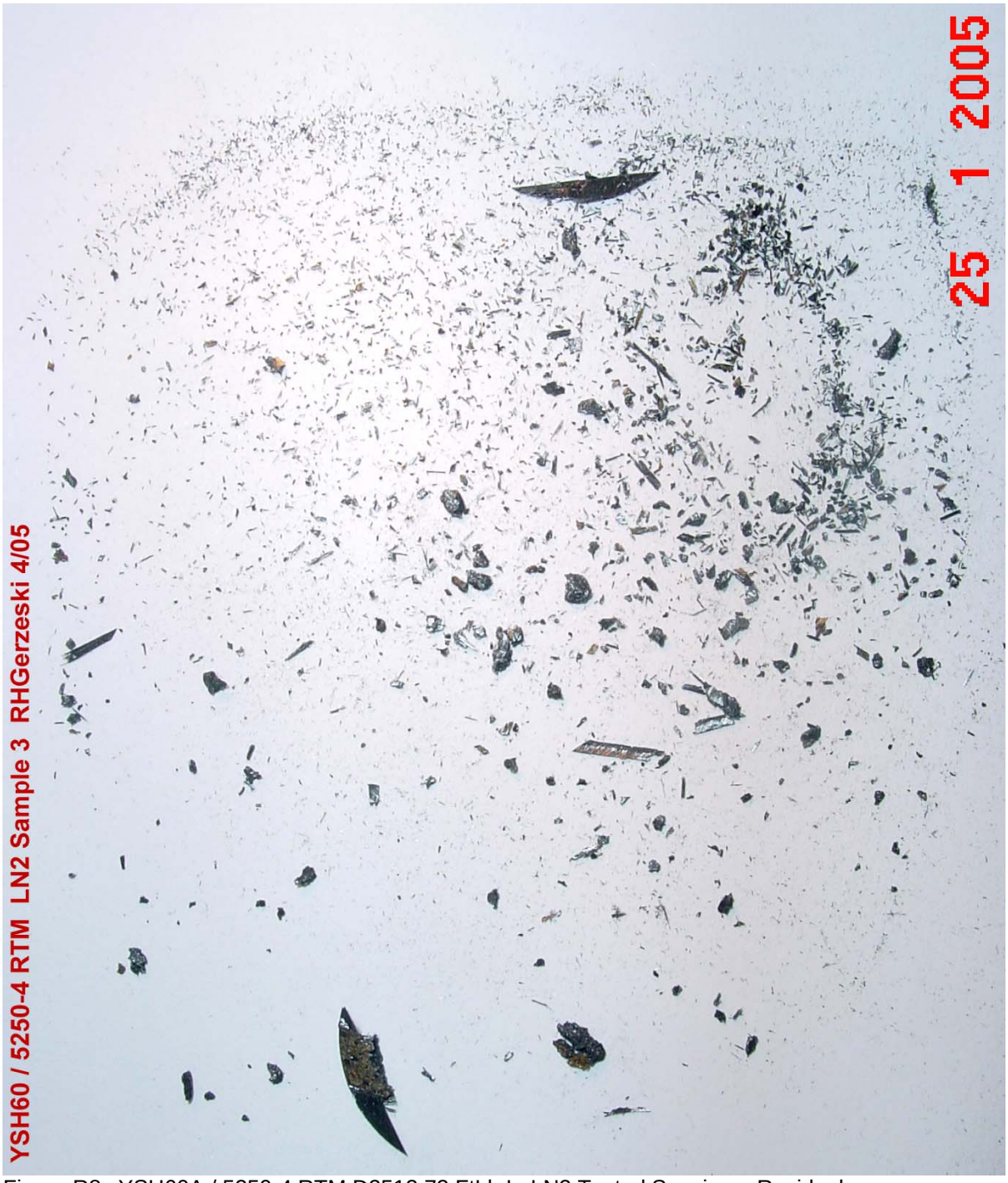


Figure R8c YSH60A / 5250-4 RTM D2512 72 FtLb In LN2 Tested Specimen Residuals

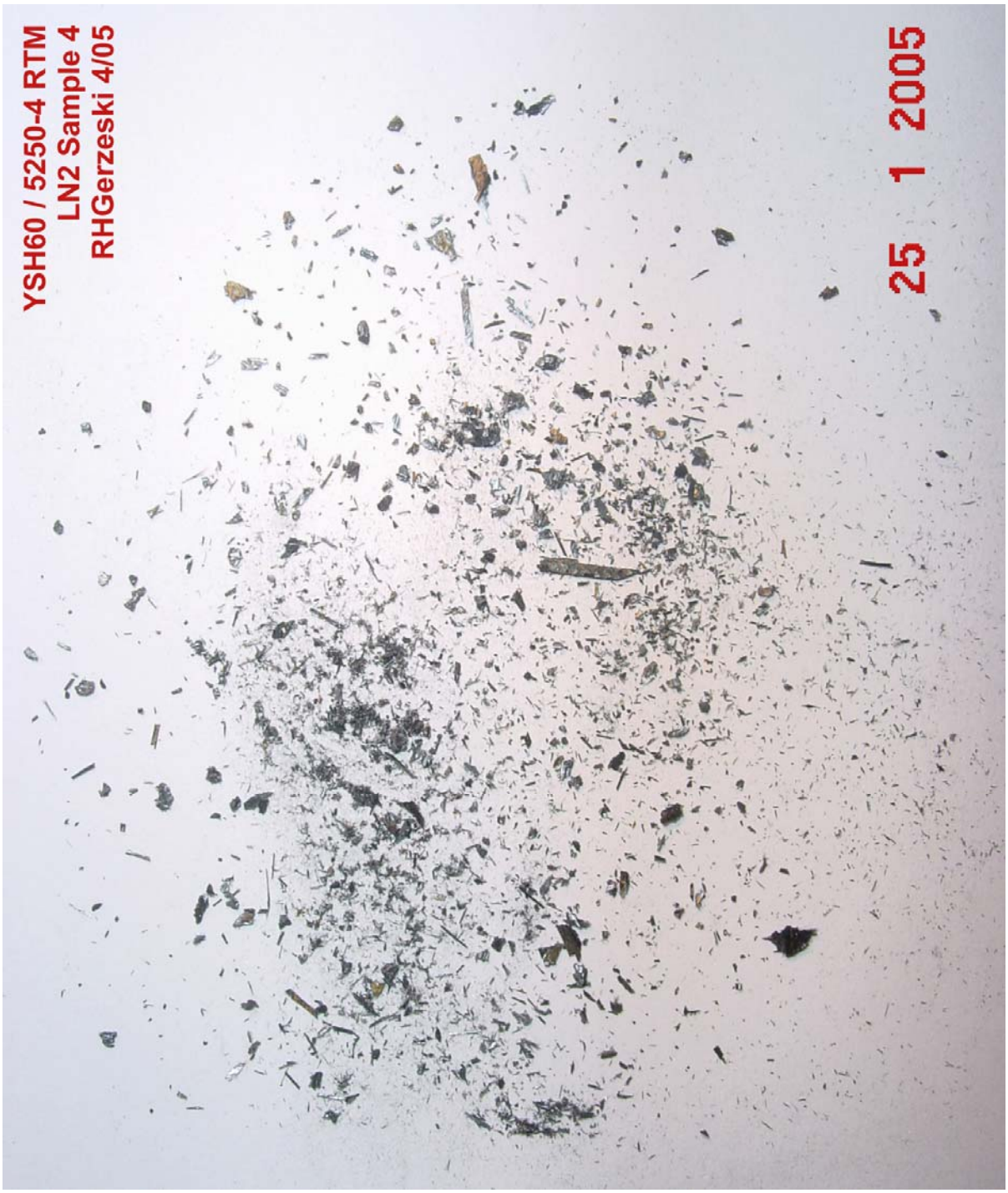


Figure R8d YSH60A / 5250-4 RTM D2512 72 FtLb In LN2 Tested Specimen Residuals

Appendix: Residuals: Discs



Figure R9a 5250-4 RTM D2512 72 FtLb LOX Tested Specimen Disc Residuals



Figure R9b 5250-4 RTM D2512 72 FtLb LOX Tested Specimen Disc Residuals

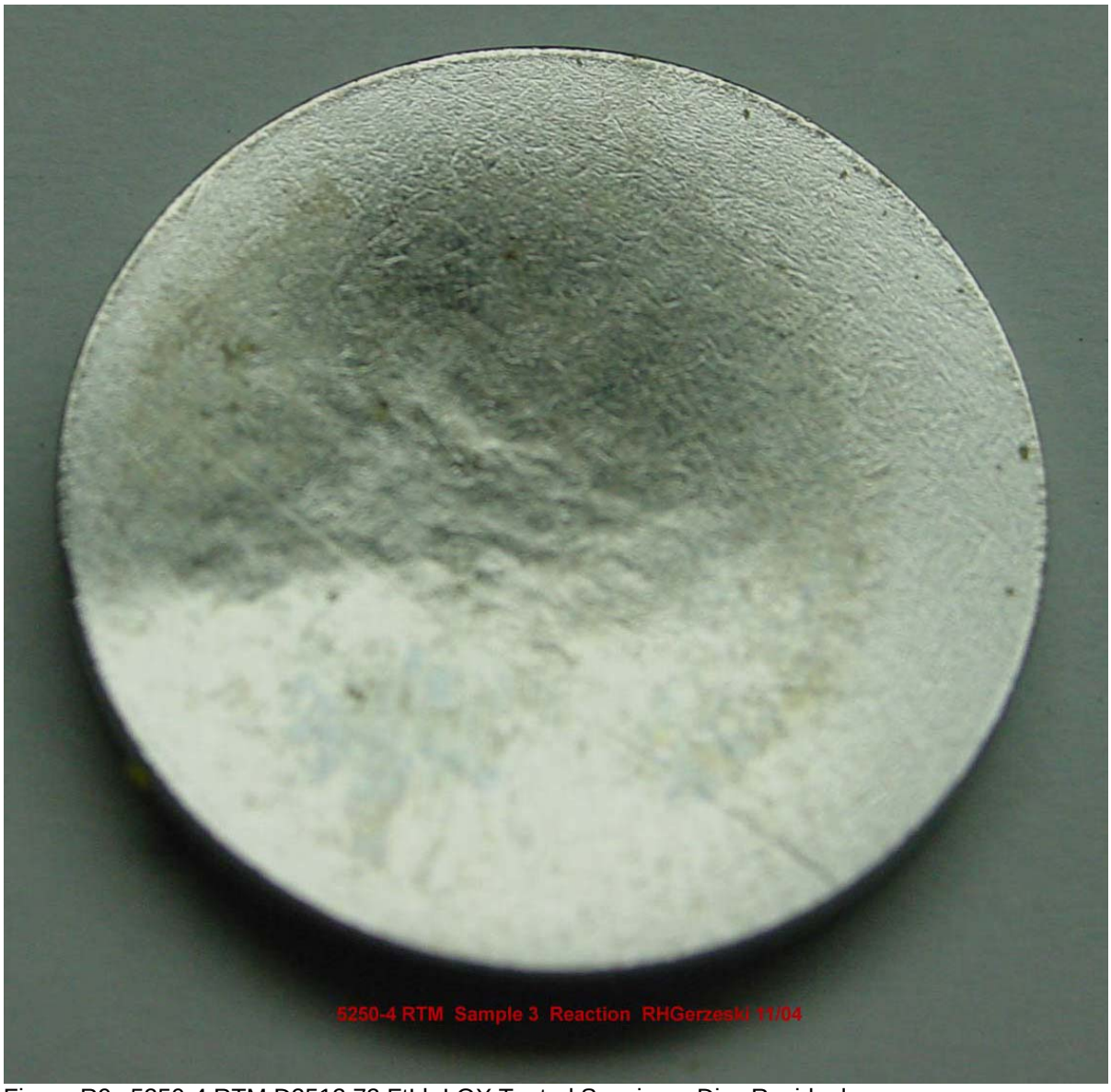


Figure R9c 5250-4 RTM D2512 72 FtLb LOX Tested Specimen Disc Residuals



Figure R9d 5250-4 RTM D2512 72 FtLb LOX Tested Specimen Disc Residuals



Figure R9e 5250-4 RTM D2512 72 FtLb LOX Tested Specimen Disc Residuals



Figure R9f 5250-4 RTM D2512 72 FtLb LOX Tested Specimen Disc Residuals



Figure R9g 5250-4 RTM D2512 72 FtLb LOX Tested Specimen Disc Residuals



Figure R9h 5250-4 RTM D2512 72 FtLb LOX Tested Specimen Disc Residuals



Figure R9i 5250-4 RTM D2512 72 FtLb LOX Tested Specimen Disc Residuals



Figure R9j 5250-4 RTM D2512 72 FtLb LOX Tested Specimen Disc Residuals



Figure R9k 5250-4 RTM D2512 72 FtLb LOX Tested Specimen Disc Residuals



Figure R9l 5250-4 RTM D2512 72 FtLb LOX Tested Specimen Disc Residuals



Figure R9m 5250-4 RTM D2512 72 FtLb LOX Tested Specimen Disc Residuals



Figure R9n 5250-4 RTM D2512 72 FtLb LOX Tested Specimen Disc Residuals



Figure R9o 5250-4 RTM D2512 72 FtLb LOX Tested Specimen Disc Residuals



Figure R9p 5250-4 RTM D2512 72 FtLb LOX Tested Specimen Disc Residuals



Figure R9q 5250-4 RTM D2512 72 FtLb LOX Tested Specimen Disc Residuals

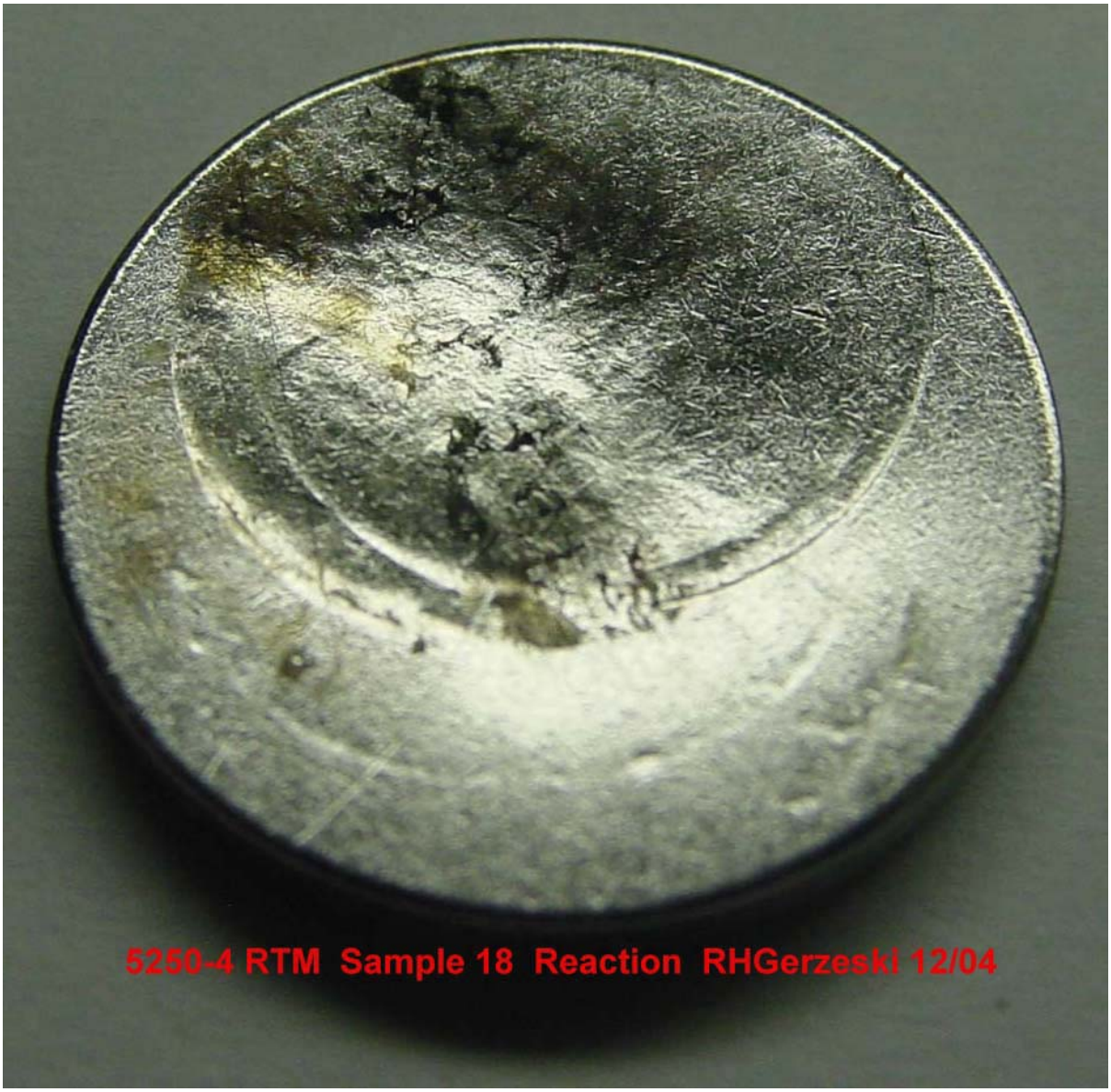


Figure R9r 5250-4 RTM D2512 72 FtLb LOX Tested Specimen Disc Residuals



Figure R9s 5250-4 RTM D2512 72 FtLb LOX Tested Specimen Disc Residuals

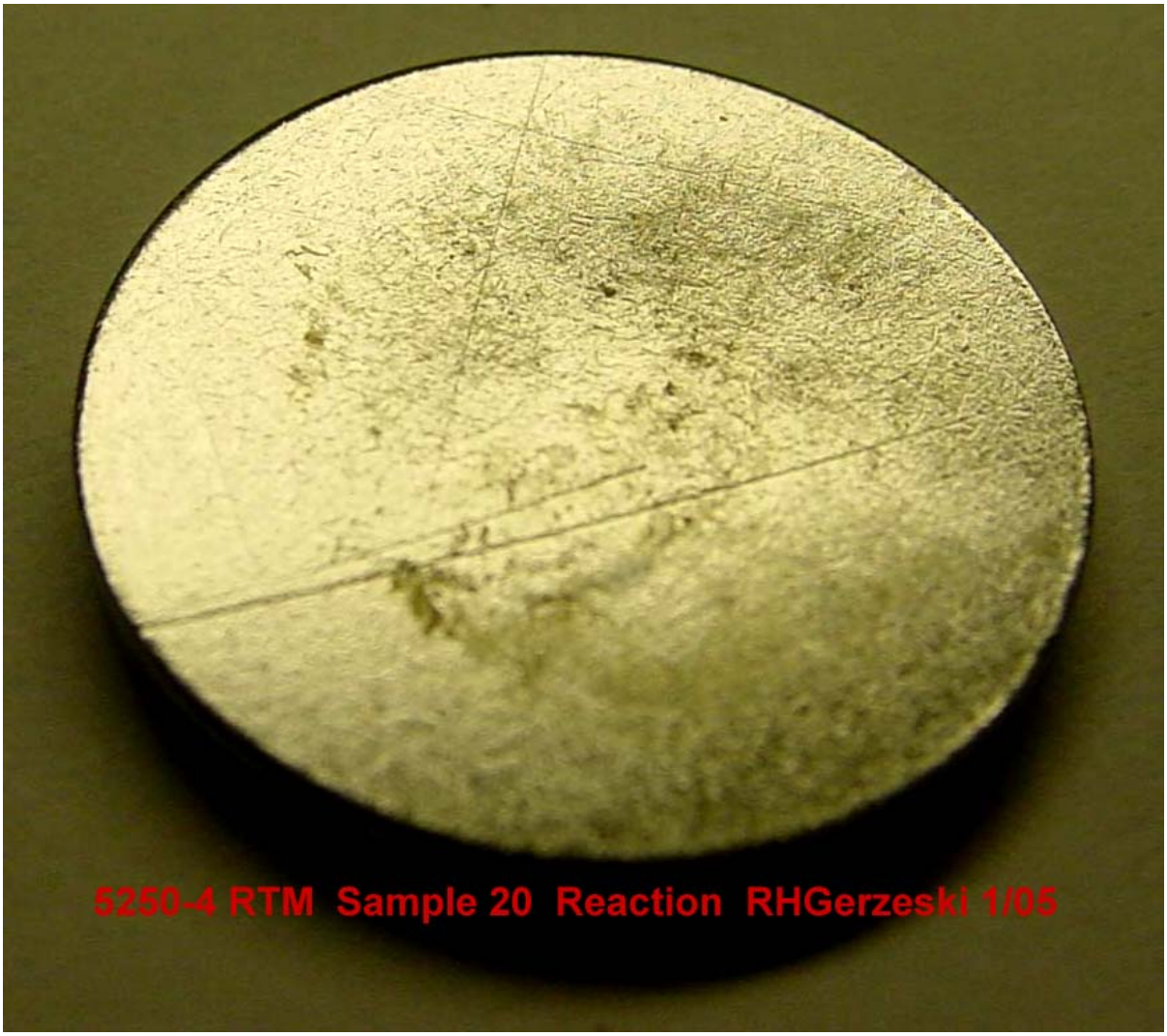


Figure R9t 5250-4 RTM D2512 72 FtLb LOX Tested Specimen Disc Residuals



Figure R10a 5250-4 RTM D2512 72 FtLb In LN2 Tested Specimen Disc Residuals



Figure R10b 5250-4 RTM D2512 72 FtLb In LN2 Tested Specimen Disc Residuals



Figure R10c 5250-4 RTM D2512 72 FtLb In LN2 Tested Specimen Disc Residuals



Figure R11a T650-35-UC309 / 5250-4 RTM D2512 72 FtLb LOX Tested Specimen Disc Residuals



Figure R11b T650-35-UC309 / 5250-4 RTM D2512 72 FtLb LOX Tested Specimen Disc Residuals

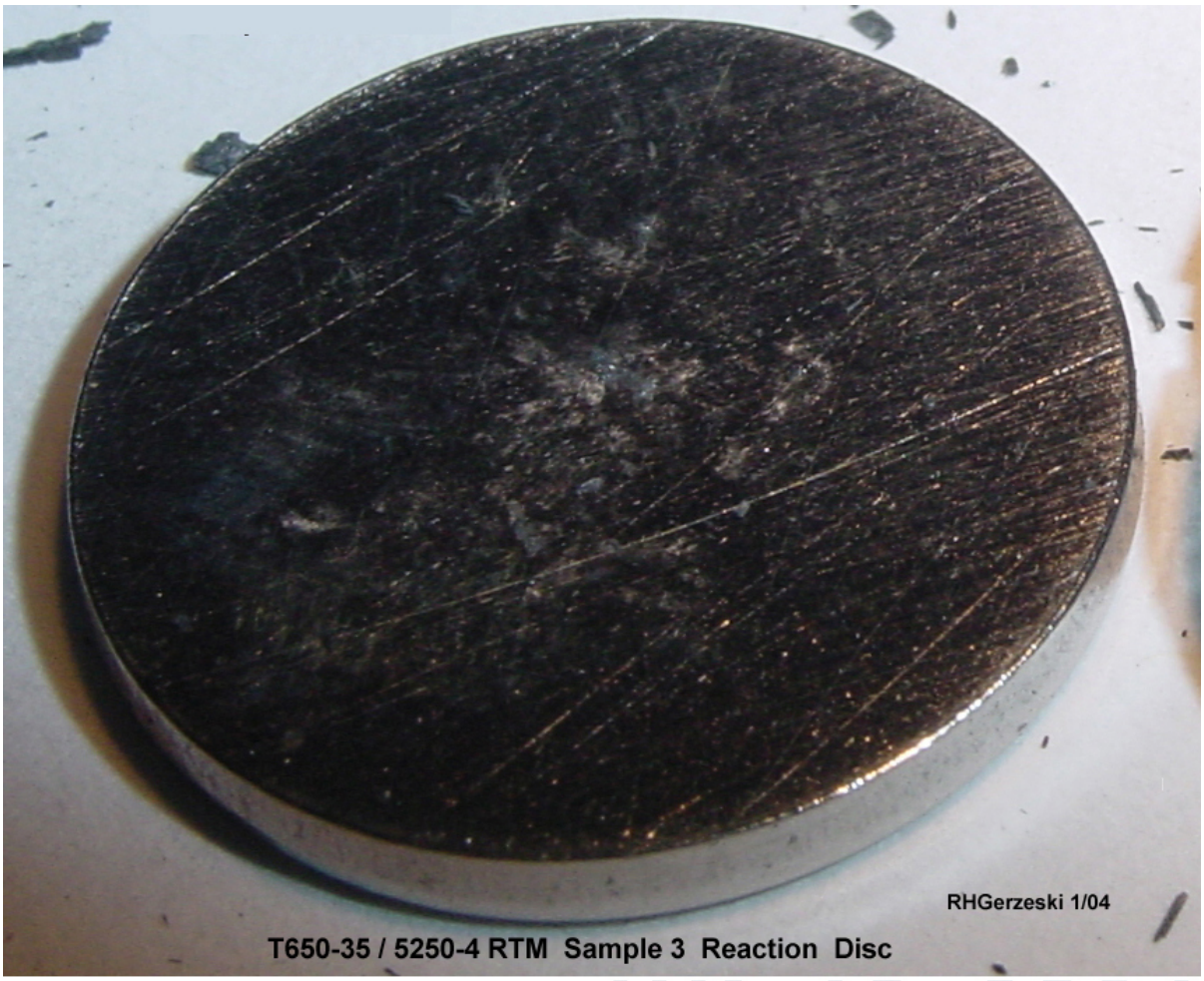


Figure R11c T650-35-UC309 / 5250-4 RTM D2512 72 FtLb LOX Tested Specimen Disc Residuals



Figure R11d T650-35-UC309 / 5250-4 RTM D2512 72 FtLb LOX Tested Specimen Disc Residuals



Figure R11e T650-35-UC309 / 5250-4 RTM D2512 72 FtLb LOX Tested Specimen Disc Residuals



Figure R11f T650-35-UC309 / 5250-4 RTM D2512 72 FtLb LOX Tested Specimen Disc Residuals



Figure R11g T650-35-UC309 / 5250-4 RTM D2512 72 FtLb LOX Tested Specimen Disc Residuals



Figure R11h T650-35-UC309 / 5250-4 RTM D2512 72 FtLb LOX Tested Specimen Disc Residuals



Figure R11i T650-35-UC309 / 5250-4 RTM D2512 72 FtLb LOX Tested Specimen Disc Residuals



Figure R11j T650-35-UC309 / 5250-4 RTM D2512 72 FtLb LOX Tested Specimen Disc Residuals



Figure R11k T650-35-UC309 / 5250-4 RTM D2512 72 FtLb LOX Tested Specimen Disc Residuals



Figure R11l T650-35-UC309 / 5250-4 RTM D2512 72 FtLb LOX Tested Specimen Disc Residuals



Figure R11m T650-35-UC309 / 5250-4 RTM D2512 72 FtLb LOX Tested Specimen Disc Residuals



Figure R11n T650-35-UC309 / 5250-4 RTM D2512 72 FtLb LOX Tested Specimen Disc Residuals

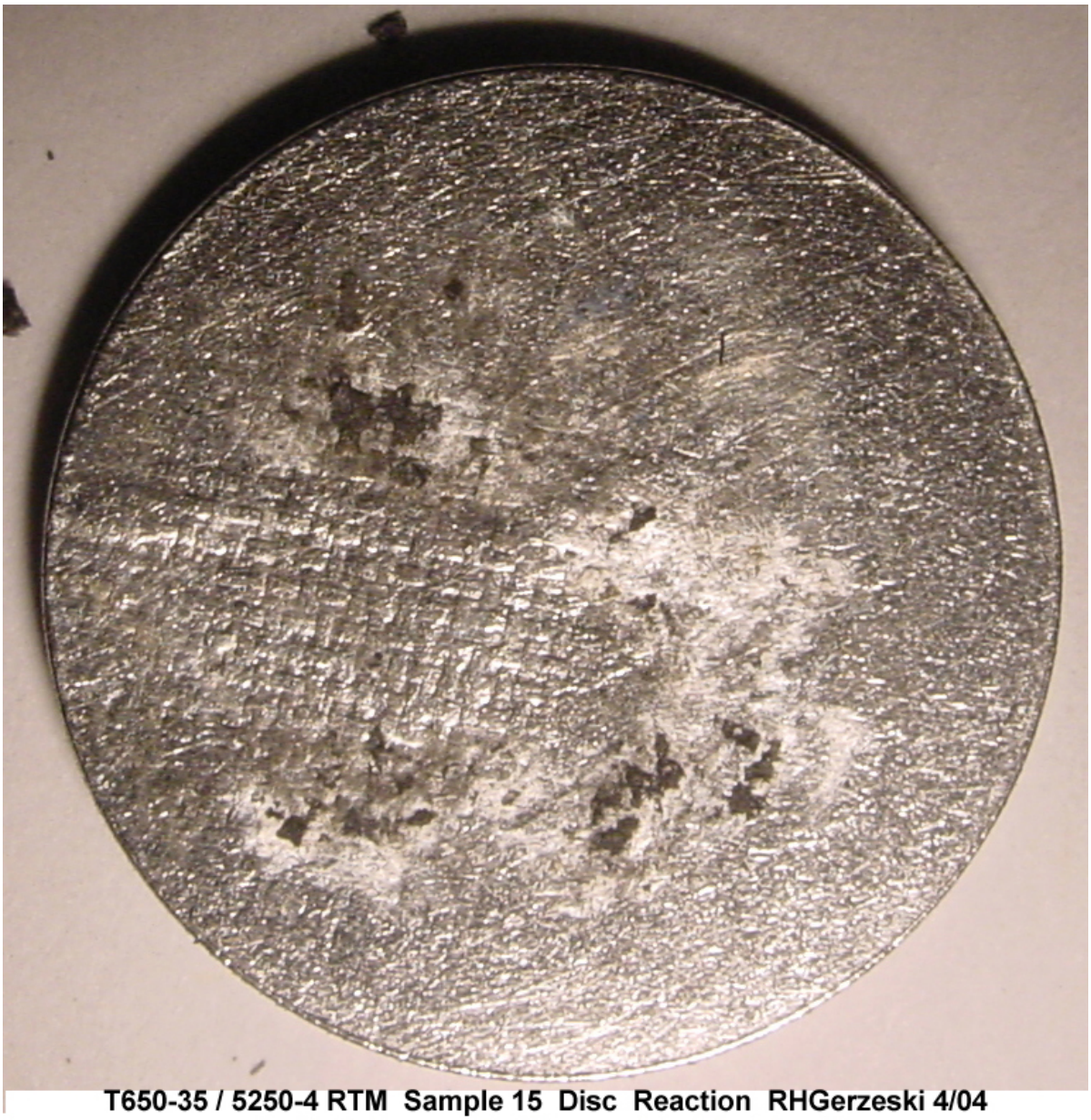


Figure R11o T650-35-UC309 / 5250-4 RTM D2512 72 FtLb LOX Tested Specimen Disc Residuals

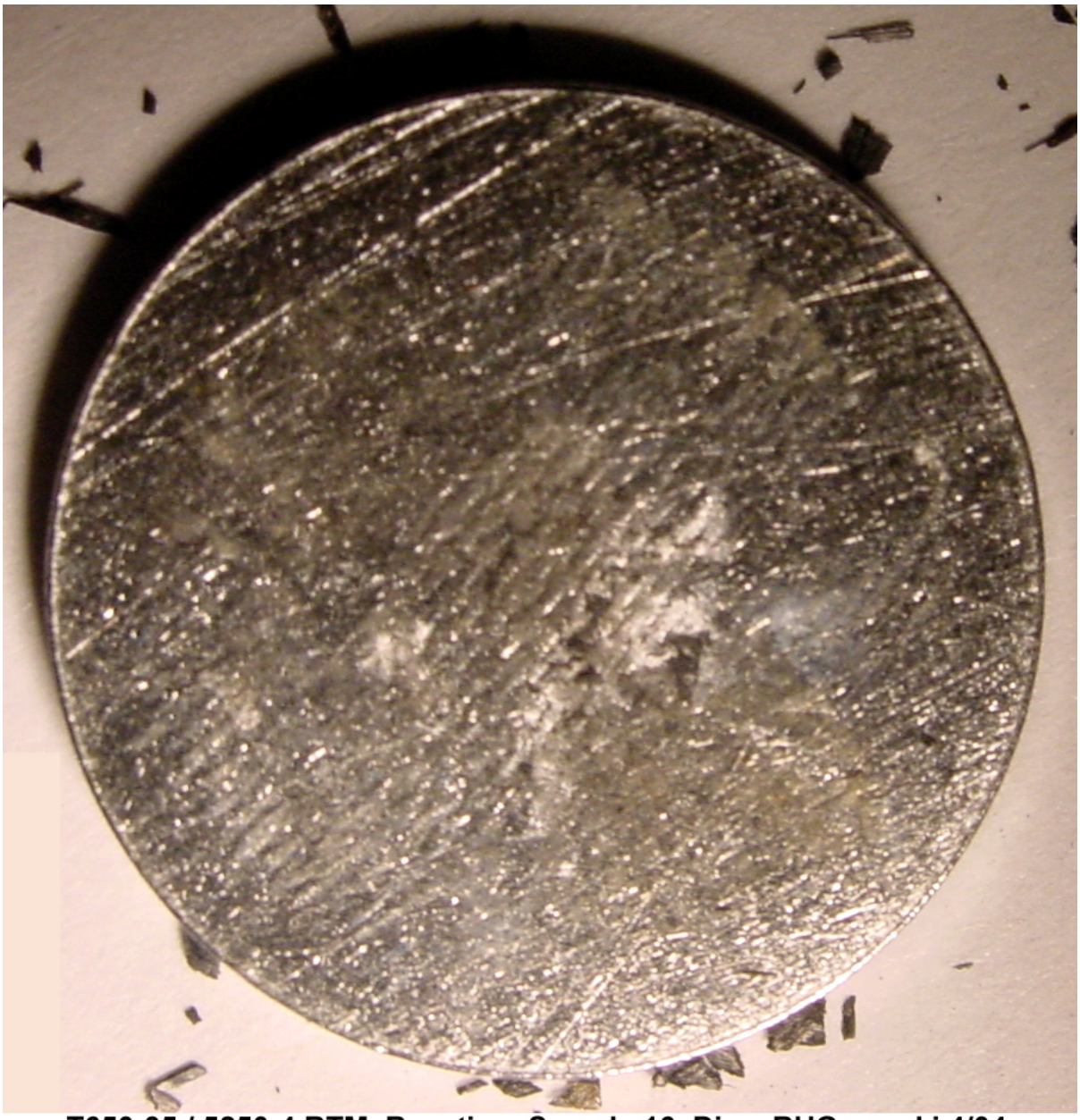


Figure R11p T650-35-UC309 / 5250-4 RTM D2512 72 FtLb LOX Tested Specimen Disc Residuals



Figure R11q T650-35-UC309 / 5250-4 RTM D2512 72 FtLb LOX Tested Specimen Disc Residuals



Figure R11r T650-35-UC309 / 5250-4 RTM D2512 72 FtLb LOX Tested Specimen Disc Residuals



Figure R11s T650-35-UC309 / 5250-4 RTM D2512 72 FtLb LOX Tested Specimen Disc Residuals



Figure R11t T650-35-UC309 / 5250-4 RTM D2512 72 FtLb LOX Tested Specimen Disc Residuals

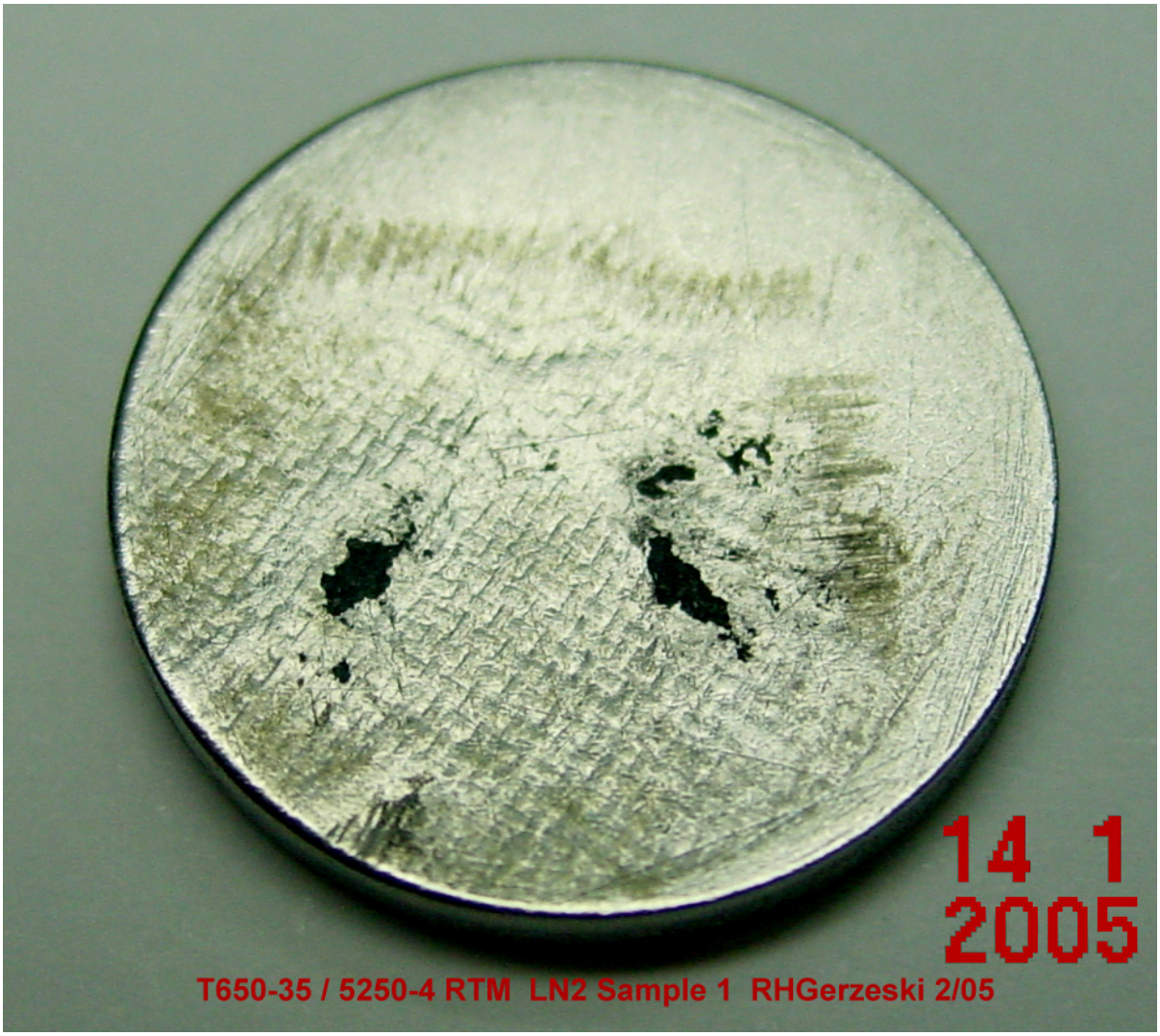


Figure R12a T650-35-UC309 / 5250-4 RTM D2512 72 FtLb In LN2 Tested Specimen Disc Residuals



Figure R12b T650-35-UC309 / 5250-4 RTM D2512 72 FtLb In LN2 Tested Specimen Disc Residuals

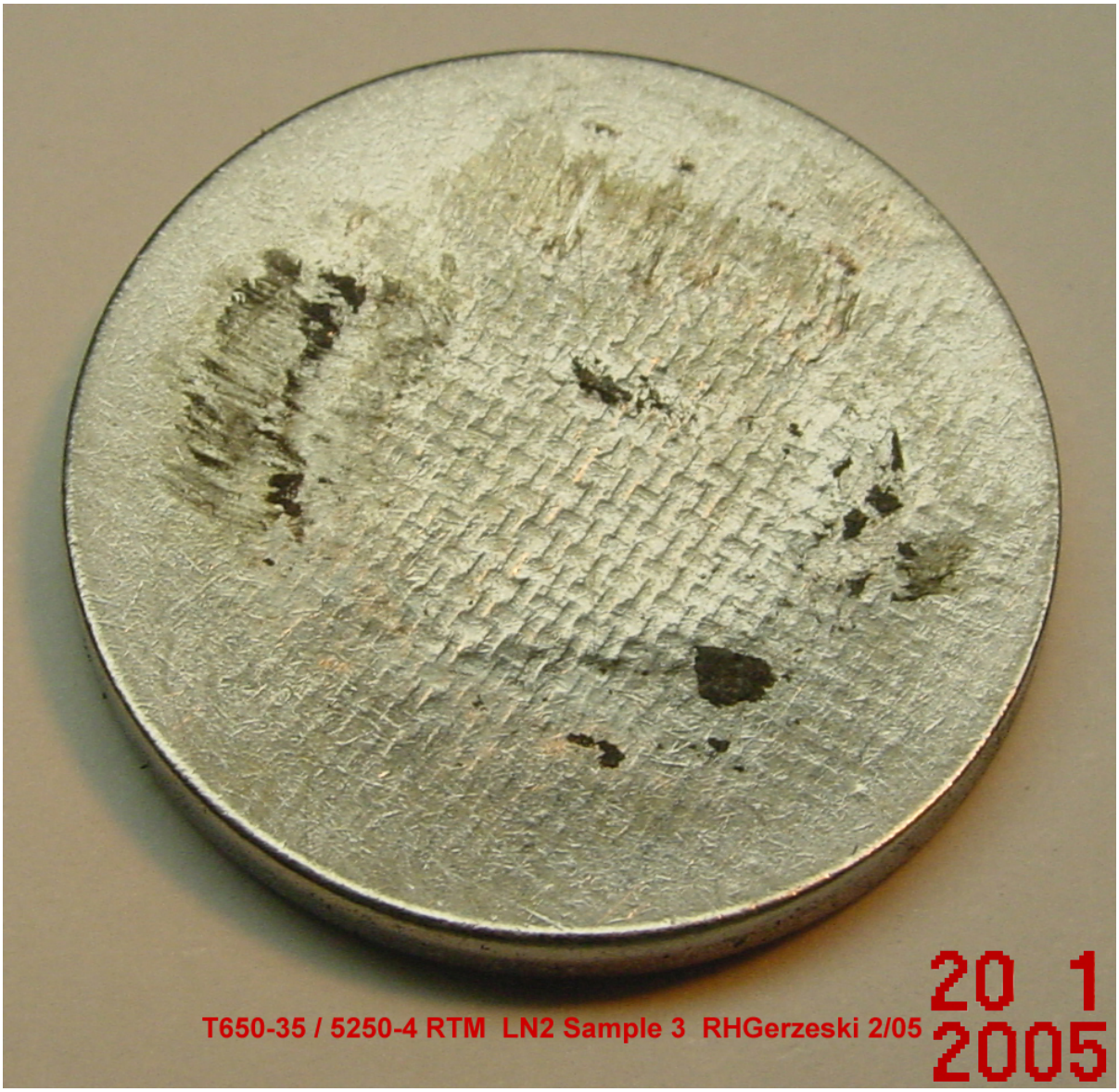


Figure R12c T650-35-UC309 / 5250-4 RTM D2512 72 FtLb In LN2 Tested Specimen Disc Residuals



Figure R13a YSH50A / 5250-4 RTM D2512 72 FtLb LOX Tested Specimen Disc Residuals



Figure R13b YSH50A / 5250-4 RTM D2512 72 FtLb LOX Tested Specimen Disc Residuals



Figure R13c YSH50A / 5250-4 RTM D2512 72 FtLb LOX Tested Specimen Disc Residuals



Figure R13d YSH50A / 5250-4 RTM D2512 72 FtLb LOX Tested Specimen Disc Residuals



Figure R13e YSH50A / 5250-4 RTM D2512 72 FtLb LOX Tested Specimen Disc Residuals



Figure R13f YSH50A / 5250-4 RTM D2512 72 FtLb LOX Tested Specimen Disc Residuals



Figure R13g YSH50A / 5250-4 RTM D2512 72 FtLb LOX Tested Specimen Disc Residuals



Figure R13h YSH50A / 5250-4 RTM D2512 72 FtLb LOX Tested Specimen Disc Residuals



Figure R13i YSH50A / 5250-4 RTM D2512 72 FtLb LOX Tested Specimen Disc Residuals



Figure R13j YSH50A / 5250-4 RTM D2512 72 FtLb LOX Tested Specimen Disc Residuals



Figure R13k YSH50A / 5250-4 RTM D2512 72 FtLb LOX Tested Specimen Disc Residuals



Figure R13l YSH50A / 5250-4 RTM D2512 72 FtLb LOX Tested Specimen Disc Residuals



Figure R13m YSH50A / 5250-4 RTM D2512 72 FtLb LOX Tested Specimen Disc Residuals



Figure R13n YSH50A / 5250-4 RTM D2512 72 FtLb LOX Tested Specimen Disc Residuals



Figure R13o YSH50A / 5250-4 RTM D2512 72 FtLb LOX Tested Specimen Disc Residuals



Figure R13p YSH50A / 5250-4 RTM D2512 72 FtLb LOX Tested Specimen Disc Residuals

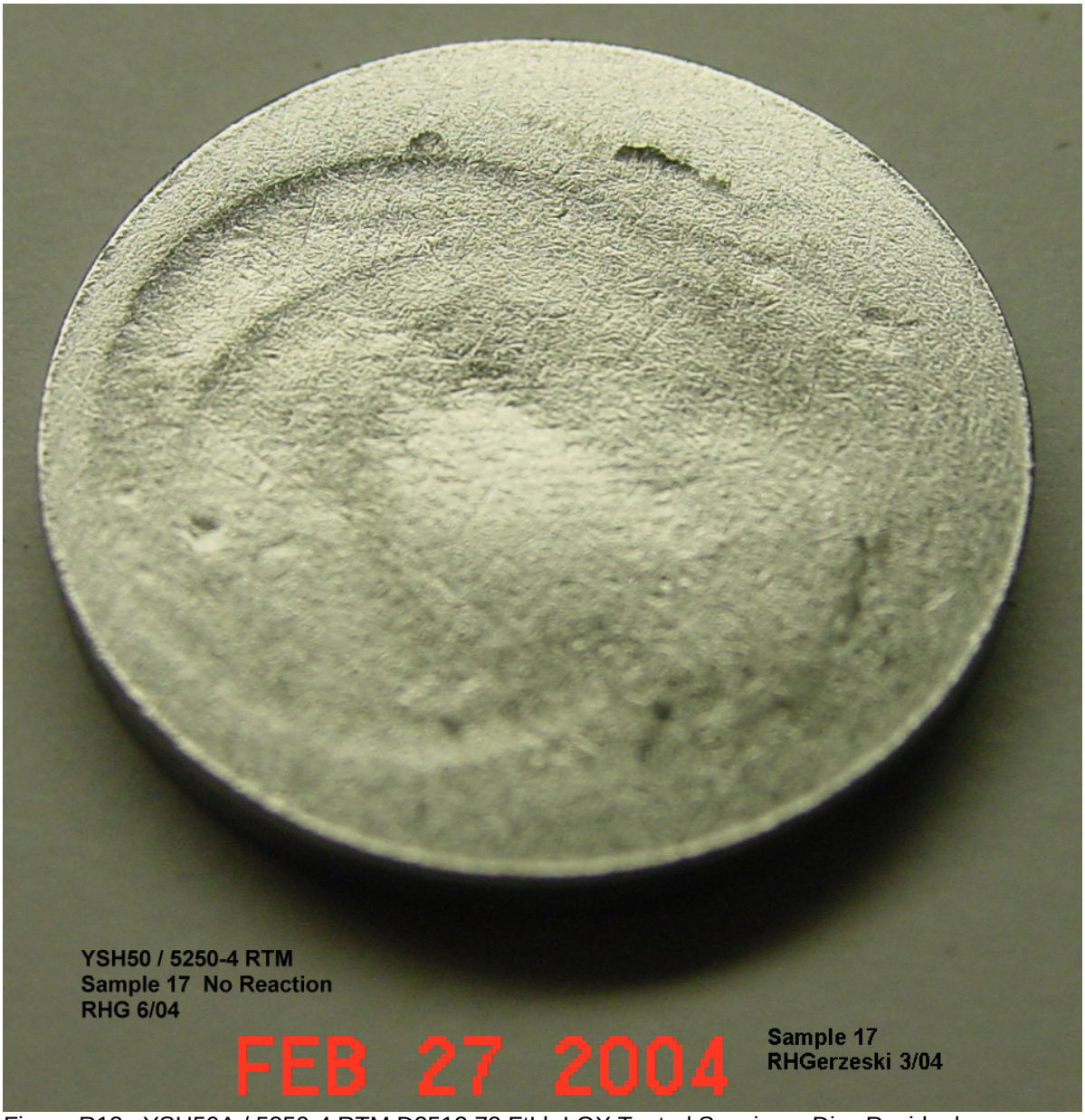


Figure R13q YSH50A / 5250-4 RTM D2512 72 FtLb LOX Tested Specimen Disc Residuals



Figure R13r YSH50A / 5250-4 RTM D2512 72 FtLb LOX Tested Specimen Disc Residuals



Figure R13s YSH50A / 5250-4 RTM D2512 72 FtLb LOX Tested Specimen Disc Residuals



Figure R13t YSH50A / 5250-4 RTM D2512 72 FtLb LOX Tested Specimen Disc Residuals



Figure R14a YSH50A / 5250-4 RTM D2512 72 FtLb In LN2 Tested Specimen Disc Residuals



Figure R14b YSH50A / 5 250-4 RTM D2512 72 FtLb In LN2 Tested Specimen Disc Residuals



Figure R14c YSH50A / 5250-4 RTM D2512 72 FtLb In LN2 Tested Specimen Disc Residuals

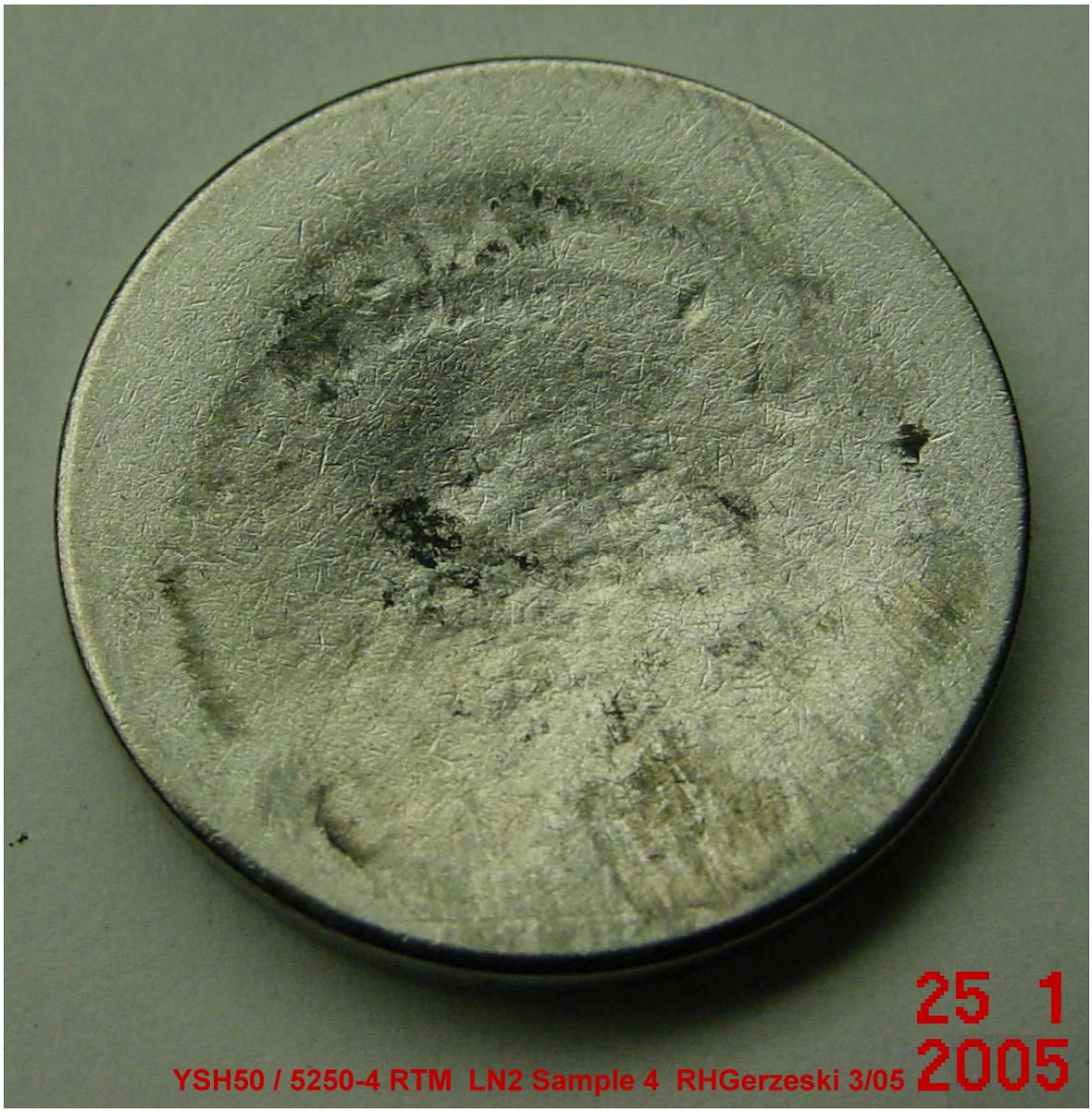


Figure R14d YSH50A / 5250-4 RTM D2512 72 FtLb In LN2 Tested Specimen Disc Residuals



Figure R15a YSH60A / 5250-4 RTM D2512 72 FtLb LOX Tested Specimen Disc Residuals



Figure R15b YSH60A / 5250-4 RTM D2512 72 FtLb LOX Tested Specimen Disc Residuals



Figure R15c YSH60A / 5250-4 RTM D2512 72 FtLb LOX Tested Specimen Disc Residuals

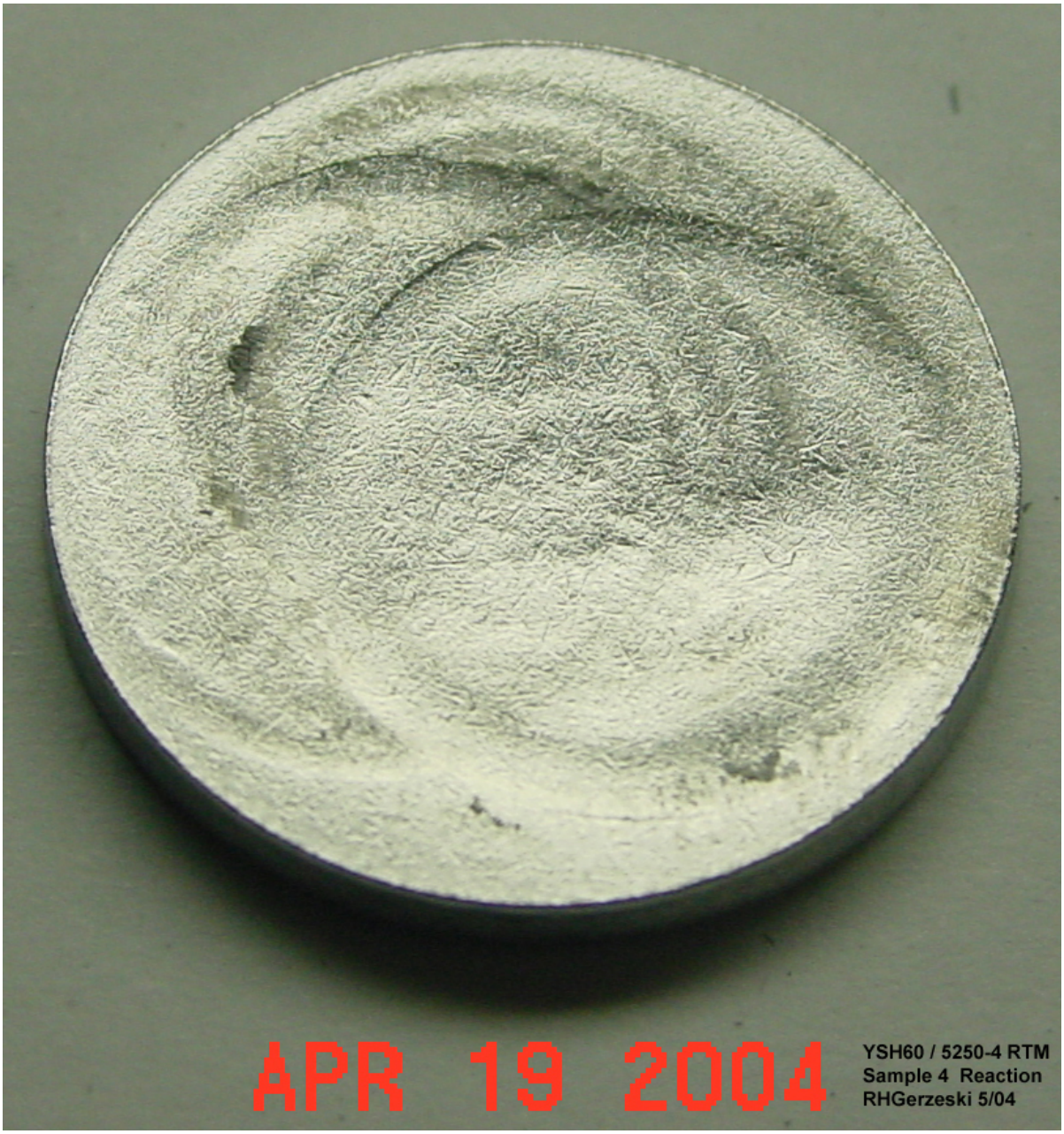


Figure R15d YSH60A / 5250-4 RTM D2512 72 FtLb LOX Tested Specimen Disc Residuals



Figure R15e YSH60A / 5250-4 RTM D2512 72 FtLb LOX Tested Specimen Disc Residuals

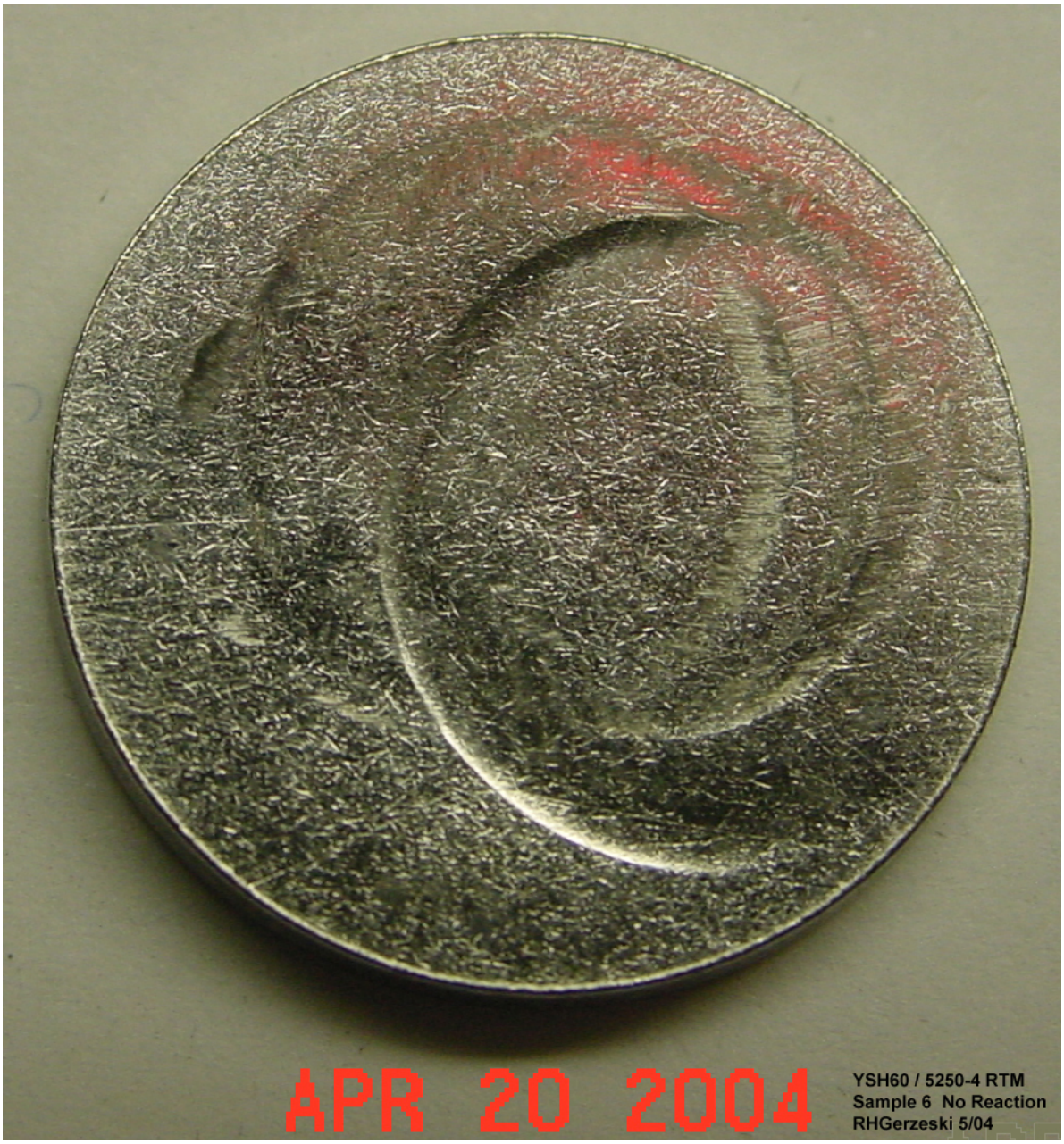


Figure R15f YSH60A / 5250-4 RTM D2512 72 FtLb LOX Tested Specimen Disc Residuals



Figure R15g YSH60A / 5250-4 RTM D2512 72 FtLb LOX Tested Specimen Disc Residuals



Figure R15h YSH60A / 5250-4 RTM D2512 72 FtLb LOX Tested Specimen Disc Residuals



Figure R15i YSH60A / 5250-4 RTM D2512 72 FtLb LOX Tested Specimen Disc Residuals



Figure R15j YSH60A / 5250-4 RTM D2512 72 FtLb LOX Tested Specimen Disc Residuals



Figure R15k YSH60A / 5250-4 RTM D2512 72 FtLb LOX Tested Specimen Disc Residuals



Figure R15l YSH60A / 5250-4 RTM D2512 72 FtLb LOX Tested Specimen Disc Residuals



Figure R15m YSH60A / 5250-4 RTM D2512 72 FtLb LOX Tested Specimen Disc Residuals

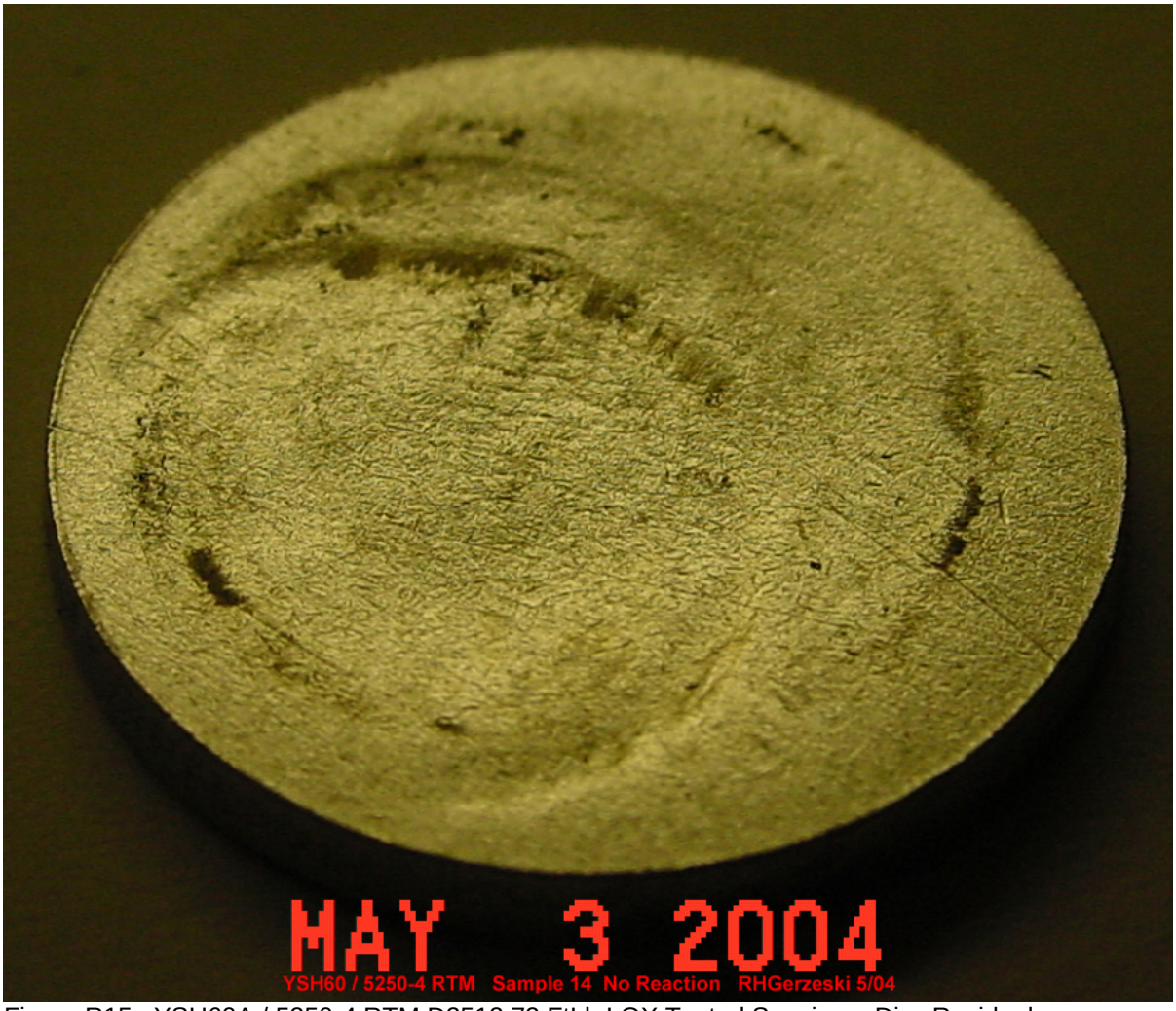


Figure R15n YSH60A / 5250-4 RTM D2512 72 FtLb LOX Tested Specimen Disc Residuals



Figure R15o YSH60A / 5250-4 RTM D2512 72 FtLb LOX Tested Specimen Disc Residuals



Figure R15p YSH60A / 5250-4 RTM D2512 72 FtLb LOX Tested Specimen Disc Residuals

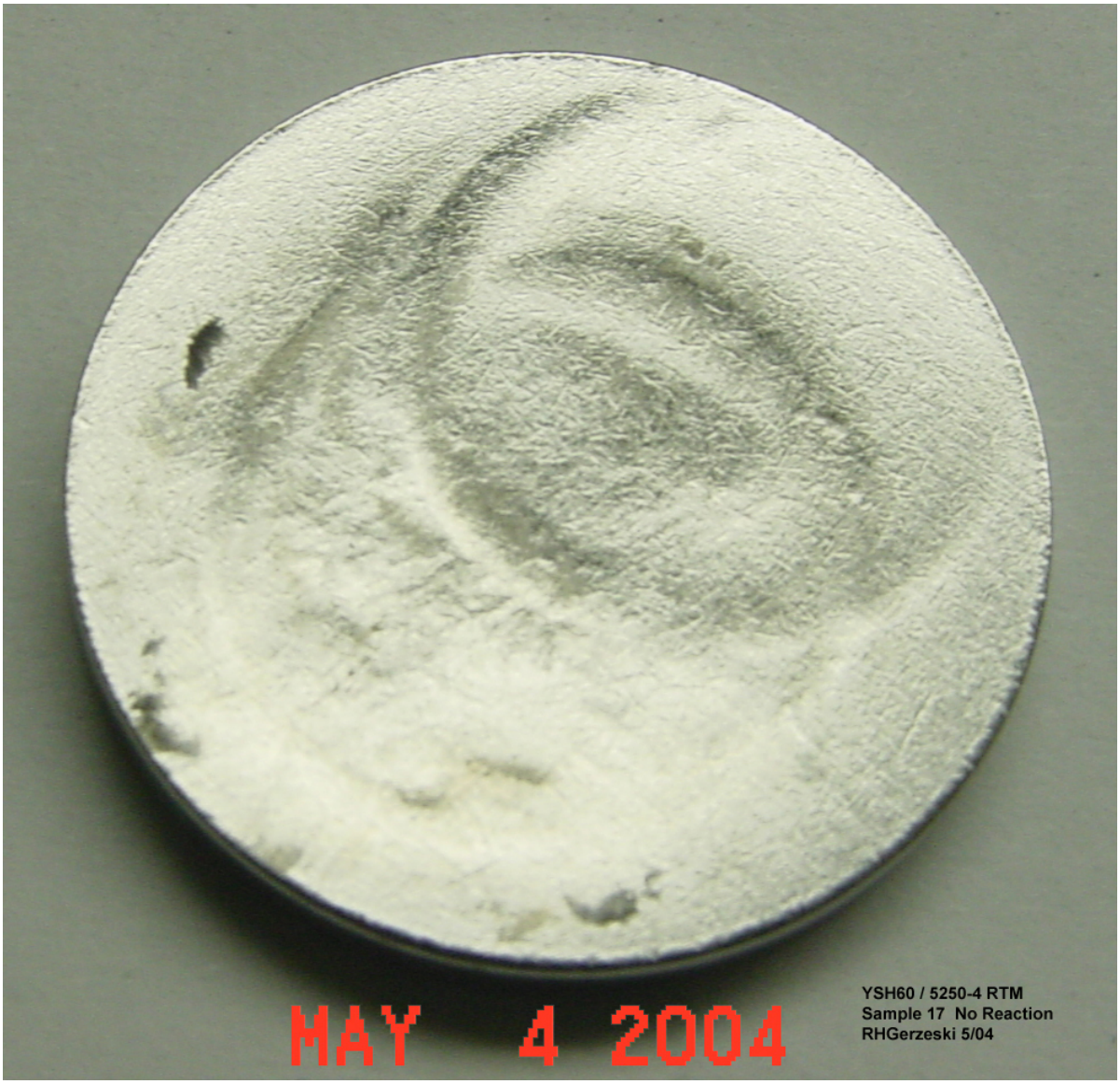


Figure R15q YSH60A / 5250-4 RTM D2512 72 FtLb LOX Tested Specimen Disc Residuals



Figure R15r YSH60A / 5250-4 RTM D2512 72 FtLb LOX Tested Specimen Disc Residuals



Figure R15s YSH60A / 5250-4 RTM D2512 72 FtLb LOX Tested Specimen Disc Residuals



Figure R15t YSH60A / 5250-4 RTM D2512 72 FtLb LOX Tested Specimen Disc Residuals



Figure R16a YSH60A / 5250-4 RTM D2512 72 FtLb In LN2 Tested Specimen Disc Residuals



Figure R16b YSH60A / 5 250-4 RTM D2512 72 FtLb In LN2 Tested Specimen Disc Residuals



Figure R16c YSH60A / 5250-4 RTM D2512 72 FtLb In LN2 Tested Specimen Disc Residuals



Figure R16d YSH60A / 5250-4 RTM D2512 72 FtLb In LN2 Tested Specimen Disc Residuals

Appendix: Residuals: Cup

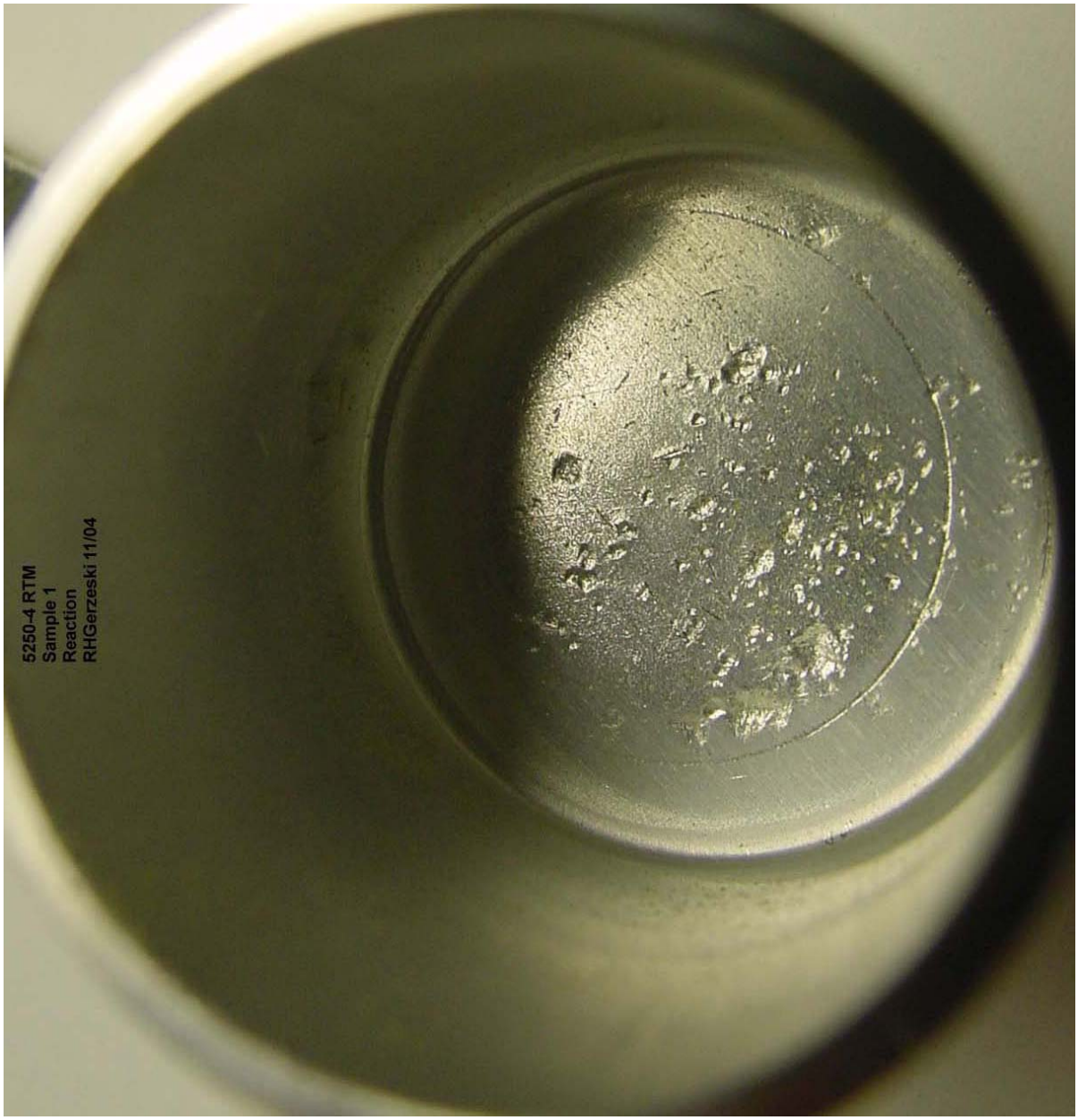


Figure R17a 5250-4 RTM D2512 72 FtLb LOX Tested Specimen Cup Residuals



Figure R17b 5250-4 RTM D2512 72 FtLb LOX Tested Specimen Cup Residuals

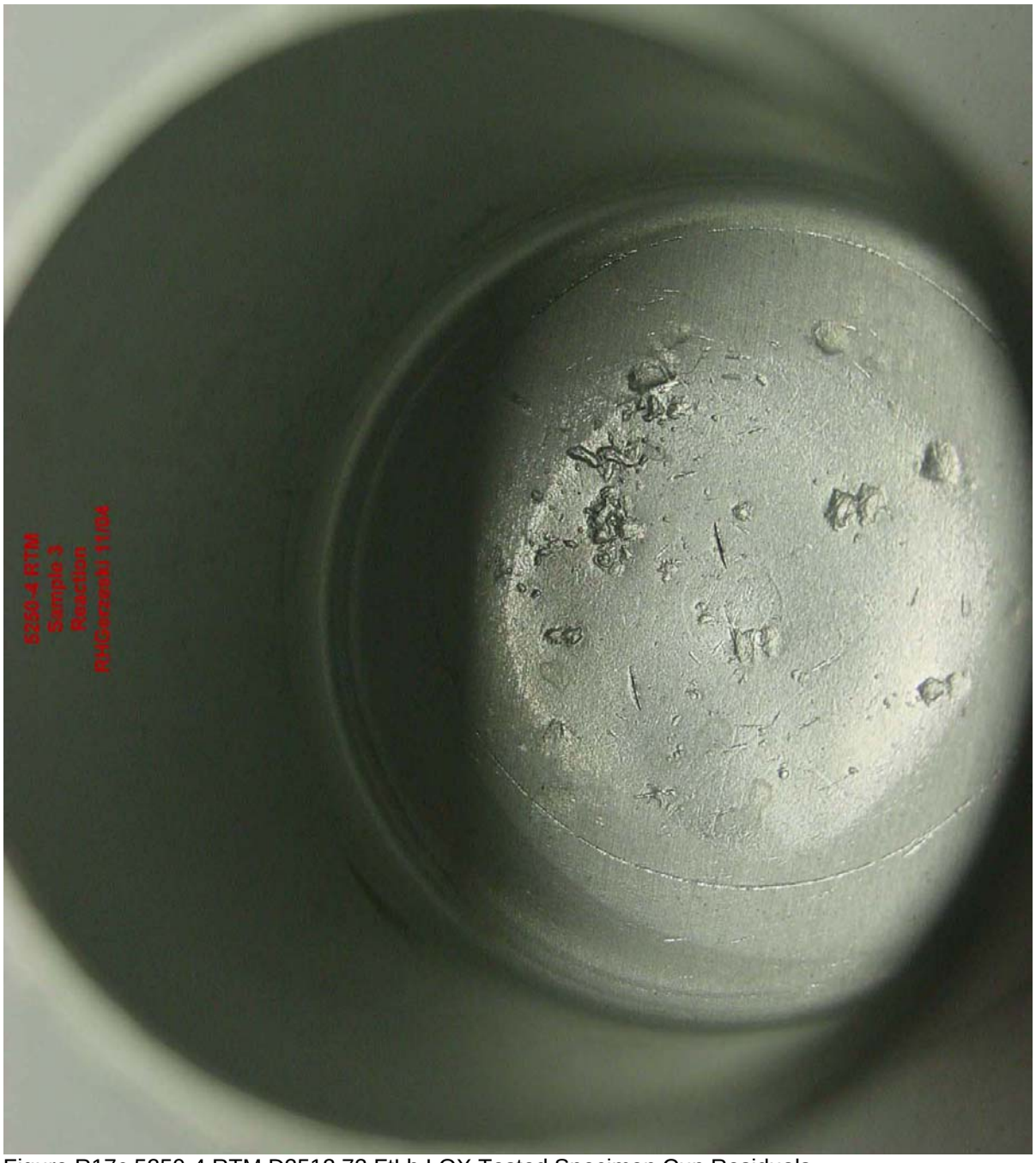


Figure R17c 5250-4 RTM D2512 72 FtLb LOX Tested Specimen Cup Residuals



Figure R17d 5250-4 RTM D2512 72 FtLb LOX Tested Specimen Cup Residuals



Figure R17e 5250-4 RTM D2512 72 FtLb LOX Tested Specimen Cup Residuals

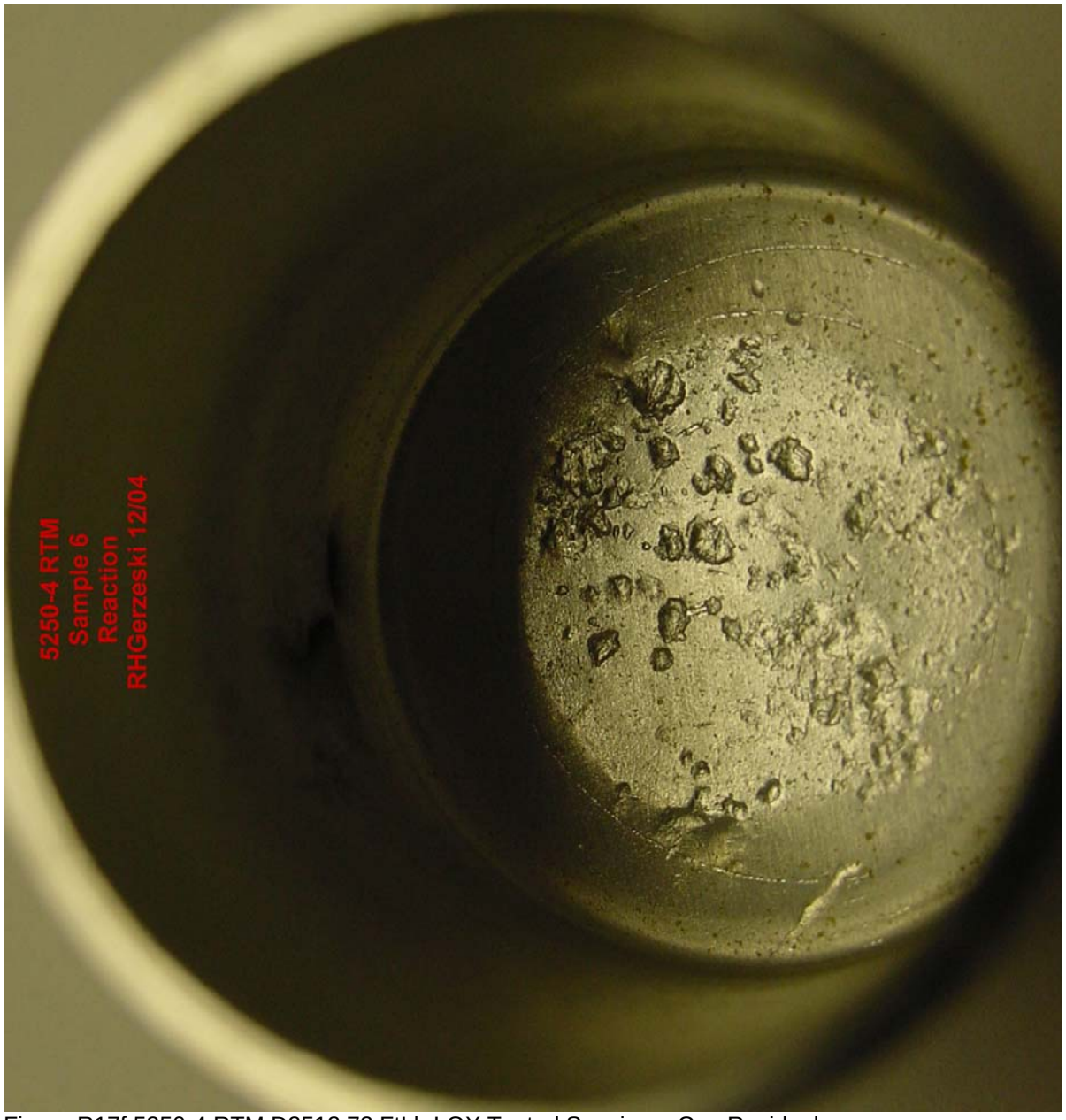


Figure R17f 5250-4 RTM D2512 72 FtLb LOX Tested Specimen Cup Residuals

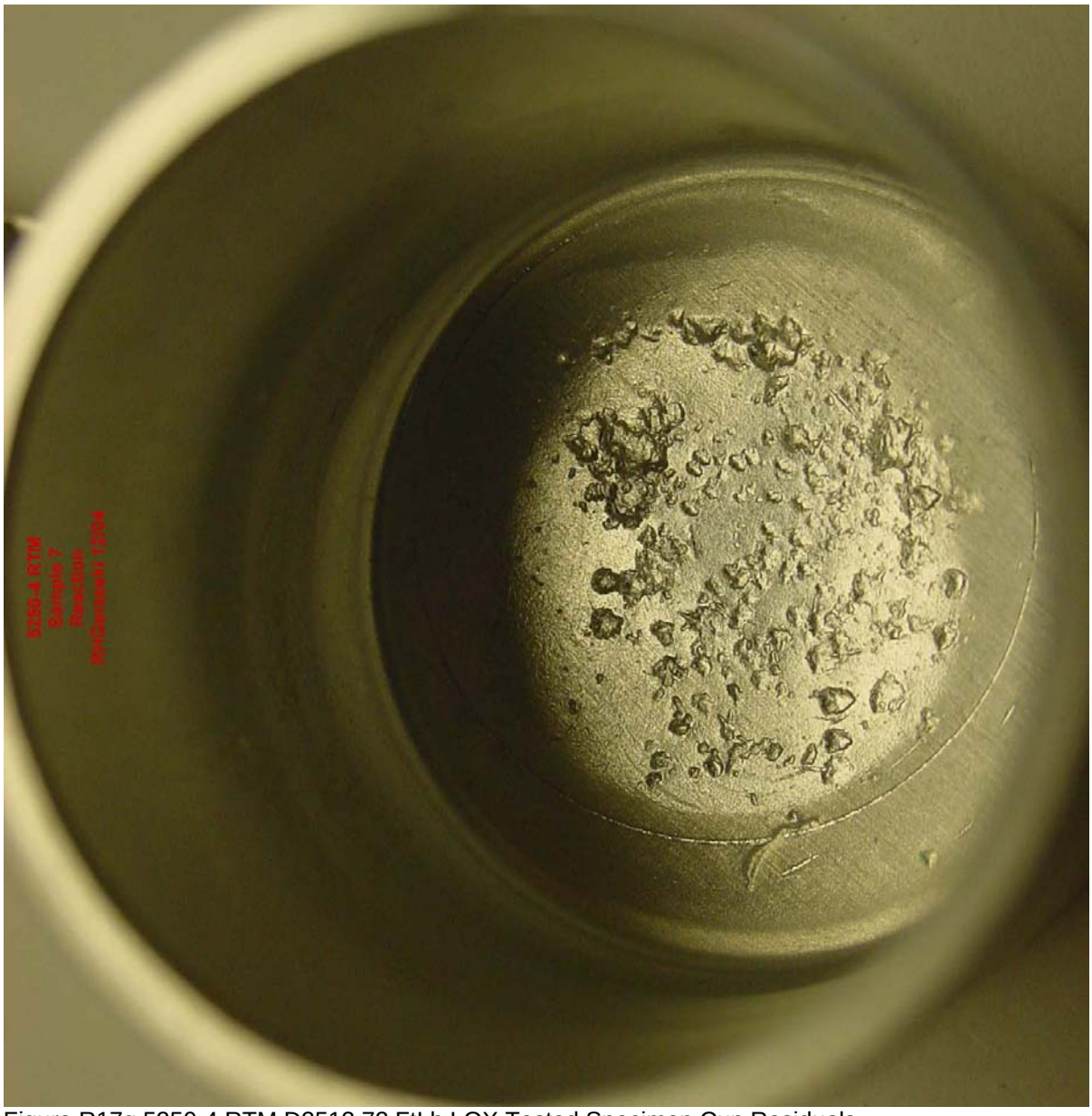


Figure R17g 5250-4 RTM D2512 72 FtLb LOX Tested Specimen Cup Residuals



Figure R17h 5250-4 RTM D2512 72 FtLb LOX Tested Specimen Cup Residuals

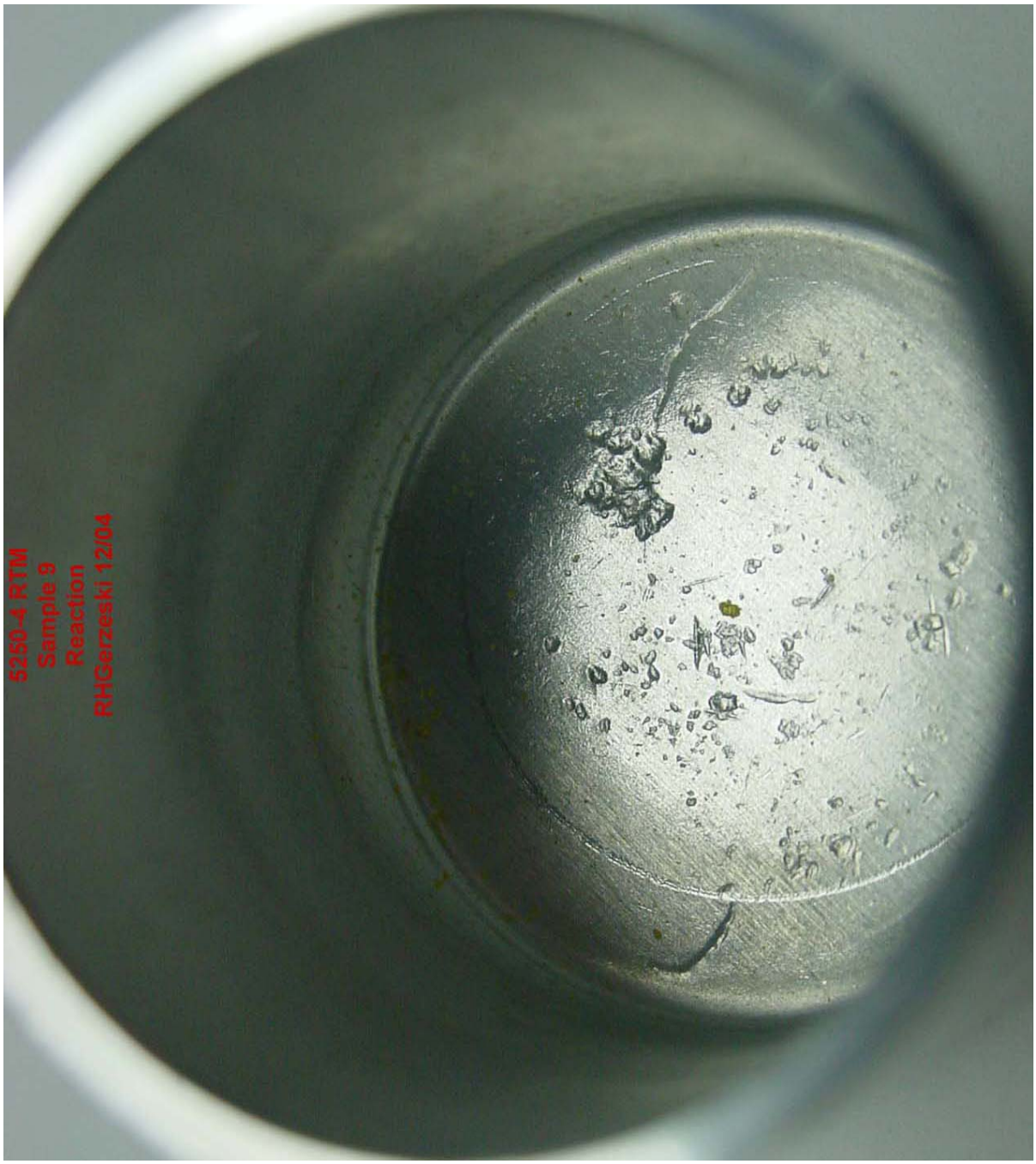


Figure R17i 5250-4 RTM D2512 72 FtLb LOX Tested Specimen Cup Residuals

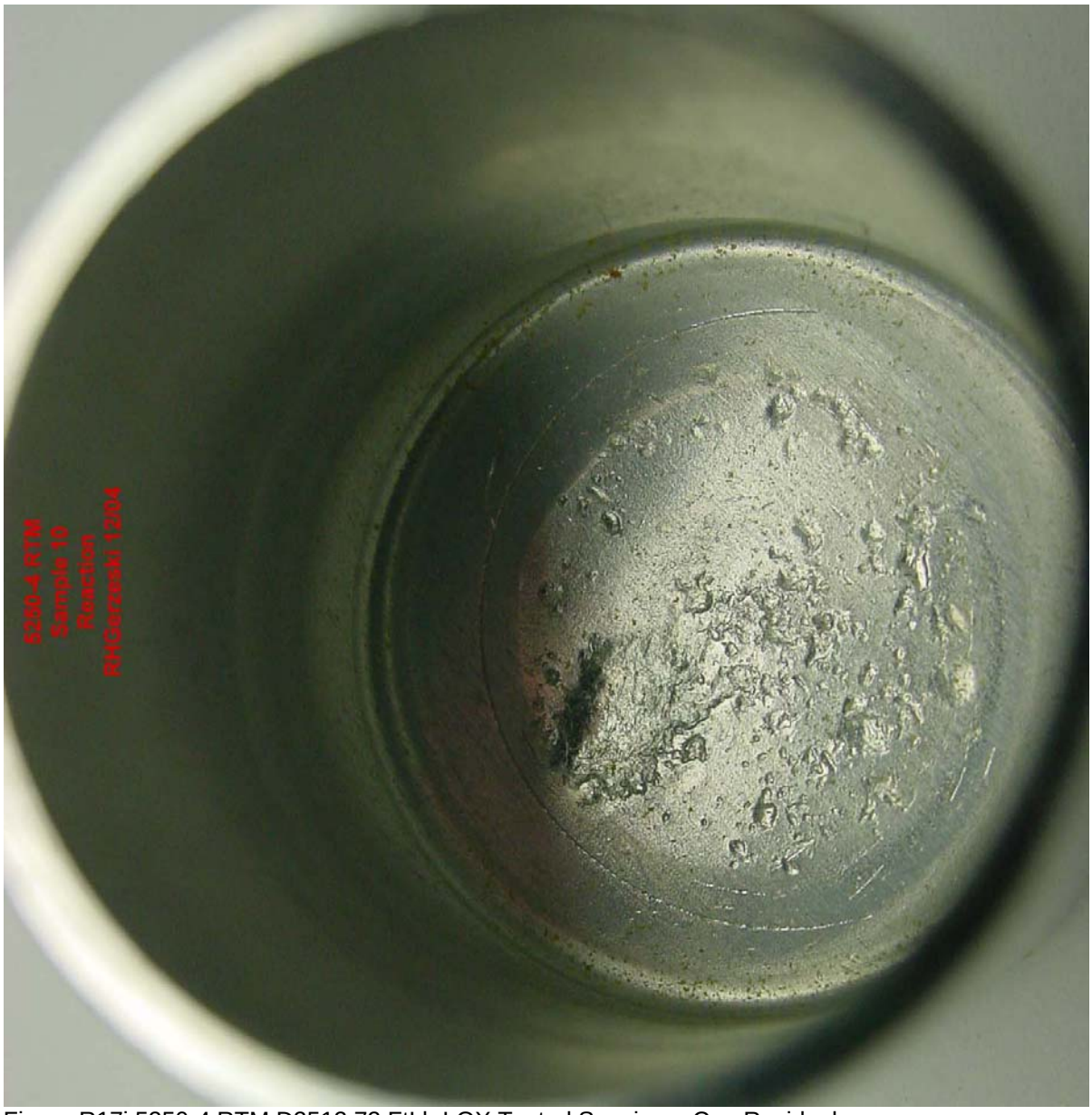


Figure R17j 5250-4 RTM D2512 72 FtLb LOX Tested Specimen Cup Residuals

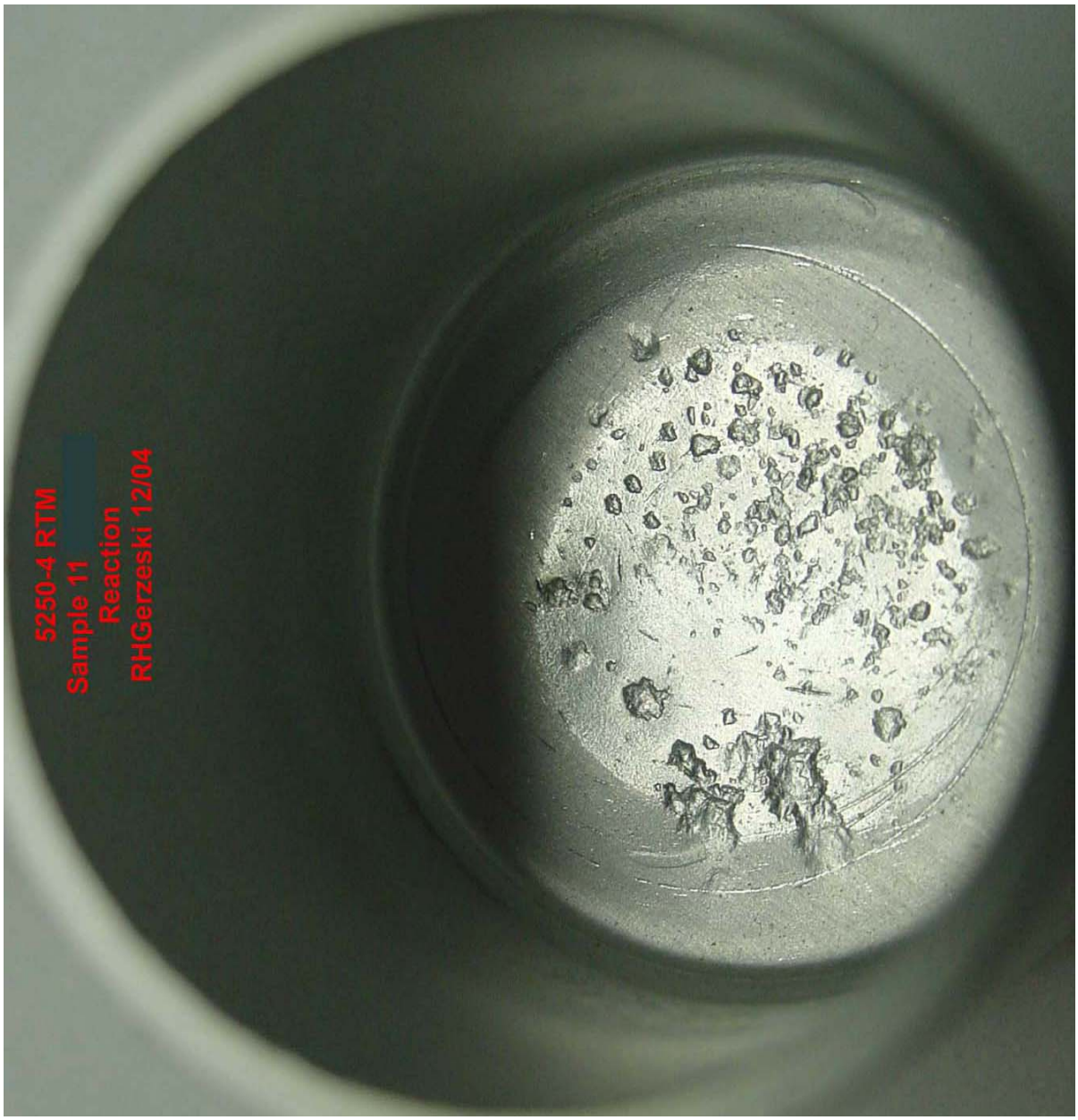


Figure R17k 5250-4 RTM D2512 72 FtLb LOX Tested Specimen Cup Residuals



Figure R17l 5250-4 RTM D2512 72 FtLb LOX Tested Specimen Cup Residuals

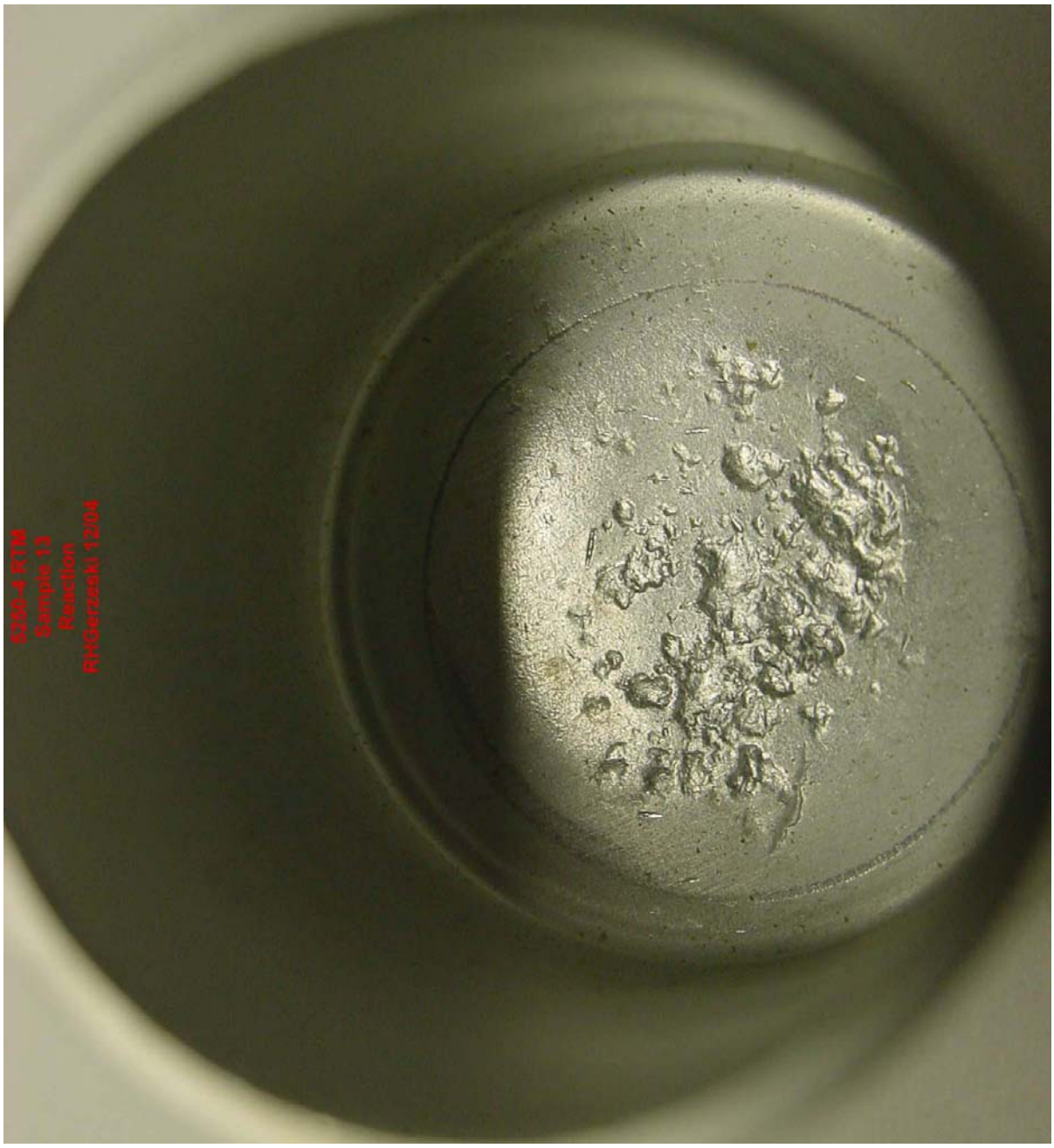


Figure R17m 5250-4 RTM D2512 72 FtLb LOX Tested Specimen Cup Residuals



Figure R17n 5250-4 RTM D2512 72 FtLb LOX Tested Specimen Cup Residuals

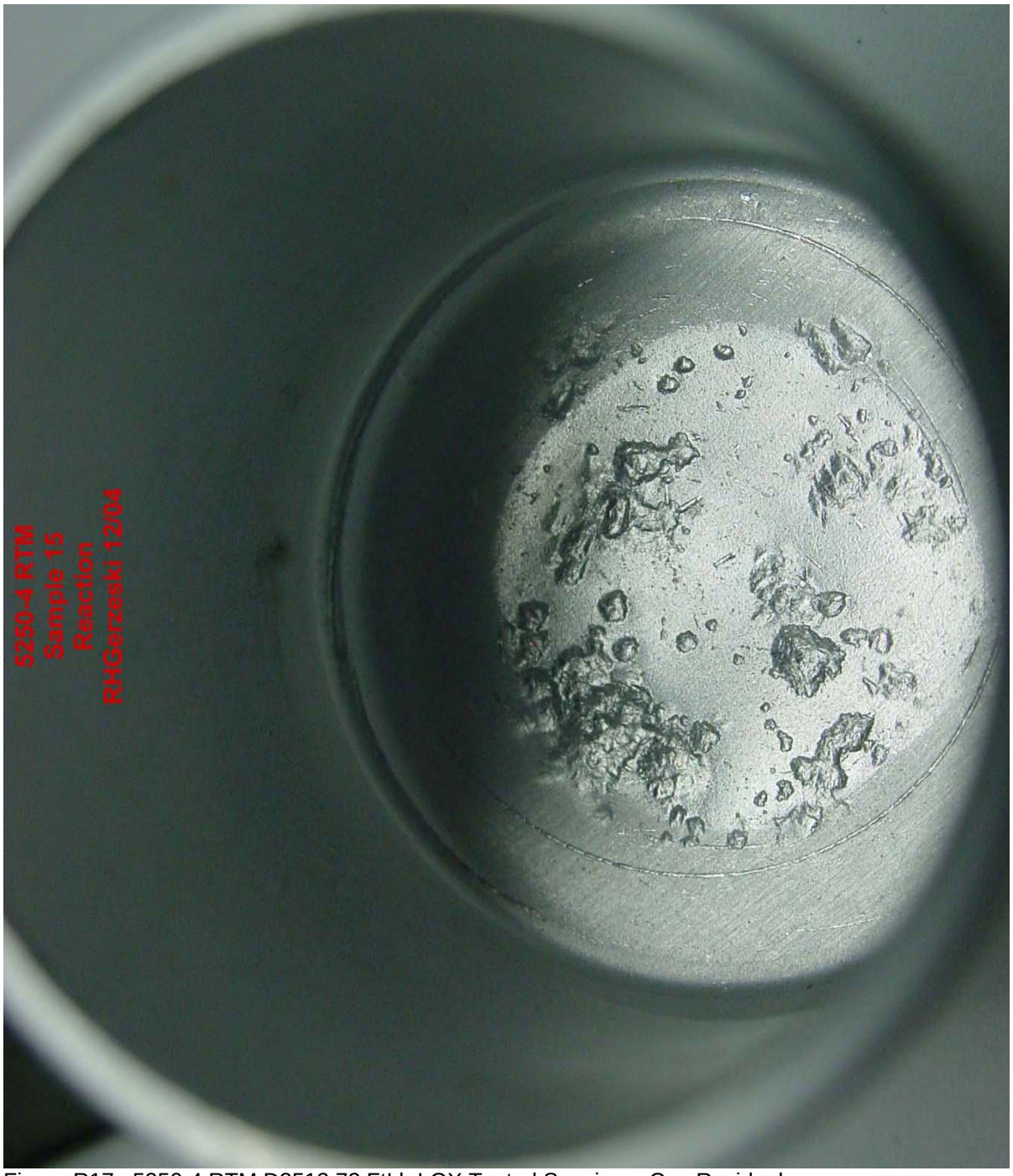


Figure R17o 5250-4 RTM D2512 72 FtLb LOX Tested Specimen Cup Residuals



Figure R17p 5250-4 RTM D2512 72 FtLb LOX Tested Specimen Cup Residuals

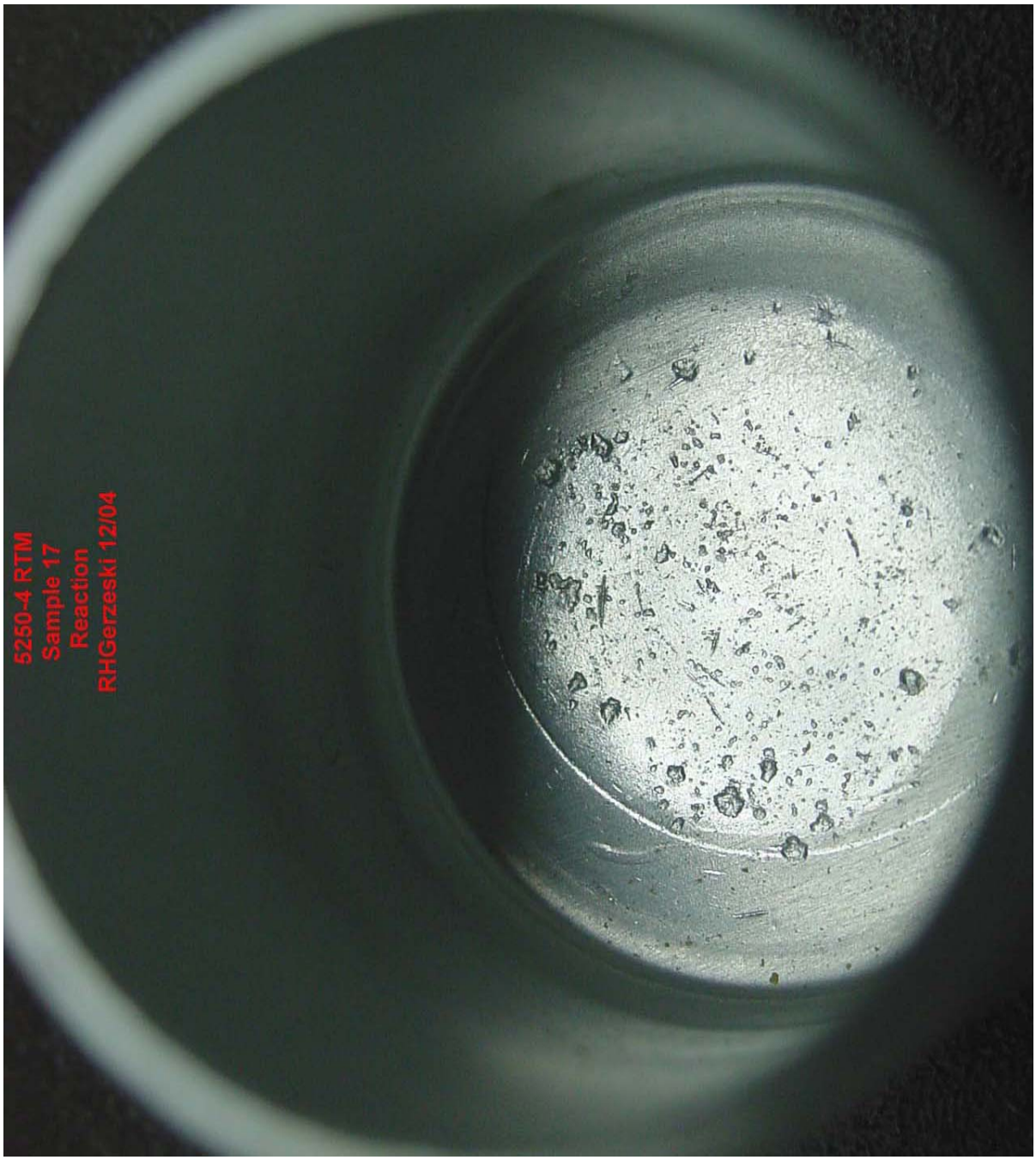


Figure R17q 5250-4 RTM D2512 72 FtLb LOX Tested Specimen Cup Residuals

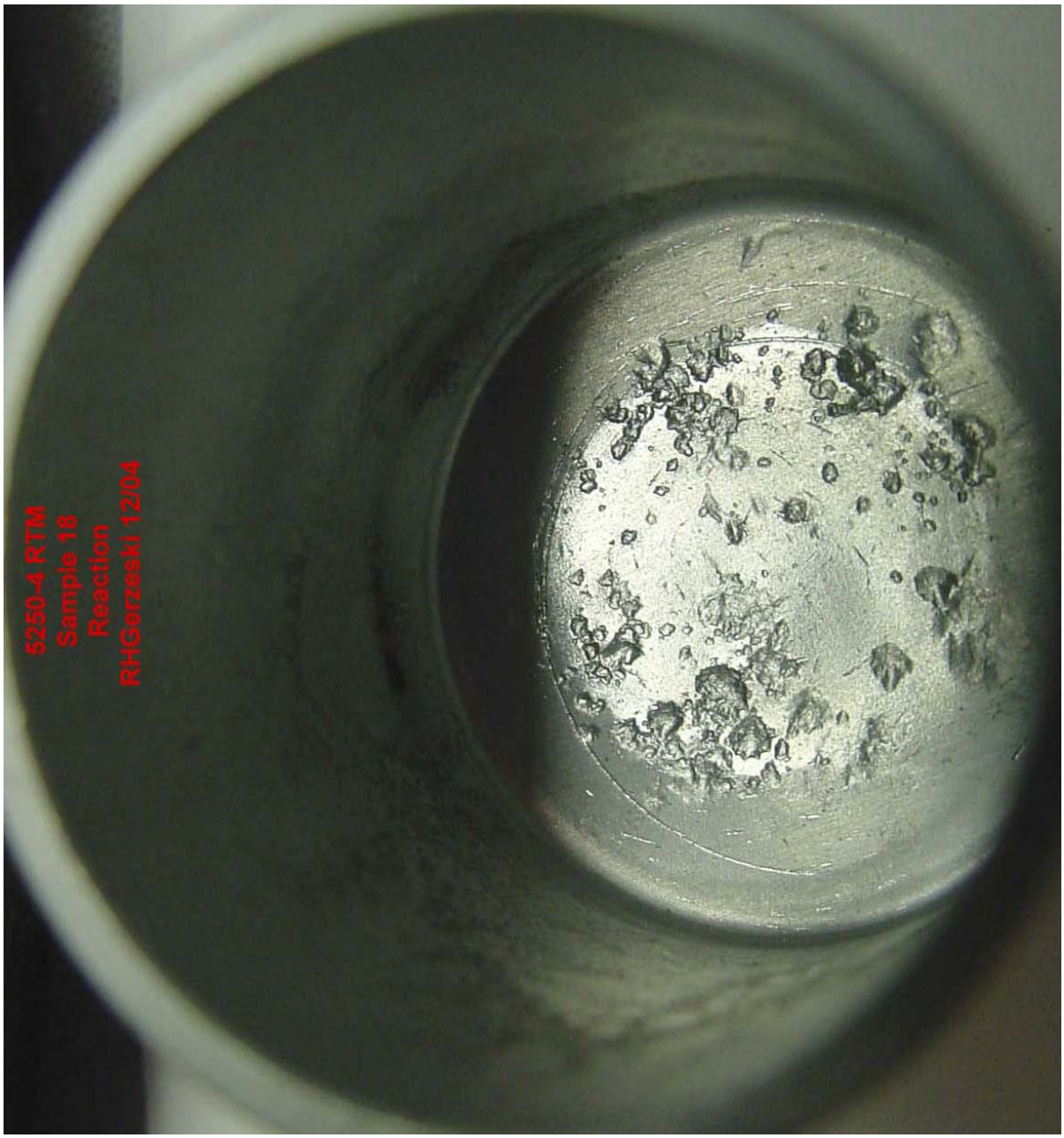


Figure R17r 5250-4 RTM D2512 72 FtLb LOX Tested Specimen Cup Residuals

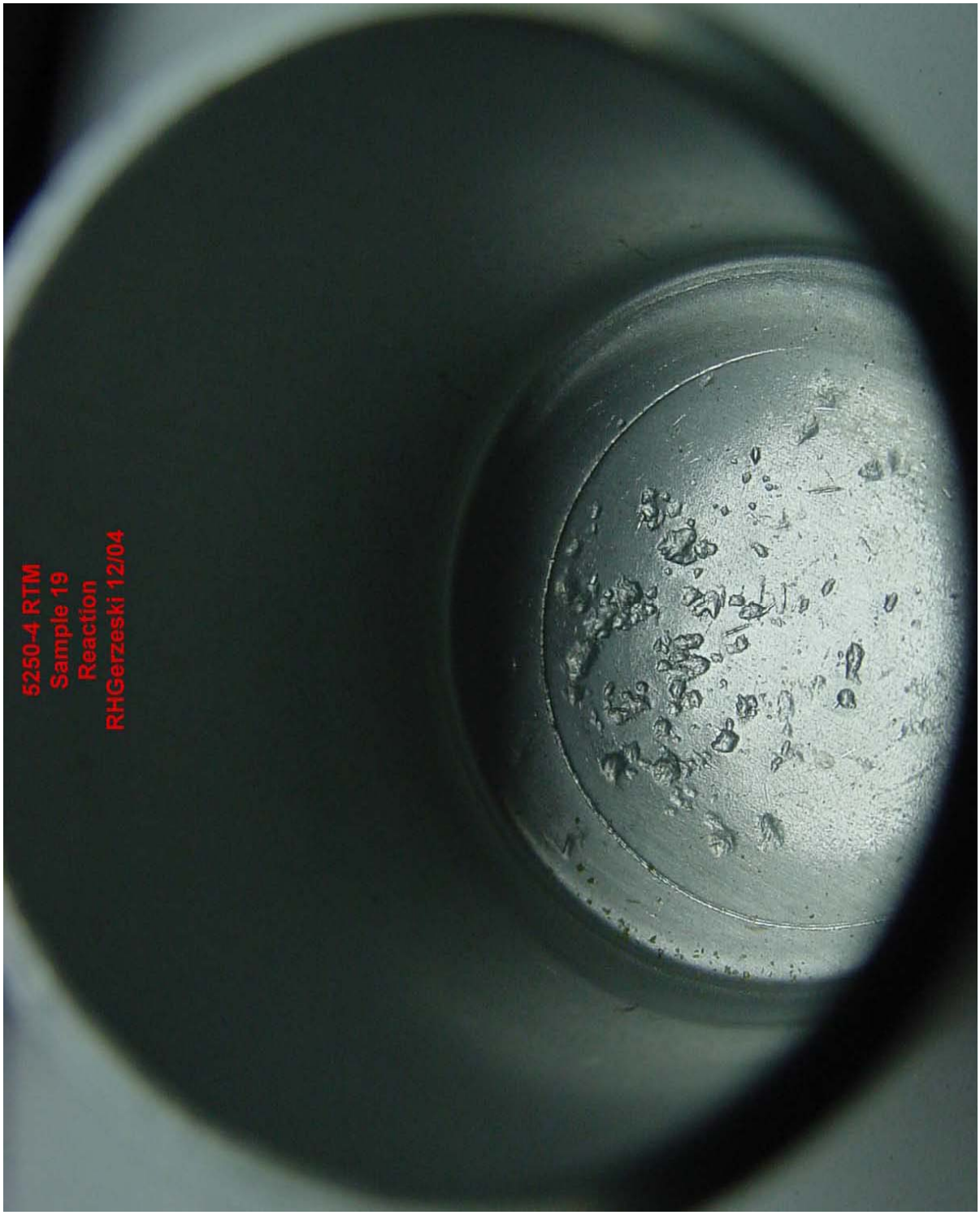


Figure R17s 5250-4 RTM D2512 72 FtLb LOX Tested Specimen Cup Residuals

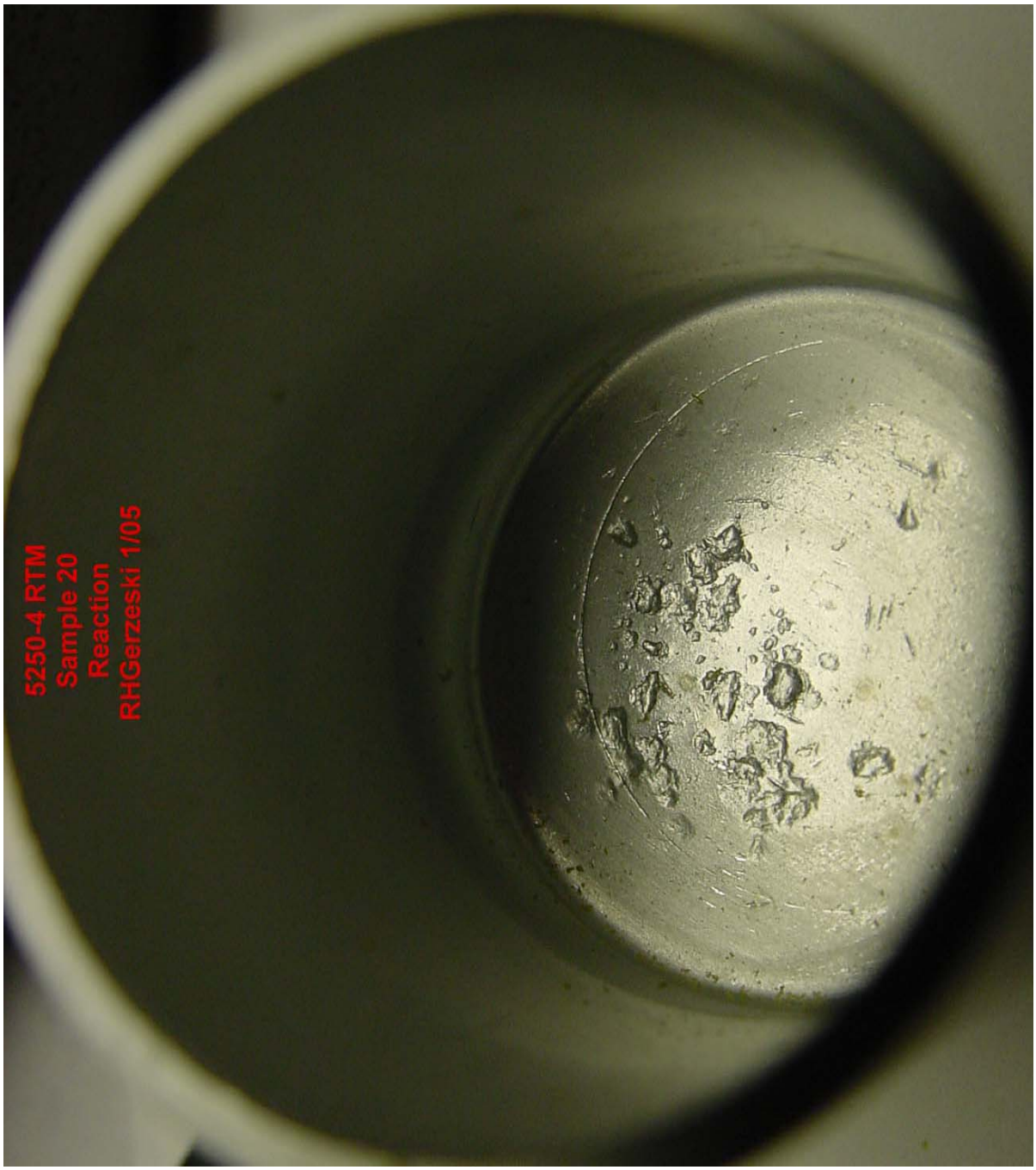


Figure R17t 5250-4 RTM D2512 72 FtLb LOX Tested Specimen Cup Residuals

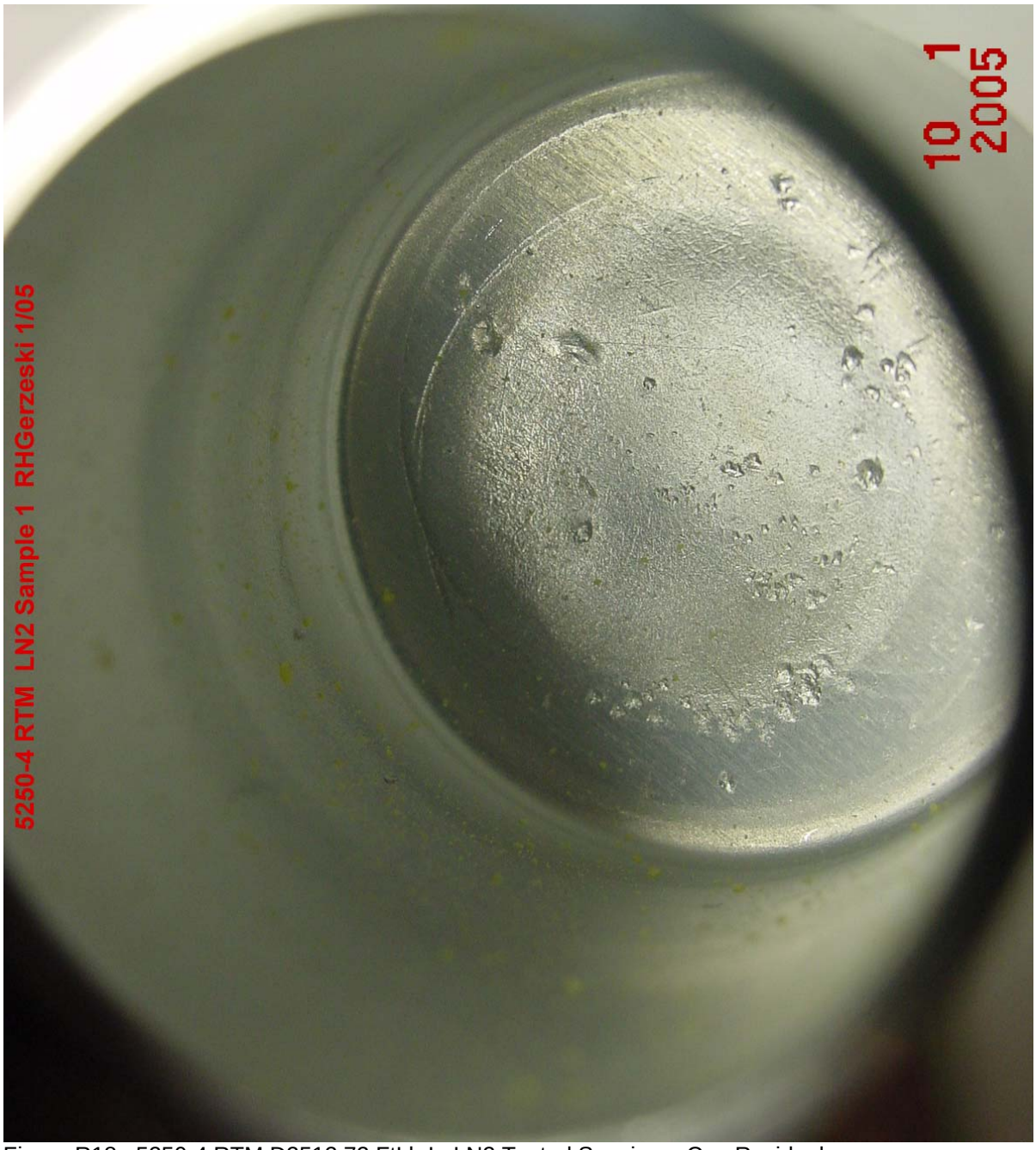


Figure R18a 5250-4 RTM D2512 72 FtLb In LN2 Tested Specimen Cup Residuals

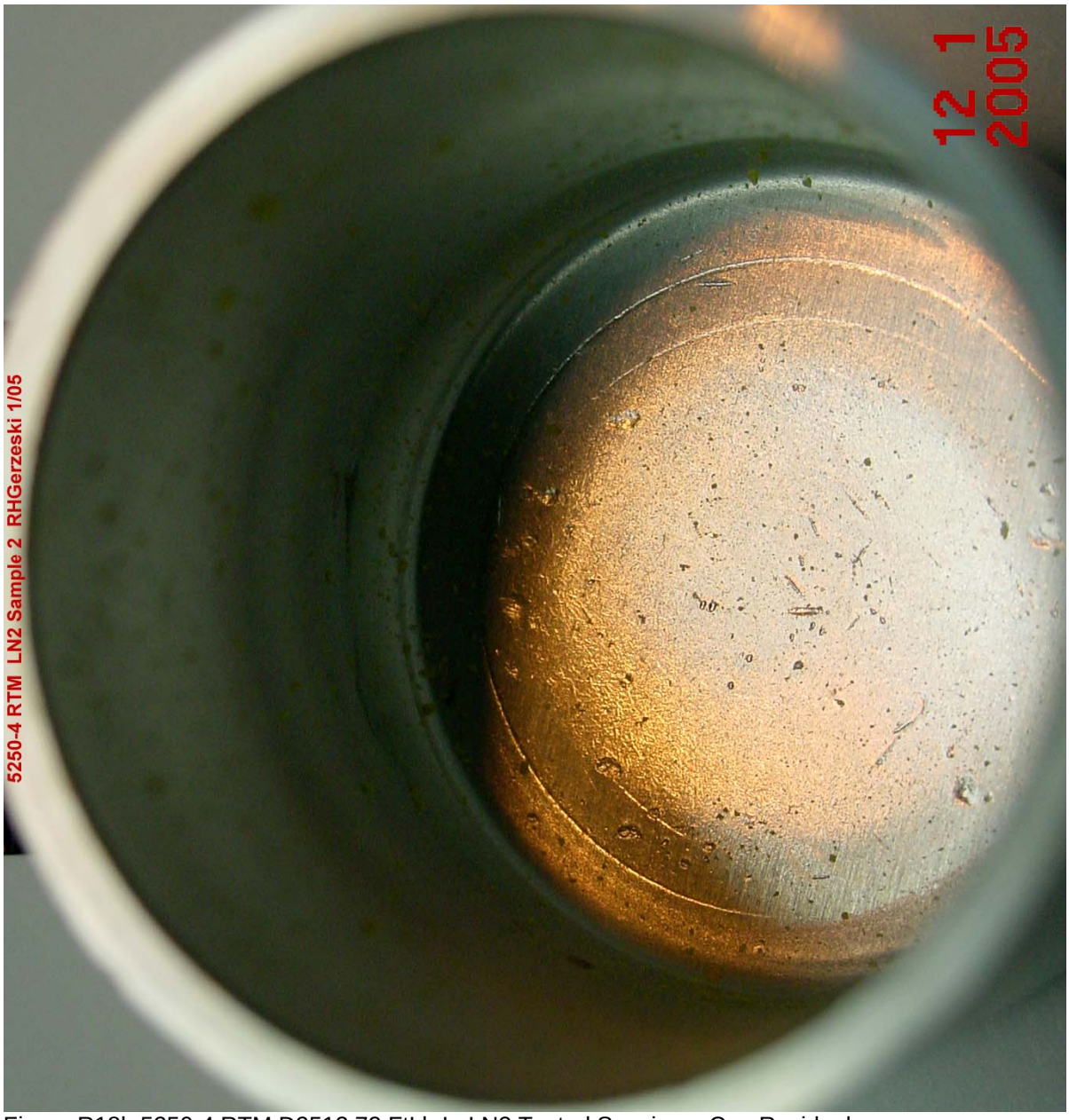


Figure R18b 5250-4 RTM D2512 72 FtLb In LN2 Tested Specimen Cup Residuals



Figure R18c 5250-4 RTM D2512 72 FtLb In LN2 Tested Specimen Cup Residuals

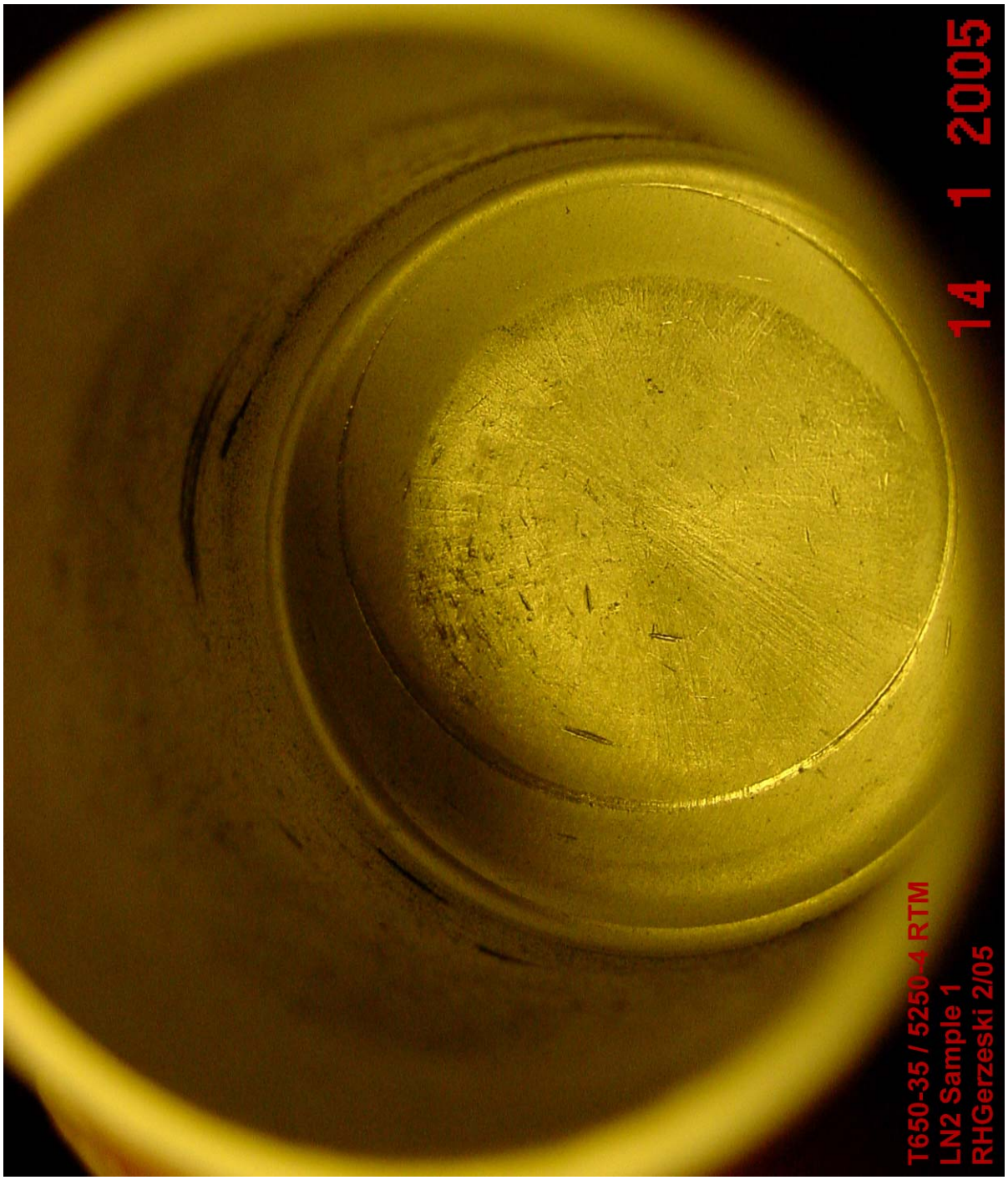


Figure R19a T650-35-UC309 / 5250-4 RTM D2512 72 FtLb In LN2 Tested Specimen Cup Residuals



Figure R19b T650-35-UC309 / 5250-4 RTM D2512 72 FtLb In LN2 Tested Specimen Cup Residuals



Figure R19c T650-35-UC309 / 5250-4 RTM D2512 72 FtLb In LN2 Tested Specimen Cup Residuals



Figure R20a YSH50A / 5250-4 RTM D2512 72 FtLb LOX Tested Specimen Cup Residuals



Figure R20b YSH50A / 5250-4 RTM D2512 72 FtLb LOX Tested Specimen Cup Residuals



Figure R20c YSH50A / 5250-4 RTM D2512 72 FtLb LOX Tested Specimen Cup Residuals



Figure R20d YSH50A / 5250-4 RTM D2512 72 FtLb LOX Tested Specimen Cup Residuals



Figure R20e YSH50A / 5250-4 RTM D2512 72 FtLb LOX Tested Specimen Cup Residuals



Figure R20f YSH50A / 5250-4 RTM D2512 72 FtLb LOX Tested Specimen Cup Residuals



Figure R20g YSH50A / 5250-4 RTM D2512 72 FtLb LOX Tested Specimen Cup Residuals



Figure R20h YSH50A / 5250-4 RTM D2512 72 FtLb LOX Tested Specimen Cup Residuals



Figure R20i YSH50A / 5250-4 RTM D2512 72 FtLb LOX Tested Specimen Cup Residuals



Figure R20j YSH50A / 5250-4 RTM D2512 72 FtLb LOX Tested Specimen Cup Residuals



Figure R20k YSH50A / 5250-4 RTM D2512 72 FtLb LOX Tested Specimen Cup Residuals

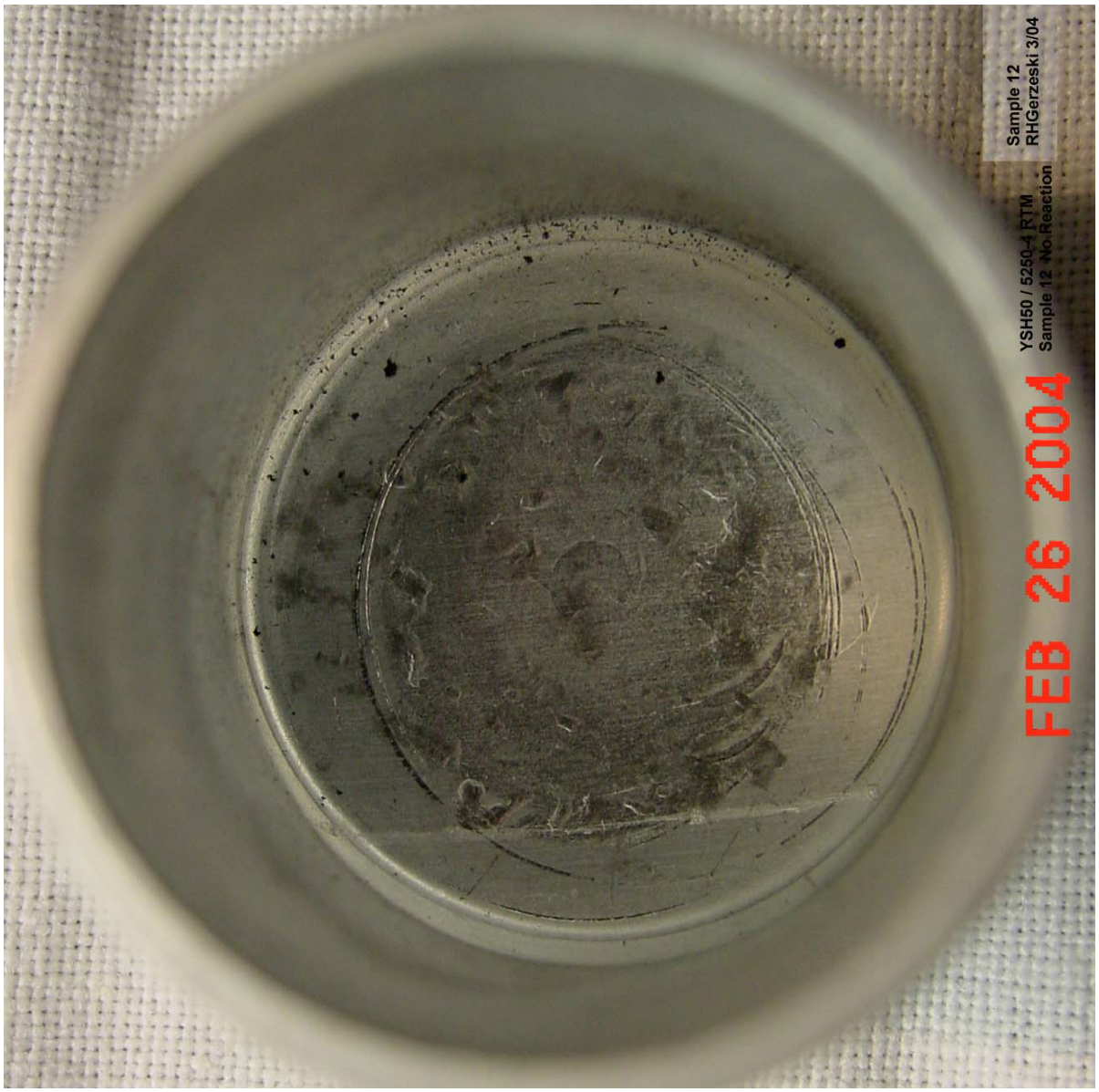


Figure R20l YSH50A / 5250-4 RTM D2512 72 FtLb LOX Tested Specimen Cup Residuals



Figure R20m YSH50A / 5250-4 RTM D2512 72 FtLb LOX Tested Specimen Cup Residuals



Figure R20n YSH50A / 5250-4 RTM D2512 72 FtLb LOX Tested Specimen Cup Residuals

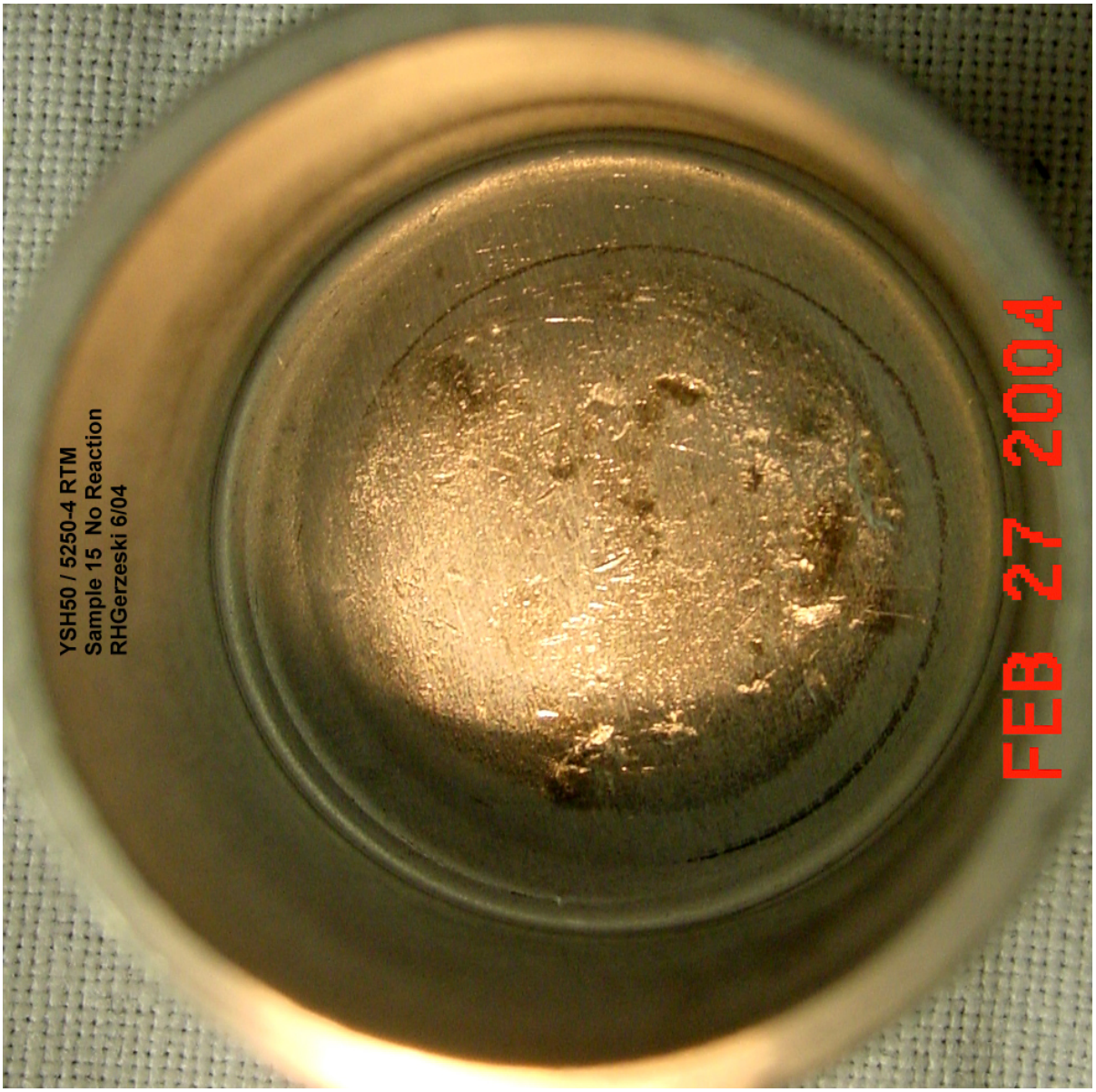


Figure R20o YSH50A / 5250-4 RTM D2512 72 FtLb LOX Tested Specimen Cup Residuals



Figure R20p YSH50A / 5250-4 RTM D2512 72 FtLb LOX Tested Specimen Cup Residuals



Figure R20q YSH50A / 5250-4 RTM D2512 72 FtLb LOX Tested Specimen Cup Residuals

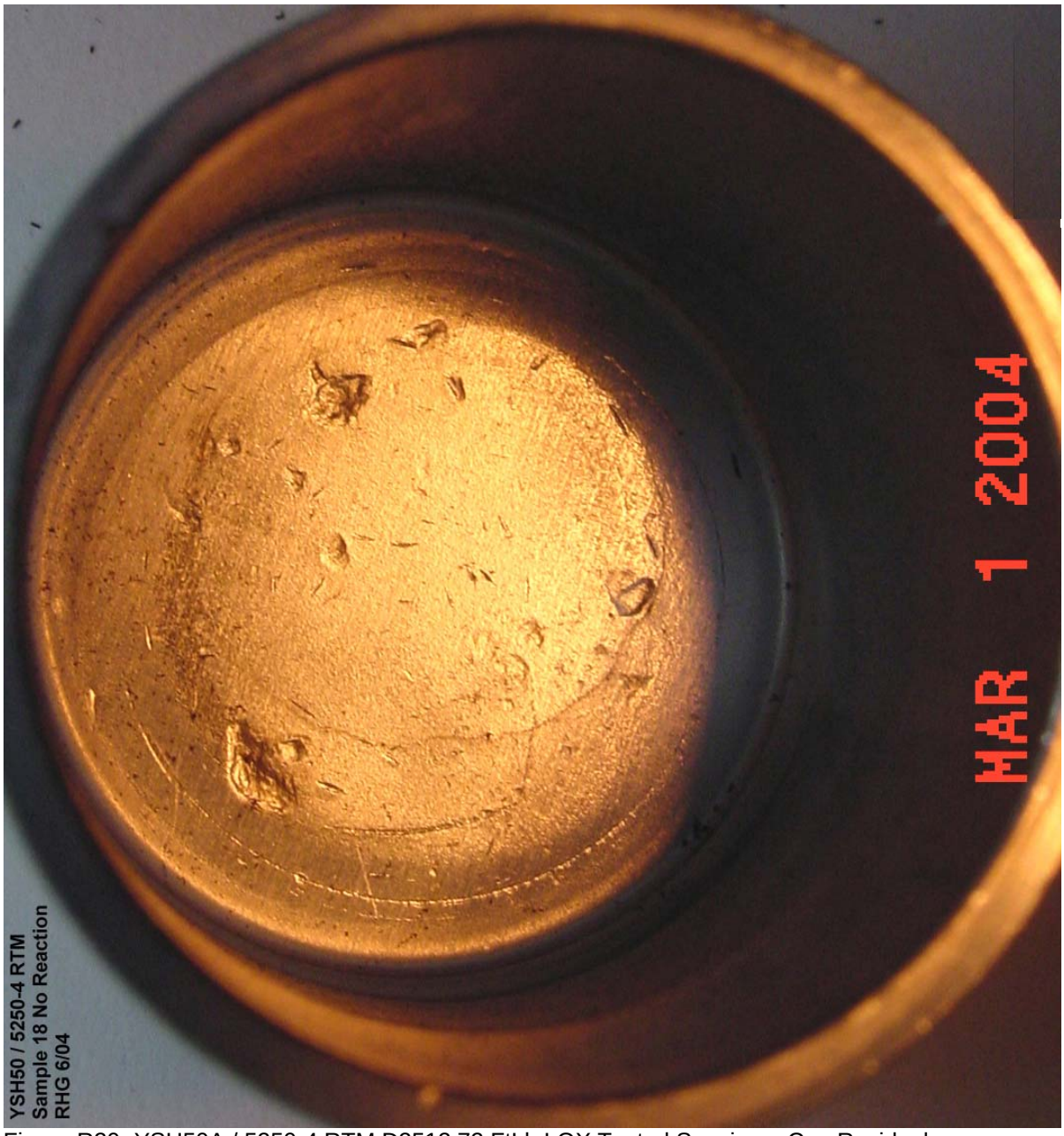


Figure R20r YSH50A / 5250-4 RTM D2512 72 FtLb LOX Tested Specimen Cup Residuals

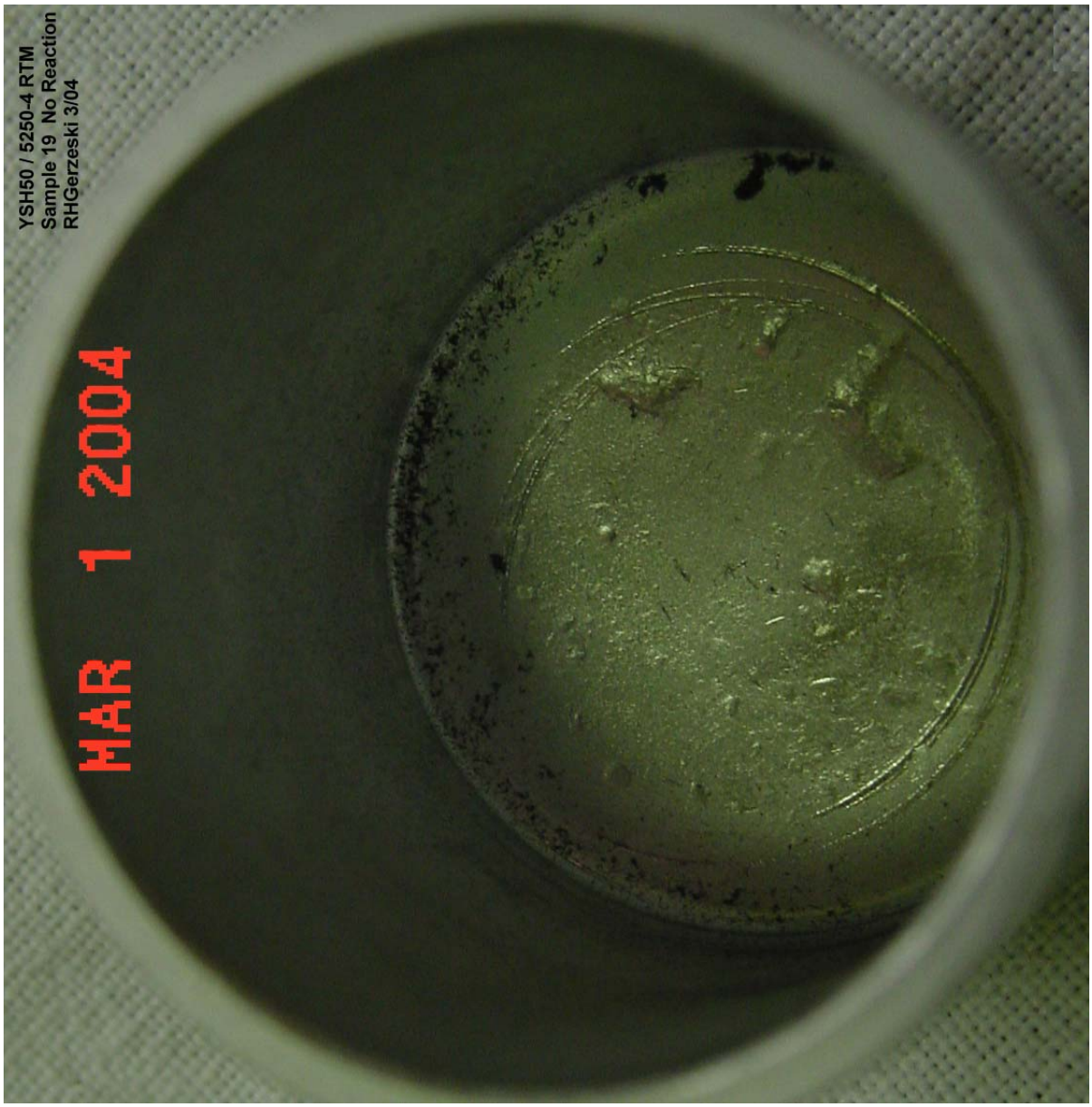


Figure R20sYSH50A / 5250-4 RTM D2512 72 FtLb LOX Tested Specimen Cup Residuals



Figure R20t YSH50A / 5250-4 RTM D2512 72 FtLb LOX Tested Specimen Cup Residuals



Figure R21a YSH50A / 5250-4 RTM D2512 72 FtLb In LN2 Tested Specimen Cup Residuals

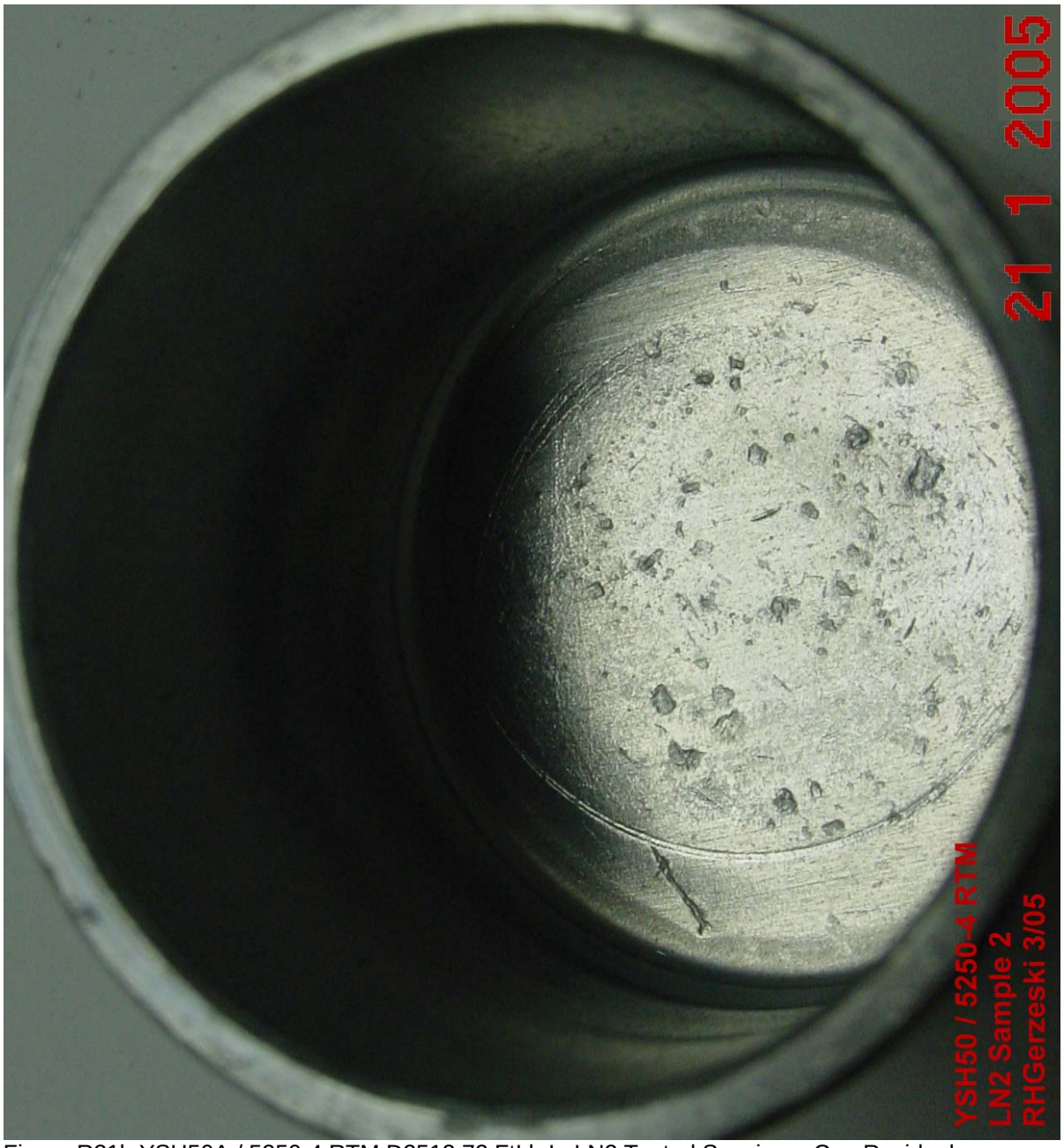


Figure R21b YSH50A / 5250-4 RTM D2512 72 FtLb In LN2 Tested Specimen Cup Residuals

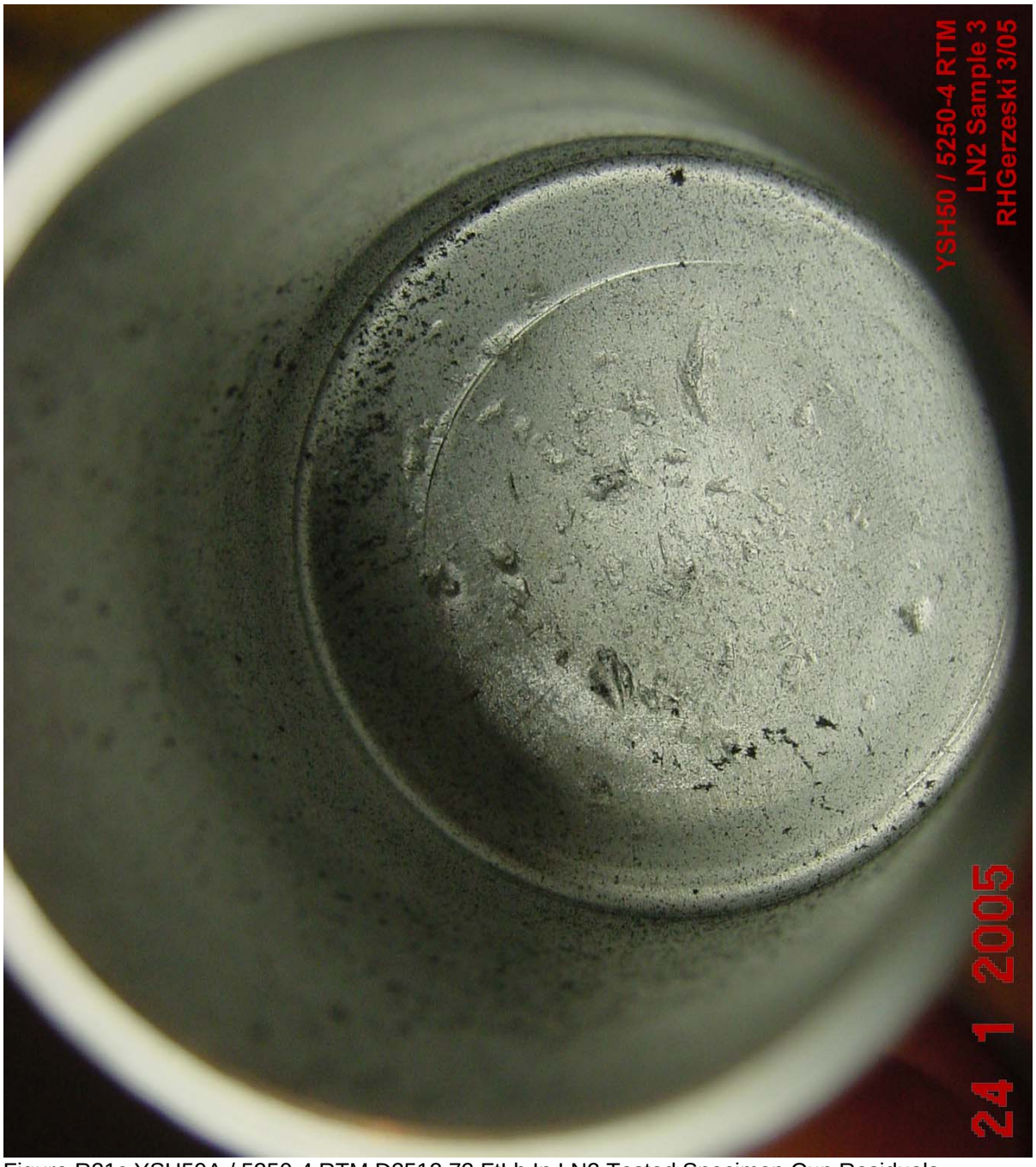


Figure R21c YSH50A / 5250-4 RTM D2512 72 FtLb In LN2 Tested Specimen Cup Residuals

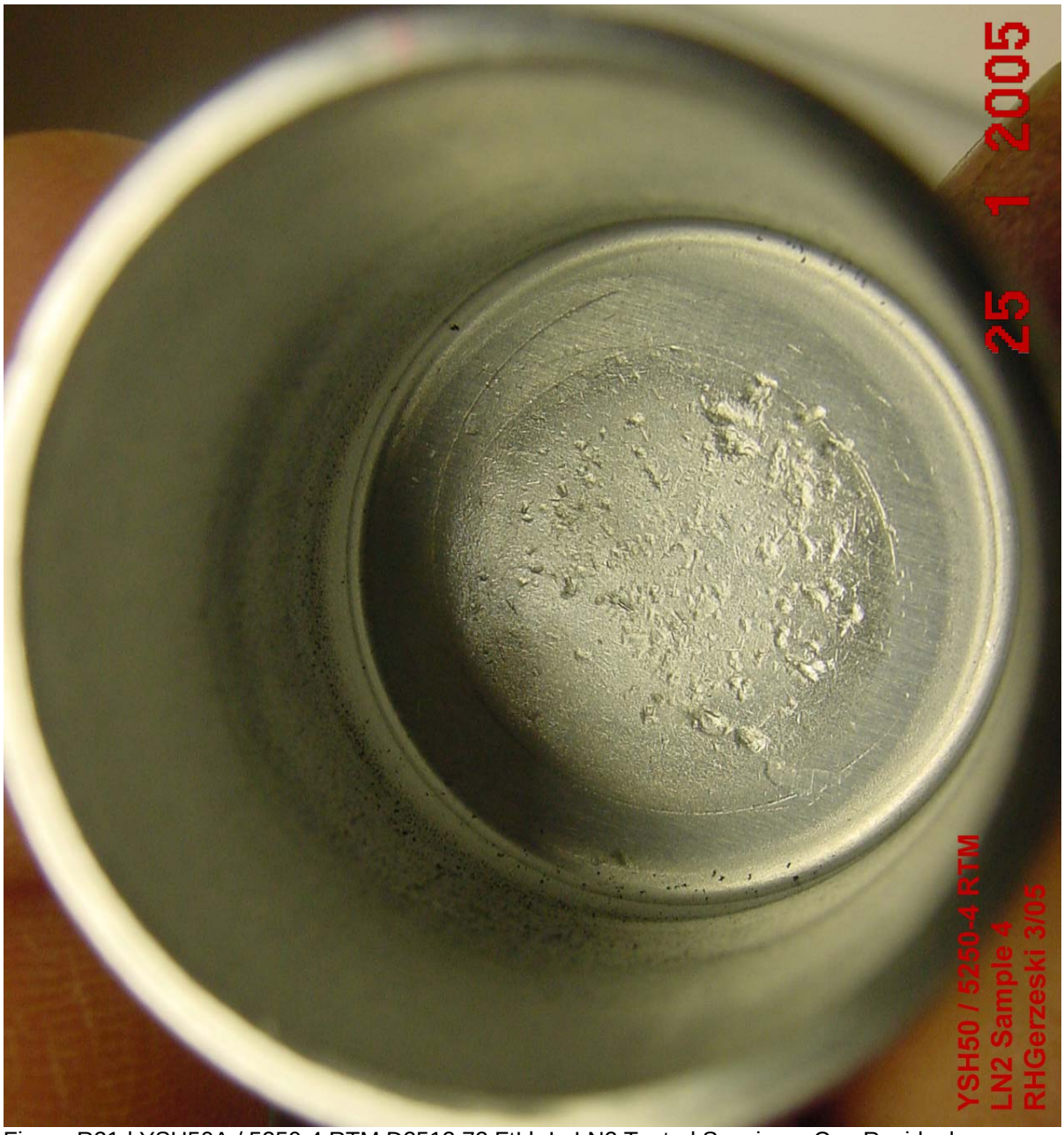


Figure R21d YSH50A / 5250-4 RTM D2512 72 FtLb In LN2 Tested Specimen Cup Residuals



Figure R22a YSH60A / 5250-4 RTM D2512 72 FtLb LOX Tested Specimen Cup Residuals



Figure R22b YSH60A / 5250-4 RTM D2512 72 FtLb LOX Tested Specimen Cup Residuals



Figure R22c YSH60A / 5250-4 RTM D2512 72 FtLb LOX Tested Specimen Cup Residuals



Figure R22d YSH60A / 5250-4 RTM D2512 72 FtLb LOX Tested Specimen Cup Residuals



Figure R22e YSH60A / 5250-4 RTM D2512 72 FtLb LOX Tested Specimen Cup Residuals

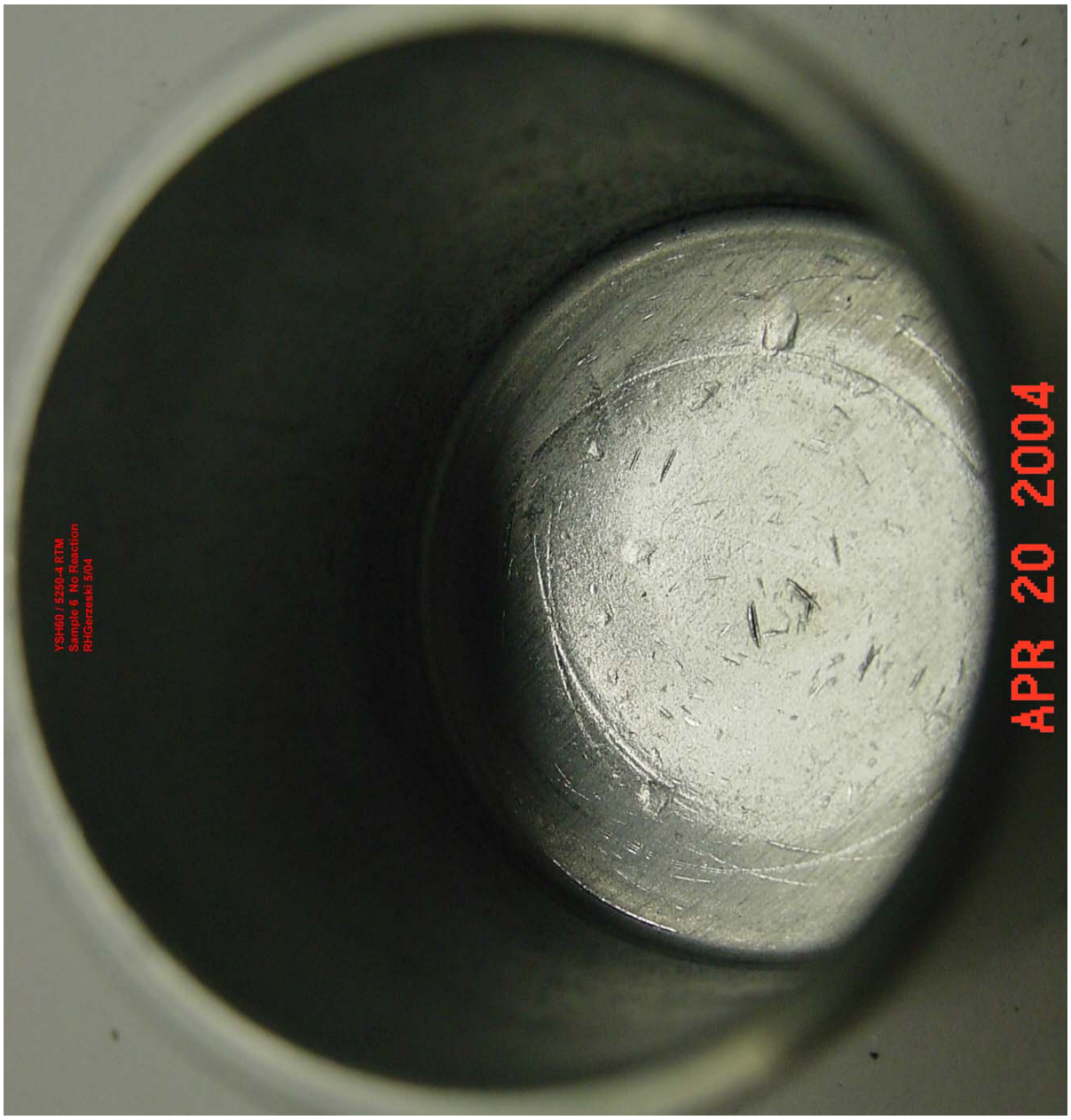


Figure R22f YSH60A / 5250-4 RTM D2512 72 FtLb LOX Tested Specimen Cup Residuals



Figure R22g YSH60A / 5250-4 RTM D2512 72 FtLb LOX Tested Specimen Cup Residuals



Figure R22h YSH60A / 5250-4 RTM D2512 72 FtLb LOX Tested Specimen Cup Residuals



Figure R22i YSH60A / 5250-4 RTM D2512 72 FtLb LOX Tested Specimen Cup Residuals



Figure R22j YSH60A / 5250-4 RTM D2512 72 FtLb LOX Tested Specimen Cup Residuals

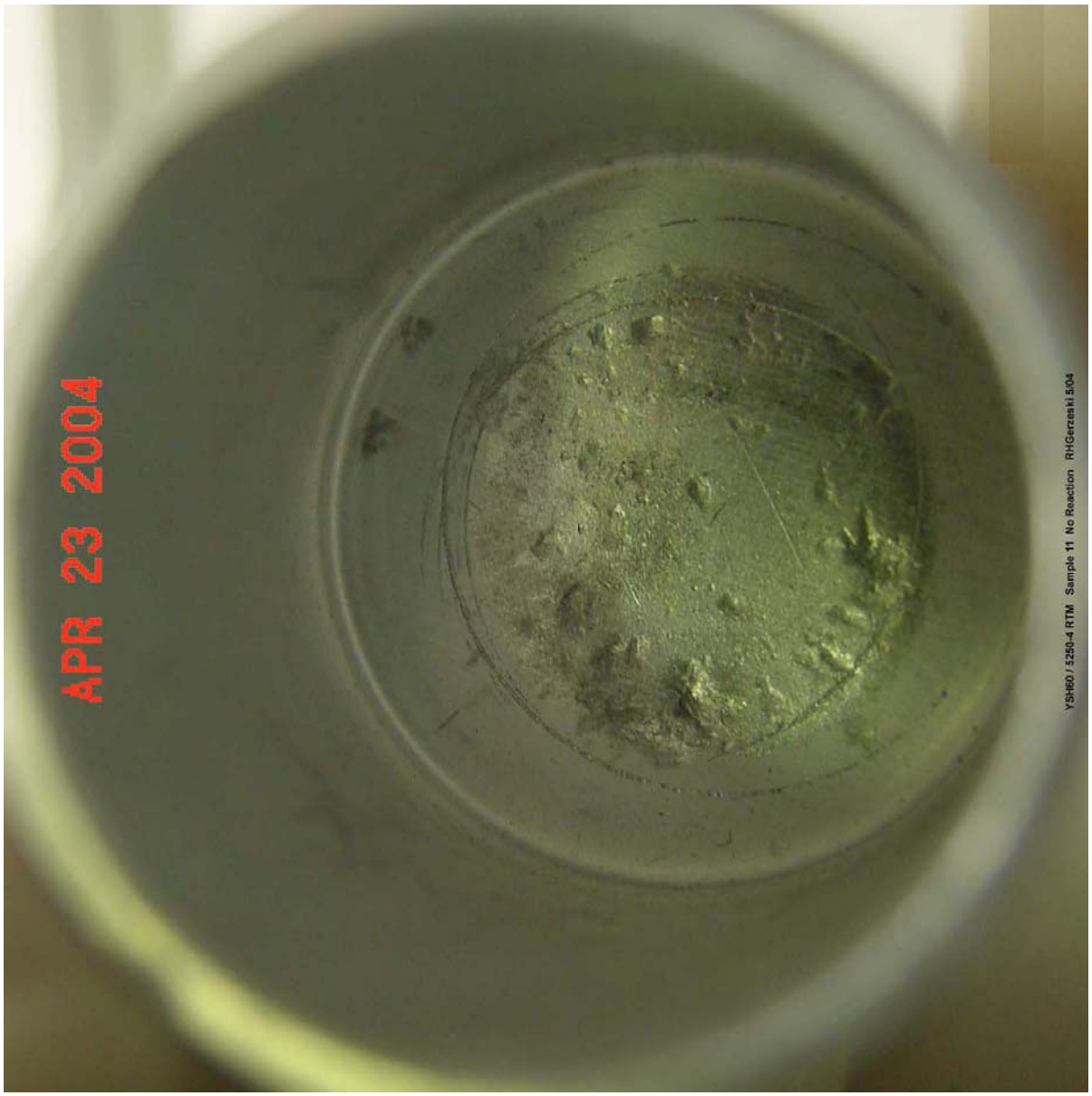


Figure R22k YSH60A / 5250-4 RTM D2512 72 FtLb LOX Tested Specimen Cup Residuals

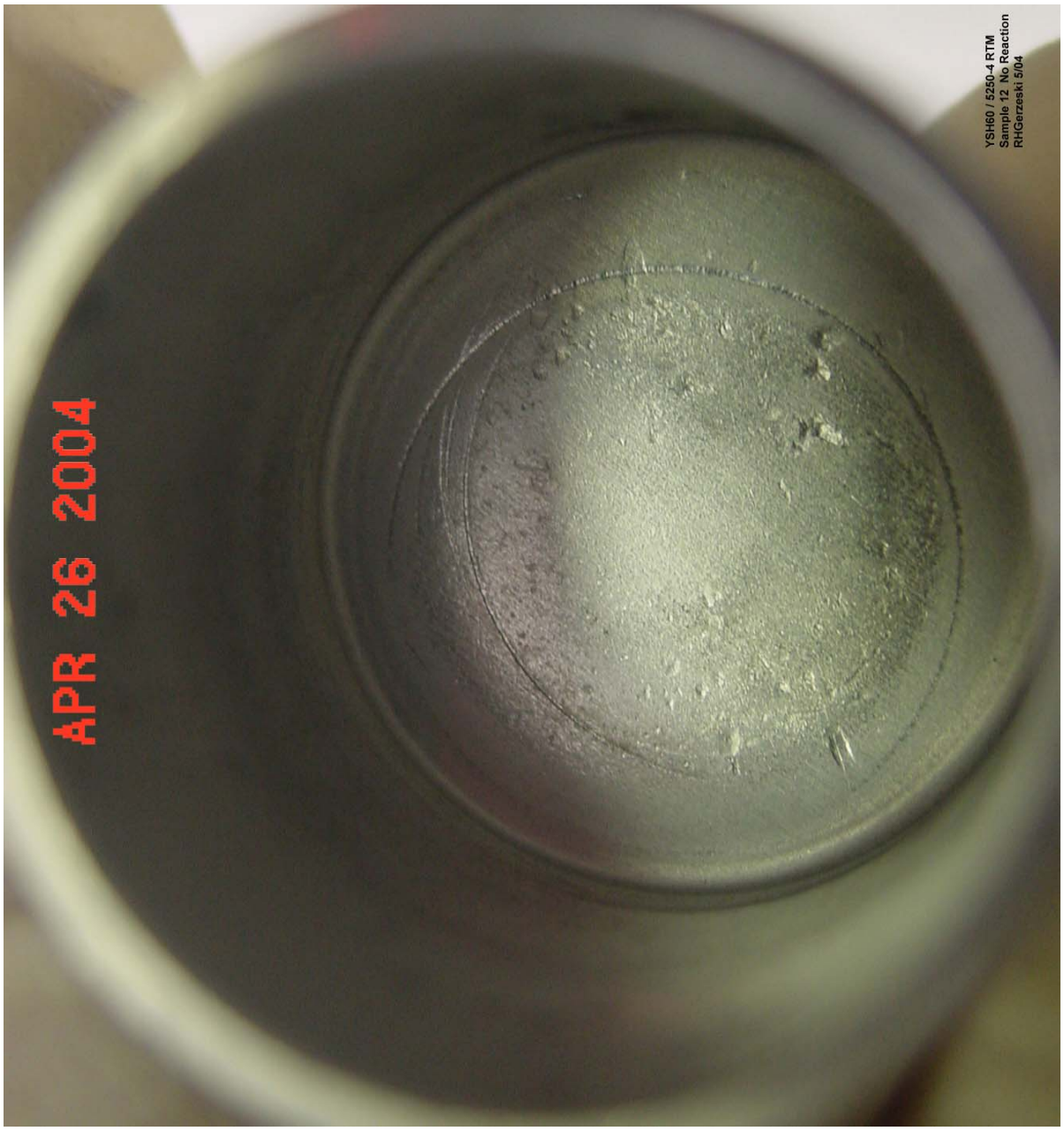


Figure R22l YSH60A / 5250-4 RTM D2512 72 FtLb LOX Tested Specimen Cup Residuals



Figure R22m YSH60A / 5250-4 RTM D2512 72 FtLb LOX Tested Specimen Cup Residuals



Figure R22n YSH60A / 5250-4 RTM D2512 72 FtLb LOX Tested Specimen Cup Residuals

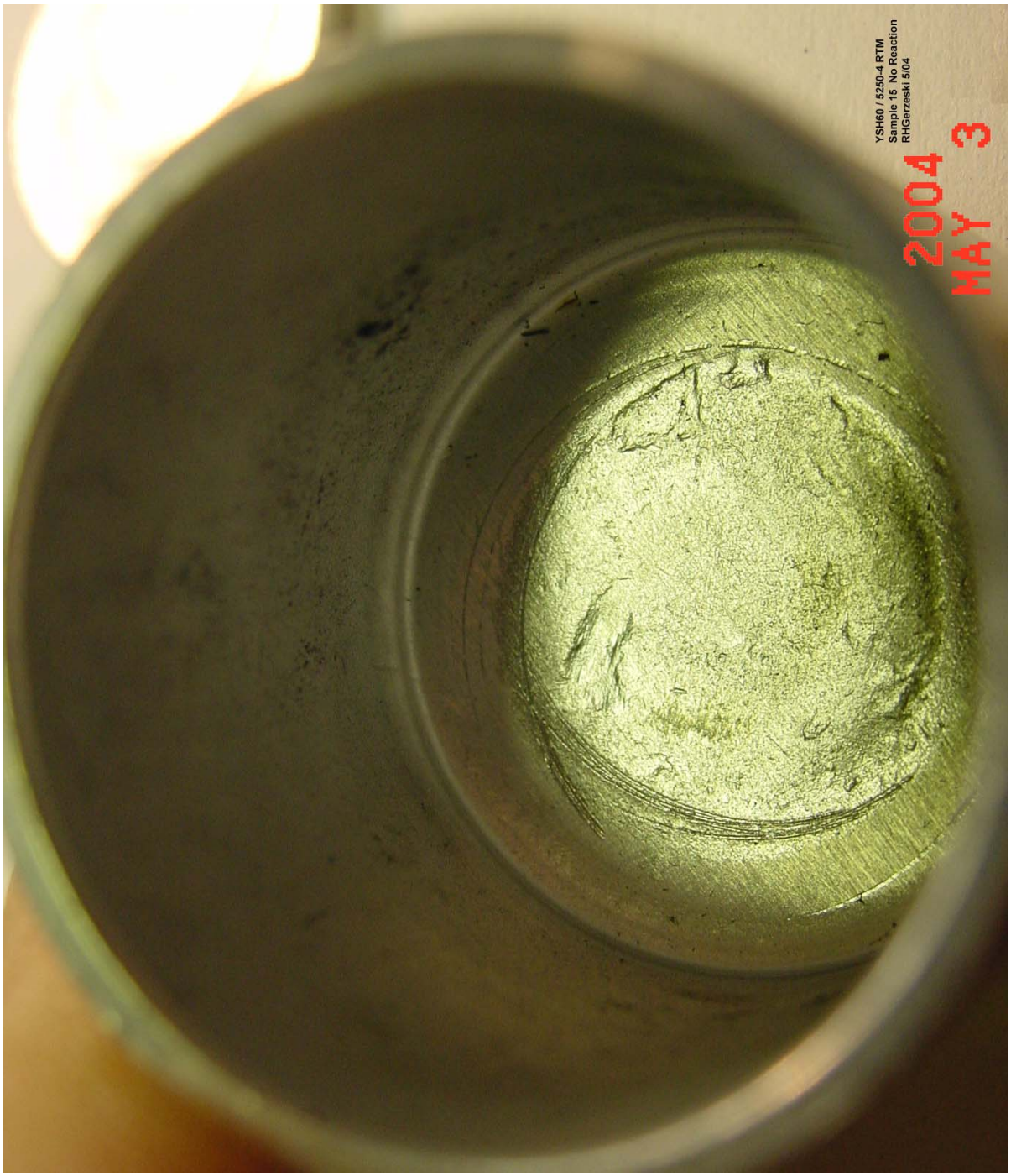


Figure R22o YSH60A / 5250-4 RTM D2512 72 FtLb LOX Tested Specimen Cup Residuals



Figure R22p YSH60A / 5250-4 RTM D2512 72 FtLb LOX Tested Specimen Cup Residuals

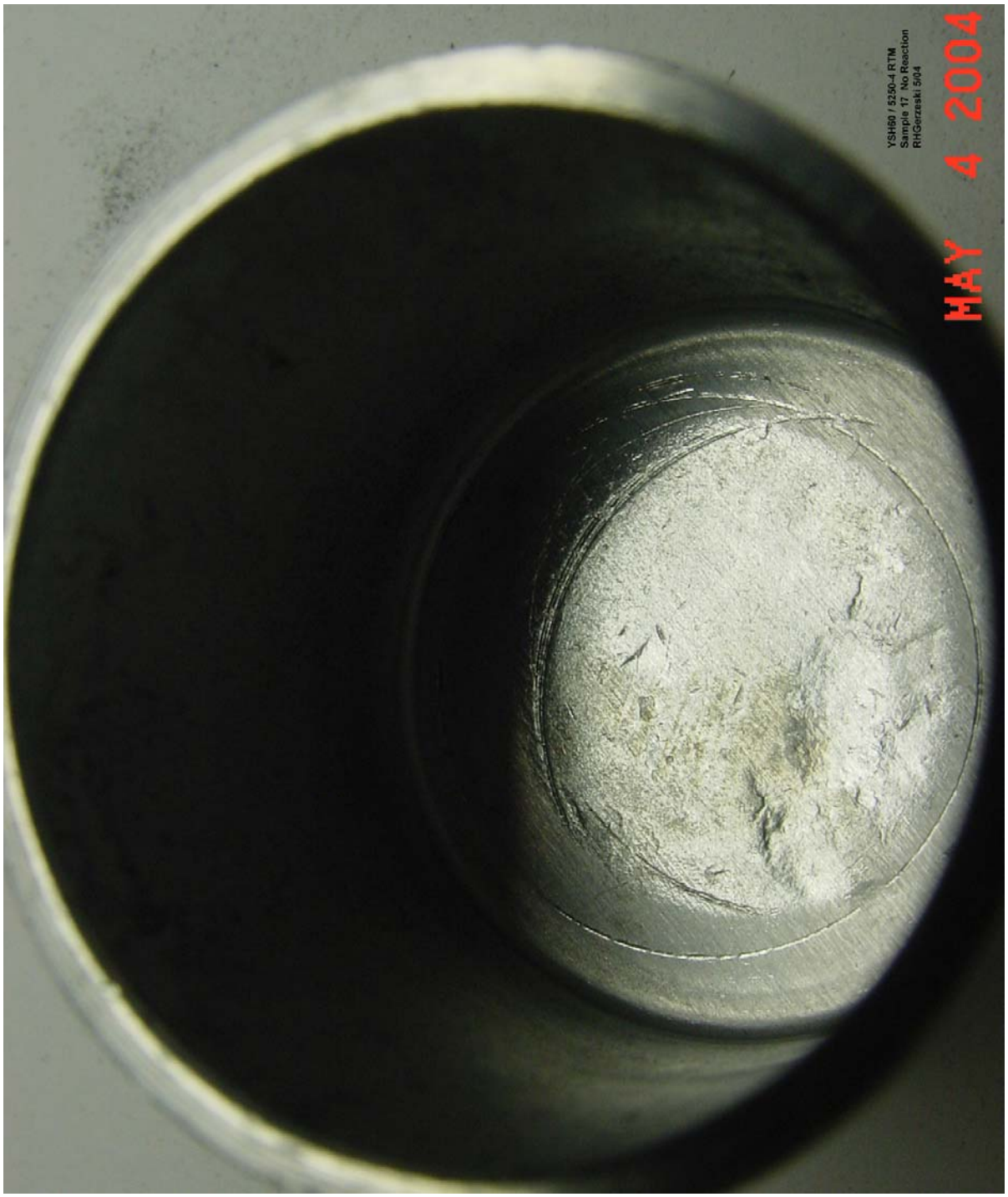


Figure R22q YSH60A / 5250-4 RTM D2512 72 FtLb LOX Tested Specimen Cup Residuals



Figure R22r YSH60A / 5250-4 RTM D2512 72 FtLb LOX Tested Specimen Cup Residuals



Figure R22s YSH60A / 5250-4 RTM D2512 72 FtLb LOX Tested Specimen Cup Residuals



Figure R22t YSH60A / 5250-4 RTM D2512 72 FtLb LOX Tested Specimen Cup Residuals



Figure R23a YSH60A / 5250-4 RTM D2512 72 FtLb In LN2 Tested Specimen Cup Residuals



Figure R23b YSH60A / 5250-4 RTM D2512 72 FtLb In LN2 Tested Specimen Cup Residuals

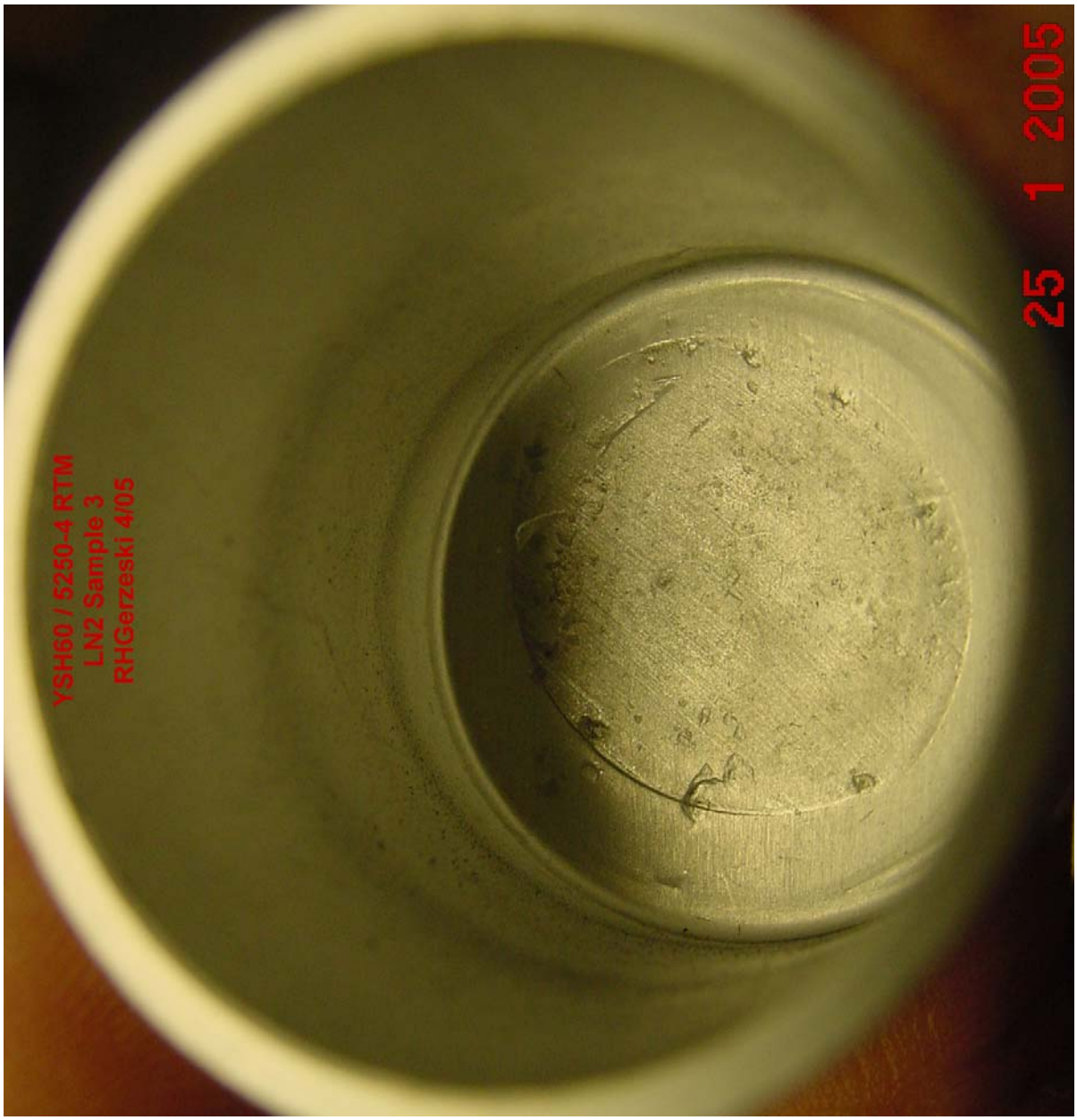


Figure R23c YSH60A / 5250-4 RTM D2512 72 FtLb In LN2 Tested Specimen Cup Residuals



Figure R23d YSH60A / 5250-4 RTM D2512 72 FtLb In LN2 Tested Specimen Cup Residuals



Figure R24a T650-35-UC309 / 5250-4 RTM D2512 72 FtLb LOX Tested Specimen From Moat Residuals



Figure R24b T650-35-UC309 / 5250-4 RTM D2512 72 FtLb LOX Tested Specimen From Moat Residuals



Figure R24c T650-35-UC309 / 5250-4 RTM D2512 72 FtLb LOX Tested Specimen From Moat Residuals



Figure R24d T650-35-UC309 / 5250-4 RTM D2512 72 FtLb LOX Tested Specimen From Moat Residuals



Figure R25a YSH50A / 5250-4 RTM D2512 72 FtLb LOX Tested Specimen From Moat Residuals



Figure R25b YSH50A / 5250-4 RTM D2512 72 FtLb LOX Tested Specimen From Moat Residuals



Figure R26a YSH60A / 5250-4 RTM D2512 72 FtLb LOX Tested Specimen From Moat Residuals



Figure R26b YSH60A / 5250-4 RTM D2512 72 FtLb LOX Tested Specimen From Moat Residuals



Figure R26c YSH60A / 5250-4 RTM D2512 72 FtLb LOX Tested Specimen From Moat Residuals



Figure R26d YSH60A / 5250-4 RTM D2512 72 FtLb LOX Tested Specimen From Moat Residuals

Appendix: Residuals: Return Bag Tagging



Figure R27a-i 5250-4 RTM D2512 LOX Tested Specimen Return Bag Tags Residuals



Figure R27a-ii 5250-4 RTM D2512 LOX Tested Specimen Return Bag Tags Residuals

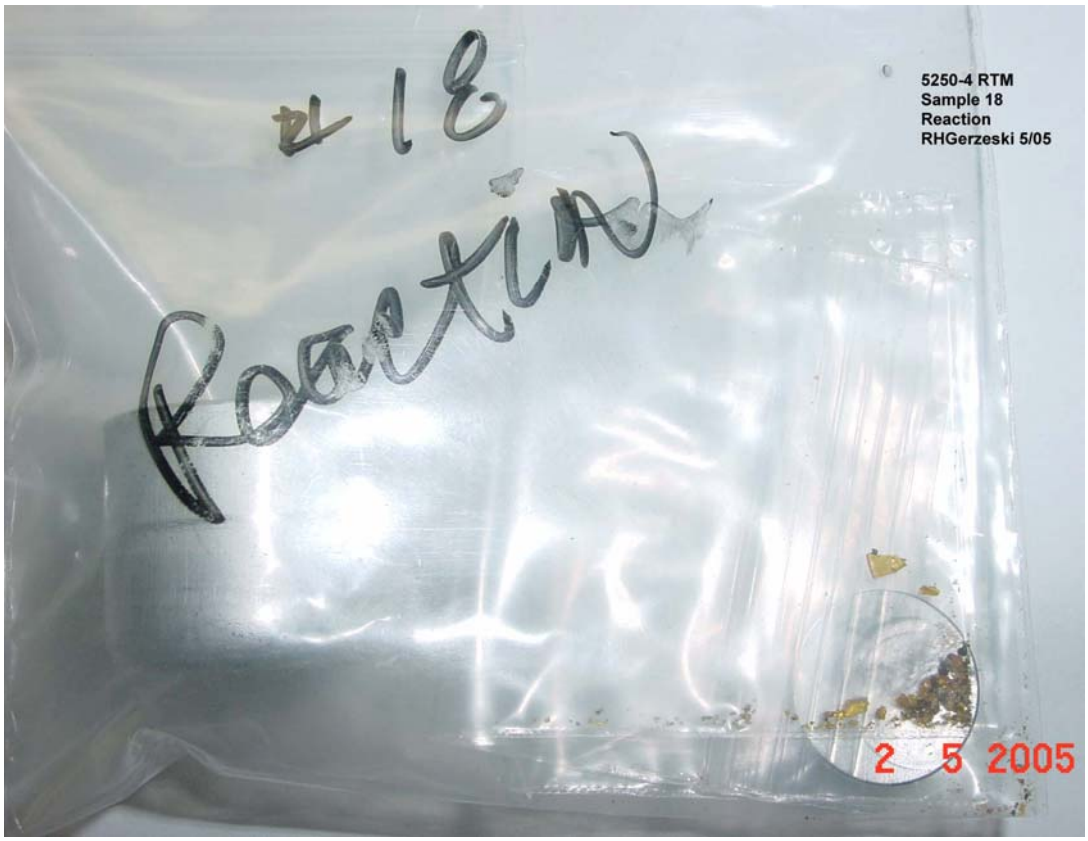


Figure R27a-iii 5250-4 RTM D2512 LOX Tested Specimen Return Bag Tags Residuals

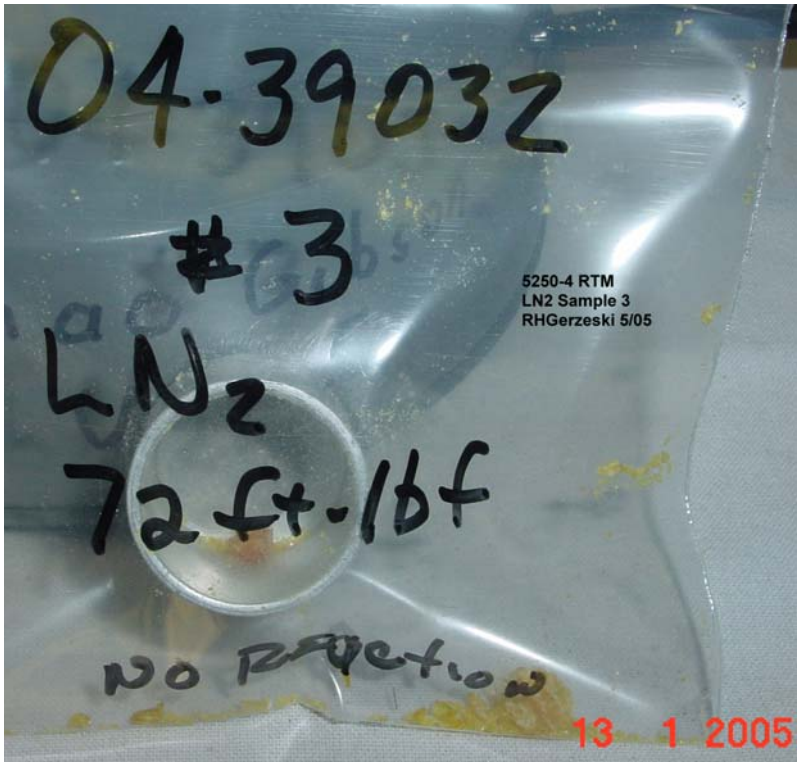


Figure R27b 5250-4 RTM D2512 LN2 Specimen Return Bag Tags Residuals

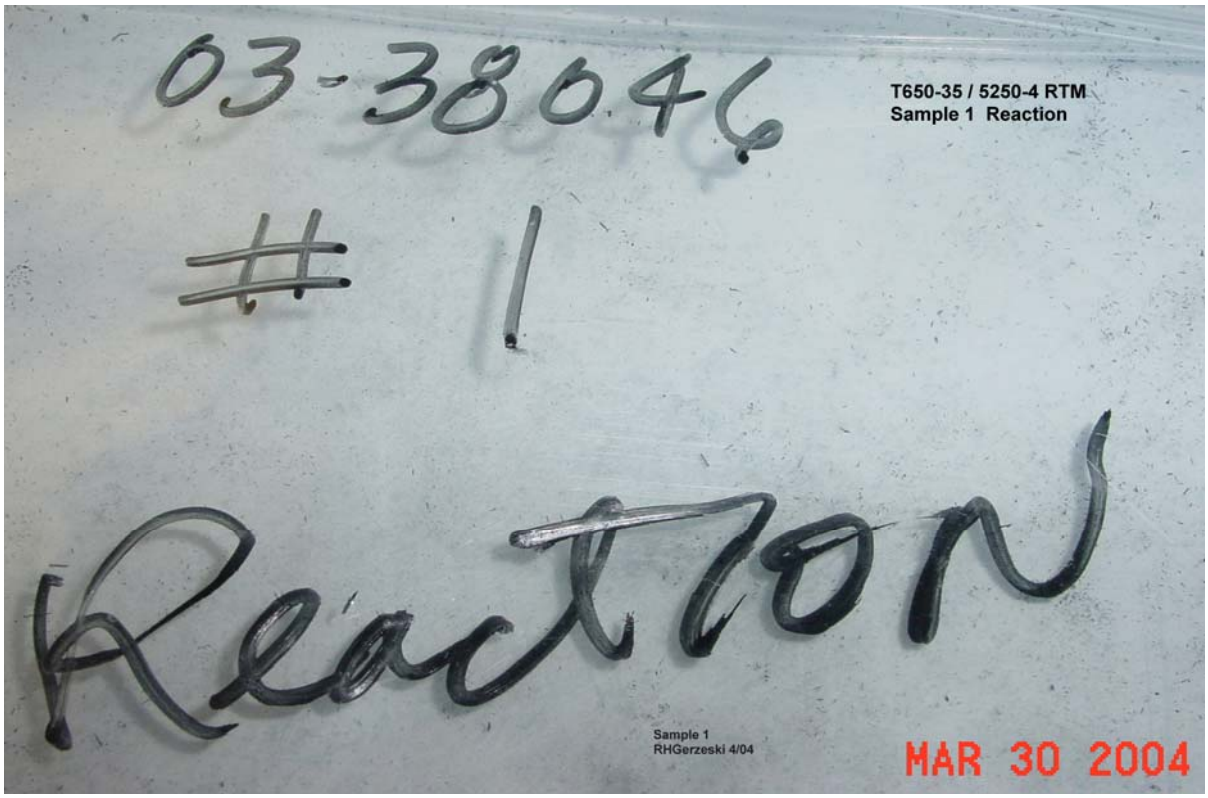


Figure R28a-i T650-35-UC309 / 5250-4 RTM D2512 LOX Tested Specimen Return Bag Tags Residuals

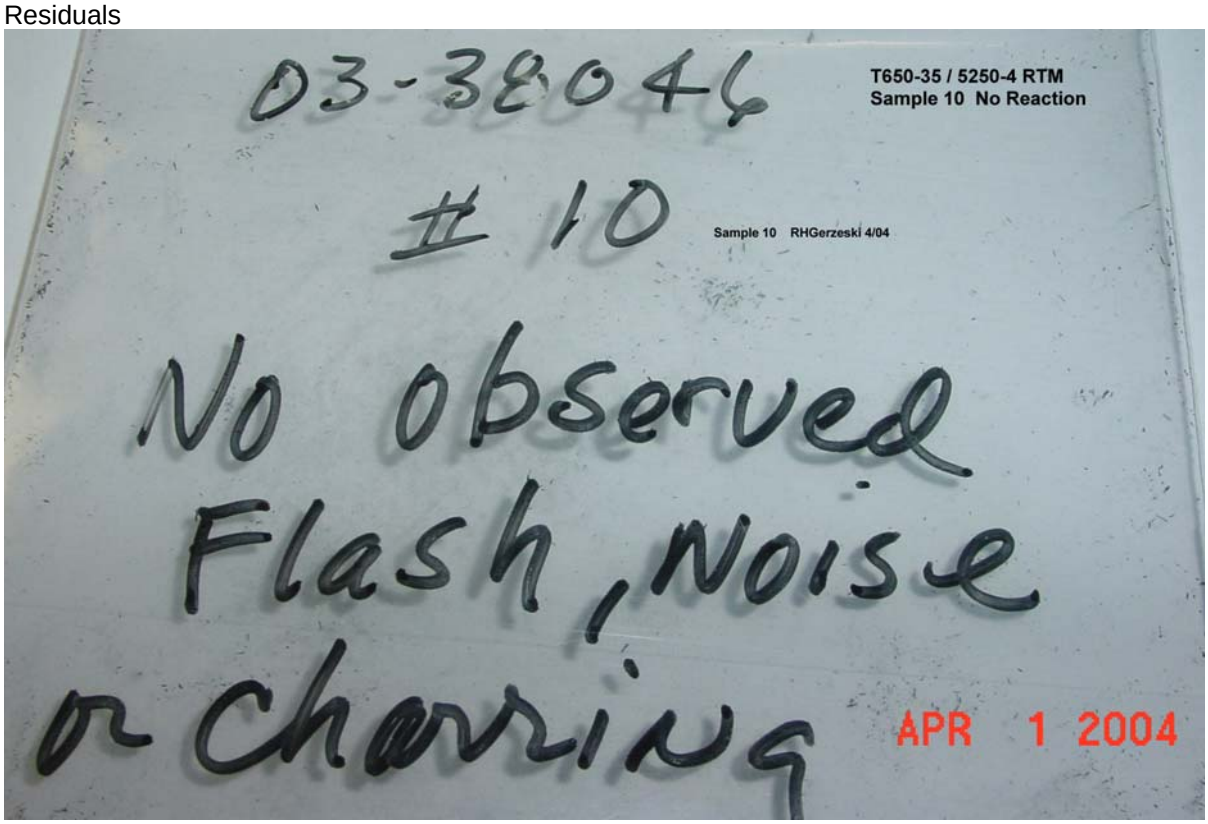


Figure R28a-ii T650-35-UC309 / 5250-4 RTM D2512 LOX Tested Specimen Return Bag Tags Residuals

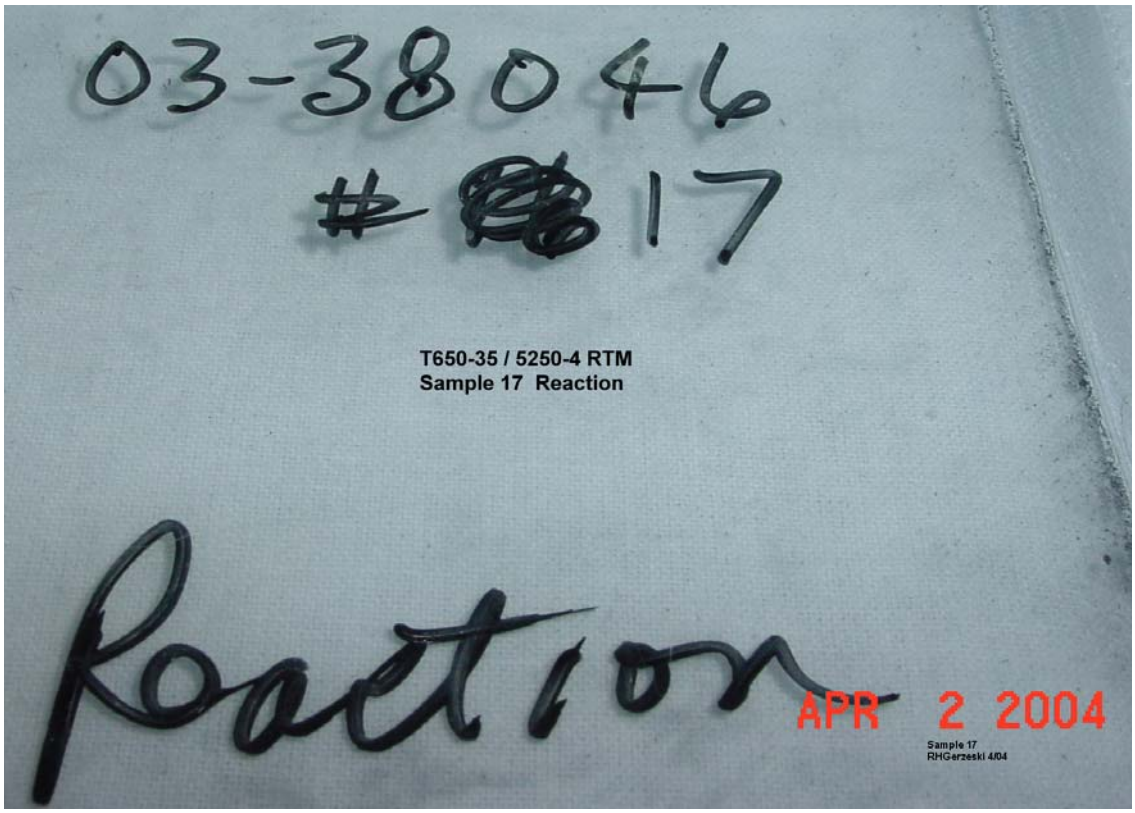


Figure R28a-iii T650-35-UC309 / 5250-4 RTM D2512 LOX Tested Specimen Return Bag Tags Residuals

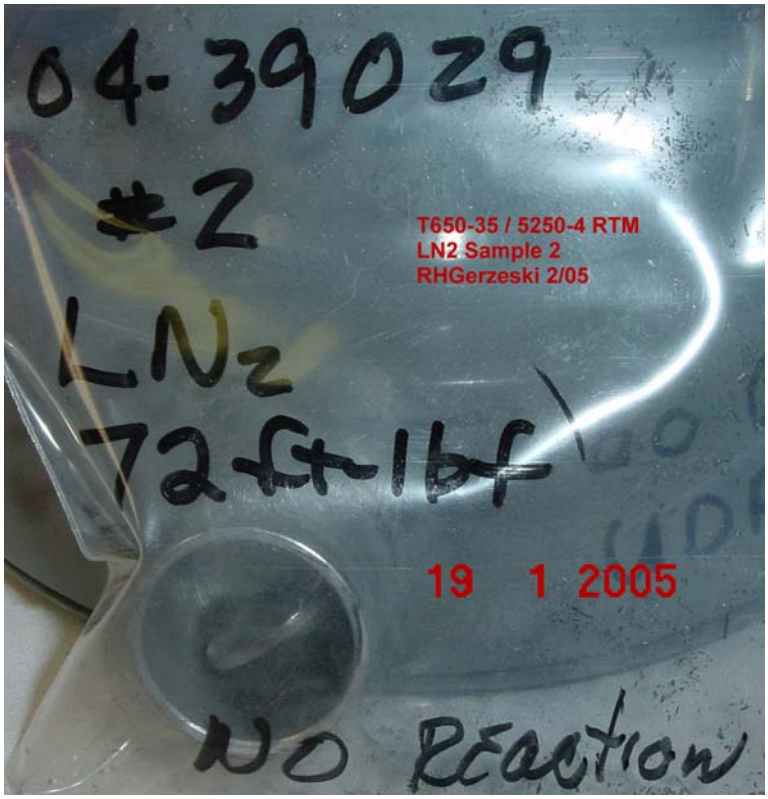


Figure R28b T650-35-UC309 / 5250-4 RTM D2512 LN2 Tested Specimen Return Bag Tags Residuals

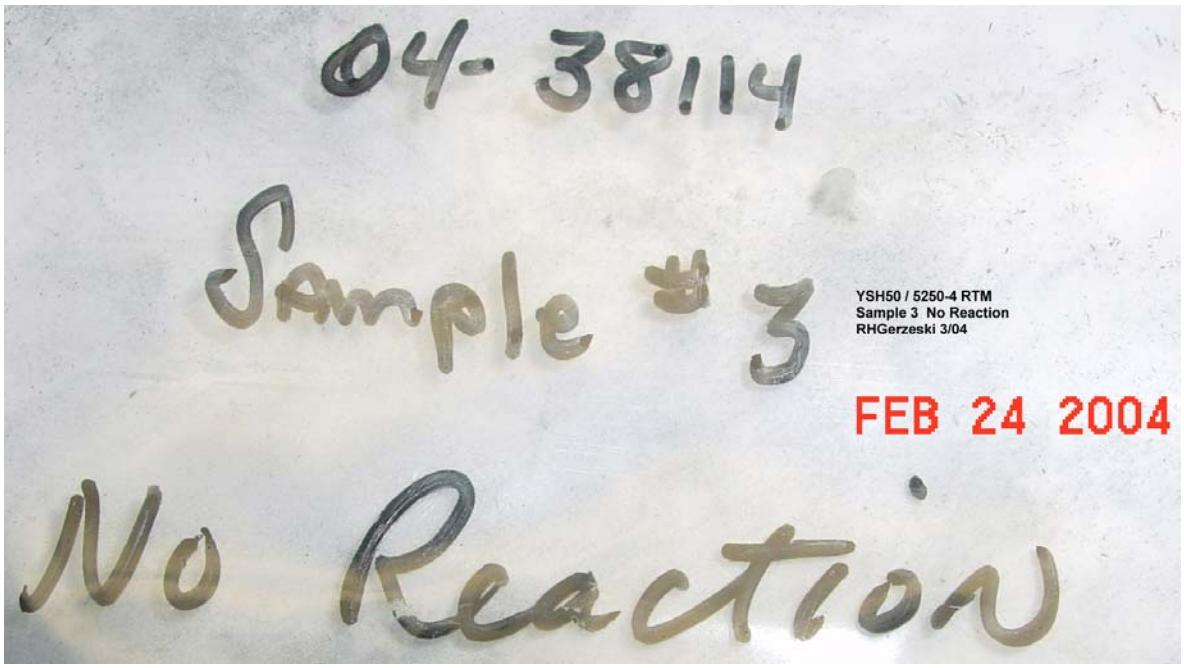


Figure R29a-i YSH50A / 5250-4 RTM D2512 LOX Tested Specimen Return Bag Tags Residuals

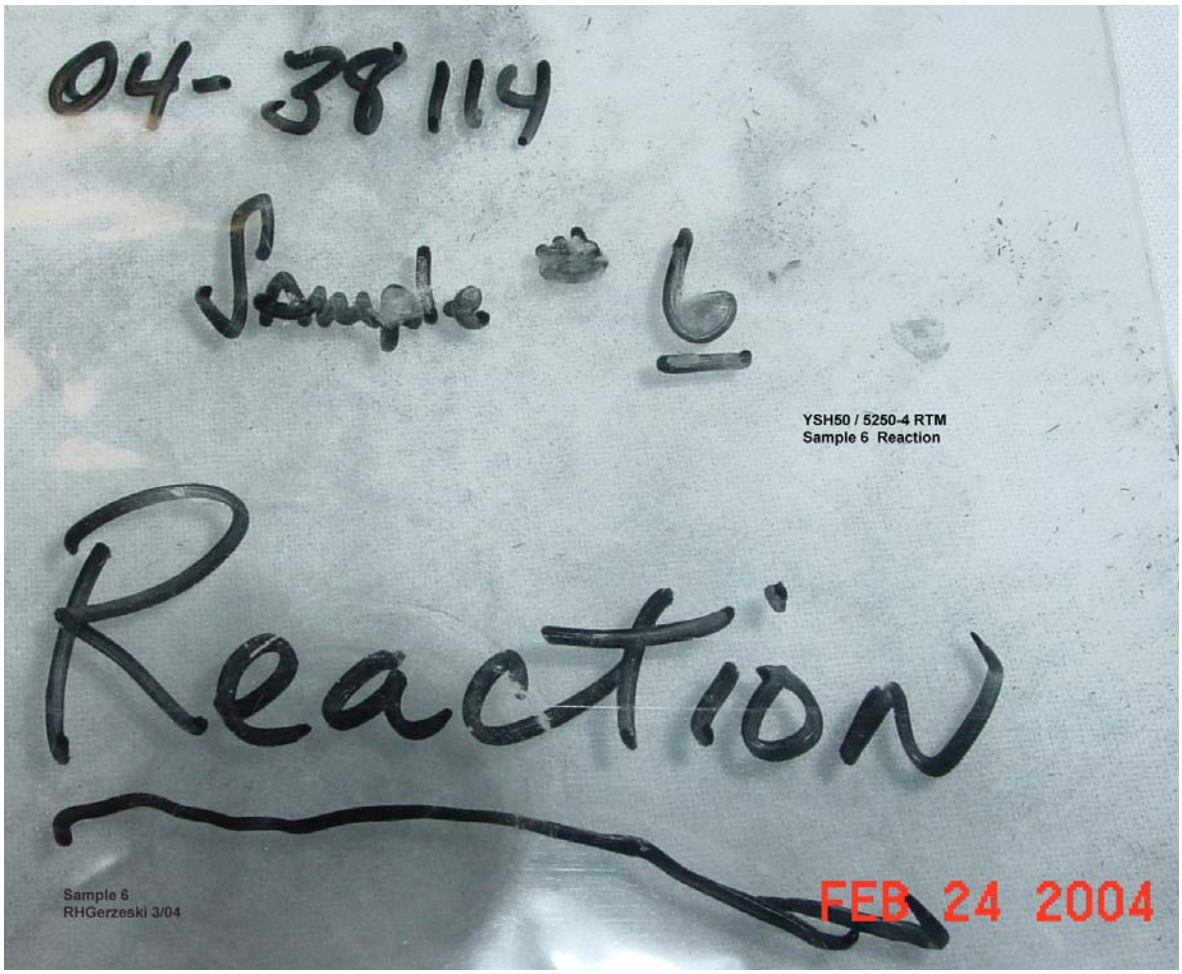


Figure R29a-ii YSH50A / 5250-4 RTM D2512 LOX Tested Specimen Return Bag Tags Residuals

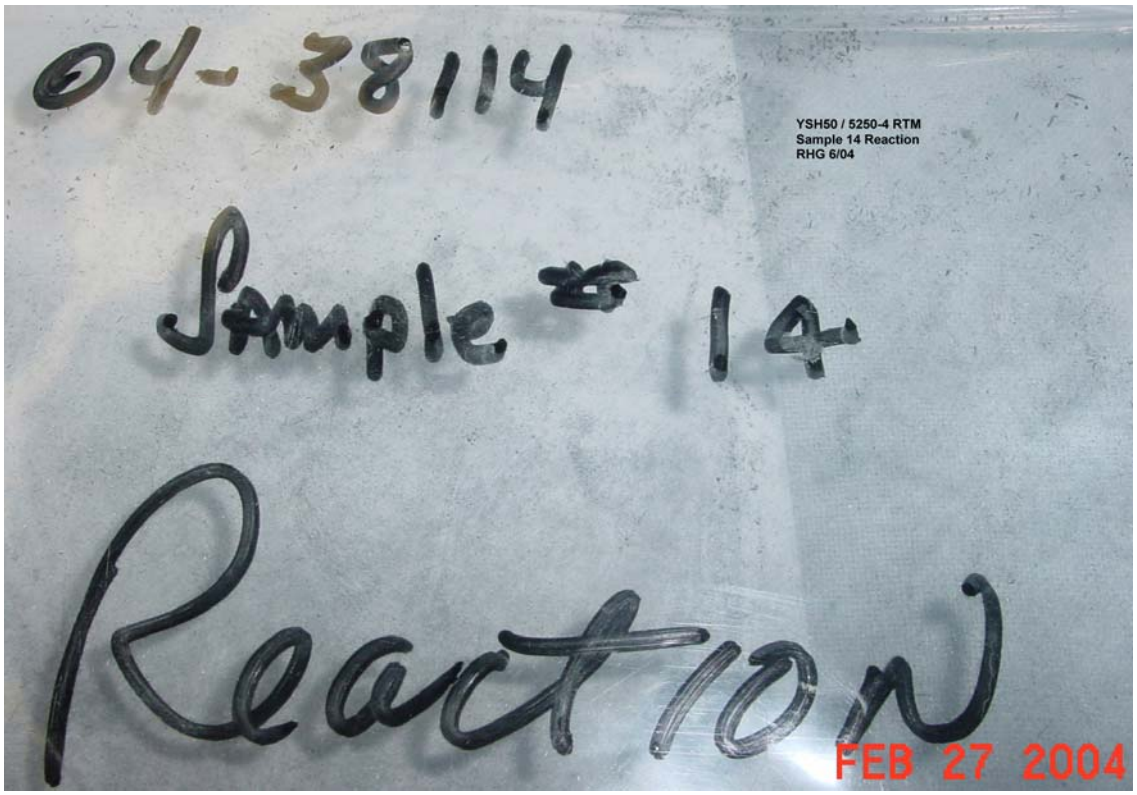


Figure R29a-iii YSH50A / 5250-4 RTM D2512 LOX Tested Specimen Return Bag Tags Residuals

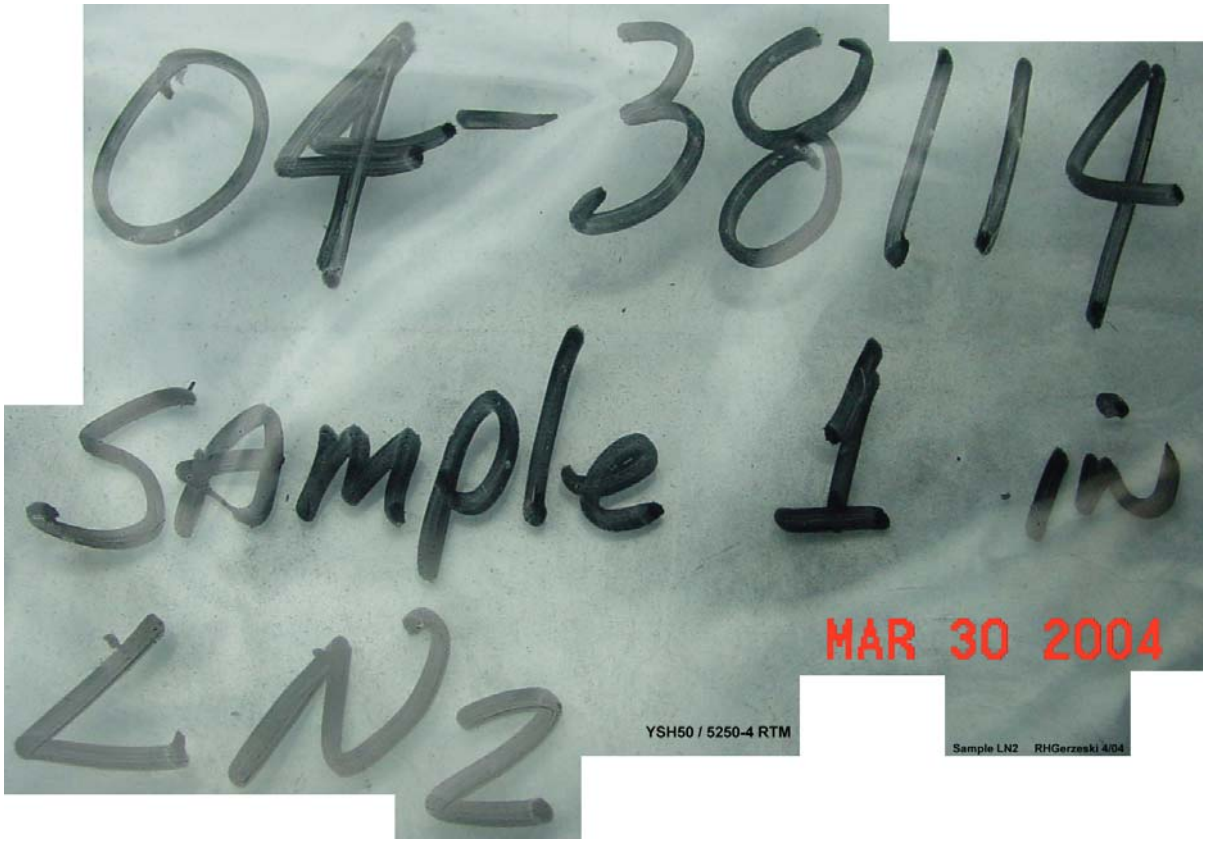


Figure R29b-i YSH50A / 5250-4 RTM D2512 LN2 Tested Specimen Return Bag Tags Residuals

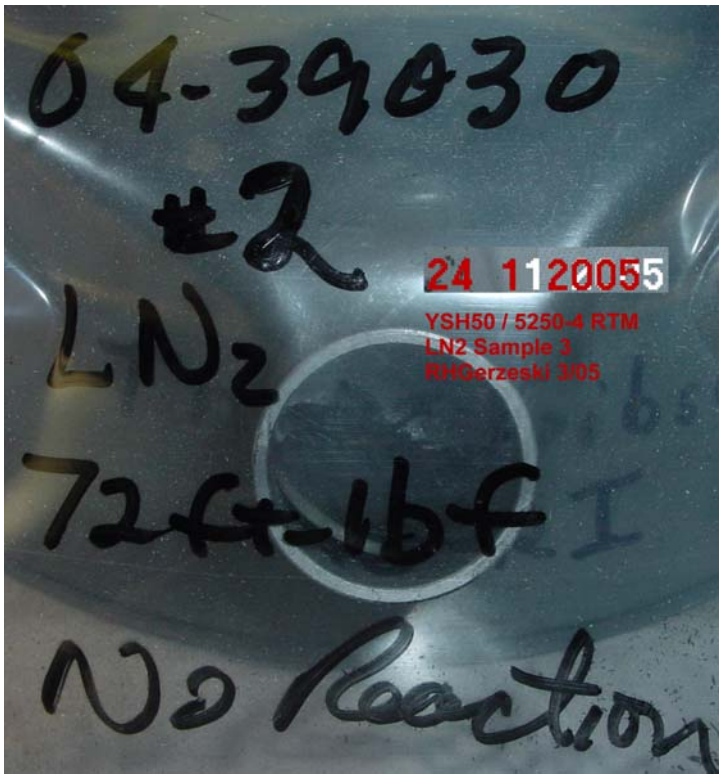


Figure R29b-ii YSH50A / 5250-4 RTM D2512 LN2 Tested Specimen Return Bag Tags Residuals

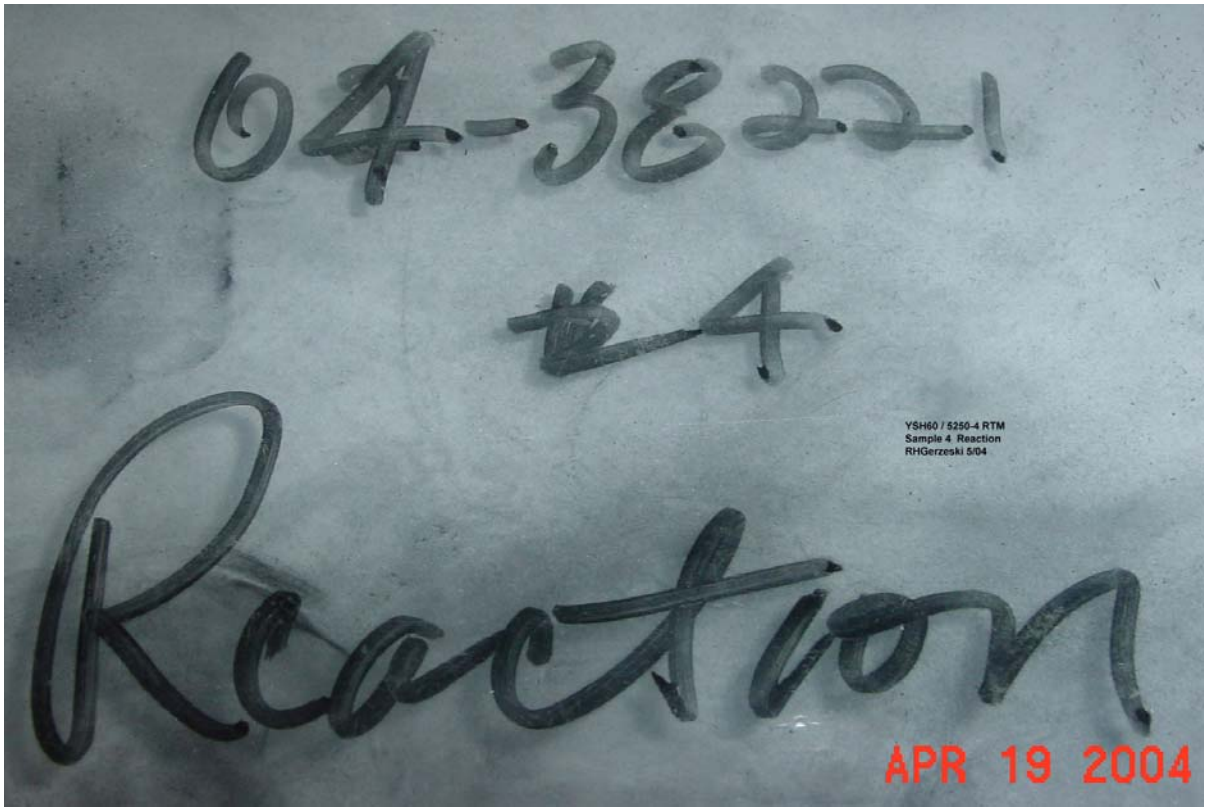


Figure R30a-i YSH60A / 5250-4 RTM D2512 LOX Tested Specimen Return Bag Tags Residuals

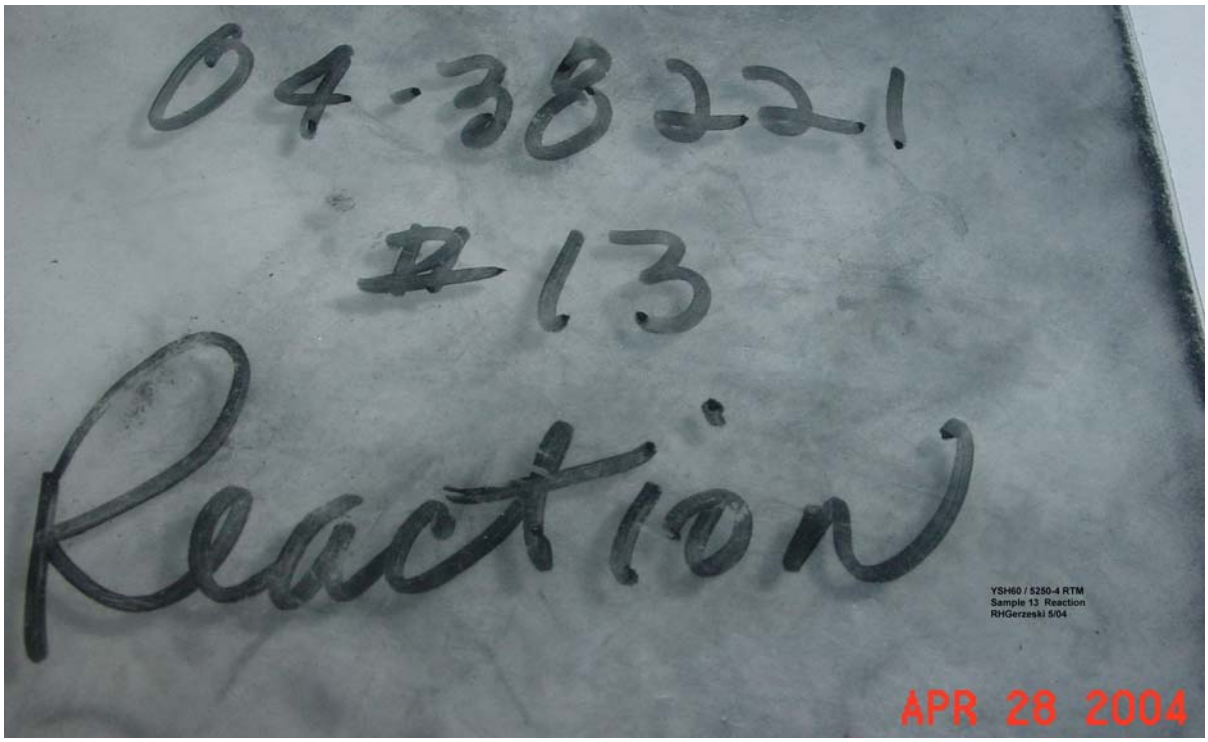


Figure R30a-ii YSH60A / 5250-4 RTM D2512 LOX Tested Specimen Return Bag Tags Residuals

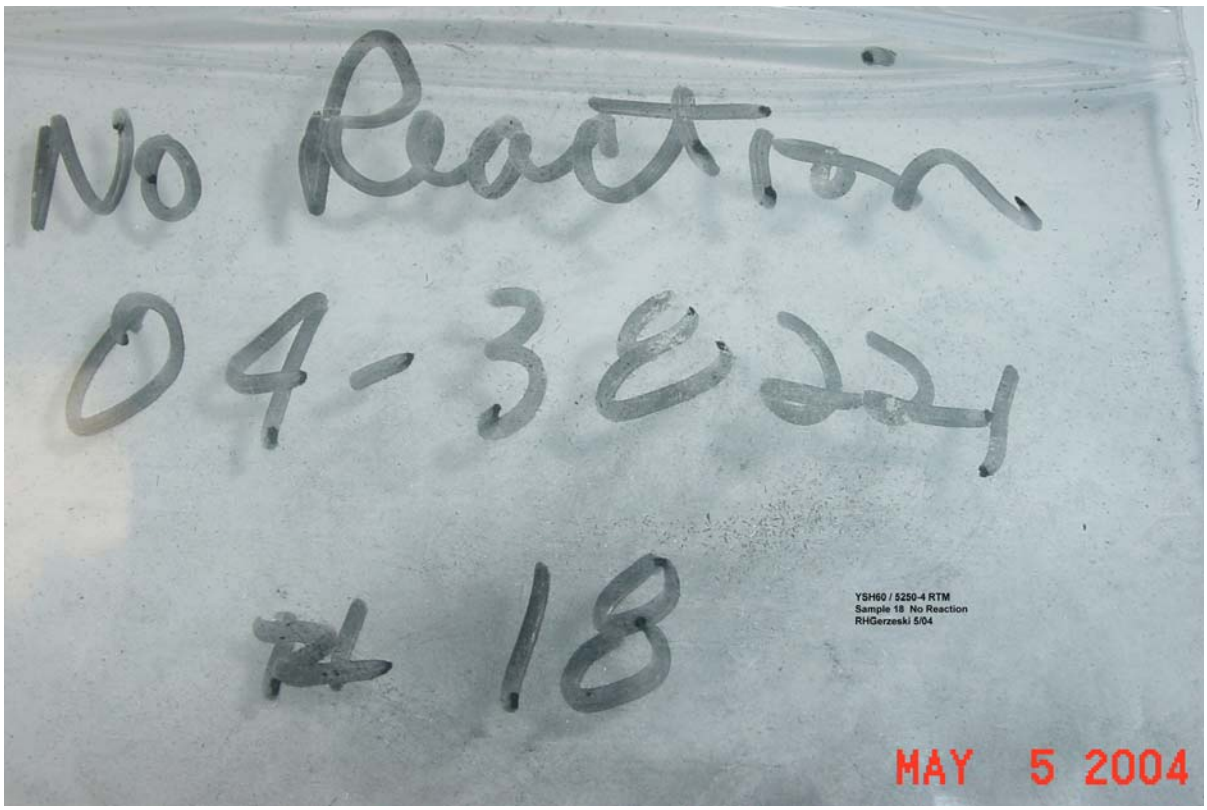


Figure R30a-iii YSH60A / 5250-4 RTM D2512 LOX Tested Specimen Return Bag Tags Residuals

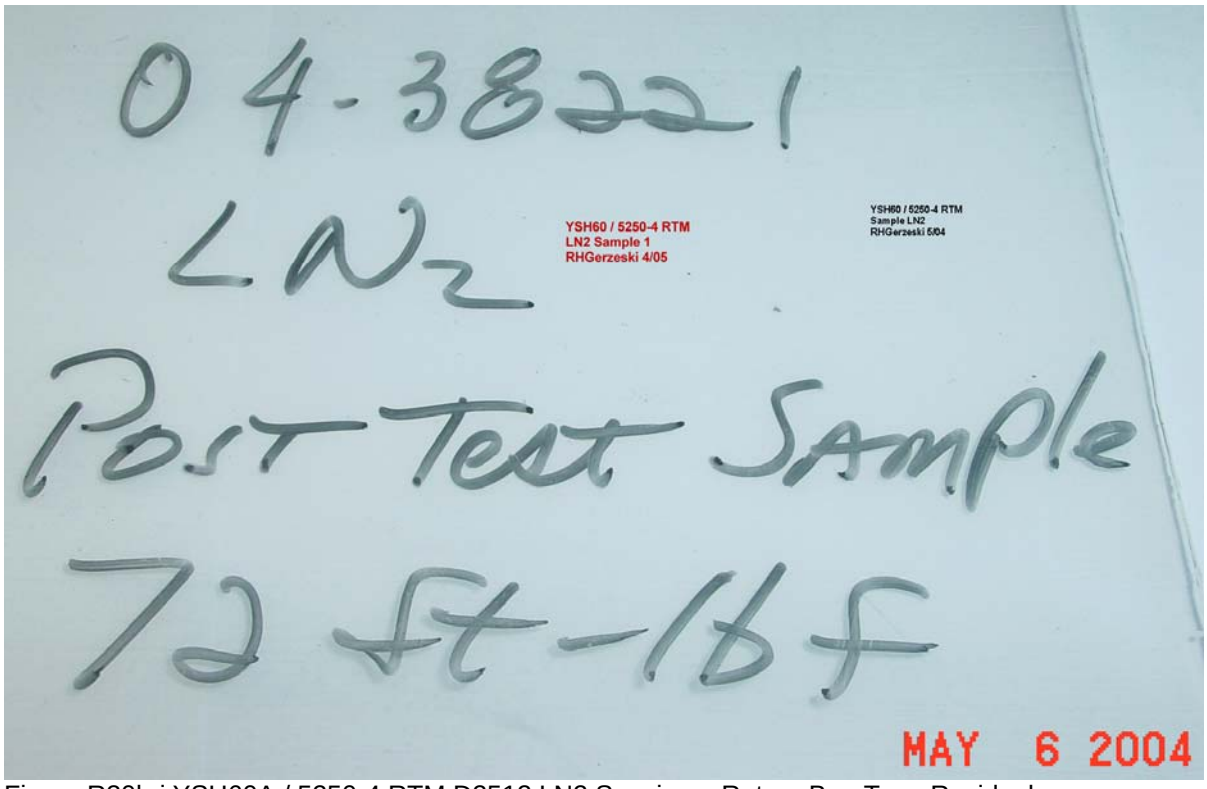


Figure R30b-i YSH60A / 5250-4 RTM D2512 LN2 Specimen Return Bag Tags Residuals

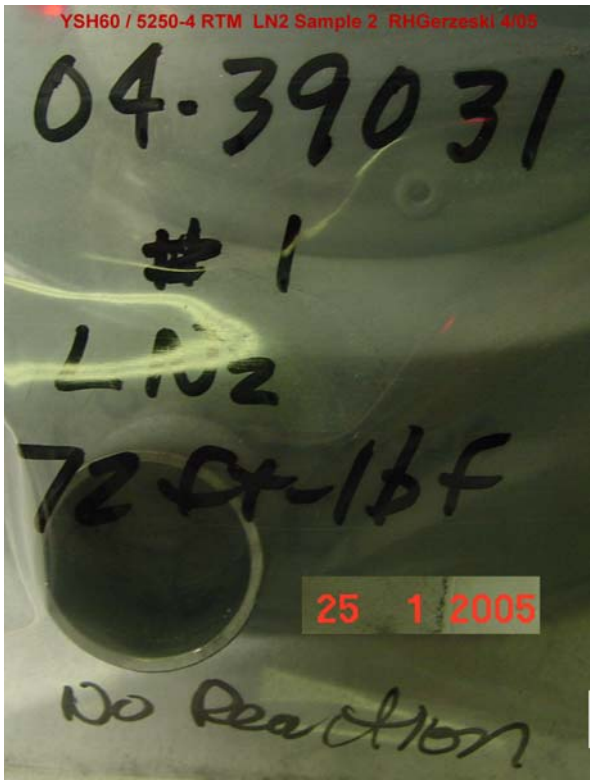


Figure R30b-ii YSH60A / 5250-4 RTM D2512 LN2 Specimen Return Bag Tags Residuals

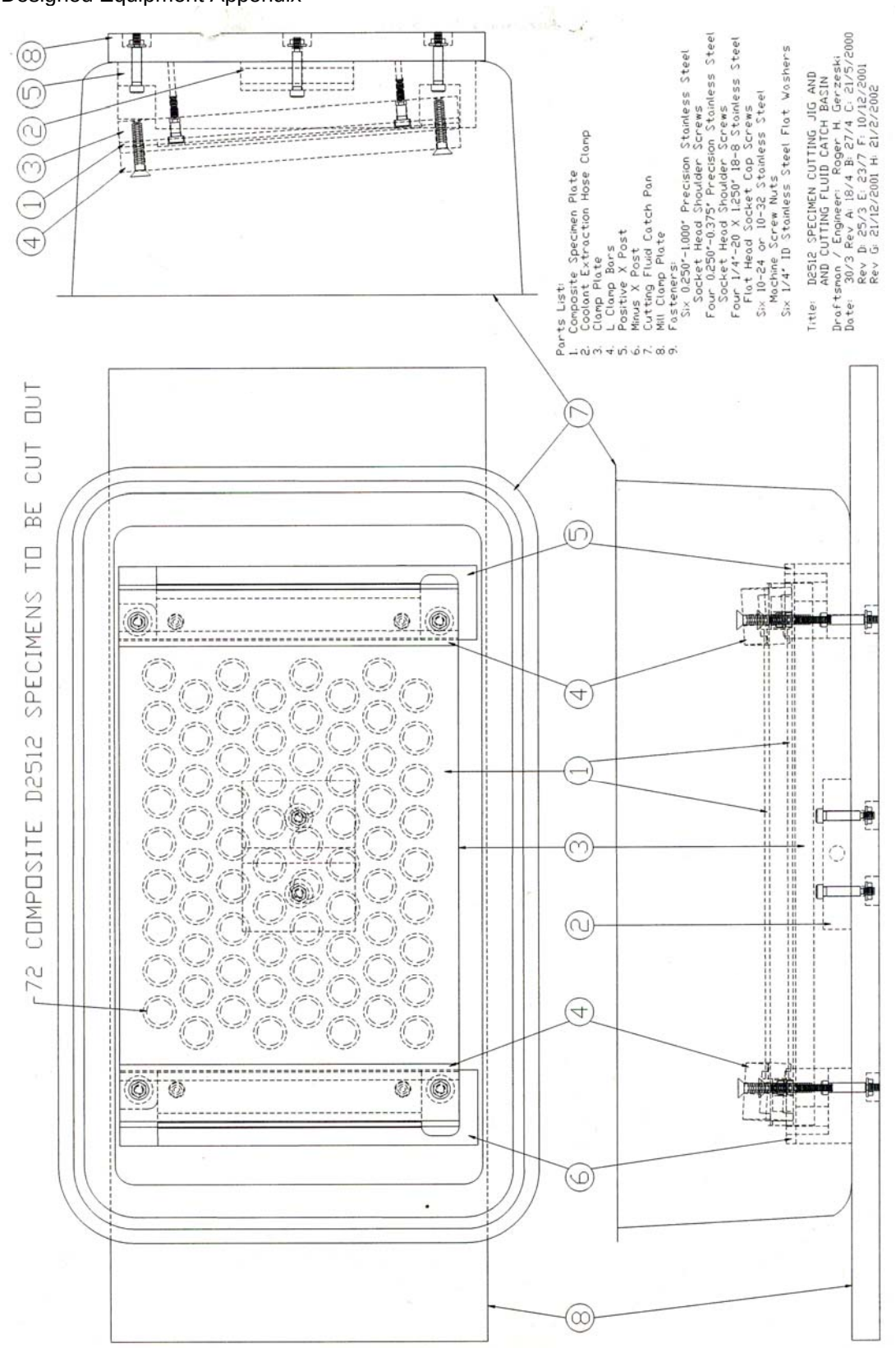


Figure D1-a, Designed Specimen Plate Holding Jig: Assembly

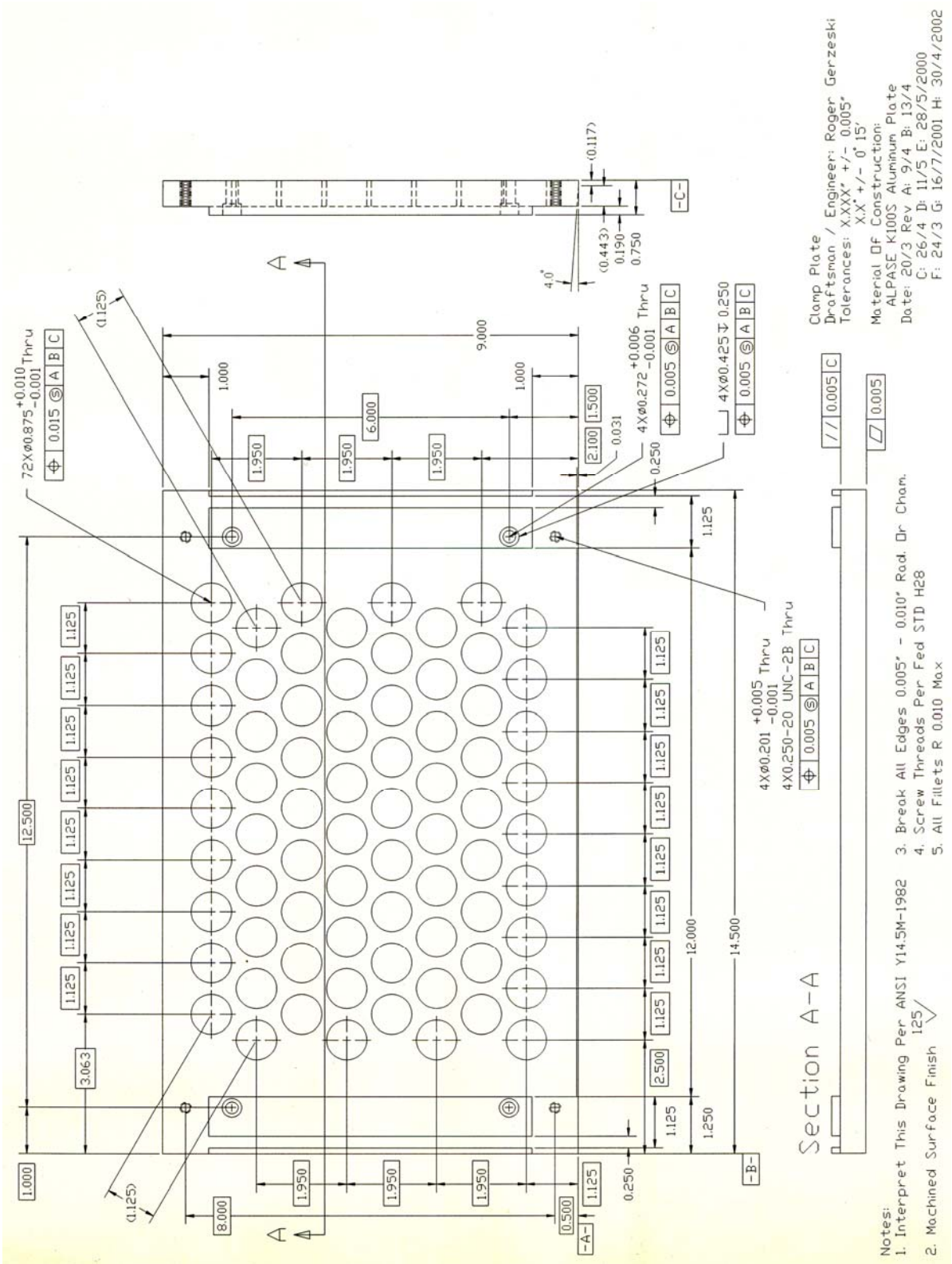


Figure D1-b-i, Designed Specimen Plate Holding Jig: Clamp Plate

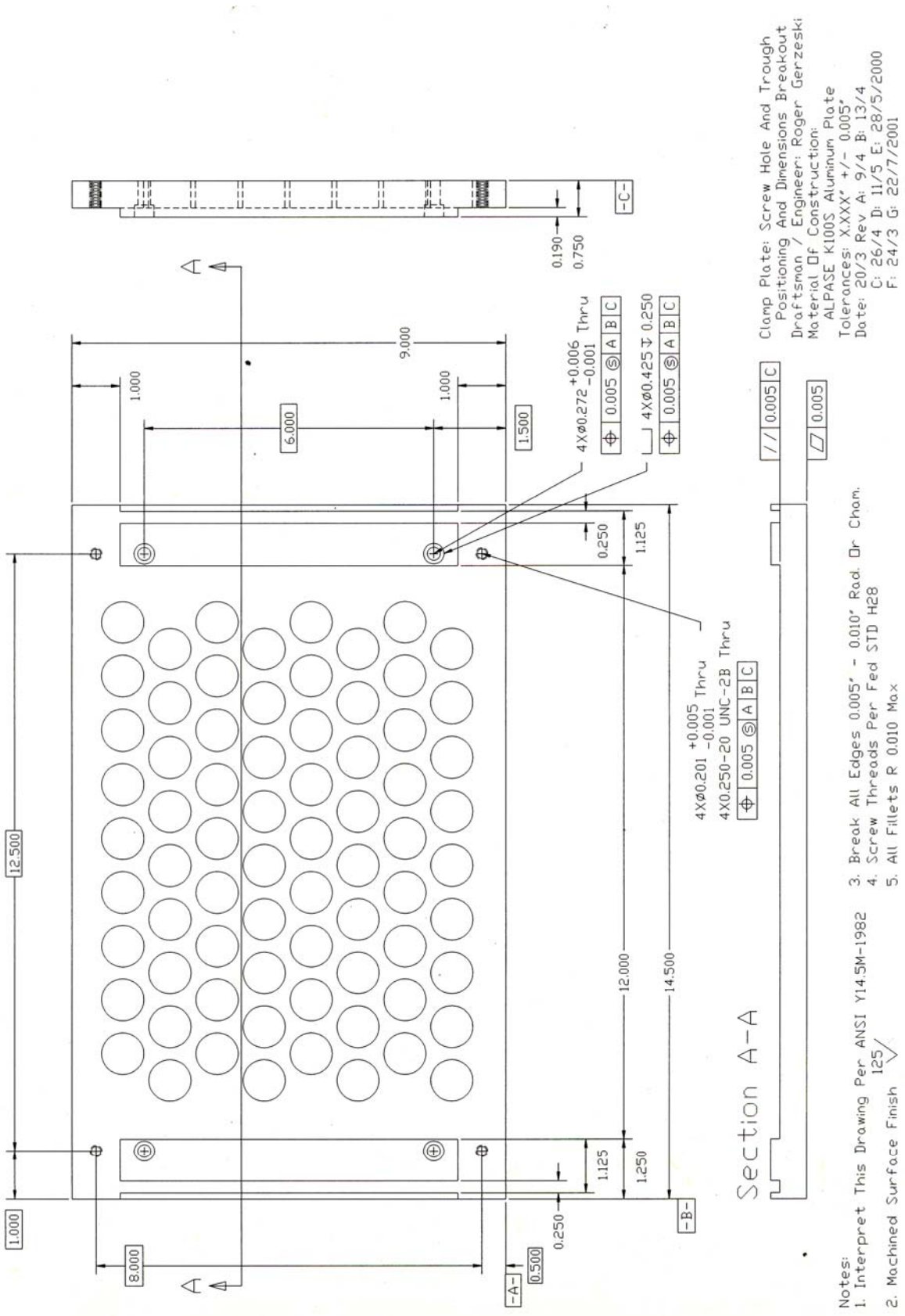


Figure D1-b-ii, Designed Specimen Plate Holding Jig: Clamp Plate: Screw Hole And Trough Positions

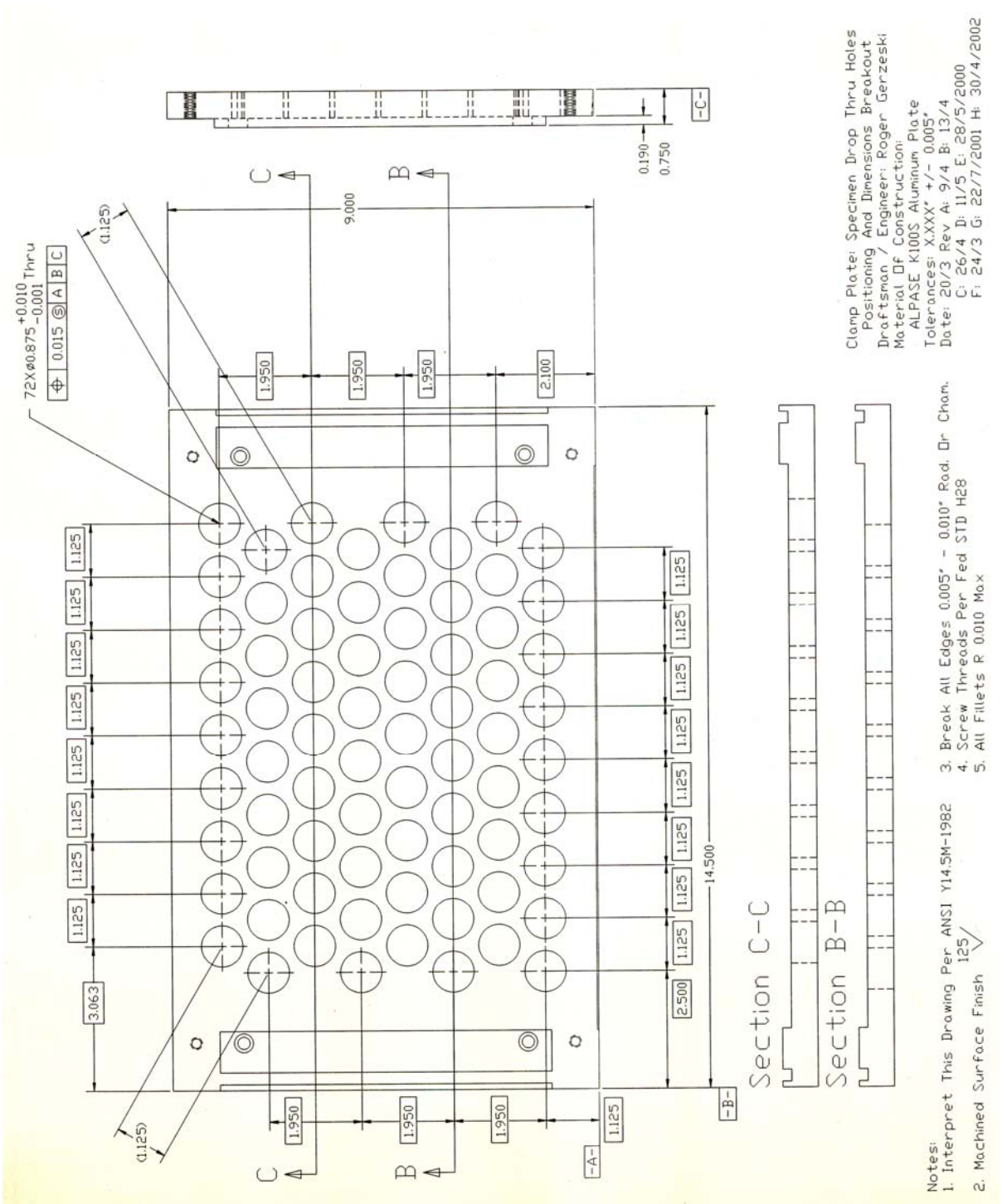


Figure D1-b-iii, Designed Specimen Plate Holding Jig: Clamp Plate: D2512 Specimen Drop Thru Hole Positions

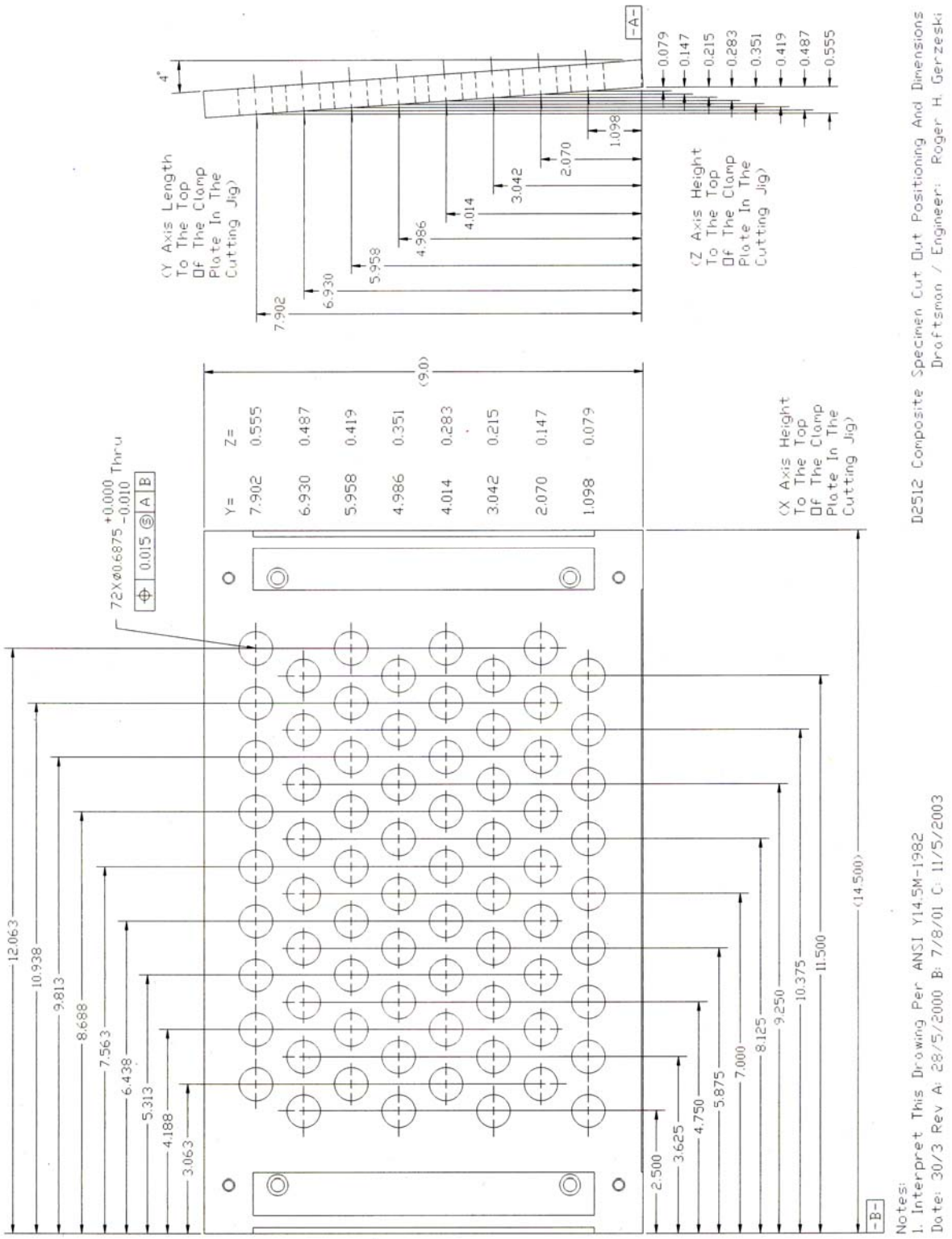


Figure D1-b-iv, Designed Specimen Plate Holding Jig: Clamp Plate: D2512 Specimen Cutting Positions

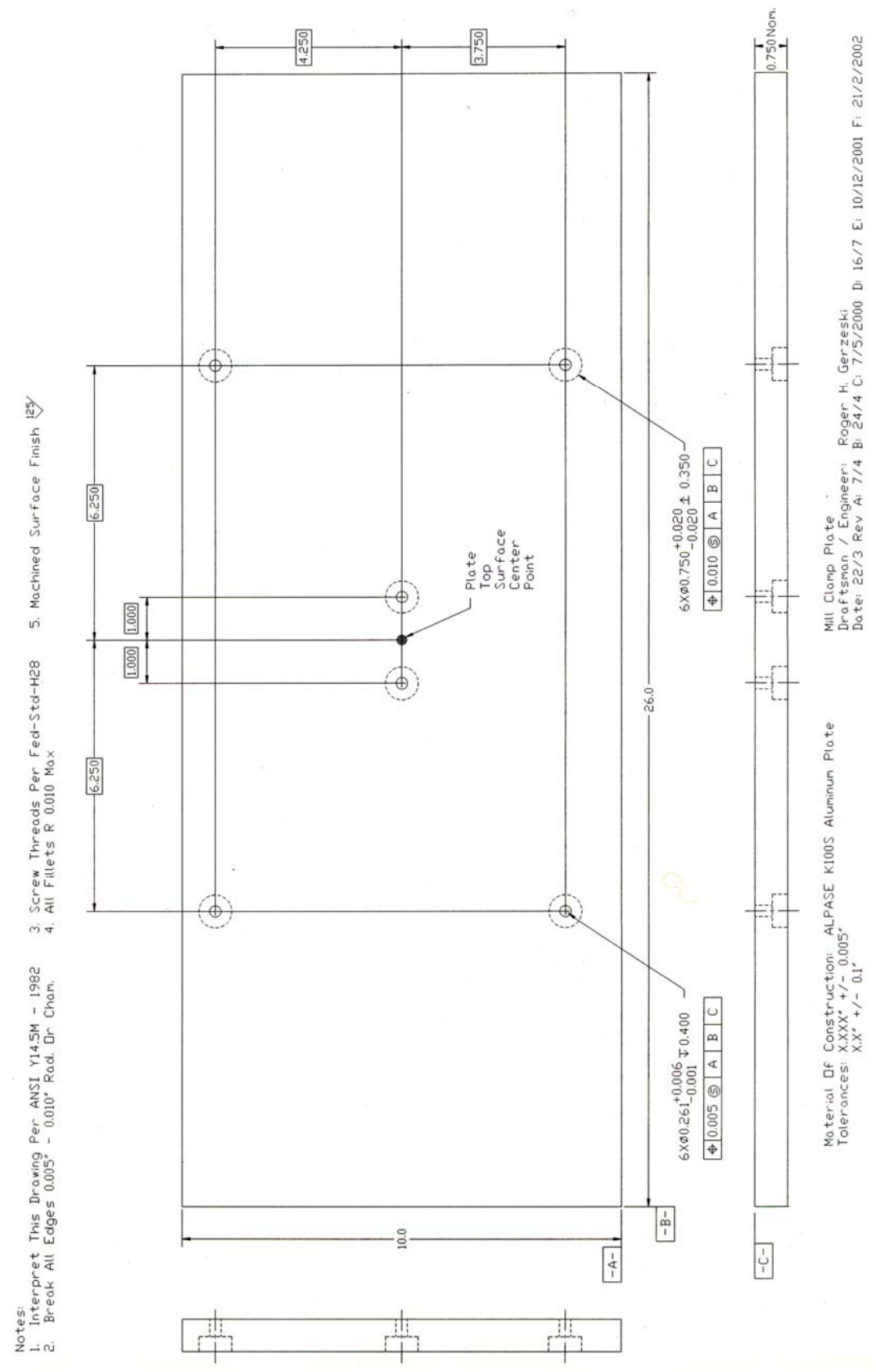


Figure D1-c, Designed Specimen Plate Holding Jig: Mill Clamp Plate

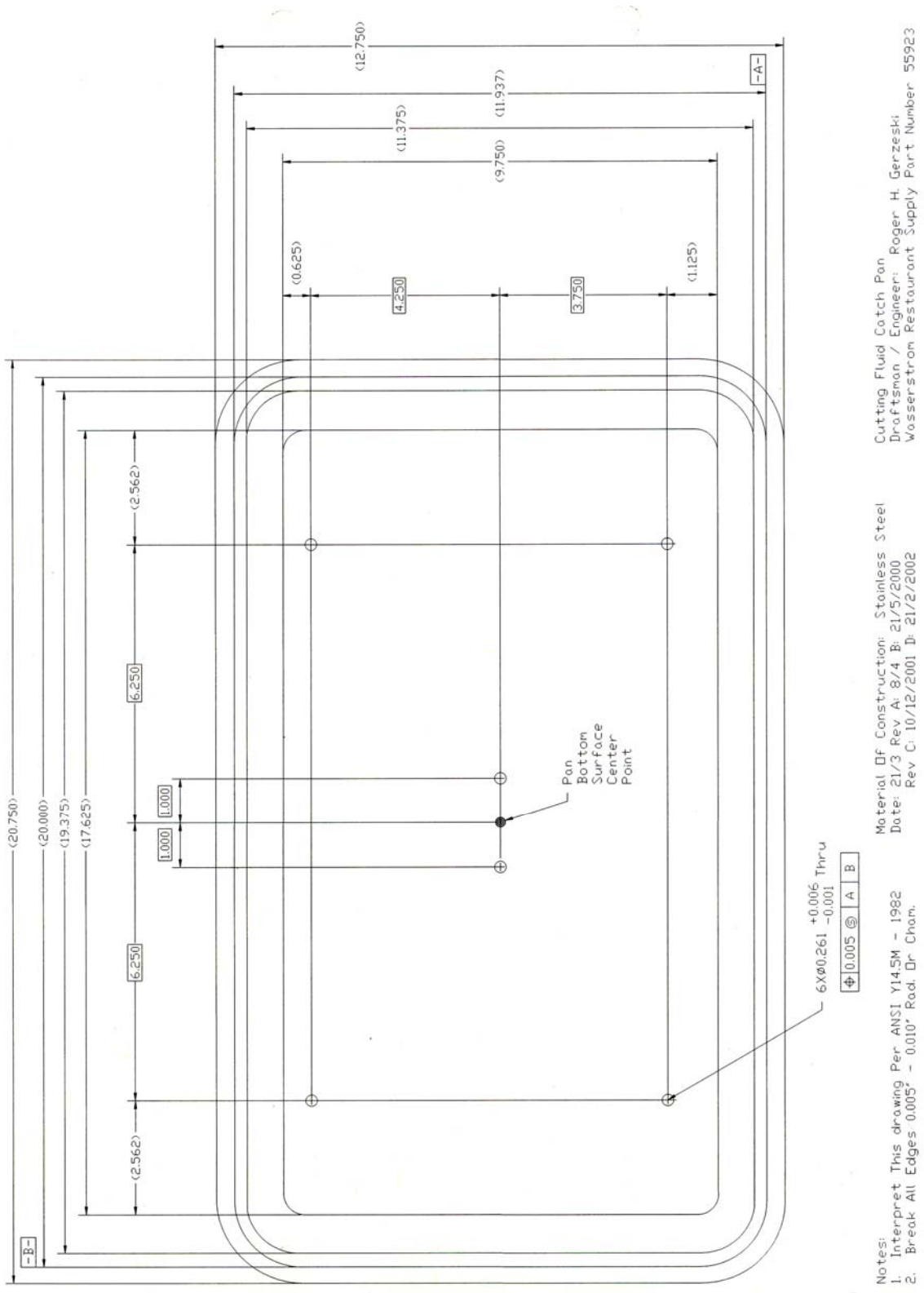


Figure D1-d, Designed Specimen Plate Holding Jig: Cutting Fluid Catch Pan

Figure D1-e, Designed Specimen Plate Holding Jig: Coolant Extraction Hose Clamp

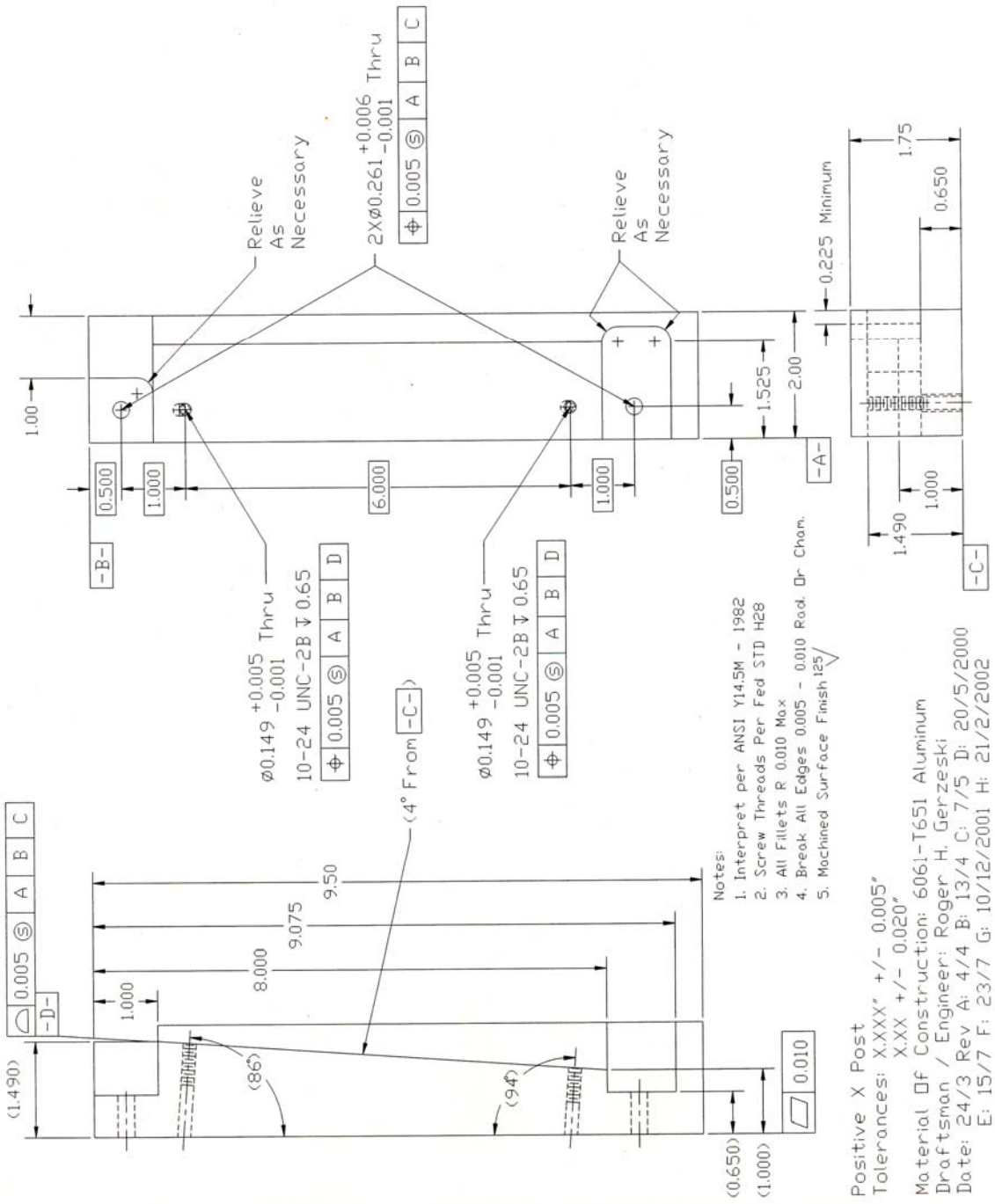


Figure D1-f, Designed Specimen Plate Holding Jig: Positive X Post

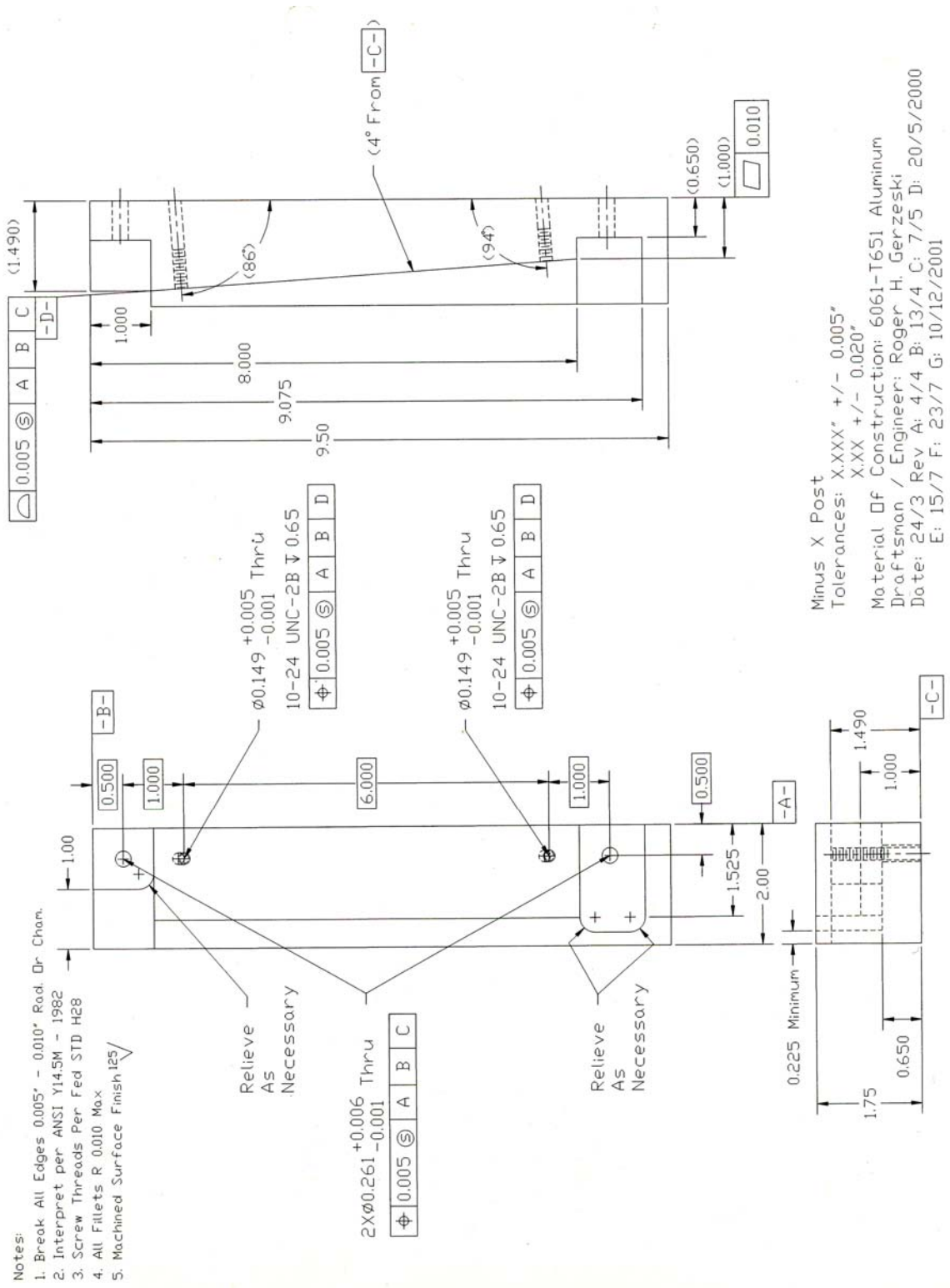


Figure D1-g, Designed Specimen Plate Holding Jig: Minus X Post

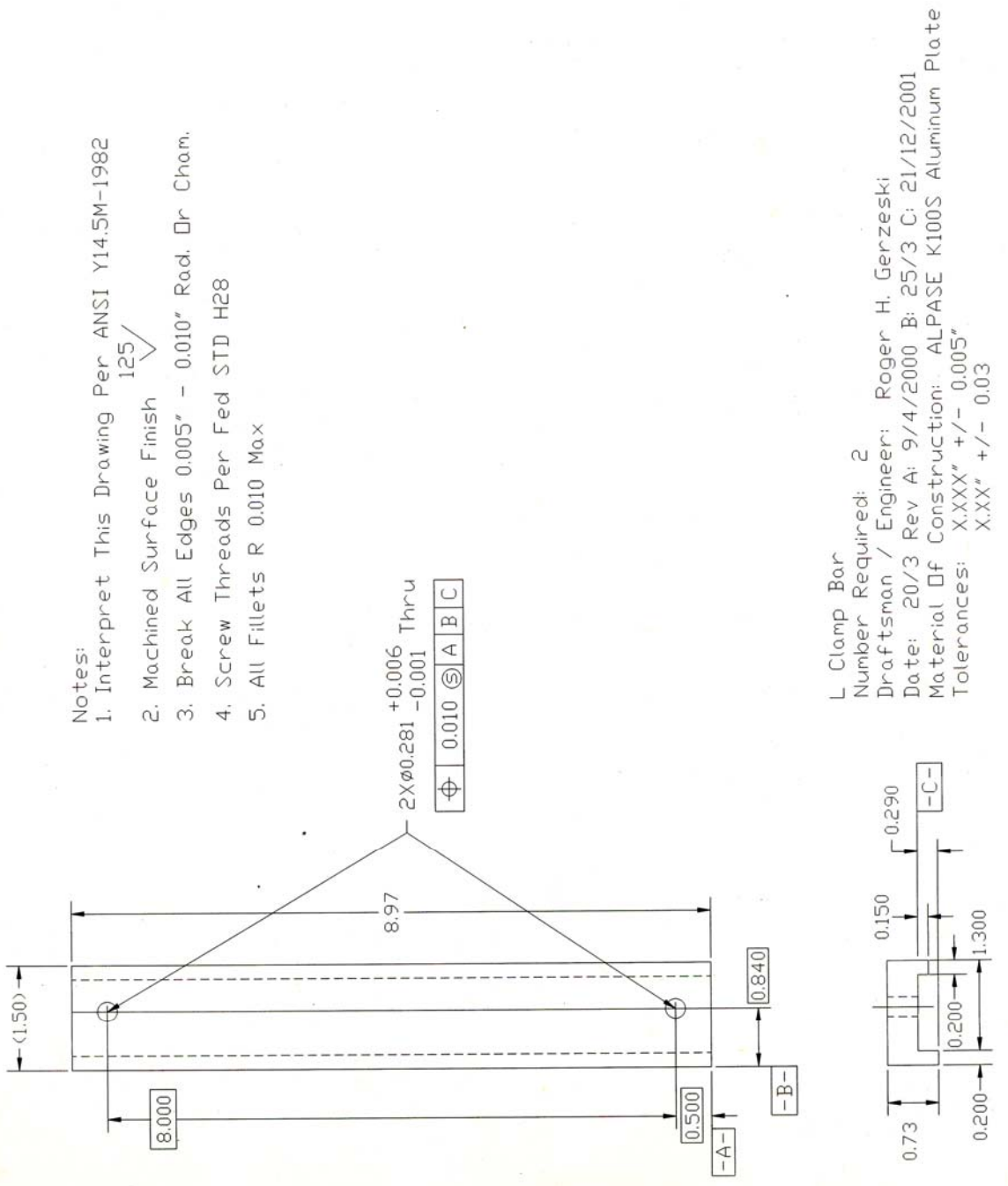


Figure D1-h, Designed Specimen Plate Holding Jig: L Clamp Bar

Figure D2, Diamond Core Drill

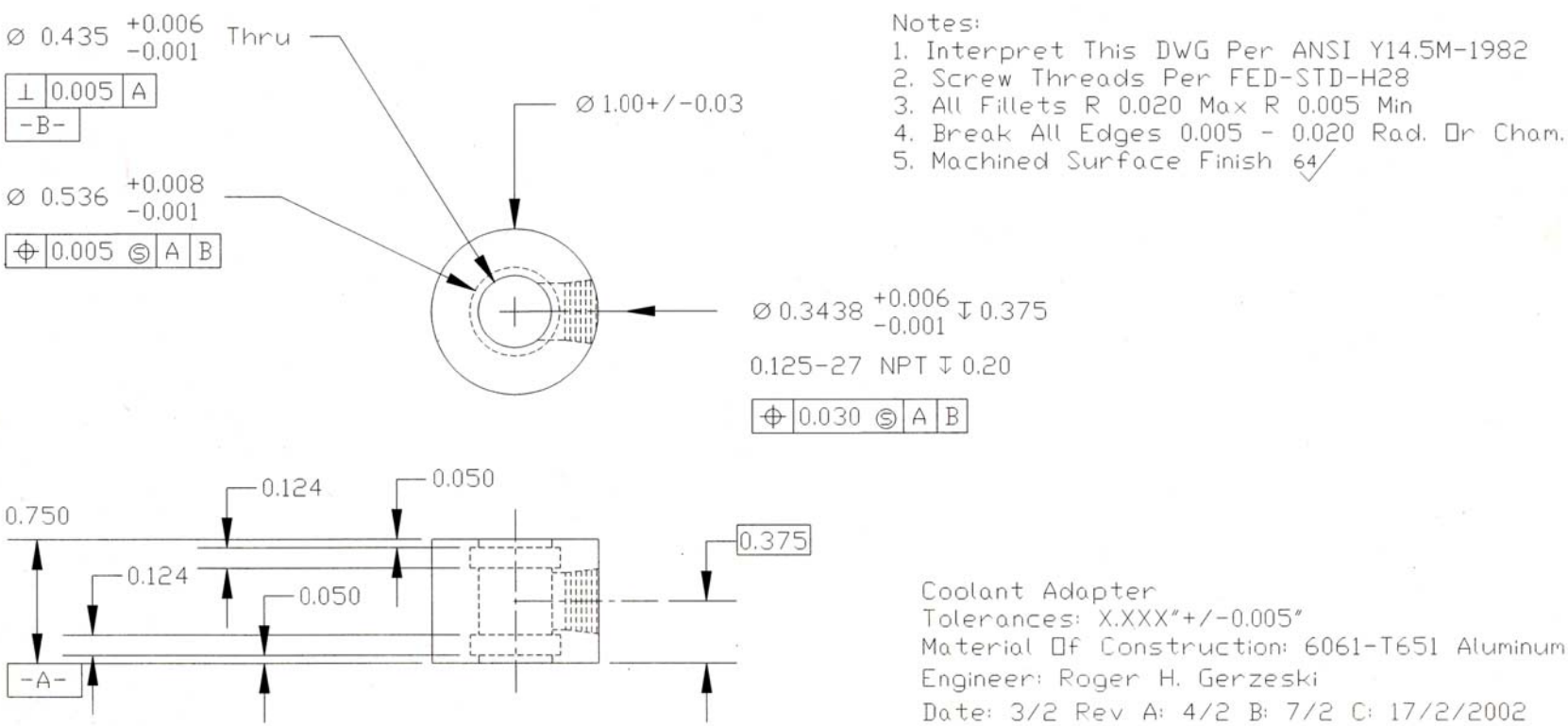


Figure D3, Coolant Adapter

Figure D4, Core Drill Wash Stand And Storage

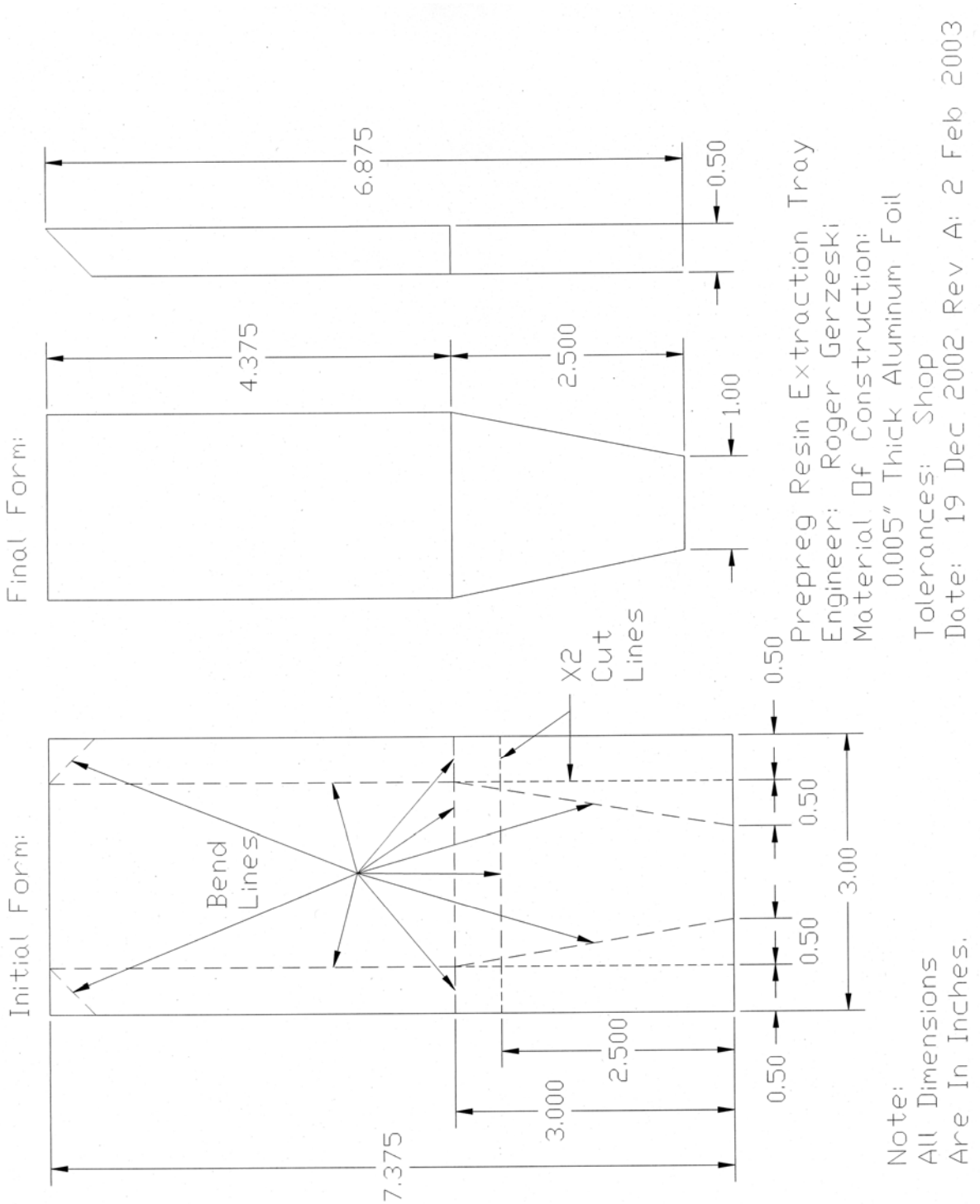


Figure D5-i, Resin Extraction Tray

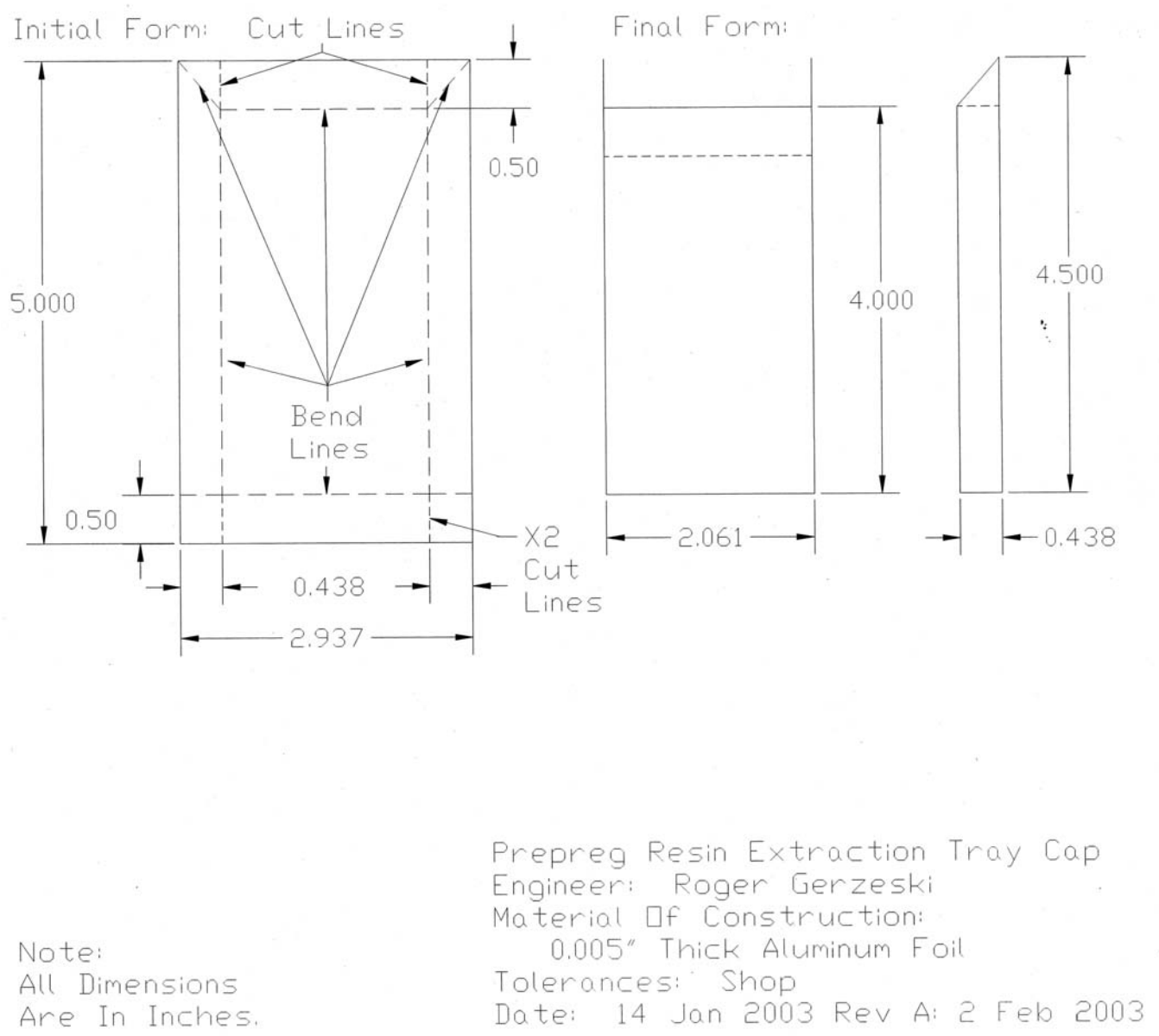


Figure D5-ii, Resin Extraction Tray Cap